RIKEN Accelerator Progress Report

2007

vol. 41

BOOK & CD-ROM

独立行政法人理化学研究所 仁科加速器研究センター
RIKEN Nishina Center for Accelerator-Based Science

RIKEN Accelerator Progress Report 2007

vol. **41**

BOOK & CD-ROM

独立行政法人理化学研究所　仁科加速器研究センター

RIKEN Nishina Center for Accelerator-Based Science
Wako, Saitama, 351-0198 JAPAN

GURAVURE & HIGHLIGHTS OF THE YEAR

The first electron scattering experiment using the SCRIT prototype

SCRIT Collaboration:

T. Emoto, Y. Furukawa[a], K. Ishii[b], S. Ito, T. Koseki[c], K. Kurita[a], A. Kuwajima[a], T. Masuda[b], A. Morikawa[a], M. Nakamura, A. Noda[d], T. Ohnishi, T. Shirai[e], T. Suda, H. Takeda, T. Tamae[a], H. Tongu[d], M. Wakasugi, S. Wang and Y. Yano

This year, there was a remarkable progress for the SCRIT collaboration. After nearly five years of intensive R&D studies of the SCRIT scheme using a prototype at KSR, Kyoto University, we have succeeded in trapping a sufficient number of ions and in reaching a sufficiently high luminosity for electron scattering experiments under the SCRIT scheme. The SCRIT has now proved to be a definite means for never-before-performed electron scattering off short-lived unstable nuclei. We finally prayed open the door to the structure studies of those nuclei by electron scattering.

The first observation of elastically scattered electrons was made in the April experiment.[1)] It was estimated that we trapped approximately 7 x 10^6 ions. By observing the elastically scattered electrons at the scattering angle of 30º, the luminosity was determined to be 2.4 x 10^{25} /cm^2/s.

In the December experiment, we further succeeded in increasing the luminosity to 10^{26} /cm^2/s by a finer control of the externally injected ion beam. The stored beam current of KSR was approximately 75 mA, and the ion trapping duration was 53 ms. This luminosity made it possible to perform the first electron scattering experiment by the SCRIT scheme: the measurement of the angular distribution of elastic electron scattering from 30º to 60º. These experiments completely mimicked the short-lived nuclei whose lifetime is in the order of 100 ms

Figure 1 shows the SCRIT prototype. Pulsed Cs ions were extracted from the ion source with the kinetic energy of 4.05 kV, and were merged at the deflector with the circulating electron beam thereby becoming trapped by the electron beam. They were, then, automatically guided towards the electrodes, where the mirror potential is formed for the longitudinal trap. The mirror potential was controlled in such a way that the pulsed Cs ions were introduced inside, and trapped for 53 ms with the kinetic energy of less than 2 eV. The ions were, then, released from the trap followed by the measurements of the number of trapped ions and their mass-to-charge distribution using the analyzer. This injection-trap-release cycle was repeated at a frequency of 17 Hz. For the repetitive measurement of scattered electrons with and without Cs ions, the Cs ions were injected every two cycles.

The scattered electrons emerging to the air through the 1-mm-thick Be window were detected using the electron detection system consisting of a drift chamber, plastic scintillators, and three sets of calorimeters. The calorimeters were energy-calibrated using 120 MeV electrons elastically scattered from the position-controllable 50 μm W wire. This whole system is installed at the 2 m straight section of the KSR as shown in Fig. 2.

In Fig. 3, the energy and vertex distributions of electrons detected by the pure-CsI calorimeter placed at the scattering

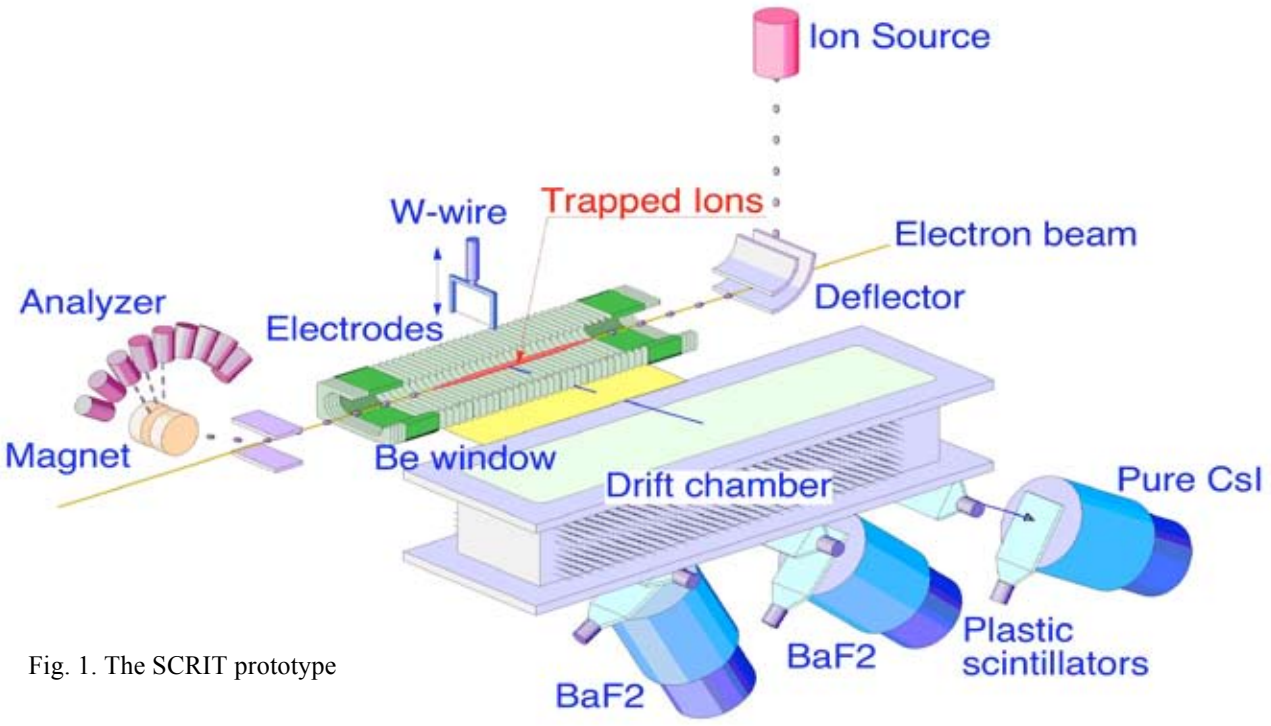

Fig. 1. The SCRIT prototype

angle of 30º are shown. Figure 3 (a) shows the vertex distribution of electrons whose energy is larger than 80 MeV. The blue (red) line shows that with (without) trapped Cs ions. Clear enhancement of electron events due to the trapped Cs ions is seen in the trap region. Figure 3 (c) shows the energy spectrum of electrons coming from the trap region. There is again a clear enhancement at around 120 MeV when the Cs ions are trapped (blue line). Since the spectrum shape of scattered electrons from the trapped Cs ions is found to be consistent with the response function of the calorimeter to 120 MeV determined using the W wire, we conclude that they are elastically scattered electrons from the trapped Cs ions.

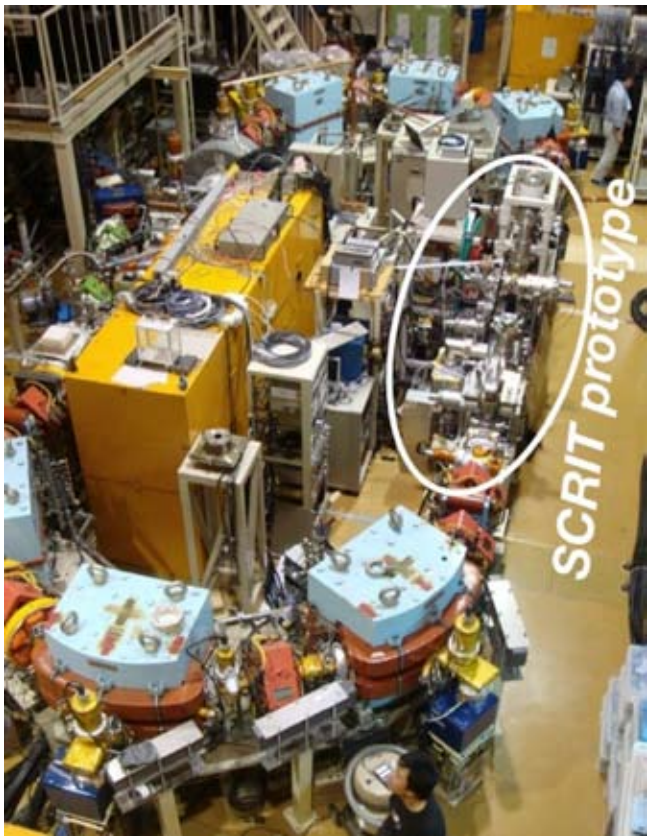

Fig. 2. Kyoto Storage Ring (KSR)

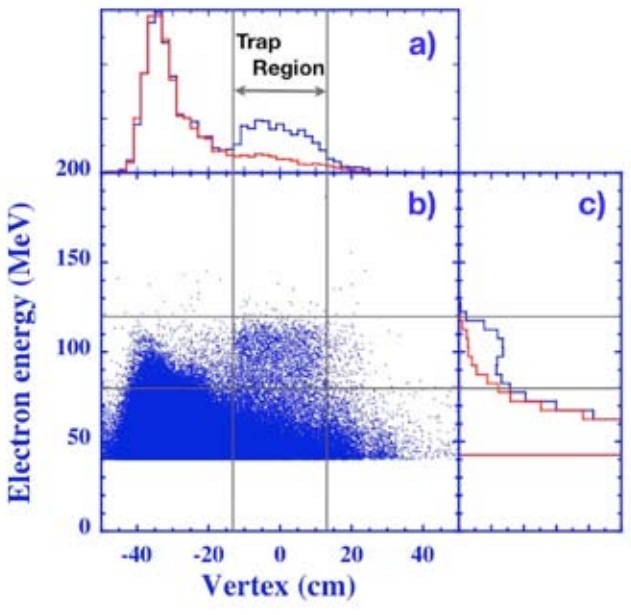

Fig. 3. Energy and vertex distributions of electrons detected by the pure CsI calorimeter. The blue (red) line in (a), (b) shows the events with (without) the trapped Cs ions.

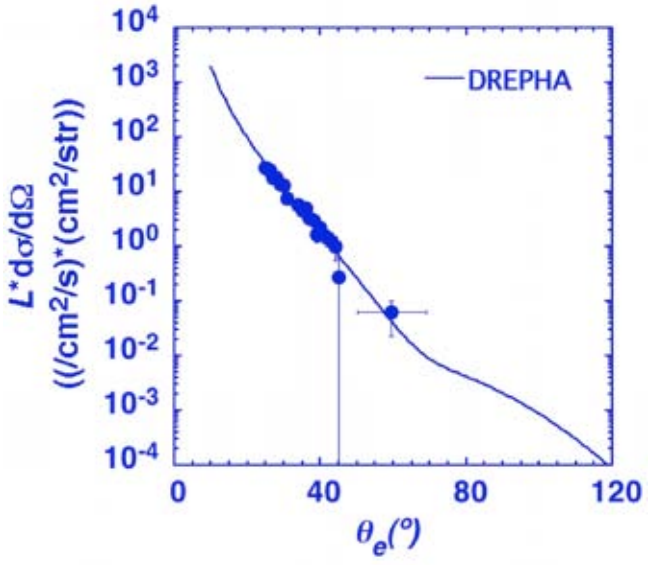

Fig. 4. Angular distributions of the scattered electrons from the trapped Cs ions. L and $d\sigma/d\Omega$ are the luminosity and the differential cross section, respectively.

Since the trap region was extended to 260 mm, a wide scattering angular range from 30º to 60º was covered. Figure 4 shows the angular distribution of the elastic scattering after correcting for the detector acceptance and the measuring time. The solid line in the figure shows the result of a distorted wave calculation of elastic electron scattering off ^{133}Cs. A good agreement of the angular dependence over nearly three orders of magnitude with the calculation confirms the measurement of elastic scattering.

Reference

1) M. Wakasugi *et al.*, Phys. Rev. Lett. **100,** 164801 (2008).

[a] Laboratory of Nuclear Science, Tohoku University
[b] Department of Physics, Rikkyo University
[c] Accelerator Laboratory, KEK
[d] Institute of Chemical Research, Kyoto University
[e] National Institute of Radiological Sciences

New isotopes ^{125}Pd and ^{126}Pd produced by projectile-fission of 345 A·MeV ^{238}U

T. Ohnishi, T. Kubo, K. Kusaka, K. Yoshida, A. Yoshida, M. Ohtake, Y. Yanagisawa, N. Fukuda, H. Takeda, N. Aoi, H. Suzuki [*1], Y. Mizoi [*2], Y. Yano, Y. Yamaguchi, K. Yoneda, H. Otsu, S. Takeuchi, D. Kameda, T. Sugimoto, Y. Kondo, H. Scheit, Y. Gono, H. Sakurai, T. Motobayashi, M. Matsushita [*3], K. Ieki [*3], T. Nakao [*1], H. Kimura [*1], T. Kuboki [*4], T. Yamaguchi [*4], T. Suzuki [*4], A. Ozawa [*5], T. Moriguchi [*5], Y. Yasuda [*5], T. Nakamura [*6], T. Nannichi [*6], T. Shimamura [*6], Y. Nakayama [*6], H. Geissel [*7], H. Weick [*7], J. A. Nolen [*8], O. B. Tarasov [*9], A. S. Nettleton [*9], D. P. Bazin [*9], B. M. Sherrill [*9], D. J. Morrissey [*9], and W. Mittig [*10]

[NUCLEAR REACTION Be(^{238}U, x) E = 345 MeV/nucleon, In-flight fission, New isotopes ^{125}Pd and ^{126}Pd, In-flight RI beam separator]

BigRIPS[1] is a new superconducting in-flight radioactive isotope (RI) beam separator at the RI Beam Factory (RIBF)[2], which provides various RI beams produced by in-flight fission or projectile fragmentation of heavy ions including uranium. It was completed and came into operation in 2007. In the first experiment using the BigRIPS, we searched for new isotopes that are very neutron-rich nuclei at around $Z = 50$ produced in the in-flight fission of ^{238}U at 345 MeV/nucleon, and the new isotopes ^{125}Pd and ^{126}Pd were found.

The in-flight fission of fissile beams[3] was used to produce neutron-rich nuclei that are far from stability. The advantages of this reaction have been demonstrated by experiments at GSI[4,5] using the ^{238}U beam. In these experiments, more than one hundred new isotopes were identified in a single experiment. The BigRIPS has been designed with large acceptances in both angle and momentum using superconducting magnets. Owing to its large acceptances, the BigRIPS can use its advantage of high production cross sections of neutron-rich isotopes from in-flight fission reaction and a good collection efficiency of fission fragments, approximately 50%.

A ^{238}U beam was accelerated up to an energy of 345 MeV/nucleon, using the newly constructed accelerator complex consisting of the linear accelerator RILAC and the four cyclotrons RRC, fRC, IRC, and SRC[2]. The uranium beam reacted with a 7-mm-thick Be target, and its intensity, monitored by measuring light charged particles recoiling out of the target, was 4×10^7 particle/sec on average. Fission fragments emitted near zero degrees were collected and analyzed using the BigRIPS. The BigRIPS consists of two stages. At the first stage, the fragments were separated by selecting magnetic rigidity ($B\rho$). The transmitted fragments were identified event by event at the second stage. During the experiment, several settings of $B\rho$ ranging from 7.0 Tm to 7.6 Tm were employed in order to determine the production yields of neutron-rich isotopes near the known limits.

Particle identification was performed at the second stage using the measured $B\rho$, energy loss (ΔE), and time of flight (TOF). TOF was measured using two plastic scintillation counters placed on the first (F3) and last (F7) focal planes of the second stage with a central flight length of 47 m. Both focal planes are achromatic. The scintillation counters were 0.2 mm thick and 100×100 mm^2 in area. At F7, two 0.35-mm-thick Si detectors with an active area of 50×50 mm^2 were installed to measure ΔE. To measure $B\rho$ precisely, the trajectory of the fragments was reconstructed from the positions and angles measured in two position-sensitive PPACs[6] at the achromatic focal plane (F3) and two more at the intermediate dispersive focal plane (F5) of the second stage. The effective area of the PPACs was 240×150 mm^2. First-order ion-optical transfer matrices were obtained experimentally with the RI beams and primary uranium beam, and they were used for the trajectory reconstruction. The $B\rho$ of the fragments on the central trajectory was determined using the magnetic fields of the dipoles measured using NMR probes and the central trajectory radii of the dipoles deduced from the magnetic field-map data. To confirm the particle identification, delayed γ rays from isomeric states in some of the products were measured using two clover-type high-purity germanium detectors located at F7.

Figure 1 shows a two-dimensional plot of the atomic number Z versus the mass-to-charge ratio A/Q at $B\rho$=7.395 Tm with a momentum acceptance of $\Delta P/P$=±1%. In Fig. 1, the events that their charge state did not change at F3 and F5 were selected by gating on the reconstructed $B\rho$. The relative root-mean-square (rms) resolution for Z and A/Q for Pd (Z=46) isotopes was 0.55% and 0.041%, respectively. Z was determined from ΔE and TOF, while A/Q was

[*1] Department of Physics, The University of Tokyo
[*2] Division of Electronics and Applied Physics, Osaka Electro-Communication University
[*3] Department of Physics, Rikkyo University
[*4] Department of Physics, Saitama University
[*5] Institute of Physics, University of Tsukuba
[*6] Department of Physics, Tokyo Institute of Technology
[*7] Gesellschaft für Schwerionenforshung (GSI)
[*8] Algonne National Laboratory (ANL)
[*9] Michigan State University (MSU)
[*10] Grand Accelerateur National d'Ions Lourds (GANIL)

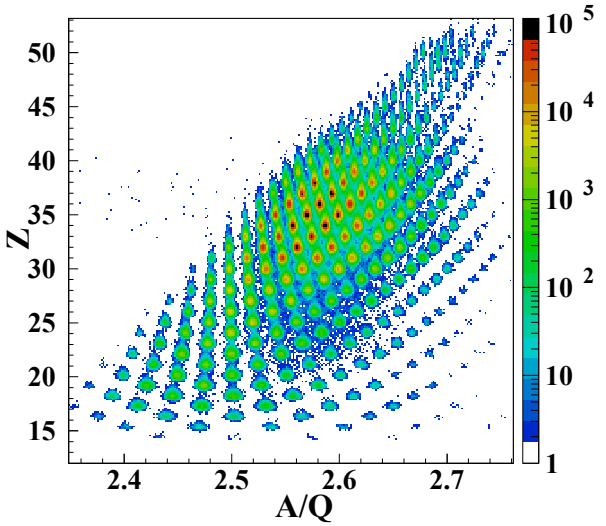

Fig. 1. Two-dimensional plot of Z versus A/Q at $B\rho$=7.395 Tm with momentum acceptance of $\Delta P/P = \pm 1\%$. In this figure, the events in which their charge state do not change at F3 and F5 are shown.

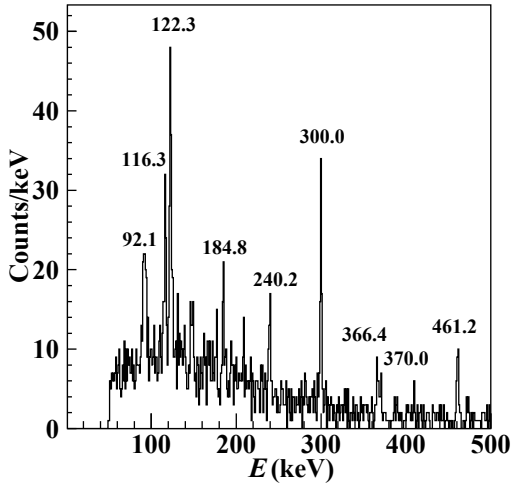

Fig. 2. Energy spectrum of delayed γ rays gated on ^{96}Rb. The labeld γ rays are corresponding to those from the decay of the isomeric state in ^{96}Rb.

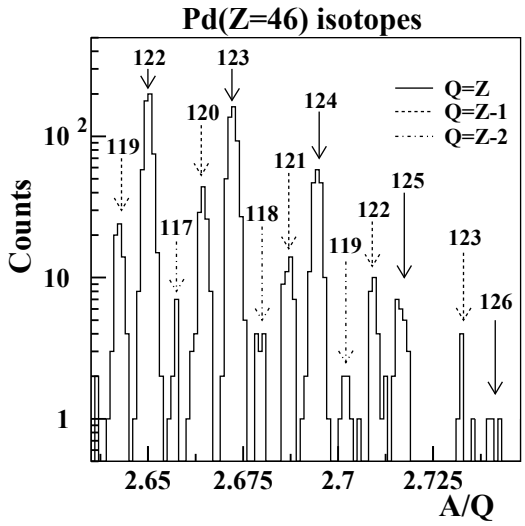

Fig. 3. A/Q spectrum of Pd isotopes around new isotopes. The Z gate is set to 46 $\pm 1.5\sigma$(0.38). The peaks are labeled using mass numbers and charge states.

deduced from TOF and $B\rho$. The calibration of TOF and ΔE was performed using fragments that have the central $B\rho$ value. The effect of the small energy loss in the F5 PPACs was included in deducing the velocity of the fragments. Particle identification was confirmed using delayed γ rays from the decay of the isomeric state in ^{96}Rb with an excitation energy of 1135 keV and a half-life of 2.0 μsec[7], as shown in Fig. 2.

An A/Q plot for Pd isotopes around new isotopes is shown in Fig. 3. This plot was obtained from the two-dimensional Z versus A/Q plot shown in Fig. 1 by gating with a Z gate set to 46 $\pm$ 0.38 (1.5σ), where σ represents the absolute rms Z resolution. Peaks for fully stripped (Q=Z), H-like (Q=$Z-1$), and He-like (Q=$Z-2$) ions are separated from each other. As shown in the figure, the new isotope ^{125}Pd is clearly identified at $A/Q = 2.717$, and the centroid position of ^{125}Pd peak is 6.2σ apart from that of ^{122}Pd^{45+} which is the nearest nuclei, where σ, the absolute rms A/Q resolution, is 0.0011. The total yield of ^{125}Pd is 22 counts. The production of the new isotope ^{126}Pd is also clearly seen in Fig. 3, although its yield is 3 counts. The total beam dose was 3.6×10^{12} at approximately 25 hours of irradiation time.

In summary, we performed the first experiment at the BigRIPS, and found the new isotopes ^{125}Pd and ^{126}Pd. This result shows the high performance of the BigRIPS in the production, separation, and particle identification of unstable nuclei. More detailed description is reported in ref. 8, and further data analysis is in progress to extract the cross sections of isotope production.

References

1) T. Kubo et al.: Nucl. Instr. and Meth. B**204**, 97(2003).
2) Y. Yano: Nucl. Instr. and Metsh. B**261** 1009(2007).
3) J. Benlliure et al.: Nucl. Phys. A**628** 458(1998).
4) M. Bernas et al.: Phys. Lett. B**331**, 19(1994).
5) M. Bernas et al.: Phys. Lett. B**415**, 111(1997).
6) H. Kumagai et al.: Nucl. Instr. and Meth. A**470**, 562(2001).
7) J. A. Pinston et al.: Phys. Rev. C**71**, 064327(2005).
8) T. Ohnishi et al.: J. Phys. Soc. Jpn. **77**, 083201(2008).

New innovative technology in plant breeding using heavy-ion beams

T. Abe, Y. Kazama, H. Takehisa, H. Ichida, K. Nishihara, Y. Hayashi, H. Ryuto, N. Fukunishi and T. Kambara

Induced mutations are highly effective in enhancing genetic variation in plants and have been successfully applied to the development of improved and new cultivars. The number of cultivars that have been bred by this method exceeds 2600 worldwide. Heavy-ion beam irradiation, which has been developed in Japan, is one of the most remarkable mutation technologies. We have put 6 new flower cultivars in the market in Japan, USA, Canada and EU since 2001 (Fig. 1 to 3). The year 2007 is memorable for the creation of a new color in the flower of a cherry named "Nishina Zao" (Fig. 4) using heavy-ion beams, which became the first plant that RIKEN registered under the Seeds and Seedlings Law. Besides "Nishina Zao", eight new flowers such as "Olivia Pure White" (dianthus, Fig. 5), "Reiko Pink" and "Reiko Pink Ring" (delosperma, Fig. 6), "Summer Wave" series (torenia) and others will begin sales in 2008 to 2009. A short overview of the technology follows.

Fig. 1. A flower bed in front of the RIKEN cafeteria. These flowers were created by ion beam irradiation. "Temari Momo", "Temari Bright Pink", "Temari Sakura Pink" and "Surfinia Rose Veind" from the center.

Fig. 2. New color of torenia "Summer wave pink white".

Fig. 3. New color of dahlia "World".

Fig. 4. New color of cherry "Nishina Zao".

Fig. 5. New color of dianthus "Olivia Pure White".

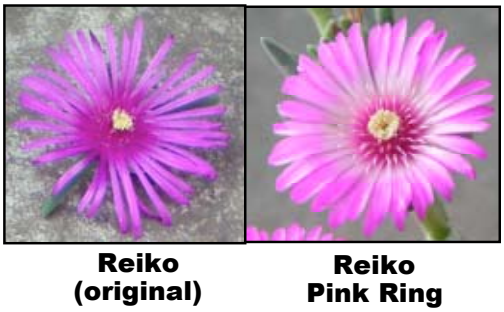

Fig. 6. New color of delosperma "Reiko Pink Ring".

Ion beams with high linear energy transfer (LET) have higher biological effects than low-LET radiation such as gamma and X-rays. Heavy-ion cancer therapy was advanced from 1986 at the RIKEN Ring Cyclotron (RRC) by the collaboration of radiation oncologists, physicists, and biologists. Encouraged by the above experience, our plant scientist group started to use the RRC for radiation biology research in 1989. We soon found that the ion beam is highly effective in causing mutagenesis of seed embryos at a particular stage during fertilization without damage to other plant tissues when an ovule-sized collimator (5-10 mm diameter) was used. We isolated many types of mutant in tobacco including albino, variegated, salt-resistant, and herbicide-resistant phenotypes.[1-3] We concluded that atomic ions accelerated to high energies induce mutations at high efficiency and wide variation even under low exposure doses and short irradiation time. A passage of an ion induces double-strand breaks at a few sites on the DNA, and a mutant lacking a gene is produced with high probability.[4-6] Then the mutants can be selected as a new variety in which the target characteristics are modified while other existing valuable characteristics are retained.[7, 8] The time for breeding can be shortened significantly to two or three years.

The LET of ions in matter has a sharp peak at the end of the range, which is called the Bragg peak (BP). In the case of cancer therapy, the BP is adjusted to the target malignant cells so that the ions deliver more dose in the target while considerably less dose to the surrounding normal tissues. In the case of plant biology, on the other hand, a uniform dose distribution is a key to the systematic study, and thus, to the improvement of the mutation efficiency. We selected sufficiently high beam energy to avoid the effect of BP and realize a uniform dose distribution. An LET of 30 keV/μm was found to be the most effective for mutation induction in *Arabidopsis* (Fig. 7)[4] and the deletion size obtained using Fe ions was larger than that using C ions in a microorganism.[9]

In parallel to these research studies, we have organized a heavy-ion plant research consortium with 120 national user groups and 11 international ones, which include agricultural experimental stations, universities, seed companies and flower companies. Recently, we have shown various results in plant physiology, genetics, botany, and agricultural science from our extensive studies using mutants of many species in the plant kingdom. We isolated 4 strains of salt-resistant rice and one of them can be grown in a saline paddy field and can produce good grains.[10, 11] Other crops have been developed using the technology, including semidwarf buckwheat that is shorter and sturdier than normal[12] and resistant to typhoon winds, sterile tomato (Fig. 8)[13] and wheat[6, 14], which are bioresources for gene analysis that enable the molecular understanding of the mechanisms of flowering. The ion beam irradiation technique enables the isolation of unique mutants that have never been obtained by conventional methods.

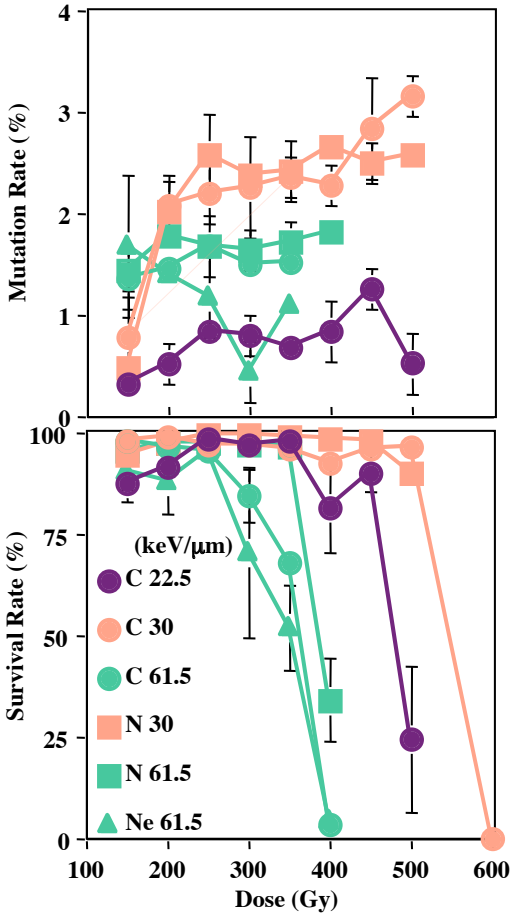

Fig. 7. Effects of heavy-ion beams on survival rate and mutation induction in *Arabidopsis*.

Fig. 8. Sterile mutant of tomato.

Referemces
1) T. Abe et.al.: RIKEN Accel. Prog. Rep. **29**, 165 (1996)
2) T. Abe et.al.: RIKEN Accel. Prog. Rep. **30**, 127 (1997)
3) T. Abe et.al.: RIKEN Accel. Prog. Rep. **31**, 148 (1998)
4) Y. Kazama et.al.: Plant Biotech. **25**, 113-117 (2008)
5) Y. Kazama et.al.: RIKEN Accel. Prog. Rep. **41**, 225 (2008)
6) K. Murai et.al.: RIKEN Accel. Prog. Rep. **41**, 233 (2008)
7) K. Suzuki et.al.: RIKEN Accel. Prog. Rep. **35**, 129 (2002)
8) M. Sugiyama et.al.: RIKEN Accel. Prog. Rep. **41**, 229 (2008)
9) H. Ichida et.al.: RIKEN Accel. Prog. Rep. **41**, 224 (2008)
10) Y. Hayashi et.al.: RIKEN Accel. Prog. Rep. **41**, 234 (2008)
11) Y. Hayashi et.al.: RIKEN Accel. Prog. Rep. **40**, 253 (2007)
12) T. Morishita et.al.: RIKEN Accel. Prog. Rep. **41**, 232 (2008)
13) S. Imanishi et.al.: RIKEN Accel. Prog. Rep. **41**, 231 (2008)
14) K. Murai et.al.: RIKEN Accel. Prog. Rep. **39**, 136 (2006)

Installation of production target system for BigRIPS separator

Atsushi Yoshida, Yoshitaka Yamaguchi, Kanenobu Tanaka, Yoshiyuki Yanagisawa and Toshiyuki Kubo

The production target system for the projectile fragment separator (BigRIPS) has been installed. It was constructed on the basis of its design studies and R&D experiments.[1-4)]

The target chamber has a replaceable unit structure to facilitate its maintenance under a high-radiation environment. On a side wall of the chamber, a target flange unit is mounted, which is a core component of this target system. The target flange unit is an all-in-one vacuum flange (Fig. 1). That is, two sets of water-cooled rotating disk target units, beam diagnostic devices of a Faraday cup (FC) and a beam profile monitor, a ladder-shaped target, and a view port for target monitoring are mounted on the same vacuum flange. Below the chamber, a vacuum pump unit that consists of a gate valve, a turbo pump, and a rotary pump is mounted. For maintenance, the target flange unit and the vacuum pump unit are disassembled using a remote-handling maintenance cart running on rails. Then, nothing remains in the chamber and we can replace all the target components.

Fig. 1. a) Target flange unit. b) Target vacuum chamber and vacuum pump unit. c) Internal view of the disk target unit containing a motor and water inlet tubes.

The maintenance procedure of the target flange unit will be carried out to change the disk target, or in the case of a failure, the target components. The remote-handling cart holds the target flange unit, and then the pneumatic flange lock actuators placed on the unit are released. After breaking the vacuum of the target chamber, the cart transports the flange through an access tunnel to a temporary storage area where spare target units are kept ready (Fig. 2). At the temporary storage area, the target flange is inserted into a shielding container and allowed to cool for several weeks. A simulator chamber is used for checking in advance the proper operation of the newly installed target flange unit.

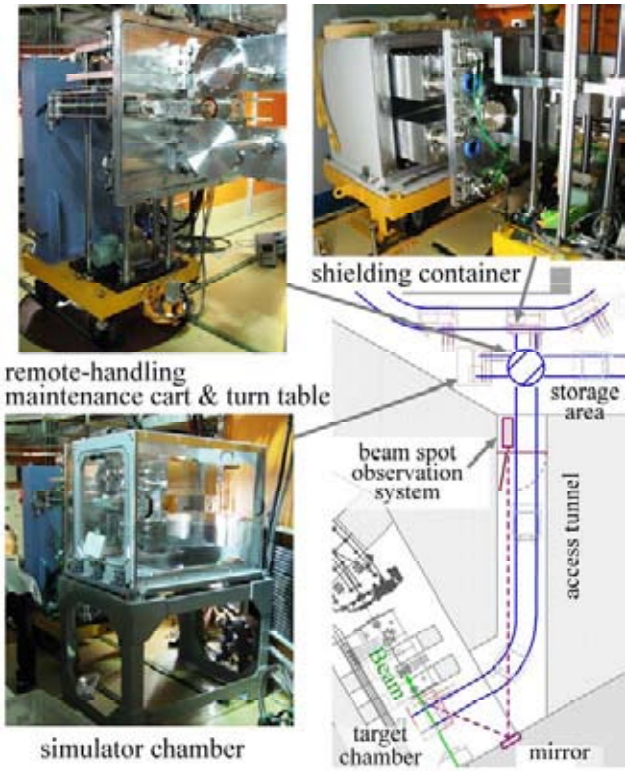

Fig. 2. Remote handling target maintenance system.

Two types of targets are provided on the target flange (Fig. 1-a). For low-beam-power experiment, namely, up to a few kilowatts of energy loss in a target, the ladder-shaped target with water cooling, which is a fixed target, is provided. Four target plates shaped as a small disk of 20 mm diameter with up to 20 mm thickness are available for mounting the fixed target holder. For high-beam-power experiments, two sets of water-cooled rotating disk target units are provided. A disk target shaped as a large disk of 30 cm diameter with up to 15 mm thickness is available for mounting the disk target unit. A wide variety of targets with different thicknesses should be prepared. Those thicknesses should be flexible by as much as 10-50 % of the stopping range of the primary beams in a target material. It is in the range of a few millimeters up to several centimeters for U to C primary beams onto a beryllium target. For this purpose, step-shaped disk targets whose circumference edge of 30 mm width has a step shape are provided. And each of the two rotating disk target units can be moved perpendicular to the beam axis by 60 mm. Using two step-shaped disks simultaneously, a wide variety of target thickness control becomes available.

As a guideline for the proper use of the fixed target and

rotating disk target, the beam spot temperature on both targets is calculated. For the fixed target, its beam spot temperature (Tr1) is analytically calculated using a formula based on the cylindrical temperature gradient model.

$Tr1 = Tr2 + dE * \ln(r2 / r1) / (2\pi * \kappa * Ltg)$,

where r1 is the beam spot radius on the fixed target and dE is the energy loss in the cylinder-shaped target of r2 radius and Ltg thickness. κ indicates the thermal conductivity of the target material. Here, an ideal water cooling is assumed, i.e., the temperature at the side wall of the target cylinder is kept the same as the cooling water temperature (Tr2). The calculated beam spot temperature on a Be target as a function of the primary beam intensity of U to C is plotted (Fig. 3). For light primary beams up to Ar, the temperature is always much below the melting temperature of the Be target material up to the goal intensity of 1 particle μA (pμA) at this facility. In this respect, the fixed target is safely applicable for these light primary beams. For the heavy primary beams of Kr to U, the fixed target is also applicable up to the intensity of a few 100 pnA. However, we should surely use the rotating target for primary beams of Kr to U with the intensity near to 1 pμA. For the rotating target, its beam spot temperature is calculated using the ANSYS code by using the RIKEN Super Combined Cluster (RSCC). The result for a Be disk target of 30 cm diameter and 4.4 mm thickness rotating at 500 rotation per minute (rpm) for the U beam is plotted with dashed line in Fig. 3 and compared with the result of the fixed target. Using the rotating disk target, we can achieve an approximately tenfold gain in the primary beam intensity.

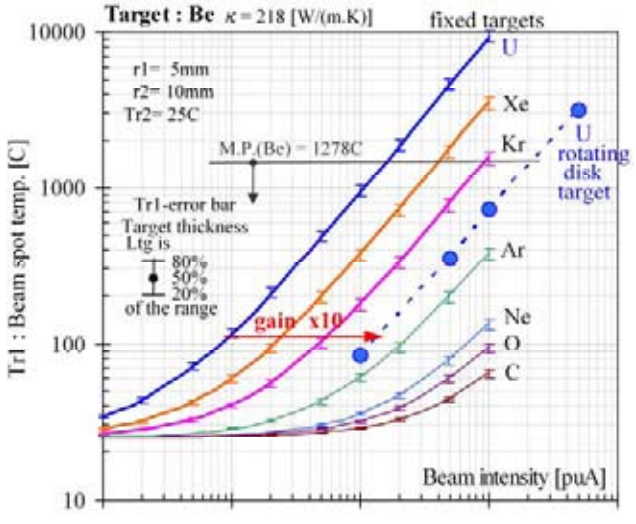

Primary beam	238U	136Xe	86Kr	40Ar	22Ne	18O	13C	
energy	350	350	350	400	400	400	400	[MeV/A]
Target	7.4	10.5	14.6	33.4	59.6	76.3	98.0	[mm]
thickness : Ltg *	1.4	1.9	2.7	6.2	11.0	14.1	18.1	[g/cm2]
Energy loss : dE	30.8	17.1	10.5	5.5	3.0	2.5	1.8	[kW/1pμA]

*) Here, Ltg is selected as 50% of the stopping range of the primary beam.

Fig. 3. Calculated beam spot temperature on a Be target as a function of the primary beam intensity of U to C.

A beam spot observation system has been introduced (Fig. 4). To reduce the radiation damage to this system, it is placed at the entrance of the target access tunnel, where it is 11 m away from the target chamber (see Fig. 2). In the light path, a reflection mirror and a vacuum view port using a sapphire window are assembled. A CCD camera with a telescope lens monitors the position and size of the beam spot. An infrared thermoviewer[5] with a silicon telescope lens monitors the temperature distribution around the beam spot within a circle of 5 cm diameter. Its achieved position resolution was 0.5 mm on the target. A laser pointer can be used to indicate the beam spot position on the targets. Besides this system, an infrared fiberscope[6] with a 35 m fiber has also been installed. It is used to measure the average areal temperature around the beam spot within a circle of 5 mm diameter. An infrared sensor and a laser spot projector are assembled at one end of the fiber located in the low-radiation environment. To avoid failure of the thermoviewer due to radiation damage, we normally use the viewer only at the start of the experiment. Then, we remove the viewer and use the fiberscope for continuous temperature monitoring.

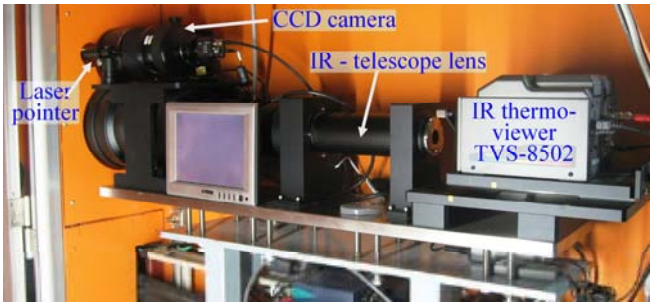

Fig. 4. Beam spot observation system.

To monitor the beam intensity, the FC in the target chamber, a scattered particle monitor, and a Fast Current Transformer (FCT)[7] are available. The FC is made of a conical tungsten cup of 15 mm thickness and 28 mm aperture. The scattered particle monitor consisting of 3 layers of plastic scintillators of 1 mm thickness detects scattered charged particles from a target. It is placed at an angle of 120 degrees from the beam axis and 68 cm from the target. The FCT is assembled at the entrance beam duct of the target chamber. The scattered particle monitor and the FCT are calibrated using the FC with a low-intensity beam of up to a few 100 enA, destructively. Then the beam intensity is measured by the monitor and the FCT, nondestructively.

References

1) A. Yoshida et al.: RIKEN Accel. Prog. Rep. 34,188(2001), 35,152(2002), 37,295(2004), 38,296(2005).
2) A. Yoshida et al.: Nucl. Instrum. & Methods Phys. Res. A 521, 65 (2004)
3) A. Yoshida: PSI Proceedings, 81(2008)
4) A. Yoshida et al.: Nucl. Instrum. & Methods Phys. Res. A, 590,204(2008)
5) TVS-8502, Nippon Avionics Co., http://www.avio.co.jp/
6) IR-FAQI, Chino Co., http://www.chino.co.jp/
7) M. Wada et al.: RIKEN Accel. Prog. Rep. 38,170(2005).

Helium-gas cooling of carbon stripper foils

H. Hasebe, H. Ryuto, N. Fukunishi, A. Goto, M. Kase, and Y. Yano

Carbon foils (C-foils) are extensively used as charge strippers for high-intensity heavy-ion beams at the RIKEN RI beam factory (RIBF). However, the C-foil lifetime is limited. One of the main causes of the short lifetime of carbon stripper foils is assumed to be the heat deposited by beams. A helium-gas-cooled rotating target is used as a target of the gas-filled recoil separator (GARIS). To examine the possibility of applying the gas-cooling mechanism to carbon stripper foils, a beam test was performed.

Figure 1 shows a photograph of multilayer C-foils[1] placed on small target holders of the GARIS rotating target. The thickness of the C-foil is 0.29 mg/cm^2. There are 5 poly-monochloro-para-xylylene (Parylene) layers and 5 carbon layers in the foil, which is normally used as a carbon stripper foil between the RIKEN ring cyclotron (RRC) and the fixed-frequency ring cyclotron (fRC) [2), 3)].

A beam test was performed on January 8-9, 2008. The measurement was carried out by irradiating the C-foils with a 5.04 MeV/u $^{70}Zn^{16+}$ beam at an intensity of 0.9 pμA that was delivered from the RIKEN heavy-ion linear accelerator (RILAC). The beam was focused on a 3 mm-x-15 mm rectangular self-supporting C-foil. The vacuum of the target chamber was approximately 1 x 10^{-6} Torr, and it became 0.5 Torr when helium gas was introduced. The irradiation time was 2 h for each C-foil.

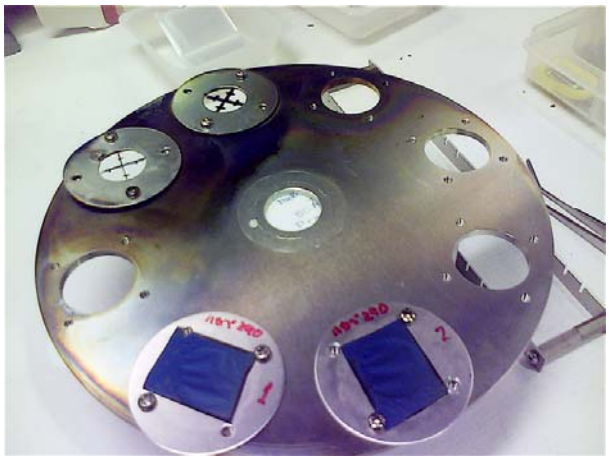

Fig. 1. Two C-foils installed on the small target holder of GARIS.

Figure 2 shows C-foils after the beam test. The left foil was irradiated with helium gas, and the right foil was irradiated without gas. The irradiation trace of the right foil (4 mm x 15 mm) is slightly larger than that of the left foil (3 mm x 15 mm). When helium gas was used, the color of the multilayer C-foil changed from blue to green. Neither C-foil broke, but pin holes appeared at the edge of the foils, possibly because some of the beam hit the foil holder. No difference in foil lifetime was observed.

Fig. 2. Photograph of C-foils after the beam irradiation. The left foil was irradiated with helium gas and the right foil was irradiated without gas.

Fig. 3. Photograph of AFM (easy Scan 2 by Nanosurf AG).

Figure 4 shows images of C-foils observed using the AFM[4] introduced in July 2007 (see Fig. 3), and the maximum area of the images is 1 μm. Figures 4 (a) to 4(d) show images of a C-foil that was neither irradiated nor placed in helium gas, a foil irradiated without helium gas, a nonirradiated C-foil placed in helium gas, and a foil irradiated with helium gas, respectively.

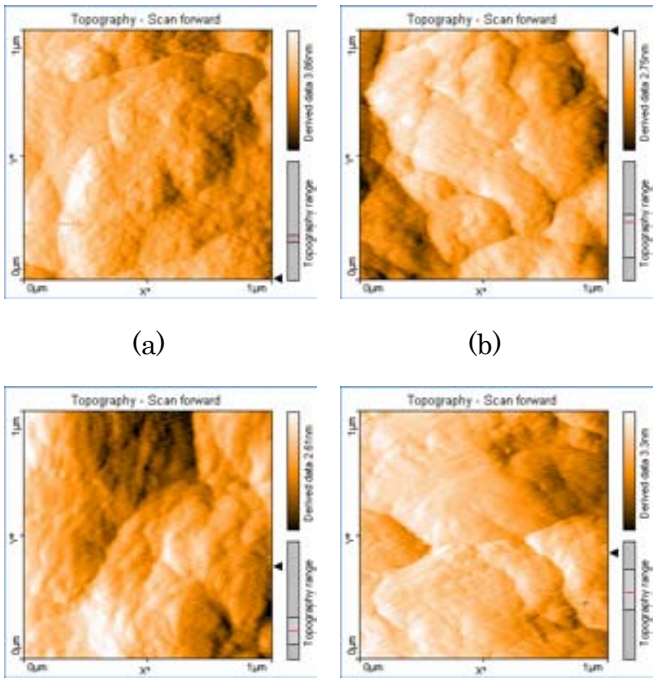

(a) (b)

(c) (d)

Fig. 4. AFM images of C-foils: (a) neither irradiated nor placed in helium gas, (b) irradiated without helium gas, (c) not irradiated but placed in helium gas, (d) irradiated with helium gas.

Foils (a) and (c) show slight unevenness because Parylene covers their surface. The Parylene is evaporated by the heat deposited by the beam. Therefore, some unevenness is observed clearly in foils (b) and (d). Foil (b) shows the carbon surface most clearly, and damage caused by the beam was not observed on the carbon surface. Because the beam shape was different in both cases, the cooling effect by the helium gas could not be judged by this beam irradiation test.

References

1) H. Hasebe, H. Ryuto, N. Fukunishi, A. Goto, M. Kase, and Y. Yano: RIKEN Accel. Prog. Rep. **40,** 128 (2007).
2) H. Ryuto, N. Fukunishi, H. Hasebe, N. Inabe, S. Yokouchi, O. Kamigaito, A. Goto, M. Kase, and Y. Yano: Proceedings of 2005 Particle Accelerator Conference, Knoxville, Tennessee, 2005, p. 3751.
3) H. Ryuto, H. Hasebe, N. Fukunishi, A. Goto, M. Kase, and Y. Yano: in this Progress Report.
4) Nanosurf AG
URL: http://www.nanosurf.com/

Observing dynamical supersymmetry breaking by euclidean lattice simulations

I. Kanamori, F. Sugino*1 and H. Suzuki

[Dynamical supersymmetry breaking, lattice gauge theory, Monte Carlo simulation]

It is widely believed that supersymmetry is relevant in particle physics beyond the standard model and it is spontaneously broken by some mechanism. If supersymmetry is not spontaneously broken at the lowest order of the perturbation theory, it remains so at all orders of the perturbation theory. There still exists, however, a possibility that supersymmetry is spontaneously broken nonperturbatively. A precise study of such *dynamical supersymmetry breaking* remains elusive because we have no universal framework that defines supersymmetric (particularly gauge) theories at a nonperturbative level.

In this work, we propose a method to observe the dynamical supersymmetry breaking in the euclidean lattice gauge theory, in the light of recent developments on lattice formulation of supersymmetric theories (for a review, see ref. 1)) and use it to examine the dynamical supersymmetry breaking in the two-dimensional $\mathcal{N} = (2,2)$ super Yang-Mills theory (2d $\mathcal{N} = (2,2)$ SYM). This seemingly simple supersymmetric system defies a straightforward low-energy description by several reasons and it is even conjectured by some authors[2] that supersymmetry is dynamically broken in this system with the gauge group $\mathrm{SU}(N_c)$.

The global supersymmetry is spontaneously broken if and only if ground-state energy is strictly positive.[3] In principle, therefore, one can determine whether the supersymmetry breaking occurs if ground-state energy can be computed. Recall that the thermal average of the Hamiltonian H with the inverse temperature β is expressed as

$$\frac{\mathrm{Tr}\, He^{-\beta H}}{\mathrm{Tr}\, e^{-\beta H}} = \frac{\int_{\mathrm{aPBC}} \mathrm{d}\mu\, He^{-S}}{\int_{\mathrm{aPBC}} \mathrm{d}\mu\, e^{-S}} \equiv \langle H \rangle_{\mathrm{aPBC}}, \quad (1)$$

where S is the euclidean (i.e., imaginary-time) action. On the right-hand side, the time-period of the system is taken to be β. What is very important in eq. (1) is the boundary condition in the temporal direction. It must be periodic for all bosonic variables and antiperiodic (aPBC) for all fermionic variables. In the low-temperature limit $\beta \to \infty$, only the ground state(s) contribute to eq. (1) and the ground-state energy E_0 will be given by $E_0 = \lim_{\beta\to\infty} \langle H \rangle_{\mathrm{aPBC}}$.

To embody this simple idea in Euclidean lattice formulation, we have to correctly choose a possible additive constant in the Hamiltonian H. For this, we adopt a relation $H \equiv iQ\overline{Q}/2$ as a working hypothesis, where

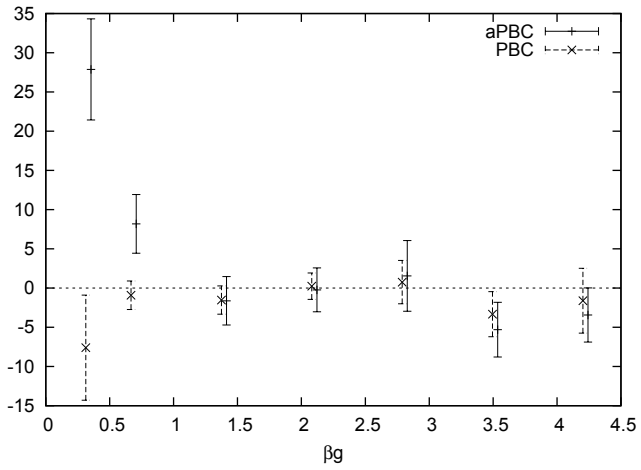

Fig. 1. The expectation values of the hamiltonian density (in a unit of g^2) with the anti-periodic (aPBC) and periodic (PBC) conditions, as a function of the physical temporal size of the system βg, where g is the gauge coupling constant in two dimensions. The physical spatial size is fixed to be $Lg = 1.4142$.

Q is the fermionic transformation and $\overline{Q}$ is the Noether charge associated with the transformation $\overline{Q}$ conjugate to Q. If the lattice formulation one adopts possesses Q as the manifest symmetry, this definition of the Hamiltonian is consistent with a topological property of the Witten index. We tested the prescription in models of supersymmetric quantum mechanics[3] and obtained very promising results. For 2d $\mathcal{N} = (2,2)$ SYM, we used a lattice formulation proposed in ref. 4), in which the fermionic symmetry Q is manifestly realized. Our results, which were obtained using the RIKEN Super Combined Cluster (RSCC), are shown in Fig. 1. The gauge group is SU(2). We regard this as a strong numerical evidence that supersymmetry is not spontaneously broken in this system. For details, we refer to ref. 5).

References

1) J. Giedt: PoS **LAT2006**, 008 (2006).
2) K. Hori and D. Tong: J. High Energy Phys. **05**, 079 (2007).
3) E. Witten: Nucl. Phys. **B 188**, 513 (1981).
4) F. Sugino: J. High Energy Phys. **03**, 067 (2004).
5) I. Kanamori, F. Sugino and H. Suzuki: arXiv:0711.2099 [hep-lat]; arXiv:0711.2132 [hep-lat].

*1 Okayama Institute for Quantum Physics

Production of ^{255}No via the ^{238}U(^{22}Ne,5n)^{255}No Reaction Using the Gas-Jet Transport System Coupled to GARIS

H. Haba, T. Akiyama, D. Kaji, H. Kikunaga,[*1] K. Morimoto, K. Morita, T. Nanri,[*2] K. Ooe,[*1] N. Sato, A. Shinohara,[*1] D. Suzuki,[*2] T. Takabe,[*1] I. Yamazaki,[*2] A. Yokoyama,[*2] and A. Yoneda

Recently, a gas-jet transport system was installed at the focal plane of the RIKEN gas-filled recoil ion separator GARIS to start superheavy-element (SHE, $Z \geq 104$) chemistry.[1] The performance of the system was first appraised using ^{206}Fr and ^{245}Fm produced in the ^{169}Tm(^{40}Ar,3n)^{206}Fr and ^{208}Pb(^{40}Ar,3n)^{245}Fm reactions, respectively.[1] The results revealed that the GARIS/gas-jet system is a promising tool for next-generation SHE chemistry, i.e., identifying SHE nuclides under extremely low-background conditions with high efficiency of the gas-jet transport. In order to produce SHE nuclides with long half-lives for chemical experiments, further asymmetric fusion reactions based on actinide targets such as ^{238}U and ^{248}Cm should be considered. As a first step, we have produced an isotope of element 102, ^{255}No, in the ^{238}U(^{22}Ne,5n)^{255}No reaction using the GARIS/gas-jet system.

A $^{238}U_3O_8$ target of 368 μg cm^{-2} thickness was prepared by electrodeposition onto a 1.27 mg cm^{-2} Ti backing foil. The $^{22}Ne^{7+}$ ion beam was extracted from the RIKEN Linear Accelerator, RILAC. The beam energy was 113.8 MeV at the center of the target. The typical beam intensity was 4 particle μA. The reaction products of interest were separated in-flight from the beam and the majority of the nuclear transfer products by GARIS and then guided into the gas-jet chamber of 70 mm i.d. × 60 mm depth through a Mylar window of 1.1 μm thickness, which was supported by a circular-hole grid with 72% transparency and 60 mm diameter. GARIS was filled with helium gas at a pressure of 38 Pa. The magnetic rigidity of GARIS was set at 1.93 Tm.

In the gas-jet chamber, the reaction products were stopped in helium gas, attached to KCl aerosols generated by the sublimation of KCl powder at 620 °C, and continuously transported through a Teflon capillary (1.59 mm i.d. × 4 m length) to a rotating wheel system, MANON, for α spectrometry. The helium flow rate was 1.0 L min^{-1}, and the inner pressure of the chamber was 38 kPa. In MANON, the reaction products were deposited onto Mylar foils of 0.68 μm thickness and 20 mm diameter placed at the periphery of a 40-position stainless-steel wheel of 420 mm diameter. After the aerosol collection, the wheel was stepped at 90-s intervals to position the foils between seven pairs of Si PIN photodiodes (Hamamatsu S3204-09). To evaluate the number of ^{255}No atoms that passed through the Mylar window of GARIS, the gas-jet chamber was replaced with a detector chamber equipped with a 12-strip Si detector of size 60 × 60 mm^2 (Hamamatsu 12CH SD).

*1 Graduate School of Science, Osaka University

*2 Faculty of Science, Kanazawa University

The sum of α-particle spectra measured in the seven top detectors of MANON is shown in Fig. 1. A beam dose of 2.81×10^{17} was accumulated. As shown in Fig. 1, 7.620–8.312 MeV α peaks[2] of ^{255}No are clearly seen under the low-background condition, indicating that the gas-jet transport of ^{255}No was successfully conducted after the physical separation by GARIS. The decay curve of the α peaks of ^{255}No is shown in the inset of Fig. 1. The half-life was determined to be 3.4±0.8 min, which is in agreement with the value of 3.1±0.2 min in the literature.[2] By comparing the spectrum measured with the 12-strip Si detector, the gas-jet transport efficiency of ^{255}No was evaluated to be 84±9%. The transport efficiency of GARIS was about 5% for the focal plane of 60 mm diameter, referring to the cross section of 90 nb.[3] Since MANON was placed in the target room in this experiment, some background events caused by large numbers of neutrons during the irradiation can be seen in Fig. 1. Recently, we have constructed a chemistry laboratory isolated from the target room by a 50-cm concrete shield where the background level is expected to be two orders of magnitude lower than that in the target room. In the near future, the production of SHE nuclides such as ^{261}Rf, ^{265}Sg, ^{269}Hs, and ^{283}112 for chemical experiments will be investigated using the ^{238}U and ^{248}Cm targets.

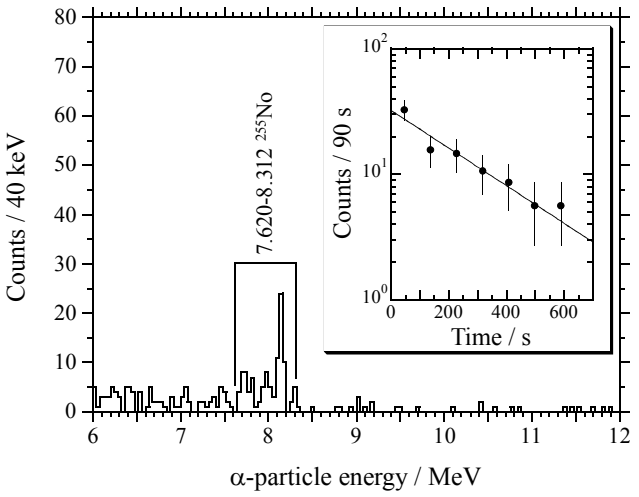

Fig. 1. Sum of α-particle spectra measured in the seven top detectors of MANON. The inset shows a decay curve of ^{255}No.

References

1) H. Haba et al.: J. Nucl. Radiochem. Sci. 8, 55 (2007).
2) R. B. Firestone and V. S. Shirley: *Table of Isotopes, 8th ed.* (John Wiley & Sons, New York, 1996).
3) H. Haba et al.: Eur. Phys. J. D 45, 81 (2007).

Systematic study of ^{9,10,11}Li with the tensor and pairing correlations

T. Myo,[*1] Y. Kikuchi,[*2] K. Katō,[*2] H. Toki,[*1] and K. Ikeda

[Nuclear structure, Unstable nuclei, Tensor force, Cluster model]

So far, many experiments have been performed on ^{11}Li and the surrounding nuclei in order to understand the exotic structures of these nuclei. We summarize the experimental data for ^{11}Li as: a) The halo neutrons have almost equal amount of the s-wave component with respect to that of p-wave[1]. b) Precise measurements of the various radius are obtained[2,3]. c) The $E1$ strength distribution has a peak near the threshold[4]. d) The electromagnetic properties show the exotic structures of ^{11}Li[5].

The challenge from the theoretical side is the mechanism of a large s-wave component for the halo neutrons, namely the disappearance of the $N = 8$ magic number. However, conventionally, most of the studies of ^{11}Li had to assume that the $1s_{1/2}$ single particle state is brought down by hand to the $0p_{1/2}$ state. It is therefore the real challenge for theorists to understand this breaking of magicity.

In the previous study[6], we have considered newly the tensor correlation in ^{11}Li based on the extended three-body model, where the tensor correlation in the ^{9}Li core is described fully in the tensor-optimized shell model[7]. It was found that the tensor and pairing correlations in ^{9}Li inside ^{11}Li are Pauli-blocked by additional two neutrons, which makes the $(1s)^2$ and $(0p)^2$ configurations close to each other to mix about equal amount of two configurations. As a result, we naturally explained the breaking of magicity and the halo formation for ^{11}Li with 47% of the $(1s)^2$ component. We also reproduced the Coulomb breakup strength and the charge radius of ^{11}Li.

In this report, following the previous study[6], we demonstrate the reliability of our framework by performing a detailed systematic analysis of the structures of ^{9,10,11}Li. For the dipole strength of ^{11}Li into ^{9}Li+n+n state, we observe the low energy peak shown in Fig. 1. We investigate the effect of the final state interactions between the ^{9}Li+n+n system, by which either the core-n or nn interactions is cut off, respectively, or both of them are cut off, namely, the plane wave treatment, shown in Fig. 1. The results show that the plane wave gives the small strength, which indicates the importance of the final state correlations. Among the final state correlations, the core-n and nn interactions give comparable contributions. This means that both two correlations are important to explain the three-body breakup mechanism of ^{11}Li.

We also show the Q moments of the ^{9}Li and ^{11}Li in Table 1. Only the absolute value is reported for ^{11}Li in the experiments[5]. The present model describes well the observations. It is found that the difference between the values of ^{9}Li and ^{11}Li is small. This trend is different from the the charge radius case, in which the enhancement in ^{11}Li is caused by the recoil effect coming from the large ^{9}Li-2n distance as 5.69 fm[6]. We here discuss the recoil effect in the Q moment of ^{11}Li by expanding its operator into the core part, the ^{9}Li-2n relative motion part. In our wave function of ^{11}Li, 2n almost form the 0^+ state with around 99%. Hence, the Q moment from the relative motion part almost vanishes because of the rank condition. This means that the recoil effect is negligible and the Q moment of ^{11}Li comes from the ^{9}Li core part. It is desired that further experimental data are obtained for the Q moment of ^{11}Li.

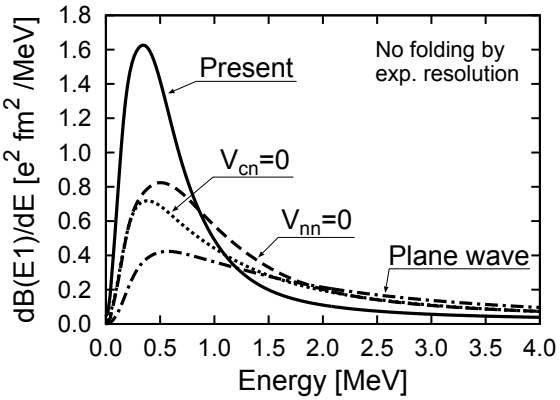

Fig. 1. Effect of the final state interactions on the $E1$ transition strength of ^{11}Li into the ^{9}Li+n+n system.

Table 1. Q moments of ^{9}Li and ^{11}Li in units of e fm^2.

	^{9}Li	^{11}Li
Present	-2.65	-2.80
Experiment[5]	-2.74 ± 0.10	3.12 ± 0.45 ($\|Q\|$)

References

1) H. Simon et al.: Phys. Rev. Lett. **83**, 496 (1999).
2) A. V. Dobrovolsky et al.: Nucl. Phys. A**766**, 1 (2006).
3) R. Sánchez et al.: Phys. Rev. Lett. **96** 033002 (2006).
4) T. Nakamura et al.: Phys. Rev. Lett. **96**, 252502 (2006).
5) E. Arnold et al.: Z. Phys.A**349**, 337 (1994).
6) T. Myo et al.: Phys. Rev. C**76**, 024305 (2007).
7) T. Myo et al.: Prog. Theor. Phys. **118**, 257 (2007).

*1 Research Center for Nuclear Physics, Osaka University
*2 Graduate School of Science, Hokkaido University

μSR detection of soft mode toward exotic magnetic ground state in bond-disordered quantum spin system IPA-Cu($Cl_{0.35}Br_{0.65}$)$_3$†

T. Goto*[1], T. Kanada*[1], T. Saito*[1], A. Oosawa*[1], H. Manaka*[2], T. Suzuki and I. Watanabe

Disorder often introduces a nontrivial effect into quantum spin systems. A small of holes destroy the uniform Néel order in the parent compound of high-T_C cuprates, and a small amount of nonmagnetic impurities stabilizes the Néel state in spin Peierls systems. Furthermore, there is a theoretical prediction of the appearance of an exotic ground state Bose glass in disordered Boson systems. Although the possibility of the experimental detection of the Bose-glass phase by either macroscopic or microscopic probes was repeatedly suggested in the solid solution of different two spin-gap systems, details still remain to be clarified.

The compound $(CH_3)_2CHNH_3$-Cu(Cl_xBr_{1-x})$_3$ abbreviated as IPA-Cu(Cl_xBr_{1-x})$_3$ is a solid solution of the two spin-gap ladder systems IPA-$CuCl_3$ and IPA-$CuBr_3$ with different spin gaps of Δ=14 and 98 K, respectively. It has been reported that experiments on macroscopic quantities show a magnetic order at low temperatures when x is within the limited region between 0.44 and 0.87, and otherwise a gapped behavior. We have investigated microscopically the ground state of the sample with x=0.35 by muon spin relaxation (μSR).

Single crystals with x=0.35 have been grown by an evaporation method[1]. Measurements of μSR have been carried out at the Riken-RAL Muon Facility in the U.K. using a spin-polarized pulsed surface muon (μ^+) with a momentum of 27 MeV/c. The incident muon beam was directed parallel to the b*-axis, which was perpendicular to one of the three outer planes with the largest area, the so-called C-plane[1].

Typical relaxation curves of muon spin polarization under zero and finite longitudinal fields (LFs) are shown in Fig. 1. The relaxation over the entire temperature and field region is described by a function containing two components expressed as

$$A_1 G_{KT}(t, \Delta)\exp(-t/\lambda_1)+A_2\exp(-t/\lambda_2), \qquad (1)$$

where G_{KT} is the Kubo-Toyabe function with the static field distribution width at the muon site Δ, the relaxation rates λ_1 and λ_2, and the component amplitudes A_1 and A_2. No muon spin rotation due to a static field produced by a magnetic order was observed in any temperature or field region. The amplitude fraction of λ_2, the larger component was around $A_2/(A_1+A_2) \approx 0.1$ at 8 K, increased with decreasing temperature and reached 0.4 at 0.3 K. The temperature dependences of the two relaxation rates under various LFs are shown in Fig. 2.

The existence of the two components in relaxation curves indicates that a microscopic phase separation occurs in this system. That is, active spins with an antiferromagnetic correlation are considered to be restricted in islands surrounded by singlet sea. Actually, λ_1 is comparable to the end member system of IPA-$CuCl_3$, though the characteristic fluctuation frequency decreases appreciably. The significant increase in relaxation rate at low temperatures shows that the ground state of the system is magnetic and still does not show any magnetic order.

The field dependence of the relaxation rate in Fig. 2 shows that the Fourier spectrum of the spin fluctuation changes from white noise like at a high temperature of approximately 8 K to steep peak weighed at around zero energy at low temperatures. This behavior is interpreted to be the soft mode toward the possible phase transition at the absolute zero, or toward an exotic phase, such as the Bose-glass phase.

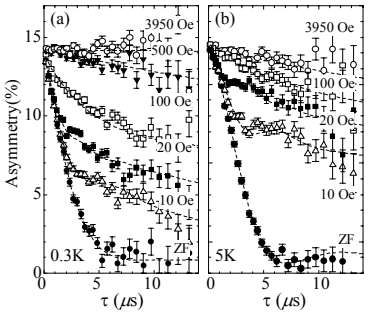

Fig. 1. Typical relaxation curves under various magnetic fields at (a) 0.3 K and (b) 5 K. Dashed curves correspond to the fitting function in Eq. (1).

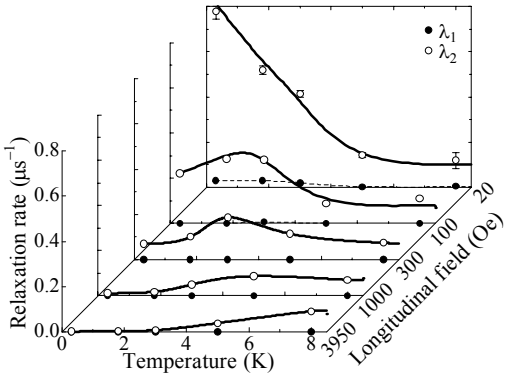

Fig. 2 Temperature dependences of two relaxation rates λ_1 and λ_2 under various longitudinal fields. Solid and dashed curves serve as visual guides.

References

1) H. Manaka *et al.* : Phys. Rev. B**63**, 104408 (2001).
2) T. Saito *et al.* : Phys. Rev. B**74**, 134423 (2006).
3) T. Adachi *et al.* : J. Phys. Soc. Jpn. **76**, 083701 (2007).

† Condensed from the article submitted to Phys. Rev. **B**

*1 Faculty of Science and Engineering, Sophia University
*2 Graduate School of Science and Engineering, Kagoshima University

Tenth-Order QED Contributions to Electron $g-2$

T. Aoyama,[*1] M. Hayakawa,[*2] T. Kinoshita,[*3] and M. Nio

[QED, anomalous magnetic moment, electron]

The anomalous magnetic moment of electron, called $g-2$, has been playing a central role in the testing of the validity of Quantum Electrodynamics (QED). A Harvard team has very recently reported the result of a new measurement of the electron anomaly $a_e = (g-2)/2$[1)]

$$a_e = 1\ 159\ 652\ 180.73\ (0.28) \times 10^{-12}\ (0.24\ \text{ppb}). \quad (1)$$

This value has a uncertainty that is 2.7 and 15 times smaller than those of previous measurements carried out in 2006[2)] and in 1987[3)], respectively.

To match the experimental precision, the theory requires the QED contributions of up to the tenth order of perturbation theory.[4)] The largest uncertainty of the current theory comes from the yet-uncalculated tenth-order contribution. There are 12672 vertex Feynman diagrams contributing to the tenth-order g–2. They are further divided into 32 gauge-invariant sets as shown in Fig. 1. The contributions from 17 sets, Sets I(a–f), II(a,b), II(f), VI(a–c), VI(e,f), and VI(i–k), were previously determined by us.[6)] Evaluation of the remaining 15 sets is very tough, because they require many ultraviolet (UV) renormalization terms as well as infrared (IR) subtraction terms. Thus far, we have developed the automatic code generation system to carry out such a complex and gigantic calculation without making a single error.

Part of the automation system, called GENCODEN, deals with a Feynman diagram without a fermion loop.[7)] Given one-line information specifying a diagram, GENCODEN generates a set of FORTRAN programs, which is ready to proceed to numerical evaluation. While debugging GENCODEN, we found an error in the old calculation of the eighth-order contribution and corrected it.[4)] This revision of the theory seriously affected the value of the fine-structure constant α determined from the measured $g-2$ and the theory.[5)]

With the help of GENCODEN, we obtained the tenth-order contributions from Sets III(a), III(b), and IV. The numerical evaluation of Set V requires enormous computational power and is still being evaluated on RIKEN's supercomputing system (RSCC).

The other part of the automation system, GENCODEVPN, takes care of a vacuum polarization diagram consisting of a single lepton loop. This enables us to evaluate swiftly Sets I(g–i) and II(c,d).

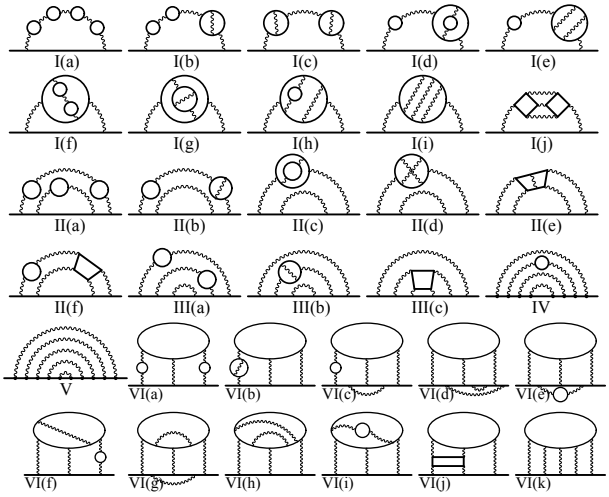

Fig. 1. Feynman diagrams contributing to the tenth-order lepton $g-2$. Typical diagrams from 32 gauge-invariant sets are shown. An external photon vertex is omitted for simplicity. There are 12672 vertex diagrams in total.

Set I(j) has a structure totally different from the other diagrams. It was evaluated by one of us (M. H.) and his collaborator, N. Watanabe, and the result will be reported elsewhere.

Only five Sets II(e), III(c), VI(d), and VI(g,h) involving a light-by-light scattering amplitude are currently left untouched. We have, however, found no technical difficulty in evaluating these sets. We hope we can report the entire contribution of the tenth-order terms very soon.

*1 Institute of Particle and Nuclear Studies, High Energy Accelerator Research Organization (KEK)
*2 Department of Physics, Nagoya University
*3 Laboratory for Elementary-Particle Physics, Cornell University

References

1) D. Hanneke, S. Fogwell, and G. Gabrielse: Phys. Rev. Lett. **100**, 120801 (2008).
2) B. Odom, D. Hanneke, B. D'Urso, and G. Gabrielse: Phys. Rev. Lett. **97**, 030801 (2006).
3) R. S. Van Dyck, Jr., P. B. Schwinberg, and H. G. Dehmelt: Phys. Rev. Lett. **59**, 26 (1987).
4) T. Aoyama, M. Hayakawa, T. Kinoshita, and M. Nio: Phys. Rev. Lett. **99**, 110406 (2007); T. Aoyama, M. Hayakawa, T. Kinoshita, and M. Nio: Phys. Rev. D **77**, 053012 (2008).
5) G. Gabrielse, D. Hanneke, T. Kinoshita, M. Nio, and B. Odom: Phys. Rev. Lett. **97**, 030802 (2006); *ibid* **99**, 039902 (2007).
6) T. Kinoshita and M. Nio: Phys. Rev. D **73**, 053007 (2006); M. Nio, T. Aoyama, M. Hayakawa, T. Kinoshita: Nucl. Phys. Proc. Suppl. **169**, 238 (2007).
7) T. Aoyama, M. Hayakawa, T. Kinoshita, and M. Nio: Nucl. Phys. B **740**, 138 (2006); *ibid* **796**, 184 (2008).

Study of low-lying states in ^{32}Mg

S. Takeuchi, N. Aoi, H. Baba,[*1] T. Fukui,[*2] Y. Hashimoto,[*3] K. Ieki,[*4] N. Imai,[*5] H. Iwasaki,[*6] S. Kanno,[*4] Y. Kondo,[*3] T. Kubo, K. Kurita,[*4] T. Minemura,[*5] T. Motobayashi, T. Nakabayashi,[*3] T. Nakamura,[*3] T. Okumura,[*3] T. K. Onishi,[*6] S. Ota,[*2] H. Sakurai,[*6] S. Shimoura,[*1] R. Sugou,[*4] D. Suzuki,[*6] H. Suzuki,[*6] M. K. Suzuki,[*6] E. Takeshita,[*4] M. Tamaki,[*1] K. Tanaka, Y. Togano,[*4] and K. Yamada

[nuclear structure, in-beam γ-ray spectroscopy]

Experimental studies on the collectivity in ^{32}Mg using the Coulomb excitation have focused on the low-lying excited state.[1)] The small excitation energy and large B($E2;2^+ \rightarrow 0^+$) value of the first 2^+ (2_1^+) state suggest that ^{32}Mg has a large nuclear quadrupole deformation.[1,2)] For further study of the collectivity in ^{32}Mg, the locations and spin parities (J^π's) of excited states above the 2_1^+ state are important. Although the excitation energies of higher states were measured by β-γ spectroscopy,[3,4)] the J^π's for those states are still unknown. In the present study, their J^π's have been investigated through the measurement of differential cross sections in the proton inelastic scattering from ^{32}Mg on the basis of inverse kinematics.[5)]

Figure 1 shows a level scheme of ^{32}Mg deduced by the present γ-γ analysis. The dotted lines are for the known levels, while the solid lines indicate the levels tentatively assigned by this study. On the basis of this level scheme, measured γ-ray spectra were analyzed with response functions for the individual γ transitions. Each response function was obtained by Monte Carlo simulations. The angular distributions of scattered ^{32}Mg for the excitation to each state were extracted using the γ-ray intensities deduced from this analysis.

Figure 2 shows the experimental angular distributions determined for the excitation to the 885 keV and 2321 keV states, indicated by the filled and open circles, respectively. The data are compared with the coupled-channel calculations performed using the code ECIS97[6)] with the KD02 optical-potential parameters.[7)] The dashed and dotted curves for the 2321 keV state correspond to the calculation assuming, respectively, 4^+ and 3^-, which are plausible candidates for J^π. The symmetric rotational model was assumed for the two-step transition ($0_1^+ \rightarrow 2_1^+ \rightarrow 4_1^+$) and one-step hexadecapole one ($0_1^+ \rightarrow 4_1^+$) for the case of 4_1^+, whereas the harmonic vibrational model was employed to calculate the one-step transition to 3_1^-. The angular distributions for the transition to the 2_1^+ state and 2321 keV state are well reproduced simultaneously by the calculation assuming 4_1^+ for the 2321 keV state rather than the one with the assumption of 3_1^-. Assuming $J^\pi = 4_1^+$ for the 2321 keV state, β_2 and β_4 parameters in the symmetric rotational model were deduced to be 0.408(22) and 0.112(29), respectively.

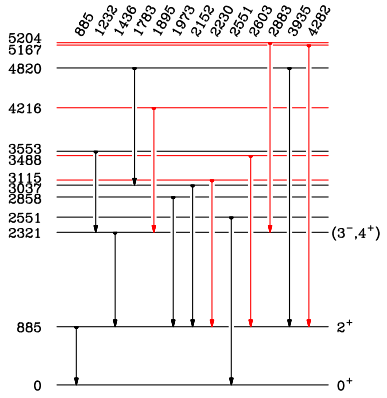

Fig. 1. Reconstructed level scheme for ^{32}Mg deduced from present studies of the ^{32}Mg+p inelastic scattering. For details, see text.

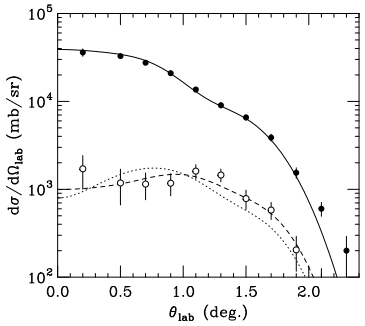

Fig. 2. Angular distributions for the excitation to the 885 keV and 2321 keV states in ^{32}Mg. For details, see text.

*1 Center for Nuclear Study, University of Tokyo
*2 Department of Physics, Kyoto University
*3 Department of Physics, Tokyo Institute of Technology
*4 Department of Physics, Rikkyo University
*5 Institute of Particle and Nuclear Studies, High Energy Accelerator Research Organization (KEK)
*6 Department of Physics, University of Tokyo

References

1) T. Motobayashi et al.: Phys. Lett. B **346**, 9 (1995).
2) C. Detraz et al.: Phys. Rev. C **19**, 164 (1979).
3) G. Klotz et al.: Phys. Rev. C **47**, 2502 (1993).
4) C. M. Mattoon et al.: Phys. Rev. C 75, 017302 (2007).
5) S. Takeuchi et al.: J. Phys.:Conf. Ser. **49**, 153 (2006).
6) J. Raynal: unpublished *coupled-channel code ECIS97*.
7) A. J. Koning, J. P. Delaroche,: Nucl. Phys. A **713**, 231 (2003).

Acceleration-Voltage Calibration of RIKEN Heavy-Ion Linac

Nobuhisa Fukunishi, Masaki Fujimaki, Yoshihide Higurashi,
Naruhiko Sakamoto, Masanori Wakasugi, Tamaki Watanabe and Masayuki Kase

The RIKEN Heavy-ion linac[1] (RILAC) is the first-stage accelerator of the RI Beam Factory (RIBF) accelerator complex. After the first-beam extraction of the RIBF, the transmission efficiency of ions accelerated by the RIBF has been very low. For example, the total transmission efficiency was 0.1% for a uranium beam acceleration although the charge stripping efficiency was 4 - 5%.[2,3] There are many problems to be addressed and one of them is how to improve the transmission efficiency of the RILAC, which is typically 30%. The RILAC consists of six acceleration cavities and its preinjector system consists of a buncher, FC-RFQ,[4] and a rebuncher. We should adjust 18 parameters (9 voltages and 9 phases) of rf fields to obtain an appropriate transmission efficiency (~70%) that is predicted by numerical simulation. However, the precise voltage calibration of the RILAC has not been performed. Hence, we decided to calibrate acceleration voltages of the rf cavities using a time-of-flight (TOF) method.

Assume that we are interested in the voltage calibration of the sixth cavity of the RILAC. The voltage and phase of the sixth cavity are usually monitored by measuring the output signals of a phase-pickup electrode placed in the cavity with a vector voltmeter. It means that the voltage and phase are relatively well known, but their absolute values are not. To determine their absolute values, it is useful to measure the beam energies. Under the condition that parameters except for the voltage and phase of the sixth cavity are fixed, the average energy of the ions accelerated by the sixth cavity depends only on the voltage and phase of the sixth cavity. This dependence is calculated numerically as shown in Fig. 1.

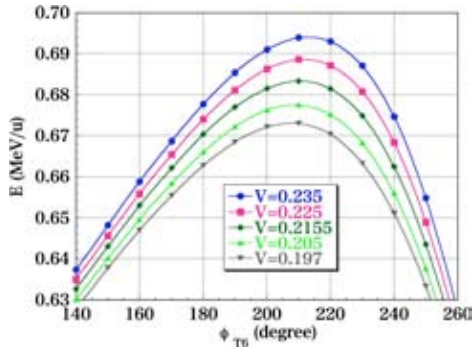

Fig. 1. Simulation results of output energies of the sixth cavity of the RILAC for various acceleration conditions. The unit of the acceleration voltage (V) is MV.

In our measurements, the average energy of the ions is determined on the basis of the ions arriving at two plastic scintillators placed at an appropriate interval. By collecting data on the average energies for various voltages and phases, and comparing them with the simulation, we can determine the two parameters what we want. One is the voltage ratio of an actual rf field to an output voltage of the phase-pickup electrode. The other is the phase shift between the actual rf field and the phase recorded using the vector voltmeter. These two quantities are easily determined by the least-square fitting. The injection energy to the sixth cavity should be measured because the energy dependence shown in Fig. 1 changes owing to the injection energy.

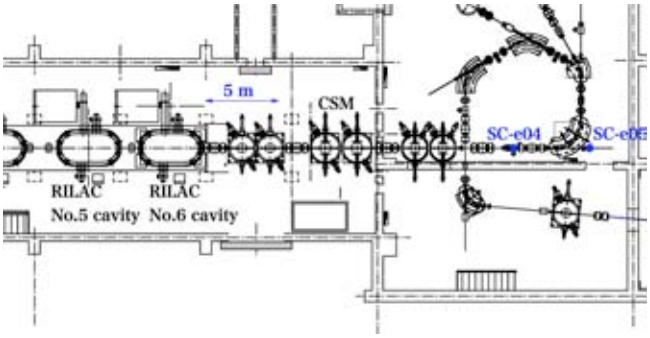

Fig. 2. Schematic layout of the TOF measurement. Two plastic scintillators were placed at the e04 and e05 chambers (SC-e04 and SC-e05).

Measurements were performed on September 27 and October 1, 2007 for the sixth and fifth cavities, respectively. We employed a system developed by the authors M. W. and T. W.[5] to measure the beam energies in the RIBF, and two plastic scintillators were placed at the e04 and e05 chambers as shown in Fig. 2. In the case of the voltage calibration of the fifth cavity, the voltage of the sixth cavity was set to zero. We did not carry out measurements for the other cavities because the distances from the cavity to be calibrated to the scintillators were too long. In the present configuration, a beam is widely spread in the longitudinal direction owing to its energy spread.

Examples of measured time spectra are shown in Fig. 3. The average beam energy was determined to be 0.661 MeV/nucleon in this case. Results obtained in a series of TOF measurements are summarized in Fig. 4 with the results of the least-square fitting. We carried out measurements for three different acceleration voltages for

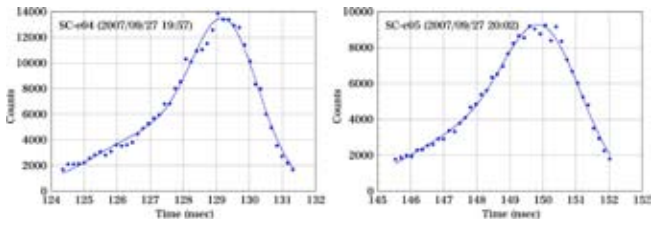

Fig. 3 Examples of time spectra measured using plastic scintillators e04 (SC-e04) and e05 (SC-e05). The vertical axis shows the time from a scintillator's signal to a stop pulse (RF). The lines are the results of the least-square fitting in which a two-component Gaussian distribution is employed.

the sixth cavity for 10 hours. In contrast, it took 8 hours to collect the TOF data shown in Fig. 4 for the fifth cavity. We found that some of the data included large errors, which are marked in Fig. 4. In these data, the time of flight from the cavity to be calibrated to the SC-e04 was inconsistent with that from the cavity to the SC-e05. It means that the injection energy to the cavity to be calibrated was slightly changed during the TOF measurement. Small voltage changes in the second cavity were repeatedly detected during the measurements. When we recognized a voltage change, we restarted a TOF measurement. The existence of data with large errors indicates that we sometimes failed to recognize the voltage changes. These data were excluded from the least-square fitting.

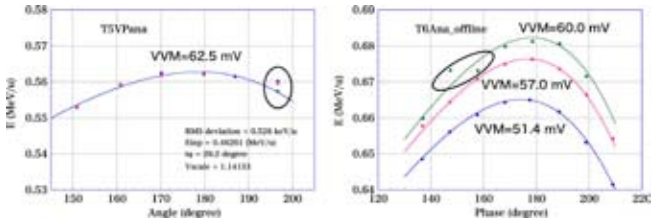

Fig. 4. Summary of TOF measurements for the fifth (left) and the sixth (right) cavities of the RILAC. The points indicate the observed energies. The lines are the results of the least-square fitting. The abbreviation "VVM" denotes output voltage of the vector voltmeter. Data inside the ellipses include large errors.

From the results of the least-square fitting, relations between the actual acceleration voltage and the output voltage of the phase-pickup electrode measured using the vector voltmeter are summarized as follows.

$$V_6\,(\mathrm{kV}) = 1.42 \times VVM_6\,(\mathrm{mV}) = 1.05\ \mathrm{Vset}\,(\mathrm{kV})$$
$$V_5\,(\mathrm{kV}) = 1.14 \times VVM_5\,(\mathrm{mV}) = 0.87\ \mathrm{Vset}\,(\mathrm{kV})$$

The symbols V_i and VVM_i (i=5,6) represent the actual voltage and the output voltage of the VVM, respectively. The symbol Vset denotes a setting value of the voltage in the rf control system of the RILAC. It should be noted that these relations hold only for 18.25-MHz acceleration.

The uncertainties of the scaling factors in these relations were also estimated. The error in measuring the distance from the SC-e04 to SC-e05 is considered to be ±0.1%, which results in a ±0.2% error in energy determination. The errors that originated from the least-square fitting to determine the peak positions of time spectra are typically 0.2 nsec, which corresponds to ±0.1% in energy determination. These errors correspond to a voltage error of at most ±0.2% because the sixth (fifth) cavity contributes to the energy difference between the sixth (fifth) and fifth (fourth) cavities. In addition, the root-mean-square deviations of the least-square fitting shown in Fig. 4 are 0.07 % and 0.09% for the sixth and fifth cavity, respectively. Hence, we conclude that the scaling factors in the equations typically include ±0.5% errors.

The present results demonstrate that the voltage calibration using a TOF method works well. We should continue voltage calibrations for the remaining cavities. It is necessary to move the plastic scintillators upstream to shorten the distance from the RILAC. On the other hand, the direct extension of the present method to the second and first cavities may be difficult because their output energies are too low. It is a future challenge to establish a method of voltage calibration for the low-energy section of the RILAC and its preinjectors.

References

(1) M. Odera et al.: Nucl. Instrum. Methods **A227**, 187 (1984)
(2) A. Goto et al.: Proc. 18th Int. Conf. on Cyclotrons and their Applications 3 (2007).
(3) N. Fukunishi et al.: "Brief Summary of Uranium Acceleration Tests in RI Beam Factory II", in this progress report.
(4) O. Kamigaito et al.: Rev. Sci. Instrum. **70**, 4523 (1999).
(5) T. Watanabe et al.: Proc. PASJ4-LAM32, August 2007, Wako-shi Saitama, WP37.

Quarkonium Melting Above Deconfinement†

Á. Mócsy*1 and P. Petreczky*1,*2

In a recent paper[1)] we analyzed in detail the quarkonium spectral functions. This analysis has shown that spectral functions calculated using potential model for the non-relativistic Green's function combined with perturbative QCD can describe the available lattice data on quarkonium correlators both at zero and finite temperature in QCD with no light quarks[1)]. Charmonia, however, were found to be dissolved at temperatures significantly lower than quoted in lattice QCD studies, and in contradiction with other claims made in recent years from different potential model studies. Fig 1 shows the pseudoscalar charmonium spectral function at different temperatures above deconfinement as obtained using the physically motivated potential ($V_1(r,T)$ in[1)]). There are no resonance like structures, only a large threshold enhancement. This enhancement above free quark propagation is an indication of a remaining correlation between the charm and anticharm quark. In Fig 1 we also show the lattice charmonium spectral function of Ref.[2)] (solid black curve). The first bump in the spectral function calculated on the lattice is consistent with the threshold enhancement obtained from the potential model. Furthermore, the spectral function integrated from 2.7GeV to 4.5GeV does not change between $T = 0$ and $1.5T_c$, neither on the lattice, nor in our results.

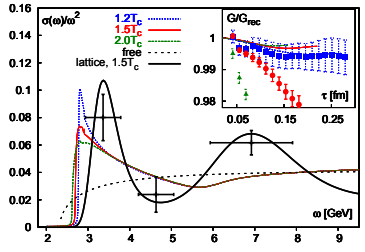

Fig. 1. Charmonium spectral function at different temperatures from[1)] and from lattice QCD at $1.5T_c$[2)].. The error-bars on the lattice spectral function correspond to the statistical error of the spectral function integrated in the ω-interval corresponding to the horizontal error-bars. The insets show the corresponding ratio G/G_{rec}[1)] together with the results from lattice calculations[2)].

In[3)] we extended the analysis to real QCD with one strange quark and two light quarks using new lattice QCD data on quark-antiquark free energy obtained with small quark masses[4)], and estimated the upper limit on the dissociation temperatures of the different charmonium and bottomonium states. There is an uncertainty in choosing the quark-antiquark potential at finite temperature. The more extreme choice, still compatible with lattice data[4)], leads to the largest possible binding energy. In this most binding potential some of the quarkonium states survive above deconfinement, but their strongly temperature-dependent binding energy is significantly reduced. This is shown in Fig. 2. Here binding energy is defined as the distance between the position of the resonance peak and the continuum threshold. Due to the reduced binding energy thermal activation can lead to the dissociation of quarkonia, even when the corresponding peak is present in the spectral function. From the binding energy using the analysis of[5)] we estimate the thermal width[3)]. When the thermal width is significantly

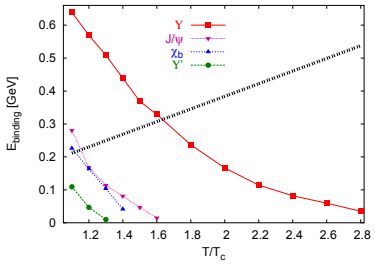

Fig. 2. Upper limit of the binding energy of quarkonium states.

larger than the binding energy no peak structure will be present in the spectral functions, even though the simple potential model calculation predicts a peak. Therefore, we define a conservative dissociation temperature by the condition $\Gamma > 2E_{bin}$. The obtained dissociation temperatures are summarized in the table: all quarkonium states, except the $1S$ bottomonium, will melt at temperatures considerably smaller than previous estimates.

state	χ_c	ψ'	J/ψ	Υ'	χ_b	Υ
T_{dis}	$\leq T_c$	$\leq T_c$	$1.2T_c$	$1.2T_c$	$1.3T_c$	$2T_c$

*1 RIKEN-BNL Research Center, Brookhaven National Laboratory, Upton, NY 11973 USA
*2 Physics Department, Brookhaven National Laboratory, Upton, NY 11973 USA

References

1) Á. Mócsy, P. Petreczky, Phys. Rev. D **77**, 014501 (2008)
2) A. Jakovac, P. Petreczky, K. Petrov, A. Velytsky, Phys. Rev. D **75**, 014506 (2007)
3) Á. Mócsy, P. Petreczky, Phys. Rev. Lett. **99**, 211602 (2007)
4) K. Petrov [RBC-Bielefeld Collaboration], arXiv:hep-lat/0610041.
5) D. Kharzeev, L. D. McLerran, H. Satz, Phys. Lett. B **356**, 349 (1995)

CONTENTS

5. Particle Physics

6. Development of Accelerator Facility

7. Instrumentation

III. Research Activities II (Material Science and Biology)

1. Atomic and Solid State Physics (ion)

2. Atomic and Solid State Physics (Muon)

I. PREFACE

Preface

This volume No. 41 of RIKEN Accelerator Progress Report compiles the yearly research activities conducted in 2007 by the laboratories and the groups of RIKEN Nishina Center for Accelerator-Based Science, or simply RIKEN Nishina Center (RNC). It also contains progress reports submitted by users of RI Beam Factory (RIBF) and RIKEN –RAL (Rutherford and Appleton Laboratory, UK) muon facility which RNC operates and are open to the international community.

The outstanding achievements of this year are selected by the editorial committee, and are presented in "Frontispiece" and "Highlights of the Year".

The RNC was inaugurated on April 1, 2006 and is presently organized into the following five divisions, one group and two affiliated research centers abroad: Accelerator Division, Nuclear Physics Research Division, User Liaison and Support Division, Sub Nuclear System Research Division, Accelerator Applications Research Division, Safety Management Group, RIKEN BNL (Brookhaven National Laboratory, US) Research Center (RBRC) and RAL Facility Office.

The RIKEN Nishina center is RIKEN's first research center named after our pioneering scientist, Dr. Yoshio Nishina. He was a multi-faced scientist who exhibited expertise in many fields including theoretical physics, experimental nuclear and cosmic-ray physics, accelerator building, and accelerator applications such as radiation biology and nuclear chemistry. Today, such a versatile scientist is rarely to be found. Thus, RIKEN Nishina center, as a collective of experts, covers each and all of these fields.

For readers' convenience, the organization chart of RNC is illustrated in the following pages.

The change that took place within the organization this year are as follows: on March 1, Dr. Toshiyuki Kubo was promoted as the group director of Experimental Installations Operation Group, Dr. Toshimi Suda as the group director of User Liaison and Support Group, and Dr. Tadashi Kambara as the group director of Accelerator Applications Research Group; on March 31, Dr. Koichiro Asahi who doubled as the professor of the Tokyo Institute of Technology and the chief scientist of Applied Nuclear Physics Laboratory resigned from the latter position, while his laboratory's researchers still continue their works in RNC; on June 1, Dr. Shuichi Enomoto was appointed as the leader of Metallomics Research Unit; and on August 1, Dr. Takashi Nakatsukasa was appointed as the associate chief scientist of Theoretical Nuclear Physics Laboratory in Nuclear Physics Research Division.

The RIBF project has made some amazing progress following the big success in extracting the first beam of a 345 MeV/nucleon $^{27}Al^{10+}$ from SRC at 16:00 on December 28, 2006: at 3:00 on March 15 2007, the first RI beams were generated through projectile-fragmentation of a 345 MeV/nucleon $^{86}Kr^{31+}$ beam, and a variety of RI beams were identified by BigRIPS; at 21:00 on March 23, we succeeded in accelerating a $^{238}U^{86+}$ beam up to 345 MeV/ nucleon; and then, at 6:40 on March 27, we identified a large variety of RI beams produced through the in-flight fission of the 345 MeV/nucleon uranium beam.

With the aim of presenting a flash report on the first outcome from the RIBF during the International Nuclear Physics Conference 2007 (INPC07) which was held at Tokyo Japan on June 3-8 2007, the first test experiment was conducted by a Japanese, German, American and French joint international team in the last week of May 2007 immediately preceding the conference. The flash report was successfully presented as an extra talk during the conference. The experiment led to the discovery of new very neutron-rich ^{125}Pd isotopes which were clearly identified by BigRIPS among a large variety of RI beams produced through the in-flight fission of the 345 MeV/nucleon uranium beam. Not only did this achievement make a great launch in the exciting exploration of nuclear world which has been inaccessible to date, but also marked a dramatic debut of the RIBF. The discovery was also historically memorable in light of the fact that the year of 2007 commemorated the 70^{th} anniversary of the commissioning of Nishina's small cyclotron which was Japan's first and RIKEN's No.1 cyclotron. The newly operational SRC is RIKEN's No.9 cyclotron.

Program advisory committees for nuclear physics (NP-PAC) and for materials and life science (ML-PAC) have been newly formed to evaluate scientific merits of experimental proposals. The NP-PAC which is jointly formed with Center for Nuclear Study (CNS), the University of Tokyo, is chaired by Prof. W. F. Henning, GSI and consists of 9 foreign members and 7 Japanese members to review proposals for RIBF including CRIB experimental installation operated by CNS. The ML-PAC, chaired by Prof. R. Kiefl, University of British Columbia, Canada, and consisting of 4 foreign members and 11 Japanese members reviews proposals for RIBF or RIKEN-RAL muon facility. The first ML-PAC and NP-PAC were held on Feb. 1 and on Feb. 9, respectively. Both are held twice a year.

Yasushige Yano
Director,
RIKEN Nishina Center for Accelerator-Based Science

Organization

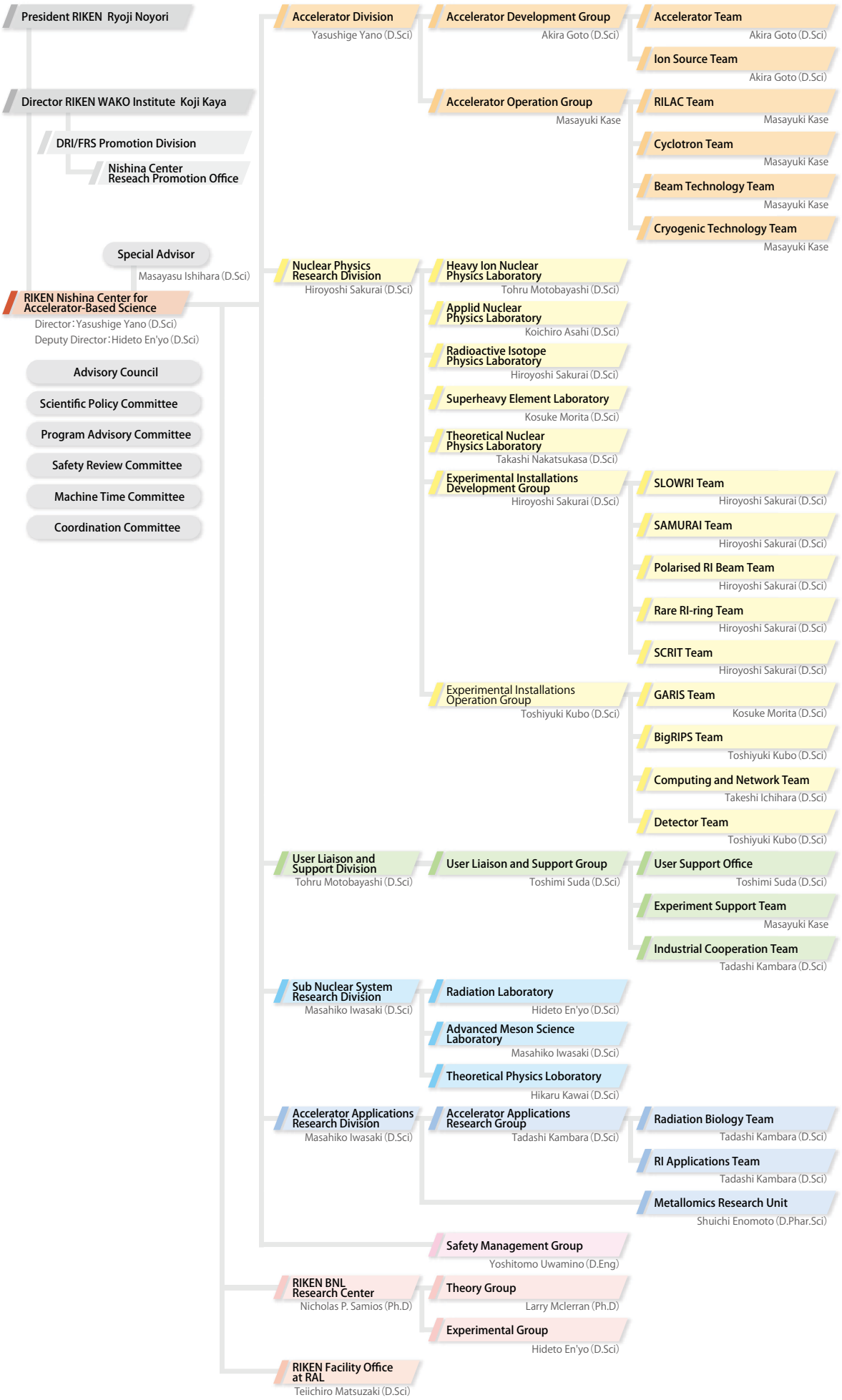

II. RESEARCH ACTIVITIES I
(Nuclear-Particle Physics)

1. Nuclear Physics

Gamma-ray measurements for particle identification

T. Nakao,[*1] D. Kameda, T. Kubo,, T. Ohnishi, N. Aoi, N. Fukuda, Y. Gono, Y. Kondo, K. Kusaka, T. Motobayashi, M. Ohtake, H. Otsu, H. Sakurai, H. Scheit, T. Sugimoto, H. Takeda, S. Takeuchi, Y. Yamaguchi, Y. Yanagisawa, Y. Yano, K. Yoneda, A. Yoshida, K. Yoshida, H. Kimura,[*1] H. Suzuki,[*1] Y. Mizoi,[*2] M. Matsushita,[*3] T. Kuboki,[*4] T. Suzuki,[*4] T. Yamaguchi,[*4] T. Moriguchi,[*5] A. Ozawa,[*5] Y. Yasuda,[*5] T. Nakamura,[*6] Y. Nakayama,[*6] T. Nannichi,[*6] T. Shimamura,[*6] H. Geissel,[*7] H. Weick,[*7] T. Nettleton,[*9] J. Nolen,[*8] D. Bazin,[*9] D. Morrissey,[*9] B. Sherrill,[*9] O. Tarasov,[*9] and W. Mittig,[*10]

[BigRIPS, Particle Identification, Isometric state measurement]

In BigRIPS[1)2)], the measurement of γ- rays emitted from isomeric states of the reaction products is very useful for particle identification. This is a report on γ- ray measurements on the BigRIPS commissioning with 345MeV/nucleon U beams in 2007.

The γ- rays were detected using two clover-type Ge detectors (Clover) that were located around the F7 focal plane of BigRIPS. The geometry is schematically shown in Fig. 1. To stop beams, we used an 8mm-thick Al stopper that was tilted by about 45 degrees from the beam line. We also used a certain-thickness Al degrader upstream of it if necessary. The energy calibration was performed with a ^{152}Eu standard γ source on the Al stopper. The absolute photo-peak efficiency of each Clover was roughly estimated with the calibration data as shown in Fig. 2. About a 2% efficiency for 1MeV γ- ray in the total of the two Clovers was acheived. In the add-back mode, the efficiency was improved to 3.5%.

When we selected particles with delayed γ events in the time period of 350-3000ns, only the events including isomeric states were clearly seen on the dE versus time-of-flight plot (PI plot). Then, the calibration of the PI plot was performed after confirming the γ- ray energy spectrum gated with the particle of interest in the PI plot, which show clear photo-peaks at the known γ energies.

Figure 3 shows the Z versus A/Q plots that were already calibrated using the ^{88}Br isomeric state. The γ-ray energy information from Clover (fig. 4) shows that the gated position is ^{88}Br. Fig. 5 shows the decay curve of the isometric state in ^{88}Br. In this experiment, depending on the BigRIPS setup, ^{79}As, ^{83}Br, ^{95}Kr, ^{96}Rb, ^{97}Sr, ^{98}Y, ^{99}Zr, ^{106}Nb, ^{130}Sn, ^{131}Sb, ^{136}Sb, ^{130}Te, ^{132}Te, ^{134}Te, ^{135}Te, ^{133}I and ^{136}Xe isomers were also observed.

*1 Department of Physics, The Univ. of Tokyo
*2 Division of Electronics and Applied Physics, Osaka Electro-Communication Univ.
*3 Department of Physics, Rikkyo Univ.
*4 Department of Physics, Saitama Univ.
*5 Institute of Physics, Univ. of Tsukuba
*6 Department of Physics, Tokyo Institute of Technology
*7 Gesellschaft für Schwerionenforshung (GSI)
*8 Algonne National Lab. (ANL)
*9 Michigan State Univ.
*10 Grand Accelerateur National d'Ions Lourds

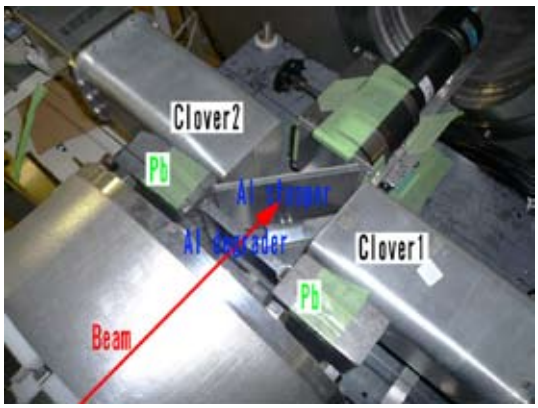

Fig. 1. Experimental setup at F7.

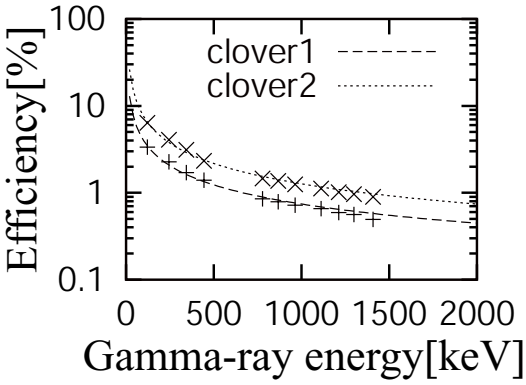

Fig. 2. Efficiency plots of Clover. The higher efficiency of "Clover 2" is due to the position of the γ source on the Al stopper in the calibration.

Table 1 shows preliminary results of isomer ratios of ^{88}Br and ^{135}Te. The isomer ratio was estimated using the photo-peak counts of the γ energy spectra and the particle counts on the Z vs A/Q plot. In the derivation, we only considered i) the Ge efficiency involving the probability of γ decay in the time period, ii) electron conversion and iii) decay of the isomeric states in flight. Note that the error in the isomer ratio is merely statistical, and does not include systematic errors.

For a future experiment using the ZeroDegree spec-

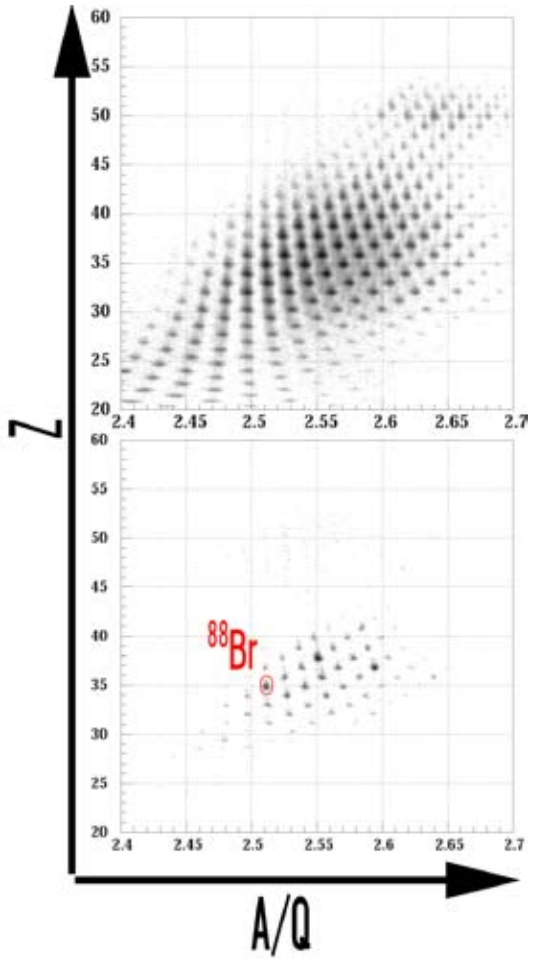

Fig. 3. Particle identification plot.

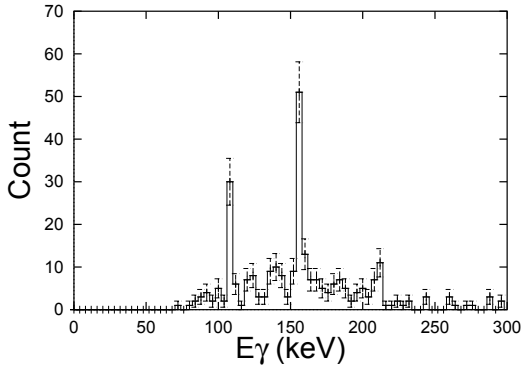

Fig. 4. γ-ray energy of ^{88}Br. Two γ energy peak are seen at 111keV and 159keV.

trometer[3] downstream of BigRIPS, we are developing a new setup for the measurement of isomeric γ- rays in the same place.

References

1) T. Kubo: Nucl. Instr. and Meth. , B 204, 97 (2003).

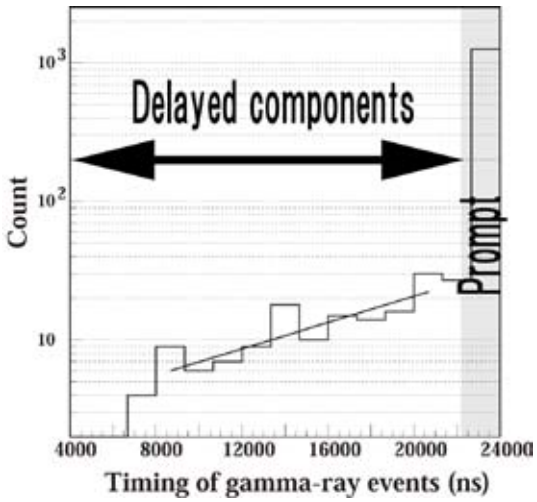

Fig. 5. Decay scheme of ^{88}Br.

Table 1. Isomer ratio of ^{88}Br and ^{135}Te.

	^{88}Br		^{135}Te	
Eγ(keV)	111	159	325	1180
Multipolarity	E2	M1	(E2)	(E2)
Isomer ratio(%)	6.61±1.7	7.49±1	4.11±0. 67	2.93±0.22

2) T. Kubo et al. : IEEE Trans. Appl. , Supercond. , 17, 1069 (2007).
3) Y. Mizoi et al. : RIKEN Accel. Prog. Rep. , 38, 297 (2005).

Observation of elastic electron scattering at the SCRIT prototype

T. Suda, T. Emoto, K. Ishii[1], S. Ito, K. Kurita[1], A. Kuwajima[2], T. Tamae[2], M. Wakasugi, S. Wang and Y. Yano

[SCRIT, elastic electron scattering, angular distribution]

This year, we have been continuing R&D studies of the SCRIT scheme[1)] by using a prototype at KSR, Kyoto University. A big progress of this year was that we have succeeded in trapping a sufficient number of externally injected Cs ions inside the electron beam and clearly observed electrons elastically scattered by the ions. In addition to the identification of elastic scattering, the angular distribution has also been successfully measured.

In this report, we present the results of the R&D studies carried out this year. The electron beam energy was 120 MeV, and the averaged stored beam current was 80 mA. Note that the results presented in this report are still preliminary.

The energy of scattered electrons has been measured using three calorimeters set at the scattering angles, θ_e, of 30°, 40° and 60°. The energy calibration of these calorimeters has been performed using elastically scattered electrons from the W-wire target[2)] and cosmic rays.

Figure 1 (a-c), shows electron energy spectra for θ_e=30°, 40° and 60°. The solid (dashed) line denotes the spectrum measured when the Cs ions are (are not) trapped. The vertex cut obtained with the track information by the drift chamber is applied to select electron events from the trap region.

Clear enhancement due to the Cs ions is observed in the energy spectra at E_e ∼100 MeV for θ_e=30° and 40°. Here, the lower energy region, $E_e \leq$ 80 MeV, and higher energy region, $E_e \geq$120 MeV, of these spectra are due to electromagnetic-shower background that originated from the short beam lifetime of KSR (∼100 s at 80 mA) and cosmic ray, respectively. Those backgrounds are independent of the Cs ion trapping. Indeed, the energy spectra at these E_e regions are identical.

Figure 1(d), shows subtracted energy spectra. Those for both θ_e=30° and 40° are consistent with the response functions of the calorimeters for 120-MeV electrons measured using the W-wire target[2)]. Thus, one can conclude that they are elastically scattered electrons from the trapped Cs ions.

Figure 2 shows the angular distribution of the differential cross section for elastic scattering. The solid line shows the results of a distorted wave calculation (DWBA), which is normalized to the data at θ=30°. The good agreement further confirms the success of the elastic scattering measurement using the SCRIT scheme. By knowing the elastic cross section for Cs, the achieved luminosity was determined to be 1.2 × $10^{26}/cm^2/s$, with the estimated number of trapped ions being 3.6 × 10^7.

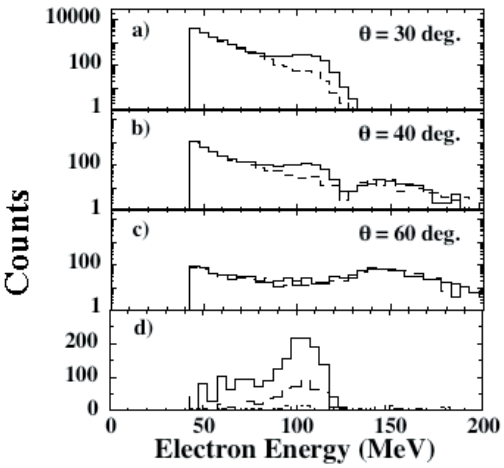

Fig. 1. Electron energy spectra. The solid (dashed) line denotes the spectrum with (without) the trapped Cs ions. The subtracted spectra are shown in d). The solid (dashed, dotted) line shows for θ_e= 30° (40°, 60°).

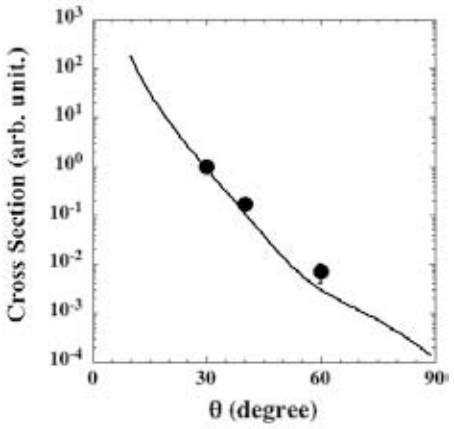

Fig. 2. Angular distribution for elastic-scattering cross section. The solid line shows the result of a DWBA calculation normalized to the data at θ_e=30°.

References

1) M. Wakasugi, T. Suda, and Y. Yano: Nucl. Instrum. Methods **A532**, 216 (2004).
2) Y. Furukawa et al.: RIKEN Accel. Prog. Rep. 40 (2007).

*1 Rikkyo University
*2 Tohoku University

Pumping ^{229m}Th by hollow-cathode discharge [V]

H. Haba, M. Hara,[*1] T. T. Inamura, Y. Kasamatsu,[*2] H. Kikunaga, T. Mitsugashira,[*1] T. Nakanishi,[*3] T. Ohtsuki,[*4] A. Shinohara,[*5] Y. Suzuki,[*1] K. Takamiya,[*6] S. Watanabe,[*1] A. Yokoyama,[*3] and H. Yuki[*4]

[Nuclear structure, NEET by electric discharge, alpha decay]

This is the final report of our five-year endeavor at Oarai to search for evidence of an extremely low-lying isomer in ^{229}Th, which is believed to be at several electron volts. Since it was first postulated by Kroger and Reich,[1] a large number of groups have attempted to obtain direct evidence of the isomer by various techniques but in vain. All of them made use of nuclear de-excitation to populate the isomer ^{229m}Th. On the contrary, our method is an entirely atomic process, as described previously,[2,3] i.e., NEET through electric discharge in a hollow-cathode tube. There is a great advantage over methods used by previous investigators because there are no unknown nuclear effects in the process.

As was mentioned in our last report,[3] we managed to start measurements with a new setup 30 seconds after switching off the hollow-cathode discharge. We measured α particles in the energy region of the α decay of ^{229}Th as a function of time, as shown in Fig. 1. (It should be stated that the half-life of the ground state of ^{229}Th is known to be 7340 y.) Simultaneously, α particles from the daughter nuclides of ^{229}Th, which are well known, were recorded for comparison (see Fig. 2). There is a considerable difference in the time dependence between them, and clear time-dependent α yields are seen in the region of minutes in the ^{229}Th α-energy range. This appears to show a sign of NEET to ^{229m}Th. Although we could not observe individual α lines characteristic of the isomer decay with the present setup, we should be able to extract the isomer half-life in this way after a precise determination of the level of background that is seen in Fig. 1.

Details will be published elsewhere before long.

*1 Oarai Branch, Institute for Materials Research, Tohoku University
*2 Advanced Science Research Center, JAEA, Tokai
*3 Graduate School of Natural Science and Technology, Kanazawa University
*4 Laboratory of Nuclear Science, Tohoku University
*5 Graduate School of Science, Osaka University
*6 Research Reactor Institute, Kyoto University

References

1) L. A. Kroger and C. W. Reich: Nucl. Phys. **A259**, 29 (1976).
2) T. T. Inamura et al.: Hyp. Interact. **162**, 115 (2005).
3) H. Haba et al.: RIKEN Accel. Prog. Rep. **40**, 38 (2007).

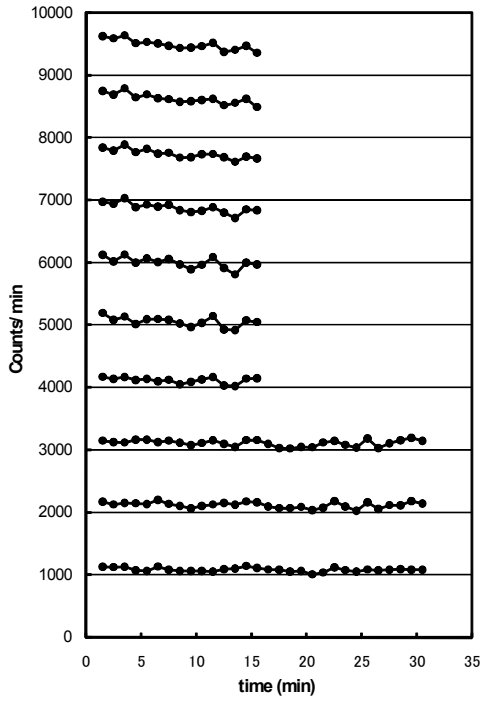

Fig. 1. Total ^{229}Th α yields in the energy range of 1107.4-5099.4 keV as a function of time. The bottom curve is for the 1st measurement after the 1st 5-min discharge. The data were successively added up to the 10th measurement (top curve).

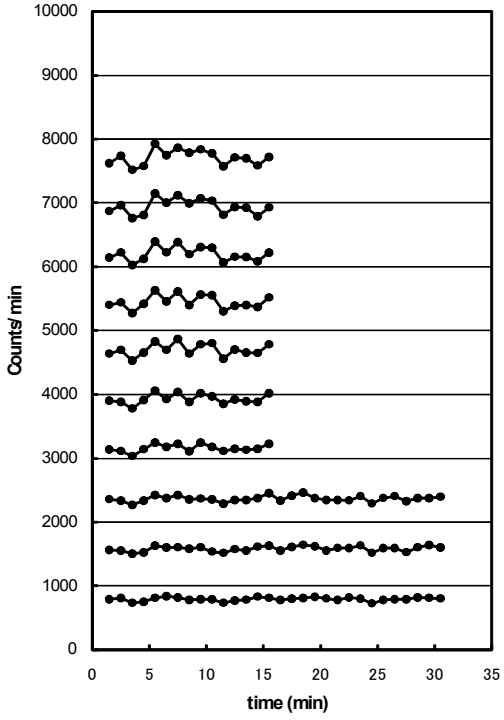

Fig. 2. Total α yields in the energy range of 5104.6-8702.0 keV from the daughter nuclides (^{225}Ac, ^{221}Fr, ^{217}At, and ^{213}Po) of ^{229}Th as a function of time. The presentation is the same as in Fig. 1.

Investigation of the ^{26}Si(p,γ)^{27}P reaction via Coulomb dissociation

Y. Togano,[*1] T. Gomi,[*2] T. Motobayashi, Y. Ando,[*1] N. Aoi, H. Baba, K. Demichi,[*1] Z. Elekes,[*3] N. Fukuda, Zs. Fülöp,[*3] U. Futakami,[*1] H. Hasegawa,[*1] Y. Higurashi, K. Ieki,[*1] N. Imai,[*4] M. Ishihara, K. Ishikawa,[*5] N. Iwasa,[*6] H. Iwasaki,[*7] S. Kanno, Y. Kondo,[*5] T. Kubo, S. Kubono,[*8] M. Kunibu,[*1] K. Kurita,[*1] Y. U. Matsuyama,[*1] S. Michimasa, [*8] T. Minemura, [*9] M. Miura,[*5] H. Murakami,[*1] T. Nakamura,[*5] M. Notani,[*10] S. Ota,[*8] A. Saito,[*8] H. Sakurai, M. Serata,[*1] S. Shimoura,[*8] T. Sugimoto, E. Takeshita, S. Takeuchi, K. Ue,[*7] K. Yamada, Y. Yanagisawa, K. Yoneda, and A. Yoshida

[^{208}Pb(^{27}P,p^{26}Si)^{208}Pb, Coulomb dissociation, Nuclear astrophysics]

The stellar reaction ^{26}Si(p,γ)^{27}P was studied via Coulomb dissociation. This reaction is a candidate process affecting the resultant nuclear abundances of ^{26}Al and isotopes of similar atomic mass in explosive hydrogen burning since the reaction destroys ^{26}Si which otherwise decays to produce ^{26}Al. The galactic γ line at 1.8 MeV associated with ^{26}Al β^+ decay has been observed by satellite telescopes.[1)] This is evidence of ongoing nucleosynthesis in the Galaxy because its half life of about 10^6 years is much shorter than the period of Galactic evolution. No direct measurement of ^{26}Si(p,γ)^{27}P has been made so far due to the short lifetime of ^{26}Si and the small cross section of the reaction. To overcome this difficulty we applied the Coulomb dissociation method, which can extract the cross section of the relevant stellar reaction with relatively low beam intensity. The aim of the present work is to determine the ^{26}Si(p,γ)^{27}P reaction rate via Coulomb dissociation and estimate the reaction flow around ^{26}Si and ^{26}Al during the explosive hydrogen burnings.

The experiment was performed using RIPS at RIKEN Nishina Center. Details of the experimental setup are described in Ref. 2. The radiative widths Γ_γ of the three resonant states, whose energies are 0.315, 0.805, and 1.374 MeV, were obtained. The E2 component of Γ_γ for the lowest resonant state, 0.315 MeV, was experimentally determined to be $(8.4 \pm 1.5)^{-5}$ eV. The M1 component was estimated using the measured E2 width and a shell model calculation, as described in Ref. 2, and the total Γ_γ was obtained to be $(4.2 \pm 1.3) \times 10^{-3}$ eV. The widths for the other two states were determined to be $(3.2 \pm 0.6) \times 10^{-4}$ eV for the 0.805 MeV state and $(5.9 \pm 1.5) \times 10^{-4}$ eV for the 1.374 MeV state.

The astrophysical reaction rate for the ^{26}Si(p,γ)^{27}P reaction was extracted from the obtained radiative widths. Figure 1 shows the stellar temperature dependence of the rate. The three solid curves represent the present results for the three resonant states. Each pair of dotted curves represents the margin of error associated with each result. The dashed curve shows the direct capture component. This figure indicates that the resonant capture through the 0.315 MeV state is the dominant process between 0.1 GK and 4 GK and those through the 0.805 MeV and 1.374 MeV states give negligible contributions in this temperature range. This result is consistent with the estimations by Caggiano et al.[3)] and Guo et al.[4)] within the margins of error. Compared with the ^{26}Si β^+ decay rate, the capture reaction rate is faster when ^{26}Si produced through the ^{25}Al(p,γ)^{26}Si reaction in novae.

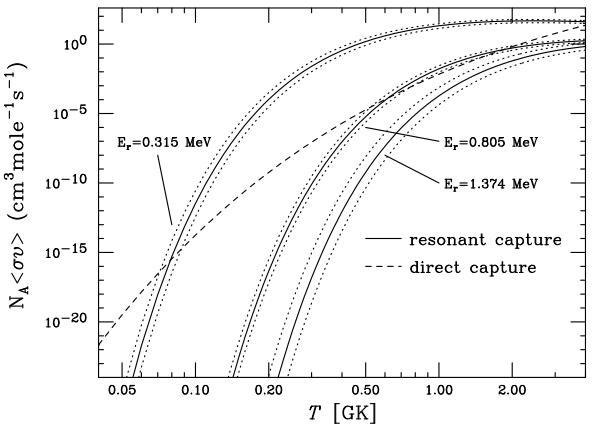

Fig. 1. Temperature dependence of the reaction rate for the ^{26}Si(p,γ)^{27}P reaction. The solid and dashed curves represent the resonant and direct capture components, respectively. Dotted curves show the margins of the error for each resonant capture through each excited state in ^{27}P.

*1 Department of Physics, Rikkyo University
*2 National Institute of Radiological Sciences
*3 Institute of Nuclear Research of the Hungarian Academy of Sciences (ATOMKI), Hungary
*4 Institute of Particle and Nuclear Studies, High Energy Accelerator Research Organization (KEK)
*5 Department of Physics, Tokyo Institute of Technology
*6 Department of Physics, Tohoku University
*7 Department of Physics, University of Tokyo
*8 Center for Nuclear Study, University of Tokyo
*9 National Cancer Center
*10 Argonne National Laboratory, USA

References

1) R. Diehl et al.: Astron. Astrophys. Suppl. **97**, 181 (1993).
2) Y. Togano et al.: Eur. Phys. J. A **27**, s01, 233 (2006).
3) J. A. Caggiano et al.: Phys. Rev. C **64**, 025802 (2001).
4) B. Guo et al.: Phys. Rev. C **73**, 048801 (2006).

One-neutron removal reactions of ^{18,19}C

Y. Kondo, T. Nakamura,[*1] Y. Satou,[*1] N. Aoi, N. Endo,[*2] N. Fukuda, T. Gomi, Y. Hashimoto,[*1] M. Ishihara, S. Kawai,[*3] M. Kitayama,[*2] T. Kobayashi,[*2] Y. Matsuda,[*2] N. Matsui,[*1] T. Motobayashi, T. Nakabayashi,[*1] T. Okumura,[*1] H. J. Ong,[*4] T. K. Onishi,[*4] H. Otsu, H. Sakurai, S. Shimoura,[*5] M. Shinohara,[*1] T. Sugimoto, S. Takeuchi, M. Tamaki,[*5] Y. Togano,[*3] and Y. Yanagisawa

[Nuclear structure, unstable nuclei, momentum distribution]

The one-neutron removal reaction in inverse kinematics is a powerful tool for investigating unstable nuclei. For instance, the momentum distribution of the core fragment, which reflects spatial extension of a removed neutron, is useful for probing the halo structure. Furthermore, spins and parities (J^π) and spectroscopic factors can be deduced from the momentum distribution and partial cross sections by employing a reaction theory, such as the eikonal model and continuum discretized coupled-channel (CDCC) calculation. We applied this technique to the one-neutron removal reactions of ^{18,19}C, aiming at the deduction of J^π of the excited states in ^{17,18}C and spectroscopic factors.

The experiment was carried out using the RIPS beam line at RIKEN. ^{18,19}C beams were produced by projectile fragmentation of a primary ^{22}Ne beam at 110 MeV/nucleon on a Be target. The ^{18}C (^{19}C) beam bombarded a liquid hydrogen target with an average thickness of 120 mg/cm^2 at around 80 (70) MeV/nucleon. Further experimental details can be found elsewhere.[1)]

Figure 1 shows the energy spectrum of the γ ray emitted from ^{17}C produced by one-neutron removal from ^{18}C. We observed two excited states at 0.21 MeV and 0.33 MeV, which, in the previous study,[2)] were tentatively assigned to $1/2^+$ and $5/2^+$, respectively. In order to examine the J^π assignments, the momentum distributions are analyzed. Figure 2 displays the transverse momentum distributions of ^{17}C measured in coincidence with the 0.21 MeV and 0.33 MeV γ rays. The distribution for the 0.21 MeV state is consistent with the CDCC calculation assuming neutron removal from the 1s orbit in ^{18}C, while that for the 0.33 MeV state is well described by the calculation under the assumption of 0d-neutron removal. These agreements confirm the $1/2^+$ and $5/2^+$ assignments for the 0.21 MeV and 0.33 MeV states, respectively.

The analysis of the one-neutron removal reaction of ^{19}C is now in progress. Spins and parities of the excited states in ^{18}C, which are unknown except for the 2^+_1 state, will be deduced from momentum distributions. In addition, spectroscopic factors will be extracted from the partial cross sections of processes feeding individual states of the residual nuclei ^{17,18}C in the one-neutron removal reactions of ^{18,19}C by comparing them with the single-particle cross sections calculated by the CDCC method.

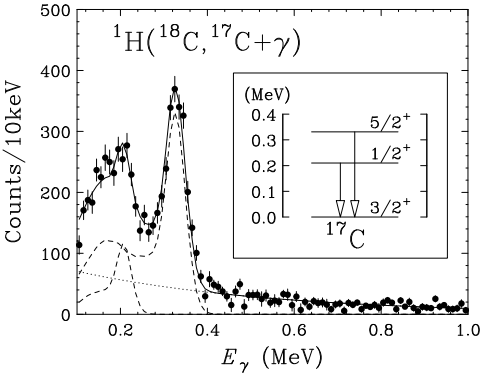

Fig. 1. Energy spectrum of the γ ray emitted from ^{17}C in the one-neutron removal reaction of ^{18}C. The dashed lines represent the response functions of the γ-ray detectors obtained by the GEANT simulation, while the dotted line denotes the exponential background. Inset illustrates the level scheme of ^{17}C and the observed γ transitions.

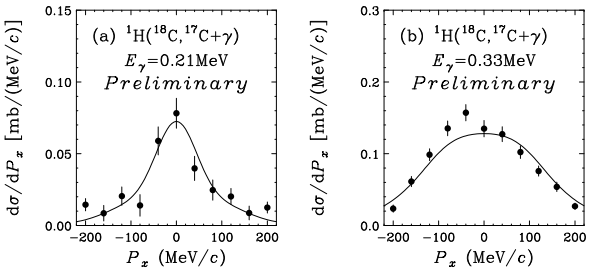

Fig. 2. Transverse momentum distributions in coincidence with the (a) 0.21 MeV and (b) 0.33 MeV γ rays emitted from ^{17}C produced by one-neutron removal from ^{18}C. The solid lines stand for the theoretical distributions for the (a) 1s and (b) 0d neutron removals calculated by the CDCC method.

*1 Department of Physics, Tokyo Tech
*2 Department of Physics, Tohoku University
*3 Department of Physics, Rikkyo University
*4 Department of Physics, University of Tokyo
*5 Center for Nuclear Study, University of Tokyo

References
1) Y. Kondo et al.: RIKEN Accel. Prog. Rep. **39**, 45 (2006).
2) Z. Elekes et al.: Phys. Lett. B**614**, 174 (2005).

In-beam γ-ray spectroscopy using the very neutron-rich ^{36}Mg beam

S. Michimasa,[*1] Y. Yanagisawa, K. Inafuku,[*2] N. Aoi, Z. Elekes,[*3] Zs. Fülöp,[*3] Y. Ichikawa, N. Iwasa,[*2] K. Kurita,[*4] M. Kurokawa, T. Machida,[*4] T. Motobayashi, T. Nakamura,[*5] T. Nakabayashi,[*5] M. Notani,[*6] H. J. Ong,[*7] T. K. Onishi,[*8] H. Otsu, H. Sakurai, M. Shinohara,[*5] T. Sumikama,[*9] S. Takeuchi, K. Tanaka, Y. Togano,[*4] K. Yamada, M. Yamaguchi,[*10] and K. Yoneda

[Nuclear reactions: ^{1}H(^{36}Mg,$^{34-36}$Mgγ)]

We report here on the in-beam γ-ray spectroscopy using the very neutron-rich ^{36}Mg beam and a hydrogen target. The ^{36}Mg nucleus is located in the middle of the shell closures of $N = 20$ and 28 and is closer to the neutron drip line than nuclei belonging to the so-called 'island of inversion'. In previous experimental studies on neutron-rich magnesium isotopes, ^{32}Mg was reported to be a well-deformed nucleus,[1] and the disappearance of the magicity at $N = 20$ was indicated. The deformation of ^{34}Mg was reported to be larger than that of ^{32}Mg.[2] The present study is an experiment to investigate the low-lying excited states in ^{36}Mg.

The experiment was performed at the unstable nuclear beam line RIPS in RIKEN. Ions of ^{48}Ca were accelerated up to 63 MeV/nucleon using the acceleration scheme of RFQ-RILAC-CSM-RRC and impinged on a 150-μm ^{181}Ta plate. A radioactive ^{36}Mg beam was isotopically separated by RIPS. Particle identification of the secondary beam was performed by a standard method based on the energy loss, time of flight and magnetic rigidity. The secondary beam bombarded a liquid hydrogen target[3] of 105 mg/cm^2. To obtain a sufficient mass resolution for the reaction products, the TOF spectrometer[4] was placed downstream of the secondary target. The scattered particles were detected using a telescope placed at the end of the spectrometer. The de-excitation γ ray from the inelastically scattered particle was detected using 160 NaI(Tl) scintillators (DALI2)[5] surrounding the secondary target. Further details on the experiment setup were described in ref. 6.

Reaction products of the ^{36}Mg beam from the secondary target are identified with an accuracy of 0.4 amu (σ) as shown in Fig. 1(a). Figures 1(b–d) show the γ-ray spectra in the proton inelastic and neutron removal channels assigned by the identification of the reaction products. A γ line at around 0.7 MeV in Fig. 1(b) is assigned to be the $2_1^+ \rightarrow 0_1^+$ transition in ^{34}Mg, since its energy is consistent with that shown in the previous works.[2] In Fig. 1(d), a γ line is located at approximately 0.7 MeV. The corresponding γ line is, however, not identified significantly in Fig. 1(c). Therefore, the 0.7-MeV line in Fig. 1(d) is identified to be the transition in ^{36}Mg. Since this γ-ray energy is consistent with an excitation energy of the 2_1^+ state in ^{36}Mg reported recently in ref. 7,the line is assigned to be the $2_1^+ \rightarrow 0_1^+$ transition.

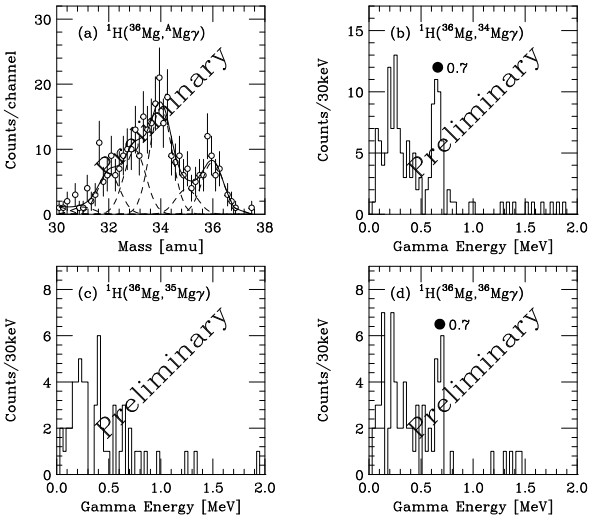

Fig. 1. (a) Particle identification of outgoing magnesium isotopes in coincidence with the ^{36}Mg beam. (b-d) Gamma-ray spectra in the (^{36}Mg,^{34}Mg), (^{36}Mg,^{35}Mg) and (^{36}Mg,^{36}Mg) reactions, respectively.

Data analysis is now in progress to deduce the deformation length of ^{36}Mg.

*1 Center for Nuclear Study, University of Tokyo
*2 Department of Physics, Tohoku University
*3 ATOMKI, Hungary
*4 Department of Physics, Rikkyo University
*5 Department of Physics, Tokyo Institute of Technology
*6 Argonne National Laboratory, USA
*7 RCNP,Osaka University
*8 Department of Physics, University of Tokyo
*9 Department of Physics, Faculty of Science and Technology, Tokyo University of Science
*10 National Institute of Advanced Industrial Science and Technology

References

1) T. Motobayashi et al.: Phys. Lett. B **346**, 9 (1995).
2) H. Iwasaki et al.: Phys. Lett. B **522**, 227 (2001).
3) H. Ryuto et al.: Nucl. Instrum. Methods Phys. Res. A **555**, 1 (2005).
4) N. Aoi et al.: RIKEN Accel. Prog. Rep. **38**, 176 (2005).
5) S. Takeuchi et al.: RIKEN Accel. Prog. Rep. **36**, 148 (2003).
6) S. Michimasa et al.: RIKEN Accel. Prog. Rep. **40**, 8 (2007).
7) A. Gade et al.: Phys. Rev. Lett. **99**, 072502 (2007).

Lifetime measurements of 2_1^+ states in ^{16,18}C

H. J. Ong, N. Imai,[*1] D. Suzuki,[*2] H. Iwasaki,[*2] H. Sakurai, T. K. Onishi,[*2] M. K. Suzuki,[*2] S. Ota,[*3] S. Takeuchi, T. Nakao,[*2] Y. Togano,[*4] Y. Kondo,[*5] N. Aoi, H. Baba, S. Bishop, Y. Ichikawa,[*2] M. Ishihara, T. Kubo, K. Kurita,[*4] T. Motobayashi, T. Nakamura,[*5] T. Okumura,[*5] and Y. Yanagisawa.

[NUCLEAR REACTIONS: ^{9}Be(^{18}C,^{18}C*)^{9}Be, lifetime measurement, RSM]

Measurement of the reduced $E2$ transition probability, $B(E2)$, from the first excited 2^+ (2_1^+) state to the ground 0^+ ($0_{\rm gs}^+$) state in an even-even nucleus is an important tool for studying proton collectivity. Recently, an anomalously small $B(E2)$ value was reported for the neutron-rich ^{16}C nucleus from the lifetime measurement of its 2_1^+ state ($\tau(2_1^+)$)[1]. The result indicates a suppressed proton contribution to the transition strength. Subsequent studies using the Coulomb-nuclear interference[2] and the proton inelastic scattering[3] suggest a neutron-dominant quadrupole collective motion in ^{16}C. To explore the possibility of the neighboring ^{18}C having the same behavior, we have carried out an experiment to determine the $B(E2)$ value of ^{18}C.

Here, we report the lifetime measurement of the 2_1^+ state in ^{18}C by means of an upgraded recoil shadow method (RSM)[1] incorporating the in-beam γ-ray spectroscopy. The remeasurement of $\tau(2_1^+)$ in ^{16}C is also reported.

The experiment was performed at RIKEN Nishina Center. Secondary beams of ^{16,18}C were produced in two separate measurements through projectile fragmentation of a 110-MeV/nucleon ^{22}Ne primary beam, and separated by the RIPS beam line[4]. The ^{16,18}C beams with typical intensities of 6.5×10^4 and 2.3×10^4 particles per second, respectively, were directed at and inelastically excited by a 370-mg/cm^2 ^{9}Be target placed at the exit of the RIPS beam line. The energies of the ^{16,18}C beams before the target were 72 and 79 MeV/nucleon. For ^{16}C, an additional measurement with a 40-MeV/nucleon beam was performed to determine the angular distribution of the γ rays in order to incorporate it into the experiment data in Ref.[1].

Scattered particles were detected using a double-layer plastic scintillator hodoscope[5] placed 4 m downstream of the secondary target; particle identification was done by means of the TOF-ΔE-E method based on the timing information and the energy deposit measured with the hodoscope.

To implement the RSM concept, we placed a thick γ-ray shield around the target. The shield was a 5-cm-thick lead slab with an outer frame of 24×24 cm^2 and an inner hole of 5.4 cmϕ. The de-excitation γ rays from the inelastically excited ^{16,18}C nuclei were detected in coincidence with the scattered ^{16,18}C by an array of 130 NaI(Tl) detectors, which form part of the DALI1[6] and DALI2[7]. The array consisted of ten layers surrounding the target. Depending on the lifetime, the detection efficiency of the γ rays varies in each layer due to the attenuation by the lead shield. Measurements were also performed without the lead shield to determine the angular distribution of the γ rays. The number of full-energy-peak events measured by the i-th layer NaI(Tl) detectors during the measurement with (without) the lead shield is denoted by $N^i_{\rm wPb}$ ($N^i_{\rm woPb}$). The $\tau(2_1^+)$ values of ^{16,18}C were determined by comparing the measured $N^i_{\rm wPb}/N^i_{\rm woPb}$ ratios with $\tau(2_1^+)$-dependent ratio functions obtained with Monte Carlo simulations.

The mean lifetime of the 2_1^+ state in ^{18}C thus determined was 18.9 ± 0.9(stat) $\pm$ 4.4(syst) ps. For ^{16}C, the remeasured $\tau(2_1^+)$ was about 18 ps. The discrepancy between the present result and the previous result (about 77 ps) in Ref.[1] was explained by incorporating the γ-ray angular distribution measured in this work into the previous data. Taking into account all available data, $\tau(2_1^+)$ for ^{16}C was determined to be 18.0 ± 1.6(stat) $\pm$ 4.7(syst) ps. The $\tau(2_1^+)$ values correspond to $B(E2)$ values of 2.6 ± 0.2(stat) $\pm$ 0.7(syst) e^2fm^4 (about 1.1 W.u.) and 4.3 ± 0.2(stat) $\pm$ 1.0(syst) e^2fm^4 (about 1.5 W.u.) for ^{16,18}C, respectively. The small $B(E2)$ value for ^{18}C, which is comparable to the value of 3.7 e^2fm^4 for the neutron-closed-shell ^{14}C nucleus, indicates that the phenomenon of hindered $E2$ strength observed in ^{16}C persists in ^{18}C.

For more details, see RIKEN-NC-NP-16 (ISSN 1881-7394) or http://arxiv.org/abs/0711.4062v1.

*1 KEK
*2 Department of Physics, University of Tokyo
*3 Center for Nuclear Study, University of Tokyo
*4 Department of Physics, Rikkyo University
*5 Tokyo Institute of Technology

References

1) N. Imai et al.: Phys. Rev. Lett. **92**, 062501 (2004).
2) Z. Elekes et al.: Phys. Lett. **B586**, 34 (2004).
3) H. J. Ong et al.: Phys. Rev. C **73**, 024610 (2006).
4) T. Kubo et al.: Nucl. Instrum. Methods B **70**, 309 (1992).
5) I. Hisanaga et al.: RIKEN Accel. Prog. Rep. **31**, 162 (1998).
6) T. Nishio et al.: RIKEN Accel. Prog. Rep. **29**, 184 (1996).
7) S. Takeuchi et al.: RIKEN Accel. Prog. Rep. **36**, 148 (2003).

Study of neutron-rich ^{23}O and the disappearance of N=20 magicity

Z. Elekes,[*1] Zs. Dombrádi,[*1] S. Bishop, Zs. Fülöp,[*1] J. Gibelin,[*2] T. Gomi, Y. Hashimoto,[*3] N. Imai, N. Iwasa,[*4] H. Iwasaki,[*5] G. Kalinka,[*1] Y. Kondo,[*3] A. A. Korsheninnikov,[*8] K. Kurita,[*6] M. Kurokawa, N. Matsui,[*3] T. Motobayashi, T. Nakamura,[*3] T. Nakao,[*5] E. Yu. Nikolskii,[*8] T. K. Ohnishi,[*5] T. Okumura,[*3] S. Ota,[*7] A. Perera, A. Saito,[*5] H. Sakurai,[*5] Y. Satou,[*3] D. Sohler,[*1] T. Sumikama, D. Suzuki,[*5] M. Suzuki,[*5] H. Takeda,[*7] S. Takeuchi, Y. Togano[*6] and Y. Yanagisawa

[nuclear structure, unstable nuclei, transfer reaction]

The stability of shell closures is determined by the size of shell gaps which are measured as the energy difference between the single-particle states belonging to different major shells. From ^{30}Si to ^{24}O, the N=20 shell gap is expected to gradually decrease, and N=14 and N=16 shell gaps develop instead.[1)] Therefore, the aim of this study is to determine the location of the excited states in ^{23}O, which directly gives the single-particle energies suitable for deducing the size of the N=16 and N=20 shell closures, via invariant mass spectroscopy combined with the (d,p) neutron transfer reaction.

The experiment was carried out at RIKEN, where a 94 A·MeV primary beam of ^{40}Ar with 60 pnA intensity collided with a ^{9}Be production target of 3 mm thickness. The total intensity of the produced secondary beam was approximately 1500 cps with an average ^{22}O intensity of 600 cps. The separation of ^{22}O particles was complete. This secondary beam was transmitted to a CD_2 target of 30 mg/cm^2. The reaction occurred at an energy of 34 A·MeV. The scattered particles were detected and identified by a 2×2 matrix silicon telescope placed 96 cm downstream of the target. The first two layers were made of strip detectors (with 5 mm width for each strip) to measure the x and y positions of the fragments. The protons emitted backward in the reaction were detected by 156 CsI(Tl) scintillator crystals and were read out by photodiodes. The neutrons originating from the decay of the produced ^{23}O nuclei excited above the neutron separation energy were detected by a neutron wall. The energy of the neutrons was deduced from the TOF, while the position of the collision was determined by identifying the rod that fired (in the vertical direction) and by the time difference between the two photomultipliers attached to the ends of the rods (in the horizontal direction).

The excitation energy spectrum of ^{23}O shown in Fig. 1 was reconstructed from the momentum of the neutrons and the heavy ion ^{22}O by calculating the invariant mass and using the known neutron separation energy (2.74 MeV). Two peaks are clearly visible at 4.00(2) MeV and 5.30(4) MeV in the spectrum. The

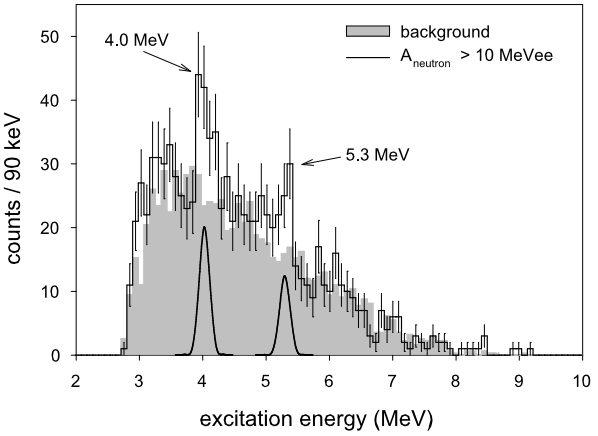

Fig. 1. Reconstructed excitation energy spectrum of ^{23}O. $A_{neutron}$>10 MeV. The shaded spectrum represents the background.

(d,p) reaction populates the single-particle states of ^{23}O. The ground state of this nucleus has been experimentally determined to be the neutron $s_{1/2}$ state.[2,3)] From a comparison with shell model calculations,[4,5)] the first excited state is the neutron $d_{3/2}$ state, the energy of which gives the N=16 shell closure to be 4 MeV. This is sufficiently large to explain why ^{24}O is the last bound oxygen isotope. The second excited state observed in the present experiment does not have any counterpart in the sd model space,[4)] and corresponds to a state from the fp shell.[5)] Its energy relative to the $d_{3/2}$ state allows us to determine the strength of the N=20 shell closure to be 1.3 MeV and provides direct evidence for the disappearance of the N=20 shell closure at Z=8.

References

1) T. Otsuka et al.: Phys. Rev. Lett. **87**, 082502 (2001).
2) D. Cortina-Gil et al.: Phys. Rev. Lett. **93**, 062501 (2004).
3) C. Nociforo et al.: Phys. Lett. **B605**, 79 (2005).
4) B.A. Brown, W.A. Richter et al.: Phys. Rev. **C74**, 034315 (2006).
5) T. Otsuka et al.: Nucl. Phys. **A685**, 100 (2001).

† Condensed from article in Phys. Rev. Lett. **98**, 102502 (2007)

*1 Institute of Nuclear Research (ATOMKI)
*2 Institut de Physique Nucléaire
*3 Tokyo Institute of Technology
*4 Tohoku University
*5 University of Tokyo
*6 Rikkyo University
*7 Kyoto University
*8 Kurchatov Institute

Proton core polarization in neutron-rich nucleus ^{74}Ni

S. Kanno,[*1] N. Aoi, D. Bazin,[*2] M. D. Bowen,[*2] C. M. Campbell,[*2] J. M. Cook,[*2] D.-C. Dinca,[*2] A. Gade,[*2] T. Glasmacher,[*2] H. Iwasaki,[*3] T. Kubo, K. Kurita,[*1] T. Motobayashi, W. F. Mueller,[*2] T. Nakamura,[*4] H. Sakurai,[*3] H. Suzuki,[*3] S. Takeuchi, J. R. Terry,[*2] K. Yoneda[*2] and H. Zwahlen[*2]

[Nuclear Structure, ^{74}Ni(p,p′ γ), Inelastic scattering, Unstable nuclei]

The neutron-rich nucleus ^{74}Ni has been studied by proton inelastic scattering to explore the evolution of $Z = 28$ core polarization in the very neutron-rich Ni isotopes in the vicinity of ^{78}Ni.

The experiment has been performed at the National Superconducting Cyclotron Laboratory at Michigan State University. Unstable nuclei including ^{74}Ni were produced by the projectile fragmentation reaction of a ^{86}Kr primary beam with a typical intensity of 20 particle nA impinging on a 399-mg/cm^2-thick ^{9}Be target at 140 MeV/nucleon. The ^{74}Ni beam was selected by the A1900 fragment separator[1] and bombarded a liquid hydrogen target[2] with a thickness of 213 mg/cm^2 to induce proton inelastic scattering in inverse kinematics. The intensity of ^{74}Ni was typically 0.45 particles per second, and the beam energy at the center of the target was 81 MeV/nucleon. Inelastically-scattered ^{74}Ni was identified with the high-resolution S800 spectrograph[3]. For the identification of populated states, de-excitation γ rays were measured by an array of position-sensitive NaI(Tl) detectors[4,5] surrounding the target.

A clear peak corresponding to the $2^+ \rightarrow 0^+$ transition was observed at 1020(11) keV in the de-excitation γ-ray spectrum, which is consistent with the value (1024(1) keV) obtained in the β-decay experiment of ^{74}Co[6]. Taking into account correction for feeding from upper excited states, we have obtained the angle-integrated cross section for the 2^+ state of ^{74}Ni to be 14(5) mb. The uncertainty contains the statistical one (30%) and the ambiguity of the feeding correction (20%).

A quadrupole deformation parameter β_2 was deduced to be 0.19(4) by comparing the observed cross section with the distorted-wave Born approximation calculation. Two calculations using global optical potentials were performed[7,8]. The average of the two results was taken, while the discrepancy (4%) was taken into account in the systematic error. Figure 1 shows the extracted β_2 values along with the ones of other Ni isotopes. Filled and open circles show those obtained from the cross section of the proton inelastic scattering ($\beta_{p,p'}$)[9,10] and those from the B(E2) value (β_C) [11–15], respectively. Both $\beta_{p,p'}$ and β_C represent the degree of collectivity and normally take similar values. Indeed, for $^{56\sim64}$Ni, $\beta_{p,p'}$ and β_C are very close to each other as shown in Fig. 1. We compare the obtained $\beta_{p,p'}$ of ^{74}Ni with β_C of lighter Ni isotopes. Hereafter, both $\beta_{p,p'}$ and β_C are referred to as β_2. The β_2 value of ^{74}Ni is comparable to the large β_2 of ^{70}Ni[15], which is about twice as large as that of ^{68}Ni. The collectivity is induced in ^{74}Ni by the filling of the neutron into the $g_{9/2}$ orbital, as was observed in ^{70}Ni.

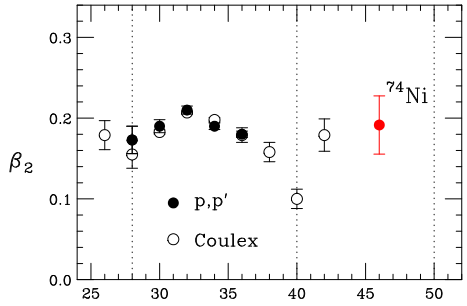

Fig. 1. β_2 systematics for Ni isotopes as a function of the neutron number. The data are taken from refs[9–15]. See text for details.

*1 Rikkyo University
*2 Michigan State University
*3 University of Tokyo
*4 Tokyo Institute of Technology

References

1) D. J. Morrissey et al.: Nucl. Instrum. Methods B **204**, 90 (2003).
2) H. Ryuto et al.: Nucl. Instrum. Methods A **555**, 1 (2005).
3) D. Bazin et al.: Nucl. Instrum. Methods B **204**, 629 (2003).
4) N. I. Kaloskamis et al.: Nucl. Instrum. Methods A **330**, 447 (1993).
5) B. C. Perry et al.: Nucl. Instrum. Methods A **505**, 85 (2003).
6) C. Mazzocchi et al.: Phys. Lett. B **622**, 45 (2005).
7) R. L Varner et al.: Phys. Rep. **201**, 57 (1991).
8) A. J. Koning and J. P. Delaroche: Nucl. Phys. A **713**, 231 (2003).
9) G. Kraus et al.: Phys. Rev. Lett. **73**, 1773 (1994).
10) E. Fabrici et al.: Phys. Rev. C **21**, 844 (1980).
11) K. Yurkewicz et al.: Phys. Rev. C **70**, 054319 (2004).
12) K. Yamada et al.: Eur. Phys. J. A **25, s01**, 409 (2005).
13) Y. Yanagisawa et al.: AIP Conf. Proc. 455 (ENAM98), Bellaire, Michigan (1998) p. 610.
14) S. Ramman, C.W. Nestor, Jr., and P. Tikkanen: At. Data Nucl. Data Tables **78**, 1 (2001).
15) O. Perru et al.: Phys. Rev. Lett. **96**, 232501 (2006).

On the Analysis of High-Energy Coulomb Excitation Experiments

H. Scheit, A. Gade,[*1] T. Glasmacher,[*1] and T. Motobayashi

Coulomb excitation (CE) of radioactive heavy-ion beams on high-Z targets at intermediate to relativistic beam energies ($E/A > 30$ MeV) is an important and now widely used method to study the structure of nuclei furthest from stability and a wealth of experimental information was obtained in laboratories worldwide since the method was first applied in 1995[1]. Even at these high beam energies it is possible to suppress the influence of the strong interaction in the excitation process, by rejecting events with small impact parameter, and to extract largely model independent nuclear structure information.

Experimentally, usually the de-excitation γ ray yields after CE are measured and from these the excitation cross sections are deduced. It is important to note that the deflection angle of the outgoing scattered particle is restricted either by the experimental setup (e.g. Ref.[2]) or during the off-line analysis of the data, which are recorded event-by-event[3]. The so imposed maximum scattering angle θ_{max} corresponds to a certain minimum impact parameter b_{min} which is chosen to exceed the sum of the radii of projectile and target by several femtometer, ensuring the dominance of the Coulomb interaction in the excitation process. The angle integrated CE cross section depends strongly on the chosen maximum scattering angle θ_{max}, which is therefore an important parameter in the analysis.

In order to extract the relevant quantities, namely the reduced transition probabilities $B(\pi\lambda)$ and in particular $B(E2)$ values, various analysis techniques are used: (*i*) distorted-wave theory (using the ECIS code used e.g. in[1]), (*ii*) the semi-classical theory of Winther and Alder[4] used e.g. in Refs.[2,3]), and (*iii*) the virtual photon method[5]. More than one method has been applied to certain nuclei and consistent results were obtained.

Recently, a new approach was proposed[6] and previously published results[1–3] were called into question in Ref.[7] claiming that either only non-relativistic, or only partially relativistic, expressions are used or the effect of the orbit of the nuclei, due to their Coulomb repulsion, is not fully accounted for. Using their model, changes in the calculated cross sections of up to 30% were reported with respect to results from the literature.

We were able to show, however, that the observed differences are solely the use of erroneous input parameters, which is illustrated in the figure. Here the experimental results are shown for various data-sets

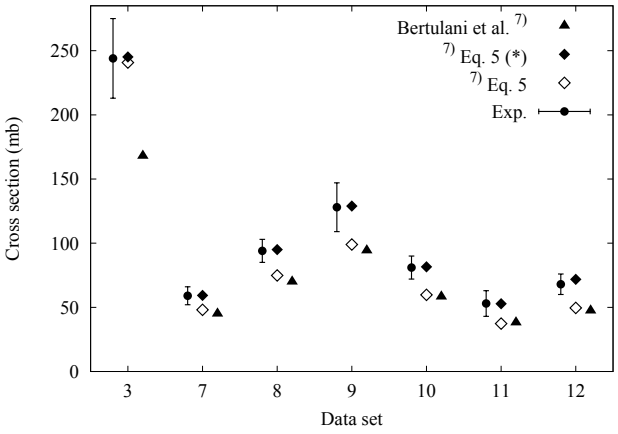

Fig. 1. Experimental CE cross sections. The number on the abscissa corresponds to the "Data set" of table 1 of Refs.[7,8]. The circles show the experimental cross sections σ_{exp} and the filled diamonds the cross sections calculated by us according to Eq. (5) of Ref.[7]. The open diamond shows the result of our own application of Eq. (5) of Ref.[7] using the input parameters listed in Ref.[7]. The triangles show the results published in Ref.[7].

(see Refs.[7,8] for details) together with 3 different theoretical calculations. The agreement between the circles and the diamonds shows that even with Eq. (5) of Ref.[7] the original results are reproduced. After further investigation we concluded that the mentioned discrepancies are due to an interchange of center-of-mass and laboratory angles and the use of the incident beam energy instead of the mid-target beam energy[8].

In fact, the expressions given for σ_{app} in Ref.[7] are analytically identical to the ones of Winther and Alder[4] as shown in the Appendix of Ref.[8]. Since for all experimental cross sections shown in the figure the semi-classical theory of Winther and Alder was employed during the analysis of the data, the results according to Eq. (5) of Ref.[7] must be identical to the original results provided the proper input parameters are used.

References
1) T. Motobayashi et al., Phys. Lett. B **346**, 9 (1995).
2) H. Scheit et al.,Phys. Rev. Lett. **77**,3967 (1996).
3) A. Gade et al., Phys. Rev. C **68**, 014302 (2003).
4) A. Winther et al., Nucl. Phys. A **319**, 518 (1979).
5) C. A. Bertulani et al., Phys. Rep. **163**, 299 (1988).
6) C. A. Bertulani et al., Phys. Rev. C **68**, 044609 (2003).
7) C. A. Bertulani et al., Phys. Lett. B **650**, 233 (2007).
8) H. Scheit et al., Phys. Lett. B **659**, 515 (2008).

† Condensed from H. Scheit et al., PLB 659, 515 (2008)

*1 NSCL and Department of Physics & Astronomy, Michigan State University, East Lansing, Michigan, USA

Spectroscopy of ^{7}He and ^{11}Be via d(^{8}He,t)^{7}He and d(^{12}Be,t)^{11}Be reactions

E. Yu. Nikolskii,[*1] A. A. Korsheninnikov, H. Otsu, H. Suzuki,[*2] K. Yoneda, H. Baba, K. Yamada, Y. Kondo,[*3] N. Aoi, M. S. Golovkov,[*4] A. S. Fomichev,[*4] S. A. Krupko,[*4] M. Kurokawa, E. A. Kuzmin,[*5] I. Martel,[*6] W. Mittig,[*7] T. Motobayashi, T. Nakamura,[*3] M. Niikura,[*8] S. Nishimura, A. A. Ogloblin,[*5] P. Roussel-Chomaz,[*7] A. Sanchez-Benitez,[*6] Y. Satou,[*3] S. I. Sidorchuk,[*4] T. Suda, S. Takeuchi, K. Tanaka, G. M. Ter-Akopian,[*4] Y. Togano,[*9] and M. Yamaguchi

[Nuclear reactions, d(^{8}He,t)^{7}He, d(^{12}Be,t)^{11}Be, unstable nuclei]

We measured the one-neutron transfer reactions d(^{8}He,t)^{7}He and d(^{12}Be,t)^{11}Be at forward laboratory angles (11^0–22^0) using the ^{8}He (42 A MeV) and ^{12}Be (71 A MeV) beams and deuteron target. The experiment was performed at the fragment separator RIPS at RIKEN. Details of the experimental setup are described in ref. 1. Here we present the preliminary data obtained using the dE and DSD detectors of the recoil telescope.

In Fig. 1(a), the inclusive triton spectrum from the reaction d(^{8}He,t) and the spectrum of tritons detected in coincidences with ^{6}He (b) are shown as a function of energy above ^{6}He + n threshold (spectrum measured in coincidences with neutrons emitted downstream has a similar character and is not shown here). The strong peak represents the ^{7}He ground state that is unstable with respect to the ^{6}He + n decay with $E_d \simeq 0.44$ MeV. The width of the peak (FWHM $\approx$ 1.7 MeV) determines the experimental resolution (natural width of ^{7}He$_{g.s.}$ is small, $\Gamma = 0.16$ MeV) that is closed to the results of the Monte-Carlo simulation. No excited states of ^{7}He were observed in the obtained spectra. Most probably, a state in ^{7}He at $E_{^6He+n} = 3.3$ MeV[2] that decays mainly into ^{4}He+3n is not seen here due to low statistics and high background level. It could be manifested in coincidences with ^{4}He, but the downstream detection system had low acceptance for alpha particles. The ^{7}He$_{g.s.}$ peak was a good reference to control the experimental conditions in the data analysis to search for ^{7}H in the same experiment.[3]

The triton spectra measured with ^{12}Be beam are presented in Figs. 1(c) and 1(d). Figure 1(c) shows the inclusive data and Fig. 2(d) represents the spectrum of tritons measured in coincidences with Be isotopes in hodoscope. (Note here that (1) we cannot identify masses for Z=4 and (2) the detection efficiency for ^{11}Be was $\sim$ 2.5 times lower than that for ^{10}Be). It is seen that in the inclusive spectrum (c) the background is high and the events from the reaction on deuterium itself are located in the energy region of $E^*_{^{11}Be} \approx 1.5 \div 5.0$ MeV. This structure has a two maxima at $\sim$ 2.5 and $\sim$ 4.0 MeV, which are seen more clearly in Fig. 1(d) where the background is significantly suppressed. The interesting feature of these spectra is that an excitation of the ground and first excited state (0.32 MeV) of ^{11}Be is not clearly seen. Probably, the second level at 1.78 MeV that could be revealed in the Be-coincidences (the threshold ^{10}Be + n lies at $E^*_{^{11}Be} = 0.502$ MeV) is also weakly excited, and the observed structure corresponds to the known states at 2.69 and 3.89 (or 3.96) MeV.[4]

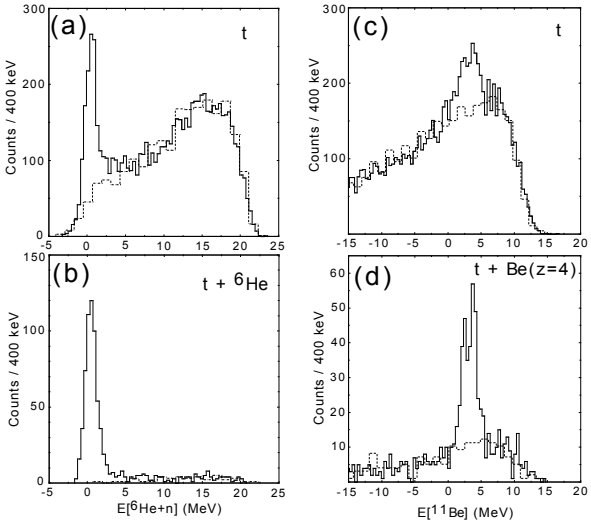

Fig. 1. Energy spectra of tritons from the reactions: (a) – d(^{8}He,t), (b) – d(^{8}He,t^{6}He), (c) – d(^{12}Be,t), (d) – d(^{12}Be,tBe). The dashed histograms show the empty-target background. See text for details.

*1 On leave from Kurchatov Institute, Russia
*2 Department of Physics, University of Tokyo
*3 Department of Physics, Tokyo Institute of Technology
*4 Joint Institute for Nuclear Research, Russia
*5 Kurchatov Institute, Russia
*6 Departamento de Fisica Aplicada, Universidad de Huelva, Spain
*7 GANIL, Caen Cedex, France
*8 Center for Nuclear Study, University of Tokyo
*9 Department of Physics, Rikkyo University

References

1) E. Nikolskii et al.: RIKEN Accel. Prog. Rep. **40**, 21 (2007).
2) A. A. Korsheninnikov et al.: Phys. Rev. Lett. **82**, 3581 (1999).
3) E. Yu. Nikolskii et al.: in this report.
4) F. Ajzenberg-Selove: Nucl. Phys. A **506**, 1 (1990).

Search for ^{7}H in ^{2}H + ^{8}He collisions

E. Yu. Nikolskii,[*1] A. A. Korsheninnikov, H. Otsu, H. Suzuki,[*2] K. Yoneda, H. Baba, K. Yamada, Y. Kondo,[*3] N. Aoi, M. S. Golovkov,[*4] A. S. Fomichev,[*4] S. A. Krupko,[*4] M. Kurokawa, E. A. Kuzmin,[*5] I. Martel,[*6] W. Mittig,[*7] T. Motobayashi, T. Nakamura,[*3] M. Niikura,[*8] S. Nishimura, A. A. Ogloblin,[*5] P. Roussel-Chomaz,[*7] A. Sanchez-Benitez,[*6] Y. Satou,[*3] S. I. Sidorchuk,[*4] T. Suda, S. Takeuchi, K. Tanaka, G. M. Ter-Akopian,[*4] Y. Togano,[*9] and M. Yamaguchi

[Nuclear reactions, d(^{8}He,^{3}He)^{7}H, unstable nuclei]

The exotic superheavy hydrogen ^{7}H with an extreme fraction of neutrons $N/Z = 6$ has been the object of experimental studies in the last several years. In a previous RIKEN experiment, evidence for the formation of the ^{7}H state near the t+4n threshold was obtained[1)]. Here we report the preliminary results of a new attempt to search for ^{7}H using a different reaction — d(^{8}He,^{3}He)^{7}H.

The experiment was performed at the fragment separator RIPS in RIKEN. The secondary beam of ^{8}He with an average energy of 42 A MeV and an intensity of 1.4×10^{5} pps bombarded a deuteron target. As a target, we used a gas cryogenic target filled with deuterium gas at a temperature of 30 K and a pressure of 0.5 atm resulting in a target thickness of 2.4×10^{20} deuterons/cm^{2}. Recoiling ^{3}He were detected at forward angles ($11^{0} \leq \theta_{lab} \leq 22^{0}$) using the RIKEN telescope of position-sensitive (strip) Si detectors with an additional dE-layer, which was an assembly of six thin ($\sim$40 μ) Si counters. Besides ^{3}He, we also detected tritons and neutrons from the decay $^{7}\mathrm{H} \rightarrow \mathrm{t} + 4\mathrm{n}$, using the downstream detection system. Details of the experimental setup are described in Ref. 2.

Figure 1 shows the ^{7}H excitation spectrum measured in coincidences with tritons from the decay of the residual ^{7}H system (data from dE and DSD detectors of the telescope were used). The spectrum is shown as a function of energy above the t+4n threshold. The dashed histogram shows the normalized background obtained from an empty-target measurement. Curves 1, 2, and 3 show nonresonant continuums, which were obtained by the calculation of 5-body (t + n + n + n + n), 3-body (t + ^{2}n + ^{2}n), and 2-body (t + ^{4}n) phase volumes, respectively. Curve 2 can be considered as an extreme case in which relative motion in both neutron pairs is described by delta function. Curve 3 is the most extreme case that can be considered as a motion of a triton and tetraneutron with a zero binding energy. The curves are normalized in the point of the histogram at E = 17.8 MeV. In the calculation, detection efficiency and experimental resolution (FWHM $\approx$ 1.9 MeV) were taken into account.

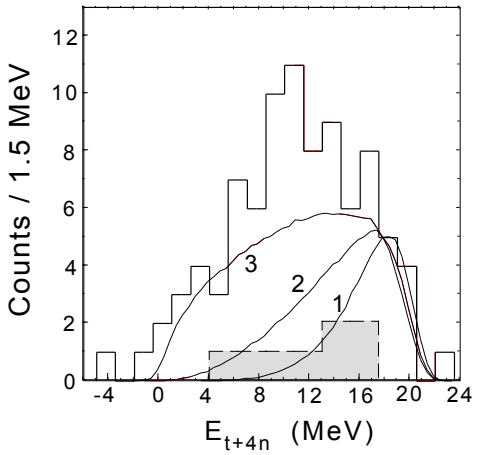

Fig. 1. Spectrum of ^{7}H from the reaction d(^{8}He,^{3}Het). The dashed histogram shows the empty-target background. Curves represent nonresonant continuums. See text for details.

Unfortunately, the obtained statistics is low and does not allow us to perform a detailed analysis of the ^{7}H spectrum. However, some remarkable features can be noted. First, the spectrum structure at low energies cannot be described by curves 1 or 2, but has the shape that is similar or even steeper than that for curve 3. Second, no clear evidence for the ^{7}H peak at low energies is observed in this reaction, but the spectrum has some "shoulder" around $\sim$2 MeV. And third, the spectrum probably has peculiarity at $\sim$10.5 MeV. Note, the simultaneously measured reactions d(^{8}He,t)^{7}He[3)] and d(^{12}Be,^{3}He)^{11}Li show well-defined peaks corresponding to the ground states of ^{7}He and ^{11}Li. Further analysis is in progress.

*1 On leave from Kurchatov Institute, Russia
*2 Department of Physics, University of Tokyo
*3 Department of Physics, Tokyo Institute of Technology
*4 Joint Institute for Nuclear Research, Russia
*5 Kurchatov Institute, Russia
*6 Departamento de Fisica Aplicada, Universidad de Huelva, Spain
*7 GANIL, Caen Cedex, France
*8 Center for Nuclear Study, University of Tokyo
*9 Department of Physics, Rikkyo University

References

1) A. A. Korsheninnikov et al. : Phys. Rev. Lett. **90**, 082501 (2003).
2) E. Nikolskii et al. : RIKEN Accel. Prog. Rep. **40**, 21 (2007).
3) E. Yu. Nikolskii et al. : in this report.

Momentum distributions of ^{18,19}C fragments from ^{20}C breakup reaction

Y. Hashizume,[*1] K. Tanaka, A. Ozawa,[*1] T. Yamaguchi,[*2] T. Suzuki,[*2] T. Aiba,[*3] N. Aoi, H. Baba, M. Fukuda,[*4] K. Inafuku,[*5] N. Iwasa,[*5] T. Izumikawa,[*6] K. Kobayashi,[*2] M. Komuro,[*2] Y. Kondo,[*7] M. Kurokawa, T. Matsuyama,[*3] S. Michimasa,[*8] T. Nakabayashi,[*7] S. Nakajima,[*2] T. Ohtsubo,[*3] R. Shinoda,[*2] M. Shinohara,[*7] H. Suzuki,[*9] M. Takechi, E. Takeshita, S. Takeuchi, Y. Togano,[*10] K. Yamada, T. Yasuno,[*1] M. Yoshitake,[*2] T. Kubo, T. Nakamura,[*7] Y. Sakurai, and T. Motobayashi

The longitudinal momentum distributions of ^{18,19}C from a ^{20}C breakup reaction involving a proton target have been measured at approximately 40 A MeV by a direct time-of-flight (TOF) technique. The momentum distributions of neutron-removal fragments from neutron-rich carbon isotopes have been measured systematically up to A=19. The experiment was carried out at RIPS.[1] Figure 1 shows the experimental setup, which was essentially the same as that used for reaction cross-section measurements of ^{22}C.[2] An ^{40}Ar primary beam of 100 particle nA was provided from RIKEN Ring Cyclotron and bombarded on a 333 mg/cm^2 Ta production target. The nuclides in secondary beams were identified event by event by the TOF between two plastic scintillators located at F2 and F3 focal planes and the value of ΔE obtained from two silicon detectors (Si) of 100 μm thickness at F3. We employed liquid hydrogen with 205 mg/cm^2 thickness as a reaction target. Outgoing particles were identified by the TOF-ΔE-E method using two plastic scintillators at F3 and F4 for the TOF, Si detectors of 320 μm thickness for ΔE, and a 5 inchϕ NaI(Tl) scintillator for E. We used a superconducting triplet quadrupole[3] to transport beams and residues from F3 to F4.

The momentum resolution was estimated to have an RMS value of 24 MeV/c by measuring the unreacted ^{20}C beam detected at F4. The longitudinal momentum distributions of the fragments were obtained from the TOF spectra between F3 and F4. The momentum broadening of the incident ^{20}C beam was corrected using the position information of the PPAC placed at dispersive focal plane F1. Background events, which are caused by reactions inside the detectors after the reaction target, were estimated by measurements without the target and subtracted by the same method as that used in the previous study.[4] The transmission of ^{18,19}C between F3 and F4 was simulated using the code MOCADI[5] since the magnetic field of the quadrupoles between F3 and F4 was optimized for the magnetic rigidity of ^{20}C by measurements of the reaction cross section of ^{20}C.[2] The momentum distributions of ^{18}C and ^{19}C fragments from the ^{20}C breakup reaction in the present analysis are shown in Fig. 2. The solid lines show fitting results using Gaussian curves. The widths of the momentum distributions for ^{18}C and ^{19}C are in agreement with the predictions by the Goldhaber model with RMS vakues of 90 MeV/c and 124 MeV/c, respectively, within the statistical experimental error. Further studies are in progress.

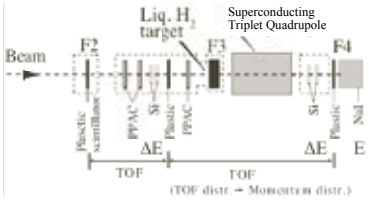

Fig. 1. Experimental setup at RIPS. The momentum distributions of fragments were obtained from TOF spectra between F3 and F4. Detectors located at F2, F3, and F4 were used for particle identification.

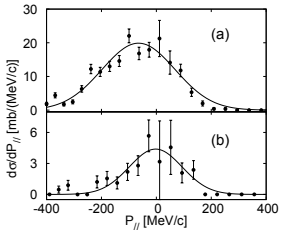

Fig. 2. Present results for the longitudinal momentum distributions of ^{18}C (a) and ^{19}C (b) in the projectile rest frame. Solid curves represent fitting results using Gaussian curves.

*1 Institute of Physics, University of Tsukuba
*2 Department of Physics, Saitama University
*3 Department of Physics, Niigata University
*4 Department of Physics, Osaka University
*5 Department of Physics, Tohoku University
*6 RI Center, Niigata University
*7 Department of Physics, Tokyo Institute of Technology
*8 Center of Nuclear Study, University of Tokyo
*9 Department of Physics, University of Tokyo
*10 Department of Physics, Rikkyo University

References

1) T. Kubo et al.: Nucl. Instrum. Methods B **70**, 309 (1992).
2) K. Tanaka et al.: RIKEN Accel. Prog. Rep. **40**, 20 (2006).
3) N. Aoi et al.: RIKEN Accel. Prog. Rep. **38**, 176 (2005).
4) T. Yamaguchi et al.: Nucl. Phys. A **724**, 3 (2003).
5) N. Iwasa et al.: Nucl. Instrum. Methods B **126**, 284 (1997).

g-Factor measurement of the isomeric state of ^{32}Al

D. Kameda, K. Takase,[*1] H. Ueno, A. Yoshimi, T. Nagatomo, Y. Hasama,[*1] H. Watanabe, M. Uchida,[*1] N. Hatakeyama,[*1] T. Inoue,[*1] S. Kagami,[*1] K. Suzuki,[*1] C. Nakano,[*1] H. Kawamura,[*2] T. Toyoda,[*2] K. Narita,[*2] J. Murata,[*2] D. Nagae,[*3] K. Shimada,[*4] and K. Asahi[*1]

[Nuclear structure, spin-aligned RI beam, TDPAD, nuclear moments]

The g factor of nuclear magnetic moment is sensitive to single particle orbits occupied by valence protons or neutrons. It often plays a decisive role in determining nuclear configurations. In ^{32}Al, the isomeric state of $T_{1/2} = 200(20)$ ns was reported at an energy level of 956 keV[1]. The isomer emits two γ rays of 222 keV and 734 keV at the same time in the cascade decay via the first excited state of 734 keV. The decay scheme suggests that the spins and parities for the isomer and first excited state are 4^+ and 2^+, respectively. The ordering of the two states, however, is not reproduced by conventional *sd*-shell models. To obtain clear information about the low-lying shell structure of ^{32}Al, we performed the g-factor measurement of the isomeric state by the time differential perturbed angular distribution (TDPAD) method with a spin-aligned ^{32}Al beam.

The ^{32}Al beam was produced by the fragmentation of ^{40}Ar at an energy of 95 MeV/nucleon with a 315-mg/cm^2-thick Be target. Using the RIPS, the obtained ^{32}Al fragments were separated to other products and delivered to the TDPAD setup. To produce spin alignment in ^{32}Al, the outgoing momentum p of ^{32}Al was restricted to the high-momentum wing of $p/p_0 = 1.02 - 1.05$, where p_0(= 12.4 GeV/c) corresponds to the peak in the yield. The isotopic purity of ^{32}Al was estimated to be 82 % by the particle identification. The beam was stopped in a 0.5-mm-thick indium sample by using a 1-mm-thick Al energy degrader and a 14-mm-diameter collimator, which were located 20 cm upstream of the sample. The beam intensity, which was around 17 k particles/s, was monitored using a plastic scintillator behind the collimator. The experimental layout is shown in Fig. 1. The γ rays were detected using four coaxial high-purity Ge detectors, the relative efficiencies of which were around 30 %, and two 5.5" $\times$ 5.5" NaI(TI) scintillators. In data acquisition, we considered only the γ events triggered by the particle within a 1.2 μs time window, which was provided by the plastic scintillator. The timing of the particle, $t = 0$, was determined from a prominent peak of the γ time spectrum. A static magnetic field B_0 was applied to the sample to observe the oscillation of the γ-ray anisotropy due to Larmor precession. Two different magnitudes, as $B_0 = 471$ and 215 mT, were adopted.

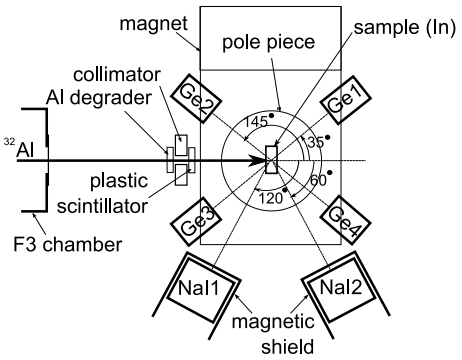

Fig. 1. TDPAD experimental layout.

Figure 2 shows the obtained energy spectrum for the "Ge 3" detector. The photo peaks of the γ rays of 222 keV and 734 keV were clearly observed. Using the 222 keV γ-ray yield, the isomer ratio was estimated to be $R \sim 80$ %, taking into account the decay in flight. (The absolute efficiency for the 222 keV γ ray was considered 0.19 % according to the calibration with standard γ sources.) In the inset in Fig. 2, the decay curve of the 222 keV γ ray is shown, together with that for the "Ge 2" detector. From the results of fitting analysis of a decay curve for all Ge detectors, the precise half-life was obtained as $T_{1/2} = 186.9(7)$ ns. Further analysis is now in progress.

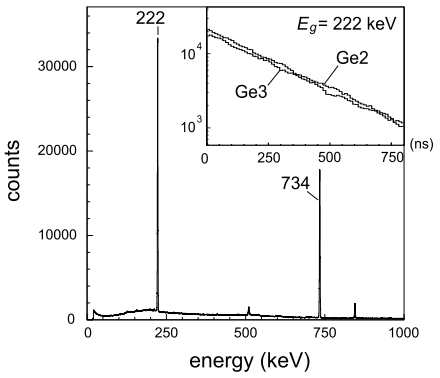

Fig. 2. Energy spectrum of "Ge 3" and decay curves gated by 222 keV γ rays in inset.

*1 Department of Physics, Tokyo Institute of Technology
*2 Department of Physics, Rikkyo University
*3 Advanced Science Research Center, Japan Atomic Energy Agency
*4 Cyclotron and Radioisotope Center, Tohoku University

References

1) M. Robinson et al.,: Phys. Rev. C **53**, R1465 (1996).

Effect of delayed γ rays on β-ray angular distribution of ^{20}F

T. Nagatomo, K. Matsuta,[*1] K. Minamisono,[*2] T. Sumikama,[*3] M. Mihara,[*1] A. Ozawa,[*4] Y. Tagishi,[*4] R. Matsumiya,[*1] M. Fukuda,[*1] M. Yamaguchi,[*4] T. Yasuno,[*4] H. Ohta,[*4] Y. Hashizume,[*4] H. Fujiwara[*1] and T. Minamisono[*5]

[Alignment correlation term, G parity, β-NMR]

The nuclear spin alignment correlation terms in the β-ray angular distribution of the mirror nuclei are suitable for testing the G-parity symmetry[1] in the weak interaction. Recently, we measured the alignment terms for ^{20}Na[2] and ^{20}F[3] mirror partners from the anisotropy of β rays emitted from the spin-aligned ^{20}Na and ^{20}F, respectively. For details of the experiments, please refer to the respective articles. Both ^{20}Na and ^{20}F nuclei dominantly decay to the first 2^+ excited state of ^{20}Ne, and then the delayed $E2$ γ rays are emitted. In spite of using a plastic scintillation counter as a β-ray-energy detector, the γ-ray-detection efficiency was not zero. That is the reason why it was unavoidable that the γ rays were observed as a pileup. In addition, because the daughter nuclei ^{20}Ne were also aligned, we have to take the anisotropic emission of the $E2$ γ rays into account. We found that the effect of the γ-ray anisotropy was not negligible compared with the very small alignment terms, practically for ^{20}F. In the present analysis, we estimated the effect of delayed γ rays on the observed alignment correlation term of ^{20}F nuclei. The effect of the delayed γ rays were derived as following. The $E2$ γ rays are distributed as

$$W(\theta_\gamma) \propto 1 - \frac{5}{14}\mathcal{A}P_2(\cos\theta_\gamma) + \frac{8}{7}\mathcal{Q}P_4(\cos\theta_\gamma) \equiv 1 + G_\gamma(\theta_\gamma), \quad (1)$$

where θ_γ is the γ-ray emission angle with respect to the orientation axis, P_n is the Legendre function, and $\mathcal{A}$ ($\mathcal{Q}$) is the rank 2 (4) nuclear spin alignment. The degrees of the alignments were observed as $\mathcal{A} = 22.3(2)\%$ and $\mathcal{Q} = -3.2(3)\%$ from the β-ray-asymmetry change by means of the β-NMR method. Because the delayed γ rays were detected as a pileup in β-ray-energy signals, the effect of γ-ray anisotropy δ_γ as a function of β-ray energy E is described as

$$\delta_\gamma(E) = G_\gamma(\theta_\gamma)\,[1 - S_\beta(E)/S_{\beta+\gamma}(E)]\,. \quad (2)$$

In Eq.(2), G_γ is determined in Eq.(1), $S_\beta(E)$ and $S_{\beta+\gamma}(E)$ are the β-ray energy spectra. The former is the ideal energy spectrum without any delayed-γ-ray pileup and the latter includes the pileup. In order to estimate these energy spectra, we employed a Monte-Carlo simulation of the electron-gamma shower in materials (EGS4), which was modified by Hirayama *et al.* to be applicable to low-energy γ rays[4].

The observed alignment correlation term for ^{20}F is shown as open circles in Fig. 1, as a function of the observed β-ray energy[3]. The endpoint energy was observed as 5.12 MeV, because of the energy loss in the δE-detectors and the MgF_2 crystal into which the ^{20}F were implanted. The effect of delayed γ-ray pileup δ_γ(E) is shown as a curve with a width that represents uncertainty arising the errors of $\mathcal{A}$ and $\mathcal{Q}$. From Fig. 1, the estimated γ-ray effect was found to be consistent with the data around the endpoint energy of 5.12 MeV, where β-γ pileup was dominantly observed. We have confirmed the effect of γ-ray pileup δ_γ, and we show the alignment term from which the δ_γ is subtracted as the closed circles in Fig. 1. The analysis to test the G parity symmetry is in progress.

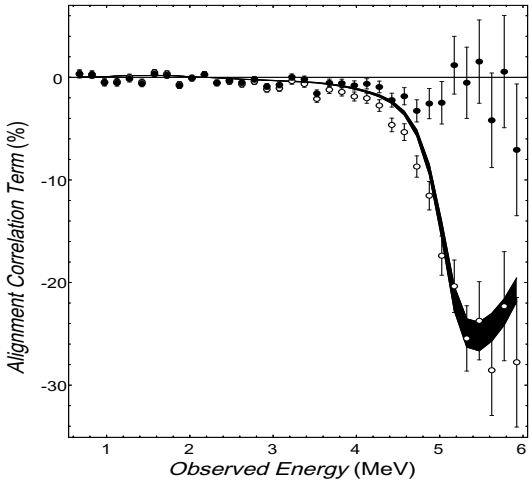

Fig. 1. The observed alignment correlation term of ^{20}F (open circles) compared with the estimated effect of delayed-γ pileup δ_γ. The closed circles represent the data with the effect δ_γ subtracted.

*1 Department of Physics, Osaka University
*2 National Superconducting Cyclotron Laboratory, Michigan State University
*3 Department of Physics, Tokyo University of Science
*4 Department of Physics, University of Tsukuba
*5 Department for the Application of the Nuclear Technology, Fukui University of Technology

References

1) S. Weinberg: Phys. Rev. **115**, 1375 (1958).
2) K. Minamisono et al.: Hyperfine Interactions **159**, 265 (2004).
3) T. Nagatomo et al.: submitted to Hyperfine Interactions.
4) H. Hirayama: KEK Internal **99**-5 R/D(1999).

Precision spectroscopy of laser-cooled $^{7,10}Be^+$ in online ion trap

T. Nakamura, M. Wada, K. Okada,[*1] A. Takamine, P. Schury, Y. Yamazaki, Y. Kanai, T. M. Kojima, A. Yoshida, T. Kubo, S. Ohtani,[*3] K. Noda,[*4] I. Katayama,[*5] V. Lioubimov,[*6] H. Wollnik,[*7] and H. A. Schuessler[*6]

[laser spectroscopy, laser cooling, $^{10}Be^+$, $^{7}Be^+$]

Precision laser spectroscopy of unstable beryllium isotopes has been in progress at the prototype slow radioactive ion beam facility (SLOWRI) of RIKEN. In year 2006, we measured the $2s\ ^2S_{1/2} \rightarrow 2p\ ^2P_{3/2}$ transition of $^{7,10}Be^+$ in the online trap and determined the absolute transition frequency of the infinite heavy-mass nucleus ν^∞ and the differential mass polarization parameter κ of beryllium ion for the first time.[1]. However the accuracy of the transition frequency was limited to the order of 50 MHz owing to the fact that the measurements were performed under gas-cooled condition, which is not sufficient to derive the charge radii of beryllium isotopes. Laser cooling is an important prerequisite to achieving a sufficiently high accuracy, for example, 300 kHz, as well as to determine the hyperfine splitting constant via laser-microwave double resonance spectroscopy.[2]

In 2007, we worked on improving trapping efficiency by employing a newly developed carbon-OPIG device[3] as well as the accuracy of laser spectroscopy by introducing the laser cooling scheme and the optical frequency comb system. Although the available accelerator beam time was very limited and the key devices such as pumping lasers and frequency synthesizers broke down one after another during different beam times, we achieved laser cooling of $^{7,10}Be^+$ ion for the first time.

Figure 1 show a spectrum of laser-cooled $^{10}Be^+$ with a beat signal frequency between the dye laser and the frequency comb. The 313 nm (957 THz) uv laser radiation for cooling was synthesized from the second harmonics of a 626 nm (479 THz) dye laser. The absolute frequency of the dye laser can be determined from the optical frequency comb as follows. The comb radiation is a mode-locked femtosecond laser at 250 MHz repetition rate ($f_{\rm rep}$). This radiation consists of thousands of narrow peaks with an exact interval of repetition rate in the frequency domain. The frequency difference between the dye laser radiation and one of the comb peaks can be observed as an interference beat signal frequency, $f_{\rm beat}$. The dye laser frequency is obtained as $f_{\rm dye} = nf_{\rm rep} \pm f_{\rm beat} \pm f_{\rm offset}$, where n is an integer indicating n-th comb peak from the origin and $f_{\rm offset}$

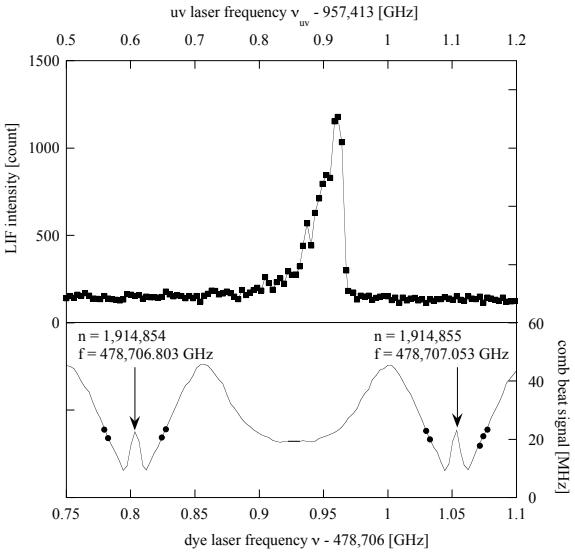

Fig. 1. Fluorescence intensity of trapped $^{10}Be^+$ ions as function of laser frequency (top) and beat signal frequency between dye laser and optical frequency comb (bottom).

is the offset frequency of the first comb peak. The index n and the polarities are determined, for example, from the iodine absorption signal. The half width at the half maximum of the laser cooled spectrum is as small as 30 MHz, which is more than 30-fold narrower than the gas-cooled spectrum. However, so far we are reluctant to determine the absolute transition frequency from this spectrum, because an asymmetry of the peak causes ambiguity and the optical pumping was not perfect owing to a problem in the polarizer wave plate. A narrower symmetric spectrum can be obtained using a low-power probe laser in addition to the cooling laser. Determination of absolute transition frequency is planned in the next beam time. By laser cooling, we determined ion temperature to be less than 0.1 K, which corresponds to a 10^{14}-fold decrease in the kinetic energy of ions, which was initially 1 GeV when produced in the reaction.

*1 Department of Physics, Sophia University
*2 Graduate School of Art and Science, University of Tokyo
*3 Institute for Laser Science, University of Electro-Comm.
*4 National Institute for Radiological Science
*5 High Energy Accelerator Research Organization (KEK)
*6 Department of Physics, Texas A&M University, USA
*7 II. Physikalisches Institute, Giessen University, Germany

References

1) T. Nakamura et al.: Phys. Rev. A **74**, 052503 (2006).
2) T. Nakamura et al.: Opt. Commun. **205**, 239 (2002).
3) A. Takamine et al.: RIKEN Accel. Prog. Rep. **40**, 147 (2007).

Towards the determination of nuclear charge radii for Be isotopes†

A. Takamine, M. Wada, T. Nakamura, K. Okada*1, P. H. Schury, Y. Yamazaki*2, Y. Kanai, T. M. Kojima, A. Yoshida, T. Kubo, S. Ohtani*3, K. Noda*4, I. Katayama*5, H. A. Schuessler*6, V. Varentsov*7, and H. Wollnik*8

[SLOWRI, charge radius, laser spectroscopy]

In recent years, the charge radii of halo nuclei have been determined by precision measurements using laser spectroscopy. The charge radii of the two-neutron halo nucleus ^{6}He and the four-neutron halo nucleus ^{8}He were determined in a magneto-optical trap at Argonne National Laboratory.[1,2] The charge radius of the two-neutron halo nucleus ^{11}Li was determined by two-photon spectroscopy by the ToPLiS group from GSI.[3] Up to now, no charge radii for radioactive Be isotopes have been determined. We aim to systematically study the charge radii of Be isotopes including the one-neutron halo nucleus ^{11}Be.

An atomic energy level E is expressed as

$$E = E_\infty - \frac{\mu}{M}E_\infty + \frac{\mu}{M}K + F\langle r_c^2\rangle \ , \qquad (1)$$

where E_∞ is the energy under the assumption that the nucleus is an infinitely heavy point charge, μ is the reduced electron mass, M is the nuclear mass, $K{=}\sum_{i<j}^{3}\mathbf{p}_i\cdot\mathbf{p}_j/\mu$ is the mass polarization parameter, F is the field shift constant, and $\langle r_c^2\rangle$ is the mean-square charge radius. The charge radius is determined by a high-resolution measurement at an atomic transition energy and theoretical calculations of K and F with sufficient accuracies. K can so far only be provided for two- or three-electron systems. Calculations for the singly charged Be isotopes are on going.

We have developed a prototype of a universal facility for realizing slow radioactive ion beams (SLOWRI). Energetic radioactive Be isotopes provided by a projectile fragment separator are decelerated and thermalized in a gas catcher cell. Then the ions are transported into a high vacuum region by a carbon-OPIG[4] and collected into a linear Paul trap cooled by He buffer gas. Inside the trap the velocity of the Be^+ ions are further reduced by laser cooling using a UV laser at 313 nm, which is resonant to the $2^2S_{1/2}$-$2^2P_{3/2}$ transition. We have already succeeded in trapping and laser cooling several hundreds $^{7,10}Be^+$ ions in the trap. Moreover the 2s $^2S_{1/2}$-2p $^2P_{3/2}$ transition energies for $^{7,10}Be^+$ were measured with high accuracies of $\sim10^{-8}$,[5] which was insufficient accuracy to deduce the charge radii.

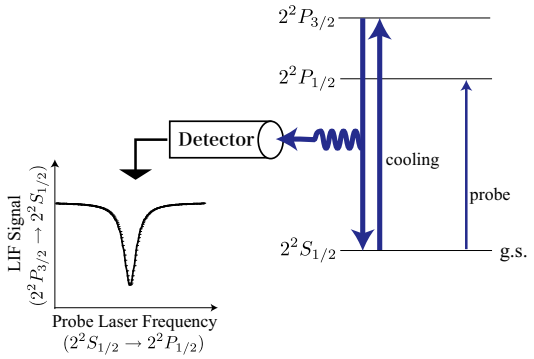

Fig. 1. Optical-optical double resonance in Be^+.

In experiments to determine the nuclear charge radii we plan to utilize the optical-optical double resonance spectroscopy method.[6] In the laser-cooling process, ions are optically pumped and strong laser-induced fluorescence is observed. If we use a probe laser to low-intensity radiation resonant to the $2^2S_{1/2}$-$2^2P_{1/2}$ transition, part of the population of ions is transferred to the $2^2P_{1/2}$ state and we then observe a reduction in the laser-induced fluorescence signal (Fig. 1). The cooling and probe lasers are alternately irradiated using acousto-optic modulators to avoid the power broadening by the cooling laser light.

The probe laser frequency is calibrated by the clockwork optical frequency comb.[7] Moreover, the probe laser will be stabilized by frequency locking to the beat frequency signal between the laser frequency and the comb frequency. An acousto-optic frequency shifter rapidly sweeps the probe laser frequency.

In 2008 we will perform on-line experiments and measure the $2^2S_{1/2}$-$2^2P_{1/2}$ transition frequencies of ^{7,10,11}Be with an accuracy of 0.4 MHz to determine the nuclear charge radii with an accuracy of 1%.

*1 Department of Physics, Sophia University
*2 Graduate School of Arts and Sciences, University of Tokyo
*3 Institute for Laser Science, University of Electro-Communications
*4 National Institute for Radiological Science
*5 Institute of Particle and Nuclear Studies, High Energy Accelerator Research Association, KEK
*6 Department of Physics, Texas A&M University
*7 Kholopin Radium Institute
*8 II. Physikalisches Institute, Justus-Liebig-Universitaet

References

1) L.-B. Wang et al.: Phys. Rev. Lett. **93**, 142501 (2004).
2) P. Mueller et al.: Phys. Rev. Lett. **99**, 252501 (2007).
3) R. Sanchez et al.: Phys. Rev. Lett. **96**, 033002 (2006).
4) A. Takamine et al.: RIKEN Accel. Prog. Rep. **40**, 147 (2007).
5) T. Nakamura et al.: Phys. Rev. A **74**, 052503 (2006).
6) D. J. Wineland et al.: Opt. Lett. **5**, 245 (1980).
7) T. Udem et al.: Nature **416**, 233 (2002).

Probing Asymmetric Nuclear Matter at RIBF

T. Murakami,[*1] S. Ebesu,[*1] E. Takada,[*2] T. Akiyama,[*3] Y. Haki,[*3] Y. Hara,[*3] K. Ieki,[*3] Y. Ikeda,[*3] A. Kitabata,[*3] K. Narita,[*3] K. Ninomiya,[*3] M. Nitta,[*3] M. Matsushita,[*3] J. Murata,[*3] H. Ooishi,[*3] T. Toyoda,[*3] H. Kawamura, Y. Nakai, S. Nishimura, and H. Sakurai

[EOS, centrality filter, pion range counter]

The nuclear Equation of State (EOS) is one of the most fundamental properties of nuclear matter and describes the relationships among the energy, pressure, temperature, density and isospin asymmetry $\delta = (\rho_n - \rho_p)/\rho$ for a nuclear system[1)]. The EOS is customarily divided into two parts, namely a symmetric matter contribution that is independent of δ and a symmetry energy term that is proportional to the δ^2.

The EOS of asymmetric nuclear matter also dictates many properties of neutron stars and of type II supernovae. Experimental information about the EOS, especially the symmetry energy term, at high densities can help to predict neutron star observables such as stellar radii, moments of inertia, maximum masses, and neutron star cooling rates.

Detailed studies of pion production in nucleus-nucleus collisions at intermediate energies provide unique opportunities to establish meaningful constraints on the density dependence of the symmetry energy at high densities $\rho > \rho_0$ where present constraints are least stringent. Calculations predict that the relative densities of neutrons and protons in the dense interior of a central nucleus-nucleus collision reflect the pressure of the symmetry energy[2,3)] and that the softer EOS results in a larger $Y(\pi^-)$ /$Y(\pi^+)$ yield ratio. The highest sensitivity of pion production to the symmetry energy is predicted to appear below the free nucleon-nucleon production threshold[4)]. It is, therefore, well suited to study the pion production systematically using beams at RIBF.

Measurements of $Y(\pi^-)$ /$Y(\pi^+)$ yield ratios would at least require a centrality trigger and a pion detector. A TPC together with a large acceptance magnet system is certainly ideal for these measurements and is under serious consideration, but would require years to realize. In the meantime, we decided to construct a simpler setup including a portable centrality filter and a pion range counter to perform pioneering works in such a direction.

Figure 1 shows a prototype of the pion range counter made of four 3 cm thick plastic scintillators read by fast PMTs. Also shown in Fig.2 is a centrality filter under an assembly consisted of 60 small slabs of plastic scintillators read by two flat-panel multianode-PMTs via optical fibers. It should provide information on a light-charged particle multiplicity. We have just finished a test of them using 400 MeV/nucleon ^{20}Ne beams from HIMAC. Very preliminary results indicate that π^+ events can be clearly identified by selecting double pulse signals corresponding to $\pi^+ \rightarrow \mu^+ + \nu_\mu$ decays. We would like to start pion production experiments using them after increasing the total number of plastics in the range counter to 8 or 9 in 2008.

References

1) P. Danielewicz, R. Lacey, W.G. Lynch,: Science **298**, 1592 (2002).
2) B.A. Li, C.M. Ko, and Z. Ren: Phys. Rev. Lett. **78**, 1644 (1997).
3) V. Baran, M. Colonna, M. Di Toro, and V. Greco: Phys. Rev. Lett. **86**, 4492 (2001).
4) Q. Li, Z. Li, S. Soff, R. K Gupta, M. Bleicher, and H. Stöcker: J. Phys. G **31**, 1359 (2005).

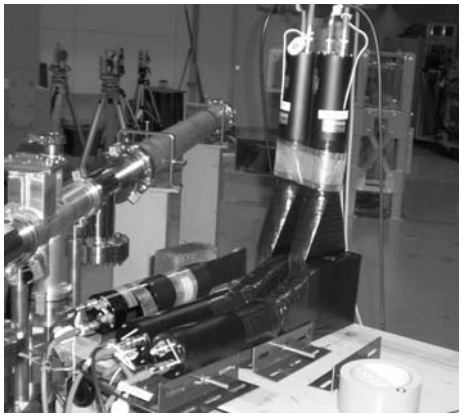

Fig. 1. Picture of prototype pion range counter

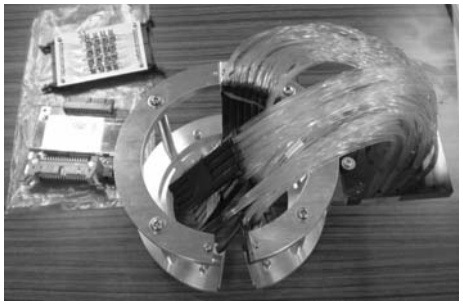

Fig. 2. Picture of multiplicity filter viewed through optical fibers during assembly

[*1] Department of Physics, Kyoto University, Kyoto, Japan
[*2] Department of Accelerator and Medical Physics, NIRS, Chiba, Japan
[*3] Department of Physics, Rikkyo University, Tokyo, Japan

Analyzing Power Measurement for the Proton Elastic Scattering on ^{8}He at 71 A MeV

S. Sakaguchi,[*1] T. Uesaka,[*1] T. Wakui,[*2] N. Aoi, Y. Ichikawa,[*3] K. Itoh,[*4] M. Itoh,[*2] T. Kawabata,[*1] T. Kawahara,[*5] Y. Kondo,[*6] H. Kuboki,[*3] T. Nakamura,[*6] T. Nakao,[*3] Y. Nakayama,[*6] S. Noji,[*3] H. Sakai,[*3] Y. Sasamoto,[*1] M. Sasano,[*3] K. Sekiguchi, T. Shimamura[*6] and Y. Shimizu[*1]

[Polarized proton solid target, Elastic scattering, Helium isotope]

Recently, much interest has been focused on the spin-dependent interaction in unstable nuclei. One of the most direct ways to see such interaction is to study the spin-orbit part of the optical potential between protons and unstable nuclei. For this purpose, we measured the analyzing power of the proton elastic scattering on ^{6}He[1)] and ^{8}He at 71 A MeV in 2005 and 2007. The aim of the measurements is to deduce and compare the spin-orbit potentials between protons and ^{4,6,8}He particles. From the systematics of the potentials, the effects of excess neutrons on the spin-orbit interaction will be investigated. Details of the $\vec{p}$–^{8}He elastic scattering measurement are reported.

The experiment was carried out using the RIKEN Projectile-fragment Separator (RIPS). The ^{8}He beam was produced by a fragmentation reaction of an ^{18}O beam with an energy of 100 A MeV bombarded onto a 13 mm^2 Be target. The energy and intensity of the beam was 71 A MeV and 1.5×10^5 pps, respectively. As a secondary target, we used the polarized proton solid target that was specially developed for RI-beam experiments.[2,3)] The target material was a single crystal of naphthalene with a thickness of 4.3×10^{21} protons/cm^2. Recoiled protons were detected using multiwire drift chambers (MWDCs) and CsI (Tl) scintillators placed on the left and right sides of the beam line. Each MWDC was located 180 mm away from the target and covered a scattering angle of $50° - 70°$ in the laboratory system. A CsI scintillator with a sensitive area of 135 mm^H $\times$ 60 mm^V was placed just behind the MWDC. Leading particles were detected using another MWDC and $\Delta E - E$ plastic scintillator hodoscopes with thicknesses of 5 and 100 mm.

The absolute value of the target polarization was determined by measuring the spin-dependent asymmetry ($P_y A_y$) of the $\vec{p}$–^{4}He elastic scattering at 80 A MeV. Figure 1(a) shows the analyzing power (A_y) of the $\vec{p}$–^{4}He scattering. Open circles represent previously measured data.[4)] Closed ones show the present data, where the target polarization (P_y) is determined to be $11.0 \pm 2.5\%$. Figure 1(b) shows the target polarization during the scattering experiment.

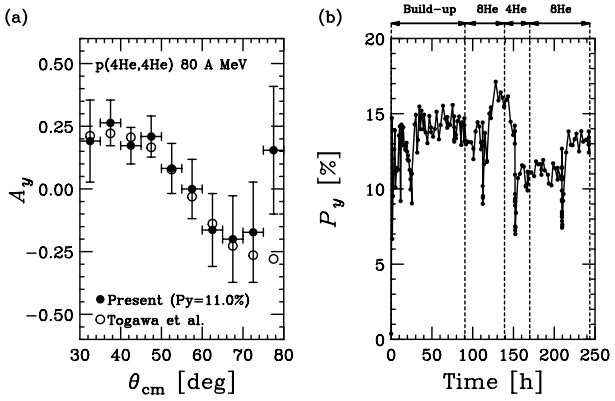

Fig. 1. (a) Analyzing power of the $\vec{p}$–^{4}He elastic scattering at 80 A MeV is shown. See text for detail. (b) Target polarization monitored by the pulsed NMR method.

The $\vec{p}$–^{8}He measurement was carried out with the same experimental setup as the $\vec{p}$–^{4}He measurement. In the $\vec{p}$–^{8}He measurement, leading particles were identified by the $\Delta E - E$ method to exclude break-up events. Figure 2 shows the scattering angle correlation of protons and ^{8}He particles. A clear locus of elastic scattering events is seen with good signal/background ratio. Differential cross section and analyzing power will be deduced in the future analysis.

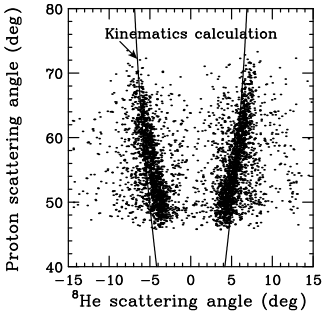

Fig. 2. Scattering angle correlation of protons and ^{8}He particles. Elastic scattering events are clearly identified.

*1 Center for Nuclear Study, University of Tokyo
*2 Cyclotron and Radioisotope Center, Tohoku University
*3 Department of Physics, University of Tokyo
*4 Department of Physics, Saitama University
*5 Department of Physics, Toho University
*6 Department of Physics, Tokyo Institute of Technology

References

1) S. Sakaguchi *et al.*, "Spin-orbit potential in ^{6}He studied with polarized proton target" at International Nuclear Physics Conference 2007 (INPC2007), Tokyo
2) T. Wakui *et al.*, NIM A **550**, 521 (2005).
3) T. Uesaka *et al.*, NIM A **526**, 186 (2004).
4) H. Togawa *et al.*, RCNP Annual Report, 1 (1987).

Production of spin-polarized ^{17}N beam via inverse-kinematics transfer reaction

K. Shimada,[*1] K. Asahi,[*2] K. Suzuki,[*2] T. Arai,[*2] M. Takemura,[*2] T. Inoue,[*2] K. Takase,[*2] S. Kagami,[*2] N. Hatakeyama,[*2] C. Nakano,[*2] Y. Hasama,[*2] Y. Kobayashi, H. Ueno, A. Yoshimi, D. Kameda, T. Nagatomo, S. Kubono,[*3] H. Yamaguchi,[*3] Y. Wakabayashi,[*3] G. Amadio,[*3] S. Hayakawa,[*3] Y. Kurihara,[*3] J. Murata,[*4] H. Kawamura,[*4] T. Toyoda,[*4] T. Sugimoto,[*5] and D. Nagae[*6]

A method of producing a spin-polarized ^{17}N beam via low-energy inverse-kinematics reactions has been developed[1–3]. According to Brink's matching conditions[4], the probability of nucleon transfer increases when the velocity of the nucleon does not change significantly before and after the transfer. As a result, the probability acquires a strong dependence on the z-component of nucleon orbital angular momenta before and after the transfer, when the coordinate system used has $\boldsymbol{z} \| \boldsymbol{k_f} \times \boldsymbol{k_i}$, where $\boldsymbol{k_i}$ ($\boldsymbol{k_f}$) is the relative momentum in the initial (final) channel. Yamamoto and Kubo show a possibility of a large spin polarization for the nuclei produced via an inverse-kinematics nucleon-transfer reaction[5]. The sign of the polarization depends on whether the reaction is near-side or far-side dominant. The kinematical matching condition becomes different between the near-side and far-side trajectories, and consequently, the cross section also becomes very different between them. Thus, a large spin polarization may occur.

In this report, we show the dependence of the polarization of ^{17}N on the emission angle. The spin-polarized ^{17}N beam was produced via a ^{9}B(^{18}O,^{17}N) reaction with a low-energy in-flight isotope separator CRIB[6], and its spin polarization was measured utilizing the β-NMR technique. The experimental setup used is shown in Fig. 1, and details were explained in Refs. 1–3. In this experiment the acceptance of the emission angle was limited using rotations of the CRIB by 0.0, 2.6 and 5.0° and slits placed after the target in the F0 chamber. In addition, the β-NMR apparatus was moved F3 to a double achromatic plane F2 for the rotation of the CRIB. To select a small Q-value channel, where the polarization increases[3], the momentum acceptance of the ^{17}N beam was limited to (1.0045–1.0295)p_0 with slits located in the momentum-dispersive plane, where p_0 is the peak in the momentum distribution of the ^{17}N beam. The observed β-ray asymmetry as a function of the emission angle in the center-of-mass system are shown in Fig. 2. The observed polarization is not a systematic error, because the sign of the polarization reversed when the angle was reversed.

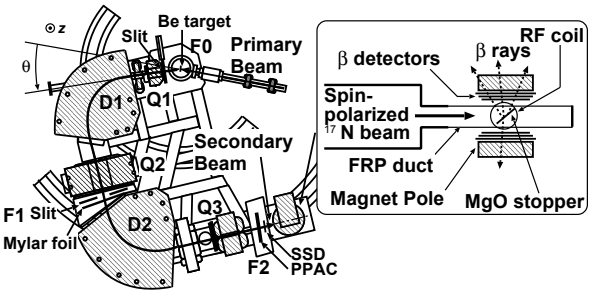

Fig. 1. Schematic view of CRIB and β-NMR apparatus.

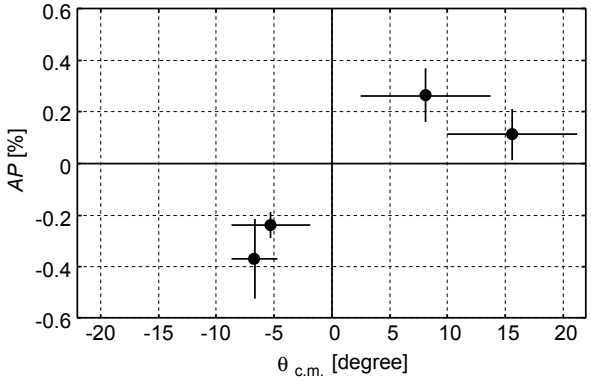

Fig. 2. Observed β-ray asymmetry as a function of the emission angle in the center-of-mass system.

We investigated the dependence of the polarization of ^{17}N produced via the inverse-kinematics low-energy transfer reaction on the Q value[3] and emission angle, although the maximum magnitude of the polarization obtained to date is small. A search for larger-maximum-magnitude polarization at various energies of ^{18}O is planned.

References

1) K. Shimada et al.: AIP Conf. Proc. **915**, 857 (2007).
2) K. Shimada et al.: RIKEN Accel. Prog. Rep., **40** (2007).
3) K. Shimada et al.: CNS Ann. Rep. 2006, **31** (2007) 31.
4) D. M. Brink: Phys. Lett. **40B**, 37 (1972).
5) Y. Yamamoto and K. Kubo: Phys. Rev. C **49**, 360 (1994).
6) Y. Yanagisawa et al.: Nucl. Instrum. Methods Phys. Res. A **539**, 74 (2005).

*1 Cyclotron and Radioisotope Center, Tohoku University
*2 Department of Physics, Tokyo Institute of Technology
*3 Center for Nuclear Study, University of Tokyo
*4 Department of Physics, Rikkyo University
*5 Japan Atomic Energy Agency
*6 Japan Synchrotron Radiation Research Institute

Feasibility Study of Direct Measurement of the ^{21}Na(α,p)^{24}Mg Stellar Reaction

D. N. Binh,[*1] L. H. Khiem,[*2] H. Yamaguchi,[*1] Y. Wakabayashi,[*1] S. Hayakawa,[*1] A. Kim,[*3] and S. Kubono[*1]

[RI beam, Novae, X-ray burst]

Under high-temperature conditions in novae and X-ray bursts, nucleosynthesis in the NeNa cycle leads to the synthesis of the astronomically important ^{22}Na nucleus. Its beta decay leads to the emission of a 1.275 MeV gamma ray. This gamma ray is possibly observable during nova events. However, the observed ^{22}Na abundance was much smaller than that predicted using current models of ONe novae.[1] The predicted ^{22}Na abundance might be reduced by the ^{21}Na(α,p)^{24}Mg reaction bypassing the production of ^{22}Na. It is a breakout process from the NeNa cycle, and makes the reaction flow bypassing the waiting point at ^{22}Mg.[2] It is also important to understand the early stage of the rp-process.[3] The purpose of this study is to perform a direct measurement of the ^{21}Na(α,p)^{24}Mg reaction for the first time using the CNS Radioactive Isotope Beam separator (CRIB) of the University of Tokyo at RIKEN campus. Recently, we have performed a test experiment to study the feasibility of the (α,p) reaction measurement.

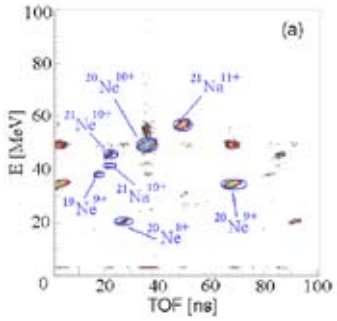

Fig. 1. Particle identification at F2

The experiment was performed by using a low-energy ^{21}Na beam from CRIB.[4] The ^{21}Na secondary beam was produced via the ^{2}H(^{20}Ne,^{21}Na)n reaction. The ^{20}Ne^{6+} primary beam was accelerated by the AVF cyclotron of RIKEN. The momenta of the ^{21}Na particles were selected using a slit at a momentum-dispersive focal plane F1 and then the beam was focused achromatically at the second focal plane F2. The particles were clearly identified at F2 by the E-TOF method and presented in Fig. 1 (a). The purity of ^{21}Na^{11+} obtained at F2 was 8.5%. To further separate ^{21}Na^{11+} from other contaminant particles, the Wien filter was used at ± 100 kV.[5] After using the Wien filter, the purity of the ^{21}Na beam was 98.5% and the ^{21}Na^{11+} beam intensity was 4 x 10^3 pps when the primary beam intensity was 370 enA. All the experimental setups of the reaction measurement were installed in the F3 chamber downstream of the Wien filter. The helium gas target of 30 mm length was filled with helium gas at 1 atm. The ΔE-E telescope consisted of a 70-μm-thick ΔE counter followed by a 1.5-mm-thick E counter. It was placed 15.2 cm away from the gas target at 0^o. The reaction products from the helium gas target, which were detected using the ΔE-E telescope, are shown in Fig. 2.

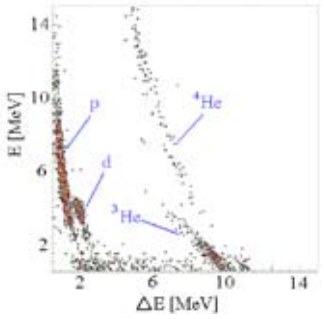

Fig. 2. ΔE-E spectrum at F3

The protons were identified and distinguished from other particles by ΔE-E particle identification. However, they were produced not only by the (α,p) reaction but also by other processes, which are elastic scattering on hydrogen nuclei of Mylar foils of the PPACs and a proton background, which was induced at the Wien filter. The proton expected from the (α,p) can be distinguished from the background by measuring its time-of-flight. In conclusion, the ^{21}Na beam was produced with the sufficiently high purity and intensity for the planned ^{21}Na(α,p)^{24}Mg experiment, and the protons from the relevant (α,p) reaction were observed in a preliminary measurement.

References

1) M. Hernanz: Proc. 5th INTEGRAL Workshop, Munich, Germany, 2004.
2) J. L. Fisker *et al.*, Astro. J. 608, 61 (2004).
3) S. Kubono, Nucl. Phys A **558**, 305 (1995).
4) S. Kubono *et al.*, Eur. Phys. J. A **13**, 217 (2002).
5) S. Kubono *et al.*, Nucl. Phys A **758**, 733c (2005).

*1 Center for Nuclear Study, Graduate School of Science, University of Tokyo
*2 Institute of Physics and Electronics, Viet Nam Academy of Science and Technology
*3 Department of Physics, Ewha Womans University

Development of ^{46}Cr secondary beam

Y. Wakabayashi,[*1] H. Yamaguchi,[*1] S. Hayakawa,[*1] Y. Kurihara,[*1] S. Nishimura, D. N. Binh,[*1*2] Y. Gono, and S. Kubono[*1]

[β-decay, unstable nuclei beam]

For the rapid proton capture process (*rp*-process) in X-ray burst and the core-collapse stage of supernova, proton-rich *pf*-shell nuclei far from stability play important roles[1]. Studies of the β and electron capture decays of these proton-rich *pf*-shell nuclei are of great astrophysical interest. These decays involved in the charged-current processes, e.g., $p \rightarrow n + e^+ + \nu$, are predominated by the Fermi and Gamow-Teller (GT) transitions. Information on GT transitions can be derived directly from β-decay measurements. To determine the accurate B(GT), it is important to determine the feeding ratio and half-life of the β-decay accurately.

In this study, the final purpose of the experiment is to measure the properties of ^{46}Cr, namely, i) the total half-life of β-decay with an accuracy better than 10 %, ii) the decay branching ratios to the ground state (Fermi transition) and GT states measured accurately, and iii) higher excited GT states if they exist.

Experimental runs to develop a ^{46}Cr secondary beam were performed using the low-energy RI beam separator (CRIB)[2,3] of the Center for Nuclear Study (CNS), University of Tokyo. A primary beam of $^{36}Ar^{10+}$ at 3.6 MeV/nucleon bombarded ^{12}C at 0.845 mg/cm^2. The primary beam was degraded to 3.0 MeV/u by a 2.2-μm-thick Havar foil placed in front of the primary target, because of the maximum production of ^{46}Cr. To separate the contaminants in the secondary beam, the Wien filter (W.F.) was used at a high voltage of $\pm$80 kV. A microchannel plate (MCP) was placed at the final focal plane (F3) to monitor the beam position. We used a window a 0.7-μm-thick Mylar covered by thin aluminum and CsI. For particle identification (PI), a monolithic Si detector[4] was placed behind the MCP. This Si detector consists of 1.5-μm-thick and 500-μm-thick layers that are used as ΔE and E counters, respectively.

Figure 1 shows PI obtained from the experimental runs. Several fusion products were observed together with ^{36}Ar of a primary beam component. It was found that the purity of ^{46}Cr was 1.2 % and the intensity was 2.4 particle per second (pps) with the primary beam of 20 particle nA. The purities and intensities of other nuclides in the secondary beam are also summarized in Table 1.

From the experimental results for ^{46}Cr, we may obtain an intensity of 24 pps and 5.2x10^6 particles in a total of 6.5 days with the primary beam of 200 particle nA, which is available from the AVF cyclotron. These values are considered to be sufficient for obtaining the accuracy described above. In the near future, we plan to perform an experiment to measure the properties of ^{46}Cr.

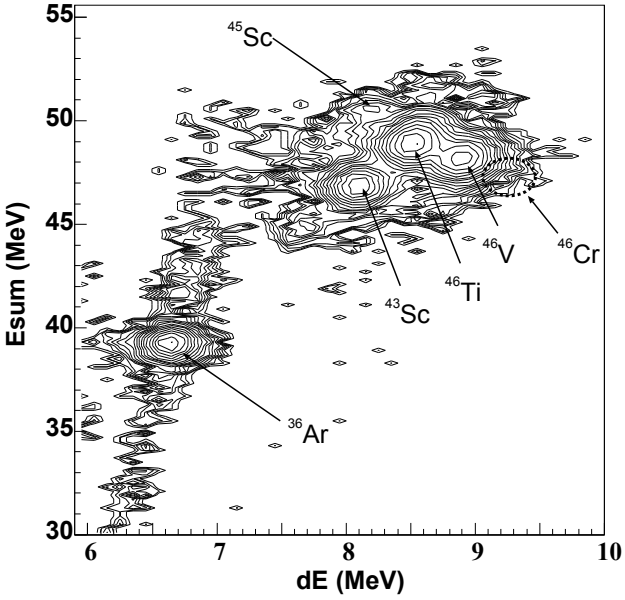

Fig. 1. ΔE-E spectrum obtained by the monolithic Si detector placed at F3.

Table 1. Purities and intensities of nuclides with primary beam of 20 particle nA, where purities and intensities are shown in units of % and pps, respectively.

Nuclide	^{46}Cr	^{46}V	^{45}Ti	^{46}Ti	^{43}Sc	^{45}Sc	^{36}Ar
Purity	1.2	28.6	3.0	38.2	13.1	0.9	15.4
Intensity	2.4	57.3	6.2	76.6	26.4	1.8	33.2

References

1) K. Langanke and G. Martinez-Pinedo, Rev. Mod. Phys. **75**, 819 (2003).
2) S. Kubono et al., Eur. Phys. J. A **13**, 217 (2002).
3) Y. Yanagisawa et al., Nucl. Instrum. Methods Phys. Res. A **539**, 73 (2005).
4) A. Musumarra et al., Nucl. Instrum. Methods Phys. Res. B **409**, 414 (1998).

*1 Center for Nuclear Study, University of Tokyo
*2 Institute of Physics and Electronic, Vietnam Academy of Science and Technology

2. Nuclear Physics(Theory)

Resonances of ^{7}He using the complex scaling method

T. Myo,[*1] K. Katō,[*2] and K. Ikeda

[Nuclear structure, Unstable nuclei, Resonance, Cluster model]

Development of the radioactive beam experiments provides us with much information of the unstable nuclei far from the stability. Recently, many experiments of ^{7}He, the unbound nuclei, have been reported[1–6]. However, there are still found contradictions in the observed energy levels and the excited states are not settled for their spins and energies. The ^{7}He excited states are experimentally suggested to appear as two or three particle resonances above the ^{4}He+3n threshold energy, because the subsystem ^{6}He is a Borromean nucleus and breaks up easily into ^{4}He+n+n.

Theoretically, when we discuss the structures of the ^{7}He resonances, it is important to describe the many-body decay properties concerned with subsystems consistently, in which the subsystems also have their particular decay widths such as ^{5}He+2n channels. This condition was not emphasized so far in the studies of ^{7}He. The ^{7}He resonant spectroscopy is desired to be investigated with the appropriate treatments of the decay properties concerned with ^{5,6}He.

The purpose of this theoretical study is to carry out the resonance spectroscopy of ^{7}He with the simultaneous descriptions of ^{5,6}He imposing the accurate boundary conditions of many-body decays. Here, we employ the cluster orbital shell model of the four-body ^{4}He+n+n+n system under the orthogonality condition model, in which the open channel effects for the ^{6}He+n, ^{5}He+2n and ^{4}He+3n decays are taken into account explicitly. We describe the many-body resonances under the correct boundary conditions for these decay channels using the complex scaling method. We employ the Hamiltonian, which reproduces the ^{4}He-n scattering data and the ^{6}He energies, shown in Fig. 1[7].

As a result, we found five resonances of ^{7}He shown in Fig. 1, which are dominantly described by the p shell configurations and the small contributions come from the sd shell. The ground and the $5/2^-$ states are reproduced well, while the slight overbinding is seen for the ground state by 0.2 keV in comparison with the experiments. The $3/2^-_2$ state is predicted very close to the $5/2^-$ state in Fig. 2. The $1/2^-$ state is also predicted as a four-body resonance with a low excitation energy having a relatively large decay width of around 2 MeV. We further investigate the spectroscopic factor (S factor) of the ^{6}He-n component for ^{7}He resonances in Table 1. The S factors are useful to understand the coupling between ^{6}He and the additional neutron in ^{7}He. It is found that the ^{6}He(2^+_1) state contributes largely in the several states of ^{7}He.

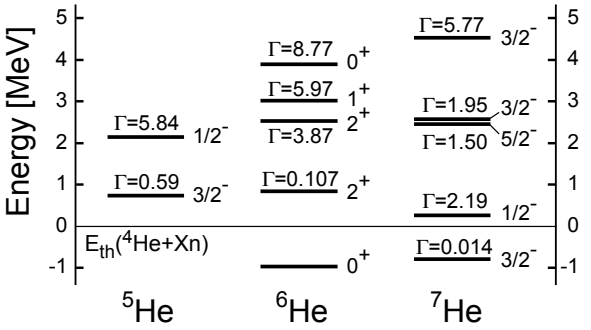

Fig. 1. Energies and decay widths of the ^{5,6,7}He states measured from the ^{4}He+Xn threshold ($X = 1, 2, 3$).

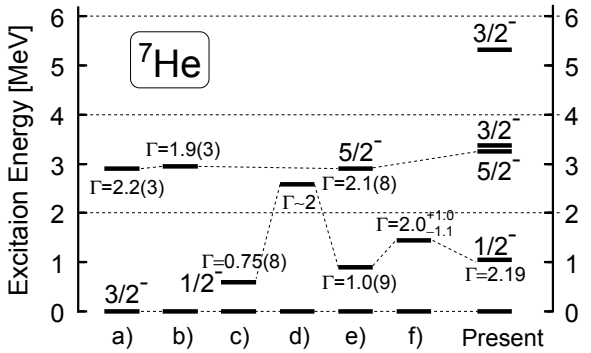

Fig. 2. Excitation spectra of ^{7}He in comparison with the experiments (a)[1], b)[2], c)[3], d)[4], e)[5], f)[6]).

Table 1. S factors of the ^{6}He-n components in ^{7}He.

	^{6}He(0^+_1)-n	^{6}He(2^+_1)-n
$3/2^-_1$	$0.75 + i0.10$	$1.51 - i0.40$
$3/2^-_2$	$0.03 + i0.03$	$1.78 + i0.06$
$3/2^-_3$	$0.01 + i0.03$	$0.02 + i0.05$
$1/2^-$	$0.25 - i0.47$	$0.13 - i0.08$
$5/2^-$	$0.00 + i0.00$	$1.37 - i0.15$

† Condensed from the article in Phys. Rev. C **76**, 054309 (2007)

*1 Research Center for Nuclear Physics, Osaka University
*2 Graduate School of Science, Hokkaido University

References

1) A. A. Korsheninnikov et al.: Phys. Rev. Lett. **82**, 3581 (1999).
2) G. Bohlen et al.: Phys. Rev. C**64**, 024312 (2001).
3) M. Meister et al.: Phys. Rev. Lett. **88**, 102501 (2002).
4) A. H. Wuosmaa et al.: Phys. Rev. C **72**, 061301 (2005).
5) F. Skaza et al.: Phys. Rev. C **73**,044301 (2006).
6) N. Ryezayeva et al.: Phys. Lett. B**639**, 623 (2006).
7) T. Myo, K. Katō, K. Ikeda: Phys. Rev. C**76**, 054309 (2007).

Exotic molecular structures in highly excited states of ^{12}Be †

M. Ito, N. Itagaki,[*1] H. Sakurai, and K. Ikeda,

[Nuclear structure, cluster model, unstable nuclei]

It is well known that various deformed structures appear in excited states of nuclear systems. The strongly deformed states have been discussed from two different viepoints so far; one is the deformation of the self-consistent mean field, while the other is the decomposition into sub units, clustering. Examples of the former and latter cases are known as the superdeformed (SD) band and molecular resonances (MRs), respectively.

In this report, we propose a new type of *superdeformed* structure based on a cluster picture in a light neutron-rich ($N > Z$) nucleus, and demonstrate that the proposed superdeformed state coexists with the MRs. The Be isotopes are the candidates manifesting such coexistence phenomena. These are typical examples of two-center superdeformed systems that build on an α+α rotor of ^{8}Be[1].

To investigate the coexistence phenomena between the MRs and the new type of superdeformed state, the intrinsic structures and their coupling to the scattering states should be treated in a unified manner, because the MRs are realized as unbound states above the particle-decay thresholds. For this purpose, we proposed a microscopic model, the generalized two-center cluster model (GTCM)[2,3]. In this study, we apply the GTCM for ^{12}Be with the α+α+4N structure.

In the GTCM, the total wave function is expressed as a linear combination of the "atomic orbitals" (AOs) around two α cores. The α particle is described using the $(0s)^4$ configuration and the valence neutrons are specified using the atomic orbitals in which the neutrons are localized at one of the α cores with $0p$ orbitals. In the calculation, the α–α distance S and the mixing weights among the AOs are treated as variational parameters. In the region where two α-cores are near, the total system is expected to form the molecular orbital (MO) structure[1] such as π^-, σ^+,..., whereas in the region where two core nuclei are far apart, the molecular orbitals smoothly change into product wave functions consisting of atomic orbitals.

Because of the smooth connection, we obtain whole energy spectra from the bound states to the unbound ones as shown in Fig. 1 (J^π=0^+). In this figure, the scattering matrix (S-matrix) for the two-neutron transfer reaction, α+^{8}He$_{g.s.}$ → ^{6}He$_{g.s.}$+^{6}He$_{g.s.}$, is also shown. The S-matrix is calculated by Kamimura's method[4]. The obtained 0^+ states are classified into three categories. **(i) MO states.** There appear two bound states below the α+^{8}He$_{g.s.}$ threshold (0^+_1 and 0^+_2). Here, the four neutrons are in MO motion around the two α cores ($(\pi^-_{3/2})^2(\sigma^+_{1/2})^2$ and $(\pi^-_{3/2})^2(\pi^-_{1/2})^2$). **(ii) MR states.** The resonance states, 0^+_3, 0^+_4, and 0^+_6, have the MR characteristics of corresponding threshold (α+^{8}He, ^{6}He+^{6}He, and ^{5}He+^{7}He, respectively). **(iii) Covalent SD state.** In the 0^+_5, two neutrons form the covalent bond of $(\sigma^+)^2$, while the other two neutrons form the atomic structure of ^{5}He+^{5}He. This state has a large clustering ($S \sim 5$ fm) due to the $(\sigma^+)^2$ formation, and hence, it should be called the "superdeformation with the covalent neutrons".

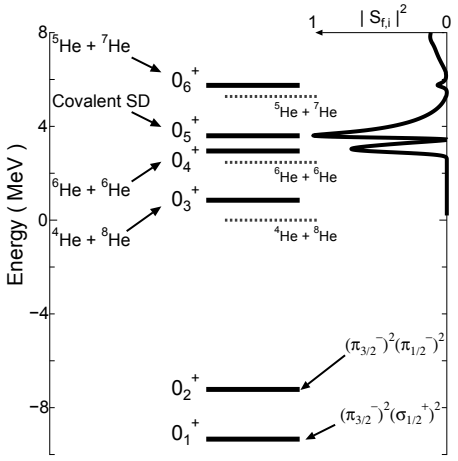

Fig. 1. Energy spectra for J^π=0^+. The dotted lines represent the threshold energy of the open channels considered in the calculation.

As shown in Fig. 1, the superdeformation with covalent neutrons and the ^{X}He+^{Y}He molecular resonances coexist within a small energy interval, say approximately 4 MeV. This is the first study pointing out the coexistence phenomena of molecular resonances and superdeformations, which can be generally observed in light neutron-rich nuclei. Systematic studies are now proceeding.

References

1) N. Itagaki and S. Okabe, Phys. Rev. C **61**, 044306 (2000); N. Itagaki, S. Okabe and K. Ikeda, Phys. Rev. C **62**, 034301 (2000), and references therein.
2) M. Ito, K. Kato and K. Ikeda, Phys. Lett. B**588**, 43 (2004).
3) Makoto Ito, Phys. Lett. B**636**, 293 (2006); *ibid*, Mod. Phys. Lett. A **21**, 2429 (2006).
4) K. Hamaguchi et al., Phys. Lett. B **650**, 268 (2007).

† Condensed from a paper submitted to Physical Review Letters (2007).

*1 Department of Physics, University of Tokyo

Inelastic proton scattering and neutron quadrupole transitions of ^{12}Be†

M. Takashina*1 and Y. Kanada-En'yo*1

[Nuclear reaction]

In the recent progress of nuclear structure research, various exotic phenomena have been revealed in unstable nuclei. For example, the disappearance of magic numbers has been discovered. Concerning the $N = 8$ magic number, ^{12}Be has been attracting a great deal of interest. Theoretically, the deformation of ^{12}Be is considered to be a key factor in the vanishing of the magic number[1]. The deformation is favored in neutron-rich Be because of the prominent cluster structure with a 2α core, and the molecular orbital picture[2] well describes systematically the low-lying states. In this picture, when the cluster is sufficiently developed, the neutron *sd*-orbital gains energy and becomes an intruder. As a result, the ground state of ^{12}Be is a largely deformed state with the dominant intruder configuration of *sd* mixing. Because of the deformation, the neutron transition is expected to be strong in the ground band.

Proton inelastic scattering can be a good probe for investigating neutron excitation in the ground band, because the proton-neutron interaction is stronger than the proton-proton interaction. Recently, a $^{12}\mathrm{Be}(p,p')^{12}\mathrm{Be}^*$ experiment in inverse kinematics was performed by Iwasaki et al.[3]. The data were analyzed by the reaction calculation based on a simple collective model, and the result of this experiment was revealed to indicate the broken shell closure.

In the usual reaction model for stable nuclei, it is assumed that the radial shape of the neutron transition density $\rho^n_{\rm tr}(r)$ is the same as that of the proton one $\rho^p_{\rm tr}(r)$. The analysis by Iwasaki et al.[3] also relies on this assumption. However, one should take into account the difference between $\rho^p_{\rm tr}(r)$ and $\rho^n_{\rm tr}(r)$ for neutron-rich nuclei. Therefore, in the present study, we investigate proton inelastic scattering on ^{12}Be using a microscopic procedure that can include the difference between $\rho^p_{\rm tr}(r)$ and $\rho^n_{\rm tr}(r)$. We adopt the microscopic coupled-channel (MCC) method based on the antisymmetrized molecular dynamics (AMD) wave function.

We prepare three kinds of AMD wave functions (i) - (iii), which give different neutron transition strengths. The values of proton and neutron transition strengths, B_p and B_n, respectively, are summarized in Table 1. In the present study, the proton-^{12}Be potential is calculated using the single-folding model. For the effective NN potential, we adopt the JLM (Jeukenne-Lejeune-Mahaux) potential[4]. The results of the MCC calculations are shown in Fig. 1. The best result is obtained with AMD (ii), which gives the neutron transition strength $^{12}\mathrm{Be}(2^+_1 \to 0^+_1)$ of B_n=37 fm^4.

Table 1. Transition strengths of ^{12}Be calculated by AMD.

^{12}Be	(i)	(ii)	(iii)
$B^{(2)}_p(2^+_1 \to 0^+_1)$ (fm^4)	14	13	15
$B^{(2)}_n(2^+_1 \to 0^+_1)$ (fm^4)	52	37	74

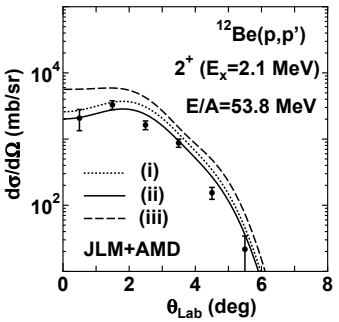

Fig. 1. Angular distribution of p+^{12}Be(g.s. $\to 2^+_1$) inelastic scattering. The solid circles are the experimental data. The dotted, solid and dashed curves are the results of MCC using AMD (i), (ii) and (iii), respectively.

On the other hand, B_n derived by Iwasaki et al.[3] is 18 fm^4, which is half of our value. This discrepancy may be due to their use of the Bernstein formula, in which the difference in the radial dependence between $\rho^p_{\rm tr}(r)$ and $\rho^n_{\rm tr}(r)$ is not taken into account. In order to see the effect of the difference, we search the neutron transition strength B_n for the $\rho^n_{\rm tr}(r) \propto \rho^p_{\rm tr}(r)$ case by artificially neglecting the difference. As a result, we obtain the transition strength of B_n=11 $\pm$ 3 fm^4. Therefore, we conclude that the difference in the radial dependence between the proton and neutron transition densities should be considered carefully in the analysis of the inelastic scattering of unstable nuclei.

References
1) Y. Kanada-En'yo and H. Horiuchi, Phys. Rev. C 68, 014319 (2003).
2) W. von Oertzen, M. Freer and Y. Kanada-En'yo, Phys. Rep. 432, 43 (2006).
3) H. Iwasaki et al., Phys. Lett. B 481, 7 (2000).
4) J.-P. Jeukenne, A. Lejeune and C. Mahaux, Phys. Rev. C 16, 80 (1977).

† Condensed from the article in Phys. Rev. C77, 014604 (2008)

*1 Yukawa Institute for Theoretical Physics, Kyoto University

Reaction cross sections of carbon isotopes incident on a proton†

B. Abu-Ibrahim,[*1] W. Horiuchi,[*2] A. Kohama, and Y. Suzuki,[*3]

[Nuclear reaction, total reaction cross sections, unstable nuclei]

Reactions of unstable neutron-rich nuclei with a proton target are of current interest since such reactions are at present the major means to sensitively probe the matter densities of exotic nuclei, particularly the region of nuclear surface. If one appropriately selects incident energies, protons could be more sensitive to neutron distributions than to proton distributions of nuclei.

The structure of carbon isotopes has recently attracted much attention. Several studies have been carried out experimentally [1] and theoretically.[2] For example, the structure of ^{22}C has been studied by two (W.H. and Y.S.) of the present authors using a three-body model of ^{20}C+n+n. They showed that it has a Borromean character.[3]

In this work, we systematically study the total reaction cross sections of carbon isotopes with N = 6-16 on a proton target for a wide range of incident energies, ranging from 40 to 1000 A MeV. Emphasis is put on the difference between a proton target and a carbon target. The calculations include the reaction cross sections of ^{19,20,22}C at 40 AMeV, the data of which have recently been obtained at RIKEN.[4] This study is an extension of our previous work on similar processes, but using a carbon target.[5]

We formulate this problem using the Glauber theory. The inputs are the parameters of nucleon-nucleon profile functions and the wave functions (densities) of carbon isotopes. The parameters of nucleon-nucleon scattering are determined from available experimental data, and we treat the interactions of proton-proton and proton-neutron separately.

To describe the intrinsic structure of carbon isotopes, we use a Slater determinant generated from a phenomenological mean-field potential, which we used in our previous work,[5] and construct the density distributions. The center-of-mass motions are appropriately taken into account. To go beyond the simple mean-field model, we adopt two types of dynamical model: One is a core+n model for odd-neutron nuclei, and the other is a core+n+n model for ^{16}C and ^{22}C.

For ^{22}C, we generate several densities that are constructed from the wave functions yielding different separation energies of 0.489, 0.361, 0.232, and 0.122 MeV for the last two neutrons. All of these energies lie within the error bar of the experimental value of 0.423±1.140 MeV. The reaction cross sections calculated using these densities are 957, 969, 985, and 1005 mb, respectively, for proton-^{22}C at 40 MeV. Since the preliminary data of proton-^{22}C reaction cross section has been reported to be around 1000 mb with a large uncertainty,[4] all of our predictions are consistent with the data, but the larger two values, 985 and 1005 mb, are favorable. If so, the data suggest a very small S_{2n}.

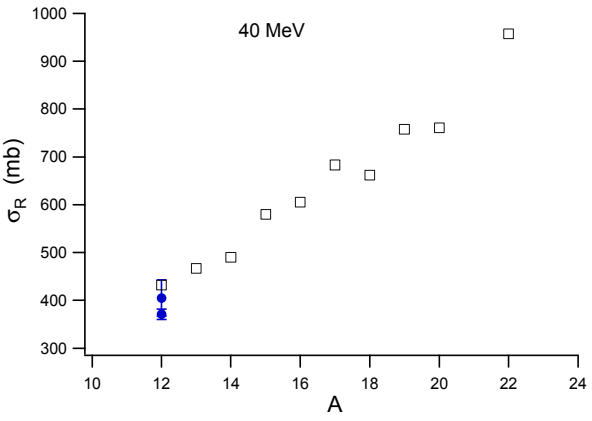

Fig. 1. Reaction cross sections for carbon isotopes at 40 MeV. The solid circles are the data for $A \simeq 12$: The upper one indicates natural carbon at 42 MeV, and the lower is ^{12}C at 40 MeV. The energy is converted to that in the case of a proton target. The preliminary data for ^{22}C is about 1000 mb with a large uncertainty.[4]

Finally, we carry out a simple estimation of the contribution of the neutron and the proton to the total reaction cross sections. The major contribution to $\sigma_{\rm R}$ comes from the surface region. Moreover, we point out that a proton target can probe the surface region of neutron-rich nuclei better than a ^{12}C target particularly at a lower incident energy.

References

1) N. Imai *et al.*: Phys. Rev. Lett. **92**, 062501 (2004).
2) N. Itagaki, T. Otsuka, K. Ikeda and S. Okabe: Phys. Rev. Lett. **92**, 142501 (2004).
3) W. Horiuchi and Y. Suzuki: Phys. Rev. C **74**, 034311 (2006).
4) K. Tanaka *et al.*: QW-005 in *INPC2007 Abstracts* and private communication.
5) W. Horiuchi, Y. Suzuki, B. Abu-Ibrahim, and A. Kohama: Phys. Rev. C **75**, 044607 (2007); Erratum: *ibid.* C **76**, 039903(E) (2007).

† Condensed from the article in Phys. Rev. C. **77**, 034607 (2008)

*1 Department of Physics, Cairo University, Egypt
*2 Graduate School of Science and Technology, Niigata University
*3 Department of Physics and Graduate School of Science and Technology, Niigata University

Competition and coexistence of normal and intruder states in exotic Na isotopes from β decay study

Y. Utsuno,[*1] T. Otsuka,[*2] T. Mizusaki,[*3] and M. Honma[*4]

[NUCLEAR STRUCTURE, shell model, unstable nuclei]

It is of considerable interest to determine the boundary of the so-called "island of inversion"[1] denoting the region where the $N = 20$ magic structure is broken. This is mainly because its location is quite sensitive to the $N = 20$ shell gap theoretically, leading to the further understanding of how the shell gap evolves in exotic nuclei.[2] For the "western" boundary of the island, i.e., that along a fixed isotope chain, we have shown that, for the Na isotope chain, a strong mixing occurs at $N = 18$ and the intruder state almost completely dominates the ground state at $N = 19$ from the nuclear moment of the ground state.[2] This indicates a more extended island than the original[1] and a markedly narrowing $N = 20$ shell gap to explain it.

It is most likely that the normal and intruder states coexist near the boundary. The information has been available for neutron-rich Na isotopes from recent experiments on the β decay.[3,4] Since not only the energy levels but also their $\log ft$ values provide useful information, in the present study, we investigated the β decay matrix elements by the Monte Carlo shell model (MCSM) calculation with the SDPF-M interaction[5], which was carried out as a RIKEN-CNS collaboration project on large-scale nuclear structure calculations using the Alphleet and Alphleet-2 computer systems.

The calculation of the β decay matrix element in MCSM is not as straightforward as other one-body transitions such as electromagnetic transitions because the standard formula to calculate the one-body transition density based on the Thouless' theorem is not applicable owing to the orthogonality between the initial and final states. We thus derived a formula to calculate the matrix element of $\langle\Phi'|c^\dagger_p c_n|\Phi\rangle$ for the β decay.

Figure 1 shows the energy levels and $\log ft$ values compared between experiment and shell-model calculations. For ^{29}Na, it was pointed out that two states at approximately 1.5 MeV should be strongly affected by the intruder states because there are no corresponding levels from the *sd*-shell model. The MCSM calculation reproduced those two levels containing an intruder component of more than 50%. In this work, we also reproduced their $\log ft$ values excellently, providing a firm confirmation of this conclusion. Since the $\log ft$ value is sensitive to the probability of the intruder states (note that it is infinity if the parent and daughter have completely different *npnh* states), the agreement supports the strong mixing there obtained by MCSM. Similarly, a good agreement for ^{30}Na has made it clear that the 924 keV state is dominated by the normal state.

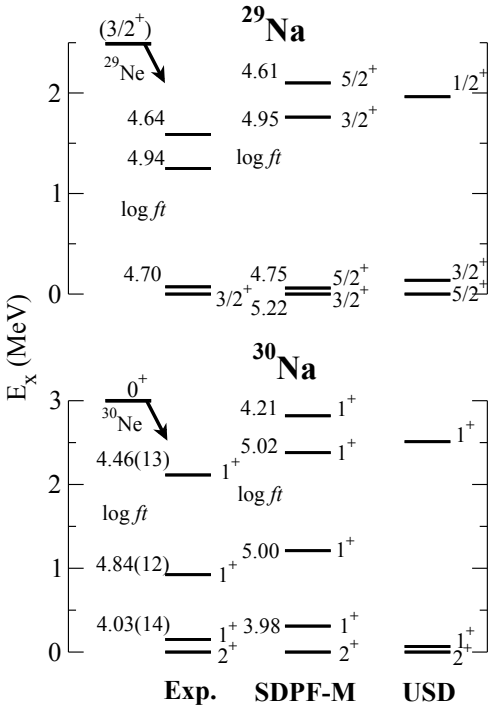

Fig. 1. Energy levels of ^{29}Na and ^{30}Na compared among experiment (Exp.), the MCSM calculation with the SDPF-M interaction (SDPF-M) and the *sd*-shell model with the USD interaction (USD) together with their $\log ft$ values. Only the levels that can be fed via allowed β decay are presented as well as the ground state. For the calculation of $\log ft$ values, g_A/g_V is quenched by a factor 0.9.

*1 Advanced Science Research Center, Japan Atomic Energy Agency
*2 Department of Physics and Center for Nuclear Study, University of Tokyo
*3 Institute of Natural Sciences, Senshu University
*4 Center for Mathematical Sciences, University of Aizu

References

1) E. K. Warburton, J. A. Becker and B. A. Brown: Phys. Rev. C **41**, 1147 (1990).
2) Y. Utsuno, T. Otsuka, T. Glasmacher, T. Mizusaki, and M. Honma: Phys. Rev. C **70**, 044307 (2004).
3) V. Tripathi et al.: Phys. Rev. Lett. **94**, 162501 (2005).
4) V. Tripathi et al.: Phys. Rev. C **76**, 021301(R) (2007).
5) Y. Utsuno, T. Otsuka, T. Mizusaki, and M. Honma: Phys. Rev. C **60**, (1999).

Shell-model description of neutron-rich Ca isotopes

M. Honma,[*1] T. Otsuka,[*2] T. Mizusaki,[*3]

[NUCLEAR STRUCTURE, shell model, unstable nuclei]

The evolution of the shell structure characterized by appearance and/or disappearance of magic numbers in nuclei far from the stability line has been one of the most interesting subjects in the nuclear structure physics. It has been pointed out that one possible origin of such a change of the shell structure is the tensor force.[1] The shell model is useful in that sense for theoretical investigations of this problem, because the shell-model Hamiltonian can properly inherit the tensor interaction from the microscopic G-matrix.

We developed an effective interaction GXPF1[2] for pf-shell nuclei by modifying the microscopic G-matrix interaction in an empirical way so as to fit available experimental energy data. The GXPF1 and the revised version GXPF1A[3] have been successfully applied for the study of many nuclei including neutron-rich ones. One interesting prediction by the GXPF1(A) is the development of a new shell closure at $N = 34$ in Ca isotopes in addition to that at $N = 32$. The latter one has been established experimentally and can be seen also in other isotopes such as Ti and Cr. On the other hand, it is still difficult to clarify experimentally the existence of such a magic structure in ^{54}Ca. Theoretically, since the development of the $N = 34$ shell gap strongly depends on details of the effective interaction, further improvement of the Hamiltonian is desired for more precise and reliable predictions.

Recently, new experimental data have been published for low-lying energy levels of $^{51-53}$Ca.[4] These data can provide important information for improving the effective interaction, especially for two-body matrix elements related to the $p_{1/2}$ and the $p_{3/2}$ orbits which could not be determined in the GXPF1(A). In order to obtain better fit to the new data, we have modified the GXPF1A in the following three parts: (1) the single-particle energy for the $p_{1/2}$ orbit is shifted up by 0.3 MeV, resulting in the single-particle energies -8.6240, -5.6793, -1.3829 and -3.8370 MeV for the $f_{7/2}$, $p_{3/2}$, $f_{5/2}$ and $p_{1/2}$ orbits, respectively, (2) $T = 1$ diagonal two-body matrix element for the $p_{3/2}$-$p_{1/2}$ orbits are modified so that the quadrupole-quadrupole interaction becomes stronger, and (3) the pairing matrix elements related to the $p_{1/2}$ orbits are readjusted.

The calculated energy levels for Ca isotopes obtained by using the modified interaction GXPF1B are shown in Fig.1. In ^{51}Ca, the GXPF1A(B) predicts a $3/2^-$ ground state and a $7/2^-$ state at 3.5 MeV excitation energy. These states correspond to neutron one-hole states on top of the ^{52}Ca core, and are in reasonable agreement with the experimental results. On the other hand, the excitation energies of the $1/2^-$ and the $3/2^-_2$ states are shifted up significantly from the GXPF1A to the GXPF1B, giving rise to much better correspondence with the new experimental data. In ^{52}Ca, the GXPF1A predicts almost degenerate 1^+ and 2^+ states corresponding to the $(p_{3/2})^{-1}(p_{1/2})^1$ doublet at around 2.3 MeV. These states are separated by 0.7 MeV with the GXPF1B, showing a reasonable correspondence with the experimental data. As for the ^{53}Ca, the ground state is tentatively assigned as $(1/2^-)$, and the first excited state appears at 2.2 MeV. The GXPF1A(B) predicts a $1/2^-$ ground state and a $3/2^-$ state at 2.1 MeV, suggesting good agreement with the experimental data.

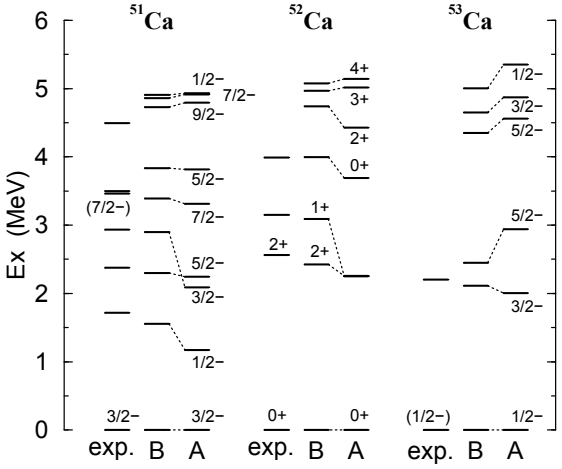

Fig. 1. Energy levels of Ca isotopes. Experimental data (exp.) are compared to shell-model results obtained by a code MSHELL[5] with the effective interactions GXPF1A and GXPF1B.

By using the GXPF1B, the excitation energy of the 2^+_1 state of ^{54}Ca is calculated to be 2.6MeV, which is almost the same as that of ^{52}Ca, predicting again the development of the $N = 34$ shell gap.

References

1) T. Otsuka, et al.: Phys. Rev. Lett. **95**, 232502 (2005).
2) M. Honma, et al.: Phys. Rev. C **65**, 061301(R) (2002); Phys. R ev. C **69**, 034335 (2004).
3) M.Honma et al.: Eur. Phys. J. A **25** Suppl. 1, 499 (2005).
4) F. Perrot et al.: Phys. Rev. C **74**, 014313 (2006).
5) T. Mizusaki: RIKEN Accel. Prog. Rep. **33**, 14 (2000).

*1 Center for Mathematical Sciences, University of Aizu
*2 Department of Physics and Center for Nuclear Studies, University of Tokyo
*3 Institute of Natural Sciences, Senshu University

Difference between interaction cross sections and reaction cross sections†

A. Kohama, K. Iida,[*1] and K. Oyamatsu[*2]

[Nuclear reaction, interaction cross section, reaction cross section, unstable nuclei]

Measurements of interaction cross sections have been performed for stable and light unstable nuclei[1] and are planned for heavy unstable nuclei in radioactive ion beam facilities, such as RIKEN RI Beam Factory. The interaction cross section, $\sigma_{\rm I}$, for a nucleus incident on a target nucleus is defined as the total cross section for all processes associated with proton and/or neutron removal from the incident nucleus. This definition of $\sigma_{\rm I}$ leads to the relation $\sigma_{\rm I} = \sigma_{\rm R} - \sigma_{\rm inel}$, where $\sigma_{\rm R}$ is the total reaction cross section and $\sigma_{\rm inel}$ is the cross section for inelastic channels.

Recently, we have systematically analyzed the proton elastic scattering and reaction cross section data for stable nuclei at a proton incident energy of $T_p \sim$ 800–1000 MeV on the basis of a "black-sphere picture" of nuclei.[2] This picture is originally expected to provide a decent description of the reaction cross section for any kind of incident particle that tends to be attenuated in nuclear interiors. We showed that for proton beams incident on stable nuclei, the cross section of a black sphere of radius a $(= \pi a^2)$, which was determined by fitting the angle of the first elastic diffraction peak calculated for proton diffraction by a circular black disk of radius, a, to the measured value, is consistent with the measured total reaction cross section.[2] This consistency suggests that the black sphere radius corresponds to a reaction radius inside which the reaction with incident protons occurs. This feature is also true for nucleus-nucleus total reaction cross sections.

In this work, we revisit the commonly accepted notion that the difference between interaction and reaction cross sections is negligible at relativistic energies. To analyze the difference, we concentrate on the reactions of stable projectiles on a carbon target and construct "pseudo data" for the reaction cross sections using a phenomenological black-sphere model of nuclei[2] since empirical data are very limited at high energies. In the model, the absorption cross section is written by

$$\sigma_{\rm BS} = \pi \left(a_{\rm P} + a({\rm C})\right)^2 , \qquad (1)$$

where $a_{\rm P}$ is the black-sphere radius of a projectile nucleus. a(C) is the black-sphere radius of the target C nucleus obtained from the measured angle of the first diffraction maximum in proton elastic scattering.[2] For proton incident energies higher than $\sim$ 800 MeV, a(C) $= 2.69 \pm 0.07$ fm. We have basically verified the validity of our assumption of $\sigma_{\rm R} \cong \sigma_{\rm BS}$ using the currently available $\sigma_{\rm R}$ data for ^{9}Be, ^{12}C, and ^{27}Al incident on ^{12}C.

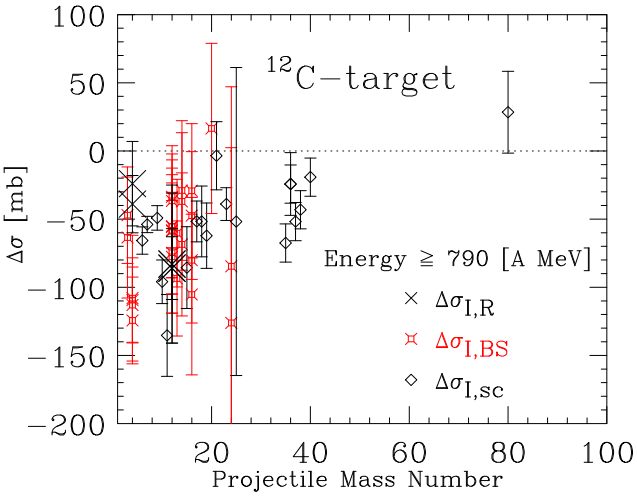

Fig. 1. $\Delta\sigma_{\rm I,R} = \sigma_{\rm I} - \sigma_{\rm R}$ (crosses), $\Delta\sigma_{\rm I,BS} = \sigma_{\rm I} - \sigma_{\rm BS}$ (squares), and $\Delta\sigma_{\rm I,sc} = \sigma_{\rm I} - \sigma_{\rm scaling}$ (diamonds) for a carbon target as a function of projectile mass. $\sigma_{\rm scaling}$ is obtained by substituting $a \simeq 1.2135A^{1/3}$ [fm] for $a_{\rm P}$ in Eq. (1). This scaling of the black-sphere radius a was found for stable nuclei ranging from He to Pb.[2]

The comparison with the empirical interaction cross sections suggests a significant difference between the reaction and interaction cross sections for *stable* nuclei. Actually, for stable nuclei incident on a carbon target, there is a significant difference between real $\sigma_{\rm I}$ data and pseudo $\sigma_{\rm R}$ data even at relativistic energies (Fig. 1).

We find that this difference is consistent with the fact that $\sigma_{\rm I} < \sigma_{\rm R}$. From the figure, as expected, we find that the difference is mostly negative. The average of the difference over various projectiles is about −60.4 mb. This difference would lead to possible uncertainties of about 0–0.3 fm in estimates of nuclear matter radii if relying on the $\sigma_{\rm I}$ data alone.

† Condensed from the article in arXiv:0803.0187[nucl-th]

*1 Department of Natural Science, Kochi University
*2 Department of Media Theories and Production, Aichi Shukutoku University

References

1) A. Ozawa, T. Suzuki, and I. Tanihata: Nucl. Phys. **A693**, 32 (2001).
2) A. Kohama, K. Iida, and K. Oyamatsu: Phys. Rev. C **72**, 024602 (2005).

Neutron skin effect on proton pairing correlation

M. Yamagami and Y. R. Shimizu*1

[Neutron-rich nuclei, pairing correlation, rotational excitation]

The neutron skin effect on proton pairing correlation in neutron-rich Mg isotopes is investigated by the Woods-Saxon potential plus the Bogoliubov pairing model[1]. We emphasize the necessity of the isovector density dependence in the pairing effective force for the description of collective phenomena in neutron-rich nuclei.

In the present study, the pairing field is treated self-consistently by using the density-dependent contact interaction,

$$v^{\tau}_{pair}(\boldsymbol{r},\boldsymbol{r}') = V_0 \frac{1-P_\sigma}{2}\left[1-\eta\left(\frac{\rho^{\tau}_{*}(\boldsymbol{r};\varpi)}{\rho_0}\right)\right]\delta(\boldsymbol{r}-\boldsymbol{r}').$$

We extend the density dependence to $\rho^{\tau}_{*}(\boldsymbol{r};\varpi) = \rho(\boldsymbol{r}) + \tau_3\varpi\rho_1(\boldsymbol{r})$, instead of the usual isoscalar density $\rho(\boldsymbol{r}) = \rho_p(\boldsymbol{r}) + \rho_n(\boldsymbol{r})$. Here the isovector density is $\rho_1(\boldsymbol{r}) = \rho_n(\boldsymbol{r}) - \rho_p(\boldsymbol{r})$, $\tau_3 = 1(-1)$ for the neutron (proton) pairing force, and P_σ is the spin exchange operator. The parameters η and $\rho_0 = 0.16$ fm^{-3} control the density dependence, and the extra parameter ϖ represents the neutron skin effect in the pairing force.

The proton pairing gaps in $^{24-40}$Mg obtained using the surface ($\eta = 1.0$) and mixed ($\eta = 0.5$) pairing forces with $\varpi = 0.0$ and 0.5 are shown in Fig. 1. The result using the volume pairing ($\eta = 0.0$) is also plotted. The Woods-Saxon potential with fixed deformation $\beta_2 = 0.3$ is used for the p-h mean field.

Using the surface pairing force with $\varpi = 0.0$, the neutron and proton pairing gaps have the same value in ^{24}Mg. However, the proton gap suddenly becomes zero as the neutron number increases. This is attributed to the neutron skin effect. Since the proton-neutron pairing interaction is not included, the strong effect of the neutron skin on the proton pairing may not be reasonable. The isovector density dependence prevents the quenching of the proton pairing gap. The isovector density dependence is also important for the mixed pairing force, although the effect is not as large as that in the case of the surface pairing force.

The sensitivity to ϖ is much weaker in the neutron pairing, because the neutron density is dominant around the surface region. On the other hand, the neutron pairing is very sensitive to the isoscalar density dependence due to the different low-density effect on the pairing forces around the surface region[1].

To investigate the effect of the isoscalar and isovector density dependences of the pairing force on the rotational excitations, the energies of the 2^+ states are estimated by the formula $E(2^+) = 6\hbar^2/2\mathcal{J}$. The moment of inertia $\mathcal{J}$ is evaluated by the cranking formula.

*1 Department of Physics, Kyushu University

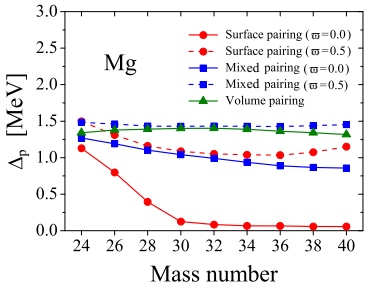

Fig. 1. Proton pairing gaps in $^{24-40}$Mg obtained with surface, mixed and volume pairing forces with $\varpi = 0.0$ and 0.5 are compared. The strengths V_0 are fixed so as to obtain the same neutron pairing gap in ^{30}Mg.

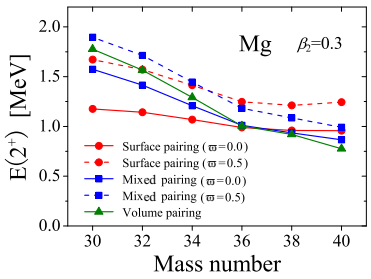

Fig. 2. Energies of the 2^+ states in $^{30-40}$Mg. The pairing force parameters are the same as those in Fig. 1.

As shown in Fig. 2, the 2^+ energies are almost constant in the case of the surface pairing. As the parameter η becomes smaller, the energies decrease rapidly due to the weakened neutron pairing around the neutron drip line. On the other hand, while maintaining the same systematic trend, the 2^+ energies shift toward higher energy with $\varpi \neq 0$.

The systematic information of the rotational 2^+ states can be utilized to explore the unique role played by the pairing correlation in neutron rich nuclei. It is also expected that the pairing properties around the neutron drip line can be used to determine the density dependence of the pairing force, which has not been well determined using the knowledge of the β-stable nuclei.

References

1) M. Yamagami and Y. R. Shimizu: submitted to Phys. Rev. **C** (2008).

Finite amplitude method for the RPA solution†

T. Nakatsukasa, T. Inakura,*1 and K. Yabana,*2

[Nuclear structure, random-phase approximation]

In order to describe the dynamical properties in the nuclear response to external fields, the random-phase approximation (RPA) is a leading theory applicable to both low-lying states and giant resonances. RPA is a microscopic theory and can be obtained by linearizing the time-dependent Hartree-Fock (TDHF) equation, or equivalently, the time-dependent Kohn-Sham equation in density-functional theory. The linearization produces a self-consistent residual interaction, $v = \delta^2 E[\rho]/\delta\rho^2$, where E and ρ are the energy-density functional and the one-body density, respectively. The standard solution of the RPA is based on the matrix formulation of the RPA equation, which involves a large number of particle-hole matrix elements of the residual interaction, $v_{ph',hp'}$ and $v_{pp',hh'}$. Since the realistic nuclear energy functional is rather complicated, it is very tedious and difficult to calculate all the necessary matrix elements. Although there have been numerous studies on HF-plus-RPA calculations, because of this complexity it has been common in practice to neglect some parts of the residual interactions. RPA calculations with full self-consistency are becoming a current trend in nuclear structure studies, however, they are only essentially for spherical nuclei at present. The applications to deformed nuclei are still very few. We propose a new practical method of solving the RPA equation in the self-consistent Hartree-Fock (HF) theory.

The basic idea of the present method is analogous to linear-response calculations in a time-dependent manner (real-time method)[1]. In the real-time method, the time evolution of a TDHF state involves only the action of the HF Hamiltonian, $h[\rho(t)]$, on single-particle orbitals, $|\psi_i(t)\rangle$ $(i = 1, \cdots, A)$. Although the real-time method is very efficient for obtaining nuclear responses in a wide energy range, its numerical instability caused by zero modes was a problem for linear-response calculations[1]. Zero-energy modes related to symmetry breaking in the HF state are easily excited, which often prevents the calculation of the time evolution for a long period. Therefore, it is desirable to develop a corresponding method in the frequency (energy) representation. This can be achieved by introducing a small parameter η and calculating the induced field as

$$\delta h(\omega) = \frac{1}{\eta}\left(h\big[\langle\psi'|, |\psi\rangle\big] - h[\langle\phi|, |\phi\rangle]\big)\right), \qquad (1)$$

where $\langle\psi'_i| = \langle\phi_i| + \eta\langle Y_i(\omega)|$ and $|\psi_i\rangle = |\phi_i\rangle + \eta|X_i(\omega)\rangle$. Its Hermitian conjugate, $\delta h^\dagger(\omega)$, may also be expressed as Eq. (1), but with $\langle\psi'_i| = \langle\phi_i| + \eta\langle X_i(\omega)|$ and $|\psi_i\rangle = |\phi_i\rangle + \eta|Y_i(\omega)\rangle$. Here, $|X_i(\omega)\rangle$ and $|Y_i(\omega)\rangle$ are forward and backward amplitudes, respectively.

Using this numerical differentiation, the RPA equations can be easily calculated by the action of the HF Hamiltonian. We employ a well-established iterative method to obtain their solutions (CGM/Bi-CGM). The most advantageous feature of the present approach is that it only requires operations of the HF Hamiltonian, $h\big[\langle\psi'|, |\psi\rangle\big]$. These operations are usually included in computational programs of the static HF calculations. The only extra effort necessary is to estimate the HF Hamiltonian with different bra and ket single-particle states, $\langle\psi'_i|$ and $|\psi_i\rangle$. Therefore, a minor modification of the static HF computer code will provide a numerical solution of the RPA equations. We name this numerical approach the finite amplitude method (FAM).

The accuracy of the FAM is tested for the BKN interaction. The BKN interaction is sufficiently simple for us to easily perform an exact RPA calculation. Figure 1 shows results calculated by the proposed method (FAM) and those using the exact RPA for a quadrupole-strength distribution in deformed ^{20}Ne. These two different calculations provide identical results. This proves that the numerical differentiation in the FAM is sufficiently accurate in practice.

References

1) T. Nakatsukasa and K. Yabana, Phys. Rev. C **71**, 024301 (2005).

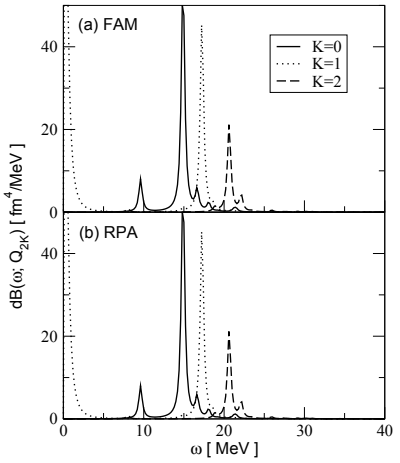

Fig. 1. Isoscalar quadrupole-strength distribution for ^{20}Ne, calculated by the FAM (a) and using the RPA (b).

† Condensed from the article in Phys. Rev. C **76**, 024318 (2007)

*1 Institute of Physics, University of Tsukuba
*2 Center for Computational Sciences, University of Tsukuba

Particle-number-projected thermal pairing*

N. Dinh Dang

[NUCLEAR STRUCTURE, thermal fluctuations, pairing, superfluid-normal phase transition, BCS theory, Richardson model, Lipkin-Nogami method, particle-number projection]

The BCS theory and its generalization, the Hartree-Fock-Bogoliubov (HFB) theory at finite temperature, describe well the superfluid-normal (SN) phase transition from the superconducting state to the normal one in infinite systems. However, when the BCS and HFB theories are applied to small systems such as atomic nuclei, modifications are required since the finiteness of the systems causes large quantal and statistical fluctuations, whose effects are ignored in these theories.

Quantal fluctuations (QF) within the BCS (HFB) theory include particle-number fluctuations. The latter exist even at zero temperature because of the violation of particle number in the BCS ground-state wave function. To eliminate this defect of the BCS (HFB) theory various methods of particle-number projection (PNP) have been proposed. These PNP methods are classified as the projection after variation (PAV) and variation after projection (VAP). In the PAV, the BCS (HFB) wave function is used to calculate the projected energy of the system, whereas the VAP determines the wave function by minimizing the projected energy. Among the VAPs, the one proposed by Lipkin and Nogami is quite popular because it is give a rather good description and, at the same time, is computationally simple albeit approximate.

Statistical fluctuations (SF) in the pairing field have been studied within the approaches based on Landau's (macroscopic) theory of phase transitions and the static-path approximation. The results of these studies show a nonvanishing pairing gap as a function of temperature in the presence of SF. The recently proposed modified BCS (MBCS) theory and its generation, the modified HFB (MHFB) theory[1)], take into account the effects due to quasiparticle-number fluctuations (QNF) based on a microscopic foundation. It has been shown for the first time within the MBCS theory that it is the QNF that smoothes out the sharp SN phase transition and leads to the nonvanishing thermal pairing in finite systems.

Since the effects of QF are still neglected within the MBCS (MHFB) theory, to give a conclusive answer to the question for SN phase transition in finite systems it is necessary to perform PNP in combination with the MBCS (MHFB) theory. This is done in the present paper by using the Lipkin-Nogami (LN) method and PAV. The calculations carried out within the Richardson model show that the PAV-MBCS theory offers predictions closer to the exact results than those obtained within the modified LN method for the pairing gap (See Fig. 1), energy of the system, and other thermodynamic characteristics such as heat capacity and entropies. The application to a realistic heavy nucleus ^{120}Sn with an open shell for neutrons shows small effects caused by PNP, which do not change the qualitative picture of smoothing out the sharp SN phase transition due to the QNF within the MBCS theory. It is now possible to confirm that the sharp SN phase transition in finite nuclei at finite temperature is smoothed out, and this is the consequence of the large QNF due to the finiteness of the system, as has been microscopically proved within the MBCS theory.

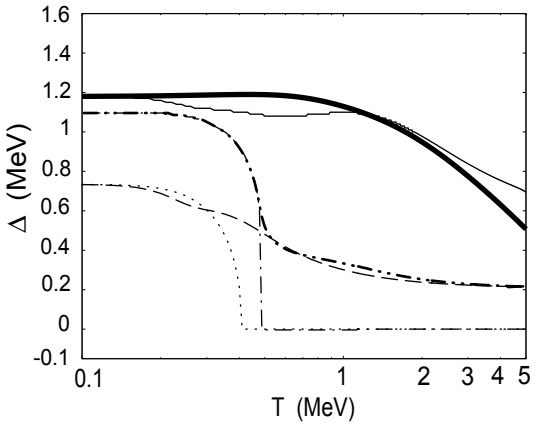

Fig. 1. Pairing gaps as functions of temperature obtained within the Richardson model for $\Omega = N + 1 = 11$ with the level distance equal to 1 MeV and pairing interaction parameter $G = 0.4$ MeV. The BCS and MBCS solutions are shown by the dotted and dashed lines, respectively. The results obtained within the LN and modified LN methods are denoted by the dot-dashed and double-dot-dashed lines, respectively. The thin solid line shows the PAV-MBCS effective gap $\Delta_{\rm PNP}$, while the thick solid lines stand for the exact result.

References

1) N. Dinh Dang and V. Zelevinsky, Phys. Rev. C 64, 064319 (2001); N. Dinh Dang and A. Arima, Phys. Rev. C 67, 014304 (2003); N. Dinh Dang and A. Arima, Phys. Rev. C 68, 014318 (2003); N. Dinh Dang, Nucl. Phys. A 784, 147 (2007).

* Condensed from Phys. Rev. C **76**, 064320 (2007).

Thermal pairing assisted by quasiparticle-number fluctuation

N. Dinh Dang and N. Quang Hung

[NUCLEAR STRUCTURE, thermal fluctuations, pairing, superfluid-normal phase transition, BCS theory, Richardson model, Lipkin-Nogami method, particle-number projection, quasiparticle RPA, neutron-rich isotopes.]

Because of its simplicity, the Bardeen-Cooper-Schrieffer (BCS) theory, which explains the conventional superconductivity, has been widely employed as the first step in nuclear structure calculations that include pairing forces. However, the application of the BCS theory to small systems such as atomic nuclei needs to be carried out with a certain care since quantal and thermal fluctuations are not negligible in finite systems, especially when the number of particles is small.

In the recently proposed self-consistent quasiparticle random-phase approximation (SCQRPA) for multilevel systems[1)], the derivation of the SCQRPA is based on a set of renormalized BCS equations. These equations include the corrections due to the quasiparticle-number fluctuation (QNF) and the SCQRPA. The latter come from the so-called screening factors, which are the expectation values $\langle \mathcal{A}_j^\dagger \mathcal{A}_{j'}^\dagger \rangle$ and $\langle \mathcal{A}_j^\dagger \mathcal{A}_{j'} \rangle$ in the correlated ground state. Here $\mathcal{A}_j^\dagger \equiv \alpha_j^\dagger \alpha_{-j}^\dagger$ is the product of two time-reversal conjugated quasiparticle operators, $\alpha_j^\dagger$ and $\alpha_{-j}^\dagger$, corresponding to the j-th orbital. The present study extends this approach to nonzero temperature T. The equations for the pairing gap and particle number, which include the effect of QNF at $T \neq 0$, are found within this approach as:

$$\Delta_j = G \sum_{j'} \left[\Omega_{j'} \langle \mathcal{D}_{j'} \rangle + 2\delta_{jj'} \frac{n_j(1-n_j)}{\langle \mathcal{D}_j \rangle} \right] u_{j'} v_{j'} \ , \quad (1)$$

$$N = 2 \sum_j \Omega_j \left[v_j^2 \langle \mathcal{D}_j \rangle + \frac{1}{2} \big(1 - \langle \mathcal{D}_j \rangle \big) \right] , \quad \Omega_j = j + \frac{1}{2} \ , \quad (2)$$

where $\langle \mathcal{D}_j \rangle = 1 - 2n_j$, $n_j = [\exp(\epsilon'_j/T) + 1]^{-1}$, $\epsilon'_j = \epsilon_j + \frac{G}{\sqrt{\Omega_j \langle \mathcal{D}_j \rangle}} \sum_{j'} \sqrt{\Omega_{j'}} (u_{j'}^2 - v_{j'}^2)(\langle \mathcal{A}_j^\dagger \mathcal{A}_{j'}^\dagger \rangle + \langle \mathcal{A}_j^\dagger \mathcal{A}_{j'} \rangle)$, and $\langle \ldots \rangle$ denotes the grand canonical ensemble average. This approach is called finite-temperature BCS1 (FTBCS1) theory to be distinguished from the usual FTBCS one. The coupling to quasiparticle-pair vibrations within the SCQRPA is carried out by using the method of double-time Green's functions. The particle-number violation is removed making use of the approximated projection within the Lipkin-Nogami (LN) method. The numerical calculations of pairing gaps, total energies, and heat capacities are performed within a double-fold equidistant multilevel model and realistic nuclei ^{56}Fe and ^{120}Sn. The results obtained show that, in the region of moderate and strong couplings, the sharp transition between the superconducting and normal phases is smoothed out, resulting in a thermal pairing gap, which does not collapse at the BCS critical temperature T_c, but has a tail, which extends to high T. The dynamic coupling of quasiparticles to SCQRPA vibrations significantly improves the agreement with the results of exact calculations and those obtained within the finite-temperature quantal Monte Carlo method for ^{56}Fe[2)]. The corrections given by the LN method to the pairing gap are significant only at low T (See Fig. 1).

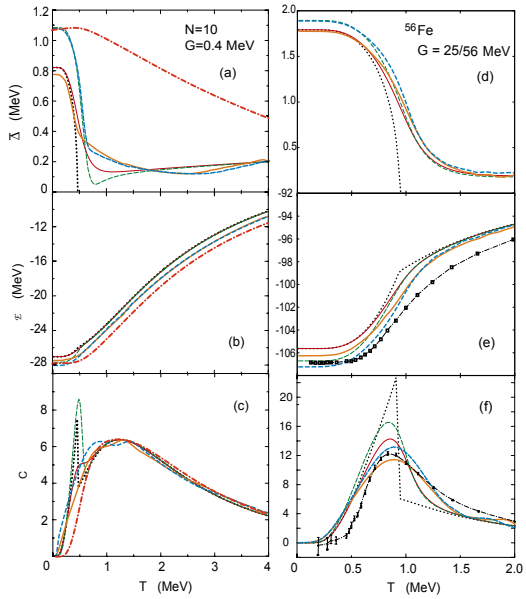

Fig. 1. Level-weighted pairing gaps $\bar{\Delta} \equiv \sum_j \Omega_j \Delta_j / \sum_j \Omega_j$, total energies $\mathcal{E} \equiv \langle H \rangle$, and heat capacities $C \equiv \partial \mathcal{E} \partial T$ as functions of temperature T, obtained for $N = 10$ [(a) – (c)], and ^{56}Fe [(d) – (f)]. The dotted, thin solid, thick solid lines show the FTBCS, FTBCS1, and FTBCS1+SCQRPA results, respectively. The predictions by the FTLN1 and FTLN1+SCQRPA are presented by the thin and thick dashed lines, respectively. The dash-dotted lines in (a) – (c) denote the exact results, whereas those in (e) and (f) stand for the predictions of the finite–temperature quantal Monte Carlo method.

References

1) N. Quang Hung and N. Dinh Dang, Phys. Rev. C **76**, 054302 (2007).
2) S. Rombouts, K. Heyde, and N. Jachowicz: Phys. Rev. C **58**, 3295 (1998).

Effects of thermal fluctuations and angular momentum on nuclear pairing properties

N. Quang Hung and N. Dinh Dang

[NUCLEAR STRUCTURE, angular momentum, thermal fluctuations, pairing, superfluid-normal phase transition, BCS theory.]

The effect of angular momentum on pairing correlations in nuclei at finite temperature T was studied in Ref.[1] within the BCS theory. For simplicity, the angular momentum projection M was introduced instead of the total one. The calculations carried out within the uniform model showed that, at $T = 0$, the pairing gap decreases as angular momentum M increases, and vanishes at the critical value M_c. This is the so-called Mottelson-Valatin effect. At a constant M value, the pairing gap decreases with increasing T, and collapses at the critical temperature T_c. However, at some values of $M \geq M_c$, there appears a temperature region $T_{c1} \leq T \leq T_{c2}$, in which the pairing gap reappears at $T = T_{c1}$, increases with T to reach a maximum, then decreases again to vanish at $T = T_{c2}$. This effect is so-called " anomalous pairing or thermally assisted pairing correlation ". In the formalism involving the BCS theory including the angular momentum, the effects of quantal and thermal fluctuations were neglected. However, these fluctuations are known to be significant in small systems such as nuclei.

Recently, an approach called the self-consistent quasiparticle random-phase approximation (SCQRPA) [2] has been proposed for a multilevel pairing model. Within this approach, the correlations due to the quasiparticle number fluctuations (QNF) and quantal fluctuations such as the QRPA are included into the equations for pairing gap and particle number. As the result, the total pairing gap, Δ_j, depends on levels and is divided into two parts. The first part, Δ, is the same as the BCS gap, while the second one, $\delta\Delta_j$, depends on levels and includes the QNF. This approach is called the BCS1 theory to be distinguished from the conventional BCS one. Very recently, it has been extended to finite temperature and called the FTBCS1 theory[3].

In the present work, we include the angular momentum M into the FTBCS1 equations to study its effects on thermal pairing in nuclei. The numerical calculations are carried out within a doubly degenerate equidistant model with a constant pairing interaction G.

The results obtained show that, at constant values of M, the pairing gaps given by the FTBCS1 theory do not collapse at T_c as predicted by the FTBCS one but decrease monotonously with increasing T and never vanish even at very high T (See Fig. 1-(a) and (c)). This feature is caused by the QNF. The effect of anomalous pairing is also seen within the FTBCS1 but

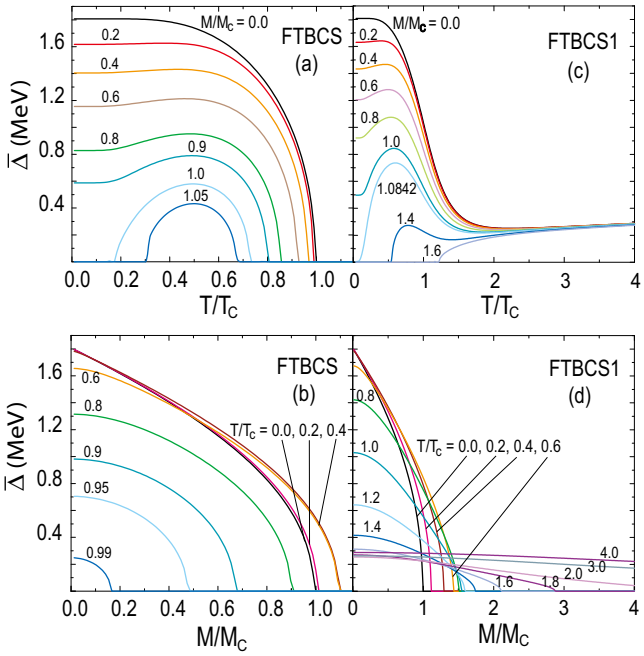

Fig. 1. Level-weighted pairing gaps as functions of T for various angular momentum projections M [(a),(c)] and as functions of M for various T [(b),(d)] obtained within the FTBCS (left) and FTBCS1 (right) using the doubly degenerate equidistant model for $\Omega = N = 10$ with the level distance equal to 1 MeV and constant pairing interaction parameter $G = 0.6$ MeV.

in such a way that the gap reappears at $T = T_{c1}$ and remains finite at $T > T_{c1}$ (See Fig. 1-(c)). At $T = 0$, the FTBCS and FTBCS1 pairing gaps for different M are the same because the QNF are zero in this case (See Fig. 1-(b) and (d)). However, the critical angular momentums M_c within the FTBCS1 are shifted up to higher values than those predicted by the FTBCS. At high T, the FTBCS1 pairing gaps are finite even at very high M (See Fig. 1-(d)).

References

1) L. G. Moretto: Phys. Lett. B **35**, 397 (1971); L. G. Moretto: Nucl. Phys. A **185**, 145 (1972).
2) N. Quang Hung and N. Dinh Dang: Phys. Rev. C **76**, 054302 (2007).
3) N. Dinh Dang and N. Quang Hung: submitted to RIKEN. Accel. Prog. Rep. **41** (2008).

Shape mixing in low-lying states of ^{68}Se and ^{72}Kr†

N. Hinohara,[*1] T. Nakatsukasa, M. Matsuo,[*2] and K. Matsuyanagi[*1]

[Nuclear structure, large-amplitude collective motion, proton-rich nuclei]

The shapes of nuclei along the $N = Z$ line change significantly as the numbers of protons and neutrons change. In ^{68}Se and ^{72}Kr, the ground and excited states corresponding to oblate and prolate shapes have been found experimentally. From the viewpoint of collective dynamics based on the mean-field theory, it is expected that the oblate and prolate shapes are mixed by the many-body tunneling effect through the potential barrier lying between two local minima in the potential energy landscape. The adiabatic self-consistent collective coordinate method[1] is a microscopic theory of large-amplitude collective motion based on the time-dependent Hartree-Bogoliubov (TDHB) theory, and enables us to extract the collective degrees of freedom (collective path) from the TDHB manifold under the assumption that the large-amplitude collective motion of interest is slow. Recently, the method has been rigorously formulated, in which the gauge invariance with respect to the particle number fluctuation degrees of freedom is taken into account (gauge-invariant ASCC method).[2]

We investigated the oblate-prolate shape coexistence/mixing phenomena in low-lying states of ^{68}Se and ^{72}Kr by the gauge-invariant ASCC method and the pairing-plus-quadrupole Hamiltonian including the quadrupole-pairing interaction. The collective path extracted by the ASCC method runs approximately along the valley that exists in the triaxially deformed region and connects the oblate and prolate local minima in the collective potential energy surface. The collective Hamiltonian that describes the coupled collective motion of the large-amplitude vibration responsible for the oblate-prolate shape mixing and the three-dimensional rotation of the triaxial shape is microscopically constructed in the collective subspace. The excitation spectra, the spectroscopic quadrupole moments, and the E2 transition properties of the low-lying states are calculated for the first time by the ASCC method. The calculation produces an oblate ground-state band and an excited prolate band. The basic pattern of shape coexistence/mixing phenomena are qualitatively reproduced using the one-dimensional collective path in the two-dimensional (β, γ) plane. It should be emphasized that the collective path, potential, and mass parameters are all self-consistently extracted from the many-dimensional TDHB manifold. We can conclude that the TDHB collective dynamics of the shape coexistence/mixing phenomena in these nuclei is essentially controlled by the single collective coordinate microscopically derived by the ASCC method.

It is also shown that the low-lying states can be reproduced significantly better by including the quadrupole pairing interaction. The reason for this is that the time-odd component of the mean field generated by the quadrupole pairing interaction enhances the collective mass of the vibrational motion and the moments of inertia of the rotational motion, which lowers the energy of the collective excitation. This component is included in the collective mass derived by the ASCC method, but it is ignored in the Inglis-Belyaev cranking mass.

The shape mixing in collective wave functions is analyzed. It is found that the shape mixing in collective wave functions attenuates as angular momentum increases. This implies that, even when the potential barrier is very low, the rotational dynamics play an important role in localizing the wave functions around the oblate and prolate minima at finite angular momenta ($I > 0$).

References

1) M. Matsuo, T. Nakatsukasa and K. Matsuyanagi: Prog. Theor. Phys. **103**, 959 (2000).
2) N. Hinohara, T. Nakatsukasa, M. Matsuo and K. Matsuyanagi: Prog. Theor. Phys. **117**, 451 (2007).

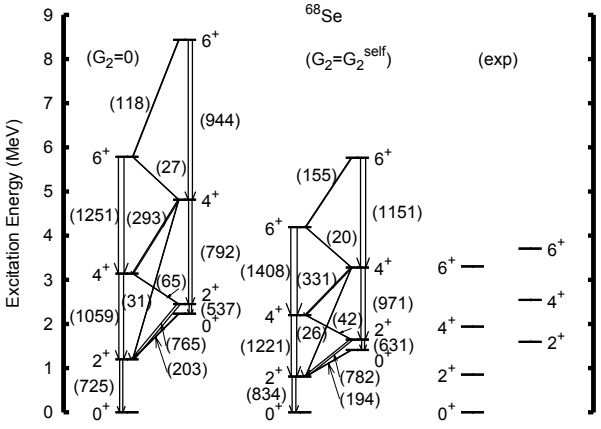

Fig. 1. Excitation spectra of low-lying states of ^{68}Se calculated by ASCC method, both neglecting (left) and including (middle) quadrupole pairing in microscopic Hamiltonian. Experimental data are shown in the right panel. The numbers in the parentheses indicate the values of B(E2) in units of $e^2\mathrm{fm}^4$.

† Condensed from the article in Prog. Theor. Phys. **119**, 59 (2008)

*1 Department of Physics, Kyoto University
*2 Department of Physics, Niigata University

Correlation between eigenenergies and sorted diagonal elements of a large dimensional hamiltonian matrix

N. Yoshinaga [*1] and A. Arima[*2]

[Shell model, matrix diagonalization, Gaussian orthogonal ensemble]

Most many-body problems are reduced to problems of how to obtain eigenenergies of a large dimensional hamiltonian matrix. However, eigenenergies of a large dimensional hamiltonian matrix are quite difficult to obtain. There are various methods to obtain eigenenergies. One is the exact diagonalization of a matrix. Usually, the Lanczos method is quite practical to obtain a few lowest energies, but the dimension of the matrix is limited up to 10^8 even using big computers. The Monte Carlo method is one of the promising methods and attract considerable attention, although it takes a lot of computational time. Recently, we have found an approximate strong linear correlation between eigenenergies and matrix elements $(h_{ii}, i = 1, \ldots, D)$ sorted according to values from smaller to larger ones $(h_{11} < h_{22} < \ldots < h_{DD})$ where D is the dimension of the matrix.[1)] Here, we have in mind the matrices of two-body shell model interactions and Gaussian orthogonal ensemble. Using the linear relation between eigenenergies and diagonal matrix elements, we can statistically obtain much eigenenergies without any diagonalization of the hamiltonian. First, let us assume the functional dependence of the eigenenergy E_i in terms of sorted diagonal elements h_{ii}. Namely, we assume that the functional relation $E_i = f(h_{ii})$ holds statistically. Since the number of states for a given energy interval is the same for both eigenenergies and diagonal elements, we have the relation,

$$\mathrm{P}(E_i)\, dE_i = \rho(h_{ii})\, dh_{ii}, \tag{1}$$

where $\mathrm{P}(E_i)$ and $\rho(h_{ii})$ are the density of states for E_i and h_{ii}, respectively. Immediately, we have the differential equation,

$$\mathrm{P}(E_i)\, f'(h_{ii}) = \rho(h_{ii}), \tag{2}$$

where $f'(h_{ii}) = \frac{dE_i}{dh_{ii}}$. Once $\mathrm{P}(E_i)$ and $\rho(h_{ii})$ are given, Eq. (2) can be solved.

Realistic two-body interaction. The eigenenergies for a realistic two-body shell model interaction are known to follow the Gaussian distribution.[2)] In this case, it is natural to assume that we have

$$\mathrm{P}(E) = \frac{D}{\sqrt{2\pi}\Sigma} \exp\left[-\frac{\left(E-\overline{E}\right)^2}{2\Sigma^2}\right], \tag{3}$$

and

$$\rho(h) = \frac{D}{\sqrt{2\pi}\sigma} \exp\left[-\frac{\left(h-\overline{h}\right)^2}{2\sigma^2}\right]. \tag{4}$$

Then, Eq. (2) is easily solved to give a linear function,

$$E_i = a h_{ii} + b, \tag{5}$$

where $a = \frac{\Sigma}{\sigma}, b = -\frac{\Sigma}{\sigma}\overline{h} + \overline{E}$.

Gaussian orthogonal ensemble. In this case, the distribution of diagonal matrix elements for dimension D matrix is given as

$$\rho(h) = \frac{D}{\sqrt{2\pi}\sigma} \exp\left[-\frac{h^2}{2\sigma^2}\right]. \tag{6}$$

The distribution of eigenenergies is given as

$$\mathrm{P}(E) = 1/\pi\sqrt{A^2 - E^2}, \tag{7}$$

where we have $A = 2D$. The lowest eigenenergy is given as $E = -\sqrt{D} = -\sqrt{2N}$. Assuming the functional dependence, the differential equation becomes

$$\frac{D}{\sqrt{2\pi}} \exp\left[-\frac{h^2}{2}\right] = 1/\pi\sqrt{A^2 - (f(h))^2}\, f'(h). \tag{8}$$

By integrating, we have

$$\frac{D}{\sqrt{2\pi}} \int_{-\infty}^{h} \exp\left[-\frac{h^2}{2}\right] dh =$$

$$\frac{D}{\pi}\left[\left(\arcsin\left(\frac{f}{A}\right) + \frac{\pi}{2}\right) + \frac{f}{A}\sqrt{1 - \left(\frac{f}{A}\right)^2}\right]. \tag{9}$$

It turns out that the solution is well-simulated using a hyperbolic function.

In this paper, we have shown the functional dependences of eigenenergies as functions of sorted diagonal elements for realistic nuclear shell model (NSM) hamiltonian (soft chaotic case) and the GOE hamiltonian (hard chaotic case). In the NSM case, the function is approximately linear, while it is simulated as a hyperbolic-tangent function in the GOE case as the dimension of the matrix approaches infinity. Most many-body problems in many physical fields are reduced to eigenvalue problems for given Hamiltonians. It is expected that the present method statistically provides a useful tool for studying many-body problems.

[*1] Department of Physics, Saitama University
[*2] Science Museum, Japan Science Foundation

References

1) J. Shen, A. Arima, Y. Zhao N. Yoshinaga: to be submitted.
2) T. A. Brody, J. Flores, J. B. French, P. A. Mello, A. Pandey, and S. S.Wong: Rev. Mod. Phys. **53**, 385 (1981).

A simple description of doublet bands in mass around 100

K. Higashiyama[*1] and N. Yoshinaga[*2]

[Nuclear structure, quadrupole coupling model, chopsticks configurations]

The $\Delta I = 1$ doublet bands built on the $\nu h_{11/2} \otimes \pi h_{11/2}$ configuration in doubly-odd nuclei around the mass $A \sim 130$ were investigated in terms of the pair-truncated shell model.[1,2] The calculations reproduce well the experimental energy levels and ratios $B(M1; I \rightarrow I-1)/B(E2; I \rightarrow I-2)$ for the yrast states. The analysis of the wave functions reveals a new band structure, which results from the chopsticks configurations of two angular momenta of the unpaired neutron and the unpaired proton, weakly coupled with the quadrupole collective excitations of the even-even core.

To confirm their structure, we have recently proposed a much simpler model, the quadrupole coupling model (QCM).[3,4] In the model, a system of one neutron in the orbital j_ν and one proton in the orbital j_π is specified as the state $|j_\nu j_\pi; L\rangle$, where L is the angular momentum of the two-particle state. The collective-core state is denoted as $|R\rangle$, where R indicates the angular momentum of the core state. A total wave function of any doubly-odd nucleus is written as a product of the collective-core state and the two-particle state,

$$|\Phi(RL; I)\rangle = [|R\rangle \otimes |j_\nu j_\pi; L\rangle]^{(I)}, \qquad (1)$$

where I is the total spin. The model Hamiltonian employed in the present calculation consists of the Hamiltonian of the collective core and the quadrupole-quadrupole interactions between the collective core, the neutron, and the proton. In this work, we apply the QCM to the $\Delta I = 1$ doublet bands with the $\nu h_{11/2} \otimes \pi g_{9/2}$ configuration in the mass $A \sim 100$ region.

In Fig. 1, we compare the theoretical energy levels of the QCM with the experimental data for ^{106}Rh. In the experiment, the 6_1^- state appears to be lower in energy than the 8_1^- state. In the QCM calculation, this state is predicted to be higher in energy than the 8_1^- state. For the yrast states with spins greater than 7, the calculated energy levels are in excellent agreement with the experiment. Concerning the yrare states, the QCM calculation reproduces the observed levels at correct positions.

In Fig. 2, we compare the theoretical ratios $B(M1; I \rightarrow I-1)/B(E2; I \rightarrow I-2)$ for the yrast states with the experimental values. The theoretical result gives a successful description of the large-amplitude staggering of the $B(M1)/B(E2)$ ratios.

By analyzing the QCM wave functions, it is found

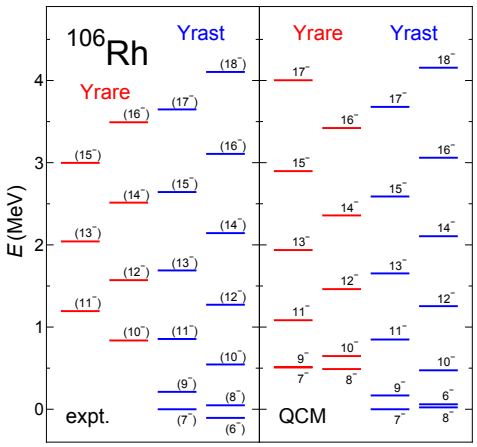

Fig. 1. Experimental energy levels of ^{106}Rh (expt.) compared with those of the QCM calculation.

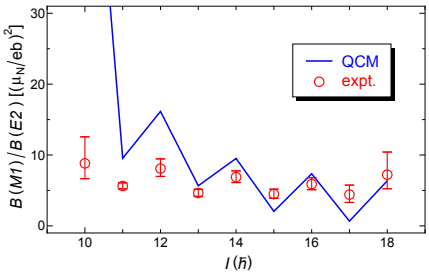

Fig. 2. Comparison of the $B(M1; I \rightarrow I-1)/B(E2; I \rightarrow I-2)$ ratios in the QCM with the experimental data (expt.).

that the main structure of the $\Delta I = 1$ doublet bands in the mass $A \sim 100$ region is described in terms of a weak coupling of the chopsticks configurations of two angular momenta of the unpaired nucleons, to the quadrupole collective excitations of the core. The excitation mechanism of these doublet bands is very similar to that in the mass $A \sim 130$ region predicted in the previous studies.[1–4]

*1 Department of Physics, Chiba Institute of Technology
*2 Department of Physics, Saitama University

References

1) K. Higashiyama and N. Yoshinaga: Prog. Theor. Phys. **113**, 1139 (2005).
2) K. Higashiyama, N. Yoshinaga, and K. Tanabe: Phys. Rev. C **72**, 024315 (2005).
3) N. Yoshinaga and K. Higashiyama: Eur. Phys. J. A **30**, 343 (2006); **31**, 395 (2007).
4) K. Higashiyama and N. Yoshinaga: Eur. Phys. J. A **33**, 355 (2007).

GCM description of rotational motions in ^{182}Os

Y. Hashimoto*1 and T. Horibata*2

[3D-CHFB, tilted-axis rotation, generator coordinate method]

In the past two decades, experimentalists have accumulated data that support the theoretical assumptions of the existence of general types of nuclear rotational motion.[1] When the axial symmetry is lost in the nuclear mean field, a general type of rotational motion occurs, in which the rotational axis is not parallel to the principal axis (PA) with the largest moment of inertia but fluctuates around the PA,[2,3] which is called the wobbling motion. ¿From a theoretical viewpoint, a much more general type of rotation is expected, where the rotational axis is located away from any of the principal axes.[4,5] This is called tilted-axis rotation (TAR).[6] The three-dimensional cranking model plays a central role in the study of the wobbling motion and TAR.

To clarify the microscopic mechanism of the general type of nuclear rotational motion, we studied the osmium nucleus ^{182}Os by the cranked Hartree-Fock-Bogoliubov (HFB) method and the generator coordinate method (GCM) on the basis of the HFB solutions. The model Hamiltonian used in the present calculation is the pairing plus quadrupole (P+QQ), as used in ref. 6. The parameters in the model Hamiltonian are the interaction strengths for the quadrupole-quadrupole and the pairing interactions, whose values are the same as those used in the previous calculations shown in ref. 7.

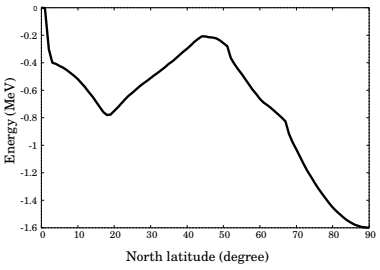

Fig. 1. Cranked-HFB energy with respect to tilt angle with angular momentum J = 24$\hbar$.

In Fig. 1, we show the energy curve with the angular momentum J = 24$\hbar$ when the axis of rotation is tilted from $\theta = 0°$ to 90°, where $\theta = 0°$ (90°) means that the axis of rotation is perpendicular (parallel) to the symmetry (z-) axis. Starting from the unstable ground band (g-band) state at $\theta = 0°$, we found a local minimum point at $\theta = 19°$, which is expected to be a "t-band" with K=8$\hbar$.[1] We found another minimum point at $\theta = 90°$. Since the energy curve has several points at which the first derivative of the curve with respect to the angle θ is discontinuous (e.g., $\theta = 3°, 42°, \cdots$), we might have structural changes in the nucleus at the points on the curve.

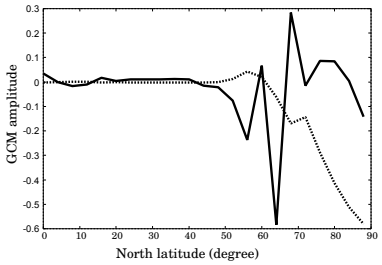

Fig. 2. Amplitudes of the two GCM solutions with the lowest (dotted curve) and the second lowest (solid curve) energies. Angular momentum is J = 24$\hbar$.

We carried out the GCM calculation on the basis of the HFB solutions along the energy curve in Fig. 1. In Fig. 2, we show the amplitudes of the two GCM solutions with the lowest and the second lowest energies. The lowest energy solution (dotted curve) shows that the HFB local minimum solution at the angle θ =90° is stable. On top of the stable HFB solution at the angle θ =90°, we find a GCM solution (solid curve) suggesting the existence of an excited state, which is expected to be a precession mode.[8] The quantum mechanical investigations on the excitational modes in terms of the GCM, including the cases with much larger amplitudes built on the set of distinctive structures pointed above, are now in progress.

*1 Graduate School of Pure and Applied Sciences, University of Tsukuba, Tsukuba, Ibaraki 305-8571, Japan
*2 Department of Software and Information Technology, Aomori University, Aomori, Aomori 030-0943, Japan

References

1) For example, P. M. Walker et al.: Phys. Lett. B309, 17 (1993).
2) A. Bohr and B. R. Mottelson: *Nuclear Structure*, Vol.II (Benjamin, Reading, MA, 1975).
3) S. Frauendorf: Rev. Mod. Phys. 73, 463 (2001).
4) A. K. Kerman and N. Onishi: Nucl. Phys. A361, 179 (1981).
5) N. Onishi: Nucl. Phys. A456, 279 (1986).
6) T. Horibata and N. Onishi: Nucl. Phys. A596, 251 (1996).
7) T. Horibata, M. Oi, N. Onishi, and A. Ansari: Nucl. Phys. A646, 277 (1999); A651, 435 (1999).
8) Y. R. Shimizu, M. Matsuzaki, and K. Matsuyanagi: Phys. Scr. T125, 134 (2006).

Existence of a one-body barrier revealed in deep subbarrier fusion†

T. Ichikawa, K. Hagino,*1 and A. Iwamoto*2

[Fusion reactions, coupled-channel model, medium-mass nuclei]

For medium-heavy mass fusion reaction at deep subbarrier energies, experimental fusion cross sections steeply fall-off, as compared with those calculated using the standard coupled-channel (CC) model.[1] Those unexpected deviations, referred to as the fusion hindrance, have been systematically observed below a certain threshold incident energy, which depends on a colliding system. The physical origin of the steep fall-off has not yet been understood.

One important aspect of the deep subbarrier fusion is that the inner turning point of the Coulomb barrier is smaller than the touching point for projectile and target. That is, the projectile and target overlap with each other in the classically forbidden region, and the composite system formed should penetrate through the residual Coulomb barrier. From this viewpoint, the threshold incident energies correlate with the potential energy at the touching point, $V_{\rm Touch}$, because the density overlap takes place at incident energies below $V_{\rm Touch}$.

In this respect, we systematically evaluated the potential energies at the touching point using various phenomenological potential models, and showed that the touching energy $V_{\rm Touch}$ indeed clearly correlates with the experimental threshold incident energies $E_{\rm s}$ estimated by Jiang *et al.* This result indicates that the steep fall-off of fusion cross sections can be attributed to the overlapping of the target and projectile nuclei.

To describe this, we propose a two-step model that phenomenologically supplements the standard CC model. That is, the two-step model consists of the capture process calculated using the standard CC model until the colliding nuclei contact each other, which is followed by the penetration of the residual potential in the overlap region to reach a compound state. The latter works only at incident energies below $V_{\rm Touch}$. Details of this model are discussed in ref. 5. The fusion cross section is, then, given by

$$\sigma(E) = \frac{\pi\hbar^2}{2\mu E}\sum_{\ell}(2\ell+1)T_{\ell}(E)P_{\rm 1bd}(E,\ell), \qquad (1)$$

where μ and E denote the reduced mass and the incident energy in the center-of-mass system, respectively. T_ℓ is the capture probability for the two-body process, which is calculated using the computer code `CCFULL`[2]. $P_{\rm 1bd}$ is the penetrability of the potential in the overlap region, which is calculated using the WKB approximation with the coordinate-dependent inertia mass.

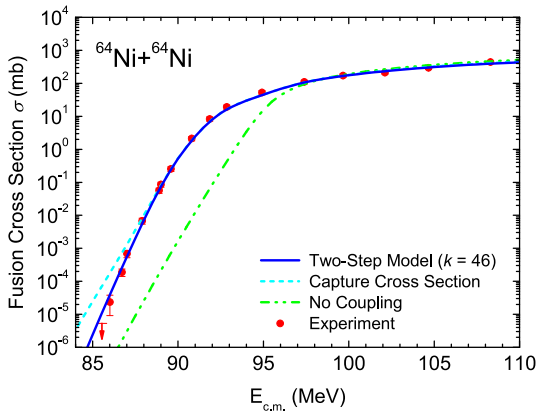

Fig. 1. Fusion cross sections for the ^{64}Ni+^{64}Ni reaction calculated using the two-step model. The filled circles denote the experimental fusion cross section, taken from ref. 1. The solid line denotes the fusion cross section. The dashed line denotes the corresponding capture cross section. The dash-dot-dotted line shows the result in the absence of the channel coupling effect.

For nuclear shapes and densities in the overlap region, we assume neck formations between the target- and projectile-like nuclei, on the basis of the macroscopic fission approach. We describe the shapes using the Lemniscatoids parametrization[3] and calculate the potential energies using the Yukawa-plus-exponential model.[4] For the inertia mass, we employ the irrational-flow mass calculated using the Werner-Wheeler approximation.

Figure 1 shows the fusion cross section for the ^{64}Ni+^{64}Ni reaction thus obtained. The result of the two-step model, denoted by the solid line, is consistent with the experimental data. We conclude that the overlaps between the colliding nuclei are responsible for the steep fall-off of the fusion cross section. In this way, the two-step model can naturally explain not only the fusion cross section but also the threshold incident energy.

References

1) C. L. Jiang et al.: Phys. Rev. Lett. **93**, 012701 (2004).
2) K. Hagino et al.: Phys. Commun. **123**, 143 (1999).
3) G. Royer et al.: J. Phys. **G8**, L159 (1982).
4) H. J. Krappe et al.: Phys. Rev. C **20**, 992 (1979).
5) T. Ichikawa et al.: Phys. Rev. C **75**, 057603 (2007).

† Condensed from articles in Phys. Rev. C**75**, 057603 (2007) and Phys. Rev. C**75**, 064612 (2007).

*1 Department of Physics, Tohoku University
*2 Japan Atomic Energy Agency

3. Hadron Physics

Measurement of direct photon via internal conversion in $\sqrt{s} = 200$ GeV p+p collisions at RHIC-PHENIX

Y.L. Yamaguchi,[*1] Y. Akiba,[*2] A. Toia,[*3] T. Dahms,[*3] T. Gunji,[*1] F. Kajihara[*1] and H. Hamagaki,[*1]

[Direct photon, Internal conversion, Low pT]

Direct photon is a unique probe to investigate properties of Quark Gluon Plasma (QGP) since photons penetrate a dense and hot partonic matter created by heavy ion collisions. Special interest is given to thermal photons from the QGP which are considered to be the primary contributor at the low energy region in the inclusive photon spectrum[1].

A measurement of 'real' direct photon using an electromagnetic calorimeter is notoriously difficult in the energy region below 4 GeV since the systematic errors can not be reduced due to a large hadron background, particularly π^0. Recently an alternative method using a 'virtual' direct photon measurement via internal conversion was demonstrated to provide the photon yield with less systematic error in Au+Au collisions[2]. For e^+e^- pairs from virtual photon decays can be obtained by a drift chamber with a reliable estimation of components from hadronic decays using the Kroll–Wada formula[3]. The same method is applicable to the direct photon yield in p+p collisions, which serves as a vital reference to the direct photon yield in Au+Au collisions. Current status of the analysis in $\sqrt{s} = 200$ GeV p+p collisions at RHIC-PHENIX is provided in this report.

One of the most important points in this analysis is to compare a ratio of the yield in a proper mass window to that in a very low mass region such as 0 to 30 MeV between the real mass spectrum and the hadronic decayed mass spectrum calculated by the Monte Carlo calculation. If any excess over the calculation is observed, it indicates the evidence of direct photon.

For real events, the correlated pair mass spectrum is obtained after combinatorial background subtraction using an event mixing method. However the contribution of cross pairs from $\pi^0, \eta \rightarrow 2\gamma(\text{or } \gamma e^+e^-) \rightarrow e^+e^-e^+e^-$ and double Dalitz decay cannnot be subtracted since they are correlated. Thus the cross pair contribution is considered in simulation as well as the other effects on real data such as eID efficiency, geometrical acceptance and momentum smearing in the low pT region. The systematic errors from different sources are listed in Tab. 1. Finally we obtain the ratios of the yield in 90–300 MeV to that in 0–30 MeV for both real and simulated hadronic component. Figure 1 shows the ratios of the yield for real and simulated hadronic component as a function of pT. The obtained ratios are almost consistent. Then a ratio of the direct photon yield to the inclusive photon yield (R_{γ^*}) are calculated from the obtained ratios as shown in Fig. 2. This result shows there might be a small amount of the direct photon in p+p collisions.

Table 1. Systematic errors from different sources.

Source	Sys.Error
eID efficiency	8%
acceptance	6%
cross pairs	6%
particle ratio	7%

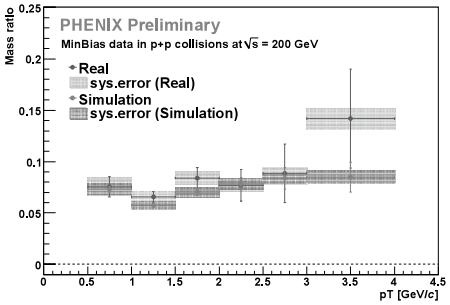

Fig. 1. The ratios of the yield in 90–300 MeV to that in 0–30 MeV for real and simulated hadronic component.

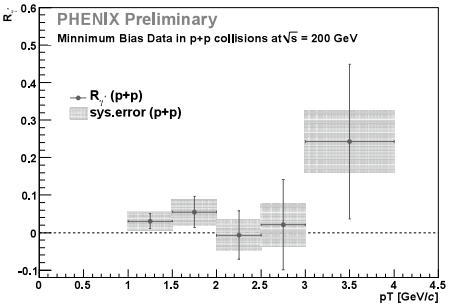

Fig. 2. The ratio of the direct photon yield to the inclusive photon yield in p+p collisions.

We hope to finalize soon the result in p+p collisions with more statistics. Hence, the comparison of the direct photon yield in p+p and Au+Au collisions will become possible.

*1 Center for Nuclear Study (CNS), University of Tokyo
*2 RIKEN (The Institute of Physical and Chemical Research)
*3 Department of Physics and Astronomy, Stony Brook University, SUNY

References

1) S. Turbide, *et al.,*: Phys. Rev. C **69** 014903 (2004).
2) Y. Akiba for the PHENIX collaboration: RIKEN Accel. Prog. Rep. **39**, 190 (2006).
3) N.M. Kroll and W. Wada: Phys. Rev. **98** 1355 (1955).

Measurement of ω mesons via radiative decay mode in $\sqrt{s_{NN}}$=200GeV Au+Au collisions at RHIC-PHENIX

M.Ouchida*[1]

The measurement of low-mass vector mesons under extreme conditions created by relativistic heavy-ion collisions is an intriguing study being carried out as a part of the quest to observe the QCD phase transition to quark gluon plasma. Properties such as the mass and width of vector mesons are expected to be modified at low p_T which can be used as a probe of the chiral symmetry restoration. Furthermore, hadron suppression due to jet quenching which is considered to be an effect of QGP, should be observed in the spectra of vector mesons.

We measured ω mesons ($782\mathrm{GeV/c^2}$)[1)] via the radiative decay mode ($\omega \rightarrow \pi^0\gamma$, $\pi^0 \rightarrow 2\gamma$) in $\sqrt{s_{NN}}$=200GeV Au+Au collisions at RHIC-PHENIX. The main challenge of this analysis is to handle the huge combinatorial background necessary for reconstructing particles from the three-body decay mode. The focus of the analysis is on a feasibility study using both simulation and real data to search for the optinal parameters that improve $S/\sqrt{B}$. For example, the momentum and energy range of π^0 and γ are optimized to reconstruct ω. To estimate the remaining background, we consider three background sources, correlated and uncorrelated backgrounds (BG2 and BG1, respectively) and the K_s^0 contribution (BG3), then each amount of background is determined by fitting. The total background can be successfully subtracted from the foreground as shown in Fig. 1.

*1 Hiroshima University

The ω invariant yield is defined as

$$E\frac{d^3N}{dp^3} = \frac{1}{BR \cdot N_{evt}} \cdot \frac{1}{2\pi\epsilon p_T} \cdot \frac{dN_\omega^{meas}}{dp_T dy}, \qquad (1)$$

where BR is the branching ratio (8.92 %)[1)], N_{evt} is the number of events for each centrality, ϵ is the total efficiency and N_ω^{meas} is the number of measured ω mesons.

To evaluate the efficiency ϵ, we performed a single ω event simulation using event generators based on Monte Carlo codes. The PHENIX implementation of the GEANT-based simulation and the event particle tracking software system, PISA were used to consider the detector response.

The results for ω meson production for each *centrality* (the value used to characterize the heavy-ion collisions) is shown in Fig. 2. Lines represent estimated yields from p+p collisions scaled by the number of collisions without a nuclear matter effect. The figure suggests that data points become lower than the lines for higher centrality, i.e., hadron suppression.

In summary, we were able to extract ω via the radiative decay mode in Au+Au by overcoming the huge combinatorial background by applying an optional cut and the subtraction of multiple backgrounds. The result suggests that ω meson production might be suppressed in central Au+Au collisions at high p_T region.

References

1) Particle Data Group; J. Phys. **G33**, 1 (2006).

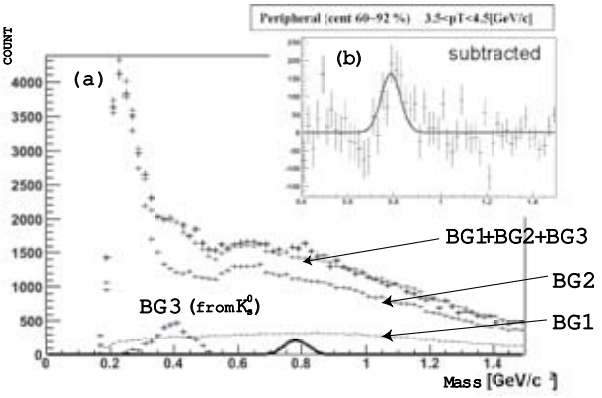

Fig. 1. (a) Invariant mass spectra of 3 γ. Three background sources, BG1, BG2 and BG3, are shown with the foreground. Solid Gaussian lines denote ω peaks when the mean and width are fixed values extracted by the simulation. (b) After subtracting BG1+BG2+BG3 from the foreground. The solid line is the fitted function when the mean and width are fixed.

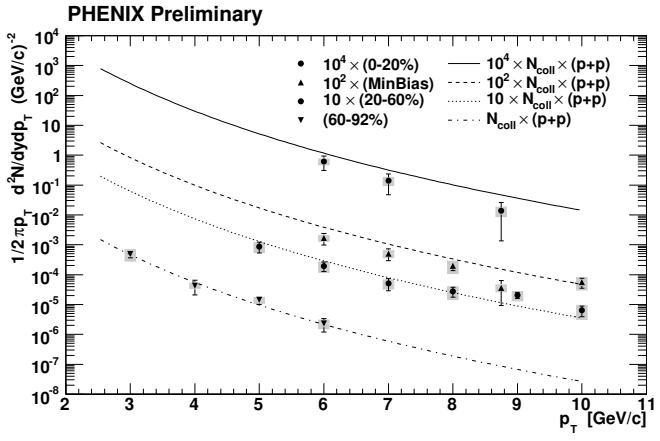

Fig. 2. ω meson production in Au+Au. The centrality increases from the bottom to the top. The minimum bias trigger (MinBias) is the trigger accepting 92% of the geometrical cross section.

Azimuthal anisotropy measurement of direct photon in $\sqrt{s_{NN}} = 200$ GeV Au+Au collisions at RHIC-PHENIX

K. Miki *1

[PHENIX, RHIC, QGP, Direct Photon, Flow]

In the heavy-ion collision experiment at the Relativistic Heavy-Ion Collider (RHIC), strong suppression is observed at high transverse momenta (p_T) hadron yields in central Au+Au collisions compared with p+p collisions when using the scaling law of the number of binary nucleon-nucleon collisions[1]. The observed high-p_T suppression is attributed to the energy loss of hard-scattered partons passing through the high-density matter[2]. On the other hand, the non suppression of the high-p_T direct photon (non hadronic decay photon) yield is observed in $\sqrt{s_{NN}} = 200$ GeV Au+Au collisions[3]. Since photons do not interact strongly with other particles, they have a long mean free path and can thus provide information on the states in which they were emitted.

Although the measurements of direct photons as penetrating probes allow us to more reliably study hot and dense matter, there are many photon sources in addition to hard-scattered photons in heavy-ion collisions. In non central collisions, the collision region is expected to have spatial anisotropy, and have an ellipsoid shape. Different pressure gradients and particle densities of the participants cause different anisotropies of the particle emission, depending on the production processes of photons. Therefore, the azimuthal anisotropy parameter v_2 is a powerful tool for exploring the source of direct photons.

The second harmonic coefficient parameter v_2 of the azimuthal distribution of the particles produced in heavy-ion collisions is defined by

$$\frac{dN}{d\phi} \propto 1 + 2v_2 \cos(2(\phi - \Phi_{RP})), \tag{1}$$

where ϕ is the emission angle of the particle and Φ_{RP} is the direction of the reaction plane, which is determined by another anisotropy existing in the forward particle flow. If more particles are emitted in the minor-axis direction of the ellipsoid, v_2 should have a positive sign. The photons resulting from initial Compton-like hard scattering are expected to exhibit a zero v_2 if they do not interact with the hot dense matter. The v_2 of photons from parton fragmentation are expected to have a similar v_2 to hadrons because of the suppression of high-p_T hadrons. On the other hand, the photons resulting from the energy loss of parton jets in the hot dense medium caused by Bremsstrahlung should negative v_2, because the partons emitted in the direction of the major ellipsoidal axis of the collision region should produce more Bremsstrahlung photons.

The anisotropy of direct photons ($v_2^{\mathrm{dir.}}$) is defined as hadron decay photons v_2 (v_2^{decay}) subtracted from all of the measured photons v_2 ($v_2^{\mathrm{inc.}}$) with each the number of measured photons as weight. v_2 for direct photons is estimated from Eq.(2),

$$v_2^{\mathrm{dir.}} = \frac{(N^{\mathrm{inc.}}/N^{\mathrm{decay}}) \cdot v_2^{\mathrm{inc.}} - v_2^{\mathrm{decay}}}{(N^{\mathrm{inc.}}/N^{\mathrm{decay}}) - 1} \tag{2}$$

Figure 1 shows v_2 for π^0 and direct photons as a function of p_T (0 to 10 [GeV/c]). The strong suppression of neutral hadrons by the jet-quenching effect makes it possible to extract v_2 for direct photons when $p_T > 4$ GeV/c. v_2 for direct photons is found to be consistent with a value of zero within statistical and systematic errors. This result supports the hypothesis that the most effective part of direct photons originates from initial Compton-like hard scattering. To study the effect of another emission source, it is necessary to perform more detailed calculations with larger samples and compare the results with other analysis results.

References
1) K. Adcox et al. : Phys. Rev. Lett. **88**, 022301 (2002).
2) S. S. Adler et al. : Phys. Rev. **C76**, 034904 (2007).
3) S. S. Adler et al. : Phys. Rev. Lett. **94**, 232301 (2005).

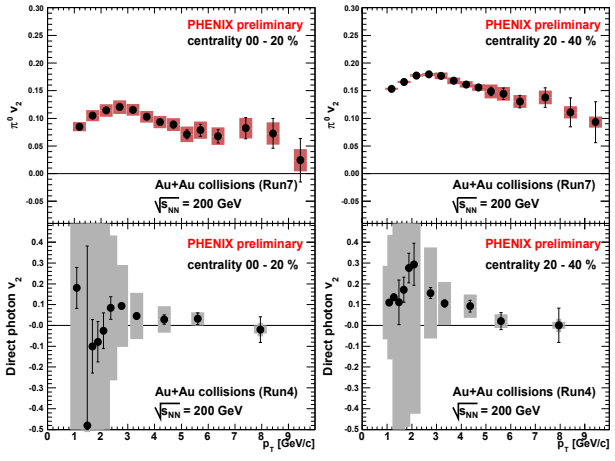

Fig. 1. v_2 for π^0 and direct photons as a function of p_T. Black bars show the statistical error and boxes show the systematic error. $\pi^0 v_2$ is estimated using the Run7 data set (new plot) using the RXNP detector (new detector).

*1 Graduate school of Pure and Applied sciences, University of Tsukuba

PHENIX's Central Track Beam Shift and Momentum Scale Corrections on Run-06's $\sqrt{(s)} = 200$ pp Collisions

A. Morreale,*1

1 Introduction

The inner PHENIX charged tracking system consists of Drift Chambers (DC) and Pad Chambers (PC1), which measure charged particle trajectories in the θ and ϕ direction to thus obtain 3 momentum of the particle. The DC are cylindrically shaped and located in the region from 2 to 2.4 m from the collision point and 2 m along the beam direction. This places them in a residual magnetic field with a maximum of 0.6 kG. [1] Since there is no magnetic field tracking within the DC and the PC region, charged tracks in the central spectrometers are reconstructed assuming a collision vertex in the geometrical center of the detector. Hit associations in the DC and PC1 in conjunction with a track reconstruction model is used to associate hits within a window of the track. In order to obtain accurate momentum reconstruction of charged tracks, offline corrections are made to the collision vertex. Displacement of the collision vertex from the detector's center can be caused by shift of the beam axis, or detector misalignment as the central spectrometres can roll in the x direction during detector access periods and normal beam operations. This vertex displacement (offsets) affect the x and y coordinates as these are related to the r-ϕ slope which are in turn used during momentum track reconstruction.[1]

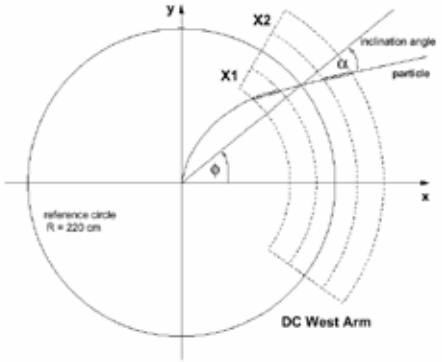

Fig. 1. Charged tracking in the detector region is calculated by using a hough transform of the tracks left by passing particles in the drift chamber, an assumption made is that the track is straight in the detector region.

*1 Department of Physics, University of California at Riverside

2 Beam Shift Calibration Procedure

To calculate the amount the collision vertex which is off-centered in the data taken during 2006 proton proton running, zero magnetic field runs were studied. These runs are taken under zero magnetic field settings in the PHENIX detector, therefore charged particles will not bend. To center the distribution of the shifted vertex of the expected straight tracks, the α and ϕ of charged tracks recorded on the drift chamber was studied. Since tracks are expected to be straight in the central arms, and any ϕ-dependance of the measured track's azimuthal angle (α) gives an indication and a numerical measurement of the offsets in x (XOffset) and y (YOffset).

Two main components were corrected in this analysis: an actual beam shift and a misalignment caused by the detector central arms being moved. A beam shift is indicated by an YOffset and XOffset different than zero but in equal magnitude in east and west arms. An non-zero XOffset that has different magnitudes in the west and east arms, is an indication of a detector misalignment. Corrections to both effects are done. In addition, a momentum scale correction was extracted from the offset measurements.

The α vs ϕ plots were used by transforming from polar coordinates to extract XOffset and YOffset.

The actual offset was defined as in eq(1). The XOffset West(East)and YOffset obtained using this method can be found in Table 1.

$$\Delta\alpha = \frac{XOffset * \sin(\phi)}{R_{DC}} + \frac{YOffset * \cos(\phi)}{R_{DC}} \quad (1)$$

R_{DC} = Drift chamber radius = 220 cm.

XOffset	West	fill 7621:	-0.27 cm
XOffset	East	fill 7621:	-0.03 cm
YOffset		fill 7621:	0.19 cm
XOffset	West	fill 7641:	-0.29 cm
XOffset	East	fill 7641:	-0.05 cm
YOffset		fill 7641:	0.20 cm

Table 1. XOffsets and YOffsets found

Offsets in the x and y coordinate were found, as Table 1 shows, and corrected for in the 2006 longitudinal proton-proton beam data sample. The stability of the offsets throught the whole data set was tested by checking at well known charged particle spectra in diffrent data ranges. If the offsets were not stable, a change in the mass position, and/or mass spectra resolution would be detected by looking at an charge

dependant shift in the mass squared m^2 value for protons and anti protons. Protons and anti-protons are well known charged particles in the PHENIX detector that are often used for calibration purposes. Once the beam shift offsets had been found and tested for stability then the momentum scale was extracted. Testing for stability was done by comparing the mass spectra of protons and anti protons in all the data. Comparison of mass values to published values from the Particle Data Group (PDG) physics booklet publication was also performed[2].

3 Momentum Scale

Charge separated m^2 distributions from momentum p < 1.8 to p > 1.0 were studied. Mass peaks were obtained and signal + background was fitted to a polynomial degree 2 + gaussian. The m^2 was identified using Phenix Time of flight(TOF), the mass value obtained from the fit for protons and antiprotons was 0.906 ±0.001. These measurement of the protons and antiprotons mass gave a momentum scale correction, as the m^2 tof variable is directly related to the momentum of the particle via:

$$m^2 = p^2 * \sqrt{t^2/(L^2 - 1)} \quad (2)$$

where t and L are known variables indicating time of flight of particle and distance from collision to detector respectively. The m^2 of 0.906 GeV^2 compared to the PDG value of 0.880 GeV^2 gave a scale of 0.97, or 3% from unity. This deviation was used as a momentum scale correction. A secondary cross check was performed by looking at high pT $\pi^{\pm}$ candidates firing the in the Ring Imaging Čerenkov counter (RICH). This cross check verified that the RICH threshold turn-on curve for charged pions could be clearly seen unshifted around 5 GeV/c (pion threshold is 4.7GeV/c). Similar to the proton and anti-proton inspection, mismatch of the turn-on curve for π^+ and π^- would indicate a beam shift component remaining. Charged pions do not make use of the time of flight , but rather use the RICH detector for identification.

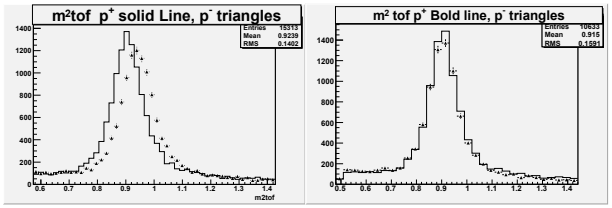

Fig. 2. m2tof of p(solid line) and antip(tringles) before(left) and after(right) corrections

4 Results and Conclusions

Beam Shift and Momentum scale corrections on the longitudinal 2006 proton proton data at $sqrt(s) = 200GeV$ were obtained. The beam shift offsets obtained can be seen on Table 1, the momentum scale correction was found to be 0.97. The calibration of the these corrections were made available to the PHENIX collaboration after being tested using known particle species: protons/antiprotons and $\pi^{\pm}$. Both methods showed that the corrections were valid over the whole data set meant to calibrate.

References

1) K. Adcox et al., *PHENIX central arm tracking detectors*, NIM A499 489-507, 2003
2) W.-M.Yao et al. (Particle Data Group), J. Phys. G 33, 1 (2006) and 2007 partial update for the 2008 edition

PHENIX local polarimeter analysis in polarized proton-proton collisions at $\sqrt{s} = 200$GeV from RHIC Run-6

S. Dairaku*[1] for the PHENIX Collaboration

[Spin, Asymmetry]

One of the main goals of the PHENIX experiment is to determine the polarized gluon distribution function in a proton.[1)] To achieve this objective, we use polarized proton-proton collisions. We determine the polarized gluon distribution function by measuring double longitudinal-spin asymmetries during the production of various particles. In RHIC rings, proton beams are vertically polarized. Therefore, we need to change the direction of the beam polarization from the vertical direction to the longitudinal direction using spin rotator magnets. A local polarimeter is used for evaluating how correctly the proton beams are longitudinally polarized when the spin rotator is on.

When the spin rotator is off, the proton beams are vertically polarized at the PHENIX interaction region, and the local polarimeter can measure the significant single transverse-spin asymmetry (A_N) for forward neutron production,[2)] which is calculated by

$$A_N \equiv \frac{1}{P}\frac{\sigma_\uparrow - \sigma_\downarrow}{\sigma_\uparrow + \sigma_\downarrow} = \frac{1}{P}\frac{\sqrt{N_L^\uparrow N_R^\downarrow} - \sqrt{N_L^\downarrow N_R^\uparrow}}{\sqrt{N_L^\uparrow N_R^\downarrow} + \sqrt{N_L^\downarrow N_R^\uparrow}}, \qquad (1)$$

where P is the absolute polarization value measured by the RHIC polarimeters, and $N_{L(R)}^{\uparrow(\downarrow)}$ is the number of neutrons scattered to the left (right) when the direction of the beam polarization is vertically upwards (downwards). We identify forward neutrons using a zero degree calorimeter (ZDC) and measure the scattering direction of the neutrons using a shower maximum detector (SMD) by detecting the shower shape in the ZDC.

When the spin rotator is on, the local polarimeter measures the asymmetries A_{LR} and A_{UD}, which are the left-right and up-down asymmetries of the forward neutron production, respectively. We can calculate the fraction of the residual transverse component of the beam polarization ($\frac{P_T}{P}$) as

$$\frac{P_T}{P} = \sqrt{\left(\frac{A_{LR}}{A_N}\right)^2 + \left(\frac{A_{UD}}{A_N}\right)^2}. \qquad (2)$$

If the proton beams are longitudinally polarized correctly, $\frac{P_T}{P}$ should be ~ 0, and the fraction of the longitudinal component ($\frac{P_L}{P}$), which is calculated by

$$\frac{P_L}{P} = \sqrt{1 - \left(\frac{P_T}{P}\right)^2}, \qquad (3)$$

should be ~ 1.

Figures 1 and 2 show the azimuthal angle ϕ dependence of the asymmetry A_N for forward neutron production for two RHIC rings (the so-called blue ring and yellow ring, respectively) when the spin rotator was off. We can see the clear sinusoidal shape of the vertically polarized beams.

The analysis is ongoing, and the final values of the transverse component ($\frac{P_T}{P}$) and the longitudinal component ($\frac{P_L}{P}$) will be reported in the near future.

References

1) G. Bunce et al.: Ann. Rev. Nucl. Part. Sci. **50**, 525 (2000).
2) Y. Fukao et al.: Phys. Rev. B **650**, 325 (2007).

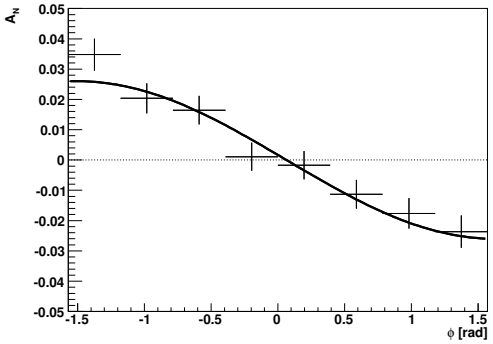

Fig. 1. Azimuthal angle ϕ dependence of the asymmetry for forward neutron production for the blue ring when the spin rotator was off.

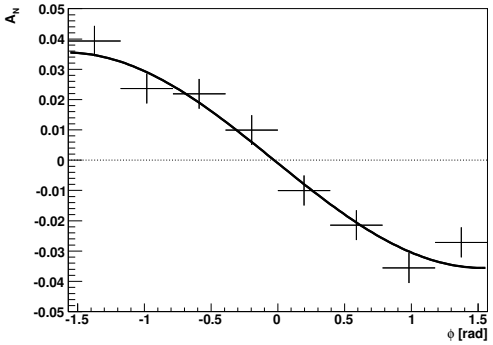

Fig. 2. Azimuthal angle ϕ dependence of the asymmetry for forward neutron production for the yellow ring when the spin rotator was off.

*1 Department of Physics, Kyoto University, Japan

Longitudinal spin transfer to $\bar{\Lambda}$ in $\sqrt{s}$=200 GeV longitudinally polarized proton-proton collisions

R.Han*1

1 Introduction

The spin transfer to hyperon in experiments for the study of nucleon spin, which connects to spin dependent quark to hyperon fragmentation function and is also a potential probe for the spin structure of nucleon, has been widely used to study various aspects of spin effects in high-energy reactions through the self spin-analyzing parity violating decay of hyperon[1]. Among hyperons, Λ and its antiparticle $\bar{\Lambda}$ are more appropriate to be studied for their self-analyzing power and larger cross section. $\bar{\Lambda}$ is also found to be sensitive to the polarization of the antistrange sea of the nucleon[2].

2 $\bar{\Lambda}$ Production at RHIC/PHENIX

The PHENIX experiment is the largest of the four experiments currently performed to gather data at the Relativistic Heavy Ion Collider (RHIC). $\bar{\Lambda}$ is reconstructed via it weak decay $\bar{\Lambda} \rightarrow \bar{p}\pi^+$ with a branch ratio of 64%. We reconstructed $\bar{\Lambda}$ from pp collisions extracted from the data collected during the 2002-2003 run period (Run-3) of RHIC/PHENIX with one beam polarization reaching 36%.

The invariant mass spectrum is plotted in the figure below. In total, 60308 $\bar{\Lambda}$ signal and 52253 background events are reconstructed in the mass range of 1.110 $GeV/c^2 \sim$ 1.122 GeV/c^2. $\bar{\Lambda}$ events with comparative statistics are also generated for the study of spin transfer.

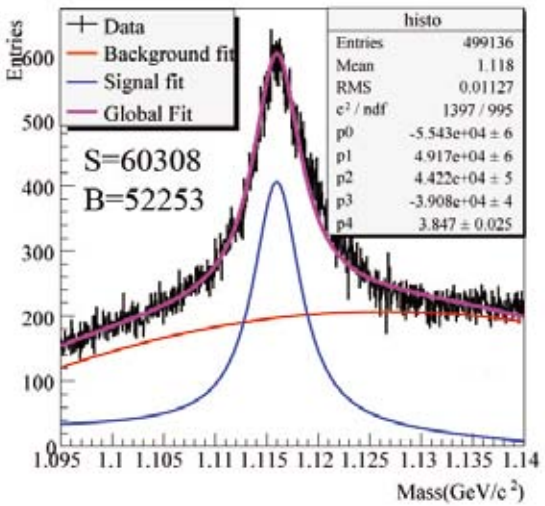

*1 School of Nuclear Science and Engineering, North China Electric Power University, Beijing

3 Spin Transfer to $\bar{\Lambda}$

The spin transfer to $\bar{\Lambda}$ can be analyzed through the angular distribution of the decay proton in the $\bar{\Lambda}$ rest frame

$$\frac{dN}{dcos\Theta_{\bar{p}\bar{\Lambda}}} \sim (1+\alpha P_B \cdot D_{LL} \cos\Theta_{\bar{p}\bar{\Lambda}}) \cdot a(\kappa, \cos\Theta_{\bar{p}\bar{\Lambda}}); (1)$$

where $a(\kappa, \cos\Theta_{\bar{p}\bar{\Lambda}})$ is the acceptance correction function; $\Theta_{\bar{p}\bar{\Lambda}}$ is the angle between the momentum of the decay antiproton and $\vec{e}_3$ in the $\bar{\Lambda}$ rest frame, where $\vec{e}_3$ is defined as the direction of the $\bar{\Lambda}$ momentum in the laboratory frame. α is the decay asymmetry in the $\bar{\Lambda}$ rest frame, and P_B is the beam polarization, where D_{LL} is the spin transfer from the proton to $\bar{\Lambda}$, the first "L" being the initial longitudinal polarized proton and the second one means the longitudinal polarized $\bar{\Lambda}$ produced in the collision. The preliminary result of spin transfer to $\bar{\Lambda}$ from Run3 data has been approved by PHENIX collaboration.

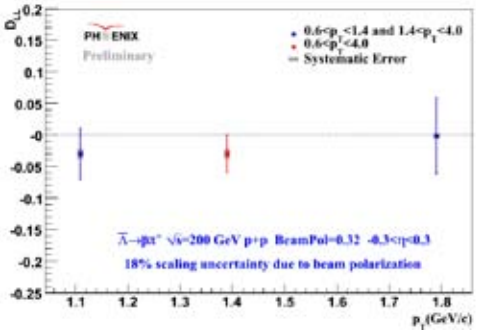

The observed spin transfer to $\bar{\Lambda}$ is consistent with zero within statistical uncertainties, as qualitatively expected from the small average x_F and p_T. Quantitative theoretical predictions exist for transverse momenta p_T larger than 8 GeV. It should be noted that at lower p_T, for which preliminary data exist, the cross section is not well described by current pQCD calculations. The preliminary study shows that 1.5M $\bar{\Lambda}$ events could be reconstructed from the PHENIX run5 data set. By including run5 data, we expect to increase statistics by a factor of three and to obtain a more solid physics output on spin transfer analysis.

References

1) C. X. Liu and Z. T. Liang: Phys. Rev. D 62, 094001 (2000); Q. H. Xu, C. X. Liu and Z. T. Liang: Phys. Rev. D65, 114008 (2002); H. Dong, J. Zhou and Z. T. Liang: Phys. Rev. D 72, 033006 (2005).
2) Qinghua Xu for the STAR collaboration, hep-ex/0512058,2005.

Single spin asymmetry of di-hadron production in transversely polarized pp collision at $\sqrt{s} = 200$ GeV

R. Yang,[*1] M. Große Perdekamp,[*1] and R. Seidl

The transversity distribution is one of the three parton distribution functions of the proton at leading twist. It can be interpreted as the difference between the number of quarks that have spin parallel and antiparallel to the proton spin inside a transversely polarized proton. Compared with the other two distribution functions, the quark momentum distribution function and the quark helicity distribution, experimental knowledge on transversity distribution is still very limited.

Due to the chiral odd nature of the transversity distribution, it cannot be probed directly in inclusive deep-inelastic scattering (DIS). One solution is to couple the transversity distribution with another chiral-odd function such as the transversity distribution itself or a chiral-odd, spin-dependent fragmentation function. As an example, Ref. 1 demonstrated a global QCD analysis of transversity distribution using single spin asymmetry measured from semi-inclusive DIS[2)3)] and the corresponding spin-dependent fragmentation function measured in e^+e^- experiment[4)].

At the PHENIX experiment at the Relativistic Heavy Ion Collider (RHIC), the single spin asymmetry of di-hadron production measured in transversely polarized proton-proton collisions can be taken as an input for the global QCD analysis. The asymmetry is defined as

$$A(\phi) = \frac{1}{P}\frac{N_\uparrow/L_\uparrow - N_\downarrow/L_\downarrow}{N_\uparrow/L_\uparrow + N_\downarrow/L_\downarrow} \quad (1)$$

where $N_\uparrow$ and $N_\downarrow$ are the counts of di-hadron pairs, $L_\uparrow$ and $L_\downarrow$ are the luminosities of the beam with the arrows indicating polarization direction of the proton beam, and P is the beam polarization. This asymmetry is calculated in different ϕ bins, where the angle ϕ is an azimuthal angle between the polarization direction and the direction of the hadron plane. Since a $\sin(\phi)$ modulation is expected[5)], the measured asymmetry must be fit with a sine function

$$A(\phi) = A_{UT}\sin(\phi) \quad (2)$$

to obtain the analyzing power A_{UT} which is a convolution of transversity distribution function and a spin-dependent fragmentation function:

$$A_{UT} \propto \delta q(x) \otimes H_1^\sphericalangle(z, m^2). \quad (3)$$

$H_1^\sphericalangle$ is the spin-dependent fragmentation function of di-hadron production. It is usually referred to as "interference fragmentation function" (IFF) in the literature. The measurement of IFF is an ongoing effort at the BELLE experiment by observing asymmetries in azimuthal angles of pion pair production in back-to-back jets in e^+e^- collisions. Based on existing pion phase shift data, the sign of $H_1^\sphericalangle$ might change where the invariant mass of the pion pair is close to 780 MeV/c^2, or the ρ meson mass[6)]. Therefore, the analyzing power A_{UT} is also calculated for 5 different invariant mass bins from 0.5 MeV/c^2 to 2 MeV/c^2.

Proton-proton collision data at $\sqrt{s} = 200$ GeV taken in 2006 was used for this measurement. The integrated luminosity is 2.7 pb^{-1} and beam polarization is 55%. Events are selected by a photon trigger with threshold of 1.4 GeV. For this analysis, the di-hadron pairs have been chosen to be $\pi^0\pi^{+/-}$ and $\pi^+\pi^-$ pairs. Neutral pions and charged pions are measured by the central arm of the PHENIX detector. When counting the pairs of pions, it is required that each pion has $p_T > 1$ GeV/c, and both come from the same detector arm. To reduce background from meson decay and conversion electrons at high p_T, an additional constraint of $p_T < 6$ GeV/c has been applied for the charged pions. Figure 1 shows the statistical uncertainties of the analyzing power for $\pi^0\pi^{+/-}$ and $\pi^+\pi^-$ pairs. This is an ongoing analysis and the plan is to have the results approved by the PHENIX spin working group and to show the results in late 2008.

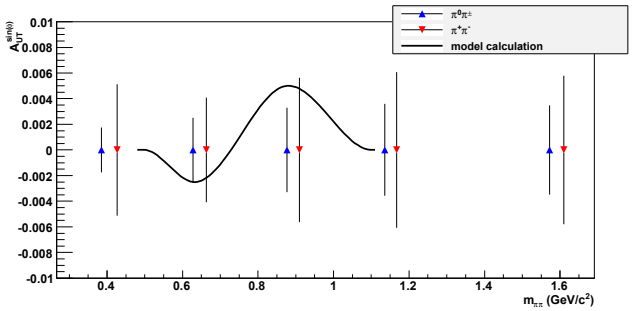

Fig. 1. Expected statistical uncertainties of the single spin asymmetry. The curve is an prediction based on the transversity taken from Ref. 1 and the fragmentation function from Ref. 6.

*1 University of Illinois, USA

References
1) M. Anselmino et al.: Phys. Rev. D **75**, 054032 (2007).
2) A. Airapetian et al.: Phys. Rev. Lett. **94**, 012002 (2005).
3) E. S. Ageev et al.: Nucl.Phys. B **765**, 31 (2007).
4) R. Seidl et al.: Phys. Rev. Lett. **96**, 232002 (2006).
5) A Bacchetta et al.: Phys.Rev. D **70**, 094032 (2004).
6) R. Jaffe et al.: Phys. Rev. Lett. **80**, 1166 (1998).

Longitudinal Double Spin Asymmetries in Forward Rapidity with Prompt Muon in Polarized p+p Collisions at $\sqrt{s}$=200GeV†

X. Wang[*1*3], H. Liu[*2] and M. Liu[*2]

[Spin, Single muons, Asymmetry]

Deep-inelastic scattering (DIS) experiments with polarized leptons and polarized nucleons have shown that the spins of quarks and anti-quarks account for only approximately 25% of the nucleon spin[1]. The rest of the proton spins must be carried by the gluons and orbital angular momentum. Measurements of the scale dependence of the inclusive nucleon spin structure function and recent semi-inclusive DIS data[2] have shown the coarse constraint in the possible gluon spin contribution. Furthermore, heavy quark production in polarized p+p collision at RHIC energy is dominated by the gluon-gluon interaction, thus providing direct access to the (polarized) gluon distribution in the proton.

We report the feasibility of measuring the longitudinal double spin asymmetries of single muon production at forward rapidity in polarized p+p collisions. PHENIX has two spectrometers designed for measuring muon production over the pseudorapidity range $1.2 < |\eta| < 2.4$. The muon arms start with a thick hadron absorber to reduce the hadronic background for muon measurements. Muon arms consist two Muon Trackers (Mutr) and two Muon Identifiers (MuID). Muons can be produced from D or B meson through semi-leptonic decay (prompt muon). The main backgrounds of prompt muons are punch-through hadrons and muons from light hadron decay. The inclusive asymmetry A_{LL}^{incl} is given as

$$A_{LL}^{incl} = \frac{1}{P_B \cdot P_Y} \frac{N^{++} - R \cdot N^{+-}}{N^{++} + R \cdot N^{+-}} \quad (1)$$

$$A_{LL}^{prompt} = \frac{A_{LL}^{incl} - r \cdot A_{LL}^{BG}}{1 - r}, \quad (2)$$

$$\delta A_{LL}^{prompt} = \frac{\sqrt{(\delta A_{LL}^{incl})^2 + r^2 \cdot (\delta A_{LL}^{BG})^2}}{1 - r}, \quad (3)$$

where r is the background fraction and A_{LL}^{BG} is the asymmetry of the background. Figure 2 shows the prompt- to-background ratio. Comprehensive hadron simulation was carried out to understand the hadron component at different MuID layers. After the track quality cut was applied, we observed that the tracks stopped at layer 2 or 3 are mostly hadrons (as shown in the right-hand plot of fig.1). The hadrons that stopped at MuID layer 2 or 3 are used to study the background asymmetry.

*1 New Mexico State University, Las Cruces, NM, USA
*2 Los Alamos National Laboratory, Los Alamos, NM, USA
*3 Hua-Zhong Normal University, Wuhan, China

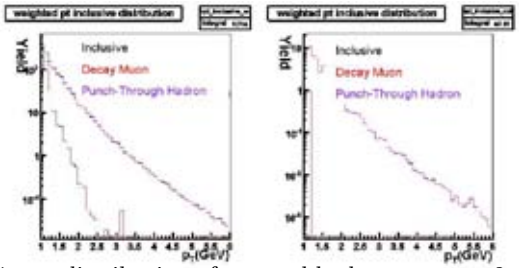

Fig. 1. p_T distribution of stopped hadrons at gaps 2 and 3 from simulation(left:before cut; right:after cut)

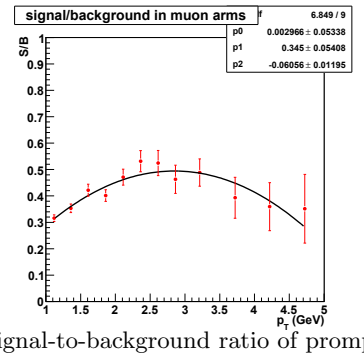

Fig. 2. Signal-to-background ratio of prompt muons.

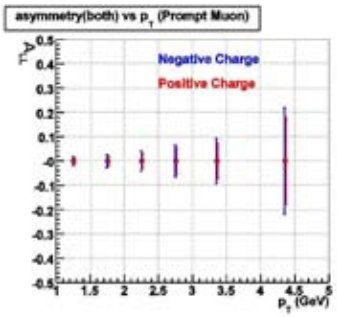

Fig. 3. Prompt muon A_{LL} vs. p_T.

Runs 5 and 6 data are used to perform this analysis. This work is now in progress and the results are expected to be released in a few months. Figure 3 shows the statistical sensitivity of prompt muon A_{LL} vs p_T.

References

1) J. Ashman et al., Phys. Lett. B **206**, 364 (1988); Nucl. Phys. B**328**, 1 (1989); E. Hughes and R. Voss, Annu. Rev. Nucl. Part. Sci. 49, 303 (1999).
2) HERMES Collaboration, Phys. Rev. Lett. **84**, 2584 (2000); COMPASS Collaboration, Phys. Lett. B **633**, 25 (2006).

Measurement of Longitudinal Double-Spin Asymmetries of Back-to-Back Dimuons in Polarized p+p Collisions at $\sqrt{s}$=200 GeV

H. Liu, M. Liu and C. M. Camacho*[1] for the PHENIX Collaboration

[Spin, Back-to-Back Dimuons, Asymmetry]

Understanding the contribution of the polarized gluons to the proton spin is one of the key steps toward resolving the proton spin puzzle. At the Relativistic Heavy Ion Collider (RHIC) energy, heavy quark production is dominated by the gluon-gluon interaction; thus, measurements of the heavy flavor production in the polarized p+p collisions will enable us to study the polarized gluon distributions. In this report, we present the status of longitudinal double-spin asymmetries in back-to-back (B2B) dimuons production in the polarized p+p collisions at RHIC. The B2B dimuons have been measured using the PHENIX muon spectrometers at forward and backward rapidities ($1.2 < |\eta| < 2.4$) where two muons go into opposite arms. Monte Carlo simulations with PYTHIA event generator have shown that the B2B dimuons in the mass range of $5 < M < 10$ GeV, mostly come from heavy quark decays, through the channels $D\bar{D} \rightarrow \mu^+\mu^-$ and $B\bar{B} \rightarrow \mu^+\mu^-, \mu^-\mu^-, \mu^+\mu^+$.

The longitudinal double-spin asymmetry A_{LL} is measured as

$$A_{LL} = \frac{1}{P_b P_y} \frac{N^{++} - RN^{+-}}{N^{++} + RN^{+-}}, \quad (1)$$

where P_b and P_y are the beam polarizations for blue and yellow beams, respectively, $N^{++}(N^{+-})$ is the B2B dimuons yield from the same (opposite) helicity beam collisions, and $R = L^{++}/L^{+-}$ is the relative luminosity measured with the beam-beam counter (BBC) and the zero-degree calorimeter (ZDC) at very forward rapidity.

For the heavy quarks production at RHIC, the asymmetry is proportional to the gluon polarization,

$$A_{LL} \sim \frac{\Delta g(x_1)}{g(x_1)} \times \frac{\Delta g(x_2)}{g(x_2)} \times a_{LL}^{gg \rightarrow Q\bar{Q}}, \quad (2)$$

where $\Delta g(x)$(g(x)) is the (un)polarized gluon distribution, and $a_{LL}^{gg \rightarrow Q\bar{Q}}$ is the partonic asymmetry. In the case of the B2B dimuons, $x_1 \sim x_2$, and $A_{LL} \propto [\Delta g(x)/g(x)]^2$. The mass distribution of B2B dimuons is shown in figure 1. The measured inclusive asymmetry A_{LL}^{incl} is related to A_{LL}^{B2B} by

$$A_{LL}^{B2B} = \frac{A_{LL}^{incl} - r \cdot A_{LL}^{BG}}{1 - r}, \quad (3)$$

$$\delta A_{LL}^{B2B} = \frac{\sqrt{(\delta A_{LL}^{incl})^2 + r^2 \cdot (\delta A_{LL}^{BG})^2}}{1 - r}, \quad (4)$$

*1 Los Alamos National Laboratory, Los Alamos, NM, USA

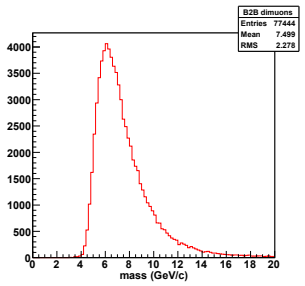

Fig. 1. Invariant mass distribution of B2B dimuons at $\sqrt{s} = 200$ GeV detected using the PHENIX muon spectrometers.

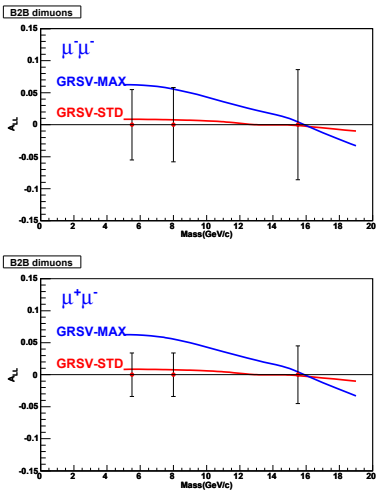

Fig. 2. A_{LL}^{incl} vs. mass in B2B dimuons production at $\sqrt{s} = 200$ GeV.

where r is the background fraction, and A_{LL}^{BG} is the background asymmetry.

Figure 2 shows the sensitivity of the inclusive B2B dimuon A_{LL}^{incl} vs. the mass from the 2006 RHIC polarized p+p run. The experimental statistical sensitivities are compared with two gluon polarization models, GRSV standard (red curve) and maximum gluon polarization (blue curve), calculated at LO for $B\bar{B}$ production.[1–3] $\mu^-\mu^-$ pairs are free from $D\bar{D}$ contribution and are expected mostly from $B\bar{B}$ decays, while the $\mu^+\mu^-$ sample contains more non-$B\bar{B}$ events. The analysis is in progress and preliminary results will be published in the near future.

References

1) A. P. Contogouris *et al.*: Phys. Lett. B **246**, 524 (1990).
2) M. Karliner *et al.*: Phys. Lett. B **324**, 209 (1994).
3) M. Gluck *et al.*: Phys. Rev. D **63**, 094005 (2001).

Measurement of Double Longitudinal Spin Asymmetry (A_{LL}) in Direct Photon Production in $\sqrt{s} = 200$ GeV Proton-Proton Collisions at PHENIX

R. Bennett,[*1] K. Okada, and T. Horaguchi[*2]

Production of direct photon in $\sqrt{s} = 200$ GeV pp collisions at RHIC is one of the important channels PHENIX will employ to determine the polarized gluon distribution. To establish the theoretical understanding of this process, we compare the direct photon total cross section measured using our data, with the perturbative QCD calculations at next-to-leading order. This comparison shows good agreement between data and theoretical calculations over a broad range in photon transverse momentum (P_T)

The double helicity spin asymmetries, A_{LL}, is evlauate from the 2005 dataset based on a luminosity of 2.7 pb^{-1} and polarization 50%. Since the direct photon A_{LL} is linear in ΔG, the gluon contribution to the spin of the proton, it is sensitive to both the sign and magnitude of ΔG. It will serve as a complementary measurement to the π^0 A_{LL} analysis . A_{LL} is calculated using the following formula.

$$A_{LL} = \frac{1}{|P_B||P_Y|}\frac{N_{++} - RN_{+-}}{N_{++} + RN_{+-}} \ , \quad R = \frac{N_{++}}{N_{+-}} \qquad (1)$$

Where $P_B(P_Y)$ is the polarization of the blue (yellow) beam. $N_{++}(N_{+-})$ are direct photon yields during like (unlike) sign helicity crossings. R is the relative luminosity, which is the ratio of the production rates.

The extraction of direct photon A_{LL} relies on, first purifying the sample by considering only isolated photons as direct photon candidates. Photons originating from hadronic decays (π^0, η, ω...) will be found in close proximity to other jet material, as opposed to the direct photon which should remain isolated. A 0.5[rad] cone is defined around any candidate photon. A photon is considered isolated if the sum of the energy inside the cone is less then 10% of the energy of the candidate photon. This effectivly removes photons originating from hadronic decays while leave behind a cleaner direct photon sample.[1)] The cut is most efficient at high P_T. Next, photons originating from hadronic decays (mostly $\pi^0 \to \gamma\gamma$) which pass the isolation cut are removed. These are hadronic decays in where the energy asymmetry of the photons is so great that the pair pass the isolation cut. These photons are identified by creating mass-pairs of photons which pass the cut. Any photon which forms a pair of $135 \pm 30 MeV$ are simply removed from the isolated photon sample. We denote these photons by n_{π^0} .

Finally we correct the assymetry for hadronic decays in which one photon has missed the PHENIX acceptance. We estimate this from the total number of π^0's where both decay photons are in PHENIX acceptance, $N_{\pi^0}^{tagged}$. $N_{\pi^0}^{tagged}$ is then scaled by the probability that one photon will miss our acceptance ($R_{\pi^0}^{miss}$). $R_{\pi^0}^{miss}$ is estimated by a Monte Carlo simulation. We then assume other hadronic decays (η, ω...) will have similar behavior as the π^0 and their contribution can be calculated by comparing their branching ratios to that of the π^0. We denote all one-miss hadrons by, N^{bg}. The direct photon asymmetry and uncertainty are corrected by:

$$A_{LL}(direct-\gamma) = \frac{A_{LL}(iso - n_{\pi^0}) - rA_{LL}^{bg}}{1-r}, r = \frac{N_{bg}}{N_{iso-n_{\pi^0}}} \qquad (2)$$

$$\Delta A_{LL}(sig)^2 = \frac{\Delta A_{LL}^2(iso - n_{\pi^0}) + r^2 \Delta A_{LL}^2(bg)}{(1-r)^2} \qquad (3)$$

Here, $A_{LL}(iso - n_{\pi^0})$ is the asymmetry of the sample of isolated photons minus photons originating from hadronic decays that still pass the isolation cut. A_{LL}^{bg} is the asymmetry of the one-miss hadrons. r is the ratio of the number of one-miss hadrons to the number of isolated photons minus n_{π^0}. The uncertainy of each point is then evaluated in this manner.

Fig. 1, shows we are unable to distinguish the several GRSV model curves. It is important to note that although we are statistically limited at the moment, we have shown that we have a consistent method for measuring the double longitudinal spin asymmetry and as gains are made in both luminosity and polarization this measurement will certainly complement the results of the neutral pion asymmetry analysis.

References

1) S.S. Adler et al.: Phys. Rev. Lett. (98), 012002 (2007)

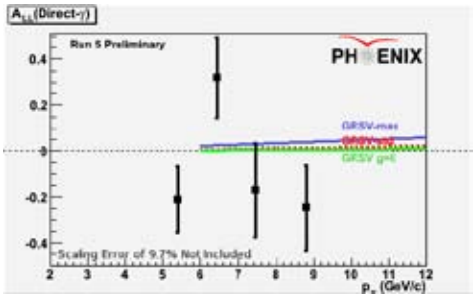

Fig. 1. Direct Photon A_{LL} as a function of P_T with curves for GRSV theoretical models

*1 Department of Physics, State University of New York at Stony Brook
*2 Department of Physics, Hiroshima University

Run06 Polarization in Proton-Proton Operation at RHIC Using the Hydrogen Jet Polarimeter

K. Boyle,[*1] I. Alekseev,[*2] A. Bravar,[*3] G. Bunce,[*4*5] C.M. Camacho,[*6] S. Dhawan,[*7] A. Dion,[*2] K.O. Eyser,[*8] R. Gill,[*4] W. Haeberli,[*9] A. Hoffman,[*10] H. Huang,[*4] H. Liu,[*6] M.X. Liu,[*6] Y. Makdisi,[*4] I. Nakagawa, H. Okada,[*4] K. Sakashita,[*11] E. Stephenson[*12] D.N. Svirida,[*1] T. Wise,[*9] J. Wood,[*4] and A. Zelenski[*4]

[polarized proton, silicon strip detector, RHIC, polarimetry, CNI, forward elastic scattering]

A necessary ingredient in the RHIC spin program is high polarization that is precisely measured. A polarized Hydrogen jet polarimeter[1)] is used to make an absolute measurement of the beam polarization, which is needed to normalize the results from the proton-Carbon polarimeters.[2)] In the 2006 RHIC run (Run06), the RHIC spin goal of less than 5% total relative uncertainty in the polarization of a single beam was achieved at beam energy of 100 GeV.

The Hydrogen jet is designed to study protons elastically scattered at low recoil energy (T_R) nearly perpendicular to the beam direction. In this low recoil energy region of a few MeV, the asymmetry due to the Coulomb nuclear interference effect is expected to be maximal. In a polarized hydrogen target, two different asymmetries can be measured: ε_T, the target asymmetry where the target is taken as polarized and the beam unpolarized, and ε_B, the beam asymmetry where the beam is taken as polarized and the target unpolarized. The analyzing power, which is a physics quantity, is the same in both cases, and so we can relate target and beam polarization as

$$P_B = \frac{\varepsilon_B}{\varepsilon_T} P_T \qquad (1)$$

where P_T (P_B) is the target (beam) polarization. P_T is monitored by a Breit-Rabi polarimeter and was maintained at 92.4±1.8% throughout both Run05 and Run06.

Figure 1 compares the Run05 and Run06 measured target and beam asymmetries as a function of the struck proton's recoil energy for the two beams (called "Blue" and "Yellow"). The target asymmetry is consistent between the two years, whereas the difference in beam asymmetry indicates the increased polarization in Run06. In Run6, the average polarization was $53.2 \pm 0.9 \pm 1.3\%$ and $52.7 \pm 0.8 \pm 1.3\%$ in the Blue and Yellow beams, respectively.

Polarization was also measured during a short 31 GeV run in Run06. Figure 2 shows the target and beam asymmetries measured with the "Blue" beam. Large backgrounds in the "Yellow" running period prevented asymmetry measurements, and so only blue was measured. Blue beam was used to normalize both beams in during the 31 GeV run.

References

1) H. Okada *et al.*, Phys. Lett. B **638**, 450 (2006).
2) O. Jinnouchi *et al.*, RHIC/CAD Accelerator Physics Note 171, 2004.

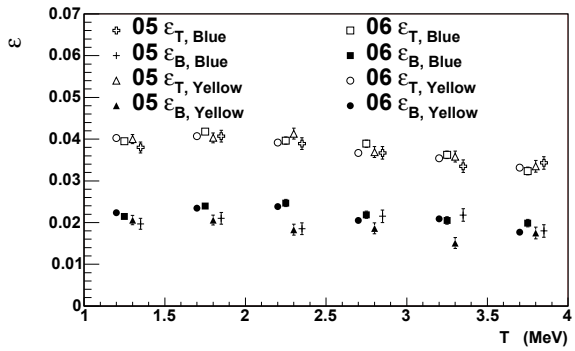

Fig. 1. Target (open) and beam (filled) asymmetry vs. recoil energy at 100 GeV from Run05 and Run06 (top).

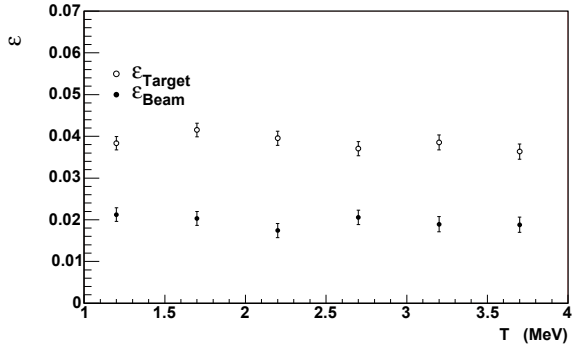

Fig. 2. Target (open) and beam (filled) asymmetry vs. recoil energy at 31 GeV (bottom) from Run06.

*1 State University of New York - Stony Brook, Stony Brook, NY 11794
*2 Institute for Theoretical and Experimental Physics, Russia
*3 University of Geneva, 1205 Geneva, Switzerland
*4 Brookhaven National Laboratory, USA
*5 RIKEN-BNL Research Center, BNL, USA
*6 Los Alamos National Laboratory, Los Alamos, NM 87545
*7 Yale University, USA
*8 University of California, Riverside, USA
*9 University of Wisconsin, USA
*10 Massachusetts Institute of Technology, Cambridge, MA 02139
*11 Tokyo Institute of Technology, Tokyo 152-8551, Japan
*12 Indiana University Cyclotron Facility, USA

A Study on the Relative Luminosity for Helicity Asymmetry Measurement in Polarized *pp* Collisions at $\sqrt{s} = 62.4$ GeV at RHIC-PHENIX

K. Aoki*[1] for the PHENIX Collaboration

One of the main goals of the RHIC-PHENIX experiment is to study the structure of proton spin through the double helicity asymmetry (A_{LL}) of particle production in polarized pp collisions. In Run 2006, we measured $\pi^0 A_{LL}$ at $\sqrt{s} = 62.4$GeV in addition to $\sqrt{s} = 200$GeV.[1)] The results significantly extended the sensitivity of the polarized gluon distribution to higher Bjorken-x. A_{LL} is calculated as

$$A_{LL} = \frac{1}{P_1 P_2} \frac{N_{++} - R N_{+-}}{N_{++} + R N_{+-}}, \quad \text{where} \quad R = \frac{L_{++}}{L_{+-}}. \quad (1)$$

$P_{1(2)}$ is the polarization of two colliding beams, $N_{++(+-)}$ is the particle yield in parallel (antiparallel) helicity bunch crossings, and R is relative luminosity. A precise determination of R is essential for the A_{LL} measurement since the uncertainty of R propagates as $\delta A_{LL} \sim \frac{1}{2P_1P_2}\delta R$. The average polarization was $\langle P_1 \cdot P_2 \rangle = 0.23$ in Run 2006 at $\sqrt{s} = 62.4$GeV.

The achieved accuracy would be $\delta R = 1.3 \times 10^{-3}$ ($\delta A_{LL} = 2.8 \times 10^{-3}$) if analysis similar to that at $\sqrt{s} = 200$GeV[2)] was performed. The value of δA_{LL} is more than half of the statistical uncertainty of $\pi^0 A_{LL}$ at the lowest p_T, where the statistics are the highest. We discuss how we improved the accuracy of R.

The PHENIX Beam-Beam Counter (BBC) covers $3.0 < |\eta| < 3.9$ with full azimuthal coverage and detects charged particles.[3)] The Zero Degree Calorimeter (ZDC) covers the forward direction (< 2.8mrad) and detects neutral particles.[3)] BBC and ZDC serve as independent luminosity measures. They are placed symmetrically to the plane $\eta = 0$ and the different components are named BBCN, BBCS and ZDCN, ZDCS.

A Local-Level 1 (LL1) trigger, BBCLL1[NoCut], is defined as the coincidence between BBCN and BBCS hits. BBCLL1[30cm] is defined as BBCLL1[NoCut] with an additional offline vertex position cut with $|z| < 30$cm. ZDCLL1[30cm] and ZDCLL1[150cm] are defined in a similar way.

BBCLL1[30cm] counts are used to calculate R. By comparing it with the other luminosity measures, δR is evaluated. Let $N_{A(B)}(i)$ be the counts of trigger A(B) in bunch crossing i. $r(i) = N_A(i)/N_B(i)$ should be constant if the two triggers are ideal luminosity measures. The assumption was tested by a fit[2)], where possible spin dependences are taken into account. We use BBCLL1[30cm] as trigger B in this article. ZDC[30cm] was chosen for trigger A at $\sqrt{s} = 200$GeV.[2)] At $\sqrt{s} = 62.4$GeV, the ratio ZDC[30cm]/BBCLL1[30cm] is an order of magnitude smaller. Even with the use of ZDC[150cm] (three times higher statistics than that of ZDC[30cm]), the achieved accuracy was $\delta A_{LL} = 2.8 \times 10^{-3}$ and is statistically limited.

Trigger	62.4GeV	200GeV
BBCLL1(NoCut) in ZDCwide	1.3×10^{-2}	(*) 2.1×10^{-1}
ZDCwide in BBCLL1(NoCut)	3.8×10^{-5}	(*) 6.7×10^{-3}
BBCLL1(NoCut) in pZDC	(*) 1.9×10^{-1}	N/A
pZDC in BBCLL1(NoCut)	(*) 1.2×10^{-2}	N/A

Table 1. Event overlap. Triggers with (*) are used in the analysis.

For improvement of the accuracy, a trigger pZDC defined as (BBCN||BBCS)&&(ZDCN||ZDCS), was introduced and used as trigger A. BBCLL1[30cm] has a vertex cut, while pZDC does not. The fit across bunches using these triggers produced a large χ^2, partially due to the vertex width variation in each bunch crossing. This effect was corrected using the vertex distribution width obtained by a Gaussian fit to the vertex distribution. After the correction, $\tilde{\chi^2}(=\chi^2/NDF)$ of the fit was greatly reduced, although it was still larger than unity (at most $\sim$10). This was taken into account by enlarging the fit error by $\sqrt{\tilde{\chi^2}}$. The achieved accuracy was $\delta A_{LL} \sim 1.4 \times 10^{-3}$, which is two times more accurate than the results using ZDC[150cm].

Since pZDC uses a common detector with BBCLL1, the dependence on each other should be evaluated. For the study, event overlap was investigated. Let "A in B" be the fraction of events that are collected by trigger B and which fire trigger A at the same time. To avoid the effect from the difference of the vertex cut, BBCLL1(NoCut), ZDC[150cm], and pZDC were compared and are summarized in Table 1. The effect of a 150cm cut is small since a typical vertex distribution has a width of $\sigma \sim 60$cm. ZDCLL1 in BBCLL1 at 200GeV (pZDC in BBCLL1) is $\sim$ 0.7% (1.2%). BBCLL1 in ZDCLL1 is $\sim$ 21% (19%). Thus, the event overlap at $\sqrt{s} = 62.4$GeV is at a similar level to that at $\sqrt{s} = 200$GeV.

*1 Department of Physics, Kyoto University, Japan

References
1) K. Aoki et al.: RIKEN Accel. Prog. Rep. **40**, 79 (2007).
2) K. Tanida et al.: RIKEN Accel. Prog. Rep. **37**, 227 (2003).
3) K. Adcox et al.: Nucl. Instrum. Methods A **499**, 469 (2003).

Double Helicity Asymmetry of Inclusive Charged Hadron Production in Proton Proton Collisions at $\sqrt{s} = 62.4$ GeV at PHENIX

A. Datta,[*1] D. Kawall,[*1,*2]

[Double Helicity, Asymmetry, Longitudinal Polarization]

Introduction

The gluon contribution to the spin of the proton is

$$\Delta G(Q^2) = \int_0^1 \Delta g(x, Q^2) dx,$$

where Δg is the polarized gluon distribution, x is the momentum fraction, and Q is the resolution scale.

At PHENIX, spin asymmetries are measured for several processes sensitive to $\Delta g(x, Q^2)$. Hadron production in pp scattering at $\sqrt{s} = 62.4$ GeV with transverse momentum (p_T) below 5 GeV/c is dominated by quark-gluon scattering at leading order in perturbative QCD (pQCD), providing sensitivity to the gluon helicity distribution in the proton. In the rapidity range ($-0.35 < \eta < 0.35$) covered by the PHENIX central arm detectors[2], scattering of quarks and gluons with momentum fractions 0.05 - 0.2[1] are probed. The cross-sections and double-spin asymmetry for single inclusive charged hadrons in this kinematic regime are important for constraining Δg, and for comparison with threshhold resummation calculations[1].

Hadron Selection and Background Reduction

Integrated luminosity of $\sim 0.08\ pb^{-1}$ of minimum bias triggered data (triggered on any inelastic process) of longitudinally polarized pp collisions at $\sqrt{s} = 62.4$ GeV were recorded at RHIC in 2006. Charged tracks reconstructed from Drift Chamber (DC)[2] and the 1st layer of the Pad Chamber (PC1)[2] with the additional requirement of a matching hit on either PC3 or the electromagnetic calorimeter[2] are selected. An offline vertex cut of 30 cm on both sides of the nominal center of the interaction region is imposed to remain within the acceptance of the tracking detectors. Transverse momenta are reconstructed using the DC, and are corrected for spatial shifts of the DC arms. Runs with large dead areas or high noise in the DC are eliminated from the analysis.

Electrons and positrons from conversion of photons mostly coming from π^0 decays are one source of the background. The Ring Imaging Cherenkov (RICH) detector at PHENIX has a high momentum threshold for hadrons (4.7 GeV/c for pions) and less than 100 MeV/c threshold for $e^{\pm}$. RICH veto is used to separate $e^{\pm}$ tracks from hadron tracks in the desired transverse momentum range ($0.2 \leq p_T \leq 4.5$ GeV/c). Muons from charged hadron decays are another source of the background and they are eliminated by track selection procedure and momentum cuts.

Predictions From Theory

Next-to-leading order pQCD calculations of A_{LL} for mid-rapidity charged hadrons at $\sqrt{s} = 62.4$ GeV have been performed by W. Vogelsang *et al.* for several GRSV models with factorization and renormalisation scales $\mu = p_T$. Figure 1 shows predictions of A_{LL} for inclusive positively charged hadrons for three different scenarios: 'GRSV-max' ($\Delta G(1GeV^2) = 1.9$), 'GRSV-standard' ($\Delta G(1GeV^2) = 0.4$), and '$\Delta g = 0$' ($\Delta G(1GeV^2) = 0.1$). Also shown on the plot are the anticipated experimental uncertainties on A_{LL}, estimated from the observed charged hadron yields.

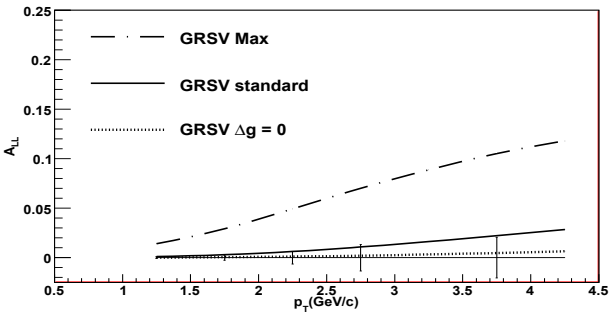

Fig. 1. GRSV predictions of A_{LL} for positively charged hadrons from pp ($\sqrt{s} = 62.4GeV$) and projected uncertainties for integrated luminosity of 0.08 pb^{-1}.

Conclusion

With the uncertainties anticipated on A_{LL}, we will be able to test the (currently disfavored) GRSV-max predictions[1] for consistency with the data at more than 3 σ. An attempt to distinguish between the two other input polarised gluon distributions will require more statistics, and distinguishing between them remains inconclusive for the moment.

References

1) D. de Florian, W. Vogelsang and F. Wagner, Phys. Rev. D **76**, 094021 (2007).
2) K. Adcox *et al.* (PHENIX Collaboration), Nucl. Instr. and Meth. A **499**, Pages 469-479, 489-507, 521-536 (2003).

[*1] Department of Physics, University of Massachusetts, Amherst, USA
[*2] RIKEN-BNL Research Center, Brookhaven National Laboratory, Upton, NY, USA

A study of high-p_T photons in the PHENIX electromagnetic calorimeter

K. Okada

In high-energy nuclear collision experiments, the detection of photons is one of the key issues. Because photons only interact with media electromagnetically, a photon produced by direct process provides information on the initial condition of the collision with little disturbance. Even for the hadronic probe, the major hadronic production process, the neutral pion (π^0), is identified with its decay products, which are photons.

At the RHIC-PHENIX experiment, the main photon detector is the electromagnetic calorimeters (EMCals) in the central rapidity region[1]. There are two types of calorimeters: the lead scintillator (PbSc) and the lead glass (PbGl). The cell size of PbSc (PbGl) is 53 (40) [mm] and is located 5 [m] from the collision point. It provides a high resolution in the vertical plane; however, there is no longitudinal segmentation.

Two photons from a π^0 start to merge at the π^0 energy of about 10 GeV, and it becomes difficult to identify a single photon cluster. In PHENIX, three approaches have been taken to address this photon-merging issue. The first is by carrying out a full simulation. The second is based on photon cluster shape parametrization according to test beam results. The third uses actual collision data. This report describes the third approach and gives a comparison between the three approaches.

The analysis is based on 4 pb^{-1} of proton+proton ($p+p$) collision data collected in 2006. In a $p+p$ collision, the particle multiplicity is so low that the effect of the overlap of two independent photon clusters can be safely ignored. Here we focus on the medium-energy region where the two photons from π^0 do not completely merge so that the cluster shape is expected to be different from that of a single photon. All clusters in the EMCal are divided into four categories by a cluster shape cut and a charged track match. If the cluster comprises merged photons from a π^0, it should not pass the photon shape cut or be matched to a charged track. However, this category also contains other objects: background not related to collisions, single photons that failed the photon shape cut, and neutral hadrons. Background not related to collisions is subtracted using the time-of-flight information. At higher energy, the contribution from the background is larger. It is about 10% at 15 GeV. The single-photon contribution is estimated by the number of clusters with a photon shape and no track match and the photon-shape-cut efficiency. The neutral hadron contribution is estimated by scaling the number of clusters matched to a track.

Figure 1 shows the number of clusters of the four categories in the PbSc as a function of cluster energy after the subtraction of the background not related to the collisions. From this figure, the category of (not photon shape and no track match) shows an excess starting at approximately 10 GeV, which indicates the contribution of π^0 photon merging (π^0_{merge}).

As a comparison, the number of π^0s identified by two clusters (π^0_{sep}) is used. Figure 2 shows the ratio of π^0_{sep} to ($\pi^0_{sep}+\pi^0_{merge}$). In the same figure, the results of two other analyses are also shown. As the cluster energy increases, more π^0 photons merge and fewer π^0 are identified by the separated photons, thus this ratio decreases. Since the PbGl has finer segmentation, the onset is higher than that of PbSc. All three independent approaches are in good agreement, although the analysis described in this report has a large statistical uncertainty at the high-energy region.

References

1) K.Adcox et al.: Nucl. Inst. Meth. A**499**, 469 (2003).

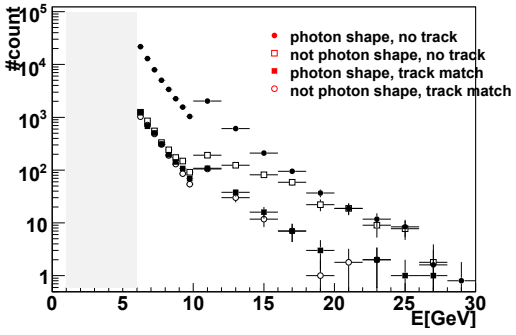

Fig. 1. Number of clusters after background subtraction (PbSc).

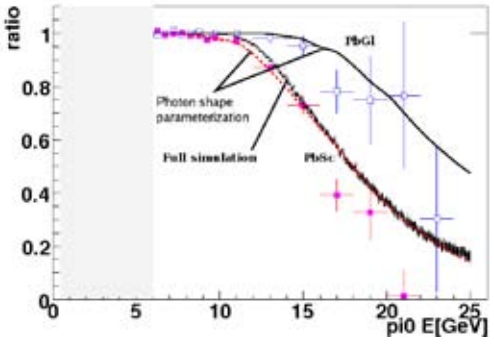

Fig. 2. Ratio of π^0_{sep} to ($\pi^0_{sep}+\pi^0_{merge}$) as a function of E_{π^0}.

Transversely Polarized Proton Spin Measurements in p+p Collisions with the PHENIX detector†

Mickey Chiu, Department of Physics, Brookhaven National Laboratory, Upton NY 11973

Early measurements of double longitudinal asymmetries at RHIC, when both protons are longitudinally polarized, have shown that the contribution to the proton's spin from gluon spin is perhaps not very large[1–3], and might be much less than the 70% remainder of the proton's spin that is unknown. In addition to longitudinally polarized spin measurements, one can also study the spin asymmetries which result when colliding transversely polarized protons. At the RHIC collision energy of $\sqrt{s} = 200$ GeV, NLO pQCD can accurately describe the invariant cross-sections in unpolarized collisions even at forward rapidities[4], so while it is not theoretically known how at the moment, the hope is that orbital angular momentum can be probed by measuring such myriad effects as the Sivers effect, Collins effect, and higher twist effects in tranversely polarized proton collisions, *in a region where the theory is quantitatively understood.*

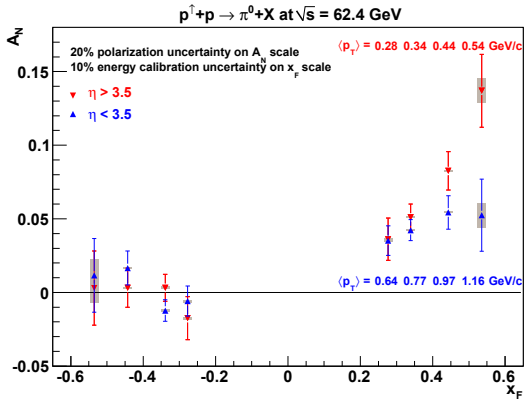

Fig. 1. The x_F dependence of neutral pion analyzing power $A_N^{\pi^0} = \frac{1}{P}\frac{N^\uparrow - N^\downarrow}{N^\uparrow + N^\downarrow}$ at $\sqrt{s} = 62$ GeV, for two different pseudorapidity bins

The most recent transversely polarized proton run at RHIC, in 2006, yielded an integrated luminosity of approximately 2.7 pb^{-1} at a $\sqrt{s} = 200$ GeV and approximately 20 nb^{-1} at a $\sqrt{s} = 62$ GeV, with an average beam polarization of about 50%. In this 2006 run, a new $PbWO_4$ based electromagnetic calorimeter, the Muon Piston Calorimeter (MPC), was installed at forward rapidities ($3.1 < \eta < 3.7$) in the south arm of PHENIX[6], in time for the transverse running at $\sqrt{s}$ = 62 GeV. This new detector allows for more interesting studies of transverse spin effects since many of the non-zero asymmetries are at larger rapidities, presumably because at forward rapidities one probes larger x_F and therefore have sensitivity to valence quark orbital motion effects.

After masking out noisy towers, correcting the tower by tower gains, clustering towers, and setting the energy scale using the mininum ionizing peak, one can reconstruct the π^0in the MPC. The background from combinatoric pairs is subtracted out using mixed events. After this, one can count the left-right asymmetry A_N in the production of π^0's relative to the spin direction of the proton. In figures 1 and 2 the single spin asymmetry A_N is plotted as a function of x_F and p_T, respectively, for our sample of π^0's in the MPC. One can see that there is a significant asymmetry. For this sample the statistics begin to run out at a p_T of 1.5 GeV/c, and in any case, due to the low collision energies there is a kinematic limit of $p_T \sim 3$ GeV/c for this lower collision energy. The low p_T that is reached does bring into question the ability to interpret the results, since a perturbative QCD treatment of the data may not be valid. This question can be explored further by comparing the production cross-section to the NLO pQCD prediction.

In conclusion, PHENIX has measured the single spin transverse asymmetry of π^0, $h^\pm$, and J/Ψ, covering an x_F from 0 to 0.6, and at two different collision energies. In the future, we expect approximately 25% of the polarized proton running at RHIC will be in the transverse mode, and the prospects for transverse asymmetry measurements at PHENIX are quite good. The north MPC was installed in time for the 2008 run, doubling the coverage at forward rapidities, while a compact tungsten-silicon based calorimeter covering pseudorapidity from 1 to 3, the Nose-Cone Calorimeter, is planned as an upgrade for installation in 2011. With the better coverage from the new detectors and higher statistics, one can make more differential measurements in order to decouple the possible contributions to the transverse single spin asymmetry.

References

1) S. S. Adler *et al.* [PHENIX Collaboration], Phys. Rev. Lett. **93**, 202002 (2004)
2) S. S. Adler *et al.* [PHENIX Collaboration], Phys. Rev. D **73**, 091102 (2006)
3) B. I. Abelev *et al.* [STAR Collaboration], Phys. Rev. Lett. **97**, 252001 (2006)
4) J. Adams *et al.* [STAR Collaboration], Phys. Rev. Lett. **92**, 171801 (2004)
5) S. S. Adler *et al.* [PHENIX Collaboration], Phys. Rev. Lett. **95**, 202001 (2005)
6) M. Chiu [PHENIX Collaboration], AIP Conf. Proc. **915**, 539 (2007)

Multiple Collision Effects on Relative Luminosity Measurement at PHENIX

A. Datta,[*1] D. Kawall,[*1,*2]

[Luminosity, Asymmetry, Spin]

Introduction

PHENIX measures asymmetries, A_{LL}, in particle production from collisions of polarized proton beams :

$$A_{LL} = \frac{1}{P_1 P_2} \frac{N_a/L_a - N_b/L_b}{N_a/L_a + N_b/L_b}.$$

Here N_a is the particle yield from beam helicity states $++$ and $--$, and N_b is that for $+-$ and $-+$. $L_{a,b}$ are the corresponding beam luminosities. P_1, P_2 are beam polarizations. The asymmetries are of physics interest because of their sensitivity to the polarization of quarks and gluons in the proton. Measuring the physics asymmetry requires the measurement of the relative luminosity $R = L_a/L_b$ of the colliding beams to higher precision than the expected asymmetries in particle production.

Current Method of Determining *R*

PHENIX has Beam Beam Counters[1)] (BBCs) at ± 144 cm from the center of the nominal interaction region (IR). If a *pp* collision occurs, the average hit time is constructed in the BBC arms north and south of the vertex. The difference in average hit time of each side is used to reconstruct the vertex position z:

$$z = \frac{T^S_{av} - T^N_{av}}{2} * c,$$

where c is the velocity of light in vacuum.

The rate of events occurring between ± 30 cm of the nominal IR center is a measure of the luminosity. This method counts at most one event per bunch crossing, even if there were multiple events. This leads to an underestimate of the luminosity. However, if events occur simultaneously at $z > 30$ cm and $z < -30$ cm, the two events are reconstructed as a single event at their midpoint, leading to an overestimate of the luminosity.

Effects of Multiple Collisions on BBC Response

To see which of the competing effects is dominant, we sought the BBC detection efficiency to inelastic collisions occurring at different vertex locations (see Fig. 1). The event generator PYTHIA was used to simulate inelastic *pp* collisions at $\sqrt{s} = 200$ GeV. The resulting particles were tracked and the BBC response simulated using PISA, the PHENIX detector simulator.

*1 Department of Physics, University of Massachusetts, Amherst, USA
*2 RIKEN-BNL Research Center, Brookhaven National Laboratory, Upton, NY, USA

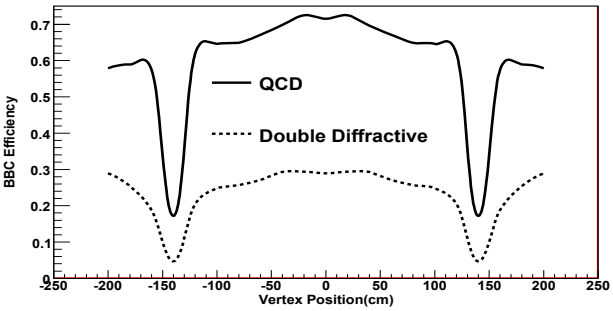

Fig. 1. BBC efficiency for some of the inelastic processes.

The BBC response to multiple events per bunch crossings could be simulated by using the BBC efficiency to the individual events. To do this, we formed the convolution in space and time of bunches of ions with properties consistent with those at RHIC. This yields a "true" temporal and spatial distribution of events. Multiple collisions per crossing could be simulated by choosing two or more events from this "true" distribution. The BBC response to each event is determined from its true vertex location (Fig. 1), then the average hit time in each BBC arm is determined, yielding the inferred vertex position. Since we know the true rate of events inside ± 30 cm, and the inferred (*i.e.* observed by BBC) rate of events inside ± 30 cm, we can determine the error in the luminosity calculation. To the extent that the bunch shapes are the same for like and unlike helicity bunches, the size of the error depends on the event rate and the vertex distribution.

Results

We can express the correction δR to the relative luminosity R as : $\delta R = R \times (r_a - r_b) \times f$. Here r_a, r_b are collision probabilities for the different helicity configurations a or b. Typical values are $R \approx 1$, $r_a \approx$ collision frequency/crossing frequency $\approx$ 2 kHz/78 kHz, and $|r_a - r_b|/r_a \approx 0.02$ and f (which is bunch shape and acceptance dependent) ≈ 0.5. This yields corrections $\delta R \leq 2 \times 10^{-4}$. This correction is expected to increase as the collider luminosity increases.

References

1) M. Allen et al. (PHENIX Collaboration), Nucl. Instr. and Meth. A **499**, Pages 469-479, 549-559 (2003).

Accessing Gluon Spin Contributions at Low-x through Double Longitudinal Spin Asymmetries

M. Grosse-Perdekamp,[*1] J. Koster,[*1] A. Veicht[*1]

A major research goal of the Relativistic Heavy Ion Collider and its two large experiments, STAR and PHENIX, is determining the polarized gluon distribution function ($\Delta g(x)$). These measurements are carried out using the double longitudinal spin asymmetry (A_{LL}) from either inclusive hadron or jet yields produced in the polarized proton-proton collisions. The double longitudinal spin asymmetry does not make a direct measurement of the parton momentum fraction x, but is sensitive to an integral of $\Delta g(x)$ over an x range determined by the choice of observable. The neutral pion A_{LL} measured at PHENIX during Run 05 and Run06, shown in Fig 1., have been used in a global QCD analysis and constrain the total gluon spin contribution to the proton ($\Delta G = \int_0^1 \Delta g(x)dx$) to be small for one model framework. The present data however still fits other models that have a large ΔG, such as the Gehrmann-Stirling Model C[2], equally well. In order to differentiate between the models new approaches are needed which limit the x range of the probed gluon.

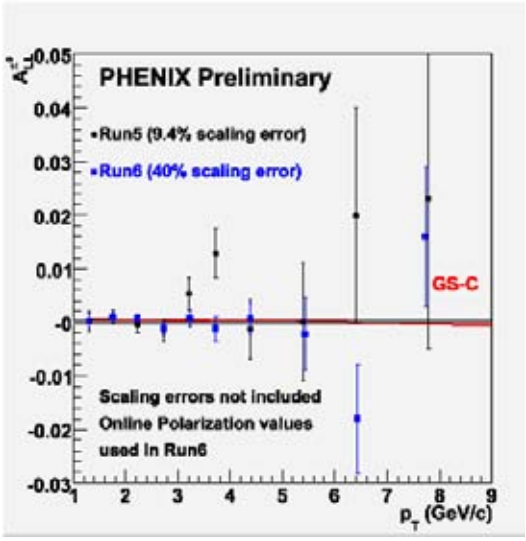

Fig. 1. PHENIX $\pi^0 A_{LL}$ from Run 05 and 06 proton-proton collisions at $\sqrt{s} = 200\,\mathrm{GeV}$, and the Gehrmann Stirling Model C predicted $\pi^0 A_{LL}$

The current PHENIX measurements are done with a single hadron at mid-rapidity which selects a broad range in the sampled $x_{1,2}$, that is roughly $0.03 \leq x_{1,2} \leq 0.3$. The need for measurements with a different range in x is illustrated in Figures 1 and 2. Figure 1 shows the predicted asymmetry based on the

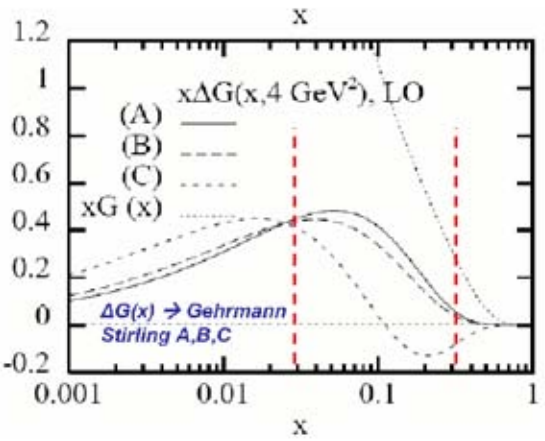

Fig. 2. Gehrmann Stirling Models A, B and C. The vertical dashed lines indicate the x range probed in current measurements.

Gehrmann-Stirling Model C[2] of the polarized gluon distribution which has a node but still contributes a total gluon spin contribution of 1. This model or any distribution which rises at sufficiently small x can be consistent with the present data set.

The small x region holds potentially large gluon spin contributions. Taking the unpolarized gluon distribution as a bound for the polarized gluon distribution gives an upper bound for the spin contributions. The CTEQ 6.5M unpolarized gluon distribution at a Q^2 of the maximum spin contribution for the range $0.01 < x < 0.03$ range is 4.9 $\hbar$ for $Q^2 = 4\,\mathrm{GeV}^2$ while for the $0.3 < x < 1$ range the maximum contribution is only 2.7×10^{-2} for Q^2=100 GeV^2.

Two ongoing analyses using existing data from Run 06 will access lower average x by using data from a new forward electromagnetic calorimeter. The first analysis will measure a single hadron A_{LL} while the second will require two hadrons: one in the forward region and the other in the central region.

References

1) M. Hirai, S. Kumano and N. Saito: Phys. Rev. , D74 2006.
2) T. Gehrmann and W.J. Stirling: Phys. Rev. , D53 1996.
3) K. Boyle: Proc. of the 17th Internation Spin Physics Symp., Vol. 915 (2007) p. 335-338.

*1 University of Illinois at Urbana-Champaign

Sampling fractions study for the Nose-Cone Calorimeter

O. Chvála*1

The Nose-Cone Calorimeter (NCC) is a new detector planned as a forward upgrade of PHENIX experiment at RHIC at BNL. This detector will expand PHENIX acceptance of γ and π^0 measurement from the current range of $\eta \pm 0.35$ adding the region of $1 < \eta < 3$.

NCC detector is a tungsten–silicon (W-Si) sampling calorimeter, its face is located 41 cm from the nominal PHENIX vertex. The NCC is approximately disk-shaped with a radius of 50 cm. Each tower composes of silicon sensors segmented to 15×15 mm pads. The detector is 19 cm thick, subdivided into three longitudinal segments: EM1, EM2 measuring electromagnetic showers; and a HAD segment, to identify and reject hadronic background. In addition, EM1 segment contains two layers of finely segmented 2D silicon strips at depths of 2 radiation lengths (X_0) and $3\,X_0$ for high energy π^0 identification (PI1 and PI2). Total depths of the two EM segments is $8\,X_0$ each, and $19\,X_0$ for the HAD segment. The NCC is designed to be a tracking calorimeter. Clusters of hits in the consecutive longitudinal segments together with information from the PIs and an independent vertex position measurement are fitted to form NCC tracks.

Large phase space coverage of the NCC together with its lateral and longitudinal segmentation necessitates rapidity and energy dependent calibrations of sampling fractions, energy deposits and shower shapes used to reconstructs shower energies and to identify particles responsible for a shower. A significant part of the corresponding analyzes was done during my stay at the RIKEN institute. This report describes how these calibrations performed.

The NCC is designed to measure electromagnetic showers, primarily photons, direct or a meson (mostly π^0) decay products. The calibrations described in this report correspond to electromagnetic showers. Calibration for hadrons and jets can be done following the same procedure.

1 Sampling fractions

Energy deposits in the calorimeter are sampled by pads comprising silicon sensors. Consecutive pads in an NCC segment are connected to form a sub-tower. The energy collected by the silicon pads is only a fraction of the energy deposited in the corresponding calorimeter volume, since most of the energy is deposited in the passive tungsten radiator.

The sampling fraction, the ratio of the detected energy to the total energy deposited, depends on the shower composition, which varies with the depth and the shower energy. It also varies with η as the shower depth changes by about 1.4 from nearly perpendicular impact at high η to a (pseudo)rapidity of about one, modifying the sampling fraction. The sampling fraction of an EM shower therefore depends on the NCC segment, the shower energy and the incident angle of the shower on the detector. The sampling fraction also depends on energies of tracking cutoffs in the GEANT3 simulation.

The sampling fractions were studied by a detailed GEANT3 simulation of the NCC calorimeter. The sampling fractions for the three NCC segments are shown in Fig. 1a for the EM1, Fig. 1b for the EM2, and Fig. 1c for the HAD segment, as a function of η and energy of the shower. The sampling fractions are used iteratively in the track reconstruction algorithm as a look-up table with fast bilinear interpolation.

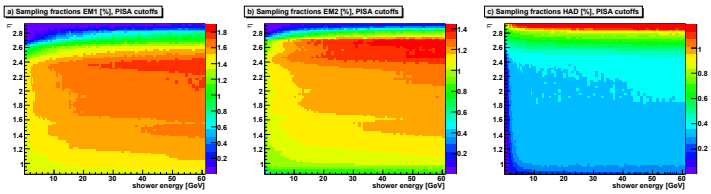

Fig. 1. Sampling fractions in percent for a) EM1, b) EM2, c) HAD segment as a function of the shower energy and the angle. Importance of both angular and energy dependence is clearly visible.

2 Energy calibration

After the tracks are formed, the final stage energy correction is applied. This accounts for leakage at the calorimeter edges, nonlinearity at low energies, and calibration of the reconstruction losses. The energy calibration factor $\xi(E, \eta)$ is defined as a ratio of the true shower energy over the reconstructed energy of the shower; the reconstructed shower energy comprises of sampled energy deposits in each sub-tower in the calorimeter segments weighted by the sampling fraction and the reconstruction algorithm. Fig. 2 shows $\xi(E, \eta)$ as a function of the reconstructed shower energy and angle.

3 Conclusion

We studied energy and rapidity dependence of the sampling fraction and energy calibration of NCC using a detailed GEANT simulation during SPINFEST at RIKEN. It can be observed in Fig. 2 that the sam-

*1 Dept. of Physics and Astronomy, University of California in Riverside, Riverside, CA 92521, USA

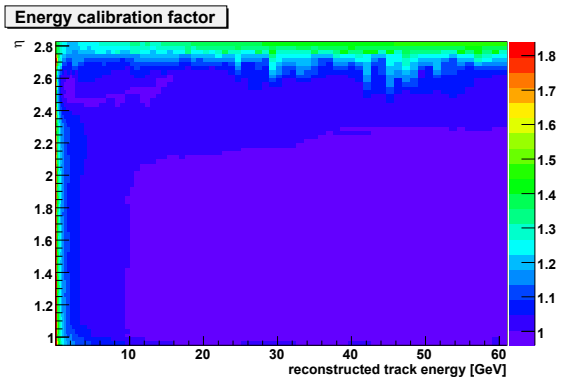

Fig. 2. Energy calibration for electromagnetic showers as a function of the shower energy and η

pling fractions shown in Fig. 1 work well and they are appropriate for the NCC detector. The final stage energy calibration corrections remain significant only at edge regions and for low energy γs, as expected from the detector geometry and presence of cutoffs in the shower development simulations.

4 Acknowledgments

I would like to express my thanks to the RIKEN institute, Kensuke Okada, Yuji Goto, Astrid Morreale and other PHENIX collaborators for allowing me to work at this workshop at RIKEN and for making it a very pleasant stay.

4. Hadron Physics(Theory)

Global QCD Analysis of Fragmentation Functions

D. de Florian,[*1] R. Sassot,[*1] M. Stratmann

[hadronization, global QCD analysis, theoretical uncertainties]

The last few years have seen a growing interest in accurate parameterizations for fragmentation functions driven by the increasing role of one-particle inclusive measurements as a QCD laboratory for the spin and flavor structure of the nucleon, nuclear modifications of parton densities and fragmentation functions, and, in general, as a window to the non-perturbative regime so far little explored.

Until recently, fragmentation functions have been extracted exclusively from singe-inclusive electron-positron annihilation data[1]. Such a procedure has many inherent uncertainties: e^+e^- data provide no information on how to disentangle quark from antiquark fragmentation and the gluon fragmentation is only weakly constrained from QCD scaling violations. Here we report on the results of a first *global QCD analysis* [2], where we have determined individual fragmentation functions for quarks and antiquarks for all flavors, as well as gluons, from a much larger set of data. Hadron production in semi-inclusive deep-inelastic scattering (SIDIS) and proton-proton collisions has the advantage of charge separated final states and sensitivity to different scales, energy fractions z, and combinations of fragmentation functions than e^+e^- data.

In order to accommodate the additional data, we adopt a more versatile functional form for the input fragmentation functions than in previous extractions,

$$D_i^H(z,\mu_0) = N_i z^{\alpha_i}(1-z)^{\beta_i}[1+\gamma_i(1-z)^{\delta_i}], \qquad (1)$$

where the initial scale μ_0 in Eq. (1) is taken to be $\mu_0 = 1\,\mathrm{GeV}$ for the light partons and the quark masses for charm and bottom. To reduce the number of parameters to those that can be effectively constrained by the data, we are still forced to make some plausible assumptions. For instance, we impose isospin symmetry for the sea fragmentation functions in the case of pions, i.e., $D_{\bar{u}}^{\pi^+} = D_d^{\pi^+}$, but we allow for slightly different normalizations in the $q+\bar{q}$ sum $D_{d+\bar{d}}^{\pi^+} = N D_{u+\bar{u}}^{\pi^+}$. Similar assumptions are made in the case of kaons, protons, and the remaining charged hadrons, see[2].

The resulting fits are in good agreement with all data analyzed[2], see, e.g., Figs. 1 and 2. This is a crucial test of the fundamental universality property of fragmentation functions usually assumed in QCD calculations. Differences to previous analyses[1] are most apparent when compared to data that imply charge separation, especially in the case of kaons, and, in general, for observables sensitive to the gluon fragmentation at large energy fractions z. In order to reliably estimate the uncertainties characteristic of the fragmentation functions obtained in our fits, we apply the Lagrange multiplier technique[2] to the χ^2-profiles for the truncated second moments $\int_{z_{\min}}^1 z D_i^H(z)dz$. For pions the relative uncertainties are found to be about 3% and 10% for "favored" (valence) and "unfavored" (sea) or gluon fragmentation functions, respectively. The uncertainties in kaon fragmentation functions are typically twice as large as those for pions[2]. In the near future, precision data from BELLE are expected to further reduce the uncertainties by allowing for the first time to study scaling violations in e^+e^- data.

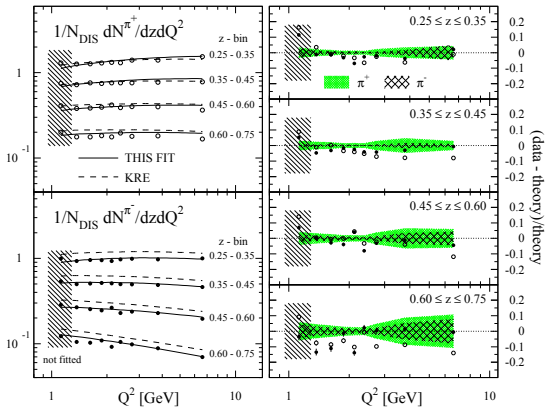

Fig. 1. Comparison with $\pi^\pm$ SIDIS data from HERMES.

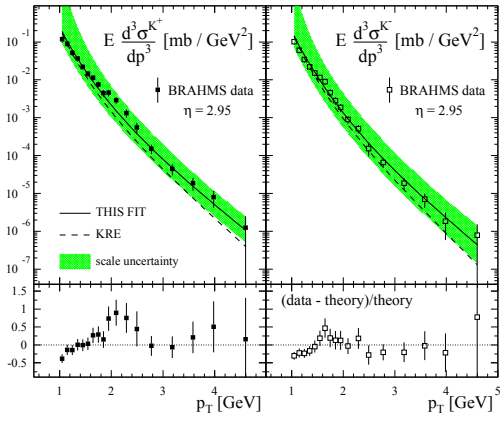

Fig. 2. Comparison with $pp \to K^\pm X$ data from BRAHMS.

References

1) S. Kretzer, Phys. Rev. **D62**, 054001 (2000); S. Albino *et al.*, Nucl. Phys. **B725**, 181 (2005); M. Hirai *et al.*, Phys. Rev. **D75**, 094009 (2007).
2) D. de Florian, R. Sassot, and M. Stratmann, Phys. Rev. **D75**, 114010 (2007); **D76**, 074033 (2007).

*1 Dep. de Fisica, Universidad de Buenos Aires, Argentina

Isospin dependence of the EMC effect†

W. Bentz,[*1] I. C. Cloët,[*2] and A. W. Thomas[*3]

[NUCLEAR STRUCTURE FUNCTIONS, Isospin dependence, Effective Quark Theories]

In this work we investigate the dependence of the EMC ratio

$$R_A = \frac{F_{2A}}{ZF_{2p} + NF_{2n}} = \frac{\frac{4}{9}f_{u/A} + \frac{1}{9}f_{d/A}}{\frac{4}{9}f^{(0)}_{u/A} + \frac{1}{9}f^{(0)}_{d/A}} \qquad (1)$$

on the ratio Z/N of the nucleus A. Here F_{2A} is the spin independent nuclear structure function, and F_{2p}, F_{2n} are the spin independent free nucleon structure functions. The quark distributions in the nucleus are denoted as $f_{q/A}$ $(q = u, d)$, and the distributions in the absence of nuclear effects are $f^{(0)}_{q/A} = Z/Af_{q/p} + N/Af_{q/n}$, where $f_{q/N}$ are the quark distributions in the nucleon $(N = p, n)$.

We evaluate the nuclear quark distributions in nuclear matter. The equation of state for nuclear matter is constructed in the mean field approximation[1)], including self consistent isoscalar scalar (σ), isoscalar vector (ω^0), and isovector vector (ρ^0) fields. The individual nucleons are described as quark-diquark bound states in the NJL model, where we take into account the scalar (0^+) and axial vector (1^+) diquarks. The strengths of the diquark interactions are adjusted to the mass and the axial vector coupling constant of a free nucleon. The couplings of the vector fields (ω^0 and ρ^0) to the nucleon are adjusted to the saturation density and the symmetry energy for the case $N = Z$. The quark distributions in the nucleus are evaluated as the convolution of the nucleon distributions in the nucleus and the quark distributions in the nucleon[2)].

In Figs. 1 and 2 we show the EMC ratios for several fixed ratios Z/N. The baryon density used in the calculation is the saturation density for each value of Z/N. The data shown in the figures refer to the nuclear matter extrapolation of isoscalar nuclei.

On the neutron rich side (Fig. 1), the EMC effect increases as Z/N decreases from 1 to 0.6, while for $Z/N < 0.6$ the effect decreases in the valence quark region. This can be understood as follows: Because of the isovector mean field, the u (d) quarks feel an additional attraction (repulsion) as we go to the neutron rich side. This additional binding means that the medium modifications of the u distribution become larger as we go to the neutron rich side. Because of the bigger charge of the u quark, the EMC effect will tend to increase (see Eq.(1)). However, at the same time the overall magnitude of the u distribution decreases relative to the d distribution, and eventually the smaller medium modification of the d distribution leads to a decreasing EMC effect.

On the proton rich side, the EMC effect decreases with increasing Z/N, see Fig.2. In this case, the binding (medium modification) of the u (d) distribution becomes smaller (larger) as we replace neutrons by protons, and at the same time the overall magnitude of the u distribution becomes dominant over the d distribution. Therefore the EMC effect gradually decreases on the proton rich side.

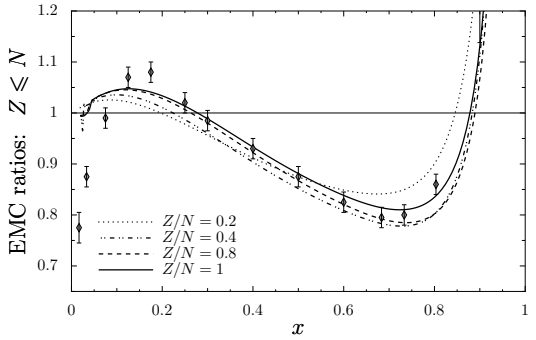

Fig. 1. EMC ratios for $Z/N < 1$.

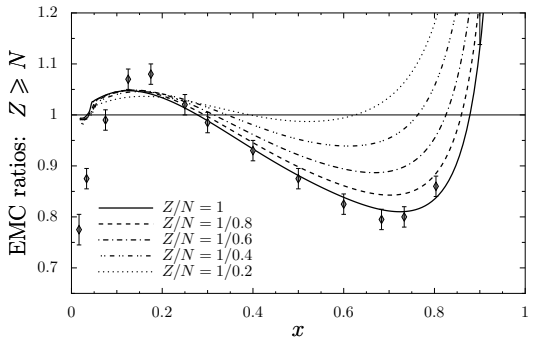

Fig. 2. EMC ratios for $Z/N > 1$.

References

1) W. Bentz and A.W. Thomas, Nucl. Phys. **A 696** (2001) 138.
2) I.C. Cloët, W. Bentz and A.W. Thomas, Phys. Lett. **B 642** (2006) 210.

† Condensed from an article by I.C. Cloët, W. Bentz, and A.W. Thomas, to be published.

*1 Department of Physics, Tokai University, Kanagawa, Japan
*2 Argonne National Laboratories, Argonne, IL, U.S.A.
*3 Jefferson Laboratories, Newport News, VA, U.S.A.

On the DLY Relation for Fragmentation Functions†

W. Bentz,[*1] T. Ito,[*1] A. W. Thomas[*2] and K. Yazaki[*3]

[FRAGMENTATION FUNCTIONS, Drell-Levy-Yan Relation, Effective Quark Theories]

The Drell-Levy-Yan (DLY) relation[1)] expresses the quark fragmentation function $D_q^h(z)$ by the quark distribution function $f_q^h(x)$ in the unphysical region of the Bjorken variable ($x > 1$). Here we outline two independent derivations of this relation, referring to the case of the nucleon ($h = N$), and give numerical examples, which indicate that the predictions for $D_q^h(z)$ based on this relation and a simple effective quark theory are smaller than the empirical values by factors of ten to hundred.

We consider the Green function $< p_n|T\left(\mathcal{O}(0)\Psi_N(p)\right)|0>$, where $\Psi_N(p)$ is the Fourier transform of the nucleon field operator, $\mathcal{O}$ is a local field operator, and $|p_n>$ is a hadronic state. If $\Gamma(p, p_n)$ denotes the amputated Green function, the spectral representation (or reduction formula) leads to the following relations:

$$\begin{aligned} < p_n|\mathcal{O}|p> &= \overline{\Gamma}(p, p_n)\, u_N(p) \\ < \overline{p}, p_n|\mathcal{O}|0> &= \pm\overline{\Gamma}(-p, p_n)\, v_N(p)\,. \end{aligned} \tag{1}$$

Here $|p>$ ($|\overline{p}>$) denotes a nucleon (antinucleon) state with 4-momentum p^μ, and u_N, v_N are the nucleon spinors. The plus (minus) sign holds if $\mathcal{O}$ is a fermion (boson) type operator.

If we take $\mathcal{O}$ to be the current operator in the definition of the hadronic tensors $W^{\mu\nu}$ and $\overline{W}^{\mu\nu}$ for the processes $ep \to e'X$ and $e^+e^- \to pX$, respectively, Eq. (1) gives $\overline{W}^{\mu\nu}(p, q) = -W^{\mu\nu}(-p, q)$, which leads to the DLY relation

$$D_q^h(z) = \pm\frac{z}{6}\, f_q^h(\frac{1}{z})\,. \tag{2}$$

For $h = N$ ($h = \pi$) the minus (plus) sign holds. We can also take $\mathcal{O}$ to be the quark field in the operator definitions of $f_q^h(x)$ and $D_q^h(z)$, and Eq. (1) again leads to (2). One important observation from Eq.(2) is the following: For the case of the nucleon, the generalized distribution *must* cross zero at $x = 1$, but for the pion it *must not* cross zero because both the distribution and the fragmentation functions should be positive.

As an illustration, we show the generalized u distribution for the π^+ and proton in Figs. 1 and 2. Here we use a simple NJL model description of the pion as a $q\overline{q}$ state, and the nucleon as a quark-scalar diquark state. It is particularly evident from Fig.2 that the "tail" of the distribution ($x > 1$) is extremely small. Indeed, the fragmentation function predicted by Eq.(2) turns out to be smaller than the empirical one by factors of ten to hundred, and a similar - though less severe - problem occurs for the pion, too. Because the distributions for $x < 1$ describe the empirical ones very well[2)], this is a puzzling problem. We found that sea quark effects, induced by the pion cloud, do not improve the situation.

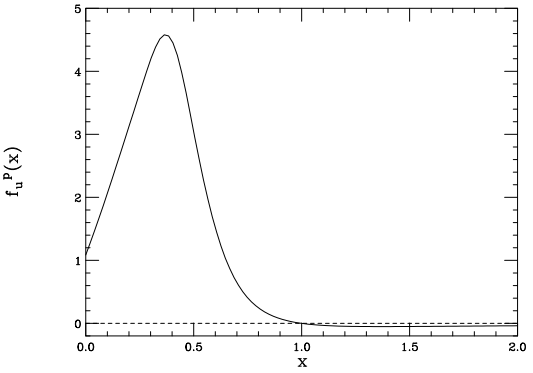

Fig. 1. Generalized u distribution in proton.

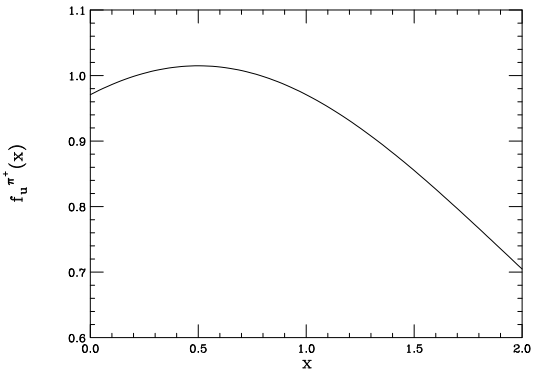

Fig. 2. Generalized u distribution in π^+.

References

1) S.D. Drell, D.J. Levy and T.M. Yan, Phys. Rev. **187** (1969) 2159; **D1** (1970) 1617.
2) I.C. Cloet, W. Bentz and A.W. Thomas, Phys. Lett. **B 642** (2006) 210.

† Condensed from an article by T. Ito, W. Bentz, A.W. Thomas and K. Yazaki, to be published.

*1 Department of Physics, Tokai University, Kanagawa, Japan
*2 Jefferson Laboratories, Newport News, VA, U.S.A.
*3 Department of Mathematics, Tokyo Woman's Christian University, Japan

Change in Shear Viscosity as Color Ionization of QCD

Y. Hidaka and R. Pisarski*1

[Quark gluon plasma, nonequilibrium system]

The experimental results on heavy-ion collisions at RHIC have clearly indicated a new regime. Much interest has been focused on collective properties, particularly elliptical flow, which appear to be well described by a system in which the ratio of the shear viscosity, to the entropy, is small.

Of particular interest is the transition from a gaseous plasma, in which ionization is complete, to a regime in which ionization is only partial. As the fraction of ionization decreases, the system forms a condensed phase, which is usually a liquid; at higher densities still, then a solid.

We suggest that in a non-Abelian gauge theory, the renormalized Polyakov loop characterizes the degree of ionization of color charge. Lattice simulation[1] indicates that while the theory is confined for $T \leq T_c$, the ionization of color is essentially complete by a few times T_c. Thus, color charge is only partially ionized in this relatively narrow temperature window[2]. We term this a "semi"-QGP.

In this report, we consider how shear viscosity changes in semi-QGP[3]. In perturbative calculation [4,5], the shear viscosity changes simply from the running of QCD coupling with temperature. We ignore this, to concentrate on how it depends on how it changes as the Polyakov loop does.

To include the effect of the Polyakov loop, we characterize eigenvalues of the temporal Wilson line as a timelike component of the gauge field A_0, which is diagonal in color: $A_0^{cl} = Q^a/g$, where g is the gauge coupling constant for an SU(N_c) gauge theory, and $a = 1...N_c$. The Wilson line is $L = \exp(iQ/T)$; thus, the Polyakov loop in the fundamental representation is $\ell = \mathrm{tr}L/N_c$. Thermal vacuum is given not by a fixed Q, but by a distribution. For example, the confined phase at infinite N_c shows a completely flat eigenvalue distribution, which ensures that all Polyakov loops vanish in the confined phase, $\langle \mathrm{tr}\, L^n \rangle = 0$ for all $n \geq 1$.

Viscosity can be obtained by solving the Boltzmann equation[4,5] in the background using the constant A_0. We estimate viscosity in the pure gauge theory with a large number of colors for simplicity. In this case, viscosity is described as a function of the Polyakov loop. Since the expectation value of Polyakov loop is less than one in semi-QGP, one can expand viscosity for a small Polyakov loop. We find a simple result for a small Polyakov loop as

$$\frac{\eta(L)}{\eta_{\mathrm{pert.}}} = \frac{2|\langle\ell\rangle|^2}{1+|\langle\ell\rangle|^2}\frac{\zeta(2)\zeta(4)}{\zeta^2(5)} \simeq 3.31\frac{|\langle\ell\rangle|^2}{1+|\langle\ell\rangle|^2}\,, \quad (1)$$

*1 Department of Physics, Brookhaven National Laboratory

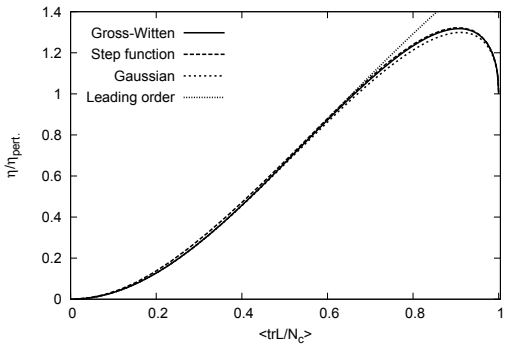

Fig. 1. Numerical results for viscosity divided by perturbative viscosity with several ansatz of color eigenvalue densities. Leading order stands for Eq.(1).

where $\zeta(n)$ is the Riemann zeta-function. $\eta_{\mathrm{pert.}}$ is the perturbative viscosity, $\eta_{\mathrm{pert.}} \simeq 27.1T^3/(g^4 \ln g^{-1})$[4,5] without the background. In Fig. 1, we show numerical results for $\eta(L)/\eta_{\mathrm{pert.}}$ with assumptions of eigenvalue distribution, which are step-function-, Gross-Witten-[6] and Gaussian-type distributions. The differences between these eigenvalue distributions are very small. We also plot the ratio of viscosity in Eq. (1). The result is in good agreement with numerical results up to $\langle\ell\rangle = 0.7$. This indicates that a higher representation of color is negligible in semi-QGP. We find that shear viscosity is suppressed near T_c or at a small ℓ, as shown in Fig. 1. This implies that the ratio of shear viscosity to entropy increases significantly in semi-QGP. This increase in viscosity/entropy may be important in proceeding from RHIC to LHC energies. A bump is observed near $\ell \simeq 0.9$. The value is 25% larger than the perturbative value. The physical interpretation has not been determined yet, but this will be clarified in our future work[3].

References

1) S. Gupta, K. Hubner and O. Kaczmarek, [arXiv:0711.2251].
2) R. D. Pisarski, Phys. Rev. D **74**, 121703 (2006).
3) Y. Hidaka and R. Pisarski in preparation.
4) M. Le Bellac, *Thermal Field Theory* (Cambridge University Press, Cambridge, 2000).
5) P. Arnold, G. D. Moore and L. G. Yaffe, Jour. High Energy Phys. **0011**, 001 (2000); *ibid.* **0305**, 051 (2003).
6) D. J. Gross and E. Witten, Phys. Rev. D **21**, 446 (1980).

Nucleon axial charge in (2+1)-flavor dynamical DWF QCD

Y. Aoki,[*1] T. Blum,[*2*1] H.-W. Lin,[*3] M.-F. Lin,[*4] S. Ohta,[*5*6*1] S. Sasaki,[*7] R.J. Tweedie,[*8] T. Yamazaki,[*2] and J.M. Zanotti[*8] for RBC and UKQCD Collaborations

[Quantum Chromodynamics, Hadron Physics, Nucleon Structure]

The isovector axial charge, g_A, of nucleon is defined as the axial vector form factor at zero four-momentum transfer, $g_A = G_A(q^2 = 0)$. The axial vector form factor is given by the nucleon matrix element of the axial vector current, $A^a_\mu = \overline{\psi}\gamma_\mu\gamma_5(\tau^a/2)\psi$, with up- and down-quark doublet ψ,

$$\langle n'|A^a_\mu|n\rangle = \overline{u}_{n'}[\gamma_\mu G_A(q^2) + iq_\mu G_P(q^2)]\gamma_5(\tau^a/2)u_n,$$

where G_P is the induced pseudoscalar form factor, τ^a an isospin Pauli matrix, and q the momentum transfer, $q_\mu = p^n_\mu - p^{n'}_\mu$. The axial charge is known experimentally, as $g_A = 1.2695(29)$[1], from neutron beta decay. That the value deviates from unity is an outcome of spontaneous breaking of chiral symmetry in quantum chromodynamics (QCD), and as such plays a pivotal role in understanding nucleon structure.

The RBC and UKQCD Collaborations recently completed a refined lattice-QCD calculation of this quantity using the "2+1" flavors of dynamical domain-wall fermion (DWF) ensembles with strange quark with a mass slightly heavier than physical, four values for degenerate up and down light quark mass that correspond to pion mass of $m_\pi = 0.33$-0.67 GeV, and on two volumes with spatial size $L = 1.8$ and 2.7 fm[2,3]. These ensembles consist the most accurate theoretical calculation of hadron physics to date, with the best chiral and flavor symmetries provided by DWF quarks at a sufficiently high lattice cutoff combined with reasonably large volumes. This allows us a detailed investigation of the systematics associated with nucleon structure calculations, most notably the finite-volume effect (FVE) in the axial charge which the RBC collaboration pioneered in quenched DWF calculations[4].

Our results are summarized in Fig. 1, and compared with some earlier ones. We find unexpectedly large FVEs at the smallest value of m_π. Further, the present results exhibit a scaling with the single variable $m_\pi L$ which we also discovered in previous two-flavor DWF and Wilson fermion calculations. Using this scaling to eliminate the finite-volume effect, we obtain $g_A = 1.20(6)(4)$ at the physical pion mass, where the first and second errors are statistical and systematic. This large FVE with dynamical quarks suggests

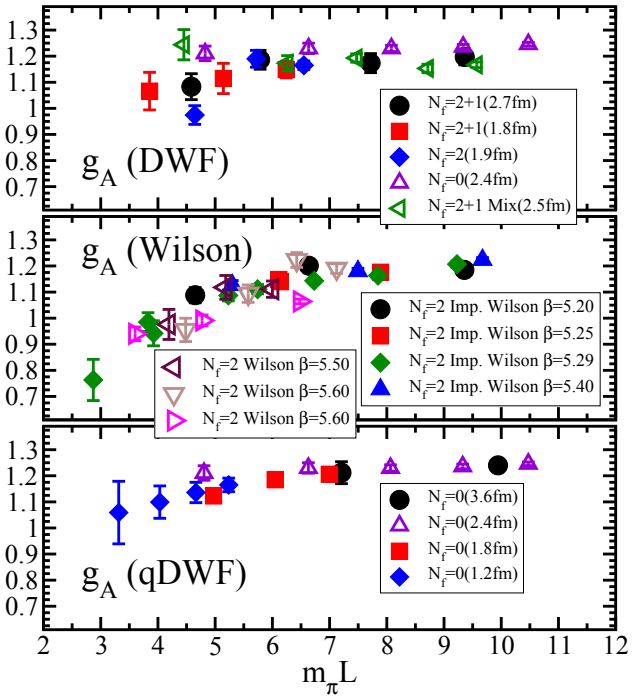

Fig. 1. Finite-volume effect (FVE) and $m_\pi L$ scaling in nucleon axial charge, g_A. Top, middle, and bottom panels are respectively dynamical DWF, dynamical Wilson, and quenched DWF results. For details, see ref.[5] and references cited there in: We observe significant finite-volume effect at the lightest mass in the top. The effect scales well with a single variable, $m_\pi L$.

we need larger lattice volumes for satisfactory lattice calculations of nucleon structure at realistic up- and down-quark mass values. See a letter article, ref.[5], for further details. We thank the members of the RBC and UKQCD Collaborations for ensemble generation and analyses, and RIKEN, USDOE, PPARC, BNL, Columbia and Edinburgh Universities for providing the resources essential to complete this research.

*1 RIKEN BNL Research Center, BNL, USA
*2 Physics Department, University of Connecticut, USA
*3 Thomas Jefferson National Accelerator Facility, USA
*4 Center for Theoretical Physics, MIT, USA
*5 Institute of Particle and Nuclear Studies, KEK
*6 Physics Department, SOKENDAI Graduate University
*7 Physics Department, University of Tokyo
*8 School of Physics, University of Edinburgh, UK

References

1) W.-M. Yao et al., Journal of Physics, G 33, 1 (2006).
2) C. Allton *et al.* [RBC and UKQCD Collaborations], Phys. Rev. D **76**, 014504 (2007).
3) P. Boyle [RBC and UKQCD Collaborations], PoS (LATTICE 2007) 005; arXiv:0710.5880 [hep-lat].
4) S. Sasaki, K. Orginos, S. Ohta and T. Blum, Phys. Rev. D **68**, 054509 (2003).
5) T. Yamazaki *et al.*, [RBC and UKQCD Collaborations], Phys. Rev. Letters 100, 171602 (2008).

Dynamical QCD simulation with θ terms†

T. Izubuchi,[*1] S. Aoki,[*1*2] K. Hashimoto,[*1] Y. Nakamura,[*3] T. Sekido[*1] and G. Schierholz[*2]

[Strong CP problem, electric dipole moment, θ vacuum]

Nonperturbative prediction of the Neutron's Electric Dipole Moment (NEDM) with the Strong CP violating θ term, $S_\theta = i\frac{\theta}{32\pi^2}\int \epsilon_{\mu\nu\tau\rho}F_{\mu\nu}F_{\tau\rho}d^4x = i\theta Q_{\rm top}$, has been recognized as a challenging, yet very interesting, task for lattice QCD for 19 years. *The Strong CP Problem*, the potential inconsistency between the mysteriously small experimental NEDM and anticipations for a natural size of vacuum angle $\theta \sim \mathcal{O}(1)$, may be exposing one of the most prominent unnaturalness in nature. To seek a breakthrough on this difficult calculation, we introduce the CP violation according to S_θ in the probability of QCD ensemble generation for the first time, then measure observables without reweighting to see whether the new calculation method has better control over the statistical and systematic errors. To keep the Boltzmann weight positive semidefinite, θ is analytically continued to pure imaginary, $\theta \to -i\theta$, which can be reverted assuming θ is small.

To measure NEDM, a constant electric field, $\vec{E}$, is applied to Nucleon, and the energy, m_N, dependence on its spin polarization, $\vec{S}$, is measured,

$$m_N(\vec{E},\vec{S}) - m_N(\vec{E},-\vec{S}) = 2id_N(\theta)\vec{S}\cdot\vec{E} + \mathcal{O}(E^3) \ . \quad (1)$$

We use the ordinary Euclidean $U(1)$ field background rather than its *Minkowski* space version used in the original calculation,[1)] which is reported to be susceptible to the systematic error induced at the periodic boundary in temporal direction.[2)] To avoid the boundary effect and also to safely neglect the $\mathcal{O}(E^3)$ in eq. (1), a *uniform and weak electric field* invented some time ago[3,4)] is used.

Our lattice quark is the two flavors of the RG-improved clover fermion, $\psi(x)$, which is set to be unphysically heavy, $m_\rho/m_\pi \sim 0.85$, for the feasibility study of the novel method. The θ term is rotated into a parity-violating "mass" term in the quark action, $\frac{\theta}{2}\bar{\psi}(x)\gamma_5\psi(x)$. A thermalized statistical ensembles with $\theta = 0.4$ and 0.0 are accumulated for $\tau = 2,000$ in the molecular dynamics time unit each in the Hybrid Monte Carlo simulations with Sexton-Weingarten, and Hasenbush accelerations. The gauge action of our choice is the RG-improved gauge action a la Iwasaki with $\beta = 2.1 (a^{-1} \sim 2\text{GeV})$ for $16^3 \times 32$ lattice.

When $e^{-S_\theta} = e^{-\theta Q_{\rm top}}$ is turned on, the negative topological charge, calculated from the $\mathcal{O}(a^2)$-improved combination of APE-smeared 1×1 and 2×1 plaquettes, should appear more frequently than the positive charge for $\theta > 0$. Indeed, the histogram of $Q_{\rm top}$ for $\theta = 0.4$ comes out shifted in the negative direction. The mean topological charge becomes negative, $\langle Q_{\rm top}\rangle = -7.9$, leaving the width of the distribution approximately unchanged; a clear signature of CP violation is successfully implemented in the simulation.

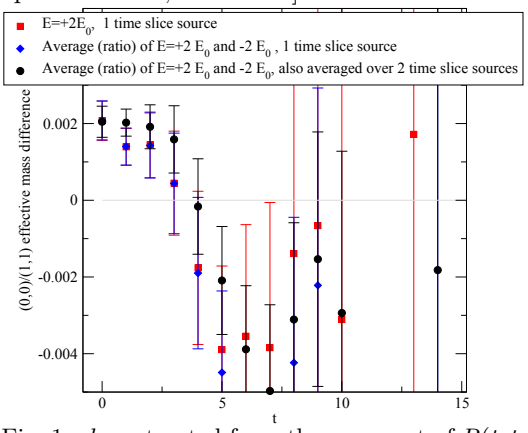

Fig. 1. d_N extracted from the exponent of $R(t, t_{src}; E)$ determined at t. The applied external electric fields are $E = +2E_0$ (red), $E = -2E_0$ (blue), and the appropriate average over $E = \pm 2E_0$ (black).

The polarized Neutron propagator is measured on 100 independent configurations under the external electric field, that is, a multiple of $E_0 = 2\pi/(L_z L_t) \times 3 \simeq 0.0368$ in the z direction. The quark charges are set as $q_{\rm up} = 2/3$ and $q_{\rm down} = -1/3$. As an example of physical signal, Fig. 1 shows the spin-dependent ratio of the propagators,

$$R(t, t_{src}; E) = \lim_{t\to\text{large}} \frac{\langle N_\uparrow(t)\overline{N}_\uparrow(t_{src})\rangle_{\theta,E}}{\langle N_\downarrow(t)\overline{N}_\downarrow(t_{src})\rangle_{\theta,E}} \propto e^{-d_N\theta E t}. \quad (2)$$

The results are only on two parameter points, and could be susceptible to systematic errors, such as excited state contaminations, precise normalization of θ, and $\mathcal{O}(\theta^2, E^2)$. However, the improved signal-to-noise ratio for the novel method is encouraging considering the relatively small statistics. A more demanding simulation with domain-wall fermions or overlap fermion might be free from (some of) such systematic errors.

† Condensed from the article in PoS (LATTICE 2007) 351.
*1 Institute for Theoretical Physics, Kanazawa University
*2 Institute of Physics, University of Tsukuba
*3 John von Neumann Institute NIC/DESY Zeuthen, Germany
* This work was made possible with the computational resources provided by the Large-Scale Simulation Program No. 07-14 (FY2007) of the High-Energy Accelerator Research Organization (KEK), the RIKEN Super Combined Cluster (RSCC), and QCDOC at RBRC and Columbia University.

References
1) S. Aoki and A. Gocksch: Phys. Rev. Lett. **63**, 1125 (1989), Erratum-ibid.65:1172,1990.
2) E. Shintani *et al.*: Phys. Rev. **D75**, 034507 (2007), [hep-lat/0611032].
3) U. M. Heller: Nucl. Phys. Proc. Suppl. **4**, 417 (1988).
4) E. Brown: Phys. Rev. **133**, A1038 (1964).

5. Particle Physics

$B_0 - \overline{B_0}$ mixing in static limit with domain wall fermions†

Y. Aoki*1

Experimental efforts made it possible to determine the oscillation frequencies of $B_d^0 - \overline{B_d^0}$ and $B_s^0 - \overline{B_s^0}$ precisely. The Kobayashi-Maskawa matrix elements V_{td} and V_{ts} can be obtained through these results, once the hadronic matrix elements are calculated. In the standard model, the oscillation frequency reads

$$\Delta m_q = [\text{known factor}] \cdot |V_{tq}^* V_{tb}|^2 \mathcal{M}_q, \qquad (1)$$

where q is either d or s, $\mathcal{M}_q$ is the B_q^0–$\overline{B_q^0}$ mixing matrix element

$$\mathcal{M}_q = \left\langle \bar{B}_q^0 \right| [\bar{b}\gamma^\mu(1-\gamma_5)q][\bar{b}\gamma_\mu(1-\gamma_5)q] \left| B_q^0 \right\rangle \qquad (2)$$

which needs to be calculated in QCD. By historical reason matrix element sometimes is written with mass m_{B_q} and decay constant f_{B_q} being factorized as $\mathcal{M}_q = \frac{8}{3} m_{B_q}^2 f_{B_q}^2 B_{B_q}$, which defines the bag parameter B_q. Lattice QCD provides an ideal framework to calculate these low energy matrix elements.

In lattice calculation the $SU(3)$ breaking ratio $\xi = f_{B_s}\sqrt{B_{B_s}}/f_{B_d}\sqrt{B_{B_d}} \propto \sqrt{\mathcal{M}_s/\mathcal{M}_d}$ can be obtained more precisely than the each matrix element, since the large fraction of the statistical and systematic errors cancel in the ratio. Through ξ (theory) and $\Delta m_s/\Delta m_d$ (experiment), the ratio $|V_{td}/V_{ts}|$ is determined. $|V_{td}/V_{ts}|$ provides an important constraint on the unitarity triangle. As the error of the ratio from the experiment is small (sub-percent), the error of the lattice calculation of ξ dominates the width of the allowed range from $|V_{td}/V_{ts}|$.

To be free from the uncontroled quenching error, the full $2+1$ flavor lattice QCD calculation of ξ is indispensable. The RBC/UKQCD collaborations have been trying to calculate the mixing employing static approximation in the heavy quark effective theory (HQET) with the $2+1$ flavor domain wall fermions for the light flavors. The first results has been reported in[2]. We are working to improve this results to obtain much more precise number of the matrix element. The key issures to achieve this will be a) to have smaller quark mass for the extrapolation of the u, d quarks to the physical point, where larger physical volume must be used to make the finite volume effect negligible; b) to determine matrix elements and the mixing coefficient of higher dimensional operator to get lid of $O(a)$ discritization error, where a is the lattice spacing (We have shown this error is substantial for decay constants and the matrix elements in our first study[2]); c) to perform non-perturbative renormalization of the operator, and further, non-perturbative estimate of the coefficients of the higher dimensional operators. c) is quite challenging, but we have started investigating it. b) is underway via lattice perturbation theory. In this report, we show the results dealing with issue a) which was made possible by large scale simulation on QCDOC at RIKEN-BNL Recearch Center.

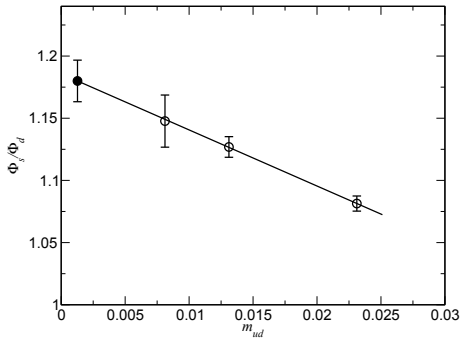

Fig. 1. Ratio of decay constants Φ_s/Φ_d as a function of m_{ud}, where $\Phi_q = f_{B_q}/\sqrt{m_{B_q}}$ for $q = d$, s. Solid symbols show the values extrapolated to the physical point by linear fit.

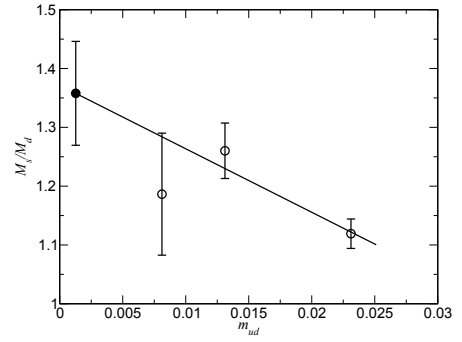

Fig. 2. Ratio M_s/M_d of the $B^0 - \overline{B^0}$ mixing matrix elements $M_q = \mathcal{M}_q m_{B_q}$ renormalized at m_b with $\overline{\text{MS}}$, NDR as functions of m_{ud}.

The results are summalized in Fig. 1 (the ratio of the decay constants) and Fig. 2 (the ratio of the matrix elements). The obtained $SU(3)_f$ breaking ratio is $\xi = \sqrt{\mathcal{M}_s/\mathcal{M}_d}(m_{B_s}/m_{B_d}) = 1.16(4)$, which is improved but, still consistent with 1.11(7) (APE smearing) and 1.14(8) (HYP smearing for static quark actions) obtained with larger statistics, but larger mass and smaller volume study.

References

1) Y. Aoki, J. Wennekers, PoS(Lattice 2007) 345-1–7.
2) C. Albertus, et al., PoS(Lattice 2007) 376-1–7.

† Condensed from the article[1]

*1 RIKEN-BNL Research Center

Z_N^d symmetry breaking in simulation of twisted Eguchi-Kawai model†

Tomomi Ishikawa, Tatsuo Azeyanagi,[*1] Tomoyoshi Hirata[*1] and Masanori Hanada[*2]

In 1982, Eguchi and Kawai introduced an important and interesting idea, which is now called *Eguchi-Kawai equivalence*[1]. In this equivalence, the existence of the global $\mathbb{Z}_N^d$ symmetry plays a crucial role. However, it was found that the symmetry is actually broken in the weak coupling region for $d > 2$[2]. To avoid this problem, the modified version of this model, twisted Eguchi-Kawai model (TEK model), was proposed[3]. The TEK model is a single hypercubic model, whose action is

$$S_{TEK} = -\beta N \sum_{\mu \neq \nu} Z_{\mu\nu} \mathrm{Tr}\, U_\mu U_\nu U_\mu^\dagger U_\nu^\dagger, \qquad (1)$$

where U_μ $(\mu = 1, .., 4)$ are link variables and $Z_{\mu\nu} = \exp(2\pi i n_{\mu\nu}/N), n_{\mu\nu} = -n_{\nu\mu} \in \mathbb{Z}_N$. The classical solution $U_\mu^{(0)} = \Gamma_\mu$ is called a "twist eater" and guarantees the existence of the $\mathbb{Z}_N^4$ symmetry in the weak coupling limit. If we use the standard twist $n_{\mu\nu} = L\,\epsilon_{\mu\nu}$, where $L = \sqrt{N}$ and $\epsilon_{\mu\nu}$ is an antisymmetric tensor, this single hypercubic model can describe the planar Yang-Mills (YM) theory with the L^4 lattice. In the intermediate coupling region, it is unclear whether the symmetry is unbroken because there is no guarantee that the symmetry is preserved. Numerical simulations performed during the early days of introduction of this model, however, showed that the symmetry is unbroken throughout the entire coupling region. It has promoted the belief that the TEK model indeed works. Surprisingly, some indications of $\mathbb{Z}_N^4$ symmetry breaking have recently been reported in several contexts concerning the TEK model[6,7]. Our work presented in this article is along this line. We concentrate on investigating the locations of symmetry breaking from the weak coupling side in the (β, N) plane and show the continuum limits as YM cannot be taken. [a]

Now we give an estimation for the $\mathbb{Z}_N^4$ symmetry breaking point from the weak coupling side β_c. We assume that the breaking at this point is a transition from the twist-eater phase $U_\mu = \Gamma_\mu$ to the identity configuration phase $U_\mu = \mathbb{1}_N$. The classical energy difference between these configurations can easily be calculated from action (1) as $\Delta S \simeq 2\pi^2\beta \sum_{\mu\neq\nu} n_{\mu\nu}^2 = 24\pi^2\beta N$. Going away from the weak coupling limit, the system shows quantum fluctuations. We expect that the $\mathbb{Z}_N^4$ symmetry is broken if the fluctuation

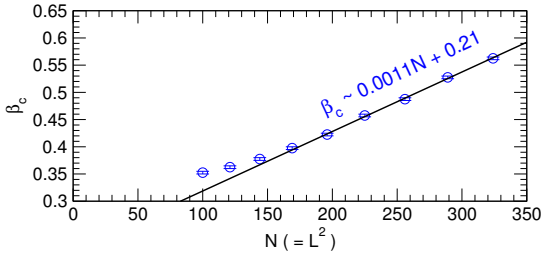

Fig. 1. β_c^L versus N. The line is obtained by fitting using $N \geq 169$ data.

around the twist-eater configuration exceeds the energy difference ΔS. Because the system describes $O(N^2)$ interacting gluons, it is natural to assume that their quantum fluctuations provide an $O(N^2)$ contribution to the effective action. Combining this assumption with ΔS, we can estimate the breaking point β_c as

$$\beta_c \sim N. \qquad (2)$$

To determine whether this approximation really holds, we present numerical simulation data in Fig. 1. The breaking point β_c is simply obtained by observing the expectation value of the Polyakov line with a cold start. In this figure, we can observe a clear linear dependence of β_c on N, as similarly obtained using eq. (2), in the larger N region. Thus, the EK equivalence is valid only in the region $\beta > \beta_c \sim N$. As is well known, the one-loop perturbative calculation of the YM lattice theory shows that its beta function behaves as $\beta \sim \log a^{-1}$ near the weak coupling limit, where a is the lattice spacing. Then, the continuum limit of the YM system with the fixed physical size $l = aL$ can be obtained using the scaling $\beta \sim \log N$. To obtain a large N limit with an infinite volume, we should keep β lower than that obtained using eq. (2), where the $\mathbb{Z}_N^4$ symmetry is broken.

From our theoretical observation combined with numerical simulation, we conclude that the TEK model does not have the continuum limit as the YM theory and further modifications are required in actual simulations.

† Condensed from the article in JHEP **0801** (2008) 025 and PoS (LATTICE 2007) 054.

*1 Department of Physics, Kyoto University, Japan
*2 Department of Particle Physics, Weizmann Institute of Science, Israel

a) Note that this model also describes gauge theories on noncommutative spaces. Even in this case, we can show the same conclusion as in the case of the YM.

References

1) T. Eguchi and H. Kawai, Phys. Rev. Lett. **48** (1982) 1063.
2) G. Bhanot *et al.*, Phys. Lett. B **113** (1982) 47.
3) A. Gonzalez-Arroyo and M. Okawa, Phys. Lett. B **120** (1983) 174; Phys. Rev. D **27** (1983) 2397.
4) H. Aoki *et al.*, Nucl. Phys. B **565** (2000) 176.
5) J. Ambjorn *et al.*, JHEP **9911** (1999) 029; Phys. Lett. B **480** (2000) 399; JHEP **0005** (2000) 023.
6) W. Bietenholz *et al.*, JHEP **0610** (2006) 042.
7) M. Teper and H. Vairinhos, Phys. Lett. B **652** (2007) 359.

A novel asymptotic formula for spin asymmetries at small transverse momentum

H. Kawamura, J. Kodaira,[*1] and K. Tanaka[*2]

[Perturbative QCD, soft gluon resummation, spin asymmetry]

Mechanism of the soft gluon effects is well understood for inclusive hadronic production of color-singlet particles, $h_1 + h_2 \to F(Q, Q_T, y, \cdots) + X$, where F is observed particles with the invariant mass Q, transverse momentum Q_T, rapidity y and other kinematical variables. When $Q_T \ll Q$, the real emission of gluons are strongly suppressed and the incomplete cancellation of the soft singularities between the real emission and the virtual corrections yields the logarithmically enhanced corrections $\propto \alpha_s^n \ln^m(Q^2/Q_T^2)$ $(m \leq 2n-1)$, which make the conventional perturbation useless. Resummation of these corrections is performed in the impact parameter b space, conjugate of the Q_T space (see, *e.g.* Ref.[1]) for details), to ensure the transverse momentum conservation. The resummed cross section is expressed by the inverse Fourier transform as

$$\frac{d\sigma^{\rm res.}}{dQ^2 dQ_T^2} \propto \int db \frac{b}{2} J_0(bQ_T) e^{S(b,Q)} \cdots , \qquad (1)$$

where $J_0(bQ_T)$ is a Bessel function and the ellipses include the convolutions of the coefficient functions with the parton distribution functions for incoming hadrons evaluated at the scale $\mu = b_0/b$ with $b_0 = 2e^{-\gamma_E}$. The soft gluon corrections are resummed in the Sudakov factor $e^{S(b,Q)}$ and the exponent can be written as

$$S(b,Q) = \frac{1}{\alpha_s(Q^2)} h^{(0)}(\lambda) + h^{(1)}(\lambda) + \cdots , \qquad (2)$$

where $\lambda = \alpha_s(Q^2)\beta_0 \log(b^2Q^2/b_0^2)$ and $\beta_0 = (11N_c - 2N_F)/(12\pi)$. The first term $h^{(0)}$ resums the leading logarithmic (LL) terms $(m = 2n-1)$ and the second term $h^{(1)}$ resums the next-to-leading logarithmic (NLL) terms $(m = 2n-2, 2n-3)$ and so on. The integrand of (1) is valid in the perturbative region $b \lesssim 1$GeV, and in order to complement the effects from the nonperturbative region $b \gg 1$ GeV, we introduce a nonperturbative function via a replacement $e^{S(b,Q)} \to e^{S(b,Q) - g_{NP} b^2}$ with a parameter $g_{NP} \simeq 0.5$ GeV.

The asymptotic behavior of (1) at $Q_T = 0$ for $Q^2 \to \infty$ limit was studied by the saddle-point method at the LL level without a nonperturbative function in the early developments of transverse momentum resummation[2]. The LL asymptotic formula is valid only for a very large Q^2 and does not approach the exact cross section in $Q^2 \to \infty$ limit. In Ref.[1,3], we extended the evaluation including the NLL contributions such as $h^{(1)}$ in (2) and b dependence of the parton distribution functions, and also the nonperturbative function $e^{-g_{NP}b^2}$. The NLL result is by no means useful to evaluate the production rate at $Q_T = 0$ due to the phase space suppression, but is useful to evaluate the spin asymmetries in the small Q_T region where the resummed cross sections dominates the whole cross sections in both polarized and unpolarized channels[3]. For example, the double-spin asymmetry of the dilepton production in transversely polarized hadronic collision is evaluated as

$$\mathcal{A}_{TT}(Q_T) \equiv \frac{\Delta_T d\sigma / dQ^2 dQ_T^2 dy d\phi}{d\sigma / dQ^2 dQ_T^2 dy d\phi} \qquad (3)$$

$$\simeq \frac{\cos(2\phi)}{2} \frac{\delta H\left(x_1^0, x_2^0;\ b_0^2/b_{SP}^2\right)}{H\left(x_1^0, x_2^0;\ b_0^2/b_{SP}^2\right)} , \qquad (4)$$

where the prefactor $\cos(2\phi)/2$ is the characteristic dependence of the transversely polarized cross section on the azimuthal angle ϕ of one of the outgoing leptons, and $(\delta)H(x_1, x_2; \mu^2)$ denotes the sum of the products of the (transversity) density distributions: $(\delta)H(x_1, x_2; \mu^2) = \sum_q e_q^2 \left[(\delta)q_{h_1}(x_1, \mu^2)(\delta)\bar{q}_{h_2}(x_2, \mu^2) + (1 \leftrightarrow 2)\right]$. $x_{1,2}^0 = \sqrt{Q^2/S}e^{\pm y}$ denote the DY scaling variables. The surprisingly simple form of (4) indicates that the soft gluon corrections largely cancel between polarized and unpolarized cross sections, and the remnant at the NLL level reside only in the unconventional scale b_0/b_{SP} of parton distributions, which is determined by the saddle-point in (1) at $Q_T = 0$. Note that this scale remains in the $Q^2 \to \infty$ limit and the asymptotic formula (4) approaches the exact asymmetry $\mathcal{A}_{TT}(Q_T)$ in this limit. Actually, it shows a good agreement with $\mathcal{A}_{TT}(Q_T)$ in the small Q_T region even in realistic cases, for example, with the kinematics of RHIC and J-PARC for pp collisions[3] and with the GSI kinematics for $p\bar{p}$ collisions[4]. Therefore, the formula (4) can be useful for extracting the transversity from experimental data.

*1 Theory Division, High Energy Accelerator Organization (KEK), deceased.
*2 Department of Physics, Juntendo University

References
1) Prog. Theor. Phys. **118**, 581 (2007).
2) G. Parisi and R. Petronzio, Nucl. Phys. **B154**, 427 (1979).
3) H. Kawamura, J. Kodaira and K. Tanaka, Nucl. Phys. **B777**, 203 (2007).
4) H. Kawamura, J. Kodaira and K. Tanaka, arXive:0801.0026.

Four-dimensional lattice chiral gauge theories with anomalous fermion content†

Y. Kikukawa*1 and H. Suzuki

[Chiral gauge theories, lattice gauge theory, gauge anomaly]

Regarding the continuum field theory, it has been discussed that chiral gauge theories with Weyl fermions in anomalous gauge representations, the so-called anomalous gauge theories, can consistently be quantized, provided that some of gauge bosons are permitted to acquire (bare) mass. Such theories in four dimensions are inevitably non-renormalizable and must be regarded as a low-energy effective theory with a finite UV cutoff. It has also been argued (on the basis of the perturbation theory) that the UV cutoff has an upper bound given by gauge boson mass, up to a proportionally constant.[1)]

On the other hand, on the basis of a general lattice framework of chiral gauge theories,[2,3)] it has been found that the fermion sector of a wide class of anomalous gauge theories, which includes all four-dimensional anomalous theories, cannot consistently be defined on the lattice under some assumptions.[4)] The essence of this observation (in four dimensions) can be summarized as follows.

Theorem 1 *Let the gauge group G be compact and semisimple. Then the following four requirements are incompatible:*

(1) A lattice Weyl determinant reproduces the gauge anomaly in the classical continuum limit.
(2) Only gauge invariant restrictions are placed on link variables.
(3) The modulus of a lattice Weyl determinant is gauge invariant.
(4) A lattice Weyl determinant is a (at least) C^2-class function of link variables.

This statement asserts that there is no lattice formulation of anomalous gauge theories that fulfills all the four seemingly natural requirements. This, however, raises a question: Presently, we know of only a low-energy (compared with, for example, the Plank scale) spectrum of fermions with which gauge anomalies are fortunately cancelled. It is quite possible, however, that a new heavy fermion that would give rise to an additional gauge anomaly will be discovered. Cannot such an anomalous theory be formulated on the lattice? Or, do we have to determine an anomaly-free fundamental theory very precisely to study low-energy dynamics of chiral gauge theories of our concern? This appears very unnatural.

In this work, we obtained an (at least partial) answer to the above-mentioned question. We show that the fermion sector of anomalous gauge theories can consistently be formulated on the lattice, if all gauge bosons are assumed to have non-zero masses. More precisely, we explicitly construct a consistent Weyl fermion integration measure as described in refs. 2) and 3) in the vacuum sector of the configuration space of link fields, by introducing bare mass terms of gauge bosons. This corresponds to evading the nogo theorem by neglecting requirement (2). Technically, such mass terms remove very random gauge degrees of freedom that cause obstructions to a consistent fermion integration measure.

The mass term of gauge bosons we introduce is not invariant under lattice gauge transformations. However, the gauge invariance is anyhow broken by fermions in an anomalous gauge representation. Introduction of a bare mass term is in fact very natural because, as is wellknown, the gauge anomaly induces mass for gauge bosons through higher-order diagrams even if bare mass is set to be zero. In this manner, at least for cases that all gauge bosons are massive, we have a picture in the lattice gauge theory that is consistent with expectations in the continuum theory.[1)]

Not only for clarifying the above-mentioned theoretical issue, our lattice construction may also be used for practical purposes. For example, this framework may be used to determine at a nonperturbative level an upper bound on the UV cutoff in low-energy effective theories with an anomalous fermion content. If we further introduce the Stückelberg or Wess-Zumino scalar field, this framework provides also a lattice definition of a four-dimensional nonlinear sigma model with the Wess-Zumino-Witten (WZW) term. Because in our construction we used a lattice Dirac operator that satisfies the Ginsparg-Wilson relation,[5)] such as the overlap Dirac operator,[6,7)] the WZW term has expected topological properties.

† Condensed from the article in J. High Energy Phys. 0710, 018 (2007)
*1 Institute of Physics, University of Tokyo

References

1) J. Preskill: Ann. Phys. (NY) **210**, 323 (1991), and references cited therein.
2) M. Lüscher: Nucl. Phys. **549**, 295 (1999).
3) M. Lüscher: Nucl. Phys. **568**, 162 (2000).
4) K. Matsui and H. Suzuki: J. High Energy Phys. **01**, 051 (2005).
5) P. H. Ginsparg and K. G. Wilson: Phys. Rev. **D 25**, 2649 (1982).
6) H. Neuberger: Phys. Lett. **B 417**, 141 (1998).
7) H. Neuberger: Phys. Lett. **B 427**, 353 (1998).

Two-dimensional $\mathcal{N} = (2, 2)$ super Yang-Mills theory on computer†

H. Suzuki

[Supersymmetry, gauge theory, Monte Carlo simulation]

It will be very exciting if a nonperturbative issue in supersymmetric gauge theories (such as the possibility of dynamical supersymmetry breaking) can be studied numerically at one's will. In the case of the lattice gauge theory—a unique framework to date for such a nonperturbative study of gauge theories, however, supersymmetry cannot be manifestly realized. A latticized spacetime inevitably breaks infinitesimal translations that are a part of the supersymmetry algebra. What one can expect *at best* is the restoration of supersymmetry in the limit in which the lattice spacing is set to zero (the continuum limit). Despite the great efforts made towards the numerical study of the four-dimensional $\mathcal{N} = 1$ super Yang-Mills theory,[1,2] so far no conclusive evidence of restoration of supersymmetry in the continuum limit has been observed. Given this situation, to test various ideas, it should be useful to examine low-dimensional supersymmetric gauge theories in detail, which have a much simpler ultraviolet (UV) structure and for which it is relatively easy to accumulate high statistics in Monte Carlo simulations.

In this work, we carried out a preliminary numerical study of a lattice formulation of the two-dimensional $\mathcal{N} = (2, 2)$ super Yang-Mills theory (2d $\mathcal{N} = (2, 2)$ SYM), proposed by Sugino[3] with the gauge group SU(2). (For recent reviews on lattice formulation of supersymmetric theories, see refs. 4) and 5).) The advantage of this formulation is that a fermionic symmetry, corresponding to one of four supercharges in the target continuum theory, is manifestly preserved even with finite lattice spacings and finite volume. Because of this exact fermionic symmetry, full supersymmetry is expected to be restored in the continuum limit *without any local counterterms*.

We developed a code of a hybrid Monte Carlo simulation using a C++ library, FermiQCD/MDP.[6,7] We mainly studied various one-point supersymmetric Ward-Takahashi (WT) identities. These are precisely the same set of WT identities numerically analyzed by Catterall[8] on the basis of his own lattice formulation of 2d $\mathcal{N} = (2, 2)$ SYM. A typical result is shown in Fig. 1 in which the expectation values of the total action density are plotted as a function of the lattice spacing a. (All dimensionful quantities are normalized by the two-dimensional gauge coupling constant g.) Because of the manifest fermionic symmetry, the expectation value must be zero for all lattice spacings. The result is consistent with this expectation within

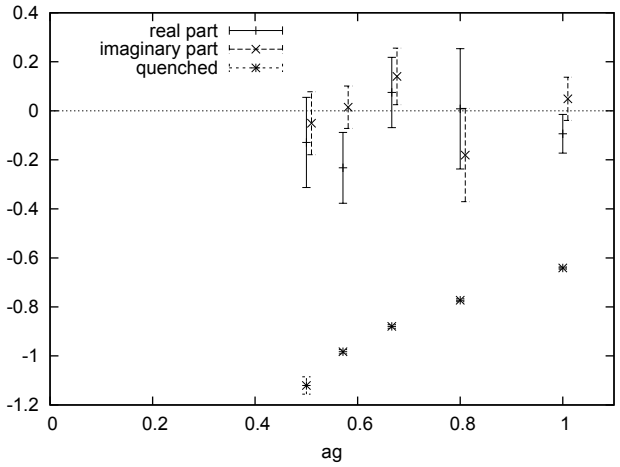

Fig. 1. Expectation values of the total action density in unit of g^2 as function of lattice spacing a.

almost 1σ for all values of ag and strongly indicates the correctness of our algorithm and code. The result of quenched approximation (in which the quantum effect of fermions is removed) is also shown and one can clearly observe the distinction from the supersymmetric case. In our numerical simulation, WT identities implied by the exact fermionic symmetry of the formulation are reproduced with fair accuracy and, for most of these identities, we clearly observe the quantum effect of dynamical fermions. For WT identities expected only in the continuum limit, the results seem to be consistent with the behavior expected from supersymmetry, although we do not see a clear distinction from the quenched (i.e., non-supersymmetric) simulation. We also measured the expectation values of renormalized gauge-invariant bi-linear operators of scalar fields to illustrate how this type of numerical study can be useful.

† Condensed from the article in J. High Energy Phys. 0709, 052 (2007)

References

1) I. Montvay: Int. J. Mod. Phys. **17**, 2377 (2002), and references cited therein.
2) F. Farchioni and R. Peetz: Eur. Phys. J. **C 39**, 87 (2005).
3) F. Sugino: J. High Energy Phys. **03**, 067 (2004).
4) D. B. Kaplan: Nucl. Phys. **129** (Proc. Suppl.), 109 (2004).
5) J. Giedt: PoS **LAT2006**, 008 (2006).
6) M. Di Pierro: Comput. Phys. Commun. **141**, 98 (2001).
7) M. Di Pierro and J. M. Flynn: PoS **LAT2005**, 104 (2006).
8) S. Catterall: J. High Energy Phys. **04**, 015 (2007).

Comments on solutions for nonsingular currents in open string field theories†

I. Kishimoto and Y. Michishita*

[Nonperturbative techniques; string field theory, D branes, Conformal field theory, algebraic structures, Supersymmetry]

The string field theory is expected to be a candidate for nonperturbative formulation of the string theory. Various studies using the string field theory are useful not only for understanding the string theory from the unified viewpoint but also for developing the string field theory itself. The study of analytic solutions of string field theories is important for understanding nonperturbative phenomena in the string theory. There have been various attempts to solve the equations of motion of string field theories. In particular, since Schnabl constructed an analytic solution[1] for tachyon condensation in Witten's cubic bosonic open string field theory, there have been a number of new developments in this field. Recently, new analytic solutions for marginal deformations using nonsingular currents have been proposed by Schnabl[2] and Kiermaier et al.[3] They can be regarded as an application of the technical methods developed by Schnabl.[1] As a generalization of these solutions to Berkovits' Wess-Zumino-Witten (WZW)-type open superstring field theory, new analytic marginal solutions to the equation of motion have also been developed by Erler[4] and Okawa.[5]

We consider a generalization of an expression of the solution for marginal deformations given by Schnabl,[2] in both Witten's bosonic string field theory and Berkovits' WZW-type superstring field theory. We construct a class of new solutions to the equation of motion $Q_{\rm B}\Psi + \Psi * \Psi = 0$ in the bosonic string field theory and $\eta_0(e^{-\Phi}Q_{\rm B}e^{\Phi}) = 0$ in the superstring field theory.

In the bosonic string field theory, we found that by taking a BRST invariant and nilpotent string field $\hat{\psi}$, namely, $Q_{\rm B}\hat{\psi} = 0$ and $\hat{\psi} * \hat{\psi} = 0$, we can generate a class of solutions to the equation of motion with

$$\Psi^{(\alpha,\beta)}(\hat{\psi}) = P_\alpha * \frac{1}{1+\hat{\psi} * A^{(\alpha+\beta)}} * \hat{\psi} * P_\beta. \qquad (1)$$

Here, $\{P_\alpha\}_{\alpha\geq 0}$ is a BRST invariant commutative monoid, which satisfies $Q_{\rm B}P_\alpha = 0$, $P_\alpha * P_\beta = P_{\alpha+\beta}$, $P_{\alpha=0} = I$ (I: identity state) and $A^{(\gamma)}$ ($\gamma \geq 0$) is an associated string field, which satisfies $Q_{\rm B}A^{(\gamma)} = I - P_\gamma$. An example of such string fields $(P_\alpha, A^{(\alpha)})$ can be constructed concretely using wedge states. In particular, if we take $\hat{\psi} = U_1^\dagger U_1 \lambda c J(0)|0\rangle$ with a nonsingular current J as a BRST invariant and nilpotent string field, where U_1 is composed of Virasoro operators associated with the identity state, we can reproduce Schnabl/KORZ's marginal solution with eq. (1) with $\alpha = \beta = 1/2$. Furthermore, we can reproduce the Schnabl's solution for tachyon condensation[1] using $\lim_{\lambda\to\infty}\Psi^{(1/2,1/2)}(\lambda Q_{\rm B}U_1^\dagger U_1 B_1^L c_1|0\rangle)$.

In the superstring field theory, using a string field $\hat{\phi}$ such as $\eta_0 Q_{\rm B}\hat{\phi} = 0, \hat{\phi} * \hat{\phi} = 0, \hat{\phi} * \eta_0\hat{\phi} = 0, \hat{\phi} * Q_{\rm B}\hat{\phi} = 0$, we can generate a class of solutions to the equation of motion using the following formula:

$$\Phi^{(\alpha,\beta)}(\hat{\phi}) = \log(1 + P_\alpha * f * P_\beta)\,, \qquad (2)$$

$$f \equiv (e^{\hat{\phi}} - 1)\frac{1}{1 - \eta_0\hat{A}^{(\alpha+\beta)} * (e^{-\hat{\phi}}Q_{\rm B}e^{\hat{\phi}})}\,, \qquad (3)$$

where $\{P_\alpha\}_{\alpha\geq 0}$ is a BRST and η_0-invariant commutative monoid and $\hat{A}^{(\gamma)}$ ($\gamma \geq 0$) is an associated string field, which satisfies $\eta_0 Q_{\rm B}\hat{A}^{(\gamma)} = I - P_\gamma$. As an explicit example, if we take the wedge state as P_α, its associated string field $\hat{A}^{(\gamma)}$ is constructed as $\hat{A}^{(\gamma)} = \int_0^\gamma d\alpha\Big(\log\frac{\alpha}{\gamma}\Big)\Big(\frac{\pi}{2}J_1^{--L} + \alpha\frac{\pi^2}{4}\tilde{G}_1^{-L}B_1^L\Big)P_\alpha$ with $J^{--}(z) = \xi b(z)$ and $\tilde{G}^- = [Q_{\rm B}, J^{--}(z)]$. In particular, $\Phi^{(1/2,1/2)}(\lambda U_1^\dagger U_1 c\xi e^{-\phi}\psi(0)|0\rangle)$, where $\psi(z)$ is a fermionic component of a nonsingular supercurrent, corresponds to Erler/Okawa's solutions.

Actually, the eqs. (1) and (2) give maps from one solution to another in the bosonic string and superstring field theory respectively. Moreover, $\hat{\psi} \mapsto \Psi^{(\alpha,\beta)}(\hat{\psi})$ and $\hat{\phi} \mapsto \Phi^{(\alpha,\beta)}(\hat{\phi})$ form commutative monoids with respect to compositions of maps. It is interesting to apply our maps (1) and (2) to generating various solutions. We have also investigated gauge transformations among solutions generated using these maps and found formal expressions of gauge parameter string fields. Such gauge transformations seem to become singular because they relate simple but singular solutions on the basis of the identity state to regular solutions with a finite width of worldsheet. It is an important problem to define the regularity of string fields more carefully and examine that of our generated solutions and the gauge parameters that relate them.

† Condensed from the article in Prog. Theor. Phys., **118**, 347 (2007).

* High Energy Accelerator Research Organization (KEK)

References

1) M. Schnabl: Adv. Theor. Math. Phys. **10**, 433 (2006).
2) M. Schnabl: Phys. Lett. B **654**, 194 (2007).
3) M. Kiermaier, Y. Okawa, L. Rastelli and B. Zwiebach: JHEP **0801**, 028 (2008).
4) T. Erler: JHEP **0707**, 050 (2007).
5) Y. Okawa: JHEP **0709**, 084 (2007).

Prospects of Open Charm Production at GSI-FAIR and J-PARC

J. Riedl,[*1] A. Schäfer,[*1] M. Stratmann

[heavy flavor production, perturbative QCD, NLO corrections, charge asymmetry]

The study of heavy flavors has become a versatile tool to probe different aspects of QCD, ranging from heavy flavor parton densities and the hadronization of heavy quarks to the dynamics of (spin-dependent) hard-scattering. Equally significant improvements of the heavy quark tagging methods in experiment and the theoretical framework have been achieved. For the latter, next-to-leading order (NLO) accuracy with full dependence on the heavy quark mass m_Q is the state-of-the-art throughout.

Here, we will focus on a first exploratory study of open charm production in $\bar{p}p$ and pp collisions at the future GSI-FAIR and J-PARC facilities[1)] with maximum c.m.s. energies $\sqrt{S}$ of about 14.5 and 10 GeV, respectively. Such experiments have the potential to further our understanding of the underlying QCD dynamics and the applicability of perturbative methods at moderate c.m.s. energies so far little explored. To study the possible relevance of all-order resummations, we provide[1)] differential charm yields at NLO accuracy, including estimates of theoretical uncertainties due to variations of the charm quark mass or the renormalization and factorization scales, see, e.g., Fig. 1. Most of the large NLO corrections displayed in the middle panel of Fig. 1 can be attributed to the large uncertainties in the LO and NLO gluon distributions at large momentum fractions x. It is interesting to note that the dominant production channel for charm is gluon-gluon fusion in pp collisions at J-PARC, see the bottom panel of Fig. 1, but quark-antiquark annihilation in $\bar{p}p$ collisions at GSI-FAIR[1)].

Another interesting, though experimentally challenging observable is the so called "charge asymmetry", which describes the difference of cross sections for producing a heavy quark Q or a heavy anti-quark $\bar{Q}$ at a certain point in phase-space: $A_C \equiv (d\sigma^Q - d\sigma^{\bar{Q}})/(d\sigma^Q + d\sigma^{\bar{Q}})$. This asymmetry probes a certain subset of NLO radiative corrections and vanishes at the LO approximation, see[1)]. This feature makes it an important test of QCD hard scattering dynamics. It should be mentioned that routinely used event generators based on LO matrix elements cannot predict this interesting effect. A first measurement of A_C for top production has been recently reported by the CDF collaboration. We estimate the size of A_C for charm quarks at GSI-FAIR and J-PARC, see Fig. 2, and, for the first time, compute the corresponding charge asymmetry also for polarized hadroproduction[1)].

Provided that longitudinally polarized beams and targets will be available at GSI-FAIR and/or J-PARC, studies of the double-spin asymmetry $A_{LL} \equiv d\Delta\sigma/d\sigma$ could provide unique insight in the distributions describing the polarization of (anti-)quarks and gluons in the nucleon at medium-to-large momentum fractions x, which are difficult to access at collider energies. The expected size of A_{LL} strongly depends on the unknown gluon polarization at J-PARC[1)]. GSI-FAIR mainly probes the fairly well known u, d valence quark polarizations, and A_{LL} is estimated to be around 10%.

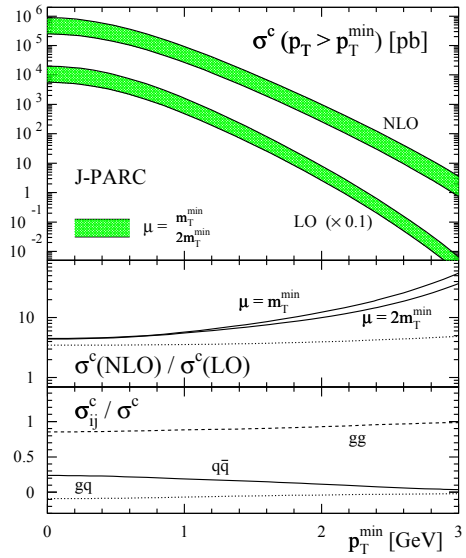

Fig. 1. Open charm cross section at J-PARC.

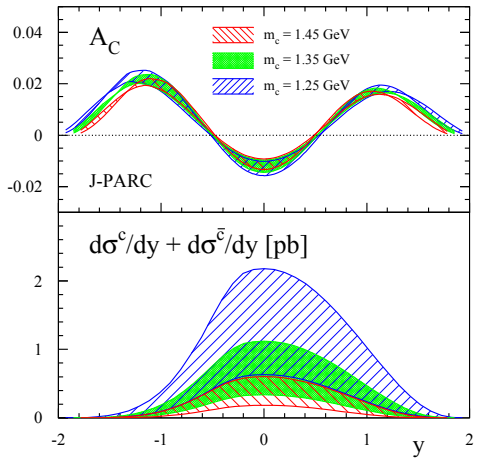

Fig. 2. Charge asymmetry A_C for charm at J-PARC.

References

1) J. Riedl, A. Schäfer, and M. Stratmann, Eur. Phys. J. **C52**, 987 (2007).

*1 Institut für Physik, Universität Regensburg, Germany

6. Development of Accelerator Facility

Acceleration Tests of Uranium Beam in RIBF (I)

Nobuhisa Fukunishi, Masaki Fujimaki, Tadashi Fujinawa, Akira Goto, Hiroo Hasebe, Yoshihide Higurashi, Kumio Ikegami, Eiji Ikezawa, Naohito Inabe, Tadashi Kageyama, Osamu Kamigaito, Masayuki Kase, Masanori Kidera, Shigeo Kohara, Misaki Kobayashi-Komiyama, Makoto Nagase, Keiko Kumagai, Takeshi Maie, Takahide Nakagawa, Jun-ichi Ohnishi, Hiroki Okuno, Hiromichi Ryuto, Naruhiko Sakamoto, Masanori Wakasugi, Tamaki Watanabe, Kazunari Yamada, Shigeru Yokouchi and Yasushige Yano

The uranium beam is one of the most important beams in the RI Beam Factory[1] (RIBF), because it is suitable for effectively producing very neutron-rich isotopes with mass numbers around 90 and 130. In addition, the uranium beam is one of the most difficult beams for us to accelerate because a five-step acceleration including a three-step charge-stripping process is required as shown in Fig. 1. Hence, beam commissioning tests of three newly constructed cyclotrons, the Fixed-Frequency Ring Cyclotron[2] (fRC), the Intermediate-Stage Ring Cyclotron[3] (IRC) and the Superconducting Ring Cyclotron[4] (SRC), have been performed mainly using uranium beams as summarized in Table 1.

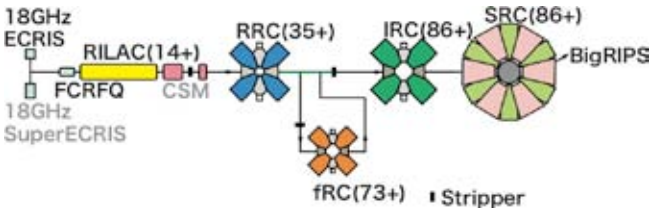

Fig. 1. Acceleration scheme of a uranium beam in the RIBF. The numbers in the parentheses are the charge states of uranium ions. The acceleration energies of the RILAC, RRC, fRC, IRC and SRC are 0.67, 11, 50, 114 and 345 MeV/nucleon, respectively.

Table 1. Operational statistics of RIBF beam commissioning in the period from July 2006 to June 2007. Operation times listed include waiting times caused by mechanical problems.

Accelerator used	Beam	Operation Time
RILAC, RRC	11-MeV/u U	8 days
RILAC,RRC,fRC	50 MeV/u U	60 days
RILAC,RRC,IRC	114-MeV/u Kr	17 days
SRC without fRC	345-MeV/u Al	16 days
SRC without fRC	345-MeV/u Kr	23 days
SRC with fRC	345-MeV/u U	36 days

During the period from July 2006 to November 2006, the fRC was commissioned and the injectors of the fRC were also tested for uranium beam acceleration. On July 24, 2006, we succeeded in accelerating a uranium beam to 50 MeV/nucleon, which corresponded to the designed extraction energy of the fRC, but failed to extract it because the beam intensity of 50 MeV/nucleon was only 3 nA. The transmission efficiency of the fRC was nearly 1%.

At this stage of the beam commissioning tests, our beam diagnostics system had not been established. Hence, it was difficult to quantitatively explain the reasons for this extremely low transmission efficiency. However, the following reasons were factors. First, the rebuncher[5] placed between the RIKEN Ring Cyclotron (RRC) and the fRC did not work. Its high-power tests were scheduled in August 2006. Secondly, we failed to form a precise isochronous magnetic field because we could not detect the signals of the beam passing through phase-pickup electrodes. We used an oscilloscope to detect preamplified signals but the signal-to-noise ratio was too low. Thirdly, the energy spread of the uranium beam injected into the fRC far exceeded the acceptance of the fRC. The energy spread originating from the nonuniformity of the charge stripper foil placed between the RRC and the fRC was estimated to be more than 1%. Finally, the lifetime of the first-step charge stripper placed downstream of the RIKEN heavy-ion linac (RILAC) was too short, that is less than 10 minutes, for a 0.67 MeV/nucleon uranium beam with an intensity of 10 μA. The lifetime problem had been already pointed out in Ref. 6. In addition, our beam tuning-techniques remained primitive.

All the problems mentioned above had been greatly reduced by March 2007. The rebuncher placed between the RRC and the fRC became operational in September 2006. Using the rebuncher, we succeeded in extracting a 50 MeV/nucleon uranium beam on September 29, 2006. To obtain precise isochronous fields, we have added noise filters and employed a lock-in amplifier to observe signals in noisy environments. Using the improved phase probe, we succeeded in forming an isochronous magnetic field with a standard deviation of less than 0.15 nsec in November 2006. To reduce the energy spread of uranium beams injected into the fRC, we have reduced the stripper thickness from 0.6 mg/cm^2 to 0.3 mg/cm^2. This modification has resulted in a change in the most probable charge state from 73+ to 71+ and a 1.5% increase in the injection energy of the fRC, which corresponds to a 10 mm increase in the injection radius of the fRC. Hence, we moved two injection apparatus (the electro-static inflector and the magnetic inflector 1) outwards at the end of November 2006. To solve the first-stripper problem, the acceleration scheme has

been changed from the upper scheme in Fig. 2 to the lower one, which has been realized by a new method developed for the RIKEN 18 GHz ECR[7] ion source. In this method, a rod of uranium metal was used instead of UF_6 gas. An acceleration-deceleration technique was also employed in the extraction region of the ion source[8]. These improvements successfully increased the beam intensity of uranium beams as shown in Fig. 3.

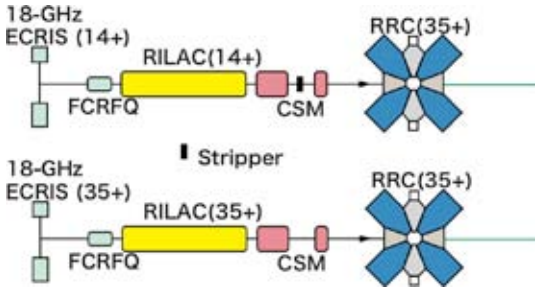

Fig. 2. Original (upper) and modified (lower) acceleration schemes of the RILAC-RRC section.

During the period from the end of November 2006 to February 2007, beam commissioning tests of the IRC and SRC were performed without using the fRC. We succeeded in extracting a 114 MeV/nucleon krypton beam from the IRC on November 25, 2006 and a 345 MeV/nucleon aluminum beam from the SRC on December 28, 2006. Following these successes, 345 MeV/nucleon uranium beams were successfully extracted from the SRC on March 23, 2007. However, the intensities of the 345 MeV/nucleon uranium beams were limited as shown in Fig. 3.

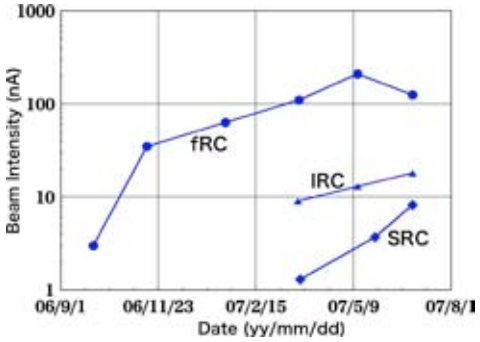

Fig. 3. Uranium beam intensities obtained in the beam commissioning tests. The beam intensities were measured by Faraday cups, which were not well calibrated for uranium beams. Hence, the intensities shown here were overestimated by a factor of two or three. The decrease in the fRC-extracted beam intensity in July 2007 was caused by introducing a new Faraday cup.

The first experiment of the RIBF using 345 MeV/nucleon uranium beams was scheduled in May 2007. To increase the beam intensity, the beam rebunching system between the RILAC and the RRC was modified because the bunch length of the uranium beam injected into the RRC was not sufficiently short. To compress the beam bunches, it was necessary to move a rebuncher downstream because the magnification factor of the longitudinal beam size from the RILAC to the RRC is determined by the ratio of the distance between the RILAC and the rebuncher to that between the rebuncher and the RRC. In contrast, the longitudinal acceptance of the rebuncher becomes small upon moving it downstream. To solve this poblem, we inserted an additional rebuncher into the S6 region as shown in Fig. 4. This rebuncher was originally placed between the AVF cyclotron and the RRC that was used in the AVF-RRC operation. We also moved the rebuncher originally placed in the J4 region upstream as shown in Fig. 4. Because of this modification, we succeeded in the single-turn extraction of an 11 MeV/nucleon uranium beam from the RRC. After these preparations, the first experiment of the RIBF was performed, wihch resulted in the discovery of a new isotope ^{125}Pd.

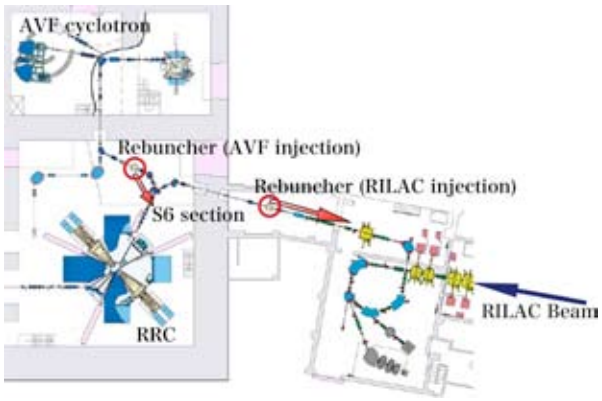

Fig. 4. Layout of rebunchers for the RRC before and after the replacement performed in April 2007. Arrows show where rebunchers were moved.

References

(1) Y. Yano: "The RIKEN RI Beam Factory Project: A Status Report", Nucl. Instr. Meth. B (2007), doi:10.101b/ j.nimb.2007.04.174 .
(2) T. Mitsumoto et al.: Proc. 17th Int. Conf. On Cyclotrons and Their Applications, 384 (2004).
(3) J. Ohnishi et al.: Proc. 17th Int. Conf. On Cyclotrons and Their Applications, 197 (2004).
(4) H. Okuno et al.: Proc. 17th Int. Conf. On Cyclotrons and Their Applications, 373 (2004).
(5) T. Aoki et al.: Proc. of PASJ3-LAM31, August 2006, Sendai, FP20.
(6) H. Ryuto et al.: Proc. 17th Int. Conf. On Cyclotrons and Their Applications, 307 (2004).
(7) T. Nakagawa et al.: Nucl. Instrum. Methods B 226, 392 (2004).
(8) Y. Higurashi et al.: Proc. of PASJ4-LAM32, August 2007, Wako-shi Saitama, FO14.

Acceleration Tests of Uranium Beam in RIBF (II)

Nobuhisa Fukunishi, Masaki Fujimaki, Tadashi Fujinawa, Akira Goto, Hiroo Hasebe, Yoshihide Higurashi, Kumio Ikegami, Eiji Ikezawa, Naohito Inabe, Tadashi Kageyama, Osamu Kamigaito, Masayuki Kase, Masanori Kidera, Shigeo Kohara, Misaki Kobayashi-Komiyama, Makoto Nagase, Keiko Kumagai, Takeshi Maie, Takahide Nakagawa, Jun-ichi Ohnishi, Hiroki Okuno, Hiromichi Ryuto, Naruhiko Sakamoto, Masanori Wakasugi, Tamaki Watanabe, Kazunari Yamada, Shigeru Yokouchi and Yasushige Yano

The first experiment of the RIBF was successfully completed with the discovery of a new isotope, ^{125}Pd. However, the typical beam intensity of uranium beams extracted from the SRC during the experiment was as low as 2 ~ 3 nA and the total transmission efficiency from the ion source to the SRC extraction was 0.1%[1]. Taking into account the total charge-stripping efficiencies of 4 ~ 5%, more than 97% of ions were lost during acceleration. The reasons for this extremely low transmission efficiency have been understood partially based on data obtained in a series of tests performed after the first experiment.

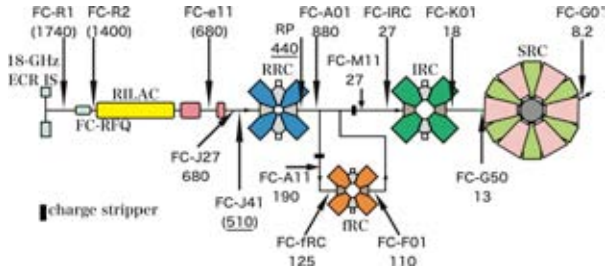

Fig. 1. Beam intensities observed (lower column, nA) and names of beam monitors used (upper column) at various positions of RIBF. The data shown in Fig. 1 were measured at two different times. The data obtained in the earlier measurement (shown with parentheses) were normalized to the later data. Here, we use the abbreviations FC and RP for a Faraday cup and a radial probe, respectively.

We summarize in Fig. 1 the beam intensities obtained on June 29, 2007. The positions of beam-intensity monitors are schematically shown in Fig. 1. Note that the beam intensities shown in Fig. 1 are not calibrated as it is easily determined by comparing the beam intensities before (680) and after the RRC acceleration (880). We think that only two beam monitors, the FC-J41 and RRC-RP are reliable (within accuracy of 10%) because they sufficiently suppress secondary electrons emitted by uranium ion irradiation. The FC-J41 has a flat distribution of suppression voltage. The magnitude of the suppression voltage is 1 kV. The radial probe (RP) of the RRC experiences an isochronous magnetic field of 1.5 Tesla, which is sufficient to suppress secondary electrons. All the other Faraday cups could not effectively suppress secondary electrons. A comparison between the data of the RRC-RP (440 nA) and FC-A01 (880 nA) implies that our Faraday cups overestimate beam intensity typically by a factor of two for a medium-energy uranium beam. On the other hand, the production rates of secondary particles at the BigRIPS indicated that the FC-G01 overestimated beam intensity by a factor of three[2]. In addition to the uncertainties of absolute values, five types of Faraday cup were used and the suppression efficiency of secondary electrons differed between the five types. As a result, it is difficult to reliably estimate the partial transmission efficiency of the RIBF accelerator complex.

For convenience in discussion, we assumed that the data from the fRC injection (FC-fRC) to the SRC extraction (FC-G01) were overestimated by a factor of two. We also used 0.17 and 0.27 as charge stripping efficiencies of the first and second charge-stripping processes, respectively. These values were determined by measuring charge-state fractions[3]. Imperfections of charge strippers, for example, the existence of pinholes, are not taken into account in the present assumption and hence partial transmission efficiencies may be underestimated. Under these assumptions, partial transmission efficiencies are determined as summarized in Table 1

Table 1. Estimated transmission efficiencies of various sections in uranium acceleration test. (2007/07/3)

Ion source – RILAC end	29%
RILAC end – RRC extraction	86%
RRC extraction – fRC injection	41%
fRC injection – fRC extraction	88%
fRC extraction – IRC injection	75%
IRC-injection – IRC extraction	67%
IRC extraction – SRC injection	72%
SRC injection – SRC injection	63%

The transmission efficiency from the ion source to the RILAC end is estimated by numerical simulation. It is 70% for a uranium beam with its transverse emittance of 150π mm mrad (4σ value) under an assumption that an energy spread at R1 is negligible. The preliminary results of transverse emittance (90% emittance) were 140π and 250π mm mrad for the horizontal and vertical directions, respectively. This may be the reason for the observed low transmission efficiency. One of the other reasons for the low

transmission efficiency is that the vacuum pressure is not sufficiently low and uranium ions capture electrons particularly in the low-energy beam transport line from the ion source to the FC-RFQ. It will be tested in 2008.

For other sections, we measured various quantities, such as profiles and time structures of the beam to understand observed transmission efficiencies. Figure 2 shows the time structures of the fRC-injected (D15) and IRC-extracted (K01) beams.

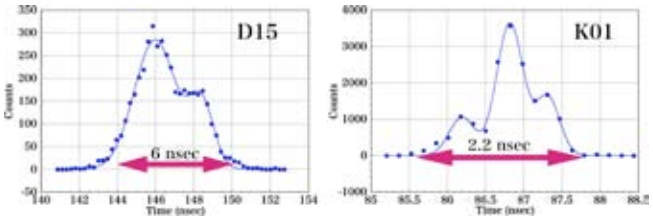

Fig. 2. Time structures of beam after first charge stripping process (D15) and beam extracted from IRC (K01). Plastic scintillators were used in the measurements. The vertical axis show a time difference defined as (rf signal) – (scintillator signal). The position of the D15 scintillator is about 40 meters downstream of the first charge stripper.

The K01 data indicate that the phase width (2.2 nsec) of the IRC-extracted beam was 29 degrees, which corresponds to a phase width of 43 degrees in IRC injection taking into account the phase compression effect[4, 5] due to the radial distribution of acceleration voltage in the IRC. The phase acceptance of the IRC is designed to be 20 ~ 25 degrees with the use of a flat-top resonator. However, the flat-top resonator was not used in this acceleration test because its leakage fields might give serious damage on the electric inflector placed in the same valley region of the IRC. Without using the flat-top resonator, the phase acceptance of the IRC is at most 10 degrees and the phase width of the IRC-injected beam was more than four times of the accepted value. This explains why the total transmission efficiency from the IRC-injection to the SRC extraction was 30%. This longitudinally expanded beam structure was a consequence of a large energy spread of the beam. One possible reason for this is that the thickness uniformity of the second stripper is poor. Another possible reason is that we failed to adjust the phase of an rf-field generated by the flat-top resonator of the fRC. To distinguish between the two possibilities, we have additionally installed a plastic scintillator between the fRC and the second charge stripper.

The time spread (~ 6 nsec) of the D15 data in Fig. 2 corresponds to an energy spread of 1.4%. If it was true, the stripper foil used was seriously damaged. We made additional measurements in October 2007 and the results are shown in Fig. 3. In the data noted by “RIKEN”, we used a homemade carbon foil, which was the same type of carbon foil used in the test shown in Fig. 2. The energy spread caused by the “RIKEN” stripper was estimated to be 0.55% (4σ value), which was beyond the acceptance (0.2%) of the rebuncher placed between the RRC and the fRC. It is necessary to reduce the energy spread. One candidate solution is to use the diamond-like carbon foil developed by the TRIUMF group[6], the result of which is also shown in Fig. 3. In addition, one of the authors (H. H.) has also started to improve homemade stripper foils.

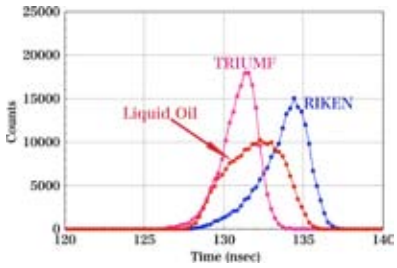

Fig. 3. Time spectra of beams measured at D18 after charge stripping (2007/10/2).

In addition to the problems mentioned above, there may be additional problems. Step-by-step improvements are necessary to obtain good transmission efficiencies. Problems mentioned here have been solved partially. For example, Faraday cups with high precisions have been introduced. They were verified in a krypton acceleration test performed in November 2007. In the test, we also succeeded in the correct use of the IRC’s flat-top resonator. As a result, the transmission efficiency of the IRC was improved. Table 2 shows a summary of the transmission efficiencies of the accelerators used in the krypton acceleration test. No sizable beam losses were detected for beam transfer lines. On the other hand, the transmission efficiencies of the RILAC and SRC were still low. In the next stage of the beam commissioning, detailed studies of the RILAC and SRC are required.

Table 2. Transmission efficiencies of RIBF accelerators for 345-MeV/nucleon-krypton beam. (2007/11/4)

RILAC	28%
RRC	89%
IRC	82%
SRC	45%

References

(1) A. Goto et al.: Proc. of 18th Int. Conf. on Cyclotrons and their Applications, 3 (2007).
(2) N. Aoi: private communication.
(3) H. Ryuto et al.: Proc. of 18th Int. Conf. on Cyclotrons and Their Applications, 314 (2007).
(4) R.W. Mueller and R.W. Mahr: NIM, **86**, 241 (1970).
(5) W. Joho: Particle Accelerators, **6**, 41 (1970).
(6) TRIUMF Carbon Foil Laboratory.

Effect of biased disc on plasma potential of RIKEN 18 GHz ECR ion source

W. Takai, H. Higashijima, T. Nakagawa, Y. Higurashi, M. Kidera, A. Goto and Y. Yano

Recently, several laboratories have measured the plasma potential and reported its importance, because a lower plasma potential provides a higher beam intensity of the highly charged heavy ions.[1,2] One of the new methods for plasma potential measurement is based on retarding electric field and successfully applied to measuring the plasma potential of ECR ion sources under the various conditions (i.e., gas pressure, RF power, and gas mixing).[2]

In 1999, we observed that the beam intensities of highly charged Ar ions are strongly dependent on negatively biased disc position.[3] However, the effect of disc position on ECR plasma is not clear yet. To understand this mechanism, we need further investigation. For this reason, as a first step toward understanding the mechanisms, we investigated the effect of a biased disc on plasma potential measured using the new method described in ref. 2.

In this experiment, we used the RIKEN 18 GHz ECR ion source. Detailed information and performance of the ion source were described in ref. 4. The extraction voltage was fixed to 8 kV.

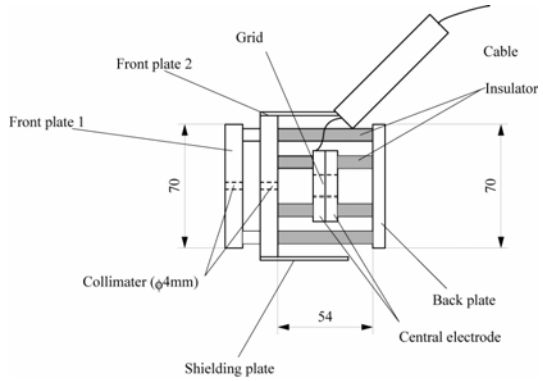

Fig. 1. Schematic drawing of device for plasma potential measurement.

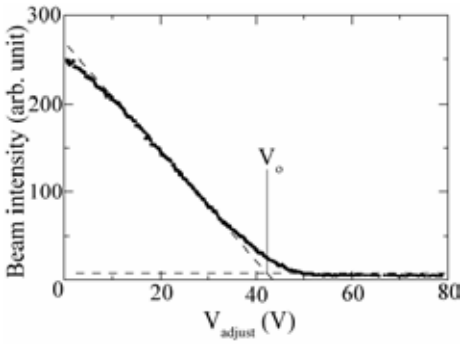

Fig. 2. Beam intensity of multicharged Ar ions as function of V_{adjust}.

Figure 1 shows the device for measuring plasma potential. The beam was collimated by double slits (diameter; 2 mm) as shown in Fig.1. The mesh size was 1×1 mm^2 with a wire diameter of 0.2 mm. The power supply for the mesh was floating at a high voltage of the ion source (V_{source}), which eliminates the possible measurement error of source potential. When an ion passes through the collimators, the ion is decelerated by the potential difference ($V_{mesh}= V_{source}+ V_{adjust}$) between second collimator and the mesh. V_{adjust} is the voltage regulated by the power supply. The ions which have a high enough kinetic energy can pass through the mesh and reach the back plate. The current of ions that pass through the mesh is measured by the back plate.

Figure 2 shows the typical beam intensity of Ar^{9+} ions as a function of V_{adjust}. The RF power was 460 W. The kinetic energy of Ar ions higher than qV_{source} is mainly due to plasma potential and the thermal energy of ions in the plasma, where q is the charge of heavy ions. In Fig. 2, we can observe the region in which current decreases linearly until it starts to saturate. We define V_0 as the voltage at the intersection of the linear fit and the horizontal line corresponding to the average current after saturation. The voltage V_0 includes the effect of the plasma potential and the thermal energy of the ions.

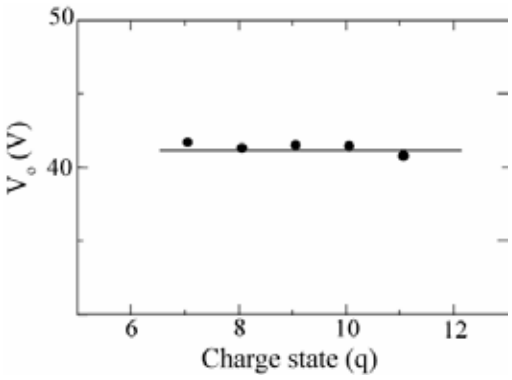

Fig. 3. V_0 for multicharged Ar ions

Figure 3 shows V_0 as a function of the charge state of Ar. It is clearly shown that the V_0 is constant and independent of the charge state. In a previous study, we observed that V_0 decreased with increasing charge and became constant above q=5.[5] If we assume that the ion temperature is more or less constant and independent of the charge state for multicharged heavy ions, the effect of thermal energy of lower-charge-state Ar ions on V_0 is stronger than that of higher-charge-state Ar ions. It means that the thermal energy is not dominant factor in the V_0 for higher charge state of Ar ions in our experiment. For these reasons, we chose V_0 for higher-charge-state of Ar ions (q=9) as a plasma potential.

Figure 4 shows the beam intensity of Ar^{9+} ions as a

function of V_{adjust} at the disc positions L=4.80 and 5.01 cm. The disc position of L is defined in fig. 5.

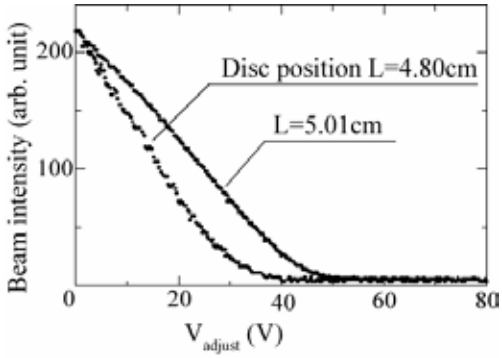

Fig. 4. Beam intensity of multicharged Ar ions as function of V_{adjust} at disc position L=4.80 and 5.01 cm

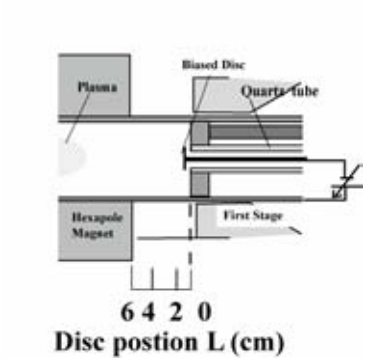

Fig. 5. Schematic drawing of RF injection side of RIKEN 18 GHz ECR ion source and biased disc.

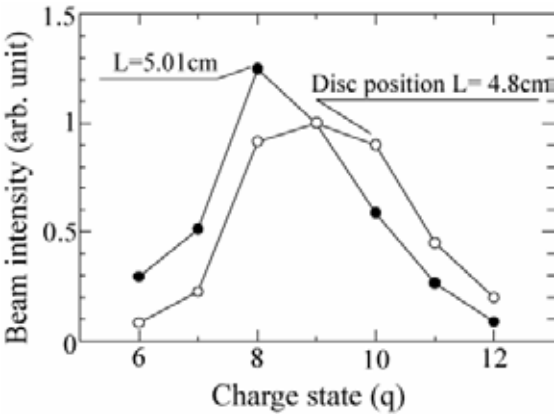

Fig. 6. Charge state distributions of Ar ions at disc position L = 4.80 and 5.01 cm

It was observed that the plasma potential at L=5.01 cm was higher than that at L=4.80 cm. Simultaneously, we measured the charge distribution of Ar ions. Figure 6 shows the charge distributions at two disc positions. The RF power was 400W. The gas pressure was $7x10^{-7}$ Torr. The average charge state of Ar ions at L=4.80cm was higher than that at L=5.01cm. It seems that the lower plasma potential provides higher-average-charge state. To investigate this effect systematically, we measured the plasma potential and average charge state of Ar ions at various disc positions. Figure 7 shows the plasma potential (closed circles) and average charge state of Ar ions (open circles) as a function of disc position. It was observed that the plasma potential and average charge state of Ar ion s were strongly oscillated by moving the biased disc, and average charge became lower at higher plasma potential. Figure 8 shows the average charge vs. plasma potential. It is clearly observed that the average charge decreases with increasing plasma potential.

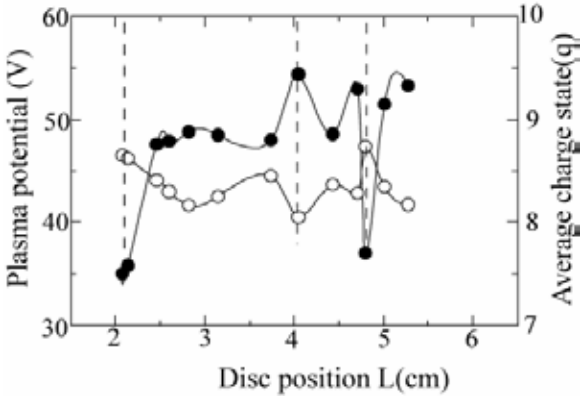

Fig. 7. Plasma potential (closed circles) and average charge state of Ar ions (open circles) as a function of disc position

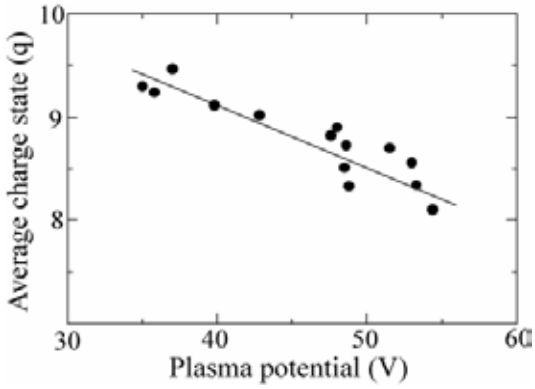

Fig. 8. Plasma potential vs. average charge state

References

1)Z. Q. Xie et al: Rev. Sci. Instrum. 65, 2947(1994)
2)O. Tarvainen et al: Rev. Sci. Instrum. 75, 3138 (2004)
3) S. Biri et al: Nucl. Instrum. Methods B152, 386 (1999)
4)T. Nakagawa et al: Nucl. Instrum. Methods. B226,392(2004)
5)H. Higashijima et al: accepted for publication in Rev. Sci. Instrum.

Production of U beam from RIKEN 18 GHz ECRIS

Y. Higurashi, T. Nakagawa, H. Haba, M. Kidera, T. Aihara*, Tamura*, A. Goto and Y. Yano

One of the important challenges for the RIKEN RI beam factory project is to produce an intense beam of U ions.[1] For this reason, we attempted to produce highly charged U ion beam with RIKEN 18 GHz ECRIS. In 2006, we successfully produced ~2 eμA U^{35+} ion beam by the sputtering method[2,3] and the beam was accelerated up to ~345 MeV/u using accelerator complex.
However, the beam intensity was still low compared with the required beam intensity (15 pμA). Therefore, we need to further improve the ion source performance to increase the beam intensity.

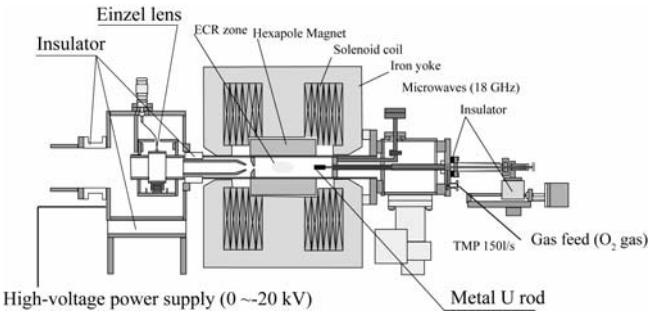

Fig.1. Schmatic of the accel-decel extraction system of RIKEN 18 GHz ECRIS.

In 2007, as a first step to increase the beam intensity, we adopted the accel-decel extraction system to increase the extraction current. Figure 1 shows the schematic drawing of the accel-decel extraction system of the RIKEN 18 GHz ECRIS. The extraction electrode was isolated from the ground potential. A negative voltage was supplied to the electrode to increase the extraction voltage between the plasma chamber and the extraction electrode. To test the effect of the accel-decel extraction system on the beam intensity, we measured the beam intensity of highly charged Xe ions. We used Xe ions because the Xe ion beam production is easier to tune than that for U ions beam. The voltage supplied to the plasma chamber was fixed at 5.6 kV. To obtain a 345 MeV/u uranium beam from the accelerator complex of the RIKEN RIB factory project, the extraction voltage of the ion source for the U^{35+} ion beam has to be set at 5.6 kV to match the acceleration condition. Figure 2 shows the beam intensity of highly charged Xe ions as a function of negative voltage supplied to the extraction electrode. The ion source was tuned to maximize the beam intensity at each extraction voltage. It is clearly seen that the beam intensities increased by increasing the negative voltage up to a certain level and keeping it.

*SHI Accelerator Service Ltd

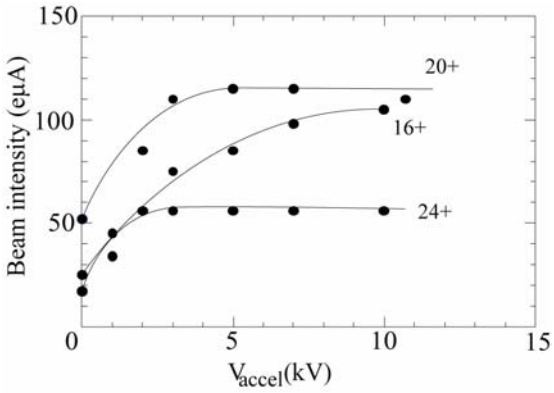

Fig. 2. Beam intensities of highly charged Xe ions as a function of negative voltage of extraction electrode

In addition to the accel-decel extraction system, we also used a larger U rod ($6\times6\times25mm^3$) which was twofold larger than the rod ($3\times6\times25mm^3$) used in 2006 to increase the number of emitted neutral U atoms.

Figure 3 shows the typical charge distribution of the highly charged U ions, which was measured using the faraday cup that was placed downstream of the analyzing magnet. The ion source was tuned for the production of the U^{35+} ion beam. The RF power was 550 W. Oxygen gas was used as the ionized gas. The voltages supplied to the plasma chamber and extraction electrode were 5.6 and -6.7 kV, respectively. Under this condition, we obtained ~4 eμA of U^{35+} ion beam. For a short time, we obtained a ~5 eμA of U^{35+} beam in the test experiment.

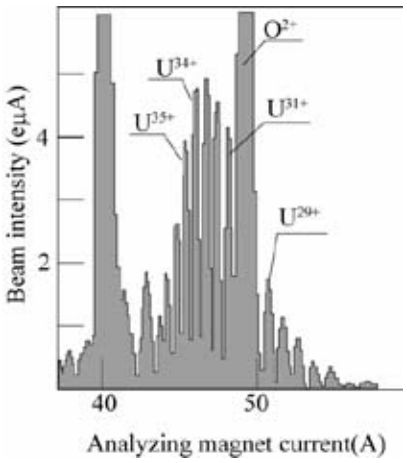

Fig. 3. Charge state distribution of the U ions.

References
1)Y. Yano: Nucl. Instrum. Methods B261,1009(2007)
2)Y. Higurashi et al.,: accepted for publication to Rev. Sci. Instrum.
3)Y. Higurashi et al.,: RIKEN Acc. Prog. Report 40,117(2006)

Design and construction of superconducting coils for RIKEN 28 GHz ECR ion source

Jun-ichi Ohnishi, Takahide Nakagawa, Yoshihide Higurashi, Hiroki Okuno, Kensuke Kusaka, and Akira Goto

The construction of the superconducting coil system for the 28 GHz ECR ion source[1] began at a factory of Mitsubishi Electric Corporation in October 2007. It consists of six solenoids SL1~SL6 and a set of sextupole coils as shown in Fig. 1.[2] The maximum axial magnetic fields are 3.8 T at the RF injection side and 2.2 T at the beam extraction side. The sextupole magnetic field is approximately 2 T on the inner surface of the plasma chamber (r = 75 mm). The coils use a NbTi-copper conductor and are bath-cooled in liquid helium.

The design of the superconducting coil was modified during the construction design. The parameters of the new design are shown in Table 1. Although each sextupole coil in the original design has a saddle form that fits a bore cylinder, it was changed to a flat shape to make the winding of the coil easy. Because this change decreases the sextupole magnetic field, the inscribed radius of the coils was reduced to 98.5 mm from 102 mm at the expense of the thickness of the vacuum insulation of the cryostat. Figure 2 shows the Ic performance of the conductor with a rectangular shape used for coils other than SL3 and SL4 and the load points for the solenoid SL1 and the sextupole. The maximum experience field of the sextupole coils is 7.4 T and it is 6.5 T except for the field component of the current direction.

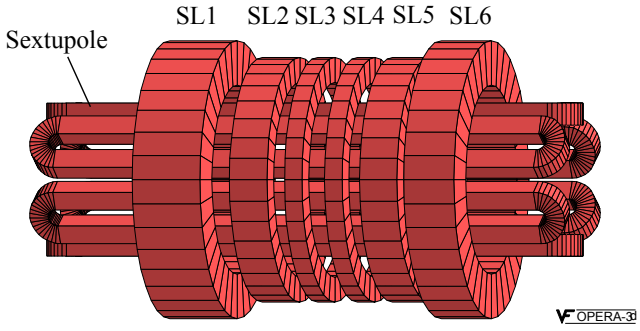

Fig. 1. Arrangement of the superconducting solenoid and sextupole coils.

The sextupole coils are very difficult to design and fabricate because of the following reasons: the experience magnetic field is high, the magnetic force is strong and inhomogeneous, they are assembled from six long racetrack coils, and the inside space is narrow. The longitudinal distributions of the magnetic force acting on the straight region of the sextupole coils are shown in Fig. 3. Because the expansion magnetic force in the azimuth direction is generated by not only the self-field but also the radial magnetic field of the solenoids, it changes along the beam axis and its direction is opposite for the coils of N and S poles. Figure 4 shows a cross section of the sextupole straight part. To minimize the movement of the coils caused by the inhomogeneous and large magnetic force, the coils are fixed with stainless steel wires wound with very high tension of about 580 MPa. The tension is decreased by about 25% after cooling because of the difference in the thermal shrinkage factor. The deformation of the coils was calculated by ANSYS.[3] Assuming that the remaining tension after the cooling was 460 MPa and the thickness of the wire region was 2 mm, the maximum displacement of the coils was calculated to be 0.19 mm and the movement of the coils by excitation was 0.03 mm.

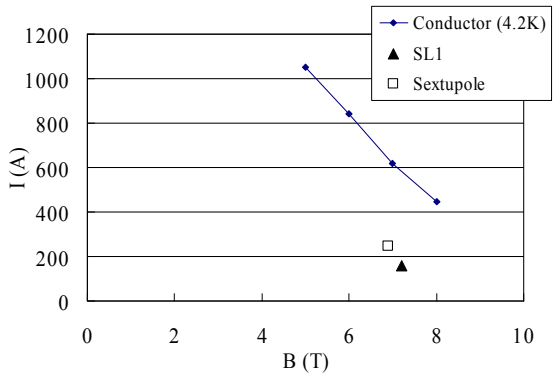

Fig. 2. Ic of the conductor and load points of the SL1 and the sextupole.

Table 1. Parameters of the superconducting coils.

	SL 1	SL 2	SL 3	SL 4	SL 5	SL 6	Sextupole
Inner radius (mm)	170	175	175	175	175	170	102
Outer radius (mm)	250	220	220	220	220	250	142
Length (mm)	135	75	35	35	75	100	1073
Conductor size (mm)	0.82 x 1.15	0.82 x 1.15	φ1.09	φ1.09	0.82 x 1.15	0.82 x 1.15	0.82 x 1.15
Cu/NbTi ratio	1.3	1.3	6.5	6.5	1.3	1.3	1.3
No. turns	9124	2778	1305	1305	2778	6830	1216
Current (A)	162	182	109	109	155	132	271
Bmax (T)	7.2	5.2	3.1	3.0	4.8	5.4	7.4(6.5)
Ic (A)	203	298	229	233	278	223	349
Iop/Ic	0.80	0.61	0.47	0.47	0.56	0.59	0.78
Inductance (H)	34.0	4.0	1.0	1.0	4.0	20.0	6.9

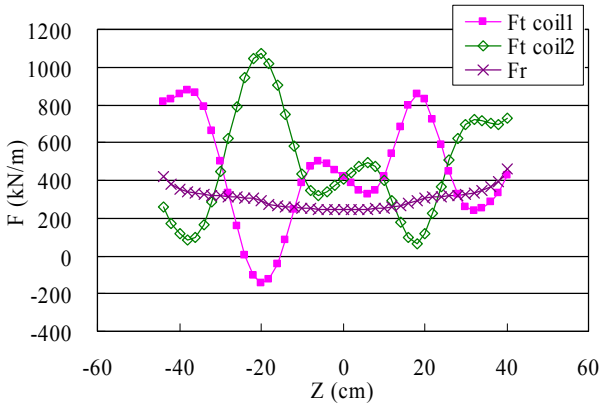

Fig. 3. Magnetic force acting on the sextupole coils. Fr indicates radial direction and Ft the expansion force in azimuth direction. Coil 1 and coil 2 differ in terms of the pole direction.

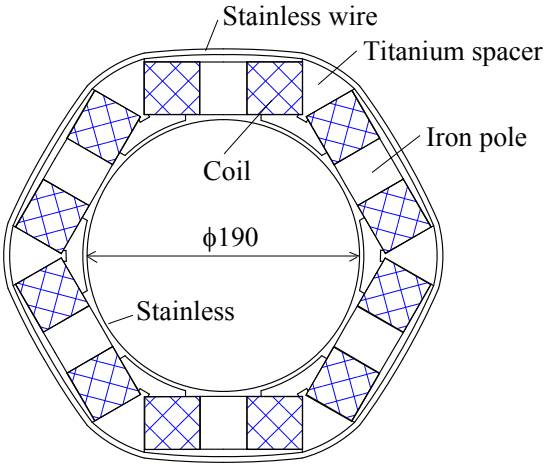

Fig. 4. Cross section of the straight part of the sextupole coil.

The quench protection is made by connecting both ends of each coil with clamp diodes, and resistors are not used. The sextupole coils are protected by each of the six coils because the maximum voltage from the ground becomes larger than 2000 V when they are protected collectively. Figure 5 shows the currents of the six solenoids and the temperature of the SL1 calculated by QUENCH[4] when the SL1 quenched during the nominal operation of all the solenoids. The temperature rise of the SL1 was 115 K and the maximum voltage between the layers was about 50 V. On the other hand, Fig. 6 shows the currents of the sextupole coils when one of the six coils quenches. It is found that all the coils quench in order because the currents of the neighbors of the quench coil are increased. The maximum temperature rise of the six coils was about 120K. Because the unbalance of the currents between the coils is generated during quenches, the sextupole must have been designed to withstand the anisotropic magnetic force.

The winding of the sextupole and the solenoid coils began in January 2008. The excitation test of the coil

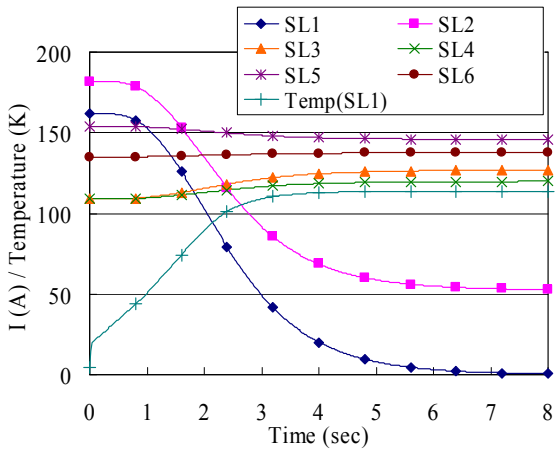

Fig. 5. Calculated current and temperature changes of the solenoid coils after the SL1 quenched.

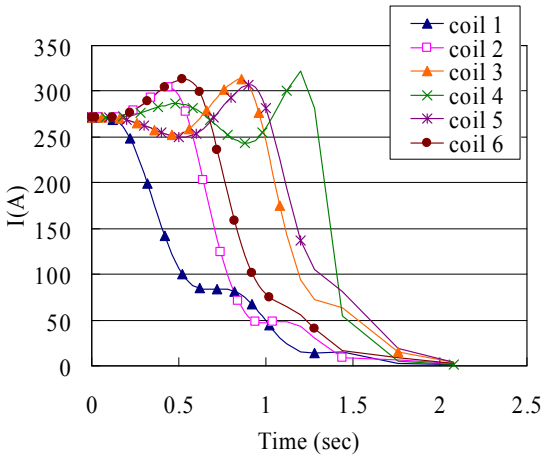

Fig. 6. Calculated current waveforms of six coils of the sextupole after coil 1 quenched. The numbering of the coils is in the order of the azimuth direction.

assembly alone is planned in May and the total system with a recondensed cryostat will be completed in September.

References

1) T. Nakagawa et al.: RIKEN Accel. Prog. Rep. **40**, 118 (2007).
2) J. Ohnishi et al.: High Energy Physics and Nuclear Physics **31**, suppl. 1, 37 (2007).
3) http://ansys.com.
4) M. N. Wilson: Rutherford Laboratory Report, RHEL/M151 (1968).

Optimization of low-energy beam transport under space charge

Y. Sato,[*1] Y. Higurashi, T. Nakagawa, M. Kidera, and A. Goto

To achieve an intense heavy-ion beam, we can shorten the length of low energy beam transport (LEBT) system under the space charge domain. In this report, we discuss the effect of changing the length with using IGUN software, which can simulate a beam from the ion source in the space charge domain[1)]. Our simulation model is inspired by the LEBT of the 18 GHz ECR ion source (ECRIS) at RIKEN[2)]. We recall that there is no treatment for ion space charge compensation in our LEBT system. Therefore, we assume that our LEBT is in the space charge domain upstream of the analyzing bending magnet.

To set the ion beam from ECRIS, we refer to the measured beam distribution at the Faraday cup after the bending magnet of RIKEN in June 2007. We assume that the ion beam at ECRIS consists of 140 μA of O^{2+}, 250 μA of O^{3+}, 260 μA of O^{4+}, 190 μA of O^{5+}, 110 μA of O^{6+}, 50 μA of O^{7+} and 2.4 μA of U^{35+}. The plasma Debye length is assumed to be 0.212 mm. The total beam current becomes 1 mA. In this paper, we focus on the LEBT upstream of the analyzing bending magnet. The IGUN software treats cylindrical problems. Therefore, the model geometry is cylindrical and close to that at RIKEN. The effect of the quadrupole magnet next to the analyzing bending magnet is neglected. We can expect the effect of the quadrupole magnet on beam emittance to be smaller than that of other upstream components. The model components in the IGUN are the plasma and extraction electrodes, the solenoidal components of magnetic field from ECRIS, the focusing solenoid, the Einzel lens, and deceleration. The solenoidal magnetic field is modeled from the simulation using FEMM (Finite Element Method Magnetics) software[3)].

We compare three types of LEBT from ECRIS to the bending magnet: (I) possibly shortest LEBT for RIKEN 18 GHz ECRIS, (II) the current LEBT for RIKEN 18 GHz ECRIS, and (III) the previous LEBT for RIKEN 18 GHz ECRIS. Their properties are listed in Table 1. The solenoid field and the voltage of the center of the Einzel lens are optimized to minimize the r-r' emittance of the U^{35+} beam in front of the bending magnet in each LEBT.

The r-r' diagram at the entrance of the bending magnet in each LEBT is shown in Figs. 1, 2, and 3. The optimized RMS emittances of the U^{35+} beam at the entrance of the bending magnet in LEBTs are 180 mm mrad for LEBT (I), 270 mm mrad for LEBT (II), and 230 mm mrad for LEBT (III). We found that a 0.5 m shorter LEBT can achieve an around 30 percent lower emittance beam under the space charge domain. Therefore, we must set our LEBT length as short as possible if there is no treatment to compensate the ion space charge effect in the LEBT.

*1 yoichisato@riken.jp

References

1) R. Becker and W. B. Herrmannsfeldt: Rev. Sci. Instrum.63, 2756 (1992).
2) N. Inabe, M. Kase, O. Kamigaito, Y. Miyazawa, M. Hemmi, T. Chiba, A. Goto, Y. Batygin, and Y. Yano: RIKEN Accel. Prog. Rep **28**, 166 (1995).
3) D. Meeker: in *Finite Element Method Magnetics, User's Manual* ♯ (http://femm.foster-miller.net /Archives/doc/manual42.pdf).

Table 1. Parameters of model LEBTs.

ELEMENT	Position	Properties
(I) SHORT LEBT		
Plasma outlet radius	0 mm	5 mm
Plasma electrode	0 mm	5.6 kV
Extraction electrode	30 mm	-10.5 kV
Einzel center lens 60 mm	265 mm	+4.45 kV
Deceleration	600 mm	0 V
Entrance of bending magnet	1004 mm	
(II) NEW LEBT		
Plasma outlet radius	0 mm	5 mm
Plasma electrode	0 mm	5.6 kV
Extraction electrode	30 mm	-10.5 kV
Solenoid 360 turns, 280 mm	250 mm	200 A
Einzel center lens 60 mm	660 mm	-6 kV
Deceleration	967 mm	0 V
Entrance of bending magnet	1550 mm	
(III) OLD LEBT		
Plasma outlet radius	0 mm	5 mm
Plasma electrode	0 mm	5.6 kV
Extraction electrode	30 mm	-10.5 kV
Einzel center lens 60 mm	265 mm	+0.6 kV
Deceleration	600 mm	0 V
Solenoid 360 turns, 280 mm	630 mm	20 A
Entrance of bending magnet	1550 mm	

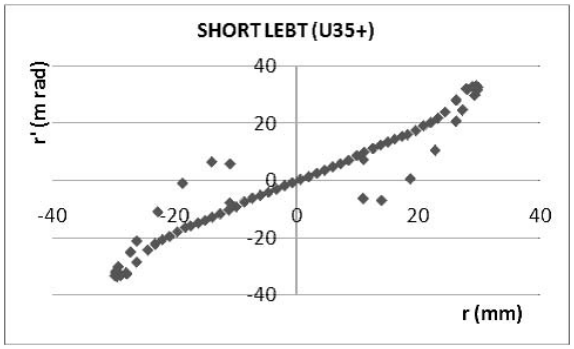

Fig. 1. The r-r' diagrams of U^{35+} in front of bending magnet for Short LEBT.

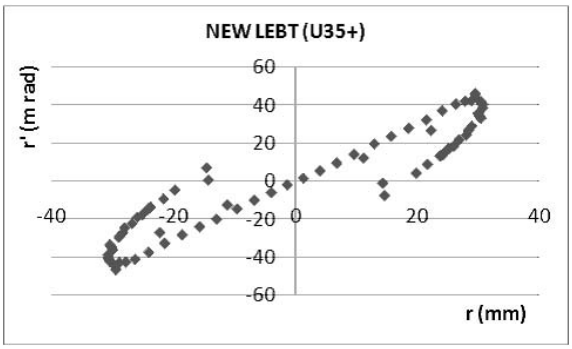

Fig. 2. The r-r' diagrams of U^{35+} in front of bending magnet for New LEBT.

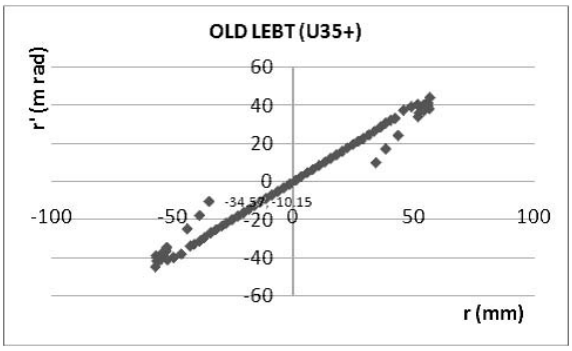

Fig. 3. The r-r' diagrams of U^{35+} in front of bending magnet for Old LEBT.

Material inspection for field emission of electrons in cavity of RILAC booster

O. Kamigaito and T. Kobayashi

In May 2005, strong X-rays were radiated from the last cavity (A6) of the RILAC booster,[1] and it became impossible to raise the cavity voltage to the required value of 300 kV. The observed phenomena resembled those in the case of the A1 cavity in December 2001: the cavity voltage did not exceed a certain level despite the excessive rf power transmitted to the cavity. In the case of the A1 cavity, it was found that the small particles produced by Teflon components emitted electrons on the surfaces of electrodes at a high electric field and generated X-rays through the bremsstrahlung process.[2] We, therefore, removed all the Teflon components from the booster cavities in 2002. However, the generation of X-rays from the A6 cavity implies that there are still other origins of electron emission.

We collected a lot of very tiny particles scattered in the A6 cavity and analyzed them by scanning electron microscopy (SEM) and energy dispersion X-ray analysis (EDX). Figure 1 shows a typical X-ray spectrum obtained by EDX, which shows that the main component is silver with a small contribution of carbon.

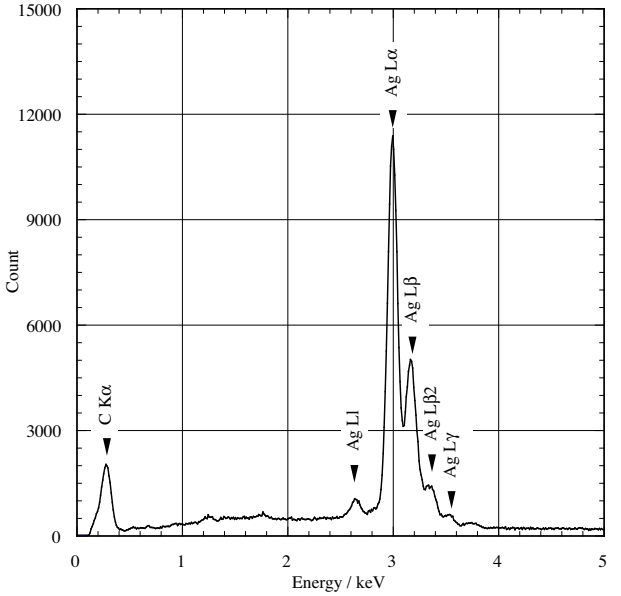

Fig. 1. Typical X-ray spectrum.

The only component containing silver in the booster cavities is the sliding contacts used around the frequency tuner and rf feeder, as shown in Fig. 2. This component also contains 5% carbon. Therefore, the tiny particles must come from the sliding contacts around the tuner, which always moves during the operation.

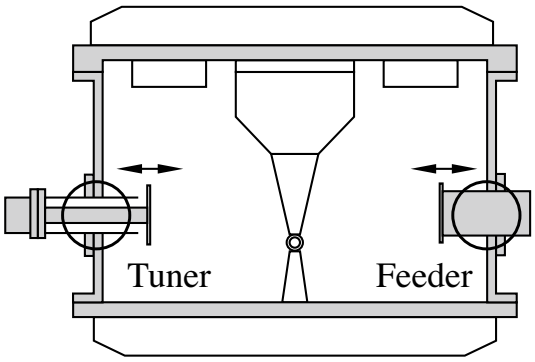

Fig. 2. Cross-sectional view of booster cavity A6. Sliding contacts are used around the tuner and feeder.

References

1) O. Kamigaito, M. Kase, N. Sakamoto, Y. Miyazawa, E. Ikezawa, N. Fukunishi, S. Kohara, M. Fujimaki, M. Hemmi, T. Chiba, Y. Chiba, H. Ryuto, A. Goto, and Y. Yano: Rev. Sci. Instrum. **76**, 013306-1 (2005).
2) O. Kamigaito, H. Hasebe, T. Aihara, T. Ohki, H. Yamauchi, A. Uchiyama, K. Oyamada, S. Kohara, N. Sakamoto, E. Ikezawa, M. Kase, and Y. Yano: RIKEN Accel. Prog. Rep. **36**, 285 (2003).

Reconditioning of four-rod cw RFQ for new injector to RI-beam factory

O. Kamigaito, E. Ikezawa, T. Fujinawa, H. Fujisawa,[*1] S. Yokouchi, K. Oyamada,[*2] H. Yamauchi,[*2] T. Ohki,[*2] T. Aihara,[*2] M. Tamura,[*2] A. Uchiyama,[*2] N. Sakamoto, M. Kase, A. Goto, and Y. Yano

A new injector system for the RI-beam factory[1] has been proposed, which enables the performance of experiments on the super-heavy elements[2] and RI-beam factory independently.[3] This injector system, consisting of an ECR ion source, an RFQ linac, and three drift-tube linacs (DTLs), is expected to accelerate heavy ions of M/q=7 up to an energy of 680 keV/u. The resonant frequencies of the RFQ and DTLs have been chosen to be 36.5 MHz, which is twice that of the RRC. Figure 1 shows a schematic diagram of the new injector system.

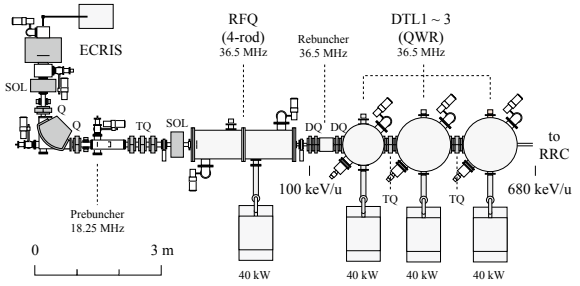

Fig. 1. Schematic diagram of new injector system.

In November 2007, an RFQ system including two post accelerators and their RF amplifiers was transferred to RIKEN through the courtesy of Kyoto University. This RFQ system was originally developed by Nissin Electric Co., Ltd. in 1993.[4] Since the termination of its acceleration tests in the company, the RFQ system has been maintained in the Advanced Research Center for Beam Science, Kyoto University for several years.

The RFQ linac, based on a four-rod structure, accelerates heavy ions of M/q=16 up to an energy of 84 keV/u in the cw mode with an rf frequency of 33.3 MHz. When the RFQ resonator is modified so as to have a resonant frequency of 36.5 MHz, it becomes possible to accelerate ions of M/q=7 to 100 keV/u, which is the required energy in the new injector system, without changing the vane electrodes.

After setting the RFQ system in the RIBF building, as shown in Fig. 2, we installed vacuum pumps on it and started evacuation with a newly designed control system of pumps. Figure 3 shows a schematic diagram of the pumping system. The vacuum level reached 3.5 $\times 10^{-5}$ Pa in January 2008.

*1 Advanced Research Center for Beam Science, Institute for Chemical Research, Kyoto University
*2 SHI Accelerator Service Ltd.

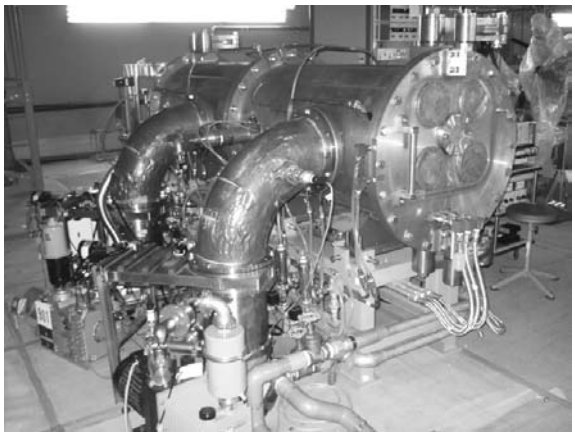

Fig. 2. Photograph of RFQ placed in RIBF building. Two turbomolecular pumps were installed.

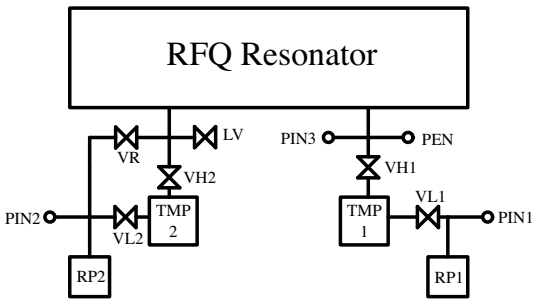

Fig. 3. Schematic diagram of pumping system.

We also measured the unloaded-Q (Q_0) of the RFQ resonator. The measured Q_0 is 5,280, which is very close to the original value of 5,400 measured in 1996.[5]

We plan to perform a high-power test using the original frequency of 33.3 MHz in June 2008, after reassembling the rf amplifier.

References

1) Y. Yano: Nucl. Instrum. Methods **B 261**, 1009 (2007).
2) K. Morita, K. Morimoto, D. Kaji et al.: J. Phys. Soc. Jpn. **73**, 1738 (2004).
3) O. Kamigaito, N. Fukunishi, T. Nakagawa, H. Saito, and A. Goto: Proc. 3rd Annual Meeting of Particle Accelerator Society of Japan and 31th Linear Accelerator Meeting in Japan, Sendai, Japan, 2006-8, p. 502.
4) H. Fujisawa: Nucl. Instrum. Methods **A 345**, 23 (1994).
5) H. Fujisawa, N. Hamamoto, and Y. Inouchi: Proc. 7th Int. Symp. Advanced Nuclear Energy Research, Takasaki, Japan, 1996-3, p. 436.

Calculations of beam transmission and quality in RIKEN AVF Cyclotron

S. B. Vorozhtsov,[*1] A. S. Vorozhtsov,[*1] E. E. Perepelkin,[*1] S. Watanabe,[*2] S. Kubono,[*2] T. Mitsumoto,[*2,*3] and A. Goto

Experimental studies, such as nuclear physics of unstable nuclei and nuclear astrophysics, are performed using the AVF cyclotron. To establish such research activities, the upgrade project of the AVF cyclotron is being conducted in collaboration between the Center for Nuclear Study (CNS) of the University of Tokyo and RIKEN. One of the issues in this project is to increase the intensity of $^{14}N^{5+}$ ion beams up to 10 pμA, which is required for obtaining sufficient yields of secondary particles.[1] The present study is thus focused on the improvements in beam transmission efficiency and beam quality in the AVF cyclotron by detailed orbit simulations.

The computer model of the electromagnetic fields of the AVF cyclotron was prepared and successfully checked against the measurements. It comprises the following structural elements: a magnet yoke, spiral sectors, center plugs, trim and harmonic coils, an inflector, an RF shield, RF Dee electrodes, a deflector and a magnetic channel (see Figs. 1 and 2). Electric and magnetic field distributions and mechanical structures were transmitted to the beam dynamics code for simulations, and particle losses on the surfaces of the system elements were estimated.

First, the simulation with respect to the beam injection and acceleration was performed for the existing geometry and originally designed operational parameters. The obtained results showed that the beam transmission efficiency agreed with the measurement; the major particle losses occurred in the center region during several turns owing to the vertical broadening of the beam. The simulation also indicated that the inflector electrode was too short to introduce the beam onto the median plane of the cyclotron, and that this caused vertical beam oscillation, also resulting in the beam loss.

The easiest way to improve the above situation is to determine better operational parameters instead of changing the present geometry of the center region. A preliminary calculation showed that the broadening of the beam could be mitigated and the beam transmission efficiency could be improved by changing the following parameters: the injection energy of the beam and the RF Dee voltage. In the simulation for 7 MeV/nucleon $^{14}N^{5+}$, the extraction voltage of the ECR ion source was decreased from 10.4 kV to 9 kV and the RF Dee voltage from 46.7 kV to 40 kV. These values were adopted in order to obtain a sufficiently small vertical angle at the exit of the inflector as well as to ensure the beam passage through the puller with the beam crossing the first acceleration gap at the positive RF phase that allows the electric focusing. It is noted that a negative phase (defocusing) at this gap was adopted in order to avoid

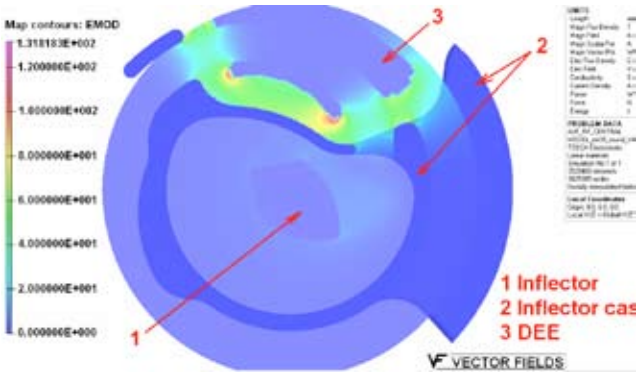

Fig. 1. Computer model for the electric field distribution in the center region.

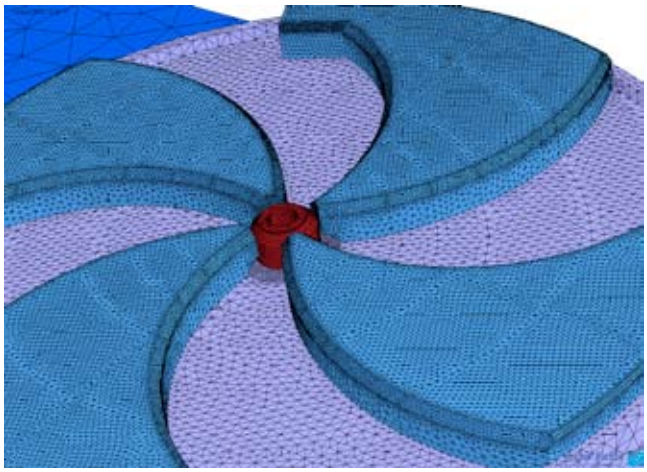

Fig. 2. Computer model for the magnetic field distribution.

overfocusing.[2,3] The magnetic field amplitude of the first trim coil was also changed by approximately 50 % to ensure beam sitting at zero RF degree in the isochronous field region. The result obtained in the calculations indicated that the beam transmission efficiency in the range from the inflector entrance to the electro-static deflector was improved from 40 % to 65 %.

References

1) M. Fukuda et al.: CNS-REP-59, 2003, p. 74.
2) A. Goto et al.: Proc. 12th Int. Conf. Cyclotrons and Their Applications, Berlin, Germany, 1989, p. 439.
3) A. Goto et al.: RIKEN Accel. Prog. Rep. **22**, 205 (1988).

*1 Joint Institute for Nuclear Research, Dubna, Russia
*2 Center for Nuclear Study, University of Tokyo
*3 Sumitomo Heavy Industries, Ltd.

Foil changer with energy adjuster function†

H. Ryuto,*1 H. Hasebe, N. Fukunishi, T. Abe, A. Goto, M. Kase, and Y. Yano

The matching between the exit energy of a cyclotron and the injection energy of the adjacent cyclotron is crucial in a heavy-ion cyclotron complex such as the RIKEN RI-beam factory. A uranium beam accelerated using the fixed-frequency ring cyclotron (fRC) loses approximately one-tenth of its kinetic energy while passing through the third stripper placed between the fRC and the intermediate-stage ring cyclotron[1]. The beam energy behind the third stripper changes because of the thickness difference of the stripper foil when the stripper foil is changed. It is a rather complicated task to fine-tune the extraction energy of the beam by changing the extraction radius, or to fine-tune the injection energy of the following cyclotron by adjusting the injection radius. To fine-tune the beam energy easily, a charge stripping foil changer that also has an energy adjuster function was fabricated.

Figure 1 shows a schematic view of the charge-stripping foil changer with an energy adjuster function (FCEA). Carbon foils are attached to foil holders. The foil holder is a 0.5-mm-thick rectangular aluminum plate with a rounded rectangular hole of 28 mm × 14 mm. The foil holders are attached to holder supports using leaf springs. The holder supports are on a pair of chain loops stretched in a cylindrical vacuum chamber. Thirty carbon foils and a beam viewer can be set in the FCEA. A part of the chain loops is used to allow beams to pass without charge stripping, and this part is also used to determine the zero point of the loops using switches. The carbon foils are changed using the maintenance port. Two motors are placed at one end of the cylindrical vacuum chamber. The other end is connected to a common vacuum chamber in the beam transport line. One of the motors is used to change the foil at the beam position by rotating the chain loops through a biaxial feedthrough and gears. The other motor is used to tilt the foil. The distance that the beam passes through the foil, that is, the effective thickness of the foil, is adjusted by changing the angle between the foil and the beam. The ions that pass through the carbon foil lose their energy approximately in proportion to the thickness of the foil; thus, the beam energy can be adjusted by tilting the foil. The maximum tilting angle is 60°. The foil can be changed while maintaining the same tilting angle.

A uranium beam was accelerated to 345 MeV/nucleon using two FCEAs at the second and third stripper sections. The FCEAs operated stably during the acceleration of the uranium beam.

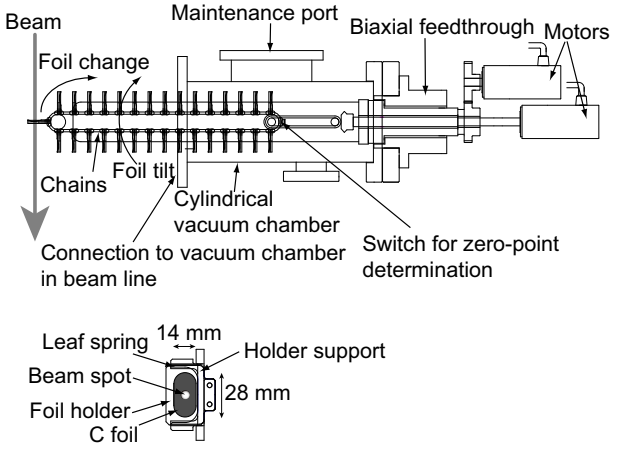

Fig. 1. Schematic view of charge-stripping foil changer with energy adjuster function showing side view and close-up view around beam spot on carbon stripper foil.

References

1) H. Ryuto, N. Fukunishi, H. Hasebe, N. Inabe, S. Yokouchi, O. Kamigaito, A. Goto, M. Kase, Y. Yano, Proceedings of the 2005 Particle Accelerator Conference, Knoxville, USA, 2005, p. 3751.

† Condensed from the article in Nucl. Instrum. Meth. A 581, 586 (2007).

*1 Present address: Photonics and Electronics Science and Engineering Center, Kyoto University.

Development of new Faraday cup for RIBF

T. Watanabe, M. Kase, M. Fujimaki, N. Fukunishi, K. Yamada, A. Yoshida and Y. Yano

New Faraday cups have been developed to measure current of heavy-ion beams for the RIKEN RI beam factory (RIBF). Ten new Faraday cups have been installed into the transport lines of the RIKEN heavy-ion linac (RILAC), the RIKEN ring cyclotron (RRC), the fixed-frequency ring cyclotron (fRC) and the intermediate-stage ring cyclotron (IRC) to measure the current of accelerated heavy-ion beams. The design of the new Faraday cups and the preliminary experimental results obtained during the commissioning of the RIBF using the heavy-ion beams are described in this report.

During beam commissioning, it is essential to keep the beam transmission efficiency as high as possible, because the production of RI beams requires an intense primary beam, and the activation of the beam transport chambers induced ed by beam loss should be avoided. In this facility, to evaluate the beam transmission efficiency, Faraday cups are used. When an accelerated particle hits the surface of a Faraday cup, secondary electrons are always generated. If these electrons leave the insulated cup area, the reading of the beam current will be incorrect owing to the number of lost electrons. Thus, preventing the escape of secondary electrons from the cup is very important for measuring the beam current precisely. Typically, this can be achieved by applying a high voltage near the entrance of the cup. We fabricated and installed old Faraday cups, which have diagonally cut shapes for cooling the cups effectively. A schematic drawing of the old Faraday cup installed into the beam transport line at the RIBF is shown in Fig. 1. The designed cooling power of the cup was 10 kW for high-energy heavy-ion beams. However, as the electric field of suppression for the secondary electron beam was asymmetrical, the measured current depended on the position of the heavy ion beam. Thus, the tuning of beam transport was difficult, because the smaller the distance between the electrode and the cup, the higher the current was read (show Fig. 1). Therefore, we decided to design and fabricate a new Faraday cup. Since the electrical field on the beam axis is lower than that on the edge, it is difficult to completely prevent the escape of the high-energy secondary electrons produced by high-energy heavy-ion beams, such as uranium beams. To resolve this technical issue, we calculated the electric field of the suppression electrode by using the MAFIA program. MAFIA is an interactive program package for the computation of electromagnetic fields and is directly based on the fundamental equations of electromagnetic fields, the Maxwell equations. To maintain the high electric potential, the length of the suppression electrode was increased. The MAFIA program can import the file format of Stereo lithography files, the so-called STL files, made by many CAD programs. Figure 2 shows the three-dimensional field distribution of the calculated electric field indicated by arrows, and Fig. 3 shows the two-dimensional contour plot of the absolute electric potential cut at the X-Y plane. The voltage applied to the suppression electrode was 1 kV.

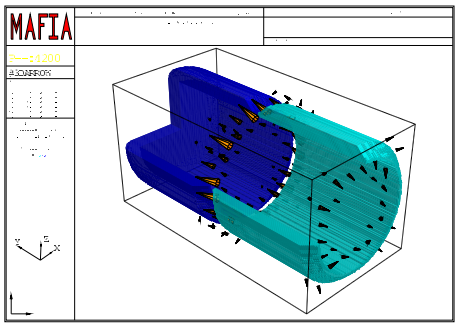

Fig. 2. Calculated three-dimensional field distribution of electric field indicated by arrows.

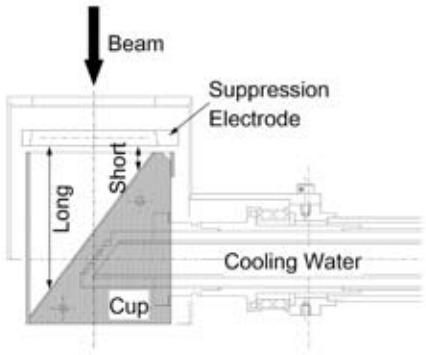

Fig. 1. Schematic drawing of old Faraday cup installed into beam transport line at RIBF.

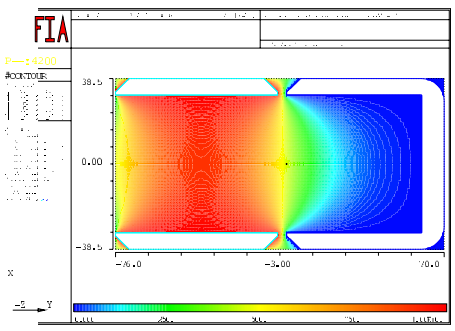

Fig. 3. Calculated two-dimensional contour plot of absolute electric potential cut at X-Y plane.

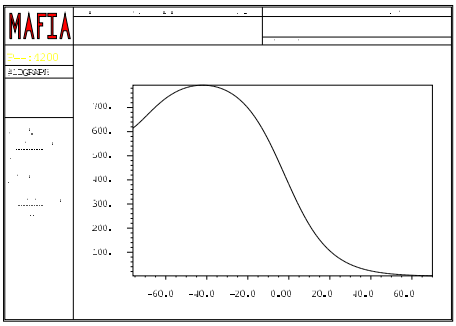

Fig. 4. Electric potential along Y-axis at position of (X=0, Z=0).

Figure 4 shows the electric potential along the Y-axis at the position of (X=0 and Z=0), and the electric potential on the beam axis of 820 V was obtained.

A schematic drawing and a photograph of the Faraday cup, which was designed on the basis of the previous calculations and installed into the beam transport line between the fRC and the IRC at the RIBF are shown in Figs. 5 and 6, respectively. The sizes and solid angles of the old and new Faraday cups are shown in Table 1. The Faraday cup is pneumatically inserted

Table 1. Size and solid angle of each faraday cup.

	Depth	Inner diameter	Solid angle
Old FC	26 (mm)	46 (mm)	0.783 (sr)
New FC	60	62	0.715

into the beam transport chamber by the pneumatic feeder when the measurement is started. The depth of the cup is 60 mm, and the inner and outer diameters of the cup are 62 mm and 77 mm, respectively. An isolated cup and a suppression electrode are connected to a BNC feedthrough and a safe high-voltage (SHV) feedthrough, which is a high-voltage (max. 5 kV) coaxial feedthrough particularly designed to protect an electric discharge from high-voltage exposure, respectively. The output current from the BNC feedthrough is connected to a current-sensitive preamplifier, which consists of lower impedance input and the conversion of the current to a voltage. A dynamic range of 120 dB depending on the beam current is obtained by a log operational amplifier. The driving control and status monitoring of the Faraday cup are controlled by the EPICS system[1].

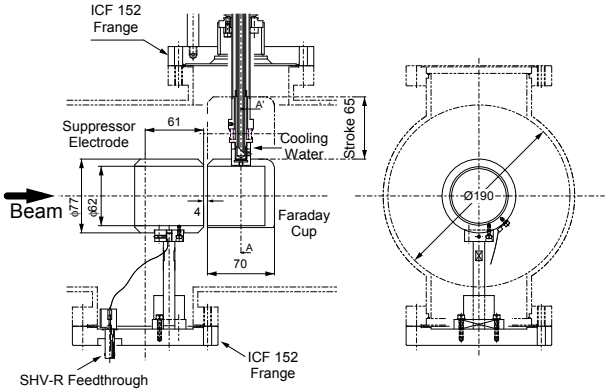

Fig. 5. Schematic drawing of new Faraday cup.

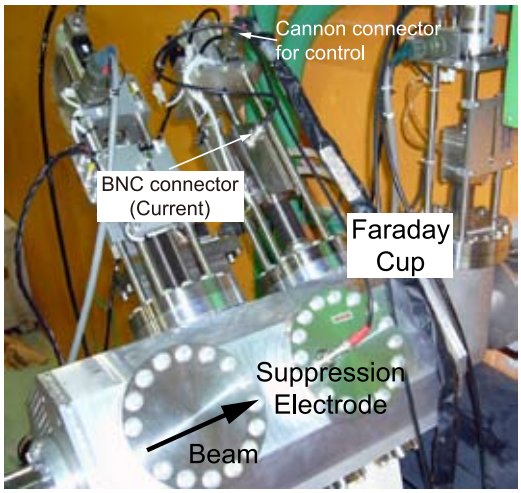

Fig. 6. Photograph of new Faraday cup.

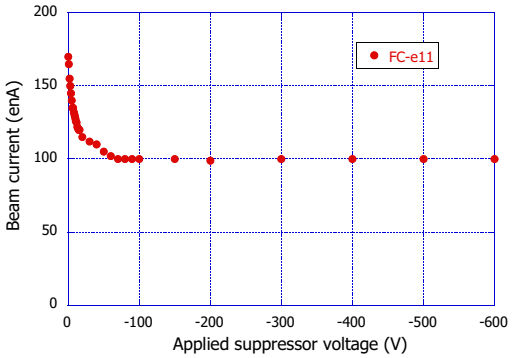

Fig. 7. Typical measurement result obtained using suppression voltage and 5.0 MeV/u $^{70}Zn^{16+}$ beam.

By applying a voltage well above the mean energy of the secondary electrons, the electrons are pushed back to the cup surface. A typical measurement result obtained using this suppression voltage and a 5.0 MeV/u $^{70}Zn^{16+}$ beam is shown in Fig. 7. From this result, the current was found to saturate over the applied voltage of 70 V.

The authors thank the operation staff for their great help.

References

1) M. Kobayashi-Komiyama et al.: RIKEN Accel. Rep. **37**, 277 (2004).

Status report on transverse emittance monitor

Yasuteru Kotaka[*1], Hiromichi Ryuto, Masaki Fujimaki, Masayuki Kase

It is essential to determine transverse emittance precisely to achieve an efficient acceleration of ion beams. An emittance monitor system for heavy-ion beam acceleration at the RIKEN RI beam factory (RIBF) has been developed.

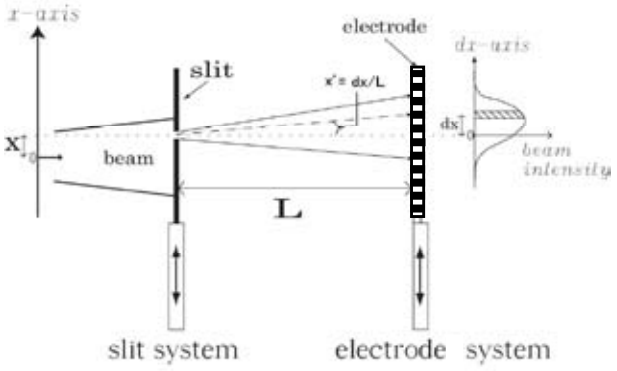

Fig.1. Schematic for measurement of transverse emittance

First, the principle of transverse emittance measurement using the emittance monitor system is described. The x-axis is set perpendicular to the beam axis (see Fig. 1). When a slit system is inserted into the beam line, ions going through a slit are detected using a set of electrodes placed behind the slit at a distance L. As a result, the angle (x') distribution at the slit's displacement (x) is measured. After performing this process along the x-axis, the x-x' distribution of beam is acquired. Transverse emittance can be calculated as the area of x-x' distribution of the beam.

Fig.2. Photograph of emittance monitor systems. The upper part shows a slit system and the lower part shows the electrode system.

Figure 2 shows a photograph of the emittance monitor system. The horizontal and vertical slits are arranged in such a way that they form a rectangle. Horizontal and vertical sets of electrodes are similarly arranged as slits. The slit and electrode systems are placed at the ports at an angle of 45 degrees from the horizontal direction, so that horizontal and vertical emittances can be measured using the same monitor. The measurable beam size is within a radius of 14.4 mm determined by the length of the slits (42 mm). The accuracy of the position setting of the slit and electrode systems is 0.012 mm at a stroke of 300 mm. The gap width between slits is 0.1 mm.

An electrode is fabricated from a Ta ribbon whose thickness is 0.1 mm. Ceramic insulators whose thickness is 0.24 mm are placed between the Ta ribbons. The resolving power of position is 0.34 mm and the beamwidth acceptance is 10.54 mm. The beam current detected using the electrode is amplified and an amplifier transports a beam current of 10 nA to a 10 V output voltage. The output voltage is digitized using an ADC whose resolution is 16 bit at 20 V.

Figures 3 and 4 respectively show the horizontal and vertical emittances measured using an ^{16}O beam accelerated to 10.3 MeV/nucleon by an AVF Cyclotron. L was 317 mm, so the angular resolution was 1.1 mrad and the acceptance of the beam angle was 33.2 mrad. Data are acquired every 0.35 mm of a stroke of 82 mm. It took 2.5 min to measure horizontal and vertical emittances. The horizontal and vertical emittances estimated from the area of the ellipses are 19.3 and 10.0 π mm･mrad respectively.

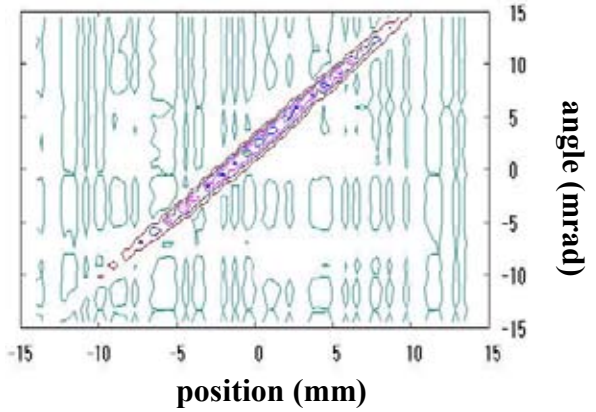

Fig.3. Horizontal emittance.

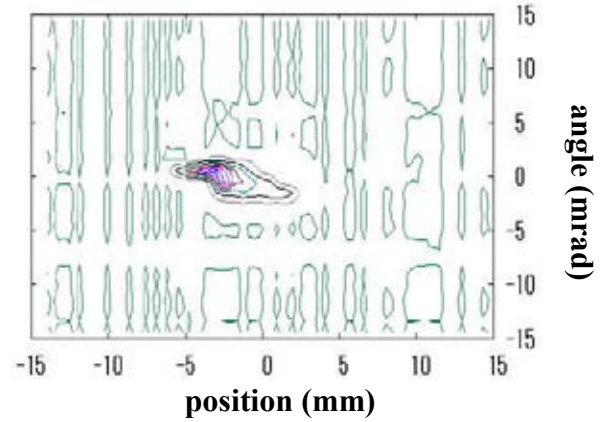

Fig.4. Vertical emittance.

[*1] SHI Accelerator Service Ltd.

Constructing High-Availability Cluster System for RIKEN RIBF Control System

A. Uchiyama,[*1] M. Kobayashi-Komiyama, and M. Kase

In the RIBF control system based on EPICS, there are various types of IOCs, such as a network-based CAMAC crate controller (CC/NET), a wireless router application platform (WRAP) and a VME board computer, to control various types of devices[1]. A CC/NET and a WRAP have GNU/Linux as their operating system, and EPICS programs are installed from the file server of a desktop PC with a mirrored disk (RAID1) system using a network file system (NFS). The VME board computer has vxWorks as its operating system, and it is available for network booting using file transport protocol (FTP). We have an exclusive server for the FTP service and network booting in our system, which is a single-server computer with no RAID system. Since these IOCs do not have disks, these are not expected to break easily. However, they will probably fail to run if the NFS server or FTP server has a problem in its system. To avoid this problem, we need to replace these servers with new ones with higher reliability. Accordingly, a purpose of our work is to improve this weak point of the system by the implementation of a high-availability cluster system (HA cluster). Generally speaking, an HA cluster is a computer cluster system promoting the reliability, availability, and serviceability (RAS) of the services provided by the cluster. In this paper we report on HA clusters for the FTP server and NFS server used by our EPICS IOCs.

Table 1. Specifications of FTP cluster.

	Active node	Standby node
CPU	Intel Celeron 2.66GHz	Intel Xeon 3050
Memory	256MByte	1GByte
OS	RHEL 4	CentOS 4.2
Software	Heartbeat, rsync, vsftpd	

Table 2. Specifications of NFS cluster.

	Active node / Standby node
CPU	Dual-Core AMD Opteron 2212HE
Memory	2GByte
OS	Scientific Linux 4.3
Software	Heartbeat, DRBD, nfsd

One of the main concepts of our system is that it is unnecessary to have a mission-critical environment in our control system except for the interlock system. In other words, we provide the service at all times for accelerator operation, but the situation allows the system to be down for a few minutes. The second concept is to construct a system with low cost. Therefore, we decided to implement failover clusters composed of an active-standby node. To build the system, open-source Heartbeat[2], DRBD[3], and rsync[4] were installed. Similarly, Red Hat Enterprise Linux clones are used for their operating systems; Scientific Linux 4.3 is installed in the NFS cluster server, CentOS 4.2 is installed in the FTP cluster server. The specifications are summarized in Tables 1 and 2.

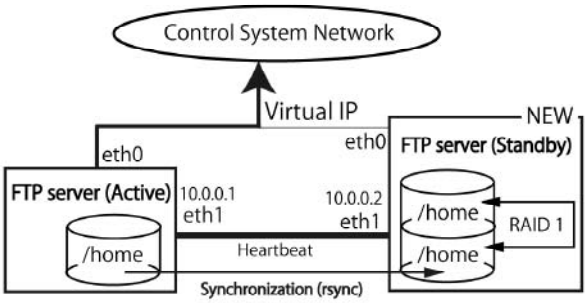

Fig. 1. FTP cluster server in RIBF control system.

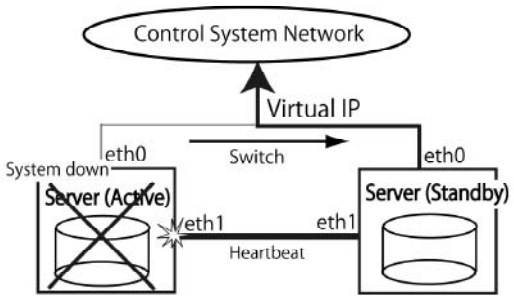

Fig. 2. Action of HA cluster during failover.

Figure 1 shows the FTP cluster server in the RIBF control system. This HA cluster consists of a new FTP server and an old one for booting the VME board computers. In this system, Heartbeat sends heartbeat packets to each server using eth1 for alive monitoring and service monitoring. This HA cluster normally provides the FTP service from eth0 of the active node through a virtual IP address. In order to avoid disk trouble during long-term operation, the RAID1 system is synchronized manually as a backup disk by using rsync. The action of the HA cluster during failover is shown in Fig. 2. Failover is the capability of switching over automatically to standby node, when the active

*1 SHI Accelerator Service Ltd.

node has a problem. In a recovery test, it was confirmed that the service switches from active node to standby node automatically without problems. Also, providing the FTP service stopped for a few seconds during the service switching at the action, because the standby node cannot take over the process file used by the FTP service of the active node.

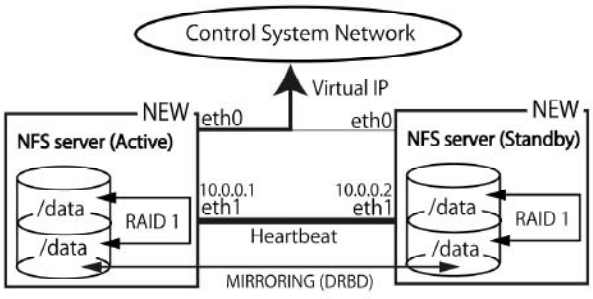

Fig. 3. NFS cluster server in RIBF control system.

Figure 3 shows the NFS cluster server in the RIBF control system. This HA cluster consists of two new servers, and all the Linux IOCs access it to share EPICS programs. In this NFS cluster, Heartbeat sends heartbeat packets as well as the FTP cluster. In addition, these RAID1 systems are synchronized automatically with each other as a mirrored disk over the network by DRBD. Therefore, this NFS cluster is not only available to switch the service without downtime in failover, but also it is extremely improbable that we lose the data stored in the NFS cluster, because this system has four same data in two RAID1 systems.

In December 2007, we started to implement the HA clusters after a recovery test. The number of IOCs is shown in Table 3. As a result, we succeeded in implementing two HA clusters for key services with low cost using only open-source software. Thus, it was confirmed that this HA system was useful in a small-scale system like ours. Note that this NFS cluster server can not only provide a failover system for the service to IOC boxes, but also provide a high-security disk system compared with a RAID1 system without an expensive disk array system.

Table 3. Number of clients connected with clusters in RIBF control system.

Service	Number of clients
FTP	5
NFS	16

In the present system, we cannot detect the occurrence of a failover until someone telnets the cluster, because the network of the control system is a standalone system disconnected from Internet, and it is not possible to send a security alert by E-mail. In the future, a security alert function will be implemented by the TCP/IP port and IP address monitoring of the cluster from the other client.

Finally, the author would like to thank Takashi Ichihara for helpful suggestions.

References

1) M. Kobayashi-Komiyama et al.: in this report.
2) http://www.linux-ha.org/
3) http://www.drbd.org/
4) http://rsync.samba.org/

Beam phase and acceleration rf monitoring system using lock-in amplifier for stable beam supply

R. Koyama,[*1] M. Fujimaki, T. Watanabe, Y. Kotaka,[*1] N. Fukunishi, M. Kase, and Y. Yano

One of the most important factors for supplying stable beams in both aspects of energy and intensity is to maintain the matching of beam phases between accelerators in a multistage acceleration system, such as the RIKEN RI Beam Factory (RIBF). However, it is known that the optimized beam phase by tuning gradually shifts with time owing to the phase drift of acceleration rf and so on. Hence, it is important to monitor the beam phase constantly, and we have developed a monitoring system using the lock-in amplifier SR844[1]. In addition, the system for monitoring the acceleration rf, which is a major cause of phase mismatching, has also been developed. The monitoring system has been introduced to the RILAC and CSM. These systems were actually used in the experiment on superheavy elements with the GARIS[2] from January to March 2008.

In the experiment, a $^{70}Zn^{16+}$ ion beam was accelerated up to 352.6 MeV and bombarded on the target of the GARIS, as shown in Fig. 1. The beam phase was

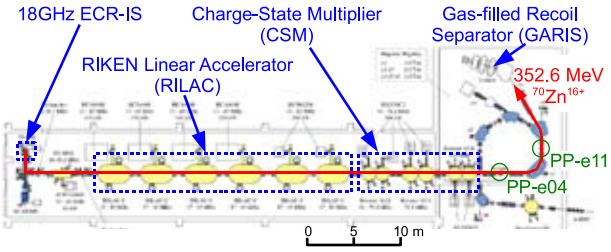

Fig. 1. Schematic top view of RILAC-GARIS course.

measured at the phase probes (PP) mounted in the sections called "e04" and "e11" using the developed SR844 system (Fig. 2) in this experiment. The system is controlled by a LabVIEW program. The phase and amplitude of the beam bunch signal are plotted as a function of time on the front panel of the program and written in an output file. The program also beeps out a warning when the beam phase or intensity changes beyond the permissible range. It should be noted that a third-harmonic acceleration rf is used as the reference signal of the developed SR844 system. Figure 3 shows the frequency component of the signal from PP-e11. The peaks observed also under beam-off conditions correspond to leakage rf and its larger harmonics from the RILAC and CSM cavities. The beam bunch signal has a much higher harmonic component than the leakage rf. Therefore, if we select a frequency with a high S/N ratio, we can perform

[*1] SHI Accelerator Service, Ltd.

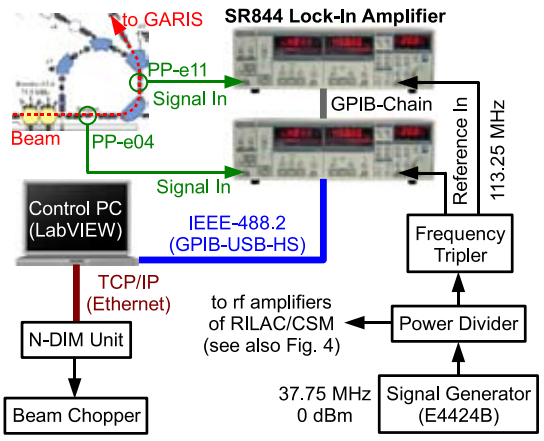

Fig. 2. Block diagram of beam-phase-monitoring system using developed SR844 system.

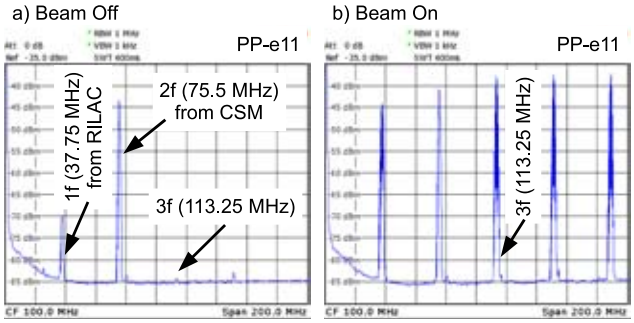

Fig. 3. Frequency component of signal from PP-e11 observed using spectrum analyzer under a) beam-off, and b) beam-on conditions.

measurements with negligible leakage rf effects. We have monitored the third-harmonic frequency component of the beam bunch signal in this experiment. In addition, signals other than the beam bunch signal, such as the third-harmonic leakage rf, are rejected by numerically subtracting the I/Q component measured using the developed SR844 system under beam-off conditions from that measured under beam-on conditions using the program.

The newly developed rf monitor is expected to have a higher measurement accuracy by utilizing the developed SR844 system than the old monitoring system using a vector volt meter 8508A. An accurate and automated monitoring system is efficient in determining which cavity causes the beam phase shift. This system is also controlled by the LabVIEW program, and the rf

voltages and phases of all cavities are plotted as a function of time on the front panel with switching and written in the output file. We can easily determine which cavity we should tune, when the beam phase changes, by monitoring the correlation between the beam phase and the acceleration rf using these systems.

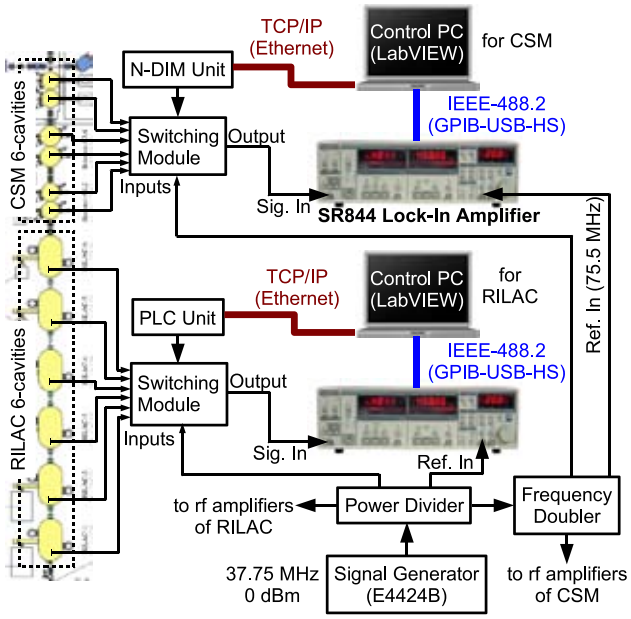

Fig. 4. Block diagram of rf-monitoring system using developed SR844 system for RILAC and CSM.

Figure 5 shows examples of the beam phase and acceleration rf obtained using the developed SR844 system. The fluctuations of the beam phase and acceleration rf normalized by the optimized value of the required energy are plotted as a function of time in this figure. The operation performed is summarized as follows: 1) The beam phase drifted over the limit value and a warning was beeped out from the developed SR844 system. 2) We checked consistency between the beam phase observed using the developed SR844 system and the beam energy measured by a beam user. 3) We changed manually the phase of the RILAC-#5 because only its phase drifted among those of other cavities. 4) The beam phase monitored using the developed SR844 system recovered to the phase optimized to the required energy. 5) We checked the beam energy recovered to the required one.

Figure 6 shows the improvement in the voltage stability of the CSM-A5 by exchanging its module for the voltage regulation called auto-gain control (AGC). We found that the voltage fluctuation of the CSM-A5 was periodic with a very large amplitude in comparison with those of the other CSM cavities. The fluctuation of the beam phase synchronized with that of the CSM-A5 was clarified, as shown in Fig. 6.

The developed SR844 system enabled us to determine easily the conditions of the beam phase and acceleration rf, as described above. We plan to extend the use of the system and aim at supplying more stable beams all over the RIBF. In addition, the time series analysis of the data obtained using the developed SR844 system is in progress. In this analysis, we plan to use various data, such as those obtained at a certain electric power and room temperature. We also plan to reveal the dynamics of the acceleration system of the RIBF to improve its stability.

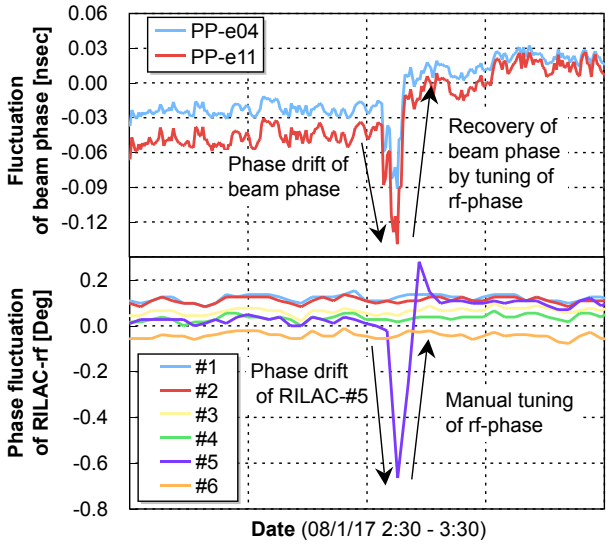

Fig. 5. Example of manual tuning for recovery of beam phase using SR844 monitoring system.

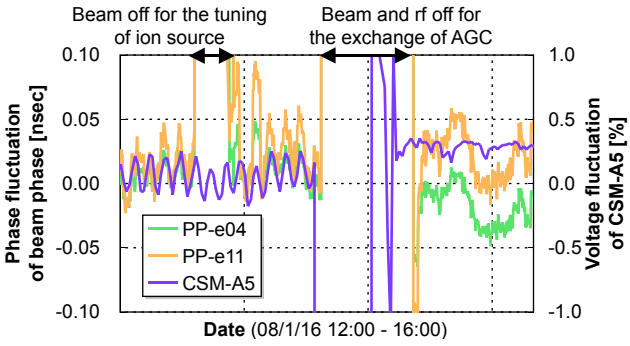

Fig. 6. Improvement in voltage stability of CSM-A5 by exchanging its module for auto gain-control (AGC).

Finally, the authors are grateful to the operation staff of SHI Accelerator Service Ltd. for their cooperation in the preparation of hardware for the SR844 monitoring system for the RILAC-GARIS course.

References

1) R. Koyama et al.: Proc. PASJ4-LAM32, Wako-shi, Saitama (2007) WP38.
2) K. Morita et al.: J. Phys. Soc. Jpn. **73**, 2593 (2004).

Comparison of vacuum systems for ring cyclotrons in RIBF

S. Yokouchi, N. Fukunishi, K. Ikegami, N. Inabe, J. Ohnishi, H. Okuno,
K. Yamada, M. Nishida,* A. Goto, M. Kase, and Y. Yano

The main accelerator of the RIKEN RI beam factory (RIBF) is a cascade of four ring cyclotrons (RCs): the RRC, the fRC, and the IRC are normal conducting cyclotrons, and the SRC is a superconducting cyclotron.[1] Vacuum systems for these RCs are designed on the basis of nearly the same concept.[2–5]

The vacuum chamber consists of magnet chambers with and without an additional chamber[2] (AC), RF resonators, flat-top (FT) resonator, and valley chambers, as shown in Table 1. The AC is provided to isolate ultrahigh vacuum for ion beams (beam vacuum) from a pole of the sector magnet, which desorbs a large amount of gas, in the RRC and IRC. The AC is not required for the fRC since the surface of a pole is coated by a thin Ni layer to reduce its outgas.[6] On the other hand, the beam vacuum is enclosed by the outer walls of a cryostat vacuum chamber in which warm poles are contained in the SRC.[7] A pneumatic expansion seal is employed for connection of the RF resonator and the magnet chamber in the IRC[4] and SRC[8]. In the RRC, this seal method was not carried out although planned. Table 2 shows the surface area of main materials for vacuum chambers exposed to beam vacuum.

The vacuum pumping system is based on cryopumps for main evacuation, turbomolecular pump (TMP) pumping systems for high-vacuum evacuation prior to main evacuation, and rough pumping systems. In addition to these systems, two kinds of differential pumping system are used: One is for evacuation of the AC (AC pumping system) in the RRC and IRC, and the other is for that of the subvacuum of the RF resonator[5] (subpumping system) in the IRC and SRC. The numbers of vacuum pumping systems are listed in Table 3. A cryopump of 10 m^3/s is used for RF resonators and valley chambers. Two 4 and 2.3 m^3/s cryopumps are used for the FT resonator of the IRC and SRC, respectively. A cryopump of 5 m^3/s, which is of the panel type and directly inserted into the stem of the RF resonator,[9] is used only for the RRC.

Each RC (ring cyclotron) has a local controller, which is equipped with a programmable logic controller, and provides a remote sequence control for the vacuum system. A module-type vacuum gauge combined with pirani gauges and cold cathode gauges is employed for monitoring vacuum pressure and interlocking vacuum process control in all RCs. At present, only SRC control is available at the RIBF control console, and others are not yet available for lack of device support programs.

The typical pumping parameters of the RCs are summarized in Table 4. The pumping factors of the SRC and fRC are slightly smaller than that of the RRC; however, the required pressure is attained in all the RCs. From the actual results of the fRC, Ni coating for a pole is proved to be a useful method for manufacturing.

Figure 1 shows the ratio of the outgas from the main material with respect to the total outgas. The predominant outgas is that from copper in the IRC and SRC, while it is that from the fluoroelastomer in the RRC and fRC. The outgas of subvacuum accounts for 35% of total gas load in the IRC, and 40% of that in the SRC. The subpumping system is capable of evacuating this outgas, as mentioned above. This function, however, does not seem to work well. A result of evacuation for an RF resonator of the SRC was as follows: the pressure of beam vacuum without subvacuum pumping (p_{bo}) was 4.4×10^{-6} Pa , and that with subvacuum

Table 1. Configuration of vacuum chambers of RCs.

Vacuum chamber	RRC	fRC	IRC	SRC
Magnet chamber with AC	4	-	4	-
Magnet chamber without AC	-	4	-	6
RF resonator	2	2	2	4
FT resonator	-	1	1	1
Valley chamber	2	2	2	2

Table 2. Inner surface areas of vacuum chambers. Values in parentheses indicate those of subvacuum[4,5]. The unit is m^2.

Material	RRC	fRC	IRC	SRC
Stainless steel	167	70	313(118)	442(245)
Copper	180	92	330(124)	605(249)
Ni-plated iron	-	45	-	-
Fluoroelastomer	3.0	2.0	2.1(0.6)	5.0(1.6)

Table 3. Numbers of vacuum pumping systems.

Pumping system	RRC	fRC	IRC	SRC
Main pump				
10 m^3/s cryopump	10	6	12	16
5 m^3/s cryopump	4	-	-	-
4 m^3/s cryopump	-	-	2	-
2.3 m^3/s cryopump	-	-	-	2
TMP pumping system	4	2	4	4
Rough pumping system	2	2	2	2
Subpumping system	-	-	4	8
AC pumping system	4	-	4	-

* SHI Accelerator Service, Ltd.

Table 4. Typical pumping parameters of RCs. Total outgas is that after 50 h of pumping calculated using the inner surface areas shown in Table 2 and the same equations for outgassing rate as those reported in Ref. 3 are used for standardization. Pumping factor is defined as the total pumping speed divided by total outgas and normalized with that of the RRC.

Parameter	RRC	fRC	IRC	SRC
Total volume (m^3)	30	16	35	90
Total outgas ($Pa \cdot m^3/s$)	5.0×10^{-4}	4.5×10^{-4}	7.0×10^{-4}	1.3×10^{-3}
Total pumping speed (m^3/s)	120	60	128	164.6
Pumping factor	1	0.64	0.88	0.59
Design pressure (Pa)	$3 \sim 4 \times 10^{-6}$	4×10^{-5}	1×10^{-5}	5×10^{-6}
Current pressure measured (Pa)	$6 \times 10^{-7} \sim 2 \times 10^{-6}$	$1 \sim 2 \times 10^{-6}$	$6 \times 10^{-7} \sim 2 \times 10^{-6}$	$1 \sim 4 \times 10^{-6}$

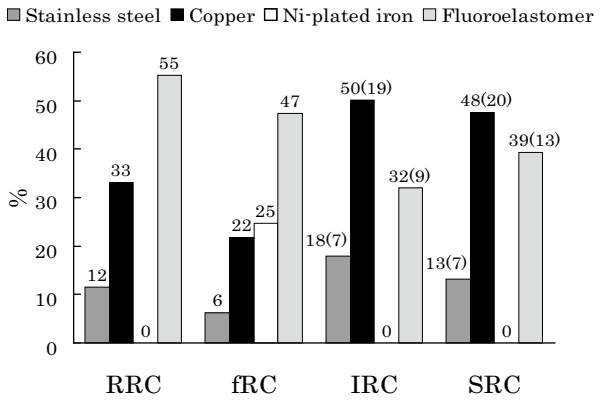

Fig. 1. Ratios of outgas from main material with respect to total outgas. Values in parentheses indicate those of subvacuum.

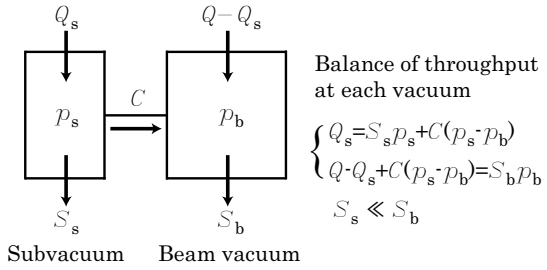

Fig. 2. Pumping model for RF resonator. Q_s and Q are the outgas of subvacuum and that of subvacuum and beam vacuum in $Pa \cdot m^3/s$, respectively. S_s and S_b are the effective pumping speed for subvacuum and that of beam vacuum in m^3/s, respectively. p_s and p_b are the pressure of subvacuum and that of beam vacuum in Pa, respectively. C is the conductance between subvacuum and beam vacuum in m^3/s. In this model S_s/S_b can be considered to be 0, since S_b is much larger than S_s.

pumping (p_b) was 4.0×10^{-6} Pa. Supposing the pumping model as is drawn in Fig. 2, p_b is given by

$$\frac{p_b}{p_{bo}} = 1 - \frac{S_s}{C + S_s}\frac{Q_s}{Q} \qquad (1)$$

p_b/p_{bo} is 0.91. Q_s/Q is considered to be approximately 0.4, although practically somewhat large. S_s, which is the total effective pumping speed of two TMPs of 0.35 m^3/s connected with a pipe of 100 mm diameter and 320 mm length (including a gate valve), is estimated to be 0.36 m^3/s. By substituting these values into Eq. (1), C is calculated to be 1.2 m^3/s. However, C must be much smaller to reduce the subvacuum gas load flowing into the beam vacuum effectively. For example, p_b/p_{bo} values are calculated to be 0.6 and 0.7 for C=0 and 0.12 m^3/s using Eq. (1). Although the copper plate of subvacuum is designed and constructed carefully so that the conductance between the subvacuum and the beam vacuum is as small as possible, it might be beyond manufacturing know-how. We must investigate the effect of the subpumping system for the IRC without delay, which has the same structure as that as the SRC.

References

1) Y. Yano: Nucl. Instr. and Meth. in Phys. Res. B261, 1009 (2007).
2) K. Ikegami et al.: RIKEN Accel. Prog. Rep. **17**, 156(1983).
3) S. Yokouchi et al.: RIKEN Accel. Prog. Rep. **38**, 279(2005).
4) J. Ohnishi et al.: Proc. 17th Int. Conf. on Cyclotrons and Their Applications, Tokyo, 197(2004-10).
5) K. Sugii et al.: RIKEN Accel. Prog. Rep. **33**, 226(2000).
6) N. Inabe et al.: Proc. 17th Int. Conf. on Cyclotrons and Their Applications, Tokyo, 200(2004-10).
7) H. Okuno et al.: RIKEN Accel. Prog. Rep. **38**, 283(2005).
8) H. Okuno et al.: RIKEN Accel. Prog. Rep. **40**, 137(2007).
9) N. Ohsako et al.: RIKEN Accel. Prog. Rep. **19**, 191(1985).

Accuracy, Linearity and Stability Tests of Old Power Supplies in RIBF

Makoto Nagase, Nobuhisa Fukunishi, Seiji Fukuzawa[*1], Eiji Ikezawa, Keiko Kumagai,
Masashi Tamura[*1], Akito Uchiyama[*1], Kazuyoshi Yadomi[*1], Hiromoto Yamauchi[*1] and Masayuki Kase

Beam tuning, especially of beam transport lines, requires many efforts of accelerator operators. It is very time consuming because a step-by-step optimization from upstream is usually performed in our facility. During the optimization, operators try and select better parameters of our accelerator complex on the basis of data on positions and profiles of a beam. However, it is possible to determine appropriate parameters, for example excitation currents of magnets, on the basis of a result of an orbit calculation starting from a reliable initial condition. For a calculation-based operation, accuracies of power supplies are essential but they have not been examined for old power supplies used in the beam transport line from the RIKEN heavy-ion linac (RILAC) and RIKEN Ring Cyclotron (RRC)[1]. Stabilities of power supplies are also important for a stable long-term operation of the RI Beam Factory (RIBF). To this end, we measured precisely output currents of the power supplies using high-precision DC current transformers (DCCT) [2, 3].

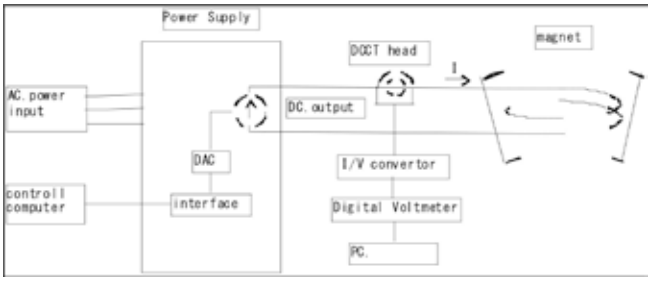

Fig. 1. Setup of the current measurements using a DCCT.

Table 1. Specifications of apparatus used in measurements.

Device	Brand and Type	Specifications
DCCT	HITEC TOPACC-T-20-MultiRange	150,300,550,1050,2000A <0.25ppm/K
	HITEC STACC-HC	3000A <1ppm/K
	DANFYSIK 866-600	600A <0.3ppm/Degree
Digital Voltmeter	KEITHLEY 2701	Resolution 6+1/2 digit
PC	Dell WinXP	LabView is installed

A setup of the measurement is schematically shown in Fig. 1. Current from a power supply is controlled by a control computer through an interface module and a digital-to-analog converter (DAC). An actual output current is detected by a DCCT and converted to voltage. Voltage is measured using a digital voltmeter and recorded in a personal computer. We summarize in Table 1 specifications of the apparatus used in the measurement.

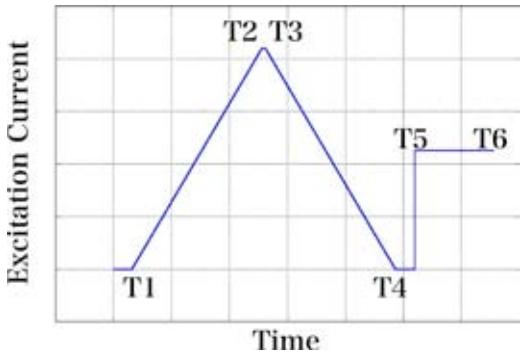

Fig. 2. Excitation pattern in measurement.

An excitation pattern of a power supply is programmed, as shown in Fig. 2. Starting from zero, current is raised linearly to its maximum at a constant rate of 0.1 A/sec or so (T1 ~ T2 in Fig. 2) and kept unchanged for a certain duration (T2 ~ T3) and decreased to be zero (T3 ~ T4). After a current is set to be the parameter used in uranium beam acceleration and kept unchanged for several hours (T5 ~ T6). The DCCT monitors continuously during the period from T1 to T6. In this excitation pattern, the linearity of power supply is checked from output currents from T1 to T2 and those from T3 to T4. The stability of power supply is measured during the period from T5 to T6. In Fig. 2, a time scale from T5 to T6 is compressed to be 1/60 for a convenience.

We applied the method described above to 33 power supplies. Nine power supplies are for dipole magnets (DMs) placed between the RILAC and the RRC, five are for injection and extraction dipole magnets of the RRC (BM1_1, BM1_2, BM2, EBM1, EBM2), two are for steering magnets (SHS60 and SVEB12) and the others are for quadrupole magnets used in the RILAC-RRC beam line. Results of the measurements are summarized in Table 2. The following should be noted.

Firstly, we found marked differences (> 1%) between setting current and actual output current for several power supplies. The largest was found in the QDJ33 power supply and the difference was –5.4%. We should modify the setting values of these power supplies on the basis of the present measurements.

Secondly, no incontinuity was observed in the linearity tests. It means that all the bits of the DACs used in the power supplies work properly. However, the linearity itself

1 SHI Accelerator Service Ltd.

is not perfect for some power supplies. The DMe5 power supply is an example of this problem. The output current was 2.9% lower than the setting current. To investigate the linearity, we first calibrate the setting currents to reproduce the measured maximum current and then subtract the output currents from the calibrated setting currents. The results are shown in Fig. 3. The nonlinearity observed is 0.4 A, which corresponds to 0.2% of the maximum current of the power supply. The difference between the setting current and the measured current should be the same for both current-increasing (T1 ~ T2) and current-decreasing directions (T3 ~ T4), in principle. However, large differences are observed, as shown in Fig. 3. It may come from the temperature dependence of the manganin resister used in the current feedback loop of the power supply.

Table 2. Summary of measurements.

The first column shows the magnet excited by the power supply tested. The second column indicates the type of current sensor used in the power supply. The word "DCCT", "manganin" and "zeranin" means a DCCT combined with a well-thermocontrolled DAC in a Peltier oven[4], a manganin resister and a zeranin resister, respectively. In the fourth column, the difference between the setting current and the actual output current at the maximum current of the power supply is shown.

Maget excited	Current sensor	Maximum current (A)	Error of current	Stability
DMe1	manganin	210	-1.00%	175ppm/21H
DMe2	DCCT	203	-1.75%	10.2ppm/6H
DMe3	manganin	210	-2.87%	234ppm/18H
DMe4	manganin	210	-2.32%	52.2ppm/17H
DMe5	manganin	210	-2.88%	94.8ppm/21H
QTe51a	manganin	150	-0.12%	22ppm/12H
DMJ34	DCCT	443.2	1.15%	12.8ppm/19H
DMS5	DCCT	448.4	0.05%	5.4ppm/19H
DMS6	DCCT	449.6	-0.21%	18.4ppm/21H
DMS7	DCCT	501.5	-0.61%	12.8ppm/19H
QDJ32	zeranin	182.2	-1.44%	74.6ppm/5H
QDJ33	zeranin	182.2	-5.44%	108ppm/5H
QDJ28a	zeranin	151.8	-0.23%	52.5ppm/5H
QDJ28b	zeranin	151.8	-0.55%	46.7ppm/5H
QDJ41a	zeranin	121.5	0.01%	20.9ppm/6H
QDJ41b	zeranin	101.2	-0.17%	26.1ppm/6H
QSJ31_34	zeranin	101.18	-0.74%	8.2ppm/6H
QSJ24	zeranin	101.16	-0.84%	27ppm/7H
QSJ25	zeranin	151.76	0.22%	32ppm/7H
QSJ26	zeranin	202.5	-0.91%	18.5ppm/7H
QSJ27	zeranin	263.05	-1.69%	10.0ppm/5H
QDJ42a	zeranin	182.2	-1.70%	102ppm/5H
QDJ42b	zeranin	141.65	-1.69%	30.5ppm/5H
QDS43a	zeranin	161.9	-1.88%	10.0ppm/7H
QDS43b	zeranin	182.25	-2.52%	60.3ppm/7H
QSS51	zeranin	161.65	-0.32%	30.2ppm/7H
SHS60	zeranin	556.3	-0.82%	174.4ppm/5H
SVEB12	zeranin	560	-1.93%	17.7ppm/7H
BM1_1	zeranin	2728	-0.10%	12.2ppm/15H
BM1_2	zeranin	2726	-0.63%	94ppm/15H
BM2	zeranin	2728	-1.46%	84.5ppm/15H
EBM1	zeranin	2530.8	-0.38%	35.9ppm/18H
EBM2	zeranin	1620.4	-0.58%	16.4ppm/15H

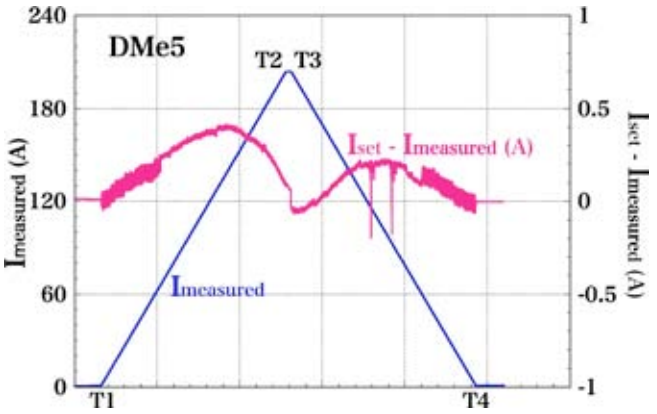

Fig. 3. Linearity of the power supply of the DMe5.

Thirdly, in the long-term stability tests, we found that the output current of the power supplies of DMe1 and DMe3 changed more than 100 ppm during the measurements. These power supplies should be improved in the near future. We also found power supplies with poor stabilities. These are for quadrupole magnets and steering magnets. For these magnets, their effects on beam quality are not so serious and the observed stabilities are acceptable. It also should be noted that a power supply in which a shunt resister is used in its current feedback loop requires 20 ~ 30 minutes to reach its thermal equilibrium. This obsrvation is due to the DMe5 power supply, as shown in Fig. 4. On the other hand, a rapid stabilization is obtained for a power supply that uses a DCCT for its current feedback loop. This is due to DMS5, as shown in Fig. 4.

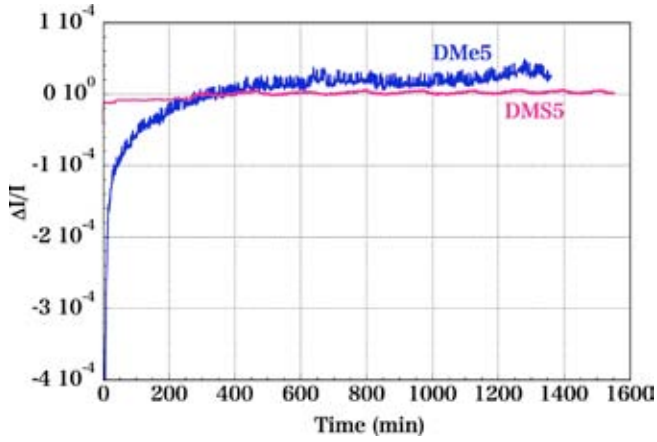

Fig. 4. Stabilities of power supplies of DMe5 and DMS5 magnets.

References

(1) K. Hatanaka et al., Proc. 11th Int. Conf. On Cyclotrons and Their Applications, 384 (1986).
(2) http://www.ppmpower.co.uk/manuprod25.htm (HITEC power protection)
(3) http://www.danfysik.com/ (DANFYSIK)
(4) M. Nagase et al., Accel. Prog. Rep. 37, 273 (2003)

Problems and solutions in operation of EIC and EDC of IRC

Keiko Kumagai, Jun-ichi Ohnishi, Naruhiko Sakamoto, and Osamu Kamigaito

The electrostatic inflector (EIC) and deflector (EDC) used for beam injection and extraction of the IRC consist of an electrode with a maximum voltage of -120 kV and a grounded septum. The gap distance between the electrode and the septum is 12 mm. The length of the electrode and the septum are 0.75 m and 1.35 m, respectively. The arrangement of the electric line of the EIC and EDC is shown in Fig. 1. The voltage of the EIC and EDC is introduced into the vacuum chamber from a ceramic feedthrough. The coaxial cables that can withstand high voltages are used for the electric line from a high voltage power supply to the feedtrough. In the case that a coaxial cable is long, it is necessary to put resistors to protect the EIC and EDC and power supplies from damage due to the stored electrostatic energy of the cable during electric discharges, which occur regularly and frequently between the electrode and the septum.

First, two oil-immersed resistors of 100 kΩ were installed 4 m away from the electrode and close to the power supplies, as shown in Fig. 1(a). The two resistors are used for decreasing the amount of stain on the electrode and the septum and minimizing damage to the power supply during electric discharges. In December 2006, immediately after the beam commissioning of the IRC started, the coaxial cables broke a few times at a place between the electrode and the resistor. It was assumed that the surge voltage was larger than 150 kV at which the cables can withstand. Since the power supplies do not require a protection resistor when the coaxial cables are shorter than 10 m, we moved the power supplies 6 m away from the EIC and EDC and removed the resistors (Fig. 1(b)). The cables did not break after these changes and we succeeded in extracting the first beam from the SRC on December 28. After that, the IRC was operated for about one month until the end of March 2007.

It was found during the operation for four months that electric discharges occurred dozens of times in one hour when the EIC and EDC were operated at voltages higher than 100 kV, the electrode and septum become dirty, and the damage to the power supplies is extensive. To overcome these problems, we installed two series resistors of 100 kΩ each inside the feedthrough of the EIC in April 2007, as shown in Fig. 1(c). The resistors are insulated with a plastic cylinder (polyacetal) in N_2 or SF6 gas. After the installation of the resistors, the amount of stain on the electrode and the septum decreased and the power supply did not break down. In addition, we prepared a 200kV-resistant coaxial cable to reuse the oil-immersed resistor as a backup of the resistors inside the feedthrough.

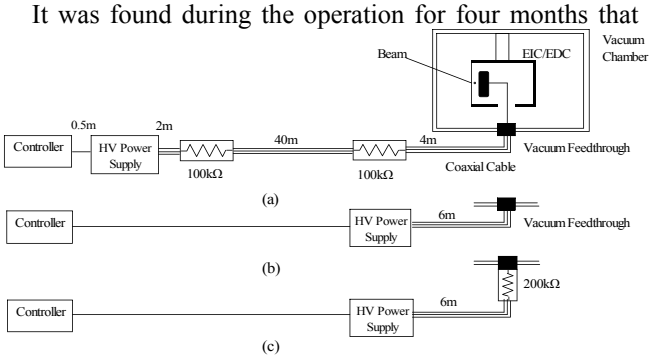

Fig. 1. Wiring of EIC and EDC and power supply. a Coaxial cables between the electrode and a resistor broke four times. (b) HV power supplies broke down three times. (c) The problem did not occur until Nov. 2007.

During the operation in May 2007, the protection resistor located in the feedthrough for the EIC burned and the insulating cylinder melted at about 30 minutes after the start of the operation of the flat-top RF resonator. Since the resonator is located at the same valley region where the EIC and EDC are installed, it was presumed that a leakage RF field of 109.5 MHz entered into the resistor through the voltage supply line and heated it. In order to prevent the RF leakage field from entering the high-voltage line, we installed a grounded thin stainless shield around it, as shown in Fig. 2. RF contact fingers are placed between the EIC and EDC and the shield because they need to be moved at a distance of 20 mm during beam adjustment. We measured the RF voltages of the leakage field on the coaxial cables before and after the installation of the shield. It was found that the RF voltage decreased to 5% for the EIC and smaller than 1% for the EDC, as shown Table 1. Therefore, it is expected that the heating in the protective resistors in the feedthrough became sufficiently small.

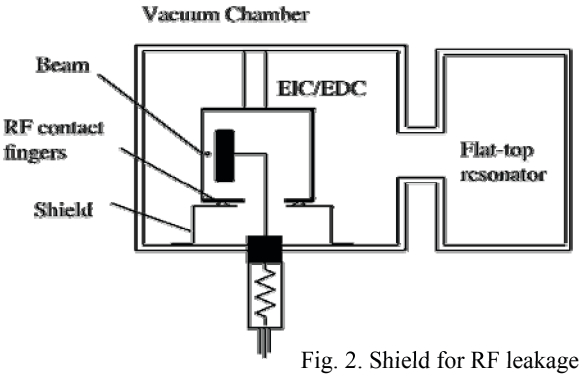

Fig. 2. Shield for RF leakage field.

Table 1. RF leakage voltages on coaxial cables measured at end of power supply. The input impedance was 1MΩ.

	EIC (Vp-p)	EDC (Vp-p)
Without shield	300	200
With shield	14.4	0.66

Status of the SRC in 2007

K. Yamada, H. Okuno, N. Fukunishi, T. Maie, J. Ohnishi, N. Sakamoto, S. Yokouchi, A. Goto, M. Kase, and Y. Yano

The first beam extraction of the superconducting ring cyclotron (SRC)[1] was accomplished at 16:00 on December 28th, 2006 using 345 MeV/nucleon $^{27}Al^{10+}$. Following this exciting event, the commissioning of a uranium beam was performed in March 2007. The SRC was successfully commissioned using 345 MeV/nucleon $^{238}U^{86+}$ on March 23rd, 2007.[2] The first experiment at the RI Beam Factory[3] was carried out from mid-May to early June 2007 using the uranium beam. In the latest study of the SRC, a ^{86}Kr beam was used. A beam current of up to 1.1 eμA for 345 MeV/nucleon $^{86}Kr^{34+}$ was attained on November 10th, 2007 on the new Faraday cup (FC-G01) located in the wall between the SRC room and the IRC room.

Various modifications were performed for the SRC between the times of machine study in 2007 as listed below. Two diagnostic devices were added in the extraction beam line of the SRC to make commissioning using the uranium beam easier. As shown in Fig. 1, a beam profile monitor with three wires (PF-G00) was installed slightly downstream of the gate valve GV-G00 that separates the vacuum of the SRC and its extraction beam line. This monitor is used to verify the beam extracted from the SRC and to adjust its trajectory in combination with the existing profile monitor PF-G01. Another device installed was a movable baffle-slit assembly attached on the center of the EBM. Subsequently, the baffle slit was replaced by a beam-stopper head. Because the radial beam pattern of the uranium beam was not distinct, probably due to the effect of secondary electrons, a single-wire electrode was mounted on each radial probe (MDP, ERP1, ERP2).

Newly designed Faraday cups for precise measurements were developed to overcome the problem that the beam intensity was overestimated by a factor of two or three due to the insufficient suppression of secondary electrons. Two Faraday cups, FC-G50 and FC-SC2, which were installed at the entrance of the injection line to the SRC and at the central region of the SRC, respectively, have been replaced by the newly designed cups.[4] On the other hand, the above-mentioned Faraday cup, FC-G01, is based on a special design illustrated in Fig. 2. It consists of a fixed main suppressor electrode, a fixed cylindrical electrode, and a cup bottom movable from upstream to downstream with respect to the beam axis. The beam stops on the cup bottom and the emitted secondary electrons are captured by the cylindrical electrode. Other electrons are returned by the electrostatic field provided by the main suppressor electrode. The subsuppressor electrode is used to trap the electrons escaping from the aperture between the cup bottom and the cylindrical electrode. The cup bottom is made of oxygen-free copper with ϕ62 mm inner diameter, and the bottom is 23 mm thick and cooled by water. This thickness is designed to fit beams from argon to uranium accelerated by the SRC. The cup bottom and part of the cylindrical electrode are shown in Fig. 3.

Because of the stray field induced by the sector magnets of the SRC, magnetic shields are required for various devices. As shown in Fig. 4, we added a magnetic shield around the injection beam line so that the injected beam could not be deflected in the shield door of the SRC. An additional magnetic shield was also in-

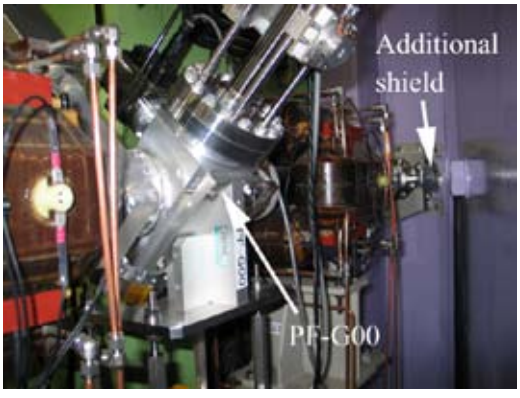

Fig. 1. Additional magnetic shield for beam duct and the wire monitor PF-G00 placed immediately after the exit of the SRC.

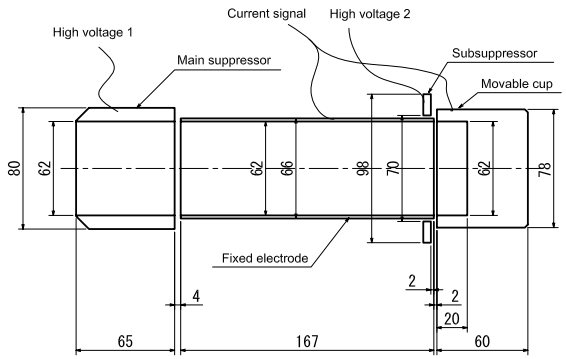

Fig. 2. Schematic diagram of new Faraday cup (FC-G01) for measuring the beam current provided by the SRC.

stalled at the extraction beam line as shown in Fig. 1. The radial probes ERP1 and ERP2 were not able to move because their gate valves closed due to the jam of solenoid valves. The solenoid valves were covered by magnetic shields. Since the coaxial switching unit for the signal of phase probes was inactive due to the strong stray field, it was mounted on a 19 inch rack of stainless steel enclosed by a magnetic shield. The turbomolecular pump and the rotary pump for the sub-vacuum pumping system[5] were shielded as shown in Fig. 5. The magnetic limit switches for the angle valve and pneumatic cylinder were replaced by mechanical switches.

In addition to the above improvements, the following devices have been introduced to make the operation easier: a cable connection panel for the vacuum gauge, a foreline trap for the rough pumping system, a vent pipe for the vacuum exhaust, a hydrostat for the SRC (and the IRC), a footstep for access to the SRC, and a basket for the annual inspection of the shield door. The electrodes of the EIC and EDC were cleaned several times to increase the maximum voltage to 120 – 130 kV. The septum electrode was polished by buffing, and an ultrasonic cleaning system was successfully adopted to improve the condition of the high-voltage electrode. Note that four RF cavities successfully generate a high voltage up to designed value[6].

There were several mechanical problems in 2007 as follows. The cooling water leaked from the juncture between the tube and the hollow conductor of the steering magnet in the SRC. The photoswitch of a preamplifier for the profile monitor located at the valley chamber was destroyed by the radiation. The high-voltage cable for the EDC was broken under mechanical stress. Sparks occurred at the resistors protecting the EIC and EDC. The sheath of the coaxial cable for the cold cathode gauge melted, which indicated excess pressure. The DC current transformer in the power supply for the SRC main coil failed. The contact fingers of the tuning panel in RF resonator No.4 burned out. In addition, the problems with the power feeder of the RF resonator, the wide-band amplifier, the final amplifier of the flat-top resonator, the PLC of the shield door controller, the trim coil power supply, and the EIC power supply occurred. These problems were resolved immediately.

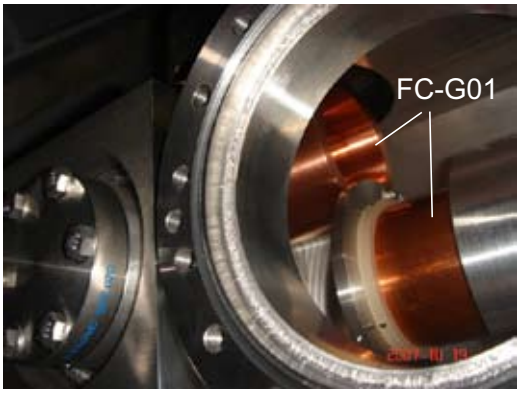

Fig. 3. FC-G01 installed in the vacuum chamber located downstream of the SRC.

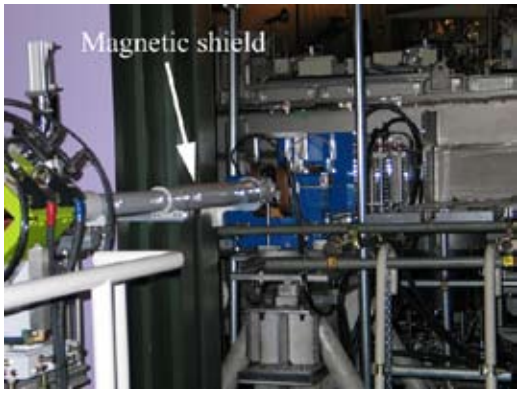

Fig. 4. Injection beam line of SRC to the valley chamber for EIC and EDC. An assembly of magnetic shields surrounds the beam line between the gate valve GV-G51 and the vertical steerer SV1.

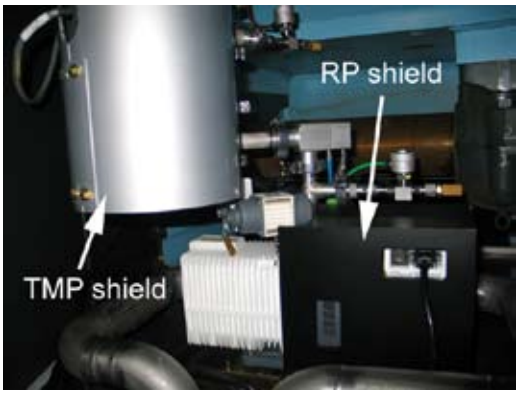

Fig. 5. Magnetic shields for the sub-vacuum pumping system located at the machine-center side of valley in the SRC.

References

1) H. Okuno et al.: IEEE Trans. Appl. Supercond.: **17**, 1063–1068, 2007.
2) N. Fukunishi: J. Particle Accelerator Society of Japan **4**, 112 (2007).
3) Y. Yano: Nucl. Instr. Meth. B **261**, 1009 (2007).
4) T. Watanabe et al.: in this report.
5) S. Yokouchi et al.: in this report.
6) N. Sakamoto et al.: in this report.

Variable-length feeder line for rf system of superconducting ring cyclotron

N. Sakamoto, O. Kamigaito, H. Okuno, M. Kase, A. Goto, and Y. Yano

The SRC consists of six superconducting sector magnets with magnetic shields, four acceleration cavities and one flat-top resonator. The acceleration cavities are equipped with rf power amplifiers located outside of the magnetic shield (see Fig. 1). The maximum gap voltage of the acceleration cavity is 500 kVp/cavity with an rf power of 100 kW at a frequency of 36.5 MHz.

The main power amplifiers are based on the tetrode SIEMENS RS2042SK coupled with the tetrode RS2012CJ with a grounded-grid circuit. The amplifiers are basically the same as those for RIKEN Ring Cyclotrons (RRC)[1]. The maximum rf power output is about 150 kW.

In the area where the amplifiers are situated, the stray magnetic field of the superconducting sector magnet is about 100 Gauss in the vertical direction. A feasibility test on the amplifier with a strong magnetic field was performed. Before connecting amplifiers to the cavities, a power test on the amplifiers at a stray field of 100 Gauss using a water-cooled dummy load (200 kW C.W.) was performed with a maximum power output of 150 kW. The power was generated quite stably and no change in plate loss was observed.

The output ports of the amplifiers are connected to cavities with a 50 Ω coaxial line of WX152D for main cavities and WX120D for a flat-top cavity. The cavities are coupled with the coaxial line by inductive couplers. The couplers are tunable to match the impedance of the cavity to 50 Ω.

The coaxial feeder-line is equipped with a sliding-system (variable length) and the amplifier is placed on a movable platform so that the length of the feeder-line varies from 7 to 8 m. This is crucial to prevent the coupling of the HOMs of the feeder line with the HOMs

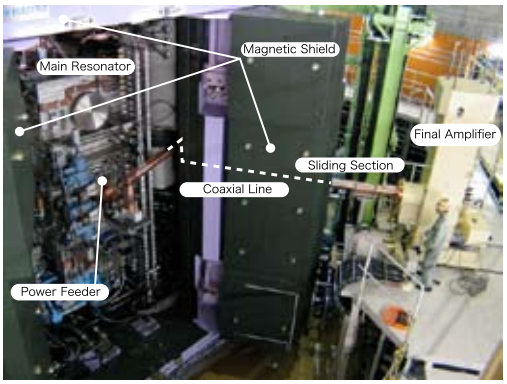

Fig. 1. Photo of the No.3 cavity and the amplifier.

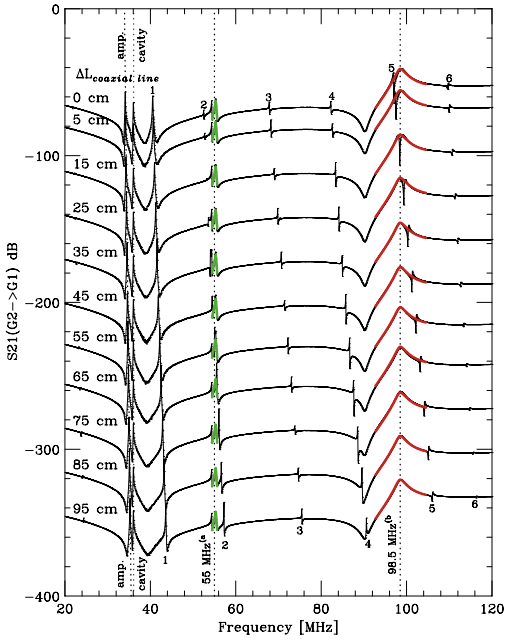

Fig. 2. Resonance modes of rf system. The cavity and amplifier are tuned to a frequency of 36.5 MHz. The resonances labeled with numbers are HOMs of the feeder coaxial line. a) The green peak is a HOM of the input circuit. b) The red peak denotes the resonance between the G1 and G2 electrodes.

of the amplifier and the cavity in the entire range of operational frequency. Fig. 2 shows the HOMs of the main rf system. The cavity and amplifier were tuned for 36.5 MHz. The S-parameter (S_{21}) between ports for the power supplies of the control grid (G1) and screen grid (G2) was measured using a network analyzer(Agilent Technology E5061A). From our experiences with the amplifiers for RRC, we know that there are two critical modes. One is the resonance of the input stubs at 55 MHz and the other is the resonance between the G1 and G2 electrodes of the power tube at 98.5 MHz. The position of 0 cm has been selected for the 36.5 MHz operation.

In summary the variable length feeder-line system works very well. Finally an acceleration voltage of 2 MV/turn at 36.5 MHz has been achieved with a total rf power of 400 kW[2].

References

1) T. Fujisawa et al., Sci. Papers I.P.C.R. 79 (1985).
2) N. Sakamoto et al., "RF System for the RIBF Superconducting Ring Cyclotron", Proc. 18th Int. Conf. on Cyclotrons and Their Applications (Giardini Naxos, 2007).

Operational Status of He Cooling System for SRC

T. Dantsuka*[1], H. Okuno, K. Yamada, K. Ikegami and M. Kase

The helium cooling system for SRC consists of four He reservoir tanks, three compressors (one for backup), a He refrigerator and a control dewar for the magnet, as shown in Fig. 1. The control dewar, which is located on the top of the SRC, gathers the pipes and cables from the six sector magnets to make a closed circuit. The cooling capacities of the helium refrigerator are 620 W at 4.5 K, and 4000 W at 70 K, and 4 g/s gas helium is used for cooling current leads. It is estimated that it takes three weeks to cool the cold masses of 142 ton from room temperature to 4.5 K with this cooling system. The cooling capacity of the system was designed to be more than 1.5 times the estimated heat loads of the whole superconducting magnets.

In 2007, it was operated for about 7000 hours. However, we encountered a problem concerning the He refrigerator, which remains to be solved. Fig. 1 shows that the flow rate of what in the He cooling system gradually decreases, increasing the temperature of the 80 K stage adsorber and decreasing the pressure of the T1 inlet. This suggests that some impurity accumulates somewhere around the first turbine. We have to stop operating the refrigerator every two months to warm it up to room temperature and remove the impurity.

We started to determine the reason for the decrease in cooling power with the help of the KEK staffs who have much experience about the long-term operation of many large helium cooling systems. As a first step, we measured impurity ratio of the helium coolant in the cooling system using devices normally used in KEK, which have high accuracies and are well-calibrated. We

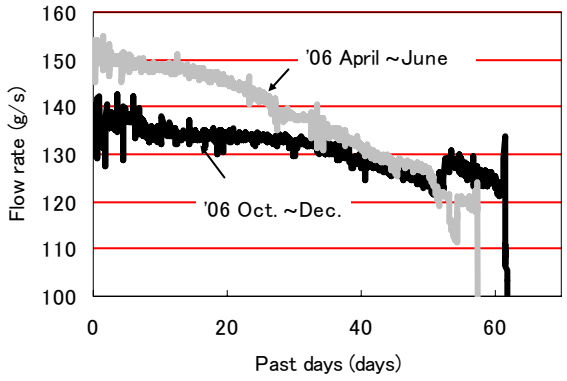

Fig. 2. Flow rate through first turbine in He refrigerator for SRC.

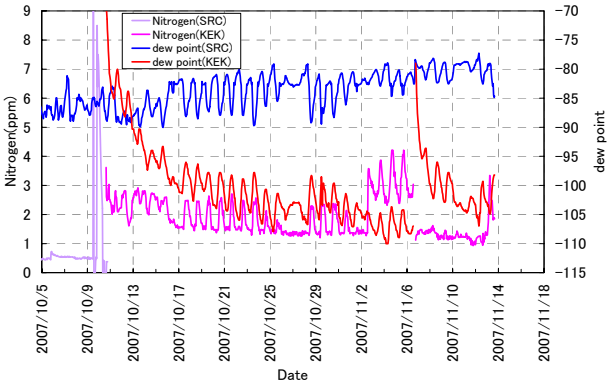

Fig. 3. Trend graph of impurity ratio of N_2 and H_2O (dew point) by two types of detector.

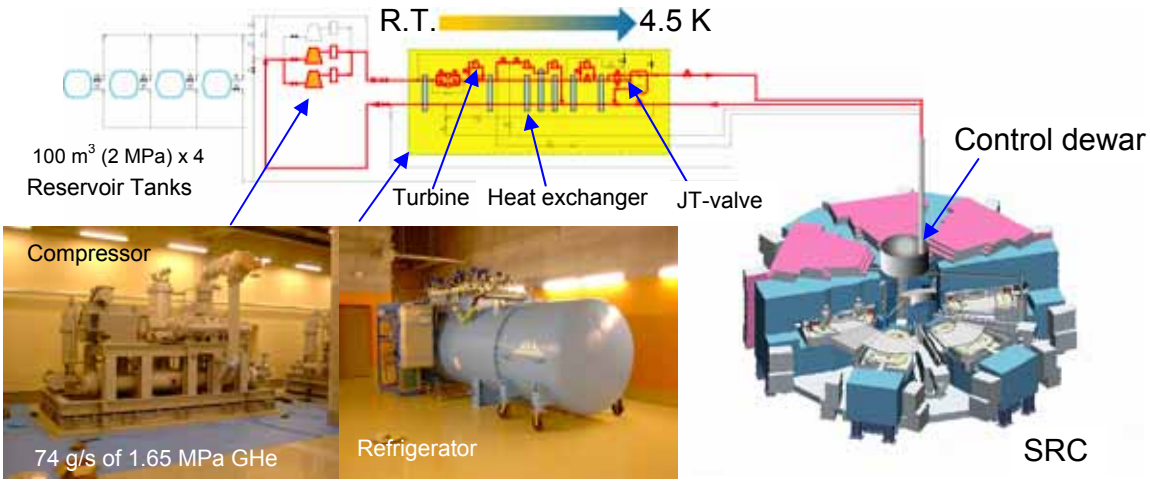

Fig. 1. Conceptual diagram of helium cooling system for SRC.

*1 Science Service

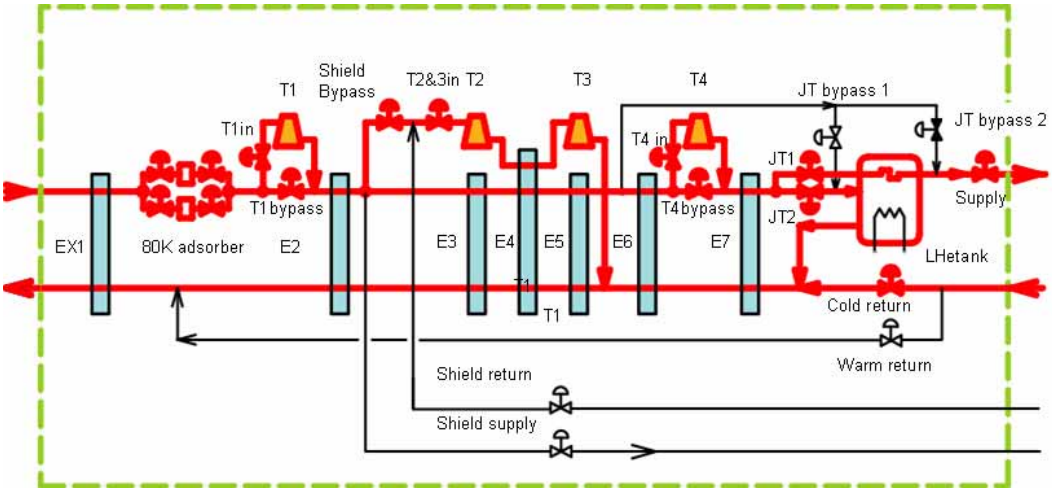

Fig. 4. Cooling Diagram of He refrigerator.

were interested in N_2 and H_2O, the boiling points of which are higher than 70 K. The measurement results show a large discrepancy between the data from KEK devices and the data from the devices normally used in the operation, as shown in Fig. 2. The dew point (H_2O impurity) impurity measured with high accuracy is 20 degrees higher than those from devices normally used for measurement. The helium coolant in the system contains N_2 impurity about three times those measured in the operation. All the data show that impurities remain in the system even when impurities were eliminated in the 80 K adsorber. This suggests that impurities reaches the helium coolant continuously.

We also measured the absolute pressure at the suction line going to the compressor where helium pressure is set to be 0.003 MPaG. The measured data showed that the accuracy of the pressure gauge used in the normal operation was low, suggesting that the system has a risk of operating at negative pressure. If the pipes have leaks, some air reaches the helium coolant. Detailed leak tests on the helium pipes are in progress.

The refrigerator has two 80 K adsorbers to allow their regeneration without stopping the refrigerator operation, as shown in Fig. 4. However, since isolation valves for the adsorbers leak, we could not regenerate them. We replace the gaskets of the valves during maintenance, expecting that we can isolate the adsorbers for regeneration, which is indispensable for long-term cooling operations.

Preliminary experiments on the hydrogen removal apparatus for the liquid helium supply and recovery system

M. Nakamura, K. Ikegami and M. Kase

In recent years, the liquid-helium supply and recovery system of the Wako campus have shown problems with hydrogen impurities in the system.[1] Occasionally, a few hydrogen impurities (ppm amounts) had been found in recovered helium gas. In such cases, the 20 K adsorber in the refrigerator can't remove all the hydrogen impurities. As a result, hydrogen can enter the liquid-helium storage vessel, and cause many serious problems. To remove the impurity hydrogen from the recovered helium gas, we have examined to install a hydrogen removal apparatus in our system. The silver-zeolite "Ag-400" made by "Molecular Products Inc." can be used as the adsorbent in our apparatus. Usually, this adsorbent is used for removing hydrogen from the vacuum spaces of cryogenic vessels and we have not found it being used in a liquid helium production system. Therefore, firstly, in the preliminary experiment, the applicability of "Ag-400" for hydrogen removal from helium gas of more than atmospheric pressure has to be confirmed. Next, the activity of "Ag-400" for hydrogen adsorption should be examined.

For the first preliminary experiment, we have used a new experimental setup. This setup is constructed using a standard mixed gas, a new test vessel, a gas flowmeter, and a pressure gauge. The standard gas was a mixture of pure helium gas with approximately 3 ppm of hydrogen gas. About 500 g of "Ag-400" was placed in the test vessel. In this experiment, the standard gas was passed through the vessel at various flow speeds and the hydrogen concentration in the filtered standard gas was analyzed by gaschromatography (Shimadzu GC-14B). Throughout the experiment, the flow speed of the standard gas and the pressure in the vessel were detected simultaneously. The results are shown in Table1.

Table 1 Hydrogen concentration in filtered gas.

Standard gas flux (L/min)	Pressure in vessel (kgf/cm^2G)	Hydrogen concentration (ppm)
1.4	0.7	0
3.6	0.8	0
9.2	1.7	0
34.1	0.6	0

We could find that the hydrogen impurity was completely removed in every case. These results suggested that the "Ag-400" can be used to remove hydrogen from the flowing helium gas of more than atmospheric pressure.

In the next experiment, the absorption activity of "Ag-400" was examined. We made a new small vessel containing about 20 g of "Ag-400", which was used instead of the former vessel. The standard gas was flowed at 1.4L/min through this small vessel in 24 h and the hydrogen concentration was detected in every 30 min. The results are shown in Fig. 1.

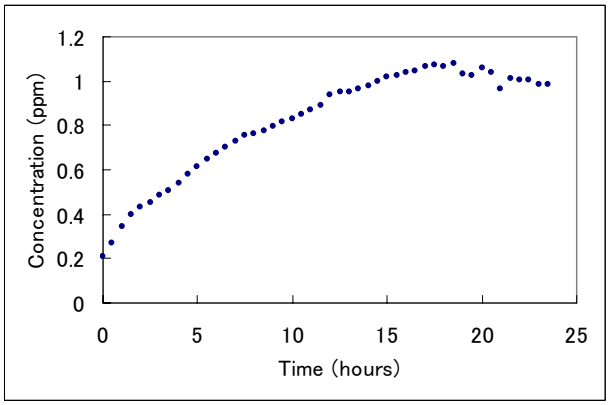

Fig. 1 Change in hydrogen concentration in filtered gas.

At the first measurement, the hydrogen concentration was found to be reduced from 3 to 0.2 ppm. Probably, a small amount of adsorbent can remove almost all the hydrogen, but not completely. After a few hours, the adsorbent activity had gradually decreased and the concentration of impurity hydrogen had increased. After about 18 h, the decrease in the adsorbent activity had stopped and the hydrogen impurity remained at about 1.0-1.1 ppm. Finally, 24 h later, the hydrogen concentration in the filtered standard gas was maintained about 1.0 ppm. This result showed that "Ag-400" can still remove the hydrogen impurity after about $2.0m^3$ of standard gas containing about 3 ppm of hydrogen was flowed.

When our system showed problems as described in a previous report, $1800m^3$ of recovered helium gas was found to contain about 1-2 ppm of impurity hydrogen.[1] However, from the results of this experiment, we can estimate that about 20-30 kg of "Ag-400" can reduce the hydrogen impurity sufficiently. Further studies are under way. In conclusion, we can predict that the hydrogen removal apparatus using "Ag-400" can be used for the liquid-helium supply and recovery system in RIKEN.

Reference

1) K. Ikegami et al.: RIKEN Accel. Prog. Rep. 38, 286 (2005).

Present Status of Liquid-Helium Supply and Recovery System

K. Ikegami, H. Okuno, M. Nakamura, T. Yoshida, T. Maie, H. Fukuda, and M. Kase

The liquid-helium supply and recovery system, which can generate liquid helium at a rate of 200 L/h from pure helium gas, has been stably operated since the beginning of April 2001. The volumes of liquid helium supplied per year are listed in Table 1. The total volume supplied gradually increased between 2001 and 2004. The volume supplied to the low-temperature physics laboratory increased more than threefold from 2004 to 2005 due to the implementation of the extensive nanoscience project. The total volume supplied in 2006 of about 100 kiloliter is almost equal to that in 2005.

The control system of the compressor for liquefying helium gas broke down at the end of October 2007 and was repaired in six days.

An observation system[1] for measuring the recovered helium gas has been running smoothly since its completion in 2005. The purity of the helium gas recovered from laboratories has improved gradually since the completion of the system. The volume of helium gas sent from each building such as the Cooperation Center Building for the Advanced Device Laboratory, the Chemistry and Material Physics Building, the Joint Laboratory Building used for the nanoscience project, the Main Research Building, which is connected to the Frontier Research Building and the Frontier Material Research Facility Building, the East Brain Science Building, the Nishina Memorial Building and the RIBF Accelerator Building on Wako campus to the liquid-helium supply and recovery system has been measured. The recovery efficiency, which is the ratio of supplied liquid helium to recovered helium gas, has been measured. The average recovery efficiency for 2006 has increased to above 78%.

Currently, the liquid-helium measuring and tally system[2] for liquid helium supplied to researchers, which was completed last year, is running smoothly.

References
1)K. Ikegami et al.: RIKEN Accel. Prog. Rep. 39, 254 (2005).
2)K. Ikegami et al.: RIKEN Accel. Prog. Rep. 40, 138 (2006).

Year	2001	2002	2003	2004	2005	2006
Laboratory & institute	Amount of supplied liquid helium (ℓ)					
Magnetic materials laboratory	3392	7024	7713	11829	15672	16512
Low-temperature physics laboratory	1270	3090	6966	9515	34713	29520
Advanced device laboratory	9977	10849	9726	7401	11264	15017
Condensed molecular materials laboratory	1939	1615	3079	5353	5912	7772
Surface chemistry laboratory	1146	1676	4533	5007	5370	5486
Brain science institute	6277	8144	5055	6292	7285	6956
Other laboratories	3535	7730	14476	9487	15717	14767
Total	27536	40182	51530	54884	95933	96030

Table 1. Volumes of liquid helium supplied to laboratories per year from 2001 to 2006.

Low-charge-state ion production using a laser ion source as primary ion injection for RHIC-EBIS

T. Kanesue,[*1] J. Tamura,[*2] and M. Okamura,[*3]

We are studying a laser ion source (LIS) for primary ion injection into RHIC-EBIS. RHIC-EBIS is a new pre-injector for the Relativistic Heavy Ion Collider (RHIC) and NASA space Radiation Laboratory (NSRL) being built at Brookhaven National Laboratory to provide a high beam current, highly charged heavy ion beam[1]. This new pre-injector has many advantages in addition to increase injection energy into the Booster synchrotron and to eliminate stripping foils before the Booster. These advantages will increase integrated luminosity at RHIC. Charge state 1+ ions are required as a primary ion source for RHIC-EBIS. A LIS that produce ions by a pulsed high power laser irradiation onto a solid state target is a candidate of external ion source. Almost all solid state targets can be used and only ions are transported and injected into the electron beam ion source (EBIS) trap region to prevent contamination in the trap region.

We attempted to optimize laser power density for the maximum yield of charge state 1+ ions by defocusing the laser beam. The second harmonics of the Nd:YAG laser (0.73 J / 5.5 ns and 532 nm wavelength) was used. The plasma total current of ^{27}Al measured by FC increased with decreasing laser power density on the target (power density was adjusted by changing the spot size of the laser). This is mainly because of the increased target area utilized. Maximum ion yield was recorded at a power density of $9.1 \times 10^8 [W/cm^2]$ which was the most defocused condition in our configuration at that time. Ion yield can be increased with more effective defocusing. Thus the charge state distributions of ^{27}Al, ^{56}Fe and ^{181}Ta were measured precisely at this power density. We used a cylindrical 90 degrees electrostatic ion analyzer to separate ion signals. The description of the measurement system is given in ref. 2. Using the obtained results and the relation $j \propto L^{-3}$ where j is the ion current density and L is the distance from the target[3], the plasma drift distance to achieve the required number of ions assuming a 10 % efficiency during the entire losses in EBIS was calculated. The calculated plasma properties under these conditiosn are shown in Table 1. The peak current of Al was too high for efficient beam transport. This can be reduced by decreasing laser power density which increases ion intensity. Another disadvantage of LIS was its large energy spread of about 100 %, which can be reduced by applying time dependent extraction voltage according to the ion energy calculated frm the simple TOF information triggered by laser light. The charge state distribution of Ta, the ion energy and the required extraction voltage are shown in Fig. 1.

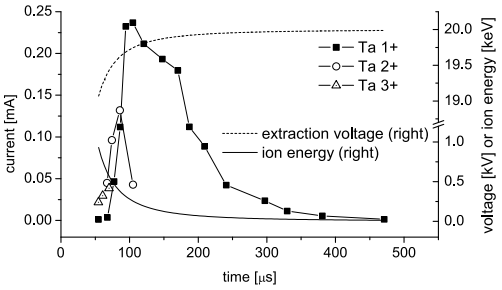

Fig. 1. Time dependence of Ta, ion energy and required extraction voltage for compensating for energy spread

- - - - -

References

1) J. Alessi et al.: Proc. PAC07, Albuquerque, 2007, p.3782
2) S. Kondrashev et al.: J. Appl. Phys. 100, 103301 (2006)
3) B. Yu. Sharkov et al.: Proc. EPAC96, Sitges, Spain, 1996, p.1550

Table 1. Number of charge state 1+ ions and drift length required to satisfy ion yields with $1cm^2$ extraction areas based on experiment

Target	Required 1+ ions for LIS	% of 1+ ions	Drift distance [m]	Pulse width [μs]	Peak current [mA]	Energy at peak current [eV]	Energy spread [eV]
^{27}Al	4.3E11	70	1.34	25	2.63	540	694
^{56}Fe	2.4E11	80	1.88	45	0.85	545	578
^{181}Ta	1.7E11	93	2.91	99	0.24	743	825

*1 Department of Applied Quantum Physics and Nuclear Engineering, Kyushu University
*2 Department of Energy Sciences, Tokyo Institute of Technology
*3 Brookhaven National Laboratory, New York, USA

7. Instrumentation

Status of BigRIPS and ZeroDegree project

T. Kubo, K. Kusaka, T. Ohnishi, K. Yoshida, A. Yoshida, N. Fukuda, M. Ohtake, Y. Yanagisawa, H. Takeda, H. Sakurai, T. Motobayashi, and Y. Yano

The BigRIPS in-flight separator[1,2] and its RI-beam delivery line,[3] called the ZeroDegree spectrometer, have been constructed as a major experimental installation in the RI beam factory (RIBF). The construction began in fiscal year 2002. BigRIPS was successfully commissioned in March 2007, the end of fiscal year 2006, while the commission of ZeroDegree is scheduled for April 2008.

Figure 1 shows a schematic layout of the BigRIPS separator and the ZeroDegree spectrometer along with the RIBF cyclotrons. The BigRIPS separator is a superconducting in-flight separator, which is employed for the production of RI beams based on the in-flight scheme. It is characterized by large acceptances and a two-stage separator scheme. The large acceptances were achieved using large-aperture superconducting quadrupoles, allowing the efficient production of RI beams not only by the projectile fragmentation but also by the in-flight fission of uranium beams, in which RI beams are produced with large spreads of both angle and momentum.

The two-stage separator scheme allows us to deliver tagged RI beams as well as to perform two-stage isotopic separation. In the former mode, the first stage is used to produce and separate RI beams, while the second stage is employed to identify RI-beam species in an event-by-event mode. In the latter mode, an energy degrader or a charge stripper is employed at both stages to improve the purity of RI beams.

The BigRIPS separator leads into the RI-beam delivery line as shown in Fig. 1. It is designed not only to transport RI beams to experimental setups placed downstream, but also to serve as a zero-degree forward spectrometer called ZeroDegree. When it is employed as a zero-degree spectrometer, a secondary target, which is surrounded by a γ-ray array detector, is placed at the beginning of the beam line. For reaction studies using RI beams, ZeroDegree analyzes and identifies projectile reaction residues in coincidence with γ-rays.

The BigRIPS magnets consist of fourteen superconducting triplet quadrupoles (STQs), in which three superconducting quadrupoles are installed in a single cryostat, and six room-temperature dipoles. They are indicated as STQ1-14 and D1-6 in Fig.1, respectively. The magnets of the RI-beam delivery line consist of nine STQs (STQ15-23) and two room-temperature dipoles (D7-8). These magnets have essentially the same design. In total, the system consists of 69 superconducting quadrupoles and eight dipoles. There are 12 focuses in the beam line, indicated as F1-12 in Fig. 1. The first stage of BigRIPS is from the production target (F0) to the F3 focus, while the second stage is from F3 to F7. The beam line from F8 to F11 forms the ZeroDegree spectrometer. Each focus is equipped with a focal plane chamber, which accommodates focal plane devices such as beam-line detectors and some beam-diagnosis devices. The primary beams are stopped at a high-power beam dump located at the first dipole D1. The first stage of BigRIPS is surrounded by radiation shields which weigh about 7000 tons.

The installation of the BigRIPS magnets, including the cryogenic systems of the STQs, was completed by April 2006, and all the magnets were successfully tested online in 2006. The installation and assembly of the other components, such as the focal plane devices, the beam-line

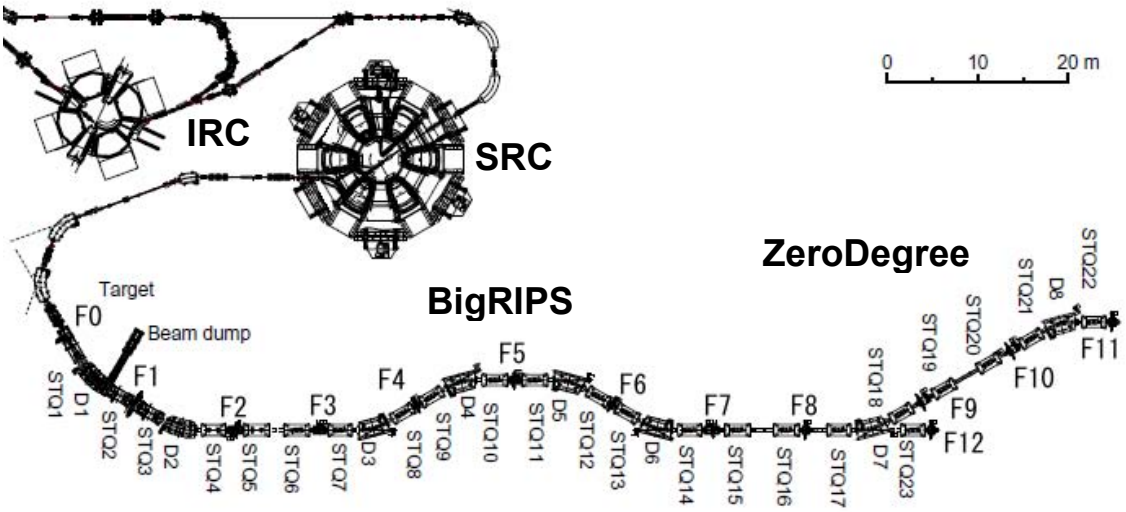

Fig. 1. Schematic layout of RI beam factory in 2007.

Fig. 2. Photographs of BigRIPS separator: a) and b) show the first and second stages of the BigRIPS separator, respectively, while c) shows the first stage after the thick radiation shields were installed.

Fig. 3. Photographs of ZeroDegree spectrometer: a) shows a view of the target position, while b) and c) show those of the intermediate and final focuses, respectively.

detector system, the control system, the production target, the beam dump, and the radiation shields, were completed by February 2007. Figure 2 shows photographs of the BigRIPS separator.

The installation and online testing of the ZeroDegree magnets and the installation of the focal plane chambers were completed by February 2007. The other components, including the beam-line detector system, were completed by December 2007; thus ZeroDegree is now ready for the commissioning. Figure 3 shows photographs of the ZeroDegree spectrometer.

We began the commissioning of BigRIPS in March 2007. The first RI beams were successfully produced on March 13th using $^{86}Kr^{31+}$ beams at 345 MeV/u. We then produced RI beams using $^{238}U^{86+}$ beams at the same energy for the first time on March 27th 2007, at the very end of fiscal year 2006.

We resumed commissioning experiments using the uranium beams on May 16th, to check and tune the performance of BigRIPS, such as the ion optics, the capability of particle identification (PID) and the transmission, as well as to tune the beam-line detector system. Once we realized a reasonable performance, particularly for PID, we switched the runs to search for new isotopes between May 24th and June 3rd 2007. Although the intensity of the uranium beams was as low as ~10^8 particle/s and the net data accumulation time was as short as one day, we observed a new isotope ^{125}Pd (Z=46) and possibly ^{126}Pd. Figure 4 shows the PID plot. This discovery demonstrated not only the high performance of the BigRIPS separator but also symbolized the successful launch of the new-generation RI beam facility. The experiments were performed by a large collaboration of about 50 physicists from Japan and other countries. Figure 5 shows some scenes shot during the experiments.

More detailed reports on the project are given elsewhere in this progress report.

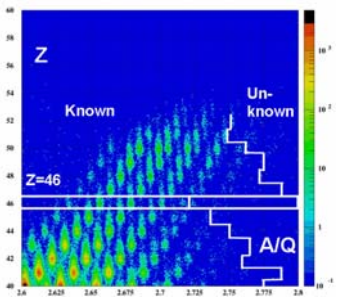

Fig. 4. Particle identification plot of RI beams obtained from the ^{238}U+Be reaction at 345 MeV/u. The vertical axis shows the atomic number Z, while the horizontal axis shows the mass-to-charge ratio A/Q of RI beams.

Fig.5 Scenes shot during the BigRIPS commissioning and the experiment to search for new isotopes.

References

1) T. Kubo: Nucl. Instr. and Meth., **B 204**, 97 (2003).
2) T. Kubo et al.: IEEE Trans. Appl., Supercond., **17**, 1069 (2007).
3) Y. Mizoi et al.: RIKEN Accel. Prog. Rep., **38**, 297 (2005).

Study of BigRIPS optics

H. Takeda, T. Kubo, T. Ohnishi, N. Fukuda, M. Matsushita,[*1] N. Aoi, K. Kusaka, K. Yoshida, Y. Yanagisawa, and H. Suzuki[*2]

BigRIPS[1] is an in-flight RI beam separator at RIBF. It is designed to produce and deliver intense RI beams in a wide region of a nuclear chart. For efficient transmission of RI beams even when the in-flight fission of uranium beams is employed as a production reaction, large acceptance is one of the important features of the BigRIPS. Large-aperture superconducting triplet-quadrupole (STQ) magnets are used to realize large acceptance. However, this feature causes the formation of wide fringing field regions around two edges of the magnets. Shapes of the fringes are varied according to the strengths of fields. It is indispensable to consider the effects of such fringe fields for a detailed analysis of BigRIPS optics, which is required to precisely reproduce transfer matrix elements. For this purpose, we used COSY INFINITY[2], which is an arbitrary order beam physics code for the study and design of an optical system. Arbitrarily shaped fringing fields can be taken into account in the code.

Field maps were measured previously at certain intervals of current. They were expressed by Enge functions. The transfer matrix elements of optical devices of the BigRIPS are calculated using the fitted Enge functions and are optimized to realize desired optical properties (e.g., dispersive/achromatic focus) at each focal plane. Figure 1 shows a horizontal beam envelope from F0 to F7 in the first-order COSY calculation.

To examine the fundamental optical properties of the BigRIPS and the predictability of COSY calculation, we measured optics data during the BigRIPS commissioning beam time. Initial- and final-phase space variables are related to matrix elements by linear transformation in the first-order optics:

$$
\begin{aligned}
x_f &= (x|x)\, x_i + (x|a)\, a_i + (x|\delta)\, \delta, \\
a_f &= (a|x)\, x_i + (a|a)\, a_i + (a|\delta)\, \delta, \\
&\cdots,
\end{aligned}
$$

where x, a, and δ are the position, angle, and magnetic rigidity of the particle with respect to the central ray. Thus, the $(x|x)$ parameter was extracted by measuring a slope parameter in the (x_i, x_f) plane with narrow gates of a_i and δ. Other parameters were obtained similarly.

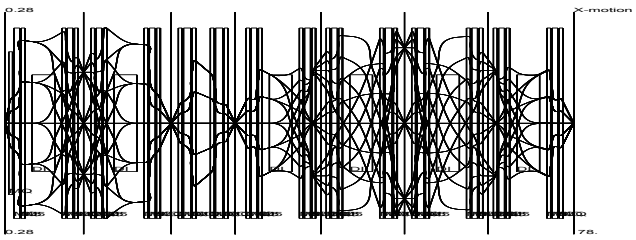

Fig. 1. Horizontal beam envelope from F0 to F7.

Measurements were performed using both primary and secondary beams. Positions and angles were determined from PPAC data. Obtained matrix elements are compared with the COSY calculation results shown in Fig. 2. Unfilled bars indicate the COSY calculated values, whereas filled bars indicate the measured values. In the case of primary beams, the positions and angles are small. Moreover, there are several discrete but narrow peaks in dispersion because charge states change at a production target and/or detector materials. Taking advantage of these features of primary beams, $(x|x)$ and $(x|\delta)$ can be measured with relatively small errors. On the other hand, the widths of positions, angles, and dispersions are large in the case of secondary beams. It is suitable for measuring the $(a|a)$ term. As expected, $(x|x)$ and $(x|\delta)$ obtained using the primary beam and $(a|a)$ using the secondary beam well agree. Other parameters were essentially small under the present optical conditions. Errors were estimated as $5 \sim 10\%$ taking into consideration the position resolutions of PPAC. Disagreements in $(x|a)$ parameters are conspicuous. They are very sensitive to certain STQ magnet strengths; thus, it is rather difficult to obtain data showing good agreement.

One of the most important purposes of an optical study is the reconstruction of beam trajectory. Considering first-order optics, δ can be reconstructed from measured positions $(F3x, F5x)$ and angle $(F5a)$ at focal planes by solving the following simultaneous equations:

$$
\begin{cases}
F5x = (x|x)\, F3x + (x|a)\, F3a + (x|\delta)\, \delta, \\
F5a = (a|x)\, F3x + (a|a)\, F3a + (a|\delta)\, \delta.
\end{cases}
$$

The goodness of reconstruction can be verified by comparing the measured $F3a$ with the reconstructed $F3a$. They agreed within 1%. A/Q values were corrected using the reconstructed δ;

$$
A/Q = \frac{B\rho_0(1+\delta)}{\gamma\beta m_u}.
$$

The magnetic rigidity at the central ray $B\rho_0$ was calibrated from measurements of NMR probes. γ and β are the Lorentz factor and velocity obtained from TOF measurements, respectively.

A/Q spectra of Zr isotopes produced by the in-flight ^{238}U fission at 345 MeV/nucleon at $B\rho = 7.4$ Tm setting are shown in Fig. 3 for comparison. The upper

*1 Department of Physics, Rikkyo University
*2 Department of Physics, University of Tokyo

Primary Beams

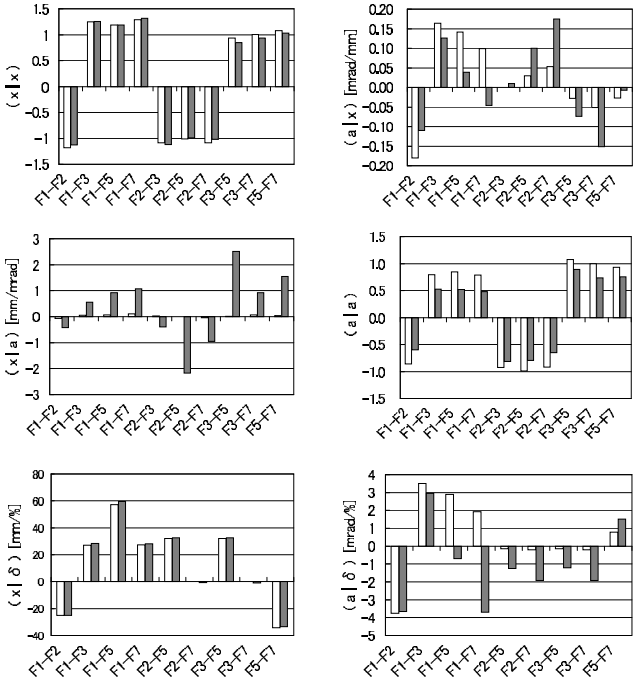

Secondary Beams

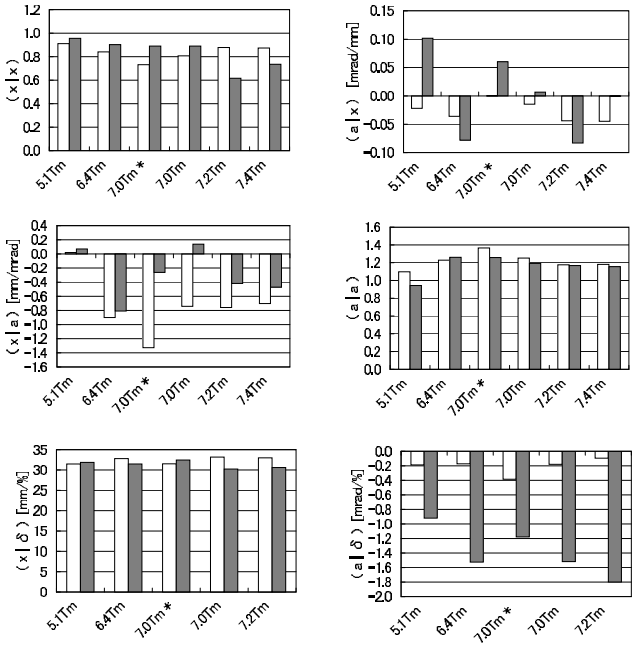

Fig. 2. First-order matrix elements are shown. Unfilled and filled bars indicate calculated and measured values, respectively. The upper half of the figure shows the matrix elements among various combinations of focal planes at $B\rho = 7.25\,\mathrm{Tm}$ primary beam setting. The matrix elements between F3 and F5 with secondary beams at various $B\rho$ settings are shown in the lower half of the figure.

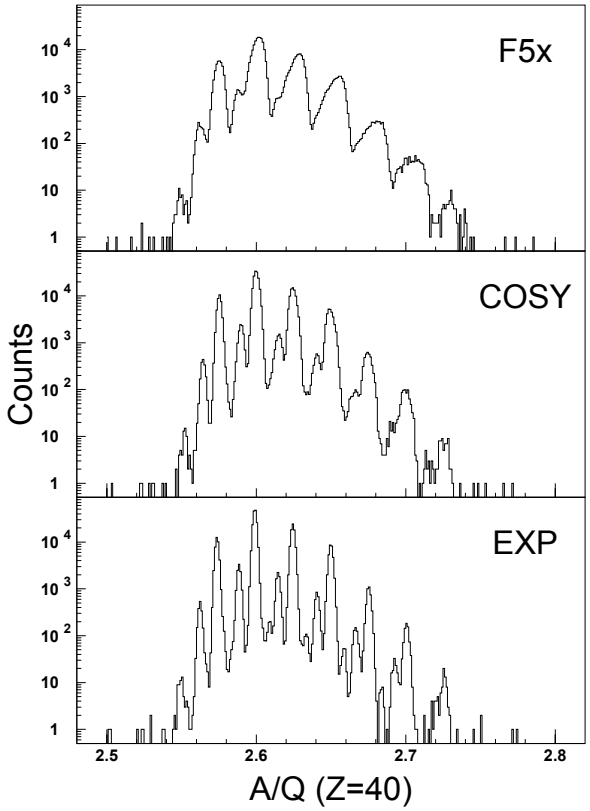

Fig. 3. The $B\rho$ reconstruction effect is demonstrated.

part shows the A/Q spectrum with δ correction using F5 position data through the $(x|\delta)\delta$ term only. The middle part shows the result of the reconstruction described above, in which the calculated (COSY) matrix elements are used. We can clearly observe that the A/Q resolution is much improved by the reconstruction. However, there seems to be room for further improvements in COSY calculation, when compared with the reconstruction results with the measured matrix elements shown in the lower spectrum.

We are now revising fringing field fittings with Enge functions and excitation curves of the magnets to improve reproducibility of the COSY calculation, particularly for $(x|a)$. Higher-order track reconstruction is also in progress.

References

1) T. Kubo: Nucl. Instr. and Meth. **B204**, 97 (2003).
2) K. Makino, M. Berz: Nucl. Instr. and Meth. **A558**, 346 (2006).
`http://bt.pa.msu.edu/index_cosy.htm`

High-power beam dump system for BigRIPS

N. Fukuda, K. Yoshida, T. Kubo, K. Kusaka, A. Yoshida, M. Ohtake, T. Ohnishi, Y. Yanagisawa, Y. Mizoi[*1], T. Okuyama[*2], and Y. Yanagi[*2]

The beam dump system for BigRIPS is a device to stop the primary beam for all desired RI beams. The system has been installed in the beam line and has been on line since the commisioning of BigRIPS started. The beam dump system is characterized by a wide coverage range of beam positions and an extremely high cooling capacity.

The primary beam is deflected over a wide range of positions in the first dipole magnet (D1) depending on the relative $B\rho$ difference between the primary beam and the selected fragment, defined as $\delta_{B\rho} = B\rho_{\rm prim}/B\rho_{\rm frag} - 1$. In order to cover the possible range from $\delta_{B\rho} = -50\%$ to $+100\%$, the beam dumps are installed over at about 2000 mm in D1, and between D1 and the second superconducting triplet quadrupole magnet, as illustrated in Fig. 1. The sidewall beam dumps are located on both sides of the optical axis in the D1 vacuum chamber. The inner- and outer-sidewall dumps cover $\delta_{B\rho}$ ranges of -50%–-24% and $+18\%$–$+100\%$, respectively. The outer-sidewall dump is also designed to work in case magnet power supplies unexpectedly turn off. The exit dumps that are installed on both sides of the optical axis at the exit of D1 are independently movable in the horizontal direction to function as a slit. They cover a $\delta_{B\rho}$ range of -30%–$+27\%$. The coverage range of $\delta_{B\rho}$ for each beam dump is shown in Fig. 2. For $|\,\delta_{B\rho}\,| \leq 10\%$, the beam dump may decrease the acceptance for desired fragments; therefore, such a $\delta_{B\rho}$ range will not be used practically.

The inner-sidewall dump is fabricated using rectangular screw tubes made of oxygen-free Cu to form a vertically inclined wall with bending along the curvature of D1, as shown in Fig. 1. The use of a screw tube as a cooling channel contributes to improving heat transfer, and the inclined shape helps decrease the power density on the surface of the beam dump[1,2]. We adopted Cu as the material because of its high thermal conductivity. For the outer-sidewall dump, swirl tubes made of Cu-Ag alloy are arranged vertically in a zigzag manner to form a bended wall. As for the outer-sidewall dump, inclination of the wall is not necessary because an expected heat flux is not very high. The swirl tube has a high heat transfer coefficient[3] similarly to the screw tube, and the Cu-Ag alloy has a good thermal conductivity and radiation hardness. Figure 3 shows a photograph of the sidewall beam dump. The specifications for the sidewall dumps are summarized in Table 1.

The exit dump is a V-shaped CuCrZr plate equipped with screw tubes as cooling channels. Its vertically inclined angle is 6°, which reduces heat flux to approximately 1/10. We adopted CuCrZr alloy, which provides a sufficient radiation hardness and a high thermal conductivity. Radiation-hard materials should be chosen for the exit dumps, because they will be irradiated frequently by uranium beams. The transverse dimension of the dump was determined to cover up to six significant charge states of uranium at the beam dump position. A photograph of the exit beam dump is shown in Fig. 4. The specifications for the exit dump are summarized in Table 2.

The maintenace of the beam dump system is an important issue, because the beam dump is expected to be damaged and to be highly radioactivated during an operation. In particular, the exit beam dump will be irradiated by intense uranium beams; thus it is expected to be damaged frequently. In order to replace the exit beam dump rapidly and safely, we implemented a maintenance mechanism that has a linear-guide rail, as shown in Fig. 1, which enables us to take the dump in and out through the cave hole in well radio-shielded environment. In addition, we employed a pillow seal system for vacuum sealing, which provides us a complete remote handling of the vacuum system. Figure 5 shows a photograph of the pillow seal.

The beam dump is cooled by pressurized water with a high flow velocity. The cooling capacity of the beam dump system is evaluated on the basis of ANSYS simulation. The maximum beam power is expected to be 83 kW, which corresponds to the case of a ^{238}U beam at 350 MeV/nucleon and 1 particle μA. The projected heat flux to the beam dump for a 83 kW beam is shown in Fig. 2. In the evaluation, the maximum beam powers that can be absorbed by the beam dumps are defined by a maximum temperature of 350°C. For the inner-sidewall beam dump, the maximum heat flux produced by a ^{238}U beam of 83 kW appears at about $\delta_{B\rho} = -30\%$. The maximum temperature in this case is obtained to be 370°C. It slightly exceeds 350°C, which, however, is in the allowable range of our criteria. On the other hand, the expected maximum heat flux on the outer-sidewall dump is not very large and can be absorbed sufficiently. For the exit beam dump, the acceptable beam powers have been expected to be 40 kW for $\delta_{B\rho} = -20\%$, 25 kW for $\delta_{B\rho} = -10\%$, and 60 kW for $\delta_{B\rho} = +10\%$. Taking into account the energy loss in the production target and the charge state distribution, the maximum beam power on the beam

*1 Division of Electronics and Applied Physics, Osaka Electro-Communication University.
*2 Toshiba Corporation

dump is equivalent to about 40 kW. The exit beam dump can, therefore, withstand a ^{238}U beam with a full intensity, except in the region of around $\delta_{B\rho} = -10\%$.

References

1) Y. Mizoi et al.: RIKEN Accel. Prog. Rep. **36**, 318 (2003).
2) K. Ezato et al.: Fusion Eng. Des. **81**, 347 (2006).
3) J. Boscary et al.: Fusion Eng. Des. **43**, 147 (1998).

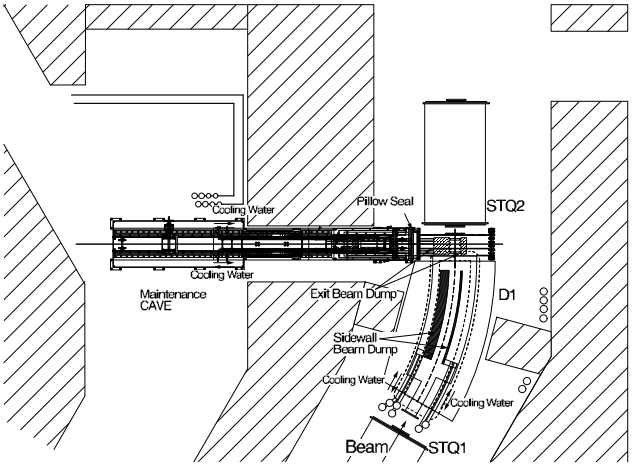

Fig. 1. Horizontal cross-sectional view of beam dump system and dipole magnet.

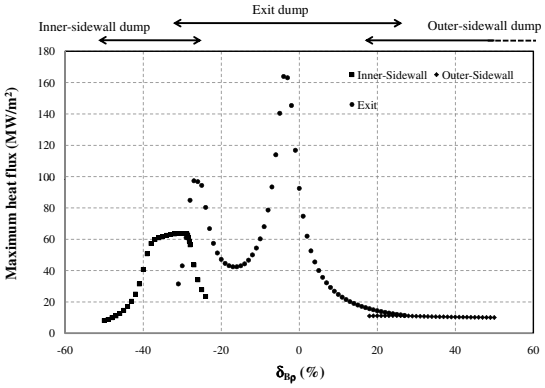

Fig. 2. Operation domain and expected maximum heat flux for beam dump. The heat flux is calculated for a beam power of 83 kW. The beam spot at the target is assumed to be $x_0 = y_0 = 0.5$ mm and $a_0 = b_0 = 5$ mrad.

Table 1. Specifications of the sidewall beam dump.

	Material	Pipe shape	Cooling channel
Inner sidewall	OF-Cu	rectangular 14 mm × 14 mm	M8-screw 23 tubes
Outer sidewall	Cu-Ag	circular ϕ 14 mm	ϕ 8 mm swirl 11 tubes

Fig. 3. Photograph of sidewall beam dump.

Table 2. Specifications of exit beam dump.

	Effective area size	Cooling channel
Inner sidewall	Horizontal: 322 mm Vertical: 66 mm	M8-screw 24 tubes
Outer sidewall	Horizontal: 120 mm Vertical: 66 mm	M8-screw 8 tubes

Fig. 4. Photograph of exit beam dump.

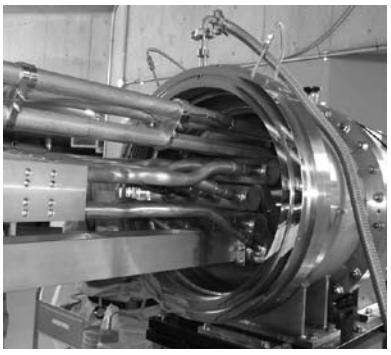

Fig. 5. Photograph of pillow seal for exit beam dump.

Signal transport system with optical fiber for RIBF

H. Kumagai, and T. Ohnishi

In RIBF, the distance between the experimental halls and the counting rooms is more than 100 m. Using a conventional coaxial cable for such a long distance, a analog signal from a detector and a digital signal from a circuit are attenuated, and consequently, the resolution of timing and pulse height for these signals decrease. To overcome this problem, we have developed a signal transport system using an optical fiber. Using this transport system, circuit tuning can be performed at the counting room while looking analog signals, and the electric ground level at the experimental hall can be isolated from that at the counting room. In addition, it is easy to add a long delay time ($>$ 100 ns) to a signal line using an optical fiber with no pulse distortion, and the required space for the delay cable is small.

Our signal transport system consists of transmitter and receiver modules. These two modules are connected with an optical fiber. Figures 1 and 2 show the conceptual design of this system and the schematic circuit drawings for the two modules, respectively. In the experimental hall, the amplitude and timing information of the electric signals from a detector or a circuit is converted to that of a laser using the laserdiode in the transmitter module, and the signals are transported through the optical fiber to the counting room with a minutely small loss. At the end, the signals are restored to their original form using the photodiode in the receiver module. The laserdiode and photodiode used are SLT4260 and SPV3203 produced by Sumitomo Electric Industries, Ltd, respectively. The driver and amplifier circuits for the diodes are originally designed by us. The cost of one channel including the transmitter and receiver modules is about 83,000 JPY. A photograph of the transmitter and receiver modules, which are packaged in an Nuclear Instrument Module (NIM) module, is shown in Fig. 3.

Figure 4 shows a typical example of signals using our transport system. The upper and lower photographs show a comparison between input and output signals with the 100 m transport through the optical fiber and conventional coaxial cable, respectively. Although the output signal through the coaxial cable is markedly attenuated, it is clearly observed that there is no difference between input and output signals in the case of the 100 m optical fiber.

Linearity is one of the important features of the signal transport system. In Fig. 5, the relationship between the input (V_i) and output (V_o) pulse heights obtained with our system is shown. It was measured using the analog signals in Fig. 4, and fitted as $V_o = 1.004V_i + 3.89 \times 10^{-5}V_i^2$. The result of the fitting

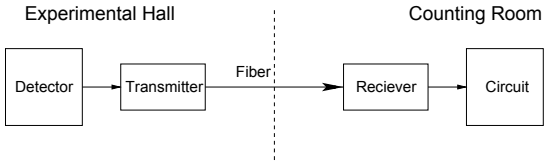

Fig. 1. Conceptual design of signal transport system with optical fiber. Electric signals from detectors at the experimental hall are transported to the counting room through the optical fiber.

shows the sufficient linearity of our system.

Time jitter was also measured using the same signals. To reduce the dependence of the timing on pulse height, a constant-fraction discriminator was used to determine the timing of the signals. Figure 6 shows the variation in the time difference between input and output signals. The standard deviation of the Gaussian fit is 11.7 ps. The time jitter of the measurement system is measured to be 10.7 ps. The intrinsic time jitter of our system is estimated to be 4.8 ps (r.m.s.), which is mainly caused by the circuit noise of the modules.

The gain of the laserdiode varies with temperature. From the measurement obtained using a constant-temperature oven, the temperature-dependent factor of the gain is 0.43% per degree. For a high counting rate more than 1 MHz, the baseline of the output signal is shifted by AC coupling inside the modules. In the case of an NIM signal with this system, the delay time caused by the base line shift is about 50 ps at 1 MHz. In order to use this system in RIBF, the radiation damage is investigated using the ^{70}Zn beam from RILAC at RIKEN. The total dose of irradiated neutrons is evaluated to be about 10^9 counts, and no effects on the performance of this system are confirmed.

In BigRIPS[1)], this signal transport system has been installed at all focal planes. In total, more than 100 channels were used for position and timing detectors. During the commissioning experiment of BigRIPS, this system was very stable. In addition, this system was applied to obtain a long delay time of about 1.5 μs. Signals were delayed without any distortion, and the space for delay cables was much smaller than that for a conventional coaxial cable.

In summary, we have developed a signal transport system with an optical fiber, and the performance of this system has been investigated. Currently, the development of a precise transport system for slow signals with a 1 μs time width is under way.

Reference

1) T. Kubo et al.: Nucl. Instr. Meth. B**204**, 97 (2003).

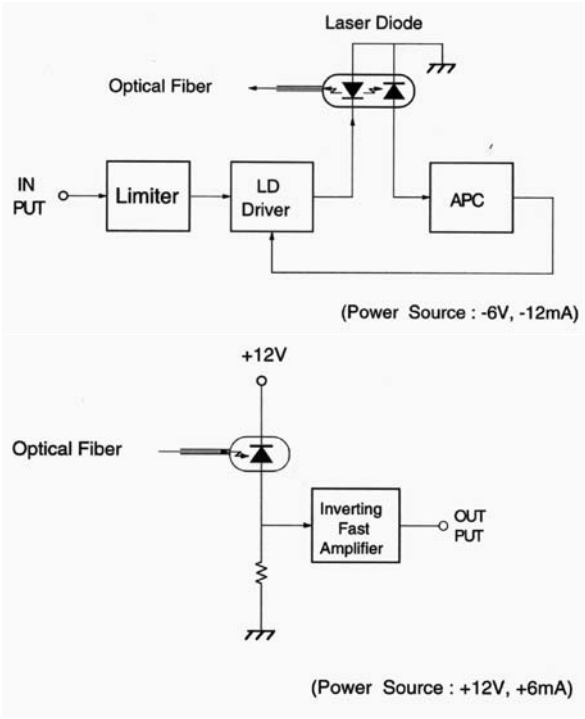

Fig. 2. Schematic circuit drawings of transmitter and receiver modules. The upper figure is a drawing of the transmitter module, while the lower one is that of the receiver module. APC is an auto-power-control module.

Fig. 3. Photograph of transmitter and receiver modules packaged in NIM module. The left and right components are the transmitter and receiver modules, respectively.

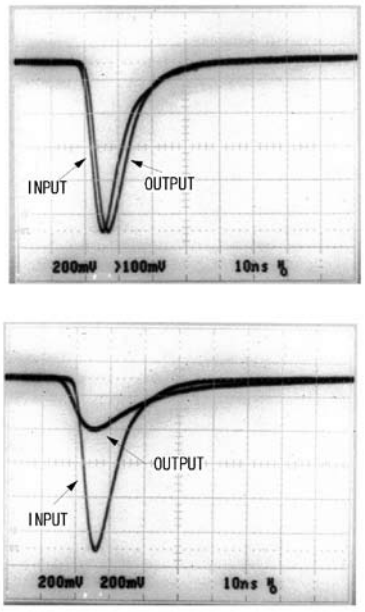

Fig. 4. Photographs of comparison between input and output signals with 100 m transport. The upper photograph shows the case of a 100 m optical fiber with our system, while the lower one shows that of a 100 m conventional coaxial cable.

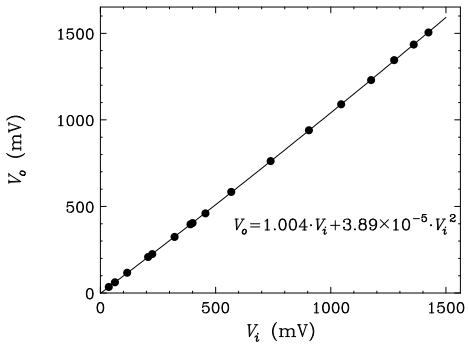

Fig. 5. Relationship between pulse heights of input V_i and output V_o signals. From the fitting result, $V_o = 1.004V_i + 3.89 \times 10^{-5}V_i^2$.

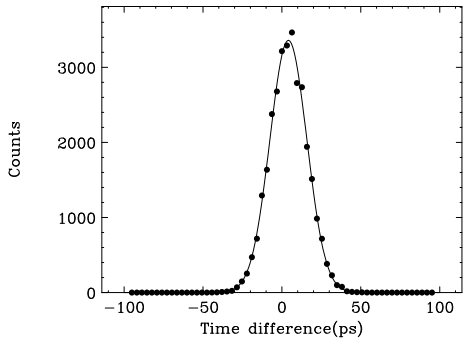

Fig. 6. Variation in time difference between input and output signals with 100 m optical fiber using our system. From the Gaussian fit, σ is 11.7 ps.

Beam-line detectors for BigRIPS

T. Ohnishi, T. Kubo, K. Kusaka, K. Yoshida, A. Yoshida, M. Ohtake, Y. Yanagisawa, N. Fukuda, H. Takeda, N. Aoi, H. Suzuki [*1], Y. Mizoi [*2], H. Kumagai, T. Suda, K. Kimura [*3], A. Ozawa [*4], T. Suzuki [*5], T. Yamaguchi [*5], H. Otsu, Y. Kondo, T. Nakao [*1], D. Kameda, Y. Gono, and Y. Yano

Beam-line detectors for BigRIPS[1] have been developed over the last several years in order to identify an RI beam event-by-event at a high counting rate. In BigRIPS, the particle identification is performed by using magnetic rigidity ($B\rho$), energy loss (ΔE), and the time of flight (TOF). Position detectors such as the delay line parallel-plate avalanche counter (PPAC)[2,3], ΔE detectors such as the silicon (Si) detector and tilted electrode gas ionization chamber (TEGIC)[4], and timing detectors such as thin plastic scintillation counters are placed at the focuses to measure $B\rho$, ΔE, and the TOF, respectively. For the confirmation of particle identification, NaI(Tl) scintillation and germanium (Ge) detectors are also used to measure the total kinetic energy and the γ rays from the isomeric state, respectively. In Fig. 1, the locations of these detectors are shown. The properties of beam-line detectors were examined by using fragments produced by the in-flight fission of a 345 MeV/nucleon ^{238}U beam at the commissioning experiment of BigRIPS.

The PPAC has been developed in order to measure the position of unstable nuclei with good detection efficiency at a high counting rate of approximately 10^6 Hz [2,3]. This counter has been already used in the RIPS[5], and its performance has been demonstrated[2,3]. For BigRIPS, two electrode sets are installed inside one PPAC in order to obtain good detection efficiency for heavy ions, and the effective area is enlarged to 240 $\times$ 150 mm^2. Figure 2 shows the outside view of the PPAC. As the detector gas for the PPAC, C_3F_8 is used due to the large energy loss and the short rise time of the signal. During the commissioning experiment at BigRIPS, the pressure of C_3F_8 was kept as 11 Torr. The operating anode bias was 890 V. At several focal planes, two PPACs with two electrode sets are installed, and the position resolution of the PPAC is estimated by using the fitted track. We fitted a straight line through three planes to identify the position of the rest plane. Figure 3 shows a typical distribution of deviations from the fitted track. The standard deviation of the Gaussian fit is 0.48 mm. Considering the propagation of error including the geometry of the PPAC, the position resolution is estimated to be 0.35 mm (r.m.s). Figure 4 shows the overall detection efficiency as a function of the atomic number (Z). This includes the PPAC efficiency of one plane and the efficiency of obtaining a position for both X and Y directions at the focal plane. For nuclei with $Z > 30$, the overall detection efficiency was almost 100%. This efficiency depends on the gas pressure and the operating bias. If we tune the condition, it increases to more than 90% for light ions[3].

The timing detector for BigRIPS is a thin plastic scintillation counter with two photomultiplier tubes (PMTs), one on each side, as shown in Fig. 5. The plastic scintillator model is BC-420, its size is 100$\times$100 mm^2, and its thickness is 0.2 mm. A Hamamatsu H-1949 PMT is used with a current booster. Two plastic scintillation counters installed at two achromatic focal planes (F3 and F7) were used for the TOF measurement. From the TOF measurement using an energy-degraded ^{238}U beam at 308 MeV/nucleon, which has a flight time of 227 ns over the 46.98 m central flight path, the intrinsic time resolution of one timing detector was measured to be 75 ps (FWHM).

For the ΔE measurement, the Si detector and TEGIC[4] installed at F7 were used. The effective area of the Si detector is 50 $\times$ 50 mm^2 and its thickness is 0.35 mm. The diameter of the effective area for the TEGIC is 200 mm. Figure 6 shows the inside view of the TEGIC. The TEGIC was operated using 760 Torr P10 (Ar 90%+CH_4 10%) gas, and its anode bias was 500 V. The measured energy resolutions of the Si detector and the TEGIC for ^{90}Sr were 1.1% (FWHM) and 0.9% (FWHM) at $B\rho$=7.2 Tm, respectively. Figure 7 shows the yield distribution in terms of the atomic number (Z) measured by using the TEGIC. For fragments in the region Z=20–50, a Z resolution of ΔZ=0.43 (FWHM) was achieved.

The NaI(Tl) scintillation detector was installed at F7. It is 3 inches in diameter and 60 mm in depth. The measured energy resolution of the NaI(Tl) scintillation detector was 1.98% (FWHM) for ^{104}Zr at $B\rho$=7.2 Tm.

The Ge detector used at BigRIPS is a four-segment clover-type detector. To confirm the particle identification, this detector was used to measure γ rays emitted from some of the products in their isomeric states, for example, 122 keV and 300 keV transitions in ^{96}Rb and 141 keV and 167 keV transitions in ^{97}Sr. More details concerning the Ge detector will be described in another report[6].

In summary, we have developed beam-line detectors for BigRIPS. It was confirmed that these detectors have sufficient resolution for the particle identification of fragments produced by the in-flight fission of ura-

*1 Department of Physics, The University of Tokyo
*2 Division of Electronics and Applied Physics, Osaka Electro-Communication University
*3 Nagasaki Institute of Applied Science
*4 Institute of Physics, University of Tsukuba
*5 Department of Physics, Saitama University

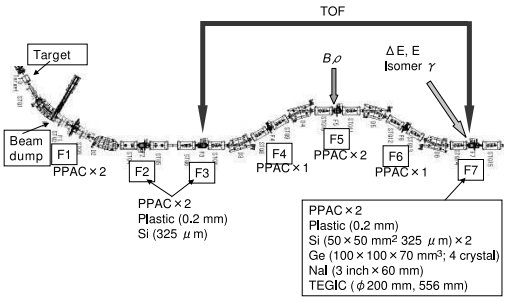

Fig. 1. Locations of beam-line detectors.

Fig. 2. Outside view of the PPAC.

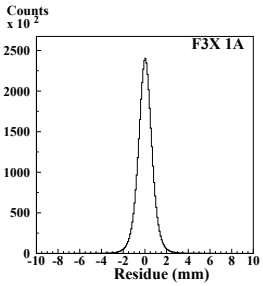

Fig. 3. Distribution of deviations from the fitted track. This distribution shows the case of an X plane at the upstream F3 PPAC. The standard deviation of the Gaussian fit is 0.48 mm.

nium. The development of better resolution and a high counting rate is in progress.

References

1) T. Kubo et al.: Nucl. Instrum. and Methods. B**204**, 97 (2003).
2) H. Kumagai et al.: RIKEN Accel. Prog. Rep. **31**, 164 (1998).
3) H. Kumagai et al.: Nucl. Instrum. and Methods. A**470**, 562 (2001).
4) K. Kimura et al.: Nucl. Instrum. and Methods. A**538**, 608 (2005).
5) T. Kubo et al.: Nucl. Instrum. and Methods. B**70**, 309 (1992).
6) T. Nakao et al.: in this progress report.

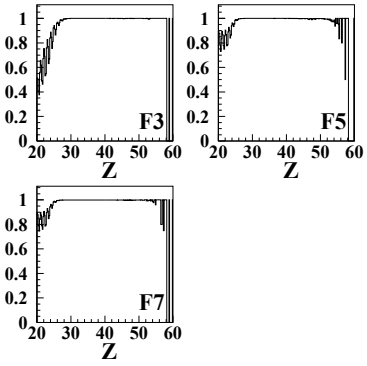

Fig. 4. Overall detection efficiency as a function of the atomic number (Z) at F3, F5, and F7. This includes the PPAC efficiency of one plane and the efficiency of obtaining a position for both X and Y directions at the focal plane.

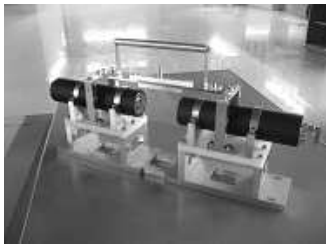

Fig. 5. Outside view of plastic scintillation counter.

Fig. 6. Inside view of the TEGIC.

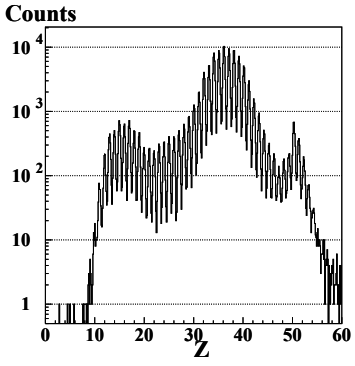

Fig. 7. Yield distribution from in-flight fission of U in terms of the atomic number Z at $B\rho$=7.2 Tm with a momentum acceptance of $\Delta P/P$=±1%, measured by using the TEGIC.

Magnetic field-map measurement of superconducting triplet quadrupole and dipole magnet for BigRIPS separator at RIKEN†

Y. Yanagisawa, K. Kusaka, T. Kubo, T. Haseyama,*1 Y.Yano, H. Suzuki, *2 and Y. Mizoi*3

The BigRIPS is one of the next-generation separators, which is aimed at achieving RI beams of greater capability, being characterized by large acceptances in its ion optics and the adoption of a two-stage separator scheme. It consists of fourteen superconducting triplet quadrupoles (STQ1-14) and six room-temperature dipoles (D1-D6). In the present report, field mapping devices for the quadrupoles and dipoles, and some results for the measured field distributions of STQ7, STQ11 (quadrupole) and D4 (dipole) are described.

Firstly, we describe the magnetic field-map measurement of STQs. We have performed the field-map measurements of STQ7 and STQ11, which represent superferric STQs. STQ7 consists of Q500, Q800, and Q500, whereas STQ11 consists of Q500, Q1000, and Q500. The nominal effective lengths of STQ7 and STQ11 are 500 mm-800 mm-500 mm and 500 mm-1000 mm-500 mm, respectively. Their pole-tip and warm bore radii are as large as 170 mm and 120 mm, respectively. The maximum pole-tip fields are also as high as 2.4 T, corresponding to a maximum field gradient of 14.1 T/m. Details of the STQs are described in Refs. 1-4.

We measured the cylindrical field map (B_r, B_θ, B_Z) along the beam axis, where B_r, B_θ, and B_z are the field components of the radial (r) direction, the azimuthal (θ) direction, and the beam line axis (z), respectively. The field mapping device is a two-motion stage, θ -Z, driven by stepping motors. The hall sensors are mounted on the arm, which moves along the z-axis in the warm bore of the magnet. The detail of the field mapping device is described in Ref.5. The stroke of the z-motion is 2810 mm. The arm is driven by a screw along the guide pipe and rotates with a guide pipe as a whole in the θ direction. We used three-axis Hall sensors (AXIS-3 AERPOC Ltd.). These axes correspond to the directions, r, θ and z. Two stepping motors are driven by the motion controller board (PCI-7332 National Instruments Co. ltd.) installed in a control PC. The Hall voltages are measured by a digital multimeter (DMM) (Keithley 2700+ 7700) with a constant current of 10 mA supplied by a current source (Yokogawa 7651). The data from the DMM are stored in PC via a GPIB interface. The motion of the Hall sensor arm is tested using a height gauge before being installed in the magnet. When the arm moves along a beam axis, the position accuracy of the radius is ±0.2 mm. It is caused by the bend and torsion of the guide pipe. Measurements are performed at z-motion steps of 10 mm and the hall sensors are rotated 360 degrees at a step of 9 degrees at each z. We performed measurement only in the clockwise direction in order to avoid possible backlash.

Figure 1 shows examples of measured field distributions for the Q800 magnet. The spatial distribution of $B_{r,2}$ whose Q800 magnet is at a radius r = 107 mm is plotted as a function of z. The $B_{r,2}$ is the quadrupole component of B_r. The origin of z-axis corresponds to the center of each magnet. The $B_{r,2}$ is obtained by decomposing the measured B_r field using the fast Fourier transform (FFT). Data are taken by exciting the measured magnet only with the current range from 20 A to 165 A (Q1000 160 A).

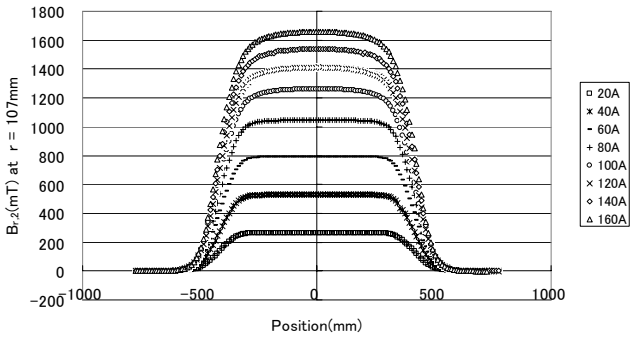

Fig. 1 Distribution of quadrupole field component $B_{r,2}$ for Q500 magnet along beam axis.

Figure 2 shows the effective lengths of the Q500, Q800 and Q1000 magnets. Effective length is obtained by integrating the $B_{r,2}$ numerically. It decreases when current exceeds 50A in all the magnets. We considered the change in effective length in the

† Condensed from the article in IEEE Trans. Appl. Superconductivity in press

*1 Japan Laser Corporation.
*2 Department of Physics, University of Tokyo
*3 Osaka-Electro Communication University

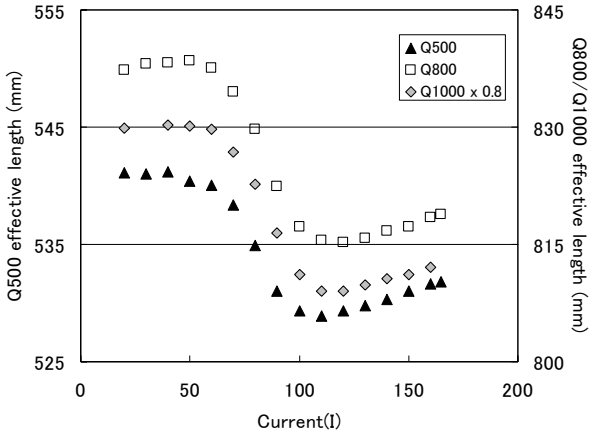

Fig. 2 Effective lengths of Q500, Q 800 and Q1000 magnets.

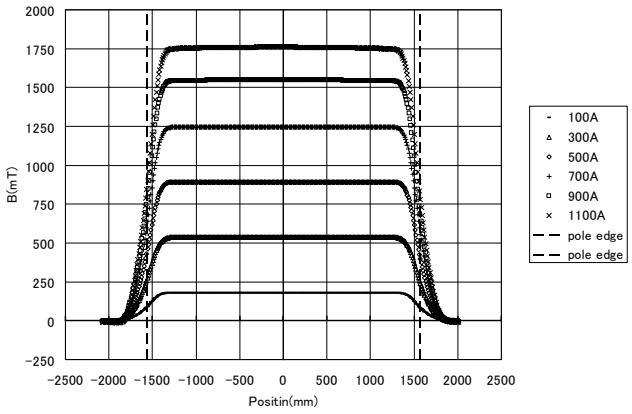

Fig. 3 Magnetic field distribution along central orbit of dipole.

ion optics calculations of the BigRIPS separator.

Secondly, we describe the magnetic field-map measurement of the dipole. The BigRIPS has six room-temperature dipole magnets with the same design. It is an H-type sector magnet. The bending angle and of radius of the sector magnet are 30 degrees and 6 m, respectively. The maximum operational field strength is 1.6 T, which corresponds to the current of 950 A. To achieve the homogeneity of the magnetic field, the corners of the pole pieces are shaped in Rogowski's cut. We used the field clamp to adjust the effective length to the arc length of the magnet.

We measured the magnetic field distribution of the B_y of D4 in the medium plane. The field mapping device consists of a base plate and a moving hall sensor holder. We set the 15 hall sensors every 20 mm in a direction perpendicular to the central orbit of the holder. The hall sensors of HGT-3010 manufactured by Lake Shore Co. ltd. with the nominal control current of 100mA are used. The holder moves along the base plate driven by ultrasonic motors. The motion controller and measurement system are the same as those used in the field mapping of STQs.

Measurements are automatically performed along the central orbit at every around 10 mm step because of the restriction of the motion controller. The position is measured by an encoder. For the confirmation of the position, a photosensor detected the pin every 1.2 degrees (about 125 mm). The measurement range is 4140 mm. We show in Fig. 3 a magnetic field distribution along the central orbit. The effective length is obtained by integrating the measured field map numerically on the medium plane. Figure 4 shows the effective length along the central orbit. Over 700A, the effective length begins to decrease and at 950A, it is smaller by approximately 10 mm.

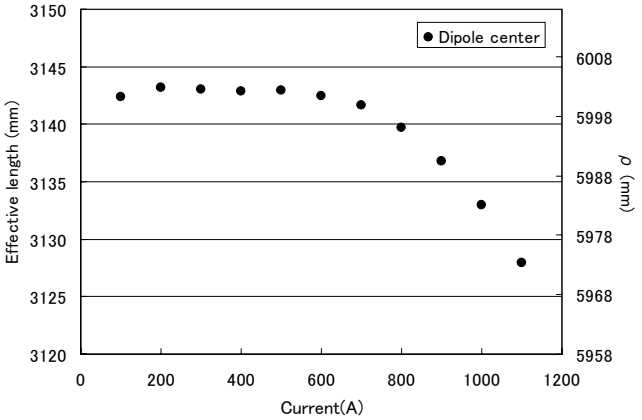

Fig. 4 Effective length of center radius of dipole.

In summary, we have carried out magnetic field-map measurements on STQ7, STQ11 and D4. For quardrupoles, we decomposed measurement field data using FFT. Ray tracing calculations of ion optics for BigRIPS using the obtained data were successfully performed last March 2006.

References

1) S. T. Kubo: Nucl. Instrum. Methods. Phys. Res., B **204**, 97 (2003).
2) T. Kubo et al.: IEEE Trans. Appl. Superconductivity, 17, 1069 (2007).
3) T. Hirumachi et al.: IEEE Trans. Appl. Superconductivity, 10, 236 (2000).
4) K. Kusaka et al.: IEEE Trans. Appl. Superconductivity, 14, 310 (2004).
5) K. Kusaka et al.: RIKEN Accel. Prog. Rep. 36, 312 (2003).

Control system of BigRIPS

K. Yoshida, T. Ohnishi, K. Kusaka, A. Yoshida, Y. Yanagisawa, M. Ohtake, N. Fukuda, and T. Kubo

The control system of BigRIPS is an integrated control system that controls and monitors magnets, beam diagnostic devices and vacuum pump stations of the BigRIPS separator and Zero Degree Spectrometer. The BigRIPS separator and Zero Degree Spectrometer consist of 69 superconducting quadrupole magnets, 8 superconducting sextapole magnets, and 8 dipole magnets, and are equipped with 80 diagnostic devices, such as slits and beam position detectors, and 22 pump stations. A system is required to control and monitor these seamlessly. The experimental physics and industrial control system (EPICS)[1] is used as the base software of the control system of BigRIPS. EPICS is a set of open source software tools and is widely used as the control system of accelerators. By utilizing EPICS, our effort to construct a control system is minimized since EPICS has been used in the accelerator control of RIBF and in the control of the RIPS separator at the RIKEN ring cyclotron facility.[2]

The configuration diagram of the BigRIPS control system is shown in Fig. 1. Two VME CPU boards of ADVME7501 manufactured by Advanet Inc. are used as the input output controller (IOC) of EPICS. Tornado 2.0.2 is utilized as the operating system of IOCs. Sun Fire V215 is used as the EPICS host computer with the Solaris 9 operating system. The host computer also acts as the boot server of the IOCs. EPICS R3.14.9 is utilized as the base software of the BigRIPS control system. Device supports for network I/O (NIO) and program logic circuits (PLC) developed by the RIKEN accelerator and KEK-RIKEN groups[3], respectively, are installed in addition to the standard I/O device support of EPICS. NIO is the remote I/O system that works as the interface between the VME-bus and power supplies of the magnets. The PLC of the Yokogawa FA-M3 series is used for the control of diagnostic devices and vacuum pump stations.

The status of the cryostats of the superconducting magnets is once collected and monitored in a sub-control system called the cryostat controller and forwarded to the IOC afterwards since the fast response of cutting off the power supply is necessary to protect the magnets when the quench of the superconducting magnets occurs. The cryostat controller consists of VME CPU board of AVME-148 operated with OS-9, FA-M3 PLCs, and their I/O modules. An Ethernet communication routine compatible with the ether unit of FA-M3 is built into the OS-9 system so that the epics IOC can communicate with the AVME-148 CPU as if it is FA-M3 PLC.

The EPICS extension software of *dm2k* is utilized as the user interface of the control system. Figure 2 shows the photograph of the display of the operator console. The magnets are set by specifying the central rigidity of the separator. The necessary currents of the magnets are calculated from the the central rigidity and beam optics parameters stored in the system. The beam optics parameters can be replaced easily by various sets of parameters through the *burt* utility of EPICS. Thus, the control system can handle various optics modes of the separator. Beam diagnostic devices, such as slits and detectors, are positioned appropriately according to the position values inputted and/or by clicking In/Out buttons in the control window of *dm2k*.

Collecting the status information and recording them are the other roles of the control system. The *channel archiver* utility is used for this purpose. About one thousand data, such as magnet currents and their statuses, slit positions, and vacuum are collected and stored in the disk of the host computer. Retrieving and plotting the data are performed through the *archive viewer* utility. In addition to the standalone program, the web interface is also installed so that we can see the retrieved data as graphs or numerical tables through both the utility program and web pages.

The error notification system is also included in the control system. The EPICS *alh* (ALarm Handler) utility works for this purpose. *Alh* is configured to ring the bell of the operator console and to send e-mails when a severe condition occurs, so that not only the operators sitting in front of the console but also persons responsible for the devices away from the console can receive the notification.

References

1) http://www.aps.anl.gov/epics/
2) K. Yoshida et al.: RIKEN Accel. Prog. Rep. **35**, 177 (2002).
3) J. Odagiri et al.: Proc. 3rd Annu. Meet. Particle Accelerator Society of Japan and 31st Linear Accelerator Meet. Japan, Sendai, 2006-8 (2006).

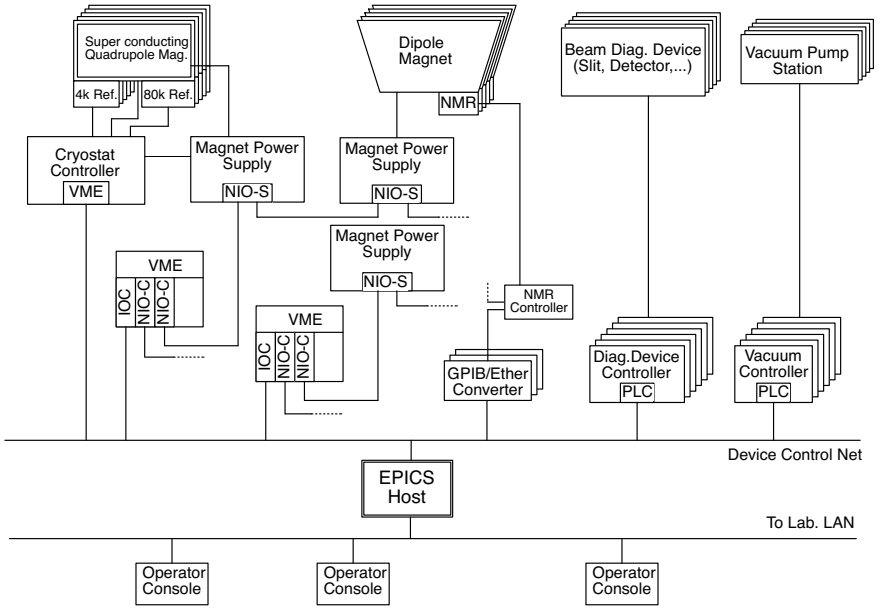

Fig. 1. Block diagram of BigRIPS control system.

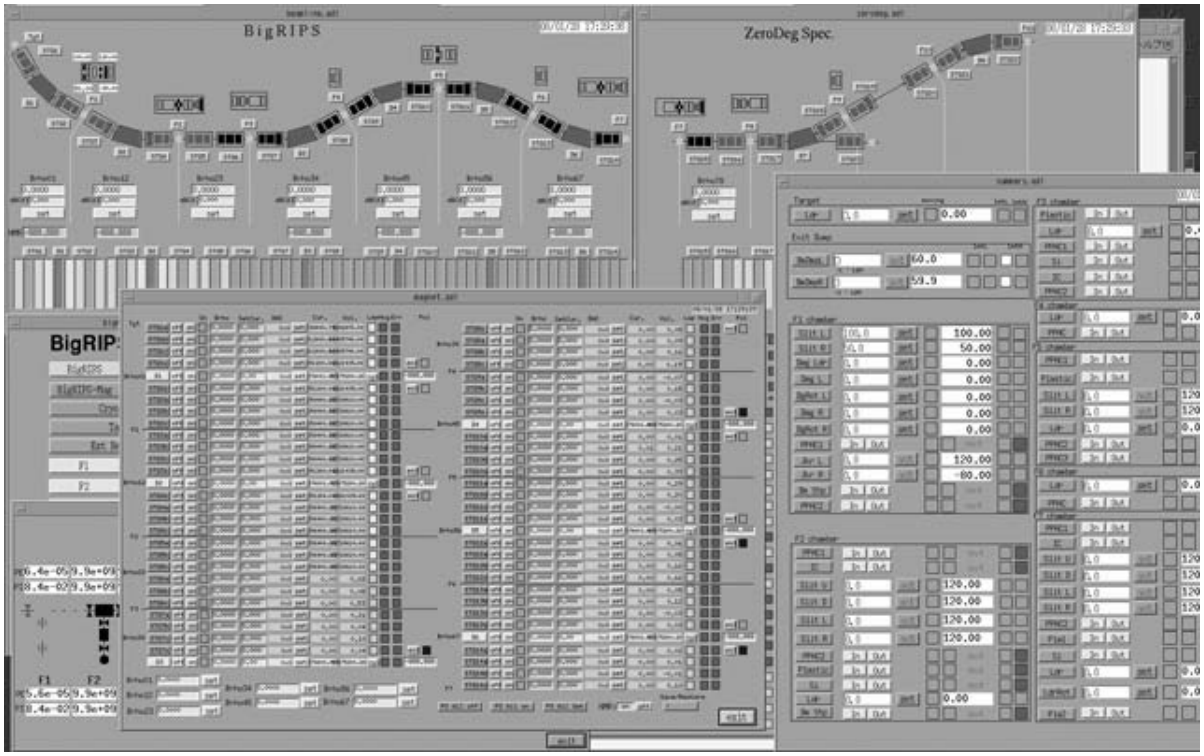

Fig. 2. Photograph of console display.

Design of high-resolution beam line for the SHARAQ spectrometer

T. Kawabata,[*1] G. P. A. Berg,[*2] T. Kubo, H. Sakai,[*3] S. Shimoura,[*1] and T. Uesaka,[*1]

The construction of the SHARAQ spectrometer was started in 2005 by the Center for Nuclear Study.[1] The SHARAQ spectrometer was designed to achieve a high momentum resolution of $\Delta p/p \sim 1/15000$ for charged particles with a magnetic rigidity of $B\rho = 6.8$ Tm. The SHARAQ spectrometer will be devoted to nuclear spectroscopic study using RI beams produced by the RI beam factory (RIBF) at RIKEN. Since the RI beams have a variety of isospin, spin, and internal energies, the RI-beam-induced reactions are expected to be useful tools to probe nuclear many-body systems.

Since the RI beams generally have a large emittance, the dispersion matching technique[2,3] must be introduced to perform high-resolution measurements. If the dispersions of the SHARAQ spectrometer and its beam line are properly "matched", the missing-mass resolution can be significantly improved and made better than the momentum spread of the RI beam.

On the basis of the notation of the computer code TRANSPORT,[4] the dispersion matching conditions are given as

$$s_{11}b_{16} + s_{12}b_{26} + s_{16} = 0, \quad (1)$$

$$s_{21}b_{16} + s_{22}b_{26} + s_{26} = 0, \quad (2)$$

where s_{ij} and b_{ij} are the beam transfer matrix elements of the SHARAQ spectrometer and its beam line, respectively. From Eqs. (1), (2), and the SHARAQ design values of s_{ij},[1] the dispersion matching conditions for the beam line transfer matrix elements are determined to be $b_{16} = -14.76$ m and $b_{26} = 4.79$ rad. It is necessary for the high-resolution spectroscopy with the secondary RI beam to construct the beam line satisfying those matching conditions.

The SHARAQ spectrometer will be installed in the E20 experimental room at RIBF. Since the RI beam emitted from the production target at F0 is achromatically focused at F3 in the normal beam transport procedure for the BigRIPS fragment separator,[5] we determined F3 to be the starting point of the SHARAQ beam line.

The SHARAQ beam line shares the magnetic elements with the BigRIPS fragment separator up to F6. After F6, the SHARAQ beam line branches from BigRIPS and bends 60° toward the target. Since the layout of the magnetic elements of the BigRIPS fragment separator has already been fixed, the layout between the branching point and the target was optimized to satisfy the dispersion matching conditions based on the first-order ion optical calculation using the computer code COSY INFINITY.[6] The optimized beam line layout is shown in Fig. 1.

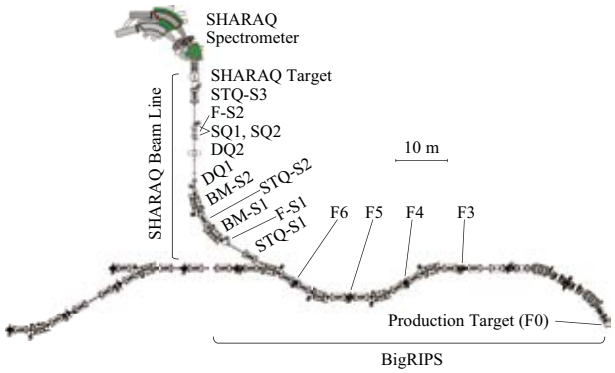

Fig. 1. Layout of the SHARAQ spectrometer and the high resolution beam line at RIBF.

In the SHARAQ beam line, the two 30° bending magnets (BM) are used with several quadrupole magnets for the beam transport from F6 to the SHARAQ target. Although most of the quadrupole magnets are superconducting triplet quadrupole magnets (STQ), the doublet (DQ) and singlet (SQ) quadrupole mangets are the normal conducting magnets.

Envelopes of the beam trajectories in the horizontal plane obtained from the first-order ion optical calculation are shown in Fig. 2(a). The trajectories for particles with $x_0 = \pm 3$ mm, $y_0 = \pm 3$ mm, $\theta_0 = \pm 10$ and 0 mr, $\phi_0 = \pm 30$ and 0 mr, and $\delta_0 = \pm 0.3\%$ at F3 are drawn.

The transfer matrix of the SHARAQ beam line obtained by the first-order ion optical calculation is tabulated in Table 1. The dispersion matching conditions are successfully satisfied, whereas the horizontal and vertical magnifications are almost unity. The off diagonal elements of b_{21} and b_{43} are kept small to reduce the angular spread caused by x_0 and y_0. Detailed description of the first-order ion optical calculation is given in Ref.[7].

Although the beam-line layout was optimized on the basis of the first-order calculation, the higher order aberration is not negligible since the secondary RI beams have a large emittance. Therefore, the precise ion optical calculation should be performed using the measured magnetic field maps of BM and STQ to examine the higher order aberration. The beam envelopes in the horizontal plane obtained from the fifth-order ion optical calculation are compared with those in the first-order calculation in Fig. 2(b). The 72 tra-

*1 Center for Nuclear Study, Graduate School of Science, University of Tokyo
*2 Department of Physics, University of Notre Dame
*3 Department of Physics, Graduate School of Science, University of Tokyo

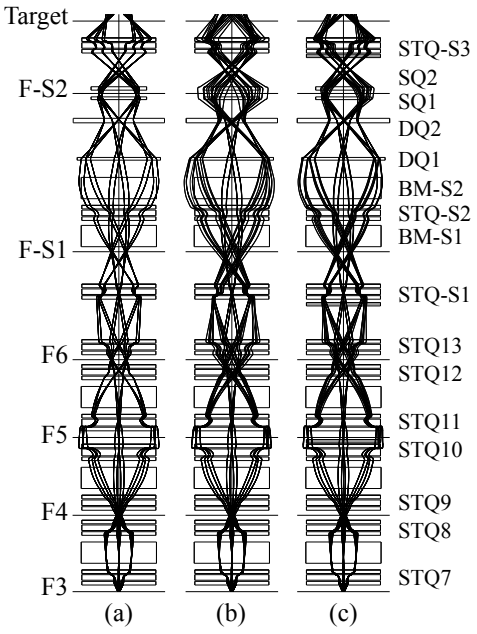

Fig. 2. Envelopes of the dispersive beam transport from F3 to the SHARAQ target in the horizontal plane. The trajectories for particles in the first-order calculation are shown in (a), whereas those in the fifth-order calculation without and with octupole magnets are in (b) and (c), respectively. The octupole magnets are indicated by the gray rectangles in (c).

$(x\|x)$ $(=b_{11})$	-0.99	$(x\|\theta)$ $(=b_{12})$	0.00
$(\theta\|x)$ $(=b_{21})$	0.08	$(\theta\|\theta)$ $(=b_{22})$	-1.03
$(x\|\delta)$ $(=b_{16})$	-14.76	$(\theta\|\delta)$ $(=b_{26})$	4.79
$(y\|y)$ $(=b_{33})$	1.24	$(y\|\phi)$ $(=b_{34})$	0.00
$(\phi\|y)$ $(=b_{43})$	-0.55	$(\phi\|\phi)$ $(=b_{44})$	0.80

Table 1. Beam transfer matrix of the SHARAQ beam line obtained by the first-order ion optical calculation. The units for the lengths and angles are m and radian, respectively.

jectories for particles with $x_0 = \pm 3$ mm, $y_0 = \pm 3$ mm, $\theta_0 = \pm 10$ and 0 mr, $\phi_0 = \pm 30$ and 0 mr, and $\delta_0 = \pm 0.3\%$ are drawn. It is clearly seen that the beam images at the focal points are strongly distorted owing to the higher order aberration. It is found that the third-order aberration is the most significant, whereas the other aberration is not large.

Since the octupole magnet is useful to correct the third-order aberration, the best layout of the octupole magnets was searched. As a result, it was found that the third-order aberration is effectively corrected when three octupole magnets are installed at F5 and at the upper streams of STQ-S1 and STQ-S3, as seen in Fig. 2(c).

To examine the beam profile on the SHARAQ target, a Monte Carlo calculation was carried out. A monochromatic beam with the momentum of $\delta_0 = 0$ or $\pm 0.3\%$ was transported from F3 to the SHARAQ target using the calculated beam transfer matrix. The beam spot and the angular spreads at F3 were assumed to have Gaussian distributions with full widths at half maximum of $\Delta x_0 = \Delta y_0 = 0.5$ mm, $\Delta\theta_0 = 10$ mr, and $\Delta\phi_0 = 30$ mr. The expected correlation between the horizontal position on the SHARAQ target and the horizontal/vertical angles at F3 is shown in Fig. 3. The left panels show the correlation when the three octupole magnets are not installed, while the right panels show the correlation when the octupole magnets are installed. Three loci seen in each panel correspond to the three assumed monochromatic beams with the fractional momentum deviations of $\delta = 0$ and $\pm 0.3\%$. It is clearly seen that the octupole magnets actually correct the higher order aberration.

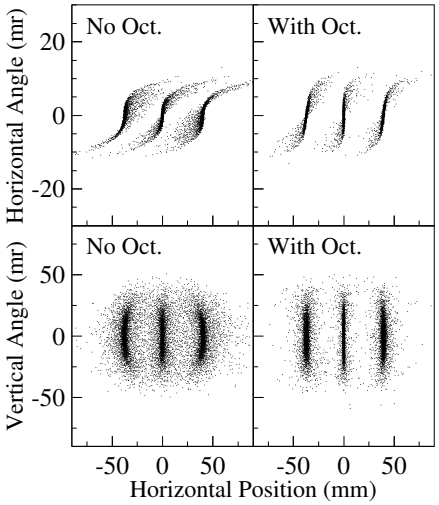

Fig. 3. Correlation between the horizontal position on the SHARAQ target and the horizontal/vertical angles at F3. The left and right panels show the correlation patterns before and after the three octupole magnets are installed.

The construction of the SHARAQ beam line will be started soon, and the first beam will be delivered to the SHARAQ spectrometer in 2009.

References

1) T. Uesaka et al.: RIKEN Accel. Prog. Rep. **40** (2007) 155.
2) B. L. Cohen: Rev. Sci. Instr. **30** (1959) 415.
3) T. Wakasa et al.: Nucl. Instrum. Methods. A **482** (2002) 79, and references therein.
4) K. L. Brown et al.: SLAC Report No. 91 Rev. 1, 1974.
5) T. Kubo: Nucl. Instrum. Methods. B **204** (2003) 97.
6) M. Berz et al.; Computer code COSY INFINITY, http://bt.pa.msu.edu/index_files/cosy.htm.
7) T. Kawabata et al.: RIKEN Accel. Prog. Rep. **40** (2007) 153.

Field measurement system of the superferric quadrupole magnets for SHARAQ spectrometer

Y. Sasamoto,[*1] K. Nakanishi,[*1] T. Uesaka,[*1] S. Shimoura,[*1] T. Kubo, H. Sakai,[*2] N. Yamazaki,[*1] and R. Yoshino,[*1]

New missing mass spectroscopy with an RI beam is planned to be conducted at RIBF with the SHARAQ spectrometer[1)2)]. The SHARAQ spectrometer is designed to achieve a resolving power of $p/\delta p = 1.5\times 10^4$ and a high angular resolution of $\delta\theta \sim 1$ mrad for particles with a maximum magnetic rigidity of $B\rho = 6.8$ Tm.

The SHARAQ spectrometer consists of three quadrupoles and two dipole magnets. The first doublet quadrupoles (SDQ) are superconducting magnets that provide a large field gradient of 14.1 T/m. The nominal effective lengths of the quadrupoles are 500 mm (Q500) and 1000 mm (Q1000). The design of SDQ is similar to that of BigRIPS triplet quadrupole magnets (STQ)[3)].

Fig. 1. Photograph of SDQ magnet.

To achieve the designed performance, field mapping is important because ion-optical calculations show that the major aberrations originate from the inhomogeneous field distribution of SDQ in the region of $r > 12$ cm[2)]. In this report, the field measurement system for the SDQ magnet is described.

In this system, we measured the voltage of a hall probe together with the following;

- temperatures of the room and around the hall probe,
- the electric current supplied to hall elements,
- the current and voltage of DC power supplies, and
- miscellaneous data for monitoring the status of a cryostat.

The diagram of the system is shown in Fig. 2. To measure the magnetic field, three-axis hall probes (Arepoc Co. Ltd., AXIS-3) were used. The temperature was measured using a platinum resistance thermometer. The electric current from a current source was monitored from the voltage of the resistor placed in series between the source and a hall probe.

Data acquisition was controlled by a Linux-based PC. Data were registered in the digital multimeter (Keithley 2701) linked to the PC with the Ethernet network communication. The hall probe mount was swept over the measured volume by a pulse motor operated via GPIB devices.

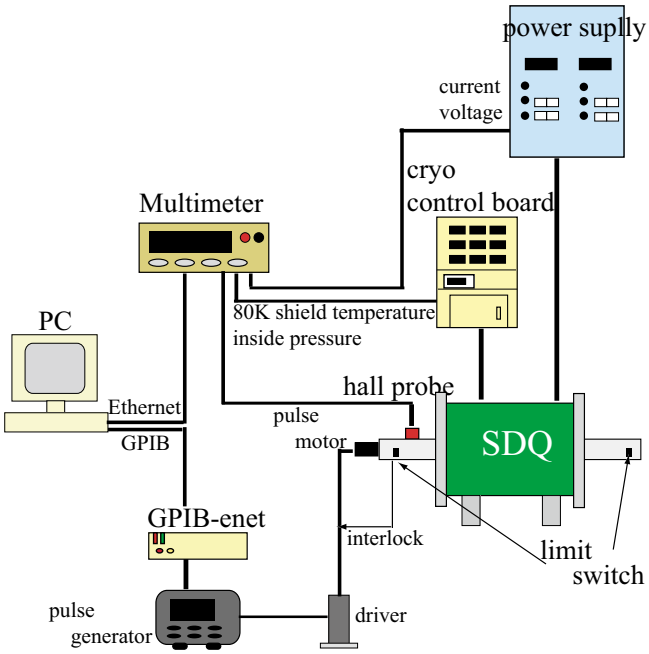

Fig. 2. Diagram of the measurement system.

The whole system including the DC power supplies is required to be sufficiently stable to measure the magnetic field with $\Delta B/B \sim 10^{-4}$. Prior to the measurement, the stability of the system was examined.

Figure 3 shows the typical current and voltage of a power supply in half a day. The current did not exhibit a significant variation, while the voltage gradually changed. The variation in voltage was found to depend on the temperature of the room. It was found that the DC power supplies were sufficiently stable to keep the magnetic field of $\Delta B/B \sim 10^{-4}$ for a few tens of hours.

Figure 4 shows a typical variation in temperature. In most cases, the variation was 0.1 $\sim$ 0.5 °C in a day. This variation results in the fluctuations of about 10^{-4} for the hall probe voltage since the temperature coefficient of the hall probe is as small as 2×10^{-4}/K.

*1 Center for Nuclear Study, University of Tokyo
*2 Department of Physics, University of Tokyo

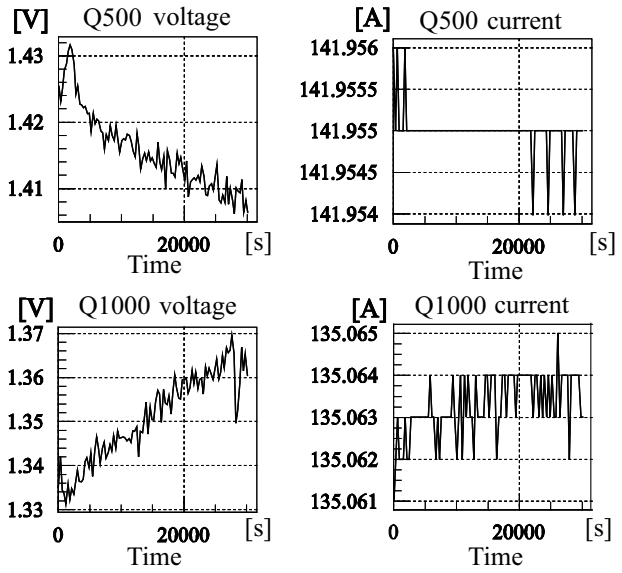

Fig. 3. Typical output of the power supply in half a day.

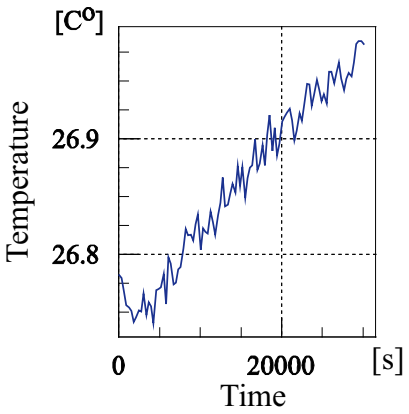

Fig. 4. Temperature around the hall probe measured by the platinum resistance thermometer.

A major variation in hall voltage was found to be due to the variation in current from the source. As is expected, the stability of the current source was consistent with the designed value of 0.01%/day; however, the current from the source sometimes varied more than the designed value of two figures. By correcting the large variation for the current source, a stability of $< 10^{-4}$ was obtained in the entire system including SDQ, as shown in Fig. 5. In the present study, it was found that the field measurement can be performed with the required accuracy using this system. More details of the method and results of the field measurement will be reported elsewhere soon.

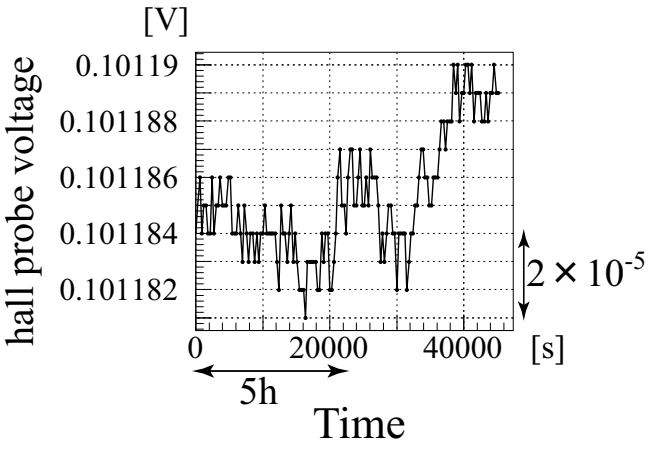

Fig. 5. Output voltage of the hall probe.

References
1) T. Uesaka et al.: CNS Ann. Rep. **2005** (2006) 61.
2) T. Uesaka et al.: RIKEN Accel. Prog. Rep. **40**, 155 (2007).
3) K. Kusaka et al.: IEEE Trans. Appl. Supercond. **14**, 310 (2004) .

AC power system for SHARAQ

Tadashi. Fujinawa, Sigele. Suzuki*, Toshiyuki. Kubo and Yasushige. Yano

Center for Nuclear Study, Graduate School of Science, The University of Tokyo (CNS) and RIKEN Nishina Center are constructing the Spectroscopy of hadronic systems with radioactive quantum beam （SHARAQ） in the basement of RIBF building. RIKEN Nishina Center will supply space and beams, and is responsible for build infrastructures, such as an electrical power supply and a water-cooling system. In this paper, we report to the electrical power supply system and the electrical equipments of the water-cooling system.

Electrical power supply system

The maximum capacity of the magnet-power sauce (DC) for SHARAQ is 1000kVA.

A dory-type transformer is 6.6kV/415V, and a △-Y connection is located in the E20 experiment room on the third basement floor in RIBF building. The transformer is highly efficient at a rated point of 98.95% and at a maximum point of 99.25% (40% of the rated point).The transformer together with a medium-voltage (MV) vacuum circuit breaker and no-fuse-breakers with an earth leakage trip element (ELCB) for 415V is covered with Japan electrical manufacturers' standard (JEM) that is called as metal-clad switchgear. This type of switchgear is very safe for humans and prevents fire.

The switchgear is connected to No.2 high-voltage substation feeder No.52RF5 by a 6.6kV-triplex-type cable with an environmental management (EM) cross-linked polyethylene insulator and a polyethylene sheath (XLPE/PE). The size of the cable is 60mm^2 and the allowable current is 160A. The actual current with the load of 1MVA is only 88A. The cable withstands a shortcut current of 22.43kA.[1] Fig. 2 shows the appearance of the switchgear.

The protection relays are installed on both feeder side (52SRF5) and incoming side (52SRF5R). The feeder side detects over current (50), short circuit-current (51) and ground directional current (67), and SHARAQ power system side detects under voltage (27), 50 and 51.

A single line diagram is shown in Fig.1

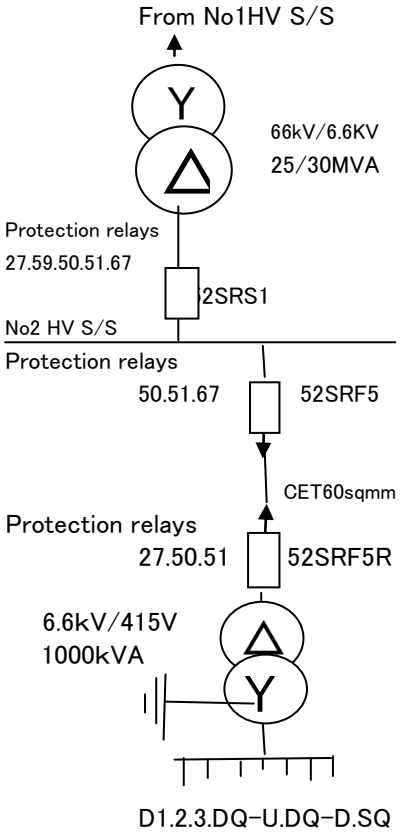

Fig. 1 Single line diagram

The control system operates with DC110V and

can also work during electrical power outage as well. The operation can be performed both locally and remotely. The remote control system with a flat-panel display is in CGS[2] center control room located in NISHINA memorial building.

Water- cooling system

The power souse for the SHARAQ water-cooling system uses existing power souse of RIBF cooling system connected to a CGS bus that provides an uninterruptible power souse. The system has three motors. The first motor is called the primary cooling water pump (30kW), which circulates deionized water (Fig. 3). The second motor is a circulating water pump (37kW) for the cooling tower. The third motor is a cooling tower fan (7.5kW). Those motors are connected to the existing motor control center (MCC) of extra units. All motors are three-phase 50Hz 415V high efficiency. The motor starters use a direct connection system, which enable a quick start and efficient restart. They are also more reliable and economical than the star-delta starter recommended by Ministry of Land Infrastructure and Transport (MLIT). The direct-type starters can only be used when the transformer's capacity is sufficiently large. Simple low-voltage (LV) starters are in the Motor Control Centre (MCC). MCC is the culmination of advancements in digital technology. The incorporation of a control data link network (CDL) converts the MCC into a superior data information system. MCC is connected to helium (He) control room with CDL. Short-circuit protection is achieved through the use of Molded Case Circuit Breakers (MCCBS=NFB) and thermal relays for over current. The above-mentioned systems require simpler hardware contraction and more straightforward operational skills. The cable capacity for the cooling tower has enough cross sections for the future extension of 2MW cooling capacity, which will be used for the rare RI mass ring and/or Self-Cooling Radioactive Ion Target (SCRIT) of experimental equipments. Those devices are planned to be built in the near future.

CONCLUSION

The electrical power supply system has been successfully operated.

This indicates that we have achieved our initial goals particularly environmental management.

Fig. 2 MV switchgear.

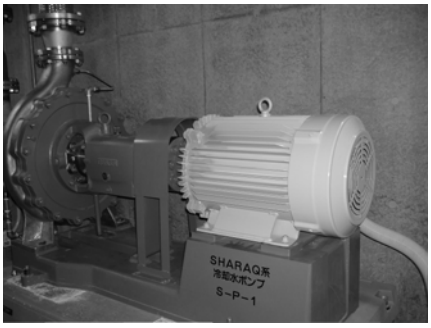

Fig.3 30kW high efficiency motor.

REFERENCE

1) T. Fujinawa et al.: RIKEN Accel. Prog. Rep.38 (2004).
2) T.Fujinawa et al.: RIKEN Accel. Prog. Rep.36 (2002)

*Shinbishi Elect

Development of the SCRIT for Electron Scattering

M. Wakasugi, T. Emoto, K. Ishii[a], S. Ito, K. Kurita[a], A. Kuwajima[b], A. Noda[c]. T. Shirai[c], T. Suda, T. Tamae[b], H. Tongu[c], S. Wang, and Y. Yano

We succeeded in developing a novel internal target (Self-Confining RI Ion Target: SCRIT) in an electron storage ring for electron scattering off unstable nuclei[1]. A prototype of the SCRIT device was installed in the Kaken storage ring (KSR) in Kyoto University. Approximately 3.6×10^7 of stable Cs ions were trapped in the SCRIT for about 53 ms at the electron beam current of 75 mA. The collision luminosity between the electron beam and the trapped Cs ions was achieved to be $10^{26}/(cm^2s)$ within 50-ms trapping time. The elastically scattered electrons from the trapped Cs ions were observed and its angular distributions were measured at the angle of 30, 40 and 60 degrees[2].

Experimental setup of the R&D study is schematically shown in Fig. 1. Pulsed Cs ion beams were accelerated vertically to 4.05 keV and bent 90 degrees into the direction of the electron beam axis. They were merged with the electron beam and guided to the SCRIT device using transverse trapping force provided by the electron beam. The SCRIT device is composed of 40 longitudinally stacked thin electrodes with 100-mm-long terminals at both ends. They form longitudinal mirror potential with a 240-mm-long trapping region.

Trapped ions in the SCRIT were extracted after a certain trapping time. They were guided into an analyzer, which measures the number of trapped ions and their charge-state distribution using a magnetic field. Channeltrons, numbered #1-#9, were used for extracted-ion counting in the analyzer. The Cs^{1+} ions were counted by channeltron #3, Cs^{2+} ions by #4, and $Cs^{3+\sim5+}$ ions by #5. Overall efficiency of the ion counting by the channeltrons was 10^{-5}.

Scattered electrons emerging from the SCRIT were detected by an electron detection system consisting of a drift chamber, pairs of plastic scintillators and calorimeters placed at the scattering angles of 30, 40 and 60 degrees. Details of the electron detection system are described in Ref. 2.

Electron beam, whose energy is 120 MeV, was injected into the KSR every 4 seconds because of the short storage lifetime, typically 100 s at 80 mA. After waiting the completion of radiation dumping, which took 2 s from the injection, the measurements were performed during the remaining 2 s. The SCRIT operation cycle composed of ion-injection, trapping and extraction was repeated during the measurement. Trapping time was varied in the range of 10-200 ms for measurement of the time evolution of the trapped ions, and the electron beam current was varied in the range of 45-75 mA to measure the current dependence.

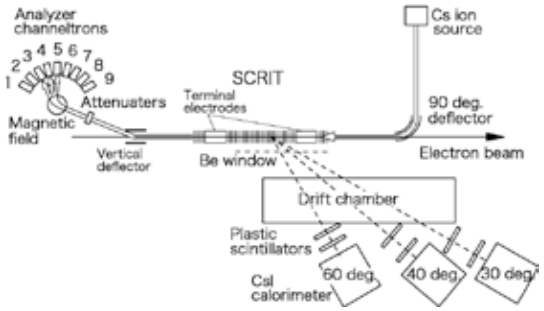

Fig. 1. Prototype of the SCRIT and the experimental setup.

Typical data for time evolution of the trapped Cs ions, the analysis is still preliminary, is shown in Fig. 2. Open symbols indicate Cs–ion yield of Cs^{1+}, Cs^{2+} and $Cs^{3+\sim5+}$ measured by channeltrons #3, #4 and #5, respectively. Closed symbol shows the number of trapped Cs ions including all charge states. Dotted and dash-dotted lines indicate time evolutions of these items calculated using rate equations[3]. The experimental data are well reproduced by the calculation. The number of initially trapped ions, N_i, and the trapping lifetime, τ_{life}, were derived from the reproductive calculation; $N_i=3.6(1) \times 10^7$, and $\tau_{life}=53(1)$ ms at the current of 75 mA.

Reproducing the time evolution of each charged state of trapped Cs ions, the collision luminosity between electron beam and trapped Cs ions can be estimated, which is shown by a solid line. It exceeds $10^{26}/(cm^2s)$ within 50-ms trapping time.

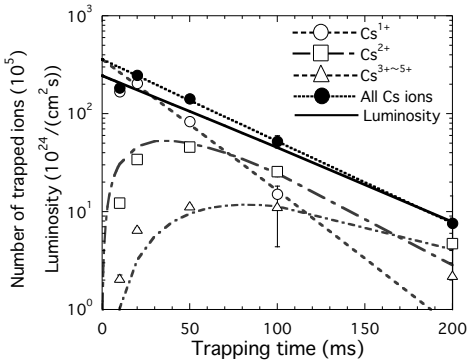

Fig. 2. Time evolution of the number of trapped ions and the collision luminosity.

References

1) M. Wakasugi et al., Phys. Rev. Lett., 100, 164801 (2008).
2) T. Suda et al., in this progress.
3) B.M. Penetrante et al., Phys. Rev. A43, 4873 (1991).

[a] Department of Physics, Rikkyo University
[b] Laboratory of Nuclear Science, Tohoku University
[c] Institute of Chemical Research, Kyoto University

Gain monitor system for the SCRIT experiment

S. Wang, T. Emoto, K. Ishii[1], S. Ito, K. Kurita[1], A. Kuwajiam[2], T. Suda, T. Tamae[2], M. Wakasugi and Y. Yano

In the SCRIT experiment at KSR of Kyoto University, three calorimeters, one CsI and two BaF_2, were employed for measuring the energy of scattered electrons. Each calorimeter consists of seven scintillation crystals. According to the cosmic-ray measurement in the pervious experiment, the peak position of cosmic-ray, corresponding to 48 MeV, was found to shift during one week measurement, as shown in Fig. 1. The probable reason is that the temperature of crystals increased during the experiment period. It is known that light output of scintillation crystal has temperature dependence, BaF_2, as an example, light output will decrease nearly 2% per ^oC at room temperature[1)]. In addition, the other part, including photomultipliers (PMT) and circuits, may also have effect on the gain stability. Therefore, we developed a gain monitor system.

Our gain monitor system includes two parts. One is a temperature monitor system which checks the temperature change of crystals and PMTs. The other part is an LED monitor system which is introduced to monitor the stability of the pulse-height measurement system.

The PMTs of CsI and BaF_2 detectors cover from 185 nm to 650 nm with the peak sensitivity at about 420 nm. Thus, a blue LED would be desirable.

The LED monitor system consisted of three parts: one blue LED, a light guide connector and optical fibers for each detector. The stability of the LED monitor system was monitored by an ^{241}Am source implanted in a NaI crystal which mounted at a PMT. The stability of the LED monitor system has been confirmed to be much better than 1% over one week measurement. By the result of the LED monitor system, the stability of PMTs and circuits has been found to be better than 1%. Therefore, the gain shift mentioned above should mainly come from the light output change of crystals.

Figure 2 shows the temperature change during the experiment. It is obvious that when KSR was in operation ("on"), the temperature increased. As seen in Fig. 2, the temperature of detectors increased almost 3^oC during 70 hours operation period. According to ref. 1, the light output of BaF_2 crystal would decrease about 6%, which is consistent with the result of cosmic-ray measurement, as shown in Fig. 1.

As a conclusion, in a long term experiment at KSR, in addition to check the pulse-height measurement system by gain monitor system, cosmic-ray measurement or elastically scattered electrons measurement from W-wire[2)] is necessary for monitoring the light output change of crystals.

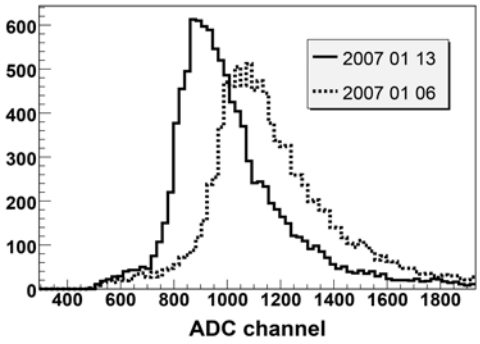

Fig. 1. ADC spectrum of cosmic-ray measurement of BaF2#1. Dashed line is at beginning of the experiment and solid line is at the end of the experiment.

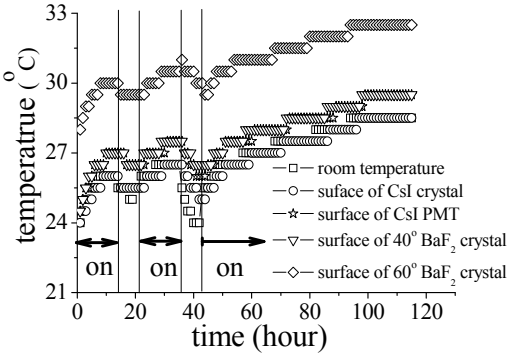

Fig. 2 The temperature changed during the experiment.

References

1) V. Nanal, et al.: Nucl. Instr. Meth. A 389 (1997) 430.
2) Y. Furukawa, et al.: RIKEN Accel. Prog. Rep. 40 (2007).

Present status of long injection beam line for rare–RI ring project

Y. Yamaguchi, A. Ozawa,[*1] I. Arai,[*1] T. Fujinawa, N. Fukunishi, A. Goto, S. Igarashi,[*1] T. Kikuchi,[*2] T. Ohnishi, T. Ohtsubo,[*4] H. Sakurai, T. Suzuki,[*3] M. Wakasugi, K. Yamaguchi,[*1] T. Yamaguchi,[*3] Y. Yasuda,[*1] and Y. Yano

We have proposed precise mass measurements of short–lived rare nuclei including the r–process region using a cyclotron–like storage ring[1]. The cyclotron–like storage ring is designed for a fixed energy of 200 MeV/nucleon ($\gamma_t = 1.214$). The short–lived rare nuclei for a wide range of momentum ($\delta p/p \sim \pm 1\%$) are injected onto their equilibrium ring orbits by dispersion matching. The ring allows us to determine the masses of such rare nuclei with an accuracy of 10^{-6} by measuring the revolution time (up to 1 ms) with the velocity measurements before the ring. To measure the velocity with the required accuracy of 10^{-4} before the ring and to inject such rare nuclei into the ring individually, a long injection beam line is indispensable.

The long injection beam line is branched off from the dispersion–matching (SHARAQ) beam line[2], which is connected to BigRIPS[3]. A start counter for the velocity measurements is located at the F3 achromatic focal plane of BigRIPS, and a stop counter is located at the R5 achromatic focal plane of the long injection beam line. The distance between those two counters is about 180 m, which gives more than 1 μs flight time for particles of 200 MeV/nucleon. Since a typical counter has a timing resolution higher than 100 ps, the long injection beam line including BigRIPS allows us to measure the velocity with an accuracy of 10^{-4}.

Figure 1 shows the present floor plan of the long injection beam line that reflects a first–order beam–optical calculation result. The long injection beam line, which starts from the branching point in Fig. 1, consists of forty–three quadrupole magnets and twenty–four dipole magnets with a 15 degree bend. We recycle all dipole magnets of TARNII[4] (TN–D). The two types of quadrupole magnet of TARNII (TN–Q) and KEK–PS (PS–Q) are recycled. The main parameters for these magnets are summarized in Table 1. The maximum dipole magnetic field strength of 1.5 T, due to the limitation of the existing power supply, does not satisfy our final demand. To excite the maximum dipole magnetic field strength up to 1.6 T, a new power supply is necessary.

We have examined the beam optics using the computer code COSY–INFINITY[5] with A/Z=3 particles of 200 MeV/nucleon. The beam trajectories of first–order optics are shown in Figs. 2, 3, and 4. The trajectories in the horizontal and vertical planes are shown

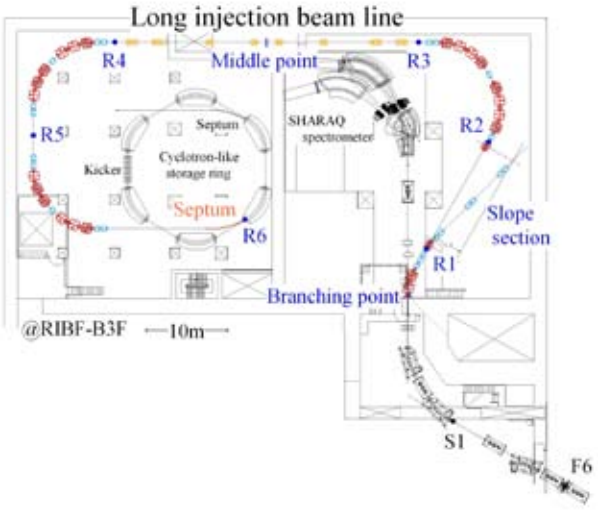

Fig. 1. Present floor plan of long injection beam line that reflects first–order beam–optical calculation result.

for $\delta x = \pm 1$ mm, $\delta y = \pm 1$ mm, $\delta\theta = \pm 8$ mrad, $\delta\phi = \pm 8$ mrad, and $\delta p/p = \pm 1$ %.

Figure 2 shows the beam trajectories from the F3 achromatic focal plane of BigRIPS, which is the starting point of our beam–optical calculation, to the branching point. The acceptance of this section is wider than that of the downstream section from the branching point. Figure 3 shows the beam trajectories from the branching point to the middle point of the long injection beam line. To branch off from the SHARAQ beam line, a particle is bent 30 degrees using two TN–D magnets and is squeezed using triplet PS–Q magnets. To change the floor level of the beam line from the SHARAQ stage to B3F, we must bend the beam line below. Thus, we use a 90–degree–rotated TN–D magnet (*i.e.*, 15 degree bend below). After the end of the slope section, the particle is bent 120 degrees using eight TN–D magnets and transported to the straight section (between R3 and R4). Twenty

Table 1. Main parameters for recycled magnet.

Model	TN–D	TN–Q	PS–Q
Number	24	20	23
Gap, Bore Diameter (mm)	80	130	100
Length (m)	1.06	0.20	0.60
B (T), B' (T/m)	1.5	7	18

*1 Institute of Physics, University of Tsukuba
*2 Department of Electrical and Electronic Engineering, Utsunomiya University
*3 Department of Physics, Niigata University
*4 Department of Physics, Saitama University

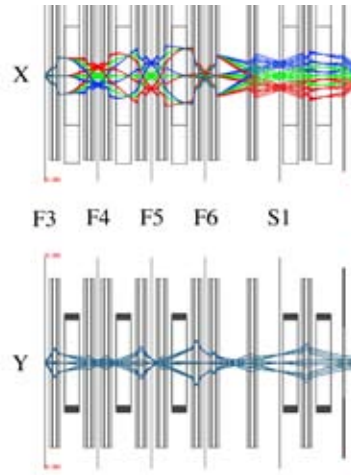

Fig. 2. Beam trajectories in horizontal (upper) and vertical (lower) planes from F3 of BigRIPS to branching point.

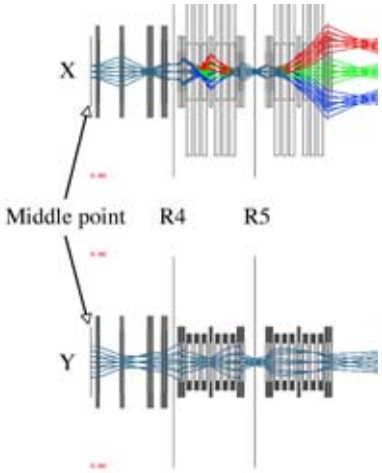

Fig. 4. Beam trajectories from middle point to R6 of long injection beam line.

TN–Q magnets are used in the straight section. Figure 4 shows the beam trajectories from the middle point to the R6 of the long injection beam line. Doubly achromatic focus is achieved at the R5 focal plane, used as a stop counter installation place for the velocity measurements. The R6 corresponds to the exit of the septum magnet for injection.

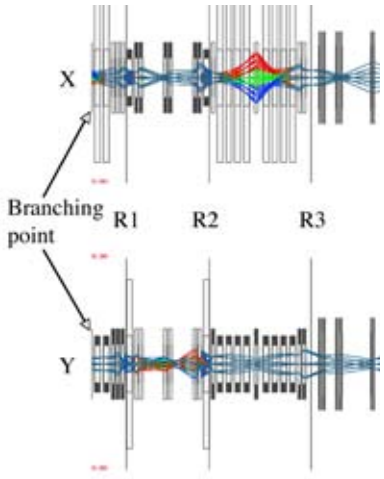

Fig. 3. Beam trajectories from branching point to middle point of long injection beam line.

To inject the rare nuclei onto their equilibrium ring orbits with small aberrations, dispersion matching is required. The preliminary result for the dispersive beam transport condition is shown in Fig. 4. The arrangement of the dispersive section (between R5 and R6) has not been fixed yet, owing to the unfinished detailed examination of the injection scheme.

We considered only the first–order effects in this paper; however, higher–order aberrations are not negligible. Such aberrations will affect not only the dispersion matching but also the velocity measurements. The evaluation of the effects of higher–order aberrations is still in progress.

References

1) Y. Yamaguchi et al.: RIKEN. Accel. Prog. Rep. **40**, 151 (2007); Y. Yamaguchi et al.: Nucl. Instrum. Methods Phys. Res. B (2008), in press.
2) T. Kawabata et al.: RIKEN. Accel. Prog. Rep. **40**, 153 (2007).
3) T. Kubo: Nucl. Instrum. Methods Phys. Res. B **204**, 97 (2003).
4) T. Katayama et al.: Particle Accel. **32**, 105 (1990).
5) M. Benz: Nucl. Instrum. Methods Phys. Res. A **298**, 473 (1990).

Development of a Portable Multi-Reflection Time-of-Flight Mass Spectrograph†

P. Schury, T. Nakamura, A. Takamine, M. Wada, H. Wollnik,*1 and Y. Yamazaki

[Mass measurements, unstable nuclei, low energy beam]

We are developing a multi-reflection time-of-flight (MRTOF) mass spectrometer for use with radioactive ion (RI) beams. The MRTOF will be attached to its own dedicated gas stopping cell, allowing the system-as-designed to be portable. This will provide flexibility in commissioning the device by making it possible to use less-demanded RI sources, such as CRIB. Once the system is shown to be fully functional, it will be able to take beam from any available source at RIKEN such as CRIB, RIPS, or BigRIPS – or even be relocated to another facility.

Figure 1 provides a sketch of the system. Energetic ions will be slowed in a solid degrader and thermalized in a helium-filled chamber. Using a proven RF-carpet technique,[1] thermalized ions will be extracted from the gas cell and injected into a radio-frequency (RF) multipole ion beam guide to be transported through a differentially pumped region. An RF quadrupole mass filter will select for a specific ion mass number, removing non-isobaric ions. The isobaric ion ensemble will then be cooled in a low-pressure gas-filled RF ion trap before being injected into the MRTOF.

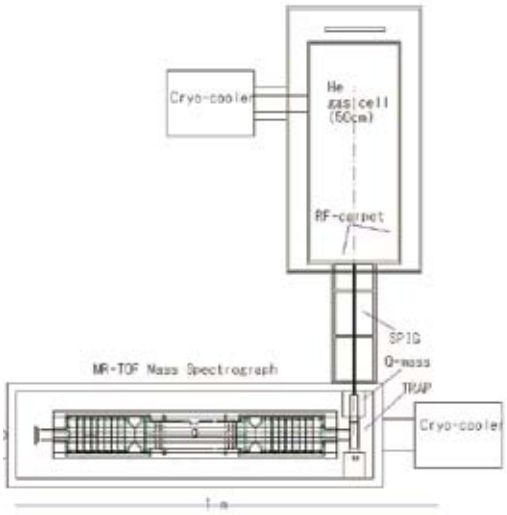

Fig. 1. Planned layout for the portable MRTOF system. The system includes a gas cell for stopping relativistic ions, an ion trap to prepare ions for injection into the MRTOF and ion guide systems for transporting thermalized ions from the gas cell to the ion trap.

Design goals for this new MRTOF device are based on what has previously been achieved in an off-line prototype.[2)3)] The off-line prototype achieved a mass resolving power of 200,000. The on-line system, still under development, is expected to be able to achieve even better resolving powers. To achieve this goal, an emphasis has been placed on achieving extremely high-stability voltage signals for the MRTOF electrodes and designing the system to minimize the likelihood of a faulty alignment of the electrodes – which could introduce systematic measurement errors.

Perhaps more importantly, for the study of the most exotic isotopes, the new system is intended to be highly efficient. The gas cell will be cryogenically cooled to reduce gas impurities which might charge exchange with either the ionized helium or the radioactive ions. While the RF-carpet technique does not transport He^+, gas impurities ionized by exchange with helium ions can lead to a powerful source of impurity ions.

As the total flight length may be as much as 1 km, the emittance strongly effects the the efficiency of the system. The energy spread of the ions directly effects of the maximum resolving power of the system. To address these issues, the ion trap will also be cryogenically cooled, which should lead to a reduction in the energy spread and emittance of the cooled ion cloud.

Figure 2 shows the mechanical layout of the MRTOF system. The system will be mounted on a heavy base of stainless steel to minimize sagging effects. To minimize effects from thermal expansion the mounting base will be water-cooled, which should provide a temperature stability of $\Delta T < 1$K, resulting in $\Delta L/L < 17$ ppm.

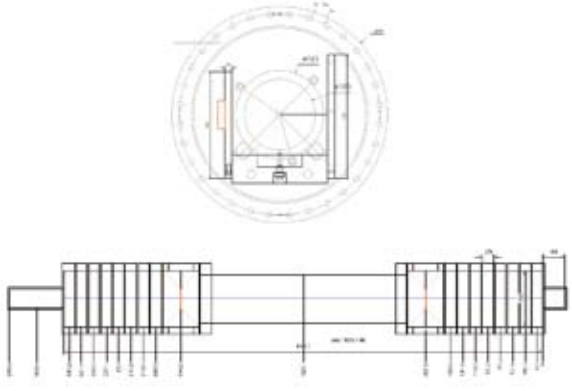

Fig. 2. Mechanical drawing of MRTOF. Lateral and transverse views are at different scales.

Due to the low rate for very exotic isotopes it is im-

*1 University of Giessen

portant that the system be stable over periods of as long as weeks in order to be able to analyze data in aggregate. For example, if operated at a mass resolving power of 200,000 the system must be constant on a level of better than 5 ppm over the course of the measurement or systematic mass shifts will occur at the level of the measurement uncertainty. In order to prevent such from occurring, much effort has gone into development of an extremely precise voltage regulation system. Figure 3 details the voltage stabilization system in a flowchart.

The voltage regulation system makes use of voltage dividers built of low temperature-coefficient resistors to provide feedback to a digital PID controller. To further improve the stability of the system the voltage dividers, ADC, and voltage reference are all to be maintained at a highly constant temperature, preferably $\Delta T < 10$ mK.

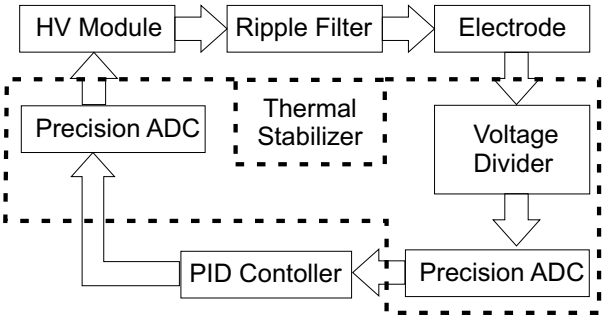

Fig. 3. Flowchart of the voltage stabilization system.

At present, development work for the portable MRTOF is ongoing. The mechanical design of the MRTOF electrodes and vacuum chamber are largely complete. The design of the cooling trap and the electrode system for transporting ions from the trap to the MRTOF is ongoing, but on-track to be complete before the end of FY2007. The electronics required for the system have been evaluated and the design of the PID controller and temperature stabilization circuits are progressing. It is presently scheduled that mechanical components will be sent for fabrication at the start of FY2008 and construction will begin in earnest by mid-FY2008 with commissioning beginning in late FY2008 or early FY2009.

References

1) M. Wada et al., Nucl. Instrum. Methods **B204**, 570 (2003)
2) Y. Ishida, M. Wada and H. Wollnik: Nucl. Instrum. Methods and Phys. Res. **B241**, 982 (2005).
3) Y. Ishida, M. Wada and H. Wollnik: RIKEN Accel. Prog. Rep. **40**, 150 (2007)

Highly accurate magnetic field measurement by new NMR equipment

Y. Yasuda,[*1] A. Ozawa,[*1] Y. Yamaguchi, I. Arai,[*1] K. Y. Hara,[*1] Y. Hashizume,[*1] T. Moriguchi,[*1] and T. Nakajima[*2]

We plan to construct a precise mass-measurement apparatus "Rare-RI Ring", which makes it possible to measure masses of exotic nuclei with a relative accuracy higher than 10^{-6} at RIBF. Rare-RI Ring consists of a long injection beam line and a cyclotron-like storage ring. We require a uniform and stable magnetic field with a 10^{-6} relative accuracy for sector magnets in our storage ring. Before constructing sector magnets, we had to examine the measurement of the magnetic field with a 10^{-6} relative accuracy. Then, we investigated the uniformity and stability of the magnetic field of a D8 magnet in a zero-degree forward spectrometer (ZDS) at 1.5 Tesla. Although the relative accuracy for the D8 magnet is 10^{-4}, which is due to the power supply, we performed the measurement at around the center of the sector magnet, which might be most uniform in the magnet. We used the newly produced NMR equipment with an external frequency synthesizer. It has a relative accuracy higher than 10^{-6} and its scope is 1.5 T±5 mT[1)].

At the beginning of the measurement, we searched the most uniform point for the magnetic field in the median plane of the D8 chamber, where we could observe the sharpest resonance signal, and called it as the reference point of measurement. We measured the magnetic field distribution around this point and a long time fluctuation at this point. A schematic view of the measured region is shown in Fig. 1. As the magnetic

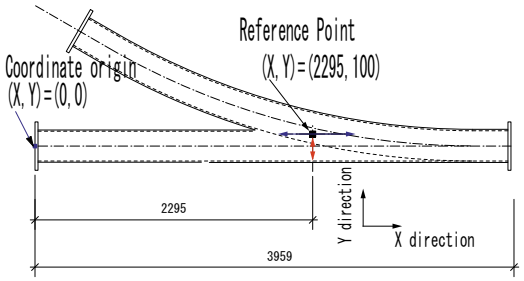

Fig. 1. Schematic view of D8 chamber. We performed our measurement around the center of the chamber.

field changes slowly for a long time, we estimated the magnetic field distribution as a relative ratio correcting a time fluctuation by the following method. The measured magnetic field at each point was considered as a function of coordinates (X, Y) and time t, and we assumed that the local magnetic field $f(X, Y, t)$ at each point in the magnet has the same time fluctuation. We obtained a polynomial function $f_r(t)$, which expresses the fluctuation of the magnetic field at the reference point as a function of time, by fitting to the

*1 Institute of Physics, University of Tsukuba
*2 ECHO ELECTRONICS CO., LTD.

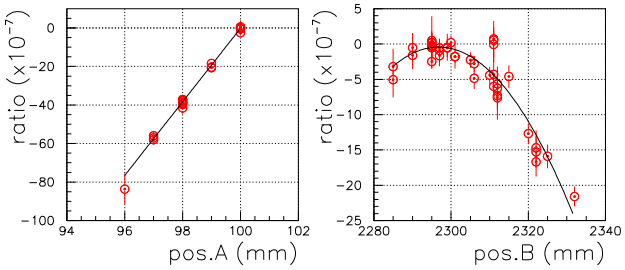

Fig. 2. The position dependences of the magnetic field around the reference point (X,Y)=(2295,100).

reference point data, and we calculated the relative ratio $\{f(X, Y, t) - f_r(t)\}/f_r(t)$ at each point. The deviation of the magnetic field crosses 10^{-6} at distances of 25 mm in the X direction and 0.5 mm in the Y direction from the reference point. The dependences of the measured magnetic field on position and direction can be understood from the pole shape and measured region.

We show one of the results of long-time measurements in Fig. 3. The resonance frequency indicates the magnitude of the magnetic field at the reference point. It decreased by 5×10^{-5} relatively 26 hours later. We also measured the temperatures of the experimental room and yoke and coil surfaces. The temperatures of the room and coil surface were kept within ±0.2°C. However, that of the yoke surface increased by about 1°C. It appears that the temperature of the yoke surface correlates to the magnetic field. The fact that the rate of linear expansion of iron is on the order of 10^{-5} may explain this correlation. We started the measurement 18 hours later after turning the power of the magnet on. Although the stability of the power supply is expected to affect the magnetic field, we could not measure it in this time.

We plan to perform a long-time measurement for about one week.

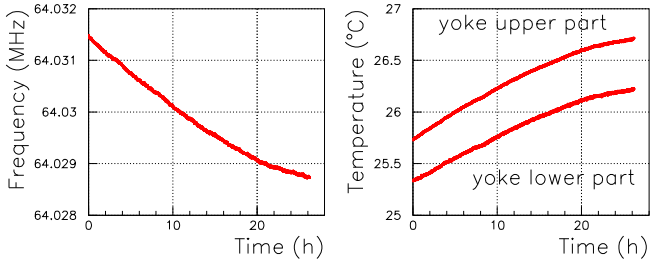

Fig. 3. Time dependences of magnetic field at reference point and temperatures of magnet yokes for 26 h.

References

1) ECHO ELECTRONICS CO., LTD., NMR EFM-15000R operating manual (2007).

Development of a cryogenic gas target system at CRIB

H. Yamaguchi,[*1] Y. Wakabayashi,[*1] G. Amadio,[*1] S. Hayakawa,[*1] H. Fujikawa,[*1] S. Kubono,[*1] J.J. He,[*2] A. Kim,[*3] and D.N. Binh,[*1]

[RI beam production, gas target]

A thick and thermostable gas target is necessary for the production of intense RI beams at CNS Radio Isotope Beam separator (CRIB)[1–3]. Recently we constructed a cryogenic gas target system, and its design and basic test results of are reported here.

Figure 1 shows the entire structure of the target system. The target gas cell located in a vacuum chamber is shown at the bottom of the figure. The cell is 80-mm-long and has a 20-mm-diameter cylindrical hole to contain the gas inside. On the beam direction sides of the cell, flanges with 2.5-μm-thick Havar foils were attached to seal the cell, using thin indium wires. The

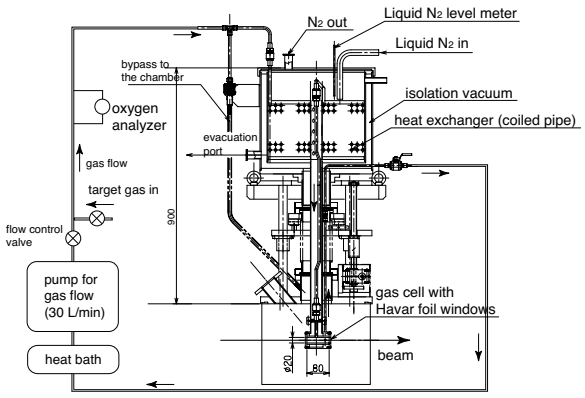

Fig. 1. Design of the cryogenic gas target system.

main features of the cryogenic gas target system are as follows.

(1) Liquid-nitrogen cooling
The target gas and window foils are cooled by liquid nitrogen. If the target is ideally cooled to the liquid nitrogen temperature (77 K), it is nearly four times thicker than a room temperature target at the same pressure. The low temperature is also desirable for stability against high power beams.

(2) Forced gas circulation
The target gas can be forced to flow using a circulation pump. It is known that the effective target thickness is reduced by irradiation with a high heat depositing beam. That is, when the heat deposition of the beam along the beam is greater than 10 mW/mm, the gas around the beam track is heated and the density of the target decreases[4]. We may be able to avoid the density-reduction effect to some extent, by maintaining the gas flow on the order of 10 standard liters per minute (slm). This feature is not implemented in the other cryogenic targets for the same purpose, such as the one at MARS[5,6].

(3) Oxygen concentration monitoring
When we circulate the hydrogen gas in the closed system, we have to be concerned with the possibility of an explosion, which can occur if air leaks into the system. Considering the explosive limits of hydrogen, the concentration of oxygen in the hydrogen gas must be lower than 5%. We have installed an oxygen analyzer for monitoring oxygen concentration during the experiment.

We performed some basic tests of the cryogenic target system producing an RI beam at CRIB. For details of CRIB and its magnets and detectors, refer to references[1–3]. In the test measurement, hydrogen gas at 760 Torr (at maximum) was used to produce RI beams. The primary beam used for production was $^{7}Li^{2+}$at 5.6 MeV per nucleon, with the maximum current of 2.7 eμA. The cryogenic target worked stably with this maximum current, which proves that the target can accept a heat load of 7.4 W (5.2 W in the hydrogen gas, the rest in the Havar window foils). The heat load was determined by measuring the maximum primary-beam current and primary-beam energy before and after the gas target. The cross section of the beam at the target was about 5 mm^2. The RI beam produced in this measurement was $^{7}Be^{4+}$at 4.0 MeV per nucleon. The target temperature was 85–90 K. The maximum target thickness in this measurement was 2.3 mg/cm^2, 3.3 times thicker than that at room temperature with the same pressure (760 Torr).

Figure 2 shows the production rates of the $^{7}Be^{4+}$ beam, measured for various primary-beam currents and circulation rates of the target gas. The production rates were normalized for the momentum acceptance of $\pm$3 %, and we confirmed that we can obtain an intense ^{7}Be beam of 2×10^{8} particles per second (pps) in the best cases. The primary-beam current was measured with a Faraday cup on the beam line.

For counting RI beams with a rate of up to around 10^{6} pps, we used a parallel-plate avalanche counter (PPAC)[7]. For beams with a much higher rate, we placed a thin (1 μm) gold foil in the beam line, and

*1 Center for Nuclear Study, Graduate School of Science, University of Tokyo
*2 School of Physics, The University of Edinburgh
*3 Department of Physics, Ewha Womans University

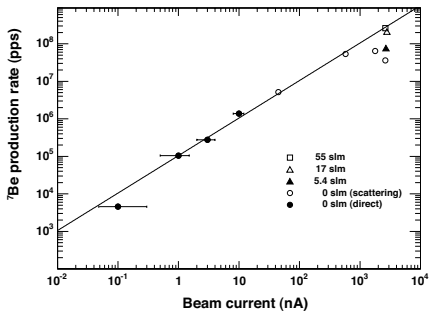

Fig. 2. Production rates of the $^7Be^{4+}$ beam measured for various primary beam currents and target gas circulation rates. For primary beams with currents less than 10 nA, the rates were directly measured with the PPAC (indicated as 'direct'). For higher current beams, the rates were determined by counting particles scattered elastically with a gold foil.

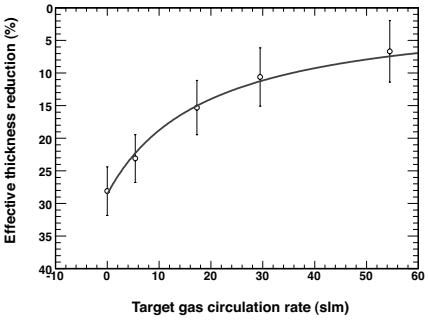

Fig. 3. Effective thickness (or density) reduction observed at the hydrogen gas target with the original thickness of 2.3 mg/cm^2 irradiated by the $^7Li^{2+}$ beam of 2.7 eμA. The reduction is denoted as the relative deviation from the original thickness, measured with a low-current beam. The error is mostly systematic.

detected elastically scattered beams with a silicon detector.

The results show a good linearity between the production rate and a primary beam current less than 1 eμA. The beam purity remained the same for this current region. However, when the beam current exceeded 1 eμA, the production rate deviated from the linearity, and the beam purity started to decrease. This is considered as the density-reduction effect caused by heat.

As we observed the beams with a fixed central momentum, the counting rate of $^7Be^{4+}$ decreases because of the following two effects, both arising when the target density is reduced. The first effect is simply the reduction of the number of the beam-production reactions, as it is nearly proportional to the target density. The second effect is the momentum shift of the produced beam. The central momentum of the beam becomes higher than that for the density without reduction, and significant portion of the beam will fall out of the momentum acceptance, optimized for low-current beam conditions.

We evaluated the second effect (momentum shift) using the counting rate, beam purity, and the relationship of the momentum and counting rate, all of which were measured in this test experiment. By excluding the second effect, the reduction of target thickness (or target density) caused from the heat deposition was calculated.

Figure 3 shows the reduction of the effective thickness against the original thickness, measured with the low-current beam, for several circulation rates. The primary beam current was around 2.7 eμA. The heat deposited from the beam was 5.2 W (corresponding to 65 mW/mm) in the gas and 2.2 W at the window foils. As shown in the figure, the target density decreased by about 30 %, when there was no gas circulation. This amount of reduction agrees with the previous measurement[4], which resulted in a reduction by 30 % for a beam of 60 mW/mm. These results illustrate that there is a density reduction effect, which could be minimized by circulating the target gas.

In summary, we obtained a very intense (2×10^8 pps) ^{7}Be beam, having the energy of (4.0 ± 0.2) MeV per nucleon. We have observed a reduction of the target density, probably due to the high heat deposition of the beam. The reduction was about 30 % at maximum, when the beam deposited heat of 65 mW/mm in the gas. We succeeded in reducing this reduction effect to about 5 % by circulating the gas at 55 slm.

References

1) S. Kubono, *et al.*: Eur. Phys. J. A **13** (2002) 217.
2) Y. Yanagisawa, *et al.*: Nucl. Instrum. Methods Phys. Res., Sect. A **539** (2005) 74–83.
3) T. Teranishi, *et al.*: Phys. Lett. B **556** (2003) 27–32.
4) J. Göerres, *et al.*: Nucl. Instrum. Methods Phys. Res **177** (1980) 295.
5) D. Semon, *et al.*: Phys. Rev. C **53** (1996) 96–105.
6) A. Azhari, *et al.*: Phys. Rev. C **63** (2001) 055803.
7) H. Kumagai, *et al.*: Nucl. Instrum. Methods Phys. Res., Sect. A **470** (2001) 562.

Development of 1-mm-thick solid hydrogen target

K. Tanaka, Y. Matsuda,[*1] S. Ishimoto,[*2] K. Ozeki, H. Sakaguchi,[*3] S. Suzuki,[*2] H. Takeda, S. Terashima, and J. Zenihiro[*4]

We have developed a solid hydrogen target (SHT) system for a project on the elastic scattering of protons with RI beams (ESPRI)[1]. The elastic scattering of radioactive nuclei can be measured through an inverse kinematics method by detecting the scattered protons from the SHT. To identify the elastic scattering, the ground state of the nuclei must be separated from any excited states clearly. Therefore, a thin SHT is necessary because the multiple scattering, energy loss and energy straggling of the recoiled protons inside the target reduce the resolution of the level energy of projectile nuclei[2]. Although we have made 3 $\sim$ 5-mm-thick SHTs previously, the use of a thinner SHT was demanded in an elastic scattering experiment for a ^{20}O nucleus[1]. We have attempted to prepare a 1-mm-thick SHT with an almost the same setup for producing the 3 $\sim$ 5-mm-thick SHTs; however, a hole has been formed in the solid hydrogen[1]. In the present study, we improved the SHT setup to obtain a 1-mm-thick and 30-mm-diameter SHT with a thin beam window foil. The major refinements are the improvement of heat transfer with aluminum foil, the inhibition of the inflow of heat through a press machinery for the beam window foil, and a more reliable measurement of window foil swelling than that in the previous setup[1] with a laser displacement sensor and an opaque film.

There was a possibility that radiation heat makes a hole in the solid hydrogen. Compared with the 3 $\sim$ 5-mm-thick of SHT, the 1-mm-thick SHT is thin; thus, it has a small path for transfering the inflowing heat. Moreover, because the heat conductivity of solid hydrogen ($\leq$ 1 W/m K) is lower than that of Cu ($\sim$1000 W/m K at 10 K), the heat flowing into the 1-mm-thick SHT was not removed to a copper cell sufficiently. To compensate the small efficiency of the thin SHT for transfering heat inflow on the SHT, we put a 100 μm aluminum foil, which has a high heat conductivity ($\leq\sim$ 2000 W/m K at $\sim$ 10 K, depending on the purity of aluminum materials), on the upstream side of the cell, as shown in Fig. 1. The aluminum foil was glued with an epoxy adhesive agent on the copper cell. However, it was easily peeled off at low temperatures because the rates of thermal expansion of aluminum foil, copper cell, and epoxy adhesive are different. To seal the cell, a 9-μm-thin aramid film was put onto the aluminum foil and glued with the adhesive around the boundary of the aluminum foil. The adhesive was put between the copper cell, the aluminum foil and the aramid film. Care was taken not to put the agent where the beam passes through the SHT.

On the downstream side of the SHT, a 12-μm-thin aluminized Mylar foil was used as the beam window. Because the angular distribution of the recoiled protons for the downstream of the SHT is measured for the ESPRI experiment, a thin material is necessary for inhibiting the multiple scattering in the foil of the beam window. Therefore, a 100-μm-thick aluminum foil can't be used on the downstream side of the SHT. Using the 100-μm-thick aluminum foil on the upstream side of the SHT, the uniform SHT was successfully produced and kept for a few days.

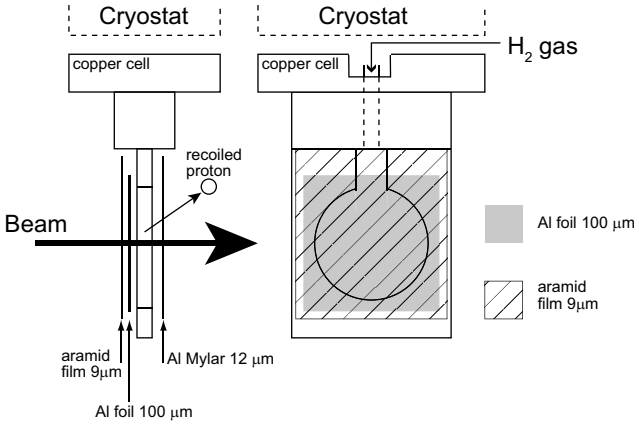

Fig. 1. Schematic view of the target cell for 1-mm-thick SHT. The diameter of the hole in the cell for the SHT was 30 mm.

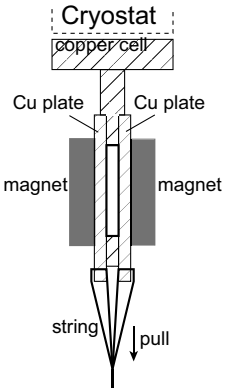

Fig. 2. Schematic view of the press machinery with the copper plate for preventing the swelling of window films.

To determine the cross sections of elastic scattering precisely, the flatness of the SHT surface is also important. However, the beam window foils swell when

*1 Department of Physics, Tohoku University
*2 High Energy Accelerator Research Organization (KEK)
*3 Department of Applied Physics, Miyazaki University
*4 Department of Physics, Kyoto University

hydrogen gas is allowed to flow into the cell. Thus, so far, we have set copper plates on both sides of the cell to press it to obtain a flat SHT. In the previous setup, the copper plates were pressed onto the cell using stainless-steel bellows, which were connected to the vacuum chamber at room temperature[1]. Because the heat inflow into the thin solid hydrogen through this setup could make a hole in it, we improved this press machinery to inhibit the inflow of heat. In this study, the previous bellows were replaced with magnet plates. The copper plates were the same as those in the previous setup. The plates and cell were sandwiched between two magnets, as shown in Fig. 2. Cotton strings were connected to the copper plates to pull down the copper plates after the solid hydrogen was formed, and then the copper plates and magnets were removed from the surface of the beam window foil to impinge ion beams. Due to the low heat conductivity and the small path for transfering the heat through the cotton strings, the amount of heat inflowed through this press machinery decreased compared with that in the previous setup. Before hydrogen gas flowed into the cell, the temperatures of the cell and plate were ∼5 K and ∼7 K, respectively. On the other hand, their temperatures in the previous setup were ∼5 K and ∼60 K, respectively, under the same conditions[1]. Using this improved press machinery, the SHT without window foil swelling was produced successfully.

The flatness of the downstream side of the target was confirmed using a laser displacement sensor KEYENCE LK-500. Figure 3 shows the setup for the flatness measurement. We measured the distance between the laser sensor and the surfaces of the SHT and cell, and then scanned horizontally along the horizontal center line of the SHT and cell. Because a transparent window did not reflect the laser light well, we used a 12-μm-thick aluminized Mylar foil. Additionally, in order to check whether a hole exists in the solid hydrogen, part of the aluminum layer on the window foil at the center and its longitudinal direction was stripped off. The surface of the SHT was flat within a 0.1 mm accuracy, as shown in Fig. 4. Owing to the structure of the vacuum chamber of the SHT, the laser sensor could not be installed on the upstream side of the cell; thus, the flatness of the upstream side of the SHT was not measured in this study. However, the total strength of the aramid film and aluminum foil is larger than that of the film of the downstream side. Therefore, we assumed the same flatness for both sides. With this setup, the existence of the uniform SHT was confirmed and the flatness was measured simultaneously.

In summary, we have developed an SHT of 1 mm thickness and 30 mm diameter successfully. Using the aluminum foil located upstream of the target cell, the efficiency of heat transfer was increased and holes were not included in the solid hydrogen. To obtain a flat SHT, the copper plates covered both sides of the cell to press the beam window foil. The flatness was confirmed with a laser displacement sensor. Because the aluminum foil glued upstream of the SHT provides some background of scattered protons, further improvements for reducing the background are under way.

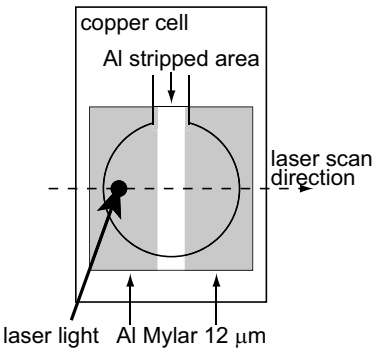

Fig. 3. Schematic view of the downstream side of the copper cell and the principle of the laser measurement for the flatness of the beam window foil. The laser sensor was scanned horizontally. Part of the aluminum layer was stripped to observe the solid hydrogen.

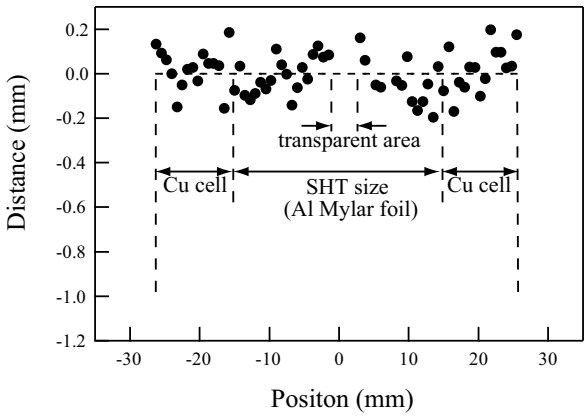

Fig. 4. Results of the flatness measurement of the beam window foil. The horizontal axis denotes the position along the target. The vertical axis denotes the displacement of the cell surface. At the center of the aluminum Mylar window foil, the foil was transparent because the aluminum layer was stripped and then the measurement was made impossible.

- - - - -

References

1) H. Takeda et al.: RIKEN Accel. Prog. Rep. **40**, 161 (2006).
2) S. Terashima et al.: RIKEN Accel. Prog. Rep. **40**, 18 (2006).

Application of Cryotarget to Laser ion Source†

J. Tamura,*1 M. Okamura,*2 and T. Kanesue,*3

We examined laser-produced plasma from rare gas target as part of a future laser ion source[1]. Features of various heavy ion generations using a pulsed laser have been studied. However, gaseous material at room temperature has not been able to be used as a laser ion source target because rare gases, which are in gas state at room temperature, need to be cooled to solid targets for laser irradiation.

We solidified Ne gas and Ar gas with a Gifford McMahon cryocooler which can cool down to 43 K at the first stage with a cooling capacity of 50 W and to 4.2 K at the second stage with the capacity of 1 W. The cryocooler cold head was placed inside of the target chamber. The rare gases are sprayed directly into a cooled volume attached to the second stage. The laser spot area was covered by a 0.08mm thickness Ta sheet to decrease damages from direct laser exposure. By irradiating the ice with a Nd:YAG laser, we could generate Ne plasma and Ar plasma. The ion currents of the plasma were measured by a Faraday cup located 2.3 m from the target. The charge state distributions of the plasma were measured by electrostatic ion analyzer located 3.7m from the target.

The obtained ion currents and its charge distributions of Ne plasma and Ar Plasma are shown in Fig. 1 and Fig. 2, respectively. The peak values of ion current density reached 1.2 mA/cm^2 for Ne and 1.6 mA/cm^2 for Ar at Faraday cup position, respectively. To explore the laser irradiation condition, the laser power and the position of the focusing lens were varied. For all the conditions, higher ionized particles expand with the higher kinetic energies and leading edges of pulse are closely related to the laser power density. The large ratio of the highly charged particle makes the plasma pulse length shorter.

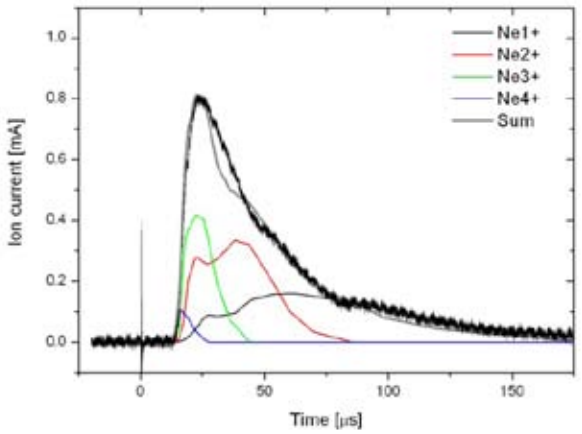

Fig. 1. Ion currents of Ne plasma at Faraday cup position. This was obtained from the laser irradiation condition with pulse energy of 1200 mJ, FWHM of 12 ns and irradiation diameter of 2.2 mm.

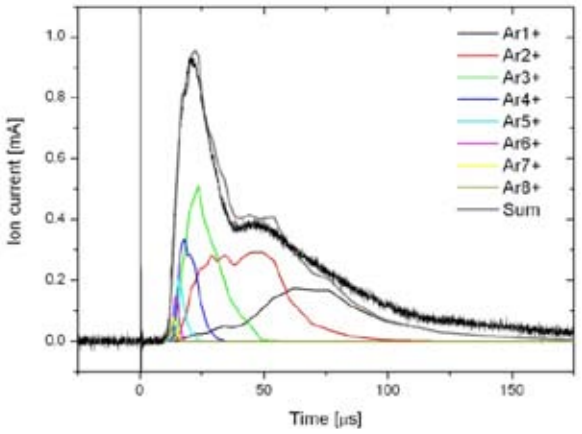

Fig. 2. Ion currents of Ar plasma at Faraday cup position. This was obtained from the laser irradiation condition with pulse energy of 1200mJ, FWHM of 6ns, irradiation diameter of 2.2mm.

We studied the effect of the thickness of the solidified target on the property of the laser plasma. There was almost no variation, although we changed the repetition rate of laser shots. It seems that only the surface layer might contribute to the plasma production. Above 1 Hz operation of laser shot, the plasma pulse shape shifted to a solid Ta plasma's shape. Also we tried to move the position of the gas feed nozzle, however we could not observe significant change of the plasma. The current and the charge state distribution were stable. The residual gas around the cooled area can be captured and is accumulated enough to provide the laser plasma with reasonable repetition rate.

We confirmed that a solidified rare gas with a 4 K cryocooler can be used as a laser ion source target driven by a Nd:YAG laser. Damages or corrosion of the optical device was not observed. If we apply the plasma to a direct plasma injection scheme[2], the expected injection current will be more than 100 mA.

---

† Condensed from the article in Rev. Sci. Instrum. **79**, 1 (2008)

*1 Department of Energy Sciences, Tokyo Institute of Technology
*2 Collider-Accelerator Department, Brookhaven National Laboratory
*3 Department of Applied Quantum Pnysics, Kyushu University

References

1) J. Tamura, M. Okamura, T. Kanesue, and S. Kondrashev, Appl. Phys. Lett. **91**, 041504 (2007).
2) H. Kashiwagi, M. Fukuda, M. Okamura, R. A. Jameson, T. Hattori, N. Hayashizaki, K. Sakakibara, J. Takano, K. Yamamoto, Y. Iwata, and T. Fujimono, Rev. Sci. Instrum. **77**, 03B305 (2006).

Performance of Polarized Proton Target in $\vec{p} + {}^8$He Scattering Experiment

T. Kawahara,[*1] T. Uesaka,[*2] T. Wakui,[*3] and S. Sakaguchi[*2]

1 Introduction

A polarized proton target for RI beam experiments has been developed at CNS[1)]. The target is operated in a low magnetic field (0.01-0.3 T) and at a high temperature (77-300 K). Protons in the crystal of aromatic molecules are polarized by the method described in Ref 1. In the first step, we excite electrons with laser light, and produce a large population difference in excited triplet states of pentacen molecules. This population difference is transferred to proton polarization by microwave irradiation.

The polarized proton solid target was applied to RI beam experiments in 2003 and 2005, during which analyzing power for $\vec{p} + {}^6$He scattering was measured at the RIKEN projectile fragment separator (RIPS). The average proton polarization was 11.5% in 2005[2)].

In order to reduce statistical errors in scattering experiments, improvement of proton polarization is crucially important. From previous studies, it is expected that the polarization is limited by the low intensity of optical excitation power. To improve optical excitation power, we have increased repetition rate and pulse width. As a result, we have succeeded in obtaining higher proton polarization.

The improved polarized proton target system was applied to a $\vec{p} + {}^8$He scattering experiment in 2007[4)]. We also mention a newly discovered phenomenon in the reversal of polarization.

2 Enhancement of optical power

Protons are polarized by repeating the optical excitation of pentacene molecules using a pulsed laser and by polarization transfer. Polarization transfer is carried out by magnetic field sweeping during microwave irradiation. These process were repeated at 2 kHz in previous studies. Repetition rate had been limited by the magnetic field sweeping system.

In the magnetic field sweeping system, current is supplied to the coil by a voltage-current(V-I) converter circuit with a high-power OpAmp PA05 (APEX). As shown in Fig. 1(a), the circuit in previous studies included an element called the Q-snabber to prevent unwanted oscillation. Since a portion of current flows into the Q-snabber, increase in frequency causes damage to the circuit due to heating of the Q-snabber. Thus the repetition rate was limited at about 2 kHz. In order to use frequencies higher than the limit, we have reconfigured the circuit design, as shown in Fig. 1(b), and stabilized the circuit without the Q-snabber. This circuit works at the repetition rate of up to several kHz.

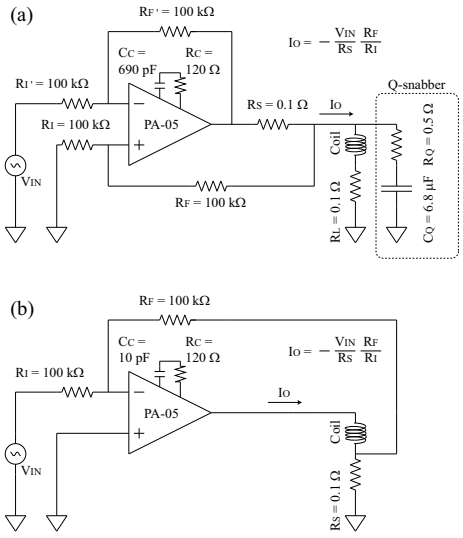

Fig. 1. Schematic view of V-I converter circuit (a) old circuit used in 2005 (b) new circuit developed in 2007.

The entire system can be operated at a repetition rate of 2.6 kHz. At this moment, the repetition rate is limited by the optical chopper used to chop the light of a constant-wave laser. The repetition rate will be increased by introducing another laser or optical chopper.

The pulse width of the laser was 20 μsec in experiments in 2003 and 2005. From the evaluation of optimum pulse width described in Ref. 1, it is expected that a longer pulse width leads to higher proton polarization. We have measured proton polarization using a pulsed laser light with different pulse widths. Figure 2(a) shows the time course of development of polarization during a $\vec{p} + {}^8$He scattering experiment in 2007. Pulse width changed during t=500-2500 min, as shown in Fig. 2(b). Here, four different widths (50, 32, 40, and 65 μsec) were tried. We operated the polarized system at a pulse width of 65 μsec after 2500 hours. A longer pulse width was not tried to avoid the depolarization effect caused by laser damage.

*1 Department of Physics, Toho University
*2 Center for Nuclear Study, Graduate School of Science, University of Tokyo
*3 Cyclotron and Radioisotope Center, Tohoku University

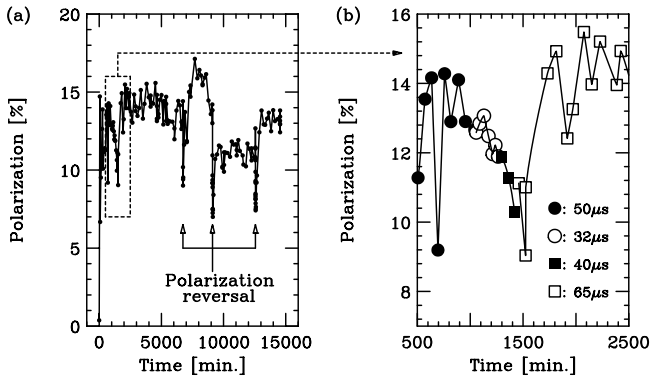

Fig. 2. Time course of development of polarization during $\vec{p}+{}^{8}$He scattering experiment

3 Target performance in $\vec{p}+{}^{8}$He scattering experiment

The time course of development of proton polarization during the $\vec{p}+{}^{8}$He scattering experiment is shown in Fig. 2. The average proton polarization was 11.1%.

We compare the pumping parameters and polarization achieved in the previous experiment (2005) and that in the $\vec{p}+{}^{8}$He scattering experiment (2007), as shown in Table 1.

Table 1. Comparison of optical parameters and polarization in $\vec{p}+{}^{6}$He scattering experiment in 2005 and $\vec{p}+{}^{8}$He scattering experiment in 2007.

	$\vec{p}+{}^{6}$He	$\vec{p}+{}^{8}$He
Laser power	22 W	18 W
Repetition rate	2 kHz	2.6 kHz
Pulse width	20 μsec	65 μsec
Average polarization	11.5±2.5%	11.1±2.5%

This polarization system was operated using two Ar-ion lasers in 2005. Each laser was driven at a repetition rate of 1 kHz, resulting in 2 kHz in total. In 2007, we operated the polarization system with one Ar-ion laser at 2.6 kHz. Although the laser power was reduced, a comparable polarization was obtained owing to the higher repetition rate of 2.6 kHz and the longer pulse width.

4 Polarization reversal

We succeeded in reversing polarization by the 180° pulse NMR method during the $\vec{p}+{}^{6}$He scattering experiment in 2005[4]. The efficiency of polarization reversal was 60%. There is a possibility of further improvement of reversal efficiency. For this purpose, we studied the spin reversal phenomenon in detail. The dependence of polarization immediately after the reversal was measured. We observed this interesting phenomenon when polarization decreases in a time constant of 15 min. This time constant is markedly different from those of spin-spin relaxation and spin-lattice relaxation. This phenomenon may be related to spin defusion. Further study will be carried out on this phenomenon.

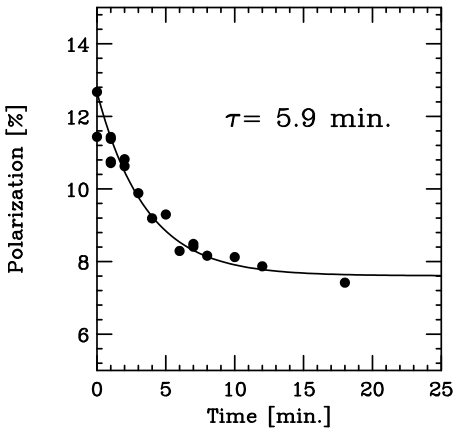

Fig. 3. Time course of development of polarization after reversal.

5 Summary and perspective

We have succeeded in increasing the repetition rate of the polarization process up to 2.6 kHz by improving a V-I converter. The improved polarized proton solid target system was applied to the $\vec{p}+{}^{8}$He scattering experiment in 2007. The average proton polarization was 11.1±2.5%. The laser pulse width was extended to 65 μsec for higher polarization. The repetition rate can be increased at least by a factor of two by introducing of a high-speed optical chopper.

We also discovered a new phenomenon that polarization decreases after the polarization reversal. We will study the origin of this phenomenon to improve efficiency of the polarization reversal.

References

1) T. Wakui, *et al.*: Nuclear Instruments and Methods in Physics Research A **550** (2005) 521,
2) S. Sakaguchi, *et al.*: RIKEN Accelerator Progress Report vol. 40 (2006).
3) S. Sakaguchi, *et al.*: RIKEN Accelerator Progress Report vol. 41 (2007).
4) T. Kawahara, *et al.*: RIKEN Accelerator Progress Report vol. 40 (2006).

Development of a super-segmented beta-counting system CAITEN†

S. Nishimura, M. Kurata-Nishimura, S. Bishop, M. Matsushita,*1 K. Ieki, *1 and H. Sakurai

[scintillation detector, beta-decay, unstable nuclei]

A new project, RIBF, has begun and has successfully demonstrated its high production yield of very neutron-rich nuclei using an intense uranium beam. β-decay study of those nuclei is one of the major methods to clarify on their nuclear structure. It is also expected to provide half-lives of neutron-rich nuclei, which play an important role in the study of the astrophysical r-process in supernova explosions.

From the practical point of view, it is required to perform decay experiments at an extremely low production yield of r-process nuclei in the cocktail beam environment. Thus, we have designed a new beta-counting system "CAITEN" dedicated for half-life measurements of rare isotopes using a novel technique[1,2]. The system CAITEN comprises two primary subsystems. One is a large cylindrical plastic scintillator (CPS: ϕ500mm $\times$ 1000mm, 20mm^t) as an active implantation target. Another is twenty-four position-sensitive photomultiplier-tubes (PSPMT: Hamamatsu H8500) array arranged inside the CPS (See Figure 1a).

The CPS consists of 4×10^5 scintillator pixels (REXON RP-408: 6x6x20mm^3 x 4×10^5) glued on a cylindrical plastic tube and this arrangement is mounted on two rotating rims. Here, the system CAITEN is designed to move the CPS vertically at a beam height (170 cm $\pm$ 50 cm) synchronized together with rotating motion at a speed of 0 $\sim$ 180 rpm using two independent stepping motors controlled by a programmable sequencer system. The idea is to reduce the density of nonassociated decay events from the previously implanted nuclei remaining in the CPS by distributing accumulated nuclei on the entire CPS surface.

The positions and timings of implanted ions and their associated decay events are measured by reconstructing the scintillation images projected on the PSPMTs. Here, the PSPMTs are supported independently and are floating inside the CPS at the beam height without having physical contact with the CPS. The segmented light guides, in the shape of cylindrical caps, are attached onto the PSPMT to minimize the air-gap distance from the inner surface of the CPS ($\sim$ 4 mm) for accurate position measurement of decay events (See Figure 1b). A compact resistive-chain electric circuit with an optional daisy chain connection to the neighboring PSPMTs is designed and is attached for each PSPMT for masked reduction of readout channels. A trigger signal is extracted by discriminating the positive signal from each H8500 dynode. The pulse height of the integrated anode signals from the PSPMTs are amplified using fast amplifiers and are measured using CAMAC ADC (Phillips H7166) to deduce position information.

We have installed the PSPMTs and CPS in the CAITEN. The mechanical control has been tested by rotating the CPS at a realistic speed. The optimization of the CAITEN is in progress using beta sources (^{90}Sr and ^{207}Bi).

References
1) S. Nishimura, et al.: Nucl. Phys. **A 718**, 214c (2003).
2) S. Nishimura, et al.: OMEG 2003, World Scientific (2003) 304.

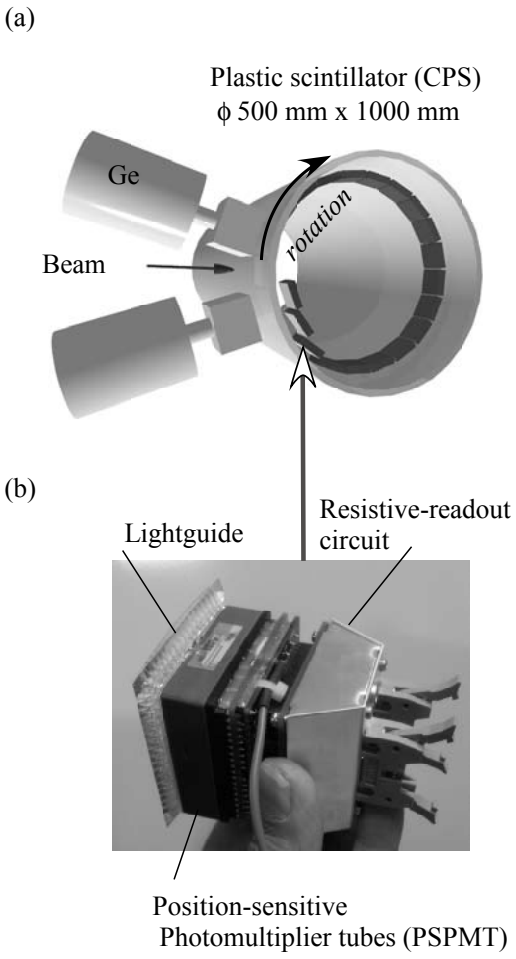

Fig. 1. (a) Schematic of CAITEN with CPS. (b) PSPMT with segmented light guide and resistive-readout circuit.

† Supported by RIKEN President's Discretionary Fund
*1 Rikkyo University

Drift and extraction of ^{16}N stopped in neon gas

A. Yoshimi, H. Ueno, T. Sugimoto,[*1] K. Shimada,[*2] D. Nagae,[*3] J. Murata[*4], H. Kawamura[*4] and K. Asahi [*5]

The stopping of an unstable nuclear beam in a gas catcher and its extraction into a vacuum area are considered to be important for next-generation RI-beam facilities. We have developed a gas catcher and an ion-guide system for an atomic beam resonance method with RI beams (RIABR) [1]. We have used neon gas as a stopping material, which has a stopping power larger than that of the widely used helium. There is no experimental data for gas catcher experiments with neon gas; thus, we attempted to stop the produced RI beam in neon gas and to drift the stopped RI ions by the DC electric field in the gas, and to extract the drifted RI ions into the vacuum area.

An RI beam of ^{16}N ($T_{1/2}$=7.13 s) was produced in this experiment at the Cyclotron Radio Isotope Center of Tohoku University. A primary beam of ^{15}N from the AVF cyclotron bombarded a CD_2 target to produce ^{16}N by the d(^{15}N, ^{16}N)p reaction. The ^{16}N with an emission angle of 1.2° – 2.6° was introduced into a stopping chamber filled with neon gas in order to reject the intense primary ^{15}N beam[2]. Figure 1 shows the stopping chamber and detector system. The incoming ^{16}N beam was introduced through an aluminum foil window and stopped in the chamber filled with 200 Torr Ne gas[3]. Part of the stopped ^{16}N tends to exist as an ionic state in the neon gas; thus, such ions can be drifted by an electric field to the vicinity of an exit orifice (ϕ 1 mm) where a gas flow also assists them to spout out into a downstream extraction chamber. A DC electrode assembly, which consists of 33 thin aluminum discs with a 5 cm bore, produced a DC electric field of 8 V/cm to the stopped ^{16}N ions. A relatively high voltage of 200 V/cm was applied at the last disc just before the extraction orifice to converge the drifted ions. The drift of the ions can be directly observed by a two-layer β-telescope located beside the chamber. The first layer consists of five plastic counters for detecting the source position of β-rays. This telescope has a position resolution of 6 cm. The drift effect of ^{16}N ions can be measured by comparing the positions when the DC field is switched on/off.

Figure 2(a) shows a typical β-decay spectrum from ^{16}N stopped in the chamber measured by the telescope. Figure 2(b) shows a change in counting ratio at each position when the DC field is applied. From this spectrum a drift efficiency from upstream (1,2) to downstream (3,4) was estimated to be 3.0%. This indicates that 97 % of the stopped RI was neutralized, because the half-life of ^{16}N is sufficiently longer than the drifting time of 0.3 s. This efficiency will be further improved by purifying the

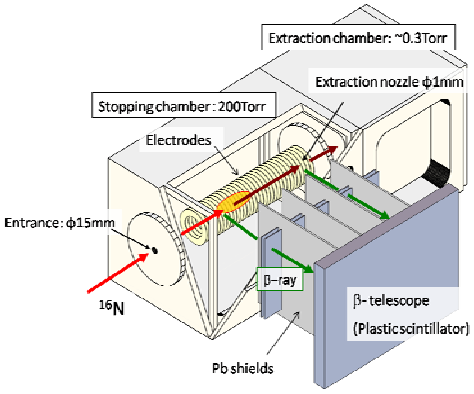

Fig. 1: Experimental setup for stop/drift/extraction of ^{16}N beam.

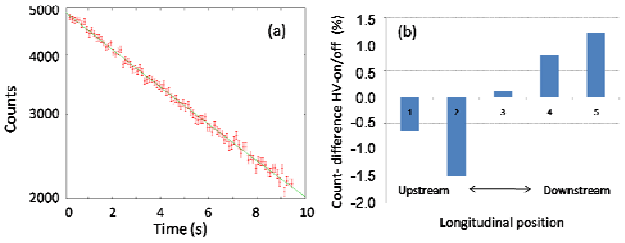

Fig. 2: (a) Beta-ray time spectrum measured by the β-telescope. (b) Difference of ^{16}N position distribution between DC field on- and off.

stopping gas and baking the stopping chamber to suppress the neutralization of the stopped RI ions. The extracted ^{16}N into the downstream chamber through a nozzle was also measured by counting β-rays from ^{16}N stopped in a stopper inside the extraction chamber. Although the extraction conditions, such as the DC field gradient before the nozzle, nozzle shape and the introduction of an RF ion guide, were not optimized, the total transmission efficiency was measured to be about 10^{-3}. This total efficiency is consistent with the observed drift efficiency and the simulation with the arrangement of the electric field. Although the extracted RI beam of about 10 pps at the vacuum chamber in this experiment is not sufficient for the development of RIABR, improvement will be performed on the basis of the obtained data.

References

1) A. Yoshimi et al.: AIP Conf. Proc. **915**, 849 (2007).
2) T. Sugimoto et al.: RIKEN Accel. Prog. Rep. **40**, 145 (2007) .
3) K. Shimada et al.: RIKEN Accel. Prog. Rep. **39**, 156 (2006).

[*1] Japan Synchrotron Radiation Research Institute （JASRI）
[*2] CYRIC, Tohoku University
[*3] Japan Atomic Energy Research Institute
[*4] Department of Physics, Rikkyo University
[*5] Department of Physics, Tokyo Institute of Technology

Development of silicon-strip detector with wide-dynamic-range readout system from 20 keV to 4 GeV†

N. Uematsu*1 and S. Nishimura*2

[Nuclear structure, shell model, unstable nuclei]

The study of very neutron rich nuclei, particularly by β and γ spectroscopy experiments, is important for shedding light on the nuclear structure near the drip line as well as for astrophysical research related to the r-process. We are now preparing an experiment using Ge semiconductor detectors in conjunction with double-sided silicon strip detectors (DSSD).

In the experiment it is necessary to stop the radioisotope nuclei in the DSSD and to efficiently detect the β particles from the stopped radioisotope. The energy deposits of the incident particles need to be measured for heavy nuclei in the DSSD with mass A $\sim$ 100 together with their associated beta particles. The expected energies of the incident particles introduced in the DSSD are expected to be up to $\sim$ 4 GeV, while β particles with energies below 20 keV must be detected simultaneously. At present, the preamp that we use can amplify energy up to about 600 MeV, because of its high gain. Thus we are currently modifying the existing readout system to cover a wide dynamic range of energies up to 4 GeV with adequate energy resolution. The overall performance of the readout system including the DSSD has been evaluated using a pulser and a β source.

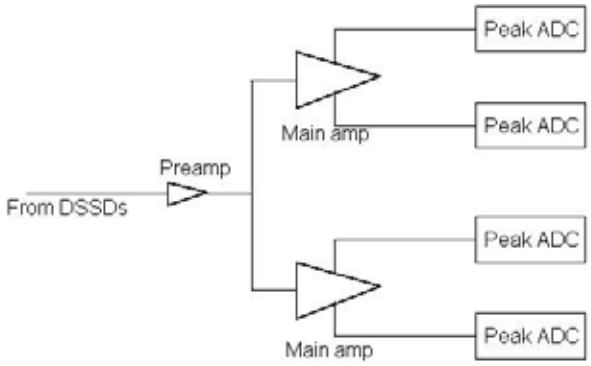

Fig. 1. Circuit diagram of new readout system. The input from DSSDs is divided in two ways after the preamp (CS AMP-3). We then use the two outputs of the main amps.

We now discuss two newly developed readout systems. The first readout system divides the dynamic range of the main amp. The ranges are from 20 keV to 40 MeV and from 4 MeV to 4 GeV to ensure adequate resolution of the readout systems. This is achieved by using main amps (CAEN N586B) with four different gains (×1, ×10, ×128, ×1280) (see Fig 1.). As a result the resolution of each amp reached 1keV/ch, 10keV/ch, 100keV/ch and 1MeV/ch, respectively. If the signal is saturated in the higher gain, the lower gain will take over to read out the signals. However, there is a disadvantage of using four samps because we need read out with good resolution.

The performance of this readout system has been tested using a 5.4 MeV α ray of ^{241}Am for energy calibration and further tested at higher energies using a pulser. A larger feedback capacitance, which decrease the gain of the preamp, is applied to the pre amp for measurement at higher energies. The results show the

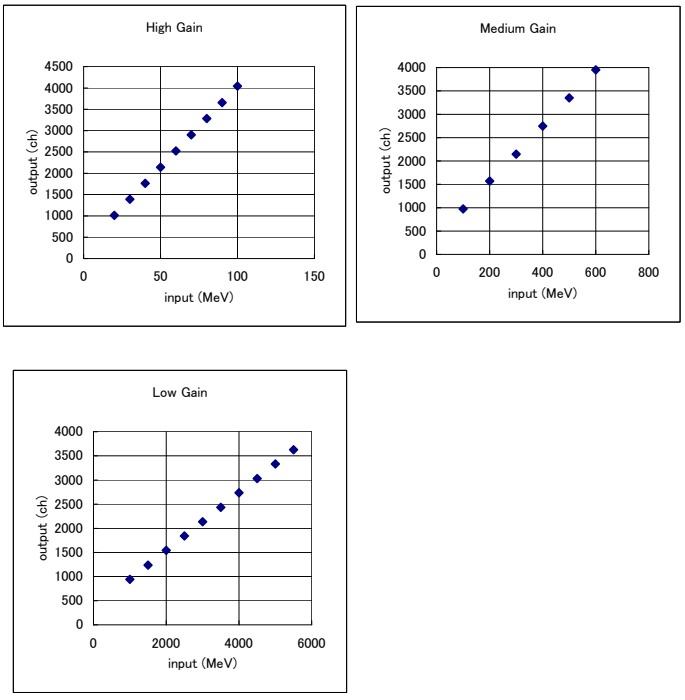

Fig. 2. Plots showing the linearity for different energy regions. The horizontal axis corresponds to input energy and the vertical axis shows the output channels using peak ADCs.

wide dynamic range of this readout system up to 4 GeV with adequate linearity throughout the energy range. The resolutions for the low-, medium-, and high- energy regions are evaluated to be 25 keV/ch, 152 keV/ch, and 1.5 MeV/ch, respectively(see Fig 2.). However, the noise for the low-energy region becomes larger from 20 keV to 120 keV, corresponding to a real-

*1 Tokyo Univ. of Science
*2 RIKEN

istic dynamic range of approximately 10^4. This effect is caused by the sensitivity of the preamp due to its lower amplification with larger feedback capacitance.

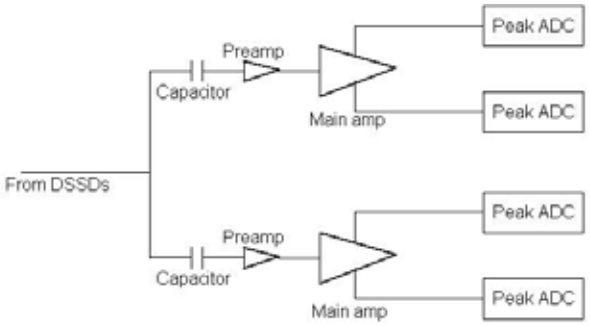

Fig. 3. Circuit diagram of the other readout system. The input from DSSDs is divided in two waya using different capacitors. We use same type of preamp. And we use the two outputs of the main amps. The capacitance is inserted into the cable core.

Instead of decreasing the gain of the preamp to cover the several GeV energy region, we have used a new system with parallel preamp readout (see Fig 3). Here, two independent preamps with different impedance circuits are prepared in order to transfer most of the charge ($\geq$ 98 %) for low-energy measurement, the remaining charge ($\leq$ 2 %) for higher-energy measurement. Considering the intrinsic capacitance and resistance for the DSSDs, effective charge collection in the readout system requires the selection of adequate capacitance ($\geq$ 10000 pF) for the high-gain part.
The results for an impedance ratio of 50 : 1 to cover low energies up to 80 MeV and higher energy up to 4 GeV are shown in Fig 4 respectively. According to our results, there is a sudden change the gain factor for the medium gain and low gain at an energy $\sim$ 500 MeV. This is caused by the saturation of the preamp in the high-gain line, where the balance of the charge transfer into two parallel lines is broken. However, a lower energy threshold of less than 60 keV was achieved. We also attempted to split the signals into two different resistances instead of two different capacitances. However, the pulse height appeared to be lower than in the case of two different capacitance, i.e, there was less sensitivity the lower-energy region.

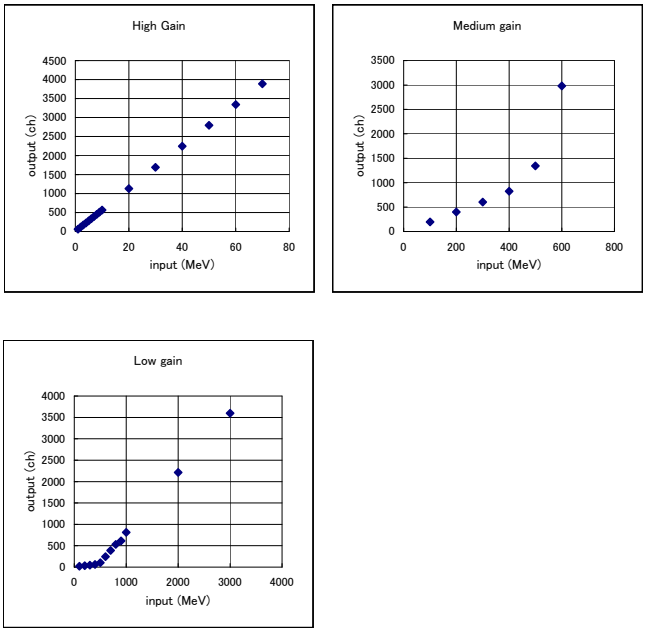

Fig. 4. Linearity of each readout line with different amplifications. The horizontal axis corresponds to input energy and the vertical axis shows the readout value in the channel using peak ADCs.

We have developed and investigated the performance of two readout methods. One uses a single preamp with lower amplification. The other uses two parallel preamps with different impedances. Although the first method exhibits good linearity in the entire region of energy for the dynamic range, we could not obtain adequate sensitivity below 100 keV for a dynamic range of about 10^4. However, the second method has a large dynamic range of $\sim 10^5$ at the expense of nonlinearity around 500 MeV. The overall performance of these methods will be investigated using a real beam in future.

Estimation of photon numbers detected in OROCHI experiment

T. Furukawa, Y. Matsuo, A. Hatakeyama,[*1] T. Ito,[*2] K. Fujikake,[*2] T. Kobayashi, and T. Shimoda[*3]

We have been developing a new laser spectroscopic method, *OROCHI*, which is an abbreviation of "Optical RI atom Observation in Condensed HelIum," with the aim of establishing a versatile method for determining the nuclear spins and moments of unstable nuclei,[1] based on the combination of superfluid helium (He II) as a stopper of the RI beam and the *in situ* laser spectroscopy of RI atoms stopped in He II to detect the laser-induced fluorescence (LIF) photons.[2] Recently, we have demonstrated that nuclear spins and moments are obtained from the measurement of Zeeman and hyperfine splittings of atoms using the laser-radiowave (RF)/microwave (MW) double-resonance method with our OROCHI technique.[3] The remaining issue to be addressed is the estimation of the RI yields required in the OROCHI experiments. In this report, we describe the estimation of the required RI yield, taking alkali Rb atoms as an example.

The LIF photon intensity emitted from one atom in He II can be estimated from the photoabsorption cross section of the atom. The cross section of the $D1$ absorption line of Rb atoms in He II is given as

$$\sigma(\nu_0) = \frac{c^2}{8\pi^2\nu_0^2} \cdot \frac{A}{\Delta\nu/2} = 1.4 \times 10^{-15}(\mathrm{cm}^2), \qquad (1)$$

where A=36.1 MHz is Einstein's A coefficient for the Rb atoms, ν_0=385.6 THz (=778.0 nm) is a peak frequency of the absorption spectrum, and $\Delta\nu$=4.0 THz is the FWHM.[4] We assume here that $\sigma(\nu)$ in the pumping laser line is constant because the absorption linewidth (4.0 THz) is sufficiently larger than the laser linewidth (10 GHz). Then the photon emission rate Γ from one atom irradiated with the pumping laser (power density: 100 mW/mm^2) can be obtained from the photon number density of the pumping laser I_l as

$$\Gamma = I_l \cdot \sigma(\nu_0) = 5.1 \times 10^4(\mathrm{photons/s}). \qquad (2)$$

The detection rate of the photons emitted from the atoms in the observation region using the optical detection system, I_{det}, is given as

$$I_{det} = I_{RI} \cdot \tau \cdot \epsilon_{stp} \cdot \Gamma \cdot \Omega \cdot \epsilon_f \cdot \epsilon_{qe}, \qquad (3)$$

where I_{RI} is the RI beam intensity, τ and ϵ_{stp} are the lifetime and stopping probability of the RI atoms in the detection region, Ω and ϵ_f are the solid angle and transmission efficiency of the optical detection system, respectively, and ϵ_{qe} is the quantum efficiency of PMT.

Now we consider our measurement omit of the low-yield ^{100}Rb isotope (τ=51 ms, I_{RI}=10 pps from BigRIPS). Assuming that the stopped range of RI atoms in He II is distributed over approximately 3 mm when the spot size of the RI beam is 10 mm ϕ, and considering the conditions of the pumping laser irradiated perpendicular to the RI beam direction (power: 1 W, spot size: 3 mm ϕ), 30% of the stopped RI atoms is pumped with a laser and then they emit LIF photons (i.e., ϵ_{stp}=0.3). The LIF photons are focused to the PMT (Hamamatsu Co.Ltd., R636-10, ϵ_{qe}: typically 10% at Rb $D1$-line LIF of 795 nm) through a set of lenses (spatial filter) and two interference filters (ϵ_f: total 10%) to reduce stray laser light. Note that the stray light is easily reduced by a factor of 10^{-5} by the interference filters because the photoabsorption line of atoms in He II is shifted 15 nm from their emission line. The first lens (diameter: 10 cm ϕ) is located 5 cm from the detection region, so that the solid angle of the detection system Ω is approximately 25%. From Eq. (3), the detection rate I_{det} is 19 counts/sec, which means that we can detect approximately two photons from one RI atom, which is much more efficient than the use of conventional laser spectroscopy ($\leq 10^{-3}$).

Figure 1 shows the simulated spectrum of ^{100}Rb microwave resonance expected in one day of measurement, with the assumptions that the spectrum shape is the same as that in our previous work,[3] the hyperfine splitting of the ground-state ^{100}Rb is equal to 3.0 GHz, and the background count rate is reduced to as low as 10 cps by the interference filters. The resonance peak can be clearly seen and the peak position is determined within 2 kHz error by simple Lorentz-shape fitting. This result suggests that we can actually determine the nuclear spin and moment of RI for a yield of 10 pps, which cannot be achieved by conventional methods. Note that the hyperfine resonance frequency of ^{100}Rb can be determined within 10 kHz error although the measurement time is only 1 h.

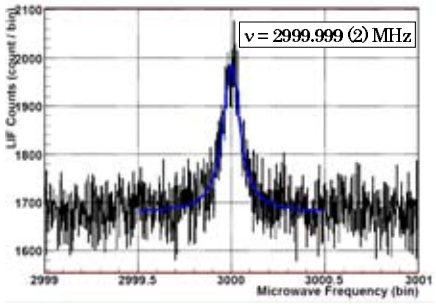

Fig. 1. Expected spectra in 1 day of measurement using ^{100}Rb beam (MW frequency sweep: 2999 - 3001 MHz).

*1 Dept. of Appl. Phys., Tokyo Univ. Agr. Tech.
*2 Inst. of Phys., Meiji University
*3 Dept. of Phys., Osaka University

References
1) T. Furukawa *et al.*: Proc. INPC07, in press.
2) T. Furukawa *et al.*: Phys. Rev. Lett. **96**, 095301 (2006).
3) T. Furukawa: Doctoral thesis, Osaka Univ. (2007).
4) Y. Takahashi *et al.*: Phys. Rev. Lett. **71**, 1035 (1993).

Network and Computing Environment for RIKEN Nishina Center

T. Ichihara, Y. Watanabe, K. Yoshida, and A. Yoshida

We have been operating Linux/Unix NIS/NFS cluster systems[1−2] at the Nishina Center. The host *RIBF* is used for the mail server and NFS server for the user home directory. Postfix is used for mail transport software and Dovecot is used for imap and pop services. These software packages enable secure and reliable mail delivery. The hosts *RIBFSMTP1* and *RIBFSMTP2* are new mail front-end servers used for tagging spam mails and isolating virus-infected mails. We have been using Spam Assassin and Sweep software in our previous mail server *RARFSMTP* and *RARFSMTP2*.[2] Since the number of spam mails has increased rapidly in recent years, occasional mail-delay problem have occurred with the CPU utilization limit. Therefore, we have replaced the software Spam Assassin and Sweep with Sophos Pure Message, which is approximately 30 times faster than the previous software. The host *RIBF00* is an ssh login server and a general-purpose computational server. In the host *RIBFDATA01*, 10 TB Fiber-channel RAID systems are served for data storage for the experiments.

For the off-line data analysis of the RIBF experiment, a prototype of the Storage Area Network (SAN) environment that shares common RAID storage via fiber-channel switches, has been installed and is being evaluated. Two sets of dual-core Opteron 1U servers and a 10 TB SATA Raid system have been installed for the development and backup of a data acquisition (DAQ) system for RIBF experiments[3].

The bandwidth of the Internet connection of RIKEN Wako campus was increased from 1 Gbps to 10 Gbps at the beginning of 2007. Therefore, a large amount of experimental data can be transferred over the Internet[4]. A data transfer rate of 340 MB/s (2.8 Gbps) has been observed between BNL and RIKEN RIBF over the Internet.

The internet streaming servers, *RIBF-WM*, which serves Windows Media streaming files, and *RIBF-QT*, which serves Quick Time streaming files, have been installed. The video recording files of the nuclear-physics series lectures[5] held at the Nishina Center have been archived and they can be accessed via the Internet Windows Media and Quick Time formats at a speed of 128 kbps, 512 kbps or 2 Mbps, depending on the conditions of the Internet connection of the client. To archive the presentations of the International Nuclear Physics Conference held at Tokyo (INPC2007), the web server *INPC2007* has been installed.

An anonymous ftp server, *FTP.RIKEN.JP*, is managed and operated at RIKEN Nishina Center. Since the server has become obsolete and is sometimes unstable, it has been replaced with a new server, SUN Enterprise V40z, which is equipped with four sets of 2.6 GHz dual-core Opteron CPUs and 16 GB Memory. A 10 TB SATA Raid system has been added to this server. Major Linux distributions are mirrored daily at ftp servers.

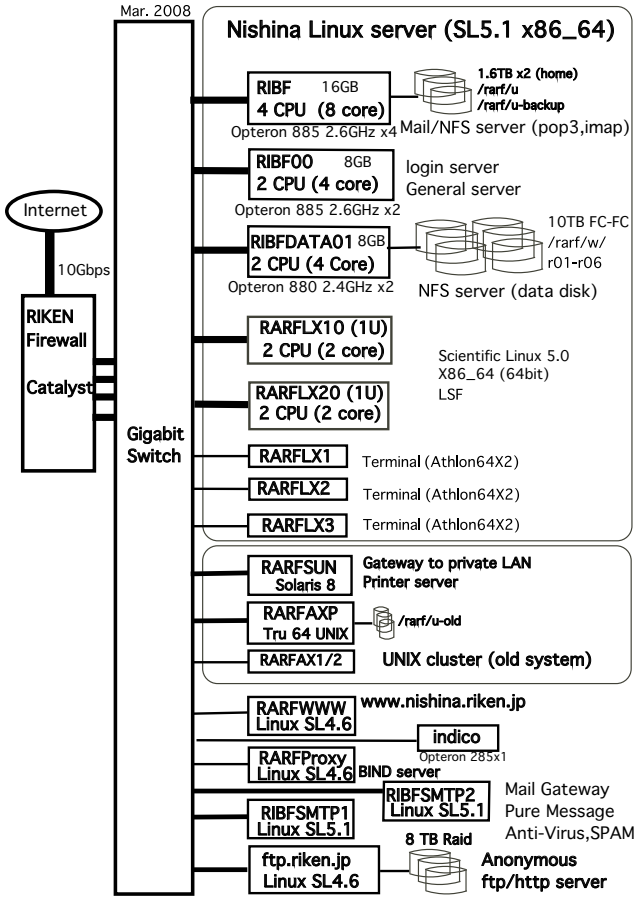

Fig. 1. Configuration of Linux/Unix server.

Figure 1 shows the current configuration of the Linux/Unix servers at Nishina Center. Most of the users of Nishina Center have e-mail addresses of the following forms:

username@ribf.riken.jp or *username@riken.jp*.

The former represents an e-mail address of the Nishina Center mail server (*RIBF*) and the latter represents an e-mail address of the RIKEN mail server.

References

1) *http://ribf.riken.jp/*
2) T. Ichihara et al. RIKEN Accel. Prog. Rep. 39 199 (2006).
3) H. Baba et al.: In this report.
4) S. Yokkaichi et al. In this report.
5) *http://www.nishina.riken.jp/video-lec/*

A new data acquisition system for RIBF

H. Baba, T. Ichihara T. Ohnishi, S. Takeuchi, K. Yoshida, Y. Watanabe, S. Ota,[*1] and S. Shimoura[*1]

A new data acquisition (DAQ) system for RIBF has been introduced. The features of this RIBF DAQ are listed as follows.

- Network distributed
- On-line event building and analysis
- Hierarchical event building
- Each detector section has a DAQ
- Parallel data readout from the CAMAC and VME modules
- Commodity hardware only (PC, OS, Ethernet, RAID, SAN, etc.)

The in-flight RI-beam separator named BigRIPS[1)] analyzes RI beams by using many beam profiling detectors placed at seven focal plane along the 77-meter-long beam line. Tagged RI beams impinge on the reaction target located at the end of BigRIPS. Downstream of the reaction target, various particle/gamma-ray detectors such as DALI[2)] and GRAPE,[3)] and several spectrometers such as ZeroDegree, SHARAQ, and SAMURAI are used. The detector section of BigRIPS is used in all experiments, but the use of the other detector section depends on the experimental conditions. Since experiments having different setups are performed one after another over several weeks, the DAQ system should have flexibility. It is important to change the combination of the DAQ for each section as quickly as possible. Therefore, we developed a new network-distributed DAQ system with the function of event building.

The configuration of the RIBF DAQ is shown in Fig. 1. The DAQ system is divided into each detector section such as BigRIPS, ZeroDegree, and DALI. The boxes represent computers. The boxes labeled CAMAC (VME) indicate CAMAC (VME) crates with a computer. Each detector section has its own event builder labeled 'slave event builder' in Fig. 1. Data obtained at the different sections are collected by the master event builder. In the stand-alone mode, each section works as an independent DAQ system.

For the event-building and analysis computers, Linux OS is used. On the other hand, RTLinux,[4)] which is a real-time expansion of Linux, is adopted for some of the front-end computers. Owing to the use of RTLinux, stable high-speed data readout is possible. For the data storage, a RAID system labeled 'storage' in Fig. 1 is installed in the storage area network (SAN). The event-builder and analyzer computers can access the RAID system at the same time via SAN. Data is processed by a software package called 'babirl DAQ'. It is newly developed and based on babarl DAQ[5–7)] which

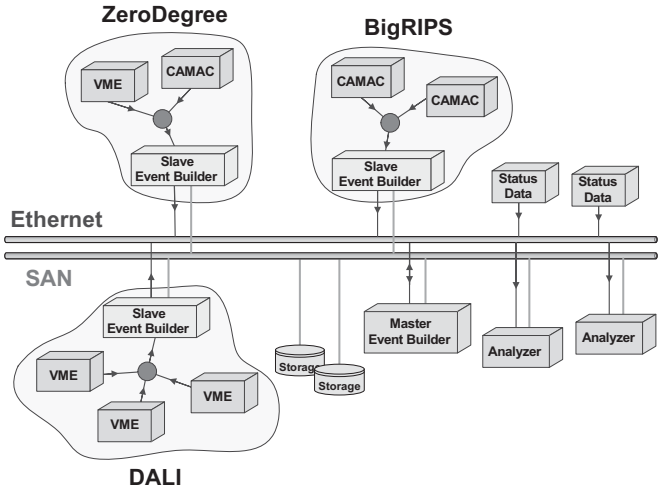

Fig. 1. The configuration of RIBF DAQ. The boxes are computers. The boxes labeled CAMAC (VME) are the front-end computers for CAMAC (VME).

was previously used at RIKEN RIPS and CRIB. The babirl DAQ package can deal with various CAMAC and VME controllers:

- CAMAC
  - TOYO CC/7700,
  - TOYO CC/NET,
  - Kinetic K3922,
- VME
  - SBS 620,
  - CAEN V2718,
  - Wiener VMEMM,
  - ADVME 8001,
  - VMIVME 7807.

In addition to CAMAC and VME, this system is able to treat data from the prototype Ubiquitous detector.[8,9)]

The data flow of this system is explained as follows. Data of the modules in each crate are collected by each CAMAC (VME) computer under the common trigger. This buffered data is called event-fragment data. The event-fragment data are transferred to slave event builder through the ethernet, and event-assembled-fragment data, which are the event data of its detector section, are built by using the event number individually counted by each CAMAC (VME) computer. To construct whole event data (event-assembled data), the slave event builder transfers event-assembled-fragment data to the master event builder. The event-assembled

*1 Center for Nuclear Study, University of Tokyo

data are stored in the storage system and transferred to the analyzer to analyze events online. An important feature is that the DAQ of each section can work as a stand-alone DAQ. Event-assembled-fragment data can also be stored in the storage system via SAN. The event builder treats not only event data but also comment data and status data such as the values of the scaler and magnetic fields of magnets and the high-voltage supply to the detectors. Status data are transferred to the event builder independently of experimental events, and are attached to the event-assembled data.

Owing to the parallel readout, the dead time of the new system is improved compared with the previous system. If the number of modules per CAMAC (VME) computer is small and the conversion times of all the modules are short enough, it is possible to achieve a dead time of less than 100 μs per event. Since it is necessary to distribute a common trigger to all CAMAC and VME modules, the dead time of the entire system depends on the CAMAC (VME) computer having the longest dead time.

The previous systems[5–7,10] use the RIKEN data format (RDF). For RIBF DAQ, a new raw-data format has been specified to satisfy the hierarchic structure and the undefined block length. It is named RIDF, which stands for RIBF data format. According to this data format, all data are stored as blocks. In some cases, blocks include other blocks as their contents. There are various types of blocks.

- Global block: contains the following blocks.
- Event block: contains a segment block and a scaler block.
- Segment block: contains acquired raw data.
- Scaler block: contains acquired scaler data.
- Status block: contains status data.
- Comment block: contains comments such as run information.

These blocks are indicated by the header words. Figure 2 shows the header rule of the RIDF. The meanings of the contents of the header word are listed below.

- Reserve bit (Re): These bits are not used at the moment.
- Layer (Ly): The layer shows the hierarchical relation of each block. Usually the layers of the global block, event block, and segment block are 0, 1, and 2, respectively.
- Class ID: Class ID is the identifier of the block.
- Size: Size is the block size including the header word in units of short word. The maximum size of one block is 8 MB; however, it is suggested less than 128 KB is used.
- Address: Address is the unique number of the computer.

The detail of RIDF is described in Ref. 11. The on-

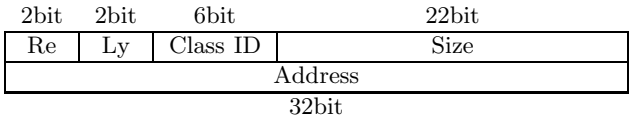

Fig. 2. The header rule of RIDF. The size of this header is 64 bits.

line/offline analysis program, ANAPAW,[5,7] which has been widely used for the analysis of RDF, has been extended to handle RIDF.

This RIBF DAQ has been operating since February 2007. Further developments of event building, analysis software, the device driver, and the status monitor are now in progress.

References

1) T. Kubo : Nucl. Inst. Meth. B **204**, 97 (2003).
2) S. Takeuchi et al.: RIKEN Accel. Prog. Rep. **36**, 148 (2003).
3) S. Shimoura et al.: Nucl. Inst. Meth. A **525**, 188 (2004).
4) M. Barabanov and V. Yodaiken: Linux Journal **34**, 19 (1997).
5) H. Baba et al.: RIKEN Accel. Prog. Rep. **34**, 221 (2001).
6) H. Baba and S. Shimoura: CNS Annual Report 2001, 53 (2002).
7) H. Baba et al.: RIKEN Accel. Prog. Rep. **37**, 187 (2004).
8) T. Watanabe et al.: RIKEN Accel. Prog. Rep. **40**, 193 (2007).
9) H. Baba et al.: RIKEN Accel. Prog. Rep. **40**, 193 (2007).
10) T. Ichihara et al.: IEEE Trans. Nucl. Sci. **36**, 1628 (1989).
11) H. Baba: RIBF DAQ Manual.

Run06 Polarization of Proton-Proton Operation at RHIC

C. Muñoz Camacho,[*1] I. Nakagawa, I. Alekseev,[*2] K. Boyle,[*3] A. Bravar,[*4] G. Bunce,[*5*6] S. Dhawan,[*7] A. Dion,[*3] K.O. Eyser,[*8] R. Gill,[*5] W. Haeberli,[*9] A. Hoffman,[*10] H. Huang,[*5] H. Liu,[*1] M.X. Liu,[*1] Y. Makdisi,[*5] H. Okada,[*5] K. Sakashita,[*11] E. Stephenson[*12] D.N. Svirida,[*2] T. Wise,[*9] J. Wood,[*5] and A. Zelenski[*4]

[polarized proton, silicon strip detector, RHIC, polarimeter, polarimetry, CNI, forward elastic scattering]

In 2006 the proton-carbon (pC) polarimeters at the Relativistic Heavy Ion Collider (RHIC) used a new target scan mode, with the measurements generally performed with vertical targets stepping in x (transverse horizontal coordinate) across the beam, with equal measurement time at each step. It allowed to measure horizontal polarization profile in each run separately (with limited statistical precision). Horizontal targets were used in a few measurements, which provided vertical polarization profile measurements.

On the first step of pC data analysis, two parameters, t_0 and dead layer (DL), were extracted for each strip in each measurement from the fit of the "banana" plot: the recoil Carbon time-of-flight (ToF) vs. energy. The DL parameter carries the meaning of "effective" dead layer and is used to correct the carbon deposited energy to obtain carbon kinetic energy[1)], and t_0 is a ToF offset. The list of quality checks (QA) included control of the width and position of the carbon (C) mass peak, as well as C mass peak position vs. its kinetic energy (which detects problems with the waveform digitizer, data adquisition and/or in the fit of "banana"), strip by strip variations of the number of events in the "banana" and consistency in bunch-by-bunch asymmetry measurements. All systematic uncertainties from the effects above were estimated to be negligible for the final fill-by-fill[a)] polarization measurements, except the energy correction effect (described by DL), which was defined to be 1.2%.

Since pC measurements, hydrogen jet measurements[2)] and RHIC experiments are each sensitive to different polarization averages across the beam (see Fig. 1), we need to measure (and then correct for) the polarization profile of each beam. The correction due to polarization profile depends on the ratio of widths of the beam intensity profile and beam polarization profile. It can be obtained by fitting the polarization vs. event rate in a scan by a function $P/P_{max} = (L/L_{max})^R$:

$$\left.\begin{aligned} L &= L_{max} \cdot e^{\frac{-x^2}{2\sigma_L^2}} \\ P &= P_{max} \cdot e^{\frac{-x^2}{2\sigma_P^2}} \end{aligned}\right\} \Rightarrow P = P_{max} \cdot (L/L_{max})^R . \quad (1)$$

Here it is assumed that both intensity and polarization profiles have gaussian shapes with widths σ_L and σ_P, correspondingly, and at least one point in the scan corresponds to beam maximum intensity; P_{max} and L_{max} are polarization and event rate at beam maximum intensity and $R = (\sigma_L/\sigma_P)^2$. This approach was used to extract the P_{max} and R parameters for each fill, which were used to calculate the average beam polarization for fixed mode (in order to normalize to hydrogen jet measurements) and for beams.

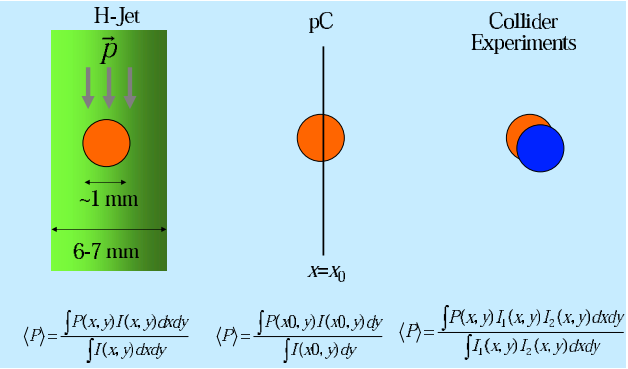

Fig. 1. Average polarization measured by hydrogen jet measurements[2)] (left), pC polarimeters (center) and collider experiments (right).

The polarization measured by the pC polarimeters $\widetilde{P_{pC}}$ in the scan mode are correlated with the peak polarization at the beam center (in both horizontal and vertical directions) P_{max}:

$$\widetilde{P_{pC}} = P_{max} \cdot C_{1X} \cdot C_{1Y} , \quad (2)$$

where C_{1X} and C_{1Y} are the profile correction factors for the horizontal and vertical directions, respectively.

*1 Los Alamos National Laboratory, Los Alamos, NM 87545
*2 Institute for Theoretical and Experimental Physics, Russia
*3 State University of New York - Stony Brook, Stony Brook, NY 11794
*4 University of Geneva, 1205 Geneva, Switzerland
*5 Brookhaven National Laboratory, USA
*6 RIKEN-BNL Research Center, BNL, USA
*7 Yale University, USA
*8 University of California, Riverside, USA
*9 University of Wisconsin, USA
*10 Massachusetts Institute of Technology, Cambridge, MA 02139
*11 Tokyo Institute of Technology, Tokyo 152-8551, Japan
*12 Indiana University Cyclotron Facility, USA

a) One fill correspond to the time the injected beams are stored in the accelerator rings, typically 6–7 hours.

Indeed,

$$C_{1X} = \frac{\int_{-\infty}^{\infty} dx\ \mathcal{P}(x)\ \mathcal{I}(x)}{\int_{-\infty}^{\infty} dx\ \mathcal{I}(x)} = \frac{\int_{-\infty}^{\infty} dx e^{-\frac{x^2}{2\sigma_L^2}} e^{-\frac{x^2}{2\sigma_P^2}}}{\int_{-\infty}^{\infty} dx e^{-\frac{x^2}{2\sigma_L^2}}} = \frac{1}{\sqrt{1+R}}\,, \quad (3)$$

and similarly for the vertical direction. On the other hand, the polarization profile needs to be weighted by both beam intensity profiles for the polarizations concerned by collider experiments P_{exp}:

$$P_{exp} = P_{max} \cdot C_{2X} \cdot C_{2Y} = \widetilde{P_{pC}} \cdot \frac{C_{2X}}{C_{1X}} \cdot \frac{C_{2Y}}{C_{1Y}}\,. \quad (4)$$

These profile corrections factors are given by:

$$C_{2X} = \frac{\int_{-\infty}^{\infty} dx\ \mathcal{P}(x)\ \mathcal{I}_1(x)\ \mathcal{I}_2(x)}{\int_{-\infty}^{\infty} dx\ \mathcal{I}_1(x)\ \mathcal{I}_2(x)}\,. \quad (5)$$

Assuming $\mathcal{I}_1(x) \approx \mathcal{I}_2(x)$, we can write:

$$C_{2X} = \frac{\int_{-\infty}^{\infty} dx\ \mathcal{P}(x)\ \mathcal{I}^2(x)}{\int_{-\infty}^{\infty} dx\ \mathcal{I}^2(x)} = \frac{1}{\sqrt{1+R/2}}\,, \quad (6)$$

and similarly for C_{2Y}. The ratio C_{2X}/C_{1X} is then given by:

$$\frac{C_{2X}}{C_{1X}} = \frac{\sqrt{1+R}}{\sqrt{1+R/2}} \approx \frac{1+R/2}{\sqrt{1+R/2}}\,, \quad (7)$$

valid for $R \ll 1$. Using the same approximations for the vertical direction, we can finally write:

$$P_{exp} = \widetilde{P_{pC}} \cdot \sqrt{1+R_X/2} \cdot \sqrt{1+R_Y/2}\,. \quad (8)$$

Fig. 2 shows final polarization results for Run06, with an average polarization value of 55%.

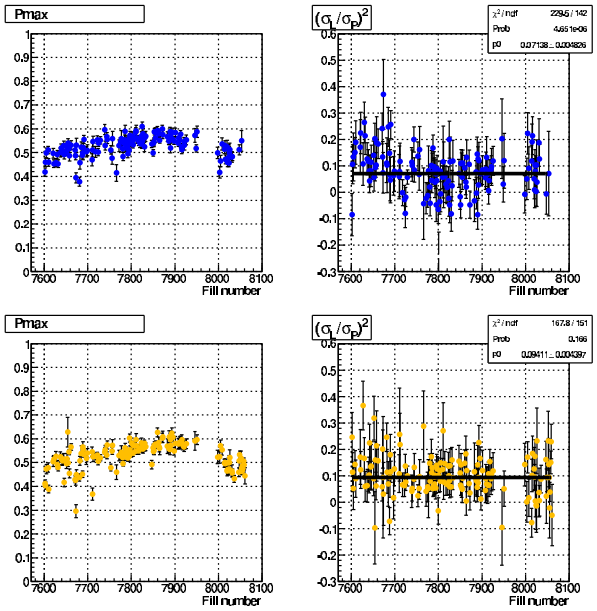

Fig. 2. Absolute polarization at beam maximum intensity (P_{max}) and profile ratio $R = (\sigma_L/\sigma_P)^2$ vs. fill number for both blue (top) and yellow (bottom) proton beams.

References

1) I. Nakagawa et al.: RIKEN Accel. Prog. Rep. **40**, (2007), and references therein.
2) K. Boyle et al.: RIKEN Accel. Prog. Rep. **41**, (2008).

CCJ Operation in 2006-2007

S. Yokkaichi, H. En'yo, Y. Goto, H. Hamagaki,[*1] T. Ichihara, S. Kametani, T. Nakamura, Y. Watanabe

1 Overview

The operation of CCJ[1,2], RIKEN Computing Center in Japan for RHIC[3] physics, started in June 2000 as the largest off-site computing center for the PHENIX[4] experiment at RHIC. CCJ was initially planned to perform three roles in PHENIX computing, 1) as the simulation center, 2) as the Asian regional center and 3) as the center of spin physics. Recently, DST (Data Summary Tape) production from raw data has become more important, especially for the p+p data. Out of the many off-site computing facilities of PHENIX, only CCJ can handle the several hundreds of TB of raw data in use of HPSS (High Performance Storage System)[5] for the time being.

A joint operation with RSCC (RIKEN Super Combined Cluster System)[6] was started in Mar. 2004. Most of our computing power is now provided by RSCC. On the other hand, the disk storage and service nodes are still located at the CCJ machine room in RIKEN Main Building and maintained by ourselves. HPSS is shared by CCJ and RSCC, while the CCJ data occupy more than 90% of the data stored in the HPSS.

Many analysis and simulation projects are being carried out at CCJ. They are shown on the web page: `http://ccjsun.riken.go.jp/ccj/proposals/`.

2 Current configuration

In the CCJ machine room, we have approximately 190 PC nodes operated using Linux, 166 nodes are used for calculation and the others are used for various services, e.g., data transfer. Each calculation node has 1 GB of memory, 10–31 GB of local disk and dual CPUs (Pentium III 700 MHz – 1.4 GHz, Pentium 4 2.0 GHz). Scientific Linux (SL) 3.0.5 is operated on the calculation nodes, similarly to at RCF (RHIC Computing Facility)[7], which is the main analysis facility for PHENIX. The upgrade to SL4 is planned in 2008. About 90 nodes are currently operational as calculation nodes and the others are waiting to be retired. Out of the operational nodes, 36 nodes have been augmented with 300 GB of local disk, on which 10 TB of nDST data are located in order to avoid the overhead of the data transfer from the data servers or HPSS. However, a user should take care to submit a job to the node on which the required nDST file is located.

Each RSCC calculation node has 2 GB of memory, 100 GB of local disk space and two Xeon 3.06 GHz processors. Out of the 1024 calculation nodes in RSCC, 128 nodes are dedicated to CCJ usage. They share the PHENIX software environment and can access the CCJ data servers as well as the nodes in the CCJ machine room.

We have two log-in servers. The older server (SUN E450) operated by Solaris 2.6, on which the mail and http servers were also running, was replaced by an HP PC server operated by SL5 in Nov. 2007. Following RCF, we have required the SSH public-key authentication in order to log-in to CCJ since Sept. 1, 2007.

We have a main server (SUN Fire V880) using Solaris 8 for the NIS/DNS/NTP server and the NFS server for the users' home region on the 8 TB SCSI-RAID.

At the end of JFY 2006, two data servers (SUN Fire V40z) and four SATA-RAID systems (9 TB each) were purchased and deployed to replace the systems retired in 2006: a PC data server, two SUN E450 data servers and 24 TB SCSI RAID disks. Each SATA-RAID is served as a single partition using LVM (Logical Volume Manager)[8] with XFS[9].

Including two above servers, we have five V40z data servers, which are operated by SL4 and connected to large RAID systems (67 TB in total). Except for the users' work regions (40 GB is assigned to each user), none of the disks can be accessed by NFS from the calculation nodes to maintain the total I/O throughput. The *rcp* command is used to access the data with a limitation on the number of *rcp* process to avoid congestion in each data server. In the first half of JFY 2007, they tended to hang up being triggered by the heavy I/O load. Particularly the server of the users' work-regions was found to hang up most frequently. We purchased a SUN M4000 operated by Solaris 10 to use as a new NFS server for the users' home- and work-regions, in expectation of the stability. It was delivered at Feb. 2008 along with a 12 TB FC-RAID system.

On the calculation nodes, the batch queuing system LSF[10] is operated. In Mar. 2008, they were upgraded from version 6.0 to 7.0. On the CCJ-dedicated nodes in RSCC, LSF version 6.0 was upgraded to 6.2 in Feb. 2008.

HPSS version 6.2 is used as a mass-storage system at CCJ and RSCC. Approximately 1.2 PB of CCJ data (200,000 files) have been stored as of Dec. 2007. Five IBM p630 servers operated using AIX are used as the HPSS core server and data/tape movers. For CCJ, eight T9940B tape drives (30 MB/s I/O with capacity 200 GB/cartridge), two T10000 drives (120 MB/s I/O with 500 GB/cartridge) and 6,110 tape cartridges are located in two StorageTek PowderHorn 9310 tape robots. A robot can handle approximately 5-6,000

*1 CNS, University of Tokyo

tapes, and thus the two robots have a capacity of 11,083 tapes and 8,620 tapes are already installed.

3 PHENIX software environment

Two AFS[11] clients are operated using OpenAFS on Linux to share the software environment of the PHENIX experiment as analysis and simulation libraries, configuration files and so on. To cope with the instability caused by OpenAFS, one client is experimentally operated as a virtual machine using Xen[12], in order to reset automatically when it hangs up.

The total size of the PHENIX software copied by AFS daily or weekly from BNL is approximately 300 GB as of Dec. 2007. All the calculation nodes are served the software by NFS, not by AFS. Using a *rsync* server on a PC, the PHENIX software environment are also shared by PHENIX collaborators in Japan. Because the PHENIX analysis libraries are compiled using the shared libraries provided by the operating system on the calculation nodes, the OS used in CCJ should be the same as that used in RCF as mentioned above. It is unrealistic to recompile the software on the other local OS by ourselves, because they contain 14 GB of CVS data, which are being updated daily.

For PHENIX analysis, PostgreSQL is used as the DB engine to store the calibration data. The total amount of data in the PHENIX-DB is 40-50 GB as of Dec. 2007. The data are copied to CCJ by request of users. Three Linux PCs are used to operate the DB in CCJ.

4 WAN and data transfer

In Oct. 2006, a 10Gbps network (Super SINET, which was integrated as SINET3 in Apr. 2007), which is maintained by NII[13], became available at RIKEN Wako Campus. Then, the bottleneck in the data transfer between CCJ and BNL became approximately 1.5 Gbps of bandwidth (B/W) between the CCJ main switch (Catalyst 4506) and the RIKEN firewall. They were connected by the aggregated two 1000BASE fibers, but the total B/W was found to be limited to 1.5 Gbps due to the firewall performance. To remove the bottleneck, a 10GBASE switch (Foundry FESX424) was newly introduced in CCJ machine room in Nov. 2007 with a 10GBASE line from the switch to the RIKEN main switch.

In the second half of JFY 2007, four PC servers (HP ProLiant DL145 G3) and four SATA-RAID disks (12 TB each) were deployed as 'buffer boxes' for the data transfer between CCJ and BNL. Each node has two buffer areas A and B, each with a 2 TB. The raw data are transferred from BNL using GridFtp[14] and stored in buffer A. When A is full, B is used to store the data and the transfer to HPSS from A is started, and vice versa.

The buffer boxes are operated by SL5 with a Grid environment (VDT[15] 1.8.1). Each server has two network I/F. One is connected to the new 10GBASE switch and communicates only with BNL. The limitation is set by the access control list on the RIKEN main switch. The other is connected to the CCJ main switch and communicates with all but BNL. Using the new setup, a 360 MB/sec transfer rate from BNL to CCJ was achieved in Jan. 2008 as shown in Fig.1.

No p+p data were obtained in PHENIX Run-7 (Nov. 2006–May 2007) and thus no raw data were transferred to CCJ in 2007. In Run-8 (Nov. 2007–Mar. 2008), 100 TB of p+p data were transferred using the new data-transfer machines in Feb. and Mar. 2008.

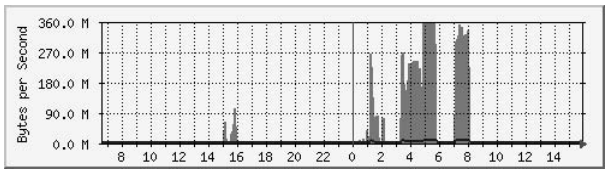

Fig. 1. Data transfer rate between CCJ and BNL achieved in Jan. 2008 with the new 10GBASE switch.

5 Outlook

After five years of operation, RSCC will be renewed in Jan. 2009. We have been taking part in the discussion on the detail of the renewal. Replacement of the tape storage system by disk storage was also discussed but was not adopted.

For CCJ, two big changes are being discussed; 1) a new tape robot for HPSS will be deployed and located in the CCJ machine room, 2) calculation nodes assigned to CCJ will be installed with large disks (the typical size is expected to be ∼1 TB), and the nDST data will be located in the same manner as that of above-mentioned local data disks in a part of CCJ calculation nodes.

References

1) http://ccjsun.riken.go.jp/ccj/
2) S. Kametani et al., RIKEN Accel. Prog. Rep. 39, 224 (2006); RIKEN Accel. Prog. Rep. 40, 197 (2007).
3) http://www.bnl.gov/rhic
4) http://www.phenix.bnl.gov
5) http://www.hpss-collaboration.org/
6) http://rscc.riken.jp
7) http://www.rhic.bnl.gov/RCF/
8) http://www.lvm.org/
9) http://www.xfs.org/
10) http://www.platform.com/products/LSF/
11) http://www.openafs.org/
12) http://www.xen.org/
13) http://www.nii.ac.jp/
14) http://www.globus.org/grid_software/data/gridftp.php
15) http://vdt.cs.wisc.edu/index.html

PHENIX silicon vertex tracker project

Y. Akiba, J. Asai, S. Chollet,[*1] V. Cianciolo,[*2] A. Deshpande,[*3,*4] B. Deepack, O. Drapier,[*1] A. Drees,[*3] H. En'yo, K. Fujiwara, F. Gastaldi,[*1] R. Granier de Cassagnac,[*1] R. Ichimiya, J. Kanaya, T. Kawasaki,[*5] M. Kawashima,[*6] M. Kasai,[*6] K. Kurita,[*6] M. Kurosawa, A. Lebedev,[*7] E. J. Mannel,[*8] R. Nouicer[*9] C. Ogilvie[*7] H. Ohnishi, M. Okumura,[*10] Y. Onuki, R. Pak,[*9] C. Pancake,[*3] P. Riedler,[*11] M. Sekimoto,[*12] E. Shafto,[*3] W. Sondheim,[*13] A. Taketani, S. Watanabe,[*10] K. Yamakoshi,[*10] and PHENIX VTX group

We are constructing a silicon vertex tracker (VTX) for the PHENIX experiment at RHIC. The primary purpose of the detector is to carry out precise measurements of heavy-quark production (charm and beauty) in $A+A$, $p(d)+A$, and polarized $p+p$ collisions. The main physics topics addressed by the VTX are as follows.

- Probing high-density partonic matter
  - Energy loss of heavy quarks (charm and bottom) in dense matter
  - Elliptic flow of heavy quarks in dense matter
  - Precise measurement of open heavy-quark production
  - Modification of jets by medium effects
- Measurements of gluon spin structure of nucleon
  - $\Delta G/G$ with heavy-quark production
  - $\Delta G/G$ with γ-jet measurement
- Nucleon structure in nuclei
  - Gluon shadowing over broad x-range

These are key measurements that are required for future RHIC programs, both for the study of the dense partonic matter produced in heavy-ion collisions and for the measurement of the nucleon spin-structure functions.

The VTX detector consists of two inner layers of silicon pixel detectors[1)] and two outer layers of silicon strip detectors. The detector covers pseudo-rapidity $|\eta| < 1.2$ and azimuth $\Delta\phi \approx 2\pi$.

The main points of progress this year are as follows.

- The US side of the project was started in US FY07. The total budget is 4.7 M US dollars over four years (FY07-FY10).
- The fabrication of the final prototype (1.5 cm) bus has been completed[2)]. The production of the bus is under way.
- A Q/A testing system of the pixel bus has been developed[3)].
- The fabrication of the final prototype of the pixel read-out board (SPIRO-2) has been completed at Ecole Polytechnique. The fabrication of the production version (SPRIO-3) is under way.
- A cosmic ray test of the final pixel system prototype was performed[4)]. The test uses a 1.5cm-wide pixel bus and a SPRIO-2 board. Clear cosmic ray tracks were observed in the test.
- Q/A of the pixel sensor module is on going.[5)]
- Q/A of the "Pilot" ASICS used in SPIRO boards is completed[6)]
- Development of a pixel detector assembly system is almost complete[7)].
- The gluing procedure of various pixel components is established[8)]
- The production of the strip sensor has been completed. Four hundred sensors have been delivered.
- Q/A of the produciton sensor is under way at BNL.
- A lab for strip sensor module assembly has been set up at BNL.
- The second prototype of the Read Out Card (ROC) of the strip system has been fabricated and tested at ORNL. The development of the third prototype of the strip system ROC (ROC-3) is under way.
- A prototype of the rad hard ASIC for strip readout, RCC, was fabricated. Testing of the RCC chip is under way at ORNL.
- The mechanical and thermal engineering work of the VTX system is under way by HYTEC, a mechanical engineering company.

*1 LLR, Ecole Polytechnique, CNRS-IN2P3, France
*2 Oak Ride National Laboratory, USA
*3 Stony Brook University, USA
*4 RIKEN BNL Research Center, USA
*5 Niigata University, Japan
*6 Rikkyo University, Japan
*7 Iowa State University, USA
*8 Columbia University, USA
*9 Brookhaven National Laboratory, USA
*10 Tokyo Metropolitan College of Industrial Technology, Japan
*11 European Organization for Nuclear Research, Switzerland
*12 High Energy Accelerator Research Organization, Japan
*13 Los Alamos National Laboratory, USA

References

1) A. Taketani et al.: RIKEN Accel. Prog. Rep. **41**, 162 (2008).
2) K. Fujiwara et al.: RIKEN Accel. Prog. Rep. **41**, 163 (2008).
3) M. Kawashima et al.: RIKEN Accel. Prog. Rep. **41**, 169 (2008).
4) M. Kurosawa et al.: RIKEN Accel. Prog. Rep. **41**, 175 (2008).
5) M. Kurosawa et al.: RIKEN Accel. Prog. Rep. **41**, 173 (2008).
6) R. Ichimiya et al.: RIKEN Accel. Prog. Rep. **41**, 171 (2008).
7) Y. Onuki et al.: RIKEN Accel. Prog. Rep. **41**, 165 (2008).
8) M. Kasai et al.: RIKEN Accel. Prog. Rep. **41**, 167 (2008).

Overview status of the Silicon Pixel detector for RHIC-PHENIX upgrade†

A. Taketani, Y. Akiba, J. Asai, N. Cassano,[*1] S. Chollet,[*2] B. Deepack, O. Drapier,[*2] A. Dress,[*1] H. En'yo, K. Fujiwara, F. Gastaldi,[*2] R. Granier de Cassagnac,[*2] R. Ichimiya, J. Kanaya, M. Kasai,[*4] T. Kawasaki,[*4] M. Kawashima,[*4] K. Kurita,[*4] M. Kurosawa, E. J. Mannel,[*5] R. Muto, H. Ohnishi, M. Okumura,[*6] Y. Onuki, C. Pancake,[*1] P. Riedler,[*7] E. Shafto,[*1] M. Sekimoto,[*8] W. Sondheim,[*9] M. Togawa, S. Watanabe[*6], and K. Yamakoshi[*6]

PHENIX is one of the major experiments at the Relativistic Heavy Ion Collider (RHIC) at the Brookhaven National Laboratory. It has been exploring the spin structure of the nucleon utilizing polarized proton-proton collisions and characteristics of the Quark Gluon Plasma created in heavy ion collisions. The Silicon Vertex Tracker (VTX)[1] will be implemented in 2010 to enhance physics capabilities. It will be installed very close to the collision point and will cover $\mid \eta \mid \leq 1.2$ and $\mid \phi \mid \sim 2\pi$ by four layers of silicon sensors. It will be able to distinguish heavy quarks from light quarks by detecting a displaced vertex due to the longer lifetime of heavy quarks, whose $c\tau$ ranges from 100 μm to 400 μm.

The VTX is composed of two inner pixel layers and two outer strip layers. We are responsible for the former. The pixel detector consists of pixel ladders, extenders, Silicon Pixel Interface Read-Out (SPIRO) boards, and Front End Modules (FEM). The pixel ladder is composed of a thermal plate including a cooling tube structure, which is made of carbon fiber, four sensor hybrid modules, and two readout buses. The sensor hybrid module comprises a silicon pixel sensor and four dedicated readout chips. The signal due to a passing charged particle is fed to the readout chip and converted to binary data. They are readout by the SPIRO board through the readout bus and extender, and transmitted to the FEM via serial optical link, which sends them to the PHENIX DAQ system. One hundred twenty sensor hybrids must be checked on a test bench before assembly. Ninety-eight modules have been tested until this year. The modules 44, 6 and 48 are identified as good, usable, and bad sensors, respectively.[2]

A Cu-Al-polyimide based bus was fabricated as a prototype. It was assembled with sensor hybrid modules and its expected functionality was confirmed. Also, the design of a preproduction version bus was finalized and the bus is now under fabrication.[3] During fabrication, the manual connectivity check for the fine pitch bus might take a long time. Therefore, an automatic bus check system was developed[4] and used for testing the fabricated bus. In addition to reducing the production time to only 10 min per bus, it identified many micro short circuits between signal lines and the plane ground. Thus, the layout of the bus was changed and its yield was improved markdly.

Digital and analog pilot chips are implemented on the SPIRO board for controlling and giving reference voltages to readout chips on the sensor hybrid modules. One hundred fifty pairs are required for the entire PIXEL detector. They were tested with test benches and their functionality was confirmed.[5]

The assembly of the pixel ladder is required to have an accuracy less than 25 μm for precise tracking. The mechanical design is almost finalized. Dedicated assembly benches and jigs have been developed. The procedures for gluing the components of the ladder to each other are established with a glue thickness of 100 $\pm$ 30 μm.[6] The possibility of breaking the bonding wire between the readout chip and the bus, due to the vibration induced by the Lorentz force at a magnetic field, was increased. We tested it at the same magnetic field and decided to encapsulate the entire bonding wire.[7]

A full chain test with a telescope of three layers of prototype pixel ladders, extender, SPIRO, FEM, and PHENIX DAQ system was performed and demonstrated the performance by utilizing cosmic ray.[8]

Electrical integration was discussed from the viewpoints of bias voltage, low voltage, and grounding issues.[9] The specifications of the power supplies were finalized.

*1 Stony Brook University, USA
*2 LLR, Ecole Polytechnique, CNRS-IN2P3, France
*3 Niigata University, Japan
*4 Rikkyo University, Japan
*5 Columbia University, USA
*6 Tokyo Metropolitan College of Industiral Technology, Japan
*7 European Organization for Nuclea Research, Switzerland
*8 High Energy Accelerator Research Organization, Japan
*9 Los Alamos National Laboratory, USA

References

1) Y.Akiba et al.:RIKEN Accel.Prog.Rep.**41**,161 (2008)
2) M.Kurosawa et al.:RIKEN Accel.Prog.Rep.**41**,173 (2008)
3) K.Fujiwara et al.:RIKEN Accel.Prog.Rep.**41**,163 (2008)
4) M.Kawashima et al.:RIKEN Accel.Prog.Rep.**41**,169 (2008)
5) R.Ichimiya et al.RIKEN Accel.Prog.Rep.**41**,171 (2008)
6) M.Kasai et al.: RIKEN Accel.Prog.Rep.**41**,167 (2008)
7) Y.Onuki et al.:RIKEN Accel.Prog.Rep.**41**,165 (2008)
8) M.Kurosawa et al.:RIKEN Accel.Prog.Rep.**41**,175 (2008)
9) E.J.Mannel et al.:RIKEN Accel.Prog.Rep.**41**,179 (2008)

Development of fine-pitch and low-material-budget readout bus for PHENIX pixel detector

K. Fujiwara, A. Taketani, M. Kawashima*1, T. Kawasaki*2 K. Yamakoshi*3, K. Takano*3, S. Watanabe*3, Y. Akiba, H. En'yo, R. Ichimiya, Y. Onuki, M. Kasai*1 and PHENIX VTX group

The PHENIX detector system at the relativistic heavy ion collider (RHIC) at Brookhaven National Laboratory will be upgraded by installing a four-layer silicon vertex tracker (VTX) by the summer of 2010.[1] The VTX consists of two inner silicon pixel detectors and two outer silicon strip detectors. The VTX will enhance the physics capabilities to enable the investigation of new hot and dense nuclear matter in heavy-ion collisions and the structure of the proton spin in polarized proton-proton collisions at the RHIC by identifying heavy quarks via the measurement of the displaced vertex.[1] Our group is responsible for making the Silicon Pixel Detector part.

The signals from pixel sensors are processed using bump-bonded readout chips and converted to binary data. One readout chip has a 32-bit data width. The binary data are transferred to a SPIRO board[?] via fine-pitch low material budget readout bus. The signal on the SPIRO board is converted to a serial optical signal and transmitted to the PHENIX DAQ system. The signal transfer bus (Pixel Bus) has been developed with several constraints from the target physics, radiation environment, and mechanical structure points of view. The development status of the Pixel Bus is described in this report.

The Silicon Pixel Detector has principally four constraints in the detector side and in the production side, ∼50 μsec of detector readout time, to avoid mechanical conflict with the neighboring detector sector, to minimize the multiple scattering and photon conversions, and to easily make and handle the Pixel Bus in the production side. In terms of the detector readout time, we have chosen to expand the number of parallel 32-bit data width in the original design of ALICE[3] to 128 bits. At first, we modified the digital PILOT chip, which has a 2 × 32-bit data width. The digital PILOT chip controls readout chips and multiplexes a data.[?] By using two digital PILOT chips for each half-ladder,[4] the Pixel Bus will have a 128-bit data bus width. Four readout chips (4 × 32-bit data width) can be read in parallel. However, this expansion requires a circuit with a four-times-denser layout from the original ALICE design on the bus. To avoid mechanical conflict with the neighborhood, a bus width of 13.9 mm is required. To minimize the multiple scattering and make the photon conversion in the detector as small as possible, the Pixel Bus has to be thin. Finally, to be satisfied with the production and handling of the bus, the bus should be made up of a technology of Flexible Printed Circuit board (FPC), which is made from a conductor of copper and aluminum and a polyimide insulator. The development of such a fine-pitch FPC is challenging but necessary for the project.

We have developed a new copper-aluminum-polyimide FPC that has 128-bit data bus width. The advantage of the Pixel Bus is not only its ability to increase the data bus width fourfold but it also has a reduced material budget. For our bus, we are aiming at less than 0.28% X_0 in the radiation length. The bus has six layers that consist of copper, aluminum and polyimide layers. It contains two signal layers, two through-hole layers for manufacturing purposes, a power and a ground layer. The bus contains 188 longitudinal lines in total. The size of the bus is 13.9 × 250 mm^2. Therefore, one signal and control line is 30 μm in width and 30 μm internal in minimum with 3 μm thickness.[6,7]

During its development, the HSPICE simulator[8] was used to evaluate the performance of the Pixel Bus, to characterize its own resistance and transmitting waveforms to simulate an ideal case. These simulated signals are compared with the signals on the produced trial bus. The behavior of the propagation signal and the crosstalk induced on the bus are estimated using the HSPICE simulator[6,7]. In the simulation, first, the geometrical model for the 2-D field solver of the Pixel Bus and the Extender is prepared as shown in Fig. 1.[6] The Extender is connected to a SPIRO board and supplies power and bias voltage to a half-ladder. Next, the library of the GTL driver in the

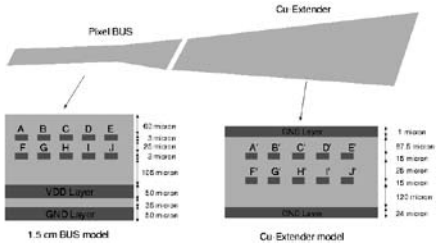

Fig. 1. Geometrical model of bus simulation.

ALICE1LHCb readout chip,[9] the GTL receiver in the Digital PILOT ASIC, and pull-up resisters with the pull-up voltage of 1.8 V are combined into the model shown in Fig. 2.[6] The top part is used for the evaluation of the propagation and the bottom part simulates crosstalk on the adjacent signal line. Then, the square

*1 Department of Physics, Rikkyo University
*2 Department of Physics, Niigata University
*3 Tokyo Metropolitan College of Industrial Technology

digital pulse with 100 nsec width and the amplitude of 1.8 V is injected as a signal from the ALICE1LHCb readout chip. It is propagated to the GTL receiver through the bus and the extender. The simulation result with 220 Ω pull-up resisters is shown in Fig. 3. It shows that the rise time of the waveform at the end of the Extender (Probe Point#2) is ∼80 nsec, with a fall time of ∼15 nsec. Since the low level of the pulse falls to 0.3 V, the noise margin is 0.5 V for the GTL threshold of 0.8 V. The maximum level of crosstalk (Probe Point#2') is 0.3 V_{PP}. Probe Point#4, which is a digital readout result, indicates that the simulated pulse has a 50% duty cycle, which is the same as the input pulse. Consequently, the Pixel Bus with the Extender and the 220 Ω pull-up resisters can transfer the data correctly.[6)]

The result of the HSPICE simulation is compared with the propagation characteristic on the produced bus with an oscilloscope. In the comparison, the propagated data signal and the crosstalk are measured on test points on the SPIRO board. The analog bandwidth of an oscilloscope is 300 MHz and the passive probe has the bandwidth of 500 MHz. The analog bandwidth is sufficiently high to observe these waveforms. Fig. 4 shows a comparison of the simulated signal with the measured signal. They agree reasonably well and the crosstalk level is sufficiently low. The

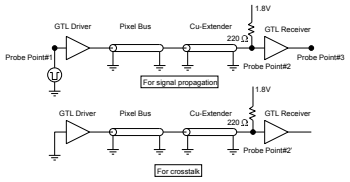

Fig. 2. HSPICE model of Pixel Bus. (Top): Model for the evaluation of propagation, (Bottom): Model for the evaluation of crosstalk.

bus resistance is measured on the prototype Pixel Bus to compare with the simulation result. The resistance of a signal line is 43.3 Ω from the simulation. The measured resistance on a data line in the signal layer is 40.7 ± 2.4 Ω, the resistance of a data line with three through-holes is 50.4 ± 2.4 Ω. Therefore, the resistance of a through-hole is estimated to be approximately (50.4 Ω-40.7 Ω)/3 ∼ 3 Ω. This is consistent with the value expected from the simulation within systematic uncertainty; thus, the prototype bus seems to satisfy our requirement.[6)] As a result, it is confirmed that the simulation agrees well with the propagation in the real bus. We tuned the pull-up resisters by this simulation method, then we concluded that 220 Ω has best propagation characteristics.

In summary, we have successfully developed a very fine pitch and low-material-budget readout bus for the VTX upgrade. A simulation method using the HSPICE simulator to evaluate the propagation property in the Pixel Bus has been established. The performance of the bus is confirmed with HSPICE simulation and the chain test.[10)] The performance satisfies the PHENIX design requirement from the electrical and mechanical viewpoints. For the mass production, a quality assurance procedure has been established.[11)] It is an electrical inspection method using a Linux PC. Finally, the mass production of the Pixel Bus will begin this year.

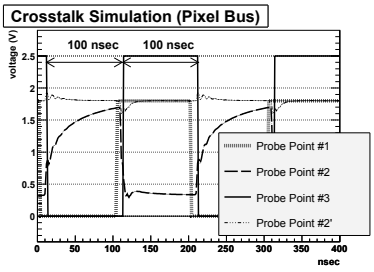

Fig. 3. Simulation result for the bus with 220 Ω of pull-up resisters.

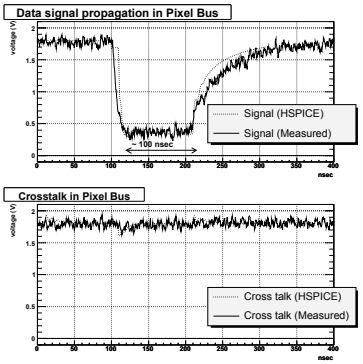

Fig. 4. Comparison of HSPICE simulation and measured result for the Pixel Bus with 220 Ω of pull-up resisters.

References

1) Y. Akiba: RIKEN Accel. Prog. Rep. **41**, 161, (2008).
2) R. Ichimiya: RIKEN Accel. Prog. Rep. **41**, 171, (2008).
3) A. Kluge et al.: Proc PIXEL 2002 Workshop (Monterey, CA) eConfC020909.
4) Y. Onuki: RIKEN Accel. Prog. Rep. **41**, 165, (2008).
5) K. Fujiwara et al.: Czech. J. Phys. **55** (12), (2005)
6) K. Fujiwara, Development of a silicon pixel tracker for an experiment of high energy heavy ion and polarized proton collisions, Doctoral dissertation, Niigata University, 2007.
7) K. Fujiwara, Conference record of IEEE in 2007.
8) Synopsys Inc: HSPICE Manual (2006).
9) W. Snoeys et al.: Nucl. Instr Meth. A**466**, 366, (2001).
10) M. Kurosawa, et al.: RIKEN Accel. Prog. Rep. **41**, 173, (2008)
11) M. Kawashima, et al.: RIKEN Accel. Prog. Rep. **41**, 169, (2008)

Development of assembly procedure for PHENIX pixel detector †

Y. Onuki, Y. Akiba, J. Asai, H. En'yo, K. Fujiwara, R. Ichimiya, H. Kano, M. Kasai,[*1] K. Kurita,[*1] M. Kawashima,[*1] M. Kurosawa, R. Muto, H. Ohnishi,
A. Taketani, Y. Yamamoto[*2] and PHENIX VTX Collaboration

The Relativistic Heavy Ion Collider (RHIC)[1] of Brookhaven National Laboratory provides collisions of polarized proton-proton $\sqrt{s}$ up to 500 GeV and heavy ion $\sqrt{s_{NN}}$ up to 200 GeV. The PHENIX[2] is one of two major experiments at RHIC. The silicon vertex tracker (VTX)[3] for the PHENIX detector will be installed in 2010 to enhance the physics capabilities for both heavy ion program and spin program. The upgrade will enable the precise measurement of the energy loss of the charm and bottom quark separately in Quark Gluon Plasma (QGP) at heavy-ion collisions. Fundamental information on gluon polarization in the proton can be extracted from the measurement of the proton beam helicity-dependent asymmetry of the heavy quark production. Both measurements are required for the identification of heavy flavor. The VTX will have a distance to the closest approach resolution better than 50 μm, which enables us to separate the decay products of the heavy and light flavor quarks, and identify the charm and bottom quarks.

The VTX consists of two major parts: the inner two layers are pixel-type sensors and the outer two layers are strip-type sensors.[4] The distance from the beam line for each layer is 25, 50, 100 and 140 mm, respectively. The inner two pixel layers have 10 and 20 pixel sensor modules (ladder) in ϕ direction. RIKEN is assigned to fabricate all the ladders. A ladder is formed using 4 sensor modules, a bus[5] that is a flexible circuit board made of copper, aluminum and polyimide, and a stave that is made of CFRP including cooling pipe.[6] We have been developing dedicated assembly fixtures for the mass production of the ladder: The assembly bench has a microscope with sufficient magnification for observing the alignment mark on the sensor module and a long-stroke X-stage with a magnetometer which can measure the position with sub-μm accuracy. The alignment jig is used by placing it on the assembly bench and fixing the sensor modules by vacuum hole one by one independently. The X-Y-θ-stage jig is used for sensor module alignment with under 10 μm accuracy. The turn jig is used flipping over the aligned sensor modules and gluing the sensor modules and stave. The details of the jigs and procedure for the alignment were already reported last year.[7] We have been improving and developing more assembly procedures particularly for gluing and stacking both the bus and stave into a ladder. Each component is glued using two-component epoxy paste adhesives, Araldite 2011, which is known as radiation-hard adhesive.[8] It is important to establish how to dispense the adhesive with a low thickness and a smooth surface without boids. Thus, we have been studying how to optimize the dispensing parameters with a programmable robot and an adhesive dispenser[9].

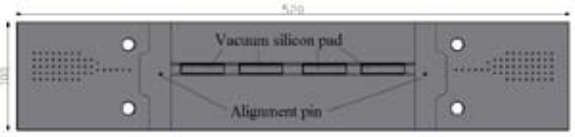

Fig. 1. The stave jig has four bushes. Each pair of diagonal holes is used for the relative position determination of the jigs to be placed properly with pins.

Fig. 2. The bus jig has many hollows on the surface for the bus's SMD (Surface Mount Device) to be placed flat. The provided two pins are put through the two bushes of the stave jig as a guide for the proper location. Two micrometers for thickness control are attached on the backside of the figure.

The stave is placed on the stave jig, which is shown in Fig. 1 and is developed this year, and then dispensed adhesive. The stave jig with a silicon pad sticks the stave by vacuum chucking. It has two alignment pins for the proper placing of the stave.

The bus-jig is also newly developed for use in placing and sticking two buses by vacuum chucking. Epoxy adhesive is dispensed on the bus on the bus jig in the same manner as that for stave gluing. Then the bus jig is placed on the stave jig to glued to each other, as shown in Fig.1. The thickness of the glue can be controlled with two micrometers provided by the bus jig. Our target thickness is $\sim$ 100 μm and it was already achieved with dummy components.[9]

Sensor modules and buses are connected by 25 μm-diameter 4 mm-long aluminum wires by wedge bonding. The PHENIX DAQ trigger is sent to four sensor modules from the bus via the bonding wires. It is also a problem for us that the CDF experiment in the Fermi National Laboratory shows[10] that the bonding

† Condensed from the article in Phys. Rev. Lett. **85**, 1827 (2000)

*1 Rikkyo University, Japan
*2 University of Electro-Communications, Japan

wire breaks because of the vibration induced Lorentz force that interacts with the wire flowing a periodic electric current in a magnetic field and the vibration was suppressed by the encapsulation of the wire with a silicon encapsulant. To look at this issue in our detector, a simple test was carried out with a magnet, which has a maximum field of 0.8 $Tesla$. The bonding wire on the test board, which has a similar shape and length was settled in the magnetic field. The field and wire configurations were the same as that in the PHENIX. The wire was terminated using the 50 Ω resistor and fed GTL level pulse to simulate the trigger synchronized current. The vibration of the wire, which is shown in Fig. 4 was observed using the CCD camera outside the magnetic field. The wire was broken by feeding $\sim 10\ mA$, $\sim 7\ KHz$ pulse within a minute. The motion images were recorded in the PC and analyzed. Fig. 5 shows the vibration amplitude depending on the GTL pulse frequency. It has clear resonance at approximately 7 KHz. It is comparable to the current PHENIX maximum trigger rate of $\sim 5\ KHz$ and has a possibility to coincide the trigger rate after PHENIX DAQ system is upgraded and the luminosity of the RHIC is improved in the future. Thus, we decided to encapsulate the entire wire with Sylgard 186 and 184 manufactured by G.E. Dow Corning to avoid the crucial vibration.

All the designs for components of a pixel ladder and assembly jigs were completed by the end of 2007 and will be manufactured in start of 2008. The production of the pixel ladder will begin in the spring of 2008.

References

1) H. Hahn et al. Nucl. Instrum. Methods Phys. A **499**, 245 (2003).
2) K. Ac et al. Nucl. Instrum. Methods Phys. Res. A **499**, 469 (2003).
3) C. Woody, Proc.18th Winter Workshop on Nuclear Dynamics, Nassau, The Bahamas 2002-1(EP Systema, 2002); J. M. Heuser, Nucl. Instrum. Methods Phys. Res. A **511**, 210 (2003); Y. Akiba, AIP Conf. Proc., **698**, 785 (2003); A. Taketani, Nucl. Instrum. Methods Phys. Res. A **541**, 137 (2005); K. Tanida, Nucl. Instrum. Methods Phys. Res. A **549**, 75 (2005)
4) J. Tojo et al. IEEE Trans. Nucl. Sci. **51**, 2337(2004); Z. Li et al. Nucl. Instrum. Methods Phys. Res. A **541**, 21 (2005); Nucl. Instrum. Methods Phys. Res. A **535**, 404 (2004). Nucl. Instrum. Methods Phys. Res. A **518**, 300 (2004)
5) K. Fujiwara et al. RIKEN Accel. Prog. Rep. **41** 163 (2008).
6) Y. Onuki et al. RIKEN Accel. Prog. Rep. **40** 205 (2006).
7) Y. Onuki et al, RIKEN Accel. Prog. Rep. **40** 171 (2007).
8) ATLAS SCT Barrel Module FDR, SCT-BM-FDR, 2001.
9) M. Kasai et al, RIKEN Accel. Prog. Rep. **41** 167 (2008).
10) G. Bolla et al, Nucl. Instrum. Methods Phys. Res. A **518**, 277 (2005);

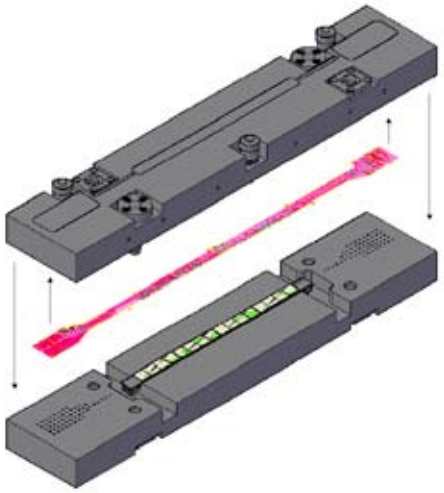

Fig. 3. Gluing two buses and four sensors on the stave.

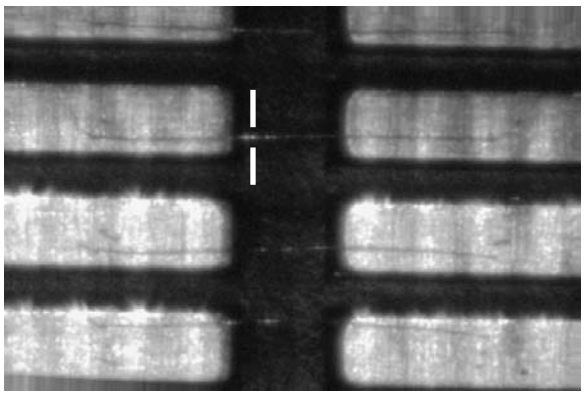

Fig. 4. Recorded movie of the vibration of wire in the circuit. Several wires can be seen as thin horizontal lines. Squares located on both sides are the lands of electrode of the circuit. Each movie was recorded in three seconds. The GTL pulse was switched off during the first, and then switched on after two seconds.

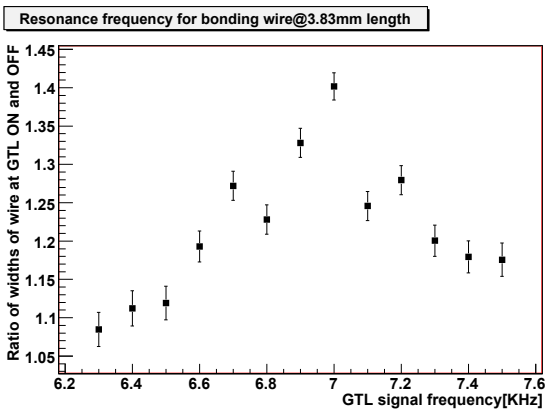

Fig. 5. Vertical axis is the ratio of the width of wires when the GTL signal is on or off. Each width of the wire comes from the sigma value fitted by Gaussian for the histogram, which is the slice at the maximum resonanced plane (vertical line) from Fig. 4.

Gluing for PHENIX silicon pixel detector

M. Kasai,[*1] Y. Onuki, Y. Yamamoto,[*2] K. Yamakoshi,[*3] A. Taketani, H. En'yo, K. Kurita,[*1] K. Fujiwara, M. Kurosawa, M. Sekimoto,[*4] M. Kawashima,[*1] R. Ichimiya, Y. Akiba, and PHENIX VTX group.

PHENIX at the Relativistic Heavy Ion Collider is an exploratory experiment for the investigation of high energy collisions of heavy ions and protons in Brookhaven National Laboratory. We will install a silicon vertex tracker (VTX) into most inner part from beam pipe in 2010. The VTX enables tagging heavy-quark production (charm and beauty) in A + A and p(d) + A, polarized p + p collisions, namely it can measure tracks from D-meson and B-meson decay and then distinguish the event including charm quark and the event including bottom one. In addition, it leads to precise measurements of reconstructing parton momentum in γ + jet event by measuring momentum of charged particle from jet.

The VTX consists of pixel sensors at inner 2 layers (10 pixel full ladders and 20 pixel full ladders which cover at r=2.5, 5.0cm with z=$\pm$10cm.) and strip sensors at outer 2 layers. Rikkyo university and RIKEN are responsible for the pixel detector. These ladders should meet following requirements from mechanical points of view.

- Dimensional uniformity of entire VTX $\leq$25μm, Pixel sensor modules alignment accuracy $\leq$10μm.
- Stress free semiconductor devices on the ladder.
- Assembly process should be done in the room temperature. However entire VTX will be operated in $0°C$.
- Glue which sticks each components on the ladder should be thin enough in order to maintain high thermal conductivity and minimize the ladder thickness.

Structure of the pixel stave[2)3)] is shown in Fig.1. It is formed by a thermal plate, four sensor modules, and two readout buses. The thermal plate[1)] is made from a CFRP plate and a cooling, which supports whole stave mechanically. The sensor module is made from a pixel sensor and four dedicated readout chips. The readout bus is a copper-aluminum-polyimide base flexible printed circuit board. The assembly procedure has to be established for mass production, 30 ladders and 10 ladders as spares.

The procedure for sensor modules alignment in pixel assembly had been established with dedicated jigs in 2006.[4)] We established the procedure to glue four dummy sensor modules and a glass plate with a uniform gluing thickness of about 100μm.

In this report, we especially describe the gluing procedure for a stave. The equipment in Fig.2 was used for gluing. Gluing is performed by a dispenser and a programmable robot. We tested several parameter sets, dispensing pressure and needle, glue direction etc, with program. A glass plate, which surface is enough smooth, and an aluminum plate are substituted for a thermal plate, and a sensor module, respectively. The aluminum plate is easy to fabricate as same size of sensor module in width, length, and heiesght, and is much cheaper than real one.

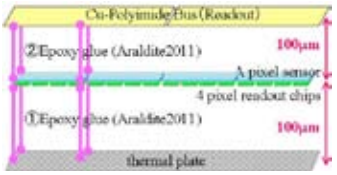

Fig. 1. Structure of a pixel stave

Fig. 2. A setup of gluing

The glass plate is placed on an alignment-jig and the dummy sensor modules are placed on a turn-jig. The turn-jig is put on the alignment-jig and the offsets between the glass plate and dummy sensor modules are adjusted with micrometers to 100μm. This is because we dispense the glue for 100μm thickness. Then the glue is dispensed on the glass plate as in Fig.3. Finally, the glass plate and the dummy sensor modules are attached. During these steps, all parameters were optimized.

(1) Getting rid of bubbles with a centrifugal machine : 3 minutes at rotation radius 16.3cm with 2400rpm.
(2) Internal diameter of the dispenser needle is 1.06mm.
(3) Dispensing pressure is 0.220MPa or 0.230MPa.
(4) Gluing direction is only way Side A $\rightarrow$ Side B (The total is 12 lines.)
Gluing distance is 25cm including extra 2.5cm

*1 Department of Physics,Rikkyo University
*2 The University of Electro-Communications
*3 Tokyo Metropolitan College of Aeronautical Engineering
*4 KEK

on both at begin and end, which is needed to maintain a uniform pressure/glue dispensing rate in the dispensing machine.

(5) Distance between the lines is 1.05mm. The sweep speed is 30mm/sec and total 12 sweeps per stave takes about 2min.

(6) This procedure is done within 15min after mixing two component epoxy in the 23°C and from 40% to 50% humidity environment.

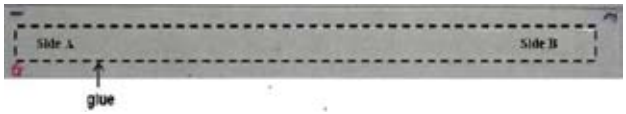

Fig. 3. The glue is dispensed on the dummy thermal plate which is made by glass plate..

These works are done in the clean room. Eleven samples are fabricated and measured. The thickness of sensor modules and glass plate are measured before gluing by using a micrometer. After gluing, total thickness is measured and glue thickness is evaluated. Fig.4 shows the average thickness of the glue of each sample. Gluing procedure with 100±30μm is established.

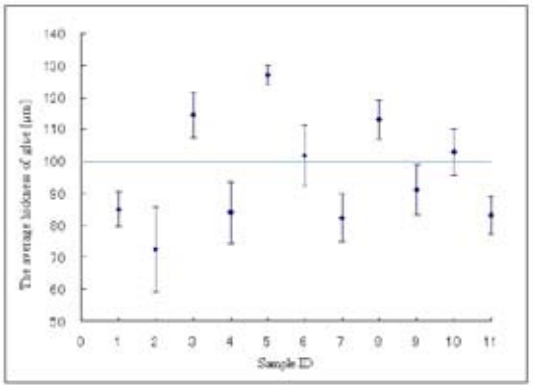

Fig. 4. Thickness of glue. The variation by the different measurement location on a sample

During defining the parameters, remaining issues are raised as listed below.

- Dispensing pressure does not reach to the intended value by 0.07MPa just after a few second from staring. The pressure affects the dispensing rate. At this moment, extra sweep length is needed to maintain flat pressure.
- Glue is dispensed as line shape and it takes a few minuets to merge into single flat plane. There are no big bubble between lines, but small (0.01∼0.1mm) bubbles might remain after gluing the glass plate and the dummy sensor modules.
- The glue at side A is about 30μm thicker than at side B.

The first and third issues are fine with current solution. But in second one, it is not easy to eliminate small bubbles. There are two concern with small bubbles in the glue. One is that bubles may expand or explode and stress silicon devices which is very fragile. Another is that heat conductivity may decrease.

The heat conductivity may be affected by the fraction of babble total volume in the total glue. It is very small effect and can be ignored. The glue dispensed on the glass plate is exposed the heat cycle by using peltier device. Temperature of the glue is monitored by an infrared themography. The lowest and highest temperature are 0°C and 40°C respectively, which are expected realistic senario of the VTX opeation. It takes about 9 minitutes for one cycle, 0°C → 40°C → 0°C. There are no observation of explosion under 7 times of heat cycle. Also it is estimated expansion of the bubble by measuring the projected bubble area with a microscope. Some pictures at each temperature are taken with a digital camera. The projected bubble area(S) in the picture is converted to a bubble radius(r) when the bubble shape is assumed as a circle whose area is S=π r^2. Fig.5 shows comparison between the measured-radius and equation of state, and Fig.6 shows comparison with the coefficient of thermal expansion. Error bars show the r.m.s. of the 6 measurements at each temperature. It seems that the thermal expansion of the bubbles is not issue for the pixel detector from these result. Additionally no damage, no glue crack, and no peal off are observed during the heat cycle.

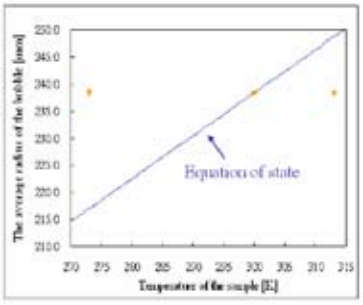

Fig. 5.

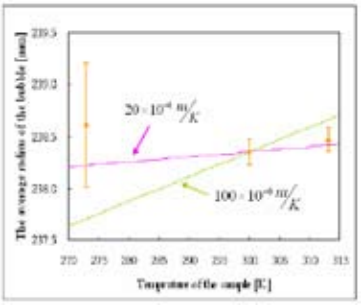

Fig. 6.

In summary, the way of diaspensing and gluing between thermal plates and sensor modules for PHENIX pixel detector is established. The glue thickness is controlled with 100±30μm. The thermal expansion of the bubbles is not issue for the pixel detector.

References

1) J. Asai: RIKEN Accel. Prog. Rep. 38, 235 (2005)
2) K. Fujiwara: RIKEN Accel. Prog. Rep. 38, 228 (2005)
3) H. Ohnishi: RIKEN Accel. Prog. Rep. 38, 230 (2005)
4) Y. Onuki: RIKEN Accel. Prog. Rep. 40, 171 (2007)

Quality assurance of fine-pitch and low-material readout bus for silicon pixel detector

M. Kawashima,[*1] K. Fujiwara, A. Taketani, K. Kurita,[*1] Y. Akiba, R. Ichimiya, Y. Onuki, M. Kasai,[*1]
M. Kurosawa M. Sekimoto and PHENIX VTX group

In the PHENIX experiment at the Relativistic Heavy Ion Collider in Brookhaven National Laboratory, the research utilizing high-energy heavy-ion collision and polarized proton collision is being advanced. We plan to install a silicon vertex detector[1] (VTX) to improve the vertex tracking performance with higher resolution of the PHENIX detector system.

The VTX consists of two inner pixel layers and two outer strip[2] layers. It is necessary to have 10 ladders at the first layer and 20 ladders at the second layer in order to surround the collision point. A ladder is an unit of the detector to which is composed of a support, pixel sensor modules including bump-bonded dedicated readout chips[3] and a readout bus[4], as shown in Fig. 1.

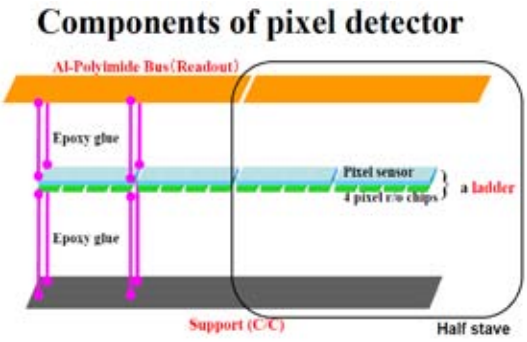

Fig. 1. Components of pixel detector: A full stave consists of 2 buses, 4 ladders, and 1 support. One half is electrically independent from the other half.

The pixel detector is required to have low material budget, compact size and high-speed readout because of the conditions of physics measurement in PHENIX experiment. The signal arising on the silicon sensor is fed to a chip and converted to binary data. They are transferred to the SPIRO[5] board via a readout bus. The SPIRO board receives parallel binary data and transmits them via a serial optical link. One readout chip has a 32-bit-wide data bus. In order to reduce the readout time, four out of eight chips are read out simulteniously. Thus the readout bus has to have a 4×32 bit-wide parallel line. It also needs other control lines and voltage reference lines, so the total number of lines is 188. However the pixel detector is at the innermost part of the PHENIX detector and it is required ti have low material budget and to be compact. We have selected a copper-aluminum-polyimide based flexible printed circuit board as the technical choice. The width of the line is 30μm and the space between two lines is 30μm. The industry-standard line/space is 100/100μm. The readout chip is electrically connected by the bonded wire, the pad of which is 100μm wide with a 120μm pitch. The number of connections to the chips per bus is 862. The SPIRO-side connection has 186 lines of connectors with 200μm.

Just after pattern etching during each layer formation, signal lines are visually checked using a microscope. Then these layers are stacked together and connected via copper plated through holes. The connectivity of the stacked bus must be tested. The bus has over 1000 pads to connect to the readout chips and the SPIRO board, so it may be very time-consumingto perform the check using prove needles. Therefore we developed a connectivity check system. The system consists of an extended bus part and PCI-based digital Input/Output boards (DI/O). The concept of the system is shown in Fig. 2. The signal lines at rth bonding pad for the readout chip are extended to the card edge connector, which can be easily connected to the outside DI by attaching cables with card edge connectors. On the SPIRO side, the lines from connector pads are extracted and fed to DO. After confirming the connectivity, these extended part are cut off. DI/Os are controlled by LINUX PC through the PCI bus. The circuit diagram of each connection is shown in Fig. 3.

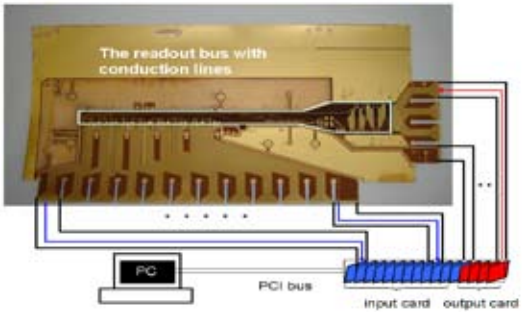

Fig. 2. Concept layout of the bus check system: The bus has extended parts which are connected to the DI/O. They are controlled by a PC.

The principle of this system is that the TTL signal us fed to a signal line on the SPIRO side and the TTL signalis recieved on the readout-chip side. It is able to predict which lines recieves the true TTL signal with a given input signal. We fed only one signal line simulteniously, and checked all sginal lines on the reaout-chip

*1 Rikkyo University

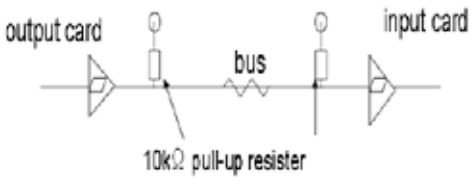

Fig. 3. Circuit diagram of each connection: A signal lines is driven by the TTL driver. The TTL level signal will be recieved at the other end. In the typical case, one signla from the SPIRO side may be distributed to one to four places on the readout-chip side.

side. This test can privide the correct connectivity. After developing the system, it was passed to the bus manufacture with an operation manual. The engineer can run it and identify the problem. It takes about 5 minutes to connect the extended part and the DI/O, and 1 minute to run the software. The check result is written into files. Hence we can share it and carry out discussions from remote locations. When the pre-production bus was manufactured, this check system was used. One out of five samples was passed. This method greatly improves the inspection stage in the production of the readout bus. Two types of problems were found. One was a simple mistake on the net list in the design stage. The other was that some lines touch the adjacent plane ground via unetched copper. This problem was solved by widened the space between the signal lines and the adjacent plane ground. The production yields were also greatly improved.

The fine-pitch and low-material-budget readout bus for the PHENIX pixel detector has been manufactured as part of the preproduction.A system for checking the electrical connectivity of the bus was developed.

References

1) Y. Akiba et al.: RIKEN Accel. Prog. Rep. 41,161(2008)
2) Z. Li, et.al.,"Novel stripixel detector for PHENIX Upgrade",NIMA 518(2004)300-304
3) A. Kluge et al.: Proc PIXEL 2002 Workshop (Monterey, CA) ConfC020909.
4) K. Fujiwara et al.: RIKEN Accel. Prog. Rep. 41,163(2008)
5) R. Ichimiya et al.: RIKEN Accel. Prog. Rep. 40,171(2007)

Analogue and Digital Pilot Testing for the silicon pixel detector of the PHENIX experiment†

R. Ichimiya, F. Gastaldi, *1 Y. Akiba, E. T. Atomssa, *1 R. Granier de Cassagnac, *1 S. Chollet, *1 O. Drapier, *1 H. E'nyo, K. Fujiwara, M. Kurosawa, E. J. Mannel, *2 H. Ohnishi, Y. Onuki, C. Pancake, *3 E. Shafto, *3 A. Taketani
and PHENIX VTX Group

As part of the upgrade program of the PHENIX detector at RHIC, a silicon VerTeX tracker (VTX) [1–4] is being developed for installation in 2010. The VTX provides vertex tracking with a resolution of $< 50\mu$m over a large coverage both in rapidity ($|\eta| < 1.2$) and in azimuthal angle ($\Delta\phi \sim 2\pi$). It consists of two inner pixel layers followed by two outer strip layers. We are responsible for the pixel layers. Each pixel layer is formed by 10 (first layer at 2.5 cm) and 20 (second layer at 5 cm) ladders. Each pixel ladder consists of two half-ladders with an active length of 11 cm covering the $\eta > 0$ and $\eta < 0$ regions. The readout system for the pixel detector is thus divided into 60 subsystems; each subsystem contains one half-ladder, as shown in Fig. 1.

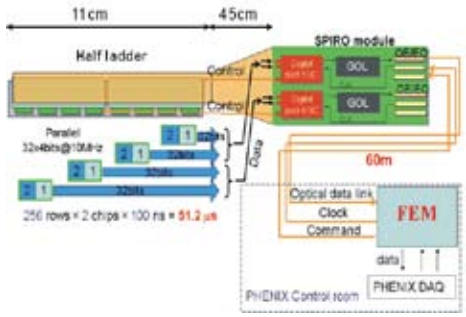

Fig. 1. Pixel detector readout scheme.

Hit data at two pixel sensors are read out by eight readout chips[6] and sent through four 32-bit wide buses on a half-ladder to a SPIRO board. The SPIRO board receives data from the pixel bus and sends it to a Front-End Module (FEM) via optical data links. The FEM receives data from the SPIRO boards, reformats it into the standard PHENIX data format and transmits it to the PHENIX DAQ system. In addition, it provides a clock, a trigger and slow control to the SPIRO boards.

1 SPIRO Board

As described above, the SPIRO board is the front-end electronics for the half-ladders. It consists of two Digital Pilot ASICs, two Analogue Pilot ASICs, a control FPGA, two GOL high-speed serializer ASICs and three OE/EO converters as shown in Fig. 2. It performs the following functions:

- Sending control signals to the half-ladder.
- Multiplexing data from the half-ladder and sending it to the FEM via optical links.
- Providing slow control of the pixel readout chips and the SPIRO board itself.
- Performs data format conversion to match the PHENIX requirement.

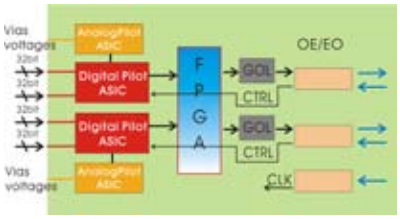

Fig. 2. Block diagram of SPIRO.

The core component of the SPIRO board is the Digital Pilot ASIC. Each of the two pixel readout chip[6] pairs presents 256×2 sequential words of data to a 32-bit bus synchronously at a beam collision clock frequency of 10 MHz as shown in Fig. 1. To meet the readout timing requirements of PHENIX, four readout chips are read out in parallel. To optimize the readout speed and space factor, PHENIX Digital Pilot ASIC[5] with twice the number of input channels was developed using the same design rules and radiation-tolerant technology as the original ALICE Digital Pilot ASIC[7]. The PHENIX Digital Pilot ASIC with 2×32 inputs can simultaneously read two 32-bit words from two pairs of pixel readout chips. Each 32-bit input handles the output from a pair of chips, which represents 512 sequential words of pixel data. An Analogue Pilot ASIC provides several reference voltages using on-chip DACs and monitors the voltages and currents of 4 pixel readout chips using an on-chip ADC. We use the ALICE Analogue Pilot ASIC without any modifications. The FPGA converts the data format to adopt the PHENIX requirement and transfers the data from the PHENIX global clock ($\approx$ 38 MHz) domain to a low-jitter local clock (40 MHz) domain using an on-chip FIFO. Two GOL ASICs serialize the 32-bit width data into 1.6 Gbps.

*1 Laboratoire Leprince-Ringuet, École Polytechnique, CNRS-IN2P3, France
*2 Columbia University, Nevis Laboratories, USA
*3 Department of Physics and Astronomy, Stony Brook University, USA

2 Digital/Analogue Pilot Testing

2.1 Test Setup

To test all 190 Digital Pilot ASICs and 204 Analogue Pilot ASICs, two inspection boards were fabricated to test each ASICs. They equipped with a QFP IC socket, control/readout ports and monitoring ports.

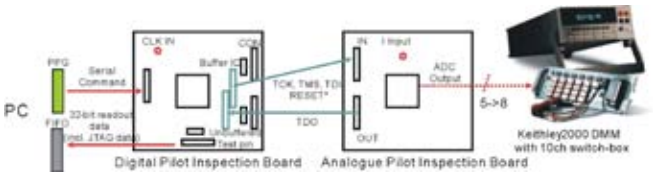

Fig. 3. Pilot ASIC Inspection Setup.

The test inspection setup basically has the same configuration as the SPIRO board. Serial commands were transmitted from an external Pulse Pattern Generator module (PPG) and fed to the Digital Pilot ASIC on the Digital Pilot Inspection board. To control and read back data from the Analogue Pilot, JTAG signal lines and a reset signal line were connected between the Digital Pilot Inspection Board and the Analogue Pilot Inspection Board with fling wires as shown in Fig. 3.

Analogue Pilot DAC output voltages were measured by a Keithley 2000 Digital Multi-Meter (DMM) with a 10 channel switch-box. Analogue Pilot ADC data were stored in its registers and read out by Digital Pilot ASIC via the JTAG path. The readout data from the Digital Pilot ASIC were read out by a FIFO module. The whole system i.e., the PPG module, the FIFO module and the Keithley 2000 DMM, was controlled by a Linux computer and all the readout data were recorded.

2.2 Analogue Pilot Inspection

The Analogue Pilot ASIC inspection consists of DAC output voltage measurement by the DMM, ADC readout via the JTAG path and the JTAG registers read/write test.

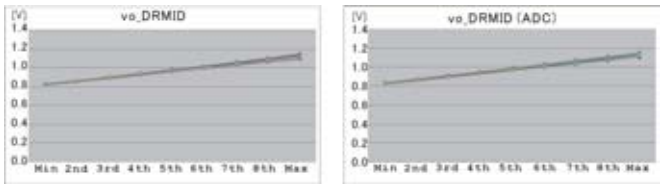

Fig. 4. DAC output voltages (left) and their readback by ADC (right).

Fig. 4 shows measured DAC output voltage for each DAC register value and the corresponding readback voltage measured by the ADC for good chips. Readback voltages obtained by the ADC agree well with the DAC output voltages. We rejected chips with out of range from either the normal output voltages or the normal readback voltages. Some chips did not respond to DAC register setting. We found that 180 good chips out of the 204 chips; there were 12 faulty chips and 12 chips with output voltages that slightly exceeded the normal ranges or with pins that were deformed.

2.3 Digital Pilot Inspection

For Digital Pilot chips, which have a direct interface with the pixel ladder, their inspection was carried out with using a half-ladder and an old prototype SPIRO board with a QFP IC socket. During this test, trigger commands were sent to the Digital Pilot chips and the data were read out. We observed the output data by scanning the threshold value of the pixel readout chip from high to low. If the Digital Pilot functions well in the test, uniform random hit patterns should be displayed as the threshold decreases. We then set test pulse mask patterns on the pixel chips, and we outputted test pulses and trigger commands. This test is to check Digital Pilot's test pulse output function and crosstalk in the Digital Pilot chip.

We found that there were 178 good chips out of the 190 chips.

3 Summary

To eliminate faulty Digital and Analogue Pilot chips used in the SPIRO board before their assembly, they were inspected. For Analogue Pilot chips, ADC output voltages were measured by a DMM and also read back by an on-chip DAC. We confirmed that the output voltages were in good agreement with readback voltages. By this inspection, we verified that we had 178 good Digital Pilot chips and 180 good Analogue Pilot chips. These are sufficient numbers for SPIRO board fabrication for the PHENIX experiment.

References

1) Y. Akiba et al.: Proposal for a Silicon Vertex Tracker (VTX) for the PHENIX Experiment, BNL-72204-2004, Physics Dept. BNL (2004).
2) Y. Akiba et al.: RIKEN Accel. Prog. Rep. **41**, 161 (2008).
3) A. Taketani et al.: RIKEN Accel. Prog. Rep. **41**, 162 (2008).
4) E. J. Mannel et al.: RIKEN Accel. Prog. Rep. **41**, 179 (2008).
5) H. Kano et al.: RIKEN Accel. Prog. Rep. **38** 237 (2005).
6) K. Wyllie: ALICE1LHCB Preliminary Users Manual Version 3/7/01, http://kwyllie.home.cern.ch/kwyllie/ALICE1LHCB.htm
7) A. Kluge: ALICE Silicon Pixel On Detector Pilot System OPS2003-The missing manual, ALICE-INT-2004-030, CERN (2005).

Quality assurance test of readout chips and pixel sensor hybrids for PHENIX

M. Kurosawa, Y. Akiba, J. Asai, B. Deepak, H. En'yo, K. Fujiwara, R. Ichimiya, J. Kanaya, M. Kasai, M. Kawashima, R. Muto, M. Okumura, Y. Onuki, P. Riedler, and A. Taketani

The PHENIX detector at RHIC-BNL has been upgraded with a silicon vertex tracker (VTX)[1] surrounding a beam pipe with four cylindrical layers. The inner two layers are silicon pixel detectors (SPDs) and the outer two layers are silicon strip detectors (SSDs). In the plan of upgrading PHENIX VTX, the RIKEN group is developing the SPD. The SPD is made up of 30 ladders, each of which consists of four sensor hybrids.[2] A sensor hybrid is an assembly of a silicon pixel sensor and four readout chips[3] (ALICE1LHCb) bump-bonded with 20-μm-diameter bumps to the sensor (bonded by VTT[a]). The readout chip has 8192 pixel cells arranged in 32 columns and 256 rows. The pixel size is 50 μm × 425 μm. In preparation for the mass production of the ladder, a quality assurance (QA) test is required for the readout chips and pixel sensor hybrids to ensure that they can be used as detectors. This report describes recent results of the QA test.

Figure 1 shows a picture of the QA system. It mainly consists of a probe station (SUSS MacroTec), a probe card, a DAQ adapter board, VME equipment for a DAQ system, and a Windows PC. A LabVIEW program running in the Windows PC is used for data taking and analysis. The measured and analyzed data are sent to a PostgreSQL database server located at a secure area accessible only from the internal RIKEN network. The database can be accessed from the web interface in the secure area.

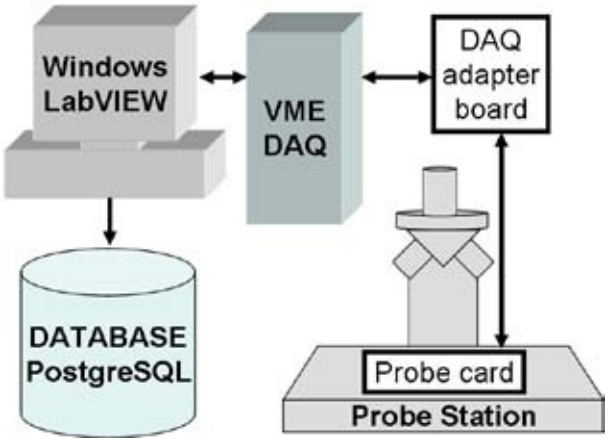

Fig. 1. QA test system in a clean room at RIKEN.

All the readout chips and hybrid sensors are tested for the following parameters.

Items to be checked for readout chips:

(1) Current consumption
- The current consumptions of analog and digital circuits of the readout chips are measured.

(2) JTAG and DAC functionality
- It is confirmed whether configuration settings in the chip are readable and writable by means of a Joint Test Action Group (JTAG) protocol.
- The digital-to-analog converter (DAC) linearity is calibrated.

(3) Mask functionality
- The noisy pixels can be masked by a mask functionality.

(4) Minimum threshold and noise level
- The minimum threshold in all pixel matrices is determined.

(5) Mean threshold and mean noise for the complete pixel matrix
- The test pulse from the pulsar inside the chip is sent to each pixel cell and the mean threshold and noise levels are determined.

Items to be checked for sensor hybrids:

(1) Same tests as those in items 1, 3 and 4 and part of JTAG functionality test in item 2
- The sensor is biased at 50 V during the measurements.

(2) Performance of SPD with β source (^{90}Sr)
- Faulty bump bonds and maximum efficiency are checked by β source measurement.

The tested readout chips and sensor hybrids are classified in three classes, Class I, II, and III. The chips and sensor hybrids classified as Class I are used for the experiment. Class II and III are not used for the experiment, but Class II is used for other purposes such as the production of a prototype ladder.

The readout chips (sensor hybrids) categorized into Class I satisfy the following criteria.

- Current consumptions lower than 350 and 270 mA for analog and digital circuits, respectively.
- A complete JTAG and DAC functionality for readout chips and a complete JTAG functionality for sensor hybrids.
- Mean threshold lower than 1800 electrons (4200

*1 Tokyo Metropolitan College of Aeronautical Engineering
a) VTT Electronics, Tekniikantie 17, Epsoo, P.O. Box 1101, FIN-02044 Epsoo, Finland

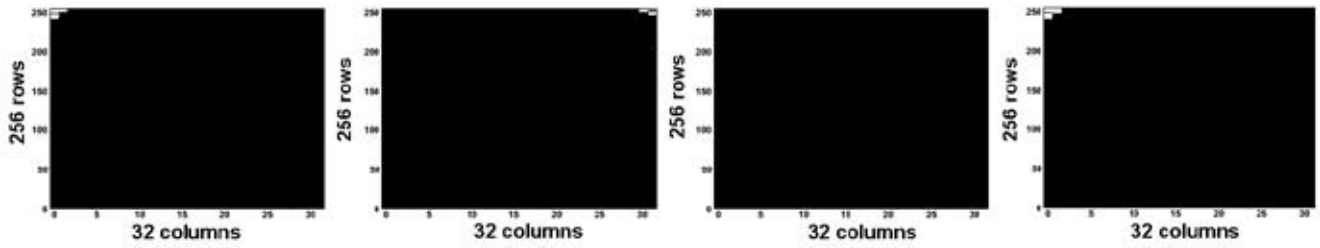

Fig. 2. Typical response of a sensor hybrid, categorized into Class I, to β rays. Good and faulty bump bonds are shown in black and white, respectively.

electrons).
- Less than 1% defect pixels in mean threshold scan (and source test).

The QA test results of the readout chips are summarized in Fig 3. About 1030 Class I readout chips of them were used for bump-bonding with a pixel sensor. The average of the mean threshold and mean noise for the Class I readout chips are about 1400 and 120 electrons, respectively.

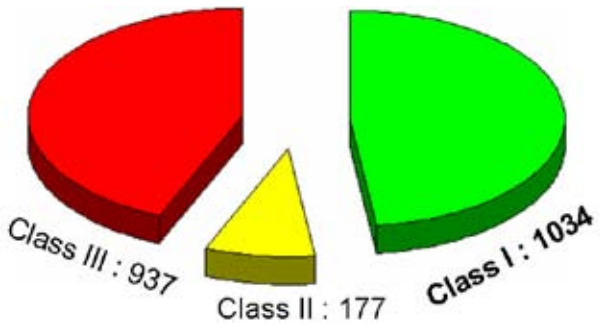

Fig. 3. QA test results of the readout chips.

Figure 4 shows the summary of QA test results. About 100 sensor hybrids have been probed and 45 Class I sensor hybrids were obtained. The average of the mean threshold and the mean noise for the Class I sensor hybrids are about 3300 and 150 electrons, respectively. A typical response to β rays from ^{90}Sr is shown in Fig. 2.

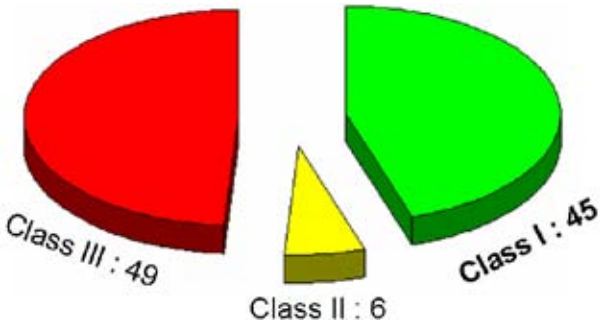

Fig. 4. QA test results of the sensor hybrids.

The main reasons of classification in Class III were a mask test error and a faulty bump-bonding, and one or two readout chips out of four readout chips on the sensor had these errors. Such Class III sensor hybrids can be repaired by a replacing bad readout chips with new ones (rework process).

We obtained 1030 readout chips and 45 sensor hybrids classified as Class I. Since a total of 120 sensor hybrids are required for the experiment, we need 75 Class I sensor hybrids more. About 50 sensor hybrids will be fabricated and 38 Class III sensor hybrids will be repaired by the rework process to obtain 75 Class I sensor hybrids. The required time of QA is about 18 sensor hybrids per month. The QA test of the required sensor hybrids for the experiment will be completed by August 2008.

References

1) Y. Akiba et al.: RIKEN Accel. Prog. Rep. **41**, 161 (2008).
2) Y. Onuki et al.: RIKEN Accel. Prog. Rep. **41**, 165 (2008).
3) K. Fujiwara et al.: RIKEN Accel. Prog. Rep. **38**, 228 (2005).

Cosmic-ray experiment with PHENIX silicon pixel sensor telescope

M. Kurosawa, K. Fujiwara, Y. Akiba, J. Asai, H. En'yo, R. Ichimiya, M. Kasai, M. Kawashima, Y. Onuki, C. Pancake,[*1] E. Shafto,[*1] A. Taketani and the PHENIX VTX Group

PHENIX is an experiment aiming to study the spin structure of nucleons and hot and dense matter at Brookhaven National Laboratory's Relativistic Heavy Ion Collider (RHIC). PHENIX is being upgraded with the introduction of a silicon vertex tracker (VTX) to extend its physics capability[1]. The VTX is composed of a four-layer barrel detector, two outer silicon strip detectors (SSD) and two inner silicon pixel detectors (SPD). The basic component of the SPD is a half ladder assembled using two sensor hybrids[2]. One sensor hybrid has four readout chips bump-bonded to a silicon pixel sensor, with pixel sizes of 50 μm in the z (row)-direction and 425 μm in the ϕ (column)-direction[3]. The sensor hybrids are wire-bonded to a readout bus[4], and the bus is connected to a readout board[5] (SPIRO), which controls the readout chips and transfers binary data to a DAQ system. The RIKEN group have developed two types of readout bus, one is a 3.0-cm-wide Cu-polyimide-based bus and the other is 1.5-cm-wide Cu-Al-polyimide-based bus. As a first step, the 3.0-cm-wide bus was fabricated to perform an electrical test by connecting it to a hybrid sensor and SPIRO board. The 3.0-cm-wide bus was fabricated by industrial-standard technology without R&D. In 2006, a full chain test was successfully performed using the 3.0-cm-wide bus, the prototype SPIRO and a front end module (FEM)[6]. In 2007, we fabricated the 1.5-cm-wide bus with new technology. To avoid a mechanical conflict during the VTX construction, the width of the bus was reduced to 1.39 cm. By using Al, the radiation length was reduced to one-quarter that of Cu. Then, to verify the functionality of the Al-polyimide bus and perform the chain test with the PHENIX readout system, a chain test using cosmic rays was carried out at Stony Brook University in September 2007.

The setup of the chain test using cosmic rays is basically the same as that of the previous experiment in 2006. We used two previous prototype half ladders (using the 3.0 cm bus) and one prototype pixel ladder (using the 1.5 cm bus). Figure 1 shows the setup of the telescope. The three prototypes are stacked lengthwise. All the half ladders are connected with the three SPIRO boards. These SPIRO boards are controlled by one FEM via optical fibers. The main roles of FEM are to send the 40 MHz clock and serial commands, and take serial data including hit information from the SPIRO boards. The trigger is made of a coincidence of self-trigger signals (FastOR) on layer 0, layer 1 and layer 2. The FastOR signal is generated when a cosmic ray hits a sensor hybrid. If the FEM receives the trigger signal, it sends a level-1 trigger to all half ladders, then hit information is sent to the SPIRO boards and stored in the FEM module. The stored data in the FEM were read out by two ways: one was by a Window PC connected with a USB interface; the other was using a granule timing module (GTM) and a data collection module (DCM). The later way is the same configuration as a PHENIX DAQ system.

In the chain test, the prototype detector and DAQ system were confirmed to be well functioning by the telescope configuration consisting of three pixel layers connected with the readout system.

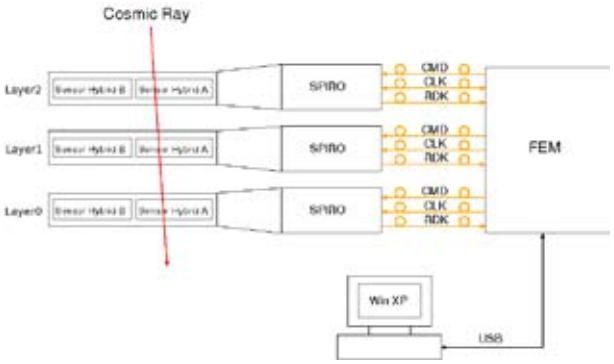

Fig. 1. Setup of cosmic-ray experiment. The vertical distance between the sensor hybrids was 60 mm. Sensor hybrid B was not used in the experiment.

A total of 75 cosmic-ray events with hit on three sensor hybrids were obtained. We estimated the intrinsic resolution of the hybrid sensor from these cosmic-ray events. A typical cosmic-ray event is displayed in Fig. 2. The top three images show the hit positions of the cosmic-ray on each sensor hybrid after clusterization. The bottom image represents a reconstructed track obtained from the least-squares fit with the hit positions (cross points) on each layer after the position alignment.

The position alignment of the sensor hybrid were carried out by translation (col_{shift}, row_{shift}, z_{shift}) and rotation (col_{rot}, row_{rot}, z_{rot}). The 'col' and 'row' indicate the column and row direction, respectively. The parameters, z_{shift}, col_{rot} and row_{rot}, were assumed to be zero because they were not effective the position alignment. The translation and rotation parameters were determined by minimizing the chi-square defined as

$$\chi^2 = \sum_{hits} \left(\frac{(col'_{trk} - col_{trk})^2}{\sigma^2_{col}} + \frac{(row'_{trk} - row_{trk})^2}{\sigma^2_{row}} \right). \quad (1)$$

The col_{trk} and row_{trk} are the intersection position

[*1] Stony Brook University, USA

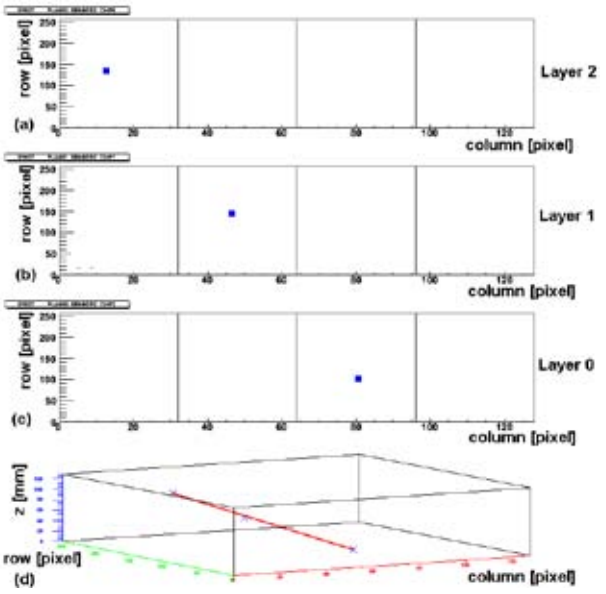

Fig. 2. Event display of typical cosmic ray event. (a)-(c) Square points represent the clusterized hit position on each layer. (d) The cross points and straight line are the hit position and reconstructed track, respectively.

of a line connecting the hit positions on layer 2 and 0. The $col^{'}_{trk}$ and $row^{'}_{hit}$ are the alignmented hit position for translation and rotation defined as below.

$$col^{'}_{trk} = col_{hit} - row_{hit} z_{rot} + col_{shift} \quad (2)$$

$$row^{'}_{trk} = row_{hit} + col_{hit} z_{rot} + row_{shift} \quad (3)$$

Here, col_{hit} and row_{hit} represent a hit position on a sensor hybrid.

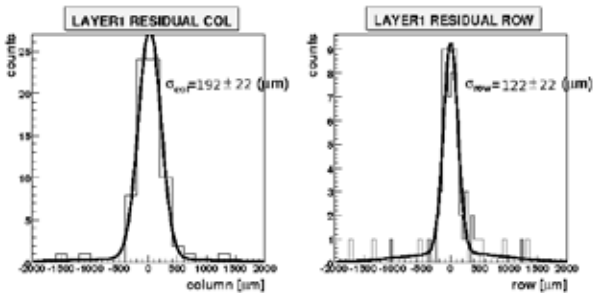

Fig. 3. (a) and (b) are the residual distributions in the column and row directions, respectively, on layer 1.

Figure 3 shows the residual distributions of layer 1 after the alignment. The residuals in the column and row directions were defined as $(col^{'}_{trk} - col_{hit})$ and $(row^{'}_{trk} - row_{hit})$, respectively. The standard deviations of these residual distributions were calculated to be 192 ± 20 μm and 122 ± 20 μm in the column and row directions, respectively. These standard deviations were used to obtain the intrinsic position resolution of a sensor hybrid.

The position resolution of the sensor hybrid is due to two components. One is the intrinsic position resolution and the other is the effect of multiple scattering in the support of the sensor hybrids. We obtained the intrinsic position resolution by estimating the effect of multiple scattering.

The procedure of the estimation for multiple scattering is same as that carried out in the analysis, last year. The resolution due to multiple scattering was calculated under the following conditions.

- The momentum of cosmic rays at ground level is used a known momentum distribution[7].
- The energy loss of the 4 GeV cosmic rays passing through concrete with an average thickness of 6 m is 2.5 GeV (The experiment was performed in an underground area of a six-story building.).
- The thickness of the scattering material is estimated to be the average thickness of the material through which the particle passed.

From the calculation under the above conditions, the resolution from the multiple-scattering effect was calculated to be 35 μm. Thus, we obtained the intrinsic position resolutions in the column and row directions to be σ_{col} = 150 ± 16 μm and σ_{row} = 94 ± 17 μm, respectively. The error is the statistical error not including the systematic error.

The measurement of cosmic rays has been performed with silicon pixel sensor hybrids and a 1.5 cm bus at Stony Brook University. Seventy-five clear tracks of cosmic rays were measured. The 1.5 cm bus has been working without problems.

References

1) Y. Akiba et al.: RIKEN Accel. Prog. Rep. **41**, 161 (2008).
2) Y. Onuki et al.: RIKEN Accel. Prog. Rep. **41**, 165 (2008).
3) K. Fujiwara et al.: RIKEN Accel. Prog. Rep. **38**, 228 (2005).
4) K. Fujiwara et al.: RIKEN Accel. Prog. Rep. **40**, 186 (2007).
5) R. Ichimiya et al.: RIKEN Accel. Prog. Rep. **40**, 176 (2007).
6) M. Kurosawa et al.: RIKEN Accel. Prog. Rep. **40**, 180 (2007).
7) J. Kremer et al.: Phys. Rev. Lett. **83**, 4241-4244 (1999).

Beam stopper and Mott polarimeter for T-violation experiment

H. Kawamura[*1], M. Fukuda[*2], Y. Hirayama[*3], D. Kameda, J. Komurasaki[*2], K. Matsuta[*2], M. Mihara[*2], J. Murata[*1], T. Nagatomo, K. Narita[*1], D. Nishimura[*2], T. Toyoda[*1], M. Uchida[*4], H. Ueno, and H. Yoshimi

[Mott polarimeter, β decay, spin polarization, symmetry]

A beam stopper and a Mott polarimeter for a time reversal violation experiment have been developed. The transverse polarization of electrons emitted from spin-polarized nuclei can be determined by measurement of the asymmetry that arises from the scatterings of the electrons from high-Z nuclei. A non-zero value of the electron transverse polarization component normal to the plane spanned by nuclear polarization and the electron momentum implies the violation of time reversal symmetry (T).

Polarized nuclei are implanted in a stopper to which an external static magnetic field is applied. The polarimeter should be closely positioned to the stopper, considering the detector solid angle. A small permanent magnet is employed instead of an electromagnet. It is not necessary to change the intensity of the magnetic field and to keep the homogeneity, unlike in β-NMR measurement. The magnetic field intensity B_0 must be as small as possible in order to minimize the bending of electron tracks. On the other hand, the polarization relaxation time T_1 has to be sufficiently longer than to the lifetime. T_1 depends on the B_0, temperature, and material of the beam stopper. In the present study, the B_0 and material dependences of T_1 are measured prior to the T-violation experiment. A polarized ^{8}Li beam is obtained via the ^{7}Li$(d,p)^8$Li reaction using the Van de Graaff accelerator of Osaka University. ^{8}Li is implanted in the metal stopper to which the external magnetic field is applied at room temperature. The polarization relaxation is measured by the β-NMR method. Determined T_1 is shown in Fig. 1. As a result, we choose Pt with greater than 500G at normal temperature as the stopper for the T-violation experiment.

Regarding the polarimeter, multi-wire drift chamber (MWDC) is utilized as an electron tracking detector[1]. The size of the MWDC is 640mm×510mm×240mm, and its effective area is 440mm×300mm. It consists of 6 sense layers (XX′UU′VV′) with a wire gap of 10mm and a pitch of 10mm. First, an offline experiment using a checking source is performed. A β-source (^{90}Sr/Y, $E_{\max}$=2.2MeV) is placed at the entrance window, and a 300-μm-thick Pb foil is placed at the opposite side window. Consequently, it is shown that the backscattering of Mott scattering of β-ray with Pb foil can be detected. Mott scattering for a backward angle has a small cross section and a large asymmetry. The figure of merit is maximized at ∼110°. The obtained angular distribution is compared with the results of a Monte-Carlo simulation (Fig. 2). The obtained width of the residual distribution is less than 10°. It is smaller than the scale of the angular dependence of the asymmetry. Therefore, it can be said that the MWDC has sufficient ability to work as a Mott polarimeter.

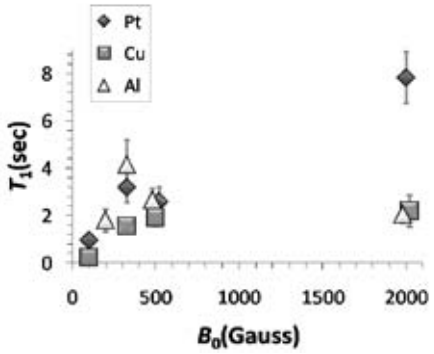

Fig. 1. T_1 vs B_0. The lifetime of ^{8}Li is 838msec. T_1 roughly becomes longer as B_0 increases. The data point of Al includes a large error owing to a low material purity, and other factors.

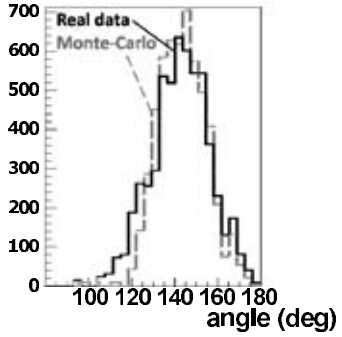

Fig. 2. Obtained angular distribution of Mott scattering.

In addition, a DAQ system and a pintle mount for online experiment have been developed. The entire Mott polarimeter consists of a beam stopper with magnets, 9 scintillation counters, and a MWDC. Currently, we have assembled the experimental apparatus, and carried out performance evaluation. The T-violation experiment at the polarized ^{8}Li beamline of KEK-TRIAC was performed in April 2008.

*1 Department of Physics, Rikkyo University, Tokyo
*2 Graduate School of Science, Osaka University
*3 Institute of Particle and Nuclear Studies, KEK, Ibaraki
*4 Department of Physics, Tokyo Institute of Technology

References

1) H. Kawamura et al.: RIKEN Accel. Prog. Rep. **40**, 167 (2007).

Development of centrality filter and pion detector for heavy ion collision experiments

M. Nitta[*1], T. Akiyama[*1], K. Ieki[*1], T. Ikeda[*1], S. Ebesu[*2], H. Oishi[*1], H. Kawamura, A. Kitabata[*1], E. Takada[*3], T. Toyoda[*1], Y. Nakai, K. Narita[*1], S. Nishimura, K. Ninomiya[*1], Y. Hara[*1], Y. Haki[*1], M. Matsushita[*1], T. Murakami[*2], J. Murata[*1] and H. Sakurai

[collision centrality, pion detector, TOF]

The physical properties of hot and dense nuclear matter in an isospin asymmetric nuclear collision are the target of study in RIBF. In order to determine the collision impact parameter, we have developed a Centrality Calorie Meter (CCM). In addition, we have also developed a pion range counter in the present study. The results of a test experiment performed at HIMAC are described. As a probe of collision centrality in a nucleus-nucleus collision, emitting particle multiplicity is often used. In the present study, instead of measuring the multiplicity, we attempt to measure the total transverse energy to obtain centrality information. A test experiment for the CCM test was performed at HIMAC in July 2007. The experimental setup is shown in Fig. 1. Pure CsI scintillators are located in the forward and sideward directions. An indium target and 400MeV/u Xe-139 beam were used. In order to confirm that the sideward CCM can function as a centrality filter, a correlation between the sideward scintillator and the forward scintillator was expected to be observed. As a result, we succeeded in finding the forward-sideward cor- relation (see Fig. 2).In a central collision, a large amount of transverse energy is emitted in the sideward direction; on the other hand, a small number of nucleons originating from the incident nuclei are injected to the forward calorimeter.

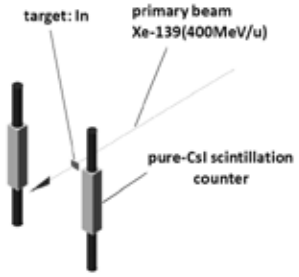

Fig. 1. The Layout of CCM

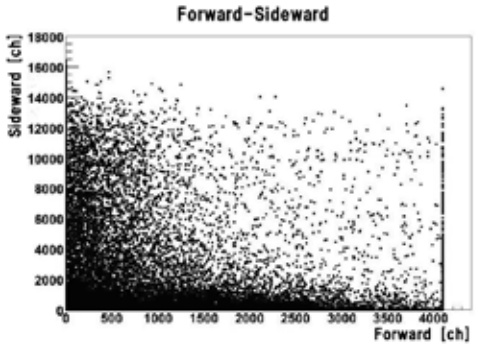

Fig. 2. Forward-sideward correlation

For the detection of the pions, $\pi^+ \rightarrow \mu^+ + \nu_\mu$ decay is used. We can identify the stopped pion events in the presence of strong back ground events by selecting the double-pulse events from the muon decay. A performance test of the pion range counter was performed in December 2007, and January 2008 at HIMAC. A 0.1-1.9mm (0.5mm) Pb target and 600MeV/u (400 MeV/u) Ne-20 beam were used on December 07 (January 08).

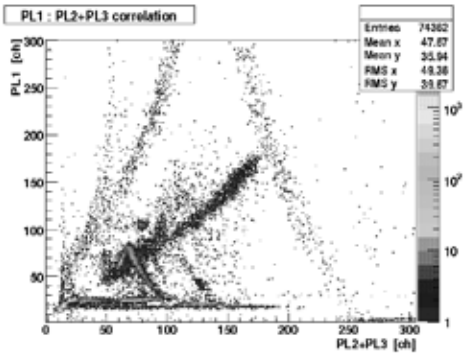

Fig. 3. Pion events observed with the pion range counter.

Four plastic scintillators were placed in a line. In addition, in order to measure the TOF and ΔE of pions, a TOF wall consisting of plastic scintillators was built. The results obtained using the range counter are shown in Fig. 3. PL1, PL2 and PL3 indicate the first, second and third scintillators respectively. The correlation between PL1 and PL2+PL3 is shown in Fig. 3. Pion events are clearly observed to form a Λ-shaped line. The "slope" of the Λ line is the penetrated pion event, and the opposite is stopped event. As shown in Fig. 4,similar results are also observed using the TOF counter.

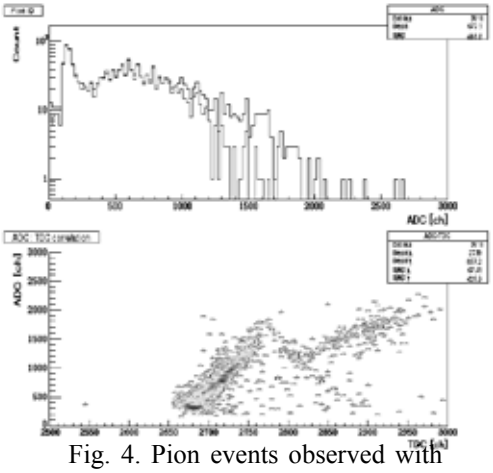

Fig. 4. Pion events observed with the TOF counter

In these experiments, it is confirmed that CCM exhibits satisfactory performance as a centrality filter and the pion range counter can identify the pion event.

*1 Department of Physics, Rikkyo University
*2 Department of Physics, Kyoto University
*3 Department of Accelerator and Medical Physics, NIRS, Chiba, Japan

Overview of the Readout Electronics for the Silicon Vertex Tracker for the PHENIX Experiment

E.J. Mannel,[*1] Y. Akiba, E.T. Atomssa,[*2] D. Bista, M. Bobrek,[*3] C.L. Britton,[*3] S. Chollet,[*2] V. Cianciolo,[*3] L.G. Clonts,[*3] A. Deshpande,[*4] O. Drapier,[*2] K. Fujiwara, F. Gastaldi,[*2] R. Granier de Cassagnac,[*2] R. Ichimiya, J. Kanaya, M. Kasai,[*5] M. Kawashima,[*5] K. Kurita,[*5] M. Kurosawa, R. Nouicer,[*6] C. Pancake,[*4] H. Pei,[*7], P. Riedler[*8] E. Shafto,[*4] A. Taketani, S. Watanabe,[*9] K. Yamakoshi,[*9] Y. Yamamoto, and the PHENIX VTX Group

[RHIC, PHENIX, Silicon Detectors, Electronics]

The PHENIX experiment at the Relativistic Heavy Ion Collider (RHIC) at Brookhaven National Laboratory has approved the silicon vertex tracker (VTX) upgrade to be installed in 2009, in preparation for initial data taking during PHENIX Run 10. The goal of the VTX upgrade is to provide precise measurements of heavy-quark production (charm and beauty) in A+A, $p(d)$+A and polarized p+p interactions at RHIC. These are essential measurements for future heavy-ion and spin-physics programs at RHIC. In addition, the precise tracking capabilities of the VTX will provide significant improvements to other PHENIX physics measurements.

The VTX consists of two detector sub-systems, the pixel detector and the stripixel detector. The VTX provides nearly full coverage in azimuth over the rapidity range of $|\eta| < 1.2$, with 50 μm resolution in the distance to closest approach. A preliminary design of the central detector is shown in Fig. 1.

The pixel detector consists of two inner barrels, each approximately 22 cm long. The first barrel with a radius of 2.5 cm is built from 10 pixel ladders, while the second barrel is built from 20 pixel ladders.[1–3] Each ladder is constructed from two half-ladders which are mounted on a carbon composite stave which provides mechanical support and cooling for the ladder. A schematic drawing of the half ladder is shown in Fig 2. Each half-ladder consists of two sensor modules mounted on a multi-layer readout bus (pixel bus). The pixel detector uses the ALICE1LHCb readout chip designed by the CERN EP-MIC group for the ALICE and LHCb experiments.[4] Four readout chips, thinned to 150 μm are bump-bonded to a sensor module. The pixel bus is a fine pitch kapton/copper/aluminum printed circuit board (PCB) providing power and control signals to the readout chips and brings data out

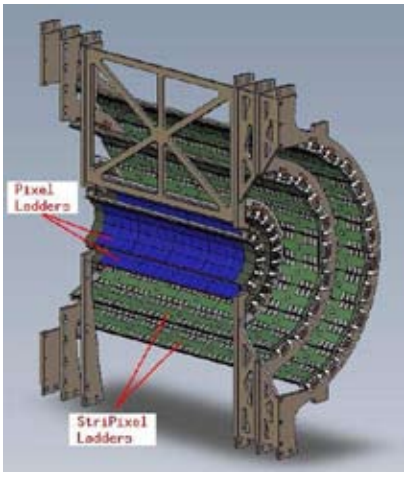

Fig. 1. A cross-section view of the proposed VTX showing the two inner pixel barrels, two outer stripixel barrels, and cooling and support structure.

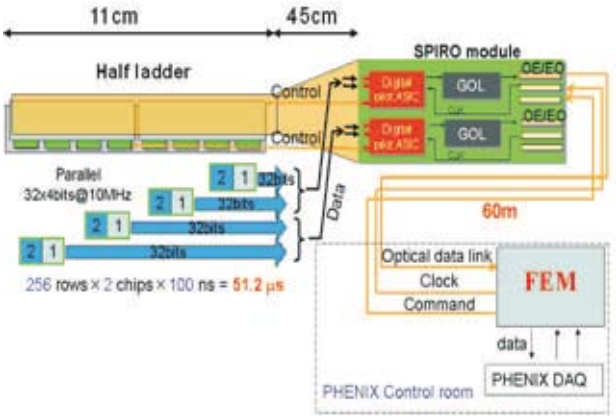

Fig. 2. A schematic overview of a pixel half-ladder.[3]

to the Silicon PIxel Read-Out (SPIRO) module on a 128 bit data bus. The half-ladder is connected via a bus extender to a SPIRO module which provides all voltages, control and timing signals and reads out the data for a half ladder. The SPIRO module is connected via optical fiber to the pixel Front End Module (FEM)

*1 Columbia University, Nevis Laboratories, USA
*2 Laboratoire Leprince-Ringuet, Ecole Polytechnique, CNRS-IN2P3, France
*3 Oak Ridge National Laboratory, USA
*4 Department of Physics and Astronomy, Stony Brook University, USA
*5 Rikkyo University, Japan
*6 Brookhaven National Laboratory, USA
*7 Iowa State University, USA
*8 CERN, CH-1211, Geneva Switzerland
*9 Tokyo Metropolitan College of Industrial Technology, Japan

which is the interface to the PHENIX data acquisition system. The pixel bus and bus-extender are being designed and built at RIKEN. The final prototype of the pixel bus is shown in Fig 3.

Fig. 3. The final prototype pixel bus prior to attachment of the sensor modules and and connectors. The 500 Yen coin provides the scale.

The SPIRO module is used to control and readout the the ALICE1LHCb chips. Two PHENIX Digital Pilot ASICs located on the SPIRO board each readout two ALICE1LHCb chips in parallel at a rate of 10 MHz, allowing a half ladder to be completely read out in 51.2 μsec, achieving a maximum data rate of $\sim$ 20kHz. The PHENIX Digital Pilot ASIC was developed by the RIKEN group using the same design rules and radiation tolerant technology as used for the ALICE Pixel Pilot ASIC.[5] Data from the PHENIX Digital Pilot chip is serialized with the Gigabit Optical Link (GOL) chip which is radiation tolerant and capable of transmitting data at 1.6 Gbits/sec.[6] The SPIRO module also has two Analog Pilot chips used for voltage control and monitoring on the half-ladder.[7] The SPIRO modules are being designed and built at LLR-Ecole Polytechnique in France.

The Pixel FEM is the interface between two SPIRO modules and the PHENIX DAQ and slow control systems. Commands, initialization parameters and clock timing information is transmitted to the SPIRO modules and pixel data is received from the SPIRO modules. In addition, the FEM formats the pixel data into standard PHENIX data packages prior to inclusion of the data into a PHENIX data stream. The pixel FEM is being designed and built at Stony Brook University.

Prototype pixel buses, bus extenders, SPIRO boards and pixel FEMs were used to build a cosmic ray test stand which was successfully tested at Stony Brook University in October of 2007. The system consisted of a 1.5 cm pre-production bus and two 3.0 cm prototype buses forming a 3 layer cosmic ray telescope. During the tests, approximately 100 cosmic ray events were observed in the telescope.[8]

The stripixel detector forms the two outer barrels of the VTX. The inner barrel with a radius of 10 cm consists of 18 ladders, and the outer barrel at a radius of 14 cm consists of 26 ladders. Each ladder contains 5 or 6 stripixel sensor modules for the inner and outer barrels of the stripixel detector respectively.

Each sensor module consists of a silicon stripixel sensor with x and u strips on the same side of the silicon sensor.[9] The u strips are rotated 4.6° with respect to the x strips to provide stereo readout of the sensor. The silicon sensor is attached to the ReadOut Card (ROC) and the modules are mounted on a carbon fiber stave which provides the mechanical support and cooling for the ladder. Each ladder is readout from one end to a stripixel FEM located near the detector which provides the interface to the PHENIX data acquisition system.

Readout of the stripixel sensor is controlled by the ROC which has 12 SVX4 chips developed at Fermi National Laboratory and Lawrence Berkeley National Laboratory.[10] Each SVX4 chip reads out 128 strips which are digitized with 8 bit ADCs, allows for on-board zero suppression, has a 46 deep pipeline buffer and is radiation hard. Control of the readout is done by the ROC Control Chip (RCC), a custom radiation tolerant ASIC designed at Oak Ridge National Laboratory. All RCCs on a ladder share a common bus which is also connected to the Pilot Module (PM). The PM passes all data between the stripixel FEM and the ladder and provides voltage regulation, filtering and distribution to the ladders. The stripixel FEM serves as the interface between the ROC's and the PHENIX DAQ and slow control systems. The ROCs, PMs and FEMs are being designed, prototyped, and built at Oak Ridge National Laboratory, and the sensor module assembly and ladder construction is being done at Brookhaven National Laboratory.

Final prototypes of the PIXEL bus, bus extender, and SPIRO modules have been built. A system test of the prototype modules was successfully completed at Stony Brook University in October 2007. Fabrication of production components is to start in the first half of 2008. We expect to start assembly of the first pixel buses in 2008, with all ladders ready for installation into the detector in time for the data taking during PHENIX Run 10 starting in 2009. Prototyping of sensor modules and read out electronics for the stripixel ladders continues with production of ladders scheduled to start in 2009, and installation scheduled to be completed in 2010 in time for PHENIX Run 11.

References

1) H. Kano, et al. : RIKEN Accel Prog. Rep. 39(2006)211
2) K. Fujiwara, et al.: RIKEN Accel Prog. Rep. 41(2008)
3) R. Ichimiyma et al.: RIKEN Accel Prog Rep. 41 (2008)
4) K. Wyllie: ALICE1LHCB Documentation (2001)
5) A. Kluge: ALICE Silicon Pixel On Detector Pilot System OPS2003-The missing manual (2005)
6) P. Moreira et al.: GOL Reference Manual (2005)
7) G. Anelli, R. Dinapoli, A. Kluge: Specification of the digital control part of the ANAPIL2 (2004)
8) M. Kurosawa, et al.: RIKEN Accel Prog. Rep. 41(2008)
9) Z. Li et al.: Nucl. Instr. and Mth. A 518 (2004), 535 (2004), 541 (2005)
10) L. Christofek et al.: SVX4 User's Manual (2003)

Development of the front-end electronics for the muon trigger in RHIC-PHENIX experiment

Y. Fukao for the PHENIX MuTr FEE Upgrade Group

The PHENIX experiment aims to reveal the spin structure of the proton. One of the mysteries in the study of the proton spin structure is the contribution of sea quarks to the proton spin. Currently, we only know that the total polarization of the sea quarks is slightly negative, and no measurement that can directly reveal the flavor of the sea quarks has been performed. Our goal is to determine the polarization of the sea quarks and their individual flavor by measuring a single helicity asymmetry in W boson production during the collisions of polarized protons. Since the W boson is produced by the weak interaction, there are many advantages of this method. One is that the theory of the weak interaction is well understood and the measurement of the asymmetry can directly connect to the polarization of the sea quarks. The second is that the W boson couples with the quark flavor selectively. The third is that quarks with negative helicity or antiquarks with positive helicity participate in the reaction due to the $V-A$ structure of the weak interaction. For these reasons, measuring the W boson is a promising method studying the spin of the sea quarks.

W bosons are measured by detecting high-momentum muons from their decay, using the muon arms in the PHENIX experiment.[1] Figure 1 shows the side view of the PHENIX detector. Two muon arms are located forward and backward of the collision point. The muon arm consists of a muon identifier (MuID) and a muon tracker (MuTr). MuID comprises five layers of chambers sandwiched by steel walls. Particles that penetrate MuID are identified as muons. MuTr comprises three stations of tracking chambers in a radial magnetic field. The two stations near the collision point include three cathode-readout strip chambers each, while the last station has two chambers. In total, there are six or four active cathode planes in each station because the cathodes of both sides are read out. The direction of the nonstereo cathode strips is radial and the stereo strips are tilted by about 10 degrees. Therefore, MuTr is sensitive to the azimuthal position of the muon. The momentum of a muon is determined from the curvature of its track. One of the greatest difficulties in measuring a W boson is that the trigger rate will be too high at the designed luminosity for 500 GeV operation to record all events in the current setup, in which muons with a momentum of more than 2.5 GeV/c can penetrate MuID and fire the trigger.

We are developing a new trigger system for the muon arm. The system performs rough particle tracking online and triggers events with straight tracks as possible high-momentum muons. To implement such a function into PHENIX, two types of hardware are planned to be installed, a resistive plate chamber (RPC) and trigger boards for MuTr (MuTRG). The trigger will be generated as a combination of RPC and MuTRG. RPC provides the two-dimensional position of the muon and three stations will be installed in each arm. One of the features of RPC is its good timing resolution of a few nsec. The timing of the new trigger will be determined by RPC. MuTRG contributes to providing the position in the azimuthal direction, which is sensitive to the momentum of the muon, with minimum modification to the PHENIX detector. Figure 2 shows a schematic diagram of MuTRG. The signal from the cathode strips of MuTr is divided into two lines. 95% of the charge of the signal is sent to the existing electronics, MuTr-FEE (front-end electronics), to measure the position offline. The remaining 5% is used for MuTRG. It is amplified and discriminated (MuTRG-AD[2]), then transmitted from the interaction region to the counting room (MuTRG-TX), where signals from several MuTRG-TX boards are merged (MuTRG-MRG). Finally, the trigger is generated in combination with RPC at the level 1 trigger board. The hit information from MuTRG is also sent to a data collection module (DCM) and recorded.

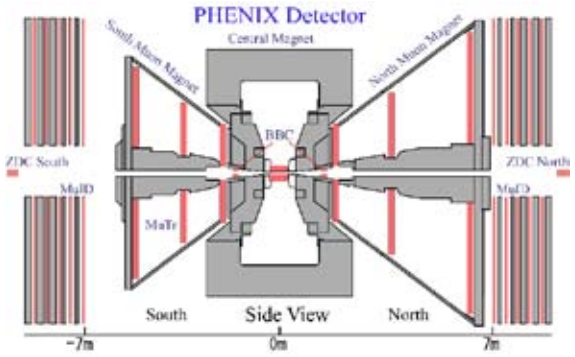

Fig. 1. Side view of the PHENIX detector.

During summer 2007, we performed a test experiment at PHENIX to evaluate MuTRG-AD and TX boards. The boards were installed in part of MuTr and the data by a cosmic ray were collected. The output of MuTRG-TX was received by a temporary interface board and sent to the PHENIX readout system. The data were recorded by a standard PHENIX DAQ and merged with the data from MuTr-FEE. The purpose of the test experiment was twofold. One was to evaluate the effect of MuTRG-AD and TX on the existing MuTr-FEE and the other was to evaluate the performance of MuTRG-AD and TX themselves.

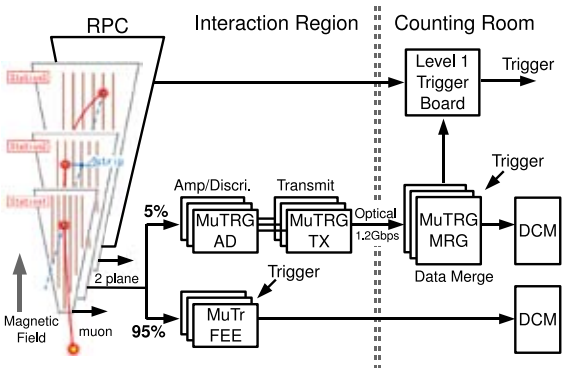

Fig. 2. Schematic diagram of MuTRG.

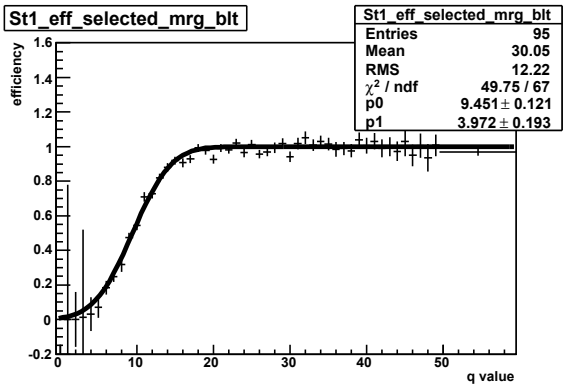

Fig. 4. Turn-on curve of MuTRG efficiency. The q value corresponds to the calibrated charge. MPV for MIP has a q value of 17. The data is fitted to a function of the Gaussian integral. $p0$ and $p1$ indicate the center and width of the rising edge, respectively.

It is important to maintain the performance of MuTr when it operates with MuTRG. Because the noise in MuTr-FEE is increased by adding MuTRG-AD, which degrades the position resolution of MuTr, the effect of MuTRG on MuTr-FEE must be minimized. Figure 3 shows the noise level of MuTr with MuTRG-AD and TX. The noise level is defined as the ratio of the pedestal RMS (root mean square) to the MPV (most probable value) for the MIP (minimum ionization particle). The noise level was increased by 30% after installing MuTRG-AD and TX. This corresponds to the degradation of the position resolution from 100 μm[a)] to 120 μm, and a simulation shows that this is acceptable. It also turned out that the position resolution is recovered by increasing the high voltage (HV) of MuTr by 25 V. In addition to studying the noise level, we evaluated the detection efficiency of MuTr and no serious problems were found.

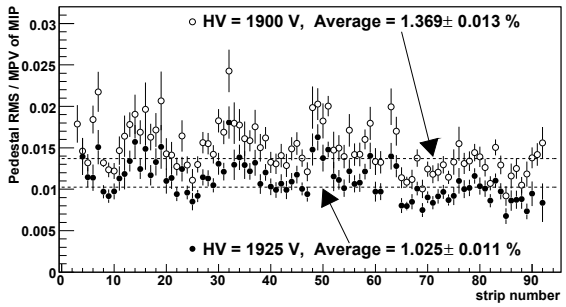

Fig. 3. Noise level for a part of MuTr after MuTRG-AD and TX were installed. The horizontal axis is the number of the cathode strip. The open circles were measured with nominal HV for MuTr (1900 V). The filled circles were measured with HV increased by 25 V. The averages over the strips are shown in the figure.

To evaluate the performance of MuTRG, we examined its efficiency, the noise in MuTRG-AD and the timing resolution, which are directly related to the rejection power of the trigger. Figure 4 shows the turn-on curve of the efficiency of MuTRG-AD. The threshold for the signal in MuTRG-AD was set so that the fake hit by noise was 1 kHz, the effect of which is negligible in terms of the rejection power. The turn-on curve was fitted reasonably well to a function of the Gaussian integral with the efficiency at the plateau fixed to 1. Based on the turn-on curve, we obtained an efficiency of 91% for MIP for the single-cathode plane. Therefore, when we take the OR of two cathodes in the same station, the efficiency becomes 99%. The timing resolution of MuTRG was evaluated to be ∼60 nsec, although the time distribution is not Gaussian but asymmetric. About 95% of the signal from MuTRG was included in a gate of 318 nsec.[b)]

From the results of the test experiment, we produced a combined board of MuTRG-AD and TX, and confirmed that the noise in both MuTr-FEE and MuTRG is consistent with the results of the test experiment. To finalize the development of MuTRG-AD and TX, we plan to carry out another test at PHENIX. The board with the combined MuTRG-AD and TX will be installed into half of MuTr in summer 2008. The development of MuTRG-MRG will also be completed at that time.[3)]

References

1) PHENIX collaboration: Nucl. Instrum. Meth. **A**499, 537, (2003).
2) K. Shoji et al.: RIKEN Accel. Prog. Rep. **4**0, 184 (2007).
3) K. R. Nakamura et al.: RIKEN Accel. Prog. Rep. **4**1, 183 (2008).

a) The position resolution of 100 μm was evaluated at a test bench.[1)] This resolution has not yet been achieved at PHENIX and a study to achieve it is underway.

b) The interval between the intersections of beams is 106 nsec at RHIC. The trigger timing is determined by RPC. However, increasing the gate for MuTRG causes a fake track and degradation of the rejection power. The gate of 318 nsec is considered acceptable on the basis of a simulation.

Specification of Data-Merging Board and Data-Collecting-Module Interface Board for Muon Trigger Upgrade at RHIC PHENIX

K. R. Nakamura*1 and the PHENIX Collaboration*2

One of the goals of the PHENIX experiment at RHIC is the understanding of the spin structure of a proton. The spin structure of a proton contains many unknown properties and one of them is the spin distribution function of each sea-quark flavor. To solve this problem, as a part of the PHENIX experiment we plan to measure the single-spin asymmetry of the W boson production cross section A_L^W of proton-proton scattering at $\sqrt{s} = 500$GeV.[1)]

For this measurement we need to detect muons produced by W boson decay in the forward and backward directions.[2)] In the PHENIX detector system, the forward muon detection is performed by a muon arm,[3)] which consists of cathode strip chambers (MuTr) for tracking and momentum measurement, and five wire-chambers (MuID) with alternating layers of steel walls for hadron absorption (Fig. 1).

In the measurement of W boson production, W bosons are identified by the detection of high-transverse-momentum muons over 20GeV/c, since in the low-momentum-region background events are dominant compared with W boson events. However, the threshold momentum of the current trigger system is up to 2.5GeV/c. When the designated RHIC luminosity of $2\times10^{32}\mathrm{cm}^{-2}\mathrm{s}^{-1}$ at $\sqrt{s} = 500$GeV is achieved, the reaction rate is expected to be 12MHz. At this threshold level of MuID, its rejection factor is about 250 and the trigger rate is 48kHz. Since the bandwidth of the PHENIX data acquisition system is 2kHz, it is still inefficient to acquire W boson data using this system. Thus, a new trigger with a rejection rate of over 6000 is needed for effective measurement. This implies the necessity of a trigger system with a higher threshold of momentum of over 20GeV/c.

A new trigger system using the MuTr signal is being developed. This system uses 5% of the Coulomb charge of the cathode strip signal to provide hit information and only produces a trigger for high-momentum muon events. The proposed system is shown in Fig. 2. Currently, the R&D of the amplifier-discriminator board (MuTRG-AD), which amplifies and discriminates 5% of the strip signal to obtain a hit signal, and that of the data-transfer board (MuTRG-TX), which serializes the 64-bit signal from the AD board for transmission from the interaction region to the counting house through an optical cable, are nearly complete.[4)] The combined AD and TX board (MuTRG-ADTX) is now being developed. The trigger system collects MuTr hit data from two cathode planes per station. Each cathode plane is covered by several MuTRG-ADTX boards. Thus, a data-merging board (MuTRG-MRG), which collects and reorders the signals of these MuTRG-ADTX according to strip ordering and transmits them to the first-level trigger board (LL1 board), which produces the trigger signal, is necessary.

The most important role of MuTRG-MRG is to merge the hit data and transmit it to the LL1 board.Since a number of MuTRG-ADTX are installed in each cathode plane, one MuTRG-MRG must be able to handle 1.2Gbps hit signals from 10 MuTRG-ADTX. Data from each MuTr-ADTX arrives synchronously with the beam clock and contains a beam-clock counter number (BCLK), which represents the event number, and hit information obtained from the MuTr strip. MuTRG-MRG checks the consistency of the BCLK from all MuTRG-ADTX. After this check, the board

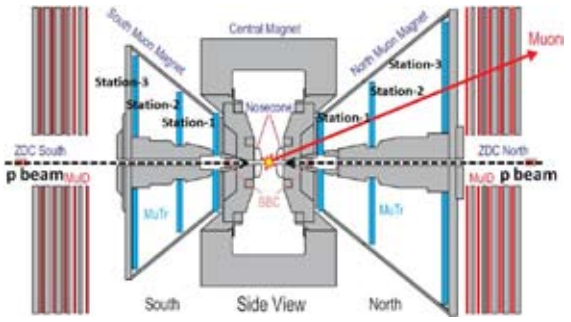

Fig. 1. Side view of forward/backward PHENIX detector system.

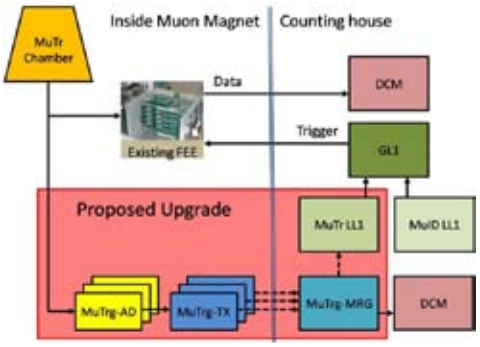

Fig. 2. Proposed upgrade of system. The R&D of MuTrg-AD and MuTrg-TX are almost complete.

*1 Department of Physics, University of Kyoto
*2 We also collaborated with O. Sasaki and M. Ikeno at KEK.

Table 1. Summary of control signals of MuTRG-MRG and ADTX through VME bus

MuTRG-MRG side	ADTX side
FPGA configuration, Reset, Initialization, Test signal input, Error detect, Mask configuration, Test signal readout, Link status, Chip control	FPGA configuration, Reset, Initialization, Test signal input, AD threshold configuration, Chip control

discards unnecessary data originating from parts of the AD boards unconnected to the chamber and reorders the residual valid data according to the strip arrangement. The hit data from the two cathode planes are compressed by using logical OR (or AND) on the two signals of the pair of strips. Finally, MuTr-MRG transmits the ordered data to the LL1 board through an optical cable at a data rate of about 2.8Gbps. Achieving the data rate is the most challenging work on the design of MuTRG-MRG. In this way MuTRG-MRG handles the data of at most 192 cathode strips.

Once the MuTRG-ADTX are installed inside MuTr, they are not directly controllable. Thus, the second important role of MuTRG-MRG is to control MuTRG-ADTX remotely. Control signals from the operator are transferred to MuTRG-MRG using a VME bus, and MuTRG-MRG distributes these signals to MuTRG-ADTX through an optical cable. Table 1 shows a summary of the control signals of MuTRG-ADTX and MuTRG-MRG.

Upon a request from the PHENIX trigger, the MuTRG-MRG sends triggered hit data to the data-collecting-module (DCM), which collects the hit data for the further analysis. Since MuTRG-MRG transmits the triggered data to the DCM after trigger is received, it must memorize the event data transmitted to the LL1 board until the trigger signal arrives. Thus, MuTRG-MRG is designed to store the data in a shift-register of more than 40 events.

An interface board is necessary to merge and serialize the triggered data from a number of MuTRG-MRG to transmit large amount of data from all the MuTRG-MRG to the DCM. This new board is called the DCM-interface board (MuTRG-DCMIF) and is now also being developed. MuTRG-DCMIF has two roles in this new system. The first one is to collect MuTRG-MRG signals and transmit serialized signals to DCM through an optical cable as mentioned above. One MuTRG-DCMIF can connect 16 MuTRG-MRG and handle the data from these 16 boards. The second role of the board is to receive control signals from the global timing module (GTM), which provides the trigger, beam clock, reset signal, initialization signal, and other features in the PHENIX DAQ system. MuTRG-DCMIF selects the trigger, beam clock, reset, and initialization signals from the GTM signal to distribute them to MuTRG-MRG, and the MuTRG-MRG transmits the reset and initialize signals to MuTRG-ADTX. In this way, the whole system can receive the GTM signals.

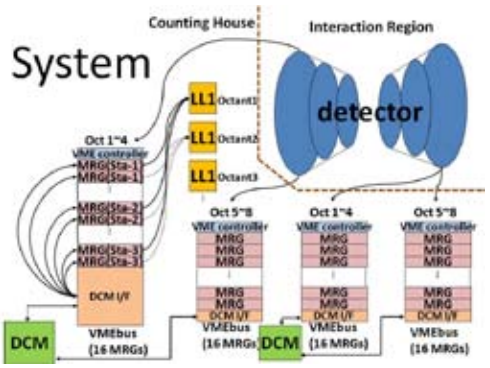

Fig. 3. System setup of MuTRG-MRG and DCM I/F boards. The hit signals bring to Counting House from Interaction Region.

The system setup of MuTRG-MRG and MuTRG-DCMIF is shown Fig. 3. Four VME crates are needed, and 16 MuTRG-MRG and one MuTRG-DCMIF are amounted on each crate. These boards are 9U in height and 280mm in depth.

The MuTRG-MRG and MuTr-DCMIF boards are now undergoing R&D. MuTRG-MRG will be complete at the beginning of April 2008, and MuTRG-DCMIF will be complete in summer 2008. Testing of the prototypes at the KEK test bench before their production and installation in the PHENIX system is scheduled for this summer.

References

1) G. Bunce et al.: Annu. Rev. Nucl. Part. Sci. **50**, 525 (2000).
2) C. Bourrely and J. Soffer: Phys. Lett. B **314**, 132 (1993).
3) URL: http://www.phenix.bnl.gov/WWW/muon/muon.html
4) Y. Fukao et al.: RIKEN Accel. Prog. Rep. **41**, 181 (2008).

III. RESEARCH ACTIVITIES II
(Material Science and Biology)

1. Atomic and Solid State Physics(ions)

First-principles electron dynamics simulation for optical breakdown of dielectrics under intense laser field

T. Otobe,[*1] M. Yamagiwa,[*1] J.-I. Iwata,[*2] K. Yabana,[*2] T. Nakatsukasa, and G. F. Bertsch[*3]

The interaction of ultrashort laser pulses with dielectrics has been a subject of intense study for both the fundamental interest as well as for possible applications. A key physical process in the interaction, the optical breakdown of the medium, is a highly nonlinear optical process but is not yet fully understood. The optical breakdown causes a reproducible structural modification of the dielectric, making the process suitable for micromachining, medical surgery, and other technical applications. However, the first-principles computational approach has not been applied to the electron dynamics for bulk systems irradiated by intense ultrashort pulses. In the present article, we report our attempt to describe the optical breakdown of dielectrics based on the time-dependent density-functional theory (TDDFT).

The TDDFT enables us to treat the ionization of both multiphoton and tunneling mechanisms. It also incorporates the dynamical screening effect, which is one of the important many-body correlations. We apply the TDDFT to diamond, a prototype of a typical insulator. Our computations are performed using a formalism that was originally developed for the calculation of the dielectric function of crystalline solids.[1] Assuming the long-wavelength limit and that the pulse laser is represented by a time-dependent spatially uniform electric field $\vec{E}_{\rm laser}(t)$, the electronic motion is described by the following time-dependent Kohn-Sham (TDKS) equation for single-particle orbitals $\psi_i(\vec{r},t)$:

$$i\hbar\frac{\partial}{\partial t}\psi_i(\vec{r},t) = \left\{\frac{1}{2m}\left(\vec{p}+\frac{e}{c}\vec{A}_{\rm tot}(t)\right)^2 + V_{\rm ion}(\vec{r}) + \int d\vec{r}'\frac{e^2}{|\vec{r}-\vec{r}'|}n(\vec{r}',t) + \mu_{\rm xc}(\vec{r},t)\right\}\psi_i(\vec{r},t), \quad (1)$$

where $n(\vec{r},t)$ is the time-dependent density given by $n(\vec{r},t)=\sum_i|\psi_i(\vec{r},t)|^2$, and $\mu_{\rm xc}(\vec{r},t)$ is the exchange-correlation potential. The orbitals $\psi_i(\vec{r},t)$ are specified by band index n and Bloch wavenumber $\vec{k}$. The time-dependent, spatially uniform vector potential $\vec{A}_{\rm tot}(t)$ is composed of the external and induced ones, $\vec{A}_{\rm tot}(t)=\vec{A}_{\rm ext}(t)+\vec{A}_{\rm ind}(t)$. The external vector potential $\vec{A}_{\rm ext}(t)$ is related to the electric field of the applied laser pulse, $\vec{E}_{\rm laser}(t)=-d\vec{A}_{\rm ext}(t)/dt$. The induced vector potential, $\vec{A}_{\rm ind}(t)$, expresses the electric field caused by the polarization.

Figure 1 shows results for diamond. The laser pulse is characterized by the maximum laser intensity, $I_0 = 1\times10^{15}$ W/cm^2, the laser frequency, $\hbar\omega = 3.1$ eV, and the pulse duration, $T = 40$ fs. The top panel (a) of Fig. 1 shows the time profile of the electric field. $\vec{E}_{\rm laser}(t)$ and $\vec{E}_{\rm tot}(t)$ are presented by dotted and solid lines, respectively. The middle panel (b) shows the number of excited electrons per carbon atom, which is defined as

$$n_{\rm ex}(t) = \sum_{nn'\vec{k}}\left(\delta_{nn'} - |\langle\phi_{n\vec{k}}|\psi_{n'\vec{k}}(t)\rangle|^2\right). \quad (2)$$

The bottom panel (c) shows the excitation energy per carbon atom as a function of time.

At the beginning, when the applied electric field is weak, the response is dielectric: $E_{\rm tot}(t)\simeq\epsilon^{-1}E_{\rm ext}(t)$, with the static dielectric constant of diamond, $\epsilon\simeq6$. At $t\approx15$ fs, the number of excited electrons and the excitation energy show a rapid increases. Simultaneously, the total electric field becomes out of phase to the applied electric field, signaling a large energy transfer. This change may indicate an optical breakdown. Detailed investigation is now in progress.

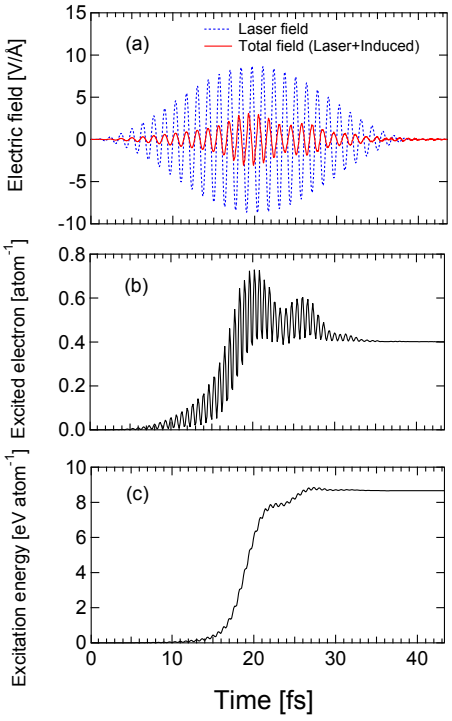

Fig. 1. TDDFT simulation for diamond under a laser pulse. See text for details.

*1 Advanced Photon Research Center, JAEA
*2 Center for Computational Sciences, University of Tsukuba
*3 INT, University of Washington, USA

References

1) G. F. Bertsch et al., Phys. Rev. B **62**, 7998 (2000).

Pulse-luminescence continuum in heavy-ion tracks in case of extremely weak atomic interaction in condensed rare gases

Kazuie Kimura, Masanori Koshimizu*[1], Hiromichi Ryuto, Keisuke Asai*[1], and Masayuki Kase

By time-resolved spectra of time resolution of 85 ps, we found unknown ultrafast luminescence from incipient track cores by 2-MeV/nucleon heavy-ion in insulator crystals. Such luminescence could be observed evidently for alkali halides and metal oxides while negligibly slight luminescence was observed in SiO_2 and none in diamonds which are formed by covalent bonds. It can be characterized as follows[1, 2]. The luminescence rises from vacuum ultraviolet region in some crystals and covers a visible end. It has a structure comprised of broad peaks. Its efficiency is largely dependent on the atomic number of the projectile ion, i.e. excitation density and also on target solids, probably their bond nature. The efficiency increases super-linearly in many cases with excitation density. This means that the luminescence is produced by multiple interactions among precursors. The lifetime of these precursors should be less than 100 ps since the deconvoluted decay curve of luminescence fit to an exponential function and has no tail. The lifetimes of known excited states are too long to be the precursors. The luminescence efficiencies is largely dependent on the target material: in case of alkali halides, the efficiency increases in the order of mass of halogens such that iodides have about 100 times stronger luminescence than fluolides. Lastly, this luminescence is independent of temperature in the range between 3K and 350 K. Almost all electronic excited states in the solids are known to be unable to survive at 350 K. Therefore, the present luminescence should be unusual one which has spectroscopic nature unchanged by temperature increase. This means that the spectrum obtained near 350 K is due to neat ultra-fast luminescence surviving after the other luminescence disappeared. Since the spectrum comprises continuum, we call the ultra-fast luminescence UFLC (ultra fast luminescence continuum). The photoemission mechanism is, we propose, stimulated emission through interaction among near-continuum states, i.e. stimulated emission of hot bands. This mechanism is the most applicable for alkali halides. Broad peaks of UFLC are interpreted due to Stokes shift similarly to self-trapped excitons. It is noted that time for hole-trapping (2ps) is much shorter than the time till electrons ejected diffuse, return to holes, and create self-trapped excitons (100ps). Also, holes in alkali halides are essentially halogen atom, X^0, which has no longer ionic bonds with surrounding ions which work as a network to diffuse excess energy. In exchange, the extremely high-dencity of continua and hot bands stimulate photo-emissions. By contrast, diamond has 4 bonds a carbon atom that can keep their networks against ionization. Therefore, the escape probability of the excess energy depends on the bond order and its strength. However, strong VUV-UFLC of MgO seems to be not interpreted by this mechanism but by extra dynamics of holes, though the detail is not described here. Now, if above network mechanism is true, what happens in liquid or solid rare gases? There are no atom-atom attractive forces except for that of van der Waals force at ground states. Since the hole is isolated, strong UFLC could be expected. We will try to measurer UFLC and its dynamical data for condensed rare gases using a cryo-monochromator shown in Fig.1. and our ion-photon time correlation system.

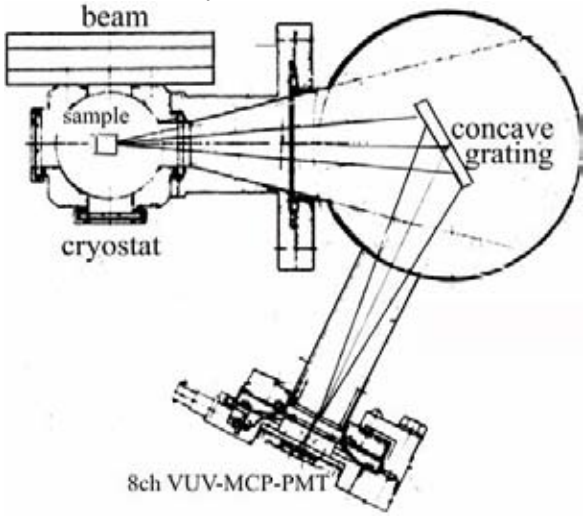

Fig.1. Cryo-monochromator; a grating is concave one with a focal length 197 mm, blaze wavelength of 50 nm and it looks at the sample directly Time-correlation system using 8ch MCP-PMT is the same as the one used in Ref. 2.

*1 graduate school of eng. Tohoku Uni.

References

1) K. Kimura, J. Kaneko, S. Sharma, W. Hong, and N. Itoh, Phys. Rev. B 60, 12626(1999)
2).K. Kimura, Nucl. Instr. Meth. Phys. Res., B 212, 123(2003)

Dynamic features of beam guiding by insulator capillaries

Y. Kanai, M. Hoshino,[*1] T. Ikeda, T. Kambara, R. Hellhammer,[*2] N. Stolterfoht,[*2] and Y. Yamazaki

The electric property of insulator surfaces can be used to guide slow ions along the axis of an insulator capillary.[1,2] Qualitatively, this guiding process can be explained as the deflection of ions by charge patches produced on the capillary surface by the preceding ion-surface collisions.[1,3] Here, we present experimental results indicating the relationship between the growth of the charge patches and the behavior of the guided ions.

We performed experiments at RIKEN with Ne^{7+} ions from a 14.5 GHz ECR ion source.[4,5] Beam energies were 3.5, 4.9, and 7 keV, and beam intensities 5 - 200 pA at the target position. The typical beam divergence was smaller than 0.5°. The diameter of the beam at the target was 1-1.5 mm. A polyethylene terephthalate (PET) foil was attached to the target holder and rotated. The PET foil included capillaries with a length of 10 μm and a diameter of 200 nm. The capillary density was 4×10^6 capillaries/cm^2. To avoid the macroscopic charging of the surface of the PET foil, Au was evaporated on the front and exit sides. We used a two-dimensional position-sensitive detector (PSD) consisting of MCPs and a wedge-and-strip anode. It was set 170 mm from the target and rotated on the horizontal plane around the target. The vacuum in the chamber was lower than 1×10^{-5} Pa.

Typical experimental results for 3.5 - 7 keV Ne^{7+} are shown in Fig. 1. Here, the PET capillary was tilted by 2.8° with respect to the incident beam direction and the beam intensity was 50 pA. The transmitted intensities and deflection angles of the beams were plotted as functions of the charge accumulating at the foil surface. The deflection angles moved along the tilted direction in accordance with the intensity evolution. Although this behavior seems to be a general feature for the beam guiding effect[4–7], a detailed study has not been done.

The increase in deflection angle with the intensity evolution in Fig. 1 may be attributed to the growth of a charge patch at the entrance region of the capillary. Moreover, the decrease in deflection angle after the maximum in Figs. 1 (a) and (b) may be attributed to the growth of another charge patch in the capillary. Plural patch formation was shown by simulation.[3] It is noted that this oscillatory behavior of the deflection angle along the tilted direction was clearly observed at low energies of 3.5 and 4.9 keV, and was not observed at 7 keV, as shown in Fig. 1. At the energy of 7 keV, the second patch may not be formed and the guided ions may be deflected only once by the patch in the entrance region.

*1 Department of Physics, Sophia University
*2 Hahn-Meitner Institute, Berlin, Germany

References
1) N. Stolterfoht et al.: Phys. Rev. Lett. **88**, 133201 (2002).
2) T. Ikeda et al.: Appl. Phys. Lett. **89**, 163502 (2006).
3) K. Schiessl et al.: Phys. Rev. A **72**, 062902 (2005).
4) Y. Kanai et al.: Nucl. Instrum. Methods B **258**, 155 (2007).
5) N. Stolterfoht et al.: Phys. Rev. A **76**, 022712 (2007).
6) N. Stolterfoht et al.: Nucl. Instrum. Methods B **225**, 169 (2004).
7) M. Fürsatz et al.: J. Phys. Conf. Series **58**, 319 (2007).

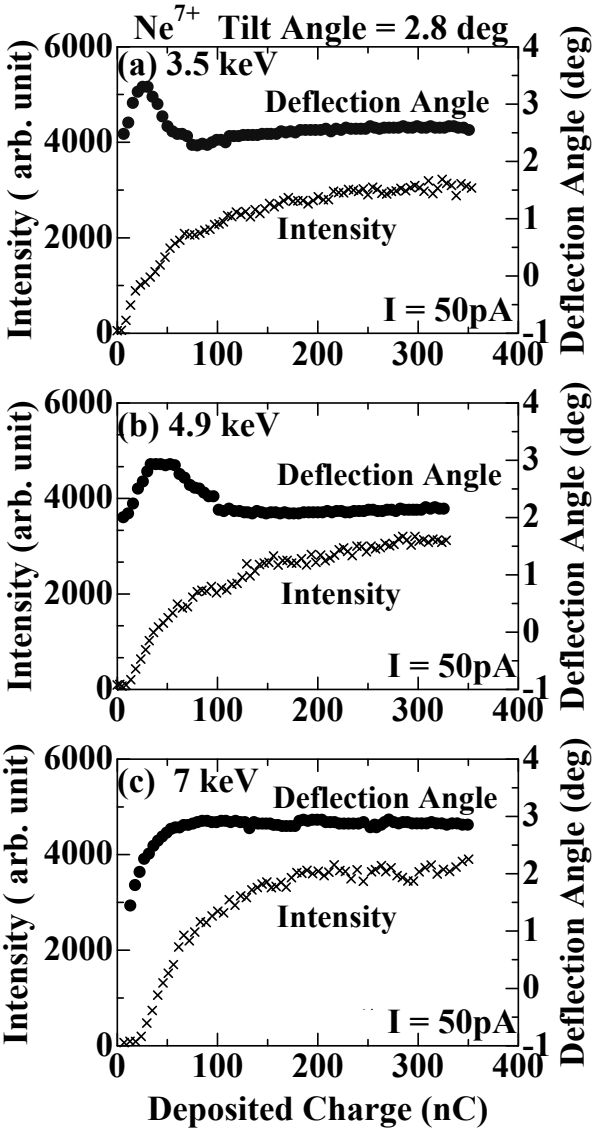

Fig. 1. Deflection angle (•) and intensity (×) evolutions of transmitted 3.5, 4.9, and 7 keV Ne^{7+} ions as functions of charge deposited at PET foil. The tilt angle was 2.8° and the beam intensity was 50 pA. The deflection angle was deduced from the peak position at the PSD.

Density enhancement of slow highly charged ion beams focused by tapered glass capillary

T. Ikeda, Y. Kanazawa,[*1] Y. Kanai, T. M. Kojima, M. Hoshino,[*1] Y. Iwai, and Y. Yamazaki[*2]

We have developed a method to produce a nanometer-sized slow highly charged ion (HCI) beam with a single tapered glass capillary. The ions entering the glass capillary hit the inner wall and consequently cause the wall to become charged. When the accumulated charge becomes sufficiently large to prevent the subsequent incident ions from touching the inner wall, the ions travel more or less parallel to the wall, and then the ions can exit from the outlet. When the diameter of the outlet is smaller than that of the inlet, a density-enhanced beam is realized. The glass capillary has the following advantages for producing a nanobeam of slow HCIs; (1) the size of the output beam is the same as the outlet inner diameter, (2) ions can be reflected from the inner wall without close collision, keeping their initial charge states, and (3) the taper can enhance the density of the output beam.

An ion beam of 8 keV Ar^{8+} was extracted from a 14.5 GHz Caprice ECR (electron cyclotron resonance) ion source at RIKEN, and injected in a glass capillary made of borosilicate[2], and finally detected by a PSD (position-sensitive detector) after a deflector (Fig. 1). The deflector was used for the charge-state analysis of transmitted ions. The outer and inner diameters of the capillary at the inlet were 2 mm and 0.8 mm, respectively, and those at the outlet were 55 μm and 0.9-24 μm, respectively. (Hereafter, $D_{\rm out}$ for the outlet inner diameter.) Aluminum foil was used to monitor incoming ion currents of 0.1 - 100 pA.

For a capillary of $D_{\rm out}$= 24 μm, the transmitted beam was obtained even when the capillary was tilted by ±87 mrad (=±5°) with respect to the beam direction. Its divergence of ±5 mrad without the charge transfer inside the capillary was observed, where the transmission rate was at most 1%. Without tilting the capillary, the maximum counts at the PSD was about 1600 cps for an entering current of 0.2 pA. The density enhancement factor σ was introduced as the ratio of N_t/S_o to N_i/S_i, where N_t is the number of transmitted ions, N_i the number of injected ions into the capillary, and S_o and S_i the geometrical outlet and inlet cross sections of the capillary, respectively. For this measurement, the density of the output beam was approximately 10-fold that of the input beam ($\sigma \sim$10)[1].

However, density enhancement may depend on beam energy, the charge state of ions, ion mass, input current intensity, outlet size, and surface conductivity of the capillary among others. We examined the input current dependence of density enhancement. Figure 2 shows the enhancement factor as a function of input current without tilting the capillary ($D_{\rm out}$= 20 μm). The measurement errors of input current and enhancement factor were due to input-beam fluctuation and were estimated to be about 10%. The enhancement factor was found to decrease from 6 to 1 with the input current varying from 0.8 pA to 30 pA. To confirm the upper limit of the enhancement, measurements with input currents less than 0.8 pA are required.

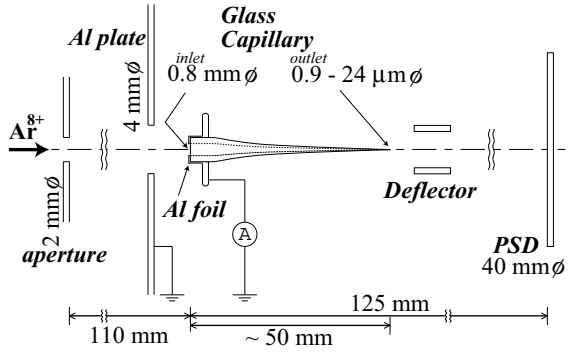

Fig. 1. Schematic view of experimental setup[1].

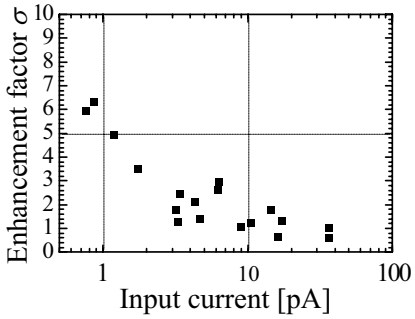

Fig. 2. Input current dependence of enhancement factor for 8 keV Ar^{8+} beam.

References

1) T. Ikeda, Y. Kanai, T. M. Kojima, Y. Iwai, T. Kambara, Y. Yamazaki, M. Hoshino, T. Nebiki, and T. Narusawa: Appl. Phys. Lett. **89**, 163502 (2006).
2) T. Ikeda, T. M. Kojima, Y. Iwai, Y. Kanai, T. Kambara, T. Nebiki, T. Narusawa, and Y. Yamazaki: J. Phys. Conf. Ser. **58**, 68 (2007).
3) T. Ikeda, Y. Kanai, T. M. Kojima, Y. Iwai, Y. Kanazawa, M. Hoshino, T. Kobayashi, G. P. Pokhil, and Y. Yamazaki: J. Phys. Conf. Ser. **88**, 012031 (2007).

*1 Department of Physics, Sophia University
*2 Also at the Institute of Physics, University of Tokyo

Precision measurement of Ar^{+*} with collinear laser spectroscopy

V.Lioubimov,[*2] M.Wada,[*1] M. Ogawa,[*3] A.Takamine,[*1,*3] T.Nakamura,[*1] P. Schury,[*1] H.Iimura,[*4] K.Okada,[*5] H.A.Schuessler,[*2] and Y.Yamazaki,[*1,*3]

Precision laser spectroscopy on a metastable $^{40}Ar^{+}$ ion beam has been performed with a collinear fast beam setup[1] and two (parallel and anti-parallel) laser radiations. Collinear laser spectroscopy has been used for systematic measurements of nuclear charge radii through the isotope shift of atomic levels. For such a purpose, one usually doesn't need absolute resonance frequencies but only needs differences of resonance frequencies among isotopes. If such relative values are concerned, a single laser radiation at fixed frequency can be used for spectroscopy and the isotope shift can be determined from the Doppler shift by scanning the beam velocity. However, a measurement of the absolute transition energy provides important additional information. Recent atomic theory can predict atomic level energies with great accuracy which allows us to deduce the absolute value of the nuclear volume effect. In particular certain atomic levels can be probes for the possible variation of the fundamental constant.[2]

We measured the $^2G_{7/2} - ^2F_{5/2}$ transition ($\lambda_0 \approx 617$ nm) of a$^{40}Ar^{+}$ metastable ions at a beam energy of 20 keV. A 20-keV Ar ion beam was provided by a plasma ion source and mass separated by a 90-degree dipole magnet. The fluorescence detection region of the beam line was located at a fixed potential of -150 V in order to avoid optical pumping before a photo multiplier detects laser induced fluorescence (LIF). The resonant frequency of such an accelerated beam is obviously very sensitive to the beam energy. The sensitivity is 13 MHz/V in the present case. The acceleration voltage was stabilized to <0.1 V using an accurate voltage divider and a software PID feedback loop. Even when the acceleration voltage was constant, we still observed noticeable velocity drifts which were mainly due to the ion source conditions. We therefore measured LIF in parallel and anti-parallel configuration simultaneously using two independent lasers. The frequencies of two radiations were also measured simultaneously using an optical frequency comb generator. A mode-locked femto second laser with a microstructure fiber provides millions of narrow peaks in the frequency domain with an exact interval of the repetition rate of the laser ($f_{\mathrm{rep}} = 250$ MHz) in the visible to IR spectral ranges. Two dye laser radiations were merged and interfered with the comb radiation and the beat signals were detected in avalanche photo detectors. Due to a slight but sufficient difference (≈ 1.5 nm) of the wavelengths of the two lasers, two beat signals can be detected independently in two detectors using a grating. The dye laser frequency is determined as $\nu_{\mathrm{dye}} = nf_{\mathrm{rep}} \pm f_{\mathrm{beat}} \pm f_{\mathrm{offset}}$, where n is an integer indicating the n-th peak of the comb and f_{offset} is the offset of the first comb peak from the origin. The signs and n can be determined from the saturation spectroscopy of I_2 molecule and f_{offset} is locked to 40 MHz.

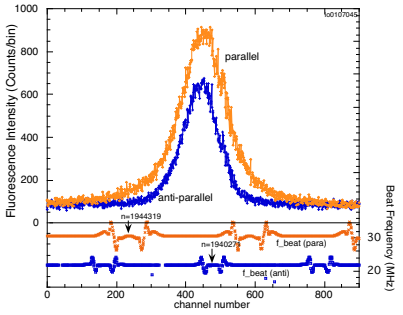

Fig. 1. LIF spectra of a $^{40}Ar^{+*}$ metastable ion beam with parallel and anti-parallel laser radiations. Absolute laser frequencies are obtained from the beat frequencies with a frequency comb.

Figure 1 shows an experimental result. The laser frequency for parallel configuration was scanned from lower to higher while the anti-parallel radiation was from higher to lower and the start frequencies were adjusted to coincide with each other. The beat frequencies were counted through band pass filters to avoid spurious counts due to the side-band signals and noise. The observed peak frequencies are described as $\nu_{\mathrm{para}} = \nu_0/\gamma(1+\beta\cos\theta_{\mathrm{p}})$ and $\nu_{\mathrm{anti}} = \nu_0/\gamma(1-\beta\cos\theta_{\mathrm{a}})$, where γ, β are the relativistic factors. Since the difference between the angles of laser radiations to the beam, $\theta_p - \theta_a$ is less than 1 mrad, the absolute transition frequency is obtained as $\nu_0 = \sqrt{\nu_{\mathrm{p}}\nu_{\mathrm{a}}}$ with high accuracy. Several measurements at different conditions showed good agreement in ν_0 while the beam velocities were different. We preliminary determined the transition frequency as $\nu_0 = 485,573,619.7(3)$ MHz. This measurement has two orders of magnitude higher accuracy than previous data.[3]

*1 Atomic Physics Laboratory, RIKEN
*2 Department of Physics, Texas A&M University
*3 Graduate School of Arts and Science, University of Tokyo
*4 Japan Atomic Energy Research Institute
*5 Department of Physics, Sophia University

References

1) V. Lioubimov et al.: RIKEN Accel. Prog. Rep. **40**, 166 (2007).
2) M. Aldenius et al.: submitted to Mon. Not. R. Astron. Soc. (2006).
3) G. Norlen: Phys. Scr. 8, 249 (1973).

Accuracy evaluation of the measurement system for determining hyperfine structure of alkali atoms in superfluid helium

K. Fujikake,[*1] T. Furukawa, Y. Matsuo, A. Hatakeyama,[*2] T. Kobayashi, A. Sasaki,[*1]
H. Odashima,[*1] and T. Shimoda[*3]

Laser spectroscopy in superfluid He (He II) is expected to be an effective method for determining the nuclear moments of unstable nuclei from their hyperfine structure. We have recently demonstrated its use for the accurate determination of nuclear moments and the hyperfine anomaly (Bohr-Weisskopf effect) of stable ^{85,87}Rb atoms in He II by laser-microwave double-resonance spectroscopy.[1,2)] The obtained hyperfine anomaly parameter is slightly different from that in free space due to the effect of surrounding He atoms. For a detailed discussion of such effects, it is necessary to evaluate the experimental error in our measurements of hyperfine structure of atoms in He II. For this evaluation we observed the hyperfine structure of ^{85}Rb atoms at room temperature in free space using the setup that was used previously for atoms in He II. We here report the comparison between the microwave hyperfine transition frequency we observed and that in the literature.[3)]

Figure 1 shows the experimental setup used for the measurement of the hyperfine transition frequency of ^{85}Rb atoms in free space. A glass cell (30 mm in diameter, 40 mm in length) containing a Rb metal sample is placed in the center of an open-top quartz container in a helium cryostat. Note that the cryostat is not cooled with any coolant. Other instruments such as the pumping laser, laser-induced fluorescence (LIF) detection system, and microwave devices are the same as those used for the experiment on atoms in He II.[4,5)] Rubidium atoms vaporized from the metal sample are optically pumped with the pumping laser tuned to the D_1 line (795 nm). During optical pumping, Rb atoms are populated in the F=2 ground state and then the atoms cease emitting LIF photons. When the microwave frequency is resonant with the hyperfine structure splitting, photon emission recovers because the polarization of atoms is decreased. To prevent the population relaxation of atoms due to wall collisions, the inside of the glass cell is coated with paraffin.[6)]

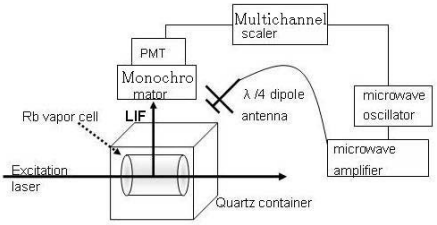

Fig. 1. Experimental setup.

A spectrum of the hyperfine transition of ^{85}Rb atoms in the ground state (F=2, m_F=0 → F=3, m_F=0) is shown in Fig. 2. We scanned the microwave frequency of the oscillator with a sweep time of ∼ 1 s and accumulated the results of about 50 LIF counts. In this experiment we used the step-sweeping mode rather than the continuous-sweeping mode used for the experiment on atoms in He II. In the continuous-sweeping mode, the output frequency of the oscillator is not phase-locked, and therefore it caused an uncertainty of a few hundred kHz in the frequency determination. In this work, the resonance frequency of the hyperfine transition, ν, is determined to be ν = 3.035734(2) GHz and is in good agreement with the previously reported value of ν = 3.035732440 GHz[3)] within the statistical error. The step-sweeping mode turned out to provide better stability of frequency than the continuous-sweeping mode , and consequently the resonance frequency of the hyperfine transition obtained in this experiment is two orders of magnitude more accurate than that in the previous experiment. We plan to determine the hyperfine structure splittings of Cs and Rb atoms in He II with improved accuracy by operating the microwave oscillator in the step-sweeping mode.

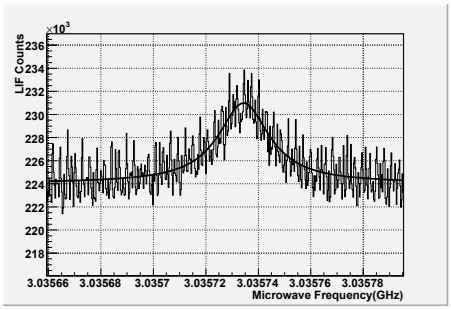

Fig. 2. Hyperfine transition spectrum of ^{85}Rb in the ground state (F=2, m_F=0 → F=3, m_F=0). Other m_F components are outside of the frequency region.

*1 Dept. of Phys., Meiji University
*2 Dept. of Appl. Phys., Tokyo University Agr. Tech.
*3 Dept. of Phys., Osaka University

References
1) T. Furukawa: Doctoral thesis, Osaka Univ. (2007).
2) T. Furukawa et al.: Proc. INPC07, in press.
3) M. Teru, R. Fortin, and J. Y. Savard: IEEE Trans. Instrum. Meas. *IM-25*, 477 (1976).
4) T. Furukawa et al.: RIKEN Accel. Prog. Rep. **40**, 212 (2007).
5) T. Itou et al.: RIKEN Accel. Prog. Rep. **40**, 213 (2007).
6) G. Singh, P. Dilavore, and C.O. Alley: Rev. Sci. Instrum. **43**, 1388 (1972).

Online TDPAC study with the $^{19}F(\leftarrow{}^{19}O)$ probe implanted in highly oriented pyrolytic graphite†

W. Sato,*[1] H. Ueno, H. Watanabe, H. Miyoshi,*[2] A. Yoshimi, D. Kameda, T. Ito,*[2] K. Shimada,*[3] J. Kaihara,*[2] S. Suda,*[2] Y. Kobayashi, A. Shinohara,*[1] Y. Ohkubo,*[4] and K. Asahi*[2]

Nuclear spectroscopic techniques combined with the probe-implantation method are very suited for the investigation of interaction between impurity atoms and host materials because of their high sensitivity. Directing our interest to this advantage, we have established an online time-differential perturbed angular correlation (TDPAC) measurement system at the RIKEN Nishina Center. The TDPAC method is a nuclear spectroscopy, which provides microscopic information on a local scale in matter through hyperfine interactions between probe nuclei and the surrounding spins and charge distribution. As a trial of the combined method at this facility, the short-lived isotope ^{19}O, a parent of a new TDPAC probe ^{19}F, was implanted in a sheet of highly oriented pyrolytic graphite (HOPG) and TDPAC measurements were performed on line. Demonstrating the applicability of this online TDPAC method, we here report successful observation of an electrostatic interaction between the probe and the surrounding carbon atoms.

Ionized ^{22}Ne was accelerated by a two-stage acceleration with the AVF cyclotron and the ring cyclotron up to 110 MeV/u at a beam intensity of 150 pnA. A variety of radioactive nuclides were produced at a Be production target by projectile-fragmentation reactions; the secondary beam of interest, ^{19}O, was separated out of these heavy ions at a purity of 98% or higher by the RIKEN projectile-fragment separator.[1] A well-focused pulsed beam of ^{19}O was implanted deep in the sample at a beam intensity of $\geq 10^5$ s^{-1}. In order to obtain better counting statistics, we used sixteen BaF_2 detectors. They were arranged in four independent detector planes for the investigation of a sample-to-detector configuration dependence of perturbation patterns for a single crystalline sample. The TDPAC measurements were performed at 18 K on the 1357-197 keV cascade γ rays from ^{19}F nuclei, whose 197 keV intermediate state with its nuclear spin and parity of $5/2^+$ has a half life of 89.3 ns.

The TDPAC spectra of $^{19}F(\leftarrow{}^{19}O)$ implanted in the HOPG sheet at 18 K are shown in Fig. 1. The spectrum in Fig. 1(a) was obtained by the detectors directed to face the two-dimensional HOPG layer at $\pi/4$ radians, and the spectrum in Fig. 1(b) obtained by those arranged in parallel with the layer. There is an apparent difference

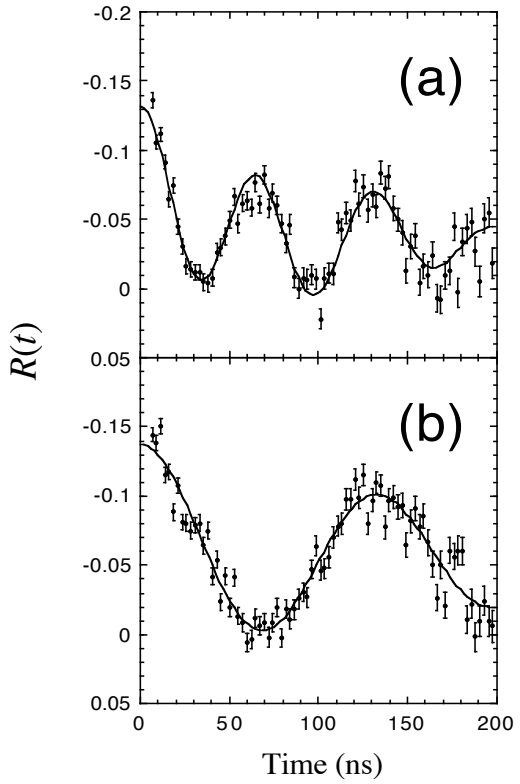

Fig. 1. TDPAC spectra of $^{19}F(\leftarrow{}^{19}O)$ in HOPG measured at 18 K for different sample to detector configurations. See the text for detail.

in the time-evolving oscillation patterns between Figs. 1(a) and 1(b), signifying the presence of a *c*-axis orientation dependence in these spectra. Assuming that the electric field gradient (EFG) is axially symmetric ($\eta = 0$) and the symmetric axis is oriented in parallel with the *c* axis, we performed least-squares fits to the spectra with theoretical equations. The fits are satisfactory for both of the perturbation functions as indicated with the solid curves in Figs. 1(a) and 1(b); that is, the *c* axis of the HOPG was found to be parallel to the axially symmetric principal axis of the EFG at the site of the probe nucleus. The EFG value at the probe nucleus was evaluated from the fits to be $|V_{zz}| = 2.91(17) \times 10^{22}$ V m^{-2}. This value is in good agreement with a theoretical value for the nucleus of ^{19}F placed in the interlayer position of point group C_{3v}, $V_{zz} = -2.938 \times 10^{22}$ V m^{-2}.[2] This agreement suggests that the incident ^{19}O atoms are initially stabilized at this site.

† Condensed from the article in Nucl. Instr. Meth. Phys. Res. B **266**, 316 (2008).

*1 Graduate School of Science, Osaka University
*2 Department of Physics, Tokyo Institute of Technology
*3 Cyclotron and Radioisotope Center, Tohoku University
*4 Research Reactor Institute, Kyoto University

References

1) T. Kubo et al.: Nucl. Instr. Meth. Phys. Res. B **70**, 309 (1992).
2) D. Surono et al.: Hyperfine Interact. **96**, 23 (1995).

Structure of Au-Pd nanoparticles synthesized by GeV ion irradiation

Iwase*1, N. Maeda*1, T. Akita*2, T. Abe, T. Kambara, H. Ryuto and F. Hori*1

Previously, we suggested that nanoparticles synthesized from Au and Pd aqueous solutions by 1.6 GeV C ion irradiation have a structure with Au cores surrounded by Pd shells [1]. In this report, we show that the Au core-Pd shell structure has directly been observed by an annular dark field scanning transmission electron microscopy (ADF-STEM).

The specimens were dilute aqueous solutions with 0.5 mM $NaAuCl_4/2H_2O$ as a precursor of Au^{3+} ions, 0.5 mM $PdCl/2NaCl/3H_2O$ as a precursor of Pd^{2+} ions, and 8 mM sodium dodecyl sulfate (SDS) as a surfactant. The specimens were sealed in polystyrene vessels and irradiated with 1.6 GeV fully-stripped carbon ions at the E5B beam line of the RIKEN ring cyclotron accelerator. The irradiation doses used were 300,1500,5000 and 10000 Gys. The irradiated solutions including Au-Pd particles were dropped on carbon films and are dried in vacuum. The Au-Pd particles dispersed on carbon films were observed by ADF-STEM. Energy dispersive X-ray spectroscopy (EDS) was also used to investigate the local composition of Au-Pd particles.

Figure 1 shows the ADF-STEM images of Au-Pd nanoparticles synthesized by 1.6 GeV carbon irradiation. As can be seen in the figure, the diameter of Au-Pd particles is within 3-8 nm, and each particle reveals a very bright region is surrounded by a weaker-contrast region. As the intensity of ADF-STEM image is nearly proportional to the square root of the atomic number of the elements, the ADF-STEM image suggests that the core of Au atoms (atomic number, 79) is surrounded by a shell of Pd atoms (atomic number, 46). This Au core-Pd shell structure was confirmed by EDS. We measured the EDS spectra at points “13” and “14” shown in Fig. 1. The intensities of the Au-Mα and Pd-Lα X-rays at the two points clearly show that the core and shell of the particle consist of Au and Pd atoms, respectively.

We have also synthesized Au-Pd nanoparticles using other irradiation methods (10 MeV pulsed electron irradiation and Co-60 γ-ray irradiation)[2]. The average size of particles synthesized by GeV ion irradiation is larger than that of particles synthesized by the electron irradiation, but smaller than that of particles synthesized by γ–-ray irradiation. Au-Pd nanoparticles synthesized by GeV ion irradiation and χ-ray irradiation clearly show a structure with a Au- core and a Pd- shell, but the particles synthesized by pulsed electron irradiation are too small to detect the core-shell structure. We are now determining which irradiation parameters (e.g,. LET and dose rate) predominate the size and structure of Au-Pd nanoparticles.

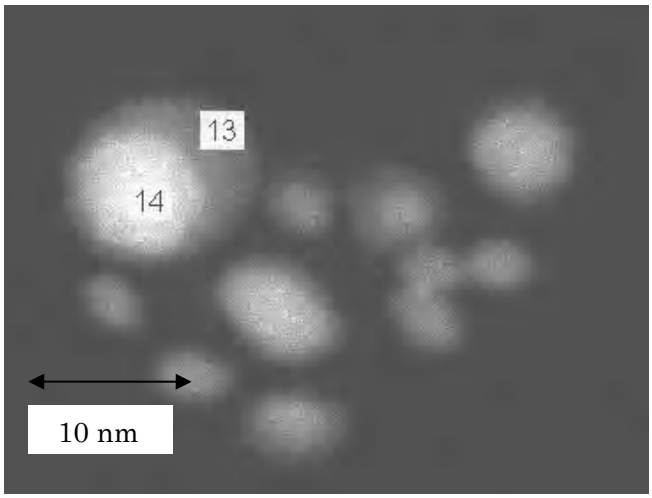

Fig. 1. ADF-STEM image of Au-Pd nanoparticles synthesized by 1.6 GeV C irradiation to the dose of 10,000 Gys.

References

1) N. Maeda, F. Hori, T. Kambara, T. Abe, H. Ryuto, A. Iwase,* RIKEN Accel. Prog. Rep. 40(2007) 202.
2) N. Maeda, T. Hiroki, F. Hori, S. Okuda, R. Taniguchi, T. Kojima, T. Kambara, T. Abe, A. Iwase: Mater. Res. Soc. Symp. Proc. Vol. 900E, 0900-O06-16.1-6.

*1 Osaka Prefecture University.
*2 National Institute of Asvanced Industrial Science and Technology (AIST)

Lattice Location of Hydrogen in β_1-V_2H†

Tatuya Hayashi,[*1] Shigetoshi Koike,[*2] Naota Higami,[*1] Kazuhiro Hirabayashi,[*1] Hiroshi Matsuba[*1]
Kiyoshi Ogiwara and Eiichi Yagi[*3]

On the basis of neutron, electron and X-ray diffraction experiments it has been reported that the β_1-V_2H has two different crystal structures, a body-centred monoclinic one and a body-centred tetragonal one with an axial ratio of c_0/a_0~1.1 (c_0 and a_0; lattice parameters in the *c*-direction and the *a*-direction, respectively) with an ordered arrangement of hydrogen atoms, depending on the condition for crystal growth. The β_1-V_2H phase exists below about 450 K, and above about 470 K it transforms to a body-centred cubic (bcc) phase (α-V_2H) with a disordered arrangement of hydrogen atoms at tetrahedral interstitial (T) sites. When tensile stress is applied during transformation from an α to a β_1-phase, it crystallizes into the tetragonal structure, while without tensile stress it crystallizes into the monoclinic structure. The lattice location of hydrogen in the tetragonal β_1-V_2H has been investigated by the neutron and X-ray diffraction methods.[1,2] By the latter method, the lattice location of hydrogen can be only indirectly deduced. It has been reported that hydrogen is located at O_z sites which are octahedral (O) sites between two adjacent V atoms aligned along c_0 axis (z-axis). The density distribution of hydrogen around an O_z site was also obtained by the neutron diffraction method.[2] Despite usefulness of a channelling method to obtain such information, no experiment has been performed for the β_1-V_2H. As a channelling method utilizing a nuclear reaction $^1H(^{11}B, \alpha)\alpha\alpha$ with a ^{11}B beam has been developed for study on hydrogen,[3] in the present work the lattice location and the density distribution of hydrogen in the tetragonal β_1-V_2H have been studied.

A β_1-V_2H single crystal was prepared in the following processes. Hydrogen was doped to a vanadium single crystal slice 0.5 mm thick from the gas phase above 573 K up to the concentration corresponding to a composition of V_2H under the tensile stress of 1.0 kg/mm^2 along the [001] direction. Thus an α-V_2H single crystal was prepared. By cooling the specimen from 483 K to room temperature at a rate of 0.1 K/min, a single domain of β_1-V_2H was prepared. During whole processes the tensile stress was being applied. The concentration of hydrogen was [H]/[M] (hydrogen-to-metal atom ratio)=0.5. Channelling analyses were performed at room temperature for [100], [110] and [101] axial channels, and (110), (100) and (001) planar channels with a $^{11}B^+$ beam of about 2.02 MeV, utilizing a resonance type of nuclear reaction of $^1H(^{11}B, \alpha)\alpha\alpha$ at about 1.8 MeV as in previous studies on H in V.[4,5] In this method hydrogen can be detected by measuring the emitted α particles, whose energy ranges from 0 to about 5 MeV.

Figure 1 shows channelling angular profiles of yields of ^{11}B ions backscattered by V atoms (B-angular profiles) and those of α articles (α-angular profiles). From the orientation dependence of the α-angular profiles it is concluded that hydrogen is located at O_z sites. It is to be noted that for the (001) channel the α-angular profile coincides with the B-angular profile, whereas for the (100) channel it does not. This result indicates that hydrogen is completely shadowed behind the (001) planes, whereas it is not completely shadowed but its density distribution is extended outside the (100) planes, i.e. in the [001] direction. The HWHM of density distribution of hydrogen around an O_z site was estimated to be less than 0.2 Å in the [001] direction and about 0.35 Å in the [100] direction. These values are smaller by about factor 2 than those obtained by neutron experiments, but very close to the theoretically obtained values.[6]

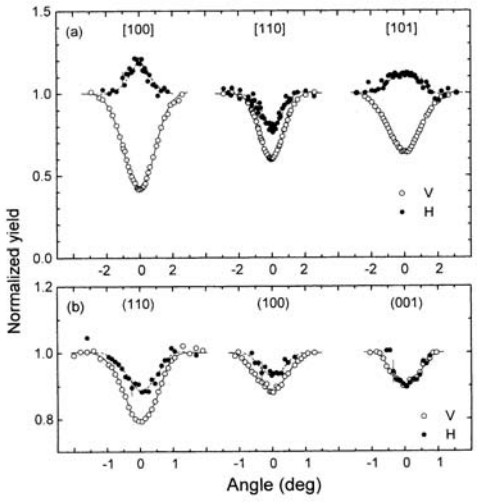

Fig. 1. Channelling angular profiles obtained at room temperature for V_2H.

References
1) Y. Noda et al.: Acta Cryst. B**42**, 529 (1986).
2) T. Kajitani and M. Hirabayashi: Z. Phys. Chem. N.F. **145**, 281 (1985).
3) E. Yagi et al.: J. Phys. Soc. Jpn **52**, 3441 (1983).
4) E. Yagi et al.: Phys. Rev. B**31**, 1640 (1985).
5) E. Yagi et al.: Phys. Rev. B**33**, 5121 (1986).
6) H. Sugimoto: J. Phys. Soc. Jpn. 53, 2592 (1984).

† Condensed from the article in J. Alloys and Compounds **446-447**, 512 (2007)

*1 School of Science and Engineering, Waseda University, Tokyo
*2 Department of Physics, Tokyo University of Science
*3 RIKEN and School of Science and Engineering, Waseda University

2. Atomic and Solid State Physics(muon)

Development of new μ-e decay counter for multichannel μSR spectrometer with intense pulsed muon beam at RIKEN-RAL

Y. Hirayama,[*1] M. Iio, K. Ishida, M. Iwasaki, Y. Matsuda, T. Matsuzaki, H. Ohnishi, H. Outa, D. Tomono, J. Kasagi[*2], H. Yamazaki[*2], R. Klein[*3] and S.N. Nakamura[*3]

Proton beam intensity upgrade is in progress at Rutherford Appleton Laboratory (RAL). Owing to this upgrade, an approximately 1.5 times higher muon beam intensity is expected at RIKEN-RAL. To handle such a high-intensity beam, a new μSR (muon spin rotation, resonance, relaxation) spectrometer must be developed. Spectrometers are generally composed of a number of positron counters and three pairs of coils. The biggest problem with the high-intensity beam is the distortion of the muon decay time spectrum caused by signal pile-up; two or more positrons are injected into the counter at the same time. To solve this problem, it is effective to increase the number of counter segments in order to reduce the incoming positron rate per counter. Since the space in the coils is limited, a small counter with a compact read-out is required for this purpose. Therefore, we developed a new counter to realize the compact read-out to increase the number of counter segments easily. At least, 282 segments are essential for reducing the number of pile-up signals compared with the present ARGUS spectrometer[1] specification.

The most important character of the counter is the use of a single wavelength shifter fiber (WSF) as a compact light guide to read photons from a scintillator instead of a bulky acrylic light guide. The photons are absorbed by WSF and those emitted in the axial direction of WSF are transmitted to a photomultiplier tube. Figure 1(a) shows the counter, which is composed of a scintillator (14×14×50 mm^3), a 75 cm WSF (Kuraray Y-11(200)M-S 1 mm) and a 16ch multianode photomultiplier tube (MAPMT, Hamamatsu H6568-10). This scintillator is designed specifically to be sensitive to a positron incidence angle. The spindly scintillator is pointed at the sample, so that positrons from the sample position penetrate through the longest path and background particles outside the target penetrate through a path shorter than the longest path. If an appropriate threshold level of output signals from the MAPMT is provided in proportion to the light output, we can preferably observe decay positrons only from the sample direction and reject background particles.

We performed an experiment at the Laboratory of Nuclear Science (LNS), Tohoku University[2] to count the number of photons from the counter and to test the positron incidence angle dependence of the light output. A 250 MeV/c positron beam penetrates a 50 mm scintillator directly. The counter was tilted at angles (θ) of 0°, 5°, 10°, 17° and 90°. Figure 1(b) shows a typical photon number distribution. We detected approximately 100 photons. The angle dependence of the light output is shown in Fig. 1(c). The vertical axis in Fig. 1(c) is normalized by the average number of photons at 0 °. The number of photons calculated from the shape of the scintillator is also shown in Fig. 1(c) with a solid line. It indicates that the calculated value is consistent with the experimental value. In addition, if the threshold level were set at 0.7, we could observe positrons with the incidence angles below 15° effectively. For the new spectrometer, we need a tighter constraint of the incidence angle. Therefore, we plan to use 10×10 × 50 mm^3 scintillators. The calculated value is also shown in Fig. 1(c) with a dotted line. To confirm background suppression using the muon beam at RIKEN-RAL, we observed a muon decay time spectrum at a high threshold level of 0.7. The constant background was not observed at this threshold level in this statistics of 8×10^6, indicating that it could be suppressed at least below 10^{-5} of the statistics at time zero.

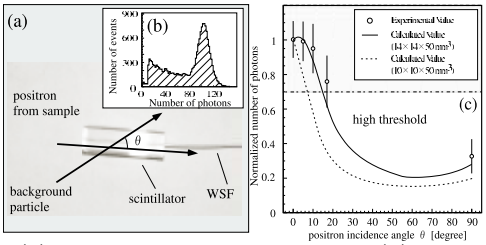

Fig. 1. (a) Picture of counter element. (b) Typical photon number distribution. (c) Angle dependence of light output. The vertical axis is the number of photons normalized by that at 0 °. Each bar with the experimental value denotes the FWHM of the photon spectrum peak at each angle.

We established the compact read-out mechanism of the counter. The construction of the new μSR spectrometer is in progress. The total number of fabricated counters is 606, which is three times larger than that of counters of a conventional ARGUS spectrometer. Pile-up events can be suppressed below 2.7 % of total events. We would like to thank the accelerator staff of LNS for providing the beams and their kind support for the experiment.

References

1) R. Kadono et al.: RIKEN Accel. Rep. **29** (1996).
2) H. Yamazaki et al.: Nucl. Instrum. Methods A **536** (2005)70.

*1 Department of Physics, Tokyo Institute of Technology
*2 Laboratory of Nuclear Science, Tohoku University
*3 Department of Physics, Tohoku University

Development of New TDC and Data Acquisition System for Next-Generation μSR

R. Kadono,[*1] A. Koda,[*1] N. Kawamura,[*1] S. Takeshita,[*1] K. H. Satoh,[*1] M. Tanaka[†],[*2] T. Uchida,[*2] Y. Yasu,[*2] S. Y. Suzuki,[*3] Y. Matsuda,[*4] T. Matsuzaki,[*4] and M. Iwasaki,[*4]

It is anticipated upon the completion of J-PARC (with 1 MW beam power) that the MUSE facility will deliver pulsed beams with an unprecedentedly high intensity: the estimated instantaneous event rates are 10^4–10^5 positrons within a mean lifetime of 2.2 μs, which is repeated at a rate of 25 Hz. To cope with the problem in handling such a high data rate, a collaboration with the KEK electronics system group has been started.

The most crucial step for the time-differential μSR measurements is to record the timing of muon-decay positrons with a precision of $\sim \pm 0.5$ ns for a relatively long period ($\sim$ 30 μs) using time-to-digital converters (TDCs). Although such devices have been commercially available (e.g, Model 3377, LeCroy), they share a common problem in that the interface for computer access is based on some specific data bus such as CAMAC or VME. These data buses have an inherent problem that their specifications become quickly obsolete, getting unsupported by electronics/computer developers. Moreover, they are not suited for high-density implementation required for the highly segmented detection system: it is anticipated that 1000$\sim$2000 positron counters are necessary for a typical μSR spectrometer to minimize the distortion of time spectra caused by the pile-up of positron events and associated loss of information, while those devices usually have only 16$\sim$32 input channels per module.

We are currently developing a new TDC module based on custom-made integrated circuits (ASICs). The ASICs for TDC have been originally developed by the KEK electronics group for use in large-scale detector systems for high-energy physics experiments; therefore they are readily modified for high-density implementation. Moreover, the development of a new hardware interface based on the ubiquitous Ethernet technology is in progress. The idea is to build the TCP protocol into a small "silicon" chip ("SiTCP", in a commercially available FPGA) for further integration to front-end devices. Presently, the Ethernet and associated TCP/IP protocol are the *de facto* standards for data exchange over a computer network, and the risk of being left behind with an obsolete data bus can thus be minimized by adopting the Ethernet as a direct interface between front-end devices and computers. The specification for the data transfer rate of the current Ethernet ($\geq$ 1 Gbps) is fast enough to handle the average event rate anticipated for the J-PARC Muon Facility.

The adoption of the Ethernet as an interface for front-end devices gives rise to the need for an unprecedented data acquisition (DAQ) system for use in a multi-CPU environment. As a first step in the development of a new DAQ system, we performed a test experiment on the SiTCP-based TDC module with a prototype DAQ system using the pulsed muon beam at RIKEN-RAL. The module consists of TDC-ASIC on a mother board which is customized for the SiTCP interface. The signal outputs from the ARGUS spectrometer (48 channels each for the backward/forward counters) were connected to TDC. Figure 1 shows a typical set of the obtained spectra, where one can observe exponential decay of counting rates without distortion over more than five decades (corresponding to the time range of ten times the muon's lifetime). Following this promising result, we are now preparing for the test of positron counters based on new photon detection devices for replacing bulky phototubes.

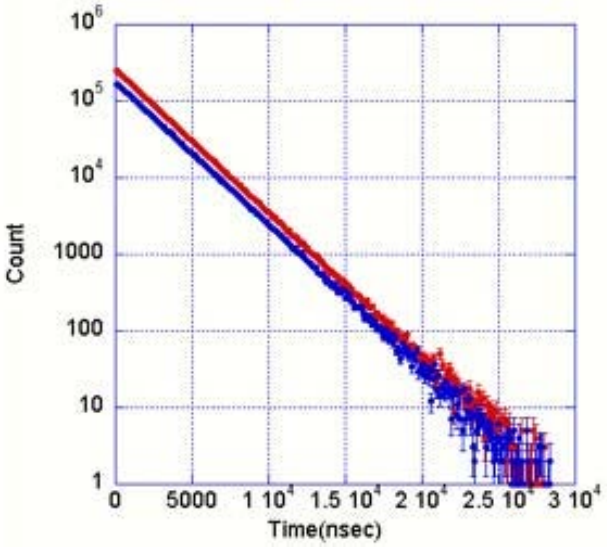

Fig. 1. Time-dependent μ-e decay spectra for the backward and forward sets of counters on the ARGUS spectrometer.

[†]Present affiliation: Dept. of Physics, Univ. of Tokyo

[*1] Inst. Materials Structure Science, KEK
[*2] Inst. Particle and Nuclear Physics, KEK
[*3] Computer Research Center, KEK
[*4] Nishina Center for Accelerator-Based Science, RIKEN

Density enhancement of muon beams with tapered glass tubes†

T. M. Kojima, D. Tomono, T. Ikeda, K. Ishida, Y. Iwai, M. Iwasaki, Y. Matsuda, T. Matsuzaki, and Y. Yamazaki*1

We have demonstrated that the beam density of 54 MeV/c muons can be increased almost by a factor of two when a tapered glass tube is inserted coaxially along the muon beam.

The experiment was performed at Port 2 of RIKEN-RAL Muon Facility at Rutherford Appleton Laboratory, U.K. The top of Fig. 1 schematically shows the experimental setup. A 50 Hz pulsed muon beam[1)] is extracted into atmosphere through thin Mylar foil and an aluminum collimator of inner diameter 40 mm and length 85 mm. A Typical beam intensity is about 10^4 muons per pulse and the beam size is about 40 mm as FWHM at 403 mm dowstream from the collimator. Positron/electron contamination is negligible. The glass tubes were made of Pyrex. The inlet diameter, $D_{\rm in}$, was 46 mm. The lengths of the tubes, L, were 100–400 mm, the outlet diameters, $D_{\rm out}$, were 3–20 mm, and the thickness was 2 mm. We prepared plastic scintillation counters with a thickness of 0.5 mm and diameters, $D_{\rm sci}$, of 5, 10, and 20 mm. One of the scintillators was placed 3 mm downstream of the tube to monitor the muon intensity. Scintillation intensities, $V_{\rm with}$ and $V_{\rm without}$, were measured with and without the glass tube, respectively, keeping all other experimental conditions the same. The energy and angular distributions of muons at the position of the scintillator were calculated with a Monte Carlo simulation,[a)] and a pair of average deposition energies $\varepsilon_{\rm with}$ and $\varepsilon_{\rm without}$ was evaluated for each set of experimental conditions. The numbers of muons that hit the scintillator, $N_{\rm with}$ and $N_{\rm without}$, are proportional to $V_{\rm with}/\varepsilon_{\rm with}$ and $V_{\rm without}/\varepsilon_{\rm without}$, respectively. The beam density enhancement factor, ξ, is given as

$$\xi = N_{\rm with}/N_{\rm without} \quad \text{for} \quad D_{\rm out} \geq D_{\rm sci} \quad (1)$$

$$= N_{\rm with}/N_{{\rm without},d\leq D{\rm out}} \quad \text{for} \quad D_{\rm out} < D_{\rm sci}, \quad (2)$$

where the suffix '$d \leq D_{\rm out}$' stands for the muon signal integrated within the area of $D_{\rm out}$ using a measured muon beam profile.

Density enhancements of 54 MeV/c muon beams were observed for all the conditions studied. The bottom of Fig. 1 shows ξ with L = 400 mm tubes as a function of $D_{\rm out}$ for $D_{\rm sci}$ = 20 mm together with the results of the numerical simulation. As seen in the figure, ξ increases from $\simeq$ 1.5 to $\simeq$ 2.3 as $D_{\rm out}$ decreases from 20 to 3 mm, and the simulation successfully reproduces the overall behavior of the experimental results. This enhancement occurs because a certain fraction of muons incident on the inner wall is reflected via small-angle scattering and transported to the outlet of the tube. It is worth noting that the density enhancement for μ^- was almost identical to that of μ^+.

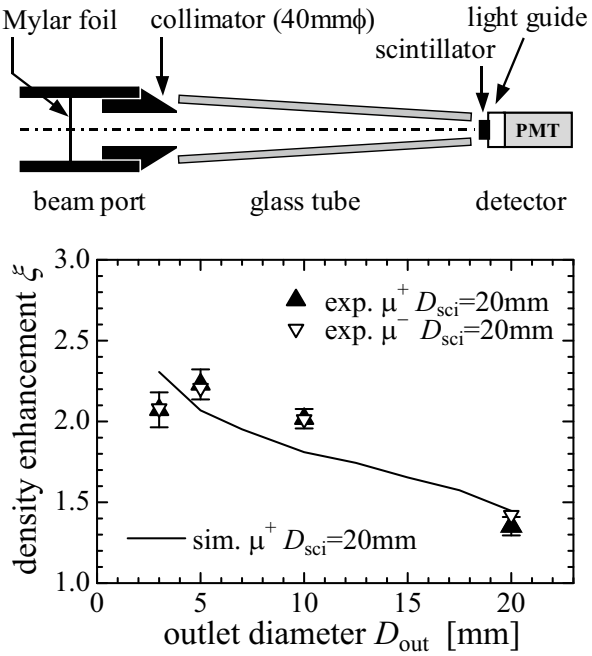

Fig. 1. Top: a schematic view of the experimental setup (not to scale). Bottom: the beam density enhancement ξ for 54 MeV/c muons with L = 400 mm tubes as a function of $D_{\rm out}$ for $D_{\rm sci}$ = 20 mm. The solid line shows the result of the simulation.

We also simulated the density enhancement under a vacuum condition for 27–81 MeV/c. The simulation shows the enhancement factor is about 2 and almost constant over the entire momentum region, including commonly used surface muons of 27 MeV/c. The simulation also suggests that the density enhancement factor improves further when the tube is made of a heavy material such as copper, lead, or gold. Preparations in this direction are in progress.

References

1) T. Matsuzaki *et al.*: Nucl. Instrum. Methods Phys. Res., Sect. A **465** (2001) 365-383.

† Condensed from the article in J. Phys. Soc. Jpn, Vol.76, 093501 (2007).

*1 Also at Graduate School of Arts and Sciences, University of Tokyo

a) In the simulation; 1) the energy loss is scaled from proton data using a semi-empirical formula, 2) the energy straggling is given by the Vavilov distribution, and 3) the angular distribution is given by the Moliere expression for multiple scattering. For simplicity, a parallel muon beam is generated having a 4 % momentum dispersion and the measured Gaussian position distribution.

Muon-catalyzed fusion in nonequilibrium mixtures of T_2 with ortho/para/normal-D_2

K. Ishida, T. Matsuzaki, Y. Matsuda, M. Iwasaki, H. Imao, K. Nagamine, N. Kawamura[*1], M. Kato[*1] and H. Sugai[*2]

[muon, fusion, deuterium, tritium]

In a muon-catalyzed fusion (μCF) cycle, muonic molecule formation is one of the key processes and it is essential that the rate should be reasonably high for a muon to catalyze many fusions during its lifetime (λ_0 = 2.2 μs). The $dt\mu$ formation is considered to proceed as follows: $(t\mu)_F + (\mathrm{DX})_{K_i\nu_i} \rightarrow [(dt\mu)xee]_{K_f\nu_f}$ ($x = d, t, \mathrm{X} = \mathrm{D}, \mathrm{T}$), where F is the hyperfine state and $K_i(K_f)$ and $\nu_i(\nu_f)$ are the rotational and vibrational states of the initial (final) channel respectively. Since the final states are only in discrete levels, the initial state must have a matching energy (the resonant condition) for the reaction to occur. Thus, the $dt\mu$ formation rate often shows an interesting, and sometimes unexpected, dependence on target conditions, such as temperature, density and molecular states.

For the understanding of the reaction, it is important to know separately the $dt\mu$ formation rate from each initial molecular state. In a measurement performed at the RIKEN-RAL Muon Facility, the cycling rate increased by 25% in the nonequilibrium state immediately after D_2+T_2 mixing and gradually decreased to the value for the equilibrated state (D_2+T_2+2DT)[1]. This result clearly shows the dominance of the resonant formation with D_2 over that with DT.

Because the resonance condition should depend on the rotational level of D_2 molecules, an experiment that varies the ortho-D_2 (rotational states K_i=0,2,...) to para-D_2 (K_i=1,3,...) ratio in the D_2/T_2 target is very important. For the $dd\mu$ formation in pure D_2, we observed a difference by a factor as large as 2 between the ortho-D_2 and para-D_2 targets[2,3]. It is predicted that the effect is even larger for the dtμ formation. Several calculations suggest that the dtμ formation rate with para-D_2 is much higher than that with ortho-D_2.

Previously, we reported μCF measurements[4] on liquid mixtures of T_2 with normal-D_2 and ortho-D_2. Recently, we have successfully produced para-rich D_2 (72% para concentration), and μCF on its mixture with T_2 has also been studied. In Fig. 1, the time dependence of the neutron disappearance rate ($\lambda_n = \lambda_0 + W\phi\lambda_c$, where W is the muon loss probability per cycle, ϕ the target density and λ_c the μCF cycling rate) compared with its value at the equilibrium state is plotted instead of λ_c itself. This is because we do not have suffiecient data to determine the absolute fusion yield, which is essential to the extraction of the cycling rate, due to the low beam intensity in the last measurement. Even though the disappearance rate almost follows the variation in cycling rate, since W is much less dependent on the target condition. It can be seen from Fig. 1 that the increase in λ_n (and λ_c) due to the nonequilibrium effect is largest with ortho-D_2 and smallest with para-rich D_2.

It is puzzling why the observed effect is opposite to theoretical calculations. One explanation could be that the $dt\mu$ formation due to the three-body collision becomes important in liquid D/T and such a collision may favor $dt\mu$ formation with ortho-D_2. We plan to confirm the D_2(para-rich)+T_2 result using D_2 of higher para concentration ($> 90\%$) under better beam conditions. Also, we plan an independent measurement focused on the ortho-para D_2 state stability by *in situ* Raman spectroscopy at JAEA. Such measurements will give us more quantitative values of the ortho-D_2 and para-D_2 contributions to $dt\mu$ formation.

References

1) K. Ishida *et al.*: RIKEN Accel. Prog. Rep. **35**, 39 (2002).
2) H. Imao *et al.*: Phys. Lett. B **632**, 192 (2006).
3) H. Imao *et al.*: Phys. Lett. B **658**, 120 (2008).
4) K. Ishida *et al.*: RIKEN Accel. Prog. Rep. **39**, 82 (2006).

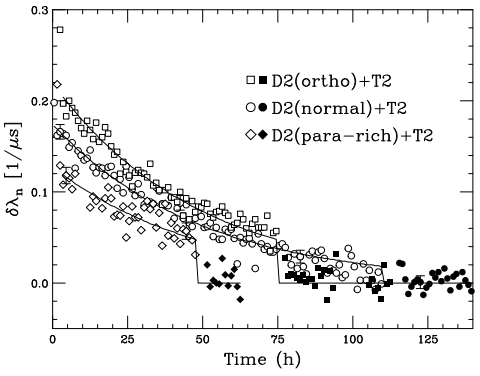

Fig. 1. Difference in neutron disappearance rate from equilibrated value as function of time after mixing D_2 and T_2. Cases using D_2(normal)+T_2, D_2(ortho)+T_2 and D_2(para-rich)+T_2 are compared. Filled symbols denote the data obtained after equilibration.

*1 Muon Science Laboratory, High Energy Accelerator Research Organization
*2 Advanced Science Research Center, Japan Atomic Energy Agency

Muon Transfer Studies in Solid D_2 with Implanted Alkali and Alkaline-Earth Ions

P. Strasser*1, A. Taniguchi*2, S. Ohya*3, H. Mochizuki*3, T. Matsuzaki, K. Ishida, Y. Matsuda, M. Iwasaki, and K. Nagamine*4

[Muonic atom spectroscopy, Solid hydrogen film, Ion implantation]

We proposed the cold hydrogen film method[1] to expand muonic atom spectroscopy by utilizing nuclear beams, including, in the future, radioactive isotope (RI) beams, to produce radioactive muonic atoms. This method will enable the study of unstable nuclei by the muonic X-ray method at facilities in which both intense μ^- and RI beams will be available. The basic concept is to stop both μ^- and nuclear beams simultaneously in a solid hydrogen film, followed by the application of the direct muon transfer reaction to higher Z nuclei to form radioactive muonic atoms.

An experimental program to perform muonic atom spectroscopy with stable ions implanted in a solid hydrogen (H_2/D_2) film has been initiated at the RIKEN-RAL muon facility to experimentally establish the feasibility of this method. Already very promising results were obtained in pure solid D_2 films with argon ions implanted non-uniformly, to study the muon transfer reaction and the diffusion process of dμ atoms. A new surface ionization type ion source has been constructed and installed on the existing μA* apparatus at port 4 with the aim of using in the future radioactive isotopes. This type of ion source is capable of producing ions from alkali and alkaline-earth metals with high efficiency. At the moment, only stable beams will be produced to optimize the new surface ion source and tune the beam transport optics. Barium and strontium ions were successfully generated from barium oxide and strontium oxide, and accelerated up to 30 keV with a new ion extraction unit. Beam intensities of 1–2 μA were obtained. The ion beam optics was tuned to transport the beam to the solid hydrogen target and optimize the beam spot to efficiently use the large muon beam size at the target position. All barium and strontium isotopes could be separated on the focal plane after the bending magnet, allowing the implantation of only one specific isotope on the target.

The first transfer experiment was performed by measuring two different targets with isotopically separated strontium ions. As shown by Monte Carlo simulations performed with SRIM, the range of 30-keV Sr ions in solid D_2 is only about 200 nm, with a range straggling of about 60 nm (FWHM). Therefore, it is very difficult to perform a uniform implantation in a thick D_2 layer.

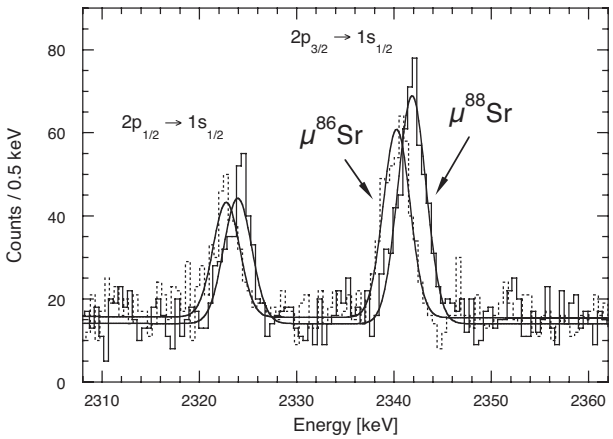

Fig. 1. Muonic strontium delayed energy spectra with 1-mm pure D_2 and about 1 ppm of ^{88}Sr (solid line) and ^{86}Sr (dotted line) ions implanted non-uniformly.

Consequently, the same procedure as that used previously to implant argon ions was utilized. Each Sr implantation was separated from the next by depositing a fixed amount of D_2 to yield a total D_2 layer thickness of 1 mm. Each implantation region was identical, and a total of 20 implantations separated by 50 μm were performed for each target, corresponding to an average Sr concentration of about 1 ppm throughout the D_2 layer. Figure 1 shows the delayed energy spectra measured by the Ge detector with 1-mm pure D_2 and ^{88}Sr ions (solid line) and ^{86}Sr ions (dotted line) implanted non-uniformly. A preliminary analysis shows that the measured isotope shift is consistent with that observed in previous experiments performed using enriched strontium isotopes in very large quantities. This experiment was performed using natural strontium oxide in the ion source, and only about 7×10^{16} ions of ^{88}Sr and 5×10^{16} ions of ^{86}Sr in the target, respectively. These experiments are still performed with a relatively large number of implanted ions, because of the relatively low μ^- beam intensity at 27 MeV/c. Future intense muon beams with higher muon flux would require fewer implanted ions. Further measurements are planned with other alkaline-earth metals and rare earth elements, and possibly long-lived radioactive isotopes in the near future.

*1 Muon Science Laboratory, IMSS, KEK
*2 Research Reactor Institute, Kyoto University
*3 Department of Physics, Niigata University
*4 University of California Riverside, CA, USA

References

1) P. Strasser et al.: Hyp. Int. 119, 317 (1999); Nucl. Instr. and Meth. A 460, 451 (2001); AIP Conf. Proc. 793, 242 (2005).

Studies of thin $Nd_{0.5}Sr_{0.5}MnO_3$ film using low-energy polarized muon beam

Y. Matsuda, P. Bakule, M. Iwasaki, T. Matsuzaki, I. Watanabe, Y. Miyake,[*1] Y. Murakami,[*2] M. Izumi,[*3] and K. Miyano[*3]

[thin film, magnetism, perovskite, μSR]

We have been carrying out μSR studies of a $Nd_{0.5}Sr_{0.5}MnO_3$ (NSMO) film. NSMO is one of the manganese oxides with a perovskite-like structure, which has been attracting interest in the last few years. Bulk crystals of NSMO are paramagnetic at room temperature, and show a ferromagnetic transition at 250 K and a successive antiferromagnetic transition at 170 K with a very sharp metal-insulator transition. It is understood that near the boundary between the ground state and the ferromagnetic-metallic state, two states are in a delicate balance. Thus, when a small external field (magnetic field, electric field, or light) is applied, the balance suddenly falls to one side, resulting in marked changes in resistivity.

A recent demonstration of such phase transition in a thin NSMO film is a large step forward for device application[1)], although the magnetic structure of the thin film is not known. The understanding of the interplay between the external conditions and the delicate balance between different magnetic states in thin films would be of great interest. There are few probes that can be used to investigate magnetic properties of thin films, and our newly build low-energy polarized muon beam line[2,3)] provides a unique opportunity. In contrast to a conventional polarized muon beam line, in which muon's kinetic energy is 4 MeV or higher, our low-energy muon beam line can supply polarized muons with variable implantation energy from 1 keV to 30 keV. This means that we can control the penetration depth of polarized muons within a few tens of nm. This experiment is the first demonstration of this technique at the RIKEN-RAL muon facility.

Since the last report in the RIKEN accelerator progress report[4)], we have made several improvements on our beam line. The stability of the magnetic field of a bending magnet in our low-energy muon beam line has been improved by replacing an old power supply to a new one. The strength of the field is now constantly monitored by a Hall probe. This has greatly improved the pointing stability of our low-energy muon beam, reducing background and eliminating a drift of the offset level on the spectrum. An unstable high-voltage power supply for one of the electrostatic quadrupoles is also replaced. The optical arrangement in the laser system to generate Lyman-α light for generation of low-energy muons[3)] has been modified so that the confocal condition of 212.5 nm and 820 nm lasers in Kr gas is improved.

In the experiment, we used four NSMO films epitaxially grown on (110)-oriented $SrTiO_3$. The thickness of the films was about 100 nm, and the size was 10 mm by 10 mm. The samples were mounted on a GM cryostat, which can cool the sample down to 10 K. We carried out zero-field μSR measurement at 300 K, 280 K, 240 K, 230 K, 225 K, 220 K, 215 K, 155 K, 110 K and 100 K. The residual magnetic field under zero-field condition was less than 2 mG.

We observed a clear change in μSR spectrum around 220 K. This corresponds to a magnetic phase transition from a paramagnetic state to a ferromagnetic state. This observation is the first demonstration of magnetic phase transition in thin films using our low-energy muon beam. We also observed a change in spectrum shape between 215 K and 155 K, and 155 K and 110 K. The former change may be related to the metal-insulator transition at 170 K previously observed in resistivity measurement of a sample[1)]. The latter may correspond to the newly discovered phase transition at 140 K, unique to this NSMO film[5)]. Unfortunately, because of 10 months long shutdown of the ISIS accelerator in 2007, we were not able to accumulate enough data to draw a conclusion on these two transitions. We have been given an extension of our allocated beam time by the last Nishina Center ML-PAC, and we are planning to continue the measurement, as well as developing work on the beam line.

*1 High Energy Accelerator Research Organization
*2 Faculty of Science, Tohoku University
*3 Research Center for Advanced Science and Technology, the University of Tokyo

References

1) M. Nakamura, Y. Ogimoto, H. Tamaru, M. Izumi, and K. Miyano: Appl. Phys. Lett. **86**, 182504 (2005).
2) P. Bakule, Y. Matsuda, M. Iwasaki, Y. Miyake, K. Nagamine, Y. Ikedo, K. Shimomura, and P. Patrick: Physica B **374-375**, 456 (2006).
3) P. Bakule, Y. Matsuda, Y. Miyake, K. Nagamine, M. Iwasaki, Y. Ikedo, K. Shimomura, P. Strasser, S. Makimura: Nucl. Inst. Meth. B 266, 335 (2008).
4) Y. Matsuda, P. Bakule, I. Watanabe, Y. Miyake, Y. Murakami, M. Izumi, K. Miyano: RIKEN Accel. Prog. Rep. **39**, 149 (2006).
5) Y. Wakabayashi, D. Bizen, H. Nakano, Y. Murakami, M. Nakamura, Y. Ogimoto, K. Miyano, H. Sawa: Phys. Rev. Lett. **96**, 017202 (2006).

Studies of vortex core in parity-violated superconductor with strong spin-orbit interactions

N. Nishida,[*1] T.U. Ito,[*1,*2] W. Higemoto,[*2] S. Kawamura,[*3] H. Takeya,[4] K. Hirata,[*4] and I. Suzuki,[*5]

[non-centrosymmetric, spin-orbit interaction, superconductivity,μ^+SR]

In a superconductor with a non-centrosymmetric crystal structure, the Cooper pair can take a parity-mixed orbital state, and spin singlet and spin triplet states can be mixed. In addition to non-centrosymmetricity, the presence of strong spin-orbit interaction removes spin degeneracy in electron bands and brings about the splitting of spin-up and spin-down bands. Thus, in non-centrosymmetric crystals with a strong spin-orbit interaction, unconventional superconductivity may be realized. Recently, in an applied magnetic field, peculiar vortex states which are very different from Abbrikosov vortex lattice have been proposed; the quasi-particle spin polarization[1] in the vortex core or FFLO-like mixed state[2] may occur. Recently, Li_2Pd_3B (Tc=6.7K)[3,4] and Li_2Pt_3B (T_c=2.43K)[5] have been discovered and are best candidates for studying effects of non-centrosymmetricity and strong spin-orbit interaction on superconductivity; the crystal structure is non-centrosymmetric and the spin-orbit interaction is about 3 times stronger in Li_2Pt_3B than in Li_2Pd_3B. The temperature dependence of the penetration depth, λ(T), has been obtained[6] through surface impedance measurements: In Li_2Pt_3B, the λ(T) has been found to exhibit a linear T dependence at low temperatures, indicating a line-node superconducting energy gap Δ, while in Li_2Pd_3B, the λ(T) levels off at low temperatures, indicating an almost isotropic Δ. To interpret these features, the "S-triplet Cooper pairing" of s-wave orbital symmetry and spin-triplet state has been proposed in Li_2Pt_3B [7]. In Li_2Pd_3B detailed μ^+SR studies have been performed[8], and the obtained λ(T) is similar to that by the surface impedance study. Recent NMR studies on Li_2Pd_3B and Li_2Pt_3B[9] have cofirmed the spin-triplet superconductivity of Li_2Pt_3B. Considering that peculiar superconductivity can be realized in Li_2Pt_3B, we performed μ^+SR experiments to observe the spin polarization of quasi-particles perpendicular to the flux line in the vortex core[1]: When μ^+ is implanted with the spin parallel to the applied magnetic field, the initial direction of μ^+ spin will be relaxed, if in the vortex core there exists quasi-particle spin polarization perpendicular to the flux line, and if not, it will not be relaxed. The only possible method for detecting this type of local spin polarization is LF-μ^+SR. The LF-

*1 Tokyo Institute of Technology
*2 Japan Atomic Energy Association
*3 Ochanomizu University
*4 National Institute of Metals
*5 RIKEN Nishina Center

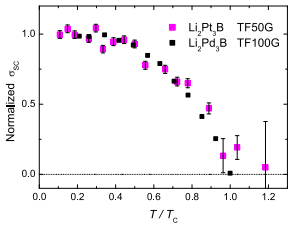

Fig. 1. σ(T) in Li_2Pt_3B and those in Li_2Pd_3B of ref.8) are plotted.

μ^+SR experiments on Li_2Pt_3B at 50 G were performed at 3 K above T_c and at 0.4 K below T_c at the RIKEN-RAL Muon Facility. An appreciable difference has not been detected within error after about 1.5×10^8 events in the spectra. The quasi-particle spin polarization in the vortex core has not been detected within the error range. To measure λ(T), the TF-μ^+SR measurements have also been performed at 50 Oe: The dephasing of muon spin precession is well described in terms of exp(-$t^2/2\sigma^2$), where $\sigma \propto 1/\lambda^2$. The normalized σ values are plotted in Fig. 1. In Li_2Pt_3B and Li_2Pd_3B, σ(T) has been found to exhibit the same temperature dependence with leveling off below $0.5 \times T_c$. This indicates that, in Li_2Pt_3B and Li_2Pd_3B, the superconductivities are not very different. The μ^+SR results are inconsistent with the results of the surface impedance or NMR experiments. The main reason for this discrepancy is unknown at the present. However, considering that Li_2Pt_3B is extremely sensitive to moisture[10], the results of the surface impedance or NMR experiments might be affected by surface conditions, while, as μ^+SR probes the inside of the sample, the results are not affected by the surface conditions.

References

1) N. Hayashi et al.: Physica **C437-438**, 96 (2006).
2) R. P. Kaur et al.: Phys. Rev. Lett. **94**, 137002 (2005).
3) K. Togano et al.: Phys. Rev. Lett. **93**, 247004 (2004).
4) H. Takeya et al.: Proc. LT-24 (2005).
5) P. Badica et al.: J. Phys. Soc. Jpn. **74**, 1014 (2005).
6) K.-W. Lee et al.: Proc. LT-24 (2005).
7) H. Q. Yuan et al.: Phys. Rev. Lett. **97**, 017006 (2006).
8) R. Khasanov et al.: Phys. Rev. **B73**, 214528 (2006).
9) M. Nishiyama et al.: Phys. Rev. Lett. **98**, 047002 (2007).
10) U. Eibenstein and W. Jung: J. Solid State Chem. **13**, 21 (1997).

Impurity-induced effect in a spin-Peierls compound TiOBr

S. Ohira-Kawamura,[*1] S. Kuroiwa,[*2] H. Kawashima,[*2] J. Akimitsu,[*2] K. Ohishi,[*3] and R. Kadono[*4]

[Spin-Peierls system, muon spin relaxation]

TiOBr has attracted interest as a new spin-Peierls (SP) system that shows two phase transitions[1]: a second-order transition accompanying the SP lattice distortion with an incommensurate (IC) structure at $T_{c2} = 47$ K and a first-order commensurate (C) SP transition at $T_{c1} = 27$ K. In contrast to another inorganic SP system $CuGeO_3$, a long-range magnetic order in an impurity-doped system $Ti_{1-x}Sc_xOBr$ has not been reported. This fact implies that the system is highly one-dimensional and interchain magnetic interactions in it are negligible. To investigate the transition temperatures for various Sc concentrations and spin dynamics in these systems, we performed μSR measurements at the RIKEN-RAL Muon Facility.

In the ZF-μSR time spectra of pure TiOBr, muon spin relaxation is markedly enhanced below 27 K. On the other hand, Sc-substituted samples do not show any remarkable enhancement of the muon spin relaxation down to 1.5 K. The time spectra are well fitted with the function $A(t) = A_s G_{KT}(\Delta, t)e^{-\lambda t}$, where Δ is the distribution width of the internal field at the muon site and λ is the relaxation rate. $G_{KT}(\Delta, t)$ is the Kubo-Toyabe function for describing the muon spin relaxation due to the nuclear dipole field. The temperature dependence of λ for $x \leq 0.01$ is depicted in Fig. 1. In these three samples, λ slightly increases below ~50 K. As temperature further decreases, only TiOBr ($x = 0$) shows a steeper increase in λ below ~27 K. This behavior is similar to the typical T dependence of λ accompanying the formation of a spin-singlet state. Therefore, in the case of a pure TiOBr system, two anomalies in λ at ~50 K and 27 K seem to correspond to the IC- and C-SP transitions ($T_{c2} = 47$ K and $T_{c1} = 27$ K). However, two other systems do not show the steep increase in λ at T_{c1}. This result indicates that the local internal fields observed in the Sc-substituted samples are different from that in TiOBr. It is expected that a small amount of impurities will markedly suppress the C-SP state of TiOBr.

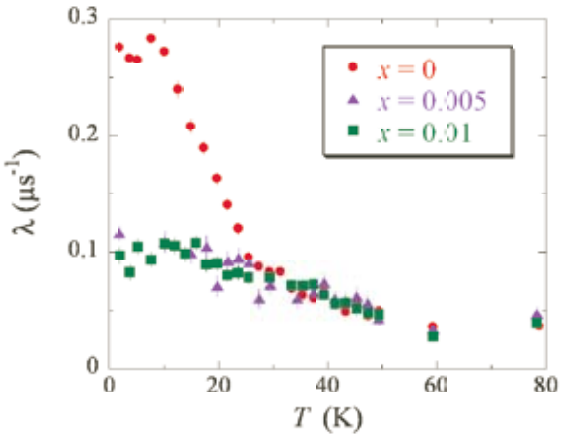

Fig. 1. Temperature dependence of the muon spin relaxation rate λ for $x = 0$, 0.005 and 0.01.

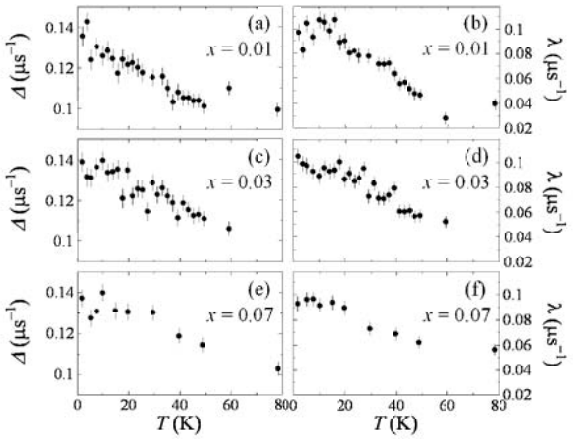

Fig. 2. Temperature dependences of distribution width of internal field Δ [(a), (c) and (e)] and relaxation rate λ [(b), (d) and (f)], for $x = 0.01$, 0.03 and 0.07.

Figures 2(a)-(f) show the temperature dependences of Δ and λ in $Ti_{1-x}Sc_xOBr$ for $x \geq 0.01$. The IC-SP transition temperature T_{c2} has been expected to decrease with increasing x to reach zero at around $x = 0.07$.[1] However, λ increases below ~50 K commonly in all measured samples with the independence of x.

Since the systems have a 2D layered structure where Ti and Sc spatially form triangular lattices, the SP transition at T_{c1} may occur to release the frustration within the 2D layers. The x-independent increase in λ below ~50 K may indicate the suppression of magnetic fluctuations, rather than the IC-SP transition.

*1 Present address: Academic & Information Board, Ochanomizu University
*2 Department of Physics, Aoyama Gakuin University
*3 Advanced Science Research Center, Japan Atomic Energy Agency
*4 Muon Science Laboratory, High Energy Accelerator Research Organization

References

1) T. Sasaki et al.: cond-mat/0509358 (2005).

Magnetic properties in spin-singlet Pd(dmit)$_2$ salts having a 2D distorted triangular lattice

S. Ohira-Kawamura,[*1] R. Kato, M. Tamura, and M. Iwasaki

[Organic conductor, 2D distorted triangular lattice, spin-singlet system, muon spin relaxation]

Organic Pd(dmit)$_2$ salts have a 2D layered structure consisting of [Pd(dmit)$_2$]$_2$ dimers, each of which possesses spin-1/2. The dimers form a distorted triangular lattice in the layers with interdimer antiferromagnetic interactions. Therefore, strong spin frustration is expected to occur there.[1)] Because of the small spatial anisotropy in the triangular lattice, the systems exhibit the character of a 2D square lattice or 1D chain at low temperatures, by releasing the frustration. We have previously performed μSR experiments on some Pd(dmit)$_2$ salts with the character of the 2D square lattice due to the small anisotropy, and we observed long-range magnetic order.[2,3)] As the next step of our study, we carried out the μSR measurement of $C_2H_5(CH_3)_3P[Pd(dmit)_2]_2$ ($P2_1/m$) to investigate its novel magnetic properties. X-ray structure analysis and magnetic susceptibility measurement suggest that this system shows a spin-singlet state such as the spin-Peierls state below 25 K,[4)] although the system has a 2D approximately triangular lattice structure rather than a 1D chain structure.

The μSR experiment was carried out at the RIKEN-RAL Muon Facility. 25 mg of the $C_2H_5(CH_3)_3P[Pd(dmit)_2]_2$ polycrystalline samples were prepared.

The ZF-μSR time spectra exhibit almost Gaussian-type time evolution of the muon spin polarization down to ~25 K. The relaxation gradually became faster at lower temperatures, and the shapes of the time spectra become exponential. The time spectra were fitted with the function $A(t) = A_0 G(\Delta, t)\exp(-\lambda t)$. The temperature dependences of the muon spin relaxation rate λ and the internal field distribution at the muon site Δ are shown in Figs. 1(a) and (b), respectively. λ is independent of temperature down to ~25 K, and then starts to increase. Δ seems to rapidly decrease concomitantly at ~25 K, because the shapes of the time spectra change from Gaussian-type to exponential. Such behavior of λ and Δ is often observed in spin-singlet systems. In fact, similar temperature dependences of λ and Δ are reported for another Pd(dmit)$_2$ salt that forms a spin-singlet state.[3)] It often happens in the spin-singlet state that dilute spins which do not dimerize yield fluctuating local fields and cause the muon spin relaxation. The increase in λ slightly below the transition temperature is thought to reflect the dynamics of the electronic spins such as the slowing down of spin flip excitations across the finite energy gap in the magnetic excitation spectrum in the spin-singlet state.[5)] Therefore, our result strongly indicates that the system exhibits a valence bond (VB) ordered state, as suggested by the previous studies.[4)] Note that such a large enhancement of the muon spin relaxation is not observed in a resonating valence bond state because the resonance frequency is too high to be detected by the μSR method. Below ~15 K, λ eventually saturates. The temperature independence of λ in this temperature region may be used to detect the local field due to some defect.

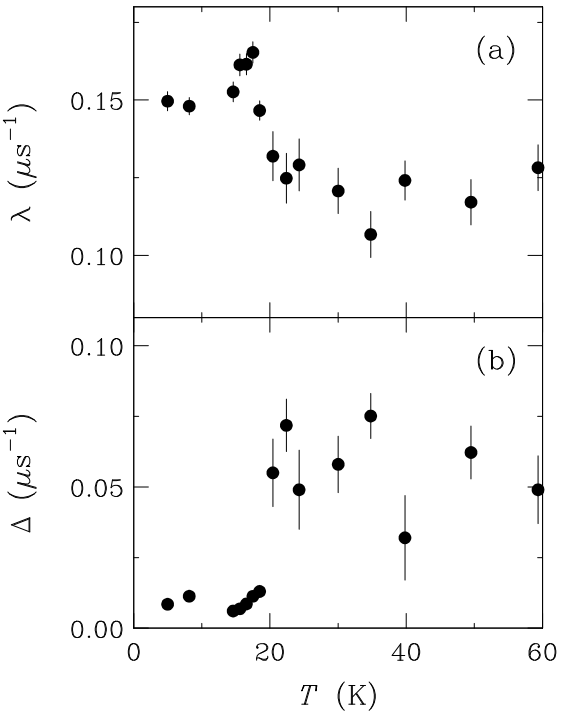

Fig. 1. Temperature dependences of (a) the muon spin relaxation rate λ and (b) the internal field distribution Δ.

References
1) M. Tamura and R. Kato: J. Phys.: Condens. Matter **14**, L729 (2002).
2) S. Ohira et al.: Phys. Rev. B **70**, 220404(R) (2004).
3) S. Ohira et al.: Physica B **374-375**, 122-125 (2006).
4) M. Tamura et al.: J. Phys. Soc. Jpn. **75**, 093701 (2006).
5) B. W. Lovett et al.: Phys. Rev. B **61**, 12241 (2000).

*1 Present address: Academic & Information Board, Ochanomizu University

Effect of randomness on the quantum spin system $Tl_{1-x}K_xCuCl_3$ with $x = 0.44$ studied by Zero-field Muon-Spin-Relaxation (ZF-μSR) method†

T. Suzuki, F. Yamada,[*1] I. Watanabe, T. Goto,[*2] A. Oosawa,[*2] and H. Tanaka,[*1]

[spin gap, magnon, Bose-Einstein condensation, randomness, Bose glass phase]

In the mixed system $Tl_{1-x}K_xCuCl_3$, which is the subject of this study, the randomness of the local potential is introduced through the difference in the value of the dominant intradimer interaction J between $TlCuCl_3$ and $KCuCl_3$, because J corresponds to the local potential of the excited spin triplets (magnons). Magnetization measurements suggest that the ground state is negative with no gap in the mixed system at zero field (ZF), although both the parent materials are non-magnetic with finite excitation gaps[1)].

The appearance of a new phase, Bose-glass phase, at lower magnetic fields at $T = 0$ is predicted by theories.[2)] According to theoretical predictions, the Bose-glass phase is produced between gapped and ordered phases. Recently, we have reported an increase in the muon-spin-relaxation rate λ at low temperatures at $x = 0.20$, which is possibly a precursor to the Bose-glass phase at $T = 0$[3)]. However, it has not yet been clarified whether or not another ground state apart from the Bose-glass phase and the gapped state appears when the randomness is enhanced with increasing the concentration of x. To investigate microscopic magnetic properties in highly random systems, we carried out the zero-field muon-spin-relaxation (ZF-μSR) measurements in $Tl_{1-x}K_xCuCl_3$ with $x = 0.44$ single crystals at the RIKEN-RAL muon facility.

Figure 1 shows ZF-μSR time spectra at each temperature. The shape of the time spectrum is changed drastically with decreasing temperature. The μSR time spectra are analyzed using the function of the stretched exponential $A_0 \exp(-\lambda t)^{\beta}$, where A_0 is the initial asymmetry and λ is the muon-spin-relaxation rate. Figure 2 shows the temperature dependence of the muon-spin-relaxation rate λ and of the power β. The relaxation rate λ rapidly increases with decreasing temperature in contrast to the case of $x = 0.20$ (open triangles). The rapid increase in the relaxation rate λ reminds us of the critical divergence toward a phase transition, and it is suggested that there exists a critical slowing down of the fluctuation frequency of the Cu-3d spins to a spin frozen state below 80 mK in zero-field. The expected spin frozen state is not the Bose-glass phase, because the saturation of the relaxation rate λ is not observed in the case of $x = 0.44$. The power β of the stretched exponential function decreases with decreasing temperature, and tends to saturate to the value of $\beta = 0.65$. By the analogy of the nuclear spin-lattice relaxation by spatially localized impurity spins[4)], it is suggested that the fast muon-spin-relaxation originates from the spatially-fixed dilute moments fluctuating in time, and that spatially separated islands, which have a finite magnetic moment large enough to cause the fast muon-spin-relaxation, appear in the singlet sea at lower temperatures.

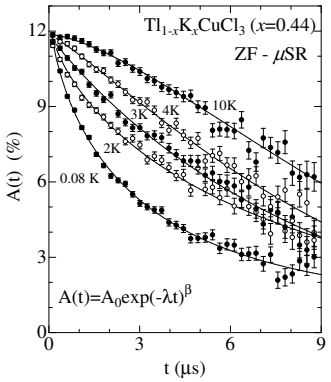

Fig. 1. Time spectrum of the zero-field muon-spin-relaxation. Solid lines indicate fitted results obtained using the stretched exponential function $\exp(-\lambda t)^{\beta}$.

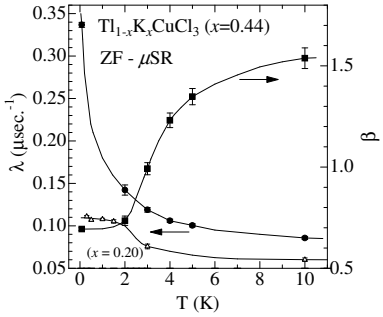

Fig. 2. Temperature dependence of the relaxation rate λ (left-hand side vertical axis, closed circles) and of the power β (right-hand side vertical axis, closed squares) for $x = 0.44$. Solid lines are guides for the eye.

References

1) A. Oosawa *et al.*: Phys. Rev. B **65**, 184437 (2002).
2) M. P. A. Fisher *et al.*: Phys. Rev. B **40**, 546 (1989).
3) T. Suzuki *et al.*: J. Phys. Soc. Jpn. **75**, 025001 (2006).
4) M. R. McHenry *et al.*: Phys. Rev. B **5**, 2958 (1972).

† Condensed from article in J. Phys. Soc. Jpn. **76**, 074704 (2007).

*1 Department of Physics, Tokyo Institute of Technology
*2 Department of Physics, Sophia University

μSR study of the impurity-induced magnetic phase in $Tl(Cu_{1-x}Mg_x)Cl_3$†

T. Suzuki, F. Yamada,*1 I. Watanabe, T. Goto,*2 A. Oosawa,*2 and H. Tanaka*1

[Keywords: Bose-Einstein condensation, quantum phase transition, impurity effect]

$TlCuCl_3$ has the magnetic ground state of spin singlets with an excitation gap of 7.5 K.[1] At low magnetic fields, magnetization decreases to zero because of the singlet ground state. At high magnetic fields, however, magnetization begins to increase below the temperature T_N. Neutron elastic scattering experiments have revealed that the field-induced Néel ordering occurs and that the vertical component of spins orders antiferromagnetically.[2] Recently, impurity-introduced $Tl(Cu_{1-x}Mg_x)Cl_3$ single crystals have been grown, and new intriguing phenomena have been reported.[3,4] The magnetic phase transition to an ordered state is observed by magnetization and specific heat measurements in the zero-field limit, and neutron elastic scattering measurements reveal that this impurity-induced ordered state is an antiferromagnetically ordered state whose magnetic structure is the same as that of the field-induced phase in $TlCuCl_3$. The purpose of this study is to investigate the microscopic magnetic properties of the impurity-induced ordered state in $Tl(Cu_{1-x}Mg_x)Cl_3$ with $x = 0.0047$ at low temperatures using the muon-spin-relaxation (μSR) technique. Measurements of μSR were performed using the LTF instrument at the Swiss Muon Source (SμS), Paul Scherrer Institut (PSI), Villigen, Switzerland. Before μSR measurements, we carried out the measurement of the temperature dependence of the specific heat in the zero field. We observed a clear peak in the temperature dependence of the specific heat of the spin system, and the phase transition point T_N is confirmed to be 0.70 K.

In order to investigate the difference in spin dynamics between temperatures below and above T_N, the longitudinal-field muon-spin-relaxation (LF - μSR) measurements were carried out at 20 mK and 1 K. Figure 1 shows the time spectrum at 20 mK at each magnetic field. Solid lines indicate fitted results using the function $A(t) = A(0)G_{KT}(\Delta, H_{LF}, t)\exp(-\lambda t)$. $G_{KT}(\Delta, H_{LF}, t)$ is the static Kubo-Toyabe function. Figure 2 shows the magnetic field dependence of the muon spin relaxation rate at 20 mK and 1 K. The obtained data for 20 mK are well fitted using the Redfield formula of $\lambda(H_{LF}) = \gamma_\mu^2 H_{loc}^2 \tau / (1 + \gamma_\mu^2 H_{LF}^2 \tau^2)$. The local magnetic field H_{loc} and the frequency of fluctuation f at muon sites are deduced to be $H_{loc} = 34$ gauss and $f = 1/\tau = 0.74$ MHz, respectively. On the other hand,

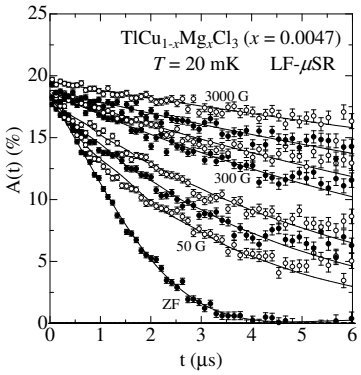

Fig. 1. Time spectrum of the longitudinal-field muon-spin-relaxation (LF - μSR) of $TlCu_{1-x}Mg_xCl_3$ with $x = 0.0047$ at 20 mK in 0, 50, 70, 100 300, 1000, 3000, 5000 gauss. Solid lines indicate fitted results.

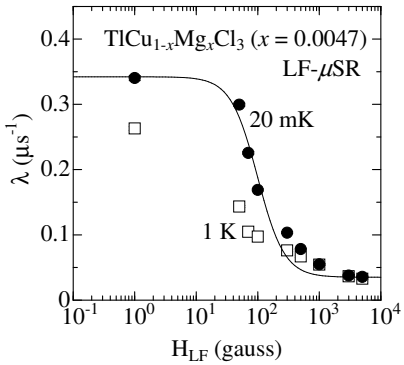

Fig. 2. Magnetic field dependence of the relaxation rate λ at 20 mK and 1 K. Solid lines indicate fitted result for 20 mK.

the magnetic field dependence of λ in the case of 1 K is broad and the cutoff structure is almost smeared. This means that muon spins feel widely spread spectrum of the local magnetic fields H_{loc} and of the frequency of fluctuation f at 1 K. These results indicate that the local magnetic fields H_{loc} and the frequency of the fluctuation at muon sites, which originate from the Cu-3d spins fluctuation, concentrate to the one component with decreasing temperature, but the Cu-3d spins in the crystal are not frozen down to 20 mK. These spins slowly fluctuate at a frequency below 1 MHz at 20 mK.

References
1) H. Tanaka *et al.*: J. Phys. Soc. Jpn. **70**, 939 (2001).
2) A. Oosawa *et al.*: Phys. Rev. B **65**, 184437 (2002).
3) A. Oosawa *et al.*: Phys. Rev. B **66**, 020405(R) (2002).
4) H. Imamura *et al.*: J. Phys. Soc. Jpn.**74**, 064423(2006).

† Condensed from the article submitted to Phys. Rev. B

*1 Department of Physics, Tokyo Institute of Technology
*2 Department of Physics, Sophia University

μSR studies of the ground state of an impure spin-ladder

A. Kikkawa,[*1] Z. Honda,[*2] K. Katsumata,[*1] I. Watanabe,[*3] T. Suzuki,[*3] and T. Matsuzaki[*3]

[μSR, spin-ladder, impurity effect]

The ground state of quantum antiferromagnets such as, a spin, $S = 1$ Heisenberg antiferromagnetic chain, a spin-Peierls compound and a two-leg spin-ladder is a singlet with an energy gap (spin-gap) to the lowest excited state due to quantum fluctuations. This non-magnetic state is called the spin liquid one. When an impurity is doped in these magnetic systems, novel phenomena appear. Examples include, the fractional spin degrees of freedom at the ends of $S = 1$ Heisenberg antiferromagnetic chain[1)] and the impurity induced long-range magnetic order in spin-Peierls and two-leg spin-ladder materials[2–4)]. To the best of our knowledge, there have been neither theoretical nor experimental studies on randomly mixed two spin ladder materials with different magnetic atoms. We have performed experimental studies on a random mixture of two spin-ladder materials, $Na_2(Co_{0.5}Fe_{0.5})_2(C_2O_4)_3(H_2O)_2$.

From our magnetic measurements on single crystals of $Na_2(Co_{0.5}Fe_{0.5})_2(C_2O_4)_3(H_2O)_2$, we find that the temperature, T, dependence of the magnetic susceptibility shows a broad peak at ~ 18 K indicating a formation of a spin-gap and an increase below ~ 6 K. The latter observation is interpreted as due to the presence of magnetic moments that do not participate in the formation of the spin liquid state. The magnetic field dependence of the magnetization is consistent with this interpretation.

In order to obtain microscopic information on this mixed ladder, we have performed μSR measurements under zero and non-zero magnetic fields applied parallel to the muon beam direction (longitudinal field, LF). Muon spin-relaxation measurements were conducted at the RIKEN-RAL Muon Facility in the UK.

Figure 1 shows the time spectra obtained at LF = 0.395 T and at the designated temperatures. We see a considerable amount of muon spin relaxation and the relaxation becomes faster with decreasing temperature. This T-dependence of the spectra is very different from that observed in pure $Na_2Co_2(C_2O_4)_3(H_2O)_2$. In the pure compound, the relaxation is extremely slow at low temperatures, reflecting the non-magnetic ground state[5)]. The present μSR measurements show clearly that magnetic moments exist at the low temperatures and cause μ-on spin relaxation. This result gives a microscopic evidence for our interpretation of the magnetic susceptibility mentioned above.

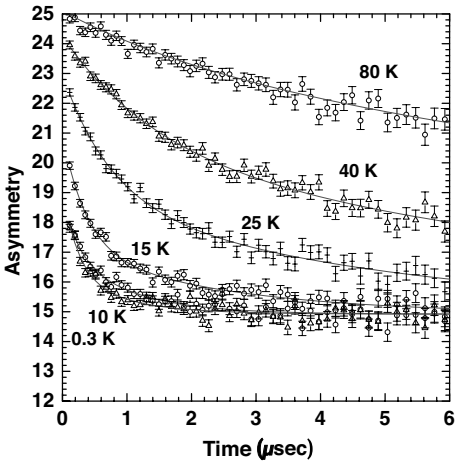

Fig. 1. Temperature dependence of the μ-on spin decay of an assembly of single crystal samples of $Na_2(Co_{0.5}Fe_{0.5})_2(C_2O_4)_3(H_2O)_2$ measured at 0.395 T. Full lines are the results of fits to the formula discussed in the text.

We fitted the spectra to a sum of two relaxation functions,

$$G_z(t) = D\exp(-\lambda_1 t) + E\exp(-\lambda_2 t) + F, \qquad (1)$$

where, D, E and F are constants, independent of time, t, and λ_1 and λ_2 are the relaxation rates. The relaxation rate thus obtained increases with decreasing T down to about 10 K and becomes almost temperature independent below about 10 K. This result is interpreted as follows: at high temperatures Co and Fe electron spins are in the paramagnetic state and the fluctuation time is too fast to be detected by μSR which has a characteristic time window from 10^{-6} to 10^{-11} seconds. With decreasing temperature, the spatial correlation among spins develops and the fluctuation of the spins becomes slow. The almost temperature independent relaxation rate at the low temperatures imply a wide distribution in relaxation times as is often observed in random magnetic systems.

*1 RIKEN SPring-8 Center, Harima Institute
*2 Faculty of Engineering, Saitama University
*3 Advanced Meson Science Laboratory, RIKEN Nishina Center

References

1) M. Hagiwara *et al.* : Phys. Rev. Lett. **65**, 3181 (1990).
2) J. P. Renard *et al.*: Europhys. Lett. **30**, 47 (1995).
3) H. Fukuyama *et al.*: J. Phys. Soc. Japan **65**, 1182 (1996).
4) M. Azuma *et al.*: Phys. Rev. B **55**, R8658 (1997).
5) A. Kikkawa *et al.*: J. Phys. Soc. Japan **76**, 023707 (2007).

μSR study around a quantum critical point in heavy fermion compounds $Ce_2RhIn_{8-x}Sn_x$

K. Ohishi,[*1] R. H. Heffner,[*1,*2] T. U. Ito,[*1,*3] W. Higemoto,[*1] E. D. Bauer,[*2] and T. Suzuki

Quantum phase transitions are induced by the application of a control parameter, typically either pressure or chemical substitution, in contrast to classical phase transitions, which are induced by thermal fluctuation. It is observed that superconductivity and/or non-Fermi liquid (NFL) behavior often occurs in the vicinity of a magnetic quantum critical point (QCP), where the Curie or Néel temperature approaches $T = 0$ K. NFL behavior includes anomalous temperature dependences of the electrical resistivity ($\Delta\rho = \rho(T) - \rho(0) \propto T^n, 1 \leq n < 2$) and the specific heat coefficient ($C/T \propto -\ln T$)[1,2], in contrast to the Fermi liquid behavior seen in ordinary metals ($\Delta\rho \propto T^2, C/T =$ constant). To study these behaviors, which appear near a QCP, the heavy fermion systems are very suitable since they can be tuned continuously from the magnetic ordered state to the paramagnetic metallic state by varying a single parameter, i.e., the strength of hybridization between conduction bands and f-electrons. Phase diagrams observed in heavy fermion systems have indeed been established experimentally for magnetic ordering, superconductivity and NFL behavior. However, at present, there is no ability to predict whether superconductivity, magnetism or both will occur in such a phase diagram, and what properties any specific ground state will possess. This is crucial for understanding why magnetic ordering and superconductivity occur together, and why superconductivity and NFL behavior appear in the vicinity of a QCP.

Ce_2RhIn_8 is a known antiferromagnet with $T_N = 2.8$ K[3], but becomes superconducting above a pressure of 1.1 GPa[4]. The magnetically ordered state is favored at low pressure. The Néel temperature is eventually depressed with increasing pressure, and superconductivity sets in above 1.1 GPa. Recently, it has been found that the chemical substitution of Sn for In in $Ce_2RhIn_{8-x}Sn_x$ depresses T_N for a critical concentration of about $x \sim 0.5$, suggesting the emergence of a QCP[5]. According to specific heat measurements above 0.4 K[5], NFL behavior in C/T was observed. Therefore, it is considered that $Ce_2RhIn_{8-x}Sn_x$ is a good candidate to study magnetism and superconductivity around a QCP because two QCPs are induced in this system.

In this beam time, we focused on Sn-doped samples, and performed zero-field (ZF) and longitudinal-field (LF) muon spin relaxation (μSR) measurements of $Ce_2RhIn_{8-x}Sn_x$ ($x = 0.5$ and 0.7) in the temperature range between 0.3 K and 10 K at the RIKEN-RAL Muon Facility in the U.K. Figure 1 shows the ZF-μSR time spectra for the $x = 0.5$ sample at various temperatures. While the relaxation rate above 2 K is almost independent of temperature, it gradually starts to increase with decreasing temperature. As shown in this figure, muon spin precession signals are not observed down to 0.3 K, suggesting the absence of magnetic ordering at this temperature. The LF-μSR measurements revealed that the internal field at 0.3 K is static at a few gauss. Although the data are not shown here, no muon spin precession has been observed in the $x = 0.7$ sample. The relaxation rate observed in $x = 0.7$ is smaller than that in $x = 0.5$. While the detailed analysis is in progress, it is likely that the suppression of magnetic ordering occurs in both $x = 0.5$ and 0.7 samples. Further experiments at lower temperature are necessary to clarify the magnetic ground state of these samples.

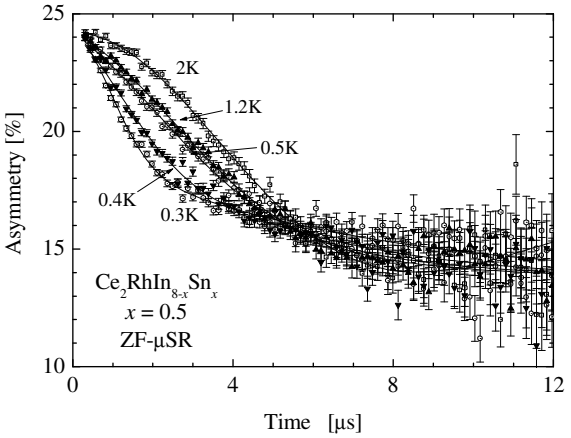

Fig. 1. ZF-μSR time spectra in $Ce_2RhIn_{8-x}Sn_x$ ($x = 0.5$) at various temperatures.

References

1) P. Coleman and A. Schofield: Nature **433**, 226 (2005).
2) T. Park et al.: Nature **440**, 65 (2006).
3) J. D. Thompson et al.: J. Magn. Magn. Mater. **266-230**, 5 (2001).
4) M. Nicklas et al.: Phys. Rev. B **67**, 020506(R) (2003).
5) E. D. Bauer: Unpublished results.

*1 Advanced Science Research Center, Japan Atomic Energy Agency
*2 Los Alamos National Laboratory, USA
*3 Department of Physics, Tokyo Institute of Technology

Quasi-Static Internal Field Observed by μSR in $La_{2-x}Sr_xCuO_4$

I. Watanabe, T. Adachi[*1] S. Yairi[*1] Y. Koike[*1] and K. Nagamine[*2]

[μSR, High-T_c, Cu-Spin Dynamics, Spin Gap]

The origin of high-T_c superconductivity remains controversial and lots of experimental and theoretical studies that have been carried out over past 20 years. We have continuously studied Cu-spin dynamics in high-T_c oxides using the muon-spin relaxation (μSR) technique. The μSR technique is a unique method of sensing spin dynamics within the middle-frequency range between 10^{-6} and 10^{-11} sec. Using the zero-field (ZF) μSR measurement of polycrystalline samples of $La_{2-x}Sr_xCuO_4$ (LSCO), we have clarified a close relationship between the mobility of holes and the dynamics of the internal field at the muon site[1,2]. To obtain more detailed information on the dynamics of the internal field at the muon site, we have carried out precise μSR measurement in longitudinal fields (LF) with statistics higher than conventional statistics[2]. LF-μSR measurement has been performed at the RIKEN-RAL Muon Facility in the UK. A special setup called a "fly-past" mode, improves the signal-to-noise ratio, has been developed to measure small changes in μSR time spectra. Polycrystalline samples of LSCO with x=0.115 have been prepared by the conventional solid-state reaction method[1,2]. The sample has shown a static magnetically ordered state below apriximatelly 10 K[1,2].

Figure 1 shows the LF dependence of time spectra at 50.8 K. The time spectrum of ZF shows a Gaussian-type depolarization behavior and recovers with increasing LF, and becomes almost flat above 20 G. The time spectra have been analyzed using the analysis function of $A_0 e^{-\lambda t} G_Z(\Delta, t, H_{loc})$ (Ref. 2). Here, A_0 is the initial asymmetry and $G_Z(\Delta, t, H_{loc})$ is the Gaussian-type Kubo-Toyabe function[2]. In Fig. 3, a calculated time spectrum with LF = 5 G and $\lambda = 0$ is shown by a red line. The measured data with the same condition is highlighted by blue circles. Clearly, there is a difference between the obtained and calculated spectra. This difference proves the nonzero value of λ.

Figure 2 shows the LF dependence of λ at 50.8 K. λ decreases with decreasing LF. Its LF dependence shows a convex shape in the log-log plot. To obtain quantitative information from this data, the Redfield equation is applied[3–5]. The Redfield equation is expressed;

$$\lambda(H_{LF}) = \frac{2\gamma_\mu^2 H_{loc}^2 \tau_c}{1 + \gamma_\mu^2 H_{LF}^2 \tau_c^2}, \quad (1)$$

where τ_c is the correlation time of the internal field at the muon site, γ_μ the gyromagnetic ratio of a muon spin ($\gamma_\mu = 2\pi \times 13.55$ MHz/kG), and H_{loc} the internal field fluctuating with the frequency of ω_c ($= 1/\tau_c$) at the muon site.

After obtaining the best fit using the Redfield equation, τ_c and H_{loc} have been obtained to be about 0.07 MHz and 1.8 G, respectively. In paticular, the obtained frequency is at the low end of the μSR characteristic time window. Therefore, the current study proves the existence of a small quasi-static internal field in LSCO well above the magnetic transition temperature.

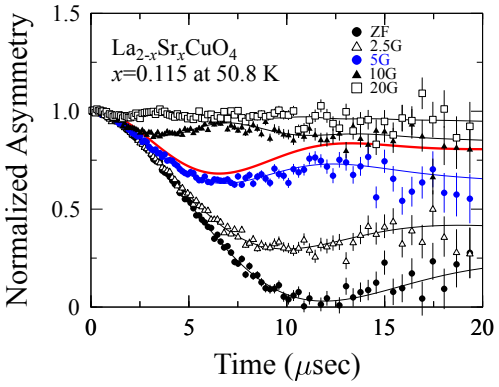

Fig. 1. Longitudinal-field μSR time spectra of $La_{2-x}Sr_xCuO_4$ with x=0.115 at 50.8 K.

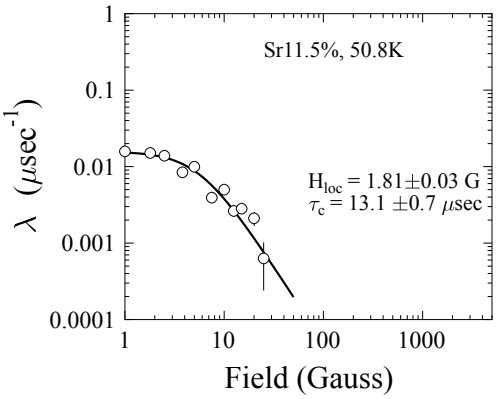

Fig. 2. Longitudinal-field dependence of λ of $La_{2-x}Sr_xCuO_4$ with x=0.115 at 50.8K.

*1 Department of Applied Physics, Graduate School of Engineering, Tohoku University.
*2 Physics Department, University of California, Riverside (UCR), USA.

References

1) I. Watanabe *et al.*, J. Low Temp. Phys. **131**, 331 (2003).
2) I. Watanabe *et al.*, to be published in Phys. Rev. B.
3) W. Higemoto *et al.*, Phys. Lett. A **243**, 80 (1998).
4) I. Watanabe *et al.*, Phys. Rev. B **62**, 14524 (2000).
5) T. Saito *et al.*, Phys. Rev. B **74**, 134423 (2006).

Effect of Pressure on a Static Magnetically Ordered State of Cu Spins in $La_{2-x}Sr_xCu_yZn_{1-y}O_4$ with $x = 0.13$ and $y = 0.0025$ Studied by μSR

I. Watanabe, T. Adachi*1, Y. Ishii, T. Kawamata, Y. Koike*1, and D. Andreica*2

[μSR, High T_c, Cu Spin Dynamics, Pressure]

One of the fascinating models for describing the mechanism of high-T_c superconductivity is the so-called stripe model of spins and holes[1]. An important point for understanding this model is to investigate the dynamics of stripes. It has been reported that stabilized stripes are easily destabilized by a low pressure of about 2 kbar[2]. On the other hand, we have proved in our previous μSR study that a small amount of non-magnetic impurities stabilizes dynamically fluctuating stripes in $La_{2-x}Sr_xCuO_4$ at around x=0.13, where the hole concentration is about 1/8 per Cu[3]. Therefore, we have carried out a μSR measurement at a high-pressure of about 8 kbar in order to investigate the effect of pressure on the dynamics of stripes.

The polycrystalline Zn-substituted sample, $La_{2-x}Sr_xCu_{1-y}Zn_yO_4$, with x=0.13 and y=0.0025 has been prepared by a typical solid-state reaction method. In this sample, the stabilization of stripes is observed below 7 K, although no sign of the stabilization of stripes is observed in the case of y=0. Thus, this sample is expected to be located at the boundary between the stabilized and dynamically fluctuating states of stripes. If the dynamics of stripes depends on the pressure, the disappearance of the stabilized state of stripes would be observed in this sample at a pressure of the order of a few kbar. The high-pressure μSR measurement was carried out at PSI in Switzerland using a clump-type cell made of CuBe. The applied pressure in this study was 8.1 kbar. μSR time spectra at a transverse field (TF) of 50 G were measured with changing temperature.

Figure 1 shows a photograph of the high-pressure cell available at PSI. The cell is cooled in the He-gas atmosphere down to about 2 K. Muons with a high momentum were injected into the sample through the wall of the cell. Figure 2 shows temperature dependences of the amplitude of the muon-spin precession in TF = 50 G at 0 and 8.1 kbar. The precession amplitude decreases with decreasing temperature below 15 K. This tendency is the same as that observed in our previous study[4]. Thus, the decrease in the precession amplitude of the muon spin indicates the stabilization of stripes. As observed in Fig. 2, the temperature dependence of the precession amplitude of the muon spin obtained at 8.1 kbar is similar to that measured in the atmosphere. Thus, it is concluded from this study that pressure does not affect on the dynamics of stripes at least up to about 8 kbar. Additional high-pressure experiments using other samples are now planned in order to obtain more information about the pressure dependence of the stabilization of stripes.

Fig. 1. Pressure cell available at PSI and used in this study.

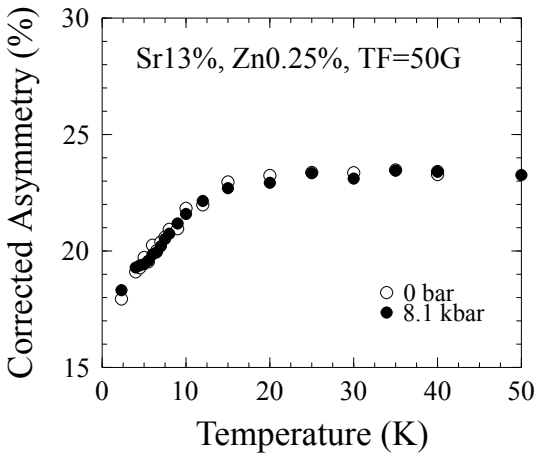

Fig. 2. Temperature dependences of the amplitude of the muon-spin precession of $La_{2-x}Sr_xCu_{1-y}Zn_yO_4$ with x=0.13 and y=0.0025 in TF = 50G at 0 and 8.1 kbar.

*1 Department of Applied Physics, Graduate School of Engineering, Tohoku University
*2 PSI, Switzerland, and Department of Physics, Babes-Bolyai University, Romania

References

1) J. M. Tranquada *et al.*; *Nature* (London) **375**, 561 (1995).
2) S. Arumugam *et al.*; Phys. Rev. Lett. **88**, 247001 (2002).
3) I. Watanabe *et al.*; Phys. Rev. B **65**, R180516 (2002).
4) T. Adachi *et al.*; Phys. Rev. B **69**, R184507 (2004).

Suppression of antiferromagnetic order by impurity-doping in the electron doped $Pr_{1-x}LaCe_xCuO_4$

Masaki Fujita,[*1] Aya Hino,[*2] Toshiaki Takagi,[*2] Isao Watanabe,[*3] and Kazuyoshi Yamada[*1,*4]

Electron-hole symmetry of a pairing mechanism is one of the central issues in a research on high-T_c superconductivity. Since either type of carrier doping into Mott insulators induces high-T_c superconductivity, it is widely considered that the spin correlations play a crucial role in the superconducting mechanism. To reveal the universal nature of spin correlations on underlying CuO_2 planes, impurity effects have been extensively studied for the high-T_c superconductors. In a prototypical hole-doped (n-type) superconductor $La_{2-x}Sr_xCuO_4$ (LSCO), evidence for the existence of spatially modulated spin correlations (stripe correlations) and/or the magnetic quantum phase transition was revealed in the superconducting phase by a systematic μSR measurement.[1,2] To understand such a novel magnetism revealed by impurity substitution in carrier-doped Mott insulators and its relevance to the high-T_c superconductivity, comparative studies betweeen hole-doped and electron-doped (n-type) systems are indispensable.

To gain further insight into this problem, we have performed zero-field μSR measurements on the electron-doped system $Pr_{1-x}LaCe_xCu_{1-y}Zn_yO_4$[3] at RIKEN-RAL Muon Facility, Rutherford Appleton Laboratory in the UK. As shown in Fig. 1, the Zn-free sample shows a clear rotation component in the μSR time spectrum at $T\sim$6 K, indicating the existence of a static magnetic order at low temperature. However, upon Zn doping, the time spectrum changes into an exponential-type one with faster depolarization. This result indicates the suppression of the development of spin correlations at low temperature by Zn doping. The onset temperature for the appearance of static magnetic order (T_N) as a function of Zn concentration is plotted in Fig. 2 for y=0, 0.04 and 0.08. T_N decreases monotonically upon Zn doping for all systems with fixed Ce concentration. Furthermore, no clear evidence of appearance of magnetic order was observed in the superconducting phase at low temperature down to 6 K. These results suggest the reduction of spin correlations by Zn doping and different from the behavior in the hole-doped system in which an anomalous enhancement of spin correlations is confirmed at adequate Zn concentrations. Therefore, the nature of static or low-energy spin fluctuations in the n-type system would be quite different from those in the p-type system. A monotonic reduction of spin correlations and no appearance of magnetic order after vanishing the superconductivity suggest that the non magnetic Zn impurity in the electron-doped system simply acts as a vacancy of spins on underlying CuO_2 planes, resulting into the dilution of Cu spins by Zn doping.

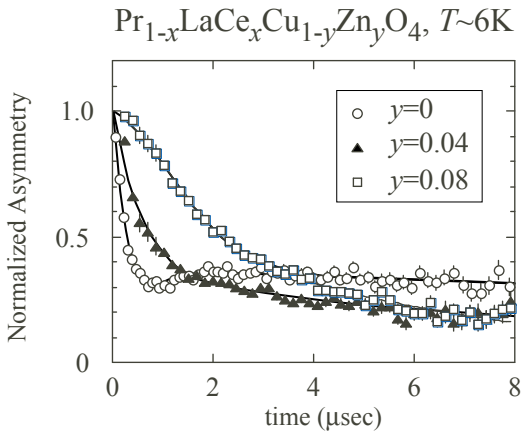

Fig. 1. ZF-μSR time spectra for Zn-doped PLCCO with y = 0 (circles), 0.04 (triangles), and 0.08 (squares).

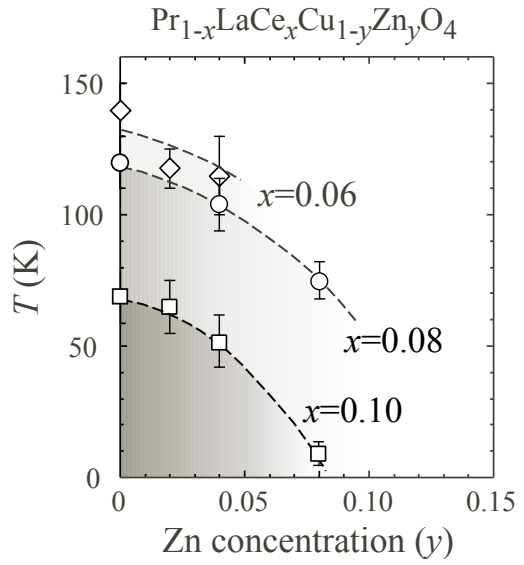

Fig. 2. Zn-concentration dependence of the magnetic transition temperature for x=0.06 (diamonds), 0.08 (circles) and 0.10 (squares).

*1 Institute for Materials Research, Tohoku University, Japan
*2 Department of Physics, Tohoku University, Japan
*3 RIKEN Advanced Meson Science Laboratory
*4 World-Premier-International Research Center Initiative, Tohoku University, Japan

References

1) I. Watanabe *et al.*, Phys. Rev. B **62**, R11985 (2000).
2) Risdiana *et al.*, Phys. Rev. B **77**, 054516 (2008).
3) M. Fujita *et al.*, Phys. Rev. B **67**, 014514 (2003).

μSR Study of Proton Dynamics in 9-Hydroxyphenalenone Derivatives

Tomoyuki Mochida,[*1,2] Masaru Oyama,[*1,2] Tadashi Sugawara,[*3] Isao Watanabe, Yasuyuki Ishii, Takao Suzuki, Takayuki Kawamata, and Teiichiro Matsuzaki

In this study, we elucidate the nature of the phase transitions in molecular crystals of 9-hydroxyphenalenone derivatives. These are interesting materials for investigating hydrogen/deuterium dynamics and its consequences on phase transitions in hydrogen-bonded ferroelectrics.[1, 2] At room temperature, the molecules undergo rapid tautomerization coupling with intramolecular hydrogen transfer between the two oxygen atoms (Fig. 1). By applying μSR, we investigate the distribution or order-disorder of the hydrogen/deuterium along the hydrogen bond and how they are correlated with the phase transitions.

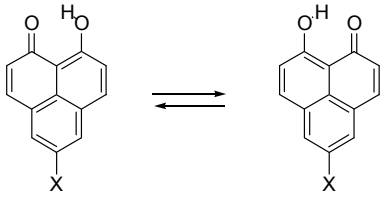

Fig. 1. Tautomerization of 9-hydroxyphenalen-1-one derivatives.

As the first step, we investigated how the hydrogen/deuterium dynamics in the 5-bromo derivative (X = Br) can be detected by μSR. The phase sequences of the 5-bromo compound (**1**-*h*) and its deuteroxy analogues (**1**-*d*) have been examined in detail:[3–5] **1**-*h* exhibits no phase transition, but **1**-*d* exhibits successive phase transitions at T_I = 34 K and T_C = 22 K. The absence of phase transition in **1**-*h* has been ascribed to hydrogen tunneling.[4,5] Previously, preliminary μSR measurements for **1**-*d* were performed at PSI for 1 day, but the relaxation time turned out to be too long for the instruments. This time, we performed μSR measurements at RAL for two days, and could evaluate the relaxation time for both **1**-*h* and **1**-*d*.

The temperature dependence of the relaxation rates for **1**-*d* under zero magnetic field is shown in Fig. 2. A significant increase in the relaxation rate was observed at approximately 36 K, which may reflect the ordering of the deuterium associated with the phase transition. However, a more detailed analysis is necessary to unambiguously ascribe the origin of this enhancement. To exclude the contribution of muonium, relaxation rates were measured under a longitudinal magnetic field at 4000 G. A marked enhancement of the relaxation rate was observed at approximately 200 K. The origin of the enhancement is of special interest. A similar tendency of the relaxation rates for **1**-*h* was observed, but the results are preliminary owing to beam-time limitation.

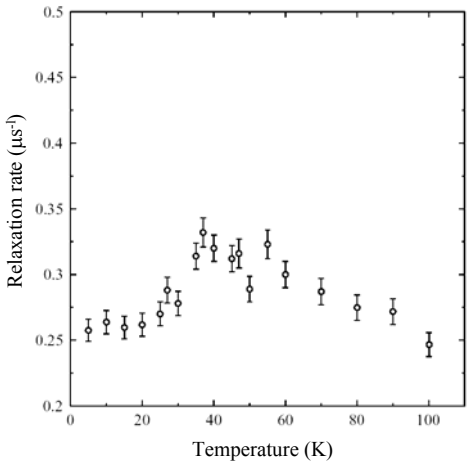

Fig. 2. Temperature dependence of muon relaxation rate in 5-bromo-9-deuteroxyphenalen-1-one (**1**-*d*).

For further studies, we need to collect more accurate data for **1**-*h* for the discussion of the isotope effect. We further plan to investigate the hydrogen/deuterium dynamics in the 5-methyl derivatives, which exhibit unusual low-temperature structures.[6] Since these materials are the organic version of KDP-like ferroelectrics, these investigations will provide essential information on the role of hydrogen dynamics in hydrogen-bonded ferroelectrics.

References

1) T. Mochida, D. Kuwahara, S. Miyajima, and T. Sugawara: J. Phys. Chem. B. 107, 12315 (2003).
2) T. Mochida, A. Izuoka, T. Sugawara, Y. Moritomo, and Y. Tokura: J. Chem. Phys. 101, 7971 (1994).
3) Y. Moritomo, Y. Tokura, T. Mochida, A. Izuoka, and T. Sugawara: J. Phys. Soc. Jpn. 64, 1892 (1995).
4) T. Matsuo, K. Kohno, A. Inaba, T. Mochida, A. Izuoka, and T. Sugawara: J. Chem. Phys. 108, 9809 (1998).
5) T. Matsuo, K. Kohno, M. Ohama, T. Mochida, A. Izuoka, and T. Sugawara: Europhys. Lett. 47, 36 (1999).
6) R. Kiyanagi, A. Kojima, H. Kimura, M. Watanabe, Y. Noda, T. Mochida, T. Sugawara, and S. Kumazawa: J. Phys. Soc. Jpn. 74, 613 (2005).

*1 Kobe University
*2 Toho University
*3 The University of Tokyo

Electronic structure and dynamical properties of hydrogen in WO_3 probed by muon

M. Mihara,[*1] K. Shimomura,[*2] I. Watanabe, Y. Ishii, T. Suzuki, J. Komurasaki,[*1] D. Nishimura,[*1] K. Nishiyama,[*2] R. Kadono,[*2] S. Takai,[*3] T. Nakano,[*1] and T. Hirose[*4]

Hydrogen in some wide gap semiconductors forms shallow donor levels and can be a source of conductivity. WO_3 is one of the candidates for the formation of shallow donor levels upon hydrogen incorporation, which is suggested by theoretical prediction based on first-principle total-energy calculations[1]. The muon spin rotation (μSR) spectroscopy is suitable for investigating the formation and electronic structure of such levels, as determined by the existence of the muonium (Mu) center shown in ZnO[2] and so on with an extremely small hyperfine coupling constant compared with the vacuum hydrogen value. Previous studies of transverse field (TF) μSR in WO_3 suggest the possibility of shallow Mu formation[3,4]. However, higher statistical data have been desired to confirm whether the shallow Mu exists in WO_3. For this purpose, TF-μSR measurements in WO_3 single crystals prepared by the Bridgeman method[5] were performed using a high-intensity pulsed positive muon beam at the RIKEN-RAL facility.

A TF-μSR spectrum at 7 K under a transverse field of 2 mT is shown in Fig. 1. No evidence of the shallow muonium formation, such as a beat pattern due to a small hyperfine field, has been shown in WO_3 within 460M-event data.

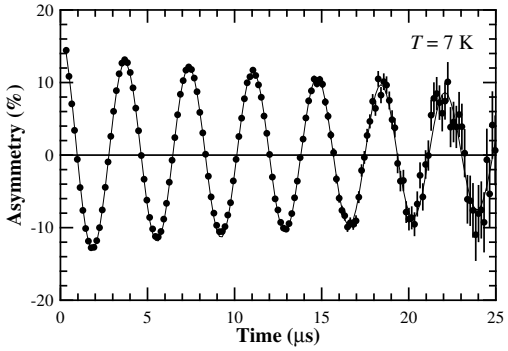

Fig. 1. TF-μSR spectrum in WO_3 single crystal grains.

Another subject is the diffusion property of hydrogen in WO_3. Hydrogen impurities in WO_3 play an important role in changing its optical properties, as observed in the nonstoichiometric compound H_xWO_3, called tungsten bronze. The hydrogen-doped (dark blue) and undoped (colorless) states in solid WO_3 thin films can be reversibly controlled by applying electric field (electrochromic effect). Here, we measured the zero field (ZF) muon spin relaxation in H_xWO_3 at RIKEN-RAL, to extract information on the basic proton diffusion process from the dynamical properties of muon in H_xWO_3, which is important for the development of the electrochromic device based on the WO_3 thin film[6].

We used two powder samples of commercial undoped WO_3 and doped H_xWO_3 synthesized by the mechanochemical method[7], in which the WO_3 powder was milled with zirconia balls and xylene for 24 h. The hydrogen concentration was estimated to be a few tens of %. To avoid an undesirable antiferromagnetism due to oxygen adsorption, the samples were degassed at 150 °C in vacuum and subsequently sealed within 30-μm-thick silver foils by glue in He atmosphere.

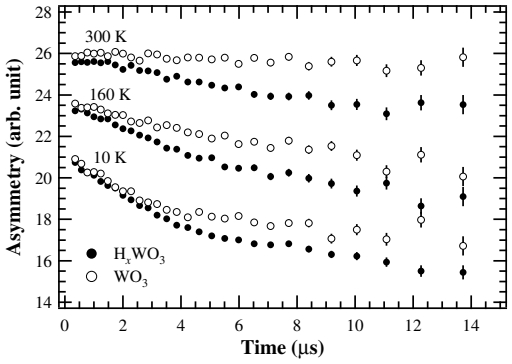

Fig. 2. ZF μSR spectra in H_xWO_3 and WO_3.

Typical spectra are shown in Fig. 2. A relatively fast relaxation was observed in the doped sample compared with the undoped sample owing to the nuclear dipolar field from protons. Data analysis is now in progress to extract the dynamical properties of muons in H_xWO_3 and further experimental studies at temperatures higher than room temperature are being planned.

*1 Department of Physics, Osaka University
*2 Institute of Material Structure Science, KEK
*3 Department of Materials Science, Tottori University
*4 Department of Physics, Kagoshima University

References
1) Ç. Kılıç et al.: Appl. Phys. Lett. **81**, 73 (2002).
2) K. Shimomura et al.: Phys. Rev. Lett **89**, 255505 (2002).
3) S. F. J. Cox et al.: Proc. Int. Conf. Phys. Semiconductors (2005) p. 193.
4) M. Mihara et al.: KEK-MSL Report (2005) p. 33.
5) T. Hirose et al.: Phys. Status Solidi (a) **203**, 608 (2006).
6) H. Yoshimura and N. Koshida: Jpn. J. Appl. Phys. **45**, 3479 (2006).
7) S. Takai et al.: Electrochemistry **72**, 876 (2004).

3. Radiochemistry and Nuclear Chemistry

Development of capillary electrophoresis apparatus for chemistry of short–lived radioactive elements

T. Kuribayashi,*[1] T. Yoshimura,*[1] K. Ooe,*[1] N. Takahashi,*[1] H. Haba, S. Enomoto, and A. Shinohara*[1]

The chemistry of heavy actinides has recently received attention and has been performed to determine the periodicity of elements. Studies of the properties of these elements have been limited owing to low production rates and short lifetimes of nuclides. For solution chemistry of these elements, two methods, ion exchange and solvent extraction have been applied.[1)] From the significance of heavy actinide chemistry, it is important to establish a new methodology to investigate the chemical properties of such actinides. Capillary zone electrophoresis is highly promising for the chemistry of the heavy actinides since this method rapidly separates chemical species with high resolution.[2)] In this study we applied capillary electrophoresis as a rapid chemical apparatus for short-lived radioactive elements.

The mobility of each of the lanthanides (Ce, Pm, Sm, Eu, Gd, Dy, Yb, and Lu) was determined using lanthanide multitracers, which were produced in ^{197}Au(^{14}N,X) reactions at the E3b course of the RIKEN Ring Cyclotron. A fused silica capillary 30 cm in length and 100 μm in inner diameter was used. The applied voltage was +15.0 kV. The electrolyte used was an aqueous solution of 12 mM α-HIB (2-hydroxy-iso-butyric acid) and pH was adjusted to 3.11 with 0.35 M acetate and 10 mM creatinine. Each fraction eluted from the capillary was collected into plastic tubes and the radioactivity of each fraction was measured using a Ge semiconductor detector. No significant Cl^- dependence of mobility of each lanthanide was observed for 10^{-1} M KCl; thus, it is found that KCl aerosols delivering a short-lived nuclide in a gas-jet transport system may be unaffected by the mobility of the lanthanide. Figure 1 shows

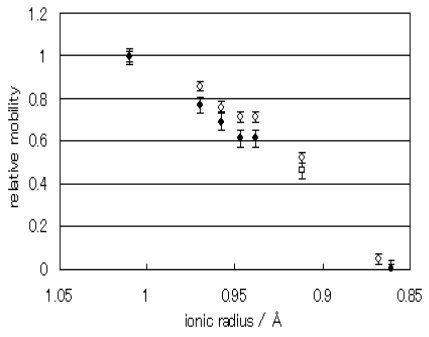

Fig. 1. Plots of relative mobility against ionic radius of lanthanide ions. (open circle: offline experiment using lanthanide multitracers, filled circle: online experiment using lanthanide multitracers, open square: ^{152}Dy).

*[1] Department of Chemistry, Graduate School of Science, Osaka University

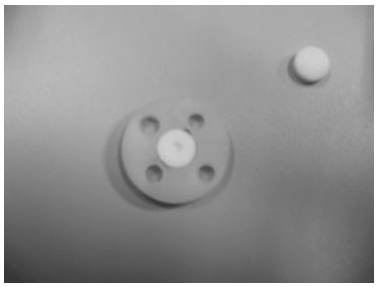

Fig. 2. Holder for collection of short-lived nuclides using a gas-jet transport system.

that the relative mobility of lanthanide ions when that of Ce was normalized as 1 and Lu as 0. Mobility decreased in the order of the atomic number. Since the equilibrium constant with α-HIB becomes larger with decreasing ionic radius of the metal ion, the amount of the effective charge of the metal complex with α-HIB decreases with increasing atomic number.[3)]

For the experiment using the KCl gas-jet transport system installed at an accelerator,[1)] a holder to collect the short-lived radioactive element was designed (Figure 2). This holder has a small dip with 1.5 mm in radius and 3 mm in depth. The short-lived nuclide collected in this holder is dissolved in a small amount of water (2 μL) to give a comparative concentrated solution and the nuclide is efficiently introduced into the capillary. The experiment was performed using the AVF cyclotron at the research center of nuclear physics (RCNP) in Osaka University. In this experiment, a ^{152}Dy ($t_{1/2}$ = 2.37 h) tracer was produced in the reaction of ^{140}Ce(^{16}O,4n)^{152}Dy. ^{152}Dy produced by an irradiation for 10 min was collected on the holder and was dissolved into a solution containing the lanthanide multitracers at pH 3. The experimental condition to obtain the mobility of ^{152}Dy was the same as that to determine mobility described above (offline experiment) except for an applied voltage of +20.0 kV. The mobility of ^{152}Dy is in agreement with those of the offline experiment. From these results it is found that this methodology is valid for the chemistry of short-lived nuclides. In the future we will perform the chemistry of heavy actinides using this system.

References

1) M. Schädel: Angew. Chem. Int. Ed. **45**, 368 (2006).
2) Y. Kitamoto et al.: RIKEN Accel. Prog. Rep. **39**, 112 (2006).
3) T. Hirokawa et al: J. Chromatogr. **312**, 11 (1984).

Preparation of rotating ^{238}U target of GARIS

H. Kikunaga,[*1] H. Haba, D. Kaji, and K. Morita

We plan to the study chemical properties of superheavy elements (SHEs) with atomic numbers $Z \geq 104$ by using the gas-jet transport system coupled to the gas-filled recoil ion separator GARIS at the RIKEN Linear Accelerator Facility (RILAC).[1] SHE nuclides with long half-lives for chemical experiments are commonly produced by hot-fusion reactions on actinide targets such as ^{238}U, ^{248}Cm, and ^{249}Bk. Thus, the actinide targets in the oxide form, which are stable for high-intensity heavy-ion bombardments for long beam times, are prepared by electrodeposition from organic solutions (molecular-plating method). In this paper we report on a procedure of preparing a large and uniform U_3O_8 target by electrodeposition for irradiations using a rotating target system of GARIS.

The details of the electrodeposition cell used in this work are described in Ref. [2]. A Ti backing foil of 3 μm thickness placed on a water-cooled Ti block was used as the cathode, whereas a Pt plate of 0.1 mm thickness on another Ti block was used as the anode. A Teflon spacer perforated in the shape of a banana and of 10 mm thickness was sandwiched by the electrodes sealed using silicon rubbers perforated in the same banana shape and of 1 mm thickness. The active target area was 7.85 cm^2.

Prior to electrodeposition, a uranium material in the chemical form of $UO_2(NO_3)_2 \cdot 6H_2O$ was purified by an ion exchange method in hydrochloric acid. 0.01 M HNO_3 (5.5 μL) containing 2.6 mg of ^{238}U was mixed with 12 mL of 2-propanol, and the mixture was filled into the electrodeposition cell. Electrodeposition was carried out by applying a voltage of 800 V at an increasing current density from 1 to 6 mA cm^{-2} for 20 min. During the electrodeposition, the Ti blocks were continuously water-cooled at 10–15 °C. After the electrodeposition, the target was sintered in an electric furnace to obtain uranium oxide. The temperature in the furnace was raised up to 600 °C in 20 min, and thereafter the power was turned off. The target thickness of 312 ± 15 μg cm^{-2} averaged for the 16 targets was determined by α spectrometry of ^{238}U. The average deposition yield was 95±4%. Figure 1 shows a photograph of the ^{238}U target mounted on the Al frame. The uniformity of the target was investigated using an imaging plate Fujifilm BAS-MS2040. The imaging plate was exposed by the targets for 9 days. The areal weight distribution of the target is shown in Fig. 2 for each 1.0 mm × 1.0 mm pixel. It was found that the standard deviation of thickness is only 3% except for the 2 mm outer edge of the target.

The 16 ^{238}U targets were arranged on the rotating wheel of 30 cm diameter and were irradiated with the 113.8-MeV ^{22}Ne beam with beam currents up to 4.3 particle μA to produce ^{255}No *via* the ^{238}U(^{22}Ne,5*n*)^{255}No reaction.[3] A total beam dose of 2.5×10^{18} was accumulated. The target wheel was rotated during the irradiation at 3000 rpm and cooled with helium gas filled in GARIS at a pressure of 38 Pa. After the irradiation, no damage or losses of the target material were observed by α spectrometry. In the near future, we will develop a rotating Cm_2O_3 target to produce SHE nuclides for chemical experiments such as ^{261}Rf, ^{265}Sg, and ^{269}Hs.

[*1] Present address: Graduate School of Science, Osaka University

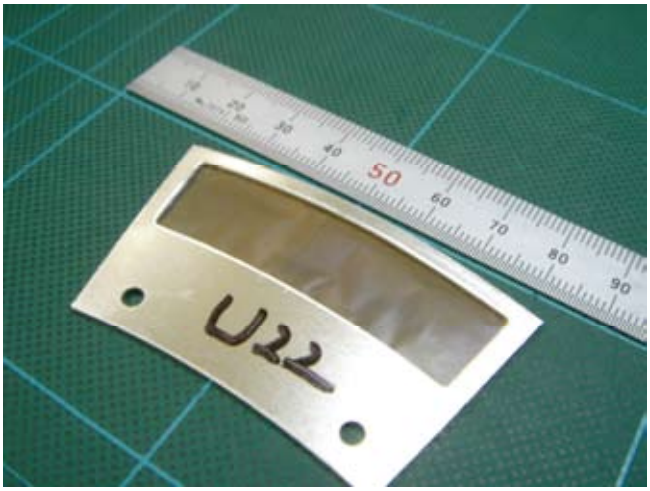

Fig. 1 Photograph of ^{238}U target.

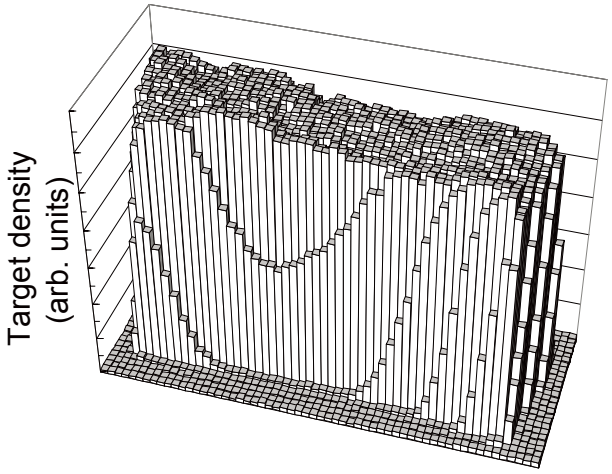

Fig. 2 Areal weight distribution of ^{238}U target for each 1.0 mm × 1.0 mm pixel measured with imaging plate Fujifilm BAS-MS2040.

References

1) H. Haba et al.: J. Nucl. Radiochem. Sci. 8, 55 (2007).
2) H. Haba et al.: RIKEN Accel. Prog. Rep. 39, 109 (2006).
3) H. Haba et al.: a separate paper of this report.

Anion-exchange behavior of Nb, Ta, and Pa as homologues of Db in HF/HNO_3 solutions†

Y. Kasamatsu,*1 A. Toyoshima,*1 H. Toume,*1 K. Tsukada,*1 H. Haba, and Y. Nagame*1

To find suitable conditions for the experimental study of the anion-exchange behavior of element 105, dubnium (Db), we have investigated the anion-exchange behavior of the group 5 elements Nb and Ta and their pseudo homologue Pa in HF/HNO_3 media by a batch method using radiotracers of ^{95}Nb, ^{179}Ta, and ^{233}Pa.

Niobium-95 ($T_{1/2}$ = 34.97 d) and ^{179}Ta ($T_{1/2}$ = 665 d) were produced by proton bombardments of Zr and Hf metallic foil targets with natural isotopic abundance, respectively, using the RIKEN K70 AVF cyclotron. The incident energy of the proton beam was 14 MeV with a beam current of approximately 5 μA. The radioactive tracers were prepared by an anion-exchange separation from the target materials and other by-products. Protactinium-233 ($T_{1/2}$ = 27.0 d) was chemically separated from its α-decay parent ^{237}Np ($T_{1/2}$ = 2.144×10^6 y) by the anion-exchange method.

Before the measurements of the distribution coefficients (K_d) in the anion-exchange reaction, the adsorption of the elements on the surfaces of experimental tools made of perfluoroalkoxy (PFA) and polypropylene (PP) was investigated in HF and HF/HNO_3 solutions with $[F^-] > 10^{-6}$ M. The time dependence of the adsorption of the radiotracers on the PFA and PP tubes was observed. We found that the adsorption of the group 5 elements on both PP and PFA surfaces is negligible within 1 week in the solutions.

The K_d values on the anion-exchange resin were subsequently investigated in HF/0.1 M HNO_3 solutions. In a PP test tube, 8–200 mg of the dried resin and 3 mL of HF/HNO_3 solution containing 30–50 μL of the tracer solution were mixed. Then, the tube was shaken for a certain time (shaking time). After centrifugation, 1 mL of the solution was pipetted into a small PP container and subjected to γ-ray spectrometry using a Ge detector. The same treatment was conducted without the resin to determine the reference radioactivity of the solution. The radioactivity of each isotope on the resin was determined by subtracting the radioactivity in the supernatant solution from the reference radioactivity of the solution. The K_d values were evaluated from the ratio of the radioactivity in the resin to that in the solution as

$$K_d = \frac{A_r V_s}{A_s W_r}, \quad (1)$$

where A_r and A_s are the radioactivities (Bq) in the resin and solution, respectively, V_s is the volume of the solution (mL), and W_r is the mass of the dry resin (g). We investigated the dependence of the K_d value on the shaking time in HF/HNO_3 solutions with HF concentrations of 10^{-4}, 10^{-3}, 10^{-2}, 1, and 10 M to obtain the K_d values in equilibrium. From the results, the shaking time in the anion-exchange experiments was determined to be 15 min for the solutions with HF concentration $[F^-] \geq 10^{-4}$ M, while it is at least 5 h for solutions with 10^{-5} M $\leq [F^-] < 10^{-4}$ M, and 1 day for those with $[F^-] < 10^{-5}$ M. Under such experimental conditions, the K_d values of Nb, Ta, and Pa were determined in various concentrations of HF/0.1 M HNO_3 (1×10^{-6} M $\leq [F^-] < 2 \times 10^{-2}$ M). Variations of the K_d values of Nb, Ta, and Pa as a function of $[F^-]$ are shown in Fig. 1. The K_d values of the elements increase with increasing $[F^-]$, which reflects the successive formation of anionic fluoro complexes. The decrease in the K_d values in the concentrated $[F^-]$ region is due to the displacement of the anionic fluoro complexes of the group 5 elements on the resin through the HF_2^- anions.[1)]

As shown in Fig. 1, clear differences in the anion-exchange behavior among Nb, Ta, and Pa were observed under the studied conditions, suggesting that each element forms different anionic fluoro complexes.[1,2)] From the present results, we propose that a chemical experiment on Db in HF/HNO_3 media would be appropriate for the study of the fluoride complexation of Db.

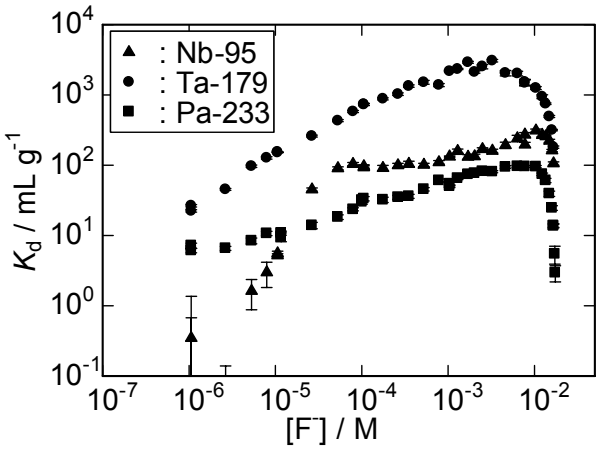

Fig. 1. Variations of the K_d values of Nb, Ta, and Pa on the anion-exchange resin as a function of the fluoride ion concentration.

References

1) R. Caletka and V. Krivan: J. Radioanal. Nucl. Chem. **142**, 359 (1990).
2) O. L. Keller and A. C. Strode: Inorg. Chem. **5**, 367 (1966).

† Condensed from the article in J. Nucl. Radiochem. Sci. **8**, 69 (2007).

*1 Advanced Science Research Center, Japan Atomic Energy Agency.

4. Radiation Chemistry and Biology

Ion irradiation in liquid of μm^3 region for cell surgery†

Y. Iwai, T. Ikeda, K. Maeshima, T. M. Kojima, T. Kobayashi,
T. Nebiki,*1 G. P. Pokhil,*2 T. Narusawa,*1 N. Imamoto, and Y. Yamazaki

A typical animal cell is about 50 μm in diameter and composed of complex intracellular organelles and assembled macromolecules, which range in size from more than 1 μm (e.g., chromosomes, mitochondria, and nuclear compartments) down to 100 nm (e.g., centriole, and nuclear pore complex) or less. Several research groups have been intensively working on the preparation of ∼MeV microbeams for biological applications. In a conventional scheme, a well-focused energetic ion beam is extracted in air via a vacuum isolation window, then injected into a biological cell in water.[1,2] Another straightforward scheme involves passing energetic ions through a micron-sized aperture with or without a thin window at the end.[3–5] The drawbacks of these schemes are as follows: (i) a relatively large cylindrical volume is damaged along the beam trajectory in addition to the targeted point; (ii) serious energy and angular stragglings are induced during passage through the vacuum isolation window and air, which deteriorates beam quality, and as a result determines the lower limit of beam size at the target, and (iii) real-time control/monitoring of the bombarding point is not easy even when a micron-sized beam is prepared. To overcome such technical but serious problems, we have developed a scheme using a tapered glass capillary with a thin window at its outlet.[6,7] This scheme can realize pinpoint energy deposition and a three-dimensional selection of the bombarding point by observing the outlet through a microscope with micron precision or better in an arbitrary position of a living cell or in any liquid object.

Figure 1(a) shows an illustration of the microbeam preparation setup including an X-Y stage, which is aligned by the upstream micrometers with respect to the beam line. The beam is first trimmed by a square aperture of 1×1 mm^2 formed by four rectangular aluminum plates, then injected into a tapered glass capillary on a capillary holder and passed through a thin window at the outlet of the capillary. This end window enables the whole beam line to be kept under vacuum and, at the same time, a microbeam can be injected into a liquid target in a well-defined position in front of the capillary. The tapered glass capillary is ∼50 mm long (Fig. 1(b)) with inlet and outlet diameters of 0.8 mm and several micrometers, respectively.[6,7] The downstream micrometers are used to align the capillary to the beam axis in steps of 0.5 mrad. The capillary outlet is placed in the focus of an optical microscope, which is installed on a three-dimensional stage. Figures 1(c) and 1(d) show an optical microscope image and a scanning ion microscope (SIM) image near the capillary outlet, respectively. As expected, this window was vacuum-tight and the outlet could be safely dipped in liquid.

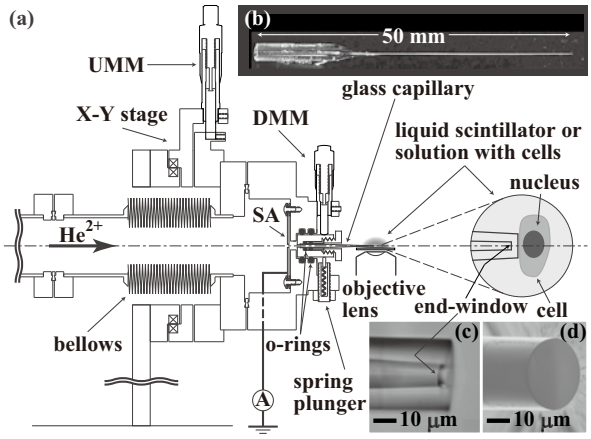

Fig. 1. (a) Schematic drawing of microbeam preparation setup. Upstream micrometer (UMM), downstream micrometer (DMM), and square aperture (SA). (b) Photograph of tapered glass capillary, (c) microgram of capillary outlet, and (d) diagonal image of capillary outlet by SIM.

Ion beams of 3 and 4 MeV He^{2+} from an electrostatic tandem accelerator at Kochi University of Technology were charge-state-selected by an analyzing magnet, and then transported to the microbeam preparation setup described above. Figure 2(a) shows a microscopy image observed using a charge-coupled device (CCD) camera when a 3 MeV He^{2+} beam was injected into a droplet of a liquid scintillator (BICRON BC-501A) through a tapered glass capillary with a thin window. A diffuse white area is clearly visible downstream of the window showing ions that were injected into a volume of about μm^3 in the liquid scintillator through the thin window. The open circles and crosses in Fig. 2(a) show the observed scintillation intensity projected along and perpendicularly to the beam axis, respectively. Figure 2(b) shows the simulated energy deposition in the window and scintillator by the computational code "stopping and range of ions in matter," SRIM-2006.[8] The dashed line in Fig. 2(a) shows the scintillation intensity distribution evaluated taking into account the conversion efficiency from the energy deposition to the scintillation.

† Condensed from the article in Appl. Phys. Lett. **92**, 023509 (2008)

*1 Kochi University of Technology
*2 Skobeltsyn Institute of Nuclear Physics, Moscow State University, Russia

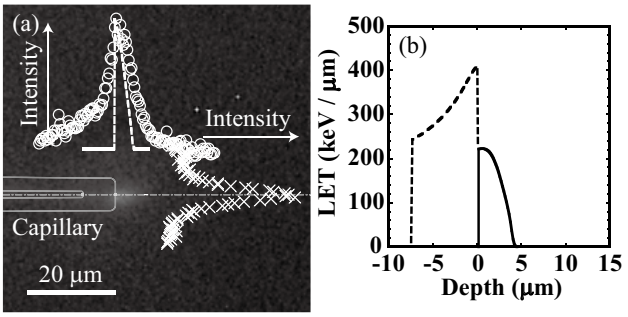

Fig. 2. (a) Scintillation due to 3 MeV He^{2+} beam entering tapered glass capillary with end-window thickness of 7.5 μm and outlet diameter of 1.6 μm. The thin solid curves show an outline of the capillary. The open circles and crosses show the projected scintillation intensity along and perpendicular to the beam axis, respectively. The dashed line shows the scintillation intensity distribution evaluated taking into account the conversion efficiency from the energy deposition to the scintillation. (b) Linear energy transfer (LET) calculated by SRIM-2006[8] with 3 MeV He^{2+} beam entering capillary with end-window thickness of 7.5 μm. The dashed and solid lines show the LET in the end window and liquid scintillator, respectively.

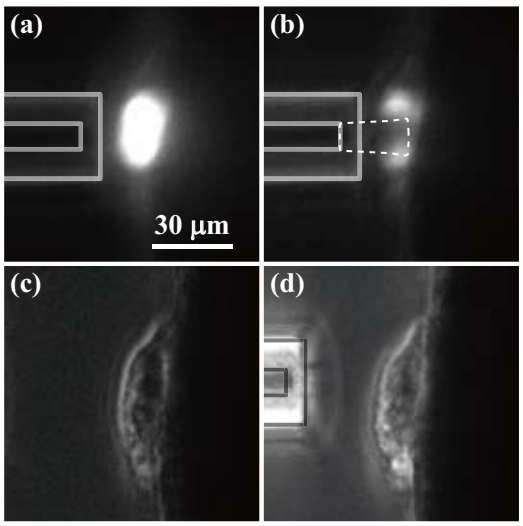

Fig. 3. Fluorescence images of HeLa cell nucleus labeled with histone H2B-GFP.[9] (a) Before and (b) after irradiation with 4 MeV He^{2+} beam entering tapered glass capillary with end-window thickness of 7.3 μm and outlet diameter of 9.6 μm. (c) and (d) are the phase contrast images of (a) and (b), respectively. The solid and dashed lines show an outline of the capillary and a calculation of the energy deposition region by SRIM-2006.[8] In (c) and (d), the capillary is far from the cell to prevent it sticking to the cell.

The focusing factor ξ, which is the ratio of the beam density at the outlet to that at the inlet, was measured as a function of the outlet diameter $D_{\rm out}$ in the range of 1.5-9.6 μm. The transmitted ion current was measured with a Faraday cup covering the capillary outlet. On the other hand, the incident current entering the capillary was evaluated by replacing the tapered capillary with a Faraday cup having the same inlet diameter as the capillary. It was found that ξ increases monotonically similarly to $\xi \propto D_{\rm out}^{-1.3}$, and reaches, as high as 1000, which is another important aspect of the tapered glass capillary compared with a conventional scheme employing a simple aperture.

As the second demonstration, a real biological cell, a HeLa cell whose nucleus was labeled with a fusion protein of histone H2B and green fluorescent protein[9] (GFP), was bombarded by a microbeam. The microbeam was prepared using 4 MeV He^{2+} incident to a tapered glass capillary with an end window of 7.3 μm thickness and 9.6 μm outlet diameter (see Figs. 1(c) and 1(d)). Figures 3(a) and 3(b) show the fluorescence images of the nucleus before and after irradiation of a transmitted current of $\sim$100 pA for $\sim$7 s, respectively, which clearly show that the bombarded volume was optically inactivated without affecting global cell morphology (see phase contrast images in Figs. 3(c) and 3(d) before and after bombardment, respectively).

In summary, we have demonstrated that a tapered glass capillary with a thin end window can deposit energy in a well-selected volume of a microscopic region in a cell. A tool enabling "surgery" in an arbitrary region of a cell is now available, providing a technique for studying various functions of intracellular structures independently. According to the simulations performed by SRIM-2006, the bombardment region in the cell can further be reduced, e.g., down to 100 nm or so when a 20 keV He^{2+} beam is injected into a tapered capillary with an end-window thickness of 100 nm and an outlet diameter of 100 nm.[10] The combination of a low-energy ion injector and an optical microscope would lead to the development of a desktop cell surgery system.

References

1) G. Dollinger et al.: Nucl. Instrum. Methods Phys. Res. B **231**, 195 (2005).
2) M. Heiß et al.: Radiat. Res. **165**, 231 (2006).
3) G. Randers-Pehrson et al.: Radiat. Res. **156**, 210 (2001).
4) M. Folkard et al.: Nucl. Instrum. Methods Phys. Res. B **210**, 302 (2003).
5) Y. Kobayashi et al.: Nucl. Instrum. Methods Phys. Res. B **210**, 308 (2003).
6) T. Nebiki et al.: J. Vac. Sci. Technol. A **21**, 1671 (2003).
7) T. Ikeda et al.: Appl. Phys. Lett. **89**, 163502 (2006).
8) J. F. Ziegler, computer code SRIM-2006.01 (http://www.srim.org/).
9) H. Kimura et al.: J. Cell Biol. **153**, 1341 (2001).
10) T. Kaito, U.S. Patent No.6740368 (25 May 2004).

DNA damage response after heavy-ion irradiation in mammalian quiescent cells

M. Izumi and T. Tsukada

Since the majority of the cells in the body exist in a quiescent state, it is in quiescent cells where most DNA damage occurs. However, it is uncertain whether DNA damage in quiescent cells is repaired or converted into mutations during quiescence or how proliferation is involved in both pathways when proliferation is stimulated.[1)]

In radiation therapy, a beam of X-rays or accelerated particles is used to kill cancer cells or slow their growth rate. Radiation therapy often causes side effects, because several important tissues that exist in the path of the radiation beam or the surrounding normal cells may be affected. In addition, recent evidence suggests that the accumulation of DNA damage is important for the aging of stem cells and progenitor cells.[2)] Therefore, it is important to understand how quiescent cells respond to DNA damage caused by ionizing radiation.

The histone H2AX protein is a variant member of the H2A family of histones and is distinguished from other H2A histones by a unique carboxy-terminal sequence. This sequence is highly conserved among species and is rapidly phosphorylated in response to DNA double-strand breaks within a minute after exposure to ionizing radiation.[3)] Phosphorylated histone H2AX directly interacts with many components involved in DNA repair and checkpoint pathways, including Mre11/Rad50/Nbs1 complex, Brca1, NFBD1, and 53BP1, and stimulates the accumulation of these proteins around DNA double-strand breaks. Furthermore, phosphorylated histone H2AX recruits chromatin remodeling factors and cohesin complex, which facilitate the homologous recombination repair.

To assess the risk of heavy ion, we examined the phosphorylation of histone H2AX after heavy-ion irradiation in mammalian cells. Mouse NIH 3T3 cells were synchronized in the quiescent state by serum starvation as previously descibed[4)] and irradiated with 3 or 10 Gy of carbon ions. Then the cell extracts were prepared in the presence of phosphatase inhibitors, and phosphorylated histone H2AX was detected by immunoblotting (Fig. 1).

In quiescent cells, the amount of phosphorylated histone H2AX transiently increased after irradiation and decreased with the half-life of less than 2 h in NIH 3T3 cells. On the other hand, the amount of phosphorylated histone H2AX decreased more slowly in cycling cells than in quiescent cells, although the initial amounts of phosphorylated histone H2AX were almost the same. The same results were obtained when the cells were irradiated with 10 Gy of argon ions.

Because the accumulation of phosphorylated histone H2AX is a hallmark of checkpoint response, it is assumed that checkpoint pathway of DNA damage in quiescent cells does not work efficiently. Now we are trying to directly quantify the amount of DNA damage and clarify the time course of actual DNA repair in quiescent cells using the Comet assay.

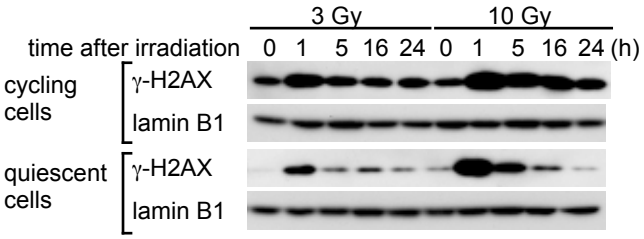

Fig. 1 Western blot analysis of phosphorylated H2AX (γ-H2AX) after heavy-ion irradiation. NIH 3T3 cells were synchronized in the quiescent state by serum starvation for 2 days. Either asynchronously growing cells or synchronized cells were irradiated with 10 Gy of carbon ions, and whole cell extracts were prepared at indicated time points and subjected to immunoblotting. As a loading control, lamin B1 was detected.

References

1) J. H. Bielas and J. A. Heddle: DNA Repair 3, 711 (2004).
2) D. J. Rossi et al.: Cell Cycle 19, 2371 (2007).
3) C. Thiriet and J. J. Hayes: Mol. Cell 18, 617 (2005).
4) H. Miyazawa et al.: J. Biol. Chem. 268, 8111 (1993).

Cell-killing effect of low dose of high-LET heavy ions

M. Tomita,[*1] T. Tsukada, and M. Izumi

Ionizing radiation is well known to induce DNA double-strand breaks (DSBs), which are one form of lethal DNA damage. Accelerated heavy ions with high linear energy transfer (LET) can induce complex clustered DNA damage involving two or more DSBs. The complexity of clustered DNA damage shows strong LET dependence.[1] The higher cell-killing effect of high-LET radiation has practical implications in applications to radiation cancer therapy and in assessing risks in a space environment. Radiation-induced bystander responses are defined as responses in cells that have not been directly targeted by radiation but are in the neighborhood of cells that have been directly exposed.[2] Radiation-induced bystander responses came into the spotlight after the report of Nagasawa and Little (1992),[3] who demonstrated that after exposure to a low dose of α-particles, a larger proportion of cells showed biological damage than that estimated to have been hit by the α-particles. In a space environment, astronauts are exposed to low fluencies of high-LET radiation. In addition, normal cells surrounding a tumor also undergo exposure in heavy-ion cancer therapy. Thus, bystander responses induced by a low dose of high-LET radiation are an important problem in radiation biology. In our study we aim to clarify the molecular mechanisms and biological implications of bystander responses induced by low doses of high-LET radiation. In this study, we show that the cell-killing effect of high-LET iron (Fe) ions is significantly higher than that of low-LET X-rays in the low-dose region.

Figure 1A shows the clonogenic surviving fraction of normal human lung embryonic fibroblast WI-38 cells irradiated with 250 kV X-rays or 90 MeV/u Fe ions at 1000 keV/μm. WI-38 cells were plated on a 25 cm^2 cell culture flask for one week before irradiation to form confluent monolayers. The surviving fraction was determined by a colony formation assay. The radiosensitivity of WI-38 cells to Fe ions was higher than that to X-rays (Fig. 1A). The doses resulting in 10% cell survival (D_{10}), calculated from the cell survival curves, were 4.02 Gy and 3.36 Gy for X-rays and Fe ions, respectively. The RBE relative to X-rays was 1.19. Figure 1B indicates the surviving fractions at doses of less that 1.0 Gy. The survival curve for Fe ions was also calculated for doses under 1.0 Gy. At lower doses, the surviving fraction for Fe ions was significantly lower than that for X-rays. The values of D_{95} were 0.128 and 0.040 for X-rays and Fe ions, respectively. The RBE was 3.2. Our present results suggest that a low dose of high-LET radiation can induce cell death efficiently in comparison with low-LET radiation.

The average number of ion tracks per nucleus was calculated as 0.72 in the nuclei of human TK6 lymphoblastoid cells irradiated with 3 Gy of Fe ions.[4] Thus, nonirradiated cells exist in the same population at doses less than 3 Gy. To clarify whether the high cell-killing effect of a low dose of high-LET radiation is caused by the induction of bystander responses, we are currently attempting to detect DSBs induced in nonirradiated cells cultured on CR39.

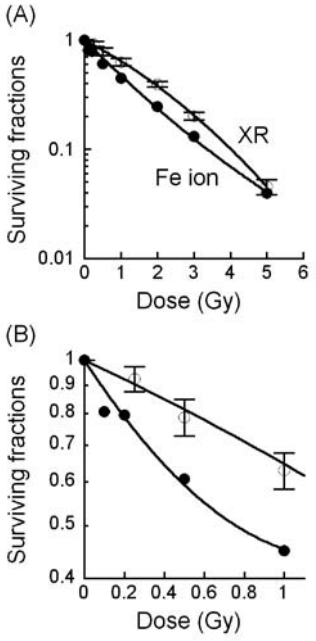

Fig. 1. Cell survival curves of normal human fibroblast WI-38 cells. Confluent monolayers of normal human fibroblast WI-38 cells were irradiated with 250 kV X-rays and 90 MeV/u Fe ions (1000 keV/μm). Cells were harvested and plated 24 h after irradiation. Surviving fractions (SFs) were normalized to those for nonirradiated controls. In A, all SFs obtained in this study were fitted by the linear-quadratic (LQ) model. In B, SFs at doses under 1.0 Gy were fitted by the LQ model. Error bars of the SFs of X-irradiated cells represent the standard errors of the means (SEMs), which were obtained from three independent experiments.

References
1) D. T. Goodhead: J. Radiat. Res. **40**, Suppl. 1 (1998).
2) K. M. Prise et al.: Radiat. Prot. Dosimetry **99**, 223 (2002).
3) H. Nagasawa and J. B. Little: Cancer Res. **52**, 6394 (1992).
4) S. Goto et al.: Radiat. Res. **158**, 678 (2002).

*1 Central Research Institute of Electric Power Industry

Induction of Bystander Effect by Carbon-Ion Irradiation of Human Cells

F. Yatagai, H. Matsumoto[*1], M. Honma[*2], and T. Abe

It is important to elucidate the effects of ionizing radiation (IR) induced not in the cells directly hit by IR but in their neighboring cells, which is generally known as the "bystander effect". Ion-bean irradiation is considered to be a powerful tool for experiments on the bystander effect, because non-hit cells can be easily distinguished from hit cells.

Unirradiated cells of a human lymphoblastoid, TK6, were incubated with a conditioned medium (CM), which was obtained by the centrifugation of the cell suspension after exposure to a 2 Gy of carbon-ion beam135 MeV/u (Fig. 1). As a control, a normal medium (NM) was prepared from an unirradiated cell suspension (Fig. 1).

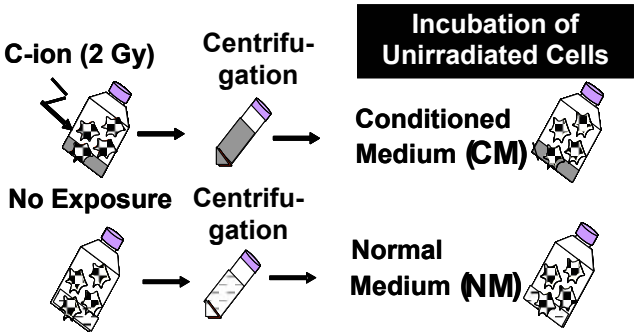

Fig. 1 Schematic illustration of the cell treatments by radiation exposure, centrifugation, and incubation

The spontaneous frequency of thymidine kinase deficient (TK^-) mutations observed in the cells cultured with CM was lower than that obtained with NM. As shown in Table1, the reduction rate was only about 20% of the original level of total mutations, but this rate becomes as high as about 60% if we restrict our consideration to EMs, which were induced relatively early. However, this type of reduction of TK^- spontaneous mutation frequency (MF) was not observed using a tumor suppressor (p53) gene deficient cell line, NH32 (a derivative of TK6).

a) TK6 (p53+)

Medium	EM (X10^{-6})	LM (X10^{-6})	Total (X10^{-6})
NM	1.04 ± 0.30	1.20 ± 0.11	2.27 ± 0.33
CM	0.38 ± 0.12	1.39 ± 0.25	1.77 ± 0.32
P-value (T-test)	0.24	0.58	0.51

EM (Early Mutant)
LM (Late Mutant)

b) NH32 (p53-)

Medium	EM (X10^{-6})	LM (X10^{-6})	Total (X10^{-6})
NM	13.8 ± 10.0	12.9 ± 1.6	26.8 ± 11.8
CM	12.1± 4.8	10.9 ± 3.2	23.0 ± 8.1
P-value (T-test)	0.80	0.43	0.49

EM (Early Mutant)
LM (Late Mutant)

Table1 Spontaneous TK mutation frequencies (MFs) of TK6 and NH32 cells obtained with NM and CM

[*1] High Energy Med. Res., Fukui Univ.
[*2] National Institute of Health Sciences

The mutational classes of the TK^- mutants isolated from TK6 cells were determined by loss of heterozygosity (LOH) analysis[1] (Fig. 2). The relative proportion of non-LOH mutations recovered in the CM collection was lower than that for NM, accounting for the reduced TK^- MF caused by using CM.

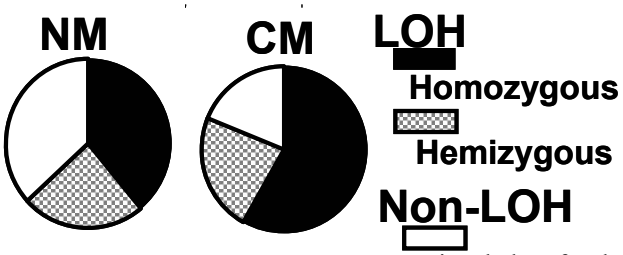

Fig. 2 Relative proportion of each mutational class for the TK^- spontaneous mutants isolated from the TK6 cell, 54 and 48 mutant clones for NM and CM, respectively.

The further characterization of LOH mutants by chromosome mapping[1] did not show any significant differences in the extent of LOHs (the deleted or replaced region of chromosome 17) between the two mutant collections, NM and CM. We also examined whether the site-specific DNA double-strand break (DSB) in the *TK* gene introduced by the expression of I-SceI restriction enzyme can be repaired more efficiently by using CM. Both repair pathways, non homologous endjoining and homologous recombination, were barely affected by the incubation medium. These results support the above possibility that the cells cultured in CM acquire the ability to reduce the occurrences of non-LOH mutations, mostly point mutations, compared with the culture in NM.

Using the same LOH analysis system, the mutagenic response of TK6 cells exposed to X-rays with a challenge dose, 2 Gy, was found to be reduced in cells previously exposed to X-rays with a priming low-dose, 5 cGy.[2] The reduced fraction mainly consisted of non-LOH mutations, as observed here. Considering the consequence of this typical radioadaptive response, the phenomenon observed here might be regarded as an example of a bystander-adaptive response, which can be defined as a response that reduces the mutagenic effects of a stress in the bystander (non-hit) cells. We are now elucidating the molecular mechanisms underlining this interesting phenomenon, for example, an essential requirement of the p53 function and a possible involvement of NO radicals.

References

1) F. Yatagai et al.: Mutat. Res. **560**, 133-145 (2004).
2) F. Yatagai et al.: Mutat. Res. **638**, 48-55 (2008).

Antiarrhythmic effect of single heavy-ion irradiation on diseased canine heart

K. Yoshioka*1, M. Amino*1, D. Fujibayashi*1, S. Tanaka*2, K. Naito*2, Y. Shinozaki*2, M. Sakai*3, S. Yamazaki*3, Y. Furusawa*4, K. Tsukada*5, T. Tsukada*6, M. Izumi*6, T. Kambara*6, and T. Tanabe*1.

Modalities currently available for the treatment and prevention of life-threatening ventricular tachyarrhythmias (VT/VF) are antiarrhythmic drugs, catheter ablation, and the implantable cardioverter/defibrillator (ICD). The prevention of sudden death of postinfarction patients consists of revascularization, optimal pharmacological therapy (including beta-blockers, ACE inhibitors, and statins), and the placement of an ICD. Antiarrhythmic drugs, including amiodarone (SCD-HeFT), have failed to decrease mortality in postinfarction patients. The usefulness of these therapeutic options is limited by either low efficiency, intolerable side effects, or the impairment of the quality of life (QOL) of the recipient. Fundamentally innovative antiarrhythmic strategies are, therefore, a matter of great concern to cardiologists. There is a need for novel therapies aimed at alleviating myocardial changes caused by the ischemic process and remodeling, and decreasing the propensity of this group of patients to ventricular arrhythmias.

Radiation therapy employed for the treatment of diseased hearts is still limited. Catheter-based intracoronary β-radiation has been shown to be effective and safe for the prevention of in-stent restenosis [1]. By using a similar catheter-based radiation technique, Guerra et al. created linear lesions at the cavotricuspid isthmus region in dogs [2]. They concluded that β–radiation holds promise as an alternative energy source for ablation therapy for atrial flutter and fibrillation. To our knowledge, the present study is the first report showing the potential usefulness of targeted external heavy-ion radiation (THIR) in the treatment and prevention of ventricular arrhythmias. An interesting case report already exists regarding the use of radiation therapy for primary tumors of the heart; Aoka et al [3] applied external heavy-ion (C-ion) radiation to a patient with a malignant cardiac angiosarcoma, and demonstrated a marked reduction of the tumor size, indicating the clinical feasibility and usefulness of THIR in the treatment of diseased hearts.

We have previously reported that the application of THIR (15Gy, HIMAC, Chiba, Japan) to rabbit hearts (anterior-lateral wall, 3×3 cm^2 area) reduced ventricular vulnerability in association with an improvement of the conduction velocity and spatial homogeneity of repolarization according to analysis by epicardial mapping [4-6].

However there is no information on the body surface parameter obtained by 12-leads electrocardiology (ECG) for THIR in large animals under the condition of a close chest experiment. Single heavy-ion irradiation ($^{12}C^{6r}$, 135MeV/nucleon, 15Gy) was applied to a 5×5 cm^2 limited area of the anterior-lateral wall of a diseased canine heart. Myocardial infarction (MI) was produced by the trans-catheter approach using a microsphere injection to the coronary artery in the left ventricle (LV) followed by 2 weeks of irradiation (MI+THIR, n=4). Electrophysiological changes in the LV were examined by analyzing the signal-averaged ECG before MI and after irradiation up to 60 days. Because it has been said that a late potential (LP) indicates the conduction delay and instability of the depolarization of LV, and which means the vulnerability to a fatal ventricular arrhythmia. LP parameters consisted of filtered QRS duration (f-QRS)(ms), root-mean-square 40ms (RMS40ms)(μV), and low amplitude (<40 μV) terminal signals (LAS40μV)(ms) were calculated using the time-domain method. An age matched canine without MI was used as a control (CON+THIR, n=4).

It was demonstrated that MI caused a significant worsening of LP; decreases in RMS40 (by 67%) and increases in LAS40 (by 56%) had occurred 7 days after the operation. However, THIR significantly improved the value of RMS40 (by 22%) and LAS40 (by 30%) 14 days after irradiation, and its effect lasted over 60 days. These effects of THIR were reversed in CON+THIR. The QRS-duration was not affected by THIR in both MI and the control. In summary, a single application of THIR to canine hearts causes a significant improvement of the conduction delay in MI. This long-lasting effect of modifying the depolarization abnormality is expected to enhance its potential therapeutic benefit as a novel strategy for treating life-threatening ventricular arrhythmias in structural heart diseases.

References

[1] J. J. Popma et al.: Circulation **106**, 1090 (2002).
[2] P. G. Guerra et al.: Circulation **110**, 911 (2004).
[3] Y. Aoka et al.: Lancet Oncol. **5**, 636 (2004).
[4] K. Yoshioka et al.: Circulation **101**, 1060 (2000).
[5] M. Amino et al.: Cardiovascular Res. **72,** 412 (2006).
[6] K. Yoshioka et al.: Circ. J. **70**, 1200 (2006).

*1 Department of Cardiology, Tokai University School of Medicine
*2 Department of Research Support Center, Tokai University
*3 Fukuda Denshi Company
*4 National Institute of Radiological Sciences
*5 Nippon Veterinary and Life Science University
*6 RIKEN

Carbon-ion beam sensitivity of DSB repair-deficient mutants of *Neurospora crassa*

L.Q. Ma*, S. Hatakeyama*, Y. Kazama, H. Ichida, Y. Hayashi, T. Abe and H. Inoue*

DNA double-strand breaks (DSBs) are induced by exposure to ionizing radiation and genotoxic chemicals. If they fail to repair expeditiously, DSBs can lead to deleterious chromosomal disorders, such as gross chromosomal rearrangement, the loss of chromosome arms and aneuploidy. Since DSBs should be repaired to maintain the genome integrity, two major repair pathways function in eukaryotic cells: homologous recombination repair (HR) and nonhomologous end-joining (NHEJ). Genetic evidence suggests that HR and NHEJ are independent and that these pathways work competitively to repair DSBs. Further analyses revealed that the MRX (Mre11-Rad50-Xrs2) complex provides as an early response initiating the two DSB repair pathways. Each member of the NHEJ, HR and MRX complexes is highly conserved in eukaryotes. The filamentous fungus *Neurospora crassa* also has almost all their members. We are interested in how HR, NHEJ and MRX combine to repair the DNA damage in *Neurospora* arising from carbon-ion irradiation. Three DSB repair-deficient mutants were examined, *mei-3*, *mus-52* and *uvs-6*, which have a mutation in the homolog genes of budding yeast RAD51 (HR), YKU80 (NHEJ) and RAD50 (MRX), respectively.

Sensitivity to carbon-ion irradiation was evaluated as follows. About $2x10^7$ conidia from a one-week culture were placed on a cellulose acetate membrane and irradiated with carbon ions at various doses of 0 to 400 Gy. The irradiated samples were suspended in a phosphate buffer and plated at 1,000 conidia per plate. After incubation at 30˚C for 3 days, the number of colonies on each plate was counted. The survival curve of each strain is shown in Fig.1. The sensitivity of the wild-type strain is indicated by closed circles. The *mei-3* mutant (*closed triangles*) was more sensitive to the carbon-ion beam than the wild-type strain. The *uvs-6* mutant (*closed diamonds*) showed the highest sensitivity to the carbon-ion beam among the tested strains. On the other hand, the *mus-52* mutant (*closed squares*) exhibited a unique pattern of sensitivity; at doses lower than 100 Gy, the *mus-52* mutant was slightly more sensitive than the wild type, but it exhibited less sensitivity than the wild type at higher doses. This tendency was in good agreement with the survival curves obtained from an X-ray irradiation experiment (data not shown).

The frequency of induced mutations was determined by measuring the number of forward mutations occurring in the *ad-3* (*adenine-3*) loci. A conidial suspension from each sample was inoculated into a 5-liter Florence flask at 5 x 10^5 viable conidia per flask. The flask was cultured in the dark at 30˚C with low aeration. Under these conditions, each conidium produces a bead like colony after 1 week. If genetic alterations occur in the *ad-3* loci, it causes the accumulation of a purple pigment as a metabolic intermediate of adenine. The mutation frequencies of the wild type and *mus-52* are shown in Table 1. Purple colonies were obtained at two doses, 100 and 200 Gy, but not at lower or higher doses. The *mus-52* mutant exhibited lower mutation frequency than the wild type. However, the data are insufficient for us to discuss the mutagenic effect of the carbon-ion beam. Further experiments should be carried out at a narrower dose range. The mutation spectrum generated in *ad-3* loci is currently being determined by DNA sequencing. The results data will be reported soon.

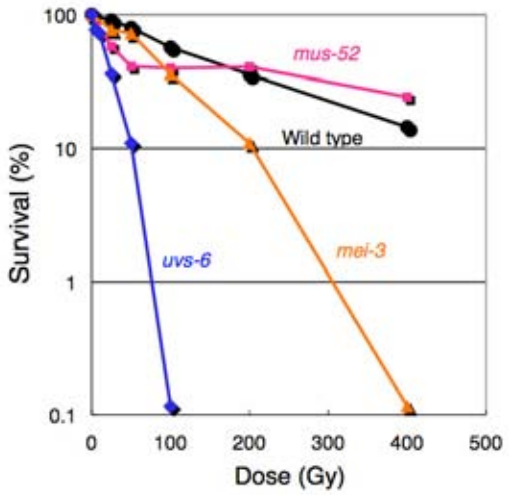

Fig.1 Sensitivity to carbon-ion beam

Table 1. Mutation frequency (per 10^6 conidia)

Strain	100 Gy	200 Gy
Wild type	49.0	56.0
mus-52	35.5	35.0

*Laboratory of Genetics, Saitama University

Molecular characterization of microbial mutations induced by carbon- and iron-ion beam irradiation†

H. Ichida, T. Matsuyama, H. Ryuto, N. Fukunishi, T. Abe, and T. Koba*1

DNA double-strand breaks (DSBs) represent the most serious form of DNA damage. It has been demonstrated previously that densely ionizing (high linear energy transfer; high-LET) radiation, such as neutrons and α-particles, can have a greater biological effect than sparsely ionizing (low-LET) X-rays or γ-rays[1]. However, little is currently known about the characteristics of the mutations induced by highly accelerated ion beams at the molecular level, although the mutagenic efficacy is known to be dependent on the radiation dose and on the energy and charge of the produced ions[2]. To investigate the molecular characteristics of heavy-ion beam induced mutations, we established a *Mesorhizobium loti* derivative that harbors a single intact copy of the levansucrase (*sacB*) gene construct within its genome. In exogenous *sacB*-expressing strains growing in selective medium, the living cells must be SacB-deficient. Therefore, we can efficiently observe the gene disruption events by selecting sucrose-tolerant colonies after irradiation.

The reporter strain, *M. loti* Line #1, was irradiated with carbon (135 MeV/nucleon, LET: 23–60 keV/μm) and iron (90 MeV/nucleon, 640 keV/μm) ion beams, and sucrose-tolerant mutants were collected. Sequencing analysis of the *sacB* fragments amplified from these mutants showed that single nucleotide mutations such as base substitutions and excisions, insertions, and deletions had occurred in each case. To evaluate the effects of the ion beam irradiation on DNA and minimize the detection of artifacts, we focused on 56 completely independent insertion and deletion events that would not be affected by any bias resulting from cell division.

The distribution of the mutated positions is depicted in Fig. 1. In insertion lines, fragments of approximately 1188 bp were identified within the *sacB* regions. The sequences of these inserts were essentially identical in all of these lines, but their positions appeared to be dispersed around the *sacB* promoter and coding regions (Fig. 1, rectangles). Sequence analysis of the junctions revealed two to four nucleotide duplications at both termini in all of the lines. These nucleotides were identical for the inserted fragments and *sacB*, representing signs of microhomology-based repair. The primary structure around the junction sites flanking the inserts consisted of AT at the possible microhomology sites followed by G(A/T)CGT(GA/AG)ACTCAT(T/A)A(C/A)CGC.

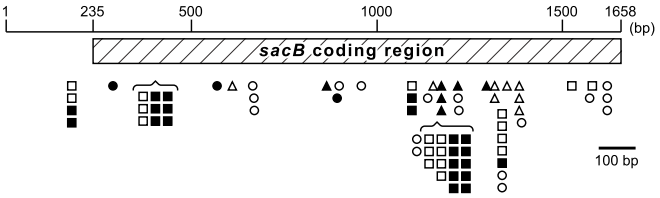

Fig. 1. Distribution of mutation positions. Circles: single nucleotide mutations; rectangles: insertions; triangles: deletions. Open symbols: carbon-ion mutations; filled symbols: iron-ion mutations.

This structure was completely conserved in all of the insertion lines and may have contributed to the homologous recombination pathway.

In the deletion lines (Fig. 1, triangles), no duplicated or homologous nucleotides were found at either of the deletion termini, indicating that they may have been induced independently of homologous recombination. Recent biochemical and bioinformatic analyses have revealed the existence of functional homologues of eukaryotic non-homologous end joining (NHEJ) proteins in bacteria, although this process had long been thought to be restricted to eukaryotes[3]. It is thus a reasonable interpretation that these deletions were induced when DNA lesions were repaired by NHEJ. Sequence analysis further showed that the deletion size range was 43–203 bp with the use of carbon ions and 119–641 bp with iron ions. The size of the deletion therefore appeared to be dependent on the LET, with carbon and iron ions producing deletions of different sizes.

In the postgenome era, reverse genomics is a useful approach, but is almost completely dependent on transgenic techniques, such as gene targeting by artificial recombination techniques. Heavy-ion beams therefore provide an effective alternative because they can generate length mutations that can be rapidly detected by general molecular techniques.

References

1) D. Goodhead: J. Radiat. Res. **40**, 1–13 (1999).
2) G. Horneck et al.: Adv. Space Res. **14**, 315–329 (1994).
3) T. Wilson et al.: Trends Biochem. Sci. **28**, 62–66 (2003).

† Condensed from the article in Mutation Research, **639**, 101–107 (2008).

*1 Graduate School of Science and Technology, Chiba University

Development of an effective system for detecting DNA damage induced by heavy-ion beam

Y. Kazama, H. Saito, M. Fujiwara, T. Matsuyama, Y. Hayashi, H. Ryuto, N. Fukunishi and T. Abe

Heavy-ion beams have high linear energy transfer (LET). In contrast to electron irradiation, which has low LET and causes closely spaced single-strand breaks, accelerated particles in heavy-ion beams are thought to produce closely positioned DNA damages and double-strand breaks upon piercing DNA strands. However, there is still little experimental evidence of a correlation between LET and the effect on deletion size in the plant kingdom. As a first step toward studying the LET-dependence on deletion size, we developed an effective system to characterize ion-induced DNA mutations in plants. We established a visual screening system for the detection of DNA damage. In this system, we used a stable transgenic *Arabidopsis* line that has a single-copy yellow fluorescent protein (YFP) gene and constitutively expresses the YFP. When the *YFP* gene is mutated by heavy-ion beam irradiation, its loss of function or expression can easily be detected by the disappearance of YFP signals under microscopy.

To produce such a transgenic line, the *YFP* gene fused with the N-terminal presequence of a mitochondrial *HSP60* and the NOS terminator under the cauliflower mosaic virus 35S (*CaMV35S*) promoter was introduced into *Arabidopsis thaliana* (L.) Heynh. ecotype Columbia (Fig. 1). A total of 324 transformants (T_1) were selected, and 47 plants exhibited bright YFP fluorescence from the whole seedling under a fluorescence stereomicroscope. One of them, designated FY2-9, was a stable transgenic line that had a single-copy fluorescent protein gene at a single chromosome locus.

Dry seeds of *YFP*-homozygous FY2-9 were irradiated with C, Ne, Ar, and Fe ions at a dose range of 5 to 200 Gy. These ions were accelerated to 135, 135, 95, and 90 MeV/nucleon, and their LETs were 22.5, 61.5, 290, and 640 keV/μm, respectively. In total, 5,183 seeds (M_1) were irradiated and the M_2 plants were screened for mutants that had no YFP signal. Four, five, two, and five seedlings were obtained from M_2 populations mutagenized with C, Ne, Ar, and Fe, respectively. The highest mutation rates were observed at doses of 200 Gy (1.10%), 200 Gy (0.82%), 10 Gy (0.44%), and 50 Gy (0.65%) in the above irradiation treatments, respectively. All the putative mutant plants showed normal growth and development, and none of the progeny exhibited YFP fluorescence. These data suggest that this visual screening system is highly efficient for screening mutants with DNA mutations.

We focused on mutant no. 104, which was irradiated with C at a dose of 200 Gy. When PCR analysis was performed on the total genomic DNA of FY2-9 and no. 104, single DNA products of 1,620 and 633 bp were amplified, respectively. Sequence analysis of the 633-bp product revealed that no. 104 contained a 985-bp deletion, which included a 3' part of the *CaMV35S* promoter, the presequence region, YFP, and a 5' part of the NOS terminator (Fig. 1). In addition, 12 base changes occurred upstream of the deletion site (data not shown). Five of these were transitions and the others were transversions. Moreover, a 49-bp fragment called the filter DNA[1] was inserted at the rejoined site (Fig. 1). In previous studies using *Arabidopsis*, either point like mutations or rearrangements by C-ion irradiation using the AVF cyclotron of Takasaki Ion Accelerators for Advanced Radiation Application were detected.[2] In contrast, C-ion irradiation using RIKEN Ring Cyclotron induced a complex pattern of mutations, a single large deletion, and many point mutations. The investigation of mutations in the other isolated mutants is in progress.

References

1) V. Gorbunova and A. A. Levy: Trends Plant Sci. **4**, 263 (1999).
2) N. Shikazono et al.: J. Exp. Bot. **56**, 587 (2005).

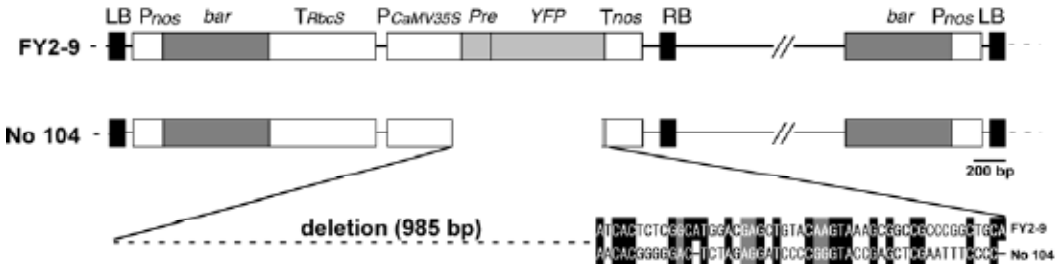

Fig. 1. Structures of the *YFP* transgene in FY2-9 and mutated region in no.104. LB: T-DNA left border, RB: T-DNA right border, P*nos*: *NOS* promoter, *bar*: bialaphos-resistance gene, T*RbcS*: *RbcS* terminator, P*CaMV35S*: *CaMV35S* promoter, *Pre*: N-terminal presequence of a mitochondrial *HSP60*, *YFP*: yellow fluorescent protein gene, T*nos*: *NOS* terminator.

† Condensed from the article in Biosci. Biotechnol. Biochem. **71**, 2864 (2007).

Radiation effect and partial deletion of the Y-chromosome by heavy ion beam in *Silene latifolia*

K. Ishii,* K. Nishihara,* K. Yamanaka,* N. Ishi,* A. Koizumi,* Y. Kazama, T. Abe, and S. Kawano*

Silene latifolia (white campion) of Caryophyllaceae is a dioecious plant in which males have one X-chromosome and one Y-chromosome and females have two X-chromosomes. The Y-chromosome contains three regions: gynoecium-suppressing function(s) (GSF), stamen-promoting function(s) (SPF), and male-fertility function(s) (MFF). *S. latifolia*, which has an XY sex-determination system, is a representative model plant for studying plant sexuality and searching for plant male-determining genes. We are aiming to establish a versatile screening method for detecting sex-reversal mutants yielded by chromosomal deletions. In this study, we examined the relationship between the effect of radiation on growth and chromosomal deletions induced by irradiating carbon-ion beam.

Hypoplasia, which appears in the first generation (M1) of plants grown from directly irradiated seeds is known as the "radiation effect". The number of dividing cells in the meristem is decreased, which delays plant growth, because they are fatally damaged by the irradiation of a carbon-ion beam. Seeds were irradiated with a 135 MeV/u carbon-ion beam with absorbed doses ranging from 20 to 200 Gy. We first examined the relationship between hypoplasia and chromosomal deletions. The number of individuals with both cotyledons and true leaves was counted three weeks after seeding to construct a survival curve (Fig. 1, ●). The survival rates of the seeds irradiated at up to 75 Gy ranged from 100% to 85%. The survival rates of seeds irradiated at more than 75 Gy decreased as the amount of absorbed dose increased. The survival rate of seeds irradiated at 200 Gy was 18%. Although the seeds irradiated at 200 Gy germinated to produce cotyledons or true leaves, they exhibited extreme hypoplasia and hardly grew even after five weeks (△). For irradiation ranging from 20 to 150 Gy, the growth inhibition was almost proportional to the absorbed dose. Growth rates after three weeks (○) and five weeks ranged from 8 to 90%. However, three months after transplanting in a farm field, the growth rate of the plants germinated from seeds irradiated at doses of as high as 150 Gy recovered to nearly 50% and the plants grew to 50 cm in height. The growth inhibition by irradiation appears to be limited to the early stages of growth. Almost all of the hypoplasia appearing in this generation of plants grown from seeds directly irradiated with a heavy-ion beam is expected to not be inherited by the next generation (M2).

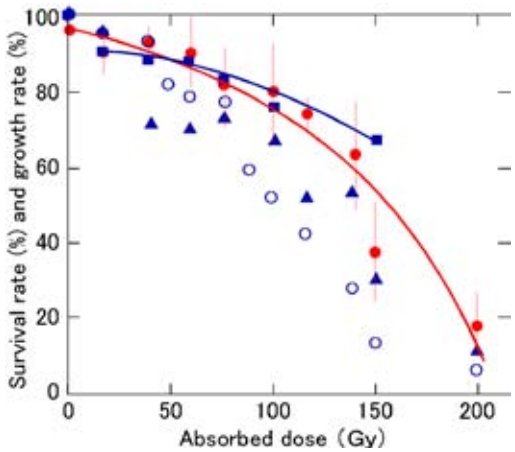

Fig. 1 Survival rates and growth rates of seedlings raised from the irradiated seeds. The survival rates (●) were estimated for three weeks after seeding. The growth rates of three weeks (○) and five weeks (▲) after seeding , and three months after transplanting in a farm field (■) were measured for individuals irradiated at different absorbed doses (Gy).

* Department of Integrated Biosciences, Graduate School of Frontier Sciences, University of Tokyo

The male of *S. latifolia* is suitable for checking chromosomal deletions by PCR because it has one X-chromosome and one Y-chromosome. We examined 60 individuals, which were irradiated with doses ranging from 80 to 200 Gy, using 36 STS markers (20 Y-chromosome-, 7 X-chromosome-, and 9 autosome-specific markers). This range of irradiation resulted in plants growing at less than 60% of the standard growth rate. In an individual irradiated at 150 Gy (A36-0), the chromosomal region containing MS2, ORF191, *SlY1*, ScX11, *SlY3*, MS4, and *SlssY* was deleted (Fig. 2). Each of the four true leaves of A36-0 was a chimera of the cells possessing deleted chromosomal DNA and wild-type chromosomal DNA.

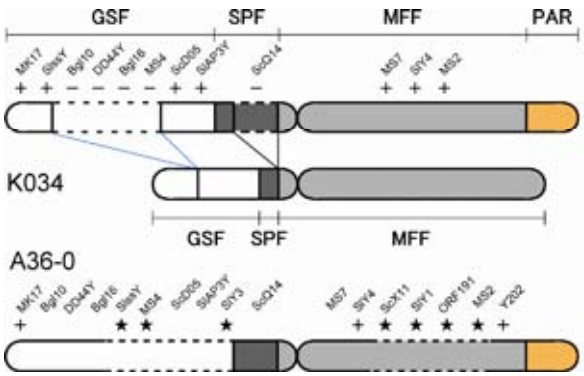

Fig. 2 Scheme of Y-chromosome-specific STS markers and their deletion sites. K034 is a spontaneous mutant.1) A36-0 was obtained in this study by heavy-ion-beam irradiation. ★ indicates the deletion regions of A36-0.

References

1) A. Koizumi et al.: Plant Cell Physiol. **48**, 1450-1461 (2007)

High-efficiency improvement of transgenic torenia flowers by ion beam irradiation

K. Sasaki*, R. Aida*, H. Yamaguchi*, T. Narumi*, Y. Hayashi, H. Ryuto, N. Fukunishi, T. Abe and N. Ohtsubo*

Although genetic engineering and ion beam breeding have beneficial features, both still have practical or technical disadvantages in the production and commercialization of transgenic plants on demand. For example, public release of genetically engineering products may experience problems such as cost of commercialization and overcoming public resistance. Likewise, ion beam breeding is hampered by low reproducibility—it is difficult to obtain the same mutant in different experiments. Such deficiencies might be compensated in part by combining these procedures thereby improving the risk-cost/benefit ratio and to identify the genes that produce valuable mutant phenotypes.

To develop an efficient way to produce and release transgenic flowers to the public domain, as well as to improve the risk-cost/benefit ratio of product commercialization, we performed ion beam irradiation of wild-type and genetically modified torenia (*Torenia fournieri* Lind. 'Crown Violet') plants in which petal color and pattern had been modified by controlling two anthocyanin biosynthesis-related genes encoding chalcone synthase (*CHS*) and dihydroflavonol-4-reductase (*DFR*)[1]. The transgenic line CS400-29 contains a transgene encoding torenia chalcone synthase gene (*CHS*) under the control of cauliflower mosaic virus 35S RNA promoter (p35S). Similarly, CA411-3 and CA411-7 contain p35S::antisense-*CHS*, DS405-2 contains p35S::*DFR* (DFR is dihydroflavonol- 4-reductase) and DA416-20 contains a p35S::antisense-*DFR* gene.

Ion beams of $^{12}C^{6+}$ (1.62 GeV, LET 22.5 KeV μm^{-1}, 5–80 Gy) and $^{20}Ne^{10+}$ (2.70 GeV, LET 61.5 KeV μm^{-1}, 5–30 Gy) were applied to 11,500 leaf disks from wild type and five transgenic lines, and over 3,200 regenerated flowering plants were then investigated for visible phenotypes. The mutation rate after whole irradiation averaged 10.4% (Table 1), and the maximum rate in the initial screening was 44.2% (^{20}Ne, 30 Gy). Mutant phenotypes were observed mainly in flowers and showed wide variation in color and shape (Figure 1). Mutation efficiencies for petal color and coloration pattern were higher in transgenic plants than in wild-type plants, while those for petal shape and corolla divergence were almost equivalent in the two plant groups. Mutation spectrums in petal color in transformant-based mutants were obviously wider than those in wild-type plants.

We propose that the combination of genetic engineering and ion beam irradiation greatly facilitates improvement of agrobiological and commercial traits within a short period.

Table 1. Mutation rates of ion-beam irradiated plants.

Original lines	^{12}C No. Plants	Mutated	Rate (%)	Original lines	^{20}Ne No. Plants	Mutated	Rate (%)
WT	398	27	6.8	WT	420	22	5.2
CA400-29	142	19	13.4	CA400-29	252	22	8.7
CS411-3	252	35	13.9	CS411-3	255	20	7.8
CS411-7	314	30	9.6	CS411-7	290	21	7.2
DA405-2	117	22	18.8	DA405-2	247	25	10.1
DS416-20	259	40	15.4	DS416-20	295	55	18.6
^{12}C subtotal	1482	173	11.7	^{20}Ne subtotal	1759	165	9.4
WT	818	49	6.0				
TG	2423	289	11.9				
Total	3241	338	10.4				

Reference

1) R. Aida et al.: Plant Sci. 153, 33 (2000)

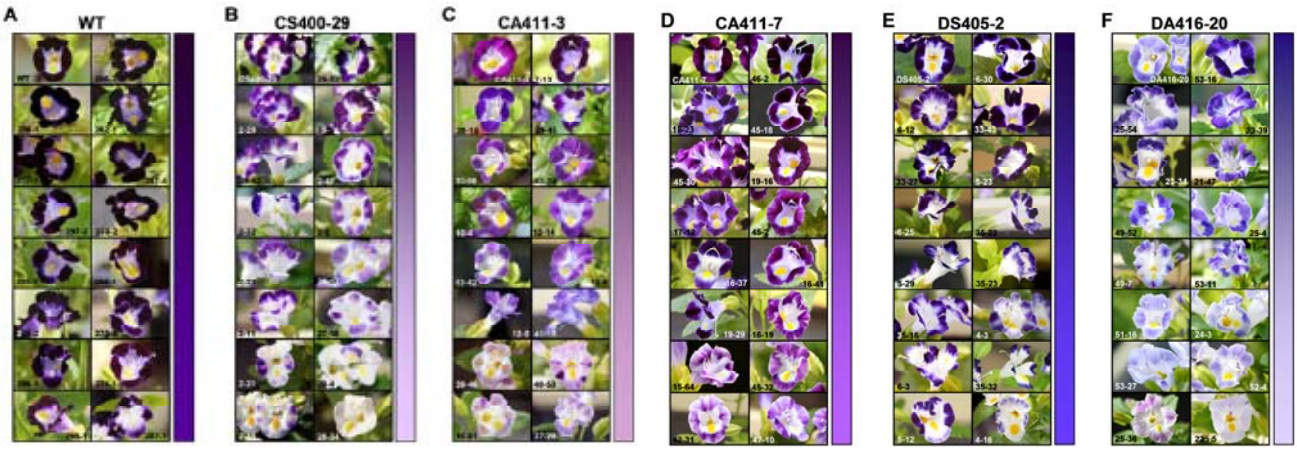

Figure 1. Morphological and color variations induced by heavy-ion beam irradiation. The original flower of each plant material is shown in the top-left corner of the colomn. A representation of the mutation spectrum in each irradiation experiment is shown as a color chart beside the colomn.

* National Institute of Floricultural Science

Condensed from the article in Plant Biotechnol. **25(1)**, 45 (2008).

Analysis of a class B gene-deficient like torenia mutant produced by ion beam irradiation

K. Sasaki*, R. Aida*, T. Niki*, H. Yamaguchi*, T. Narumi*, T. Nishijima*, Y. Hayashi, H. Ryuto, N. Fukunishi, T. Abe and N. Ohtsubo*

We propose that the combination of genetic engineering and ion beam irradiation greatly facilitates improvement of agrobiological and commercial traits within a short period, and heavy-ion beam irradiation was applied to genetically modified torenia (*Torenia fournieri* Lind. 'Crown Violet') plants carrying anthocyanin biosynthesis-related transgenes.

Among the mutants, we unexpectedly obtained a class B gene-deficient like mutant, 53-31. Because the molecular and/or genetic mechanisms of floral developmental control are poorly understood in torenia, we chose the mutant for our analysis. The 53-31 mutant was obtained by the ^{20}Ne (30 Gy) ion beam irradiation of DS416-20[1] plant which carrying 35S:: dihydroflavonol-4-reductase (*DFR*) gene. In this mutant, petals (Figure 1A-d, -e) were changed into sepals (Figure 1A-f), as seen in B-class mutants of snapdragon and *Arabidopsis*. We assumed that the torenia class B genes *GLOBOSA* (*TfGLO*) and/or *DEFICIENS* (*TfDEF*), which are orthologs of *PISTILATA* (*PI*) and *APETALA3* (*AP3*) in *Arabidopsis*, respectively, would be deficient in the 53-31 mutant. Then, we examined the expression of the *TfGLO* and *TfDEF* genes using the first, second and fourth whorls of the mutant, by RT-PCR analysis (Figure 1B). The results indicated that only *TfGLO* expression was not detected after 28 cycles of RT-PCR in all whorls. To investigate whether this mutant phenotype was caused by a mutation in the *TfGLO* gene, we next determined the genomic sequence of *TfGLO* and its 1.4 kb promoter region in WT plants. Comparison of the 693 bp *TfGLO* cDNA and the genomic sequence showed that *TfGLO* has five exons and four introns (Figure 1C). The introns are 135, 662, 212 and 199 bp long. Consequently, specific mutation was not seen in the genomic sequence of *TfGLO* in the 53-31 mutant, even after the 1.4 kb promoter region had also been sequenced (data not shown).

The result indicated that such a phenotype (Figure 1A-c) is caused by deficiency in the expression of only *TfGLO* among these two class B genes. Although we expected a specific mutation in the genomic sequence of *TfGLO* which resulted in loss of its expression, we found no such candidate within the sequence that included the 1.4 kb promoter region (Figure 1C). In *Arabidopsis*, the *AP1*, *LEAFY* (*LFY*) and unusual floral organs (*UFO*) genes have been reported to participate in the expression of class B genes. Since *AP1*, *LFY*, and *UFO* have yet been cloned in torenia, we are now trying to clone these regulatory genes and intend to investigate their expression for future analysis.

Molecular and/or genetic research in torenia is rather difficult because its genomic sequence has not been determined. However, we isolated many floral phenotype mutants of torenia by ion beam irradiation. For some mutants, we will be able to identify the deficient gene that causes the mutant phenotype by reference to the abundant information on regulatory genes and/or enzymes in other model plants. We expect that increasing amounts of information on the mechanisms by which floral development is controlled in torenia will accumulate in the future.

Reference

1) R. Aida et al.: Plant Sci. **153**, 33 (2000).

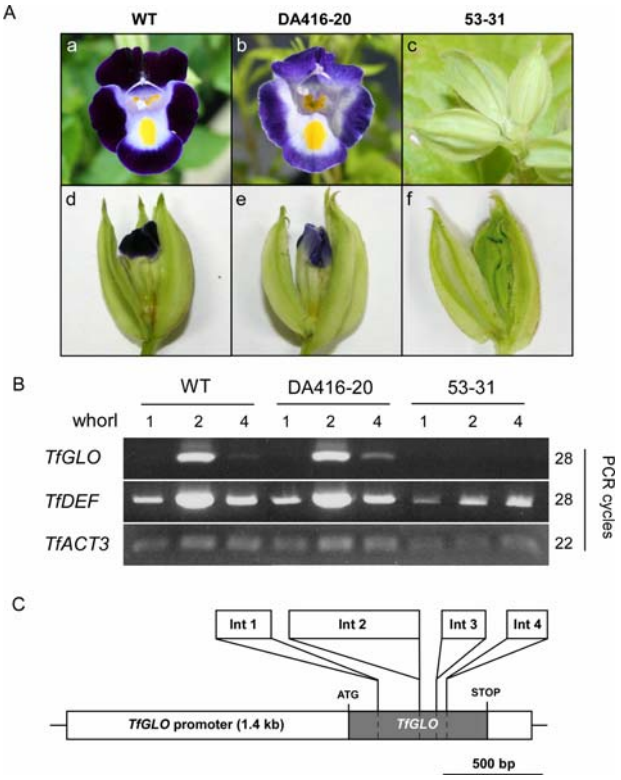

Figure 1. Analysis of mutants obtained by heavy ion beam irradiation. (A) Photographs of WT (a), DA416-20 transgenic line (b) and 53-31 mutants (c) obtained from the DA416-20 line. Photographs of second whorls in WT (d), DA416-20 (e), and 53-31 mutants (f). (B) RT-PCR analysis of class B genes *TfGLO* (AB359952) and *TfDEF* (AB359951) in whorls 1, 2, and 4 of WT, DA416-20 and 53-31 plants. The torenia actin gene, *TfACT3* (AB330989), was used as an internal control. (C) Genomic structure of *TfGLO* gene. ATG, initiation codon. STOP, stop codon. Gray box indicates the coding region of *TfGLO* (693 bp). The lengths of the introns are in the order, 135, 662, 212, and 199 bp.

* National Institute of Floricultural Science

Condensed from the article in Plant Biotechnol. **25**, 81 (2008).

Development of flower colour mutant of *Dianthus chinensis* var. *semperflorens* by heavy-ion beam irradiation

M. Sugiyama,* Y. Hayashi, N. Fukunishi, H. Ryuto, T. Terakawa* and T. Abe

Dianthus chinensis var. *semperflorens* is a caryophyllaceous plant known as 'Tokonatsu' in Japan. It is a dwarf (about 10 to 15 cm high) perpetual flowering plant grown by garden farming or container gardening. Traditionally, new cultivars of *D. chinensis* var. *semperflorens* are developed by selective breeding utilizing a naturally occurring bud mutation process or by crossbreeding. Recently, an artificial induction of mutations by heavy-ion beam irradiation has been used in plant breeding. Some new cultivars of ornamental plants such as *Verbena hybrida* and *Petunia hybrida* have been developed by heavy-ion beam irradiation.[1, 2] In this study, we attempt to develop a flower colour mutant of *D. chinensis* var. *semperflorens* by heavy-ion beam irradiation.

The flower of *D. chinensis* var. *semperflorens* cv. 'White Eye' (WE) exhibits a concentric red ring over the underlying white colour (Fig.1A). WE was used as the plant material for our study. Stems of WE propagated *in vitro* were cut into approximately 3-5 mm segments, each carrying axillary buds. The stem segments were cultured on MS medium containing 0.5 mg/l kinetin and 0.1 mg/l naphthylacetic acid for 15 days. They were then irradiated with a $^{12}C^{6+}$ ion beam (135 MeV/nucleon, LET 23 KeV/μm) at doses of 20, 25, 30, 35, 40, 60 and 80 Gy. The irradiated samples were transplanted on a fresh MS medium for plant elongation and rooting. Fifty days after the irradiation, the plants were transferred to flower pots and grown in a greenhouse. After four months of culture, the viability of the irradiated sample and the mutations in flower morphology were examined.

The effects of the heavy-ion beam irradiation are shown in Table 1. The survival rate of the plant decreased as radiation dose increased. All the plants irradiated at 80 Gy died. At doses below 80 Gy, several types of mutants were detected among the surviving specimens. Some control specimens developed a uniformly coloured mutated purplish pink flower probably caused by somaclonal variation during culture *in vitro*. Heavy-ion beam irradiation at 20 to 60 Gy augmented the occurrence of this flower colour mutant. Furthermore, the irradiation diversified the flower morphology in terms of colour and form. Mutants with flowers that showed various colour patterns differing from the original were obtained at 20 to 40 Gy (data not shown). Mutants that were altered in only flower form and in both flower colour and form were obtained at 25 to 35 Gy and 25 to 40 Gy, respectively. Two specimens producing a mutated white flower, obtained at 30 and 35 Gy, were selected for further evaluation (Fig. 1B). These specimens produced mutated white flowers along with the original flower type, suggesting that they were chimeras. A branch carrying a mutated white flower was cut from these specimens and grown separately to isolate the white flower characteristics. Finally, some isolates that produce only white flowers were obtained. The isolates originating from the specimen obtained at 30 Gy took more time to bloom than those originating from the specimen obtained at 35 Gy. These isolates were almost identical to the original plant in other phenotypic characteristics (Table 2).

In *D. chinensis* var. *semperflorens*, it has been difficult to develop new cultivars producing white flowers by traditional breeding methods because this characteristic is uncommon in this plant. The present results show that heavy-ion beam irradiation is effective for developing new cultivars of this species. The application for new-variety registration for the isolate with white flowers, which was bred from the specimen obtained at 35 Gy, was filed with the Japanese Ministry of Agriculture, Forestry and Fisheries in 2007.

Fig. 1. Original flower (A) and mutated white flower (B) of *D. chinensis* var. *semperflorens* cv. 'White Eye'.

Table 1. Effects of $^{12}C^{6+}$ ion beam irradiation on *D. chinensis* var. *semperflorens* cv. 'White eye'

Dose (Gy)	Number of plants irradiated	Number of plants surviving	Survival rate (%)	Number of mutants producing flowers with indicated colour: Purplish pink		Colours other than purplish pink		Number of mutants showing mutation in only flower form		Number of mutants showing mutations in both flower colour and flower form	
				No.	(%)§	No.	(%)§	No.	(%)§	No.	(%)§
Control	100	90	90	15	(16.7)	0	(0.0)	0	(0.0)	0	(0.0)
20	100	74	74	40	(54.1)	4	(5.4)	0	(0.0)	0	(0.0)
25	300	223	74	112	(50.2)	20	(9.0)	7	(3.1)	1	(0.4)
30	300	175	58	93	(53.1)	19	(10.9)	9	(5.1)	4	(2.3)
35	400	127	32	59	(46.5)	23	(18.1)	6	(4.7)	2	(1.6)
40	100	34	34	16	(47.1)	4	(11.8)	0	(0.0)	1	(2.9)
60	100	5	5	4	(80.0)	0	(0.0)	0	(0.0)	0	(0.0)
80	100	0	0	−	(−)	−	(−)	−	(−)	−	(−)

§ Frequency of mutants (%) = (Number of mutants/Number of plants surviving) × 100

Table 2. Phenotypic comparison between wild type and white-flower mutant obtained at 35Gy§

	Plant height of blooming	Flower diameter	Petal width	Length of maximum leaf	Width of maximum leaf
Wild type	94.1±5.2	31.2±3.1	15.6±1.4	55.3±4.3	8.1±0.9
White flower mutant	102.7±5.2	31.2±1.7	13.9±0.8	60.5±1.9	8.3±0.5

§ Values represent the mean (mm) ± standard error of 8 individuals.

*Hokko Chemical Industry Co., Ltd.

References

1) K. Suzuki et al.: RIKEN Accel. Prog. Rep. 35, 129 (2002)
2) K. Miyazaki et al.: RIKEN Accel. Prog. Rep. 35, 130 (2002)

Induction of floral-color mutation by C-ion irradiation in spray-type chrysanthemum

N. Wakita [1], Y. Kazama, Y. Hayashi, H. Ryuto, N. Fukunishi, K. Yamamoto [1], S. Ijichi [2] and T. Abe

A spray-type chrysanthemum is one of the major cut flowers and a special product of Wadomari town. Wadomari town has developed original varieties of spray-type chrysanthemum with various floral colors by crossbreeding since 2001. However, it is desired to produce more varieties with new floral colors to meet a wide variety of consumer needs. Recently, heavy-ion beam irradiation has been utilized for breeding of various plants. [1)] In this study, we performed heavy-ion beam irradiation of chrysanthemum to induce new floral-color mutants.

Forty stem segments from 18 original varieties of chrysanthemums were irradiated with C ions (135 MeV/nucleon, LET 22.5 keV/μm) at doses of 3 Gy and 6 Gy. The irradiation doses were selected on the basis of previous research. [2)] After irradiation, the stem segments were transplanted to an experimental field. The survival rates of irradiated plants were all 100%. Newly developed stem segments from each irradiated plant were removed, retransplanted in the field, and further studied for mutation in the experimental field. The number of retransplanted segments was 125-389 in each irradiation experiment.

Among the 18 varieties, 10 exhibited flower-color mutations (Table 1). The other eight varieties showed no mutation. The mutation rates ranged from 0.35% to 6.40%. One of the varieties, Kazumi Fantasy showed a higher mutation rate and a wider spectrum than any other varieties.

In addition to mutants showing flower-color changes, those showing color-pattern changes were obtained in the irradiation experiment on Kazumi Harmony and Kazumi Liebe. In these mutants, the white area on the rims of petals expanded (Fig. 1). All of the flowers of these mutants showed the same type of color-pattern change. Investigation of the stability of these mutations is in progress.

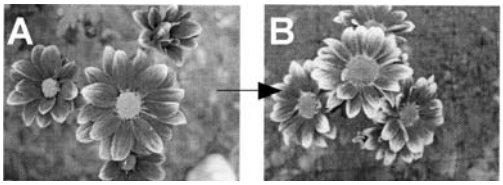

Fig. 1 Color-pattern mutant. A, flowers of an original variety of chrysanthemum, Kazumi Harmony. B, flowers of a color-pattern changing mutant. White areas of petals were expanded in the mutant.

References

1) T. Abe et al.: 18th Inter. Conf. Cyclotrons Their Appli. *in press* (2008)

2) K. Suzuki et al.: RIKEN Accel. Prog. Rep. **37**, 152 (2004).

Table1. Flower-color mutation induced by C-ion beam

Variety	Dose	No. of Plants[a]	Flower color		No. of Mutants	Mutation Rate (%)
			Original	Mutant		
Kazumi Soleil	3 Gy	217	Yellow	Greenish yellow	1	0.46
	6 Gy	172			5	2.91
Kazumi Venus	3 Gy	162	Bright yellow	Yellow	0	0
	6 Gy	135			2	1.48
Kazumi Harmony	3 Gy	170	Deep purplish pink	Deep yellowish red	0	0
	6 Gy	160			2	1.25
Kazumi Liebe	3 Gy	229	Dull yellowish pink	Dull pink	1	0.44
	6 Gy	228			4	1.75
Kazumi Rosso	3 Gy	211	Purplish pink	Dull purplish pink	0	0
	6 Gy	209			1	0.48
Kazumi Fantasy	3 Gy	125	Reddish yellow	Orange, Strong reddish orange, Pale yellow	4	3.20
	6 Gy	172			11	6.40
Kazumi Sakura	3 Gy	126	Pinkish white	White, Pale purplish pink	1	0.79
	6 Gy	196			2	1.02
Kazumi Elf	3 Gy	132	White	Greenish yellow	1	0.76
	6 Gy	137			3	2.19
Kazumi Espoir	3 Gy	163	Light orange	Strong red	0	0
	6 Gy	172			1	0.58
Kazumi Accord	3 Gy	282	Yellowish white	Pale greenish yellow	1	0.35
	6 Gy	389			2	0.51

[a] No. of retransplanted segments

1 Wadomari Cho agricultural experimental station

2 Mayor of Wadomari town

Analysis of libraries of 'Micro-Tom' tomato mutations induced by heavy-ion bombardment†

S. Imanishi, A. Noguchi, T. Hiraga, M. Nagata, Y. Hayashi, N. Fukunishi, H. Ryuto, T. Abe and I. Honda

Fruit setting, development, and ripening are complex, genetically programmed processes. Identifying the factors that control these processes is important for understanding the mechanisms of reproductive development. We induced mutations in the tomato (*Solanum lycopersicum*) cultivar 'Micro-Tom' by heavy-ion irradiation (HII), recently established as an effective method for inducing mutations in plants, and constructed mutation libraries.

Dry seeds of tomato were irradiated by ^{12}C or ^{20}Ne-ion beams accelerated to 135 MeV/nucleon with RRC. The linear energy transfer values of the ^{12}C and ^{20}Ne ions were 22.7 and 64.2 keV/μm. The lethal dose 50 (LD_{50}) was found to be higher than 200 Gy for both ions (Fig. 1). Sweet pepper, which also belongs to the Solanaceae family, was irradiated by ^{12}C or ^{20}Ne-ion beams with RRC under the same conditions and did not germinate under the 200 Gy irradiation[1]. Although the condition of irradiation was different, the LD_{50} of the tomato cultivar 'First' was reported to be 50 Gy with C ions accelerated with the AVF cyclotron in TIARA[2]. 'Micro-Tom' showed a low sensitivity to a high HII dose; however a direct comparison with these results is thought be difficult.

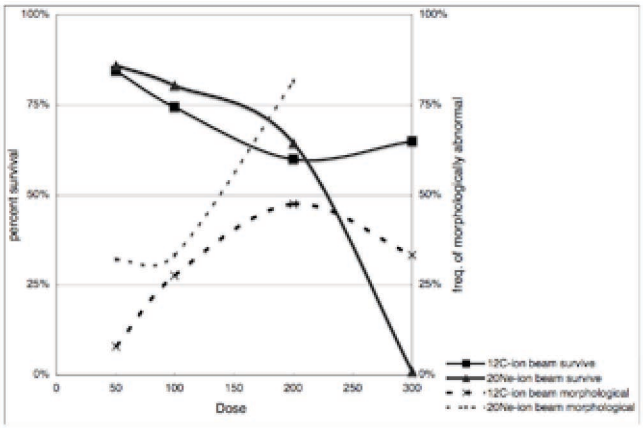

Fig. 1. 'Micro-Tom' M_1 generation raised from the seeds irradiated with accelerated heavy-ion.

By screening 6,794 M_1 plants, we found various mutations, including those affecting the sizes of plants, leaves, or fruits, and one conferring a broccoli-like inflorescence. This M_1 mutant (Fig. 2) resembles that tomato *anantha* mutant, in which the development of floral primordia is surpressed before organogenesis[3-5]. Because we could not obtain seeds from this mutant, inheritance and segregation of the trait are unknown, while the phenotype of *anantha* has been shown to be caused by a recessive mutation[4]. The isolation of monogenic homozygous recessive mutants in the M_1 generation has not commonly been described in other mutational studies using many plant species, although our group isolated such mutants in sweet pepper by M_1 plant selection in HII mutational studies[1]. Furthermore, we found several morphological mutants in the M_1 generation. Most of these mutations are not inherited in the M_2 generation, as reported[1], whereas about 3% of the M_2 progenies derived from seeds irradiated with ion beams showed abnormalities the same as those observed in the M_1 generation. We continue the analysis of the mode of inheritance of the mutations.

Fig. 2. An M_1 mutant in which all inflorescences look like broccoli.

To date, we have visually phenotyped 1,610 M_2 families (five sibs per line) in the field, and found 262 plants differing from the wild type (WT) in one or more characteristics. The fruit of one plant was larger than that of WT. These results suggest that such mutation libraries could be powerful tools for explaining the reproductive development of plants.

References

1) I. Honda et al.: Euphytica **152**, 61 (2006).
2) M. Masuda et al.: Acta. Hort. **637**, 257 (2004).
3) J. Helm: Züchter **21**, 89 (1951).
4) E. F. Paddock and L. Alexander: Ohio J. Sci. **52**, 327 (1952).
5) K. D. Allen and M. Sussex: Planta **200**, 254 (1996).

† Condensed from the article in Acta. Hort. **745**, 485-489 (2007)

National Institute of Vegetable and Tea Science (NIVTS), National Agriculture and Food Research Organization (NARO)

Semidwarf mutants of Tartary buckwheat induced by heavy-ion beam irradiation

T. Morishita*[1], Y. Miyazawa*[2], H. Saito, Y. Hayashi, H. Ryuto, N. Fukunishi and T. Abe

Recently, heavy-ion beams have been regarded as a new mutagen for plant breeding because of their high linear energy transfer (LET) and high relative biological effectiveness (RBE). We previously reported the biological effects and mutation induction by ion beams in buckwheat[1) 2)]. We obtained semidwarf mutants named IRBFT-45, 63, 67 and 77. The semidwarf type is important for improving lodging resistance and yielding ability in buckwheat breeding. These semidwarf mutants were obtained by irradiating dry Tartary buckwheat (var. Rotundatum) seeds with 40 Gy of carbon (23 keV/μm, $^{12}C^{6+}$), 100 Gy of carbon (39 keV/μm, $^{12}C^{6+}$), 30 Gy of iron (624 keV/μm, $^{56}Fe^{24+}$) and 20 Gy of argon (280 keV/μm, $^{40}Ar^{17+}$) ions (Table 1). The phenotype of IRBFT-45 is semidwarf and other semidwarf mutants exhibited similar phenotype as IRBFT-45 (Fig. 1). The plant height of these mutants are from one-half to one-third of Rotundatum. Furthermore main stem length and 1000-grain weight are lower than those of Rotundatum. Among the mutants, IRBFT-67 showed the highest 1000-grain weight (Table 2). Because of their lodging resistance, it seems that these mutants will become good breeding materials.

References

1) T. Morishita et al.: RIKEN Accel. Prog. Rep. 36, 137 (2003)
2) T. Morishita et al.: RIKEN Accel. Prog. Rep. 40, 255 (2007)

Table 1. Semidwarf mutant lines of Tartary buckwheat.

Mutant	Original	Ion Species	LET (keV/μm)	Dose (Gy)
IRBFT-45	Rotundatum	$^{12}C^{6+}$	23	40
IRBFT-63	Rotundatum	$^{12}C^{6+}$	39	100
IRBFT-67	Rotundatum	$^{56}Fe^{24+}$	624	30
IRBFT-77	Rotundatum	$^{40}Ar^{17+}$	280	20

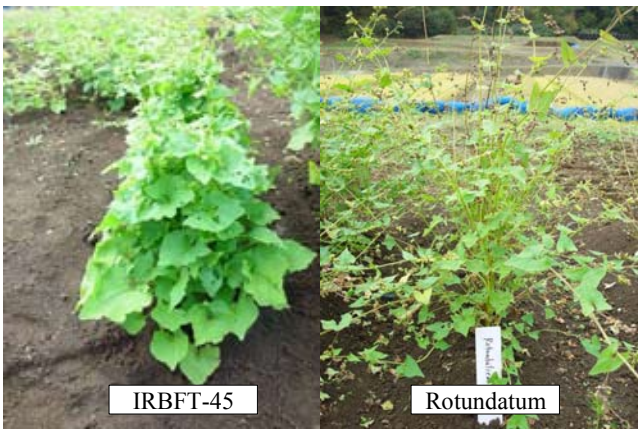

Fig. 1.Semi-dwarf mutant IRBFT-45 (left) and original variety Rotundatum (right). Other mutants (IRBFT-63,67,77) are similar phenotype as IRBFT-45.

Table 2. Characteristics of semidwarf mutants of Tartary buckwheat

Mutant	Year	Generation	Plant height (cm)	Main stem length (cm)	No. of nodes	No. of branches	1000-grain weight (g)	Resistance of lodging
IRBFT-45	2003	M3	64.0	64.0	15.0	9.0	14.5	very high
	2004	M4	—	—	—	—	15.9	—
	2005	M5	63.7	57.7	20.9	8.6	15.0	very high
	2006	M6	59.6	57.7	21.9	9.3	16.9	very high
IRBFT-63	2004	M3	—	—	—	—	16.3	—
	2005	M4	58.7	48.8	16.0	7.3	15.8	very high
	2006	M5	57.8	52.8	15.2	7.3	16.7	very high
IRBFT-67	2004	M3	—	—	—	—	17.8	—
	2005	M4	60.9	57.0	17.6	7.7	17.0	very high
	2006	M5	52.1	47.8	14.6	7.8	17.5	very high
IRBFT-77	2005	M2	—	—	—	—	15.5	—
	2006	M3	37.7	33.9	16.7	9.0	16.4	very high
Rotundatum (Original)	2003	—	114.5	109.8	19.5	6.8	21.1	medium
	2004	—	—	—	—	—	20.5	—
	2005	—	108.5	102.2	18.8	7.8	19.6	medium

Resistance of lodging is evaluated by field observation.

*1 National Institute of Agrobiological Sciences
*2 Grad. Sch. Life Sci., Tohoku Univ.

Detection of deletion region of the ion-beam-induced einkorn wheat (*Triticum monococcum*) mutant, *maintained-vegetative-phase*

K. Murai*[1], N. Shitsukawa*[1], C. Ikari*[1], S. Shimada*[1], S. Kitagawa*[1], K. Sakamoto, H. Saito, H. Ryuto, N. Fukunishi, S. Takumi*[2], S. Nasuda*[3] and T. Abe

The timing of the phase transition from vegetative to reproductive growth is associated with the heading time, one of the most important traits in cereal crops. In hexaploid common wheat (*Triticum aestivum*), the heading time is genetically determined and has three characteristic components: a vernalization requirement, photoperiod sensitivity, and narrow-sense earliness (earliness per se), that is, an autonomous promoting pathway. To develop mutant for heading-time genes, einkorn wheat (*T. monococcum*) strains KU104-1 and KU104-2 were used in ion-beam treatment experiments. The seeds were subjected to accelerated ions of $^{14}N^{7+}$ with 135 MeV/nucleon energy in a dose of 50 Gy nitrogen ion-beam treatment and then sown in a field. The ears of M_1 plants were bagged and the harvested selfed seeds of each ear were used to produce the M_2 lines. We identified the *maintained-vegetative-phase* (*mvp*) mutant by its inability to transit from the vegetative to the reproductive phase.[1)] We obtained two *mvp* mutant lines: the first was found in 1921 M_2 line plants of KU104-2; the second was found in 1326 M_2 line plants of KU104-1. These lines were named *mvp-1* and *mvp-2*, respectively. *mvp* mutants continued to grow vegetatively and never underwent the transition to the reproductive growth phase. After vernalization treatment, *mvp* plants grew vegetatively for more than 4 years in a growth chamber under-long day conditions (16 h light/8 h dark) at 20 °C. In our previous study, we showed that *WAP1* (wheat *APETALA1*) is a key gene in the regulatory pathway that controls the phase transition from vegetative to reproductive growth in common wheat.[2)] *WAP1* is an ortholog of the *VRN1* gene that is responsible for vernalization insensitivity in einkorn wheat. PCR analysis of the genomic DNA from wild-type (WT) einkorn wheat and the *mvp* mutants was performed using the *WAP1*/*VRN1* -specific primer set WAP1-553L (5'-AAGATCAGACTCAGCCTCAA-3') and WAP1-1003R (5'-TTCACATAAACAACATCCCA-3'). No *VRN1* gene fragment was amplified from the *mvp* mutants indicating that this region of the *VRN1* gene had been deleted by the ion-beam treatment. To determine the size of the deleted region in the *VRN1* gene of the *mvp-1* mutant, we carried out PCR analyses using primer sets designed from the chromosome 5AL BAC 231A16 of the einkorn wheat strain DV92. The twenty primer sets covering the *VRN1* coding and promoter regions did not amplify any DNA fragments from the *mvp-1* mutant, but 2 primer sets located outside this region (65228-66046 and 84799-85280) amplified DNA fragments (Fig. 1). These results indicate that the deletion is about 19 kb in length and includes the *VRN1* coding and promoter regions in the *mvp-1* mutant. To examine the relationship between the *VRN1* deletion genotype and the *mvp* phenotype, we performed PCR analysis of an M_3 generation that was derived from an *mvp* heterozygous M_2 plant, segregating for *mvp* and normal phenotypes. In the M_3 generation, *mvp* and normal plants segregated in a ratio of 1:3 for both *mvp-1* and *mvp-2* mutations. Genomic DNA was isolated from each M_3 plant grown in the field, and the presence or absence of the *VRN1* gene was assessed using the *VRN1*-specific primer set, 81655L (5'-TCGTGGAGAAGCAGAAGGC-3') and 82017R (5'-GTTGATGTGGCTCACCATCC-3'), designed from the BAC sequence of DV92. We found that the *VRN1*-deleted genotype perfectly co-segregated with the *mvp* phenotype for both *mvp-1* and *mvp-2* mutations. These results indicate that the *mvp* phenotype was caused by the deletion in the *VRN1* gene and that *mvp-1* and *mvp-2* are allelic. The *mvp* mutation resulted from the deletion of the *VRN1* coding and promoter regions, demonstrating that *WAP1*/*VRN1* is an indispensable gene for phase transition in wheat. Furthermore, this study indicates that ion-beam treatment is useful for isolating mutants with single-gene deletion.

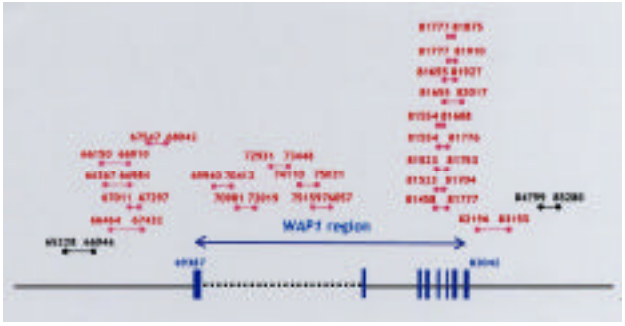

Fig. 1 PCR analysis of the *VRN1* region in wild-type (WT) and *mvp-1* mutant. Primer sets are indicated by a combination of Arabic figures based on the sequence of the chromosome 5AL BAC 231A16 of the *T. monococcum* strain DV92. Red lines indicate amplified DNA fragments not detected in *mvp-1* mutants. Black lines indicate amplified DNA fragments detected in both WT and *mvp-1* mutant plants.

References

1) N. Shitsukawa et al.: Genes Genet. Syst. **82**, 167 (2007).
2) K. Murai et al.: Plant Cell Physiol. **44**, 1255 (2003).

*1 Department of Bioscience, Fukui Prefectural University, *2 Department of Agrobioscience, Graduate School of Agricultural Science, Kobe University, *3 Division of Applied Biosciences, Graduate School of Agriculture, Kyoto University

Characterization of salt-tolerant mutants of rice induced by heavy-ion irradiation

Y. Hayashi, H. Takehisa, Y. Kazama, C. Kanba*1, S. Ohbu, H. Ryuto, N. Fukunishi, H. Tokairin, K. Ohkoshi*2, Y. Yoshino*2, T. Sato*1 and T. Abe

Salinity is a serious worldwide soil problem in rice-growing areas because salinity stress affects the growth and productivity of crops. In our previous paper, we reported salt-tolerant mutant lines of rice induced by C ion irradiation[1]. The 6-99 and 19-74 lines grew taller than untreated line, and the 19-55 line maintained its greenness in a saline paddy field. In this study, we characterized these salt-tolerant mutants of rice.

Three lines of salt-tolerant mutants (6-99, 19-55 and 19-74) and WT (*Oryza sativa* L. cv. Nipponbare) were examined. The plants were grown in a control paddy field and a saline paddy field. The salt concentration of floodwater was regulated by flooding the saline paddy field with salt water (Na^+ 120mM) or fresh water every week. The salt concentration during the experimental period of 2006 was maintained from 20 to 65mM Na^+ and that of 2007 was maintained from 25 to 100mM Na^+.

We recorded the shoot length, yield components (number of panicles, number of grains, percentage of ripening, grain weight) and grain appearance. Most yield components were measured by counting the panicles on the main culms. Grain appearance was measured by a rice inspector (SATAKE RGQI10A or Kett RN500) using dehulled grains. Eating quality was graded on a 5-point scale from 1 (bad) to 5 (good). The eating quality of WT grown in the control paddy field was assigned the standard value of 3. A panel of at least 10 judges selected at random evaluated the eating quality.

The 6-99 and 19-74 lines exhibited high shoot length, but there were no differences in the relative rate of shoot length in the saline paddy field between the mutant lines and WT (Table 1). For the relative rates of grain number and fertility, no differences between the mutant lines and WT were observed. For the 1000-grain weight, the 6-99 and 19-74 lines did not show a significant reduction in the saline paddy field compared with WT. Grain appearance is one of the most important factors in evaluating the quality of rice. The grain appearance of WT was significantly degraded in the saline paddy field, particularly under the higher salt concentration in 2007. The grain appearance of the 6-99 and 19-74 lines in the saline paddy field were better than that of WT (Fig. 1). In the eating quality test, the scores of WT and the 6-99 line were equivalent in the control paddy field. Each score for the saline paddy field was decreased; however, the score of the 6-99 line was higher than that of WT (Table 2). These results indicate that the two mutant lines 6-99 and 19-74 were less affected by salinity stress. These mutants are expected to be useful for understanding the mechanisms controlling the salt-tolerance of rice plants. Physiological and genetic analyses are in progress.

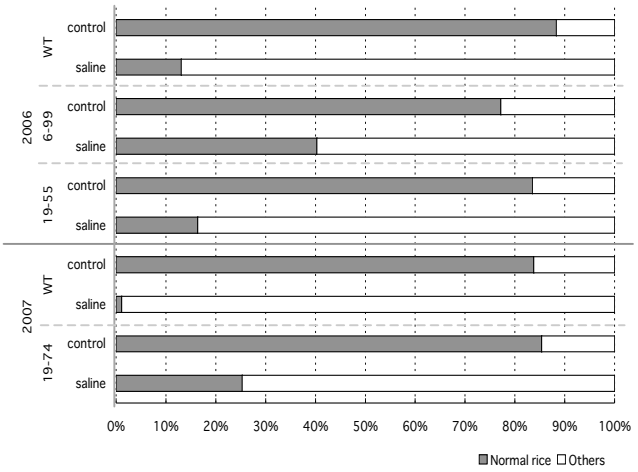

Fig.1 Grain appearance of brown rice in control and saline paddy fields measured by rice inspector.

Reference
1) Y. Hayashi et al.:RIKEN Accel. Prog. Rep. **40**, 253 (2007).

Table 1. Shoot length and yield components in control and saline paddy fields.

		Shoot length (cm)	Panicle number (/plant)	Grain number (/ panicle)	Fertility (%)	1000-grain weight (g)
WT[b]	control	100	17.7	98.7	96.6	26.6
	saline	88.2 (88%)[a]	26.7 (151%)	93.6 (95%)	89.9 (93%)	20.2 (76%)
6-99L[b]	control	113	13.3	97.9	95.7	27.5
	saline	102 (90%)	19.7 (148%)	94.7 (97%)	93.5 (98%)	22.9 (83%)
19-55[b]	control	97.2	18.2	99.8	96.0	27.0
	saline	86.0 (89%)	25.8 (142%)	95.5 (96%)	90.7 (94%)	20.9 (77%)
WT[c]	control	96.0	25.8	97.6	91.5	27.1
	saline	70.2 (73%)	17.2 (67%)	63.0 (65%)	85.8 (91%)	17.4 (64%)
19-74[c]	control	108	15.6	104.0	91.6	27.5
	saline	79.0 (74%)	14.2 (91%)	67.0 (64%)	81.1 (89%)	21.1 (77%)

[a] :Relative rate in the saline paddy field (saline/control × 100). [b] :Harvest in 2006. [c] :Harvest in 2007.

Table 2. Scores of eating quality test.

	Control Paddy field	Saline Paddy field
Nipponbare	3	2.63 ± 0.18
6-99	3.06 ± 0.16	2.86 ± 0.15
19-55	2.67 ± 0.31	1.61 ± 0.21

*1 Graduate School of Life Sciences, Tohoku University
*2 Chiba Prefectural Agriculture Research Center

Identification of blast resistance gene in Indica-type rice, Kasalath, using chromosome segment substitution lines.

H. Takehisa, M. Yasuda*[1], Y. Fukuta*[2], H. Nakashita*[1], T. Sato*[3], T. Abe

Rice blast caused by the fungal pathogen *Magnaporthe grisea* (*M. grisea*) is one of the most devastating rice diseases worldwide. The identification and utilization of resistance genes have been proven to be the most effective and economical approach to controlling rice blast disease. The indica cultivar Kasalath has been extensively used as a model cultivar known to be resistant to many Japanese blast fungus races. To determine the resistance mechanisms of Kasalath, we identified the blast resistance gene(s) to *M. grisea* race Hoku1 (Japanese blast fungus) by using chromosome segment substitution lines (CSSLs).

We used 52 CSSLs. The CSSLs were developed from backcrosses of rice varieties Nipponbare and Kasalath. The genotype of each line was determined using 214 RFLP markers distributed along the 12 rice chromosomes. Therefore, these CSSLs can be used as a permanent mapping population. The seeds were imbibed in distilled water at 30℃ for 2 days. Germinated seeds were sown on a synthetic culture soil (Gouseibaido No.3; Mitui-Toatu, Ltd., Tokyo, Japan) in seedling cell trays (30 cm×60 cm) in a greenhouse for 2 weeks before inoculation. Four-leaf-stage plants were used for the experiments. Pretreatment with water was performed by drenching the soil. Five days after pretreatment, challenge inoculation with Hoku1 was performed on the pretreated leaves. In the rice blast assay, plants were sprayed with Hoku1 conidia suspension (105 spores/mL), kept at 100% humidity for 16 h, and then incubated for 5days in a greenhouse (25°C). Infection on leaf-4 was calculated 5 days after inoculation. The disease reaction of the inoculated plants was evaluated 12 days after challenge inoculation.

Kasalath and Nipponbare exhibited resistance and susceptibility to Hoku1, respectively. There were 10 resistant lines and 42 susceptible lines among the 52 CSSLs. Two resistant lines (CSSLs 27 and 28) had the Kasalath chromosome segment on chromosome 6 (Figure1, A). This indicated that there was a blast resistance gene on chromosome 6 of Kasalath. However, the 8 other lines (CSSLs 2, 5, 20, 26, 29, 32, 38, and 41) with a Kasalath segment on chromosome 6, exhibited susceptibility. These results suggest that the Kasalath blast resistance gene was located between the *C1478* marker and the *R2123* marker according to these genotypes. Moreover, 7 other resistant lines (CSSLs 9, 12, 13, 47, 48, 49 and 50) had the Kasalath segment on chromosome 11 (Fig. 1, B). However, 6 other lines (CSSLs 2, 18, 43, 44, 46 and 51) with the Kasalath segment on chromosome 11 showed susceptibility. These results suggest that the resistance gene was located between the *S14061* marker and the *C535* marker in chromosome 11 according to these genotypes and that Kasalath has two genes that express resistance to Hoku1.

Near the two genes are the loci of the resistance genes *Piz* and *Pia*, respectively (Table 1, A and B). The monogenic lines carrying *Pia* showed susceptibility to Hoku1 (data not shown). Therefore, it is considered that the Kasalath blast resistance gene on chromosome 11 is a novel gene. In contrast, each monogenic line carrying *Piz*, *Piz-t, Piz-5* and *Pi9* at the *Piz* locus showed resistance to Hoku1 (data not shown). However, when these monogenic lines showed resistance to other blast isolates, Kasalath showed susceptibility to them (data not shown). This means that Kasalath did not have *Piz*, *Piz-t, Piz-5* and *Pi9*. These results suggest that the Kasalath blast resistance genes at chromosomes 6 and 11 might be novel. In our study, we identified the novel blast resistance gene in Kasalath using CSSLs.

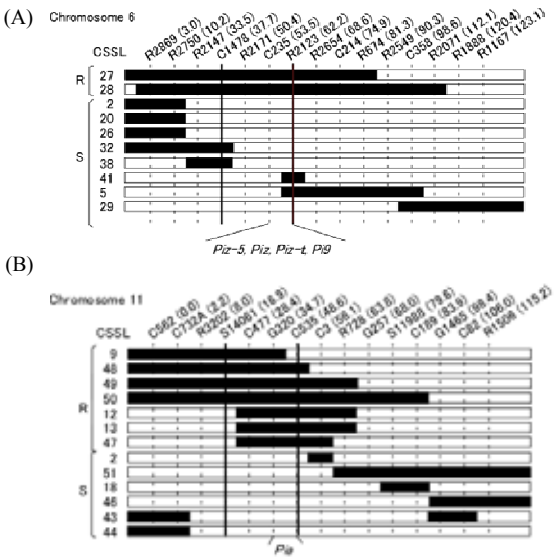

Figure1. Graphical genotypes of CSSLs which had the Kasalath chromosome segments on chromosome 6 (A) and 11 (B), respectively. The accession number of CSSL, the DNA markers (slanting numbers) and genetic distance (the numbers in parentheses) were according to the database of Rice Genome Research Center. White and black bars indicated the Nipponbare and Kasalath chromosome, respectively. *Pi-genes* were known blast resistance genes. R = resistant; S = susceptible

*1 RIKEN Discovery Research Institute
*2 JIRCAS
*3 Graduate School of Life Science, Tohoku University

IV. OPERATION RECORDS

1. Operation of RIBF

RILAC operation

E. Ikezawa, T. Ohki,* M. Kase, O. Kamigaito, T. Nakagawa, N. Sakamoto, H. Okuno, M. Wakasugi, N. Fukunishi, M. Kobayashi-Komiyama, M. Kidera, Y. Higurashi, H. Ryuto, T. Watanabe, K. Yamada, S. Kohara, M. Fujimaki, M. Nagase, T. Kageyama, S. Yokouchi, T. Aihara,* H. Yamauchi,* A. Uchiyama,* K. Oyamada,* R. Koyama,* M. Tamura,* A. Goto, and Y. Yano

* SHI Accelerator Service Ltd.

Throughout this reporting period, RILAC has been in steady operation and has supplied various ion beams for various experiments. Table 1 shows some statistics for the RILAC operation from January 1 through December 31, 2007. For the beam commissioning of the RI Beam Factory (RIBF), 0.67 MeV/nucleon ^{238}U and 2.68 MeV/nucleon ^{86}Kr ion beams accelerated by RILAC were injected intensively into the RIKEN Ring Cyclotron (RRC) 11 times in total from January through November 2007. Therefore, the percentage of the beam service time for injection into RRC was approximately 96% of the total RILAC beam service time. A ^{238}U ion beam was used for the first time in a research experiment at RIBF. The mechanical troubles encountered hardly affected the operation time schedule throughout this reporting period.

Table 1. Statistics for RILAC operation from January 1 through December 31, 2007.

Operation time of RILAC	3338.5 hr
Beam service time of RILAC	2497.5 hr
Mechanical trouble	0.0 hr
Beam service time of RILAC standalone	100.5 hr
Beam transport to RRC	2397.0 hr

Table 2. Beam service time of RILAC standalone allotted to each beam course in the No. 1 target room of RILAC in 2007.

Beam course	Total time (hr)	%
e2	40.5	40.3
e3	60.0	59.7
e4	0.0	0.0
Total	100.5	100.0

Table 2 shows a summary of the beam service time of the RILAC standalone allotted to each beam course (e2, e3, and e4) in the No. 1 target room of RILAC in 2007. Compared with one year ago, the beam service time of the RILAC standalone decreased by approximately 96%, because the beams commissioned by RIBF were mainly provided and research experiments on the heaviest elements, which are performed by standalone operations, were not carried out.

Table 3 shows statistics for the operation times of the 18 GHz ECR ion source (18G-ECRIS) and the superconducting ECR ion source (SC-ECRIS) in 2007. The percentages of the operation times allocated to 18G-ECRIS and SC-ECRIS were approximately 97% and 3% of the total ion source operation time, respectively. The ion beams of 6 elements were used in various experiments, beam acceleration tests, and beam commissioning.

Table 3. Operation statistics for two ion sources (18G-ECRIS and SC-ECRIS) in 2007. The operation times using SC-ECRIS are indicated in parentheses.

Ion	Mass	Charge state	Total time (hr)
Mg	26	7	143.0 (0.0)
Ar	40	11	0.0 (55.5)
Kr	86	18	728.0 (0.0)
Xe	136	20	12.0 (57.0)
Os	188	24	81.0 (0.0)
U	238	14, 35	2262.0 (0.0)
	Total		3226.0 (112.5)

We carried out the following improvements and overhauls during this reporting period.

1) The beam transport line between 18G-ECRIS and the analyzing magnet was modified. An electrostatic focusing system, which combined an accelerating electrode and a decelerating electrode, was newly installed.

2) The beam transport line between RILAC and RRC was modified. An existing rebuncher was moved from the connecting room between RRC and RILAC to the No. 2

target room of RILAC. In addition, another rebuncher was moved from the injection beam line slightly after AVF to immediately before RRC and after the merging point of two injection beam lines from AVF and RILAC. Some quadrupole magnets, Faraday cups, beam profile monitors and phase probes were also newly installed to complement the existing ones.

3) Coaxial cables for the rf reference signal and for the detection signals of rf amplifiers and rf cavities were replaced with new ones.

4) A system to monitor the beam phase and the voltage and phase of the acceleration rf was developed using a lock-in amplifier (model SR844). This system helps us to recover the beam phase easily from the shift by readjusting the rf parameters. Details of the system are reported elsewhere in this issue.[1)]

5) A vacuum chamber of the 90° bending magnet (DMe1) was replaced by a new one. The internal surface of the new chamber was reinforced with 1-mm-thick tantalum plates. A beam monitor was equipped in the new chamber to detect stray beams.

6) Three pumps and a heat exchanger of the water cooling system were overhauled. The other water pumps were subjected to a simple inspection.

7) Plate power supplies at the final stages of rf systems were subjected to annual inspection.

8) Flow switches for the lower-limit detection in the No. 1 rf power amplifier were replaced with new ones, because they were worn out after many years of operation.

We experienced the following mechanical problems during this reporting period.

1) SC-ECRIS suffered insulation failure between the plasma chamber and the solenoid coil.

2) The No. 1 rf power amplifier was splashed with water due to a puncture of the nylon tube.

References

1) R. Koyama et al.: in this issue.

AVF operation

Masayuki Kase, Noritoshi Tsukiori*2, Tadashi Kageyama, Yukimitsu Ohshiro*1,
Nobuhisa Fukunishi, Takahide Nakagawa, Osamu Kamigaito, Hiromichi Ryuto, Hiroki Okuno, Naruhiko Sakamoto,
Masanori Kidera, Masanori Wakasugi, Misaki Kobayashi-Komiyama, Yoshihide Higurashi, Makoto Nagase,
Shigeo Kohara, Shigeru Yokouchi, Kazunari Yamada, Takeshi Maie, Kiyoshi Kobayashi*2, Ryuichi Ohta*2,
Minoru Nishida*2, Kunikazu Masuda*2, Yasuteru Kotaka*2, Seiji Fukuzawa*2, Takeshi Nakamura*2, Ryo Koyama*2,
Kazuyoshi Yadomi*2, Shigeru Ishikawa*2, Makoto Hamanaka*2, Kazuo Miyake*2, Akira Goto, and Yasushige Yano
*1 Center of Nuclear Science, the University of Tokyo
*2 SHI Accelerator Service Ltd.

Table 1 shows the statistical data of the AVF cyclotron (AVF) operation from January to December 2007 together with the data obtained in the previous year. The total operation time in 2007 was the almost same as that in 2006. The operation of AVF-RRC has been at low level since 2006, because the RRC was frequently operated with the RILAC for RIBF commissioning.

The total operation in the AVF stand-alone in 2007 decreased by 20% compared with that in 2006. However, experiments in CRIB were performed very actively in 2007. 13 types of the CRIB experiments, which have been under control of the Center of Nuclear Study of the University of Tokyo (CNS), were carried out in 2007. The backlog of CRIB experiments, which had been approved by PAC became few.

The annual beam-time for student experiments as part of curriculum of the University of Tokyo were performed four times as usual in the second half of 2007.

Supply of RI, in agreement between RIKEN and Japan Isotope association, started officially in October 2007. Concerning this, the beam times for production of two types of RI, ^{65}Zn and ^{109}Cd, were carried out at the C03 beam course in November and December, respectively.

The upgrading of the AVF is in progress in cooperation with CNS. In this program, the more attractive beam has been pursued, with high energy and with strong intensity. It will expend the availability of RI beams at CRIB and strengthen the capability of ri production using an intense and energetic proton beam at C03. In 2007, the following two projects were in progress. First the beam trajectory in the AVF injection area was investigated to get higher energy efficiently in the single-harmonics mode in cooperation with DSR of Russia. Second a high rf voltage became available in higher frequency range by adjusting the capacitance of the coupling condenser in the rf amplifier.

Table 1. Statistical data of AVF operation in 2006 – 2007.

Year	2006	2007
Total operation time	3963 hr	3669 hr
Beam tuning	853 hr (22 %)	767 hr (21 %)
Injection to RRC	1051 hr (27 %)	1235 hr (34 %)
AVF stand-alone	2059 hr (52 %)	1667 hr (45 %)
Beam course (AVF stand-alone)		
E7a (CRIB)	1275 hr (62 %)	1289 hr (77 %)
E7b	257 hr (12 %)	0 hr (0 %)
C03	527 hr (26 %)	378 hr (23 %)

RRC operation

Masayuki Kase, Noritoshi Tsukiori*2, Eiji Ikezawa, Tadashi Kageyama, Nobuhisa Fukunishi, Takahide Nakagawa, Osamu Kamigaito, Hiromichi Ryuto, Hiroki Okuno, Naruhiko Sakamoto, Masanori Kidera, Masanori Wakasugi, Misaki Kobayashi-Komiyama, Yoshihide Higurashi, Makoto Nagase, Shigeo Kohara, Masaki Fujimaki, Shigeru Yokouchi, Kazunari Yamada, Yukimitsu Ohshiro*1, Kiyoshi Kobayashi*2,Ryuichi Ohta*2, Minoru Nishida*2, Kunikazu Masuda*2, Yasuteru Kotaka*2, Seiji Fukuzawa*2, Takeshi Nakamura*2, Ryo Koyama*2, Kazuyoshi Yadomi*2, Shigeru Ishikawa*2, Makoto Hamanaka*2, Kazuo Miyake*2, Akira Goto, and Yasushige Yano

*1 Center of Nuclear Science, the University of Tokyo.

*2 SHI Accelerator Service Ltd.

Table 1 shows the statistical data of the RIKEN Ring Cyclotron (RRC) operation for the year 2007, together with those in 2005 and 2006. The total operation time in 2007 recovered up to 70% of that for 2005, after it had recorded the minimum of 40% in 2006 in the 20-year history of the RRC operation.

After the first beam of 345MeV/u ^{27}Al had been successfully extracted at the end of 2006, the RIBF commissioning followed in 2007 under the condition that the budget of power rates was limited only to a four-month operation in FY 2007 and that some of it was used for the new injector development in advance. Two kinds of beam were tested in RIBF, ^{86}Kr and ^{238}U. A total of 1845 hr was spent in the RIBF commissioning. In the case of Kr beam, the RRC provides the beam into the IRC, and in the case of U beam, into fRC.

On the other hand, the beam service time of the RRC for delivering beams directly to users in the Nishina building decreased markedly to 687 hr, being 42% of 2006 and only 16% of 2005. Owing to budgetary problems, the RRC operation was stopped intentionally even in time intervals between the RIBF beam tests. In July, which is one of three months when the special high rate summer power cost is imposed in weekdays, biological experiments were conducted in a weekend to save on the power cost.

Among the large backlogs of the RIPS (E6) experiments, which had been approved by the PAC, three of them were scheduled as a beam time in 2007 according to priority. One is the experiment on the vector analyzing power measurement for the p-^{8}He elastic scattering by using a 100MeV/n ^{18}O beam, which was conducted during the so-called golden week from the end of April to the beginning of May 2007. The second is that on the nuclear moment measurements of the isomeric state of ^{32}Al using a 95 MeV/n ^{40}Ar beam in the middle of October 2007. The third is a series of 1.5-day experiments on the development on the ion-trap technology, which ran five times in total in 2007.

An unscheduled shutdown of the RRC due to the machine troubles was a total of 100hr in 2007. 37% was due to the vacuum troubles in beam probes and another 37% was due to the troubles of magnet power supplies. A shutdown due to troubles in the rf system marked only 13%.

Table 1. Operation statistical data of RRC from 2005 - 2007.

Year	2007	2006	2005
Operation time of RRC	3757 hr	2853 hr	5730 h
Beam service time	687 hr	1628 hr	4201 h
RIBF commissioning	1845 hr	496 hr	-
Machine troubles	150 hr	75 hr	1394 h
Nuclear physics experiments	48 %	65 %	78 %
Non-nuclear physics experiments	52 %	35 %	22 %
RILAC-RRC operation	72 %	36 %	33 %
AVF-RRC operation	28 %	64 %	67 %

Operation of the tandem accelerator

T. Kobayashi and K. Ogiwara

The tandem accelerator (Pelletron, 1.7MV) was operated for a total of 85 days for experiments during the annual reporting period from Jan.1 to Dec.31, 2007. A total of 35 days was spent for machine inspection, troubleshooting, beam test and recovery for electric power failure.

Compared to the previous year, the operation days decreased by 15% because a group studying semiconductor crystal growth control terminated the evaluation experiments. An application for constructing a new beam line for capillary beam focusing was accepted at the operation meeting.

The accelerated ion species in this period are H^+, He^+ and B^+ with energies from 1.5 to 2.5 MeV summarized in table 1.

Experimental studies on the following subjects were performed, and are still in progress.

(1) Nuclear reaction analysis (NRA) using $^1H(^{11}B,\alpha)2\alpha$ reaction (54days)

(a) The state of hydrogen in Nb-based and Ta-based alloys, and V as investigated by the channeling method

(b) Effect of irradiation on the state of hydrogen in metals

(2) Particle-induced X-ray emission (PIXE) (12days)

(a) Development and application of a highly sensitive high-resolution in-air PIXE system for chemical state analysis

(b) Trace element analysis of biological and environmental samples using energy dispersive X-ray spectrometry

(3) The analysis using elastic scattering (19days)

(a) Rutherford backscattering spectrometry (RBS) analysis of polymers, carbon materials.

(b) Ion channeling RBS analysis of epitaxial thin films grown on Si substrates.

(c)Elastic recoil detection (ERD) analysis of diamond-like carbon (DLC) thin films and ion-implanted polymers for determining hydrogen distribution.

Table 1 The beam conditions and the analysis techniques of the tandem accelerator

Ion	Energy [MeV]	Beam current [nA]	Analysis	Operation time [days]
$^1H^+$	1.6 – 2.5	30 – 50	PIXE	12
$^4He^+$	1.5 – 2.3	3 – 18	RBS, ERDA	19
$^{11}B^+$	2.0	1.0 – 1.5	NRA	54

Status of RIBF Control System

Misaki Kobayashi-Komiyama, Akito Uchiyama,[*1] Takeshi Nakamura,[*1] Masaki Fujimaki, and Masayuki Kase

The current structure of the EPICS-based control system of the RIKEN RI-Beam Factory (RIBF) is shown in Fig. 1. Three components have been improved since last year. The first improvement is that the server computer for the control of N-DIM, PLC, GP-IB devices and a network-based CAMAC crate controller (CC/NET) was replaced with high-availability cluster system. In this paper, a high-availability cluster system refers to a system in which all programs running on it continue to run without any interruption even if a computer malfunctions, and all programs and data are stored in the system without any loss in the cause of a malfunction. We constructed such a system using two sets of new server computers, each one including a RAID1 system (DELL PowerEdge SC1435). During normal operation, all control programs run on the main computer, and the other computer is on standby. Both computers send a heartbeat signal each other every two seconds to determine each other's status. When the main computer has a problem, the second computer immediately takes over all its tasks without any interruptions and starts running them. This changeover is performed very smoothly, and no change in the beam operation is detected by the users.

The second improvement is the upgrade of the server computer for NIO control to a high-availability cluster system. In this case, we constructed the system using the current server computer as the main computer, and we set up a new standby computer (DELL PowerEdge 860). Details of these improvements are discussed in Ref.1. As a result of these improvements, a reduction in the probability of beam service interruption due to computer malfunction is expected and system maintenance is expected to be simpler and lesstime-consuming.

The final improvement is the replacement of an old CAMAC crate controller with a CC/NET. In our control system, an old CAMAC crate controller is controlled by a VME computer, which is difficult to maintain because of its age. The purpose of this replacement is to retire the VME computer. There are six CAMAC crates in the Nishina building and one in the Linac building, and one of the crate controllers in the Nishina building and the Linac controller were replaced with CC/NETs about four years ago. The remaining crate controllers in the Nishina building were replaced this year. In this replacement, we stopped using crate number 2 and rearranged the cables from the devices for use in a crate number 1. The current crate number 1 was moved from room B of magnet power supplies (BPS) to the front of BPS in the corridor. All the DIM are now controlled using CC/NET and we are tuning the system so that it operates stably.

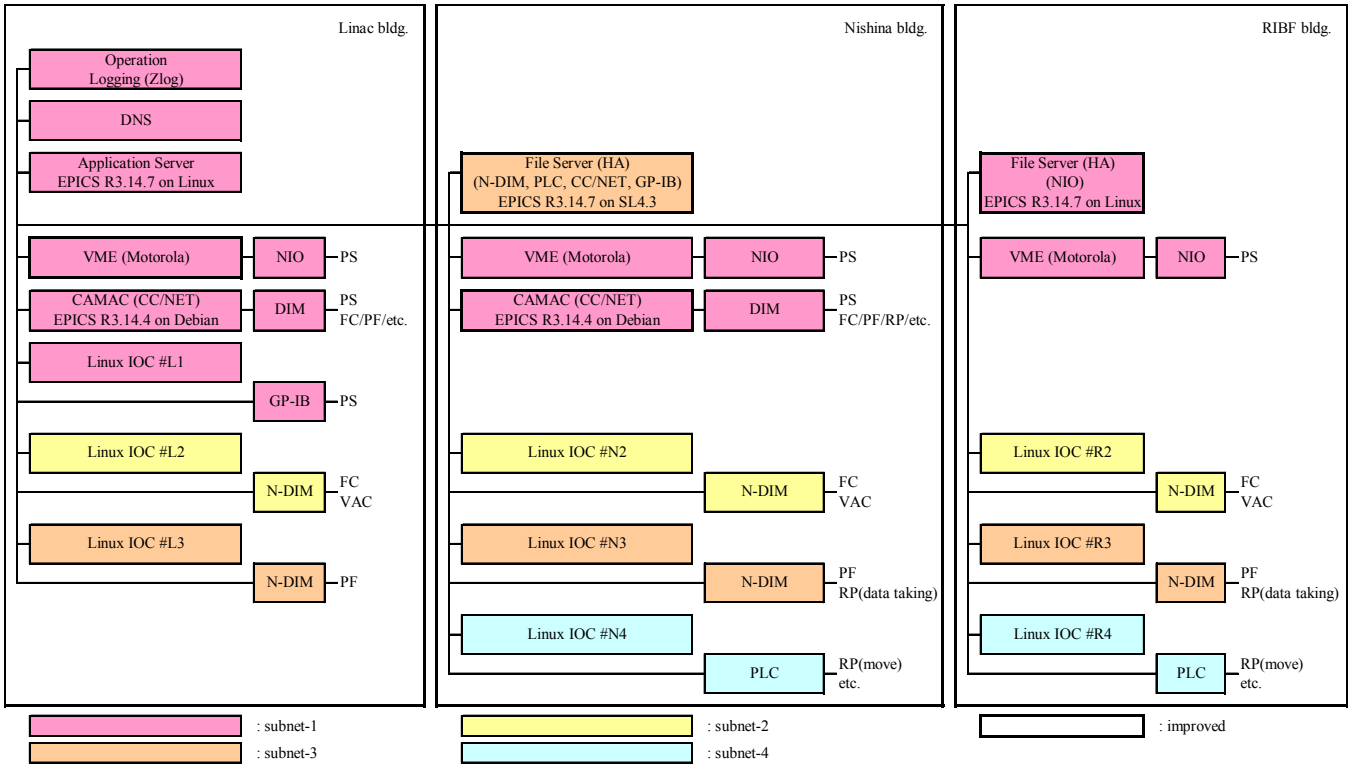

Fig. 1. Structure of RIBF control system.

[*1] SHI Accelerator Service, Ltd

The arrangement of the Beam Interlock System (BIS) has been progressed. Many new interlock signals from devices such as magnet power supplies or vacuum gate valves in beam transport lines were connected to the BIS. In addition, we set up a network router between the network of the EPICS control system and the BIS to monitor signals from the BIS in the EPICS program. The BIS is composed of Melsec PLCs, and its GUIs were developed using Melsec Soft GOT programs. Many useful GUIs have been prepared to monitor the signals of the BIS; however, there are no GUIs for monitoring the status of DI channels grouped by DO channels. In other words, there are no GUIs for monitoring the relation between a DI/AI channel and a DO channel at a glance. We know the recent histories of twenty interlock signals in a line at the BIS monitor, and all the history can be found in files; thus, when a Faraday cup is inserted into a beam transport line by BIS, we can use them to discover the faulty channel number. However, when multiple Faraday cups are inserted into a line at the same time and multiple faulty channels are listed on a monitor, we need another file to determine their relationship. We often have such an experience, particularly when we change the setup of accelerators for a new experiment. Thus, we decided to create a new GUI to determine the relation between the DI/AI and DO channels in EPICS because we are not familiar with SoftGOT programs. To obtain BIS information, an EPICS program sends a command to a PLC of the BIS. We speculated that the speed of communication among the BIS stations would be reduced by this new program; however, it had no effect on the speed. We created GUIs to monitor the DI channels grouped by DO channels, which is very useful during a beam operation.

We are now investigating the construction of a database for all parameters of the accelerators, EPICS signals and non-EPICS signals, in which they are recorded in a single time axis. We have found one possible system, and have started its construction and testing.

References

1) A.Uchiyama et al.: in this report.

Present Status of the BigRIPS Cryogenic Plant

K. Kusaka, M. Ohtake, T. Kubo, K. Yoshida, A. Yoshida, T. Ohnishi, Y. Yanagisawa, N. Fukuda, Y. Yano,
M. Nobutoki,[*1] H. Ito,[*2] N. Kakutani,[*2] T. Tsuchihasi,[*2] and K. Sato[*2]

The BigRIPS separator[1] is characterized by its superconducting triplet quadrupoles (STQs). The five STQs (STQ1 – STQ5) on the first stage of BigRIPS are cooled by a large liquid helium cryogenic plant, which consists of a Linde-TCF50S refrigerator, a Maekawa 315 kW compressor unit, one 10 m^3 and two 100 m^3 helium buffer tanks, a 2000 L liquid helium Dewar vessel, and a 50-m-long transfer line as its main components. The whole cryogenic system, including the STQ's was fabricated by Toshiba Corporation and Taiyo Nippon Sanso Corporation, and installed in the RIBF building in the beginning of 2004. The design of the system is described in ref. 2.

A stand-alone test of the cold box and heat-load measurements of the transfer line were performed in March and April 2004.[3] The first cooling operation of the whole system was performed in October and November 2004.[4] The pressure of the isolation vacuum of the transfer line increased in the refrigerator-mode operation, and a helium leakage was discovered. The origin of the leak turned out to be a pinhole in the cryogenic valve of STQ1. The leak was fixed and some improvements of the 70 K shield of the transfer line and the valve boxes were performed from April to August 2005. Heat-load measurements were carried out again in August 2005. The improved results and the estimated excess cooling capacity are summarized in Table 1.

The second cooling operation was performed in May and June 2006. After one week of purification operation and a stand alone test of the cold box, STQ1-STQ5 were cooled from the room temperature to 4 K in 16 days, and it took another 4 days to fill the cryostats and the Dewar vessel with liquid helium. Figure 1 shows the cooling curves of the STQs together with the temperature of the supply helium and return helium.

Within 43 days of continuous operation in the refrigerator mode, excitation tests of STQs, and the simultaneous excitation of all the BigRIPS magnets were successfully performed without quenching. We also verified that the magnetic axis of STQs did not differ from the optical axis. The transfer of liquid helium from the Dewar vessel to the STQ1 cryostat, in the case of quenching, was performed and the resulting transfer rate was estimated to be 180-200 L/h. Utilizing the spare heater installed in each cryostats, liquid-level control tests were performed while varying the power of the spare heaters. By introducing a new control sequence of the 4 K return valve to keep the pressure of the 4 K return-line constant (~0.038 MPaG), we have succeeded in the automated control of the liquid helium level in the cryostats.

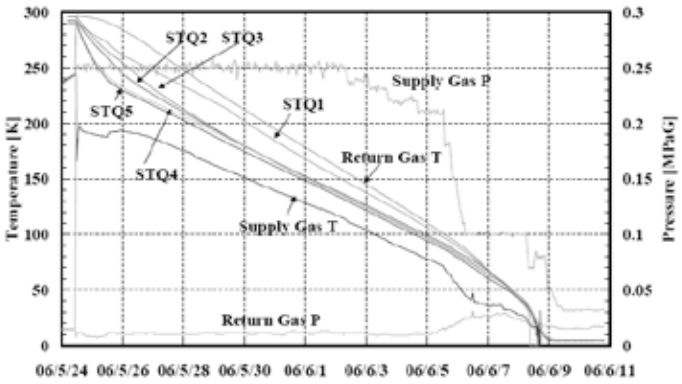

Fig. 1. Cooling curves of STQs in the precooling period. The temperature and pressure of the supply gas and return gas are also shown.

Continuous operation of the BigRIPS cryogenic plant started in October 2006. The operational record from October 2006 to July 2007 is summarized in Fig. 2. The beam time of the BigRIPS commissioning is also shown.

Table 1. Cooling capacity and heat loads of the BigRIPS cryogenic plant.

	4K Load		80K Load	
	Design	Measured	Design	Measured
Transfer line (total) [W]	101	101	403	486
(items: Transfer tube / Valve box (STQ1-5))	(61.5 / 39.5)	(47 / 54)	(358 / 45)	(362 / 124)
Liquefier load for current leads [W] ([g/s])	88 (0.91)	70 (0.71)	-	-
Cryostat load (STQ1-5) [W]	18	16	225	225
Total heat load [W]	207	187	628	711
Cooling capacity of cold box [W]	390	509.3	700	906.5
Excess cooling capacity [W]	183	322.3	72	195.5

*1 Taiyo Nippon Sanso Corporation
*2 Toshiba Corporation

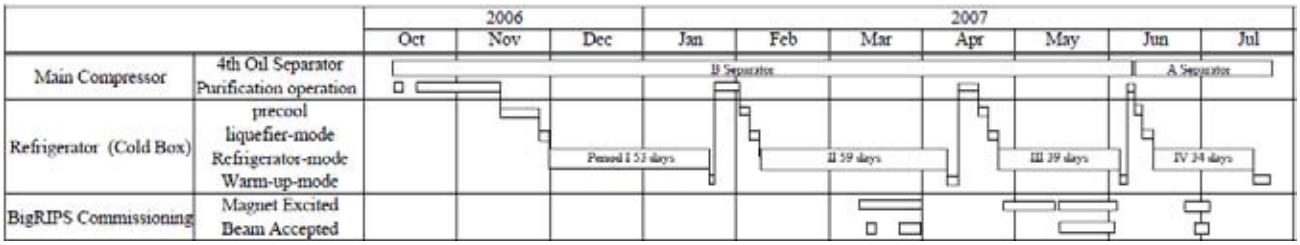

Fig. 2. Operational record of the BigRIPS cryogenic plant.

In the first operation cycle from October 2006 to January 2007, contamination of the helium gas occurred on October 11, 2006, which was caused by the incorrect operation of the gas-analyzer system attached to the cryogenic plant. After 23 days of the purification, including the evacuation of all the lines in the cold box, the room-temperature gas lines around the compressor unit, and the power-lead gas lines, the impurity concentrations of the helium gas were improved to N_2: 0.4-0.5 ppm, H_2O: ~0.1 ppm, and O_2: ~0.5 ppm, although the N_2 concentration at the beginning of the purification was too large (> 200 ppm) to measure.

The precooling was started on November 17, 2006. Since the temperature of STQ1 was 271 K, which was much higher than those of STQ2-STQ5 (175-196 K), we started the precooling operation so that the cold gas from the cold box circulated only in the transfer lines. The magnets were connected to the system when the temperature of the supply gas and return gas matched that of the magnets. This took place after 15 days of precooling and 4 days in the liquefier mode with an average liquefaction rate of ~50 L/h.

After 3 weeks of steady operation in the refrigerator mode, the power of the heater in the phase separator (PS), which corresponds to the excess cooling capacity, started decreasing gradually and the temperature of the 70 K-shield supply gas began to rise. On the 40th day in the refrigerator mode, the power of the PS heater dropped to zero and the liquid level in the PS started decreaseing. We stopped the refrigerator after 53 days of operation in the refrigerator mode, since we could not keep the liquid helium levels in cryostats STQs constant. The temperature and pressure of the 70 K-shield supply gas were ~90 K and ~1.55 MPaG, whereas they were ~55 K and ~1.58 MPaG at the beginning of the steady operation, respectively.

We initiated the warm-up operation by disconnecting STQs from the cold box. Evaporating gas was sent to the buffer tank using the recovery compressor. After stopping the expansion turbines, we closed the valves of the 80 K adsorbers to separate the first and second heat exchanger sections (EX1 and EX2), where impurities in the helium gas blocked the gas flow from the cold end. To increase the speed of the warm-up process we introduced dry nitrogen gas into the isolation vacuum of the cold box up to a pressure of 5 Torr. We measured the impurity concentrations on-line during the warm-up operation and the peak N_2, H_2O, and O_2 concentrations were 21 ppm, 2 ppm, and 4 ppm, respectively. We also analyzed the gas in the EX1 and EX2 sections off-line using a gas chromatograph. Only the N_2 concentration was measured to be 13 ppm.

After evacuating high-pressure section of the cold box we performed a purification operation such that the impurity concentrations in the helium gas were improved to N_2: 0.6-0.7 ppm, H_2O: ~0.0 ppm, and O_2: ~0.9 ppm. We then started the precooling operation. It took 12 days for the warm-up and the purification and 7 days for the precooling and the liquefier-mode operation.

As shown in Fig. 2, we have repeated the warm-up of the cold box and have recooled the magnets in the same way as that in the first operation cycle in accordance with the BigRIPS beam time schedule. Figure 3 shows the flow rate of the first expansion turbine T1 in the steady-operation period I-IV, shown in Fig. 2, which is a measure of cooling capacity. Although the T1 flow rate depends on the pressure at the entrance of T1, which can be set manually, it is mainly determined by the 70 K-shield pressure upstream of the T1 entrance. The unusual decreasing tendency of the shield pressure with time can be seen in Fig. 3.

We realize that the purity control of the helium gas is very important. We are introducing a gas chromatography system, a dew point meter, and an oxygen sensor to measure impurity concentrations. A new method of controlling the suction pressure of the compressor using a precise pressure sensor is also being introduced to avoid the possible penetration of air into low-pressure lines.

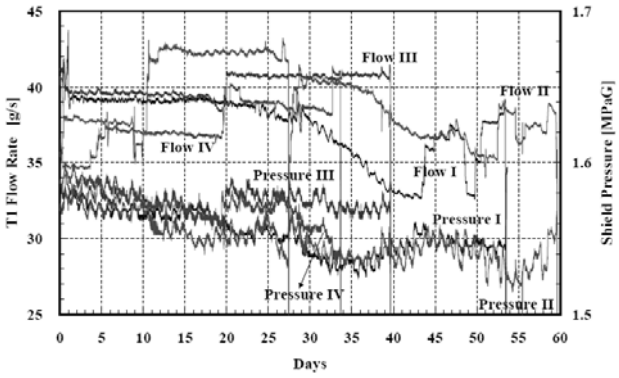

Fig. 3. T1 flow rates as functions of the operation period in the refrigerator mode. Labels I - IV denote the operation periods shown in Fig. 2. The temperature and pressure of the supply gas and return gas are also shown.

References

1) T. Kubo et al: IEEE Transactions on Appl. Supercond. **17**, 1069 (2007).
2) T. Kubo et al.: RIKEN Accel. Prog. Rep. **36**, 316 (2003).
3) T. Kubo et al.: RIKEN Accel. Prog. Rep. **38**, 289 (2005).
4) K. Kusaka et al.: RIKEN Accel. Prog. Rep. **38**, 291 (2005).

Present Status of STQ system in BigRIPS and RI-Beam Delivery Line

K. Kusaka, M. Ohtake, T. Kubo, K. Yoshida, A. Yoshida, T. Ohnishi, Y. Yanagisawa, N. Fukuda, Y. Yano,
H. Ito,* T. Miyase,* N. Kakutani,* T. Tsuchihasi,* and K. Sato*

The BigRIPS separator and the RI-Beam delivery line in the RIBF project are characterized by the superconducting triplet quadrupoles (STQs).[1] Although the five STQs (STQ1 ~ STQ5) on the first stage of the BigRIPS are cooled by a large liquid helium cryogenic plant[1,2], all the STQs on the second stage of the BigRIPS (STQ6~STQ14) and those of the RI-beam delivery line (STQ15~STQ23) are cooled by a stand-alone refrigeration system with small cryocoolers on their cryostat.[1,3]

All the STQs of the BigRIPS separator (STQ1~14) were fabricated and tested at Toshiba factory. Since the infrastructures of the RIBF facility, such as cooling water systems, were not ready for operation, they were warmed up and shipped to RIKEN in 2004. Only the five STQs (STQ1~STQ5) were installed on site and the rest (STQ6~STQ14) were stored in the BigRIPS hall in the RIBF accelerator building.

From February 2005 to February 2006, STQ6~STQ14 were cooled down from room temperature to 4 K and the GM coolers for 80K-shield and high-T_c superconducting (HTSC) power leads and GM/JT coolers for the 4K vessel began continuous operation. The precooling of the cold mass from room temperature to 80K was performed by transferring 3000~5000 L of liquid nitrogen into the cryostat with the GM cooler in operation. The precooling from 80 K to liquid helium temperature was performed by transferring ~2000 L of liquid helium from dewars (Fig. 1). After we confirmed the liquid helium in the helium vessel using the liquid level sensor, the GM/JT cooler was mounted on the cryostat. Figure 2 summarizes the amount of the transferred cryogen in the precooling of STQ6~STQ14.

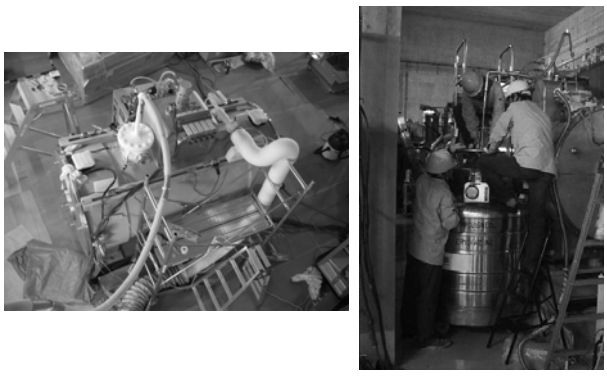

Fig. 1. Precooling by transferring liquid nitrogen (left). Transferring liquid helium from dewar (right).

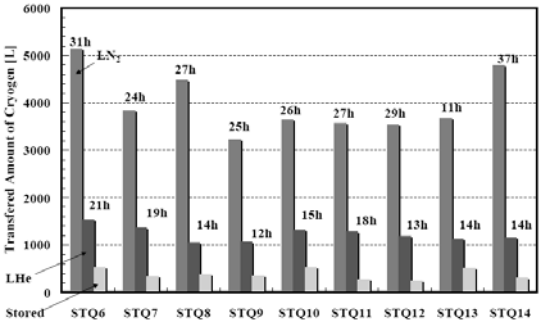

Fig. 2. Summary of amounts of transferred liquid nitrogen and liquid helium in precooling STQ6~STQ14. The total transfer times are also indicated.

STQ15, which is the first focusing element of the RI-delivery beam line, was fabricated in 2004~2005 and shipped to RIKEN in early 2005. STQ15 was shipped in a cooled state and kept at liquid-helium temperature in the BigRIPS hall by operating small cryocoolers. The installation of the STQ6~STQ15 on site began in January 2006. All the STQ's were installed and aligned in their cooled state. The installation and alignment of all the BigRIPS magnets and most of the cabling and plumbing were completed in the spring of 2006.

Excitation tests on STQ6~STQ14 were performed from May to June 2006. Excitation tests of STQ1~STQ5, cooled by the BigRIPS cryogenic plant, were also performed in the same period. The fine tuning of power supplies and interlock tests on the cryo-control panel (CCP) were also performed.

In the excitation tests on the Q500D of STQ9, an over-voltage of the HTSC power lead PL4 was detected. Although the temperatures of all the HTSC power leads PL1~PL5 were in the range of the design values 55~66 K, the voltage of PL4 at an excitation current of 2 A was measured to be 3 mV, which is much larger than the conventional value. The material of the HTSC power lead is Bi2223 whose T_C and I_C are ~80 K and 500~600A at 77 K, respectively, so that the voltage of the HTSC power lead in the STQs must be less than 1 mV even at a nominal excitation current of 142A.

STQ9 was then warmed up from July to August and the current lead port was opened. When the temperature of the cold mass became ~120 K (~1.5 month after stop running the cryocoolers), dry nitrogen gas was introduced in the isolation vacuum of the STQ9 cryostat. It took 2 months to warm the cold mass from 4 K to room temperature. The HTSC power leads PL2, PL4, and PL5

* Toshiba Corporation

were replaced with new ones, and we confirmed that PL4 was broken. Although the normal PL resistance at room temperature is within 10~20 mΩ, that of PL4 was measured to be ~167 mΩ. PL2 and PL5 were replaced to avoid possible damage that could be caused by the replacement of PL4. After the replacement, the isolation vacuum of the STQ9 cryostat was evacuated, and precooling was performed at the end of August 2006. The precooling took one week and 2000 L of liquid helium was consumed. By measuring the liquid helium consumption rate (~2.5L/h), the 4K heat load of the cryostat was confirmed to be the same as the result of the factory test (1.8W). Excitation tests were successfully performed in September 2006. A training quench of the SX coil occurred once at a current of +55 A, when it was simultaneously excited with Q500D (I = 142 A).

In the on-site excitation tests, held in the early summer of 2006, the temperatures of the HTSC power leads of STQ11 and STQ13 were found to be more than 10 K higher than that of other STQs. In September 2006, we performed another set of excitation tests on STQ6~STQ15 to measure the temperature rise ΔT of the HTSC power leads. Exciting Q500U and Q500D of each STQs one hour with a current of 142 A, the temperatures of all the power leads and the GM cooler head were recorded. It was found out that the ΔTs of the PL1, PL2, and PL4 on the STQ11 cryostat and the ΔT of the PL1 on the STQ13 cryostat exceeded ~4 K, while that of other power leads was less than 3 K, which is euqal to the design value. We have decided to warm STQ11 and STQ13 up in order to investigate the reason f or the large ΔT.

From mid October to November 2006, STQ11 and STQ13 were warmed up and thermal contacts of the power leads to the cooling Cu plate, where the GM cooler head is attached, were investigated with the current lead ports open. Since the beam time of the BigRIPS commissioning was planned in the beginning of 2007, STQ11 and STQ13 were warmed up within a month by introducing dry nitrogen gas into their isolation vacuum when all the liquid helium in the helium vessel evaporated. In both STQ11 and STQ13, the thermal contacts between the power leads and the cooling plate turned out to be insufficient. Although the bus bar attached to the HTSC power lead must be tightly connected to the cooling plate together with an aluminum nitride plate with indium, which is used as an electric insulator, some of the fastening bolts were loose. All contacts between the HTSC power lead and the cooling Cu plate and the contact of the thermo-couples to the current lead were improved, and STQ11 and STQ13 were recooled untill early December of 2006.

One-week continuous excitation tests on STQ11 and STQ13 together with STQ8 and STQ10 were performed in December 2006. STQ8 and STQ10 were chosen for the tests since their results of ΔT measurement were worse than the others. We confirmed that the fixed power leads of STQ11 and STQ13 were sufficiently cooled. However, the temperature of the PL4 of STQ8 turned out to be 12 K higher than that of the GM cold head, and ΔT was measured to be 6 K. Since we did not have sufficient time to warm up and fix STQ8 untill the BigRIPS commissioning, we replaced the compressor (U108) of the GM cooler with a larger one (U110) to enhance the cooling capacity of the GM cooler.

From March to June 2007, all the BigRIPS magnets were excited in time for the commissioning experiment of BigRIPS. Figure 3 shows a long-term trend of the power lead temperature of STQ8. During the commissioning period, all the STQs except STQ8 had stable operations. On May 28, 2007, the temperature of the PL4 of the STQ8 exceeded 70 K, which is set to the alarm level of the CCP-interlock system. We found that the temporarily replaced compressor U110 had oil leak and that the exposure pressure dropped to 1.5 MPaG from its typical value of 2.2 MPaG. To continue the commissioning beam time, we used the original U108 compressor with an exposure pressure of 1.9 MPaG. Although the PL4 temperature was only 3 K below the alarm level, we finish the commissioning without further problems.

From July to August, not only STQ8 but also STQ10 and STQ15 were warmed up and fixed of their thermal contact with the HTSC power leads. As stated above, the PL4 temperature is 14 K higher than that of the GM cooler head before the fixing. After the fixing of thermal contact, all the power lead temperatures approached within the range of 3 K from the GM head.

After the fixing of STQ8, STQ10, and STQ15, all the power leads of the BigRIPS STQs have been well cooled when the compressors and GM coolers were maintained on schedule. To establish the scheduled maintenance of GM/JT coolers, a series of R&D tests on the GM/JT cooler have been continuously performed since August 2007.

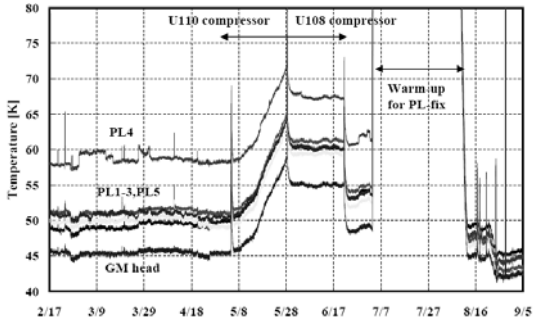

Fig. 3. Long-term trend of temperature of STQ8 power leads and GM cooler head. The sudden drop in temperature on June 21 was due to a recharge of the cryogen gas to the compressor, so that the exposure pressure changed from 1.9 MPaG to 2.2 MPaG.

References

1) T. Kubo et al: IEEE Transactions on Appl. Supercond.,Vol. 17, 1069 (2007).
2) K. Kusaka et al.: RIKEN Accel. Prog. Rep. 41, 244(2008).
3) K. Kusaka et al.: IEEE Transactions on Appl. Supercond., Vol. 14, 310 (2004).

Radiation Safety Management at RIBF

Y. Uwamino, S. Fujita, H. Sakamoto, R. Hirunuma Higurashi, H. Mukai[*1], A. Horigome, T. Yamaki, K. Igarashi, K. Nakano, N. Yukawa and Y. Sato

The cyclotrons of RRC and AVF were overhauled on schedule in the summer of 2007 after the end of operations with a 63 MeV/nucleon ^{40}Ar beam at RRC and with a 6 MeV/nucleon ^{19}F beam at AVF. Residual radioactivity was measured at various locations using an ionization-chamber γ-ray survey meter. The dose rate at the RRC deflector was found to be 4 mSv/h on September 18, 2007, which is 57 days after the end of operation, and that at the AVF deflector was found to be 13.5 mSv/h on August 20, 2007, which is 21 days after the end of operation. Figure 1 shows the variations in the dose rates at these deflectors since 1986. Owing to the long decay time of 57 days at RRC this year, the dose rate is smaller than the average of recent years. The beam intensity of AVF was increased for radioisotope production and dose rate also increased.

Residual radioactivity was measured along the beam lines after almost each experiment. The spots **a**–**x**, marked with solid circles in Fig. 2, are the places where the dose rates exceeded 20 μSv/h. Table 1 shows a summary of the observed dose rates and gives the dates on which the measurements were performed. The maximum dose rate was found to be 800 μSv/h at the RIKEN projectile-fragment separator (RIPS) target in the beam distribution corridor denoted by **q** in Fig. 2.

We continuously monitored the radiation in and around the RIBF facility using neutron and γ-ray area monitors, and the results at the site boundary and outside of the radiation controlled area are shown in Fig. 3. The data are average dose rates for each month including natural background radiation. The notations (g) and (n) denote gammas and neutrons, respectively. The environmental monitoring posts of Nos. 1-4 are placed near the site boundary. No. 1 is close to the Wako Daiyon Elementary School, No. 2 is in front of the Nishina building, No. 3 is close to Route 254 and No. 4 is close to the BSI Central Building. The computer room at the boundary of the radiation controlled area is on the ground floor immediately above a bending magnet that guides the beams from the RRC vault to the distribution corridor.

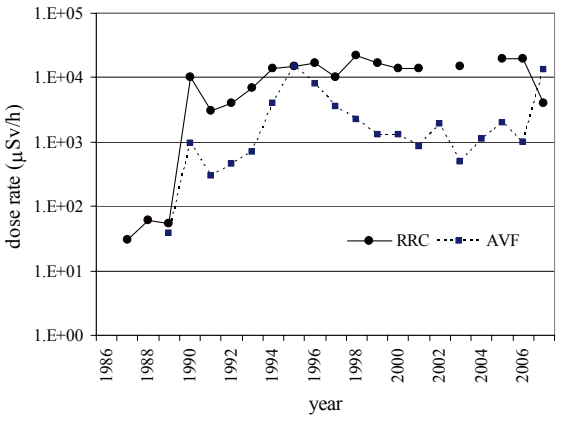

Fig. 1. Variation in dose rates at the deflectors of RRC and AVF since 1986.

Owing to the low background level, neutron dose is strongly affected by accelerator operation, and this situation is clear in the neutron dose in the computer room denoted "Comp. room (n)" in Fig. 3.

No accelerator was operated in August and September, and the dose rates at this period were assumed as the natural background. The net accumulated dose, that is, the dose after the subtraction of the background, of neutrons and gammas in the computer room in the year 2007 was 4.2 μSv, which was much lower than the allowable dose limit (5000 μSv/y). The variation in the annual dose for these 9 years is shown in Fig. 4. The value increased until 2005 and decreased thereafter owing to the operation conditions of RRC, that is, a short operation time for the RIBF construction and a dominant beam time of the low-energy uranium acceleration.

The variations in dose rates at the site boundary are very small owing to the small effect of the accelerator operation due to the long distances and thick shields. Since the amp gain of the No. 3 γ-ray monitor was corrected during the

Table 1. Summary of dose rates measured along beam lines with ionization-chamber survey meters. The points **a-x** indicate the measurement locations shown in Fig. 2.

Point	Dose rate (μSv/h)	Date (dd/mm)	Particle	Energy (MeV/u)	Intensity (enA)	Period (days)
a	110	31/8	B-11	4.6	1500	2
b	150	12/1	C-12	135	50	1.5
c	60	31/8	B-11	4.6	1500	2
d	400	31/8	B-11	4.6	1500	2
e	90	31/8	C-13	100	3700	1.5
f	90	31/8	C-13	100	3700	1.5
g	450	31/8	C-13	100	3700	1.5
h	180	30/11	C-12	135	200	0.5
i	60	12/1	C-12	135	50	1.5
j	50	12/1	C-12	135	50	1.5
k	25	27/7	C-13	100	3700	1.5
l	20	27/7	C-13	100	3700	1.5
m	50	27/7	C-13	100	3700	1.5
n	120	27/7	C-13	100	3700	1.5
o	100	27/7	C-13	100	3700	1.5
p	500	27/7	C-13	100	3700	1.5
q	800	27/7	C-13	100	3700	1.5
r	30	30/11	C-12	135	200	0.5
s	60	12/11	Kr-86	345	790	5
t	70	12/11	Kr-86	345	790	5
u	40	5/7	N-14	135	2400	2
v	400	5/7	N-14	135	2400	2
w	25	5/7	N-14	135	2400	2
x	200	12/11	Kr-86	345	790	5

*1 Japan Environment Research Corp.

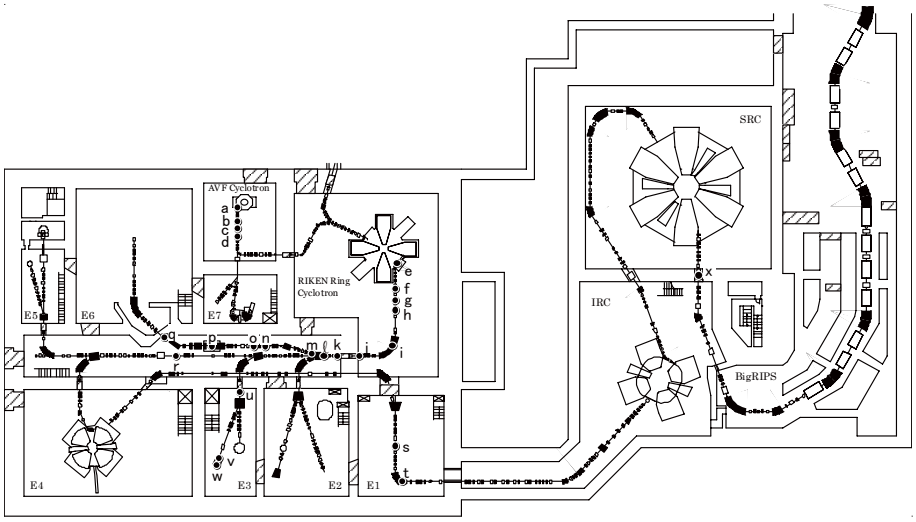

Fig. 2. Layout of RIBF beam line at Nishina building and RIBF accelerator building. Measurement locations of residual radioactivity are indicated by solid circles denoted **a**-**x**.

annual maintenance carried out in August, the dose rate shows a ramp in September, and the indicated dose rate up to August is smaller than the actual value. The net accumulated dose at any point of 2007 was smaller than the detection limit of about 20 μSv/y, which is mostly caused by the fluctuation in the natural γ radiation. The γ background is affected, for example, by rainfall, which collects the natural radioactivity of radon and its daughters in the air. The detection limit of neutrons is much smaller than that of gammas, and the maximum net accumulated dose of neutrons was 0.9 μSv/y, which was observed at No. 2. The shielding calculation[1] showed that the γ dose is comparable to or smaller than the neutron dose; nonetheless, the annual dose of neutrons and gammas at the site boundary was much smaller than the legal allowable limit (1000 μSv/y).

In addition to radiation safety, we took measures to cope with possible suffocation risk at the BigRIPS tunnel and SRC vault where a huge amount of helium is used in the superconducting magnets. The constructed device is a suffocation-safety interlock system (SIS) which is connected to the Houshasen ("radiation" in Japanese) Interlock System (HIS). If a low air concentration of oxygen or a quench at a magnet is detected, an alarm siren sounds and the beam is blocked in the latter case. The access doors and ventilation fans of the BigRIPS tunnel are controlled by SIS. The air concentration of the radioactive gas in the tunnel is also read by SIS, and the doors and fans are controlled depemding on this concentration.

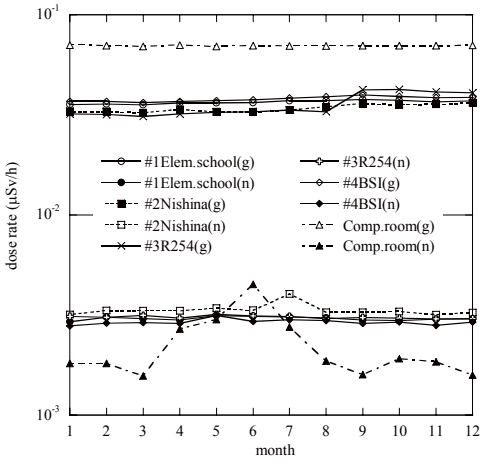

Fig. 3. Monthly dose rates at site boundary (#1 through #4) and boundary of radiation controlled area in 2007. (g) and (n) denote gammas and neutrons, respectively.

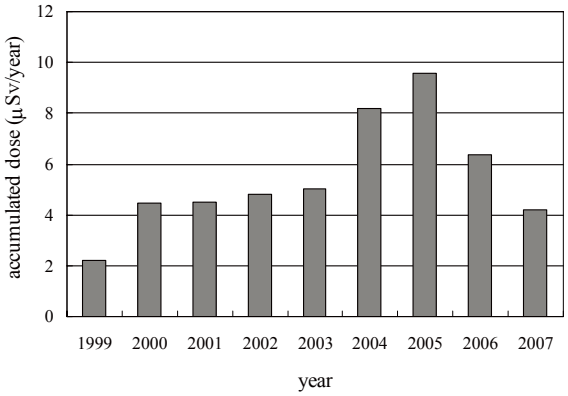

Fig. 4. Variation in accumulated leakage radiations at boundary of radiation controlled area since 1999.

Reference

1) Y. Uwamino, N. Fukunishi and K. Oishi: Proc. 9th Int. Conf. on Radiation Shielding, Tsukuba, Japan, 1999-10 (Sup. 1 J. Nucl. Sci. Technol., 2000), p146.

V. RECORDS OF LABORATORIES, GROUPS, AND TEAMS (Activities and Members)

Events of Nishina Center from Jan. 2007 to Mar. 2008

2007

16, Jan.	Commemorative lecture by Prof. T. D. Lee "Symmetry and Dynamical Symmetry, Commemorate the Decoration of the Order of the Rising Sun, Gold and Silver Star (Koshiba Hall, Univ. of Tokyo)"
16, Jan.	A Signing Ceremony for Memorandum of Understanding for RIKEN-BNL collaboration
16, Jan.	The 14th Meeting of The Management Steering Committee of RIKEN BNL Collaboration
9-10, Feb.	The 1st Program Advisory Committee for Nuclear Physics Experiments at RI Beam Factory
1, Feb.	The 1st Program Advisory Committee Meeting for Materials and Life
5, Feb.	The film shoot of the Hollywood movie "Jumper"
9-10, Feb.	The 1st Program Advisory Committee Meeting for Nuclear Physics experiments
12, Mar.	First successful extraction of Kr beam from the SRC
15, Mar.	First successful extraction of RI beam from BigRIPS
23, Mar.	First successful extraction of U beam from the SRC
25, Mar.	THE RIBF Users Informal Meeting
6, Apr.	Two isotopes of element 112 were observed at RIKEN using GARIS
3, Jun.	Symposium for Centennial Celebration of Hideki Yukawa
3, Jun.	International Nuclear Physics Conference (INPC2007)
3, Jun.	Discovery of very Neutron-rich new isotope Pd 125 (Z=46, N=79).
25-26, Jul.	The 2nd Program Advisory Committee Meeting for Materials and Life Science at RIKEN Nishina Center
1-3, Aug.	4th Annual Meeting of Particle Accelerator Society of Japan and the 32nd Linear Accelerator Meeting in Japan
12-13, Sep,	The 2nd Program Advisory Committee meeting for Nuclear Physics Experiments at RI Beam Factory
30, Oct.	First Shipment of RI (^{65}Zn, ^{109}Cd) used by AVF Cyclotron
29, Nov.	Nishina Memorial Lecture: Search for New Elements

2008

18, Jan.	Tree Planting Ceremony of "Nishina Zao"
18-19, Feb.	The 3rd Program Advisory Committee meeting for Nuclear Physics Experiments at RI Beam Factory
27-28, Mar.	The 3rd Program Advisory Committee Meeting for Materials and Life Science at RIKEN Nishina Center

Accelerator Team

1. Abstract

Our aim is to operate and develop the accelerator-complex system, mainly the rf systems, of the RI Beam Factory. We focus on further efficient use of the RI Beam Factory through R&D associated with a new injector for parallel operation of both RI beam factory experiments and the super-heavy elements experiment. Another objective of our team is to carry out an upgrading project of the AVF cyclotron on the expansion of region of its acceleration beam energies as well as the increase in beam intensity.

2. Major Research Subjects

(1) Operation and development of the accelerator-complex system
(2) R&D of a new injector for the RRC
(3) Upgrading project of the AVF cyclotron

3. Summary of Research Activity

(1) Operation and development of the accelerator system

O. Kamigaito, N. Sakamoto, S. Kohara, J. Ohnishi and A. Goto

We perform operation, maintenance and development of the RIBF accelerator system: mainly radio-frequency acceleration system. We also perform beam commissioning of the new accelerators.

(2) Development of a new injector for the RRC

O. Kamigaito, N. Sakamoto, Y. Sato and A. Goto

We are performing design and fabrication of a new injector for the RRC in order to make the efficient use of the accelerator beam time by making it possible to simultaneously conduct both experiments using RI's and the super-heavy-element search experiment. We are in charge mainly of design and development of linacs as well as the low-energy beam transport line of a superconducting ECR ion source.

(3) Upgrading of the AVF cyclotron

A. Goto

We are advancing the project of modification of the center region of the AVF cyclotron in collaboration with CNS, Univ. of Tokyo, in order to expand the region of its available acceleration energies as well as to increase the beam intensity. We are performing orbit simulations in detail for that purpose. We have already completed upgrade of the performance of the coil power supplies, improvement of the radio-frequency acceleration system, etc.

Team Leader
Akira GOTO

Members
Osamu KAMIGAITO
Shigeo KOHARA
Kiyoshi OGIWARA
Jun-ichi OHNISHI
Naruhiko SAKAMOTO

Contract Researcher
Yoichi SATO

Visiting Scientists
Mitsuhiro FUKUDA (RCNP, Osaka Univ.)
Masatoshi ITO (CYRIC, Tohoku Univ.)
Yoshitaka IWASAKI (SAGA Light Source)

Satoshi KURASHIMA (JAEA, Takasaki)
Nobumasa MIYAWAKI (JAEA, Takasaki)
Hajime SAITO (SHI Accel. Serv. Ltd.)

Research Consultants
Yoshiaki CHIBA
Shoushichi MOTONAGA

Students
Student trainees
Keisuke ITOH (Grad. Sch. Sci. Eng., Saitama Univ.)
Hiroaki MATSUBARA (Grad Sch. Sci., Osaka Univ.)
Ryo MATSUO (Grad. Sch. of Sci., Tohoku Univ.)
Yuji TAMESHIGE (Grad Sch. Sci., Osaka Univ.)

Ion Source Team

1. Abstract

Our aim is to operate and develop the ECR ion sources for the accelerator-complex system of the RI Beam Factory. We focus on further upgrading the performance of the RI Beam Factory through the design and fabrication of a superconducting ECR heavy-ion source for high-intensity uranium ions.

2. Major Research Subjects

(1) Operation and development of the ECR ion sources

(2) Development of a superconducting ECR heavy-ion source for high-intensity uranium ions

3. Summary of Research Activity

(1) Operation and development of ECR ion sources

T. Nakagawa, M. Kidera, Y. Higurashi, H. Haba, T. Kageyama and A. Goto

We routinely produce and supply various kinds of heavy ions such as zinc ions for the 113th-element experiment as well as uranium ions for RIBF experiments. We also perform R&D's to meet the requirements for stable supply of high-intensity heavy ion beams.

(2) Development of a superconducting ECR ion source for use in production of a high-intensity uranium beam

T. Nakagawa, J. Ohnishi, M. Kidera, Y. Higurashi, Y. Sato and A. Goto

The RIBF is required to supply uranium beams with very high intensity so as to produce RI's. We have designed and are fabricating an ECR ion source with high magnetic field and high microwave-frequency, since the existing ECR ion sources have their limits in beam intensity. The coils of this ion source are designed to be superconducting for the production of high magnetic field. We are also designing the low-energy beam transport line of the superconducting ECR ion source.

Team Leader

Akira GOTO

Members

Hiromitsu HABA
Tadashi KAGEYAMA
Takahide NAKAGAWA

Contract Researcher

Yoshihide HIGURASHI
Masanori KIDERA

Visiting Scientists

Takehiro MATSUSE (Fac.Text. Sci. Technol.,Shinshu Univ)

Student Trainee

Hiroyuki HIGASHIJIMA (Grad. Sch.. Sci., Rikkyo Univ.)

RILAC Team

1. Abstract

The operation and maintenance of the RIKEN Heavy-ion Linac (RILAC) have been carried out. There are the two modes, the standalone mode, in which the beam is delivered directly to the low-energy beam user in the RILAC, and the injection mode, in which the RILAC beam is injected to the RIKEN Ring Cyclotron (RRC). The RILAC is composed of two ion sources, the frequency-variable RFQ linac, six frequency-variable cavities, and six energy booster cavities (CSM). The maintenance of these devices is important to keep the log-term stability of RILAC beams.

2. Major Research Subjects

(1) The long term stability of the RILAC operation.
(2) Improvement of efficiency of the RILAC operation.

3. Summary of Research Activity

The RIKEN Heavy-ion Linac (RILAC) is a frequency-tunable linac. The RILAC is composed of two Heavy-ion ECR ion sources, RFQ linac, six main cavities, and six energy booster cavities. Thousands hours are spent in a year for delivering many kinds of heavy-ion beams to various experiments.

The RILAC has two operation modes: the stand-alone operation delivering low-energy beams directly to experiments and the injection mode operation supplying beams into the RIKEN Ring Cyclotron (RRC). In the first mode, the RILAC supplies very important beam to the nuclear physics experiment of “the research of super heavy elements”. In the second mode, the RILAC plays very important role as upstream end of the RIBF accelerators.

The maintenance is very important in order to keep the high quality performance of the RILAC. Improvements are always carried out for the purpose of more efficient operation.

Team Leader
Masayuki KASE

Member
Eiji IKEZAWA

Research Consultants
Toshiya CHIBA
Masatake HEMMI
Yoshitoshi MIYAZAWA

Cyclotron Team

1. Abstract

We are carryng out the operation and maintenance of five cyclotorons in RIKEN (AVF cyclotron, Riken Ring cyclotoron:RRC, fRC, IRC, and super-conducting cyclotron:SRC). We are trying to deliver stably a high-energy and high intensity beam to experiments.

2. Major Research Subjects

(1) Operation technology of cyclotrons.
(2) Maintenance of cyclotrons.
(3) Maintenance of super-conducting cyclotron.

3. Summary of Research Activity

We are carryng out the operation and maintenance of five cyclotorons in RIKEN (AVF cyclotron, Riken Ring cyclotoron:RRC, fRC, IRC, and super-conducting cyclotron:SRC). We are trying to deliver stably a high-energy and high intensity beam to experiments. Detailed research subjects are the following,

Operation technology of cyclotrons.
Maintenance of cyclotrons.
Maintenance of superconducting ring cyclotron..

Team Leader
Masayuki KASE

Members
Naohito INABE
Keiko KUMAGAI
Makoto NAGASE
Hiroki OKUNO

Research Ascociat
Kazunari Yamada

Beam Technology Team

1. Abstract

In order to realize the efficient acceleration in RIBF accelerators, the operation is being improved by doing various computer simulations. For this purpose, related technology (beam diagnosis, computer control, and charge stripper) was developed.

2. Major Research Subjects

(1) Improvement on the beam transmission along the multi-stage accelerator system.
(2) Development of beam diagnosis.
(3) Development of computer control.
(4) Development of charge stripper for high intensity heavy ion beam.

3. Summary of Research Activity

(1) Development of the beam diagnostic technology.
(2) Development of the charge-stripping foil.
(3) Development of the computer control system of accelerator.
(4) Investigation of beam behavior in accelerators.

Team Leader
Masayuki KASE

Members
Masaki FUJIMAKI
Nobuhisa FUKUNISHI
Sachiko ITO
Tamaki WATANABE

Contract Technical Scientist
Misaki KOBAYASHI-KOMIYAMA

Visiting Scientists
Masanori KOSHIMIZU (Grad. Sch. Eng., Tohoku Univ.)
Hideo MIKAMI (SHI Accel. Serv. Ltd.)
Hiromichi RYUTO (Photonics and Electronics Science and Engineering Center, Kyoto Univ.)

Research Consultants
Kazuie KIMURA
Mutsuko SASAKI

Cryogenic Technology Team

1. Abstract

We are operating the helium cryogenic system in the south area of RIKEN Wako campus and delivering the liquid helium to users in RIKEN. We are trying to collect efficiently gas helium after usage of liquid helium.

2. Major Research Subjects

(1) The high efficiency of the liquid herium production cycle.
(2) Optimization of the large-scaled superconductinf cyclotron.

3. Summary of Research Activity

We are operating the herium cryogenic system located in the south area of Wako campass of RIKEN. We are producing liquid helium and supplying them to RIKEN inside users. For the purpose of efficient operation, we are trying to collect the gas after the use of liquid helium.

Team Leader
Masayuki KASE

Members
Kumio IKEGAMI
Masato NAKAMURA

Technical Staff-I
Hiroo HASEBE
Takeshi MAIE

Part-time Staff
Kazushiro NAKANO

Research Consultant
Ken-ici KATO

Heavy Ion Nuclear Physics Laboratory

1. Abstract

With fast RI beams provided by the RIBF cyclotron complex, ,we study exotic behavior of nuclei far from the stability valley, explosive nuclear burning in high-temperature and high-density environment in stars and early universe, and nuclear reactions related to solar neutrino production. For that purpose, we develop various experimental methods based on intermediate-energy inelastic scattering including Coulomb excitation, Coulomb dissociation, transfer- and fragmentation-reactions coupled with g-ray and particle-decay measurements. We perform also study of the three-nucleon forces by precise measurements of elastic scattering and breakup reactions of few-nucleon systems and development of new technics including new laser-spectroscopy for exotic nuclei. Developments of radiation detectors such as semiconductor detectors and scintillation detectors, data processing methods, and construction of experimental equipment, together with theoretical studies on nuclear structure and nuclear reaction, are also made.

2. Major Research Subjects

(1) Spectroscopy of unstable nuclei with direct reactions
(2) Development of radiation detector systems with high precision and high efficiency
(3) Study of astrophysical nuclear reactions with fast beams of unstable nuclei
(4) Development of laser spectroscopy for unstable nuclei
(5) Theoretical studies on nuclear structure and nuclear reactions

3. Summary of Research Activity

3.1. γ-spectroscopy

Proton inelastic scattering on neutron rich nuclei was studied using a new γ-spectroscopy technique to investigate the evolution of shell structure.

(1) 30Ne, 36Mg

Proton inelastic scatterings on 30Ne and 36Mg were performed. 36Mg is the most neutron-rich magnesium isotope ever studied experimentally in or beyond the island of inversion region. The study of 30Ne aims at further study of the enhanced collectivity expected from the observed low excitation-energy of its 2+ state.

(2) 18,20C

Proton inelastic scattering to excite the first 2+ states in 18,20C was studied aiming at studying the mechanism of decoupling of proton and neutron collectivity observed in 16C.

3.2. Spectroscopy using breakup reactions.

(1) Invariant mass spectroscopy of nuclei in the vicinity of the neutron drip line

(a) Strong E1 transitions at low excitation energies (soft E1 excitation) were observed for 11Li by a new Coulomb breakup experiment.

(b) Inelastic-scattering, one-neutron knockout, and charge exchange reactions of 14Be were measured for proton and 12C targets. The transition to the first 2+ state of 14Be at Ex=1.55 MeV was measured, which showed smaller deformation lengths compared to 12Be. The invariant mass spectrum of 13Be in the one-neutron knockout channel showed two peaks. The peak at higher energy around Ex=2 MeV has a d-wave property.

(c) Invariant mass spectra were obtained by the breakup and inelastic scattering of 6He, 17C, and 19C on proton targets. New peaks were found for neutron-rich carbon isotopes.

(2) Invariant mass spectroscopy of proton-rich nuclei

Coulomb dissociation of the proton-rich nuclei 23Al, 27P on 208Pb was measured. Relative energy spectra

for 22Mg+p, 26Si+p were obtained. The breakup cross sections are converted to the radiative proton-capture cross sections, which provide useful information for the astrophysical network calculation on the explosive nucleosynthesis in novae and X-ray bursts.

(3) Missing mass spectroscopy of very neutron-rich light nuclei

Missing mass spectroscopy of exotic systems 7H, 6H and 4n was performed using 8He beam and deuteron target The reaction channels d(8He,3He)7H, d(8He,4He)6H, and d(8He,6Li)4n were mainly aimed at. The reference peak in the d(8He,t)7Heg.s. channel was clearly observed.

3.3. Nuclear reaction study using the high-resolution spectrograph SMART

(1) Necessity of the three-nucleon-force is shown to reproduce the deuteron-proton elastic scattering cross section. To further investigate the three-nucleon-force, spin transfer coefficients for deuteron-proton breakup reactions were measured.

(2) Many experiments have been performed to test experimentally Bell's inequality. However, tests using hadron systems are limited. We tested Bell's inequality in the proton-neutron system by measuring the spin-correlation between the proton-neutron pair in 1S0-state which was produced by the 2H(d,pn) reaction.

3.4. Laser spectroscopy and laser ablation of atoms with stable and unstable nuclei

(1) A new laser spectroscopy technique for atoms trapped in superfluid helium is being developed. We have successfully measured very long spin relaxation time (> 2 s) and hyperfine coupling constants of 133Cs atoms in superfluid helium.

(2) Tags of stable isotope collected from a bio-sample by laser ablation were successfully identified by time-of-flight technique.

3.5. SCRIT development

Feasibility studies of a novel experimental scheme has been performed, SCRIT (Self-Confining RI Target), which makes it possible to study the internal structure of exotic nuclei by electron scattering. A prototype has been installed at the electron storage ring, KSR, of Kyoto University. What we have completed this year are following; i) construction of a scattered electron calorimeter made of pure CsI crystals, ii) installation in the SCRIT chamber ultra-thin W and C wires for luminosity calibration and detector calibration, iii) installation of a recoil detector which aim at measuring a Time-Of-Flight of the recoiled nucleus by electrons for its mass determination. Newly constructed and/or installed devices all work fine. We are now ready to detect elastically scattered electrons from the SCRIT target.

3.6. SAMURAI development

SAMURAI (Superconducting Analyzer for Multi-particle from Radio Isotope Beams) is a large-acceptance multi-particle spectrometer we proposed to construct at RIBF. Its major part is of a large-gap superconducting magnet with 7 Tm of bending power. SAMURAI enables momentum analysis of heavy projectile fragments and projectile-rapidity protons with large angular and momentum acceptance. SAMURAI also affords projectile-rapidity neutron measurements with large angular acceptance in coincidence with heavy projectile fragments.

In this fiscal year, a workshop was held to establish the collaboration framework and to clarify roles of each group and issues to be solved. A summary document which includes direction of magnet design, current status of particle detectors and neutron detectors, outline of the experimental projects, was issued for the TAC meeting.

3.7. Theoretical studies of nuclear physics

Theoretical works are also promoted for the following subjects in strong cooperation with the experimental approaches.

(1) Cluster Aspect of Nuclear Physics: Roles of the tensor, deuteron-like and di-neutron cluster correlation.

(2) Nuclear matter density distributions and nuclear radii: Description of proton-nucleus elastic scattering by a "black sphere" picture.

(3) Nuclear structure study using nuclear reactions: Analysis of 16C + 208Pb inelastic scattering using the 16C wave function calculated by the anti-symmetrized molecular dynamics (AMD).

(4) Mechanism of reactions involving unstable nuclei studied by a microscopic reaction theory: Analysis of the 6He+209Bi breakup reaction based on the four-body Continuum Distcretized Coupled Channels (CDCC) method.

(5) Nuclear structure at finite temperature: A self-consistent formulation of particle-particle RPA and a model with thermal fluctuation to calculate the width of low-temperature giant resonances.

Head

Tohru MOTOBAYASHI

Members

Nori AOI
Akihisa KOHAMA
Yukari MATSUO
Toshimi SUDA
Yasushi Watanabe
Yoshiyuki Yanagisawa
Ken-ichiro YONEDA

Special Postdoctoral Researchers

Hidetada BABA
Takeshi FURUKAWA
Shoko KANNO
Yosuke KONDO
Takuma MATSUMOTO
Satoshi TAKEUCHI

Contract Researchers

Shawn BISHOP
Nguyen Dinh DANG
Kimiko SEKIGUCHI
Meiko UESAKA

Asia Program Associates

Nguyen Quang HUNG
Shuo WANG

Senior Visiting Scientists

Hisashi HORIUCHI (Grad. Sch. of Sci., Kyoto Univ.)
Kengo Ogawa
Takaharu OTSUKA (Grad. Sch. of Sci., Univ. of Tokyo,)
Hideyuki SAKAI (Grad. Sch.. of Sci., Univ. of Tokyo)
Hiroyuki SAKURAGI (Grad. Sch. of Sci., Osaka City Univ. ,)

Research Consultants

Yasuo Aoki
Kiyomi Ikeda
Toshimitsu Yamazaki
Shuhei Yamaji

Part-time Staff Ⅰ

Kiyomi Arai
Hanako Ishitobi
Miki Kanou
Hironori KUBOKI
Noriko Okayasu
tsuneyo Suzuki

Visiting Scientists

Takashi Abe
Yasuhisa ABE (RCNP, Osaka Univ.)
Shigeyoshi AOYAMA (Niigata Univ. Integrated Information Processing Center)
Ichiro ARAI (Grad. Sch. of Pure and Applied Sci., Univ. of Tsukuba,)
Yoshihiro ARITOMO (Flerov Lab. Nucl. Reactions, JINR, Russia)
Daniel BEMMERER (Tech. Univ. Berlin Inst., Germany)
Daniel BAZIN (MSU, NSCL, USA)
DIDIER BEAUMEL (Paris-XI Univ., France)
Fa BECK (Strasbourg Nucl. Inst., France)
Carlos BERTULANI (Univ. Arizona, USA)
Yorick BLUMENFELD (Paris-XI Univ., France)
Richard BOYD (Dept. of Phys., Ohio State Univ., USA)
BO CEDERWALL (Royal Insti. Tech. , Sweden)
Alan CHEN (McMaster Univ., Canada)
Silvio CHERUBINI (Catania Univ., Italy)
Alain COC (CSNSM, Orsay, France)
Tien Khoa DAO (Inst. Nucl. Sci. Tech., Center for Basic Res. Computation)
Mahananda DASGUPTA (Bompay Univ., India)
Zsolt DOMBRADI (ATOMKI, Hungary)
Zoltan ELEKES (ATOMKI, Hungary)
Henning ESBENSEN (Argonne Nat. Lab., USA)
Michael FAMIANO (MSU, NSCL, USA)
Hubert FLOCARD (Orsay Nucl. Inst., France)
Yoshihide FUCHI (KEK)
Shinichiro FUJII (CNS, Grad. Sch. Sci., Univ. of Tokyo)
Yoshitaka FUJITA (Grad. Sch. of Sci. , Osaka Univ.)
Tomonori FUKUCHI (Fac. of Sci. ,Rikkyo Univ.)
Mitsunori FUKUDA (Sch. of Sci. , Osaka Univ.)
Yoshimitsu FUKUYAMA (SPring8 Center, RIKEN)
Zsolt FULOP (ATOMKI, Hungary)
Ken-Ichi FUSHIMI (Fac.of Integrated Arts and Sci., Univ. of Tokushima)
Valdir GUIMRAES (Sao Paulo Univ. Brazil)
Taku GUNJI (Dept. Phys., Grad. Sch. Sci., Univ. Tokyo)
Kevin Insik HAHN (Ewaha Womans Univ., Korea)
Hideki HAMAGAKI (CNS, Grad. Sch. Sci., Univ. of Tokyo)
Ikuko HAMAMOTO (Lund Univ., Sweden)
Jun HASEGAWA (Tokyo Inst. of Tech., Res. Lab. for Nuclear Reactors)

Jun HASEGAWA (Tokyo Inst. of Tech., Res. Lab. for Nuclear Reactors)
Jianjun HE (Edinberg Univ.)
David HINDE (Australia Nat. Univ., Australia)
Michio HONMA (Univ. Aizu)
Takatoshi HORIBATA (Fac.of Software and Information Tech. ,Aomori Univ.)
Akos HORVATH (Eotvos Lorand Univ., Hungary)
Munetake ICHIMURA (Fac.of Computer and Information Sci., Hosei Univ.)
Eiji IDEGUCHI (CNS, Grad. Sch. Sci., Univ. of Tokyo)
Kazuo IEKI (Fac.of Sci.,Rikkyo Univ.,)
Kei IIDA (Kochi Univ. of Tech., Physical Sci.)
Nobuaki IMAI (Inst. of Particle and Nuclear Studies, KEK)
Astrid IMIG (Univ. of North Carolina, USA)
Tetsuro ISHII (JAEA)
Shigeru ISHIMOTO (Inst. of Particle and Nuclear Studies, KEK)
Naoyuki ITAGAKI (CNS, Grad. Sch. Sci., Univ. of Tokyo)
Akira IWAMOTO (JAEA)
Naohito IWASA (Dept. of Phys., Tohoku Univ.)
Hironori IWASAKI (CNS, Grad. Sch. Sci., Univ. of Tokyo)
Takuji IZUMIKAWA (Niigata Univ. RI Center)
Janos GAL (Hungarian Academy Sci., Inst. Nucl. Res., Hungary)
Toshitaka KAJINO (National Astronomical Observatory of Japan)
Nasser KALANTAR (Univ. Groningen, The Netherlands)
Gabor KALINKA (Hungarian Academy Sci., Inst. Nucl. Res., Hungary)
Yoshiko KANADA-EN'YO (Kyoto Univ., Yukawa Inst. for Theoretical Phys.)
Seigo KATO (Fac. of Sci.,Yamagata Univ.)
Kiyoshi KATO (Fac. of Sci. , Dept. of Phys., Nonlinear Phys., Hokkaido Univ.,)
Takahiro KAWABATA (CNS, Grad. Sch. Sci., Univ. of Tokyo)
Takeshi KIKUCHI (Fac.of Eng.,Utsunomiya Univ.)
Jongchan KIM (Seoul National Univ. , Korea)
Masaaki KIMURA (Grad. Sch. of Pure and Applied Sci., Univ. of Tsukuba,)
Kikuo KIMURA (Nagasaki Inst.of Applied Sci.)
Adam KISS (Eotvos Lorand Univ., Hungary)
Takeshi KOIKE (Dept. of Phys., Tohoku Univ.)
Tetsuro KOMATSUBARA (Grad. Sch. of Pure and Applied Sci., Univ. of Tsukuba,)
Alexe KORSHENINNIKOV (Inst. Generall & Nucl. Phys., Kurchatov Inst., Russia)
Evgueni KOUZMINE (Russian Res. Center, Kurchatov Inst., Russia)
Shigeru KUBONO (CNS, Grad. Sch. Sci., Univ. of Tokyo)
Kazuyoshi KURITA (Fac.of Sci.,Rikkyo Univ.,)
Chie KUROKAWA (Meme Media Lab., Hokkaido Univ.,)
Evgueni KUZMIN (JINR. Flerov Lab. of Nuclear Reaction, Russia)
Marco LA COGRATA (Catania Univ., Italy)
Karin LAGERGREN (Royal Insti. Tech. , Sweden)
Khiem LE (CNS, Grad. Sch. Sci., Univ. of Tokyo)
Alinka Lepine
Chen LI (Peking Univ., China)
Filho LICHTENTHALER
Gengjian LIN
Weiping LIU (China Inst. Atomic Energy, China)
Minliang LIU (CNS, Grad. Sch. Sci., Univ. of Tokyo)
Jingbin LU (Fac. of Sci., Kyusyu Univ. ,)
William LYNCH (MSU, NSCL, USA)

William LYNCH (MSU, NSCL, USA)
Yukie MAEDA (CNS, Grad. Sch. Sci., Univ. of Tokyo)
Kazushige MAEDA (Dept. of Phys., Tohoku Univ.)
Kensaku MATSUTA (Sch. of Sci. , Osaka Univ.)
Kenichi MATSUYANAGI (Fac. of Sci., Kyoto Univ.,)
Marco MAZZOCCO
Jie MENG (Sch. of Phys., Peking Univ., China)
Alberto MENGONI (Univ. of Tokyo)
Johannes MESSCHENDOR (Univ. of Groningen, Netherlands)
Yasuo MIAKE (Grad. Sch. of Pure and Applied Sci., Univ. of Tsukuba)
Shin'ichiro MICHIMASA (CNS, Grad. Sch. Sci., Univ. of Tokyo)
Mototsugu MIHARA (Grad. Sch. of Sci. , Osaka Univ.)
Toshiyuki MINEMURA (Inst. of Particle and Nuclear Studies, KEK)
Shiro MITARAI (Fac. of Sci., Kyusyu Univ. ,)
Toshinori MITSUMOTO
Wolfgang MITTIG (NSCL, MSU, US)
Takashi MIYACHI (Adv. Res. Inst. Sci. Eng., Waseda Univ.)
Tomoko MIYAGISHI (Natl. Inst. Radiol. Sci.)
Hiroari MIYATAKE (Inst. of Particle and Nuclear Studies, KEK)
Peter MOLLER (Los Alamos Nat. Lab., USA)
Sadao MOMOTA (Kochi Univ. of Tech., Intelligent Mechanical Systems Eng.)
Tsuneyasu MORIKAWA (Fac. of Sci., Kyusyu Univ. ,)
Ben MOTTELSON (Copenhagen NORDITA, Denmark)
Hiroyuki MURAKAMI (Fac.of Sci.,Rikkyo Univ.,)
Takayuki MYO (Theoretical Nuclear Phys., RCNP, Osaka Univ.)
Yasuki NAGAI (RCNP, Osaka Univ.)
Takashi NAKAMURA (Tokyo Inst. of Tech., Particle-, Nuclear-, and Astro-Phys.)
Kosuke NAKANISHI (CNS, Grad. Sch. Sci., Univ. of Tokyo)
Shintaro NAKAYAMA (Fac.of Integrated Arts and Sci., Univ. of Tokushima)
Evgueni NIKOLSKI (Russian Res. Center, Kurchatov Inst., Russia)
Masahiro NOTANI (Argonne Nat. Lab., USA)
Atsuko ODAHARA (Grad. Sch. of Sci. , Osaka Univ.)
Kazuyuki OGATA (Fac. of Sci., Kyusyu Univ. ,)
Alexey OGLOBLIN (Russian Res. Center, Kurchatov Inst., Russia)
Yukimitsu OHSHIRO (CNS, Grad. Sch. Sci., Univ. of Tokyo)
Takashi OHTSUBO (Dept. of Phys., Niigata Univ.)
Hiroyuki OKAMURA (CYRIC, Tohoku Univ.)
Shinsuke OTA (CNS, Grad. Sch. Sci., Univ. of Tokyo)
Masahisa OTA (Dept. of Phys., Konan Univ.)
Kazuhiro OYAMATSU (Fac.of Studies onContemporary Society,Aichi Shukutoku Univ. ,)
Kyoichiro OZAWA (CNS, Grad. Sch. Sci., Univ. of Tokyo)
Thomas PAPENBROCK
Jonathan PEARSON (McMaster Univ., Canada)
Gianluca PIZZONE (Catania Univ., Italy)
Chilakamarri RANGACHARYULU (Univ. Saskatchewan, Canada)
Stefano ROMANO (Catania Univ., Italy)
Hiroyuki SAGAWA (The Univ. of Aizu, Center for Mathematical Sci.)
Akito SAITO (Dept. Phys., Grad. Sch. Sci., Univ. of Tokyo)
Takao SAKAGUCHI (BNL, USA)
Harutaka SAKAGUCHI (Dept. of Applied Phys., Fac. of Eng., Univ. of Miyazaki)
Mitsuo SAKAI (CNS, Grad. Sch. Sci., Univ. of Tokyo)

Badawy SARHAN (Cairo Univ., Egypt)
Kimikazu SASA (Univ. of Tsukuba)
Yoshiteru SATOU (Grad. Sch. of Sci.,Tokyo Inst. of Tech.)
Ryoichi SEKI (California State Univ. , Northridge, USA)
Noritaka SHIMIZU (Grad. Sch. of Sci., Univ. of Tokyo)
Youhei SHIMIZU (Theoretical Nuclear Phys., RCNP, Osaka Univ.)
Yoshifumi SHIMIZU (Fac. of Sci., Kyusyu Univ. ,)
Susumu SHIMOURA (CNS, Grad. Sch. Sci., Univ. of Tokyo)
Cosimo SIGNORINI (Univ. of Padova, INFN, Italy)
Dorottya SOHLER (ATOMKI,Hungary)
Claudio SPITALERI (Catania, Italy)
Andreas STOLZ (MSU, NSCL, USA)
Kenji SUDA (CNS, Grad. Sch. Sci., Univ. of Tokyo)
Satoru SUGIMOTO (Grad. Sch. of Sci. , Kyoto Univ.)
Kohsuke SUMIYOSHI (Div. of Liberal Arts, Phys. Group, Numazu College of Tech.)
Yang SUN (Univ. of Notre Dame, USA)
Akihiro SUZUKI (RCNP, Osaka University)
Toshio SUZUKI (Univ. of Fukui, Fac. of Enginerring)
Toshio SUZUKI (Nihon University)
Takeshi SUZUKI (Faculity of Eng.,Saitama Univ.)
Shoji SUZUKI (Inst. of Particle and Nuclear Studies, KEK)
Nobuyuki SUZUKI (Dept. of Phys., Niigata Univ.)
Yasuyuki SUZUKI (Niigata University)
Yoshihiro TAGISHI (Univ. of Tsukuba, Inst. of Phys. ,)
Naoki TAJIMA (Univ. of Fukui, Fac. of Enginerring)
Tadayuki TAKAHASHI (JAXA)
Masatoshi TAKANO (Waseda Univ. RISE)
Masaaki TAKASHINA (Kyoto Univ., Yukawa Inst.for Theoretical Phys.)
Tadaaki TAMAE (Lab. of Nucl. Sci., Dept. of Phys.,Tohoku Univ.)
Atsushi TAMII (RCNP, Osaka Univ.)
Kazuko TANABE (Otsuma Women's Univ)
Gurgen TER-AKOPYAN (JINR. Flerov Lab. of Nuclear Reaction, Russia)
Takashi TERANISHI (Kyusyu Univ.)
Jun TERASAKI (Peking Univ., Dept. of Phys., China)
Renju THOMAS (Australia Nat. Univ., Australia)
Wendong TIAN (Shanghai Inst. Applied Phys., China)
Livius TRACHE (Texas A&M University, US)
Manyee TSANG (MSU, NSCL, USA)
Tomohiro UESAKA (CNS, Grad. Sch. Sci., Univ. of Tokyo)
Yutaka UTSUNO (JAEA)
Peter VON BRENTANO (Koln Univ., Germany)
Takahiro WADA (Fac.of Sci.and Eng.,Konan Univ.)
Yasuo WAKABAYASHI (CNS, Grad. Sch. Sci., Univ. of Tokyo)
Tomotsugu WAKASA (Fac. of Sci., Kyusyu Univ. ,)
Takashi WAKUI (Tohoku Univ. CYRIC)
Shin-ichi WATANABE (CNS, Grad. Sch. Sci., Univ. of Tokyo)
Yutaka WATANABE (Inst. of Particle and Nuclear Studies, KEK)
Zhendong WU
Shuwei XU (Chinese Academy of Sci., China)
Kazuhiro YABANA (Univ. of Tsukuba, Inst. of Phys. , Nuclear Theory Group)
Kentaro YAKO (Grad. Sch.. of Sci., Univ. of Tokyo)

Takayuki YAMAGUCHI (Saitama Univ.)
Hidetoshi YAMAGUCHI (CNS, Grad. Sch. Sci., Univ. of Tokyo)
Shoichi YAMAKA (CNS, Grad. Sch. Sci., Univ. of Tokyo)
Norio YAMAZAKI (CNS, Grad. Sch. Sci., Univ. of Tokyo)
Yanlin YE (Peking Univ., China)
Naotaka YOSHINAGA (Faculity of Sci.,Saitama Univ.)
Akira YOSHINO (CNS, Grad. Sch. Sci., Univ. of Tokyo)
Chongcheoul YUN (Chung-Ang Univ., Korea)
Tao ZHENG (Peking Univ., China)
Yong ZHENG (CNS, Grad. Sch. Sci., Univ. of Tokyo)
Shan-Gui ZHOU (Peking Univ., China)

Junior Research Associates

Naoya FURUTACHI (Grad. Sch. Of Sci., Tokyo Science University)

Student Trainees

Guengpeng AN
Yoki ARAMAKI (Grad. Sch.. of Sci., Univ. of Tokyo)
Tae-Eun CHOI (Ewaha Womans Univ., Korea)
Vincenzo CRUCILLA (Univ. of Catania, Italy)
Binh DAM (Inst. Theoretical Phys., Vietnam)
Kazuya EBISU
Koutaro FUJIKAKE (Sch. of Sci. and Tech., Meiji Univ.)
Seiya HAYAKAWA (CNS, Grad. Sch. Sci., Univ. of Tokyo)
Toshikazu HORI (Grad. Sch. of Sci. , Osaka Univ.)
Wataru HORIUCHI (Grad. Sch. of Sci.& Tech. Niigata Univ.)
Takeshi HOYA (Grad. Sch. of Pure and Applied Sci., Univ. of Tsukuba,)
Kenichi ISHII (Fac.of Sci.,Rikkyo Univ.,)
Fuming JIA
Ju Hahn LEE (Chung-Ang Univ., Korea)
Chen JUN (McMaster Univ., Canada)
Hyo-Soon JUNG (Chung-Ang Univ., Korea)
David KAHL (McMaster Univ., Canada)
Tomomi KAWAHARA (Grad. Sch. of Sci., Toho Univ.)
Tomohito KAWAMATA
Jung-Lan KIM (Ewaha Womans Univ., Korea)
Jang Youl KIM (Chung Ang Univ., Korea)
Aram KIM (Ewaha Womans Univ., Korea)
Mituhisa KITAYAMA (Dept. of Phys., Tohoku Univ.)
Nobuyuki KOBAYASHI
Junji KOMURASAKI
Takamasa KUBOKI (Grad. Sch. of Sci.& Eng., Saitama Univ.)
Kenichiro KURA (Sch. of Sci. , Osaka Univ.)
Yuzo KURIHARA (Grad. Sch. of Sci. and Eng., Tokyo Metropolitan Univ.)
Atsuhiro KUWAJIMA
Livio LAMIA (Univ. of Catania, Italy)
Ki-Woo LEE (Chung-Ang Univ., Korea)
Toshiyuki MASUE (Grad. Sch. of Sci. , Osaka Univ.)
Yohei MATSUDA (Dept. of Phys., Tohoku Univ.)
Ryohei MATSUMIYA (Grad. Sch. of Sci. , Osaka Univ.)
Kenjiro MIKI (Grad. Sch.. of Sci., Univ. of Tokyo)
Munesato MIURA

Hiroyuki MIYA
Kazutaka MIYAKAWA (Grad. Sch. of Pure and Applied Sci., Univ. of Tsukuba,)
JunYoung MOON (Chung Ang Univ., Korea)
Tetsuaki MORIGUCHI (Grad. Sch. of Pure and Applied Sci., Univ. of Tsukuba)
Yuhei MORINO (Grad. Sch.. of Sci., Univ. of Tokyo)
Yoshiaki NAKAYAMA
Takashi NANNICHI (Sch. of Sci., Tokyo Inst. of Tech.)
Daiki NISHIMURA
Shumpei NOJI (Sch. of Sci., Univ. of Tokyo,)
Susumu ODA (Grad. Sch.. of Sci., Univ. of Tokyo)
Kazuya SAITO
Satoshi SAKAGUCHI (Grad. Sch.. of Sci., Univ. of Tokyo)
Satoshi SANO (CNS, Grad. Sch. Sci., Univ. of Tokyo)
Ayako SASAKI
Masaki SASANO (Grad. Sch.. of Sci., Univ. of Tokyo)
Maria SERGI (Univ. of Catania, Italy)
KIANA SETOODEHNIA (McMaster Univ., Canada)
Tomoyuki SHIMAMURA (Sch. of Sci., Tokyo Inst. of Tech.)
Mayuko SHINOHARA (Grad. Sch. of Sci.and Eng., Tokyo Inst. of Tech.)
Ryota SHIODA (Fac.of Sci.,Rikkyo Univ.,)
Syota SUGAWARA (Sch. Sci. Eng., Waseda Univ.)
Hiroshi SUZUKI (Grad. Sch.. of Sci., Univ. of Tokyo)
Kunihiko TAJIRI (Sch. of Sci. , Osaka Univ.)
Akihisa TAKAHARA
Kana TANAKA
Yasutaka TANIGUCHI (Grad. Sch. of Sci., Kyoto Univ.)
Yasuhiro TOGANO (Fac.of Sci.,Rikkyo Univ.,)
Xinxing Xu
Yusuke YAMADA (Fac.of Sci.,Rikkyo Univ.,)
Yuji YAUCHI (Fac.of Sci., Dept. of Phys., Rikkyo Univ.,)
Jung-Sook YOO (Ewaha Womans Univ., Korea)
Akira YOSHIDA (Grad. Sch. of Sci., Kyoto Univ.)
Michiori YOSHITAKE (Grad. Sch. of Sci.& Eng., Saitama Univ.)
Chunlei ZHANG

Secretaries
Kayoko WADA

Radioactive Isotope Laboratory

1. Abstract

This laboratory explores exotic nuclear structures and dynamics in unstable nuclei that have never been investigated before, such as those with largely imbalanced proton and neutron numbers. Our aim is to develop new experimental techniques utilizing fast RI beams to discover new phenomena and properties in unstable nuclei. Another important subject is the equation-of-state of asymmetric nuclear matter, and its association with the origin of elements and with neutron stars. For instance, we are making attempts to the better understand underlyning mechanism for exotic stability-enhancements of very neutron-rich fluorine isotopes, the large deformation of the nucleus 34Mg with N=22 in spite of its vicinity to the N=20 magic neutron number and anomalous collectivity in 16C. We are further extending these studies to medium- and heavy-mass regions by developing facilities, detectors and unique methods at RIBF, thereby leading on the challenging task to find new exotic phenomena. We also perform numerical simulations of nucleosynthesis under the environment of core-collapse supernovae, and moreover quest for footprints of supernovae and solar activities in the past, embedded in Antarctic ice core, in collaboration with Cosmic radiation laboratory and National Institute of Polar Research.

2. Major Research Subjects

(1) Study of structure and dynamics of unstable nuclei through development of new methods utilizing fast RI beams

(2) Stability of exotic nuclei and exploration into limit of nuclear existence

(3) Research on equation-of-state in asymmetric nuclear matter via heavy-ion induced reaction

(4) Promotion of nuclear astrophysics in an interdisciplinary organization

3. Summary of Research Activity

(1) Program based on missing mass method

Missing mass method is an essential tool to identify and observe both bound and unbound states. Especially for highly excited states beyond particle threshold, any models of particle and gamma decay processes are not necessary in reconstructing excitation energy. Difficulties stemming from inverse kinematics are low energy of recoiled out particles from targets and high accurate measurement necessary for emission angles. To overcome the difficulties, we are developing new detection systems for proton (in)elastic scattering; ESPRI(Elastic Scattering of Proton with RI beam), and a magnetic spectrometer for particles emitted at zero degree. The two systems have been employed for light mass nuclei for matter distributions as well as spectroscopic studies.

(2) Program based on in-beam gamma spectroscopy

In the medium and heavy mass region explored at RIBF, collective natures of nuclei are one of important subjects, which are obtained through production and observation of high excited and high spin states. To populate such states, heavy-ion induced reactions such as fragmentation, fission are useful and development of in-beam gamma methods fit for the reactions is necessary. So far, we have developed two-step fragmentation method as an efficient method to identify and populate excited states, and lifetime measurements to deduce transition strength.

(3) beta spectroscopy

Beta-spectroscopy is a traditional and efficient method for nuclear spectroscopy, especially out non-yrast levels. In the light mass region, several light-mass nuclei in both neutron-rich and proton-rich region have been investigated at RIPS through beta-gamma and beta-p coincidence technique. Concerning the medium and heavy mass region available at RIBF, we are developing two position-sensitive active-stoppers to achieve low-background via position correlation; strip-silicon detectors and a cylindrical active stopper called CAITEN.

(4) Equation-of-state via heavy-ion central collisions

Eos in asymmetric nuclear matter is essentially important to understand mechanism of supernovae explosion as well as crust structure of neutron stars. We are designing an experimental setup to detect pions and multiplicity in central collisions with RIBs at the intermediate energy at RIBF.

(5) Interdisciplinary study for nuclear astrophysics

To understand the origin of elements beyond ion, interdisciplinary works are important in linking data from nuclear physics program. We are promoting simulation of nucleosynthesis in the r- process path, and investigation of Antarctic ice core to search for footprints of supernovae as well as solar activity in the past via mass spectrometer, to link data obtained from nuclear physics program.

Head
Hiroyoshi SAKURAI

Members
Takashi ICHIHARA
Takashi KISHIDA
Yoichi NAKAI
Shunji NISHIMURA
Hideaki OTSU
Heiko SCHEIT

Nishina Center Researcher
Yuko MOCHIZUKI

Research Associate
Hiroshi WATANABE

Special Postdoctoral Researcher
Maya TAKECHI
Eri TAKESHITA
Satoru TERASHIMA

Senior Visiting Scientist
Wolfgang MITTIG (GANIL, France)

Visiting Scientists
Sachiko AMARI (Washington Univ.,USA)
Koichiro ASAHI (Tokyo Institute of Technology)
Sudhee BANERJEE (Variable Energy Cyclotron Center, India)
Xiangzhou CAI (Shanghai Inst. Applied Physics, China)
Junsei CHIBA (Tokyo University of Science)
Alfred DEWALD (Univ. Cologna Insti. Nucl. Phys.)
Deqing FANG (Shanghai Inst. Applied Physics, China)
Adrian GELBERG (Univ. zu KoelnInst. Fur Kern Physik, Germany)
Wei GUO (Shanghai Inst. Applied Physics, China)
Kaoru HARA (University of Tsukuba)
Steven KARATAGLIDIS (Rhodes Univ.,South Africa)
Hiroyuki KOURA (JAEA)
Yugang MA (Shanghai Inst. Applied Physics, China)
Hideki MADOKORO (Mitsubishi Heavy Industries, Ltd)
Masayuki MATSUO (Grad. Sch. of Sci. and Tech., Niigata Univ,)
Tetsuya MURAKAMI (Kyoto Univ.)

Jiro MURATA (Rikkyo Univ.)
Tetsuo NORO (Kyusyu Univ. Fac. of Sci.)
Akira ONO (Tohoku Univ.)
Naohiko OTSUKA (JAEA)
YURI PENIONZHKEVICH (Flerov Lab. Nucl. Reactions, JINR, Russia)
Simona SCHEIT (Univ. of Tokyo)
Toshiyuki SUMIKAMA (Tokyo University of Science)
Takahiro TACHIBANA (Waseda High Sch., Waseda Univ.)
Kohji TAKAHASHI (Universite Libre de Bruxelles, Belgium)
Noboru TAKIGAWA (Fac. of Sci., Tohoku Univ.,)
Oleg TARASOV (MSU, NSCL, USA)
Ryouichi WADA (Texas A&M Univ., USA)
Juzo ZENIHIRO (Grad. Sch. of Sci., Kyoto Univ.)
Shuangquan ZHANG (Peking Univ., China)
Yumin ZHAO (Shanghai Jiao Tong Univ.)

Contract Researcher
Yasuyuki GONO

Students

Junior Research Associate
Yuichi ICHIKAWA
Taro NAKAO
Mugumi NIIKURA

Student Trainees
Shoichiro EBESU (Kyoto Univ.)
Yuhei HASHIZUME (Tsukuba Univ.)
Maki HATA (Rikkyo Univ.)
Chihiro ISHII (Tokyo University of Science)
Yoshihiko IWAO (Kyoto Univ.)
Hitomi KIMURA (Tokyo Univ.)
Hiroaki MATSUMOTO (Kyoto Univ.)
Minori NIITA (Rikkyo Univ.)
Ken-ichiro OGAWA (Tsukuba Univ.)
Kensuke OKADA (Rikkyo Univ.)
Akio SHIRAKI (Tokyo Univ.)
Daisuke SUZUKI (Tokyo Univ.)
Hirotake TAKAHASHI (Shinsyu Univ.)
Nobuya UEMATSU (Tokyo University of Science)
Hideakira YOSHII (Tokyo University of Science)
Kenta YOSHINAGA (Tokyo University of Science)

IPA
Kuoang LI (Peking Univ., China)

Visiting Rsearcher
Pieter DOORNENBAL (GSI)

Secretary
Shizuka KATO (Temporary staff)

Superheavy Element Laboratory

1. Abstract

The elements with their atomic number Z>103 are called as trans-actinide or superheavy elements. The chemical properties of those elements have not yet been studied in detail. Those elements are not exist in nature therefore, they must be produced by artificially for the scientific study of those elements. In our laboratory, we have been studying the physical and chemical properties of the superheavy elements utilizing the accelerators in RIKEN and various methods of efficient production of the superheavy elements.

2. Major Research Subjects

(1) Search for new supreheavy elements
(2) Decay spectroscopy of the heaviest nuclei
(3) Study of the chemical properties of the heaviest elements
(4) Study of the reaction mechanism of the fusion process (theory)

3. Summary of Research Activity

(1) Searching for new elements

To expand the periodic table of elements and the nuclear chart, we will search for new elements.

(2) Spectroscopic study of the nucleus of heavy elements

Using the high sensitivity system for detecting the heaviest element, we plan to perform a spectroscopic study of nuclei of the heavy elements.

(3) Chemistry of superheavy elements

Study of chemistry of the trans-actinide (superheavy element) has just started world-wide, making it a new frontier in the field of chemistry. Relativistic effects in chemical property are predicted by many theoretical studies. We will try to develop this new field.

(4) Study of a reaction mechanism for fusion process

Superheavy elements have been produced by complete fusion reaction of two heavy nuclei. However, the reaction mechanism of the fusion process is still not well understood theoretically. When we design an experiment to synthesize nuclei of the superheavy elements, we need to determine a beam-target combination and the most appropriate reaction energy. This is when the theory becomes important. We will try to develop a reaction theory useful in designing an experiment by collaborating with the theorists.

Head
Kosuke MORITA

Members
Hiromitsu HABA
Kouji MORIMOTO

Special Postdoctoral Researcher
Takatoshi ICHIKAWA
Daiya KAJI
Kazutaka OZEKI

Contract Technical Scientist
Akira YONEDA

Visiting Scientists
Kazuhiko AKIYAMA (Tokyo Metropolitan Univ.)

Masato ASAI (Japan Atomic Energy Agency)
Shin-ichi GOTO (Niigata Univ.)
Kouichi HAGINO (Tohoku Univ.)
Yoshitaka KASAMATU (Japan Atomic Energy Agency)
Hisaaki KUDO (Fac. Sci., Niigata Univ.)
Yuichiro NAGAME (Japan Atomic Energy Agency)
Tetsuya MURAKAMI (Grad. Sch. Sci., Kyoto Univ.)
Minoru SAKAMA (Tokushima Univ.)
Atsushi SHINOHARA (Osaka Univ.)
Tetsuya SATO (Japan Atomic Energy Agency)
Keisuke SUEKI (Grad. Sch. Pure Appl. Sci., Univ. Tsukuba)
Fuyuki TOKANAI (Dept. Phys., Yamagata Univ.)
Atsushi TOYOSHIMA (Japan Atomic Energy Agency)
Kazuaki TSUKADA (Japan Atomic Energy Agency)
Akihiko YOKOYAMA (Dept. Chemi., Kanazawa Univ.)
Takashi YOSHIMURA (Osaka Univ.)

Research Consultants
Takashi INAMURA
Kenji KATORI
Toru NOMURA

Students

Junior Research Associate
Takahiro AKIYAMA (Saitama Univ.)

Part-time Staff I(Research Support)
Nozomi SATO (Grad. Sch. Sci. Eng., Tohoku Univ.)

Student Trainees
Tomohiro NANRI (Dept. Chem., Kanazawa Univ.)
Itsuro YAMAZAKI (Dept. Chem., Kanazawa Univ.)

Theoretical Nuclear Physics Laboratory

1. Abstract

Nuclei are finite many-particle systems composed of protons and neutrons. They are self-bound in femto-scale (10^{-15}m) by the strong interaction (nuclear force) whose study was pioneered by Hideki Yukawa. Uncommon properties of the nuclear force (repulsive core, spin-isospin dependence, tensor force, etc.) prevent complete microscopic studies of nuclear structure. There exist number of unsolved problems even at present. In addition, radioactive beam facilities reveal novel aspects of unstable nuclei. We are tackling these old problems and new issues in theoretical nuclear physics, developing new models and pursuing large-scale calculations of quantum many-body systems. We are also strongly involved in research on other quantum many-body systems, to resolve mysteries in the quantum physics

2. Major Research Subjects

(1) Nuclear structure and quantum reaction theories
(2) First-principle calculations with the density functional theory for many Fermion systems
(3) Computational nuclear physics

3. Summary of Research Activity

(1) Large amplitude dynamics in shape coexistence phenomena

Shape coexistence phenomena in proton-rich ^{68}Se and ^{72}Kr have been studied with the adiabatic self-consistent collective coordinate method. The canonical collective variables, mass parameter, and potential were determined self-consistently. The calculation indicates importance of the triaxial degrees of freedom for the tunneling dynamics between two quasi-vacua at prolate and oblate shapes. The collective Hamiltonian was requantized to calculate excitation spectra and transition properties for the first time. The shape mixing is hindered by coupling to the rotational motion to localize collective wave functions around prolate and oblate minima.

(2) Time-dependent density funcitonal approach to nuclear photoabsorption

Nuclear photoabsorption cross sections were calculated with the finite amplitude method for the time-dependent density functional theory which we had proposed in 2007. We used the supercomputers at RIKEN, KEK, and University of Tsukuba to perform the large-scale calculations for cross sections from Be to Ni isotopes, from proton to neutron driplines. Detailed analysis is under progress.

(3) Nuclear matter density distributions and nuclear radii

We revisited the commonly accepted notion that the difference between interaction and reaction cross sections is negligible at relativistic energies. We show that the difference is clear especially in small mass number region. It could bring about uncertainties of the order of nuclear skin thickness of stable nuclei in estimates of nuclear matter radii

(4) Nuclear structure studies using nuclear reactions

We systematically studied total reaction cross sections of carbon isotopes with N=6-16 on a proton target for wide range of incident energies. The calculations include the reaction cross sections of ^{19,20,22}C at 40A MeV, the data of which had been measured at RIKEN. Our numerical results are consistent with the preliminary data, and suggest very small S_{2n} for ^{22}C.

(5) Neutron Cooper pair in deformed neutron-rich nuclei

Appearance of di-neutron correlation by neutron skin and continuum effects in neutron rich Mg and Cr isotopes is pointed out. By evaluating the moments of inertia, we show that the rotational excitations are qualitatively influenced by the di-neutron correlation and the systematic experimental information of the E2 properties can indicate the novel correlation.

(6) Molecular structure of ^{12}Be studied with the generalized two-center cluster model

We investigate the molecular structures in the unbound region and the reaction dynamics on their excitation. In this study, we employ the generalized two-center cluster model (GTCM) which can describe the atomic and molecular limits of the system with two inert-cores plus valence neutrons. We applied the GTCM to ^{12}Be and found that the various molecular configuration appear above the α+^{8}He threshold and they are strongly excited by the reaction of α+^{8}He $\rightarrow$ ^{6}He + ^{6}He.

Head

Takashi Nakatuskasa

Members

Akihisa Kohama

Special Postdoctoral Researcher

Makoto Ito

Yasuro Funaki

Contract Researcher

Masayuki Yamagami

Visiting Scientists

Tsunenori Inakura (Grad. Sch. of Pure and Applied Sci., Univ. Tsukuba)

Nicolas L.J. Michel (Dept. Phys., Kyoto Univ.)

Taiichi Yamada (Kanto Gakuin Univ.)

Takenori Furumoto (Osaka City Univ.)

Research Fellow

Kosai Tanabe

Students

Junior Research Associa

Student Trainees

Shuuichiro Ebata

Shouhei Iwasaki

Secretary

Shinko Odai

SLOWRI Team

1. Abstract

A next-generation slow radioactive nuclear ion beam facility (SLOWRI) which provides slow, high-purity and small emittance ion beams of all elements is being build as one of the principal facilities at the RIKEN RI-beam factory (RIBF). High energy radioactive ion beams from the projectile fragment separator BigRIPS are thermalized in a large gas catcher cell. The thermalized ions in the gas cell are guided and extracted to a vacuum environment by a combination of dc electric fields and inhomogeneous rf fields (rf carpet ion guide). From there the slow ion beam is delivered via a mass separator and a switchyard to various devices: such as an ion trap, a collinear fast beam apparatus, and a multi-reflection time of flight mass spectrometer. In the R&D works at the present RIKEN facility, an overall efficiency of 5% for a 100A MeV ^{8}Li ion beam from the present projectile fragment separator RIPS was achieved and the dependence of the efficiency on the ion beam intensity was investigated.

First spectroscopy experiment at the prototype SLOWI was performed on Be isotopes. Energetic ions of ^{7,10,11}Be from the RIPS were trapped and laser cooled in a linear rf trap and precision spectroscopy was performed. The evaluated ion temperature of <10 mK demonstrates that a reduction of more than 15 orders of magnitude for the kinetic energy of radioactive Be was achieved online. Precise investigation of the hyperfine structure will confirm the anomalous mean radius of the valence neutron of the so called neutron halo nucleus.

Other spectroscopy experiments using the slow RI-beams are also under progress in off-line setups. A collinear fast beam apparatus for nuclear charge radii measurements was build and tested with stable Ar+ ion beams. A multi-reflection time-of-flight mass spectrograph was build for precise and fast measurements of short-lived radioactive nuclei. A high mass resolving power of 200,000 has been achieved with a 3 ms measurement period.

2. Major Research Subjects

(1) Development and constraction of the next-generation slow RI-beam facility
(2) Precision hyperfine spectroscopy of trapped ions for magnetization distribution in a halo nuclues
(3) Nuclear charge radii measurements using ion trap and collinear fast beam apparatus
(4) Precision mass measurements of short-lived nucei using a multi-reflection TOF mass spectrograph
(5) Development of deceleration and cooling devices for energetic beams using gas cell and rf fields.
(6) Atomic physics and fundamental symmetry research investigating nuclear decay of an isolated atom

3. Summary of Research Activity

(1) Development of universal slow RI-beam facility

WADA, Michiharu, TAKAMINE, Aiko, SCHURY Peter, SONODA, Tetsu, OKADA, Kunihiro, KANAI, Yasuyuki, YOSHIDA, Atsushi, KUBO, Toshiyuki, YAMAZAKI, Yasunri, WOLLNIK, Hermann, SCHUESSLER, Hans, NODA, Koji, OHTANI, Shunsuke, KATAYAMA Ichiro

A next-generation slow radioactive nuclear ion beam facility (SLOWRI) which provides slow, high-purity and small emittance ion beams of all elements is being build as one of the principal facilities at the RIKEN RI-beam factory (RIBF). High energy radioactive ion beams from the projectile fragment separator BigRIPS are thermalized in a large gas catcher cell. The thermalized ions in the gas cell are guided and extracted to a vacuum environment by a combination of dc electric fields and inhomogeneous rf fields (rf carpet ion guide). From there the slow ion beam is delivered via a mass separator and a switchyard to various devices: such as an ion trap, a collinear fast beam apparatus, and a multi-reflection time of flight mass spectrometer. In the R&D works at the present RIKEN facility, an overall efficiency of 5% for a 100*A* MeV ^{8}Li ion beam from the present projectile fragment separator RIPS was achieved and the dependence of the efficiency on the ion beam intensity

was investigated.

(2) Laser spectroscopy of trapped radioactive beryllium isotope ions

WADA, Michiharu, TAKAMINE, Aiko, SCHURY Peter, SONODA Tetsu, OKADA, Kunihiro, KANAI, Yasuyuki, YOSHIDA, Atsushi, KUBO, Toshiyuki, YAMAZAKI, Yasunori, WOLLNIK, Hermann, SCHUESSLER, Hans, NODA, Koji, OHTANI, Shunsuke, KATAYAMA Ichiro

As a first application of the prototype SLOWRI setup, we are applying hyperfine structure spectroscopy to the beryllium isotopes to determine in particular the anomalous radius of the valence neutron of the neutron halo nucleus ^{11}Be, and to determine the charge radii of these beryllium isotopes through laser-laser double resonance spectroscopy of laser-cooled ions. Laser cooling is an essential prerequisite for these planned experiments. However, the exact resonance frequencies of the cooling transitions for radioactive beryllium isotopes are not known. In such light elements, the isotope shifts in the atomic transitions are larger than several 10 GHz and their dominant parts are due to complicated multi-electron correlations. Some theoretical works on the isotope shifts of the beryllium ion exist, however the values contradict each other at the level of accuracy needed.

The first laser spectroscopy experiments for beryllium isotopes were performed to measure the resonance frequencies of 2s $^2S_{1/2}$ - 2p $^2P_{3/2}$ transition of ^{7}Be+, ^{9}Be+ and ^{10}Be+ ions aiming at determining the specific isotope shift parameters. Then, the hyperfine structure of $^{11}Be^+$ and $^7Be^+$ ions using the laser-microwave double resonance spectroscopy were performed and A($^7Be^+$) = -742.7723(4) MHz and A($^{11}Be^+$) = -2677.308(2) MHz were determined for the first time. Precision measurements of the nuclear magnetic moments of these Be isotopes are in progress.

(3) Development of a multi-reflection TOF mass spectrograph

WADA, Michiharu, SCHURY Peter, TAKAMINE, Aiko, SONODA Tetsu, OKADA, Kunihiro, YAMAZAKI, Yasunori, WOLLNIK, Hermann,

The atomic mass is one of the most important quantity of a nucleus and has been studied in various methods since the early days of physics. Among many methods we chose a multi-reflection time-of-flight (MR-TOF) mass spectrometer. Slow RI beams extracted from the RF ion-guide are bunch injected into the spectrometer with a repetition rate of ~500 Hz. The spectrometer consists of two electrostatic mirrors between which the ions travel back and forth repeatedly. These mirrors are designed such that energy-isochrononicity in the flight time is guaranteed during the multiple reflections while the flight time varies with the masses of ions. A mass-resolving power of >200,000 has been obtained with about 500 reflections in a 30 cm length spectrometer. This mass-resolving power should allow us to determine ion masses with an accuracy of 10^{-7}. The advantages of the MR-TOF spectrometer are: 1) short measurement periods, typically 2 ms, which allows all neutron rich nuclei to be investigated, 2) the device is compact and its operation is simple, especially, it is independent from the all upstream devices, accelerators and fragment separators, 3) ions of more than isobars can be measured simultaneously, so that mass reference can easily be established in the mass spectra. In total, the number of measurable nuclides within a limited beam time would be larger than that can be achieved by other methods. It should be noted here also that this method can be used even during a low-duty parasite beam time. An on-line MR-TOF mass spectrograph with 80 cm length having an expected mass resolving power of 1,000,000 is under fabrication.

(4) Development of collinear fast beam apparatus for nuclear charge radii measurements

WADA, Michiharu, SCHUESSLER, Hans, IIMURA, Hideki, SONODA, Tetsu, SCHURY, Peter, TAKAMINE, Aiko, OKADA, Kunihiro, YAMAZAKI, Yasunori, WOLLNIK, Hermann,

The root-mean-square charge radii of unstable nuclei have been determined exclusively by isotope shift measurements of the optical transitions of singly-charged ions or neutral atoms by laser spectroscopy. Many isotopes of alkaline, alkaline-earth, noble-gases and several other elements have been measured by collinear laser spectroscopy since these ions have all good optical transitions and are available at conventional ISOL

facilities. However, isotopes of other elements especially refractory and short-lived ones have not been investigated so far.

In SLOWRI, isotopes of all atomic elements will be provided as well collimated mono-energetic beams. This should expand the range of applicable nuclides of laser spectroscopy. In the first years of the RIBF project, Ni and its vicinities, such as Ni, Co, Fe, Cr, Cu, Ga, Ge are planned to be investigated. They all have possible optical transitions in the ground states of neutral atoms with presently available laser systems. Some of them have so called recycle transitions which enhance the detection probabilities noticeably. Also the multistep resonance ionization (RIS) method can be applied to the isotopes of Ni as well as those of some other elements. The required minimum intensity for this method can be as low as 10 atoms per second.

We have built an off-line mass separator and a collinear fast beam apparatus with a large solid-angle fluorescence detector. A 617 nm transition of the metastable Ar+ ion at 20 keV was measured with both collinear and anti-collinear geometry that allowed us to determine the absolute resonant frequency of the transition at rest with more than 10^{-8} accuracy. Such high accuracy measurements for Ti and Ni isotopes are in progress.

Head
Hiroyoshi SAKURAI

Members
Michiharu Wada.

R&D team for multiparticle spectrometer

1. Abstract

Main task of R&D team for multiparticle spectrometer is to make R&D on broad range multiparticle spectrometer SAMURAI (Superconducting Analyser for Multiparticles from RadioIsotope beams), which is planned to built at BIBF for nuclear structure experiments using RI beams at RIBF. Design of the large superconducting magnet is being designed helped by various companies. Various detectors necessary for large magnetic spectrometer are being developed and tested.

2. Major Research Subjects

(1) Design of large superconducting magnet system
(2) R&D on High-accuracy/high-rate position detectors
(3) R&D on High-accuracy velocity measuring detectors
(4) R&D on High-accuracy total energy detectors

3. Summary of Research Activity

(1) Design of Large Superconducting magnetic spectrometer
(Kobayashi, Yoneda, Otsu, Kubo, Sekiguchi, Nakamura, Chiga, Iwasa, Murakami)

Basic design of large superconducting dipole magnet, which is central part of the SAMURAI system, is being made in collaboration with outside companies.

(2) R&D of Various detectors for large superconducting magnetic spectrometer
(Kobayashi, Otsu, Sato)

As necessary detectors for large superconducting magnetic spectrometer, we have developed various dectors, such as high-accuracy/high-rate position detectors, high-precision velocity detectors, high-precision total-energy detectors. Their performances have been checked using heavy-ion beams at HIMAC accelerator facility.

Head
Hiroyoshi SAKURAI

Senior Visiting Scientist
Toshio Kobayashi (Grad. Sch. Sci. Fac. Sci.,Tohoku Univ.)

Polarized RI Beam Team

1. Abstract

The team conducts the research and development on production of spin-polarized/alignment RI beams, and apply it to the research on nuclear physics and material science. The microscopic investigation of physical and chemical processes is performed by nuclear techniques which take advantage of the intrinsic nuclear properties and phenomena (spins, electromagnetic moments, decay modes etc.). In particular, the precession/resonance of a polarized/aligned nuclear spin under an external field is observed through change in the angular distribution of radiation, for the study of nuclear structures via nuclear moments. The same method, as well as the Moessbauer technique, are used for the investigation of condensed matter such as ferromagnets, fullerenes, systems with dilute magnetic impurities etc. by capitalizing radioactive nuclei as microscopic probes into them. All these research activities are to be extended to wide variety of unstable nuclei which the forth-coming facility, RI Beam Factory (RIBF), will provide. A method to produce beams of highly polarized radioactive nuclei, taking full advantage of RIBF, is being developed.

2. Major Research Subjects

(1) Production of spin-polarized RI beam with fragmentation reaction
(2) Production of spin-alignment RI beam
(3) Development of highly polarized slow RI beams
(4) Development of radioactive nuclear probes for condensed matter studies

3. Summary of Research Activity

(1) Production of fragment-induced spin polarization

In the production of RI beams with the projectile fragmentation reaction, spin-polarized RI beam can be produced in the projectile-fragmentation reaction by selecting the appropriate scattering angle and outgoing momentum. With the obtained spin-polarized nuclei, nuclear magnetic moments and electric quadrupole moments have been determined by means of the b-NMR method through the change in the angular distribution of the emitted b rays. The nuclear structure has been investigated for the nuclei far from the stability line based on this method. The sub-themes are the following.

1) Production of the spin-polarized neutron-rich Al isotopes from ^{40}Ar-primary beams and measurements of the nuclear electro-magnetic moments. (Ueno、Yoshimi、Nagatomo、Ichikawa, Kobayashi)

2) Production of the spin-polarized $^{33\text{-}34}$Al (N>20) beams from ^{36}S-primary beams and measurements of the nuclear electric-quadrupole moments (Nagatomo、Ueno、Yoshimi、Ichikawa)

3) Production of spin-polarized neutron-rich Si isotopes from ^{48}Ca-primary beams and measurements of the nuclear electro-magnetic moments. (Yoshimi、Ueno、Nagatomo、Ichikawa)

(2) Production of spin-aligned RI beams

1) Production of spin-aligned nuclei is essentially important for the study on the nuclear structure through the measurement of excited-state nuclear moments, which is also useful to material sciences. Various techniques of the production method for obtaining spin-aligned RI beams have been developed. Sub-themes are the following.

2) Production of spin-aligned ^{32m}Al beams in the projectile fragmentation and the measurement of the excited-state nuclear moment. (Ueno、Yoshimi、Nagatomo、Ichikawa)

Production of spin-aligned ^{134m}Ce beams as a probe of material science (Ueno, Yoshimi)

3) Development of a new method for the production of spin-aligned RI beams via the two-step fragmentation reactions. (Ueno, Yoshimi, Nagatomo, Ichikawa)

4) Studies on the properties of Transient Field at the high-velocity region. (Ueno, Yoshimi, Ichikawa)

5) Application of the Recoil-into-vacuum method to RI-beam experiments (Ueno, Yoshimi)

(3) Production of highly spin-polarized low-energy RI beams

New methods and devices have been developed for producing highly spin-polarized RI beams in low beam-energy region to overcome difficulties expected in the above method 1. The high spin polarization and the low beam energy are important not only for nuclear-moment measurements but also for spin-related subjects in nuclear physics, fundamental physics, and material sciences. Sub-themes are the following.

1) Development of a new atomic-beam resonance method to combine with fragmentation-based RI beams (Yoshimi, Ueno)

2) Production of low-energy spin-polarized ^{17}N beams via the transfer reactions based on the inverse kinematics and its application (Shimada, Yoshimi, Ueno)

(4) Development of RI probes and application for the condensed matter sciences

Utilizing RI beams as a probe, online Mössbauer spectroscopy and online perturbed angular correlation experiments have been carried out through the g-ray measurements. The microscopic structures, dynamics in ferromagnets, and properties of semiconductors have been investigated from the deduced internal local fields and the spin relaxation of the probe in materials. The methods and apparatus have been developed. Also, basic studies on the probe nuclei have been carried out. Sub-themes are the following.

1) (Production of high quality ^{57}Mn beams for the online Mössbauer spectroscopy (Kobayashi, Ueno, Yoshimi, Nagatomo)

2) Development of the on-line perturbed angular-correlation method with ^{19}O beams as a new probe (Kobayashi, Ueno, Yoshimi, Nagatomo, Ichikawa)

Team Leader

Hiroyoshi SAKURAI

Members

Yoshio KOBAYASHI
Hideki UENO
Akihiro YOSHIMI
Yuichi ICHIKAWA

Rare RI-ring Team

1. Abstract

We are developing the isochronous storage ring to measure the mass for rare radioactive isotopes (Rare RI ring). It is assumed that uranium is synthesized by neutron capture process after the supernovae explosion (r-process). To prove r-process, mass measurements for the rare RI are indispensable. To deduce the mass, we measure the circulation time (cyclotron frequency) for the rare RI inside the ring. RI beams produce in RIBF have some energy spread. To compensate the spread, isochronicity inside the ring is indispensable (isochronous storage ring). We will inject the rare RI one by one to the ring (individual injection) to identify the RI event-by-event. To perform the individual injection, we need a long injection line for the ring. The isochronous storage ring and the individual injection are very unique system.

2. Major Research Subjects

(1) Developments of isochronous storage ring to measure mass of rare RI
(2) Developments of detectors for mass measurements

3. Summary of Research Activity

(1) Developments of isochronous storage ring to measure mass of rare RI

We are improving conceptual designs for an isochronous storage ring, kicker magnets, and the injection line to the storage ring. The storage ring consists of six sector magnets. The edge angles of each sector magnets compensate the first order isochronism. For the kicker magnets, we fixed rough specifications. For the injection line, we performed the first order ion-optical calculations. Furthermore, we performed magnetic field measurements of a present sector magnet in BigRIPS by using NMR with high accuracy.

(2) Developments of detectors for mass measurements

The group in Saitama University performed the experiment to measure the time resolution of thin plastic-scintillators in HIMAC. The results show, for heavy ion beams with 200 A MeV, reasonably good timing resolution can be achieved even in the thin scintillator with 10 micron thickness. The group in University of Tsukuba measured a response time of Hybrid Photo Detector (HPD), which can replace with traditional Photo Multi Tube (PMT). The results show that the response time of HPD is faster than that of PMT by about 10 ns.

Team Leader
Hiroyoshi SAKURAI

Research Associate
Yoshitaka YAMAGUCHI

JRA
Shinpei NAKAJIMA (Saitama University)
Tetsuaki Moriguchi (University of Tsukuba)

Visiting Scientists
Akira OZAWA (Inst. Phys., Univ.of Tsukuba)
Yusuke YASUDA (Inst. Phys., Univ.of Tsukuba)
Ichiro ARAI (Inst. Phys., Univ.of Tsukuba)
Takeshi SUZUKI (Saitama University)
Takayuki YAMAGUCHI (Saitama University)
Takashi OHTSUBO (Niirata University)
Takashi KIKUCHI (Utsunomiya University)

SCRIT Team

1. Abstract

We aim at the investigation of internal nuclear structure of short-lived radioactive nulei (RI) by means of electron scattering. Electron scattering for RI's has never been performed duo to inability to make target of these nuclei. An electron-RI collider system, which requires a huge accelerator complex, has so far been unique solition to overcom the difficulty. We have developed a novel internal target system named SCRIT (Self-Confining RI Ion Target) in an electron storage ring to make the experiment easier with much compact experimental system.

2. Major Research Subjects

Developement of the SCRIT technology and electron scattering for unstable nuclei

3. Summary of Research Activity

Development of a novel internal target of unstable nuclei (SCRIT) in an electron storage ring for electron scattering experiment

(Wakasugi, Suda, Ito, Emoto, Nakamura, Kurita, Tamae, Noda, Shirai, Yano)

We have successfully developed a novel internal target system, which is to be used in an electron storage ring. This is named SCRIT (Self-Confining Radioactive Ion Target). This technology can localize specific ions on the electron beam axis using so-called “ion-trapping” phenomenon and form a fixed target of unstable nuclei. This will realize electron-scattering experiments for short-lived nuclei that have never been succeeded in. The R&D study of the SCRIT is now under way at the KSR in Kyoto University. We confirmed that approximately 10^7 of ^{133}Cs ions in the SCRIT device, and the angular distribution of elastically scattered electrons from the trapped Cs ions was measured. The collision luminosity was reached to be 10^{26} /cm^2/s, and the feasibility of electron scattering for unstable nuclei was completely demonstrated. The SCRIT technology will open a new application of electron rings.

Team Leader

Hiroyoshi SAKURAI

Members

Takashi EMOTO
Sachiko ITO
Masanori WAKASUGI

GARIS Team

1. Abstract

Development and maintenance of devices related to study of the superheavy elements.

2. Major Research Subjects

(1) Maintenance and development of a recoil separator.
(2) Development of rapid chemistry devices.

3. Summary of Research Activity

(1) Maintenance and development of recoil separator

A gas-filled recoil separator has been used as a main experimental device for the study of superheavy elements. We will develop and maintain the related devices. We will also offer user-support if a researcher wishes to use the devices for his/her own research program.

(2) Development of devices for fast chemistry

We do research and development of devices for fast chemistry of superheavy elements. We also offer user□support for potential users.

Team Leader
Kosuke MORITA

Members
Kouji MORIMOTO
Hiromitsu HABA

Special Postdoctoral Researcher
Daiya KAJI
Kazutaka OZEKI

Contract Technical Scientist
Akira YONEDA

Research Associate
Hidetoshi KIKUNAGA

Junior Research Associate
Takahiro AKIYAMA (Grad. Sch. of Sci.& Eng., Saitama Univ.)

BigRIPS Team

1. Abstract

This team is in charge of design, construction, development and operation of BigRIPS in-flight separator and its related experimental installations at RI beam factory (RIBF). They are employed not only for the production of RI beams but also the experimental studies using RI beams.

2. Major Research Subjects

Design, construction, development and operation of BigRIPS in-flight separator, RI-beam transport lines, and their related experimental installations

3. Summary of Research Activity

This team is in charge of design, construction, development and operation of BigRIPS in-flight separator, RI-beam transport lines, and their related experimental installations such as ZeroDegree spectrometer, at RI beam factory (RIBF). They are employed not only for the production of RI beams but also various kinds of experimental studies using RI beams.

The research subjects may be summarized as follows:

(1) General studies on RI-beam production using in-flight scheme.
(2) Studies on ion-optics of in-flight separators, including particle identification of RI beams
(3) Simulation and optimization of RI-beam production.
(4) Development of beam-line detectors and their data acquisition system.
(5) Experimental studies on production reactions and unstable nuclei.
(6) Development of superconducting magnets and their helium cryogenic systems.
(7) Development of a high-power production target system.
(8) Development of a high-power beam dump system.
(9) Development of a remote maintenance and remote handling systems.
(10) Operation, maintenance and improvement of BigRIPS separator system, RI-beam transport lines, and their related experimental installations such as ZeroDegree spectrometer and so on.

Team Leader
Toshiyuki Kubo

Members
Atsushi YOSHIDA
Koichi YOSHIDA
Masao OHTAKE
Yoshiyuki YANAGISAWA

Contract Researchers
Kensuke KUSAKA
Tetsuya OHNISHI

Research Associates
Naoki FUKUDA
Hiroyuki TAKEDA

Part-time Staff
Hidekazu KUMAGAI

Senior Visiting Scientist
Susumu SHIMOURA (CNS, Grad. Sch. Sci., Univ. of Tokyo)

Computing and Network Team

1. Abstract

Development, management and operation of the computing and network environment, mail server and data acquisition system and control of the information security of the Nishina Center for Accelerator-Based Science

2. Major Research Subjects

(1) Development, management and operation of the computing
(2) Development, management and operation of the mail server
(3) Development, management and operation of the data acquisition system
(4) Development, management and operation of the network environment
(5) Control of the information security

3. Summary of Research Activity

Development, management and operation of the computing and network environment, mail server and data acquisition system and control of the information security of the Nishina Center for Accelerator-Based Science

Team Leader
Takashi ICHIHARA

Member
Yasushi WATANABE

Detector Team

1. Abstract

This team is in charge of organizing various detector developments performed at in-house laboratories and groups, in order to improve mutual share of knowledge and experience. The team is also in charge of development and operation of various target systems.

2. Major Research Subjects

(1) Development of delay-line PPAC

(2) Development of transmitter/receiver for fast signal transmission through optical fibers

(3) Development and operation of various target system, such as cryogenic hydrogen and helium targets for nuclear physics experiments and production targets for RI-beam production.

3. Summary of Research Activity

This team is presently focusing on developments of delay-line PPAC and fast signal transmission system consisting of a pair of fast transmitter and receiver coupled with optical fibers. These two developments are essential for particle identification at BigRIPS. The team is also in charge of development and operation of various target systems.

(1) Delay-line PPAC

At BigRIPS, a purity of radioactive isotope beams (RIBs) is as low as 10% or less at medium and heavy mass region. Thus, development of detectors for high-rate use is one of goals in this team. With this respect, we have developed a position-sensitive Parallel Plate Avalanche Counter (PPAC). Delay-line read-out technique appropriate for high rate use is employed for position determination. This PPAC has two stripped-electrodes for both horizontal and vertical positions, and this configuration leads to high performance in terms of efficiency as well as position resolution. More than ten PPACs have been installed at BigRIPS, and successfully used for the first RI-beam production.

(2) Fast transmitter and receiver for optical fiber.

In general co-axial metal wires are used for fast signal transmission. Instead, we have developed a special circuit of transmitter and receiver for optical fiber.

At a new facility of RIBF, circuits for detectors are located at several focal planes of the BigRIPS, and distances between focal-planes and counting room are as long as 100 m. To introduce optical fibers in signal transmission, we focus on a common ground at each focal plane, and easily isolate the ground levels. A problem in use of optical fiber was no fast transmitter/receiver with a low cost, which are not available in market. We have developed a pair of fast transmitter and receiver for optical fibers with a semiconductor laser and photo diode. This circuit has a fast time response of more than 1GHz. Attenuation of signal amplitudes is negligibly small even at a long distance transmission of more than 100m. Many sets of transmitter/receiver with an optical fiber have been manufactured and installed for detectors at BigRIPS, and successfully used for the first RI-beam production. This fast signal transmission scheme will be standard at RIBF.

(3) Development and operation of various target systems such as cryogenic targets and production targets

Development and operation of cryogenic targets, such as liquid hydrogen and helium targets and a solid hydrogen target, are very important for nuclear physics experiments using RI beams at BigRIPS and RIBF. Development and operation of high-power production target are also crucial for RI-beam production at BigRIPS.

Head

Toshiyuki KUBO

Contract Researcher
Kanenobu TANAKA
Akira YONEDA

Part time staff I
Hidekazu KUMAGAI

Senior Visiting Scientist
Hirohiko SHIMIZU (Inst.of Materials Structure Sci., KEK)

User Support Office

1. Abstract

The RIKEN RI Beam Factory is the world preeminent facility providing the greatest opportunities for scientific researches. It is our important mission to serve for a broad range of application of a large variety of researchers so that we bring out the best performance of the RI Beam Factory. We manage to facilitate the use of RI Beam Factory to the researchers both inside and outside of RIKEN, to support experiments using the accelerator complex, to exploit industrial application researches, and to promote the RI Beam Factory to interested researchers

2. Major Research Subjects

(1) Facilitation of the use of the RI Beam Factory
(2) Support of experiments in the RI Beam Factory
(3) Promotion of the RI Beam Factory to interested researchers

3. Summary of Research Activity

In order to facilitate the use of RI Beam Factory to the researchers both inside ad outside of RIKEN, we have organized international Program Advisory Committee, consisting of world leading scientists, to review proposals, purely based on their scientific merit and feasibility, in the fields of nuclear physics (NP) and material-and-life science (ML). The NP- and ML-PAC meetings are organized twice a year. In the year 2007, we received 53 proposals in total, where over 800 researchers from worldwide are contributing.

Team Leader
Toshimi SUDA

Members
Mieko KOGURE

Technical Staff I
Narumasa MIYAUCHI

Assistant
Tomoko IWANAMI
Yuri TSUBURAI

Experimental Support Team

1. Abstract

We are supporting users of accelerators in the Nishina Center.

2. Major Research Subjects

No research.

3. Summary of Research Activity

Supporting activities are carried out for any experiments using accelerators of RILAC, AVF cyclotron, RRC and/or RIBF accelerators.

Team Leader

Masayuki KASE

Members

Nobuhisa FUKUNISHI
Naohito INABE
Osamu KAMIGAITO
Takahide NAKAGAWA
Hiroki OKUNO
Naruhiko SAKAMOTO
Masanori WAKASUGI
Tamaki WATANABE

Industrial Cooperation Team

1. Abstract

The scope of the industrial cooperation team includes industrial application of RIBF facility and research and development for industrial application of accelerator associated technologies.

2. Major Research Subjects

(1) Distribution of radioisotopes Zn-65 and Cd-109 produced at RIKEN AVF Cyclotron
(2) Application of data acquisition and signal processing technologies

3. Summary of Research Activity

(1) Commercial distribution of radioisotopes

At RIBF, various specific radioisotopes for research have been produced with the cyclotrons and used for various joint research projects. In October 2007, we have started distribution of radioisotopes Zn-65 and Cd-109 commercially to nonaffiliated users under a contract between Japan Radioisotope Association and RIKEN. Advancements of production techniques are being pursued for stable supply and quality level.

(2) Application of data acquisition and signal processing technologies

"M-sequence modulation (Takeichi et al., 2007)" enables efficient estimation of a response function from a signal time-series. We are currently working on its further developments and applications to basic and industrial research fields.

Team Leader

Tadashi KAMBARA

Members

Tomoko ABE
Shuichi ENOMOTO
Hiroshige TAKEICHI

Part time staff

Akira OTA
Yukio TSUCHIDA
Keiko YAMAZAKI
Taro YOSHIMI

Visiting Scientists

Makiko KAGA (National Inst. of Mental Health, Natl. Ctr. Neurol. Psychiat.)
Atsuko GUNJI (National Inst. of Mental Health, Natl. Ctr. Neurol. Psychiat.)
Michiteru KITAZAKI (Res. Center for Future Vehicle. Toyohashi Univ. of Tech.)
Takako SAITO (Grad. Sch. of Design, Kyushu Univ.)

Student Trainees

Yasuhisa FUJIKI (Fac. of Eng., Toyohashi Univ. of Tech.)
Shinichiro HARIYAMA (Dept. of Knowledge-based Information Eng., Toyohashi Univ. of Te
Shinichi ONIMARU (Dept. of Knowledge-based Information Eng., Toyohashi Univ. of Tech.)

Radiation Laboratory

1. Abstract

Nucleons, such as protons and neutrons, are a bound state of constituent quarks glued together with gluons. The detail structure of nucleons, however, is not well understood yet. Especially the mechanism to build up the spin of proton, which is 1/2, is a major problem in physics of the strong force. The research goal of Radiation Laboratory is to solve this fundamental question using the first polarized-proton collider, realized at RHIC, Brookhaven National Laboratory (BNL) in USA. RHIC stands for Relativistic Heavy Ion Collider, aiming also to create Quark Gluon Plasma, the state of Universe just after the Big Bang. RIKEN-BNL Research Center (RBRC) directed by N. Samios carries our core team at BNL for those exciting researches. Recent data analysis has shown that the proton spin carried by gluons is indeed small, which is a very striking finding beyond our expectations. We have been doing other pioneering researches at the domestic accelerators at RIKEN and High Energy Accelerator Research Organization (KEK), which is now proceeded to the new experiment at J-PARC. We are also performing technical developments such as novel ion sources, super conducting detectors, fine pitch pixel detectors and neutron optical devices.

2. Major Research subjects

(1) Spin physics with relativistic polarized-proton collisions at RHIC
(2) Study of nuclear matter at high temperature and/or at high density
(3) Technical developments on radiation detectors and accelerators

3. Summary of Research Activity

(1) Experimental study of spin structure of proton using RHIC polarized proton collider

[See: RIKEN-BNL Research Center Experimental Group (Heavy Ion Basic Science - Study of Spin Physics Using RHIC)]

(2) Experimental study of quark-gluon plasma RHIC heavy ion collider

[See: RIKEN-BNL Research Center Experimental Group (Heavy Ion Basic Science - Study of Spin Physics Using RHIC)]

(3) Study of nuclear medium effect on vector mesons at KEK-PS

From the experiment E325 performed at KEK-PS, we have discovered the spectral functions of vector mesons (φ, ρ and ω) are modified in nuclear matter, which are theoretically expected due to the chiral symmetry restoration. This discovery was press-released and becomes very popular, resulting in a book for general publicity and a scientific TV program. Also an award was given from RIKEN for this discovery. The second generation experiment is proposed to J-PARC and the first-stage approval was given for the physics merit and experimental feasibility. Works are ongoing for detector developments required for the new experiment. Especially several trial fabrications are done for GEM (Gas Electron Multiplier) which is a key detector to trace particles in a high rate circumstance.

(4) Study of Accelerator and Ion source

To achieve highly polarized beams in RHIC it is necessary to understand the AGS (RHIC injector synchrotron) spin dynamics. The normal-conducting partial-snake magnet, which we have developed for AGS years ago, is now in a stable operation with the other super-conducting snake magnet in AGS. After the departure of Researcher M. Okamura to BNL, this research category is moved to the collaborative work with BNL. Major equipments were transferred to BNL and became operational to continue the development of ion source with direct plasma injection scheme, with helps of two of our students.

(5) Detector development for PHENIX experiment

We have been developing the silicon vertex tracker (VTX) in order to enhance physics capability of the

PHENIX detector at RHIC. It consists of two inner layers of pixel detectors and two outer layers of strip detectors. RIKEN Radiation Laboratory group is responsible for the ladder fabrication of the pixel detector. The production of high-signal-density low-material-budget flexible printed circuit board (bus) was started followed by a check procedure using dedicated test equipments. Prototype of the ladder was assembled on the fabricated bus and showed its functionality within the full PHENIX data acquisition chain. Also the assembly procedure with 10-micron accuracy was established.

We also have been developing the momentum-sensitive trigger system for the PHENIX muon arms under the collaboration with KEK and Kyoto University. The prototype electronics was tested in the real PHENIX detector environment and its performance was confirmed.

(6) Research and development of superconductor radiation detectors

Superconductor radiation detectors are able to measure the energies of photons with a much better resolution than any type of conventional detectors. They are capable of detecting photons over a wide energy range and also charged particles. We have been developing superconducting tunnel junctions (STJs) as high-resolution radiation detectors. This year, we have started new collaborations between KEK and University of Tsukuba. With KEK, development of Aluminum-based-STJ(Al-STJ) was started to be applied for future polarization measurements of cosmic microwave background (CMB). We fabricated Al-STJs and measured their I-V curves at 0.4K. At the moment, although their properties are not so uniform, we have several good STJs which can be applicable for microwave detection. Now we are preparing an experimental environment with an adiabatic demagnetization refrigerator. With Univ. of Tsukuba, we have started to develop Hafnium-based-STJ (Hf-STJ), which will be used as infrared detector for a future neutrino-mass-measurement experiment. Since there are no reports about Hf-STJ in the world, we studied characteristics of Hf films deposited by a sputtering method. We found sputter parameters for stress-free film deposition, and that Tc of the Hf film became similar to that for a bulk by applying 300-degree heating during the Hf deposition. We are now investigating how to process Hf film to a shape of tunnel junction because conventional reactive-ion etching methods are not applicable to Hf.

(7) Neutron optics

Cold or thermal neutron beam is a high-sensitivity probe to study not only the structure of condensed matter, but also nuclear and particle physics. However, its realistic applications are still limited since the numbers of available neutron sources are small and their intensities are low. This project aims to enhance the efficiency in using those precious neutron beams by improving the neutron beam optics, in order to maximize scientific outputs within a short period of time. Base on the developed technologies, devices are fabricated and distributed to other laboratories and universities by “Riken Venture Company”, Japan Neutron Optics Inc.

This year, Micro Focusing Small Angle Neutron Scattering (mfSANS), which consists of ellipsoidal neutron mirrors and a position sensitive neutron detector developed by us, has been constructed in the research reactor JRR3M in Japan Atomic Energy Agency. We have confirmed that mfSANS works successfully.

We have started construction of a new beam line for fundamental physics research at 1MW Pulse Spallation Neutron Source in J-PARC. This beam line was designed by applying our knowledge and technique of neutron optics. We have been developing two types of neutron interferometer, one with multi-layer mirrors and the other with a silicon crystal, to measure Aharonov-Casher effect at this beam line.

(8) Theoretical study of hadron physics

A first global analysis of fragmentation functions for light mesons (pions and kaons) was performed by fitting the NLO differential cross sections to the experimental data of electron-positron annihilation, deep inelastic lepton-hadron scattering and proton-proton collisions. A similar analysis of fragmentation functions for protons and charged hadrons, which is complementary to the previous one, was also performed. These results have been published in journals and available for any studies of inclusive production of these hadrons in QCD hard scattering processes.

The photoproduction cross section of two hadrons in polarized lepton-hadron collision was calculated in the framework of perturbative QCD at the next-to-leading order accuracy and phenomenological studies of di-hadron production at HERMES and COMPASS were performed. Developing this framework to the case of hadroproduction of massive quarks, open charm production at GSI-FAIR and J-PARC was also studied.

The effects of soft gluon resummation on double-spin asymmetry for dilepton's transverse momentum spectrum in transversely polarized Drell-Yan (tDY) process were calculated at the next-to-leading logarithmic accuracy. Newly developed technique for transverse momentum resummation was studied in detail and a novel asymptotic formula for the asymmetry was derived. By performing phenomenological studies for dilepton production in tDY process at RHIC, J-PARC and GSI, the general properties of the asymmetry in pp and ppbar collisions were clarified.

The light-cone wave function (LCWF) of B mesons for exclusive decays is calculated. Performing the operator product expansion of a heavy-light non-local operator in the framework of heavy quark effective theory (HQET) including up to dimension-5 operators, the LCWF of B mesons are expressed in terms of three well-known HQET parameters. Evolution equation for the LCWF was solved analytically in coordinate space and quantities which appear in the factorization formula for exclusive B decays were calculated.

Head

Hideto EN'YO

Members

Yasuyuki AKIBA
Yuji GOTO
Itaru NAKAGAWA
Yoshie OTAKE
Hiromi SATO
Atsushi TAKETANI
Yasushi WATANABE
Satoshi YOKKAICHI

Special Postdoctoral Researchers

Yoshinori FUKAO
Kenji MISHIMA
Nobuyuki KAMIHARA

Contract Researchers

Ryo ICHIMIYA
Maki KUROSAWA
Kazuaki IKEDA
Soichiro KAMETANI
Hiroyuki KAWAMURA
Yoshiyuki ONUKI
Marco Stratmann
Kohei FUJIWARA
Masayuki NIIYAMA

Tomoaki NAKAMURA

Research Consultant

Katsuya HIROTA

Senior Visiting Scientists

Ken-ichi IMAI (Grad. Sch. of Sci., Kyoto Univ.)
Toshiaki SHIBATA (Grad. Sch. of Sci. and Eng., Tokyo Inst. of Tech. Sch. of Sci.)
Hirohiko SHIMIZU (Inst. of Materials Structure Sci., KEK)
Koichi YAZAKI (Tokyo Woman's Christian Univ.)
Takashi NAKANO(RCNP)

Visiting Scientists

Tomohiro ADACHI (DAI-ICHI KIDEN CO.,LTD)
Christine A. AIDALA (Univ. Massachusetts, Amherst, USA)
Hiroshi AKOH (National Inst. of Advanced Industrial Sci. and Tech.)
Masahiro AOYAGI (National Inst. of Advanced Industrial Sci. and Tech.)
Masayuki ASAKAWA (Grad. Sch. of Sci., Osaka Univ.)
Alexander Bazilevsky (BNL, USA)
Wolfgang BENTZ (Tokai Univ.)
Carlos CAMACHO (LANL)
Mickey CHIU (Univ. of Illinois at Urbana, USA)
Ondrej CHVALA (Unv.of California at Riverside)
Seishi DAIRAKU (Grad. Sch. of Sci., Kyoto Univ.)
Ttakumi Doi (University of Kentucky)
Dipanwita DUTTA (Nuclear Physics Division , Bhabha Atomic Research Centre)
Frank ELLINGHAUS (Univ. of Colorado, USA)
Waled EMAM (Univ. of California at Riverside, USA)
Hirotsugu FUJII (Grad. Sch./College of Arts and Sciences, Univ. of Tokyo)
Hisako FUJIMURA (Facul.Sci. , Kyoto Univ.)
Kenji FUKUSHIMA (YITP , Kyoto Univ.)
Haruhiko FUNAHASHI (Grad. Sch. of Sci., Kyoto Univ.)
Tetsuo HATSUDA (Grad. Sch. of Sci., Univ. of Tokyo)
Toshiyuki HATTORI (Res. Lab. for Nuclear Reactors, Tokyo Inst. of Tech. Sch. of Sci.)
Masashi HAZUMI (KEK)
Takeo HIGUCHI (KEK)
Masanori HIRAI (Grad. Sch. of Sci. and Eng., Tokyo Inst. of Tech. Sch. of Sci.)
Kensuke HONMA (Grad. Sch. of Sci., Hiroshima Univ.)
Takuma HORAGUCHI (Grad. Sch. of Sci., Hiroshima Univ.)
Katsuya ISHIGURO (Grad. Sch. of Natural Sci. & Tech., Kanazawa Univ.)
Noriyoshi ISHII (Grad. Sch. of Pure and Applied Sci., Univ. of Tsukuba)
Hirokazu ISHINO(Tokyo Inst.Technol.)
Barbara JAGER (Univ. Karlsruhe, Inst. Theoretical Phys., Germany)
Robert JAMESON (Goethe Universitat Frankfurt, Germany)
Osamu JINNOUCHI (Inst. of Particle and Nucl. Studies, KEK)
Masashi KANETA (Grad. Sch. of Sci., Tohoku Univ.)

Hirotsugu KASHIWAGI (Takasaki Advanced Radiation Res. Inst., JAEA)
Yuji KAWABATA (Kyoto Univ. Res. Reactor Inst.)
Takeo KAWASAKI (Grad. Sch. of Sci. and Tech., Niigata Univ.)
Akio KIYOMICHI (J-PARC, JAEA)
Yuji KOIKE (Grad. Sch. of Sci. & Tech., Niigata Univ.)
Dmitiri KOTCHETKOV (Univ. New Mexico, USA)
Shunzo KUMANO (Inst. of Particle and Nuclear Studies, KEK)
Teiji KUNIHIRO (Yukawa Inst. for Theoretical Phys., Kyoto Univ.)
Masahiko KURAKADO (Osaka Electro-CommunicationUniv.)
Han LIU (Phys. Dept. , New Mexico State Univ.)
Ming XIONG LIU (Los Alamos Nat. Lab., USA)
Yoshikazu MAEDA (RCNP , Osaka Univ.)
Keisuke MAEHATA (Fac. of Eng., Kyushu Univ.)
Yajun MAO (Peking Univ., China)
Yasuo MIAKE (Grad. Sch. of Pure and Applied Sci., Univ. of Tsukuba)
Tsutomu MIBE (KEK)
Shoichi MIDORIKAWA (Fac. of Software and Information Tech., Aomori Univ.)
Osamu MORIMATSU (Inst. of Particle and Nuclear Studies, KEK)
Takahiro MORISHIMA (KEK)
Hiroaki MYOREN (Grad. Sch. of Sci. & Eng., Saitama Univ.)
Sachio NAITO (Inst. of Materials Structure Sci., KEK)
Hiroshi NAKAGAWA (National Inst. of Advanced Industrial Sci. and Tech.)
Yoshifumi NAKAMURA (DESY, Germany)
Atsushi NAKAMURA (Information Media Center, Hiroshima Univ.)
Masashi OHNO (Sch. of Eng., Univ. of Tokyo)
Munehisa OHTANI (Inst. fuer Theoretische Physik, Universitact Regensburg, Germany)
Masahiro OKAMURA (BNL, USA)
Petra RIEDLER (CERN, Switzerland)
Koichi SAITO (Tokyo Univ. of Sci.)
Takuya SAITO (RCNP, Osaka Univ.)
Naohito SAITO (J-PARC, KEK)
Kenji SASAKI (Inst. of Particle and Nuclear Studies, KEK)
Shoichi SASAKI (Grad. Sch. of Sci., Univ. of Tokyo)
Shin-ya SAWADA (Inst. of Particle and Nuclear Studies, KEK)
Michiko SEKIMOTO (Inst. of Particle and Nuclear Studies, KEK)
Oleg SHEVCHENKO (,Joint Inst.for Nucl.Research)
Kenta SHIGAKI (Grad. Sch. of Sci., Hiroshima Univ.)
Tatsushi SHIMA (RCNP, Osaka Univ.)
Takenao SHINOHARA (Advanced Sci. Res. Center, JAEA)
Prashant SHUKLA (Nuclear Physics Division , Bhabha Atomic Research Centre)
Kazutaka SUDO (Inst. of Particle and Nuclear Studies, KEK)
Toru SUGITATE (Grad. Sch. of Sci., Hiroshima Univ.)
Mizuki SUMIHAMA (RCNP , Osaka Univ.)
Kazutaka SUMISAWA (KEK)
Tsuneo SUZUKI (Grad. Sch. of Natural Sci. & Tech., Kanazawa Univ.)

Junichi SUZUKI (Advanced Sci. Res. Center, JAEA)
Toru TAINO (Grad. Sch. of Sci. & Eng., Saitama Univ.)
Osamu TAJIMA (KEK)
Junpei TAKANO (KEK)
Manobu TANAKA (Inst. of Particle and Nuclear Studies, KEK)
Kiyoshi TANIDA (Grad. Sch. of Sci., Kyoto Univ.)
Kazuo TANIGUCHI (Fac. of Eng., Osaka Electro-Communication Univ.)
Hisayuki TORII (Grad. Sch. of Sci., Hiroshima Univ.)
Yutaka USIHIRODA (KEK)
Xiaorong WANG (New Mexico State Univ., USA)
Shizui WATANABE (Tokyo Metroporitan College of Aeronautical Engineering)
Yoshiaki YASUI (Tokyo Management College)
Imuran YOUNUS (Univ. of New Mexico, USA)

Research Fellow

Toru SEKIDO (Grad. Sch. of Natural Sci. & Tech., Kanazawa Univ.)

Students

Junior Research Associate

Kazuya AOKI (Grad. Sch. of Sci., Kyoto Univ.)
Tadaaki ISOBE (CNS, Grad. Sch. of Sci., Univ. of Tokyo)
Kentaro MIKI (Inst. Phys. , Univ.Tsukuba)
Yasuhiro MINAMIKAWA (Univ.Tokyo)
Kenichi NAKANO (Grad. Sch. of Sci. and Eng., Tokyo Inst. of Tech. Sch. of Sci.)
Misaki OUCHIDA (Facul. Science , Facul. Sci. Hiroshima Univ.)
Yoshichika SEKI (Grad. Sch. of Sci., Kyoto Univ.)
Kohei SHOJI (Grad. Sch. of Sci., Kyoto Univ.)
Jun TAMURA (Grad.Sch. at Nagatsuta , Tokyo Inst.Technol.)
Yorito YAMAGUCHI (CNS , Univ.Tokyo)

Intern

Kieran BOYLE (Dept. of Physics , SUNY at Stony Brook)
Robert BENNETT (Dept. of Physics , SUNY at Stony Brook)
Ihnjea CHOI (University of Yonsei)
Amaresh DATTA (University of Massachusetts,Amherst)
Ran HAN (School of Physics , Peking University)
John KOSTER (Department of Physics , Univ.of Illinois at Urbana-Champaign)
Astrid MORREALE (,Unv.of California at Riverside)
Masaki OKUMURA (Tokyo Metroporitan College of Aeronautical Engineering)
Kota YAMAKOSHI (, Tokyo Metroporitan College of Aeronautical Engineering)
Ruizhe YANG (Department of Physics , Univ.of Illinois at Urbana-Champaign)

Student Trainees

Kazutaka AOKI (Grad. Sch. of Sci. & Eng., Saitama Univ.)
Yusuke FUJISAWA (Grad. Sch. of Sci. & Eng., Saitama Univ.)
Masatoshi HAMADA (Fac. of Sci., Kyushu Univ.)

Masayasu HASEGAWA (Grad. Sch. of Natural Sci. & Tech., Kanazawa Univ.)
Koichi HASHIMOTO (Grad. Sch. of Natural Sci. & Tech., Kanazawa Univ.) (
Hirokazu ISHII (Grad. Sch. of Sci. & Eng., Saitama Univ.)
Taku ITO (Grad. Sch. of Sci. and Eng., Tokyo Inst. of Tech. Sch. of Sci.)
Yoshihiro IWANAGA (Facul. Science , Facul. Sci. Hiroshima Univ.)
Takeshi KANESUE (Kyushu Univ.)
Kenichi KARATSU (Grad. Sch. of Sci., Kyoto Univ.)
Miki KASAI (Coll.Sci. , Rikkyo Univ.)
Yuuji KATOU (RCNP , Osaka Univ.)
Motohiro KAWASHIMA (College of Sci., Rikkyo Univ.)
Kotaro KIJIMA (Grad. Sch. of Sci., Hiroshima Univ.)
Masahiro KONNO (Inst. Phys. , Univ.Tsukuba)
Martin LEITGAB (Univ. Vienna, Austria)
Kouichi MATSUBARA (Grad. Sch. of Sci. & Eng., Saitama Univ.)
Nathan MEANS (Dept. of Physics , SUNY at Stony Brook)
Shinji MOTOKI (Grad. Sch. of Biosphere Sci., Hiroshima Univ.)
Takahiro NAGAI (Sch. of High Energy Accel. Sci., The Grad. Univ. for Advanced Studies)
Yoshihide NAKAMIYA (Grad. Sch. of Sci., Hiroshima Univ.)
Katsuro NAKAMURA (Facul.Sci. , Kyoto Univ.)
Masaya NIHASHI(Facul. Science , Facul. Sci. Hiroshima Univ.)
Kentaro NISHIMURA (Univ.Tokyo)
Atsushi OKAMURA (Facul.Sci. , Kyoto Univ.)
Koichi SAKASHITA (Tokyo Inst.Technol.)
Shinkuro SATO (Inst. Phys. , Univ.Tsukuba)
Takahiro SAWADA (RCNP , Osaka Univ.)
Maya SHIMOMURA (National Inst. of Advanced Industrial Sci. and Tech.)
Kathrin SPENDIER (University of New Mexico)
Kenichi TAKEMASA (Inst. Phys. , Univ.Tsukuba)
Satoru UEDA (Grad. Sch. of Pure and Applied Sciences, Univ. of Tsukuba)

Secretaries

Noriko KIYAMA
Yoko SAKUMA

Advanced Meson Science Laboratory

1. Abstract

Particles like muons, pions, and kaons have finite life times, so they do not exist in natural nuclei or matters. Implanting these particles into nuclei/matters, exotic phenomena in varieties of objects can be studied from a new point of view.

Kaon is a second lightest meson which has strange-quark as a constituent quark. It is expected that if one embed a kaon into nuclei, the sizes of the nuclei become smaller and forms a high density object beyond the normal nuclear density. Study of this object could lead better understanding of the origin of the mass of the matter, and may reveal the quark degree of freedom beyond the quark-confinement. Those properties can be studied by precise heavy pionic atom research in different angle. The other example is the weak interaction in nuclear matter. It can only be studied by the weak decay of hypernuclei, which have Lambda particle in the nuclei,

Muon provides even wider variety of study from nuclear reaction to magnetism in matter. For instance, stopping positively charged muon in a material, we obtain information on the magnetic properties or the local field at the trapped site. Injecting negatively charged muon to mixture of deuterium and tritium, muon attracts surrounding atoms and is known to cause d-t fusions.

As is already clear, in our research we introduce different kind of impurities into nuclei/matters, and study new states of matter, new phenomena, or the object properties.

2. Major Research Subjects

(1) Study of meson property and interaction in nuclei
(2) Origin of matter mass / quark degree of freedom in nuclei.
(3) Condensed matter and material studies with muon
(4) Nuclear physics via muon catalyzed fusion and muonic atoms

3. Summary of Research Activity

Hadron physics at J-PARC and RIKEN-RIBF

Kaon and pion will shed a new insight to the nuclear physics. The recent discovery of deeply bound pionic atom enables us to investigate the properties of mesons in nuclear matter. At RIKEN-RIBF, we are preparing precise experimental study of the pionic atom. We are intensively preparing another next generation kaon experiments (E15 and E17) at J-PARC as day-one experiments. In these experiments, we are aiming at precise determination of the KN interaction, and clarify the nature of kaon in nuclei. By these experiments, we aim to be a world-leading scientific research group using these light meta-stable particles.

1) Deeply bound kaonic nuclei

We have performed a high precision and small ambiguity spectroscopy on the K-ppn system, strange tribaryon -S°(3115)-, at KEK (High energy accelerator research organization). We measured the momenta of protons emitted in the reaction between negatively charged K mesons and helium nuclei. Compared to the previous experiment, the mass resolution was improved by a factor of 2 and the statistical accuracy by a factor of about 10. We have newly installed detectors exclusively used for the measurement of the protons and realized small-ambiguity experiment. As a result, no structure was observed, in the spectrum, associated to the strange tribaryon with the natural width of 20 MeV/c^2, and the result was contradictory to the previous experiment. Statistical evaluation tells that the previous results are rejected by 99% confidence level. The experiment also tells us that the difficulty of the bound state search using at rest reaction, in which non-mesonic two-nucleon absorption reactions produce huge energetic nucleon background in the energy region of interest. This two-nucleon absorption process also caused the absorption width of he kaonic bound state. Thus we

proceed the search of the state in the simplest system K-pp at the kaon incident momentum of 1 GeV/c as a day-one experiment at J-PARC.

2) Deeply bound pionic and eta- nuclei

We made a spectroscopy experiment to measure deeply bound pionic states in several tin isotopes at the GSI, Germany, to investigate the pion-nucleus strong interaction. The results provided information on the iso-vector part of the strong interaction between pion and nucleus. More advanced discussion leads to the origin of the mass of matter, which is attributed to the quark condensation in the vacuum. Presently we are developing new scheme to achieve order better resolution to study pionic atom at RIKEN-RIBF.

3) Precision X-ray measurement of kaonic atom

Simultaneously with the above experiment (1), we have performed an X-ray spectroscopy of atomic $3d \rightarrow 2p$ transition of negatively charged K mesons captured by helium atoms. Many Kaonic atoms are known to be measured with various elements, however, there are very large deviations in the measured energy levels for the helium (and the oxygen) from the systematic expectations. The deviation originates in technical issues in old experiments, and new and high precision data have been long awaited for. Also, wave functions of the Kaonic atoms are expected to reflect the information on the existence of the inner structure, namely deeply bound Kaonic states. As a result of the experiment, we have succeeded in performing the spectroscopy and achieved the shift of 2+-2(stat.) +-2(syst.) eV. The obtained results reject older data beyond any doubt, and the above deviation is dissolved. Presently, aiming at the determination of the level width and yield, we are analyzing the data. To clarify the KN interaction strength, we are preparing another x-ray measurement of the kaonic helium-3 atom, which is another day-one experiment at J-PARC.

Muon science at RIKEN-RAL branch

The research area ranges over particle physics to condensed matter studies and life science. Our core activities are based on the RIKEN-RAL Muon Facility located at the Rutherford Appleton Laboratory (UK), which provides the most intense pulsed muon beam. We have variety of important research activities such as muon-catalyzed fusion (mCF) and condensed matter physics by muon spin rotation / relaxation / resonance (mSR).

(A) Condensed matter/materials studies with high energy accelerator producing particles and nuclei

A major upgrade work for mSR facility is being carried out at RIKEN-RAL muon facility reflecting growing number of collaborations with other universities and research institutes in this field. A pulsed laser system, which consists of a Nd:YAG laser and an OPO laser, has been installed to the facility under collaboration between the University of Yamanashi, KEK, and RIKEN. This will extend the scope of the mSR technique towards studies of effects induced by intense photon field, such as spin polarization of conduction electrons in semiconductors. Development of a new mSR spectrometer, which will enable us to study a sample under multiple-extreme condition, is also underway.

There are three topics of material sciences studied by the muon-spin relaxation method at the RIKEN-RAL Muon facility in 2007.

1) From measurements of the muon-spin depolarization rate in fields, quantitative values of the transition rate of electrons between iron atoms in a ironmetal complexes have been firstly obtained.

2) In a Sm-based Ru-Fe skutterudite compound, a possibility of the appearance of an ordered state of multi-pole moments has been pointed out.

3) A new condensed state of excited electronic states has been suggested in Tl-K quantum-spin systems from zero-field muon-spin relaxation method.

(B) Nuclear physics studies with muons, such as muon catalyzed fusion and muonic atoms

1) Muon catalyzed fusion (mCF)

We are studying the muon catalyzed fusion (mCF) processes in a wide range of hydrogen target conditions such as isotope mixtures and temperatures. In recent years, we studied the effect of ortho-para D_2 composition. From the precise density dependence of ddm formation rate in pure D_2 target at temperatures near the critical point (38.35 K), we have shown that the resonant ddμformation is very much dependent on the D_2 rotational levels as well as the target density. For the liquid D_2/T_2 mixture, we achieved the increase of dtm formation by using ortho-D_2 for the first time.

2) Development towards muonic atom formation with unstable nuclei

Stopping negative muons in the solid hydrogen with implanted unstable atoms, muons transfer efficiently to the implanted nuclei from muonic hydrogen to form the muonic atoms. By observing muonic X-rays at muonic atom formations, fundamental experiments on the nuclear charge density distribution are in progress. Using the newly installed surface ionization ion source, we carried out successfully the first experiment to measure an isotope energy shift of muonic X-rays originated from muonic ^{88}Sr and ^{86}Sr atoms. We also successfully observed characteristic muonic X-rays from implanted ^{138}Ba atoms.

3) Generation of ultra slow positive muon beam

We have constructed a new μSR spectrometer specialized for using low energy muon beam, whose kinetic energy is variable from a few keV to a few tens of keV. This will extend the scope of μSR technique from a bulk material to surfaces and multi-layered materials. In order to demonstrate the new spectrometer's capability, we have carried out the first μSR experiment of a thin film of a perovskite-type manganese oxide, and successfully observed changes in spectra's shape which are associated to phase transitions.

Head

Masahiko IWASAKI

Members

Katsuhiko ISHIDA
Kenta ITAHASHI
Yoshio KOBAYASHI
Yasuyuki MATSUDA
Teiichiro MATSUZAKI
Hiroaki ONISHI
Haruhiko OUTA
Isao WATANABE

Special Postdoctoral Researchers

Hidekatsu NEMURA
Takatoshi SUZUKI
Dai TOMONO
Fuminori SAKUMA

Special Contract Researcher

Masami IIO
Shinji OKADA
Takahisa KOIKE
Masaharu SATO

Contract Researchers

Pavel BAKULE
Takayuki KAWAMATA
Takao SUZUKI

Visiting Scientists

Tadashi ADACHI (Grad. Sch. Eng., Tohoku Univ.)
Yoshitami AJIRO (Grad. Sch. Sci., Kyoto Univ.)
Jun AKIMITSU (Coll. Sci. Eng., Aoyama Gakuin Univ.)
Juuichirou ARAI (Fac. Sci., Tokyo Univ. Sci.)
Shingo ARAKI (Grad. Sch. Sci., Osaka Univ.)
Kunio AWAGA (Grad. Sch. Sci., Nagoya Univ.)
George BEER (Univ. of Victoria, Canada)
HyoungChan BHANG (Seoul National Univ., Korea)
N. Ludmila BOGDANOVA (ITEP, Russia)
Prasad Tara DAS (SUNY, USA)
Masaya ENOMOTO (Grad. Sch. Arts and Sci., Univ of Tokyo)
Mark FAYFMAN (Kurchatov Institute, Russia)
Yutaka FUJII (Fac. Eng., Fukui Univ.)
Masaki FUJITA (IMR, Tohoku Univ.)
Hideto FUKAZAWA (Grad. Sch. Sci. & Tech., Chiba Univ.)
Takayuki GOTO (Fac. Sci. & Tech., Sophia Univ.)
Makoto HAGIWARA (Fac. Eng. Design, Kyoto Inst. Technol.)
Ryugo, S. HAYANO (Grad. Sch. Sci., Univ.of Tokyo)
Wataru HIGEMOTO (Advanced Sci. Res. Center, JAEA)
Masahiro HIRANO (JST)
Kazuto HIRATA (NIMS)
Emiko HIYAMA (Fac. Sci., Nara Women's Univ.)
Susumu IKEDA (KEK)
Yutaka IKEDO (Toyota Central R&D Labs.)
Fumihiro ISHIKAWA (Grad. Sch. Sci. & Tech., Niigata Univ.)
Shigeru ISHIMOTO (Inst. of Particle and Nuclear Studies, KEK)
Tomoichi ISHIWATARI (SMI, Austria)
Ryosuke KADONO (KEK)
Mineo KATO (JAEA)
Naritoshi KAWAMURA (KEK)
Jungho KIM (Seoul National Univ., Korea)
Yasushi KINO (Fac. Sci., Tohoku Univ.)
Akihiro KODA (KEK)
Yoh KOHORI (Fac. Sci., Chiba Univ.)
Yoji KOIKE (Grad. Sch. Eng., Tohoku Univ.)
Yoshitaka KUNO (Grad. Sch. Sci., Osaka Univ.)
Chow LEE (UCF, USA)
Shunsuke MAKIMURA (KEK)
Goro MARUTA (Grad. Sch. Sci., Hokkaido Univ.)
Satoru MATSUISHI (FCRC, Tokyo Tech.)
Yasuhiro MIYAKE (KEK)
Hitoshi MIYASAKA (Grad. Sch. Sci., Tohoku Univ.)
Soichiro MIZUSAKI (Coll.Sci. & Eng., Aoyama Gakuin Univ.)
Kazuhiko MUKAI (Toyota Central R&D Labs.)
Kazutaka NAKAHARA (KEK)
Takashi NAKAMURA (Tokyo Inst. of Tech., Particle, Nuclear, and Astro-Phys.)
Takayoshi NAKAMURA (RIES, Hokkaido Univ.)
Satoshi NAKAMURA (Grad. Sch. Sci., Tohoku Univ.)
Takehito NAKANO (Grad. Sch. Sci., Osaka Univ.)
Nobuhiko NISHIDA (Fac. Sci., Tokyo Tech.)

Kusuo NISHIYAMA (KEK)
Hiroshi NOZAKI (Toyota Central R&D Labs.)
Yasuo NOZUE (Grad. Sch. Sci., Osaka Univ.)
Masaaki OHBA (Grad. Sch. Eng., Kyoto Univ.)
Seiko OHIRA-KAWAMURA (Ochanomizu Univ.)
Susumu OHYA (Fac. Sci., Niigata Univ.)
Akira OSAWA (Fac. Sci. & Tech., Sophia Univ.)
Vassili PEREVOZCHIKO (VNIEF, Russia)
Leonid PONOMAREV (Kurchatov Institute, Russia)
Francis PRATT (RAL, UK)
Shin-ichi SAKAMOTO (JAEA)
Ryoichi SEKI (California State Univ. , Northridge, USA)
Kouichiro SHIMOMURA (KEK)
Vyacheslas STORCHAK (VNIIEF, Russia)
Patrick STRASSER (KEK)
Hiroyuki SUGAI (JAEA)
Jun SUGIYAMA (Toyota Central R&D Labs.)
Haruhiko SUZUKI (Grad. Sch. Nat. Sic. & Tech., Kanazawa Univ.)
Hiroyuki SUZUKI (NIMS)
Kazuyuki TAKAI (Grad. Sch. Sci. & Eng., Tokyo Tech.)
Keiji TAKEDA (ISSP, Univ. of Tokyo)
Hiroyuki TAKEYA (NIMS)
Manobu TANAKA (Inst. of Particle and Nuclear Studies, KEK)
Akihiro TANIGUCHI (KURRI, Kyoto Univ.)
Takashi TANIGUCHI (Coll.Sci. & Eng., Aoyama Gakuin Univ.)
Eiko TORIKAI (Grad. Sch. Medicine & Eng. Sci., Univ. of Yamanashi)
Akihisa TOYODA (KEK)
Kazuo UEDA (ISSP, Univ. of Tokyo)
Yun XUE (Grad. Sch. Nat. Sic. & Tech., Kanazawa Univ.)
Kazuyoshi YAMADA (IMR, Tohoku Univ.)
Arkady YUKHINCHUK (VNIIEF, Russia)
Johann ZMESKAL (SMI, Austria)

Research Consultants
Yoshinori AKAISHI
Masayasu KAMIMURA
Atsuko ITO

Students
Student Trainees
Truong Cong DUAN (Grad. Sch. Sci., Osaka Univ.)
Hiroyuki FUJIOKA (Grad. Sch. Sci., Univ. of Tokyo)
Yoshiyuki FUKUDA (Grad. Sch. Sci. & Eng., Tokyo Tech.)
Toshio HANAKI (Grad. Sch. Fac. Sci. & Tech., Tokyo Univ. Sci.)
Yuzo HIRAYAMA (Grad. Sch. Sci. & Eng., Tokyo Tech.)
Takashi ITO (Grad. Sch. Sci. & Eng., Tokyo Tech.)
Satoshi ITOH (Grad. Sch. Sci., Univ. of Tokyo)
Keishi KANADA (Grad. Sch. Sci. & Tech., Sophia Univ.)
Wakako KANEKO (Grad. Sch. Eng., Kyoto Univ.)
Hirokazu KAWASHIMA (Grad. Sch. Sci.& Eng., Aoyama Gakuin Univ.)
Noriyuki KIDA (Grad. Sch. Arts and Sci., Univ. of Tokyo)
Mijung KIM (Seoul National Univ., Korea)

Yoshihiro KUBOTA (Grad. Sch. Sci., Tohoku Univ.)
Sougo KUROIWA (Grad. Sch. Sci.& Eng., Aoyama Gakuin Univ.)
Jun MATSUMOTO (Grad. Sch. Sci., Osaka Univ.)
Hayato MOCHIZUKI (Grad. Sch. Sci. & Tech., Niigata Univ.)
Yoshifumi NAGASAKI (Grad. Sch. Fac. Sci., Kanazawa Univ.)
Keisuke OMORI (Grad. Sch. Eng., Tohoku Univ.)
ROGER PINK (SUNY at Albany, USA)
Ayumi SAITO (Grad. Sch. Sci., Tokyo Metro Univ.)
Takehiro SAITO (Grad. Sch. Sci. & Tech., Sophia Univ.)
Katsunori TAKAHARA (Inter. Grad. Sch. of Sci.& Eng., Tokyo Tech.)
Yoichi TANABE (Grad. Sch. Eng., Tohoku Univ.)
Hideyuki TATSUNO (Grad. Sch. Sci., Univ. of Tokyo)
Yoshitake TODA (Inter. Grad. Sch. of Sci.& Eng., Tokyo Tech.)
Yoko TOMITA (Grad. Sch. Sci. & Eng., Aoyama Gakuin Univ.)
Fumiko YAMADA (Grad. Sch. Sci. & Eng., Tokyo Tech.)
Heejoong YIM (Seoul National Univ., Korea)
Masanorri MIYAZAKI (The Graduate Univ. for Advance Studies(SOKENDAI))

Secretaries
Yoko FUJITA
Yuka TAKANO

Theoretical Physics Laboratory

1. Abstract

The aim of this laboratory is to reveal the laws of nature ranging from elementary particles to the universe. More precisely, the following three issues are pursued with their mutual relations emphasized:(1) Understanding the microscopic fundamental law of nature. In particular, trying to give a consistent definition of superstring and derive all the fundamental laws from one principle. (2) Understanding many-body systems. Both of the following two aspects are considered. One is the universal laws such as thermodynamics and the universality of spin systems, and the other is specific properties of individual systems such as hadrons, condensed matter, and the universe. (3) Computational science. Besides numerical analyses as an important tool for the above mentioned (1) and (2), aspects of fundamental mathematics are also pursued.

2. Major Research Subjects

(1) Constructive Definition of String Theory as Fundamental law of Physics
(2) Fundamental aspects of Quantum Field Theory and its applications
(3) High precision inspection of experimental and observational data

3. Summary of Research Activity

The ability to understand nature at its most profound level is a basic human desire. Science is founded on accumulated and tremendous efforts driven by that aspiration. The objective of our laboratory is to participate in the endeavor to better understand nature by adding our contributions to theoretical physics. The present seems to be a particularly exciting time for this as many developments appear to be about to converge and allow formation of the ultimate theory of everything.

We organize our research activities into three segments: the pursuit of the microscopic fundamental laws of physics, the study of many-body systems, and the science and technology of computation. These three aspects have an inseparable interrelation and are investigated in an integrated manner throughout the research conducted within this laboratory.

(1) Understanding the fundamental law of nature through string theory.

1) Non-perturbative effect for non-critical string

The analysis of the nonperturbative effect in the c=0 noncritical string theory defined by the one-matrix model is extended to the case of two-matrix models which provide nonperturbative definitions of $c<1$ noncritical string theories. Then, universality of nonperturbative effects including their coefficients in a generic $c<1$ noncritical string theory is achieved in the sense that they are independent of details of potentials of the two-matrix models.

2) Matrix models and curved space-time

Incorporating curved space time into matrix models is pursued. In particular, a method in which larger additional degrees of freedom is introduced to represent space-time symmetry, is proposed.

3) Domain Wall in string theory

We investigate a global structure of the moduli space of the BPS domain wall system. I particular, we are interested in the case where the dimensions of the moduli space is greater than those expected from the index theorem. We also study the T-duality between the vortices and domain walls from a string theoretical point of view. We explicitly construct a vortex solution in the Higgs phase of supersymmetric gauge theory and find an exact correspondence between the solution and D-brane configuration in the domain wall side.

4) Non BPS branes and supergravity

We investigate the correspondences between a class of classical solutions of Type II supergravity (the three-parameter solution) and D-branes in the superstring theory. In addition to the mass, the RR-charge, the

solution also carries the so-called dilaton charge, whose physical meaning was unclear. We find that the appearance of the dilaton charge is a consequence of deformations of the boundary condition from that of the boundary state for BPS D-branes. We also show that such deformed boundary states are realized as tachyonic and/or massive excitations of the open strings on D-brane systems.

5) D-branes and instantons

We have investigated instantons of four-dimensional SUSY gauge theory from the view point of superstring theory. A general prescription to construct the instanton solutions is known as the ADHM (Atiyah-Drinfeld-Hitchin-Manin) construction. In terms of superstring theory, instanton is understood as a bound state of D3-branes and D(-1)-branes. We consider a system of D3-branes and anti-D3-branes to construct the bound state via a tachyon condensation. As a result, we found that the tachyon profile contains all information on the instanton and the ADHM construction can be understood as an outcome of the gauge equivalence of this system in the low energy limit. We also applied the same method to eight-dimensional gauge theory and showed that some solitonic solution of the eight-dimensional theory can be constructed by this method.

6) Application of string theory to cosmology

qCosmological scenarios alternative to inflation motivated by string theories are known. In cyclic scenario, or ekpyrotic scenario, the universe is considered as branes sitting in higher dimensional space time. The universe is assumed to start out from a static Minkowskian space-time and experience the big-bang as the collision of pair of branes (bounce). From the observational point of view, it is of importance to study the time evolution of cosmological fluctuation through the time of big bang. We studied the problem from the point of view of local causality through the bounce. Assuming the local causality condition, we derived the most general matching condition for the fluctuation between before and after the bounce. Especially, we found it is impossible to generate scale invariant spectrum without introducing non-local causality throughout the bounce. This work made clear the physical problem to obtain the scale invariant spectrum in the bouncing cosmology. We have also studied a toy model inspired by a low-energy effective action of non-commutative field theory and estimated the range of parameters to obtain scale invariant spectrum.

Another subject pursued was the possibility of obtaining inflation due to the modification of the dispersion relation. When non-equilibrium dynamics is taken into account, we observed that the inflation can be easily realized when the energy is a decreasing function of the momentum in high-energy regime. This result provides alternative way of realizing inflation in the framework of unified theory.

(2) Quantum field theory and physics of many body systems

1) Lattice formulation of supersymmetric gauge theory

We proposed a lattice formulation of low dimensional supersymmetric gauge theories, aiming at practical implementation for numerical simulations.

2) Lattice formulation of fermions coupled to gravity

We formulated lattice Dirac operator of the overlap-type that describes the propagation of a Dirac fermion in a gravitational field. We also analyzed global gauge anomalies associated with Majorana fermions in 8k and 8k+1 dimensions.

3) Mathematical aspects of 2-dimensional gauge theories and string.

We investigate a non-perturbative correction to the N=2 supersymmetric Yang-Mills theory from the discrete matrix model point of view. We utilize the D-brane picture in superstring theory and localization theorem in order to derive the discrete matrix model from 2-dimensional Yang-Mills theory on a compact 2-cycles in the ALE space. We also find the relationship to the Dijkgraaf-Vafa theory in the continuum limit.

4) Logarithmic Confromal Field Theory

The following topics are investigated: Free field representation for LCFT with boundary; The relation

between Minimal String theory and LCFT; The relation between statistical models and LCFT.

5) Quantum field theory over the deformed commutation relation

A quantum theory of free scalar field based on the deformed Heisenberg algebra which is the correction of stringy physics is constructed.

6) Chern Simons Yang Mills Model

We have studied the Chern Simons Yang Mills Model. Non-commutative gauge theories on fuzzy spheres were obtained in such models. Fuzzy spheres look like dbrane configuration. k coincident fuzzy spheres generates the U(k) gauge group. In this direction, we are continuing effort to address some of the related issues.

(3) High precision calculation of field theory and computational science

1) High precision calculation of QED

We have announced the final result of our calculation of the electron anomalous magnetic moment. It contains up to the eighth-order of the perturbation theory of QED. The very reliable result was obtained by using high precision calculation on RIKEN's supercomputer system (RSCC).We also succeeded in automating the calculation of the tenth-order of the perturbation theory, particularly in constructing the ultra-violet subtraction terms. This is an important step to accelerate our calculation of the entire tenth-order contribution. The dominant contribution from the tenth order to the muon anomalous magnetic moment was also announced by us. In contrast to the electron, some specific Feynman diagrams give rise to the large contributions to the muon
anomaly. We explicitly evaluated about 2000 Feynman diagrams which are possible to give the leading and next-to-leading contributions.

2) Improved perturbation method and its applications

We apply improved perturbation method which is one of the variational schemes to Ising model in two-dimensions. It enables us to evaluate free energy and magnetization at strong coupling regions from weak coupling expansion even in the presence of the phase transition.

We determine approximated transition point in this scheme. In the presence of external magnetic field we can see not only stable physical states but metastable one. This reserach motivated by availability of this method to IIB matrix model which is expected to show a phase transition from 10-dimensional universe to 4-dimensional universe.

Head

Hikaru KAWAI

Members

Hiroshi SUZUKI
Koji HASHIMOTO
Tsukasa TADA

Postdoctoral Researchers

Issaku KANAMORI
Isao KISHIMOTO
Yuuichirou SHIBUSA

Contract Researchers

Makiko MATSUKAWA

Visiting Scientists

Hajime AOKI (Fac. of Sci. and Eng., Saga Univ.,)

Jiro ARAFUNE (National Inst. for Academic Degrees and Univ. Evaluation)
Zyun F. EZAWA (Grad. Sch. of Sci., Tohoku Univ.)
Kazuo FUJIKAWA (College of Sci. and Tech., Nihon Univ.,)
Amihay HANANY (Massachusetts Inst. of Tech., USA)
Masashi HAYAKAWA (Grad. Sch. of Sci., Nagoya Univ.,)
Takeo INAMI (Fac. of Sci. and Eng., Chuo Univ.,)
Nobuyuki ISHIBASI (Grad. Sch. of Pure and Applied Sci., Univ. of Tsukuba,)
Satoshi ISO (High Energy Accelerator Res. Organization)
Hiroshi ITOYAMA (Grad. Sch. of Sci., Osaka City Univ.,)
Toichiro KINOSHITA (Cornell Univ., USA)
Yoshihisa KITAZAWA (High Energy Accelerator Res. Organization)
Ivan KOSTOV (Service de Physique Theoreique, CNRS, FRANCE)
Jnanadeva MAHARANA (Inst. of Phys., INDIA)
Jun NISHIMURA (High Energy Accelerator Res. Organization)
Fumihiko SUGINO (Okayama Inst. for Quantum Phys.)
Asato TSUCHIYA (Grad. Sch. of Sci., Osaka Univ.,)
Kensuke YOSHIDA (Univ. of Rome - La Sapienza, ITALY)
Tatsumi AOYAMA (KEK)
Alexei ZAMOLODCHIKOV (Universit'e Montpellier II, FRANCE)

Research Consultants

Keiji IGI
Hironari MIYAZAWA
Yoshio YAMAGUCHI

Junior Research Associate

Secretariy

Yumi KURAMITSU
Yoko SAGIYA

Radiation Biology Team

1. Abstract

Radiation biology team studies various biological effects of fast heavy ions. It also develops new technique to breed plants by heavy-ion irradiations. Fast heavy ions can produce dense and localized ionizations in matters along their tracks, in contrast to photons (X rays and gamma rays) which produce randomly distributed isolated ionizations. These localized and dense ionization can cause double-strand breaks of DNA in cells which are not easily repaired and result in mutation more effectively than single-strand breaks. A unique feature of our experimental facility at the RIKEN Ring Cyclotron (RRC) is that we can irradiate living bodies in atmosphere or in bottles since the delivered heavy-ion beams have energies high enough to penetrate deep in matter. This team utilizes a dedicated beam line (E5B) of the RRC to irradiate cultivated cells, plants and animals with beams ranging from carbon to iron. Its research subjects cover physiological study of DNA repair, genome analyses of mutation, and development of mutation breeding of plants by heavy-ion irradiation. Some new cultivars have already been brought to the market. It also studies the physical processes of radiation effects in solutions.

2. Major Research Subjects

(1) Study on the biological effects by heavy-ion irradiation
(2) Studies on ion-beam breeding and genome analysis
(3) New medical application of heavy-ion beams
(4) Formation of nano-particles in solutions by heavy-ion irradiations

3. Summary of Research Activity

We study biological effects of fast heavy ions from the RIKEN Ring Cyclotron using 135 MeV/N C, N, Ne ions, 95 MeV/N Ar ions and 90 MeV/N Fe ions. We also develop breeding technology of plants. Main subjects are:

(1) Study and application of heavy-ion induced plant mutation

In contrast to X rays and gamma rays, fast heavy ions are found to be useful for plant breeding since they only cause localized damage on DNA and can induce mutations more effectively with lower dosage. Our team utilizes beams of fast heavy ions from the RIKEN Ring Cyclotron to develop heavy-ion breeding techniques. Genome analyses are performed to reveal the relation between genotype and phenotype.

(2) Study of heavy ion-induced damage of DNA and its repair processes

We study the double-strand break of DNA induced by heavy-ion irradiation and its repair processes. DNA double strand break (DSB) is characteristic to heavy-ion irradiation and considered to be the characteristic lesion responsible for its biological effects. Cells have two pathways to repair DSB, non-homologous end-joining

(NHEJ) and homologous recombination (HR), and it is unknown how the two pathways are involved in repairing the damage caused by heavy-ion irradiation. To elucidate it, we irradiate higher vertebrate cells lacking DNA repair proteins with C, Ar, or Fe ions and analyze them with colony formation assay and molecular biology methods.

Team Leader
Tadashi KAMBARA

Members
Tomoko ABE
Masako IZUMI

Yusuke KAZAMA
Hinako TAKEHISA
Teruyo TSUKADA

Part-time Staff I
Hideo TOKAIRIN

Part-time Staff II
Sumie OHBU

Technical Staff I
Yoriko HAYASHI

Visiting Scientists
Ryutaro AIDA (Natl. Inst. Floricult. Sci.)
Mari AMINO (Tokai University Hospital)
Chang-Hyu BAE (Sunchon Natl. Univ., Korea)
Yasuhiro CHIMI (JAEA)
Hiroyuki DAIMON (Osaka Pref. Univ.)
Makoto FUJIWARA (Grad. Sch., Col. Arts Sci., Univ. of Tokyo)
Eitaro FUKATSU (Forest tree beeding Cet.)
Koji FURUKAWA (Mukoyama Orchids Co., Ltd.)
Yoshiya FURUSAWA (Natl. Inst. Radiol. Sci.)
Toshinari GODO (Botanic Gardens Toyama)
Misako HAMATANI (Hiroshima City Agric. Forest. Promot. Cen.)
Yasuhide HARA (Kanagawa Inst. Agric. Sci.)
Masanori HATASHITA (Wakasa Wan Energy Res. Cen.)
Atsushi HIGASHITANI (Grad. Sch. Life Sci., Tohoku Univ.)
Ryoichi HIRAYAMA (Natl. Inst. Radiol. Sci.)
Akiko HOKURA (Fac. Sci., Tokyo Univ. of Sci.)
Ichiro HONDA (Natl. Agric. Res. Cen.)
Mitsugu HORITA (Hokuren Agri. Res. Inst.)
Yuji ITO (Natl. Agric. Res. Cen., Hokkaido Region)
Akihiro IWASE (Grad. Sch. Engin., Osaka Pref. Univ.)
Hiroshi KAGAMI (Shizuoka Citrus Exp. Station)
Kensuke KAGEYAMA (Fac. Engin.,Saitama Univ.)
Takeshi KANAYA (Suntory Flowers, Ltd.)
Si-Yong KANG (Dep. Rad. Plant Breed. Genet., KAERI, Korea)
Tomojirou KOIDE (Riken Vitamin Co., Ltd.)
Tsutomu KUBOYAMA (Ibaraki Univ.)
Yutaka MIYAZAWA (Grad. Sch. Life Sci., Tohoku Univ.)
Kazumitsu MIYOSHI (Fac. Bioresour. Sci., Akita Pref. Univ.)
Toshikazu MORISHITA (Inst. Rad. Breeding, Natl. Inst. Agric. Res.)
Koji MURAI (Fukui Pref. Univ.)
Daisuke NAKADA (Ela Medical Japan Co. Ltd.)
Ishikawa NORITO (JAEA)
Mio OHNUMA (Inst. Mol. Cell. Biosci., Univ. Tokyo)

Norihiro OHTSUBO (Natl. Inst. Floricult. Sci.)
Fumihisa ONO (Grad. Sch. Natural Sci. & Tech., Okayama Univ.)
Tomo OOMIYA (Hokkaido Ornamental Plants Veg. Res. Cen.)
Kenji OSAWA (Nagano Agric. Res. Cen.)
Kouichi SAKAMOTO (YUKIGUNI AGURI Co.,Ltd.)
Tadashi SATO (Grad. Sch. Life Sci., Tohoku Univ.)
Hiroaki SERIZAWA (Nagano Veg. Ornamental Crops Exp. Station)
Takiko SHIMADA (Res. Inst. Agric. Resour., Ishikawa Agric. Coll.)
Fumio SUGAWARA (Tokyo Univ. of Sci.)
Masao SUGIYAMA (Hokko Chem. Ind. Co., Ltd.)
Keita SUGIYAMA (Nat. Inst. Veg.Tea Sci.)
Kazunori SUZUKI (Plant Biotech. Inst. Ibaraki Agric. Cen.)
Masao SUZUKI (Natl. Inst. Radiol. Sci.)
Kenichi SUZUKI (Suntory Flowers, Ltd.)
Teruhiko TERAKAWA (Hokko Chem. Ind. Co., Ltd.)
Ken TOKUHARA (Dogashima Orchid Cen.)
Masanori TOMITA (CRIEPI)
Hisashi TSUJIMOTO (Fac. Agri., Tottori Univ.)
Kozo TSUKADA (Nippon Veterinary and Life Sci. Univ.)
Masao WATANABE (Fac. Agri., Tohoku Univ.)
Takuji YOSHIDA (Takii Seed Co., Ltd.)
Koichiro YOSHIOKA (Tokai University Hospital)

Research Fellows

Hideki ASAUMI (Ehime Agricultural Experiment Station)
Eikou OOYABU (Saga Pref. Agr. Res. Cen.)
Takenori SAITO (Shizuoka Tea Exp. Station)
Minoru SAITOH (Fukui Agr. Exp. Sta.)
Tsukasa SHIRAO (Kagoshima Biotechnology Inst.)
Kei-ichiro UENO (Kagoshima Biotechnology Inst.)

Students

Junior Research Associate

Hiroyuki ICHIDA (Grad. Sch. Sci. Tech.,Chiba Univ.)

Student trainees

Naoki FUKUDA (Fac. Sci., Tokyo Univ. of Sci.)
Takayuki INOUE (Dept. Phys. Rikkyo Univ.)
Teruhiko KASHIWABARA (Fac. Sci., Tokyo Univ. of Sci.)
Nobuhiro MAEDA (Grad. Sch. Eng., Osaka Pref. Univ.)
Yoshitaka MATSUMOTO (Grad. Sch. Medicine & Sch., Chiba Univ.)
Sakiko MITSUO (Fac. Sci., Tokyo Univ. of Sci.)
Kiyoshi NISHIHARA (Grad. Sch. Frontier Sci., Univ. of Tokyo)
Tatsuya ONO (Nagahama Inst. Bio-Science and Technol.)
Kazuhiro SASAKI (Grad. Sch. Life Sci., Tohoku Univ.)
Saori TAKADA (Fac. Sci., Tokyo Univ. of Sci.)

Yuka TANAKA (Nagahama Inst. Bio-Science and Technol.)
Takashi YOKOYAMA (Dept. Phys. Rikkyo Univ.)

RI Applications Team

1. Abstract

RI Applications Team performs following researches at the heavy ion accelerators of RIBF:(1) With proton from the RIKEN AVF Cyclotron, we produce radioisotopes for research of chemistry, biology, medicine, pharmaceutical and environmental sciences. The nuclides 65Zn and 109Cd are delivered to Japan Radioisotope Association for charged distribution. (2) We develop new technology of mass spectrometry for the trace-element analyses using accelerator technology to apply to the scientific research fields, such as cosmochemistry, environmental science, archaeology and so on.

2. Major Research Subjects

(1) Production of radioisotopes 65Zn and 109Cd for charged distribution,

(2) Research and development for new RI production at AVF cyclotron,

(3) The development of trace element analysis, using the accelerator techniques, and its application to geo and environmental sciences

3. Summary of Research Activity

RI applications team utilizes RIBF heavy-ion accelerators for following research subjects:

(1) Production of radioisotopes

With protons from the AVF Cyclotron, we produce radioisotopes which are used for in-house and collaboration studies. Radioisotopes of Zn-65 and Cd-109 are distributed through Japan Radioisotope Association to the general users all over Japan.

(2) R/D for RI production

We work to improve production procedure of the present Zn-65 and Cd-109 for stable supply and better quality. We also develop production techniques for other RI species which are demanded but lack supply sources.

(3) Trace element analyses with accelerator technologies

In order to achieve ultra-high sensitivities down to 10^{-15}-10^{-17} in multiple trace-element analysis, we develop technique of accelerator mass spectroscopy (AMS) at the RILAC, with a combination of an ECR ion source and a linear accelerator. We also develop a compact mass spectrometer with a stand-alone ECR ion source. There techniques are applied in fields of cosmochemistry, geochemistry, biochemistry, pharmaceutical and environmental sciences, archeology, analysis of bio-trace element and materials science.

Team Leader
Tadashi KAMBARA

Members
Shuichi ENOMOTO
Hiromitsu HABA
Kazuya TAKAHASHI

Postdoctoral Researcher
Shinji SHIGYO

Research Associate
Yousuke KANAYAMA

Part-time Staff
Takashi NYU

Temporary Staff

Ichirou SAKAMOTO
Atsushi ISHIZAWA
Yutaka EZAKI

Senior Visiting Scientists

Shuichi KIMURA (Showa Women's Univ.)

Visiting Scientists

Kazuhiko AKIYAMA (Tokyo Metropolitan Univ.)
Ryohei AMANO (Fac. Med., Kanazawa Univ.)
Wenjun DING (Colorado State Univ., USA)
Kazutoyo ENDO (Showa Pharm. Univ.)
Kaori ENOMOTO (Univ. Human Arts & Sci.)
Hiroshi HIDAKA (Fac. Sci., Hiroshima Univ.)
Seiichiro HIMENO (Fac. Pharm. Sci., Tokushima Bunri Univ.)
Takako IKEDA (Showa Women's Univ.)
Hiroko INAGE (Internat. Life Sci. Inst.)
Nobuyoshi ISHII (Natl. Inst. Radiol. Sci.)
Toshiaki ISHII (Natl. Inst. Radiol. Sci.)
Yuko ISHIKAWA (Kagawa Nutrition Univ.)
Shigenao KAWAI (Fac. Agri., Iwate Univ.)
Masuo KONDOH (Showa Pharm. Univ.)
Kenichiro MATSUMOTO (Natl. Inst. Health, USA)
Yoshitaka MINAI (Cen. Art. Sci., Musashi Univ.)
Takeshi MINAMI (Sch. Sci. Eng., Kinki Univ.)
Tomohiro NABEKURA (Fac. Pharm. Sci., Niigata Univ. Pharm. Appl. Life Sci.)
Yuichiro NAGAME (JAEA, Tokai)
Yukiko NAKANISHI (Grad. Sch. Hum. Life Sci.,Showa Women's Univ.)
Van Chuyen NGUYEN (Jpn. Women's Univ.)
Yasumitsu OGURA (Grad, Sch. Pharm. Sci., Chiba Univ.)
Jun SAITO (Iwatsu Test Instrum. Corp.)
Tomofumi SAKURAGI (Natl. Inst. Radiol. Sci.)
Hiromu SAKURAI (Kyoto Pharm. Univ.)
Hiroshi SHIMIZU (Fac. Sci., Hiroshima Univ.)
Atsushi SHINOHARA (Grad Sch. Sci., Osaka Univ.)
Hiroyuki SUZUKI (RI Res. Cen., Chiba Univ.)
Toshihiro SUZUKI (Meiji Pharm. Univ.)
Mikiko SUZUKI (Showa Women's Univ.)
Kazuo SUZUKI (Grad, Sch. Pharm. Sci., Chiba Univ.)
Keiko TAGAMI (Natl. Inst. Radiol. Sci.)
Masaaki TAKAHASHI (Grad. Sci. Agric. Biol. Sci.,Osaka Pref. Univ.)
Yoshio TAKAHASHI (Grad. Sch. Sci.,Hiroshima Univ.)
Miho TAKAHASHI (Tokyo Univ. Marine Sci. and Tech.)
Atsushi TAKEDA (Fac. Pharm. Sci., Univ. Shizuoka)
Haruna TAMANO (Fac. Pharm. Sci., Univ. Shizuoka)
Shinzo TANABE (Meiji Pharm. Univ.)
Tadayasu TOGAWA (Meiji Pharm. Univ.)
Takehiro TOMITANI (Chiba Univ.)
Atsushi TOYOSHIMA (JAEA)
Shigeo UCHIDA (Natl. Inst. Radiol. Sci.)
Kohshin WASHIYAMA (Fac. Med., Kanazawa Univ.)
Tokuko WATANABE (Aoyama Gakuin Women's Junior College)

Mineo YAMASAKI (Nara Med. Univ.)
Makoto YANAGA (Fac. Sci., Shizuoka Univ.)
Hiroyuki YASUI (Kyoto Pharm. Univ)
Akihiko YOKOYAMA (Fac. Sci., Kanazawa Univ.)
Shigekazu YONEDA (Natl. Sci. Museum)
Shozo YOSHIDA (Nara Med. Univ.)
Takashi YOSHIMURA (Grad Sch. Sci., Osaka Univ.)

Research Consultants

Yasuyuki GONO
Kuniko MAEDA

Students

Part-time Staffs

Midori SASAKI (Tokyo Univ. Fish.)
Tatsuya URABE (Tokyo Univ. Fish.)

Student Trainees

Yusuke ADACHI (Kyoto Pharm. Univ.)
Tomoko ANDO (Showa Women's Univ.)
Ai HOSODA (Internat. Christian Univ.)
Terumi KATORI (Showa Women's Univ.)
Takehiko KURIBAYASHI (Grad. Sch. Sci., Osaka Univ.)
Yohei MITSUBORI (Fac. Sci. Tech., Tokyo Univ. of Sci.)
Kazuhiro OOE (Grad. Sch. Sci., Osaka Univ.)
Mizue OZAKI (Showa Women's Univ.)
Nobuko SAJI (Showa Women's Univ.)
Mayumi SHIBANUMA (Showa Women's Univ.)
Tomomasa TAKABE (Grad. Sch. Sci., Osaka Univ.)
Masaki TAKAHASHI (Meiji Pharm. Univ.)
Yuki TASHIRO (Grad. Sch. Sci., Osaka Univ.)

Metallomics Research Unit

1. Abstract

The aim of the Metallomics Research Unit is engaged in research on metals in biology. In order to achieve the better understandings of roles, functions and regulation of metals in biological systems, we developed the multitracer technology and the multiple molecular imaging systems which is using by semiconductor Compton telescope. The Metallomics Research Unit performs following researches: (1) developments of the multitracer technology by using accelerator facilities, (2) application studies of the multitracer technology in the fields of chemistry, biology, medicine, pharmacy, nutrition, environment, agriculture, etc., (3) developments of the Gamma Ray Emission Imaging as a tool for the multi-molecular imaging apparatus, (4) investigation of drug discovery for use the multi-molecular imaging and its application studies for metallobiological researches.

2. Major Research Subjects

(1) Developments and application studies on the multitracer technology

(2) Developments of the Gamma Ray Emission Imaging as a tool for the multi-molecular imaging

(3) Investigation of drug discovery for use the multi-molecular imaging and its application studies for metallobiological researches

3. Summary of Research Activity

The Metallomics Research Unit performs following research subjects:

(1) Development and application of the multitracer technology

With high-energy heavy ions from the RIKEN Ring Cyclotron, we produces multitracers which are mixtures of various radioactive nuclides, and use them in research fields like chemistry, biology, medicine, pharmaceutical, and environmental sciences.

(2) Developments of the Gamma Ray Emission Imaging as a tool for the multi-molecular imaging

With the advent of molecular imaging technology, nuclear medical imaging modalities have been extended to visualize biological functions and processes in living subjects by labeling a radioactive nuclide on the molecular probe. However, single molecular probe might not be able to characterize the targeted disease or biological function, because biological processes in living subjects are quite complex. GREI (Gamma-Ray Emission Imaging), which is a semiconductor Compton camera, is a promising γ-ray imager being developed for multiple molecular imaging. We have already been able to obtain quite encouraging results for multiple molecular imaging by use of GREI. However, a higher spatial resolution, a shorter imaging time, and quantitativity would be required for practical use, especially for small animal imaging. We are pursuing research and development on the requirements, and they will be met in the not too distant future.

(3) Investigation of drug discovery for use the multi-molecular imaging and its application studies for metallobiological researches

Molecular imaging is a current technology to analyze the molecular dynamics in vivo, including the diagnosis for cancer, diabetes, and more diseases. We are looking for the molecular imaging probe that will detect the pre-state of several disorders.

Biometals, such as zinc, copper, iron, and manganese are important cofactors for many proteins. Imbalance of these metals is known to be involved in the development of several diseases (cancer, diabetes, and Alzheimer's disease). We are focusing on the regulation of metal transporter(s) in these diseases and are also investigating for general function of metal(s) in molecular and cell biology.

Head

Syuichi Enomoto

Research Scientist
Shinji SHIGYO
Yousuke KANAYAMA

Contract Researcher
Makoto HIROMURA
Tomonori FUKUCHI
Takashi ISHIDA

Technical Staff Ⅰ
Hatsue OBATA

Temporary Staff
Daichi SAITO

Visiting Researcher
Kaori ENOMOTO(IGARASHI)

Senior Visiting Scientist
Shuichi KIMURA (Showa Women's Univ.)

Visiting Scientists
Ryohei AMANO (Fac. Med., Kanazawa Univ.)
Tomoko ANDO (Showa Women's Univ.)
Yuko ISHIKAWA (Kagawa Nutrition Univ.)
Takako IKEDA (Showa Women's Univ.)
Hiroko INAGE (Internat. Life Sci. Inst.)
Kazutoyo ENDO (Showa Pharm. Univ.)
Yasumitsu OGURA (Grad, Sch. Pharm. Sci., Chiba Univ.)
Mizue OZAKI (Showa Women's Univ.)
Shigenao KAWAI (Fac. Agri., Iwate Univ.)
Jun SAITO (Iwatsu Test Instrum. Corp.)
Hiromu SAKURAI (Suzuka Univ. Med. Sci.)
Rie SATO (Japan Aerospace Exploration Agency)
Kazuo SUZUKI (Grad, Sch. Pharm. Sci., Chiba Univ.)
Toshihiro SUZUKI (Meiji Pharm. Univ.)
Hiroyuki SUZUKI (RI Res. Cen., Chiba Univ.)
Mikiko SUZUKI (Showa Women's Univ.)
Masaaki TAKAHASHI (Grad. Sci. Agric. Biol. Sci.,Osaka Pref. Univ.)
Yoshio TAKAHASHI (Grad. Sch. Sci.,Hiroshima Univ.)
Keiko TAGAMI (Natl. Inst. Radiol. Sci.)
Atsushi TAKEDA (Fac. Pharm. Sci., Univ. Shizuoka)
Tadayasu TOGAWA (Meiji Pharm. Univ.)
Haruna TAMANO (Fac. Pharm. Sci., Univ. Shizuoka)
Tomohiro NABEKURA (Fac. Pharm. Sci., Niigata Univ. Pharm. Appl. Life Sci.)
Yukiko NAKANISHI (Grad. Sch. Hum. Life Sci.,Showa Women's Univ.)
Seiichiro HIMENO (Fac. Pharm. Sci., Tokushima Bunri Univ.)
Jun Furukawa (Tsukuba Univ.)
Yoshitaka MINAI (Cen. Art. Sci., Musashi Univ.)
Takeshi MINAMI (Sch. Sci. Eng., Kinki Univ.)
Makoto YANAGA (Fac. Sci., Shizuoka Univ.)
Hiroyuki YASUI (Kyoto Pharm. Univ)
Shozo YOSHIDA (Nara Med. Univ.)
Masuo KONDOH (Showa Pharm. Univ.)

Kenichiro MATSUMOTO (Natl. Inst. Health, USA)
Shigeo UCHIDA (Natl. Inst. Radiol. Sci.)
Kohshin WASHIYAMA (Fac. Med., Kanazawa Univ.)
Shin WATANABE (Japan Aerospace Exploration Agency)

Research Consultants

Yasuyuki GONO

Student Trainees

Hiroyuki AONO (Grad. Sch. Sci.,Tokyo Univ.)
Ayaka AZUMA (Internat. Chirstian Univ.)
Shin-nosuke ISHIKAWA (Grad. Sch. Sci.,Tokyo Univ.)
Sho OKUYAMA (Grad. Sch. Sci.,Tokyo Univ.)
Hirokazu ODAKA (Grad. Sch. Sci.,Tokyo Univ.)
Terumi KATORI (Showa Women's Univ.)
Nobuko SAJI (Showa Women's Univ.)
Mayumi SHIBANUMA (Showa Women's Univ.)
Shinichiro TAKEDA (Grad. Sch. Sci.,Tokyo Univ.)

Secretary

Naoko HIROMURA

Safety Management Group

1. Abstract

The Nishina Center for Accelerator-Based Science possesses one of the biggest accelerator facilities in the world which consists of a heavy-ion linear accelerator and 5 cyclotrons. Uranium ions are accelerated here only in Japan. Our function is to keep the radiation level in and around the facility below the allowable limit and to control the exposure on the workers as low as reasonably achievable. We are also involved in the safety management of the Radioisotope Center where many types of experiments are performed with sealed and unsealed radioisotopes.

2. Major Research Subjects

(1)Safety management at radiation facilities of Nishina Center for Accelerator-Based Science

(2)Safety management at Radioisotope Center

(3)Radiation shielding design and development of accelerator safety systems

3. Summary of Research Activity

The Nishina Center for Accelerator-Based Science possesses one of the biggest accelerator facilities in the world which consists of a heavy-ion linear accelerator and 5 cyclotrons. Uranium ions are accelerated here only in Japan. Our function is to keep the radiation level in and around the facility below the allowable limit and to control the exposure on the workers as low as reasonably achievable. We are also involved in the safety management of the Radioisotope Center where many types of experiments are performed with sealed and unsealed radioisotopes.

Head
Yoshitomo UWAMINO

Members
Shin FUJITA
Rieko HIGURASHI HIRUNUMA
Hisao SAKAMOTO

Technical Staff I
Atsuko HIRIGOME

Assistant
Tomomi OKAYASU

Contract Officer
Hiroki MUKAI

Contract Officer
Satoshi HASHIGUCHI

Visiting Scientists
Koji OHISHI

Secretary

Tsutomu YAMAKI
Kazushiro NAKANO
Kimie IGARASHI
Yoshiko SATOU
Tsukasa SUZUKI

RIKEN-BNL Research Center
Experimental Group

1. Abstract

The RIKEN BNL Research Center (RBRC), Experiment Group studies the internal spin structure of the proton, using the first polarized proton collider at Brookhaven, RHIC, which has been promoted with RIKEN's leadership. The group leads and participates in three general areas: developing the world's highest energy polarized proton beams, developing probes of the proton's spin content, and seeking a global understanding of all proton spin data. For the proton beam, the group has developed two new methods to measuring the proton beam polarization at high energy, one using proton-Carbon Coulomb Nuclear Interference and the other using very forward neutron asymmetry discovered by our own. Recent data analysis has shown that the proton spin carried by gluons is indeed small, which is a very striking finding beyond our expectations. With collaboration with the BELLE experiment at High Energy Accelerator Research Organization (KEK), we have discovered that quark fragments can determine the spin direction of the mother quark. RHIC stands for Relativistic Heavy Ion Collider, aiming also to create Quark Gluon Plasma, the state of Universe just after the Big Bang. Until now, jet quenching effect and elliptic flows of produced particles are discovered, which have proven that the new state of dense matter is indeed created. We are proceeding to understand the nature of this matter.

2. Major Research Subjects

(1) Experimental Studies of the Spin Structure of the Nucleon
(2) Study of Quark-Gluon Plasma at RHIC
(3) Global QCD Analysis of the Spin Structure of the Nucleon

3. Summary of Research Activity

How is the spin of proton formed with 3 quarks and gluons? This is a very fundamental question in QCD, Quantum Chromo dynamics. The RHIC Spin Project has been established as an international collaboration between RIKEN and Brookhaven National Laboratory (BNL), to solve this problem by colliding two polarized protons for the first time in history. This also extended the physics capability of RHIC, Relativistic Heavy Ion Collider in BNL. At RHIC, Quark Gluon Plasma (QGP) is to be created by colliding two gold nuclei, through which we can study the state of the early Universe just after the Big Bang. In December 2001, polarized protons were successfully accelerated to 100 GeV, and collisions of transversely polarized protons were observed. Since then the spin experiment is on going.

The RIKEN-BNL Research Center was established in 1997 to support the RIKEN activities at RHIC in BNL, and also to promote theoretical studies related to RHIC, i.e. theories of strong interaction. The center's first director was T. D. Lee (Columbia University), and in October 2003, the former director of BNL, N.P. Samios, succeeded to the post of director. The center consists of a theory group lead by L. Mclerran (BNL) and an experimental group lead by H. En'yo, Chief scientist of RIKEN in Wako, who also is an associate director of RBRC.

(1) Experimental study of spin structure of proton using RHIC polarized proton collider

The first goal of the study of spin structure of proton at RHIC is to elucidate a contribution of the gluon spin in the proton spin. So far we have presented double-helicity asymmetries of neutral pions, and shown that the gluon polarization in the proton is small and the sum of gluon-spin contribution and quark-spin contribution cannot explain the total spin 1/2 of the proton spin. The remaining part must reside in the orbital-angular momentum of quarks and gluons. To finalize the smallness of the gluon-spin contribution, we need to measure the golden channel, direct-photon production, which is dominated by a single and the simplest process, gluon Compton process, in the perturbative QCD. We have been accumulating longitudinally-polarized proton

collision data to measure the double-helicity asymmetry of the direct-photon production. We have also accumulating transversely-polarized proton collision data to measure single transverse-spin asymmetries of processes which are predicted to be sensitive to the orbital-angular momentum of quarks and gluons.

In 2007 summer (June-July), the second data-analysis workshop of the PHENIX collaboration, so-called "Spin Fest", was held at RIKEN. More than 30 people from 5 countries in the world (USA, Korea, China, Holland and Japan) got together at RIKEN for active discussions and effective data analyses. Major outcomes were the double-helicity asymmetries of the neutral pion productions at 200 GeV and 62.4 GeV center-of-mass energy collisions, and single transverse-spin asymmetry of forward neutral pions at 62.4 GeV, using the 2006-run data event-reconstructed at RIKEN CC-J. The preliminary results have been presented at international conferences as the latest results of the PHENIX experiment.

Since the RHIC operation in 2008 was shortened by the DOE budget problem there was a polarized-proton collisions for only about one-month long. The RHIC accelerator achieved $2.3 \times 10^{31}/cm^2/s$ of the average luminosity and 45% of the average beam polarization at the center-of-mass energy of 200 GeV. Achieved luminosity was higher than that in 2006, but it was found that the higher luminosity made the polarization lower than that achieved in 2006. This was an issue to be solved for higher luminosity and higher polarization in the future. In 2008, we collected data with transversely-polarized proton collisions at 200 GeV to investigate single transverse-spin asymmetries of pion pairs to be visible with the interference fragmentation function, and the two-jet angular correlation. The PHENIX experiment recorded the data corresponding to 4.5 inverse picobarn of the integrated luminosity in 2008 which was about twice larger than that in 2006, and the figure of merit evaluated with the lower polarization was about comparable. All the physics data in the 2008 run were transferred to RIKEN CC-J in almost real-time via the network between US and Japan. These data will be promptly event-reconstructed and analyzed at RIKEN CC-J.

(2) Experimental study of Quark-Gluon Plasma using RHIC heavy-ion collider

The goal of high energy heavy ion physics at RHIC is study of QCD in extreme conditions i.e. at very high temperature and at very high energy density. Experimental results from RHIC have established that dense partonic matter is formed in Au+Au collisions at RHIC. The focus of the research program is now moving towards measurement of the properties of the matter.

From the fall of 2007 to the spring of 2008, RHIC had its 8^{th} year RUN (RUN8). The first part of RUN8 was deuteron + gold (d+Au) collision experiment. PHENIX recorded very high statistics d+Au data during RUN8, about 30 times of the previous d+Au run in year 2003. From the d+Au data we can study the cold nuclear effect, in particular that on J/Psi production, a key probe of Quark Gluon plasma.

The main results of PHENIX that are published in 2007 are as follows.

1) Measurements of electron pairs in p+p and Au+Au.

Electron pairs are measured in p+p and Au+Au collisions at sqrt(s_NN)=200 GeV by PHENIX experiment. In p+p collisions, the measured mass distribution is well explained by the contribution of light meson decays for the mass region less than 1 GeV. The mass spectrum above 1 GeV is dominated by correlated decay of charm and anit-charm mesons. From the yield of the electron pair continuum above 1 GeV, the total charm production cross section is deduced. The obtained cross section is in good agreement with the measurement from single electrons. In Au+Au collisions, a strong enhancement of electron pair yield above the expectation from light hadron contribution is observed for mass below 1 GeV.

2) J/Psi measurements in d+Au and Cu+Cu

Cold nuclear effects in J/PSI production in d+Au collisions are studied. The d+Au data were re-analyzed and compared with higher statistics p+p data. From the comparison, J/Psi break-up cross section in cold nuclear matter is determined. The final results of J/Psi production in Cu+Cu collision from year 2005 run of RHIC has been published.

3) High pT pi0 measurement and constraints on theory.

PHENIX measured pi0 production at high pT in Au+Au collision at 200 GeV. The new measurement has more than 10 times of statistics of the previous published results and extend the measured pT range to 20 GeV/c. The measurements shows that the pi0 production is strongly suppressed, by about a factor of five, for high pT. The suppression is consistent with that high pT scattered quarks and gluons lose significant amount of their energies in the dense matter formed in the collision. The suppression patterns are compared with the theory calculations of parton energy loss. Form the comparison, quantitative constraints on the parameters of the theories are obtained.

(3) PHENIX detector upgrade

A silicon vertex tracker (VTX) is the first of major upgrade detectors for PHENIX. The detector will be jointly constructed by RIKEN and the US/DOE. The VTX consisted of two inner layers of pixel detectors and two outer layers of strip detectors. The main points of progress in 2007 are as follows: 1) The US side of the project has been approved and the construction has started in 2007.The total budget of the US side of the project is 4.7 M US dollars over four years (FY07 to FY10) 2) A cosmic ray test of final prototype of the pixel system was performed. Clear tracks of cosmic rays are observed by three layers of pixel detectors. 3) Production of all components of the pixel system (the sensor modules, the pixel buses, SPIRO read-out board) has started. 4) Fabrication and the test of the second prototype of read-out card of the strip system, ROC-2, were completed. The fabrication and the test of the third and final prototype, ROC-3, is underway. 5) Mechanical and engineering work of the VTX system is underway. The FEM analysis of the mechanical system has been completed and the first prototype of mechanical stave of the pixel system was fabricated.

Several other detector upgrade projects of PHENIX is underway. FVTX, a forward silicon vertex detector, was proposed to DOE. After two rounds of reviews, FVTX project has been approved and its construction will start soon. Another project, nose-cone calorimeter is in the final stage of the review / approval process. A trigger system upgrade project is underway. RIKEN/RBRC is participating in the muon trigger project and also supports the nose cone calorimeter upgrade. Prototype muon trigger electronics is tested at PHENIX in 2007.

Group Leader
Hideto EN'YO

Deputy Group Leader
Gerry M. BUNCE

Members
Yuji GOTO
Takashi ICHIHARA
Atsushi TAKETANI
Yasushi WATANABE
Yasuyuki AKIBA
Itaru NAKAGAWA
Abhay DESHPANDE*2
Douglas Edward FIELDS*2
Matthias GROSS PERDEKAMP*2
Kensuke OKADA*2
David KAWALL*2
Wei XIE*2
Ralf-Christian SEIDL*2
Stefan BATHE*2

Patricia LIEBING*3
Nobuyuki KAMIHARA*4
Manabu TOGAWA*4
Kazuya Aoki (Kyoto-U)*5
Kohei Syoji (Kyoto-U)*5
Ken'ichi Nakano (T.I.Tech)*5
Jun Tamura (T.I.Tech)*5
TadaAki Isobe (CNS-U-Tokyo)*5
Yorito Tamaguchi(CNS-U-Tokyo)*5
Misaki Ouchida (Hiroshima-U)*5
Kentaro Miki (Tsukuba-U)*5
Visiting Members
Naohito SAITO (KEK)
Zheng LEE (BNL)
Ralf-Christian SEIDLE(DESY)
Kiyoshi TANIDA (Kyoto Univ.)
Akio OGAWA (BNL)
Seiji Dairaku(Kyoto-U)*6
Kenichi Karatsu (Kyoto-U)*7
Koichi Sakashita (T.I.Tech)*7
Takashi Kanesue (Kyusyu-U)*7
*1RIKEN BNL Fellow, *2 RHIC Physics Fellow,*3 Research Associate,
*4 Special Postdoctoral Researcher, *5 Junior Research Associate, *6 JSPS Student, *7 Student trainee

RIKEN-BNL Research Center
Theory Group

1. Abstract

The RIKEN BNL Research Center was established in April 1997 at Brookhaven National Laboratory in New York, USA. The Center is dedicated to study of strong interactions, including hard QCD/spin physics, lattice QCD and RHIC physics through nurturing of a new generation of young physicist. The theory group consists of three sub groups: numerical lattice QCD, perturbative QCD and phenomenological QCD. In JFY2004, the numerical lattice QCD group built a 10 TFlops QCDOC parallel supercomputer dedicated for the first-principle non-perturbative calculations of QCD. It pioneered the use of the domain-wall fermion method in QCD and we investigate various hadron physics including an important calculation of neutral Kaon CP-violations that is relevant for checking the Cabibbo-Kobayashi-Maskawa theory. The perturbative QCD group has developed various new methods required for studying hadron structures, especially in spin physics research. The phenomenological QCD group has pioneered the researches of color superconductivity, isospin density, and small-x phenomena in extreme hadronic matters.

2. Major Research Subjects

(1) Perturbative QCD
(2) Lattice QCD numerical research
(3) Phenomenological QCD

3. Summary of Research Activity

The RIKEN-BNL Research Center was established in 1997 to support the RIKEN activities at RHIC in BNL, and also to promote theoretical studies related to RHIC, i.e. theories of strong interaction. The center's first director was T. D. Lee (Columbia University), and in October 2003, the former director of BNL, N.P. Samios, succeeded to the post of director. The center consists of a theory group lead by L. Mclerran (BNL) and an experimental group lead by H. En'yo, Chief scientist of RIKEN in Wako, who also is an associate director of RBRC.

Research in the RBRC theory group focuses on a wide variety of phenomena caused by the strong interaction, one of the four fundamental interactions in nature. The strong interaction is described theoretically by Quantum Chromodynamics (QCD), and the research projects in the RBRC theory group aim to elucidate various phenomena brought about by the strong interaction from the principles of QCD. Major subjects of our research include studies (a) based on lattice QCD, (b) on spin physics based on perturbative QCD, and (c) on QCD in extreme conditions such as high temperature, high density or high energy. RBRC offers RHIC Physics Fellowships, allowing joint appointments with universities. These Fellowships enable a talented researcher to maintain a tenure track position at his/her university as well as a Fellow position at RBRC for a certain period of time. This system was established in order to increase the research potential of RBRC and to disseminate its research activities and results. At present, RBRC has cooperative agreements with BNL, Columbia University, Massachusetts Institute of Technology, the State University of New York at Stony Brook, Texas A&M University, Purdue University, Iowa State University, Kanazawa University, and University of Tsukuba.

(1) Lattice QCD

QCDOC (QCD on chip), a second-generation lattice-QCD computer, was developed in the collaboration amongst this group, Columbia University and IBM. Three units of such a machine with 10 TFlops computing power are in operation since 2005; two in BNL (RBRC and DOE) and one in Edinburgh (UK-QCD), and formed a world-wide strong collaboration for the lattice QCD studies. Such computing power enables us to perform precise calculations with 3 quark flavors with proper handling on the chiral symmetry breaking.

Several projects are on going; flavor physics for Kaon and B-meson, electro-magnetic properties of hadrons, proton decay, the nuclear force, nucleon form factors which relates to the proton spin problem, QCD thermodynamics in finite temperature/density systems as is produced in RHIC heavy-ion collisions.

(2) Perturbative QCD and spin physics

The first few years running of RHIC spin experiment have motivated much theoretical developments in 2006. For example, in order to interpret the double spin asymmetry measurements for various processes at RHIC, the global analyses from several groups have been made last year, and they all found the large positive gluon polarization is disfavored from the RHIC results. Meanwhile, there has been progress in transverse spin physics. A non-universality property was found for the transverse momentum dependent parton distribution in the dijet-correlation in proton-proton scattering, because of both initial and final state interactions effects. Azimuthal asymmetric distribution of hadrons inside a high energy jet at hadron collider has been proposed as a probe for the quark transversity distribution.

(3) Phenomenological QCD – QCD under extreme conditions –

To establish a microscopic picture of relativistic heavy ion collisions, QCD-based theoretical approaches are in progress. Especially the idea of "color glass condensation (CGC)" can be a key to understand the initial condition of heavy ion collision. We discussed a possible relation between CGC and the elliptic flow of particles which was discovered at RHIC. Other phenomenological approaches are in progress to understand the characteristics of strongly interacting quark gluon plasma (sQGP).

Group Leader

Larry McLERRAN

Deputy Group Leader

Anthony J. BALTZ

Members

Christopher DAWSON*1
Yasumichi AOKI*1
Thomas BLUM*2
Denes MOLNAR*2
Kirill TUCHIN*2
Fries RAINER*2
Tomomi ISHIKAWA*3
Feng YUAN*2
Agnes MOCSY*3
Marquet CYRILLE*3
Lichtl ADAM*3
Kenji FUKUSHIMA*4
Yoshimasa HIDAKA*4
Peter PETRECZKY*1
Taku IZUBUCHI*2
Shinya AOKI*2
Derek TEANEY*2

Visiting Members

Miklos GYULASSY (Columbia Univ., USA)
Robert L. JAFFE (Massachusetts Inst. Technol., USA)

Robert MAWHINNEY (Columbia Univ., USA)
Edward SHURYAK (State Univ. New York, Stony Brook, USA)
Shigemi OHTA (KEK)
Yoshitaka HATTA (Kyoto University)
Kei IIDA(Kochi Univ.)
Tetsufumi HIRANO (Columbia University)
Lin HUEY-WEN （Columbia University）
Masakiyo KITAZAWA (Osaka University)

Administration

Pamela ESPOSITO (Secretary)
Doris RUEGER (Assistant)
Taeko ITO (Secretary)
Susan FOSTER (Secretary)

Administrative Manager

Yoshio OKUIZUMI, Hiroshi MIYAMOTO

Deputy Administrative Manager

Ryosuke MARUYAMA

*1RIKEN BNL Fellow, *2 RHIC Physics Fellow,
*3 Research Associate, *4 Special Postdoctoral Researcher,

VI. LIST OF PUBLICATIONS & PRESENTATION

Director's Office

Publications

[Journal]

(Original Papers) *Subject to Peer Review

Sugimoto T., Nakamura T., Fukuda N., Miura M., Kondo Y., Aoi N., Baba H., Bazin D., Gomi T., Hasegawa H., Hashimoto Y., Imai N., Kobayashi T., Kubo T., Motobayashi T., Ohara M., Saito A., Sakurai H., Shimoura S., Attukalathil V. M., Watanabe K., Watanabe Y., Yakushiji T., Yanagisawa Y., Yoneda K., and Ishihara M.: "Invariant-mass spectroscopy of the neutron-drip line nucleus ^{14}Be", J. Phys.: Con. Ser. **49**, 43–44 (2006). *

Asahi K., Uchida M., Shimada K., Nagae D., Kameda D., Ueno H., Yoshimi A., Takemura M., Arai T., Takase K., Inoue T., Kawamura H., Murata J., Watanabe H., Haseyama T., Kobayashi Y., Umeya A., and Ishihara M.: "Structure of unstable nuclei from nuclear moments and decays", J. Phys.: Con. Ser. **49**, 79–84 (2006). *

Kidera M., Takahashi K., Enomoto S., Mitsubori Y., Goto A., and Yano Y.: "Development of a novel mass spectrometer equipped with an electron cyclotron resonance ion source", Eur. J. Mass Spectrom. **13**, 239–248 (2007). *

Kidera M., Takahashi K., Enomoto S., Goto A., and Yano Y.: "New fragment ion production method using super cold electrons in electron cyclotron resonance plasma", Eur. J. Mass Spectrom. **13**, 355–358 (2007). *

Motomura S., Enomoto S., Haba H., Igarashi K., Gono Y., and Yano Y.: "Gamma-Ray Compton Imaging of Multitracer in Biological Samples using Strip Germanium Telescope", IEEE Trans. Nucl. Sci. **54**, No. 3, pp. 710–717 (2007). *

Ryuto H., Hasebe H., Fukunishi N., Abe T., Goto A., Kase M., and Yano Y.: "Charge-stripping foil changer with energy adjuster function", Nucl. Instrum. Methods Phys. Res. A **581**, No. 3, pp. 586–588 (2007). *

Yano Y.: "The RIKEN RI Beam Factory Project:A status report", Nucl. Instrum. Methods Phys. Res. B **261**, 1009–1013 (2007). *

Kameda D., Ueno H., Asahi K., Takemura M., Yoshimi A., Haseyama T., Uchida M., Shimada K., Nagae D., Kijima G., Arai T., Takase K., Suda S., Inoue T., Murata J., Kawamura H., Kobayashi Y., Watanabe H., and Ishihara M.: "Measurement of the electric quadrupole moment of ^{32}Al", Phys. Lett. B **647**, 93–97 (2007). *

Shimoura S., Ota S., Demichi K., Aoi N., Baba H., Elekes Z., Fukuchi T., Gomi T., Hasegawa K., Ideguchi E., Ishihara M., Iwasa N., Iwasaki H., Kanno S., Kubono S., Kurita K., Kurokawa M., Matsuyama Y., Michimasa S., Miller K. L., Minemura T., Motobayashi T., Murakami T., Notani M., Odahara A., Saito A., Sakurai H., Takeshita E., Takeuchi S., Tamaki M., Teranishi T., Yamada K., Yanagisawa Y., and Hamamoto I.: "Lifetime of the isomeric 0_2^+ state in ^{12}Be", Phys. Lett. B **654**, 87–91 (2007). *

Sugimoto T., Nakamura T., Kondo Y., Aoi N., Baba H., Bazin D. P., Fukuda N., Gomi T., Hasegawa H., Imai N., Ishihara M., Kobayashi T., Kubo T., Miura M., Motobayashi T., Otsu H., Saito A., Sakurai H., Shimoura S., Vinodkumar A. M., Watanabe K., Watanabe Y., Yakushiji T., Yanagisawa Y., and Yoneda K.: "The first 2^+ state of ^{14}Be", Phys. Lett. B **654**, 160–164 (2007). *

Notani M., Sakurai H., Aoi N., Iwasaki H., Fukuda N., Liu Z., Yoneda K., Ogawa H., Teranishi T., Nakamura T., Okuno H., Yoshida A., Watanabe Y., Momota S., Inabe N., Kubo T., Ito S., Ozawa A., Suzuki T., Tanihata I., and Ishihara M.: "Projectile fragmentation reaction and production of nuclei near the neutron drip line", Phys. Rev. C **76**, 044605-1–044605-15 (2007). *

[Book・Proceedings]

(Original Papers) *Subject to Peer Review

Yano Y.: "Status of the riken RIB factory", Proceedings of 22nd Biennial Particle Accelerator Conference (PAC07), Albuquerque, USA, 2007–6, IEEE, Washington D.C, pp. 700–702 (2007).

Kameda D., Ueno H., Asahi K., Takemura M., Nagae D., Shimada K., Yoshimi A., Kobayashi Y., Haseyama T., Uchida M., Takase K., Arai T., Inoue T., Suda S., Murata J., Kawamura H., Watanabe H., and Ishihara M.: "Nuclear moment measurements of Neutron-rich Aluminum Isotopes Using Spin-Polarized RI beams: Determination of the Boundary of the "Island of Inversion"", Proceedings of the 17th International Spin Physics Symposium (SPIN2006), Tokyo, 2006–10, American Institute of Physics, New York, pp. 845–848 (2007). *

Stingelin L., 後藤 彰, 上垣外 修一, 坂本 成彦, 矢野 安重: "Study of new flat-top resonator for the RIKEN Ring Cyclotron", 第 3 回日本加速器学会年会・第 31 回リニアック技術研究会論文集, 仙台, 2006–8, 日本加速器学会・リニアック技術研究会, 仙台, pp. 889–891 (2006).

龍頭啓充, 長谷部裕雄, 横内茂, 福西暢尚, 後藤彰, 加瀬昌之, 矢野安重: "理研 RIBF におけるウラン加速のためのチャージストリッパー", 第 4 回日本加速器学会年会・第 32 回リニアック技術研究会論文集, 和光市, 2007–8, 第 4 回日本加速器学会・第 32 回リニアック技術研究会実行委員会, 東京, pp. 194–196 (2007).

Oral Presentations

(International Conference etc.)

Sugimoto T., Nakamura T., Fukuda N., Miura M., Kondo Y., Aoi N., Baba H., Bazin D., Gomi T., Hasegawa H., Hashimoto Y., Imai N., Kobayashi T., Kubo T., Motobayashi T., Ohara M., Saito A., Sakurai H., Shimoura S., Attukalathil V. M., Watanabe K., Watanabe Y., Yakushiji T., Yanagisawa Y., Yoneda K.,

and Ishihara M.: "Invariant-mass spectroscopy of the neutron-drip line nucleus ^{14}Be", International Symposium on Structure of Exotic Nuclei and Nuclear Forces (SENUF06), (CNS and RIKEN), Tokyo, Mar. (2006).

Kameda D., Ueno H., Asahi K., Yoshimi A., Haseyama T., Kobayashi Y., Ishihara M., Nagae D., Takemura M., Shimada K., Uchida M., Arai T., Takase K., Inoue T., Kijima G., Suda S., Murata J., Kawamura H., Narota K., Toyoda T., and Watanabe H.: "Electric quadrupole moments of neutron-rich nuclei ^{32}Al and ^{31}Al", International Symposium & School on Frontiers and Perspectives of Nuclear and Hadron Physics (FPNH07), (Tokyo Institute of Technology), Tokyo, June (2007).

Ryuto H., Hasebe H., Yokouchi S., Fukunishi N., Goto A., Kase M., and Yano Y.: "Charge strippers for acceleration of uranium beam at RIKEN RI-beam factory", 18th International Conference on Cyclotrons and their Applications (Cyclotrons 2007), (Istituto Nazionale di Fisica Nucleare), Giardini Naxos, Italy, Sept.–Oct. (2007).

(Domestic Conference)

亀田大輔, 上野秀樹, 旭耕一郎, 竹村真, 吉見彰洋, 長谷山智仁, 内田誠, 島田健司, 長江大輔, 木島剛, 新井崇雅, 高瀬研以智, 須田紳一, 井上壮志, 村田次郎, 川村広和, 小林義男, 渡邉寛, 石原正泰: "中性子過剰核 32Al の核モーメント測定–魔法数 20 の閉殻構造の破れに関連して–", 日本物理学会 2007 年春季大会, 東京, 3 月 (2007).

杉本崇, 中村隆司, 近藤洋介, 青井考, 馬場秀忠, Bazin D., 福田直樹, 五味朋子, 長谷川浩一, 今井伸明, 石原正泰, 小林俊雄, 久保敏幸, 三浦元隆, 本林透, 大津秀暁, 齋藤明登, 櫻井博儀, 下浦享, Attukalathil V. M., 渡辺極之, 渡辺裕, 薬師寺崇, 柳澤善行, 米田健一郎: "核破砕反応を用いた ^{14}Be の不変質量核分光", 京都大学基礎物理学研究所セミナー, 京都, 4 月 (2007).

杉本崇, 中村隆司, 三浦元隆, 近藤洋介, Attukalathil V. M., 青井考, 馬場秀忠, 福田直樹, 五味朋子, 石原正泰, 久保敏幸, 本林透, 大津秀暁, 櫻井博儀, 柳澤善行, 米田健一郎, Bazin D., 長谷川浩一, 今井伸明, 渡辺裕, 小林俊雄, 渡辺極之, 薬師寺崇, 下浦享, 齋藤明登: "不安定核二次ビームを用いた ^{14}Be の不変質量核分光", SPring-8 加速器セミナー, (JASRI), 播磨, 7 月 (2007).

龍頭啓充, 長谷部裕雄, 横内茂, 福西暢尚, 後藤彰, 加瀬昌之, 矢野安重: "理研 RIBF におけるウラン加速のためのチャージストリッパー", 第 4 回日本加速器学会年会・第 32 回リニアック技術研究会, 和光, 8 月 (2007).

奥野広樹, 山田一成, 池上九三男, 加瀬昌之, 矢野安重, 真家武士: "Operational Status of the He Cooling System for RIKEN SRC", 第 4 回日本加速器学会年会・第 32 回リニアック技術研究会, 和光, 8 月 (2007).

福西暢尚, 後藤彰, 稲辺尚人, 加瀬昌之, 龍頭啓充, 坂本成彦, 矢野安重: "理研 RI ビームファクトリー fRC の圧力分布計算", 第 4 回日本加速器学会年会・第 32 回リニアック技術研究会, 和光, 8 月 (2007).

奥野広樹, 山田一成, 大西純一, 福西暢尚, 横内茂, 長谷部裕雄, 池上九三男, 熊谷桂子, 坂本成彦, 上垣外修一, 長瀬誠, 藤巻正樹, 込山美咲, 後藤彰, 加瀬昌之, 矢野安重, 真家武士: "理研超伝導リングサイクロトロンの現状報告", 第 4 回日本加速器学会年会・第 32 回リニアック技術研究会, 和光, 8 月 (2007).

Accelerator Development Group

Publications

[Journal]

(Original Papers) *Subject to Peer Review

Saito F., Nagashima Y., Goto A., Iwaki M., Takahashi N., Oka T., Inoue T., and Hyodo T.: "Electrochemical transfer of 18F from 18O water to aprotic polar solvent", Appl. Radiat. Isot. **65**, 524–527 (2007). *

Ohnishi J., Nakagawa T., Higurashi Y., Kidera M., Saito H., and Goto A.: "Design of magnet system for RIKEN superconducting ECR ion source", High Energy Physics And Nuclear Physcis **31**, No. Suppl. 1, pp. 37–40 (2007).

Ryuto H., Hasebe H., Fukunishi N., Abe T., Goto A., Kase M., and Yano Y.: "Charge-stripping foil changer with energy adjuster function", Nucl. Instrum. Methods Phys. Res. A **581**, No. 3, pp. 586–588 (2007). *

[Book・Proceedings]

(Original Papers) *Subject to Peer Review

Stingelin L., 後藤 彰, 上垣外 修一, 坂本 成彦, 矢野 安重: "Study of new flat-top resonator for the RIKEN Ring Cyclotron", 第 3 回日本加速器学会年会・第 31 回リニアック技術研究会論文集, 仙台, 2006–8, 日本加速器学会・リニアック技術研究会, 仙台, pp. 889–891 (2006).

大西純一, 中川孝秀, 日暮祥英, 木寺正憲, 後藤彰: "ECR イオン源用超伝導コイルの設計", 第 4 回日本加速器学会年会・第 32 回リニアック技術研究会論文集, 日本加速器学会, 和光, pp. 745–747 (2007).

龍頭啓充, 長谷部裕雄, 横内茂, 福西暢尚, 後藤彰, 加瀬昌之, 矢野安重: "理研 RIBF におけるウラン加速のためのチャージストリッパー", 第 4 回日本加速器学会年会・第 32 回リニアック技術研究会論文集, 和光市, 2007–8, 第 4 回日本加速器学会・第 32 回リニアック技術研究会実行委員会, 東京, pp. 194–196 (2007).

Oral Presentations

(International Conference etc.)

Ryuto H., Hasebe H., Yokouchi S., Fukunishi N., Goto A., Kase M., and Yano Y.: "Charge strippers for acceleration of uranium beam at RIKEN RI-beam factory", 18th International Conference on Cyclotrons and their Applications (Cyclotrons 2007), (Istituto Nazionale di Fisica Nucleare), Giardini Naxos, Italy, Sept.–Oct. (2007).

(Domestic Conference)

龍頭啓充, 長谷部裕雄, 横内茂, 福西暢尚, 後藤彰, 加瀬昌之, 矢野安重: "理研 RIBF におけるウラン加速のためのチャージストリッパー", 第 4 回日本加速器学会年会・第 32 回リニアック技術研究会, 和光, 8 月 (2007).

福西暢尚, 後藤彰, 稲辺尚人, 加瀬昌之, 龍頭啓充, 坂本成彦, 矢野安重: "理研 RI ビームファクトリー fRC の圧力分布計算", 第 4 回日本加速器学会年会・第 32 回リニアック技術研究会, 和光, 8 月 (2007).

奥野広樹, 山田一成, 大西純一, 福西暢尚, 横内茂, 長谷部裕雄, 池上九三男, 熊谷桂子, 坂本成彦, 上垣外修一, 長瀬誠, 藤巻正樹, 込山美咲, 後藤彰, 加瀬昌之, 矢野安重, 真家武士: "理研超伝導リングサイクロトロンの現状報告", 第 4 回日本加速器学会年会・第 32 回リニアック技術研究会, 和光, 8 月 (2007).

Accelerator Team

Publications

[Journal]

(Original Papers) *Subject to Peer Review

Ohnishi J., Nakagawa T., Higurashi Y., Kidera M., Saito H., and Goto A.: "Design of magnet system for RIKEN superconducting ECR ion source", High Energy Physics And Nuclear Physcis **31**, No. Suppl. 1, pp. 37–40 (2007).

Hayashi T., Koike S., Higami N., Hirabayashi K., Matsuba H., Ogiwara K., and Yagi E.: "Lattice location of hydrogen in β_1-V_2H (tetragonal)", J. Alloys Compounds **446/447**, 512–515 (2007). *

Sekiguchi K., Sakai H., Sakamoto N., Kuboki H., Sasano M., Takahashi Y., Yako K., Kawabata T., Maeda Y., Sakaguchi S., Sasamoto Y., Suda K., Uesaka T., Okamura H., Itoh K., and Wakasa T.: "Study of Spin Parts of Three Nucleon Forces via $\vec{dp}$ Breakup Reactions at Intermediate Energies", Nucl. Phys. A **790**, 450c–453c (2007). *

[Book・Proceedings]

(Original Papers) *Subject to Peer Review

Stingelin L., 後藤 彰, 上垣外 修一, 坂本 成彦, 矢野 安重: "Study of new flat-top resonator for the RIKEN Ring Cyclotron", 第 3 回日本加速器学会年会・第 31 回リニアック技術研究会論文集, 仙台, 2006–8, 日本加速器学会・リニアック技術研究会, 仙台, pp. 889–891 (2006).

大西純一, 中川孝秀, 日暮祥英, 木寺正憲, 後藤彰: "ECR イオン源用超伝導コイルの設計", 第 4 回日本加速器学会年会・第 32 回リニアック技術研究会論文集, 日本加速器学会, 和光, pp. 745–747 (2007).

Oral Presentations

(Domestic Conference)

岩井良夫, 池田時浩, 小島隆夫, 金井保之, 和田道治, 前島一博, 今本尚子, 小林知洋, 荻原清, 成沢忠, Pokhil G. P., 山崎泰規: "蓋つき先細型キャピラリーを用いた理研マイクロビーム細胞照射装置の開発", 原子衝突研究協会第 32 回研究会, 東京, 8 月 (2007).

福西暢尚, 後藤彰, 稲辺尚人, 加瀬昌之, 龍頭啓充, 坂本成彦, 矢野安重: "理研 RI ビームファクトリー fRC の圧力分布計算", 第 4 回日本加速器学会年会・第 32 回リニアック技術研究会, 和光, 8 月 (2007).

奥野広樹, 山田一成, 大西純一, 福西暢尚, 横内茂, 長谷部裕雄, 池上九三男, 熊谷桂子, 坂本成彦, 上垣外修一, 長瀬誠, 藤巻正樹, 込山美咲, 後藤彰, 加瀬昌之, 矢野安重, 真家武士: "理研超伝導リングサイクロトロンの現状報告", 第 4 回日本加速器学会年会・第 32 回リニアック技術研究会, 和光, 8 月 (2007).

岩井良夫, 池田時浩, 小島隆夫, 金井保之, 和田道治, 前島一博, 今本尚子, 小林知洋, 荻原清, 成沢忠, Pokhil G. P., 山崎泰規: "蓋つきキャピラリーを用いた理研マイクロビーム細胞照射装置の開発", 日本物理学会第 62 回年次大会, 札幌, 9 月 (2007).

岩井良夫, 池田時浩, 小島隆夫, 金井保之, 和田道治, 前島一博, 今本尚子, 小林知洋, 荻原清, 成沢忠, Pokhil G. P., 山崎泰規: "蓋つき先細型ガラスキャピラリーを用いた細胞内および液相中微小領域へのエネルギー付与法", 第 48 回真空に関する連合講演会, (日本真空協会), 東京, 11 月 (2007).

Ion Source Team

Publications

[Journal]

(Original Papers) *Subject to Peer Review

Kidera M., Takahashi K., Enomoto S., Mitsubori Y., Goto A., and Yano Y.: "Development of a novel mass spectrometer equipped with an electron cyclotron resonance ion source", Eur. J. Mass Spectrom. **13**, 239–248 (2007). *

Kidera M., Takahashi K., Enomoto S., Goto A., and Yano Y.: "New fragment ion production method using super cold electrons in electron cyclotron resonance plasma", Eur. J. Mass Spectrom. **13**, 355–358 (2007). *

Ohnishi J., Nakagawa T., Higurashi Y., Kidera M., Saito H., and Goto A.: "Design of magnet system for RIKEN superconducting ECR ion source", High Energy Physics And Nuclear Physcis **31**, No. Suppl. 1, pp. 37–40 (2007).

[Book・Proceedings]

(Original Papers) *Subject to Peer Review

大西純一, 中川孝秀, 日暮祥英, 木寺正憲, 後藤彰: "ECR イオン源用超伝導コイルの設計", 第 4 回日本加速器学会年会・第 32 回リニアック技術研究会論文集, 日本加速器学会, 和光, pp. 745–747 (2007).

Oral Presentations

(Domestic Conference)

三堀陽平, 高橋和也, 木寺正憲, 榎本秀一, 田中龍彦, 南武志, 今津節生, 林英男: "微量元素分析に基づく、古墳等の遺構から出土した辰砂の産地推定の試み", 第 68 回分析化学討論会, (社団法人日本分析化学会), 宇都宮, 5 月 (2007).

木寺正憲, 高橋和也, 榎本秀一, 中川孝秀, 三堀陽平, 田中龍彦, 戸田勝善: "電子サイクロトロン共鳴イオン源 (ECRIS) を用いた質量分析装置の開発", 日本分析化学会第 56 年会, 徳島, 9 月 (2007).

Accelerator Operation Group

Publications

[Journal]

(Original Papers) *Subject to Peer Review

Ryuto H., Hasebe H., Fukunishi N., Abe T., Goto A., Kase M., and Yano Y.: "Charge-stripping foil changer with energy adjuster function", Nucl. Instrum. Methods Phys. Res. A **581**, No. 3, pp. 586–588 (2007). *

Shimoura S., Ota S., Demichi K., Aoi N., Baba H., Elekes Z., Fukuchi T., Gomi T., Hasegawa K., Ideguchi E., Ishihara M., Iwasa N., Iwasaki H., Kanno S., Kubono S., Kurita K., Kurokawa M., Matsuyama Y., Michimasa S., Miller K. L., Minemura T., Motobayashi T., Murakami T., Notani M., Odahara A., Saito A., Sakurai H., Takeshita E., Takeuchi S., Tamaki M., Teranishi T., Yamada K., Yanagisawa Y., and Hamamoto I.: "Lifetime of the isomeric 0_2^+ state in ^{12}Be", Phys. Lett. B **654**, 87–91 (2007). *

[Book・Proceedings]

(Original Papers) *Subject to Peer Review

龍頭啓充, 長谷部裕雄, 横内茂, 福西暢尚, 後藤彰, 加瀬昌之, 矢野安重: "理研 RIBF におけるウラン加速のためのチャージストリッパー", 第 4 回日本加速器学会年会・第 32 回リニアック技術研究会論文集, 和光市, 2007–8, 第 4 回日本加速器学会・第 32 回リニアック技術研究会実行委員会, 東京, pp. 194–196 (2007).

(Others)

込山美咲, 藤巻正樹, 長瀬誠, 加瀬昌之, 内山暁仁: "理研 RI ビームファクトリー制御系の現状", 第 4 回日本加速器学会年会・第 32 回リニアック技術研究会論文集, 東京, pp. 416–418 (2007).

Oral Presentations

(International Conference etc.)

Ryuto H., Hasebe H., Yokouchi S., Fukunishi N., Goto A., Kase M., and Yano Y.: "Charge strippers for acceleration of uranium beam at RIKEN RI-beam factory", 18th International Conference on Cyclotrons and their Applications (Cyclotrons 2007), (Istituto Nazionale di Fisica Nucleare), Giardini Naxos, Italy, Sept.–Oct. (2007).

(Domestic Conference)

龍頭啓充, 長谷部裕雄, 横内茂, 福西暢尚, 後藤彰, 加瀬昌之, 矢野安重: "理研 RIBF におけるウラン加速のためのチャージストリッパー", 第 4 回日本加速器学会年会・第 32 回リニアック技術研究会, 和光, 8 月 (2007).

奥野広樹, 山田一成, 池上九三男, 加瀬昌之, 矢野安重, 真家武士: "Operational Status of the He Cooling System for RIKEN SRC", 第 4 回日本加速器学会年会・第 32 回リニアック技術研究会, 和光, 8 月 (2007).

福西暢尚, 後藤彰, 稲辺尚人, 加瀬昌之, 龍頭啓充, 坂本成彦, 矢野安重: "理研 RI ビームファクトリー fRC の圧力分布計算", 第 4 回日本加速器学会年会・第 32 回リニアック技術研究会, 和光, 8 月 (2007).

池沢英二, 加瀬昌之, 大木智則, 藍原利光, 山内啓資, 内山暁仁, 小山田和幸, 田村匡史: "RI ビームファクトリー入射用重イオンリニアック運転状況", 第 4 回日本加速器学会年会・第 32 回リニアック技術研究会, 和光, 8 月 (2007).

奥野広樹, 山田一成, 大西純一, 福西暢尚, 横内茂, 長谷部裕雄, 池上九三男, 熊谷桂子, 坂本成彦, 上垣外修一, 長瀬誠, 藤巻正樹, 込山美咲, 後藤彰, 加瀬昌之, 矢野安重, 真家武士: "理研超伝導リングサイクロトロンの現状報告", 第 4 回日本加速器学会年会・第 32 回リニアック技術研究会, 和光, 8 月 (2007).

RILAC Team

Oral Presentations

(Domestic Conference)

池沢英二, 加瀬昌之, 大木智則, 藍原利光, 山内啓資, 内山暁仁, 小山田和幸, 田村匡史: “RI ビームファクトリー入射用重イオンリニアック運転状況”, 第 4 回日本加速器学会年会・第 32 回リニアック技術研究会, 和光, 8 月 (2007).

Cyclotron Team

Publications

[Book•Proceedings]

(Original Papers) *Subject to Peer Review

龍頭啓充, 長谷部裕雄, 横内茂, 福西暢尚, 後藤彰, 加瀬昌之, 矢野安重: “理研 RIBF におけるウラン加速のためのチャージストリッパー”, 第 4 回日本加速器学会年会・第 32 回リニアック技術研究会論文集, 和光市, 2007–8, 第 4 回日本加速器学会・第 32 回リニアック技術研究会実行委員会, 東京, pp. 194–196 (2007).

(Others)

込山美咲, 藤巻正樹, 長瀬誠, 加瀬昌之, 内山暁仁: “理研 RI ビームファクトリー制御系の現状”, 第 4 回日本加速器学会年会・第 32 回リニアック技術研究会論文集, 東京, pp. 416–418 (2007).

Oral Presentations

(International Conference etc.)

Ryuto H., Hasebe H., Yokouchi S., Fukunishi N., Goto A., Kase M., and Yano Y.: “Charge strippers for acceleration of uranium beam at RIKEN RI-beam factory”, 18th International Conference on Cyclotrons and their Applications (Cyclotrons 2007), (Istituto Nazionale di Fisica Nucleare), Giardini Naxos, Italy, Sept.–Oct. (2007).

(Domestic Conference)

中村剛, 大熊春夫, 熊谷教孝, 大島隆, 武部英樹, 松井佐久夫, 安東愛之介, 庄司善彦, 橋本智, 服部正, 熊谷桂子: “クロマティシティ変調による横方向不安定性の抑制実験”, 第 3 回日本加速器学会年会・第 31 回リニアック技術研究会, (日本加速器学会), 仙台, 8 月 (2006).

龍頭啓充, 長谷部裕雄, 横内茂, 福西暢尚, 後藤彰, 加瀬昌之, 矢野安重: “理研 RIBF におけるウラン加速のためのチャージストリッパー”, 第 4 回日本加速器学会年会・第 32 回リニアック技術研究会, 和光, 8 月 (2007).

奥野広樹, 山田一成, 池上九三男, 加瀬昌之, 矢野安重, 真家武士: “Operational Status of the He Cooling System for RIKEN SRC”, 第 4 回日本加速器学会年会・第 32 回リニアック技術研究会, 和光, 8 月 (2007).

福西暢尚, 後藤彰, 稲辺尚人, 加瀬昌之, 龍頭啓充, 坂本成彦, 矢野安重: “理研 RI ビームファクトリー fRC の圧力分布計算”, 第 4 回日本加速器学会年会・第 32 回リニアック技術研究会, 和光, 8 月 (2007).

奥野広樹, 山田一成, 大西純一, 福西暢尚, 横内茂, 長谷部裕雄, 池上九三男, 熊谷桂子, 坂本成彦, 上垣外修一, 長瀬誠, 藤巻正樹, 込山美咲, 後藤彰, 加瀬昌之, 矢野安重, 真家武士: “理研超伝導リングサイクロトロンの現状報告”, 第 4 回日本加速器学会年会・第 32 回リニアック技術研究会, 和光, 8 月 (2007).

Beam Technology Team

Publications

[Journal]

(Original Papers) *Subject to Peer Review

Kazama Y., Saito H., Fujiwara M., Matsuyama T., Hayashi Y., Ryuto H., Fukunishi N., and Abe T.: "An effective method for detection and analysis of DNA damage induced by heavy-ion beams", Biosci. Biotechnol. Biochem. **71**, No. 11, pp. 2864–2869 (2007). *

Godo T., Okuno H., Saito H., Miyazawa Y., Ryuto H., Fukunishi N., and Abe T.: "Effects of ion beam irradiation on survival and mutation induction of triploid Senno (Lychnis senno Siebold et Zucc.)", Bull.Bot.Gard.Toyama, No. 12, pp. 41–46 (2007). *

Shitsukawa N., Ikai C., Shimada S., Kitagawa S., Sakamoto K., Saito H., Ryuto H., Fukunishi N., Abe T., Takumi S., Nasuda S., and Murai K.: "The einkorn wheat (Triticum monococcum) mutant, maintained vegetative phase, is caused by a deletion in the VRN1 gene", Genes Genet. Syst. **82**, 167–170 (2007). *

Ryuto H., Hasebe H., Fukunishi N., Abe T., Goto A., Kase M., and Yano Y.: "Charge-stripping foil changer with energy adjuster function", Nucl. Instrum. Methods Phys. Res. A **581**, No. 3, pp. 586–588 (2007). *

市田裕之, 木庭卓人, 龍頭啓充, 福西暢尚, 林依子, 阿部知子, 松山知樹: "重イオンビームによって誘発される DNA 多型の解析", DNA 多型 **15**, 118–121 (2007). *

[Book・Proceedings]

(Original Papers) *Subject to Peer Review

Kanaya T., Miyazaki K., Suzuki K., Iwaki K., Ichida H., Hayashi Y., Saito H., Ryuto H., Fukunishi N., and Abe T.: "New cultivar produced by heavy-ion beam irradiation", Proceedings of the 25th Symposium on Materials Science and Engineering, Research Center of Ion Beam Technology, Hosei University, Japan, 2006–11, Research Center of Ion Beam Technology, Hosei University, Tokyo, pp. 1–6 (2007).

龍頭啓充, 長谷部裕雄, 横内茂, 福西暢尚, 後藤彰, 加瀬昌之, 矢野安重: "理研 RIBF におけるウラン加速のためのチャージストリッパー", 第 4 回日本加速器学会年会・第 32 回リニアック技術研究会論文集, 和光市, 2007–8, 第 4 回日本加速器学会・第 32 回リニアック技術研究会実行委員会, 東京, pp. 194–196 (2007).

(Others)

込山美咲, 藤巻正樹, 長瀬誠, 加瀬昌之, 内山暁仁: "理研 RI ビームファクトリー制御系の現状", 第 4 回日本加速器学会年会・第 32 回リニアック技術研究会論文集, 東京, pp. 416–418 (2007).

Oral Presentations

(International Conference etc.)

Fujinawa T.: "Desigen, installation, operation and maintenance of electrical power supply for RI beam factory", 6th International Workshop Accelerator Operations, (FERMI), Trieste, Italy, Sept. (2007).

Ryuto H., Hasebe H., Yokouchi S., Fukunishi N., Goto A., Kase M., and Yano Y.: "Charge strippers for acceleration of uranium beam at RIKEN RI-beam factory", 18th International Conference on Cyclotrons and their Applications (Cyclotrons 2007), (Istituto Nazionale di Fisica Nucleare), Giardini Naxos, Italy, Sept.–Oct. (2007).

Kazama Y., Saito H., Yamamoto Y. Y., Hayashi Y., Ichida H., Ohbu S., Ryuto H., Fukunishi N., and Abe T.: "Effects of Heavy-ion beam irradiation on mutation induction in *Arabidopsis thaliana*", 18th International Conference on Cyclotrons and their Applications (Cyclotrons 2007), Giardini Naxos, Italy, Oct. (2007).

Hayashi Y., Takehisa H., Kazama Y., Ichida H., Ryuto H., Fukunishi N., Abe T., Kamba C., and Sato T.: "Effects of ion beam irradiation on mutation induction in rice", 18th International Conference on Cyclotrons and their Applications (Cyclotrons 2007), Giardini Naxos, Italy, Oct. (2007).

Abe T., Kazama Y., Ichida H., Hayashi Y., Ryuto H., and Fukunishi N.: "Plant Breeding using the ion beam irradiation in RIKEN", 18th International Conference on Cyclotrons and their Applications (Cyclotrons 2007), Giardini Naxos, Italy, Oct. (2007).

(Domestic Conference)

神波千秋, 竹久妃奈子, 阿部知子, 林依子, 斉藤宏之, 市田裕之, 小沼亮子, 龍頭啓充, 福西暢尚, 宮沢豊, 東海林英夫, 保倉明子, 福田直樹, 中井泉, 佐藤雅志: "重イオンビーム照射により作出されたイネ塩害耐性突然変異系統の特性解析", 日本育種学会第 111 回講演会, (日本育種学会), 水戸, 3 月 (2007).

林依子, 竹久妃奈子, 風間裕介, 神波千秋, 東海林英夫, 斉藤宏之, 龍頭啓充, 福西暢尚, 宮沢豊, 阿部知子, 佐藤雅志: "イネにおける重イオンビーム照射による突然変異誘発効果", 日本育種学会第 111 回講演会, (日本育種学会), 水戸, 3 月 (2007).

風間裕介, 斉藤宏之, 宮沢豊, 金谷健至, 鈴木賢一, 林依子, 龍頭啓充, 福西暢尚, Bae C., 阿部知子: "重イオンビーム照射で作出したタバコ花色変異体の解析", 日本育種学会第 111 回講演会, (日本育種学会), 水戸, 3 月 (2007).

今西俊介, 野口有里紗, 林依子, 福西暢尚, 龍頭啓充, 永田雅靖, 本多一郎, 阿部知子: "重イオンビーム照射による極矮性トマト「マイクロトム」変異系統の整備", 第 4 回イオンビーム育種研究会, 水戸, 7 月 (2007).

武弓利雄, 阿部知子, 林依子, 山ノ内宏昭, 吉岡照高, 村松昇, 福西暢尚, 龍頭啓充: "チャ種子のイオンビーム照射効果に及ぼす線量と LET の影響", 第 4 回イオンビーム育種研究会, 水戸, 7 月 (2007).

竹久妃奈子, 林依子, 風間裕介, 神波千秋, 市田裕之, 龍頭啓充, 福西暢尚, 宮沢豊, 東海林英夫, 佐藤雅志, 阿部知子: "重イオンビーム照射により誘導されたイネ突然変異体の特性解析", イオン育種研究会, (日本原子力研究開発機構 高崎量子応用研究所), 水戸, 7 月 (2007).

龍頭啓充, 長谷部裕雄, 横内茂, 福西暢尚, 後藤彰, 加瀬昌之, 矢野安重: "理研 RIBF におけるウラン加速のためのチャー

ジストリッパー”, 第 4 回日本加速器学会年会・第 32 回リニアック技術研究会, 和光, 8 月 (2007).

福西暢尚, 後藤彰, 稲辺尚人, 加瀬昌之, 龍頭啓充, 坂本成彦, 矢野安重: “理研 RI ビームファクトリー fRC の圧力分布計算”, 第 4 回日本加速器学会年会・第 32 回リニアック技術研究会, 和光, 8 月 (2007).

奥野広樹, 山田一成, 大西純一, 福西暢尚, 横内茂, 長谷部裕雄, 池上九三男, 熊谷桂子, 坂本成彦, 上垣外修一, 長瀬誠, 藤巻正樹, 込山美咲, 後藤彰, 加瀬昌之, 矢野安重, 真家武士: “理研超伝導リングサイクロトロンの現状報告”, 第 4 回日本加速器学会年会・第 32 回リニアック技術研究会, 和光, 8 月 (2007).

竹久妃奈子, 林依子, 風間裕介, 神波千秋, 市田裕之, 龍頭啓充, 福西暢尚, 宮沢豊, 東海林英夫, 佐藤雅志, 阿部知子: “炭素イオン照射により誘導した、シワ-矮性イネ突然変異株 (*ssw*) の特性解析”, 日本育種学会第 112 回講演会, 鶴岡, 9 月 (2007).

杉山正夫, 市田裕之, 林依子, 福西暢尚, 龍頭啓充, 寺川輝彦, 阿部知子: “重イオンビーム照射によるシクラメン突然変異体の誘発”, 日本育種学会第 112 回講演会, 鶴岡, 9 月 (2007).

風間裕介, 斉藤宏之, 宮沢豊, 金谷健至, 鈴木賢一, 林依子, 龍頭啓充, 福西暢尚, Bae C., 阿部知子: “重イオンビーム照射で作出されたタバコ白花変異体について”, 日本育種学会第 112 回講演会, 鶴岡, 9 月 (2007).

寺岡毅, 澤野郁夫, 中島輝子, 加々美裕, 神尾章子, 林依子, 龍頭啓充, 福西暢尚, 阿部知子: “重イオンビーム照射がウンシュウミカンの生育に及ぼす影響”, 園芸学会平成 19 年度秋季大会, 高松, 9 月 (2007).

神波千秋, 竹久妃奈子, 林依子, 市田裕之, 小沼亮子, 龍頭啓充, 福西暢尚, 宮沢豊, 東海林英夫, 保倉明子, 福田直樹, 中井泉, 阿部知子, 佐藤雅志: “イネ塩害耐性突然変異体 6-99L の耐塩性に関わる生理要因の解明”, 第 224 回日本作物学会講演会, 金沢, 9 月 (2007).

藤原誠, 風間裕介, 斉藤宏之, 松山知樹, 林依子, 龍頭啓充, 福西暢尚, 阿部知子: “重イオンビーム照射による DNA 変異を検出・解析する効率的なシステム”, 日本農芸化学会 2008 年度大会, 名古屋, 3 月 (2008).

風間裕介, 斉藤宏之, 大部澄江, 林依子, 市田裕之, 龍頭啓充, 福西暢尚, 松山知樹, 阿部知子: “重イオンビーム照射を用いたシロイヌナズナ突然変異誘発における LET 効果”, 第 49 回日本植物生理学会年会, 札幌, 3 月 (2008).

Cryogenic Technology Team

Publications

[Journal]

(Original Papers) *Subject to Peer Review

Ryuto H., Hasebe H., Fukunishi N., Abe T., Goto A., Kase M., and Yano Y.: "Charge-stripping foil changer with energy adjuster function", Nucl. Instrum. Methods Phys. Res. A **581**, No. 3, pp. 586–588 (2007). *

[Book・Proceedings]

(Original Papers) *Subject to Peer Review

龍頭啓充, 長谷部裕雄, 横内茂, 福西暢尚, 後藤彰, 加瀬昌之, 矢野安重: "理研 RIBF におけるウラン加速のためのチャージストリッパー", 第 4 回日本加速器学会年会・第 32 回リニアック技術研究会論文集, 和光市, 2007–8, 第 4 回日本加速器学会・第 32 回リニアック技術研究会実行委員会, 東京, pp. 194–196 (2007).

Oral Presentations

(International Conference etc.)

Ryuto H., Hasebe H., Yokouchi S., Fukunishi N., Goto A., Kase M., and Yano Y.: "Charge strippers for acceleration of uranium beam at RIKEN RI-beam factory", 18th International Conference on Cyclotrons and their Applications (Cyclotrons 2007), (Istituto Nazionale di Fisica Nucleare), Giardini Naxos, Italy, Sept.–Oct. (2007).

(Domestic Conference)

龍頭啓充, 長谷部裕雄, 横内茂, 福西暢尚, 後藤彰, 加瀬昌之, 矢野安重: "理研 RIBF におけるウラン加速のためのチャージストリッパー", 第 4 回日本加速器学会年会・第 32 回リニアック技術研究会, 和光, 8 月 (2007).

奥野広樹, 山田一成, 池上九三男, 加瀬昌之, 矢野安重, 真家武士: "Operational Status of the He Cooling System for RIKEN SRC", 第 4 回日本加速器学会年会・第 32 回リニアック技術研究会, 和光, 8 月 (2007).

奥野広樹, 山田一成, 大西純一, 福西暢尚, 横内茂, 長谷部裕雄, 池上九三男, 熊谷桂子, 坂本成彦, 上垣外修一, 長瀬誠, 藤巻正樹, 込山美咲, 後藤彰, 加瀬昌之, 矢野安重, 真家武士: "理研超伝導リングサイクロトロンの現状報告", 第 4 回日本加速器学会年会・第 32 回リニアック技術研究会, 和光, 8 月 (2007).

Heavy Ion Nuclear Physics Laboratory

Publications

[Journal]

(Original Papers) *Subject to Peer Review

Sugimoto T., Nakamura T., Fukuda N., Miura M., Kondo Y., Aoi N., Baba H., Bazin D., Gomi T., Hasegawa H., Hashimoto Y., Imai N., Kobayashi T., Kubo T., Motobayashi T., Ohara M., Saito A., Sakurai H., Shimoura S., Attukalathil V. M., Watanabe K., Watanabe Y., Yakushiji T., Yanagisawa Y., Yoneda K., and Ishihara M.: "Invariant-mass spectroscopy of the neutron-drip line nucleus ^{14}Be", J. Phys.: Con. Ser. **49**, 43–44 (2006). *

Cole A., Akimunne H., Austin S., Bazin D., van den Berg A., Berg G., Brown J., Daito I., Fujita Y., Fujiwara M., Gupta S., Hara K., Harakeh M., Janecke J., Kawabata T., Nakamura T., Robert D., Sherril B., Steiner M., Ueno H., and Zegers R.: "Measurement of the Gamow-Teller Strength Distribution in 58Co via the 58Ni(t, 3He) reaction at 115 MeV/nucleon", nucl-ex **0603019**, 1–14 (2006). *

Adler S. S., Akiba Y., Bazilevsky A. V., Bunce G. M., Deshpande A., Enyo H., Fields D. E., Fox B., Fukao Y., Goto Y., Perdekamp M. G., Hasuko K., Heuser J., Horaguchi T., Ichihara T., Imai K., Ishihara M., Jinnouchi O., Kamihara N., Kaneta M., Kiyomichi A., Kobayashi H., Kurita K., Mao Y., Onishi H., Okada H., Okada K., Rykov V., Saito N., Sato H., Shibata T., Taketani A., Tanida K., Togawa M., Tojo J., Torii H., Watanabe Y., and Yokkaichi S.: "Jet structure from dihadron correlations in d+Au collisions at $\sqrt{s_{NN}} = 200$ GeV", Phys. Rev. C **73**, 054903-1–054903-27 (2006). *

Zegers R., Akimune H., Austin S., Bazin D., van den Berg A., Berg G., Brown J., Cole A., Daito I., Fujita Y., Fujiwara M., Gales S., Harakeh M., Hashimoto H., Hayami R., Hitt G., Howard M., Itoh M., Janecke J., Kawabata T., Kawase K., Kinoshita M., Nakamura T., Nakanishi K., Nakayama S., Okumura S., Richter W., Roberts D., Sherrill B., Shimbara Y., Steiner M., Uchida M., Ueno H., Yamagata T., and Yosoi M.: "The (t,3He) and (3He,t) reactions as probes of Gamow-Teller strength", Phys. Rev. C **74**, 024309-1–024309-15 (2006). *

Adler S. S., Akiba Y., Bazilevsky A. V., Bunce G. M., Deshpande A., Enyo H., Fields D. E., Fox B., Fukao Y., Goto Y., Perdekamp M. G., Hasuko K., Heuser J., Horaguchi T., Ichihara T., Imai K., Ishihara M., Jinnouchi O., Kamihara N., Kaneta M., Kiyomichi A., Kobayashi H., Kurita K., Mao Y., Onishi H., Okada H., Okada K., Rykov V., Saito N., Sato H., Shibata T., Taketani A., Tanida K., Togawa M., Tojo J., Torii H., Watanabe Y., and Yokkaichi S.: "Nuclear effects on hadron production in d+Au collisions at $\sqrt{s_{NN}} = 200$ GeV revealed by comparison with p+p data", Phys. Rev. C **74**, 024904-1–024904 -13 (2006). *

Adler S. S., Akiba Y., Aoki K., Bazilevsky A. V., Bunce G. M., Deshpande A., Enyo H., Fields D. E., Fox B., Fukao Y., Goto Y., Perdekamp M. G., Hachiya T., Hasuko K., Heuser J., Horaguchi T., Ichihara T., Imai K., Ishihara M., Jinnouchi O., Kajihara F., Kamihara N., Kaneta M., Kiyomichi A., Kobayashi H., Kurita K., Mao Y., Murata J., Onishi H., Okada H., Okada K., Rykov V., Saito N., Sato H., Shibata T., Shoji K., Tabaru T., Taketani A., Tanida K., Togawa M., Tojo J., Torii H., Tsuchimoto Y., Wagner M. M., Watanabe Y., Xie W., and Yokkaichi S.: "Improved measurement of double helicity asymmetry in inclulsive midrapidity π^0 production for polarized p+p collisions at $\sqrt{s} = 200$ GeV", Phys. Rev. D **73**, 091102-1–091102-5 (2006). *

Adler S. S., Akiba Y., Bazilevsky A. V., Bunce G. M., Deshpande A., Enyo H., Fields D. E., Fox B., Fukao Y., Goto Y., Perdekamp M. G., Hasuko K., Heuser J., Horaguchi T., Ichihara T., Imai K., Ishihara M., Jinnouchi O., Kamihara N., Kaneta M., Kiyomichi A., Kobayashi H., Kurita K., Mao Y., Onishi H., Okada H., Okada K., Rykov V., Saito N., Sato H., Shibata T., Taketani A., Tanida K., Togawa M., Tojo J., Torii H., Watanabe Y., and Yokkaichi S.: "Jet properties from dihadron correlations in p+p collisions at $\sqrt{s} = 200$ GeV", Phys. Rev. D **74**, 072002-1–072002-26 (2006). *

Adler S. S., Akiba Y., Bazilevsky A. V., Bunce G. M., Deshpande A., Enyo H., Fields D. E., Fox B., Fukao Y., Goto Y., Perdekamp M. G., Hasuko K., Heuser J., Horaguchi T., Ichihara T., Imai K., Ishihara M., Jinnouchi O., Kamihara N., Kaneta M., Kiyomichi A., Kobayashi H., Kurita K., Mao Y., Onishi H., Okada H., Okada K., Rykov V., Saito N., Sato H., Shibata T., Taketani A., Tanida K., Togawa M., Tojo J., Torii H., Watanabe Y., and Yokkaichi S.: "J/ψ Production and Nuclear Effects for d+Au and p+p Collisions at $\sqrt{s_{NN}} = 200$ GeV", Phys. Rev. Lett. **96**, 012304-1–012304-6 (2006). *

Adler S. S., Akiba Y., Bazilevsky A. V., Bunce G. M., Deshpande A., Enyo H., Fields D. E., Fox B., Goto Y., Perdekamp M. G., Hayashi N., Ichihara T., Imai K., Ishihara M., Jinnouchi O., Kamihara N., Kobayashi H., Kurita K., Mao Y., Murata J., Onishi H., Okada K., Saito N., Sato H., Shibata T., Taketani A., Tanida K., Tojo J., Torii H., Watanabe Y., and Yokkaichi S.: " Single Electrons from Heavy-Flavor Decays in p+p Collisions at $\sqrt{s} = 200$ GeV", Phys. Rev. Lett. **96**, 032001-1–032001-6 (2006). *

Adler S. S., Akiba Y., Bazilevsky A. V., Bunce G. M., Deshpande A., Enyo H., Fields D. E., Fox B., Goto Y., Perdekamp M. G., Hayashi N., Ichihara T., Imai K., Ishihara M., Jinnouchi O., Kamihara N., Kobayashi H., Kurita K., Mao Y., Murata J., Onishi H., Okada K., Saito N., Sato H., Shibata T., Taketani A., Tanida K., Tojo J., Torii H., Watanabe Y., and Yokkaichi S.: "Nu-

clear Modification of Electron Spectra and Implications for Heavy Quark Energy Loss in Au+Au Collisions at $\sqrt{s_{NN}}$ = 200 GeV", Phys. Rev. Lett. **96**, 032301-1–032301-6 (2006). ∗

Adler S. S., Akiba Y., Bazilevsky A. V., Bunce G. M., Deshpande A., Enyo H., Fields D. E., Fox B., Goto Y., Perdekamp M. G., Hayashi N., Ichihara T., Imai K., Ishihara M., Jinnouchi O., Kamihara N., Kaneta M., Kobayashi H., Kurita K., Mao Y., Murata J., Onishi H., Okada K., Saito N., Sato H., Shibata T., Taketani A., Tanida K., Tojo J., Torii H., Watanabe Y., and Yokkaichi S.: "Measurement of Identified π^0 and Inclusive Photon Second-Harmonic Parameter v_2 and Implications for Direct Photon Production in $\sqrt{s_{NN}} = 200$ GeV Au + Au", Phys. Rev. Lett. **96**, 032302-1–032302-6 (2006). ∗

Adler S. S., Akiba Y., Bazilevsky A. V., Bunce G. M., Deshpande A., Enyo H., Fields D. E., Fox B., Goto Y., Perdekamp M. G., Hayashi N., Ichihara T., Imai K., Ishihara M., Jinnouchi O., Kamihara N., Kobayashi H., Kurita K., Mao Y., Murata J., Onishi H., Okada K., Saito N., Sato H., Shibata T., Taketani A., Tanida K., Tojo J., Torii H., Watanabe Y., and Yokkaichi S.: "Common Suppression Pattern of eta and π^0 Mesons at High Transverse Momentum in Au+Au Collisions at $\sqrt{s_{NN}}$ = 200 GeV", Phys. Rev. Lett. **96**, 202301-1–202301-6 (2006). ∗

Adler S. S., Akiba Y., Bazilevsky A. V., Bunce G. M., Deshpande A., Enyo H., Fields D. E., Fox B., Fukao Y., Goto Y., Perdekamp M. G., Hasuko K., Heuser J., Horaguchi T., Ichihara T., Imai K., Ishihara M., Jinnouchi O., Kamihara N., Kaneta M., Kiyomichi A., Kobayashi H., Kurita K., Mao Y., Onishi H., Okada H., Okada K., Rykov V., Saito N., Sato H., Shibata T., Taketani A., Tanida K., Togawa M., Tojo J., Torii H., Watanabe Y., and Yokkaichi S.: "Azimuthal Angle Correlations for Rapidity Separated Hadron Pairs in d+Au Collisions at $\sqrt{s_{NN}} = 200$ GeV", Phys. Rev. Lett. **96**, 222301-1–222301-6 (2006). ∗

Adler S. S., Akiba Y., Bazilevsky A. V., Bunce G. M., Deshpande A., Enyo H., Fields D. E., Fox B., Goto Y., Perdekamp M. G., Hayashi N., Ichihara T., Imai K., Ishihara M., Jinnouchi O., Kamihara N., Kobayashi H., Kurita K., Mao Y., Murata J., Onishi H., Okada K., Saito N., Sato H., Shibata T., Taketani A., Tanida K., Tojo J., Torii H., Watanabe Y., and Yokkaichi S.: "Dense-Medium Modifications to Jet-Induced Hadron Pair Distributions in Au+Au Collisions at $\sqrt{s_{NN}} = 200$ GeV", Phys. Rev. Lett. **97**, 052301-1–052301-6 (2006). ∗

Adare A., Akiba Y., Aoki K., Asai J., Bunce G. M., Deshpande A., Enyo H., Fields D. E., Fujiwara K., Fukao Y., Goto Y., Perdekamp M. G., Horaguchi T., Ichihara T., Imai K., Inoue Y., Ishihara M., Jinnouchi O., Kamihara N., Kaneta M., Kano H., Kanoh H., Kawall D., Kiyomichi A., Kurita K., Mao Y., Murata J., Nakagawa I., Nakano K., Onishi H., Okada H., Okada K., Rykov V., Saito N., Shibata T., Shoji K., Tabaru T., Taketani A., Tanida K., Togawa M., Tojo J., Torii H., Wagner M. M., Watanabe Y., Xie W., and Yokkaichi S.: " Measurement of High-pT Single Electrons from Heavy-Flavor Decays in p+p Collisions at $\sqrt{s}$ = 200 GeV", Phys. Rev. Lett. **97**, 252002-1–252002-6 (2006). ∗

Kobayashi T., Kato T., Matsuo Y., Kurata-Nishimura M., Hayashizaki Y., and Kawai J.: "Wavelength-dependent fragmentation and clustering observed after Femtosecond Laser Ablation of solid C60", J. Chem. Phys. **127**, No. 11, pp. 111101-01–111101-03 (2007). ∗

Kurata-Nishimura M., Kato T., Matsuo Y., Kobayashi T., Oyama R., Oho Y., Kawai J., and Hayashizaki Y.: "Dependence of Femtosecond Laser Ablation for organic molecules on chosen substrate", J. Phys.: Con. Ser. **59**, 360–363 (2007). ∗

Kobayashi T., Kato T., Kurata-Nishimura M., Matsuo Y., Kawai J., Motobayashi T., and Hayashizaki Y.: "Kinetic energy of ions produced with first-, second-, and multi-shot Femtosecond Laser Ablation on a solid surface", J. Phys.: Con. Ser. **59**, 364–367 (2007). ∗

Kato T., Kobayashi T., Matsuo Y., Kurata-Nishimura M., Oyama R., Matsumura Y., Yamamoto H., Kawai J., and Hayashizaki Y.: "Comparison between femtosecond and nanosecond Laser Ablation of solution samples applied on a substrate", J. Phys.: Con. Ser. **59**, 372–375 (2007). ∗

Matsuo Y., Kobayashi T., Kurata-Nishimura M., Kato T., Motobayashi T., Kawai J., and Hayashizaki Y.: "LIF observation of neutral atoms and ions produced by Femtosecond Laser Ablation of Sm on a substrate", J. Phys.: Con. Ser. **59**, 555–558 (2007). ∗

Morita K., Morimoto K., Kaji D., Akiyama T., Goto S., Haba H., Ideguchi E., Katori K., Koura H., Kudo H., Ohnishi T., Ozawa A., Suda T., Sueki K., Tokanai F., Yamaguchi T., Yoneda A., and Yoshida A.: "Experiment on synthesis of an isotope 277112 by 208Pb + 70Zn reaction", J. Phys. Soc. Jpn. **76**, No. 4, pp. 043201-1–043201-5 (2007). ∗

Iida K., Kohama A., and Oyamatsu K.: "Formula for proton-nucleus reaction cross section at intermediate energies and its application", J. Phys. Soc. Jpn. **76**, No. 4, pp. 044201-1–044201-6 (2007). ∗

Morita K., Morimoto K., Kaji D., Akiyama T., Goto S., Haba H., Ideguchi E., Katori K., Koura H., Kikunaga H., Kudo H., Ohnishi T., Ozawa A., Sato N., Suda T., Sueki K., Tokanai F., Yamaguchi T., Yoneda A., and Yoshida A.: "Observation of second decay chain from 278113", J. Phys. Soc. Jpn. **76**, No. 4, pp. 045001-1–045001-2 (2007). ∗

Sonoda T., Fujita M., Yamazaki A., Endo T., Shinozuka T., Miyashita Y., Sato N., Goto A., Takano E., Suzuki

T., Miyake T., Tanigaki M., and Wada M.: "Development of the RF-IGISOL at CYRIC", Nucl. Instrum. Methods Phys. Res. B **254**, 295–299 (2007). *

Sekiguchi K., Sakai H., Sakamoto N., Kuboki H., Sasano M., Takahashi Y., Yako K., Kawabata T., Maeda Y., Sakaguchi S., Sasamoto Y., Suda K., Uesaka T., Okamura H., Itoh K., and Wakasa T.: "Study of Spin Parts of Three Nucleon Forces via $\vec{d}p$ Breakup Reactions at Intermediate Energies", Nucl. Phys. A **790**, 450c–453c (2007). *

Adare A., Akiba Y., Aoki K., Asai J., Bunce G. M., Deshpande A., Enyo H., Fields D. E., Fujiwara K., Fukao Y., Goto Y., Perdekamp M. G., Hachiya T., Hasuko K., Heuser J., Horaguchi T., Ichihara T., Imai K., Inoue Y., Ishihara M., Jinnouchi O., Kajihara F., Kamihara N., Kaneta M., Kanoh H., Kawall D., Kiyomichi A., Kurita K., Mao Y., Murata J., Nakagawa I., Nakano K., Onishi H., Okada H., Okada K., Wagner M. M., Watanabe Y., Xie W., and Yokkaichi S.: "Correlated production of p and $\bar{p}$ in Au+Au collisions at $\sqrt{s_{NN}} = 200$ GeV", Phys. Lett. B **649**, 359–369 (2007). *

Shimoura S., Ota S., Demichi K., Aoi N., Baba H., Elekes Z., Fukuchi T., Gomi T., Hasegawa K., Ideguchi E., Ishihara M., Iwasa N., Iwasaki H., Kanno S., Kubono S., Kurita K., Kurokawa M., Matsuyama Y., Michimasa S., Miller K. L., Minemura T., Motobayashi T., Murakami T., Notani M., Odahara A., Saito A., Sakurai H., Takeshita E., Takeuchi S., Tamaki M., Teranishi T., Yamada K., Yanagisawa Y., and Hamamoto I.: "Lifetime of the isomeric 0_2^+ state in ^{12}Be", Phys. Lett. B **654**, 87–91 (2007). *

Sugimoto T., Nakamura T., Kondo Y., Aoi N., Baba H., Bazin D. P., Fukuda N., Gomi T., Hasegawa H., Imai N., Ishihara M., Kobayashi T., Kubo T., Miura M., Motobayashi T., Otsu H., Saito A., Sakurai H., Shimoura S., Vinodkumar A. M., Watanabe K., Watanabe Y., Yakushiji T., Yanagisawa Y., and Yoneda K.: "The first 2^+ state of ^{14}Be", Phys. Lett. B **654**, 160–164 (2007). *

Fukuyama Y., Moriwaki Y., and Matsuo Y.: "Formation and dissociation of Ba^{+*} - He exciplexes at 3-25 K", Phys. Rev. A **75**, 032725-1–032725-8 (2007). *

Horiuchi W., Suzuki Y., Sarhan B. A., and Kohama A.: "Systematic analysis of reaction cross sections of carbon isotopes", Phys. Rev. C **75**, No. 4, pp. 044607-1–044607-14 (2007). *

Adler S. S., Akiba Y., Bazilevsky A. V., Bunce G. M., Deshpande A., Enyo H., Fields D. E., Fox B., Fukao Y., Goto Y., Perdekamp M. G., Hasuko K., Hayashi N., Heuser J., Horaguchi T., Ichihara T., Imai K., Ishihara M., Jinnouchi O., Kamihara N., Kaneta M., Kiyomichi A., Kobayashi H., Kurita K., Mao Y., Murata J., Onishi H., Okada H., Okada K., Rykov V., Saito N., Sato H., Shibata T., Taketani A., Tanida K., Togawa M., Tojo J., Torii H., Watanabe Y., and Yokkaichi S.: "High transverse momentum η meson production in p+p,d+Au, and Au+Au collisions at $\sqrt{s_{NN}} = 200$ GeV", Phys. Rev. C **75**, 024909-1–024909-36 (2007). *

Fujita H., Fujita Y., Adachi T., Bacher A. D., Berg G. P., Black T. C., Caurier E., Foster ., Fujimura H., Hara K., Harada K., Hatanaka K., Janecke J., Kamiya J., Kanzaki Y., Katori K., Kawabata T., Langanke K., Martinez-Pinedo G., Noro T., Robers D. A., Sakaguchi H., Shimbara Y., Shinada T., Stephenson E. J., Ueno H., Yamanaka T., Yoshifuku M., and Yosoi M.: "Isospin structure of $J^\pi = 1^+$ states in ^{58}Ni and ^{58}Cu studied by ^{58}Ni(p, p') and ^{58}Ni(^{3}He,t)^{58}Cu measurements", Phys. Rev. C **75**, 034310-1–034310-15 (2007). *

Adler S. S., Akiba Y., Bazilevsky A. V., Bunce G. M., Deshpande A., Enyo H., Fields D. E., Fox B., Fukao Y., Goto Y., Perdekamp M. G., Hasuko K., Heuser J., Horaguchi T., Ichihara T., Imai K., Ishihara M., Jinnouchi O., Kamihara N., Kaneta M., Kiyomichi A., Kobayashi H., Kurita K., Mao Y., Onishi H., Okada H., Okada K., Rykov V., Saito N., Sato H., Shibata T., Taketani A., Tanida K., Togawa M., Tojo J., Torii H., Watanabe Y., and Yokkaichi S.: "Production of ω mesons at large transverse momenta in p+p and d+Au collisions at $\sqrt{s_{NN}} = 200$ GeV", Phys. Rev. C **75**, 051902-1–051902-6 (2007). *

Gibelin J. D., Beaumel D., Motobayashi T., Aoi N., Baba H., Blumenfeld Y., Dombradi Z., Elekes Z., Fortier S., Frascaria N., Fukuda N., Gomi T., Ishikawa K., Kondo Y., Kubo T., Lima V., Nakamura T., Saito A., Sato Y., Takeshita E., Takeuchi S., Teranishi T., Togano Y., Vinodkumar A. M., Yanagisawa Y., and Yoshida A.: "Measurement of the B(E2, $0_1^+ \rightarrow 2_1^+$) in the N = 16 nucleus ^{26}Ne", Phys. Rev. C **75**, 057301-1–057391-4 (2007). *

Ichikawa T., Hagino K., and Iwamoto A.: "Existence of a one-body barrier revealed in deep subbarrier fusion", Phys. Rev. C **75**, 057603-1–057603-4 (2007). *

Ichikawa T., Hagino K., and Iwamoto A.: "Systematics of threshold incident energy for deep sub-barrier fusion hindrance", Phys. Rev. C **75**, 064612-1–064612-4 (2007). *

Nguyen H. Q. and Dang N. D.: "Self-consistent quasiparticle RPA for multi-level pairing model", Phys. Rev. C **76**, No. 5, pp. 054302-1–054302-12 (2007). *

Dang N. D.: "Particle-number-projected thermal pairing", Phys. Rev. C **76**, No. 6, pp. 064320-1–064320-13 (2007). *

Mocko M., Tsang M., Sun Z., Aoi N., Cook J. M., Delaunay F., Famiano M., Hui H., Imai N., Iwasaki H., Lynch W., Motobayashi T., Niikura M., Onishi T., Rogers A. M., Sakurai H., Stolz A., Suzuki H., Takeshita E., Takeuchi S., and Wallace M.: "Projectile fragmentation of 86Kr at 64 MeV/nucleon", Phys. Rev. C **76**, 014609-1–014609-10 (2007). *

Adler S. S., Akiba Y., Bazilevsky A. V., Bunce G. M.,

Deshpande A., Enyo H., Fields D. E., Fox B., Goto Y., Perdekamp M. G., Hayashi N., Ichihara T., Imai K., Ishihara M., Jinnouchi O., Kamihara N., Kobayashi H., Kurita K., Mao Y., Murata J., Onishi H., Okada K., Saito N., Sato H., Shibata T., Taketani A., Tanida K., Tojo J., Torii H., Watanabe Y., and Yokkaichi S.: "Measurement of density correlations in pseudorapidity via charged particle multiplicity fluctuations in Au+Au collisions at $\sqrt{s_{NN}}$ = 200 GeV", Phys. Rev. C **76**, 034903-1–034903-33 (2007). *

Adler S. S., Akiba Y., Bazilevsky A. V., Bunce G. M., Deshpande A., Enyo H., Fields D. E., Fox B., Goto Y., Perdekamp M. G., Hayashi N., Ichihara T., Imai K., Ishihara M., Jinnouchi O., Kamihara N., Kobayashi H., Kurita K., Mao Y., Murata J., Onishi H., Okada K., Saito N., Sato H., Shibata T., Taketani A., Tanida K., Tojo J., Torii H., Watanabe Y., and Yokkaichi S.: "Detailed study of high-p_T neutral pion suppression and azimuthal anisotropy in Au+Au collisions at $\sqrt{s_{NN}} = 200$ GeV", Phys. Rev. C **76**, 034904-1–034904-26 (2007). *

Notani M., Sakurai H., Aoi N., Iwasaki H., Fukuda N., Liu Z., Yoneda K., Ogawa H., Teranishi T., Nakamura T., Okuno H., Yoshida A., Watanabe Y., Momota S., Inabe N., Kubo T., Ito S., Ozawa A., Suzuki T., Tanihata I., and Ishihara M.: "Projectile fragmentation reaction and production of nuclei near the neutron drip line", Phys. Rev. C **76**, 044605-1–044605-15 (2007). *

Adare A., Akiba Y., Aoki K., Asai J., Bunce G. M., Deshpande A., Enyo H., Fields D. E., Fujiwara K., Fukao Y., Goto Y., Perdekamp M. G., Horaguchi T., Ichihara T., Imai K., Inoue Y., Ishihara M., Jinnouchi O., Kamihara N., Kaneta M., Kanoh H., Kawall D., Kiyomichi A., Kurita K., Mao Y., Murata J., Nakagawa I., Nakano K., Onishi H., Okada H., Okada K., Rykov V., Saito N., Shibata T., Shoji K., Tabaru T., Taketani A., Tanida K., Togawa M., Tojo J., Torii H., Wagner M. M., Watanabe Y., Xie W., and Yokkaichi S.: "Inclusive cross section and double helicity asymmetry for π^0 production in $p+p$ collisions at $\sqrt{s} = 200$ GeV: Implications for the polarized gluon distribution in the proton", Phys. Rev. D **76**, 051106-1–051106-7 (2007). *

Adler S. S., Akiba Y., Bazilevsky A. V., Bunce G. M., Deshpande A., Enyo H., Fields D. E., Fox B., Goto Y., Perdekamp M. G., Hayashi N., Ichihara T., Imai K., Ishihara M., Jinnouchi O., Kamihara N., Kobayashi H., Kurita K., Mao Y., Murata J., Onishi H., Okada K., Saito N., Sato H., Shibata T., Taketani A., Tanida K., Tojo J., Torii H., Watanabe Y., and Yokkaichi S.: "Measurement of single muons at forward rapidity in $p+p$ collisions at $\sqrt{s} = 200$ GeV and implications for charm production", Phys. Rev. D **76**, 092002-1–092002-24 (2007). *

Elekes Z., Dombradi Z., Aoi N., Bishop S., Fulop Z., Gibelin J. D., Gomi T., Hashimoto Y., Imai N., Iwasa N., Iwasaki H., Kalinka G., Kondo Y., Korsheninnikov A. A., Kurita K., Kurokawa M., Matsui N., Motobayashi T., Nakamura T., Nakao T., Nikolski E. Y., Onishi T., Okumura T., Ota S., Perera P., Saito A., Sakurai H., Sato Y., Sohler D., Sumikama T., Suzuki D., Suzuki M., Takeda H., Takeuchi S., Togano Y., and Yanagisawa Y.: "Spectroscopic study of neutron shell closures via nucleon transfer in the near-dripline nucleus ^{23}O", Phys. Rev. Lett. **98**, No. 10, pp. 102502-1–102502-4 (2007). *

Adler S. S., Akiba Y., Bazilevsky A. V., Bunce G. M., Deshpande A., Enyo H., Fields D. E., Fox B., Fukao Y., Goto Y., Perdekamp M. G., Hasuko K., Heuser J., Horaguchi T., Ichihara T., Imai K., Ishihara M., Jinnouchi O., Kamihara N., Kaneta M., Kiyomichi A., Kobayashi H., Kurita K., Mao Y., Onishi H., Okada H., Okada K., Rykov V., Saito N., Sato H., Shibata T., Taketani A., Tanida K., Togawa M., Tojo J., Torii H., Watanabe Y., and Yokkaichi S.: "Measurement of Direct Photon Production in p+p Collisions at $\sqrt{s} = 200$ GeV", Phys. Rev. Lett. **98**, 012002-1–012002-6 (2007). *

Adler S. S., Akiba Y., Bazilevsky A. V., Bunce G. M., Deshpande A., Enyo H., Fields D. E., Fox B., Goto Y., Perdekamp M. G., Hayashi N., Ichihara T., Imai K., Ishihara M., Jinnouchi O., Kamihara N., Kobayashi H., Kurita K., Mao Y., Murata J., Onishi H., Okada K., Saito N., Sato H., Shibata T., Taketani A., Tanida K., Tojo J., Torii H., Watanabe Y., and Yokkaichi S.: "Evidence for a long-range component in the pion emission source in Au+Au Collisions at $\sqrt{s_{NN}} = 200$ GeV", Phys. Rev. Lett. **98**, 132301-1–132301-6 (2007). *

Adare A., Akiba Y., Aoki K., Asai J., Bunce G. M., Deshpande A., Enyo H., Fields D. E., Fujiwara K., Fukao Y., Goto Y., Perdekamp M. G., Hachiya T., Hasuko K., Heuser J., Horaguchi T., Ichihara T., Imai K., Inoue Y., Ishihara M., Jinnouchi O., Kajihara F., Kamihara N., Kaneta M., Kano H., Kanoh H., Kawall D., Kiyomichi A., Kurita K., Mao Y., Murata J., Nakagawa I., Nakano K., Onishi H., Okada H., Okada K., Rykov V., Saito N., Sato H., Shibata T., Shoji K., Tabaru T., Taketani A., Tanida K., Togawa M., Tojo J., Torii H., Tsuchimoto Y., Wagner M. M., Watanabe Y., Xie W., and Yokkaichi S.: "Scaling properties of azimuthal anisotropy in Au+Au and Cu+Cu collisions at $\sqrt{s_{NN}} = 200$ GeV", Phys. Rev. Lett. **98**, 162301-1–162301-6 (2007). *

Adare A., Akiba Y., Aoki K., Asai J., Bunce G. M., Deshpande A., Enyo H., Fields D. E., Fujiwara K., Fukao Y., Goto Y., Perdekamp M. G., Hachiya T., Hasuko K., Heuser J., Horaguchi T., Ichihara T., Imai K., Inoue Y., Ishihara M., Jinnouchi O., Kajihara F., Kamihara N., Kaneta M., Kano H., Kanoh H., Kawall D., Kiyomichi A., Kurita K., Mao Y., Murata J., Nakagawa I., Nakano K., Onishi H., Okada H., Okada K., Rykov V., Saito N., Sato H., Shibata T., Shoji K., Tabaru T., Taketani A., Tanida K., Togawa M., Tojo J., Torii H., Tsuchimoto Y.,

Wagner M. M., Watanabe Y., Xie W., and Yokkaichi S.: "Energy loss and flow of heavy quarks in Au+Au collisions at $\sqrt{s_{NN}}$ = 200 GeV", Phys. Rev. Lett. **98**, 172301-1–172301-6 (2007). *

Adler S. S., Akiba Y., Bazilevsky A. V., Bunce G. M., Deshpande A., Enyo H., Fields D. E., Fox B., Fukao Y., Goto Y., Perdekamp M. G., Hasuko K., Heuser J., Horaguchi T., Ichihara T., Imai K., Ishihara M., Jinnouchi O., Kamihara N., Kaneta M., Kiyomichi A., Kobayashi H., Kurita K., Mao Y., Onishi H., Okada H., Okada K., Rykov V., Saito N., Sato H., Shibata T., Taketani A., Tanida K., Togawa M., Tojo J., Torii H., Watanabe Y., and Yokkaichi S.: "Centrality dependence of π^0 and η production at large transverse momentum in $\sqrt{s_{NN}}$ = 200 GeV $d+Au$ Collisions", Phys. Rev. Lett. **98**, 172302-1–172302-7 (2007). *

Adare A., Akiba Y., Aoki K., Asai J., Bunce G. M., Deshpande A., Enyo H., Fields D. E., Fujiwara K., Fukao Y., Goto Y., Perdekamp M. G., Horaguchi T., Ichihara T., Imai K., Inoue Y., Ishihara M., Jinnouchi O., Kamihara N., Kaneta M., Kanoh H., Kawall D., Kiyomichi A., Kurita K., Mao Y., Murata J., Nakagawa I., Nakano K., Onishi H., Okada H., Okada K., Rykov V., Saito N., Shibata T., Shoji K., Tabaru T., Taketani A., Tanida K., Togawa M., Tojo J., Torii H., Wagner M. M., Watanabe Y., Xie W., and Yokkaichi S.: "J/Ψ production versus transverse momentum and rapidity in p+p collisions at $\sqrt{s_{NN}}$ = 200 GeV", Phys. Rev. Lett. **98**, 232002-1–232002-6 (2007). *

Adare A., Akiba Y., Aoki K., Asai J., Bunce G. M., Deshpande A., Enyo H., Fields D. E., Fujiwara K., Fukao Y., Goto Y., Perdekamp M. G., Hachiya T., Hasuko K., Heuser J., Horaguchi T., Ichihara T., Imai K., Inoue Y., Ishihara M., Jinnouchi O., Kajihara F., Kamihara N., Kaneta M., Kanoh H., Kawall D., Kiyomichi A., Kurita K., Mao Y., Murata J., Nakagawa I., Nakano K., Onishi H., Okada H., Okada K., Rykov V., Saito N., Sato H., Shibata T., Shoji K., Tabaru T., Taketani A., Tanida K., Togawa M., Tojo J., Torii H., Tsuchimoto Y., Wagner M. M., Watanabe Y., Xie W., and Yokkaichi S.: "J/Ψ production versus centrality, transverse momentum, and rapidity in Au+Au Collisions at $\sqrt{s_{NN}}$ = 200 GeV", Phys. Rev. Lett. **98**, 232301-1–232301-6 (2007). *

Adare A., Akiba Y., Aoki K., Asai J., Bazilevsky A. V., Bunce G. M., Deshpande A., Enyo H., Fields D. E., Fox B., Fujiwara K., Fukao Y., Goto Y., Perdekamp M. G., Hachiya T., Hasuko K., Heuser J., Horaguchi T., Ichihara T., Imai K., Inoue Y., Ishihara M., Jinnouchi O., Kajihara F., Kamihara N., Kaneta M., Kanoh H., Kawall D., Kiyomichi A., Kobayashi H., Kurita K., Mao Y., Murata J., Nakagawa I., Nakano K., Onishi H., Okada H., Okada K., Rykov V., Saito N., Sato H., Shibata T., Shoji K., Tabaru T., Taketani A., Tanida K., Togawa M., Tojo J., Torii H., Tsuchimoto Y., Wagner M. M., Watanabe Y., Xie W., and Yokkaichi S.: "System size and energy dependence of jet-induced hadron pair correlation shapes in Cu+Cu and Au+Au collisions at $\sqrt{s_{NN}}$ = 200 GeV and 62.4 GeV", Phys. Rev. Lett. **98**, 232302-1–232302-7 (2007). *

Afanasiev S., Akiba Y., Aoki K., Bunce G. M., Deshpande A., Enyo H., Fields D. E., Fukao Y., Goto Y., Perdekamp M. G., Hachiya T., Hasuko K., Heuser J., Horaguchi T., Ichihara T., Imai K., Ishihara M., Jinnouchi O., Kajihara F., Kamihara N., Kaneta M., Kiyomichi A., Kurita K., Murata J., Onishi H., Okada H., Okada K., Rykov V., Saito N., Sato H., Shibata T., Shoji K., Tabaru T., Taketani A., Tanida K., Togawa M., Tojo J., Torii H., Tsuchimoto Y., Wagner M. M., Watanabe Y., Xie W., and Yokkaichi S.: "Elliptic flow for ϕ Mesons and (Anti)deuterons in Au+Au collisions at $\sqrt{s_{NN}}$ = 200 GeV", Phys. Rev. Lett. **99**, 052301-1–052301-6 (2007). *

Adare A., Akiba Y., Aoki K., Asai J., Bunce G. M., Deshpande A., Enyo H., Fields D. E., Fujiwara K., Fukao Y., Goto Y., Perdekamp M. G., Hachiya T., Hasuko K., Heuser J., Horaguchi T., Ichihara T., Imai K., Inoue Y., Ishihara M., Jinnouchi O., Kajihara F., Kamihara N., Kaneta M., Kanoh H., Kawall D., Kiyomichi A., Kurita K., Mao Y., Murata J., Nakagawa I., Nakano K., Onishi H., Okada H., Okada K., Rykov V., Saito N., Sato H., Shibata T., Shoji K., Tabaru T., Taketani A., Tanida K., Togawa M., Tojo J., Torii H., Tsuchimoto Y., Wagner M. M., Watanabe Y., Xie W., and Yokkaichi S.: "Transverse momentum and centrality dependence of dihadron correlations in Au+Au collisions at $\sqrt{s_{NN}}$ = 200 GeV: Jet quenching and the response of partonic matter", Phys. Rev. C **77**, 011901-1–011901-6 (2008). *

Adler S. S., Akiba Y., Bazilevsky A. V., Bunce G. M., Deshpande A., Enyo H., Fields D. E., Fox B., Fukao Y., Goto Y., Perdekamp M. G., Hasuko K., Heuser J., Horaguchi T., Ichihara T., Imai K., Ishihara M., Jinnouchi O., Kamihara N., Kaneta M., Kiyomichi A., Kobayashi H., Kurita K., Mao Y., Onishi H., Okada H., Okada K., Rykov V., Saito N., Sato H., Shibata T., Taketani A., Tanida K., Togawa M., Tojo J., Torii H., Watanabe Y., and Yokkaichi S.: "Centrality dependence of charged hadron production in deuteron+gold and nucleon+gold collisions at $\sqrt{s_{NN}}$ = 200 GeV", Phys. Rev. C **77**, 014905-1–014905-13 (2008). *

(Review)

松尾由賀利, 福山祥光, 森脇喜紀: "レーザー誘起蛍光法によるイオン - 原子分子低温衝突断面積の測定", 原子衝突研究協会誌しょうとつ **4**, No. 5, pp. 3–14 (2007).

[Book・Proceedings]

(Original Papers) *Subject to Peer Review

Dang N. D.: "Superfluid-normal phase transition in finite systems and its effect on damping of hot giant resonances", Proceedings of Predeal Summer School in Nuclear Physics: Collective Motion and Phase Transitions in Nuclear Systems, Predeal, Romania, 2006–8〜

9, World Scientific, Singapore, pp. 253–270 (2007). ∗

(Review)

Dang N. D.: "Giant resonances under extrem conditions", Proceedings of International Conference on Current problems in nuclear physics and atomice energy (NPAE-Kyiv2006), Kiev, Ukraine, 2006–5〜6, Kiev Institute for Nuclear Research of National Academy of Sciences of Ukraine, Kiev, pp. 70 –79 (2007).

Oral Presentations

(International Conference etc.)

Sugimoto T., Nakamura T., Fukuda N., Miura M., Kondo Y., Aoi N., Baba H., Bazin D., Gomi T., Hasegawa H., Hashimoto Y., Imai N., Kobayashi T., Kubo T., Motobayashi T., Ohara M., Saito A., Sakurai H., Shimoura S., Attukalathil V. M., Watanabe K., Watanabe Y., Yakushiji T., Yanagisawa Y., Yoneda K., and Ishihara M.: "Invariant-mass spectroscopy of the neutron-drip line nucleus ^{14}Be", International Symposium on Structure of Exotic Nuclei and Nuclear Forces (SENUF06), (CNS and RIKEN), Tokyo, Mar. (2006).

Nagatomo T., Minamisono K., Matsuta K., Levy C. D., Sumikama T., Ozawa A., Tagisi Y., Mihara M., Ogura M., Matsumiya R., Fukuda M., Yamaguchi M., Behr J. A., Jackson K. P., Fujiwara H., Ohta H., Yasuno T., Hashizume Y., and Minamisono T.: "Alignment Correlation Terms In β-Ray Angular Distributions From Spin Aligned ^{20}F And ^{20}Na", 17th International Spin Physics Symposium (SPIN2006), (Kyoto University), Kyoto, Oct. (2006).

Shimada K., Nagae D., Asahi K., Arai T., Takemura M., Inoue T., Takase K., Kagami S., Hatakeyama N., Kobayashi Y., Ueno H., Yoshimi A., Kameda D., Nagatomo T., Sugimoto T., Kubono S., Yamaguchi H., Wakabayashi Y., Amadio G., Hayakawa S., Murata J., and Kawamura H.: "Production of Polarized Radioactive Beams via The Inverse-kinematics Reactions and Their Applications", 17th International Spin Physics Symposium (SPIN2006), (Kyoto University), Kyoto, Oct. (2006).

Dang N. D.: "Thermal pairing in nuclei", 9th International Spring Seminar on Nuclear Physics, Challenges Facets of Nuclear Structure, (University of Naples), Neapel, Italy, May–May (2007).

Sarhan B. A., Horiuchi W., Kohama A., and Suzuki Y.: "Reaction cross sections of carbon isotopes incident on proton and ^{12}C target", 5th International Workshop on Direct Reaction with Exotic Beams (DREB2007), Wako, May–June (2007).

Shimada K., Nagae D., Asahi K., Arai T., Takemura M., Inoue T., Takase K., Kagami S., Hatakeyama N., Kobayashi Y., Ueno H., Yoshimi A., Kameda D., Nagatomo T., Sugimoto T., Kubono S., Yamaguchi H., Wakabayashi Y., Amadio G., Hayakawa S., Murata J., and Kawamura H.: "Production of low-energy spin-polarized ^{17}N beam with CRIB", 15th International Conference on Electromagnetic Isotope Separators and Techniques Related to their Applications (EMIS2007), (GANIL, IN2P3/CNRS and DSM/CEA), Deauville, France, June (2007).

Shimada K., Nagae D., Asahi K., Takemura M., Arai T., Inoue T., Takase K., Kagami S., Hatakeyama N., Kobayashi Y., Ueno H., Yoshimi A., Kameda D., Nagatomo T., Sugimoto T., Kubono S., Yamaguchi H., Wakabayashi Y., Amadio G., Hayakawa S., Murata J., and Kawamura H.: "First production of spin-polarized radioactive nuclear beam with CRIB", International Nuclear Physics Conference (INPC2007), Tokyo, June (2007).

Dang N. D.: "Giant resonances under extreme conditions", International Nuclear Physics Conference (INPC2007), (Science Council of Japan, RIKEN and others), Tokyo, June (2007).

Kohama A., Iida K., and Oyamatsu K.: "Reaction cross section and nuclear radius in the black-sphere picture", International Nuclear Physics Conference (INPC2007), (Science Council of Japan, RIKEN and others), Tokyo, June (2007).

Sarhan B. A., Horiuchi W., Kohama A., and Suzuki Y.: "Reaction cross sections of carbon isotopes incident on proton and ^{12}C target", International Nuclear Physics Conference (INPC2007), (Science Council of Japan, RIKEN and others), Tokyo, June (2007).

Furukawa T., Matsuo Y., Hatakeyama A., Ito T., Fujikake K., Kobayashi T., and Shimoda T.: "High Precision Laser Spectroscopy of Rb and Cs Atoms in Superfluid helium", 25th International Conference on Photonic, Electronic and Atomic Collisions (ICPEAC 2007), Freiburg, Germany, July (2007).

Fukuyama Y., Moriwaki Y., and Matsuo Y.: "Temperature Dependences of Formation Rate Constant and Dissociation Cross Section of Ba^{+*} - He Exciplexes at 3 - 25 K", 25th International Conference on Photonic, Electronic and Atomic Collisions (ICPEAC 2007), Freiburg, Germany, July (2007).

Shimada K., Nagae D., Asahi K., Inoue T., Takase K., Kagami S., Hatakeyama N., Kobayashi Y., Ueno H., Yoshimi A., Kameda D., Nagatomo T., Sugimoto T., Kubono S., Yamaguchi H., Wakabayashi Y., Amadio G., Hayakawa S., Murata J., and Kawamura H.: "Production of spin-polarized ^{17}N beam using inverse-kinematics low-energy transfer reactions", 14th International Conference on Hyperfine Interactions and 18th International Symposium on Nuclear Quadrupole Interactions, Foz de Iguazu, Brazil, Aug. (2007).

Matsuo Y., Kobayashi T., and Nakajima T.: "Experimental observation and control of ultrafast spin-polarization using fs laser pulses", 16th International Laser Physics Workshop (LPHYS'07), Leon, Mexico, Aug. (2007).

Sekiguchi K.: "Three Nucleon Scattering Experiments

from RIKEN", 11th International Conference on Meson-Nucleon Physics and the Structure of the Nucleon (MENU2007), (IKP, ForschungZentrum of Juelich), Juelich, Germanry, Sept. (2007).

Morita K., Morimoto K., Kaji D., Akiyama T., Goto S., Haba H., Ideguchi E., Kanungo R., Katori K., Kikunaga H., Koura H., Kudo H., Ohnishi T., Ozawa A., Sato N., Suda T., Sueki K., Tokanai F., Xu H., Yamaguchi T., Yoneda A., Yoshida A., and YuLiang Z.: "Experiment on searching for the heaviest elements at RIKEN", 3rd International Conference on the Chemistry and Physics of the Transactinide Elements (TAN 07), (Paul Scherrer Institut and Bern University), Davos, Switzerland, Sept. (2007).

Kobayashi T., Kashihata A., Bonet C., Tear S. P., and Baba H.: "Structural analysis of rare-earth silicide nanostructures on Si(001) using three-dimensional medium-energy ion scattering", 9th European Conference on Accelerators in Applied Research and Technology, (Istituto Nazionale di Fisica Nucleare), Florence, Italy, Sept. (2007).

Kato T., Nishimura M., Oho Y., Sano T., Hayashizaki Y., Kawai J., Kobayashi T., and Matsuo Y.: "Ion extraction from Ablation Plasma produced with an intense Femtosecond Laser Pulse", 9th International Conference on Laser Ablation (COLA2007), Tenerife, Spain, Sept. (2007).

Kobayashi T., Matsuo Y., Kato T., Nishimura M., Hayashizaki Y., and Kawai J.: "Observation of charge transfer among atoms and ions in Laser Ablation Plasma", 9th International Conference on Laser Ablation (COLA2007), Tenerife, Spain, Sept. (2007).

Kurata-Nishimura M., Kato T., Oho Y., Sano T., Hayashizaki Y., Kawai J., Matsuo Y., and Kobayashi T.: "Study of Femtosecond Ablation Mechanism by observing Plume expansion", 9th International Conference on Laser Ablation (COLA2007), Tenerife, Spain, Sept. (2007).

Matsuo Y., Kurata-Nishimura M., Kato T., Oho Y., Sano T., Hayashizaki Y., Kawai J., and Kobayashi T.: "Substrate Dependence of Ion Motion in Femtosecond Laser Ablation Plume observed by Planer Laser-induced Flourescence", 9th International Conference on Laser Ablation (COLA2007), Tenerife, Spain, Sept. (2007).

Kobayashi T., Matsuo Y., Kato T., Nishimura M., Hayashizaki Y., and Kawai J.: "Wavelength dependence of production species obtained by Femtosecond Laser Ablation of C_{60}", 9th International Conference on Laser Ablation (COLA2007), Tenerife, Spain, Sept. (2007).

Kobayashi T., Kashihata A., Imai M., Miyamura Y., and Baba H.: "Strain analysis of a SiGe layer on a Si(001)substrate using threedimensional medium-energy ion scattering", 18th International Conference on Ion Beam Analysis, (University of Hyderabad), Hyderabad, India, Sept.–Sept. (2007).

Sekiguchi K.: "Scattering at Intermediate Energies: n Epoch-making Experimental Study of the Three Nucleon Force", International Symposium on New Facet of Three Nucleon Force: 50 years of Fujita-Miyazawa Three Nucleon Force (FM50), (University of Tokyo), Tokyo, Oct. (2007).

(Domestic Conference)

市川隆敏, 萩野浩一, 岩本昭: "超低入射エネルギーでのサブバリア核融合断面積における融合阻害と慣性質量の効果", 日本物理学会 2006 年秋季大会, 奈良, 9 月 (2006).

西村美月, 加藤俊幸, 小林徹, 松尾由賀利, 小山理恵子, 於保祐子, 河合純, 林崎良英: "基板上に塗布した試料におけるフェムト秒レーザーアブレーションメカニズムの解明", 第 54 回応用物理学関係連合講演会, 相模原, 3 月 (2007).

堀内渉, 鈴木宜之, Sarhan B. A., 小濱洋央: "炭素同位体の反応断面積の系統解析", 日本物理学会 2007 年春季大会, 八王子, 3 月 (2007).

杉本崇, 中村隆司, 近藤洋介, 青井考, 馬場秀忠, Bazin D., 福田直樹, 五味朋子, 長谷川浩一, 今井伸明, 石原正泰, 小林俊雄, 久保敏幸, 三浦元隆, 本林透, 大津秀暁, 齋藤明登, 櫻井博儀, 下浦享, Attukalathil V. M., 渡辺極之, 渡辺裕, 薬師寺崇, 柳澤善行, 米田健一郎: "核破砕反応を用いた ^{14}Be の不変質量核分光", 京都大学基礎物理学研究所セミナー, 京都, 4 月 (2007).

加藤俊幸, 小林徹, 倉田-西村美月, 於保祐子, 佐野卓磨, 小山理恵子, 林崎良英, 松尾由賀利, 河合純: "フェムト秒レーザーアブレション飛行時間質量分析法 (fsLA-TOF-MS) の開発", 第 55 回質量分析総合討論会, (日本質量分析学会), 広島, 5 月 (2007).

藤掛浩太郎, 古川武, 松尾由賀利, 畠山温, 伊藤龍浩, 佐々木彩子, 小林徹, 下田正: "超流動ヘリウム中におけるアルカリ金属 Rb,Cs 原子の超微細構造精密測定", 原子・分子・光科学 (AMO) 第 4 回討論会, 東京, 6 月 (2007).

市川隆敏, 萩野浩一, 岩本昭: "深部サブバリア入射エネルギー反応で現れる融合阻害への断熱的アプローチ", 日本原子力研究開発機構研究会第 315 回基礎科学セミナー, 東海, 6 月 (2007).

杉本崇, 中村隆司, 三浦元隆, 近藤洋介, Attukalathil V. M., 青井考, 馬場秀忠, 福田直樹, 五味朋子, 石原正泰, 久保敏幸, 本林透, 大津秀暁, 櫻井博儀, 柳澤善行, 米田健一郎, Bazin D., 長谷川浩一, 今井伸明, 渡辺裕, 小林俊雄, 渡辺極之, 薬師寺崇, 下浦享, 齋藤明登: "不安定核二次ビームを用いた ^{14}Be の不変質量核分光", SPring-8 加速器セミナー, (JASRI), 播磨, 7 月 (2007).

今中雅士, 冨田成夫, 神田俊, 藤枝光輝, 工藤博, 笹公和: "20MeV 陽子線照射およびコロナ放電による水液滴の生成", 第 24 回エアロゾル科学・技術研究討論会, (日本エアロゾル学会), Wako, 8 月 (2007).

松本琢磨, 上村正康, 江上智晃, 井岸康統, 緒方一介, 八尋正信: "離散化チャネル結合法による 6He, 6Li 分解反応解析", 日本物理学会第 62 回年次大会, 札幌, 9 月 (2007).

藤掛浩太郎, 古川武, 松尾由賀利, 畠山温, 佐々木彩子, 小林徹, 小田島仁司, 下田正: "超流動ヘリウム中における原子の超微細構造 II：気体 Rb を用いた共鳴周波数校正", 日本物理学会第 62 回年次大会, 札幌, 9 月 (2007).

Sarhan B. A., 堀内渉, 小濱洋央, 鈴木宜之: “陽子ー炭素同位体全反応断面積の系統的解析”, 日本物理学会第 62 回年次大会, 札幌, 9 月 (2007).

市川 隆敏, 萩野 浩一, 岩本 昭: “Systematics of threshold incident energies for deep sub-barrier fusion hindrance in medium-heavy mass region”, 日本物理学会第 62 回年次大会, 札幌, 9 月 (2007).

古川武, 松尾由賀利, 畠山温, 伊藤龍浩, 藤掛浩太郎, 佐々木彩子, 小林徹, 下田正: “超流動ヘリウム中での RI 原子のレーザー分光実験における光収量計算”, 日本物理学会第 62 回年次大会, 札幌, 9 月 (2007).

福山祥光, 安田伸広, 金廷恩, 村山美乃, 田中義人, 木村滋, 守友浩, 鳥海幸四郎, 大島隆, 上岡隼人, 田中均, 松永利之, 児島理恵, 山田昇, 加藤健一, 小原真司, 高田昌樹: “ピンポイント構造計測による DVD 記録材料の時分割構造評価”, 日本物理学会第 62 回年次大会, 札幌, 9 月 (2007).

成田圭吾, 村田次郎, 川村広和, 豊田健司, 松多健策, 福田光順, 三原基嗣, 西村大樹, 小柴順治, 石川大貴, 亀田大輔: “時間反転対称性検証実験のための ^{8}Li の T1（スピン-格子緩和時間）と磁場依存性”, 平成 19 年度京都大学原子炉実験所専門研究会「原子核プローブ生成とそれを用いた物性研究 (III)」, 大阪府熊取町, 11 月 (2007).

佐々木彩子, 古川武, 藤掛浩太郎, 小林徹, 畠山温, 下田正, 小田島仁司, 松尾由賀利: “超流動ヘリウム中における In 原子の励起スペクトル：光ポンピング実現をめざして”, 第 4 回「停止・低速不安定核を用いた核分光研究」研究会, 仙台, 12 月 (2007).

古川武, 畠山温, 藤掛浩太郎, 佐々木彩子, 小林徹, 下田正, 松尾由賀利: “OROCHI オンライン実験計画とその物理”, 第 4 回「停止・低速不安定核を用いた核分光研究」研究会, 仙台, 12 月 (2007).

中務孝, 矢花一浩, 稲倉恒法, 日野原伸生, 松尾正之, 松柳研一: “密度汎関数アプローチによる原子核数値シミュレーション”, シンポジウム「未来の素粒子・原子核数値シミュレーション」, (高エネルギー加速器研究機構), つくば, 12 月 (2007).

古川武, 松尾由賀利, 畠山温, 藤掛浩太郎, 佐々木彩子, 小林徹, 下田正: “”OROCHI” project - a novel laser spectroscopy method of RI atoms in superfluid helium -”, Workshop on Advance in Physics with ISOL-based/Fragmentation-based RI Beams, (東京工業大学), 東京, 2 月 (2008).

成田圭吾, 村田次郎, 川村広和, 豊田健司, 松多健策, 福田光順, 三原基嗣, 西村大樹, 小柴順治, 石川大貴, 亀田大輔, 平山賀一: “Development of a polarization holding stopper for a T-Violation experiment”, 日本物理学会第 63 回年次大会, 東大阪, 3 月 (2008).

佐々木彩子, 古川武, 藤掛浩太郎, 小林徹, 畠山温, 下田正, 小田島仁司, 松尾由賀利: “超流動ヘリウム中に植え込まれた In 原子の励起スペクトル測定”, 日本物理学会第 63 回年次大会, 東大阪, 3 月 (2008).

松尾由賀利, 小林徹, 中嶋隆: “超短パルスレーザー誘起スピン偏極 (IV)：超高速スピン偏極の実時間観測と制御”, 日本物理学会第 63 回年次大会, 東大阪, 3 月 (2008).

西村美月, 松尾由賀利, 小林徹, 河合純, 林崎良英: “フェムト秒レーザーアブレーションによるイオン放出プロセスの解明”, 第 55 回応用物理学会関係連合講演会, (応用物理学会), 船橋, 3 月 (2008).

Radioactive Isotope Physics Laboratory

Publications

[Journal]

(Original Papers) *Subject to Peer Review

Kambara T., Kanai Y., Kojima T., Nakai Y., Yoneda A., Yamazaki Y., and Kageyama K.: "Elastic waves from fast heavy-ion irradiation on solids", J.Acoust.Emiss. **24**, 97–103 (2006). *

Sugimoto T., Nakamura T., Fukuda N., Miura M., Kondo Y., Aoi N., Baba H., Bazin D., Gomi T., Hasegawa H., Hashimoto Y., Imai N., Kobayashi T., Kubo T., Motobayashi T., Ohara M., Saito A., Sakurai H., Shimoura S., Attukalathil V. M., Watanabe K., Watanabe Y., Yakushiji T., Yanagisawa Y., Yoneda K., and Ishihara M.: "Invariant-mass spectroscopy of the neutron-drip line nucleus ^{14}Be", J. Phys.: Con. Ser. **49**, 43–44 (2006). *

Ueno H., Kameda D., Nagae D., Takemura M., Asahi K., Takase K., Yoshimi A., Sugimoto T., Nagatomo T., Shimada K., Uchida M., Arai T., Inoue T., Murata J., Kawamura H., and Narota K.: "Nuclear-moment measurements at RIKEN and perspectives in RIBF", AIP Conf. Proc. **915**, 841–844 (2007). *

Ueno H., Kameda D., Nagae D., Takemura M., Asahi K., Arai T., Shimada K., Takase K., Sugimoto T., Nagatomo T., Uchida M., Inoue T., Yoshimi A., Kawamura H., and Narota K.: "Nuclear moments of neutron-rich aluminum isotopes", Eur. Phys. J. Special Topics **150**, 185–186 (2007). *

Mizuno T., Majima T., Tsuchida H., Nakai Y., and Itoh A.: "Molecular orientation effects in CO fragmentation induced by charge-changing collisions of 6 MeV O^{4+} ions", J. Phys.: Con. Ser. **58**, 173–176 (2007). *

Kanai Y., Nakai Y., Iwai Y., Nishio K., Masuda H., and Yamazaki Y.: "Auger electrons emitted from nitrogen ions passing through a metallic microcapillary", J. Phys.: Con. Ser. **58**, 335–338 (2007). *

Morita K., Morimoto K., Kaji D., Akiyama T., Goto S., Haba H., Ideguchi E., Katori K., Koura H., Kudo H., Ohnishi T., Ozawa A., Suda T., Sueki K., Tokanai F., Yamaguchi T., Yoneda A., and Yoshida A.: "Experiment on synthesis of an isotope 277112 by 208Pb + 70Zn reaction", J. Phys. Soc. Jpn. **76**, No. 4, pp. 043201-1–043201-5 (2007). *

Morita K., Morimoto K., Kaji D., Akiyama T., Goto S., Haba H., Ideguchi E., Katori K., Koura H., Kikunaga H., Kudo H., Ohnishi T., Ozawa A., Sato N., Suda T., Sueki K., Tokanai F., Yamaguchi T., Yoneda A., and Yoshida A.: "Observation of second decay chain from 278113", J. Phys. Soc. Jpn. **76**, No. 4, pp. 045001-1–045001-2 (2007). *

Sato W., Ueno H., Taniguchi A., Itsuki Y., Kasamatu Y., Shinohara A., Asahi K., and Ohkubo Y.: "Time-dependent quadrupole interactions for ^{140}Ce ions implanted in highly oriented pyrolytic graphite", J. Radioanal. Nucl. Chem. **272**, 665–668 (2007). *

Kageyama K., Kambara T., and Nakai Y.: "Detection of weak ultrasound generated by nano- and femtosecond laser irradiation using piezoelectric sensors", J. Solid Mech. Mater. Eng. **1**, No. 9, pp. 1128–1135 (2007). *

Mizuno T., Majima T., Nakai Y., Tsuchida H., and Itoh A.: "Electronic stopping and velocity effect on multiple ionization and fragmentation of C_{60} in swift heavy ion impacts", Nucl. Instrum. Methods Phys. Res. B **256**, 101–104 (2007). *

Kondo C., Masugi S., Muranaka T., Ishikawa A., Nakano Y., Azuma T., Hatakeyama A., Komaki K., Nakai Y., Yamazaki Y., Takada E., and Murakami T.: "Trajectory dependent resonant coherent excitation of planar-channeled ions in a thin Si crystal", Nucl. Instrum. Methods Phys. Res. B **256**, 157–161 (2007). *

Shimoura S., Ota S., Demichi K., Aoi N., Baba H., Elekes Z., Fukuchi T., Gomi T., Hasegawa K., Ideguchi E., Ishihara M., Iwasa N., Iwasaki H., Kanno S., Kubono S., Kurita K., Kurokawa M., Matsuyama Y., Michimasa S., Miller K. L., Minemura T., Motobayashi T., Murakami T., Notani M., Odahara A., Saito A., Sakurai H., Takeshita E., Takeuchi S., Tamaki M., Teranishi T., Yamada K., Yanagisawa Y., and Hamamoto I.: "Lifetime of the isomeric 0_2^+ state in ^{12}Be", Phys. Lett. B **654**, 87–91 (2007). *

Sugimoto T., Nakamura T., Kondo Y., Aoi N., Baba H., Bazin D. P., Fukuda N., Gomi T., Hasegawa H., Imai N., Ishihara M., Kobayashi T., Kubo T., Miura M., Motobayashi T., Otsu H., Saito A., Sakurai H., Shimoura S., Vinodkumar A. M., Watanabe K., Watanabe Y., Yakushiji T., Yanagisawa Y., and Yoneda K.: "The first 2^+ state of ^{14}Be", Phys. Lett. B **654**, 160–164 (2007). *

Mizuno T., Okamoto D., Majima T., Nakai Y., Tsuchida H., and Itoh A.: "Impact-parameter-dependent multifragmentation of C_{60} in charge-changing collisions with 2-MeV C^+ ions", Phys. Rev. A **75**, 063203-1–063203-5 (2007). *

Fujita H., Fujita Y., Adachi T., Bacher A. D., Berg G. P., Black T. C., Caurier E., Foster ., Fujimura H., Hara K., Harada K., Hatanaka K., Janecke J., Kamiya J., Kanzaki Y., Katori K., Kawabata T., Langanke K., Martinez-Pinedo G., Noro T., Robers D. A., Sakaguchi H., Shimbara Y., Shinada T., Stephenson E. J., Ueno H., Yamanaka T., Yoshifuku M., and Yosoi M.: "Isospin structure of $J^\pi = 1^+$ states in ^{58}Ni and ^{58}Cu studied by ^{58}Ni(p, p') and ^{58}Ni(^{3}He,t)^{58}Cu measurements", Phys. Rev. C **75**, 034310-1–034310-15 (2007). *

Gibelin J. D., Beaumel D., Motobayashi T., Aoi N., Baba H., Blumenfeld Y., Dombradi Z., Elekes Z., Fortier S., Frascaria N., Fukuda N., Gomi T., Ishikawa K., Kondo Y., Kubo T., Lima V., Nakamura T., Saito A., Sato

Y., Takeshita E., Takeuchi S., Teranishi T., Togano Y., Vinodkumar A. M., Yanagisawa Y., and Yoshida A.: "Measurement of the B(E2, $0_1^+ \rightarrow 2_1^+$) in the N = 16 nucleus ^{26}Ne", Phys. Rev. C **75**, 057301-1–057391-4 (2007). *

Mocko M., Tsang M., Sun Z., Aoi N., Cook J. M., Delaunay F., Famiano M., Hui H., Imai N., Iwasaki H., Lynch W., Motobayashi T., Niikura M., Onishi T., Rogers A. M., Sakurai H., Stolz A., Suzuki H., Takeshita E., Takeuchi S., and Wallace M.: "Projectile fragmentation of 86Kr at 64 MeV/nucleon", Phys. Rev. C **76**, 014609-1–014609-10 (2007). *

Notani M., Sakurai H., Aoi N., Iwasaki H., Fukuda N., Liu Z., Yoneda K., Ogawa H., Teranishi T., Nakamura T., Okuno H., Yoshida A., Watanabe Y., Momota S., Inabe N., Kubo T., Ito S., Ozawa A., Suzuki T., Tanihata I., and Ishihara M.: "Projectile fragmentation reaction and production of nuclei near the neutron drip line", Phys. Rev. C **76**, 044605-1–044605-15 (2007). *

Elekes Z., Dombradi Z., Aoi N., Bishop S., Fulop Z., Gibelin J. D., Gomi T., Hashimoto Y., Imai N., Iwasa N., Iwasaki H., Kalinka G., Kondo Y., Korsheninnikov A. A., Kurita K., Kurokawa M., Matsui N., Motobayashi T., Nakamura T., Nakao T., Nikolski E. Y., Onishi T., Okumura T., Ota S., Perera P., Saito A., Sakurai H., Sato Y., Sohler D., Sumikama T., Suzuki D., Suzuki M., Takeda H., Takeuchi S., Togano Y., and Yanagisawa Y.: "Spectroscopic study of neutron shell closures via nucleon transfer in the near-dripline nucleus ^{23}O", Phys. Rev. Lett. **98**, No. 10, pp. 102502-1–102502-4 (2007). *

Sato W., Ueno H., Watanabe H., Miyoshi H., Yoshimi A., Kameda D., Ito T., Shimada K., Kaihara J., Suda S., Kobayashi Y., Shinohara A., Ohkubo Y., and Asahi K.: "Online time-differential perturbed angular correlation study with an ^{19}O beam Residence sites of oxygen atoms in highly oriented pyrolytic graphite", Nucl. Instrum. Methods Phys. Res. B **266**, 316–322 (2008). *

[Book•Proceedings]

(Original Papers) *Subject to Peer Review

Ueno H., Kameda D., Yoshimi A., Haseyama T., Asahi K., Takemura M., Kijima G., Shimada K., Nagae D., Uchida M., Arai T., Suda S., Takase K., Inoue T., and Kawamura H.: "Production of spin-oriented unstable nuclei via the projectile-fragmentation reaction", Polarized-Sources and Targets: Proceedings of the 11th International Workshop, Tokyo, 2005–11, World Scientific, Singapore, pp. 178–183 (2007).

Kameda D., Ueno H., Asahi K., Yoshimi A., Haseyama T., Kobayashi Y., Uchida M., Miyoshi H., Kijima G., Takemura M., Nagae D., Kato G., Emori S., Oshima S., Arai T., and Tsukui M.: "Production of spin-polarized RI beams via projectile fragmentation and the application to nuclear moment measurements", Polarized-Sources and Targets: Proceedings of the 11th International Workshop, Tokyo, 2005–11, World Scientific Publishing , Toh Tuck Link, pp. 211–212 (2007).

Kameda D., Ueno H., Asahi K., Takemura M., Nagae D., Shimada K., Yoshimi A., Kobayashi Y., Haseyama T., Uchida M., Takase K., Arai T., Inoue T., Suda S., Murata J., Kawamura H., Watanabe H., and Ishihara M.: "Nuclear moment measurements of Neutron-rich Aluminum Isotopes Using Spin-Polarized RI beams: Determination of the Boundary of the "Island of Inversion"", Proceedings of the 17th International Spin Physics Symposium (SPIN2006), Tokyo, 2006–10, American Institute of Physics, New York, pp. 845–848 (2007). *

Oral Presentations

(International Conference etc.)

Sugimoto T., Nakamura T., Fukuda N., Miura M., Kondo Y., Aoi N., Baba H., Bazin D., Gomi T., Hasegawa H., Hashimoto Y., Imai N., Kobayashi T., Kubo T., Motobayashi T., Ohara M., Saito A., Sakurai H., Shimoura S., Attukalathil V. M., Watanabe K., Watanabe Y., Yakushiji T., Yanagisawa Y., Yoneda K., and Ishihara M.: "Invariant-mass spectroscopy of the neutron-drip line nucleus ^{14}Be", International Symposium on Structure of Exotic Nuclei and Nuclear Forces (SENUF06), (CNS and RIKEN), Tokyo, Mar. (2006).

Mizuno T., Majima T., Nakai Y., Tsuchida H., and Itoh A.: "Electronic stopping and velocity effect of multiple ionization and fragmentation of C60 in swift heavy ion impacts", 22nd International Conference on Atomic Collisions in Solids (ICACS 2006), (Hahn-Meitner-Institut Berlin), Berlin, Germany, July (2006).

Mizuno T., Majima T., Tsuchida H., Nakai Y., and Itoh A.: "Molecular orientation effects on ionization of CO in charge-changing collisions of 6 MeV O^{4+} ion", 13th International Conference on the Physics of Highly Charged Ions (HCI 2006), Belfast, UK, Aug.–Sept. (2006).

Nagatomo T., Minamisono K., Matsuta K., Levy C. D., Sumikama T., Ozawa A., Tagisi Y., Mihara M., Ogura M., Matsumiya R., Fukuda M., Yamaguchi M., Behr J. A., Jackson K. P., Fujiwara H., Ohta H., Yasuno T., Hashizume Y., and Minamisono T.: "Alignment Correlation Terms In β-Ray Angular Distributions From Spin Aligned ^{20}F And ^{20}Na", 17th International Spin Physics Symposium (SPIN2006), (Kyoto University), Kyoto, Oct. (2006).

Ueno H., Nagae D., Kameda D., Takemura M., Asahi K., Takase K., Yoshimi A., Sugimoto T., Shimada K., Nagatomo T., Uchida M., Arai T., Inoue T., Murata J., Kawamura H., and Narota K.: "Electric quadrupole moment of ^{31}Al", International Nuclear Physics Conference (INPC2007), (Science Council of Japan, RIKEN and others), Tokyo, June (2007).

Murata J., Asahi K., Hirayama Y., Kameda D., Kawamura H., Nagae D., Narota K., Shimada K., Toyoda T.,

Uchida M., Ueno H., and Yoshimi A.: "T-Violating transverse electron polarization in polarized nuclear beta decay", International Nuclear Physics Conference (INPC2007), Tokyo, June (2007).

Kameda D., Ueno H., Asahi K., Yoshimi A., Haseyama T., Kobayashi Y., Ishihara M., Nagae D., Takemura M., Shimada K., Uchida M., Arai T., Takase K., Inoue T., Kijima G., Suda S., Murata J., Kawamura H., Narota K., Toyoda T., and Watanabe H.: "Electric quadrupole moments of neutron-rich nuclei ^{32}Al and ^{31}Al", International Symposium & School on Frontiers and Perspectives of Nuclear and Hadron Physics (FPNH07), (Tokyo Institute of Technology), Tokyo, June (2007).

Kanai Y., Nakai Y., Lamsadze R., Iwai Y., Nishio K., Masuda H., and Yamazaki Y.: "Auger electrons from excited states of ions after passing through a metallic microcapillary", 25th International Conference on Photonic, Electronic and Atomic Collisions (ICPEAC 2007), Freiburg, Germany, July (2007).

Mizuno T., Yamada T., Nakai Y., Tsuchida H., and Itoh A.: "Ionization and fragmentation of N_2 following electron capture and loss of 2MeV C^+ ions", 25th International Conference on Photonic, Electronic and Atomic Collisions (ICPEAC 2007), (Max-Planck-Institut fuer Kernphysik), Freiburg, Germany, July (2007).

Sugimoto T., Asahi K., Kawamura H., Murata J., Nagae D., Shimada K., Ueno H., and Yoshimi A.: "Development of atomic-beam resonance method to measure the nuclear moments of unstable nuclei", 14th International Conference on Hyperfine Interactions and 18th International Symposium on Nuclear Quadrupole Interactions, (A Joint Argentina-Brazil organization), Foz do Iguacu, Brazil, Aug. (2007).

Morita K., Morimoto K., Kaji D., Akiyama T., Goto S., Haba H., Ideguchi E., Kanungo R., Katori K., Kikunaga H., Koura H., Kudo H., Ohnishi T., Ozawa A., Sato N., Suda T., Sueki K., Tokanai F., Xu H., Yamaguchi T., Yoneda A., Yoshida A., and YuLiang Z.: "Experiment on searching for the heaviest elements at RIKEN", 3rd International Conference on the Chemistry and Physics of the Transactinide Elements (TAN 07), (Paul Scherrer Institut and Bern University), Davos, Switzerland, Sept. (2007).

(Domestic Conference)

望月優子, 五十嵐誠, 高橋和也, 牧島一夫, 馬場彩, 中井陽一, 本山秀明, 神山孝吉, 鈴木啓助: "ドームふじ浅層コアのイオン詳細解析：現状と今後", 国立極地研究所研究集会「南極氷床の物理・化学・生物のフロンティア３」, 東京, 3 月 (2007).

中野祐司, 近藤力, 東俊行, 畠山温, 小牧研一郎, 中井陽一, 山崎泰規, 高田栄一, 村上健: "結晶場による 3 次元コヒーレント共鳴励起 III", 日本物理学会 2007 年春季大会, 鹿児島, 3 月 (2007).

金井保之, 中井陽一, 岩井良夫, 益田秀樹, 西尾和之, 山崎泰規: "金属マイクロキャピラリー通過後の多価イオンからの Auger 電子", 日本物理学会 2007 年春季大会, (日本物理学会), 鹿児島, 3 月 (2007).

亀田大輔, 上野秀樹, 旭耕一郎, 竹村真, 吉見彰洋, 長谷山智仁, 内田誠, 島田健司, 長江大輔, 木島剛, 新井崇雅, 高瀬研以智, 須田紳一, 井上壮志, 村田次郎, 川村広和, 小林義男, 渡邉寛, 石原正泰: "中性子過剰核 32Al の核モーメント測定–魔法数 20 の閉殻構造の破れに関連して–", 日本物理学会 2007 年春季大会, 東京, 3 月 (2007).

杉本崇, 中村隆司, 近藤洋介, 青井考, 馬場秀忠, Bazin D., 福田直樹, 五味朋子, 長谷川浩一, 今井伸明, 石原正泰, 小林俊雄, 久保敏幸, 三浦元隆, 本林透, 大津秀暁, 齋藤明登, 櫻井博儀, 下浦享, Attukalathil V. M., 渡辺極之, 渡辺裕, 薬師寺崇, 柳澤善行, 米田健一郎: "核破砕反応を用いた ^{14}Be の不変質量核分光", 京都大学基礎物理学研究所セミナー, 京都, 4 月 (2007).

杉本崇, 中村隆司, 三浦元隆, 近藤洋介, Attukalathil V. M., 青井考, 馬場秀忠, 福田直樹, 五味朋子, 石原正泰, 久保敏幸, 本林透, 大津秀暁, 櫻井博儀, 柳澤善行, 米田健一郎, Bazin D., 長谷川浩一, 今井伸明, 渡辺裕, 小林俊雄, 渡辺極之, 薬師寺崇, 下浦享, 齋藤明登: "不安定核二次ビームを用いた ^{14}Be の不変質量核分光", SPring-8 加速器セミナー, (JASRI), 播磨, 7 月 (2007).

水野智也, 山田貴啓, 中井陽一, 土田秀次, 今井誠, 柴田裕実, 伊藤秋男: "運動量イメージング法を用いた高速重イオン荷電変換衝突に伴う C_2H_2 の電離分解過程の研究", 日本物理学会第 62 回年次大会, 札幌, 9 月 (2007).

中務孝, 矢花一浩, 稲倉恒法, 日野原伸生, 松尾正之, 松柳研一: "密度汎関数アプローチによる原子核数値シミュレーション", シンポジウム「未来の素粒子・原子核数値シミュレーション」, (高エネルギー加速器研究機構), つくば, 12 月 (2007).

Superheavy Element Laboratory

Publications

[Journal]

(Original Papers) *Subject to Peer Review

Kambara T., Kanai Y., Kojima T., Nakai Y., Yoneda A., Yamazaki Y., and Kageyama K.: "Elastic waves from fast heavy-ion irradiation on solids", J.Acoust.Emiss. **24**, 97–103 (2006). *

Haba H., Akiyama T., Kaji D., Kikunaga H., Kuribayashi T., Morimoto K., Morita K., Ooe K., Sato N., Shinohara A., Takabe T., Tashiro T., Toyoshima A., Yoneda A., and Yoshimura T.: "Startup of superheavy element chemistry at RIKEN", Eur. Phys. J. D **45**, 81–86 (2007). *

Yamashita Y., Takahashi Y., Haba H., Enomoto S., and Shimizu H.: "Comparison of reductive accumulation of Re and Os in seawater - sediment systems", Geochimica Cosmochimica Acta **71**, No. 14, pp. 3458–3475 (2007). *

Haba H., Kaji D., Kikunaga H., Akiyama T., Sato N., Morimoto K., Yoneda A., Morita K., Takabe T., and Shinohara A.: "Development of gas-jet transport system coupled to the RIKEN Gas-filled Recoil Ion Separator GARIS for superheavy element chemistry", J. Nucl. Radiochem. Sci. **8**, No. 2, pp. 55–58 (2007). *

Kasamatu Y., Toyoshima A., Toume H., Tsukada K., Haba H., and Nagame Y.: "Anion-exchange behavior of Nb, Ta, and Pa as homologues of Db in HF/HNO3 solutions", J. Nucl. Radiochem. Sci. **8**, No. 2, pp. 69–72 (2007). *

Morita K., Morimoto K., Kaji D., Akiyama T., Goto S., Haba H., Ideguchi E., Katori K., Koura H., Kudo H., Ohnishi T., Ozawa A., Suda T., Sueki K., Tokanai F., Yamaguchi T., Yoneda A., and Yoshida A.: "Experiment on synthesis of an isotope 277112 by 208Pb + 70Zn reaction", J. Phys. Soc. Jpn. **76**, No. 4, pp. 043201-1–043201-5 (2007). *

Morita K., Morimoto K., Kaji D., Akiyama T., Goto S., Haba H., Ideguchi E., Katori K., Koura H., Kikunaga H., Kudo H., Ohnishi T., Ozawa A., Sato N., Suda T., Sueki K., Tokanai F., Yamaguchi T., Yoneda A., and Yoshida A.: "Observation of second decay chain from 278113", J. Phys. Soc. Jpn. **76**, No. 4, pp. 045001-1–045001-2 (2007). *

Sato W., Ueno H., Taniguchi A., Itsuki Y., Kasamatu Y., Shinohara A., Asahi K., and Ohkubo Y.: "Time-dependent quadrupole interactions for ^{140}Ce ions implanted in highly oriented pyrolytic graphite", J. Radioanal. Nucl. Chem. **272**, 665–668 (2007). *

Sonoda T., Fujita M., Yamazaki A., Endo T., Shinozuka T., Miyashita Y., Sato N., Goto A., Takano E., Suzuki T., Miyake T., Tanigaki M., and Wada M.: "Development of the RF-IGISOL at CYRIC", Nucl. Instrum. Methods Phys. Res. B **254**, 295–299 (2007). *

Fujita H., Fujita Y., Adachi T., Bacher A. D., Berg G. P., Black T. C., Caurier E., Foster ., Fujimura H., Hara K., Harada K., Hatanaka K., Janecke J., Kamiya J., Kanzaki Y., Katori K., Kawabata T., Langanke K., Martinez-Pinedo G., Noro T., Robers D. A., Sakaguchi H., Shimbara Y., Shinada T., Stephenson E. J., Ueno H., Yamanaka T., Yoshifuku M., and Yosoi M.: "Isospin structure of $J^\pi = 1^+$ states in ^{58}Ni and ^{58}Cu studied by ^{58}Ni(p, p') and ^{58}Ni(^{3}He,t)^{58}Cu measurements", Phys. Rev. C **75**, 034310-1–034310-15 (2007). *

Ichikawa T., Hagino K., and Iwamoto A.: "Existence of a one-body barrier revealed in deep subbarrier fusion", Phys. Rev. C **75**, 057603-1–057603-4 (2007). *

Ichikawa T., Hagino K., and Iwamoto A.: "Systematics of threshold incident energy for deep sub-barrier fusion hindrance", Phys. Rev. C **75**, 064612-1–064612-4 (2007). *

Sakuma F., chiba j., Enyo H., Fukao Y., Funahashi H., Hamagaki H., ieiri m., ishino m., handa h., Kitaguchi M., mihara s., Miwa K., miyashita t., Murakami T., muto r., nakura t., Naruki M., Ozawa K., sasaki o., Sekimoto M., Tabaru T., tanaka k., Togawa M., yamada s., Yokkaichi S., and yoshimura y.: "Nuclear-matter modification of decay widths in the $\phi \to e^+e^-$ and $\phi \to K^+K^-$ channels", Phys. Rev. Lett. **98**, 152302-1–152302-5 (2007). *

Sato W., Ueno H., Watanabe H., Miyoshi H., Yoshimi A., Kameda D., Ito T., Shimada K., Kaihara J., Suda S., Kobayashi Y., Shinohara A., Ohkubo Y., and Asahi K.: "Online time-differential perturbed angular correlation study with an ^{19}O beam Residence sites of oxygen atoms in highly oriented pyrolytic graphite", Nucl. Instrum. Methods Phys. Res. B **266**, 316–322 (2008). *

Oral Presentations

(International Conference etc.)

Asai M., Tsukada K., Sakama M., Ishii Y., Toyoshima A., Ishii T., Nishinaka I., Nagame Y., Kasamatsu Y., Haba H., Kojima Y., Shibata M., Hayashi H., and Sueki K.: "Alpha-gamma spectroscopy of N = 155 and 157 nuclei using a gas-jet transport technique", 3rd International Conference on the Chemistry and Physics of the Transactinide Elements (TAN 07), (Paul Scherrer Institut and Bern University), Davos, Switzerland, Sept. (2007).

Kasamatsu Y., Toyoshima A., Asai M., Tsukada K., Haba H., Ishii Y., Toume H., Nishinaka I., Akiyama K., Kikunaga H., Goto S., Ishikawa T., Kudo H., Sato W., Ooe K., Kuribayashi T., Shinohara A., Kinoshita N., Arai M., Yokoyama A., Sakama M., Sato T., Qin Z., Duellmann C. E., and Nagame Y.: "Anion-exchange behavior of element 105, Db, in HF/HNO3 media", 3rd International Conference on the Chemistry and Physics of the Transactinide Elements (TAN 07), (Paul Scherrer Institut and Bern University), Davos, Switzerland, Sept.

(2007).

Toyoshima A., Kasamatsu Y., Tsukada K., Kitatsuji A., Haba H., Ishii Y., Toume H., Asai M., Akiyama K., Ooe K., Sato W., Shinohara A., and Nagame Y.: "Electrochemical oxidation of nobelium", 3rd International Conference on the Chemistry and Physics of the Transactinide Elements (TAN 07), (Paul Scherrer Institut and Bern University), Davos, Switzerland, Sept. (2007).

Morita K., Morimoto K., Kaji D., Akiyama T., Goto S., Haba H., Ideguchi E., Kanungo R., Katori K., Kikunaga H., Koura H., Kudo H., Ohnishi T., Ozawa A., Sato N., Suda T., Sueki K., Tokanai F., Xu H., Yamaguchi T., Yoneda A., Yoshida A., and YuLiang Z.: "Experiment on searching for the heaviest elements at RIKEN", 3rd International Conference on the Chemistry and Physics of the Transactinide Elements (TAN 07), (Paul Scherrer Institut and Bern University), Davos, Switzerland, Sept. (2007).

Nagame Y., Toyoshima A., Ishii Y., Tsukada K., Asai M., Toume H., Kasamatsu Y., Nishinaka I., Sato T., Haba H., Kikunaga H., Akiyama K., Oura Y., Nakahara H., Sato W., Shinohara A., Goto S., Kudo H., Yokoyama A., Sakama M., Sueki K., Schaedel M., Bruechle W., and Kratz J. V.: "Fluoride complex formation of element 104, Rutherfordium", 3rd International Conference on the Chemistry and Physics of the Transactinide Elements (TAN 07), (Paul Scherrer Institut and Bern University), Davos, Switzerland, Sept. (2007).

Kaji D., Haba H., Kikunaga H., Morimoto K., Akiyama T., Kudo H., Ooe K., Nanri T., Sato N., Shinohara A., Suzuki D., Takabe T., Yamazaki I., Yokoyama A., Yoneda A., and Morita K.: "Performance of a gas-filled recoil separator GARIS for hot fusion study", 3rd International Conference on the Chemistry and Physics of the Transactinide Elements (TAN 07), (Paul Scherrer Institut and Bern University), Davos, Switzerland, Sept. (2007).

Haba H., Akiyama T., Kaji D., Kikunaga H., Kuribayashi T., Morimoto K., Morita K., Nanri T., Ooe K., Sato N., Shinohara A., Suzuki D., Toyoshima A., Yamazaki I., Yokoyama A., Yoneda A., and Yoshimura T.: "Present status and perspectives of superheavy element chemistry at RIKEN", 3rd International Conference on the Chemistry and Physics of the Transactinide Elements (TAN 07), (Paul Scherrer Institut and Bern University), Davos, Switzerland, Sept. (2007).

Morita K.: "Future plan of the experimental program on synthesizing the heaviest elements at RIKEN", 6th Workshop on Recoil Separator for Superheavy Element Chemistry (TASCA 07), (GSI, TUM, and PSI), Davos, Switzerland, Sept. (2007).

Haba H.: "Perspectives of the superheavy element chemistry at RIKEN GARIS", 6th Workshop on Recoil Separator for Superheavy Element Chemistry (TASCA 07), (GSI, TUM, and PSI), Davos, Switzerland, Sept. (2007).

Motomura S., Kanayama Y., Haba H., Watanabe Y., and Enomoto S.: "Multiple Nuclide Imaging in Live Mouse Using Semiconductor Compton Camera for Multiple Molecular Imaging", 2007 IEEE Nuclear Science Symposium and Medical Imaging Conference, Honolulu, USA, Oct.–Nov. (2007).

Motomura S., Kanayama Y., Haba H., Igarashi K., Hiromura M., Watanabe Y., and Enomoto S.: "Compton Camera for Multiple Molecular Imaging", International Symposium on Metallomics 2007 (ISM 2007), (The Chemical Society of Japan), Nagoya, Nov.–Dec. (2007).

Furukawa J., Haba H., Enomoto S., and Satoh S.: "Heavy Metal Accumulation in Lotus japonicas", International Symposium on Metallomics 2007 (ISM 2007), (The Chemical Society of Japan), Nagoya, Nov.–Dec. (2007).

Kanayama Y., Motomura S., Haba H., Enomoto K. (., Watanabe Y., and Enomoto S.: "Preliminary study for multiple molecular imaging: simultaneous imaging of ^{18}F-FDG, ^{54}Mn-$MnCl_2$, and ^{65}Zn-$ZnCl_2$ in normal and tumor-bearing mouse", International Symposium on Metallomics 2007 (ISM 2007), (The Chemical Society of Japan), Nagoya, Nov.–Dec. (2007).

(Domestic Conference)

市川隆敏, 萩野浩一, 岩本昭: "超低入射エネルギーでのサブバリア核融合断面積における融合阻害と慣性質量の効果", 日本物理学会 2006 年秋季大会, 奈良, 9 月 (2006).

林田清, 常深博, 高原文郎, 穴吹直久, 村上敏夫, 米徳大輔, 郡司修一, 門叶冬樹, 櫻井敬久, 柴田晋平, 滝沢元和, 三原建弘, 玉川徹, 小濱光洋, 磯部直樹, 鶴剛, 松本浩典, 谷森達, 窪秀利, 堂谷忠靖, 高橋忠幸, 斎藤芳隆, 小賀坂康志, 片岡淳, 河合誠之, 北本俊二, 深沢泰司: "X 線ガンマ線偏光観測小型衛星 Polaris 計画", 日本天文学会 2007 年春季年会, 平塚, 3 月 (2007).

米徳大輔, 小平祐宣, 青山有加, 小坂亮太, 児玉芳樹, 江村尚美, 村上敏夫, 郡司修一, 門叶冬樹, 三原建弘: "ガンマ線バースト偏光観測装置の実機モデルの製作と性能評価", 日本天文学会 2007 年春季年会, 平塚, 3 月 (2007).

穴吹直久, 森本真史, 林田清, 常深博, 郡司修一, 岸本祐二, 石垣保博, 菅野誠, 村山裕章, 門叶冬樹, 櫻井敬久, 三原建弘, 小濱光洋, 斎藤芳隆, 山上隆正: "硬 X 線偏光度検出器 PHENEX によるかに星雲の観測:2006 年三陸気球実験データ解析結果", 日本天文学会 2007 年春季年会, 平塚, 3 月 (2007).

笠松良崇, 豊嶋厚史, 當銘勇人, 塚田和明, 羽場宏光, 永目諭一郎: "105 番元素 (Db) の化学的研究を目指した Nb,Ta,Pa の HF/HNO3 溶液系における陰イオン交換実験", 日本化学会第 87 春季年会, 吹田, 3 月 (2007).

當銘勇人, 笠松良崇, 豊嶋厚史, 石井康雄, 塚田和明, 羽場宏光, 篠原伸夫, 永目諭一郎: "HF/HNO3 混合水溶液中における Nb,Ta の陽イオン交換実験：105 番元素 Db の化学的研究に向けて", 日本化学会第 87 春季年会, 吹田, 3 月 (2007).

石井康雄, 當銘勇人, 豊嶋厚史, 浅井雅人, 西中一朗, 塚田和明, 永目諭一郎, 宮下直, 森友隆, 菅沼英夫, 田代祐基, 篠原厚, 坂牧雅巳, 後藤真一, 工藤久昭, 羽場宏光, 秋山和彦, 大浦

泰嗣: “ラザホージウムの硝酸/フッ化水素酸系におけるフッ化物錯形成”, 日本化学会第 87 春季年会, 吹田, 3 月 (2007).

豊嶋厚史, 笠松良崇, 北辻章浩, 塚田和明, 石井康雄, 當銘勇人, 浅井雅人, 羽場宏光, 秋山和彦, 大江一弘, 佐藤渉, 篠原厚, 永目諭一郎: “ノーベリウムの酸化”, 日本化学会第 87 春季年会, 吹田, 3 月 (2007).

羽場宏光, 菊永英寿, 加治大哉, 佐藤望, 秋山隆宏, 森本幸司, 米田晃, 森田浩介, 高部智正, 大江一弘, 篠原厚, 南里朋洋, 鈴木大介, 山崎逸郎, 横山明彦: “超重元素化学研究に向けた GARIS 直結型ガスジェット搬送システムの性能評価”, 日本化学会第 87 春季年会, 吹田, 3 月 (2007).

高部智正, 羽場宏光, 加治大哉, 菊永英寿, 大江一弘, 田代祐基, 佐藤望, 吉村崇, 工藤久昭, 三頭聰明, 森田浩介, 篠原厚: “RIKEN における ^{248}Cm(^{22}Ne,5n)^{265}Sg 反応を用いたシーボーギウム合成実験 (1)”, 日本化学会第 87 春季年会, 吹田, 3 月 (2007).

大江一弘, 田代祐基, 高部智正, 栗林隆宏, 矢作亘, 吉村崇, 佐藤渉, 高橋成人, 高久圭二, 羽場宏光, 榎本秀一, 篠原厚: “オンライン迅速溶媒抽出システムを用いたアクチノイドの系統的研究”, 日本化学会第 87 春季年会, 吹田, 3 月 (2007).

郡司修一, 岸本祐二, 石垣保博, 門叶冬樹, 菅野誠, 伊藤智加, 村山裕章, 櫻井敬久, 三原建弘, 小濱光洋, 林田清, 森本真史, 穴吹直久, 常深博, 斎藤芳隆, 山上隆正, 岸本俊二: “硬 X 線偏光度検出器 PHENEX によるカニ星雲の偏光観測結果”, 日本物理学会 2007 年春季大会, 八王子, 3 月 (2007).

菅野誠, 郡司修一, 岸本祐二, 石垣保博, 門叶冬樹, 伊藤智加, 村山裕章, 櫻井敬久, 三原建弘, 小濱光洋, 鈴木素子, 林田清, 森本真史, 穴吹直久, 常深博, 斎藤芳隆, 山上隆正, 岸本俊二: “硬 X 線偏光度検出器 PHENEX の開発 X:斜め入射による検出器の応答”, 日本物理学会 2007 年春季大会, 八王子, 3 月 (2007).

榎本秀一, 本村信治, 金山洋介, 羽場宏光, 石澤篤: “複数核種同時γ線イメージング装置の開発と分子イメージング研究の展開”, 第 68 回分析化学討論会, (日本分析化学会), 宇都宮, 5 月 (2007).

金山洋介, 本村信治, 羽場宏光, 渡辺恭良, 榎本秀一: “Simultaneous imaging of ^{65}Zn, ^{85}Sr, and ^{131}I in living mouse using gamma-ray emission imaging system”, 第 17 回金属の関与する生体関連反応シンポジウム, (日本薬学会物理系薬学部会), 京都, 6 月 (2007).

本村信治, 金山洋介, 羽場宏光, 渡辺恭良, 榎本秀一: “半導体コンプトンカメラによる複数分子同時イメージング装置の開発：マウスにおける複数核種同時γ線イメージング”, 第 2 回日本分子イメージング学会総会・学術集会, 福井, 6 月 (2007).

市川隆敏, 萩野浩一, 岩本昭: “深部サブバリア入射エネルギー反応で現れる融合阻害への断熱的アプローチ”, 日本原子力研究開発機構研究会第 315 回基礎科学セミナー, 東海, 6 月 (2007).

金山洋介, 本村信治, 羽場宏光, 渡辺恭良, 榎本秀一: “半導体コンプトンカメラによる複数分子同時イメージング装置の開発：マウスにおける ^{65}Zn、^{85}Sr、^{131}I 同時γ線イメージング”, 第 18 回日本微量元素学会, 福井, 7 月 (2007).

榎本秀一, 金山洋介, 榎本 (（五十嵐）) 香織, 羽場宏光: “にがり成分の生体内ダイナミクスと代謝吸収過程のイメージング (1) マルチトレーサー法による 1 型糖尿病モデルマウスの微量元素代謝：にがり投与による影響”, ソルト・サイエンス研究財団第 19 回平成 18 年度助成研究発表会, (財団法人ソルト・サイエンス研究財団), 東京, 7 月 (2007).

笠松良崇, 當銘勇人, 豊嶋厚史, 塚田和明, 浅井雅人, 石井康雄, 西中一朗, 佐藤哲也, 篠原伸夫, 永目諭一郎, 羽場宏光, 菊永英寿, 秋山和彦, 後藤真一, 石川剛, 工藤久昭, 佐藤渉, 大江一弘, 栗林隆宏, 篠原厚, 木下哲一, 荒井美和子, 横山明彦, 阪間稔, Qin Z., Duellmann C. E.: “105 番元素 Db の HF/HNO3 混合水溶液中における化学挙動”, 2007 日本放射化学会年会・第 51 回放射化学討論会, (日本放射化学会), 静岡, 9 月 (2007).

菊永英寿, 笠松良崇, 羽場宏光, 加治大哉, 森本幸司, 坂本一郎: “^{90m}Nb の半減期精密測定に向けたガスジェット搬送装置の開発と性能評価”, 2007 日本放射化学会年会・第 51 回放射化学討論会, 静岡, 9 月 (2007).

栗林隆宏, 大江一弘, 尾本隆志, 藤沢弘幸, 小森有希子, 高橋成人, 吉村崇, 羽場宏光, 榎本秀一, 三頭聰明, 篠原厚: “キャピラリー電気泳動の希土類の相互分離と短寿命核種への適用”, 2007 日本放射化学会年会・第 51 回放射化学討論会, (日本放射化学会), 静岡, 9 月 (2007).

南里朋洋, 荒木幹生, 鈴木大介, 木下哲一, 菊永英寿, 羽場宏光, 横山明彦: “超アクチニド元素溶液化学のための極微量濃度における逆相クロマトグラフィーの研究”, 2007 日本放射化学会年会・第 51 回放射化学討論会, (日本放射化学会), 静岡, 9 月 (2007).

市川 隆敏, 萩野 浩一, 岩本 昭: “Systematics of threshold incident energies for deep sub-barrier fusion hindrance in medium-heavy mass region”, 日本物理学会第 62 回年次大会, 札幌, 9 月 (2007).

金山洋介, 本村信治, 福地知則, 羽場宏光, 渡辺恭良, 榎本秀一: “複数分子同時イメージング法の開発と現状”, 分子イメージング研究シンポジウム 2008「社会のニーズに向けた分子イメージング研究の展開」, (理研，放射線医学総合研究所), 東京, 1 月 (2008).

Theoretical Nuclear Physics Laboratory

Oral Presentations

(Domestic Conference)

山上雅之: “低密度・強相関系の多核子ダイナミクス”, RIBF 理論研究推進会議拡大ワークショップ, 和光, 5 月 (2007).

中務孝: “原子核密度汎関数理論の発展”, 研究会「原子核物理学の将来像」, (京都大学), 京都, 8 月 (2007).

山上雅之: “変形した中性子過剰核における対相関と回転運動”, 日本物理学会第 62 回年次大会, 札幌, 9 月 (2007).

中務孝: “実時間解法による原子核光応答計算”, 九州大学理学部原子核セミナー, 福岡, 11 月 (2007).

中務孝: “原子核光応答の時間依存密度汎関数計算”, 第 4 回「停止・低速不安定核を用いた核分光研究」研究会, 仙台, 12 月 (2007).

山上雅之: “Isovector density dependence of pairing effective interaction and the influence on rotational excitations”, RIBF ミニワークショップ「2 核子相関と不安定原子核」, 和光, 12 月 (2007).

中務孝, 矢花一浩, 稲倉恒法, 日野原伸生, 松尾正之, 松柳研一: “密度汎関数アプローチによる原子核数値シミュレーション”, シンポジウム「未来の素粒子・原子核数値シミュレーション」, (高エネルギー加速器研究機構), つくば, 12 月 (2007).

山上雅之: “重い不安定核における新奇な集団励起の理論的探索”, シンポジウム「未来の素粒子・原子核数値シミュレーション」, (高エネルギー加速器研究機構), つくば, 12 月 (2007).

Experimental Installations Development Group

Publications

[Journal]

(Original Papers) *Subject to Peer Review

Ueno H., Kameda D., Nagae D., Takemura M., Asahi K., Takase K., Yoshimi A., Sugimoto T., Nagatomo T., Shimada K., Uchida M., Arai T., Inoue T., Murata J., Kawamura H., and Narota K.: "Nuclear-moment measurements at RIKEN and perspectives in RIBF", AIP Conf. Proc. **915**, 841–844 (2007). *

Ueno H., Kameda D., Nagae D., Takemura M., Asahi K., Arai T., Shimada K., Takase K., Sugimoto T., Nagatomo T., Uchida M., Inoue T., Yoshimi A., Kawamura H., and Narota K.: "Nuclear moments of neutron-rich aluminum isotopes", Eur. Phys. J. Special Topics **150**, 185–186 (2007). *

Morita K., Morimoto K., Kaji D., Akiyama T., Goto S., Haba H., Ideguchi E., Katori K., Koura H., Kudo H., Ohnishi T., Ozawa A., Suda T., Sueki K., Tokanai F., Yamaguchi T., Yoneda A., and Yoshida A.: "Experiment on synthesis of an isotope 277112 by 208Pb + 70Zn reaction", J. Phys. Soc. Jpn. **76**, No. 4, pp. 043201-1–043201-5 (2007). *

Morita K., Morimoto K., Kaji D., Akiyama T., Goto S., Haba H., Ideguchi E., Katori K., Koura H., Kikunaga H., Kudo H., Ohnishi T., Ozawa A., Sato N., Suda T., Sueki K., Tokanai F., Yamaguchi T., Yoneda A., and Yoshida A.: "Observation of second decay chain from 278113", J. Phys. Soc. Jpn. **76**, No. 4, pp. 045001-1–045001-2 (2007). *

Kameda D., Ueno H., Asahi K., Takemura M., Yoshimi A., Haseyama T., Uchida M., Shimada K., Nagae D., Kijima G., Arai T., Takase K., Suda S., Inoue T., Murata J., Kawamura H., Kobayashi Y., Watanabe H., and Ishihara M.: "Measurement of the electric quadrupole moment of ^{32}Al", Phys. Lett. B **647**, 93–97 (2007). *

Sugimoto T., Nakamura T., Kondo Y., Aoi N., Baba H., Bazin D. P., Fukuda N., Gomi T., Hasegawa H., Imai N., Ishihara M., Kobayashi T., Kubo T., Miura M., Motobayashi T., Otsu H., Saito A., Sakurai H., Shimoura S., Vinodkumar A. M., Watanabe K., Watanabe Y., Yakushiji T., Yanagisawa Y., and Yoneda K.: "The first 2^+ state of ^{14}Be", Phys. Lett. B **654**, 160–164 (2007). *

Sato W., Ueno H., Watanabe H., Miyoshi H., Yoshimi A., Kameda D., Ito T., Shimada K., Kaihara J., Suda S., Kobayashi Y., Shinohara A., Ohkubo Y., and Asahi K.: "Online time-differential perturbed angular correlation study with an ^{19}O beam Residence sites of oxygen atoms in highly oriented pyrolytic graphite", Nucl. Instrum. Methods Phys. Res. B **266**, 316–322 (2008). *

[Book•Proceedings]

(Original Papers) *Subject to Peer Review

Ueno H., Kameda D., Yoshimi A., Haseyama T., Asahi K., Takemura M., Kijima G., Shimada K., Nagae D., Uchida M., Arai T., Suda S., Takase K., Inoue T., and Kawamura H.: "Production of spin-oriented unstable nuclei via the projectile-fragmentation reaction", Polarized-Sources and Targets: Proceedings of the 11th International Workshop, Tokyo, 2005–11, World Scientific, Singapore, pp. 178–183 (2007).

Kameda D., Ueno H., Asahi K., Yoshimi A., Haseyama T., Kobayashi Y., Uchida M., Miyoshi H., Kijima G., Takemura M., Nagae D., Kato G., Emori S., Oshima S., Arai T., and Tsukui M.: "Production of spin-polarized RI beams via projectile fragmentation and the application to nuclear moment measurements", Polarized-Sources and Targets: Proceedings of the 11th International Workshop, Tokyo, 2005–11, World Scientific Publishing , Toh Tuck Link, pp. 211–212 (2007).

Kameda D., Ueno H., Asahi K., Takemura M., Nagae D., Shimada K., Yoshimi A., Kobayashi Y., Haseyama T., Uchida M., Takase K., Arai T., Inoue T., Suda S., Murata J., Kawamura H., Watanabe H., and Ishihara M.: "Nuclear moment measurements of Neutron-rich Aluminum Isotopes Using Spin-Polarized RI beams: Determination of the Boundary of the "Island of Inversion"", Proceedings of the 17th International Spin Physics Symposium (SPIN2006), Tokyo, 2006–10, American Institute of Physics, New York, pp. 845–848 (2007). *

Oral Presentations

(International Conference etc.)

Kawamura H., Hirayama Y., Kameda D., Murata J., Narota K., Shimoyama T., Suehiro T., Toyoda T., and Uchida M.: "A New Drift Chamber based Mott Polarimeter for T-violation experiment", International Nuclear Physics Conference (INPC2007), Tokyo, June (2007).

Ueno H., Nagae D., Kameda D., Takemura M., Asahi K., Takase K., Yoshimi A., Sugimoto T., Shimada K., Nagatomo T., Uchida M., Arai T., Inoue T., Murata J., Kawamura H., and Narota K.: "Electric quadrupole moment of ^{31}Al", International Nuclear Physics Conference (INPC2007), (Science Council of Japan, RIKEN and others), Tokyo, June (2007).

Murata J., Asahi K., Hirayama Y., Kameda D., Kawamura H., Nagae D., Narota K., Shimada K., Toyoda T., Uchida M., Ueno H., and Yoshimi A.: "T-Violating transverse electron polarization in polarized nuclear beta decay", International Nuclear Physics Conference (INPC2007), Tokyo, June (2007).

Kameda D., Ueno H., Asahi K., Yoshimi A., Haseyama T., Kobayashi Y., Ishihara M., Nagae D., Takemura M., Shimada K., Uchida M., Arai T., Takase K., Inoue T., Kijima G., Suda S., Murata J., Kawamura H., Narota K., Toyoda T., and Watanabe H.: "Electric quadrupole

moments of neutron-rich nuclei ^{32}Al and ^{31}Al", International Symposium & School on Frontiers and Perspectives of Nuclear and Hadron Physics (FPNH07), (Tokyo Institute of Technology), Tokyo, June (2007).

Sugimoto T., Asahi K., Kawamura H., Murata J., Nagae D., Shimada K., Ueno H., and Yoshimi A.: "Development of atomic-beam resonance method to measure the nuclear moments of unstable nuclei", 14th International Conference on Hyperfine Interactions and 18th International Symposium on Nuclear Quadrupole Interactions, (A Joint Argentina-Brazil organization), Foz do Iguacu, Brazil, Aug. (2007).

(Domestic Conference)

亀田大輔: "原子ビーム法による低速不安定核ビーム生成に向けた開発研究", RCNP 研究会「RCNP 入射サイクロトロン更新で展開される新しい研究」, 大阪, 2 月 (2007).

亀田大輔, 上野秀樹, 旭耕一郎, 竹村真, 吉見彰洋, 長谷山智仁, 内田誠, 島田健司, 長江大輔, 木島剛, 新井崇雅, 高瀬研以智, 須田紳一, 井上壮志, 村田次郎, 川村広和, 小林義男, 渡邉寛, 石原正泰: "中性子過剰核 32Al の核モーメント測定–魔法数 20 の閉殻構造の破れに関連して–", 日本物理学会 2007 年春季大会, 東京, 3 月 (2007).

杉本崇, 中村隆司, 近藤洋介, 青井考, 馬場秀忠, Bazin D., 福田直樹, 五味朋子, 長谷川浩一, 今井伸明, 石原正泰, 小林俊雄, 久保敏幸, 三浦元隆, 本林透, 大津秀暁, 齋藤明登, 櫻井博儀, 下浦享, Attukalathil V. M., 渡辺極之, 渡辺裕, 薬師寺崇, 柳澤善行, 米田健一郎: "核破砕反応を用いた ^{14}Be の不変質量核分光", 京都大学基礎物理学研究所セミナー, 京都, 4 月 (2007).

杉本崇, 中村隆司, 三浦元隆, 近藤洋介, Attukalathil V. M., 青井考, 馬場秀忠, 福田直樹, 五味朋子, 石原正泰, 久保敏幸, 本林透, 大津秀暁, 櫻井博儀, 柳澤善行, 米田健一郎, Bazin D., 長谷川浩一, 今井伸明, 渡辺裕, 小林俊雄, 渡辺極之, 薬師寺崇, 下浦享, 齋藤明登: "不安定核二次ビームを用いた ^{14}Be の不変質量核分光", SPring-8 加速器セミナー, (JASRI), 播磨, 7 月 (2007).

成田圭吾, 村田次郎, 川村広和, 豊田健司, 松多健策, 福田光順, 三原基嗣, 西村大樹, 小柴順治, 石川大貴, 亀田大輔: "時間反転対称性検証実験のための ^{8}Li の T1（スピン-格子緩和時間）と磁場依存性", 平成 19 年度京都大学原子炉実験所専門研究会「原子核プローブ生成とそれを用いた物性研究 (III)」, 大阪府熊取町, 11 月 (2007).

成田圭吾, 村田次郎, 川村広和, 豊田健司, 松多健策, 福田光順, 三原基嗣, 西村大樹, 小柴順治, 石川大貴, 亀田大輔, 平山賀一: "Development of a polarization holding stopper for a T-Violation experiment", 日本物理学会第 63 回年次大会, 東大阪, 3 月 (2008).

SLOWRI Team

Publications

[Journal]

(Original Papers) *Subject to Peer Review

Wada M., Ishida Y., Nakamura T., Kanai Y., Kojima T., Takamine A., Yamazaki Y., Okada K., Yoshida A., Kubo T., Katayama I., Ohtani S., Varentsov V., Wollnik H., Lioubimov V., and Schuessler H. A.: "Laser spectroscopy of trapped ^{7}Be and ^{10}Be at a prototype slow RI-beam facility of RIKEN", Hyperfine Interact. **173**, 153–163 (2006). *

Sonoda T., Fujita M., Yamazaki A., Endo T., Shinozuka T., Miyashita Y., Sato N., Goto A., Takano E., Suzuki T., Miyake T., Tanigaki M., and Wada M.: "Development of the RF-IGISOL at CYRIC", Nucl. Instrum. Methods Phys. Res. B **254**, 295–299 (2007). *

Okada K., Yasuda K., Takayanagi T., Wada M., Schuessler H. A., and Ohtani S.: "Crystallization of Ca^{+} ions in a linear rf octupole ion trap", Phys. Rev. A **75**, No. 3, pp. 033409-1–033409-10 (2007). *

Polarized RI Beam Team

Publications

[Journal]

(Original Papers) *Subject to Peer Review

Ueno H., Kameda D., Nagae D., Takemura M., Asahi K., Takase K., Yoshimi A., Sugimoto T., Nagatomo T., Arai T., Uchida M., Shimada K., Inoue T., Murata J., Kawamura H., and Narota K.: "Measurement of nuclear moments at RIKEN", AIP Conf. Proc. **891**, 113–121 (2007). *

Ueno H., Kameda D., Nagae D., Takemura M., Asahi K., Takase K., Yoshimi A., Sugimoto T., Nagatomo T., Shimada K., Uchida M., Arai T., Inoue T., Murata J., Kawamura H., and Narota K.: "Nuclear-moment measurements at RIKEN and perspectives in RIBF", AIP Conf. Proc. **915**, 841–844 (2007). *

Ueno H., Kameda D., Nagae D., Takemura M., Asahi K., Arai T., Shimada K., Takase K., Sugimoto T., Nagatomo T., Uchida M., Inoue T., Yoshimi A., Kawamura H., and Narota K.: "Nuclear moments of neutron-rich aluminum isotopes", Eur. Phys. J. Special Topics **150**, 185–186 (2007). *

Sato W., Ueno H., Taniguchi A., Itsuki Y., Kasamatu Y., Shinohara A., Asahi K., and Ohkubo Y.: "Time-dependent quadrupole interactions for ^{140}Ce ions implanted in highly oriented pyrolytic graphite", J. Radioanal. Nucl. Chem. **272**, 665–668 (2007). *

Kameda D., Ueno H., Asahi K., Takemura M., Yoshimi A., Haseyama T., Uchida M., Shimada K., Nagae D., Kijima G., Arai T., Takase K., Suda S., Inoue T., Murata J., Kawamura H., Kobayashi Y., Watanabe H., and Ishihara M.: "Measurement of the electric quadrupole moment of ^{32}Al", Phys. Lett. B **647**, 93–97 (2007). *

Sugimoto T., Nakamura T., Kondo Y., Aoi N., Baba H., Bazin D. P., Fukuda N., Gomi T., Hasegawa H., Imai N., Ishihara M., Kobayashi T., Kubo T., Miura M., Motobayashi T., Otsu H., Saito A., Sakurai H., Shimoura S., Vinodkumar A. M., Watanabe K., Watanabe Y., Yakushiji T., Yanagisawa Y., and Yoneda K.: "The first 2^+ state of ^{14}Be", Phys. Lett. B **654**, 160–164 (2007). *

Fujita H., Fujita Y., Adachi T., Bacher A. D., Berg G. P., Black T. C., Caurier E., Foster ., Fujimura H., Hara K., Harada K., Hatanaka K., Janecke J., Kamiya J., Kanzaki Y., Katori K., Kawabata T., Langanke K., Martinez-Pinedo G., Noro T., Robers D. A., Sakaguchi H., Shimbara Y., Shinada T., Stephenson E. J., Ueno H., Yamanaka T., Yoshifuku M., and Yosoi M.: "Isospin structure of $J^\pi = 1^+$ states in ^{58}Ni and ^{58}Cu studied by ^{58}Ni(p, p') and ^{58}Ni(^{3}He,t)^{58}Cu measurements", Phys. Rev. C **75**, 034310-1–034310-15 (2007). *

Notani M., Sakurai H., Aoi N., Iwasaki H., Fukuda N., Liu Z., Yoneda K., Ogawa H., Teranishi T., Nakamura T., Okuno H., Yoshida A., Watanabe Y., Momota S., Inabe N., Kubo T., Ito S., Ozawa A., Suzuki T., Tanihata I., and Ishihara M.: "Projectile fragmentation reaction and production of nuclei near the neutron drip line", Phys. Rev. C **76**, 044605-1–044605-15 (2007). *

Sato W., Ueno H., Watanabe H., Miyoshi H., Yoshimi A., Kameda D., Ito T., Shimada K., Kaihara J., Suda S., Kobayashi Y., Shinohara A., Ohkubo Y., and Asahi K.: "Online time-differential perturbed angular correlation study with an ^{19}O beam Residence sites of oxygen atoms in highly oriented pyrolytic graphite", Nucl. Instrum. Methods Phys. Res. B **266**, 316–322 (2008). *

[Book•Proceedings]

(Original Papers) *Subject to Peer Review

Ueno H., Kameda D., Yoshimi A., Haseyama T., Asahi K., Takemura M., Kijima G., Shimada K., Nagae D., Uchida M., Arai T., Suda S., Takase K., Inoue T., and Kawamura H.: "Production of spin-oriented unstable nuclei via the projectile-fragmentation reaction", Polarized-Sources and Targets: Proceedings of the 11th International Workshop, Tokyo, 2005–11, World Scientific, Singapore, pp. 178–183 (2007).

Kameda D., Ueno H., Asahi K., Yoshimi A., Haseyama T., Kobayashi Y., Uchida M., Miyoshi H., Kijima G., Takemura M., Nagae D., Kato G., Emori S., Oshima S., Arai T., and Tsukui M.: "Production of spin-polarized RI beams via projectile fragmentation and the application to nuclear moment measurements", Polarized-Sources and Targets: Proceedings of the 11th International Workshop, Tokyo, 2005–11, World Scientific Publishing , Toh Tuck Link, pp. 211–212 (2007).

Kameda D., Ueno H., Asahi K., Takemura M., Nagae D., Shimada K., Yoshimi A., Kobayashi Y., Haseyama T., Uchida M., Takase K., Arai T., Inoue T., Suda S., Murata J., Kawamura H., Watanabe H., and Ishihara M.: "Nuclear moment measurements of Neutron-rich Aluminum Isotopes Using Spin-Polarized RI beams: Determination of the Boundary of the "Island of Inversion"", Proceedings of the 17th International Spin Physics Symposium (SPIN2006), Tokyo, 2006–10, American Institute of Physics, New York, pp. 845–848 (2007). *

Oral Presentations

(International Conference etc.)

Ueno H.: "Status of RI Beam Factory Project at RIKEN", 9th International Spring Seminar on Nuclear Physics, Challenges Facets of Nuclear Structure, Vico Equense, Italy, May (2007).

Kawamura H., Hirayama Y., Kameda D., Murata J., Narota K., Shimoyama T., Suehiro T., Toyoda T., and Uchida M.: "A New Drift Chamber based Mott Polarimeter for T-violation experiment", International Nuclear Physics Conference (INPC2007), Tokyo, June (2007).

Ueno H., Nagae D., Kameda D., Takemura M., Asahi K., Takase K., Yoshimi A., Sugimoto T., Shimada K., Nagatomo T., Uchida M., Arai T., Inoue T., Murata J., Kawamura H., and Narota K.: "Electric quadrupole moment of ^{31}Al", International Nuclear Physics Conference (INPC2007), (Science Council of Japan, RIKEN and others), Tokyo, June (2007).

Shimada K., Nagae D., Asahi K., Takemura M., Arai T., Inoue T., Takase K., Kagami S., Hatakeyama N., Kobayashi Y., Ueno H., Yoshimi A., Kameda D., Nagatomo T., Sugimoto T., Kubono S., Yamaguchi H., Wakabayashi Y., Amadio G., Hayakawa S., Murata J., and Kawamura H.: "First production of spin-polarized radioactive nuclear beam with CRIB", International Nuclear Physics Conference (INPC2007), Tokyo, June (2007).

Murata J., Asahi K., Hirayama Y., Kameda D., Kawamura H., Nagae D., Narota K., Shimada K., Toyoda T., Uchida M., Ueno H., and Yoshimi A.: "T-Violating transverse electron polarization in polarized nuclear beta decay", International Nuclear Physics Conference (INPC2007), Tokyo, June (2007).

Kameda D., Ueno H., Asahi K., Yoshimi A., Haseyama T., Kobayashi Y., Ishihara M., Nagae D., Takemura M., Shimada K., Uchida M., Arai T., Takase K., Inoue T., Kijima G., Suda S., Murata J., Kawamura H., Narota K., Toyoda T., and Watanabe H.: "Electric quadrupole moments of neutron-rich nuclei ^{32}Al and ^{31}Al", International Symposium & School on Frontiers and Perspectives of Nuclear and Hadron Physics (FPNH07), (Tokyo Institute of Technology), Tokyo, June (2007).

Ueno H.: "Nuclear-moment measurements of light neutron-rich nuclei utilizing fragment-induced spin-polarization and its applications", International Workshop on Nuclear Structure: New Pictures in the Extended Isospin Space (NS07), Kyoto, June (2007).

Ueno H.: "RI Beam Factory Project at RIKEN and Physics Programme on this Facility", Advanced Studies Institute: Symmetries and Spin (SPIN-Praha-2007), Prague, Czech, July (2007).

Sugimoto T., Asahi K., Kawamura H., Murata J., Nagae D., Shimada K., Ueno H., and Yoshimi A.: "Development of atomic-beam resonance method to measure the nuclear moments of unstable nuclei", 14th International Conference on Hyperfine Interactions and 18th International Symposium on Nuclear Quadrupole Interactions, (A Joint Argentina-Brazil organization), Foz do Iguacu, Brazil, Aug. (2007).

Ueno H.: "Radioactive-Isotope Beam Factory Project at RIKEN", 2007 Korean Physical Society Meeting, Jeju, Korea, Oct. (2007).

(Domestic Conference)

亀田大輔, 上野秀樹, 旭耕一郎, 竹村真, 吉見彰洋, 長谷山智仁, 内田誠, 島田健司, 長江大輔, 木島剛, 新井崇雅, 高瀬研以智, 須田紳一, 井上壮志, 村田次郎, 川村広和, 小林義男, 渡邉寛, 石原正泰: "中性子過剰核 32Al の核モーメント測定–魔法数 20 の閉殻構造の破れに関連して–", 日本物理学会 2007 年春季大会, 東京, 3 月 (2007).

藤掛浩太郎, 古川武, 松尾由賀利, 畠山温, 伊藤龍浩, 佐々木彩子, 小林徹, 下田正: "超流動ヘリウム中におけるアルカリ金属 Rb,Cs 原子の超微細構造精密測定", 原子・分子・光科学 (AMO) 第 4 回討論会, 東京, 6 月 (2007).

杉本崇, 中村隆司, 三浦元隆, 近藤洋介, Attukalathil V. M., 青井考, 馬場秀忠, 福田直樹, 五味朋子, 石原正泰, 久保敏幸, 本林透, 大津秀暁, 櫻井博儀, 柳澤善行, 米田健一郎, Bazin D., 長谷川浩一, 今井伸明, 渡辺裕, 小林俊雄, 渡辺極之, 薬師寺崇, 下浦享, 齋藤明登: "不安定核二次ビームを用いた ^{14}Be の不変質量核分光", SPring-8 加速器セミナー, (JASRI), 播磨, 7 月 (2007).

藤掛浩太郎, 古川武, 松尾由賀利, 畠山温, 佐々木彩子, 小林徹, 小田島仁司, 下田正: "超流動ヘリウム中における原子の超微細構造 II：気体 Rb を用いた共鳴周波数校正", 日本物理学会第 62 回年次大会, 札幌, 9 月 (2007).

古川武, 松尾由賀利, 畠山温, 伊藤龍浩, 藤掛浩太郎, 佐々木彩子, 小林徹, 下田正: "超流動ヘリウム中での RI 原子のレーザー分光実験における光収量計算", 日本物理学会第 62 回年次大会, 札幌, 9 月 (2007).

成田圭吾, 村田次郎, 川村広和, 豊田健司, 松多健策, 福田光順, 三原基嗣, 西村大樹, 小柴順治, 石川大貴, 亀田大輔: "時間反転対称性検証実験のための ^{8}Li の T1（スピン-格子緩和時間）と磁場依存性", 平成 19 年度京都大学原子炉実験所専門研究会「原子核プローブ生成とそれを用いた物性研究 (III)」, 大阪府熊取町, 11 月 (2007).

佐々木彩子, 古川武, 藤掛浩太郎, 小林徹, 畠山温, 下田正, 小田島仁司, 松尾由賀利: "超流動ヘリウム中における In 原子の励起スペクトル：光ポンピング実現をめざして", 第 4 回「停止・低速不安定核を用いた核分光研究」研究会, 仙台, 12 月 (2007).

古川武, 畠山温, 藤掛浩太郎, 佐々木彩子, 小林徹, 下田正, 松尾由賀利: "OROCHI オンライン実験計画とその物理", 第 4 回「停止・低速不安定核を用いた核分光研究」研究会, 仙台, 12 月 (2007).

成田圭吾, 村田次郎, 川村広和, 豊田健司, 松多健策, 福田光順, 三原基嗣, 西村大樹, 小柴順治, 石川大貴, 亀田大輔, 平山賀一: "Development of a polarization holding stopper for a T-Violation experiment", 日本物理学会第 63 回年次大会, 東大阪, 3 月 (2008).

Experimental Installations Operation Group

Publications

[Journal]

(Original Papers) *Subject to Peer Review

Wada M., Ishida Y., Nakamura T., Kanai Y., Kojima T., Takamine A., Yamazaki Y., Okada K., Yoshida A., Kubo T., Katayama I., Ohtani S., Varentsov V., Wollnik H., Lioubimov V., and Schuessler H. A.: "Laser spectroscopy of trapped ^{7}Be and ^{10}Be at a prototype slow RI-beam facility of RIKEN", Hyperfine Interact. **173**, 153–163 (2006). *

Sekiguchi K., Sakai H., Sakamoto N., Kuboki H., Sasano M., Takahashi Y., Yako K., Kawabata T., Maeda Y., Sakaguchi S., Sasamoto Y., Suda K., Uesaka T., Okamura H., Itoh K., and Wakasa T.: "Study of Spin Parts of Three Nucleon Forces via $\vec{d}p$ Breakup Reactions at Intermediate Energies", Nucl. Phys. A **790**, 450c–453c (2007). *

Gibelin J. D., Beaumel D., Motobayashi T., Aoi N., Baba H., Blumenfeld Y., Dombradi Z., Elekes Z., Fortier S., Frascaria N., Fukuda N., Gomi T., Ishikawa K., Kondo Y., Kubo T., Lima V., Nakamura T., Saito A., Sato Y., Takeshita E., Takeuchi S., Teranishi T., Togano Y., Vinodkumar A. M., Yanagisawa Y., and Yoshida A.: "Measurement of the B(E2, $0_1^+ \rightarrow 2_1^+$) in the N = 16 nucleus ^{26}Ne", Phys. Rev. C **75**, 057301-1–057391-4 (2007). *

Oral Presentations

(Domestic Conference)

杉本崇, 中村隆司, 近藤洋介, 青井考, 馬場秀忠, Bazin D., 福田直樹, 五味朋子, 長谷川浩一, 今井伸明, 石原正泰, 小林俊雄, 久保敏幸, 三浦元隆, 本林透, 大津秀暁, 齋藤明登, 櫻井博儀, 下浦享, Attukalathil V. M., 渡辺極之, 渡辺裕, 薬師寺崇, 柳澤善行, 米田健一郎: "核破砕反応を用いた ^{14}Be の不変質量核分光", 京都大学基礎物理学研究所セミナー, 京都, 4 月 (2007).

杉本崇, 中村隆司, 三浦元隆, 近藤洋介, Attukalathil V. M., 青井考, 馬場秀忠, 福田直樹, 五味朋子, 石原正泰, 久保敏幸, 本林透, 大津秀暁, 櫻井博儀, 柳澤善行, 米田健一郎, Bazin D., 長谷川浩一, 今井伸明, 渡辺裕, 小林俊雄, 渡辺極之, 薬師寺崇, 下浦享, 齋藤明登: "不安定核二次ビームを用いた ^{14}Be の不変質量核分光", SPring-8 加速器セミナー, (JASRI), 播磨, 7 月 (2007).

BigRIPS Team

Publications

[Journal]

(Original Papers) *Subject to Peer Review

Wada M., Ishida Y., Nakamura T., Kanai Y., Kojima T., Takamine A., Yamazaki Y., Okada K., Yoshida A., Kubo T., Katayama I., Ohtani S., Varentsov V., Wollnik H., Lioubimov V., and Schuessler H. A.: "Laser spectroscopy of trapped ^{7}Be and ^{10}Be at a prototype slow RI-beam facility of RIKEN", Hyperfine Interact. **173**, 153–163 (2006). *

Sugimoto T., Nakamura T., Fukuda N., Miura M., Kondo Y., Aoi N., Baba H., Bazin D., Gomi T., Hasegawa H., Hashimoto Y., Imai N., Kobayashi T., Kubo T., Motobayashi T., Ohara M., Saito A., Sakurai H., Shimoura S., Attukalathil V. M., Watanabe K., Watanabe Y., Yakushiji T., Yanagisawa Y., Yoneda K., and Ishihara M.: "Invariant-mass spectroscopy of the neutron-drip line nucleus ^{14}Be", J. Phys.: Con. Ser. **49**, 43–44 (2006). *

Morita K., Morimoto K., Kaji D., Akiyama T., Goto S., Haba H., Ideguchi E., Katori K., Koura H., Kudo H., Ohnishi T., Ozawa A., Suda T., Sueki K., Tokanai F., Yamaguchi T., Yoneda A., and Yoshida A.: "Experiment on synthesis of an isotope 277112 by 208Pb + 70Zn reaction", J. Phys. Soc. Jpn. **76**, No. 4, pp. 043201-1–043201-5 (2007). *

Morita K., Morimoto K., Kaji D., Akiyama T., Goto S., Haba H., Ideguchi E., Katori K., Koura H., Kikunaga H., Kudo H., Ohnishi T., Ozawa A., Sato N., Suda T., Sueki K., Tokanai F., Yamaguchi T., Yoneda A., and Yoshida A.: "Observation of second decay chain from 278113", J. Phys. Soc. Jpn. **76**, No. 4, pp. 045001-1–045001-2 (2007). *

Kameda D., Ueno H., Asahi K., Takemura M., Yoshimi A., Haseyama T., Uchida M., Shimada K., Nagae D., Kijima G., Arai T., Takase K., Suda S., Inoue T., Murata J., Kawamura H., Kobayashi Y., Watanabe H., and Ishihara M.: "Measurement of the electric quadrupole moment of ^{32}Al", Phys. Lett. B **647**, 93–97 (2007). *

Sugimoto T., Nakamura T., Kondo Y., Aoi N., Baba H., Bazin D. P., Fukuda N., Gomi T., Hasegawa H., Imai N., Ishihara M., Kobayashi T., Kubo T., Miura M., Motobayashi T., Otsu H., Saito A., Sakurai H., Shimoura S., Vinodkumar A. M., Watanabe K., Watanabe Y., Yakushiji T., Yanagisawa Y., and Yoneda K.: "The first 2^{+} state of ^{14}Be", Phys. Lett. B **654**, 160–164 (2007). *

Gibelin J. D., Beaumel D., Motobayashi T., Aoi N., Baba H., Blumenfeld Y., Dombradi Z., Elekes Z., Fortier S., Frascaria N., Fukuda N., Gomi T., Ishikawa K., Kondo Y., Kubo T., Lima V., Nakamura T., Saito A., Sato Y., Takeshita E., Takeuchi S., Teranishi T., Togano Y., Vinodkumar A. M., Yanagisawa Y., and Yoshida A.: "Measurement of the B(E2, $0_1^+ \rightarrow 2_1^+$) in the N = 16 nucleus ^{26}Ne", Phys. Rev. C **75**, 057301-1–057391-4 (2007). *

Notani M., Sakurai H., Aoi N., Iwasaki H., Fukuda N., Liu Z., Yoneda K., Ogawa H., Teranishi T., Nakamura T., Okuno H., Yoshida A., Watanabe Y., Momota S., Inabe N., Kubo T., Ito S., Ozawa A., Suzuki T., Tanihata I., and Ishihara M.: "Projectile fragmentation reaction and production of nuclei near the neutron drip line", Phys. Rev. C **76**, 044605-1–044605-15 (2007). *

[Book•Proceedings]

(Original Papers) *Subject to Peer Review

Ueno H., Kameda D., Yoshimi A., Haseyama T., Asahi K., Takemura M., Kijima G., Shimada K., Nagae D., Uchida M., Arai T., Suda S., Takase K., Inoue T., and Kawamura H.: "Production of spin-oriented unstable nuclei via the projectile-fragmentation reaction", Polarized-Sources and Targets: Proceedings of the 11th International Workshop, Tokyo, 2005–11, World Scientific, Singapore, pp. 178–183 (2007).

Kameda D., Ueno H., Asahi K., Yoshimi A., Haseyama T., Kobayashi Y., Uchida M., Miyoshi H., Kijima G., Takemura M., Nagae D., Kato G., Emori S., Oshima S., Arai T., and Tsukui M.: "Production of spin-polarized RI beams via projectile fragmentation and the application to nuclear moment measurements", Polarized-Sources and Targets: Proceedings of the 11th International Workshop, Tokyo, 2005–11, World Scientific Publishing , Toh Tuck Link, pp. 211–212 (2007).

Kameda D., Ueno H., Asahi K., Takemura M., Nagae D., Shimada K., Yoshimi A., Kobayashi Y., Haseyama T., Uchida M., Takase K., Arai T., Inoue T., Suda S., Murata J., Kawamura H., Watanabe H., and Ishihara M.: "Nuclear moment measurements of Neutron-rich Aluminum Isotopes Using Spin-Polarized RI beams: Determination of the Boundary of the "Island of Inversion"", Proceedings of the 17th International Spin Physics Symposium (SPIN2006), Tokyo, 2006–10, American Institute of Physics, New York, pp. 845–848 (2007). *

Oral Presentations

(International Conference etc.)

Sugimoto T., Nakamura T., Fukuda N., Miura M., Kondo Y., Aoi N., Baba H., Bazin D., Gomi T., Hasegawa H., Hashimoto Y., Imai N., Kobayashi T., Kubo T., Motobayashi T., Ohara M., Saito A., Sakurai H., Shimoura S., Attukalathil V. M., Watanabe K., Watanabe Y., Yakushiji T., Yanagisawa Y., Yoneda K., and Ishihara M.: "Invariant-mass spectroscopy of the neutron-drip line nucleus ^{14}Be", International Symposium on Structure of Exotic Nuclei and Nuclear Forces (SENUF06), (CNS and RIKEN), Tokyo, Mar. (2006).

Yoshida A., Suda T., Ohtsuki T., Yuki H., and Kubo T.:

"Status and overview of production target for BigRIPS separator at RIKEN", 23rd World Conference of the INTDS, (KEK), Tsukuba, Oct. (2006).

Kameda D., Ueno H., Asahi K., Yoshimi A., Haseyama T., Kobayashi Y., Ishihara M., Nagae D., Takemura M., Shimada K., Uchida M., Arai T., Takase K., Inoue T., Kijima G., Suda S., Murata J., Kawamura H., Narota K., Toyoda T., and Watanabe H.: "Electric quadrupole moments of neutron-rich nuclei ^{32}Al and ^{31}Al", International Symposium & School on Frontiers and Perspectives of Nuclear and Hadron Physics (FPNH07), (Tokyo Institute of Technology), Tokyo, June (2007).

Morita K., Morimoto K., Kaji D., Akiyama T., Goto S., Haba H., Ideguchi E., Kanungo R., Katori K., Kikunaga H., Koura H., Kudo H., Ohnishi T., Ozawa A., Sato N., Suda T., Sueki K., Tokanai F., Xu H., Yamaguchi T., Yoneda A., Yoshida A., and YuLiang Z.: "Experiment on searching for the heaviest elements at RIKEN", 3rd International Conference on the Chemistry and Physics of the Transactinide Elements (TAN 07), (Paul Scherrer Institut and Bern University), Davos, Switzerland, Sept. (2007).

(Domestic Conference)

亀田大輔, 上野秀樹, 旭耕一郎, 竹村真, 吉見彰洋, 長谷山智仁, 内田誠, 島田健司, 長江大輔, 木島剛, 新井崇雅, 高瀬研以智, 須田紳一, 井上壮志, 村田次郎, 川村広和, 小林義男, 渡邉寛, 石原正泰: "中性子過剰核 32Al の核モーメント測定– 魔法数 20 の閉殻構造の破れに関連して–", 日本物理学会 2007 年春季大会, 東京, 3 月 (2007).

杉本崇, 中村隆司, 近藤洋介, 青井考, 馬場秀忠, Bazin D., 福田直樹, 五味朋子, 長谷川浩一, 今井伸明, 石原正泰, 小林俊雄, 久保敏幸, 三浦元隆, 本林透, 大津秀暁, 齋藤明登, 櫻井博儀, 下浦享, Attukalathil V. M., 渡辺極之, 渡辺裕, 薬師寺崇, 柳澤善行, 米田健一郎: "核破砕反応を用いた ^{14}Be の不変質量核分光", 京都大学基礎物理学研究所セミナー, 京都, 4 月 (2007).

杉本崇, 中村隆司, 三浦元隆, 近藤洋介, Attukalathil V. M., 青井考, 馬場秀忠, 福田直樹, 五味朋子, 石原正泰, 久保敏幸, 本林透, 大津秀暁, 櫻井博儀, 柳澤善行, 米田健一郎, Bazin D., 長谷川浩一, 今井伸明, 渡辺裕, 小林俊雄, 渡辺極之, 薬師寺崇, 下浦享, 齋藤明登: "不安定核二次ビームを用いた ^{14}Be の不変質量核分光", SPring-8 加速器セミナー, (JASRI), 播磨, 7 月 (2007).

Detector Team

Publications

[Journal]

(Original Papers) *Subject to Peer Review

有吉誠一郎, 大谷知行, Dobroiu A., 松尾宏, 佐藤広海, 田井野徹, 川瀬晃道, 清水裕彦: “超伝導検出器アレイを用いたテラヘルツイメージング”, 信学技報, No. ED2006-194(2006-12), pp. 59–63 (2006).

User Liaison and Support Group

Publications

[Journal]

(Original Papers) *Subject to Peer Review

Morita K., Morimoto K., Kaji D., Akiyama T., Goto S., Haba H., Ideguchi E., Katori K., Koura H., Kudo H., Ohnishi T., Ozawa A., Suda T., Sueki K., Tokanai F., Yamaguchi T., Yoneda A., and Yoshida A.: "Experiment on synthesis of an isotope 277112 by 208Pb + 70Zn reaction", J. Phys. Soc. Jpn. **76**, No. 4, pp. 043201-1–043201-5 (2007). *

Morita K., Morimoto K., Kaji D., Akiyama T., Goto S., Haba H., Ideguchi E., Katori K., Koura H., Kikunaga H., Kudo H., Ohnishi T., Ozawa A., Sato N., Suda T., Sueki K., Tokanai F., Yamaguchi T., Yoneda A., and Yoshida A.: "Observation of second decay chain from 278113", J. Phys. Soc. Jpn. **76**, No. 4, pp. 045001-1–045001-2 (2007). *

Oral Presentations

(International Conference etc.)

Yoshida A., Suda T., Ohtsuki T., Yuki H., and Kubo T.: "Status and overview of production target for BigRIPS separator at RIKEN", 23rd World Conference of the INTDS, (KEK), Tsukuba, Oct. (2006).

Experiment Support Team

Oral Presentations

(Domestic Conference)

竹久妃奈子, 林依子, 風間裕介, 神波千秋, 市田裕之, 龍頭啓充, 福西暢尚, 宮沢豊, 東海林英夫, 佐藤雅志, 阿部知子: “炭素イオン照射により誘導した、シワ-矮性イネ突然変異株 (*ssw*) の特性解析”, 日本育種学会第 112 回講演会, 鶴岡, 9 月 (2007).

神波千秋, 竹久妃奈子, 林依子, 市田裕之, 小沼亮子, 龍頭啓充, 福西暢尚, 宮沢豊, 東海林英夫, 保倉明子, 福田直樹, 中井泉, 阿部知子, 佐藤雅志: “イネ塩害耐性突然変異体 6-99L の耐塩性に関わる生理要因の解明”, 第 224 回日本作物学会講演会, 金沢, 9 月 (2007).

Industrial Cooperation Team

Publications

[Journal]

(Original Papers) *Subject to Peer Review

Takeichi H., Koyama S., Matani A., and Cichocki A.: "Speech comprehension assessed by electroencephalography: a new method using m-sequence modulation", Neurosci. Res. **57**, No. 2, pp. 314–318 (2007). *

(Others)

Takeichi H., Koyama S., Matani A., and Cichocki A.: "Speech comprehension assessed by electroencephalography with m-sequence technique", Int. Congr. Ser. **1301**, 83–86 (2007).

竹市博臣: "時限研究会「ブレインネットワークコミュニケーション研究会」実施報告", 日本神経回路学会誌 **14**, No. 3, pp. 245–247 (2007).

竹市博臣: "時限研究会「ブレインネットワークコミュニケーション研究会」第 2 回実施報告", 日本神経回路学会誌 **14**, No. 4, pp. 326–327 (2007).

竹市博臣, 小山幸子, 眞溪歩, Cichocki A.: "m系列変調法による脳波計測：談話理解を例として", 物性研究 **87**, No. 4, pp. 608–610 (2007).

Oral Presentations

(International Conference etc.)

Takeichi H. and Koyama S.: "A study of scene perception and perceptual interaction by multiple bistability: shading-lighting", Cognitive Neuroscience Society 2006 Annual Meeting, San Francisco, USA, Apr. (2006).

Koyama S., Toyomaki A., Matsumoto H., Matsui M. F., Takeichi H., and Morotomi T.: "Auditory event-related brain potentials elicited by short gaps embedded in a continuous sound and by brief tones: a developmental study", Cognitive Neuroscience Society 2006 Annual Meeting, San Francisco, USA, Apr. (2006).

Takeichi H.: "On the computational elements of visual surface perception", The Vision Sciences Society Meeting, (Vision Sciences Society), Sarasota, USA, May (2006).

Takeichi H., Koyama S., Kimura M., Matsumoto H., Inoue Y., and Morotomi T.: "Visually evoked brain potentials associated with volumetric completion", 36th Annual Meeting of Society for Neuroscience (Neuroscience 2006), Atlanta, USA, Oct. (2006).

Takeichi H., Koyama S., Matsumoto H., Morotomi T., and Cichocki A.: "Assessment of Speech Comprehension: Applications of M-Sequence Modulation and Independent Component Analysis to Electroencephalography", 10th Tamagawa-RIKEN Dynamic Brain Forum (DBF '07), Hakuba, Mar. (2007).

Takeichi H., Koyama S., and Cichocki A.: "Measuring sentence processing by electroencephalography (EEG): new technique using m-sequence modulation", 2007 IEEE/ICME International Conference on Complex Medical Engineering, (Institute of Complex Medical Engineering), Beijing, China, May (2007).

Takeichi H., Koyama S., and Cichocki A.: "A frequency analysis of EEG response to speech modulated by m-sequence", Cognitive Neuroscience Society (CNS) 2007 Annual Meeting, New York, USA, May (2007).

Takeichi H., Takeuchi F., Terao A., Toyosawa Y., and Koyama S.: "Brain areas responsible for the intelligibility-dependent signal with 400ms latency in the m-sequence EEG technique as identified with fMRI", 7th IBRO World Congress of Neuroscience (IBRO 2007), Melbourne, Australia, July (2007).

Takeichi H. and Koyama S.: "A coherence analysis of EEG responses to spoken sentences with and without m-sequence modulation", 37th Annual Meeting of Society for Neuroscience (Neuroscience 2007), San Diego, USA, Nov. (2007).

Takeichi H. and Koyama S.: "Assessment of speech comprehension by a random probing technique", Kyushu University 21st Century COE Program 2nd International Symposium on Design of Artificial Environments, (Kyushu University), Fukuoka, Nov.–Dec. (2007).

Koyama S., Matsumoto H., Arai K., Toyomaki A., Morotomi T., and Takeichi H.: "Auditory event-related brain potentials to short temporal gaps: A developmental study", Kyushu University 21st Century COE Program 2nd International Symposium on Design of Artificial Environments, (Kyushu University), Fukuoka, Nov.–Dec. (2007).

(Domestic Conference)

竹市博臣, 竹内文也, 寺尾敦, 豊澤悠子, 小山幸子: "M系列変調法を用いた談話理解評価に関係する脳領野の fMRI による同定", 第 12 回認知神経科学会学術集会, 福岡, 7 月 (2007).

竹市博臣, 小山幸子, Cichocki A., Foster B. L., Liley D.: "An EEG-coherence analysis of fMRI data on speech comprehension", 平成 19 年度文部科学省特定領域研究「統合脳」夏のワークショップサテライトシンポジウム/「脳と心のメカニズム」第 8 回夏のワークショップ「運動と行動」, (文部科学省特定領域研究（C）統合脳，理研 BSI、他), 札幌, 8–8 月 (2007).

竹市博臣, 小山幸子, Cichocki A.: "Correlation analysis of scalp EEG responses to spoken sentences modulated by M-sequence", 第 30 回日本神経科学大会・第 50 回日本神経化学会大会・第 17 回日本神経回路学会大会 (Neuro2007), 横浜, 9 月 (2007).

松本秀彦, 諸冨隆, 豊巻敦人, 小山幸子, 竹市博臣: "連続音中の短い無音部に対する中枢聴覚処理の特徴：小・中・高生における発達変化", 日本心理学会第 71 回大会, 東京, 9 月 (2007).

竹市博臣, 小山幸子, 松本秀彦, 諸冨隆: "聴覚野におけるリアルタイム音声言語（談話）処理の脳波を用いた検討", 日本心理学会第 71 回大会, 東京, 9 月 (2007).

竹市博臣, 寺尾敦, 竹内文也, 小山幸子, 豊澤悠子, 室橋春光: "ランダムプローブ法による談話理解の客観的評価：fMRI 研究", 第 87 回北海道医学大会生体医工学分科会・第 46 回

日本生体医工学会北海道支部大会, 札幌, 9 月 (2007).

竹市博臣: “ランダムプローブ法と談話理解の脳内機構”, 第 37 回日本臨床神経生理学会・学術大会，第 44 回日本臨床神経生理学会・技術講習会, 宇都宮, 11 月 (2007).

松本秀彦, 豊巻敦人, 小山幸子, 竹市博臣, 諸冨隆: “音の持続呈示中の無音部に対する中枢聴覚処理の発達的特徴 (2)”, 第 37 回日本臨床神経生理学会・学術大会，第 44 回日本臨床神経生理学会・技術講習会, 宇都宮, 11–11 月 (2007).

竹市博臣, 小山幸子: “リアルタイム音声言語（談話）処理の脳波を用いた検討：非線形解析”, 平成 19 年度文部科学省特定領域研究「統合脳」脳と心のメカニズム第 8 回冬のワークショップ「Social Brain」, 留寿都, 1 月 (2008).

竹市博臣, 竹内文也, 寺尾敦, 小山幸子, 室橋春光: “m系列変調（劣化）音声に対する fMRI 応答（2）”, 脳機能解析学分野第 2 回シンポジウム, (北海道大学医学部), 札幌, 1 月 (2008).

竹市博臣, 小山幸子, 竹内文也, 松本秀彦, 諸冨隆: “言語理解に関する脳信号処理技術”, IIP2008 日本機械学会情報・知能・精密機器部門（IIP 部門）講演会, 東京, 3 月 (2008).

Sub Nuclear System Research Division

Oral Presentations

(International Conference etc.)

Iio M., Ajimura S., Beer G., Bhang H., Buehler P., Busso L., Cargnelli M., Chiba J., Choi S., Curceanu C., Faso D., Fujioka H., Fukuda T., Fukuda Y., Guaraldo C., Hanaki T., Hayano R. S., Hirtl A., Iliescu M., Ishikawa T., Ishimoto S., Ishiwatari T., Itahashi K., Iwasaki M., Kienle P., Marton J., Matsuda Y., Mizoi Y., Morra O., Nagae T., Onishi H., Okada S., Outa H., Pietreanu D., Sakaguchi A., Sakuma F., Sato M., Sekimoto M., Sirghi D., Sirghi F., Suzuki S., Suzuki T., Tatsuno H., Tomono D., Toyoda A., Widmann E., Yamazaki T., Yim H., and Zmeskal J.: "A general-purpose liquid target system for hadron experiments at J-PARC", International Nuclear Physics Conference (INPC2007), (International Union for Pure and Applied Physics), Tokyo, June (2007).

Iio M., Beer G., Bhang H., Buehler P., Cargnelli M., Chiba J., Choi S., Curceanu C., Fukuda Y., Guaraldo C., Hanaki T., Hayano R. S., Hirtl A., Iliescu M., Ishikawa T., Ishimoto S., Ishiwatari T., Itahashi K., Iwai M., Iwasaki M., Juhasz B., Kienle P., Marton J., Matsuda Y., Onishi H., Okada S., Outa H., Pietreanu D., Sakuma F., Sato M., Schmid P., Sirghi D., Sirghi F., Suzuki S., Suzuki T., Tatsuno H., Tomono D., Widmann E., Yamazaki T., Yim H., and Zmeskal J.: "Precise measurement of kaonic helium atoms X-rays", 12th International Conference on Hadron Spectroscopy, (INFN Laboratori Nazionali di Frascati), Rome, Italy, Oct. (2007).

(Domestic Conference)

飯尾雅実, 板橋健太, 岩崎雅彦, 應田治彦, 大西宏明, 岡田信二, 佐久間史典, 佐藤将春, 鈴木隆敏, 友野大, 松田恭幸, 山崎敏光, 石元茂, 岩井正明, 鈴木祥二, 関本美知子, 豊田晃久, 永江知文, 石川隆, 竜野秀行, 早野龍吾, 藤岡宏之, 味村周平, 阪口篤志, 福田芳之, 千葉順成, 花木俊夫, 福田共和, 溝井浩, Beer G., Bhang H., Choi S., Yim H., 石渡智一, Buehler P., Cargnelli M., Hirtl A., Kienle P., Marton J., Widmann E., Zmeskal J., Curceanu C., Guaraldo C., Iliescu M., Pietreanu D., Sirghi D., Sirghi F., Faso D., Busso L., Morra O.: "K 中間子原子核探査実験のための液体ヘリウム標的の開発 II", 日本物理学会第 62 回年次大会, 札幌, 9 月 (2007).

飯尾雅実, 味村周平, Beer G., Bhang H., Buehler P., Busso L., Cargnelli M., 千葉順成, Choi S., Curceanu C., Faso D., 藤岡宏之, 福田共和, 福田芳之, Guaraldo C., 花木俊夫, 早野龍吾, Hirtl A., Iliescu M., 石川隆, 石元茂, 石渡智一, 板橋健太, 岩井正明, 岩崎雅彦, Kienle P., Marton J., 松田恭幸, 溝井浩, Morra O., 永江知文, 岡田信二, 大西宏明, 應田治彦, Pietreanu D., 阪口篤志, 佐久間史典, 佐藤将春, 関本美知子, Sirghi D., Sirghi F., 鈴木祥二, 鈴木隆敏, 竜野秀行, 友野大, 豊田晃久, Widmann E., 山崎敏光, Yim H., Zmeskal J.: "K 中間子原子・原子核実験のための液体ヘリウム 3 標的の開発", 文部科学省科学研究費補助金特定領域研究特定領域研究「ストレンジネスで探るクォーク多体系」第 3 回総括班主催研究会 (2007), 仙台, 11 月 (2007).

Radiation Laboratory

Publications

[Journal]

(Original Papers) *Subject to Peer Review

Stave S., Nakagawa I., and A1 Collaboration .: "Lowest-Q^2 measurement of the $\gamma^* p \rightarrow \Delta$ reaction: Probing the pionic contribution", Eur. Phys. J. A **30**, 471–476 (2006). *

Takano J., Ahrens L. A., Alforque R., Bai M., Brown K., Courant E. D., Ganetis G., Gardner C. J., Glenn J. W., Hattori T., Huang H., Jain A., Luccio A. U., MacKay W. W., Okamura M., Roser T., Tsoupas N., Tepikian S., Tuozzolo J., Wood J., Zelenski A., and Zeno K.: "Helical dipole partial Siberian snake for the AGS", J. Instrum **1**, No. P11, pp. P11002-0–P11002-22 (2006). *

Adler S. S., Akiba Y., Bazilevsky A. V., Bunce G. M., Deshpande A., Enyo H., Fields D. E., Fox B., Fukao Y., Goto Y., Perdekamp M. G., Hasuko K., Heuser J., Horaguchi T., Ichihara T., Imai K., Ishihara M., Jinnouchi O., Kamihara N., Kaneta M., Kiyomichi A., Kobayashi H., Kurita K., Mao Y., Onishi H., Okada H., Okada K., Rykov V., Saito N., Sato H., Shibata T., Taketani A., Tanida K., Togawa M., Tojo J., Torii H., Watanabe Y., and Yokkaichi S.: "Jet structure from dihadron correlations in d+Au collisions at $\sqrt{s_{NN}} = 200$ GeV", Phys. Rev. C **73**, 054903-1–054903-27 (2006). *

Adler S. S., Akiba Y., Bazilevsky A. V., Bunce G. M., Deshpande A., Enyo H., Fields D. E., Fox B., Fukao Y., Goto Y., Perdekamp M. G., Hasuko K., Heuser J., Horaguchi T., Ichihara T., Imai K., Ishihara M., Jinnouchi O., Kamihara N., Kaneta M., Kiyomichi A., Kobayashi H., Kurita K., Mao Y., Onishi H., Okada H., Okada K., Rykov V., Saito N., Sato H., Shibata T., Taketani A., Tanida K., Togawa M., Tojo J., Torii H., Watanabe Y., and Yokkaichi S.: "Nuclear effects on hadron production in d+Au collisions at $\sqrt{s_{NN}} = 200$ GeV revealed by comparison with p+p data", Phys. Rev. C **74**, 024904-1–024904 -13 (2006). *

Adler S. S., Akiba Y., Aoki K., Bazilevsky A. V., Bunce G. M., Deshpande A., Enyo H., Fields D. E., Fox B., Fukao Y., Goto Y., Perdekamp M. G., Hachiya T., Hasuko K., Heuser J., Horaguchi T., Ichihara T., Imai K., Ishihara M., Jinnouchi O., Kajihara F., Kamihara N., Kaneta M., Kiyomichi A., Kobayashi H., Kurita K., Mao Y., Murata J., Onishi H., Okada H., Okada K., Rykov V., Saito N., Sato H., Shibata T., Shoji K., Tabaru T., Taketani A., Tanida K., Togawa M., Tojo J., Torii H., Tsuchimoto Y., Wagner M. M., Watanabe Y., Xie W., and Yokkaichi S.: "Improved measurement of double helicity asymmetry in inclulsive midrapidity π^0 production for polarized p+p collisions at $\sqrt{s} = 200$ GeV", Phys. Rev. D **73**, 091102-1–091102-5 (2006). *

Adler S. S., Akiba Y., Bazilevsky A. V., Bunce G. M., Deshpande A., Enyo H., Fields D. E., Fox B., Fukao Y., Goto Y., Perdekamp M. G., Hasuko K., Heuser J., Horaguchi T., Ichihara T., Imai K., Ishihara M., Jinnouchi O., Kamihara N., Kaneta M., Kiyomichi A., Kobayashi H., Kurita K., Mao Y., Onishi H., Okada H., Okada K., Rykov V., Saito N., Sato H., Shibata T., Taketani A., Tanida K., Togawa M., Tojo J., Torii H., Watanabe Y., and Yokkaichi S.: "Jet properties from dihadron correlations in p+p collisions at $\sqrt{s} = 200$ GeV", Phys. Rev. D **74**, 072002-1–072002-26 (2006). *

Adler S. S., Akiba Y., Bazilevsky A. V., Bunce G. M., Deshpande A., Enyo H., Fields D. E., Fox B., Fukao Y., Goto Y., Perdekamp M. G., Hasuko K., Heuser J., Horaguchi T., Ichihara T., Imai K., Ishihara M., Jinnouchi O., Kamihara N., Kaneta M., Kiyomichi A., Kobayashi H., Kurita K., Mao Y., Onishi H., Okada H., Okada K., Rykov V., Saito N., Sato H., Shibata T., Taketani A., Tanida K., Togawa M., Tojo J., Torii H., Watanabe Y., and Yokkaichi S.: "J/ψ Production and Nuclear Effects for d+Au and p+p Collisions at $\sqrt{s_{NN}} = 200$ GeV", Phys. Rev. Lett. **96**, 012304-1–012304-6 (2006). *

Adler S. S., Akiba Y., Bazilevsky A. V., Bunce G. M., Deshpande A., Enyo H., Fields D. E., Fox B., Goto Y., Perdekamp M. G., Hayashi N., Ichihara T., Imai K., Ishihara M., Jinnouchi O., Kamihara N., Kobayashi H., Kurita K., Mao Y., Murata J., Onishi H., Okada K., Saito N., Sato H., Shibata T., Taketani A., Tanida K., Tojo J., Torii H., Watanabe Y., and Yokkaichi S.: " Single Electrons from Heavy-Flavor Decays in p+p Collisions at $\sqrt{s} = 200$ GeV", Phys. Rev. Lett. **96**, 032001-1–032001-6 (2006). *

Adler S. S., Akiba Y., Bazilevsky A. V., Bunce G. M., Deshpande A., Enyo H., Fields D. E., Fox B., Goto Y., Perdekamp M. G., Hayashi N., Ichihara T., Imai K., Ishihara M., Jinnouchi O., Kamihara N., Kobayashi H., Kurita K., Mao Y., Murata J., Onishi H., Okada K., Saito N., Sato H., Shibata T., Taketani A., Tanida K., Tojo J., Torii H., Watanabe Y., and Yokkaichi S.: "Nuclear Modification of Electron Spectra and Implications for Heavy Quark Energy Loss in Au+Au Collisions at $\sqrt{s_{NN}} = 200$ GeV", Phys. Rev. Lett. **96**, 032301-1–032301-6 (2006). *

Adler S. S., Akiba Y., Bazilevsky A. V., Bunce G. M., Deshpande A., Enyo H., Fields D. E., Fox B., Goto Y., Perdekamp M. G., Hayashi N., Ichihara T., Imai K., Ishihara M., Jinnouchi O., Kamihara N., Kaneta M., Kobayashi H., Kurita K., Mao Y., Murata J., Onishi H., Okada K., Saito N., Sato H., Shibata T., Taketani A., Tanida K., Tojo J., Torii H., Watanabe Y., and Yokkaichi S.: "Measurement of Identified π^0 and Inclusive Photon Second-Harmonic Parameter v_2 and Implications for Direct Photon Production in $\sqrt{s_{NN}} = 200$ GeV Au + Au", Phys. Rev. Lett. **96**, 032302-1–032302-6 (2006). *

Adler S. S., Akiba Y., Bazilevsky A. V., Bunce G. M.,

Deshpande A., Enyo H., Fields D. E., Fox B., Goto Y., Perdekamp M. G., Hayashi N., Ichihara T., Imai K., Ishihara M., Jinnouchi O., Kamihara N., Kobayashi H., Kurita K., Mao Y., Murata J., Onishi H., Okada K., Saito N., Sato H., Shibata T., Taketani A., Tanida K., Tojo J., Torii H., Watanabe Y., and Yokkaichi S.: "Common Suppression Pattern of eta and π^0 Mesons at High Transverse Momentum in Au+Au Collisions at $\sqrt{s_{NN}} = 200$ GeV", Phys. Rev. Lett. **96**, 202301-1–202301-6 (2006). *

Adler S. S., Akiba Y., Bazilevsky A. V., Bunce G. M., Deshpande A., Enyo H., Fields D. E., Fox B., Fukao Y., Goto Y., Perdekamp M. G., Hasuko K., Heuser J., Horaguchi T., Ichihara T., Imai K., Ishihara M., Jinnouchi O., Kamihara N., Kaneta M., Kiyomichi A., Kobayashi H., Kurita K., Mao Y., Onishi H., Okada H., Okada K., Rykov V., Saito N., Sato H., Shibata T., Taketani A., Tanida K., Togawa M., Tojo J., Torii H., Watanabe Y., and Yokkaichi S.: "Azimuthal Angle Correlations for Rapidity Separated Hadron Pairs in d+Au Collisions at $\sqrt{s_{NN}} = 200$ GeV", Phys. Rev. Lett. **96**, 222301-1–222301-6 (2006). *

Adler S. S., Akiba Y., Bazilevsky A. V., Bunce G. M., Deshpande A., Enyo H., Fields D. E., Fox B., Goto Y., Perdekamp M. G., Hayashi N., Ichihara T., Imai K., Ishihara M., Jinnouchi O., Kamihara N., Kobayashi H., Kurita K., Mao Y., Murata J., Onishi H., Okada K., Saito N., Sato H., Shibata T., Taketani A., Tanida K., Tojo J., Torii H., Watanabe Y., and Yokkaichi S.: "Dense-Medium Modifications to Jet-Induced Hadron Pair Distributions in Au+Au Collisions at $\sqrt{s_{NN}} = 200$ GeV", Phys. Rev. Lett. **97**, 052301-1–052301-6 (2006). *

Bourgeois P., Nakagawa I., and OOPS Collaboration .: "Measurement of the Generalized Electric and Magnetic Polarizabilities of the Proton at Low Q^2 Using the Virtual-Compton-Scattering Reaction", Phys. Rev. Lett. **97**, 212001-1–212001-4 (2006). *

Adare A., Akiba Y., Aoki K., Asai J., Bunce G. M., Deshpande A., Enyo H., Fields D. E., Fujiwara K., Fukao Y., Goto Y., Perdekamp M. G., Horaguchi T., Ichihara T., Imai K., Inoue Y., Ishihara M., Jinnouchi O., Kamihara N., Kaneta M., Kano H., Kanoh H., Kawall D., Kiyomichi A., Kurita K., Mao Y., Murata J., Nakagawa I., Nakano K., Onishi H., Okada H., Okada K., Rykov V., Saito N., Shibata T., Shoji K., Tabaru T., Taketani A., Tanida K., Togawa M., Tojo J., Torii H., Wagner M. M., Watanabe Y., Xie W., and Yokkaichi S.: " Measurement of High-pT Single Electrons from Heavy-Flavor Decays in p+p Collisions at $\sqrt{s} = 200$ GeV", Phys. Rev. Lett. **97**, 252002-1–252002-6 (2006). *

Mori Y., Okaniwa T., Nakahashi M., Ariyoshi S., Otani C., Sato H., and Matsuo H.: "Development of superconductive imaging submillimeter-wave camera with nine detector elements (SISCAM-9)", Proc. SPIE-Int. Soc. Opt. Eng. **6275**, 627523-1–627523-12 (2006).

Seki Y., Kitaguchi M., Funahasi H., Taketani K., Hino M., Otake Y., and Shimiuzu H. M.: "Development of Neutron Interferometer with Wide-Gapped "BSE"s for Precision Measurements", AIP Conf. Proc. **915**, 202–205 (2007). *

Ohno M., Sato H., Mishima K., Ikeda T., and Shimizu H.: "Low energy particle detector using a superconducting transition edge sensor", IEEE Trans. Appl. Supercond. **17**, No. 2, pp. 328–331 (2007). *

Yokkaichi S., Chiba J., Enyo H., Fukao Y., Funahashi H., Hamagaki H., Ieiri M., Ishino M., Kanda H., Kitaguchi M., Mihara S., Miwa K., Miyashita T., Murakami T., Mutou R., Nakura T., Naruki M., Ozawa K., Sakuma F., Sasaki O., Sekimoto M., Tabaru T., Tanaka K., Togawa M., Yamada S., and Yoshimura Y.: "Study of in-medium meson modification in 12 GeV p+A reactions", Int. J. Mod. Phys. A **22**, No. 2/3, pp. 397–405 (2007).

Taketani K., Seki Y., Funahasi H., Hino M., Kitaguchi M., Otake Y., and Shimiuzu H. M.: "Moiré Fringes in a Nuetron Spin interferometer", J. Phys. Soc. Jpn. **76**, No. 6, pp. 064008-1–064008-7 (2007). *

Stepanyan S., Boyarinov S., Egiyan H., Guo L., Dale D., Gabrielyan M., Gan L., Gasparian A., Glamazdin A., Mecking B., Nakagawa I., Teymurazyan A., and Wood M. H.: "Energy Calibration of the JLab Bremsstrahlung Tagging System", Nucl. Instrum. Methods Phys. Res. A **572**, 654–661 (2007). *

Adare A., Akiba Y., Aoki K., Asai J., Bunce G. M., Deshpande A., Enyo H., Fields D. E., Fujiwara K., Fukao Y., Goto Y., Perdekamp M. G., Hachiya T., Hasuko K., Heuser J., Horaguchi T., Ichihara T., Imai K., Inoue Y., Ishihara M., Jinnouchi O., Kajihara F., Kamihara N., Kaneta M., Kanoh H., Kawall D., Kiyomichi A., Kurita K., Mao Y., Murata J., Nakagawa I., Nakano K., Onishi H., Okada H., Okada K., Wagner M. M., Watanabe Y., Xie W., and Yokkaichi S.: "Correlated production of p and $\bar{p}$ in Au+Au collisions at $\sqrt{s_{NN}} = 200$ GeV", Phys. Lett. B **649**, 359–369 (2007). *

Sparveis N. F., Nakagawa I., and A1 Collaboration .: "Determination of Quadrupole Strengths in the $\gamma^* p \to \Delta(1232)$ transition at $Q^2 = 0.20(\mathrm{GeV/c})^2$", Phys. Lett. B **651**, 102–107 (2007). *

Sugimoto T., Nakamura T., Kondo Y., Aoi N., Baba H., Bazin D. P., Fukuda N., Gomi T., Hasegawa H., Imai N., Ishihara M., Kobayashi T., Kubo T., Miura M., Motobayashi T., Otsu H., Saito A., Sakurai H., Shimoura S., Vinodkumar A. M., Watanabe K., Watanabe Y., Yakushiji T., Yanagisawa Y., and Yoneda K.: "The first 2^+ state of ^{14}Be", Phys. Lett. B **654**, 160–164 (2007). *

Mishima K., Utsuro M., Nagai Y., Tanaka M., Toshiro K., Fukuda Y., Kiyanagi Y., and Ooi M.: "Time-differential

observation of the ortho-para conversion of liquid D_2 under irradiation", Phys. Rev. B **75**, 014112-1–014112-12 (2007). ∗

Adler S. S., Akiba Y., Bazilevsky A. V., Bunce G. M., Deshpande A., Enyo H., Fields D. E., Fox B., Fukao Y., Goto Y., Perdekamp M. G., Hasuko K., Hayashi N., Heuser J., Horaguchi T., Ichihara T., Imai K., Ishihara M., Jinnouchi O., Kamihara N., Kaneta M., Kiyomichi A., Kobayashi H., Kurita K., Mao Y., Murata J., Onishi H., Okada H., Okada K., Rykov V., Saito N., Sato H., Shibata T., Taketani A., Tanida K., Togawa M., Tojo J., Torii H., Watanabe Y., and Yokkaichi S.: "High transverse momentum η meson production in p+p,d+Au, and Au+Au collisions at $\sqrt{s_{NN}} = 200$ GeV", Phys. Rev. C **75**, 024909-1–024909-36 (2007). ∗

Fujita H., Fujita Y., Adachi T., Bacher A. D., Berg G. P., Black T. C., Caurier E., Foster ., Fujimura H., Hara K., Harada K., Hatanaka K., Janecke J., Kamiya J., Kanzaki Y., Katori K., Kawabata T., Langanke K., Martinez-Pinedo G., Noro T., Robers D. A., Sakaguchi H., Shimbara Y., Shinada T., Stephenson E. J., Ueno H., Yamanaka T., Yoshifuku M., and Yosoi M.: "Isospin structure of $J^\pi = 1^+$ states in ^{58}Ni and ^{58}Cu studied by ^{58}Ni(p, p') and ^{58}Ni(^{3}He,t)^{58}Cu measurements", Phys. Rev. C **75**, 034310-1–034310-15 (2007). ∗

Adler S. S., Akiba Y., Bazilevsky A. V., Bunce G. M., Deshpande A., Enyo H., Fields D. E., Fox B., Fukao Y., Goto Y., Perdekamp M. G., Hasuko K., Heuser J., Horaguchi T., Ichihara T., Imai K., Ishihara M., Jinnouchi O., Kamihara N., Kaneta M., Kiyomichi A., Kobayashi H., Kurita K., Mao Y., Onishi H., Okada H., Okada K., Rykov V., Saito N., Sato H., Shibata T., Taketani A., Tanida K., Togawa M., Tojo J., Torii H., Watanabe Y., and Yokkaichi S.: "Production of ω mesons at large transverse momenta in p+p and d+Au collisions at $\sqrt{s_{NN}} = 200$ GeV", Phys. Rev. C **75**, 051902-1–051902-6 (2007). ∗

Adler S. S., Akiba Y., Bazilevsky A. V., Bunce G. M., Deshpande A., Enyo H., Fields D. E., Fox B., Goto Y., Perdekamp M. G., Hayashi N., Ichihara T., Imai K., Ishihara M., Jinnouchi O., Kamihara N., Kobayashi H., Kurita K., Mao Y., Murata J., Onishi H., Okada K., Saito N., Sato H., Shibata T., Taketani A., Tanida K., Tojo J., Torii H., Watanabe Y., and Yokkaichi S.: "Measurement of density correlations in pseudorapidity via charged particle multiplicity fluctuations in Au+Au collisions at $\sqrt{s_{NN}} = 200$ GeV", Phys. Rev. C **76**, 034903-1–034903-33 (2007). ∗

Adler S. S., Akiba Y., Bazilevsky A. V., Bunce G. M., Deshpande A., Enyo H., Fields D. E., Fox B., Goto Y., Perdekamp M. G., Hayashi N., Ichihara T., Imai K., Ishihara M., Jinnouchi O., Kamihara N., Kobayashi H., Kurita K., Mao Y., Murata J., Onishi H., Okada K., Saito N., Sato H., Shibata T., Taketani A., Tanida K., Tojo J., Torii H., Watanabe Y., and Yokkaichi S.: "Detailed study of high-p_T neutral pion suppression and azimuthal anisotropy in Au+Au collisions at $\sqrt{s_{NN}} = 200$ GeV", Phys. Rev. C **76**, 034904-1–034904-26 (2007). ∗

Notani M., Sakurai H., Aoi N., Iwasaki H., Fukuda N., Liu Z., Yoneda K., Ogawa H., Teranishi T., Nakamura T., Okuno H., Yoshida A., Watanabe Y., Momota S., Inabe N., Kubo T., Ito S., Ozawa A., Suzuki T., Tanihata I., and Ishihara M.: "Projectile fragmentation reaction and production of nuclei near the neutron drip line", Phys. Rev. C **76**, 044605-1–044605-15 (2007). ∗

Adare A., Akiba Y., Aoki K., Asai J., Bunce G. M., Deshpande A., Enyo H., Fields D. E., Fujiwara K., Fukao Y., Goto Y., Perdekamp M. G., Horaguchi T., Ichihara T., Imai K., Inoue Y., Ishihara M., Jinnouchi O., Kamihara N., Kaneta M., Kanoh H., Kawall D., Kiyomichi A., Kurita K., Mao Y., Murata J., Nakagawa I., Nakano K., Onishi H., Okada H., Okada K., Rykov V., Saito N., Shibata T., Shoji K., Tabaru T., Taketani A., Tanida K., Togawa M., Tojo J., Torii H., Wagner M. M., Watanabe Y., Xie W., and Yokkaichi S.: "Inclusive cross section and double helicity asymmetry for π^0 production in $p+p$ collisions at $\sqrt{s} = 200$ GeV: Implications for the polarized gluon distribution in the proton", Phys. Rev. D **76**, 051106-1–051106-7 (2007). ∗

Adler S. S., Akiba Y., Bazilevsky A. V., Bunce G. M., Deshpande A., Enyo H., Fields D. E., Fox B., Goto Y., Perdekamp M. G., Hayashi N., Ichihara T., Imai K., Ishihara M., Jinnouchi O., Kamihara N., Kobayashi H., Kurita K., Mao Y., Murata J., Onishi H., Okada K., Saito N., Sato H., Shibata T., Taketani A., Tanida K., Tojo J., Torii H., Watanabe Y., and Yokkaichi S.: "Measurement of single muons at forward rapidity in $p+p$ collisions at $\sqrt{s} = 200$ GeV and implications for charm production", Phys. Rev. D **76**, 092002-1–092002-24 (2007). ∗

Adler S. S., Akiba Y., Bazilevsky A. V., Bunce G. M., Deshpande A., Enyo H., Fields D. E., Fox B., Fukao Y., Goto Y., Perdekamp M. G., Hasuko K., Heuser J., Horaguchi T., Ichihara T., Imai K., Ishihara M., Jinnouchi O., Kamihara N., Kaneta M., Kiyomichi A., Kobayashi H., Kurita K., Mao Y., Onishi H., Okada H., Okada K., Rykov V., Saito N., Sato H., Shibata T., Taketani A., Tanida K., Togawa M., Tojo J., Torii H., Watanabe Y., and Yokkaichi S.: "Measurement of Direct Photon Production in p+p Collisions at $\sqrt{s} = 200$ GeV", Phys. Rev. Lett. **98**, 012002-1–012002-6 (2007). ∗

Adler S. S., Akiba Y., Bazilevsky A. V., Bunce G. M., Deshpande A., Enyo H., Fields D. E., Fox B., Goto Y., Perdekamp M. G., Hayashi N., Ichihara T., Imai K., Ishihara M., Jinnouchi O., Kamihara N., Kobayashi H., Kurita K., Mao Y., Murata J., Onishi H., Okada K., Saito N., Sato H., Shibata T., Taketani A., Tanida K., Tojo J., Torii H., Watanabe Y., and Yokkaichi S.: "Evidence for a long-range component in the pion emission

source in Au+Au Collisions at $\sqrt{s_{NN}} = 200$ GeV", Phys. Rev. Lett. **98**, 132301-1–132301-6 (2007). *

Sakuma F., chiba j., Enyo H., Fukao Y., Funahashi H., Hamagaki H., ieiri m., ishino m., handa h., Kitaguchi M., mihara s., Miwa K., miyashita t., Murakami T., muto r., nakura t., Naruki M., Ozawa K., sasaki o., Sekimoto M., Tabaru T., tanaka k., Togawa M., yamada s., Yokkaichi S., and yoshimura y.: "Nuclear-matter modification of decay widths in the $\phi \to e^+e^-$ and $\phi \to K^+K^-$ channels", Phys. Rev. Lett. **98**, 152302-1–152302-5 (2007). *

Adare A., Akiba Y., Aoki K., Asai J., Bunce G. M., Deshpande A., Enyo H., Fields D. E., Fujiwara K., Fukao Y., Goto Y., Perdekamp M. G., Hachiya T., Hasuko K., Heuser J., Horaguchi T., Ichihara T., Imai K., Inoue Y., Ishihara M., Jinnouchi O., Kajihara F., Kamihara N., Kaneta M., Kano H., Kanoh H., Kawall D., Kiyomichi A., Kurita K., Mao Y., Murata J., Nakagawa I., Nakano K., Onishi H., Okada H., Okada K., Rykov V., Saito N., Sato H., Shibata T., Shoji K., Tabaru T., Taketani A., Tanida K., Togawa M., Tojo J., Torii H., Tsuchimoto Y., Wagner M. M., Watanabe Y., Xie W., and Yokkaichi S.: "Scaling properties of azimuthal anisotropy in Au+Au and Cu+Cu collisions at $\sqrt{s_{NN}} = 200$ GeV", Phys. Rev. Lett. **98**, 162301-1–162301-6 (2007). *

Adare A., Akiba Y., Aoki K., Asai J., Bunce G. M., Deshpande A., Enyo H., Fields D. E., Fujiwara K., Fukao Y., Goto Y., Perdekamp M. G., Hachiya T., Hasuko K., Heuser J., Horaguchi T., Ichihara T., Imai K., Inoue Y., Ishihara M., Jinnouchi O., Kajihara F., Kamihara N., Kaneta M., Kano H., Kanoh H., Kawall D., Kiyomichi A., Kurita K., Mao Y., Murata J., Nakagawa I., Nakano K., Onishi H., Okada H., Okada K., Rykov V., Saito N., Sato H., Shibata T., Shoji K., Tabaru T., Taketani A., Tanida K., Togawa M., Tojo J., Torii H., Tsuchimoto Y., Wagner M. M., Watanabe Y., Xie W., and Yokkaichi S.: "Energy loss and flow of heavy quarks in Au+Au collisions at $\sqrt{s_{NN}} = 200$ GeV", Phys. Rev. Lett. **98**, 172301-1–172301-6 (2007). *

Adler S. S., Akiba Y., Bazilevsky A. V., Bunce G. M., Deshpande A., Enyo H., Fields D. E., Fox B., Fukao Y., Goto Y., Perdekamp M. G., Hasuko K., Heuser J., Horaguchi T., Ichihara T., Imai K., Ishihara M., Jinnouchi O., Kamihara N., Kaneta M., Kiyomichi A., Kobayashi H., Kurita K., Mao Y., Onishi H., Okada H., Okada K., Rykov V., Saito N., Sato H., Shibata T., Taketani A., Tanida K., Togawa M., Tojo J., Torii H., Watanabe Y., and Yokkaichi S.: "Centrality dependence of π^0 and η production at large transverse momentum in $\sqrt{s_{NN}} = 200$ GeV $d+Au$ Collisions", Phys. Rev. Lett. **98**, 172302-1–172302-7 (2007). *

Adare A., Akiba Y., Aoki K., Asai J., Bunce G. M., Deshpande A., Enyo H., Fields D. E., Fujiwara K., Fukao Y., Goto Y., Perdekamp M. G., Horaguchi T., Ichihara T., Imai K., Inoue Y., Ishihara M., Jinnouchi O., Kamihara N., Kaneta M., Kanoh H., Kawall D., Kiyomichi A., Kurita K., Mao Y., Murata J., Nakagawa I., Nakano K., Onishi H., Okada H., Okada K., Rykov V., Saito N., Shibata T., Shoji K., Tabaru T., Taketani A., Tanida K., Togawa M., Tojo J., Torii H., Wagner M. M., Watanabe Y., Xie W., and Yokkaichi S.: "J/Ψ production versus transverse momentum and rapidity in p+p collisions at $\sqrt{s_{NN}} = 200$ GeV", Phys. Rev. Lett. **98**, 232002-1–232002-6 (2007). *

Adare A., Akiba Y., Aoki K., Asai J., Bunce G. M., Deshpande A., Enyo H., Fields D. E., Fujiwara K., Fukao Y., Goto Y., Perdekamp M. G., Hachiya T., Hasuko K., Heuser J., Horaguchi T., Ichihara T., Imai K., Inoue Y., Ishihara M., Jinnouchi O., Kajihara F., Kamihara N., Kaneta M., Kanoh H., Kawall D., Kiyomichi A., Kurita K., Mao Y., Murata J., Nakagawa I., Nakano K., Onishi H., Okada H., Okada K., Rykov V., Saito N., Sato H., Shibata T., Shoji K., Tabaru T., Taketani A., Tanida K., Togawa M., Tojo J., Torii H., Tsuchimoto Y., Wagner M. M., Watanabe Y., Xie W., and Yokkaichi S.: "J/Ψ production versus centrality, transverse momentum, and rapidity in Au+Au Collisions at $\sqrt{s_{NN}} = 200$ GeV", Phys. Rev. Lett. **98**, 232301-1–232301-6 (2007). *

Adare A., Akiba Y., Aoki K., Asai J., Bazilevsky A. V., Bunce G. M., Deshpande A., Enyo H., Fields D. E., Fox B., Fujiwara K., Fukao Y., Goto Y., Perdekamp M. G., Hachiya T., Hasuko K., Heuser J., Horaguchi T., Ichihara T., Imai K., Inoue Y., Ishihara M., Jinnouchi O., Kajihara F., Kamihara N., Kaneta M., Kanoh H., Kawall D., Kiyomichi A., Kobayashi H., Kurita K., Mao Y., Murata J., Nakagawa I., Nakano K., Onishi H., Okada H., Okada K., Rykov V., Saito N., Sato H., Shibata T., Shoji K., Tabaru T., Taketani A., Tanida K., Togawa M., Tojo J., Torii H., Tsuchimoto Y., Wagner M. M., Watanabe Y., Xie W., and Yokkaichi S.: "System size and energy dependence of jet-induced hadron pair correlation shapes in Cu+Cu and Au+Au collisions at $\sqrt{s_{NN}} = 200$ GeV and 62.4 GeV", Phys. Rev. Lett. **98**, 232302-1–232302-7 (2007). *

Afanasiev S., Akiba Y., Aoki K., Bunce G. M., Deshpande A., Enyo H., Fields D. E., Fukao Y., Goto Y., Perdekamp M. G., Hachiya T., Hasuko K., Heuser J., Horaguchi T., Ichihara T., Imai K., Ishihara M., Jinnouchi O., Kajihara F., Kamihara N., Kaneta M., Kiyomichi A., Kurita K., Murata J., Onishi H., Okada H., Okada K., Rykov V., Saito N., Sato H., Shibata T., Shoji K., Tabaru T., Taketani A., Tanida K., Togawa M., Tojo J., Torii H., Tsuchimoto Y., Wagner M. M., Watanabe Y., Xie W., and Yokkaichi S.: "Elliptic flow for ϕ Mesons and (Anti)deuterons in Au+Au collisions at $\sqrt{s_{NN}} = 200$ GeV", Phys. Rev. Lett. **99**, 052301-1–052301-6 (2007). *

Adare A., Akiba Y., Aoki K., Asai J., Bunce G. M., Deshpande A., Enyo H., Fields D. E., Fujiwara K., Fukao Y., Goto Y., Perdekamp M. G., Hachiya T., Hasuko K.,

Heuser J., Horaguchi T., Ichihara T., Imai K., Inoue Y., Ishihara M., Jinnouchi O., Kajihara F., Kamihara N., Kaneta M., Kanoh H., Kawall D., Kiyomichi A., Kurita K., Mao Y., Murata J., Nakagawa I., Nakano K., Onishi H., Okada H., Okada K., Rykov V., Saito N., Sato H., Shibata T., Shoji K., Tabaru T., Taketani A., Tanida K., Togawa M., Tojo J., Torii H., Tsuchimoto Y., Wagner M. M., Watanabe Y., Xie W., and Yokkaichi S.: "Transverse momentum and centrality dependence of dihadron correlations in Au+Au collisions at $\sqrt{s_{NN}} = 200$ GeV: Jet quenching and the response of partonic matter", Phys. Rev. C **77**, 011901-1–011901-6 (2008). ∗

Adler S. S., Akiba Y., Bazilevsky A. V., Bunce G. M., Deshpande A., Enyo H., Fields D. E., Fox B., Fukao Y., Goto Y., Perdekamp M. G., Hasuko K., Heuser J., Horaguchi T., Ichihara T., Imai K., Ishihara M., Jinnouchi O., Kamihara N., Kaneta M., Kiyomichi A., Kobayashi H., Kurita K., Mao Y., Onishi H., Okada H., Okada K., Rykov V., Saito N., Sato H., Shibata T., Taketani A., Tanida K., Togawa M., Tojo J., Torii H., Watanabe Y., and Yokkaichi S.: "Centrality dependence of charged hadron production in deuteron+gold and nucleon+gold collisions at $\sqrt{s_{NN}} = 200$ GeV", Phys. Rev. C **77**, 014905-1–014905-13 (2008). ∗

有吉誠一郎, 大谷知行, Dobroiu A., 松尾宏, 佐藤広海, 田井野徹, 川瀬晃道, 清水裕彦: "超伝導検出器アレイを用いたテラヘルツイメージング", 信学技報, No. ED2006-194(2006-12), pp. 59–63 (2006).

Oral Presentations

(International Conference etc.)

Nakagawa I.: "Polarization measurements of RHIC-pp Run05 using CNI pC-Polarimeter", 17th International Spin Physics Symposium (SPIN2006), Kyoto, Oct. (2006).

Mishima K., Sato H., Shinohara T., Oku T., Yamada S., Shimizu H. M., and Morishima T.: "High polarized beam line with magnetic lens at J-PARC", European Workshop on Neutron Optics (NOP '07), (Paul Scherrer Institute), Villigen, Switzerland, Mar. (2007).

Yokkaichi S.: "Low mass dielectron measurement at J-PARC", International Nuclear Physics Conference (INPC2007), (Science Council of Japan, RIKEN and others), Tokyo, June (2007).

Nakagawa I.: "Measurement of beam polarization in CNI region through proton-carbon elastic reaction at RHIC", International Nuclear Physics Conference (INPC2007), (Science Council of Japan and others), Tokyo, June (2007).

Nakagawa I.: "Pion and kaon polarizability measurements at J-PARC", Nuclear Physics at J-PARC: Pre-Symp. of INPC 2007, Tokai-mura, Ibaraki Pref., June (2007).

Yokkaichi S.: "Low mass dielectron measurement at J-PARC: J-PARC E16 experiment", Nuclear Physics at J-PARC: Pre-symposium of INPC 2007, Tokaimura, June (2007).

Nakagawa I.: "Polarization Measurement of Run05 proton beam at RHIC", Advanced Studies Institute - Symmetries and Spin (SPIN-Praha-2007), (Charles University), Prague, Czech, July (2007).

Nakagawa I.: "PHENIX detector upgrades for spin physics", 6th Circum-Pan-Pacific Symp. on High Energy Spin Physics (Pacific-SPIN07), (University of British Columbia), Vancouver, Canada, July–Aug. (2007).

Nakagawa I.: "p-Carbon Polarimetry at RHIC", 12th Int. Workshop on Polarized Sources, Targets & Polarimetry, (BNL), Upton, USA, Sept. (2007).

Yokkaichi S.: "In-medium modification of vector mesons measured at KEK-PS", Hadron Physics at RHIC, (Asia Pacific Center of Theoretical Physics (APCTP)), Pohang, Korea, Dec. (2007).

Mishima K., Ino T., Sakai K., Shinohara T., Hirota K., Ikeda K., Sato H., Otake Y., Ohmori H., Muto S., Higashi N., Morishima T., Kitaguchi M., Hino M., Funahasi H., Shima T., Suzuki J., Niita K., Taketani K., Seki Y., and Shimiuzu H. M.: "A Design of Neutron Optics and Physics Beam Line at J-PARC BL05", 1st J-PARC International Symposium on Pulsed Neutron and Muon Sciences (IPS 08), Mito, Mar. (2008).

Mishima K., Ino T., Sakai K., Shinohara T., Hirota K., Ikeda K., Sato H., Otake Y., Ohmori H., Muto S., Higashi N., Morishima T., Kitaguchi M., Hino M., Funahasi H., Shima T., Niita K., Taketani K., Seki Y., and Shimiuzu H. M.: "The Optics of the J-PARC BL05 and Measurement of Neutron Decay", 4th International Workshop on Nuclear and Particle Physics at J-PARC (NP08), Mito, Mar. (2008).

(Domestic Conference)

四日市悟: "KEK 12GeV PS で測定された $\rho/\omega/\phi$ 中間子質量スペクトルの変化", 日本物理学会 2007 年春季大会, 八王子, 3 月 (2007).

大竹淑恵: "結晶を用いた中性子極小角散乱実験", 第 1 回 NOP ワークショップ「低速中性子光学とそれを用いた基礎物理学」, (高エネルギー加速器研究機構), つくば, 9 月 (2007).

早藤麻美, 玉川徹, 岩本慎也, 阿部幸二, 中村聡史, 中條宏隆, 佐藤哲哉, 浜垣秀樹, 山口頼人, 牧島一夫: "fine-pitch and thick-foil GEM を用いた 2 次元イメージングにおける位置分解能の性能評価", 日本物理学会第 62 回年次大会, 札幌, 9 月 (2007).

佐藤広海, 羽澄昌史, 田島 治, 後田 裕, 住澤一高, 樋口岳雄, 石野宏和: "Al-STJ の作製と評価", 第 68 回応用物理学会学術講演会, (社団法人　応用物理学会), 札幌, 9 月 (2007).

有吉誠一郎, 田井野徹, 大谷知行, 佐藤広海, 松尾宏: "テラヘルツ帯・薄膜マッチング型 STJ 検出器の原理検証", 第 68 回応用物理学会学術講演会, 札幌, 9 月 (2007).

石井宏和, 田井野徹, 大谷知行, 渋谷孝幸, 有吉誠一郎, 佐藤広海, 明連広昭, 高田進: "基板吸収型並列 STJ アレイ検出器による THz 検出器の高感度化", 第 68 回応用物理学会

学術講演会, 札幌, 9 月 (2007).

南川泰裕, Damayanthi R. M., 森文彬, 大野雅史, 高橋浩之, 佐藤広海: “動的シミュレーションを用いた多素子型超伝導転移端マイクロカロリメータの波形解析”, 日本原子力学会 2007 年秋の大会, 北九州, 9 月 (2007).

池田一昭, 佐藤広海, 広田克也, 三島賢二, 清水裕彦: “リアル曲面スーパーミラーの開発”, 日本中性子科学会第 7 回年会 (JSNS2007), (日本中性子科学会), 福岡, 11 月 (2007).

四日市悟: “電子対測定実験 (E16) と高運動量ビームライン”, RCNP ワークショップ「J-PARC ハドロン実験施設のビームライン設備拡充に向けて」, 大阪, 11 月 (2007).

Advanced Meson Science Laboratory

Publications

[Journal]

(Original Papers) *Subject to Peer Review

Ohira-Kawamura S., Shimizu Y., Kanoda K., and Saito G.: "Spin liquid state in κ-(BEDT-TTF)$_2$Cu$_2$(CN)$_3$ studied by muon spin relaxation method", J. Low Temp. Phys. **142**, 153–158 (2006). *

Hachitani K., Amanuma H., Fukazawa H., Kohori Y., Watanabe I., Kumagai K., Sekine C., and Shirotani I.: "^{31}P-NMR and μSR studies of filled skutterudite compound SmRu$_4$P$_{12}$", J. Phys. Soc. Jpn. **75**, No. Suppl., pp. 164–166 (2006). *

Ohira-Kawamura S., Tamura M., Kato R., and Iwasaki M.: "Magnetic order and charge separation in 2D distorted triangular lattice systems β'-X[Pd(dmit)$_2$]$_2$", Physica B **374/375**, 122–125 (2006). *

Hachitani K., Amanuma H., Fukazawa H., Kohori Y., Watanabe I., Kumagai K., Sekine C., and Shirotani I.: "^{31}P-NMR and μSR studies of filled skutterudite compounds RRu$_4$P$_{12}$(R: Sm, Gd)", Physica B **378/380**, 228–229 (2006). *

Hachitani K., Fukazawa H., Kohori Y., Watanabe I., Kumagai K., Sekine C., and Shirotani I.: "^{31}P-NMR and μSR studies of filled skutterudite compounds SmT_4P$_{12}$(T: Fe,Os)", Physica B **378/380**, 230–231 (2006). *

Hayashi T., Koike S., Higami N., Hirabayashi K., Matsuba H., Ogiwara K., and Yagi E.: "Lattice location of hydrogen in β_1-V$_2$H (tetragonal)", J. Alloys Compounds **446/447**, 512–515 (2007). *

Kanada K., Saito T., Osawa A., Goto T., Suzuki T., and Manaka H.: "Impurity-induced magnetic order in the mixture of two spin gap systems $(CH_3)_2CHNH_3CuCl_3$ and $(CH_3)_2CHNH_3CuBr_3$", J. Phys. Chem. Solids **68**, 2191–2194 (2007). *

Kanada K., Saito T., Osawa A., Goto T., and Suzuki T.: "^{1}H-NMR Study on the Magnetic Order in the Mixture of Two Spin Gap Systems $(CH_3)_2CHNH_3CuCl_3$ and $(CH_3)_2CHNH_3CuBr_3$", J. Phys. Soc. Jpn. **76**, No. 6, pp. 064706-1–064706-3 (2007). *

Suzuki T., Yamada F., Watanabe I., Goto T., Osawa A., and Tanaka H.: "The effect of randomness on the quantum spin system $Tl_{1-x}K_xCuCl_3$ with $x = 0.44$ studied by the Zero-field Muon-Spin-Relaxation (ZF-μSR) method", J. Phys. Soc. Jpn. **76**, No. 7, pp. 074704-1–074704-5 (2007). *

Saito T., Sasaki T., Suzuki T., Osawa A., Goto T., Awaji S., Watanabe K., and Kobayashi N.: "High-field magnetic torque measurement in the spin gap system $(CH_3)_2CHNH_3CuCl_3$", J. Phys. Soc. Jpn. **76**, No. 8, pp. 084708-1–084708-7 (2007). *

Kojima T., Tomono D., Ikeda T., Ishida K., Iwai Y., Iwasaki M., Matsuda Y., Matsuzaki T., and Yamazaki Y.: "Density enhancement of muon beams with tapered glass tubes", J. Phys. Soc. Jpn. **76**, No. 9, pp. 093501-1–093501-3 (2007). *

Kameda D., Ueno H., Asahi K., Takemura M., Yoshimi A., Haseyama T., Uchida M., Shimada K., Nagae D., Kijima G., Arai T., Takase K., Suda S., Inoue T., Murata J., Kawamura H., Kobayashi Y., Watanabe H., and Ishihara M.: "Measurement of the electric quadrupole moment of ^{32}Al", Phys. Lett. B **647**, 93–97 (2007). *

Koike T. and Harada T.: "Calculation of the ^{3}He(in-flight K^-, n) reaction for searching the deeply-bound K^-pp state", Phys. Lett. B **652**, 262–268 (2007). *

Katzgraber H. G., Herisson D., Osth M., Nordblad P., Ito A., and Aruga-Katori H.: "Finite versus zero-temperature hysteretic behavior of spin glasses: Experiment and theory", Phys. Rev. B **76**, No. 9, pp. 092408-1–092408-4 (2007). *

Urano M., Tonishi F., Inoue H., Saito T., Fujiwara T., Chiku H., Osawa A., Goto T., Suzuki T., Sasaki T., Kobayashi N., Awaji S., and Watanabe K.: "NMR study of the vortex slush phase in organic superconductor κ-(BEDT-TTF)$_2$Cu(NCS)$_2$", Phys. Rev. B **76**, 024505-1–024505-4 (2007). *

Sato W., Ueno H., Watanabe H., Miyoshi H., Yoshimi A., Kameda D., Ito T., Shimada K., Kaihara J., Suda S., Kobayashi Y., Shinohara A., Ohkubo Y., and Asahi K.: "Online time-differential perturbed angular correlation study with an ^{19}O beam Residence sites of oxygen atoms in highly oriented pyrolytic graphite", Nucl. Instrum. Methods Phys. Res. B **266**, 316–322 (2008). *

[Book•Proceedings]

(Original Papers) *Subject to Peer Review

Koike T.: "Electron population during the cascade of kaonic nitrogen atoms", Proceedings of International Conference on Exotic Atoms and Related Topics (EXA 05), Vienna, Austria, 2005–2, Austrian Academy of Science Press, Vienna, pp. 215–219 (2005). *

Kameda D., Ueno H., Asahi K., Yoshimi A., Haseyama T., Kobayashi Y., Uchida M., Miyoshi H., Kijima G., Takemura M., Nagae D., Kato G., Emori S., Oshima S., Arai T., and Tsukui M.: "Production of spin-polarized RI beams via projectile fragmentation and the application to nuclear moment measurements", Polarized-Sources and Targets: Proceedings of the 11th International Workshop, Tokyo, 2005–11, World Scientific Publishing , Toh Tuck Link, pp. 211–212 (2007).

Koike T.: "Cascade calculation of kaonic nitrogen atoms involving the electron refilling process", Proc. 3rd Asia-Pacific Conf. on Few-Body Problems in Physics (APFB05), Nakhon Ratchasima, Thailand, 2005–7, World Scientific Publishing Co. Pte. Ltd., Toh Tuck Link, pp. 171–174 (2007). *

Kameda D., Ueno H., Asahi K., Takemura M., Nagae D., Shimada K., Yoshimi A., Kobayashi Y., Haseyama

T., Uchida M., Takase K., Arai T., Inoue T., Suda S., Murata J., Kawamura H., Watanabe H., and Ishihara M.: "Nuclear moment measurements of Neutron-rich Aluminum Isotopes Using Spin-Polarized RI beams: Determination of the Boundary of the "Island of Inversion"", Proceedings of the 17th International Spin Physics Symposium (SPIN2006), Tokyo, 2006–10, American Institute of Physics, New York, pp. 845–848 (2007). *

Oral Presentations

(International Conference etc.)

Hachitani K. and Watanabe I.: "^{31}P-NMR and μSR studies of filled skutterudite compounds SmT_4P_{12}(T: Fe,Os)", International Conferenve on Strongly Correlated Electron Systems (SCES'05), (Vienna University of Technology), Vienna, Austria, July (2005).

Hachitani K. and Watanabe I.: "^{31}P-NMR and μSR studies of filled skutterudite compounds RRu$_4$P$_{12}$ (R: Sm,Gd)", International Conferenve on Strongly Correlated Electron Systems (SCES'05), (Vienna University of Technology), Vienna, Austria, July (2005).

Hachitani K.: "^{31}P-NMR and μSR studies of filled skutterudite compound SmRu$_4$P$_{12}$", 5th International Symposium on Advanced Science Research in celebration of the World Year of Physics 2005 (ASR-WYP-2005) : Advances in the Physics and Chemistry of Actinide Compounds, (JAERI), Tokai-mura, Ibaraki Pref., Sept. (2005).

Hachitani K.: "Spontaneous time reversal symmetry breakdown associated with metal-insulator transition in SmRu$_4$P$_{12}$ probed by μSR", Joint Workshop on NQP-skutterudites and NPM in multi-approarch, (Tokyo Metropolitan University), Hachioji, Nov. (2005).

Ohira-Kawamura S., Saito A., and Miyasaka H.: "Muon spin relaxation studies on Mn^{III}_2-Ni^{II} single-chain magnet and single-molecule magnet", 10th International Conference on Molecule-based Magnets (ICMM2006), Victoria BC, Canada, Aug. (2006).

Hachitani K.: "Possible octupolar order in filled skutterudite SmRu$_4$P$_{12}$ probed by ^{31}P-NMR and μSR", 1st International Symposium of Quantum Beam Science Directorate of JAEA (ICM2006 Satellite Conference), Tokai-mura, Ibaraki Pref., Aug. (2006).

Ishida K., Matsuzaki T., Imao H., Matsuda Y., Iwasaki M., Nagamine K., Kawamura N., Kato M., Sugai H., Uritani A., Harano H., Matsumoto T., and Eaton G. H.: "Muon catalyzed d-t fusion in non-equilibrated mixtures of T_2 with normal, ortho and para-rich D_2", International Conference on Muon Catalyzed Fusion and Related Topics (MCF-07), Dubna, Russia, June (2007).

Koike T. and Harada T.: "The formation of the deeply-bound K$^-$pp state in ^{3}He (in-flight K$^-$, n) reaction spectrum", International Conference on Muon Catalyzed Fusion and Related Topics (MCF-07), (Joint Institute for Nuclear Research), Dubna, Russia, June (2007).

Iio M., Ajimura S., Beer G., Bhang H., Buehler P., Busso L., Cargnelli M., Chiba J., Choi S., Curceanu C., Faso D., Fujioka H., Fukuda T., Fukuda Y., Guaraldo C., Hanaki T., Hayano R. S., Hirtl A., Iliescu M., Ishikawa T., Ishimoto S., Ishiwatari T., Itahashi K., Iwasaki M., Kienle P., Marton J., Matsuda Y., Mizoi Y., Morra O., Nagae T., Onishi H., Okada S., Outa H., Pietreanu D., Sakaguchi A., Sakuma F., Sato M., Sekimoto M., Sirghi D., Sirghi F., Suzuki S., Suzuki T., Tatsuno H., Tomono D., Toyoda A., Widmann E., Yamazaki T., Yim H., and Zmeskal J.: "A general-purpose liquid target system for hadron experiments at J-PARC", International Nuclear Physics Conference (INPC2007), (International Union for Pure and Applied Physics), Tokyo, June (2007).

Koike T. and Harada T.: "DWIA calculation of ^{3}He(K^-,n) reaction for searching K^-pp bound state", International Nuclear Physics Conference (INPC2007), (Science Council of Japan, RIKEN and others), Tokyo, June (2007).

Kameda D., Ueno H., Asahi K., Yoshimi A., Haseyama T., Kobayashi Y., Ishihara M., Nagae D., Takemura M., Shimada K., Uchida M., Arai T., Takase K., Inoue T., Kijima G., Suda S., Murata J., Kawamura H., Narota K., Toyoda T., and Watanabe H.: "Electric quadrupole moments of neutron-rich nuclei ^{32}Al and ^{31}Al", International Symposium & School on Frontiers and Perspectives of Nuclear and Hadron Physics (FPNH07), (Tokyo Institute of Technology), Tokyo, June (2007).

Koike T. and Harada T.: "The 3He(in-flight K$^-$,n) reaction spectrum form the deeply-bound K$^-$pp state", Nuclear Physics at J-PARC: Pre-symposium of INPC 2007, (KEK), Tokai village, June (2007).

Ishida K.: "Muon beam and applications - muon at RIKEN-RAL", 9th International Workshop on Neutrino Factories and Superbeams (NuFact 07), Okayama, Aug. (2007).

Iio M., Beer G., Bhang H., Buehler P., Cargnelli M., Chiba J., Choi S., Curceanu C., Fukuda Y., Guaraldo C., Hanaki T., Hayano R. S., Hirtl A., Iliescu M., Ishikawa T., Ishimoto S., Ishiwatari T., Itahashi K., Iwai M., Iwasaki M., Juhasz B., Kienle P., Marton J., Matsuda Y., Onishi H., Okada S., Outa H., Pietreanu D., Sakuma F., Sato M., Schmid P., Sirghi D., Sirghi F., Suzuki S., Suzuki T., Tatsuno H., Tomono D., Widmann E., Yamazaki T., Yim H., and Zmeskal J.: "Precise measurement of kaonic helium atoms X-rays", 12th International Conference on Hadron Spectroscopy, (INFN Laboratori Nazionali di Frascati), Rome, Italy, Oct. (2007).

Koike T. and Harada T.: "Formation of the deeply-bound K^-pp state in the ^{3}He(in-flight K^-, n) spectrum", International Conference on Chiral Symmetry in Hadron and Nuclear Physics (CHIRAL07), (Research Center for Nuclear Physics (RCNP), Osaka University), Suita, Nov.

(2007).

(Domestic Conference)

亀田大輔, 上野秀樹, 旭耕一郎, 竹村真, 吉見彰洋, 長谷山智仁, 内田誠, 島田健司, 長江大輔, 木島剛, 新井崇雅, 高瀬研以智, 須田紳一, 井上壮志, 村田次郎, 川村広和, 小林義男, 渡邉寛, 石原正泰: “中性子過剰核 32Al の核モーメント測定–魔法数 20 の閉殻構造の破れに関連して–”, 日本物理学会 2007 年春季大会, 東京, 3 月 (2007).

鈴木隆敏, Bhang H., 千葉順成, Choi S., 福田芳之, 花木俊生, 早野龍五, 飯尾雅実, 石川隆, 石元茂, 石渡智一, 板橋健太, 岩井正明, 岩崎雅彦, Kienle P., Kim J. H., 松田恭幸, 岡田信二, 大西宏明, 應田治彦, 佐藤将春, 鈴木祥二, 友野大, Widmann E., 山崎敏光, 林熙重: “^{4}He(stopped K^-, N) 反応によるストレンジマルチバリオン状態の探索”, 中間子束縛系研究会議 2007, 和光, 6 月 (2007).

鈴木隆敏, Bhang H., 千葉順成, Choi S., 福田芳之, 花木俊生, 早野龍五, 飯尾雅実, 石川隆, 石元茂, 石渡智一, 板橋健太, 岩井正明, 岩崎雅彦, Kienle P., Kim J. H., 松田恭幸, 岡田信二, 大西宏明, 應田治彦, 佐藤将春, 鈴木祥二, 友野大, Widmann E., 山崎敏光, 林熙重: “^{4}He 上の静止 K^- 反応に於けるハイパロン-核子相関によるストレンジマルチバリオン状態の探索”, 日本物理学会第 62 回年次大会, 札幌, 9 月 (2007).

松本琢磨, 上村正康, 江上智晃, 井岸康統, 緒方一介, 八尋正信: “離散化チャネル結合法による 6He, 6Li 分解反応解析”, 日本物理学会第 62 回年次大会, 札幌, 9 月 (2007).

石田勝彦, 松崎禎市郎, 松田恭幸, 岩崎雅彦, 今尾浩士, 河村成肇, 永嶺謙忠: “オルソ・パラ重水素を用いた非平衡状態 D_2/T_2 中のミュオン触媒核融合”, 日本物理学会第 62 回年次大会, 札幌, 9 月 (2007).

佐久間史典: “J-PARC における K 中間子原子核探索実験のための円筒形ドリフト・チェンバーの開発 (J-PARC E15 実験)”, 日本物理学会第 62 回年次大会, 札幌, 9 月 (2007).

飯尾雅実, 板橋健太, 岩崎雅彦, 應田治彦, 大西宏明, 岡田信二, 佐久間史典, 佐藤将春, 鈴木隆敏, 友野大, 松田恭幸, 山崎敏光, 石元茂, 岩井正明, 鈴木祥二, 関本美知子, 豊田晃久, 永江知文, 石川隆, 竜野秀行, 早野龍吾, 藤岡宏之, 味村周平, 阪口篤志, 福田芳之, 千葉順成, 花木俊夫, 福田共和, 溝井浩, Beer G., Bhang H., Choi S., Yim H., 石渡智一, Buehler P., Cargnelli M., Hirtl A., Kienle P., Marton J., Widmann E., Zmeskal J., Curceanu C., Guaraldo C., Iliescu M., Pietreanu D., Sirghi D., Sirghi F., Faso D., Busso L., Morra O.: “K 中間子原子核探査実験のための液体ヘリウム標的の開発 II”, 日本物理学会第 62 回年次大会, 札幌, 9 月 (2007).

小池貴久, 原田融: “軽い標的核における (K^-, N) 反応スペクトルの DWIA 計算”, 日本物理学会第 62 回年次大会, 札幌, 9 月 (2007).

石田勝彦: “ミュオン触媒核融合研究の現状と展望”, 物構研セミナー, (高エネルギー加速器研究機構), つくば, 10 月 (2007).

鈴木隆敏, Bhang H., 千葉順成, Choi S., 福田芳之, 花木俊生, 早野龍五, 飯尾雅実, 石川隆, 石元茂, 石渡智一, 板橋健太, 岩井正明, 岩崎雅彦, Kienle P., Kim J. H., 松田恭幸, 岡田信二, 大西宏明, 應田治彦, 佐藤将春, 鈴木祥二, 友野大, Widmann E., 山崎敏光, 林熙重: “Λ-核子相関によるストレンジマルチバリオン状態の探索”, 文部科学省科学研究費補助金特定領域研究特定領域研究「ストレンジネスで探るクォーク多体系」第 3 回総括班主催研究会 (2007), 仙台, 11 月 (2007).

飯尾雅実, 味村周平, Beer G., Bhang H., Buehler P., Busso L., Cargnelli M., 千葉順成, Choi S., Curceanu C., Faso D., 藤岡宏之, 福田共和, 福田芳之, Guaraldo C., 花木俊夫, 早野龍吾, Hirtl A., Iliescu M., 石川隆, 石元茂, 石渡智一, 板橋健太, 岩井正明, 岩崎雅彦, Kienle P., Marton J., 松田恭幸, 溝井浩, Morra O., 永江知文, 岡田信二, 大西宏明, 應田治彦, Pietreanu D., 阪口篤志, 佐久間史典, 佐藤将春, 関本美知子, Sirghi D., Sirghi F., 鈴木祥二, 鈴木隆敏, 竜野秀行, 友野大, 豊田晃久, Widmann E., 山崎敏光, Yim H., Zmeskal J.: “K 中間子原子・原子核実験のための液体ヘリウム 3 標的の開発”, 文部科学省科学研究費補助金特定領域研究特定領域研究「ストレンジネスで探るクォーク多体系」第 3 回総括班主催研究会 (2007), 仙台, 11 月 (2007).

Strasser P.: “Radioactive muonic atom studies with stopped RI beams”, 第 4 回「停止・低速不安定核を用いた核分光研究」研究会, (東北大学，理研仁科加速器研究センター，高エネルギー加速器研究機構), 仙台, 12 月 (2007).

石田勝彦: “ミュオン触媒核融合における凝集系水素の効果”, 北大低温研共同利用研究集会「低温凝集系における水素の化学と物性」, (北大低温研), 札幌, 12 月 (2007).

Strasser P.: “不安定核によるミュオニック原子生成研究”, 日本原子力研究開発機構先端基礎研究センターセミナー, 東海村, 1 月 (2008).

小池貴久, 原田融: “(K^-, N) 反応における Σ-π 崩壊しきい値付近のカスプ的構造”, 日本物理学会第 63 回年次大会, 東大阪, 3 月 (2008).

香取浩子, 三浦登, 伊藤厚子, Schoenhart M., Groessinger R., Kozlova N., Doerr K.: “絶縁体混晶スピングラス $Fe_xMn_{1-x}TiO_3$ における磁化過程の特異な磁場掃引速度依存性”, 日本物理学会第 63 回年次大会, 東大阪, 3 月 (2008).

Theoretical Physics Laboratory

Publications

[Journal]

(Original Papers) *Subject to Peer Review

Kinoshita T. and Nio M.: "Tenth-order QED contribution to the lepton $g-2$: evaluation of dominant α^5 terms of muon $g-2$.", Phys. Rev. D **73**, 053007-1–053007-21 (2006). *

Gabrielse G., Hanneke D., Kinoshita T., Nio M., and Odom B.: "New determination of the fine structure constant from the electron g value and QED", Phys. Rev. Lett. **97**, 030802-1–030802-4 (2006). *

Kawai H., Habara Y., and Ninomiya M.: "Cyclic universe a la string theory", Prog. Theor. Phys. Suppl. **164**, 7–16 (2006). *

Suzuki H.: "Two-dimensional N=(2,2) super Yang-Mills theory on computer", J. High Energy Phys. **0709**, 052-1–052-23 (2007). *

Kikukawa Y. and Suzuki H.: "Four-dimensional lattice chiral gauge theories with anomalous fermion content", J. High Energy Phys. **0710**, 018-1–018-17 (2007). *

Kinoshita T., Aoyama T., Hayakawa M., and Nio M.: "Automated evaluation of the α^5 term of lepton $g-2$: progress report", Nucl. Phys. B (Proc. Suppl.) **160**, 235–239 (2007). *

Nio M., Aoyama T., Hayakawa M., and Kinoshita T.: "QED contributions to muon g-2: tenth-order graphs", Nucl. Phys. B (Proc. Suppl.) **169**, 238–243 (2007).

Fukaya H., Aoki S., Chiu T., Hashimoto S., Kaneko T., Matsufuru H., Noaki J., Ogawa K., Onogi T., and Yamada N.: "Two-flavor lattice QCD in the epsilon-regime and chiral Random Matrix Theory", Phys. Rev. D **76**, 054503-1–054503-12 (2007). *

Aoki S., Fukaya H., Hashimoto S., and Onogi T.: "Finite volume QCD at fixed topological charge", Phys. Rev. D **76**, 054508-1–054508-11 (2007). *

Fukaya H., Aoki S., Chiu T., Hashimoto S., Hashimoto S., Kaneko T., Matsufuru H., Noaki J., Ogawa K., Okamoto M., Onogi T., and Yamada N.: "The two-flavor lattice QCD simulation in the epsilon-regime with exact chiral symmetry", Phys. Rev. Lett. **98**, 172001-1–172001-4 (2007). *

So H., Hayakawa M., and Suzuki H.: "Overlap fermion in external gravity", Proceedings of Science **LAT2006**, 047-1–047-7 (2007). *

Fukaya H., Kanamori I., Suzuki H., and Takimi T.: "Numerical results of two-dimensional N = (2,2) super Yang-Mills theory", Proceedings of Science **LAT2007**, 264-1–264-7 (2007). *

Kishimoto I. and Michishita Y.: "Comments on solutions for nonsingular currents in open string field theories", Prog. Theor. Phys. **118**, No. 2, pp. 347–369 (2007). *

(Review)

仁尾真紀子, 木下東一郎: "レプトンの異常磁気能率と量子電気力学", 日本物理学会誌 **61**, No. 8, pp. 565–572 (2006).

仁尾真紀子: "微細構造定数 α を究める", パリティ **22**, No. 02, pp. 6–13 (2007).

(Others)

仁尾真紀子: "量子電気力学の検証", 別冊・数理科学 **:** 場の量子論の拡がり-現代からみた種々相- **2006**, 34–39 (2006).

Oral Presentations

(Domestic Conference)

岸本功, 道下洋二: "Comments on solutions for nonsingular currents in open string field theories", 京都大学基礎物理学研究所研究会「弦理論と場の理論 **:** 量子と時空の最前線」, 東大阪, 8 月 (2007).

岸本功: "開弦の場の理論の解析解をめぐる最近の進展", 日本物理学会第 62 回年次大会, 札幌, 9 月 (2007).

岸本功: "Schnabl 解に対するあるゲージ不変量の計算", 理研シンポジウム「量子場の理論と対称性」, 和光, 12 月 (2007).

Accelerator Applications Research Group

Publications

[Journal]

(Original Papers) *Subject to Peer Review

Kambara T., Kanai Y., Kojima T., Nakai Y., Yoneda A., Yamazaki Y., and Kageyama K.: "Elastic waves from fast heavy-ion irradiation on solids", J.Acoust.Emiss. **24**, 97–103 (2006). *

Kanai Y., Hoshino M., Kambara T., Ikeda T., Hellhammer R., Stolterfoht N., and Yamazaki Y.: "Two-dimensional images of transmitted slow neon ions guided by nanocapillaries in polymer foils", Nucl. Instrum. Methods Phys. Res. B **258**, 155–158 (2006). *

Ichida H., Maeda K., Ichise H., Matsuyama T., Abe T., Yoneyama K., and Koba T.: "*In silico* restriction landmark genome scanning analysis of *Xanthomonas oryzae* pathovar *oryzae* MAFF 311018", Biochem. Biophys. Res. Commun. **363**, 852–856 (2007). *

Kageyama K., Kambara T., and Nakai Y.: "Detection of weak ultrasound generated by nano- and femtosecond laser irradiation using piezoelectric sensors", J. Solid Mech. Mater. Eng. **1**, No. 9, pp. 1128–1135 (2007). *

Hoshino M., Kambara T., Kanai Y., Schuch R., and Yamazaki Y.: "Multielectron processes in close collisions of slow Ne^{q+}(q=1-9) ions with Ar atoms", Phys. Rev. A **75**, 032722-1–032722-7 (2007). *

市田裕之, 木庭卓人, 龍頭啓充, 福西暢尚, 林依子, 阿部知子, 松山知樹: "重イオンビームによって誘発される DNA 多型の解析", DNA 多型 **15**, 118–121 (2007). *

(Others)

神原正: "理化学研究所 RI ビームファクトリーにおける RI 製造", Isotope News, No. 646, pp. 17–20 (2008).

Oral Presentations

(International Conference etc.)

Ichida H., Matsuyama T., Abe T., and Koba T.: "Bacterial DNA adenine methylation changes dramatically before and after establishing symbiosis", 13rd International Congress on Molecular Plant-Microbe Interactions, Sorrento, Italy, July (2007).

Kanai Y., Hoshino M., Ikeda T., Kambara T., Hellhammer R., Stolterfoht N., and Yamazaki Y.: "Dynamic features of a beam guiding by insulator capillaries", 25th International Conference on Photonic, Electronic and Atomic Collisions (ICPEAC 2007), Freiburg, Germany, July (2007).

Kazama Y., Saito H., Yamamoto Y. Y., Hayashi Y., Ichida H., Ohbu S., Ryuto H., Fukunishi N., and Abe T.: "Effects of Heavy-ion beam irradiation on mutation induction in *Arabidopsis thaliana*", 18th International Conference on Cyclotrons and their Applications (Cyclotrons 2007), Giardini Naxos, Italy, Oct. (2007).

Hayashi Y., Takehisa H., Kazama Y., Ichida H., Ryuto H., Fukunishi N., Abe T., Kamba C., and Sato T.: "Effects of ion beam irradiation on mutation induction in rice", 18th International Conference on Cyclotrons and their Applications (Cyclotrons 2007), Giardini Naxos, Italy, Oct. (2007).

Abe T., Kazama Y., Ichida H., Hayashi Y., Ryuto H., and Fukunishi N.: "Plant Breeding using the ion beam irradiation in RIKEN", 18th International Conference on Cyclotrons and their Applications (Cyclotrons 2007), Giardini Naxos, Italy, Oct. (2007).

(Domestic Conference)

神波千秋, 竹久妃奈子, 阿部知子, 林依子, 斉藤宏之, 市田裕之, 小沼亮子, 龍頭啓充, 福西暢尚, 宮沢豊, 東海林英夫, 保倉明子, 福田直樹, 中井泉, 佐藤雅志: "重イオンビーム照射により作出されたイネ塩害耐性突然変異系統の特性解析", 日本育種学会第 111 回講演会, (日本育種学会), 水戸, 3 月 (2007).

神原正: "理研 RI ビームファクトリーの高速重イオンによる応用研究", 日本物理学会 2007 年春季大会, (日本物理学会), 鹿児島, 3 月 (2007).

金井 保之, 星野 正光, 池田 時浩, 神原 正, Hellhammer R., Stolterfoht N., 山崎泰規: "絶縁体キャピラリーによるビームガイド効果の入射イオン電流依存性", 日本物理学会 2007 年春季大会, 鹿児島, 3 月 (2007).

竹久妃奈子, 林依子, 風間裕介, 神波千秋, 市田裕之, 龍頭啓充, 福西暢尚, 宮沢豊, 東海林英夫, 佐藤雅志, 阿部知子: "炭素イオン照射により誘導した、シワ-矮性イネ突然変異株 (*ssw*) の特性解析", 日本育種学会第 112 回講演会, 鶴岡, 9 月 (2007).

市田裕之, 松山知樹, 阿部知子, 木庭卓人: "根粒菌ゲノムの DNA メチル化を介した共生制御機構", 植物微生物研究会第 17 回研究交流会, 鹿児島, 9 月 (2007).

神波千秋, 竹久妃奈子, 林依子, 市田裕之, 小沼亮子, 龍頭啓充, 福西暢尚, 宮沢豊, 東海林英夫, 保倉明子, 福田直樹, 中井泉, 阿部知子, 佐藤雅志: "イネ塩害耐性突然変異体 6-99L の耐塩性に関わる生理要因の解明", 第 224 回日本作物学会講演会, 金沢, 9 月 (2007).

神原正: "理研 RI ビームファクトリー利用の現状", 第 12 回放射線プロセスシンポジウム, (放射線利用振興協会), 東京, 11 月 (2007).

風間裕介, 斉藤宏之, 大部澄江, 林依子, 市田裕之, 龍頭啓充, 福西暢尚, 松山知樹, 阿部知子: "重イオンビーム照射を用いたシロイヌナズナ突然変異誘発における LET 効果", 第 49 回日本植物生理学会年会, 札幌, 3 月 (2008).

Radiation Biology Team

Publications

[Journal]

(Original Papers) *Subject to Peer Review

Otani M., Saito H., Abe T., and Shimada T.: "Induction of mutations in sweetpotato plants by heavy-ion beam irradiation", Acta Hort. **703**, 171–173 (2006). *

Kambara T., Kanai Y., Kojima T., Nakai Y., Yoneda A., Yamazaki Y., and Kageyama K.: "Elastic waves from fast heavy-ion irradiation on solids", J.Acoust.Emiss. **24**, 97–103 (2006). *

Imanishi S., Noguchi A., Nagata M., Abe T., and Honda I.: "Construction of libraries of 'Micro-Tom' tomato mutations induced by heavy-ion bombardment", Acta Hort. **745**, 485–489 (2007). *

Ichida H., Maeda K., Ichise H., Matsuyama T., Abe T., Yoneyama K., and Koba T.: "*In silico* restriction landmark genome scanning analysis of *Xanthomonas oryzae* pathovar *oryzae* MAFF 311018", Biochem. Biophys. Res. Commun. **363**, 852–856 (2007). *

Kazama Y., Saito H., Fujiwara M., Matsuyama T., Hayashi Y., Ryuto H., Fukunishi N., and Abe T.: "An effective method for detection and analysis of DNA damage induced by heavy-ion beams", Biosci. Biotechnol. Biochem. **71**, No. 11, pp. 2864–2869 (2007). *

Godo T., Okuno H., Saito H., Miyazawa Y., Ryuto H., Fukunishi N., and Abe T.: "Effects of ion beam irradiation on survival and mutation induction of triploid Senno (Lychnis senno Siebold et Zucc.)", Bull.Bot.Gard.Toyama, No. 12, pp. 41–46 (2007). *

Shitsukawa N., Ikai C., Shimada S., Kitagawa S., Sakamoto K., Saito H., Ryuto H., Fukunishi N., Abe T., Takumi S., Nasuda S., and Murai K.: "The einkorn wheat (Triticum monococcum) mutant, maintained vegetative phase, is caused by a deletion in the VRN1 gene", Genes Genet. Syst. **82**, 167–170 (2007). *

Ikeda T., Kojima T., Iwai Y., Kanai Y., Kambara T., Nebiki T., Narusawa T., and Yamazaki Y.: "Production of a nm sized slow HCI beam with a guiding effect", J. Phys.: Con. Ser. **58**, 68–73 (2007). *

Kageyama K., Kambara T., and Nakai Y.: "Detection of weak ultrasound generated by nano- and femtosecond laser irradiation using piezoelectric sensors", J. Solid Mech. Mater. Eng. **1**, No. 9, pp. 1128–1135 (2007). *

Ryuto H., Hasebe H., Fukunishi N., Abe T., Goto A., Kase M., and Yano Y.: "Charge-stripping foil changer with energy adjuster function", Nucl. Instrum. Methods Phys. Res. A **581**, No. 3, pp. 586–588 (2007). *

Koizumi A., Amanai Y., Ishii K., Nishihara K., Kazama Y., Uchida W., and Kawano S.: "Floral development of an asexual and female-like mutant carrying two deletions in gynoecium-suppressing and stamen-promoting functional regions on the Y chromosome of the dioecious plant *Silene latifolia*", Plant Cell Physiol. **48**, No. 10, pp. 1450–1461 (2007). *

Kazama Y., Ishii C., Schroeder A. L., Shimada H., Wakabayashi M., and Inoue H.: "The Neurospora crassa *UVS-3* epistasis group encodes homologues of the ATR/ATRIP checkpoint control system", DNA Repair **7**, No. 2, pp. 213–229 (2008). *

市田裕之, 木庭卓人, 龍頭啓充, 福西暢尚, 林依子, 阿部知子, 松山知樹: "重イオンビームによって誘発される DNA 多型の解析", DNA 多型 **15**, 118–121 (2007). *

伊東靖之, 関栄一, 大越一雄, 渡邉学, 斉藤宏之, 林依子, 阿部知子: "ベゴニア類のイオンビーム照射による変異誘導", 千葉県農業総合研究センター研究報告, No. 6, pp. 75–84 (2007).

(Review)

Takehisa H. and Sato T.: "Stress, physiological and genetic factors of rice leaf bronzing in paddy fields", Japanese J. Plant Sci. **1**, No. 2, pp. 63–68 (2007).

阿部知子: "イオンビーム育種研究のこれまでの成果", 原子力 eye **53**, No. 5, pp. 25–27 (2007).

[Book・Proceedings]

(Original Papers) *Subject to Peer Review

Kanaya T., Miyazaki K., Suzuki K., Iwaki K., Ichida H., Hayashi Y., Saito H., Ryuto H., Fukunishi N., and Abe T.: "New cultivar produced by heavy-ion beam irradiation", Proceedings of the 25th Symposium on Materials Science and Engineering, Research Center of Ion Beam Technology, Hosei University, Japan, 2006–11, Research Center of Ion Beam Technology, Hosei University, Tokyo, pp. 1–6 (2007).

Oral Presentations

(International Conference etc.)

Kambara T.: "Interdisciplinary research activities at the RIBF in RIKEN", 3rd SPARC Topical Workshop, (Organizing Committee), Paris, Feb. (2007).

Ichida H., Matsuyama T., Abe T., and Koba T.: "Bacterial DNA adenine methylation changes dramatically before and after establishing symbiosis", 13rd International Congress on Molecular Plant-Microbe Interactions, Sorrento, Italy, July (2007).

Aoyama T., Morita R., Hayashi Y., Kazama Y., Abe T., Kurata T., Nishiyama T., Tanahashi T., and Hasabe M.: "Establishment of a forward genetic approach using a genome tilling array in the moss Physcomitrella patens", The Annual International Conference for Moss Experimental Research (Moss 2007), (Korea University), Seoul, Korea, Aug. (2007).

Kazama Y., Saito H., Yamamoto Y. Y., Hayashi Y., Ichida H., Ohbu S., Ryuto H., Fukunishi N., and Abe T.: "Effects of Heavy-ion beam irradiation on mutation induction in *Arabidopsis thaliana*", 18th International Conference on Cyclotrons and their Applications (Cyclotrons 2007), Giardini Naxos, Italy, Oct. (2007).

Hayashi Y., Takehisa H., Kazama Y., Ichida H., Ryuto H.,

Fukunishi N., Abe T., Kamba C., and Sato T.: “Effects of ion beam irradiation on mutation induction in rice”, 18th International Conference on Cyclotrons and their Applications (Cyclotrons 2007), Giardini Naxos, Italy, Oct. (2007).

Abe T., Kazama Y., Ichida H., Hayashi Y., Ryuto H., and Fukunishi N.: “Plant Breeding using the ion beam irradiation in RIKEN”, 18th International Conference on Cyclotrons and their Applications (Cyclotrons 2007), Giardini Naxos, Italy, Oct. (2007).

(Domestic Conference)

藤原誠, 阿部知子, 吉田茂男, 佐藤直樹, 伊藤竜一: “FtsZ1 リングおよび葉緑体分裂面形成の空間的制御における MinE の役割”, イネ・シロイヌナズナ合同ワークショップ 2005, 奈良, 7 月 (2005).

藤原誠, 箸本春樹, 阿部知子, 吉田茂男, 佐藤直樹, 伊藤竜一: “MinE による葉緑体分裂面形成の空間的制御”, 第 47 回日本植物生理学会年会, つくば, 3 月 (2006).

藤原誠, 箸本春樹, 阿部知子, 吉田茂男, 佐藤直樹, 伊藤竜一: “葉緑体分裂位置決定における MinE の役割”, 日本植物学会第 70 回大会, 熊本, 9 月 (2006).

泉雅子: “ヒト Mcm10 の機能ドメインの解析”, 第 18 回 DNA 複製・分配ワークショップ, 熱海, 10 月 (2006).

神原正: “量子ビームの特性（放射線物理として）”, 農林水産分野における量子ビームの利用シンポジウム, (農林水産先端技術産業振興センター), 東京, 2 月 (2007).

阿部知子: “量子ビームの園芸作物育種への応用”, 農林水産分野における量子ビームの利用シンポジウム, (農林水産先端技術総合研究機構), 東京, 2 月 (2007).

神波千秋, 竹久妃奈子, 阿部知子, 林依子, 斉藤宏之, 市田裕之, 小沼亮子, 龍頭啓充, 福西暢尚, 宮沢豊, 東海林英夫, 保倉明子, 福田直樹, 中井泉, 佐藤雅志: “重イオンビーム照射により作出されたイネ塩害耐性突然変異系統の特性解析”, 日本育種学会第 111 回講演会, (日本育種学会), 水戸, 3 月 (2007).

林依子, 竹久妃奈子, 風間裕介, 神波千秋, 東海林英夫, 斉藤宏之, 龍頭啓充, 福西暢尚, 宮沢豊, 阿部知子, 佐藤雅志: “イネにおける重イオンビーム照射による突然変異誘発効果”, 日本育種学会第 111 回講演会, (日本育種学会), 水戸, 3 月 (2007).

風間 裕介, 斉藤宏之, 宮沢豊, 金谷健至, 鈴木賢一, 林依子, 龍頭啓充, 福西暢尚, Bae C., 阿部知子: “重イオンビーム照射で作出したタバコ花色変異体の解析”, 日本育種学会第 111 回講演会, (日本育種学会), 水戸, 3 月 (2007).

竹久妃奈子, 福田善通, 阿部知子, 福田直樹, 小原実広, 山谷知行, 保倉明子, 中井泉, 東谷篤志, 佐藤雅志: “塩害水田におけるイネの Leaf-bronzing の発症を制御する *qLb-3* と *qLb-11* のファインマッピング”, 日本育種学会第 111 回講演会, 水戸, 3 月 (2007).

小泉綾子, 天内康人, 石井公太郎, 西原潔, 風間裕介, 阿部知子, 河野重行: “ヒロハノマンテマ無性花変異体 K034 と両性花変異体 R025 の花発達と性染色体欠損”, 第 48 回日本植物生理学会年会, 松山, 3 月 (2007).

斉藤宏之: “重イオンビームを利用した植物育種”, 地域密着型農業バイオ研究セミナー, (新潟県刈羽郡刈羽村), 新潟県刈羽村, 3 月 (2007).

福田直樹, 阿部知子, 林依子, 竹久妃奈子, 寺田靖子, 北島信行, 保倉明子, 中井泉: “放射光マイクロビームを用いたイネ耐塩性変異株 (6-99L) における Cd の蛍光 X 線二次元イメージング”, 第 4 回イオンビーム育種研究会, 水戸, 7 月 (2007).

西原潔, 風間裕介, 小泉綾子, 山中香, 河野重行, 阿部知子: “炭素イオンビーム照射により得られた雌雄異株植物ヒロハノマンテマ両性花変異体の解析”, 第 4 回イオンビーム育種研究会, 水戸, 7 月 (2007).

今西俊介, 野口有里紗, 林依子, 福西暢尚, 龍頭啓充, 永田雅靖, 本多一郎, 阿部知子: “重イオンビーム照射による極矮性トマト「マイクロトム」変異系統の整備”, 第 4 回イオンビーム育種研究会, 水戸, 7 月 (2007).

武弓利雄, 阿部知子, 林依子, 山ノ内宏昭, 吉岡照高, 村松昇, 福西暢尚, 龍頭啓充: “チャ種子のイオンビーム照射効果に及ぼす線量と LET の影響”, 第 4 回イオンビーム育種研究会, 水戸, 7 月 (2007).

竹久妃奈子, 林依子, 風間裕介, 神波千秋, 市田裕之, 龍頭啓充, 福西暢尚, 宮沢豊, 東海林英夫, 佐藤雅志, 阿部知子: “重イオンビーム照射により誘導されたイネ突然変異体の特性解析”, イオン育種研究会, (日本原子力研究開発機構 高崎量子応用研究所), 水戸, 7 月 (2007).

阿部知子: “重イオンビームによる花きの高バラエティ化と付加価値付与”, 第 25 回日本植物細胞分子生物学会大会・シンポジウム, 千葉, 8 月 (2007).

竹久妃奈子, 林依子, 風間裕介, 神波千秋, 市田裕之, 龍頭啓充, 福西暢尚, 宮沢豊, 東海林英夫, 佐藤雅志, 阿部知子: “炭素イオン照射により誘導した、シワ-矮性イネ突然変異株 (*ssw*) の特性解析”, 日本育種学会第 112 回講演会, 鶴岡, 9 月 (2007).

杉山正夫, 市田裕之, 林依子, 福西暢尚, 龍頭啓充, 寺川輝彦, 阿部知子: “重イオンビーム照射によるシクラメン突然変異体の誘発”, 日本育種学会第 112 回講演会, 鶴岡, 9 月 (2007).

阿部知子, 風間裕介, 林依子, 市田裕之, 竹久妃奈子: “イオンビーム育種の最近の成果と今後の展開”, 日本育種学会第 112 回講演会, 鶴岡, 9 月 (2007).

鈴木隆之, 北川哲, 阿部知子, 半田裕一, 村井耕二: “コムギ花成における WAP1/VRN1-WFT-VRN2 トライアングルモデル”, 日本育種学会第 112 回講演会, 鶴岡, 9 月 (2007).

風間 裕介, 斉藤宏之, 宮沢豊, 金谷健至, 鈴木賢一, 林依子, 龍頭啓充, 福西暢尚, Bae C., 阿部知子: “重イオンビーム照射で作出されたタバコ白花変異体について”, 日本育種学会第 112 回講演会, 鶴岡, 9 月 (2007).

市田裕之, 松山知樹, 阿部知子, 木庭卓人: “根粒菌ゲノムの DNA メチル化を介した共生制御機構”, 植物微生物研究会第 17 回研究交流会, 鹿児島, 9 月 (2007).

風間裕介, 藤原誠, 小泉綾子, 西原潔, 阿部知子, 河野重行: “ヒロハノマンテマのメス特異的遺伝子 *SlSUP* の解析”, 日本植物形態学会第 19 回大会, 野田, 9 月 (2007).

寺岡毅, 澤野郁夫, 中島輝子, 加々美裕, 神尾章子, 林依子, 龍頭啓充, 福西暢尚, 阿部知子: “重イオンビーム照射がウンシュウミカンの生育に及ぼす影響”, 園芸学会平成 19 年度秋季大会, 高松, 9 月 (2007).

金澤悠, 池田時浩, 金井保之, Orourke B. E., 岩井良夫, 小島隆夫, 星野正光, 神原正, 小林知洋, 田中大, 山崎泰規: “ガラスキャピラリーを用いた低速多価イオンによるナノファブリケーション”, 日本物理学会第 62 回年次大会, 札幌, 9 月 (2007).

風間裕介, 藤原誠, 小泉綾子, 西原潔, 阿部知子, 河野重行: “ヒロハノマンテマの SUPERMAN ホモログは雌花 (♀) 特異的に発現し雄蕊 (♂) の発達を抑制する”, 日本植物学会第 71 回大会, 野田, 9 月 (2007).

西原潔, 風間裕介, 藤原誠, 小泉綾子, 山中香, 阿部知子, 河野重行: “雌雄異株植物ヒロハノマンテマの X 染色体連鎖 *WUS* ホモログ *SlWUS* の発現と機能”, 日本遺伝学会第 79 回大会, 岡山, 9 月 (2007).

神波千秋, 竹久妃奈子, 林依子, 市田裕之, 小沼亮子, 龍頭啓充, 福西暢尚, 宮沢豊, 東海林英夫, 保倉明子, 福田直樹, 中井泉, 阿部知子, 佐藤雅志: “イネ塩害耐性突然変異体 6-99L の耐塩性に関わる生理要因の解明”, 第 224 回日本作物学会講演会, 金沢, 9 月 (2007).

阿部知子: “イオンビームによる園芸植物の育種”, 第 9 回加速器利用技術セミナー, (文部科学省), 長岡, 10 月 (2007).

阿部知子: “イオンビームによる園芸植物の育種”, 第 10 回加速器利用技術セミナー「健康なくらしを創造する量子ビームの活用」, (文部科学省), 郡山, 11 月 (2007).

白尾吏, 松山知樹, 上野敬一郎, 阿部知子: “イオンビーム育種により育成した秋輪ギク「今神」の品種識別”, 日本 DNA 多型学会第 16 回学術集会, 大阪, 11 月 (2007).

泉雅子: “複製開始・伸長反応におけるヒト Mcm10 の機能解析”, 第 30 回日本分子生物学会年会・第 80 回日本生化学会大会 (BMB2007), 横浜, 12 月 (2007).

阿部知子: “重イオンビームによる新規植物資源創出”, 東北大学・農学・生命化学融合シンポジウム「地球温暖化と植物」, 仙台, 12 月 (2007).

大部澄江, 風間裕介, 阿部知子: “クリーンベンチ作業の極意”, 和泊町雇用創造推進協議会講演会, 鹿児島県和泊町, 12 月 (2007).

風間裕介, 大部澄江, 阿部知子: “パパイアの雌雄性とクローン技術による大量増殖”, 和泊町雇用創造推進協議会講演会, 鹿児島県和泊町, 12 月 (2007).

風間裕介, 斉藤宏之, 山本義治, 林依子, 阿部知子: “シロイヌナズナへの重イオンビーム変異誘発における LET 効果と DNA 変異”, 日本育種学会第 113 回講演会, 川崎, 3 月 (2008).

藤原誠, 風間裕介, 斉藤宏之, 松山知樹, 林依子, 龍頭啓充, 福西暢尚, 阿部知子: “重イオンビーム照射による DNA 変異を検出・解析する効率的なシステム”, 日本農芸化学会 2008 年度大会, 名古屋, 3 月 (2008).

風間裕介, 斉藤宏之, 大部澄江, 林依子, 市田裕之, 龍頭啓充, 福西暢尚, 松山知樹, 阿部知子: “重イオンビーム照射を用いたシロイヌナズナ突然変異誘発における LET 効果”, 第 49 回日本植物生理学会年会, 札幌, 3 月 (2008).

RI Applications Team

Publications

[Journal]

(Original Papers) *Subject to Peer Review

Sato W., Ueno H., Taniguchi A., Itsuki Y., Kasamatsu Y., Shinohara A., Asahi K., Asai K., and Ohkubo Y.: "Nuclear quadrupole relaxation of ^{140}Ce implanted in highly oriented pyrolytic graphite", Phys. Rev. B **74**, No. 21, pp. 214302-1–214302-7 (2006). *

Kidera M., Takahashi K., Enomoto S., Mitsubori Y., Goto A., and Yano Y.: "Development of a novel mass spectrometer equipped with an electron cyclotron resonance ion source", Eur. J. Mass Spectrom. **13**, 239–248 (2007). *

Kidera M., Takahashi K., Enomoto S., Goto A., and Yano Y.: "New fragment ion production method using super cold electrons in electron cyclotron resonance plasma", Eur. J. Mass Spectrom. **13**, 355–358 (2007). *

Haba H., Akiyama T., Kaji D., Kikunaga H., Kuribayashi T., Morimoto K., Morita K., Ooe K., Sato N., Shinohara A., Takabe T., Tashiro T., Toyoshima A., Yoneda A., and Yoshimura T.: "Startup of superheavy element chemistry at RIKEN", Eur. Phys. J. D **45**, 81–86 (2007). *

Yamashita Y., Takahashi Y., Haba H., Enomoto S., and Shimizu H.: "Comparison of reductive accumulation of Re and Os in seawater - sediment systems", Geochimica Cosmochimica Acta **71**, No. 14, pp. 3458–3475 (2007). *

Motomura S., Enomoto S., Haba H., Igarashi K., Gono Y., and Yano Y.: "Gamma-Ray Compton Imaging of Multitracer in Biological Samples using Strip Germanium Telescope", IEEE Trans. Nucl. Sci. **54**, No. 3, pp. 710–717 (2007). *

Haba H., Kaji D., Kikunaga H., Akiyama T., Sato N., Morimoto K., Yoneda A., Morita K., Takabe T., and Shinohara A.: "Development of gas-jet transport system coupled to the RIKEN Gas-filled Recoil Ion Separator GARIS for superheavy element chemistry", J. Nucl. Radiochem. Sci. **8**, No. 2, pp. 55–58 (2007). *

Kasamatu Y., Toyoshima A., Toume H., Tsukada K., Haba H., and Nagame Y.: "Anion-exchange behavior of Nb, Ta, and Pa as homologues of Db in HF/HNO3 solutions", J. Nucl. Radiochem. Sci. **8**, No. 2, pp. 69–72 (2007). *

Takahashi M.: "The Chemical behavior of silica in water in saline area; comparison for region and evaporation process", Spectrochim. Acta Pt. A **68**, 21–28 (2007). *

[Book・Proceedings]

(Others)

Motomura S., Kanayama Y., Haba H., Watanabe Y., and Enomoto S.: "Multiple Nuclide Imaging in Live Mouse Using Semiconductor Compton Camera for Multiple Molecular Imaging", 2007 IEEE Nuclear Science Symposium Conference Record, Honolulu, USA, 2007–10〜11, IEEE, Piscataway, pp. 3741–3742 (2007).

Oral Presentations

(International Conference etc.)

Asai M., Tsukada K., Sakama M., Ishii Y., Toyoshima A., Ishii T., Nishinaka I., Nagame Y., Kasamatsu Y., Haba H., Kojima Y., Shibata M., Hayashi H., and Sueki K.: "Alpha-gamma spectroscopy of N = 155 and 157 nuclei using a gas-jet transport technique", 3rd International Conference on the Chemistry and Physics of the Transactinide Elements (TAN 07), (Paul Scherrer Institut and Bern University), Davos, Switzerland, Sept. (2007).

Kasamatsu Y., Toyoshima A., Asai M., Tsukada K., Haba H., Ishii Y., Toume H., Nishinaka I., Akiyama K., Kikunaga H., Goto S., Ishikawa T., Kudo H., Sato W., Ooe K., Kuribayashi T., Shinohara A., Kinoshita N., Arai M., Yokoyama A., Sakama M., Sato T., Qin Z., Duellmann C. E., and Nagame Y.: "Anion-exchange behavior of element 105, Db, in HF/HNO3 media", 3rd International Conference on the Chemistry and Physics of the Transactinide Elements (TAN 07), (Paul Scherrer Institut and Bern University), Davos, Switzerland, Sept. (2007).

Toyoshima A., Kasamatsu Y., Tsukada K., Kitatsuji A., Haba H., Ishii Y., Toume H., Asai M., Akiyama K., Ooe K., Sato W., Shinohara A., and Nagame Y.: "Electrochemical oxidation of nobelium", 3rd International Conference on the Chemistry and Physics of the Transactinide Elements (TAN 07), (Paul Scherrer Institut and Bern University), Davos, Switzerland, Sept. (2007).

Nagame Y., Toyoshima A., Ishii Y., Tsukada K., Asai M., Toume H., Kasamatsu Y., Nishinaka I., Sato T., Haba H., Kikunaga H., Akiyama K., Oura Y., Nakahara H., Sato W., Shinohara A., Goto S., Kudo H., Yokoyama A., Sakama M., Sueki K., Schaedel M., Bruechle W., and Kratz J. V.: "Fluoride complex formation of element 104, Rutherfordium", 3rd International Conference on the Chemistry and Physics of the Transactinide Elements (TAN 07), (Paul Scherrer Institut and Bern University), Davos, Switzerland, Sept. (2007).

Kaji D., Haba H., Kikunaga H., Morimoto K., Akiyama T., Kudo H., Ooe K., Nanri T., Sato N., Shinohara A., Suzuki D., Takabe T., Yamazaki I., Yokoyama A., Yoneda A., and Morita K.: "Performance of a gas-filled recoil separator GARIS for hot fusion study", 3rd International Conference on the Chemistry and Physics of the Transactinide Elements (TAN 07), (Paul Scherrer Institut and Bern University), Davos, Switzerland, Sept. (2007).

Haba H., Akiyama T., Kaji D., Kikunaga H., Kuribayashi T., Morimoto K., Morita K., Nanri T., Ooe K., Sato N., Shinohara A., Suzuki D., Toyoshima A., Yamazaki I., Yokoyama A., Yoneda A., and Yoshimura T.: "Present

status and perspectives of superheavy element chemistry at RIKEN", 3rd International Conference on the Chemistry and Physics of the Transactinide Elements (TAN 07), (Paul Scherrer Institut and Bern University), Davos, Switzerland, Sept. (2007).

(Domestic Conference)

望月優子, 五十嵐誠, 高橋和也, 牧島一夫, 馬場彩, 中井陽一, 本山秀明, 神山孝吉, 鈴木啓助: "ドームふじ浅層コアのイオン詳細解析：現状と今後", 国立極地研究所研究集会「南極氷床の物理・化学・生物のフロンティア３」, 東京, 3 月 (2007).

川畑俊明, 鳥山保, 高木靖雄, 川崎克則, 長谷川賢一, 前田邦子, 小栗慶之: "波長分散型粒子線誘起 X 線分析法（WD ー PIXE）による固体高分子型燃料電池中の硫黄の分析", 電気化学会第 74 回大会, (電気化学会), 野田, 3 月 (2007).

笠松良崇, 豊嶋厚史, 當銘勇人, 塚田和明, 羽場宏光, 永目諭一郎: "105 番元素 (Db) の化学的研究を目指した Nb,Ta,Pa の HF/HNO3 溶液系における陰イオン交換実験", 日本化学会第 87 春季年会, 吹田, 3 月 (2007).

當銘勇人, 笠松良崇, 豊嶋厚史, 石井康雄, 塚田和明, 羽場宏光, 篠原伸夫, 永目諭一郎: "HF/HNO3 混合水溶液中における Nb,Ta の陽イオン交換実験：105 番元素 Db の化学的研究に向けて", 日本化学会第 87 春季年会, 吹田, 3 月 (2007).

石井康雄, 當銘勇人, 豊嶋厚史, 浅井雅人, 西中一朗, 塚田和明, 永目諭一郎, 宮下直, 森友隆, 菅沼英夫, 田代祐基, 篠原厚, 坂牧雅巳, 後藤真一, 工藤久昭, 羽場宏光, 秋山和彦, 大浦泰嗣: "ラザホージウムの硝酸/フッ化水素酸系におけるフッ化物錯形成", 日本化学会第 87 春季年会, 吹田, 3 月 (2007).

豊嶋厚史, 笠松良崇, 北辻章浩, 塚田和明, 石井康雄, 當銘勇人, 浅井雅人, 羽場宏光, 秋山和彦, 大江一弘, 佐藤渉, 篠原厚, 永目諭一郎: "ノーベリウムの酸化", 日本化学会第 87 春季年会, 吹田, 3 月 (2007).

羽場宏光, 菊永英寿, 加治大哉, 佐藤望, 秋山隆宏, 森本幸司, 米田晃, 森田浩介, 高部智正, 大江一弘, 篠原厚, 南里朋洋, 鈴木大介, 山崎逸郎, 横山明彦: "超重元素化学研究に向けた GARIS 直結型ガスジェット搬送システムの性能評価", 日本化学会第 87 春季年会, 吹田, 3 月 (2007).

高部智正, 羽場宏光, 加治大哉, 菊永英寿, 大江一弘, 田代祐基, 佐藤望, 吉村崇, 工藤久昭, 三頭聰明, 森田浩介, 篠原厚: "RIKEN における ^{248}Cm(^{22}Ne,5n)^{265}Sg 反応を用いたシーボーギウム合成実験 (1)", 日本化学会第 87 春季年会, 吹田, 3 月 (2007).

大江一弘, 田代祐基, 高部智正, 栗林隆宏, 矢作亘, 吉村崇, 佐藤渉, 高橋成人, 高久圭二, 羽場宏光, 榎本秀一, 篠原厚: "オンライン迅速溶媒抽出システムを用いたアクチノイドの系統的研究", 日本化学会第 87 春季年会, 吹田, 3 月 (2007).

三堀陽平, 高橋和也, 木寺正憲, 榎本秀一, 田中龍彦, 南武志, 今津節生, 林英男: "微量元素分析に基づく、古墳等の遺構から出土した辰砂の産地推定の試み", 第 68 回分析化学討論会, (社団法人日本分析化学会), 宇都宮, 5 月 (2007).

笠松良崇, 當銘勇人, 豊嶋厚史, 塚田和明, 浅井雅人, 石井康雄, 西中一朗, 佐藤哲也, 篠原伸夫, 永目諭一郎, 羽場宏光, 菊永英寿, 秋山和彦, 後藤真一, 石川剛, 工藤久昭, 佐藤渉, 大江一弘, 栗林隆宏, 篠原厚, 木下哲一, 荒井美和子, 横山明彦, 阪間稔, Qin Z., Duellmann C. E.: "105 番元素 Db の HF/HNO3 混合水溶液中における化学挙動", 2007 日本放射化学会年会・第 51 回放射化学討論会, (日本放射化学会), 静岡, 9 月 (2007).

菊永英寿, 笠松良崇, 羽場宏光, 加治大哉, 森本幸司, 坂本一郎: "^{90m}Nb の半減期精密測定に向けたガスジェット搬送装置の開発と性能評価", 2007 日本放射化学会年会・第 51 回放射化学討論会, 静岡, 9 月 (2007).

栗林隆宏, 大江一弘, 尾本隆志, 藤沢弘幸, 小森有希子, 高橋成人, 吉村崇, 羽場宏光, 榎本秀一, 三頭聰明, 篠原厚: "キャピラリー電気泳動の希土類の相互分離と短寿命核種への適用", 2007 日本放射化学会年会・第 51 回放射化学討論会, (日本放射化学会), 静岡, 9 月 (2007).

木寺正憲, 高橋和也, 榎本秀一, 中川孝秀, 三堀陽平, 田中龍彦, 戸田勝善: "電子サイクロトロン共鳴イオン源 (ECRIS) を用いた質量分析装置の開発", 日本分析化学会第 56 年会, 徳島, 9 月 (2007).

Metallomics Reserch Unit

Publications

[Journal]

(Original Papers) *Subject to Peer Review

Kidera M., Takahashi K., Enomoto S., Mitsubori Y., Goto A., and Yano Y.: "Development of a novel mass spectrometer equipped with an electron cyclotron resonance ion source", Eur. J. Mass Spectrom. **13**, 239–248 (2007). *

Kidera M., Takahashi K., Enomoto S., Goto A., and Yano Y.: "New fragment ion production method using super cold electrons in electron cyclotron resonance plasma", Eur. J. Mass Spectrom. **13**, 355–358 (2007). *

Yamashita Y., Takahashi Y., Haba H., Enomoto S., and Shimizu H.: "Comparison of reductive accumulation of Re and Os in seawater - sediment systems", Geochimica Cosmochimica Acta **71**, No. 14, pp. 3458–3475 (2007). *

[Book・Proceedings]

(Others)

Motomura S., Kanayama Y., Haba H., Watanabe Y., and Enomoto S.: "Multiple Nuclide Imaging in Live Mouse Using Semiconductor Compton Camera for Multiple Molecular Imaging", 2007 IEEE Nuclear Science Symposium Conference Record, Honolulu, USA, 2007–10〜11, IEEE, Piscataway, pp. 3741–3742 (2007).

Oral Presentations

(International Conference etc.)

Motomura S., Kanayama Y., Haba H., Watanabe Y., and Enomoto S.: "Multiple Nuclide Imaging in Live Mouse Using Semiconductor Compton Camera for Multiple Molecular Imaging", 2007 IEEE Nuclear Science Symposium and Medical Imaging Conference, Honolulu, USA, Oct.–Nov. (2007).

Motomura S., Kanayama Y., Haba H., Igarashi K., Hiromura M., Watanabe Y., and Enomoto S.: "Compton Camera for Multiple Molecular Imaging", International Symposium on Metallomics 2007 (ISM 2007), (The Chemical Society of Japan), Nagoya, Nov.–Dec. (2007).

Enomoto S.: "Development of Multi-Elemental Molecular Imaging on Semiconductor Compton Telescope", International Symposium on Metallomics 2007 (ISM 2007), (The Chemical Society of Japan), Nagoya, Nov.–Dec. (2007).

Furukawa J., Haba H., Enomoto S., and Satoh S.: "Heavy Metal Accumulation in Lotus japonicas", International Symposium on Metallomics 2007 (ISM 2007), (The Chemical Society of Japan), Nagoya, Nov.–Dec. (2007).

Kanayama Y., Motomura S., Haba H., Enomoto K. (., Watanabe Y., and Enomoto S.: "Preliminary study for multiple molecular imaging: simultaneous imaging of ^{18}F-FDG, ^{54}Mn-$MnCl_2$, and ^{65}Zn-$ZnCl_2$ in normal and tumor-bearing mouse", International Symposium on Metallomics 2007 (ISM 2007), (The Chemical Society of Japan), Nagoya, Nov.–Dec. (2007).

(Domestic Conference)

榎本秀一: "マルチトレーサー法の生物分野における応用研究とバイオイメージング", バイオ応用技術研究ユニットワークショップ 2007「RI を用いた植物分子イメージング技術の開発と植物機能解析研究への応用」, (日本原子力研究開発機構), 高崎, 1 月 (2007).

榎本 (（五十嵐）) 香織, 木村修一, 榎本秀一: "鉄吸収に及ぼす食事性因子の影響", 第 61 回日本栄養・食糧学会大会, 京都, 5 月 (2007).

三堀陽平, 高橋和也, 木寺正憲, 榎本秀一, 田中龍彦, 南武志, 今津節生, 林英男: "微量元素分析に基づく、古墳等の遺構から出土した辰砂の産地推定の試み", 第 68 回分析化学討論会, (社団法人日本分析化学会), 宇都宮, 5 月 (2007).

榎本秀一, 本村信治, 金山洋介, 羽場宏光, 石澤篤: "複数核種同時γ線イメージング装置の開発と分子イメージング研究の展開", 第 68 回分析化学討論会, (日本分析化学会), 宇都宮, 5 月 (2007).

金山洋介, 本村信治, 羽場宏光, 渡辺恭良, 榎本秀一: "Simultaneous imaging of ^{65}Zn, ^{85}Sr, and ^{131}I in living mouse using gamma-ray emission imaging system", 第 17 回金属の関与する生体関連反応シンポジウム, (日本薬学会物理系薬学部会), 京都, 6 月 (2007).

榎本 (（五十嵐）) 香織, 金山洋介, 本村信治, 松田芳和, 榎本秀一: "牡蠣抽出物の胃液分泌能", 第 24 回微量栄養素研究会シンポジウム, 京都, 6 月 (2007).

本村信治, 金山洋介, 羽場宏光, 渡辺恭良, 榎本秀一: "半導体コンプトンカメラによる複数分子同時イメージング装置の開発：マウスにおける複数核種同時γ線イメージング", 第 2 回日本分子イメージング学会総会・学術集会, 福井, 6 月 (2007).

金山洋介, 本村信治, 羽場宏光, 渡辺恭良, 榎本秀一: "半導体コンプトンカメラによる複数分子同時イメージング装置の開発：マウスにおける ^{65}Zn、^{85}Sr、^{131}I 同時γ線イメージング", 第 18 回日本微量元素学会, 福井, 7 月 (2007).

榎本秀一, 金山洋介, 榎本 (（五十嵐）) 香織, 羽場宏光: "にがり成分の生体内ダイナミクスと代謝吸収過程のイメージング (1) マルチトレーサー法による 1 型糖尿病モデルマウスの微量元素代謝：にがり投与による影響", ソルト・サイエンス研究財団第 19 回平成 18 年度助成研究発表会, (財団法人ソルト・サイエンス研究財団), 東京, 7 月 (2007).

榎本秀一: "半導体コンプトンカメラによる複数分子同時イメージング", バイオジャパン 2007, 横浜, 9 月 (2007).

木寺正憲, 高橋和也, 榎本秀一, 中川孝秀, 三堀陽平, 田中龍彦, 戸田勝善: "電子サイクロトロン共鳴イオン源 (ECRIS) を用いた質量分析装置の開発", 日本分析化学会第 56 年会, 徳島, 9 月 (2007).

榎本秀一: "複数分子イメージング開発とその現状", 分子イメージング研究シンポジウム 2008「社会のニーズに向けた分子イメージング研究の展開」, (理研，放射線医学総合研究所), 東京, 1 月 (2008).

金山洋介, 本村信治, 福地知則, 羽場宏光, 渡辺恭良, 榎本秀一: "複数分子同時イメージング法の開発と現状", 分子イメー

ジング研究シンポジウム 2008「社会のニーズに向けた分子イメージング研究の展開」, (理研，放射線医学総合研究所), 東京, 1 月 (2008).

Safety Management Group

Publications

[Journal]

(Review)

上蓑義朋, 坂本久雄: “ウラン加速における放射線管理”, 加速器 **4**, No. 3, pp. 184–187 (2007).

Oral Presentations

(International Conference etc.)

Uwamino Y., Fujita S., Sakamoto H., Mukai H., and Horigome A.: “RIKEN Radioisotope Beam Factory (RIBF) and its radiation safety aspects”, 17th National Symposium on Radiation Physics (NSRP-17), (Indian Society for Radiation Physics), Kolkata, India, Nov. (2007).

Uwamino Y.: “An accuracy study on the shielding calculation for RIBF”, BRNS Theme meeting on: Status of Nuclear Data Related to Accelerator Driven Systems, (Variable Energy Cyclotron Center), Kolkata, India, Nov. (2007).

(Domestic Conference)

上蓑義朋: “粒子線治療施設における放射線防護と管理”, 第 7 回重粒子医科学センターシンポジウム, (放射線医学総合研究所), 千葉, 11 月 (2007).

RIKEN BNL Research Center

Publications

[Journal]

(Original Papers) *Subject to Peer Review

Aoki S.: "QCD Phases in Lattice QCD", Int. J. Mod. Phys. A **21**, No. 4, pp. 682–687 (2006).

Fukushima K.: "Gauge invariant source terms in QCD", Nucl. Phys. A **770**, 71–83 (2006). *

Fukushima K.: "Deriving the Jalilian-Marian-Iancu-McLerran-Weigert-Leonidov-Kovner equation with classical and quantum source terms", Nucl. Phys. A **775**, 69–88 (2006). *

Adler S. S., Akiba Y., Bazilevsky A. V., Bunce G. M., Deshpande A., Enyo H., Fields D. E., Fox B., Fukao Y., Goto Y., Perdekamp M. G., Hasuko K., Heuser J., Horaguchi T., Ichihara T., Imai K., Ishihara M., Jinnouchi O., Kamihara N., Kaneta M., Kiyomichi A., Kobayashi H., Kurita K., Mao Y., Onishi H., Okada H., Okada K., Rykov V., Saito N., Sato H., Shibata T., Taketani A., Tanida K., Togawa M., Tojo J., Torii H., Watanabe Y., and Yokkaichi S.: "Jet structure from dihadron correlations in d+Au collisions at $\sqrt{s_{NN}} = 200$ GeV", Phys. Rev. C **73**, 054903-1–054903-27 (2006). *

Adler S. S., Akiba Y., Bazilevsky A. V., Bunce G. M., Deshpande A., Enyo H., Fields D. E., Fox B., Fukao Y., Goto Y., Perdekamp M. G., Hasuko K., Heuser J., Horaguchi T., Ichihara T., Imai K., Ishihara M., Jinnouchi O., Kamihara N., Kaneta M., Kiyomichi A., Kobayashi H., Kurita K., Mao Y., Onishi H., Okada H., Okada K., Rykov V., Saito N., Sato H., Shibata T., Taketani A., Tanida K., Togawa M., Tojo J., Torii H., Watanabe Y., and Yokkaichi S.: "Nuclear effects on hadron production in d+Au collisions at $\sqrt{s_{NN}} = 200$ GeV revealed by comparison with p+p data", Phys. Rev. C **74**, 024904-1–024904 -13 (2006). *

Adler S. S., Akiba Y., Aoki K., Bazilevsky A. V., Bunce G. M., Deshpande A., Enyo H., Fields D. E., Fox B., Fukao Y., Goto Y., Perdekamp M. G., Hachiya T., Hasuko K., Heuser J., Horaguchi T., Ichihara T., Imai K., Ishihara M., Jinnouchi O., Kajihara F., Kamihara N., Kaneta M., Kiyomichi A., Kobayashi H., Kurita K., Mao Y., Murata J., Onishi H., Okada H., Okada K., Rykov V., Saito N., Sato H., Shibata T., Shoji K., Tabaru T., Taketani A., Tanida K., Togawa M., Tojo J., Torii H., Tsuchimoto Y., Wagner M. M., Watanabe Y., Xie W., and Yokkaichi S.: "Improved measurement of double helicity asymmetry in inclulsive midrapidity π^0 production for polarized p+p collisions at $\sqrt{s} = 200$ GeV", Phys. Rev. D **73**, 091102-1–091102-5 (2006). *

Fukushima K.: "Characterizing the Larkin-Ovchinnikov-Fulde-Ferrel phase induced by the chromomagnetic instability", Phys. Rev. D **73**, 094016-1–094016-6 (2006). *

Adler S. S., Akiba Y., Bazilevsky A. V., Bunce G. M., Deshpande A., Enyo H., Fields D. E., Fox B., Fukao Y., Goto Y., Perdekamp M. G., Hasuko K., Heuser J., Horaguchi T., Ichihara T., Imai K., Ishihara M., Jinnouchi O., Kamihara N., Kaneta M., Kiyomichi A., Kobayashi H., Kurita K., Mao Y., Onishi H., Okada H., Okada K., Rykov V., Saito N., Sato H., Shibata T., Taketani A., Tanida K., Togawa M., Tojo J., Torii H., Watanabe Y., and Yokkaichi S.: "Jet properties from dihadron correlations in p+p collisions at $\sqrt{s} = 200$ GeV", Phys. Rev. D **74**, 072002-1–072002-26 (2006). *

Adler S. S., Akiba Y., Bazilevsky A. V., Bunce G. M., Deshpande A., Enyo H., Fields D. E., Fox B., Fukao Y., Goto Y., Perdekamp M. G., Hasuko K., Heuser J., Horaguchi T., Ichihara T., Imai K., Ishihara M., Jinnouchi O., Kamihara N., Kaneta M., Kiyomichi A., Kobayashi H., Kurita K., Mao Y., Onishi H., Okada H., Okada K., Rykov V., Saito N., Sato H., Shibata T., Taketani A., Tanida K., Togawa M., Tojo J., Torii H., Watanabe Y., and Yokkaichi S.: "J/ψ Production and Nuclear Effects for d+Au and p+p Collisions at $\sqrt{s_{NN}} = 200$ GeV", Phys. Rev. Lett. **96**, 012304-1–012304-6 (2006). *

Adler S. S., Akiba Y., Bazilevsky A. V., Bunce G. M., Deshpande A., Enyo H., Fields D. E., Fox B., Goto Y., Perdekamp M. G., Hayashi N., Ichihara T., Imai K., Ishihara M., Jinnouchi O., Kamihara N., Kobayashi H., Kurita K., Mao Y., Murata J., Onishi H., Okada K., Saito N., Sato H., Shibata T., Taketani A., Tanida K., Tojo J., Torii H., Watanabe Y., and Yokkaichi S.: " Single Electrons from Heavy-Flavor Decays in p+p Collisions at $\sqrt{s} = 200$ GeV", Phys. Rev. Lett. **96**, 032001-1–032001-6 (2006). *

Adler S. S., Akiba Y., Bazilevsky A. V., Bunce G. M., Deshpande A., Enyo H., Fields D. E., Fox B., Goto Y., Perdekamp M. G., Hayashi N., Ichihara T., Imai K., Ishihara M., Jinnouchi O., Kamihara N., Kobayashi H., Kurita K., Mao Y., Murata J., Onishi H., Okada K., Saito N., Sato H., Shibata T., Taketani A., Tanida K., Tojo J., Torii H., Watanabe Y., and Yokkaichi S.: "Nuclear Modification of Electron Spectra and Implications for Heavy Quark Energy Loss in Au+Au Collisions at $\sqrt{s_{NN}} = 200$ GeV", Phys. Rev. Lett. **96**, 032301-1–032301-6 (2006). *

Adler S. S., Akiba Y., Bazilevsky A. V., Bunce G. M., Deshpande A., Enyo H., Fields D. E., Fox B., Goto Y., Perdekamp M. G., Hayashi N., Ichihara T., Imai K., Ishihara M., Jinnouchi O., Kamihara N., Kaneta M., Kobayashi H., Kurita K., Mao Y., Murata J., Onishi H., Okada K., Saito N., Sato H., Shibata T., Taketani A., Tanida K., Tojo J., Torii H., Watanabe Y., and Yokkaichi S.: "Measurement of Identified π^0 and Inclusive Photon Second-Harmonic Parameter v_2 and Implications for Direct Photon Production in $\sqrt{s_{NN}} = 200$ GeV Au + Au", Phys. Rev. Lett. **96**, 032302-1–032302-6 (2006). *

Adler S. S., Akiba Y., Bazilevsky A. V., Bunce G. M., Deshpande A., Enyo H., Fields D. E., Fox B., Goto Y., Perdekamp M. G., Hayashi N., Ichihara T., Imai K., Ishihara M., Jinnouchi O., Kamihara N., Kobayashi H., Kurita K., Mao Y., Murata J., Onishi H., Okada K., Saito N., Sato H., Shibata T., Taketani A., Tanida K., Tojo J., Torii H., Watanabe Y., and Yokkaichi S.: "Common Suppression Pattern of eta and π^0 Mesons at High Transverse Momentum in Au+Au Collisions at $\sqrt{s_{NN}}$ = 200 GeV", Phys. Rev. Lett. **96**, 202301-1–202301-6 (2006). ∗

Adler S. S., Akiba Y., Bazilevsky A. V., Bunce G. M., Deshpande A., Enyo H., Fields D. E., Fox B., Fukao Y., Goto Y., Perdekamp M. G., Hasuko K., Heuser J., Horaguchi T., Ichihara T., Imai K., Ishihara M., Jinnouchi O., Kamihara N., Kaneta M., Kiyomichi A., Kobayashi H., Kurita K., Mao Y., Onishi H., Okada H., Okada K., Rykov V., Saito N., Sato H., Shibata T., Taketani A., Tanida K., Togawa M., Tojo J., Torii H., Watanabe Y., and Yokkaichi S.: "Azimuthal Angle Correlations for Rapidity Separated Hadron Pairs in d+Au Collisions at $\sqrt{s_{NN}}$ = 200 GeV", Phys. Rev. Lett. **96**, 222301-1–222301-6 (2006). ∗

Adler S. S., Akiba Y., Bazilevsky A. V., Bunce G. M., Deshpande A., Enyo H., Fields D. E., Fox B., Goto Y., Perdekamp M. G., Hayashi N., Ichihara T., Imai K., Ishihara M., Jinnouchi O., Kamihara N., Kobayashi H., Kurita K., Mao Y., Murata J., Onishi H., Okada K., Saito N., Sato H., Shibata T., Taketani A., Tanida K., Tojo J., Torii H., Watanabe Y., and Yokkaichi S.: "Dense-Medium Modifications to Jet-Induced Hadron Pair Distributions in Au+Au Collisions at $\sqrt{s_{NN}} = 200$ GeV", Phys. Rev. Lett. **97**, 052301-1–052301-6 (2006). ∗

Adare A., Akiba Y., Aoki K., Asai J., Bunce G. M., Deshpande A., Enyo H., Fields D. E., Fujiwara K., Fukao Y., Goto Y., Perdekamp M. G., Horaguchi T., Ichihara T., Imai K., Inoue Y., Ishihara M., Jinnouchi O., Kamihara N., Kaneta M., Kano H., Kanoh H., Kawall D., Kiyomichi A., Kurita K., Mao Y., Murata J., Nakagawa I., Nakano K., Onishi H., Okada H., Okada K., Rykov V., Saito N., Shibata T., Shoji K., Tabaru T., Taketani A., Tanida K., Togawa M., Tojo J., Torii H., Wagner M. M., Watanabe Y., Xie W., and Yokkaichi S.: " Measurement of High-pT Single Electrons from Heavy-Flavor Decays in p+p Collisions at $\sqrt{s}$ = 200 GeV", Phys. Rev. Lett. **97**, 252002-1–252002-6 (2006). ∗

Yokkaichi S., Chiba J., Enyo H., Fukao Y., Funahashi H., Hamagaki H., Ieiri M., Ishino M., Kanda H., Kitaguchi M., Mihara S., Miwa K., Miyashita T., Murakami T., Mutou R., Nakura T., Naruki M., Ozawa K., Sakuma F., Sasaki O., Sekimoto M., Tabaru T., Tanaka K., Togawa M., Yamada S., and Yoshimura Y.: "Study of in-medium meson modification in 12 GeV p+A reactions", Int. J. Mod. Phys. A **22**, No. 2/3, pp. 397–405 (2007).

Adare A., Akiba Y., Aoki K., Asai J., Bunce G. M., Deshpande A., Enyo H., Fields D. E., Fujiwara K., Fukao Y., Goto Y., Perdekamp M. G., Hachiya T., Hasuko K., Heuser J., Horaguchi T., Ichihara T., Imai K., Inoue Y., Ishihara M., Jinnouchi O., Kajihara F., Kamihara N., Kaneta M., Kanoh H., Kawall D., Kiyomichi A., Kurita K., Mao Y., Murata J., Nakagawa I., Nakano K., Onishi H., Okada H., Okada K., Wagner M. M., Watanabe Y., Xie W., and Yokkaichi S.: "Correlated production of p and $\bar{p}$ in Au+Au collisions at $\sqrt{s_{NN}}$ = 200 GeV", Phys. Lett. B **649**, 359–369 (2007). ∗

Adler S. S., Akiba Y., Bazilevsky A. V., Bunce G. M., Deshpande A., Enyo H., Fields D. E., Fox B., Fukao Y., Goto Y., Perdekamp M. G., Hasuko K., Hayashi N., Heuser J., Horaguchi T., Ichihara T., Imai K., Ishihara M., Jinnouchi O., Kamihara N., Kaneta M., Kiyomichi A., Kobayashi H., Kurita K., Mao Y., Murata J., Onishi H., Okada H., Okada K., Rykov V., Saito N., Sato H., Shibata T., Taketani A., Tanida K., Togawa M., Tojo J., Torii H., Watanabe Y., and Yokkaichi S.: "High transverse momentum η meson production in p+p,d+Au, and Au+Au collisions at $\sqrt{s_{NN}}$ = 200 GeV", Phys. Rev. C **75**, 024909-1–024909-36 (2007). ∗

Adler S. S., Akiba Y., Bazilevsky A. V., Bunce G. M., Deshpande A., Enyo H., Fields D. E., Fox B., Fukao Y., Goto Y., Perdekamp M. G., Hasuko K., Heuser J., Horaguchi T., Ichihara T., Imai K., Ishihara M., Jinnouchi O., Kamihara N., Kaneta M., Kiyomichi A., Kobayashi H., Kurita K., Mao Y., Onishi H., Okada H., Okada K., Rykov V., Saito N., Sato H., Shibata T., Taketani A., Tanida K., Togawa M., Tojo J., Torii H., Watanabe Y., and Yokkaichi S.: "Production of ω mesons at large transverse momenta in p+p and d+Au collisions at $\sqrt{s_{NN}}$ = 200 GeV", Phys. Rev. C **75**, 051902-1–051902-6 (2007). ∗

Adler S. S., Akiba Y., Bazilevsky A. V., Bunce G. M., Deshpande A., Enyo H., Fields D. E., Fox B., Goto Y., Perdekamp M. G., Hayashi N., Ichihara T., Imai K., Ishihara M., Jinnouchi O., Kamihara N., Kobayashi H., Kurita K., Mao Y., Murata J., Onishi H., Okada K., Saito N., Sato H., Shibata T., Taketani A., Tanida K., Tojo J., Torii H., Watanabe Y., and Yokkaichi S.: "Measurement of density correlations in pseudorapidity via charged particle multiplicity fluctuations in Au+Au collisions at $\sqrt{s_{NN}}$ = 200 GeV", Phys. Rev. C **76**, 034903-1–034903-33 (2007). ∗

Adler S. S., Akiba Y., Bazilevsky A. V., Bunce G. M., Deshpande A., Enyo H., Fields D. E., Fox B., Goto Y., Perdekamp M. G., Hayashi N., Ichihara T., Imai K., Ishihara M., Jinnouchi O., Kamihara N., Kobayashi H., Kurita K., Mao Y., Murata J., Onishi H., Okada K., Saito N., Sato H., Shibata T., Taketani A., Tanida K., Tojo J., Torii H., Watanabe Y., and Yokkaichi S.: "De-

tailed study of high-p_T neutral pion suppression and azimuthal anisotropy in Au+Au collisions at $\sqrt{s_{NN}} = 200$ GeV", Phys. Rev. C **76**, 034904-1–034904-26 (2007). *

Fukushima K. and Hidaka Y.: "Model study of the sign problem in the mean-field approximation", Phys. Rev. D **75**, 036002-1–036002-114 (2007). *

Adare A., Akiba Y., Aoki K., Asai J., Bunce G. M., Deshpande A., Enyo H., Fields D. E., Fujiwara K., Fukao Y., Goto Y., Perdekamp M. G., Horaguchi T., Ichihara T., Imai K., Inoue Y., Ishihara M., Jinnouchi O., Kamihara N., Kaneta M., Kanoh H., Kawall D., Kiyomichi A., Kurita K., Mao Y., Murata J., Nakagawa I., Nakano K., Onishi H., Okada H., Okada K., Rykov V., Saito N., Shibata T., Shoji K., Tabaru T., Taketani A., Tanida K., Togawa M., Tojo J., Torii H., Wagner M. M., Watanabe Y., Xie W., and Yokkaichi S.: "Inclusive cross section and double helicity asymmetry for π^0 production in $p+p$ collisions at $\sqrt{s} = 200$ GeV: Implications for the polarized gluon distribution in the proton", Phys. Rev. D **76**, 051106-1–051106-7 (2007). *

Adler S. S., Akiba Y., Bazilevsky A. V., Bunce G. M., Deshpande A., Enyo H., Fields D. E., Fox B., Goto Y., Perdekamp M. G., Hayashi N., Ichihara T., Imai K., Ishihara M., Jinnouchi O., Kamihara N., Kobayashi H., Kurita K., Mao Y., Murata J., Onishi H., Okada K., Saito N., Sato H., Shibata T., Taketani A., Tanida K., Tojo J., Torii H., Watanabe Y., and Yokkaichi S.: "Measurement of single muons at forward rapidity in $p+p$ collisions at $\sqrt{s} = 200$ GeV and implications for charm production", Phys. Rev. D **76**, 092002-1–092002-24 (2007). *

Adler S. S., Akiba Y., Bazilevsky A. V., Bunce G. M., Deshpande A., Enyo H., Fields D. E., Fox B., Fukao Y., Goto Y., Perdekamp M. G., Hasuko K., Heuser J., Horaguchi T., Ichihara T., Imai K., Ishihara M., Jinnouchi O., Kamihara N., Kaneta M., Kiyomichi A., Kobayashi H., Kurita K., Mao Y., Onishi H., Okada H., Okada K., Rykov V., Saito N., Sato H., Shibata T., Taketani A., Tanida K., Togawa M., Tojo J., Torii H., Watanabe Y., and Yokkaichi S.: "Measurement of Direct Photon Production in p+p Collisions at $\sqrt{s} = 200$ GeV", Phys. Rev. Lett. **98**, 012002-1–012002-6 (2007). *

Adler S. S., Akiba Y., Bazilevsky A. V., Bunce G. M., Deshpande A., Enyo H., Fields D. E., Fox B., Goto Y., Perdekamp M. G., Hayashi N., Ichihara T., Imai K., Ishihara M., Jinnouchi O., Kamihara N., Kobayashi H., Kurita K., Mao Y., Murata J., Onishi H., Okada K., Saito N., Sato H., Shibata T., Taketani A., Tanida K., Tojo J., Torii H., Watanabe Y., and Yokkaichi S.: "Evidence for a long-range component in the pion emission source in Au+Au Collisions at $\sqrt{s_{NN}} = 200$ GeV", Phys. Rev. Lett. **98**, 132301-1–132301-6 (2007). *

Sakuma F., chiba j., Enyo H., Fukao Y., Funahashi H., Hamagaki H., ieiri m., ishino m., handa h., Kitaguchi M., mihara s., Miwa K., miyashita t., Murakami T., muto r., nakura t., Naruki M., Ozawa K., sasaki o., Sekimoto M., Tabaru T., tanaka k., Togawa M., yamada s., Yokkaichi S., and yoshimura y.: "Nuclear-matter modification of decay widths in the $\phi \to e^+e^-$ and $\phi \to K^+K^-$ channels", Phys. Rev. Lett. **98**, 152302-1–152302-5 (2007). *

Adare A., Akiba Y., Aoki K., Asai J., Bunce G. M., Deshpande A., Enyo H., Fields D. E., Fujiwara K., Fukao Y., Goto Y., Perdekamp M. G., Hachiya T., Hasuko K., Heuser J., Horaguchi T., Ichihara T., Imai K., Inoue Y., Ishihara M., Jinnouchi O., Kajihara F., Kamihara N., Kaneta M., Kano H., Kanoh H., Kawall D., Kiyomichi A., Kurita K., Mao Y., Murata J., Nakagawa I., Nakano K., Onishi H., Okada H., Okada K., Rykov V., Saito N., Sato H., Shibata T., Shoji K., Tabaru T., Taketani A., Tanida K., Togawa M., Tojo J., Torii H., Tsuchimoto Y., Wagner M. M., Watanabe Y., Xie W., and Yokkaichi S.: "Scaling properties of azimuthal anisotropy in Au+Au and Cu+Cu collisions at $\sqrt{s_{NN}} = 200$ GeV", Phys. Rev. Lett. **98**, 162301-1–162301-6 (2007). *

Adare A., Akiba Y., Aoki K., Asai J., Bunce G. M., Deshpande A., Enyo H., Fields D. E., Fujiwara K., Fukao Y., Goto Y., Perdekamp M. G., Hachiya T., Hasuko K., Heuser J., Horaguchi T., Ichihara T., Imai K., Inoue Y., Ishihara M., Jinnouchi O., Kajihara F., Kamihara N., Kaneta M., Kano H., Kanoh H., Kawall D., Kiyomichi A., Kurita K., Mao Y., Murata J., Nakagawa I., Nakano K., Onishi H., Okada H., Okada K., Rykov V., Saito N., Sato H., Shibata T., Shoji K., Tabaru T., Taketani A., Tanida K., Togawa M., Tojo J., Torii H., Tsuchimoto Y., Wagner M. M., Watanabe Y., Xie W., and Yokkaichi S.: "Energy loss and flow of heavy quarks in Au+Au collisions at $\sqrt{s_{NN}} = 200$ GeV", Phys. Rev. Lett. **98**, 172301-1–172301-6 (2007). *

Adler S. S., Akiba Y., Bazilevsky A. V., Bunce G. M., Deshpande A., Enyo H., Fields D. E., Fox B., Fukao Y., Goto Y., Perdekamp M. G., Hasuko K., Heuser J., Horaguchi T., Ichihara T., Imai K., Ishihara M., Jinnouchi O., Kamihara N., Kaneta M., Kiyomichi A., Kobayashi H., Kurita K., Mao Y., Onishi H., Okada H., Okada K., Rykov V., Saito N., Sato H., Shibata T., Taketani A., Tanida K., Togawa M., Tojo J., Torii H., Watanabe Y., and Yokkaichi S.: "Centrality dependence of π^0 and η production at large transverse momentum in $\sqrt{s_{NN}} = 200$ GeV $d+Au$ Collisions", Phys. Rev. Lett. **98**, 172302-1–172302-7 (2007). *

Adare A., Akiba Y., Aoki K., Asai J., Bunce G. M., Deshpande A., Enyo H., Fields D. E., Fujiwara K., Fukao Y., Goto Y., Perdekamp M. G., Horaguchi T., Ichihara T., Imai K., Inoue Y., Ishihara M., Jinnouchi O., Kamihara N., Kaneta M., Kanoh H., Kawall D., Kiyomichi A., Kurita K., Mao Y., Murata J., Nakagawa I., Nakano K., Onishi H., Okada H., Okada K., Rykov V., Saito N., Shibata T., Shoji K., Tabaru T., Taketani

A., Tanida K., Togawa M., Tojo J., Torii H., Wagner M. M., Watanabe Y., Xie W., and Yokkaichi S.: "J/Ψ production versus transverse momentum and rapidity in p+p collisions at $\sqrt{s_{NN}} = 200$ GeV", Phys. Rev. Lett. **98**, 232002-1–232002-6 (2007). *

Adare A., Akiba Y., Aoki K., Asai J., Bunce G. M., Deshpande A., Enyo H., Fields D. E., Fujiwara K., Fukao Y., Goto Y., Perdekamp M. G., Hachiya T., Hasuko K., Heuser J., Horaguchi T., Ichihara T., Imai K., Inoue Y., Ishihara M., Jinnouchi O., Kajihara F., Kamihara N., Kaneta M., Kanoh H., Kawall D., Kiyomichi A., Kurita K., Mao Y., Murata J., Nakagawa I., Nakano K., Onishi H., Okada H., Okada K., Rykov V., Saito N., Sato H., Shibata T., Shoji K., Tabaru T., Taketani A., Tanida K., Togawa M., Tojo J., Torii H., Tsuchimoto Y., Wagner M. M., Watanabe Y., Xie W., and Yokkaichi S.: "J/Ψ production versus centrality, transverse momentum, and rapidity in Au+Au Collisions at $\sqrt{s_{NN}} = 200$ GeV", Phys. Rev. Lett. **98**, 232301-1–232301-6 (2007). *

Adare A., Akiba Y., Aoki K., Asai J., Bazilevsky A. V., Bunce G. M., Deshpande A., Enyo H., Fields D. E., Fox B., Fujiwara K., Fukao Y., Goto Y., Perdekamp M. G., Hachiya T., Hasuko K., Heuser J., Horaguchi T., Ichihara T., Imai K., Inoue Y., Ishihara M., Jinnouchi O., Kajihara F., Kamihara N., Kaneta M., Kanoh H., Kawall D., Kiyomichi A., Kobayashi H., Kurita K., Mao Y., Murata J., Nakagawa I., Nakano K., Onishi H., Okada H., Okada K., Rykov V., Saito N., Sato H., Shibata T., Shoji K., Tabaru T., Taketani A., Tanida K., Togawa M., Tojo J., Torii H., Tsuchimoto Y., Wagner M. M., Watanabe Y., Xie W., and Yokkaichi S.: "System size and energy dependence of jet-induced hadron pair correlation shapes in Cu+Cu and Au+Au collisions at $\sqrt{s_{NN}} = 200$ GeV and 62.4 GeV", Phys. Rev. Lett. **98**, 232302-1–232302-7 (2007). *

Aoki S., Ishii N., and Hatsuda T.: "Nuclear force from lattice QCD", Phys. Rev. Lett. **99**, No. 2, pp. 22001-1–22001-4 (2007). *

Afanasiev S., Akiba Y., Aoki K., Bunce G. M., Deshpande A., Enyo H., Fields D. E., Fukao Y., Goto Y., Perdekamp M. G., Hachiya T., Hasuko K., Heuser J., Horaguchi T., Ichihara T., Imai K., Ishihara M., Jinnouchi O., Kajihara F., Kamihara N., Kaneta M., Kiyomichi A., Kurita K., Murata J., Onishi H., Okada H., Okada K., Rykov V., Saito N., Sato H., Shibata T., Shoji K., Tabaru T., Taketani A., Tanida K., Togawa M., Tojo J., Torii H., Tsuchimoto Y., Wagner M. M., Watanabe Y., Xie W., and Yokkaichi S.: "Elliptic flow for ϕ Mesons and (Anti)deuterons in Au+Au collisions at $\sqrt{s_{NN}} = 200$ GeV", Phys. Rev. Lett. **99**, 052301-1–052301-6 (2007). *

Adare A., Akiba Y., Aoki K., Asai J., Bunce G. M., Deshpande A., Enyo H., Fields D. E., Fujiwara K., Fukao Y., Goto Y., Perdekamp M. G., Hachiya T., Hasuko K., Heuser J., Horaguchi T., Ichihara T., Imai K., Inoue Y., Ishihara M., Jinnouchi O., Kajihara F., Kamihara N., Kaneta M., Kanoh H., Kawall D., Kiyomichi A., Kurita K., Mao Y., Murata J., Nakagawa I., Nakano K., Onishi H., Okada H., Okada K., Rykov V., Saito N., Sato H., Shibata T., Shoji K., Tabaru T., Taketani A., Tanida K., Togawa M., Tojo J., Torii H., Tsuchimoto Y., Wagner M. M., Watanabe Y., Xie W., and Yokkaichi S.: "Transverse momentum and centrality dependence of dihadron correlations in Au+Au collisions at $\sqrt{s_{NN}} = 200$ GeV: Jet quenching and the response of partonic matter", Phys. Rev. C **77**, 011901-1–011901-6 (2008). *

Adler S. S., Akiba Y., Bazilevsky A. V., Bunce G. M., Deshpande A., Enyo H., Fields D. E., Fox B., Fukao Y., Goto Y., Perdekamp M. G., Hasuko K., Heuser J., Horaguchi T., Ichihara T., Imai K., Ishihara M., Jinnouchi O., Kamihara N., Kaneta M., Kiyomichi A., Kobayashi H., Kurita K., Mao Y., Onishi H., Okada H., Okada K., Rykov V., Saito N., Sato H., Shibata T., Taketani A., Tanida K., Togawa M., Tojo J., Torii H., Watanabe Y., and Yokkaichi S.: "Centrality dependence of charged hadron production in deuteron+gold and nucleon+gold collisions at $\sqrt{s_{NN}} = 200$ GeV", Phys. Rev. C **77**, 014905-1–014905-13 (2008). *

RIKEN Facility Office at RAL

Oral Presentations

(Domestic Conference)

松崎禎市郎: "Anomalous temperature dependence of muon transfer rate in solid tritium studied by muon catalyzed t-t fusion", 理研シンポジウム「理研-RAL 支所ミュオン施設におけるミュオン科学研究 2007」, 和光, 7 月 (2007).

VII. LIST OF PREPRINTS

RIKEN- NC- NP

(2007 Jan. ～ 2008 Mar.)

1 W. Horiuchi, Y. Suzuki, B. Abu-Ibrahim, and A. Kohama: “Sysematic analysis of reaction cross sections of carbon isotopes”

2 K. Morita, K. Morimoto, D. Kaji, T. Akiyama, S. Goto, H. Haba, E. Ideguchi, K. Katori, H. Koura, H. Kudo, T. Onishi, A. Ozawa. T. Suda, K. Sueki, F. Tokanai, T. Yamaguchi, A. Yoneda, and A. Yoshida: “Experiments on Synthesis of an Isotope 277112 by 208Pb + 70Zn Reaction”

3 K. Morita, K. Morimoto, D. Kaji, T. Akiyama, S. Goto, H. Haba, E. Ideguchi, K. Katori, H. Koura, H. Kudo, T. Onishi, A. Ozawa. N. Sato, T. Suda, K. Sueki, F. Tokanai, T. Yamaguchi, A. Yoneda, and A. Yoshida: “Observation of Second Decay Chain from 273113”

4 Z. Elekes, Zs. Dombradi, N. Aoi, S. Bishop, Zs. Fulop, J. Gibelin, T. Gomi, Y. Hashimoto, N. Imai, N. Iwasa, H. Iwasaki, G. Kalinka, Y. Kondo, A. A. Korsheninnikov. K. Kurita, M. Kurokawa, N. Matsui, T. Motobayashi, T. Nakamura, T. Nakao, E. Yu. Nikolskii, T. K. Ohnishi, T. Okumura, S. Ota, A. Perera, A. Saito, H. Sakurai, Y. Satou, D. Sohler, T. Sumikama, D. Suzuki, M. Suzuki, H. Takeda, S. Takeuchi, Y. Togano, and Y. Yanagisawa: “Spectroscopic stucy of neutron shell closures via nucleon transfer in the near-dripline nucleus 23O”

5 J. Gibelin, D. Bernnel, T. Motobayashi, N. Aoi, H. Baba, Y. Blumenfeld, Zs. Dombradi, Z. Elekes, S. Fortier, N. Fracaria, N. Fukuda, T. Gomi, K. Ishikawa, Y. Kondo, T. Kubo, V. Lima, T. Nakamura, A. Saito, Y. Satou, E. Takeshita, S. Takeuchi, T. Teranishi, Y. Togano, A. M. Vinodkumar, Y. Yanagisawa, and K. Yoshida: “Measurement of the B(E2,0+1->2+1) in the N=16 nucleus 26Ne”

6 D. Kameda, H. Ueno, K. Asahi, M. Takemura, A. Yoshimi, T. Haseyama, M. Uchida, K. Shimada, D. Nagae, G. Kijima, T. Arai, K. Takase, S. Suda, T. Inoue, J. Murata, H. Kawamura, Y. Kobayashi, H. Watanabe, and M. Ishihara: “Measurement of the electric quadrupole moment of 23AL”

7 S. Shimoura, S. Ota, K. Demichi, N. Aoi, H. Baba, Z. Elekes, T. Fukuchi, T. Gomi, K. Hasegawa, E. Ideguchi, M. Ishihara, N. Iwasa, H. Iwasaki, S. Kanno, S. Kubono, K. Kurita, M. Kurokawa, Y. U. Matsuyama, S. Michimasa, K. Miller, T. Minemura, T. Motobayashi, T. Murakami, M. Notani, A. Odahara, A. Saito, H. Sakurai, E. Takeshita, S. Takeuchi, M. Tamaki, T. Teranishi, K. Yamada, Y. Yanagisawa, I. Hamamoto: “Lifetime of the Isomeric 0 + 2 State in 12Be”

8 T. Ichikawa, K. Hagino, and A. Iwamoto: “Existence of One-Body Barrier Revealed in Deep Sub-Barrier Fusion”

9 T. Ichikawa, K. Hagino, and A. Iwamoto: “Systematics of threshold incident energy for deep sub-barrier fusion hindrance”

10 M. Mocko, M. B. Tsang, Z. Y. Sun, N. Aoi, J. Cok, F. Delaunay, M. A. Famiano, H. Hui, N. Imai, H. Iwasaki, W. G. Lynch, T. Motobayashi, M. Niikura, T. Onishi, A. M. Rogers, H. Sakurai, A. Stolz, H. Suzuki, E. Takeshita, S. takeuchi, and M. S. Wallace: “Projectile Fragmentation of 86Kr at 64 MeV/nucleon”

11 M. B. Tsang, W. G. Lynch, W. A. Friendman, M. Mocko, Z. Y. Sun, N. Aoi, J. M. Cook, F. Delaunay, M. A. Famiano, H. Hui, N. Imai, H. Iwasaki, T. Motobayashi, M. Niikura, T. Onishi, A. M. Rogers, H. Sakurai, H. Suzuki, E. Takeshita, S. Takeuchi, and M. S. Wallace: “Gragmentation cross-sections and binding energies of neutron-rich nuclei”

12 T. Sugimoto, T. Nakamura, Y. Kondo, N. Aoi, H. Baba, D. Bazin, N. Fukuda, T. Gomi, H. Hasegawa, N. Imai, M. Ishihara, T. Kobayashi, T. Kubo, M. Miura, T. Motobayashi, H. Otsu, A. Saito, H. Sakurai, S. Shimoura, A. M. Vinodkumar, K. Watanabe,, Y. X. Watanabe, T. Yakushiji, Y. Yanagisawa, and Yoneda: “The first 2+ state of 14Be”

13 M. Notani, H. Sakurai, N. Aoi, H. Iwasaki, N. Fukuda, Z. Liu, K. Yoneda, H. Ogawa, T. Teranishi, T. Nakamura, H. Okuno, A. Yoshida, Y. X. Watanabe, S. Momota, N. Inabe, T. Kubo, S. Ito, A. Ozawa, T. Suzuki, I. Tanihata, and M. Ishihara: “Projectile fragmentation reactions and production of nuclei near the neutron

drip-line”

14 T. Gomi, K. Yoneda, Y. Ando, N. Aoi, H. Baba, K. Demichi, Z. Elekes, N. Fukuda, Zs. Fülöp, U. Futakami, Y. Higurashi, K. Ieki, N. Imai, M. Ishihara, K. Ishikawa, N. Iwasa, H. Iwasaki, S. Kanno, Y. Kondo, T. Kubo, S. Kubono, M. Kunibu, K. Kurita, Y. U. Matsuyama, S. Michimasa, T. Minemura, M. Miura, H. Murakami, T. Nakamura, M. Notani, S. Ota, A. Saito, H. Sakurai, M. Serata, S. Shimoura, T. Sugimoto, E. Takeshita, S. Takeuchi, Y. Togano, K. Ue, K. Yamada, Y. Yanagisawa, A. Yoshida, and T. Motobayashi: “Resonant proton capture on 22Mg studied by the Coulomb dessociation method”

15 B. Abu-Ibrahim, W. Horiuchi, A. Kohama, and Y. Suzuki: “Reaction cross sections of carbon isotopes incident on a proton”

16 H. Ong, N. Imai, D. Suzuki, H. Iwasaki, H. Sakurai, T. K. Onishi, M. K. Suzuki, S. Ota, S. Takeuchi, T. Nakao, Y. Togano, Y. Kondo, N. Aoi, H. Baba, S. Bishop, Y. Ichikawa, M. Ishihara, T. Kubo, K. Kurita, T. Motobayashi, T. Nakamura, T. Okumura, and Y. Yanagisawa: “Lifetime measurements of first excited states in 16,18C”

17 H. Scheit, A. Gade, T. Glasmacher, and T. Motobayashi: “On the Analysis of Internediate-Energy Coulomb Excitation Experiments”

18 Y. Satou, T. Nakamura, N. Fukuda, T. Sugimoto, Y. Kondo, N. Matsui, Y. Hashimoto, T. Nakabayashi, T. Okumura, M. Shinohara, T. Motobayashi, Y. Yanagisawa, N. Aoi, S. Takeuchi, T. Gomi, Y. Togano, S. Kawai, H. Sakurai, H. J. Ong, T. K. Onishi, S. Shimoura, M. Tamaki, T. Kobayashi, H. Otsu, Y. Matsuda, N. Endo, M. Kitayama, and M. Ishihara: “Unbound excited states in 19,17C”

19 M. Yamagami, and Y. R. Shimizu: “Spatial structure of neutron Cooper pairs in deformed neutron-rich nuclei”

20 A. Kohama, K. Iida, and K. Oyamatsu: “Difference between interaction cross sections and reaction cross sections”

VIII. LIST OF SYMPOSIA

(2007 Jan. ～ 2008 Mar.)

1 In-beam gamma spectroscopy of the doubly magic nucleus 78Ni and its vicinity 6 Feb., User Liaison and Support Group, RIKEN
2 Large-Scale Self-Consistent Nuclear Mass Calculations 23-24 Feb., User Liaison and Support Group, RIKEN
3 Analysis of 8B elastic scattering experiments 2 Mar., User Liaison and Support Group, RIKEN
4 International Workshop: Joint JUSTIPEN-LACM Meeting 5-8 Mar., Nuclear Physics Research Div., Oak Ridge (USA)
5 Channelling of hydrogen by using nuclear reactions 15 Mar., User Liaison and Support Group, RIKEN
6 Domain Wall Fermions at en Years 15-17 Mar., RIKEN BNL Research Center, USA
7 Resent development and future prospect of the GEM based tracking detector 23 Mar., Advanced Meson Science Laboratory/Cosmic Radiation Laboratory, RIKEN
8 The Fifth International Workshop on DIRECT REACTIONS WITH EXOTIC BEAMS (DREB 2007) 30 May-2 June, Wako, RIKEN, Kyushu Univ., Univ. of Tokyo
9 Itally and Japan at the Frontiers off Nuclear, Particle and Astroparticle Physics 9 June Tokyo, Embassy of Italy in Tokyo, INFN, Japan Science Foundation, KEK and RIKEN
10 Nuclear Structure: New Pictures in the Extended Isospin Space (NS07) 11-14 June, Kyoto, Kyoto Univ., Yukawa Inst. for Theoretical Phys. and RIKEN
11 The International Symposium on Physics of Unstable Nuclei (ISPUN07) 3-7 July, Vietnam, INST. I PE, GANIL, CEA Saclay, GSI, EU Asia-Link network and RIKEN
12 Muon Science Researches at the RIKEN-RAL Muon Facility 2007, 23-24 July, Wako, Advanced Meson Science Lab., RIKEN
13 String Field Theory 07 6-7 Oct. WakoTheoretical Phyics Lab., RIKEN
14 The International Symposium on New Facets of the Three Nucleon Force-50 Years of the Fujita-Miyazawa Three Nucleon Force 29-31 Oct., Tokyo, Univ. of Tokyo, RCNP and RIKEN
15 The 10th International Symposium on Origin of Matter and Evolution of Galaxies (OMEG07) - From the Dawn of Universe to the Formation of Solar System - 4-7 Dec., Hokkaido Hokkaido Univ., NAOJ, CNS, RCNP, KEK, Univ. of Tokyo and RIKEN
16 Quantum Field Theory and Symmetry, 22-23 Dec. Wako Theoretical Phyics Lab., RIKEN
17 International Joint Workshop, LACM-EFES-JUSTIPEN Meeting 23-25 Jun., Oak Ridge, USA
18 Progress of plant biology using heavy-ion accelerators, 24-25 Jun., Wako Radiation Biology Team & Industrial Cooperation Team, RIKEN

IX. LIST OF SEMINAR

（2007 Jan. ～ 2008 Mar.）

Accelerator Division

1 Peter A. Zavodszky（MSU）23 Aug. '07 "RIBF Accel. Seminar「ECRIS development at NSCL/MSU」"
2 Jeffry W Stetson（NSCL, Michigan State University）12 Dec. '07 "RIBF Accel. Seminar「Inhomogeneities in Beams Extracted from ECR Ion Sources and Resulting Considerations」"
3 Jeffry W Stetson（NSCL, Michigan State University）14 Dec. '07 "RIBF Accel. Seminar「Design and Operational Overview of the High-energy beam lines and Particle Separator at the NSCL」"
4 Peter Speadtke（GSI）10 Jan. '08 "RIBF Accel. Seminar「Extraction from ECR Ion Sources」"
5 Xia Jiawen（Institute of Modern Physics, Lanzhou, China）19 Mar. '08 "RIBF Accel. Seminar「HIRFL-CSR Facility」"
6 A. Goto et al.（Accelerator Development Group）3 Mar. '08 "CNS-RIKEN Workshop on Upgrade of AVF Cyclotron"

Nuclear Physics Research Division

1 H. Aihara（Univ. of Tokyo）17 Apr. '07 "Monthly Colloquium「Recent Results From Belle Experiment」"
2 ZHAO Yu-min（Shanghai Jiao Tong Univ.）24 Apr. '07 "RIBF Nuclear Physics Seminar「Systematic studies of low-lying structure for nuclei in A=130-150 region」"
3 E. Hiyama（Nara Women's Univ.）26 Apr. '07 "RIBF Nuclear Physics Seminar「Recent status of hypernuclear physics」"
4 M. Wakasugi（Nishina center, RIKEN）22 May. '07 "RIBF Nuclear Physics Seminar「New technique SCRIT - for RI-electron scattering experiment」"
5 O. Hashimoto（.Tohoku Univ.）28 May. '07 "Monthly Colloquium「Reaction spectroscopy of Lambda Hypernuclei by the（e, e'K+）reaction」"
6 Y. Yamaguchi（Theoretical Physics Lab., RIKEN）19 Jun. '07 "Monthly Colloquium「Dawn of Nuclear Physics」"
7 T.F. Papenbrock（Oak Ridge）20 Jun. '07 "RIBF Nuclear Physics Seminar「Ab-initio nuclear structure calculations with three-nucleon forces」"
8 T. Rotureau（Oak Ridge）20 Jun. '07 "RIBF Nuclear Physics Seminar「Shell Model Approach for nuclei around and beyond drip-lines」"
9 K. Matsuyanagi（Kyoto Univ.）27 Jun. '07 "Lecture Series Ⅱ-4「The minimum of modern theory of nuclear structure（4th）」"
10 M. Ebihara（Tokyo Metropolitan Univ.）28 Jun. '07 "RIBF Nuclear Physics Seminar「Element abundance in the solar system and the evaluation」"
11 K. Hatanaka（Research Center for Nuclear Physics, Osaka Univ.）17 Jul. '07 "Monthly Colloquium「Physics at the RCNP cyclotron facility」"
12 S. Shimoura（CNS, Univ. of Tokyo）31 Jul. '07 "Lecture Series IV-1「Practical nuclear reaction theory for experimentalists（1st）」"
13 I. Hamamoto（Lund Univ.）18 Sep. '07 "Lecture Series V-1「One-particle motion in nuclear many-body problem」"
14 H. Baba（Heavy Ion Nuclear Physics Lab., RIKEN）3 Sep. '07 "RIBF Nuclear Physics Seminar「Isoscalarexcitation in unstable nucleus 14O」"
15 R.. Hayano（Univ. of Tokyo）16 Oct. '07 "Monthly Colloquium「Weighing the antiproton」"
16 H. Miyatake（KEK）23 Oct. '07 "Monthly Colloquium「Accelerated RNB facility, TRIAC and its physics」"

17 Valery Zagrebaev（Flerov Laboratory of Nuclear Reaction, JINR, Dubna, Russia）26 Oct. '07 "RIBF Nuclear Physics Seminar「Synthesis of superheavies. State of affair and outlook.」"

18 H. Watanabe（RI Physics Lab., RIKEN）4 Oct. '07 "RIBF Nuclear Physics Seminar「Nature of transitional nuclei scrutinized with isomer spectroscopy」"

19 K. Nishijima（Chuo Univ. / Univ. of Tokyo / Kyoto Univ.）20 Nov. '07 "Monthly Colloquium「Emergence of the Second Generation in Particle Physics」"

20 N. Aoi（Heavy Ion Nuclear Physics Lab., RIKEN）27 Nov. '07 "RIBF Nuclear Physics Seminar「Shape transition in neutron-rich Cr isotopes」"

21 S. Shimoura（CNS, Univ. of Tokyo）11 Dec '07. "Lecture SeriesIV-2「Practical nuclear reaction theory for experimentalists（2nd）」"

22 T. Kishimoto（Osaka Univ.）12 Dec. '07 "Monthly Colloquium「Study of double beta decay：A quest to answer why our universe is matter dominated」"

23 J. Gibelin（Lawrence Berkeley National Lab.）25 Dec. '07 "RIBF Nuclear Physics Seminar「Recent experiments at the Berkeley 88" Cyclotron」"

24 T. Saito（GSI）3 Dec. '07 "RIBF Nuclear Physics Seminar「Hypernuclear spectroscopy with stable heavy ion beams and rare isotope beams: The HypHI project at GSI and FAIR in Germany」"

25 Nigel Orr（LPC-Caen）4 Dec. '07 "RIBF Nuclear Physics Seminar「Exploring the structure of light unbound neutron-rich nuclei」"

26 Y. Kondo（Heavy Ion Nuclear Physics Lab., RIKEN）22 Jan. '08 "RIBF Nuclear Physics Seminar「Invariant-mass spectroscopy of the neutron drip line nuclei 13,14 Be」"

27 K. Ikeda（Heavy Ion Nuclear Physics Lab., RIKEN）12 Feb. '08 "RIBF Nuclear Physics Seminar「Halo structure of 11Li generated by the tensor and pair correlations」"

28 Juha Aysto（Univ. of Jyvaskyla, FINLAND）20 Feb. '08 "Lecture Series VI「Physics with Slow- / Trapped-RI Beams--Methods, Current Researches, and Perspectives--」"

29 I. Hamamoto（Lund Univ.）27 Feb. '08 "Lecture Series V-2「One-particle motion in nuclear many-body problem」"

30 M. Taiji（Genomic Sciences Center, RIKEN）29 Jan. '08 "Monthly Colloquium「Next-Generation Supercomputer and Future High-Performance Computing」"

31 K. Ogawa（Heavy Ion Nuclear Physics Lab., RIKEN）11 Mar. '08 "RIBF Nuclear Physics Seminar「The proton-neutron interaction and high spin isomers」"

32 I. Watanabe（Advanced Meson Science Lab.）18 Mar. '08 "Monthly Colloquium「Magnetism of the High-T_C Oxides Viewed by the Muon」"

33 Jean-Michel Daugas（CEA/DIF/DPTA / SPN）4 Mar. '08 "RIBF Nuclear Physics Seminar「Magnetic moments of μ-second isomeric fragments」"

34 T. Suda（User Liaison and Support Group, RIKEN）et al. 28 Jul. '07 "Mini Workshop「Study of two neutron correlation in 6He via nucleon-exchnge reation」"

35 H. Sakaguchi（Univ. of Miyazaki）, et al. 13 Dec. '07 "Mini Workshop「Study of nucleon density distribution using G-matrix method.」"

Superheavy Element Laboratory

1 T. Ichikawa（Superheavy Element Lab., RIKEN）23 Jul. '07 "Mini Workshop「Challenges to superheavy elements」"

Theoretical Physics Laboratory

1 T. Abe（Tokyo Inst. of Tech.）17 Oct. '07 "The 1st TNP Lab. Seminar「Lattice Calculation of Thermal Properties of Neutron Matter with NN Effective Field Theory」"
2 R. Seki（California State Univ.）17 Dec. '07 "The 2nd TNP Lab. Seminar「Nuclear Effective Field Theory; A Short Introduction」"
3 K. Hagino.（Tohoku Univ.）, et al25 Dec. '07 "Mini Workshop「Two-nucleon correlations and unstable nuclei」"
4 K. Muto（Tokyo Inst. of Tech.）16 Jan. '08 "The 3rd TNP Lab. Seminar「Monopole interaction in nuclei」"
5 N.Michel（Kyoto Univ.）13 Feb. '08 "The 4th TNP Lab. Seminar「Gamow and PTG bases expansion methods for Skyrme-HFB calculations」"
6 H.Masui（Kitami Institute of Technology）13 Feb. '08 "The 5th TNP Lab. Seminar「M-scheme cluster-orbital shell model approach for oxygen isotopes」"
7 Bertrand Giraud（Saclay, France）28 Feb. '08 "The 6th TNP Lab. Seminar「A few rigorous results for the nuclear density functional theory」"
8 M. Ito, et al.19 Mar. '08"Mini Workshop「Exotic structures and reaction dynamics of highly-excited molecular resonances in light neutron-rich systems」"

Radiation Laboratory

1 M. Stratmann（RIKEN）, Jianwei Qiu（Iowa State Univ. / ANL）, S. Kumano（KEK）25 Jun. '07 "PHENIX Spinfest at RIKEN 2007"

Advanced Meson Science Laboratory

1 F. Sakuma（Advanced Meson Science Lab., RIKEN）25 Apr. '07 "Lab. Seminar「Evidence for mass modification of vector mesons at KEK-PS E325」"
2 K. Itabashi（Advanced Meson Science Lab., RIKEN）et al. 14 Jun. '07 "Mini Workshop「Workshop on Meson Bound System」"
3 Y. Kobayashi（Advanced Meson Science Lab., RIKEN）20 Jun. '07 "Lab. Seminar「Development and status of in-beam Mossbauer spectroscopy by using the neutron capture reaction」"
4 H. Nemura（Advanced Meson Science Lab., RIKEN）, et al. 17 Jul. '07 "Mini Workshop「Joint workshop on unstable and strange nuclei ---structural aspects of light exotic systems---」"
5 E. Yagi（Advanced Meson Science Lab., RIKEN）18 Jul. '07 "Lab. Seminar「The state of hydrogen in metals as observed by the channelling method」"
6 A. Ichikawa（Kyoto Univ.）18 Sep. '07 "Lab. Seminar「Current status of the neutrino oscillation phenomenon and future prospect」"
7 T. Azuma（Tokyo Metoropolitan Univ.）25 Oct. '07 "Lab. Seminar「New trends in atomic collision physics with two ion storage rings. --heavy ion medical accelerator and electrostatic ion storage ring--」"
8 T. Goto（Sophia Univ.）7 Nov. '07 "Lab. Seminar「NMR study on the local structure in high-Tc cuprates」"
9 M. Aoki（Osaka Univ.）20 Dec. '07 "Lab. Seminar「An Experiment Searching for mu-e Conversion at J-PARC」"
10 K. Suzuki（SMI）9 Jan. '08 "Lab. Seminar「Search for the kaonic nuclear cluster K^-pp in the $p+p ¥rightarrow K^+ + K^-pp$ reaction with FOPI」"
11 S. Ohira-Kawamura（Ocyanomizu Univ.）13 Feb. '08 "Lab. Seminar「Magnetism and superconductivity in novel superconductor CeCoIn5」"

Accelerator Applications Research Division

1 R. Ito（Univ. of The Ryukyus） 11 Dec. '07 "「The role for AtMinE1 in division site determination of chloroplasts」"
2 M. Fujiwara（Univ. of Tokyo） 11 Dec. '07 "「Replication of non-green plastids in Arabidopsis」"
3 T. Abe, N. Fukunishi（Nishina Center, RIKEN）, et al. 24 Jan. '08 "Progress of plant biology using heavy-ion accelerators"

Metallomics Research Unit

1 Y. Nose（Duke University, Medical Center） 4 Dec. '07 "「Physiological roles of copper-transporter Ctr1 in mice」"
2 Y. Yoshikawa（Kyoto Pharmaceutical Univ.） 4 Dec. '07 "「Development of Zn（II） complexes to treat type 2 diabetes mellitus」"
3 S. Kabuki（Kyoto Univ.） 15 Jan. '08 "「Development of an Electron Tracking Compton Gamma-Ray Camera for Nuclear Medicine 」"
4 Y. Wada（Molecular Probe Dynamics Lab. Molecular Imaging Research Program, RIKEN） 8 Feb. '08 "「Positron Emission Tomography（PET）」"
5 T. Ikeda（Atomic Physics Lab., RIKEN） 17 Mar. '08 "「Production of nanometer-sized focused ion beams with a glass capillary and selective irradiation of organelle in a living cell」"

RIKEN BNL Research Center

1 S. Arnold（BNL）, et al. 26 Apr. '07 "Parity Violating Spin Asymmetries at RHIC-BNL"
2 Haixin Huang（BNL）, et al. 30 Aug. '07 "RHIC Spin Collaboration Meeting"
3 Daniel de Florian, Lara De Nardo, et al. 8 Oct. '07 "Global Analysis of Polarized Parton Distributions in the RHIC Era"
4 K. Boyle（SBU）, et al. 15 Nov. '07 "RHIC Spin Collaboration Meeting"
5 S. Bazilevsky（BNL）, et al. 30 Nov. '07 "RHIC Spin Collaboration Meeting"

AUTHOR INDEX

RIKEN Accelerator Progress Report Vol. 41

独立行政法人理化学研究所加速器年次報告　第41巻（2008）

印　刷　平成20年（2008）9 月25日
発　行　平成20年（2008）9 月25日

発行者　独立行政法人理化学研究所　仁科加速器研究センター
代表者　矢　野　安　重
〒351-0198　埼玉県和光市広沢２番１号
電話（048）462−1111

編集者　独立行政法人理化学研究所　仁科加速器研究センター
加速器年次報告編集委員会

印刷所　勝美印刷株式会社
〒112-0002　東京都文京区小石川 1−3−7